

**NASA TECHNICAL
MEMORANDUM**



NASA TM X-2378

NASA TM X-2378

53



NASTRAN: USERS' EXPERIENCES

Colloquium held at
Langley Research Center
Hampton, Virginia
September 13-15, 1971

FACILITY FORM 602	<u>N71-36253-</u> (ACCESSION NUMBER)	<u>N71-36305</u> (THRU)
	<u>785</u> (PAGES)	<u>H1</u> (CODE)
	<u>1</u> (NASA CR OR TMX OR AD NUMBER)	<u>32</u> (CATEGORY)

NATIONAL AERONAUTICS AND SPACE ADMINISTRATION • WASHINGTON, D. C. • SEPTEMBER 1971

REPRODUCED BY
**NATIONAL TECHNICAL
INFORMATION SERVICE**
U.S. DEPARTMENT OF COMMERCE
SPRINGFIELD, VA. 22161

1. Report No. NASA TM X-2378	2. Government Accession No.	3. Recipient's Catalog No. N71-36253-
4. Title and Subtitle NASTRAN: USERS' EXPERIENCES		5. Report Date September 13, 1971 305
		6. Performing Organization Code
7. Author(s)		8. Performing Organization Report No. L-7980
9. Performing Organization Name and Address NASA Langley Research Center Hampton, Virginia 23365		10. Work Unit No. 134-14-04-01
		11. Contract or Grant No. N/A
12. Sponsoring Agency Name and Address National Aeronautics and Space Administration Washington, D.C. 20546		13. Type of Report and Period Covered Technical Memorandum
		14. Sponsoring Agency Code
15. Supplementary Notes Compendium of papers prepared for NASTRAN Users' Colloquium, September 13-15, 1971, NASA Langley Research Center		
16. Abstract This Technical Memorandum is comprised of selected papers prepared for the NASTRAN Users' Colloquium held at the NASA Langley Research Center, September 13-15, 1971. The authors discuss the application of NASTRAN to a wide variety of static and dynamic structural problems. Specifically, the papers focus on the following topics: (I) Statics, (II) Vibrations, (III) Dynamics, (IV) Structural Design, (V) Systems and Operational Problems, (VI) Evaluations and Innovations, and (VII) New Capabilities for NASTRAN. <div style="text-align: center;">REPRODUCED BY NATIONAL TECHNICAL INFORMATION SERVICE U.S. DEPARTMENT OF COMMERCE SPRINGFIELD, VA. 22161</div>		
17. Key Words (Suggested by Author(s)) NASTRAN, structures, finite element, NASTRAN Colloquium		18. Distribution Statement Unclassified - Unlimited
19. Security Classif. (of this report) Unclassified	20. Security Classif. (of this page) Unclassified	

STAR Category 32

N O T I C E

THIS DOCUMENT HAS BEEN REPRODUCED FROM THE
BEST COPY FURNISHED US BY THE SPONSORING
AGENCY. ALTHOUGH IT IS RECOGNIZED THAT CER-
TAIN PORTIONS ARE ILLEGIBLE, IT IS BEING RE-
LEASED IN THE INTEREST OF MAKING AVAILABLE
AS MUCH INFORMATION AS POSSIBLE.

PRECEDING PAGE BLANK NOT FILMED

NASTRAN: USERS' EXPERIENCES

Compendium of papers prepared for NASTRAN Users' Colloquium

September 13-15, 1971

NASA Langley Research Center

FOREWORD

NASTRAN (NASA STRUCTURAL ANALYSIS) has been available to the public since late in 1970. As a large, comprehensive, nonproprietary, general purpose, finite element computer system for structural analysis, NASTRAN is finding widespread acceptance within NASA, other government agencies, and industry.

NASTRAN is available to the public at a cost of about \$1,700, which covers reproducing and supplying the necessary system tapes and documentation. Furthermore, NASA has provided for the continuing maintenance and improvement of NASTRAN through the establishment of a NASTRAN Systems Management Office located at the Langley Research Center. At present, NASTRAN is in use at over sixty locations, including NASA centers, other government agencies, industry, and commercial computer data centers.

Because of the widespread interest in NASTRAN and because of a desire to better serve the community of NASTRAN users, the NASTRAN System Management Office organized a NASTRAN Users' Colloquium at the Langley Research Center, September 13-15, 1971. The colloquium was planned to provide to everyone concerned an opportunity to participate in a comprehensive review of the current status of NASTRAN use, including the rate of user acceptance, unique applications, operational problems, most desired modifications including new capability, and comparisons with other less comprehensive applications programs.

Individuals actively engaged in the use of NASTRAN were invited to prepare papers for presentation at the colloquium. These papers are included in this volume. Only a limited editorial review was provided to achieve reasonably consistent format and content. The opinions and data presented are the responsibility of the authors and their respective organizations.

J. P. Raney, Head
NASTRAN Systems Management Office
Langley Research Center
Hampton, Va. 23365
September 1971

Preceding page blank

CONTENTS

	Page
FOREWORD	iii
1. NASTRAN: STATUS, MAINTENANCE, AND FUTURE DEVELOPMENT OF NEW CAPABILITY by J. Philip Raney, Deene J. Weidman, and Howard M. Adelman (NASA Langley Research Center)	1
I. STATICS	
2. CALCULATION OF STRESS CONCENTRATION DUE TO A HYPERBOLOID CAVITY IN A THIN PLATE USING NASTRAN by Phillip R. Wilcox (NASA Ames Research Center)	9
3. NON-LINEAR CONSIDERATION OF GRAVITY IN A STIFFNESS TEST OF A WEAK STRUCTURE AT SMALL STRAINS by Ralph G. Barclay, Stuart L. Hanlein, John Sween, Jr., and Paul H. King (NASA Goddard Space Flight Center)	17
4. SKYLAB I NASTRAN STRESS ANALYSIS MODELS by William S. Viall (Teledyne Brown Engineering)	27
5. SOME ASPECTS OF NASTRAN SOLUTION ACCURACY by Gernot W. Haggemacher (Lockheed-California Co.)	47
6. A NASTRAN BUCKLING ANALYSIS OF A LARGE STIFFENED CYLINDRICAL SHELL WITH A CUTOUT by Richard H. Brolliar (Teledyne Brown Engineering)	65
7. NASTRAN DIFFERENTIAL STIFFNESS ANALYSIS OF AN AIRCRAFT CANOPY . . . by Robert D. Bennett (LTV-Vought Aerospace Division)	85
8. APPLICATION OF SMALL AND LARGE DISPLACEMENT THEORY TO A LARGE FLEXIBLE SOLAR ARRAY AND COMPARISON WITH STATIC TEST RESULTS . . . by Ronald P. Schmitz (Sperry Rand Corp.)	107
9. STATIC ANALYSIS OF THE 64-m (210-ft) ANTENNA REFLECTOR STRUCTURE . . by M. Smoot Katow (Jet Propulsion Laboratory)	123
10. NASTRAN-GAP: AN INTEGRATED APPROACH TO THE ANALYSIS OF RADIATION PATTERNS OF DISTORTED REFLECTORS by William L. Cook (Communications Satellite Corp.)	141

Preceding page blank

	Page
11. ANALYSIS OF A HOT ELEVON STRUCTURE	163
by H. W. Bergmann, James C. Robinson, and Howard M. Adelman (North American Rockwell Space Division and NASA Langley Research Center)	

II. VIBRATIONS

12. NASTRAN MODELING STUDIES IN THE NORMAL-MODE METHOD AND NORMAL-MODE SYNTHESIS	181
by Roy Leon Courtney (NASA Goddard Space Flight Center)	
13. GUYAN REDUCTION SOLUTIONS RECYCLED FOR IMPROVED ACCURACY	201
by Roy Levy (Jet Propulsion Laboratory)	
14. MODAL ANALYSIS OF THE MATED SPACE SHUTTLE CONFIGURATION	221
by R. K. Gieseke (General Dynamics Corp.)	
15. NORMAL MODE ANALYSIS OF THE RADIO ASTRONOMY EXPLORER (RAE) BOOMS AND SPACECRAFT	237
by K. N. Jabbour (NASA Goddard Space Flight Center)	
16. STATIC AND DYNAMIC ANALYSIS, F-14A BORON HORIZONTAL STABILIZER	251
by S. L. Huang and H. Rubin (Naval Air Development Center)	
17. ADAPTATION OF NASTRAN TO THE ANALYSIS OF THE VIKING SPACE VEHICLE	265
by Thomas C. Jones and Larry D. Pinson (NASA Langley Research Center)	
18. ACOUSTIC ANALYSIS OF SOLID ROCKET MOTOR CAVITIES BY A FINITE ELEMENT METHOD	285
by David N. Herting, Jerrard A. Joseph, Loren R. Kuusinen, and Richard H. MacNeal (The MacNeal Schwendler Corp.)	
19. PRACTICAL ANALYSIS OF PLATE VIBRATIONS USING NASTRAN	325
by Robert R. Clary (NASA Langley Research Center)	
20. MODAL ANALYSIS OF A NINE-BAY SKIN-STRINGER PANEL	343
by Robert E. Grandle and Carl E. Rucker (NASA Langley Research Center)	

III. DYNAMICS

21. STRUCTURAL DYNAMIC ANALYSIS OF ELECTRONIC ASSEMBLIES USING NASTRAN RESTART/FORMAT CHANGE CAPABILITY	363
by Ronald P. Schmitz (Sperry Rand Corp.)	

	Page
22. THE RESPONSE OF SHELLS TO DISTRIBUTED RANDOM LOADS USING NASTRAN . . .	393
by Gary K. Jones (NASA Goddard Space Flight Center)	
23. APPLICATIONS OF NASTRAN TO COUPLED STRUCTURAL AND HYDRODYNAMIC RESPONSES IN AIRCRAFT HYDRAULIC SYSTEMS	407
by James T. Howlett (NASA Langley Research Center)	
24. APPLICATION OF NASTRAN TO A SPACE SHUTTLE DYNAMICS MODEL	421
by E. A. Thornton (Old Dominion University)	
25. COMPLEX EIGENVALUE SOLUTION TO A SPINNING SKYLAB PROBLEM	439
by Jayant S. Patel and S. M. Seltzer (Teledyne-Brown Engineering Co., Inc., and NASA George C. Marshall Space Flight Center)	

IV. STRUCTURAL DESIGN

26. APPLICATION OF NASTRAN TO THE ANALYSIS OF A SPACE SHUTTLE ORBITER STRUCTURE	451
by Gary L. Giles and John H. Dutton (NASA Langley Research Center and McDonnell Douglas Corp.)	
27. NASTRAN AS ANALYSIS TOOL IN A STRUCTURAL DESIGN OPTIMIZATION PROCESS	465
by J. E. Sobieszczanski and D. D. Loendorf (NASA Langley Research Center and Langley Directorate, U.S. Army Air Mobility R&D Laboratory)	
28. STRUCTURAL ANALYSIS AND DESIGN OPTIMIZATION OF SPACECRAFT USING NASTRAN	479
by Roy L. Courtney (NASA Goddard Space Flight Center)	
29. THE USE OF NASTRAN IN THE ANALYSIS OF LARGE COMPLEX AIRFRAME STRUCTURES - MODELING TECHNIQUES AND ORGANIZATION	493
by Gernot W. Haggemacher (Lockheed-California Co.)	

V. SYSTEMS AND OPERATIONAL PROBLEMS

30. NASTRAN DOCUMENTATION FROM AN HISTORICAL VIEWPOINT	517
by Frank J. Douglas (Computer Sciences Corp.)	
31. DATA MANAGEMENT REQUIREMENTS FOR LARGE PROBLEMS	533
by Stanley D. Hansen and Harald B. Hansteen (Boeing Co.)	
32. NASA TECHNOLOGY TRANSFER: THE COMPUTER SOFTWARE DISSEMINATION PROGRAM	551
by Joseph M. Carlson (NASA Headquarters)	

	Page
33. NASTRAN EXPERIENCES OF FORT WORTH OPERATION, CONVAIR AEROSPACE DIVISION OF GENERAL DYNAMICS	553 ~
by Merle Allen (General Dynamics/Convair)	
34. A SPECIAL NASTRAN PROGRAM FOR INPUT CHECKING AND UNDEFORMED STRUCTURE PLOTING	559
by Willianna W. Smith (NASA Langley Research Center)	
35. EXPERIENCES IN NASTRAN INSTALLATION AND TRAINING	569
by Caleb W. McCormick (The MacNeal Schwendler Corp.)	
36. NASTRAN INSTALLATION: IMPLEMENTATION STEPS AND POSSIBLE PROBLEMS ENCOUNTERED	577
by Howard E. Dielmann (Computer Sciences Corp.)	
VI. EVALUATIONS AND INNOVATIONS	
37. AN EVALUATION OF CURRENT NASTRAN DISCRETE ELEMENT MODELS FOR MONOCOQUE AND SEMI-MONOCOQUE STRUCTURES	587
by Edward L. Stanton and William F. Bozich (McDonnell Douglas Astronautics Co.)	
38. SAVINGS IN NASTRAN DECOMPOSITION TIME BY SEQUENCING TO REDUCE ACTIVE COLUMNS	627
by R. Levy and S. Wall (Jet Propulsion Laboratory and Computer Sciences Corp.)	
39. NEW ELEMENT DEFINITION CAPABILITY FOR NASTRAN	633
by Myles M. Hurwitz and Michael E. Golden (Naval Ship Research and Development Center)	
40. VIBRATION STUDIES OF A FLAT PLATE AND A BUILT-UP WING	637
by James H. Starnes, Jr. (NASA Langley Research Center)	
41. PRODUCTION OF MOTION PICTURES OF A CONTINUOUSLY DEFORMING STRUCTURE USING NASTRAN	647
by Robert J. Reynolds (Convair Aerospace Div. of General Dynamics)	
42. AN INTERACTIVE COMPUTER GRAPHICS PROGRAM FOR NASTRAN	659
by Michael Cronk (General Dynamics/Convair)	
43. NASTRAN USER INTERFACES - AUTOMATED INPUT INNOVATIONS	669
by Malcolm W. Ice (Boeing Computer Services, Inc.)	

	Page
44. PROCEDURE FOR EFFICIENTLY GENERATING, CHECKING, AND DISPLAYING NASTRAN INPUT AND OUTPUT DATA FOR ANALYSIS OF AEROSPACE VEHICLE STRUCTURES	679 ✓
by Gary L. Giles and Charles L. Blackburn (NASA Langley Research Center and AVCO Aerostructures Div.)	
45. VEHICLE STRUCTURAL ANALYSIS - PRE AND POST PROCESSOR DATA HANDLING . .	697 ✓
by T. Furuike and S. Yahata (North American Rockwell Corp.)	
46. NASTRAN PLOTTING CAPABILITIES	709 ✓
by John R. McDonough (Computer Sciences Corp.)	
47. A NASTRAN POSTPROCESSOR FOR STRUCTURAL MODIFICATION REANALYSIS	737 ✓
by Roy Levy (Jet Propulsion Laboratory)	
48. CONVERGENCE OF THE NASTRAN PLATE ELEMENTS FOR SHELL STRESS ANALYSIS	749 ✓
by Michael T. Wilkinson and Robert E. Fulton (NASA Langley Research Center)	

VII. NEW CAPABILITIES FOR NASTRAN

49. SPACE SHUTTLE - THE NEED FOR SUBSTRUCTURING	769 ✓
by H. R. Grooms and S. Yahata (North American Rockwell Corp.)	
50. A DESIGN STUDY FOR THE INCORPORATION OF AEROELASTIC CAPABILITY INTO NASTRAN	779 ✓
by Robert L. Harder, Richard H. MacNeal, and Robert V. Doggett, Jr. (The MacNeal Schwendler Corp. and NASA Langley Research Center)	
51. SOLID ELEMENT REQUIREMENT FOR NASTRAN	797 ✓
by Stig Wahlstrom (The Boeing Co.)	
52. ON THE REDUCTION OF PROLIFERATION OF FINITE ELEMENT PROGRAMS	813 ✓
by T. G. Butler (NASA Goddard Space Flight Center)	

NASTRAN: STATUS, MAINTENANCE, AND FUTURE DEVELOPMENT
OF NEW CAPABILITY

By J. Philip Raney, Deene J. Weidman,
and Howard M. Adelman

NASA Langley Research Center

NASTRAN, as the largest, most comprehensive, nonproprietary, general purpose, finite element computer system for structural analysis in existence today, is finding widespread acceptance within NASA, other government agencies, and industry. The purpose of this paper is to describe the present status of NASTRAN (NASA Structural Analysis) and to outline goals and objectives for its future maintenance and development by the NASTRAN Systems Maintenance Office.

STATUS

Background

NASTRAN was developed under the direction of Mr. T. G. Butler, NASA-Goddard Space Flight Center, during the years 1965 to 1970. Upon completion of the development phase, the management of NASTRAN was transferred to the Langley Research Center. The NASTRAN Systems Management Office (NSMO) was established in the Structures Division at Langley October 4, 1970, and the first public release of NASTRAN was in November 1970.

The requirement for centralized management of NASTRAN is dictated by its range of complex system software features and extensive capabilities. As the largest, best documented, user-oriented, general purpose finite-element computer program for structural analysis, NASTRAN is without a peer in providing capability for the integrated analysis of complete aerospace vehicle structures. Twelve prepackaged "rigid formats" permit the analysis of one and the same structural model for a wide variety of static and dynamic loading conditions, including buckling, steady state frequency response, transient and random response behavior. NASTRAN consists of over 151,000 Fortran statements which translate into over 1,000,000 machine language statements. It is machine independent and operates on the IBM 360, CDC 6000 series, and the UNIVAC 1108 machine. Perhaps the most unique feature of NASTRAN is its executive system for data scheduling and overall system control. Briefly, NASTRAN is as large and complex—in a computer software sense—as the operating systems for the three machines with which it interfaces. It is, in fact, a facility, with complete documentation, which presently is in operation throughout the United States at over 60 different machine installations, with an estimated family of users numbering nearly 1,000 persons. The communal aspects of NASTRAN are obviously far-reaching.

Role of NSMO

The management of NASTRAN is the responsibility of the NASTRAN Systems Management Office (NSMO). The functions of this office span the spectrum of NASTRAN activities from maintenance to research and development.

Specifically, these functions include:

- Centralized Program Development
(Advisory Committees)

- Coordinating User Experiences
(NASTRAN Bulletin)

- System Maintenance
(Error Correction and Essential Improvements)

- Development and Addition of New Capability

- NASTRAN-Focused Research and Development

SIGNIFICANT MILESTONES

October 1970 - September 1971

When NSMO was established in October 1970, there existed a dire need for maintenance of the NASTRAN system. With the cooperation of Goddard Space Flight Center, an interim maintenance contract was negotiated with Computer Sciences Corporation through a contract in effect at GSFC. This contract provided for the essential function of error correction until a contract for full time maintenance could be negotiated through an open competition. The interim maintenance activity was restricted to the correction of over 75 errors reported to NSMO, together with all associated documentation changes. New thermal bending and hydroelastic elements previously developed by the MacNeal-Schwendler Corporation under contract to GSFC were also installed. Levels 13 and 14 were created for government testing and evaluation. The next version of NASTRAN to be released to the public through COSMIC* will be built upon the results of this interim maintenance activity and will be designated Level 15.

In June, a contract for full time maintenance of NASTRAN was awarded to the MacNeal-Schwendler Corporation. An offsite office near the Langley Research Center has been opened by MacNeal-Schwendler, and work on many items of maintenance and development has commenced.

In addition to the maintenance contract, a contract for the development of new elements and a thermal analyzer capability was awarded in June to the Bell Aerospace Company.

*Computer Software Management Information Center, Barrow Hall, University of Georgia, Athens, 30601.

Additional milestone accomplishments include holding the First Annual NASA NASTRAN Users' Colloquium at the Langley Research Center, September 13-15, 1971, and publishing in August of Vol. 1, No. 1, of the NASTRAN Users' Bulletin—a bimonthly publication of interest to the family of NASTRAN users.

MAINTENANCE

For the purpose of the present discussion, maintenance is defined to include error correction in both the NASTRAN code and documentation, support of all utility routines such as the linkage editor and conversion routines, and enhancements to the NASTRAN executive and matrix routines which will result in increased speed, efficiency, and convenience of operation. Maintenance is a systems rather than a new capability or element-oriented activity.

Utility Routines

Routines for creating new levels of NASTRAN as well as routines for converting NASTRAN from the CDC 6000 series (parent machine) to versions that will run on the IBM 360 and UNIVAC 1108 must be constantly updated as new or modified compilers and operating systems become available for any of the three NASTRAN machines. Automatic update routines are required to implement a patch to a given level. For example, a patch is presently available from COSMIC to update Level 12.0 to 12.1. The update routines are required to enable NASTRAN users to incorporate error corrections, supplied by the maintenance contractor, in a timely fashion.

Error Correction

Error correction is perhaps the single most important maintenance activity. Errors in either the code or the manuals for the standard level of NASTRAN are reported to NSMO, together with card decks and annotated output for evaluation and priority assignment. The maintenance contractor then diagnoses, isolates, and corrects the error and further validates the fix with appropriate demonstration runs. When fully corrected and validated, the correction card deck, together with card decks for other corrected errors, is made available by NSMO as a patch to the current level of NASTRAN. By faithfully reporting known and suspected errors, each member of the NASTRAN family of users benefits both himself and potentially many others. A constantly updated computerized data bank of all known NASTRAN bugs will be established by the maintenance contractor for NSMO. A sort may be performed at any time by rigid format, module, or some other significant system parameter to determine the status of a previously reported bug to determine the nature of any uncorrected bugs in a routine of interest. This coordinated, mutually beneficial, centralized error correction activity should result in a relatively trouble-free operation for NASTRAN users.

Enhancements for Efficiency

Several systems modifications to obtain greater operational speed and efficiency are presently in progress. These enhancements include:

Substructuring capability to allow the solution of larger problems than is presently practical.

Improved multiply/add (MPYAD) routines to reduce running time.

User-specified single precision for the CDC machine.

Much faster general input/output (GINO) routines.

More efficient matrix packing routines.

It is anticipated that these and other system improvements will decrease average run times for the next public release of NASTRAN (Level 15) by approximately a factor of three.

Dummy Element

A user-oriented dummy element capability is under development by the maintenance contractor. This important convenience will allow the incorporation of the mass, damping, and stiffness matrices for a new element for test, evaluation, and use in the NASTRAN environment.

NASTRAN Users' Bulletin

An important aspect of NASTRAN maintenance is timely communication with NASTRAN users concerning important developments and system improvements. The NASTRAN Users' Bulletin is designed to satisfy this requirement. Issued bimonthly, it will contain a statement from NSMO, significant user notes, news of recently reported bugs, information on the next level to be released, and unique applications of NASTRAN.

DEVELOPMENT OF NEW CAPABILITY

Significant new capability is under development for NASTRAN in addition to the system-oriented activities of the maintenance contractor. The contract with Bell Aerospace previously alluded to provides for the development of several new elements and a comprehensive capability for thermal analysis. The evaluation and selection of new capability for NASTRAN requires the cooperation of NASA Centers, other government agencies, and industry. For example, the system modifications, new elements, and thermal analyzer capability were selected from a prioritized compilation of items supplied by all of the NASA Centers. Preference has been given to the highest priority items, although some deviation is necessitated to achieve the greatest capability within a

given cost constraint. The following selected list of new element capability is under development with public release planned for early 1973:

Nonprismatic Beam Element

Triangular and Trapezoidal Cross-Section Rings with Nonaxisymmetric Deformation

General Element defined by stiffness matrix

Multilayered Triangular and Quadrilateral Plate Elements

Triangular and Quadrilateral Shell Elements

Rigid Body Element

Triangular and Quadrilateral Plates with Membrane/Flexure Coupling

Curved Beam Element

Higher Order Shell of Revolution Element for Nonaxisymmetric Loading

Higher Order Triangular and Quadrilateral Plate Elements

In addition, the following heat transfer capability is also planned: Transient and steady-state conduction, convection and radiation with automatic conversion of the temperature history to displacement and stress history.

No attempt has been made to include with the new capability discussed above numerous other activities at other NASA centers or within industry itself. Various nonstandard experimental or parochial versions of NASTRAN exist. When new capability tested in an experimental NASTRAN environment is found to be a valuable addition to the standard level of NASTRAN, it will be incorporated by NSMO.

FUTURE LEVELS OF NASTRAN

New levels of NASTRAN will be released when the number of error correction patches, system improvements, and new elements becomes excessive and dictates the generation of a complete new level. Ease and simplicity of bookkeeping and local management are prime drivers in this situation. Although no firm commitment is possible, it is anticipated that future releases of NASTRAN will occur and will include new capability generally somewhat as follows:

1972 - Level 15

Error Corrections

Substructuring

Enhancements for speed:

GINO

MPYAD

Single Optional Precision (Limited)

Matrix Packing

Dummy Element

Thermal Analyzer
(Steady State Conduction)

1973 - Level 16

Error Corrections

Complete Single Precision

New Elements Developed By
Bell Aerospace

Complete Thermal Analyzer

Later levels will include incremental additions to the comprehensive capability if this activity receives funding support.

SUMMARY

The maintenance and development of NASTRAN has been centralized at the Langley Research Center in the NASTRAN Systems Management Office (NSMO). Several important system improvements are in progress which will result in a significant reduction of average computer run time. The maintenance contractor, MacNeal-Schwendler, is also engaged in the addition of comprehensive substructuring capability. A dummy element capability which allows the test, evaluation, checkout, and temporary use of a new element in the NASTRAN environment is also underway and planned for inclusion in Level 15.

Several new elements and a comprehensive heat transfer capability are in development under a contract with the Bell Aerospace Company. These enhancements are planned for inclusion in Level 16.

In summary, NASTRAN has emerged as a powerful, generalized facility for the analysis of complex aerospace structures and is rapidly gaining acceptance from the community of aerospace and industrial users. NASA is, therefore, committed to manage and maintain the NASTRAN system as a valuable national resource.

CALCULATION OF STRESS CONCENTRATION DUE TO A HYPERBOLOID

CAVITY IN A THIN PLATE USING NASTRAN

By Phillip R. Wilcox

NASA Ames Research Center

SUMMARY

NASTRAN has been used to solve for the stress concentration in a plate due to a hyperboloid cavity under biaxial loading. Details concerning the usage of the program, modeling of the structure, and a comparison between experimental and theoretical results are presented.

INTRODUCTION

At the time NASTRAN was released to Ames Research Center, an experimental program was underway to determine the stress concentration caused by the presence of a surface cavity in a plate under uniform biaxial tension. Both hyperboloid and hemispherical cavities were then analyzed with NASTRAN, and the comparison with experimental and other theoretical work was presented in reference 1. However, since this work represents a good example of the application of NASTRAN to three dimensional problems, details concerning the usage of the program and results for one cavity shape are given herein.

SYMBOLS

a	radius of cavity at surface of plate
d	plate thickness
h	cavity depth
K	stress concentration factor at bottom of cavity
p	applied radial pressure
r	radial coordinate
z	axial coordinate

Preceding page blank

σ_r radial stress component tangent to surface
 σ_θ circumferential stress component

PROGRAM INPUT AND OUTPUT

Level 11.1.0 rigid format series L. adapted to the I.B.M. 360-67 was used in the analysis. The cavity shape that will be discussed here is a 1.047-radian hyperboloid cavity and is shown in Figure 1.

Trapezoidal and triangular ring elements were used in the analysis within the limitation of the program. NASTRAN requires, using the notation in Figure 2:

1. $r \geq 0$ for G1 & G4 of the trapezoidal element
2. $r > 0$ for G2 & G3 of the trapezoidal element
3. $r > 0$ for G1, G2, & G3 of the triangular element
4. if $r = 0$, the grid point must be restrained because of symmetry in all but the z direction, i.e. 12456
5. if $r \neq 0$, the grid point restraints are 2456

The program outputs were:

1. displacements of all grid points (a) radial (b) axial
2. stresses for all elements (a) radial (b) circumferential (c) axial (d) shear
3. nodal forces at all grid points (a) radial (b) circumferential (c) axial
4. load vectors

The trapezoidal stress outputs were for the 4 grid points and centroid, while the triangular stress outputs were for the centroid only.

The plate was first modeled with 413 elements with 804 degrees of freedom as shown in Figure 3(a) and (b). Smaller elements, Figure 3(c), subsequently were used in the neighborhood of the cavity to avoid the large discontinuity in stresses for the same grid point of four adjoining elements as shown for the coarse grid in Figure 4. This continuity in the stresses implied that we had arrived at a reasonable size for the elements. This refinement increased the model to 497 elements with 948 degrees of freedom. To vary the ratio of cavity depth to plate thickness (h/d) elements were either added or removed from the back surface of the plate.

In all there were six different model configurations run. These configurations are listed in Table I. The largest one was for a $h/d = .25$ which had 1,033 elements with 1930 degrees of freedom and required 1151 input cards.

A compressive load equal to 6.895×10^6 N/m² (1000 psi) was applied through the grid points at the edge of the plate. The method used to

calculate the load vector is illustrated in Figure 5 and summarized as follows:

$$\begin{aligned}\text{Uniform load} &= \text{Pressure} * 2\pi r \\ \text{Load vector} &= \text{Uniform load} * \Delta z \\ &\quad \text{except for the edge grid points, for which} \\ \text{Load vector} &= \text{Uniform load} * \frac{\Delta z}{2}\end{aligned}$$

COMPARISON OF NASTRAN SOLUTIONS WITH EXPERIMENTAL AND ANALYTICAL RESULTS

Figure 6 shows the comparison between the experimental and computer solution of the cavity surface and back surface stresses for $h/d = .51$. The experimental stress concentration factors at the bottom of the cavity were within 4% of that calculated by NASTRAN based on two experimental plates. NASTRAN was also compared with the analytical work that R. A. Eubanks did in 1954 for a hemispherical cavity in a semi-infinite solid (ref. 2). The stress concentration factor, K , calculated by Eubanks was 2.23 and that obtained from NASTRAN 2.3. Here again the stress concentration factor was within 4%. Since the agreement was so good, the rest of the experimental program was cancelled and the desired quantities obtained using NASTRAN.

CONCLUDING REMARKS

The results obtained here indicate that accurate values of stresses can be obtained for three-dimensional axisymmetric problems even in regions where the stresses are rapidly varying. Of course as the stress gradient increases the grid size must be decreased to maintain the same accuracy, but the use of variable size elements allows one to confine the small grid size to the region of rapidly varying stresses.

REFERENCES

1. Reed, Robert E. Jr. and Wilcox, Phillip R.: Stress Concentration Due to a Hyperboloid Cavity in a Thin Plate. NASA TN D-5955, 1970.
2. Eubanks, R.A.: Stress Concentration Due to a Hemispherical Pit at a Free Surface. J. Appl. Mech., Vol.21, No. 1, March 1954. pp. 57-62.

Table I: Model Configurations

CAVITY SHAPE	CAVITY DEPTH/PLATE THICKNESS
1.047-radian hyperboloid	0.80
	0.67
	0.51
	0.25
0.786-radian hyperboloid	0.52
Hemispherical	0.25

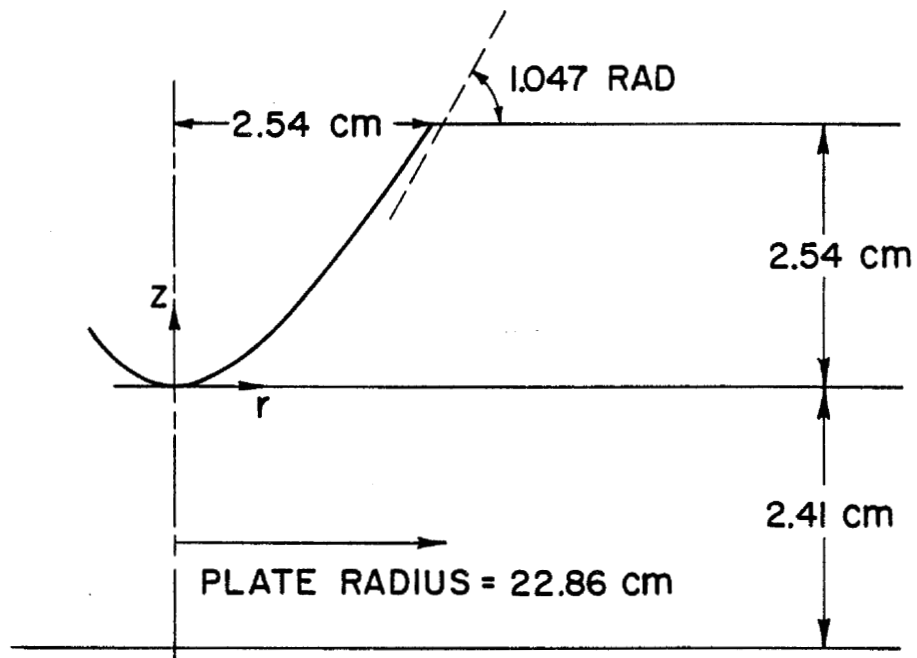


Figure 1.- 1.047-radian hyperboloid plate; $h/d = 0.51$.

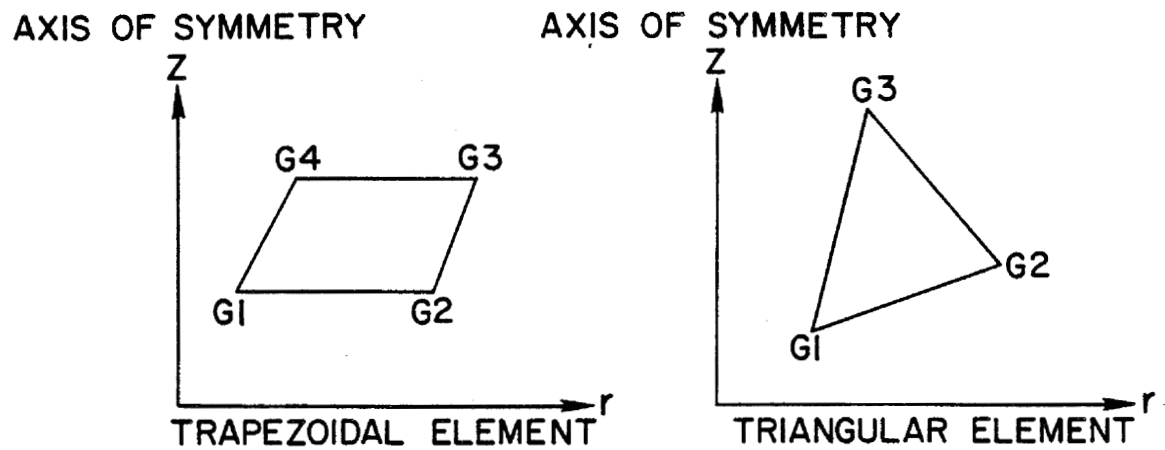


Figure 2.- Ring elements.

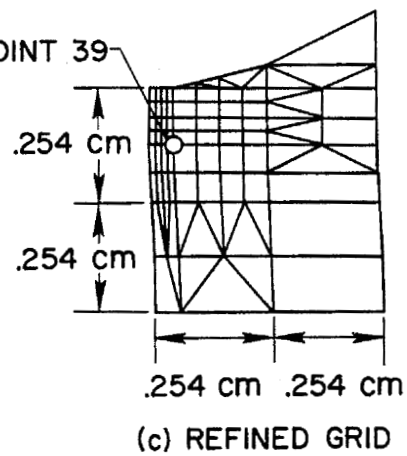
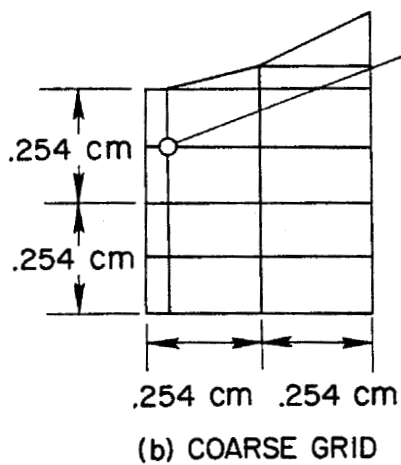
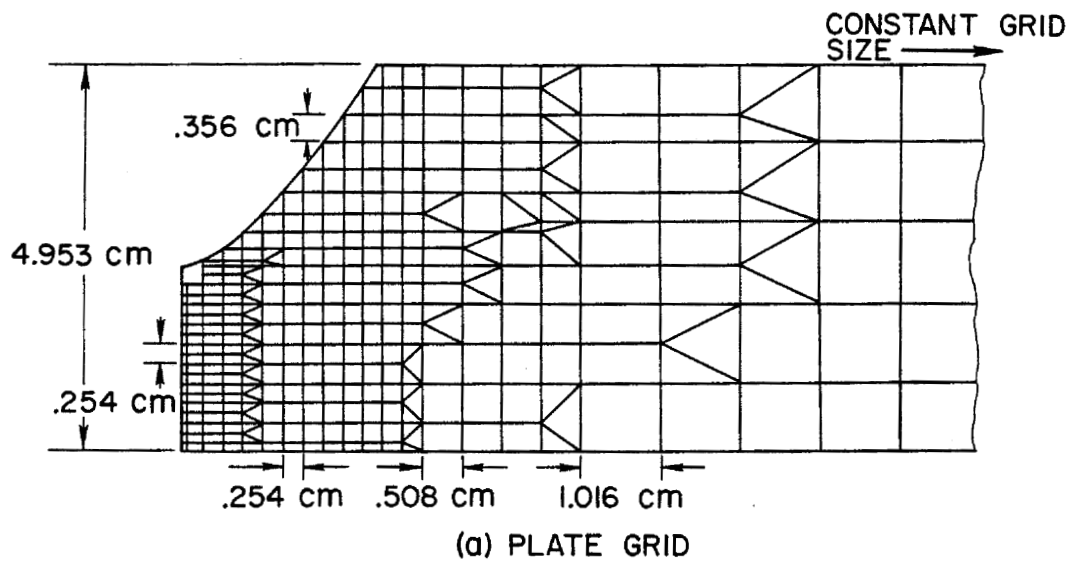


Figure 3.- Grid of 1.047-radian hyperboloid plate; $h/d = 0.51$.

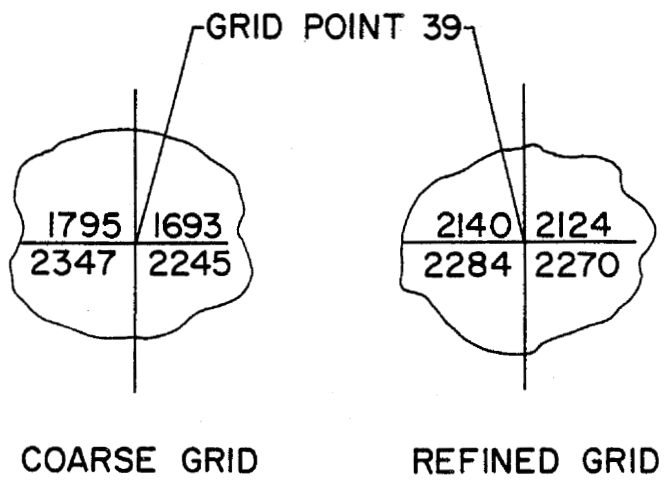


Figure 4.- Element radial stress.

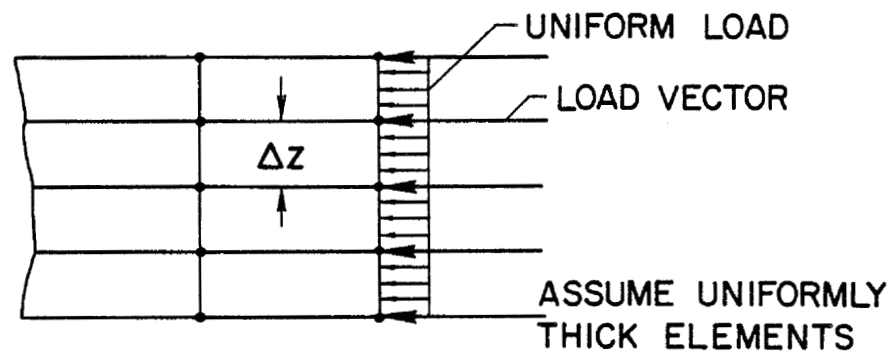
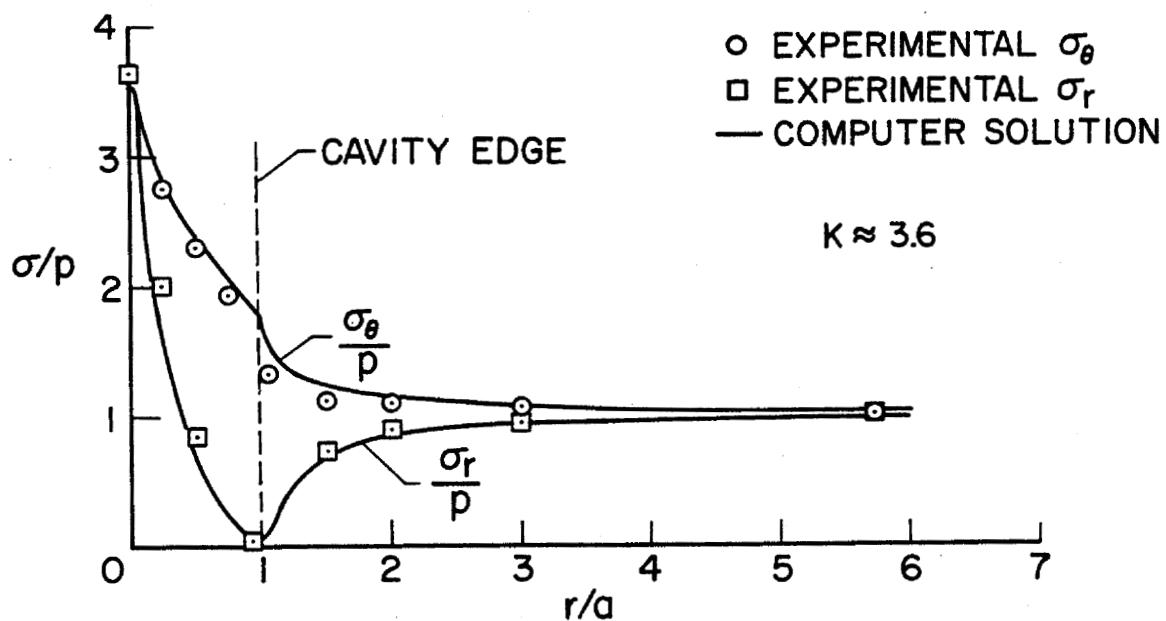
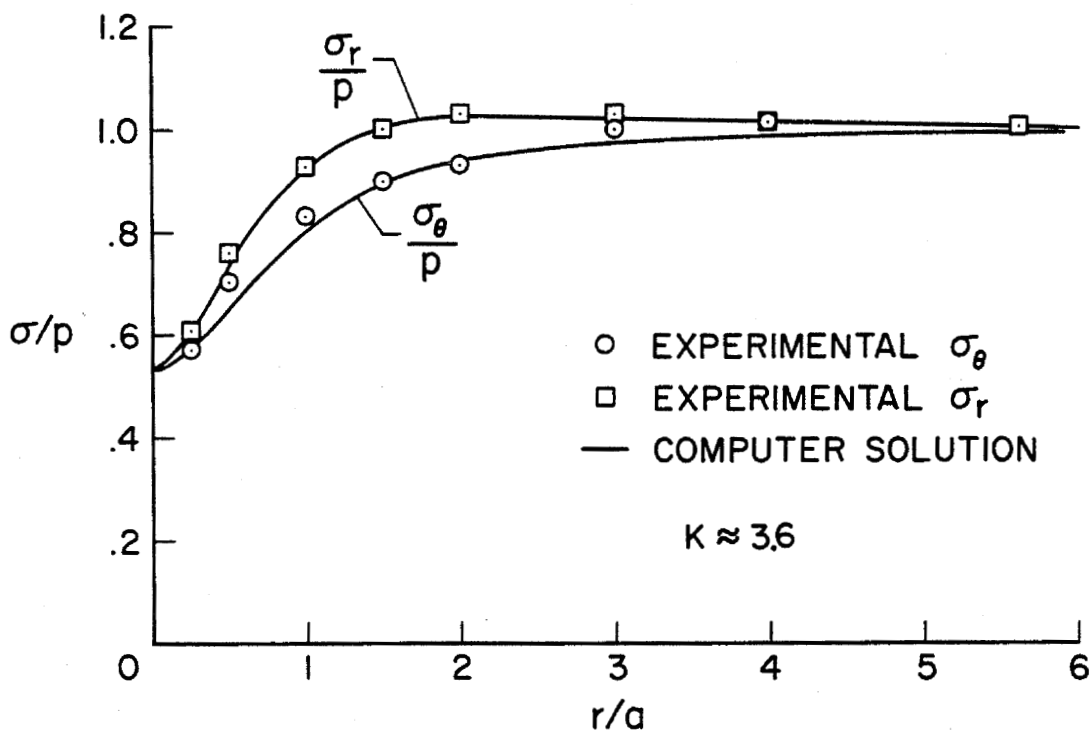


Figure 5.- Application of load vector.



(a) Cavity surface stresses.



(b) Back surface stresses.

Figure 6.- 1.047-radian hyperboloid plate; $h/d = 0.51$.

NON-LINEAR CONSIDERATION OF GRAVITY IN A STIFFNESS
TEST OF A WEAK STRUCTURE AT SMALL STRAINS

By Ralph G. Barclay, Stuart L. Hanlein,
John Sween, Jr. and Paul H. King

NASA Goddard Space Flight Center

SUMMARY

NASTRAN, NASA's finite-element structural analysis computer program, was used to calculate lateral deflections of a very weak spacecraft antenna boom, essentially a vertically-hung cantilever beam, under laboratory loading. The non-linear effect of gravity was included.

The purpose of the test was to determine the boom stiffness at extremely small strains thus simulating the strain conditions produced by dynamic lateral deflections in orbit.

The calculated deflections indicate that the determination should be possible; however, large hysteresis effects were found to be present and no stiffness results have been obtained in time for inclusion by publication date.

INTRODUCTION

On July 4, 1968, the Radio Astronomy Explorer satellite was launched. Its principal radio astronomy antennas and principal structural feature consist of four 228.6-meter (750 feet) tubular booms in an "X" configuration. Each boom was formed of beryllium copper tape which had been prestressed to curl lengthwise into a tube. For storage the tape was forced flat and wound onto its drum. In orbit, the tape is dispensed from the storage drum whereupon it immediately assumes its tubular shape. There is a seam running the length of each boom which contains interlocking teeth to limit overlapping and so improve torsional rigidity.

The "RAE" spacecraft is "gravity-gradient" stabilized which means that it orbits the earth always "pointing" toward the center of the earth. This result is caused by the fact that on the near-earth side of the spacecraft's center-of-gravity orbit the pull of gravity on the spacecraft structure is larger than the centrifugal reaction force. The reverse is true outside the center of gravity where the centrifugal reaction is larger

than the gravity force. These forces acting on the spacecraft tend to pull it into the earth-center-pointing attitude. Disturbances can cause rocking, i.e., librating, about this attitude.

After the spacecraft was fully deployed in orbit it was soon noticed that the observed libration frequencies were lower than calculated. Because the libration motion also causes a bending action in the booms, boom stiffness affects the libration frequency. From this it was postulated that the booms might be less stiff in orbit than had been measured in the laboratory where larger-than-orbit strain conditions were present. In other words, the low-strain stiffness might be different (possibly lower) than the stiffness measured at higher strains due to the overlapping, tab-meshing construction of the booms.

The main difficulty in a low-strain measurement is that the gravity load is much larger than the required low-strain loading.

SYMBOLS

R_3	NASTRAN rotation about axis perpendicular to x-y plane
T_1	NASTRAN displacement in x direction
T_2	NASTRAN displacement in y direction
E	Young's modulus
EI	stiffness
I	cross section moment of inertia
X	NASTRAN x axis (longitudinal boom axis)
Y	NASTRAN y axis (transverse boom axis)

TEST METHOD

The boom was mounted as a cantilever beam in a vertical position with the fixed end at the top. (See Figure 1.) Loading was produced by attaching a thin stick of balsa wood at the free end perpendicular to the boom. A small weight was hung on the balsa stick thus producing a moment and a downward force.

This technique of loading was chosen so as to produce deflection with a large, and somewhat uniform radius of curvature along the boom.

NASTRAN CONSIDERATIONS

Because the gravity forces on the boom are large as compared with the applied load it was necessary to consider their effect even for very small deflections. For this purpose the NONLINEAR provision of NASTRAN was used. The R_3 quantity multiplied by the segment weight yields (for small angles) the bending moment produced by gravity as the boom moves out of the vertical position.

Using the NONLINEAR provision requires the use of rigid format 9, Direct Transient Response. In order to reduce the time required to reach steady state, dampers were attached at the grid points and the load was applied gradually. See Figure 2 for NASTRAN input.

RESULTS

Figure 3 shows the NASTRAN-calculated deflections.

Figure 4 plots stiffness against tip deflection.

During laboratory testing, the unloaded shape of the boom was found not to be straight and changed when the boom was twisted ever so slightly. This effect may be important in explaining the in-orbit dynamic behaviour.

A loading sequence was carried out in which the boom returned to the unloaded shape after the load was removed. Hopefully, this data can eventually be made to yield a stiffness determination. However, since the test involved a starting shape that was not straight, a different length, and a different load, data reduction has not been completed at this time.

CONCLUSIONS

Large inelastic effects and non-straight conditions exist in this boom material.

FUTURE RESEARCH

Using relatively long lengths and precision measuring techniques it should be possible to measure some of these unusual properties of the boom material.

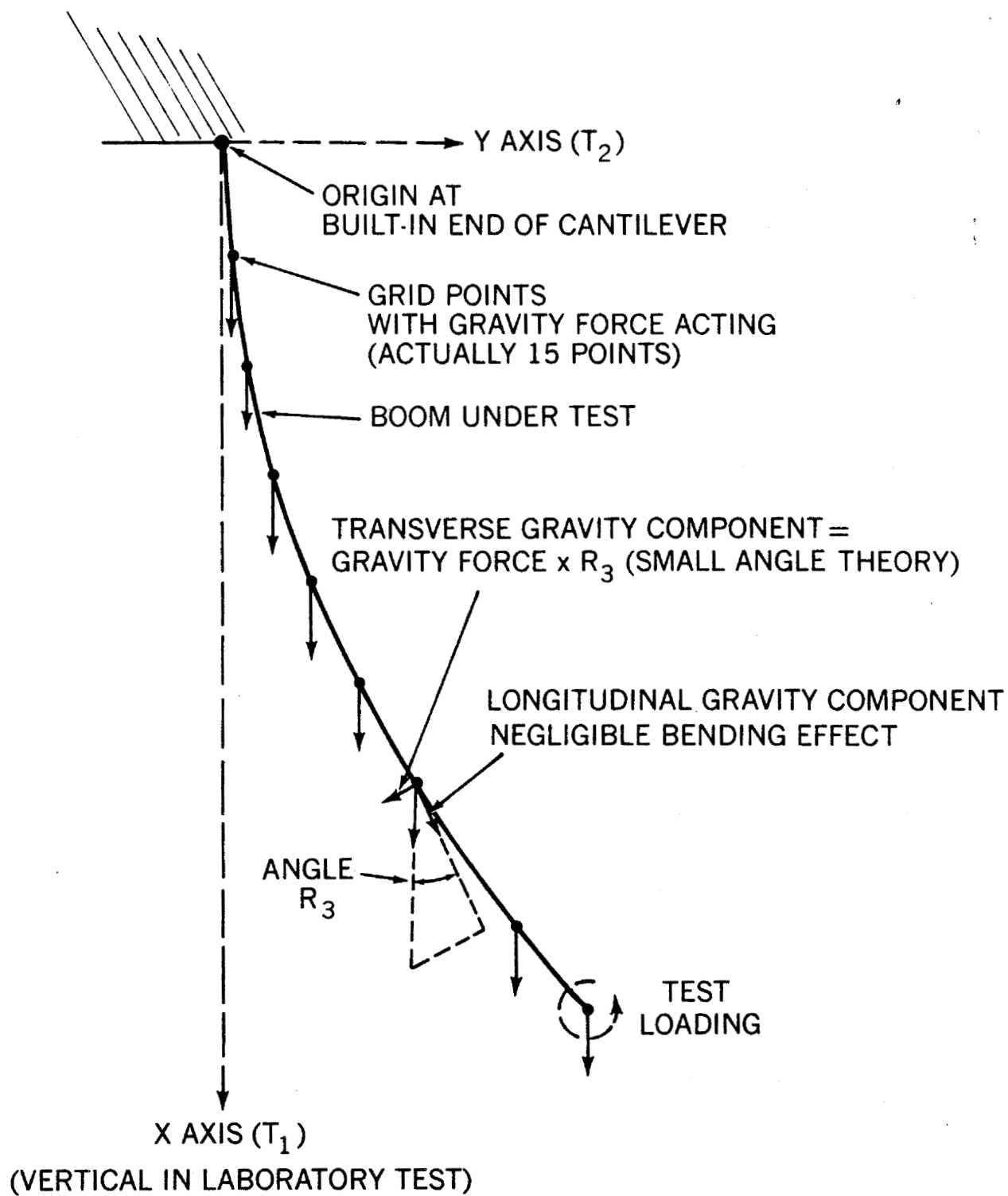


Figure 1. Loading Schematic.

ID BARCLAY,RAEEI
 APP DISP
 SOL 9.0
 TIME 20
 CEND

RAE BOOM TEST WITH APPLIED MOMENT

OCTOBER: 24, 1970

PAGE

2

BARCLAY 722

C A S E C O N T R O L D E C K E C H O

CARD

COUNT

1	TITLE = RAE BOOM TEST WITH APPLIED MOMENT
2	LABEL = BARCLAY 722
3	SET 5 = 2,3,4,5,6,7,8,9,10,11,12,13,14,15,17
4	SET 7 = 15
5	NONLINEAR = 49
6	RLLOAD = 6
7	ULOAD = 100
8	LINE=49
9	TSTEP = 4
10	DISP(SORT2) = 0
11	ULOAD = 7
12	BEGIN BULK

***USER INFO MESSAGE 207:BULK DATA NOT SORTED,XSORT WILL RE-ORDER DECK

Figure 2. NASTRAN Computer Input Data.

BARCLAY 722

SORTED BULK DATA ECHO

CARD COUNT		1	2	3	4	5	6	7	8	9	10
1	CDAR	1	1	1	2	10			2		
2	CDAR	2	1	2	3	10			2		
3	CDAR	3	1	3	4	10			2		
4	CDAR	4	1	4	5	10			2		
5	CDAR	5	1	5	6	10			2		
6	CDAR	6	1	6	7	10			2		
7	CDAR	7	1	7	8	10			2		
8	CDAR	8	1	8	9	10			2		
9	CDAR	9	1	9	10	10			2		
10	CDAR	10	1	10	11	10			2		
11	CDAR	11	1	11	12	10			2		
12	CDAR	12	1	12	13	10			2		
13	CDAR	13	1	13	14	10			2		
14	CDAR	14	1	14	15	10			2		
15	CDAMP2	2	7.00-4	2	2						
16	CDAMP2	3	7.00-4	3	2						
17	CDAMP2	4	7.00-4	4	2						
18	CDAMP2	5	7.00-4	5	2						
19	CDAMP2	6	7.00-4	6	2						
20	CDAMP2	7	7.00-4	7	2						
21	CDAMP2	8	7.00-4	8	2						
22	CDAMP2	9	7.00-4	9	2						
23	CDAMP2	10	7.00-4	10	2						
24	CDAMP2	11	7.00-4	11	2						
25	CDAMP2	12	7.00-4	12	2						
26	CDAMP2	13	7.00-4	13	2						
27	CDAMP2	14	7.00-4	14	2						
28	CDAMP2	15	7.00-4	15	2						
29	CONM2	52	2	0	8.944-2	0.0	0.0	0.0		ERA	
30	ERB	6.708-4		6.708-4		6.708-4					
31	CONM2	53	3	0	8.944-2	0.0	0.0	0.0		ERB	
32	ERB	6.708-4		6.708-4		6.708-4					
33	CONM2	54	4	0	8.944-2	0.0	0.0	0.0		ERC	
34	ERC	6.708-4		6.708-4		6.708-4					
35	CONM2	55	5	0	8.944-2	0.0	0.0	0.0		ERD	
36	ERD	6.708-4		6.708-4		6.708-4					
37	CONM2	56	6	0	8.944-2	0.0	0.0	0.0		ERE	
38	ERE	6.708-4		6.708-4		6.708-4					
39	CONM2	57	7	0	8.944-2	0.0	0.0	0.0		ERF	
40	ERF	6.708-4		6.708-4		6.708-4					
41	CONM2	58	8	0	8.944-2	0.0	0.0	0.0		ERG	
42	ERG	6.708-4		6.708-4		6.708-4					
43	CONM2	59	9	0	8.944-2	0.0	0.0	0.0		ERH	
44	ERH	6.708-4		6.708-4		6.708-4					
45	CONM2	60	10	0	8.944-2	0.0	0.0	0.0		ERI	
46	ERI	6.708-4		6.708-4		6.708-4					
47	CONM2	61	11	0	8.944-2	0.0	0.0	0.0		ERJ	
48	ERJ	6.708-4		6.708-4		6.708-4					

NOT REPRODUCIBLE

Figure 2. (cont.) NASTRAN Computer Input Data.

BARCLAY 722

SORTED BULK DATA ECHO

CARD COUNT	1	2	3	4	5	6	7	8	9	10
49	CJNM2	82	12	0	3.544-2 0.0	0.0	0.0	0.0	0.0	BRK
50	BRK	5.703-4		5.703-4		5.703-4				
51	CJNM2	83	13	0	3.544-2 0.0	0.0	0.0	0.0	0.0	BRK
52	BRK	5.703-4		5.703-4		5.703-4				
53	CJNM2	84	14	0	3.544-2 0.0	0.0	0.0	0.0	0.0	BRM
54	BRM	5.703-4		5.703-4		5.703-4				
55	CJNM2	85	15	0	3.544-2 0.0	0.0	0.0	0.0	0.0	BRN
56	BRN	5.703-4		5.703-4		5.703-4				
57	DAREA	1001	13	0	.005					
58	GRID	1		0.0	0.0	0.0		123456		
59	GRID	2		2.	0.0	0.0		3451		
60	GRID	3		4.	0.0	0.0		3451		
61	GRID	4		6.	0.0	0.0		3451		
62	GRID	5		8.	0.0	0.0		3451		
63	GRID	6		10.	0.0	0.0		3451		
64	GRID	7		12.	0.0	0.0		3451		
65	GRID	8		14.	0.0	0.0		3451		
66	GRID	9		16.	0.0	0.0		3451		
67	GRID	10		18.	0.0	0.0		3451		
68	GRID	11		20.	0.0	0.0		3451		
69	GRID	12		22.	0.0	0.0		3451		
70	GRID	13		24.	0.0	0.0		3451		
71	GRID	14		26.	0.0	0.0		3451		
72	GRID	15		28.	0.0	0.0		3451		
73	GRID	16		30.	0.0	0.0		123456		
74	MAT1	1		2.4624E91.0514E9		3.0				
75	NULIN1	49	2	2	-.0288	2	6	31		
76	NULIN1	49	3	2	-.0288	3	6	31		
77	NULIN1	49	4	2	-.0288	4	6	31		
78	NULIN1	49	5	2	-.0288	5	6	31		
79	NULIN1	49	6	2	-.0288	6	6	31		
80	NULIN1	49	7	2	-.0288	7	6	31		
81	NULIN1	49	8	2	-.0288	8	6	31		
82	NULIN1	49	9	2	-.0288	9	6	31		
83	NULIN1	49	10	2	-.0288	10	6	31		
84	NULIN1	49	11	2	-.0288	11	6	31		
85	NULIN1	49	12	2	-.0288	12	6	31		
86	NULIN1	49	13	2	-.0288	13	6	31		
87	NULIN1	49	14	2	-.0288	14	6	31		
88	NULIN1	49	15	2	-.0388	15	6	31		
89	PBAR	1	1	2.173-5	5.117-9	5.117-9	1.	4.47-4	634	
90	EQZ	5.117-9	5.117-9							
91	TABLED1	31							EQZ	
92	EQZ	-1.	-1.	0.	0.	1.	1.	ENDT		
93	TABLED1	1002							EQZ	
94	EQZ	0.	0.	70.	1.	71.	1.	ENDT		
95	TLOAD1	100	1001	0		1002				
96	ISTEP	4	1000	1.	10					
ENDDATA										

NOT REPRODUCIBLE

Figure 2. (cont.) NASTRAN Computer Input Data.

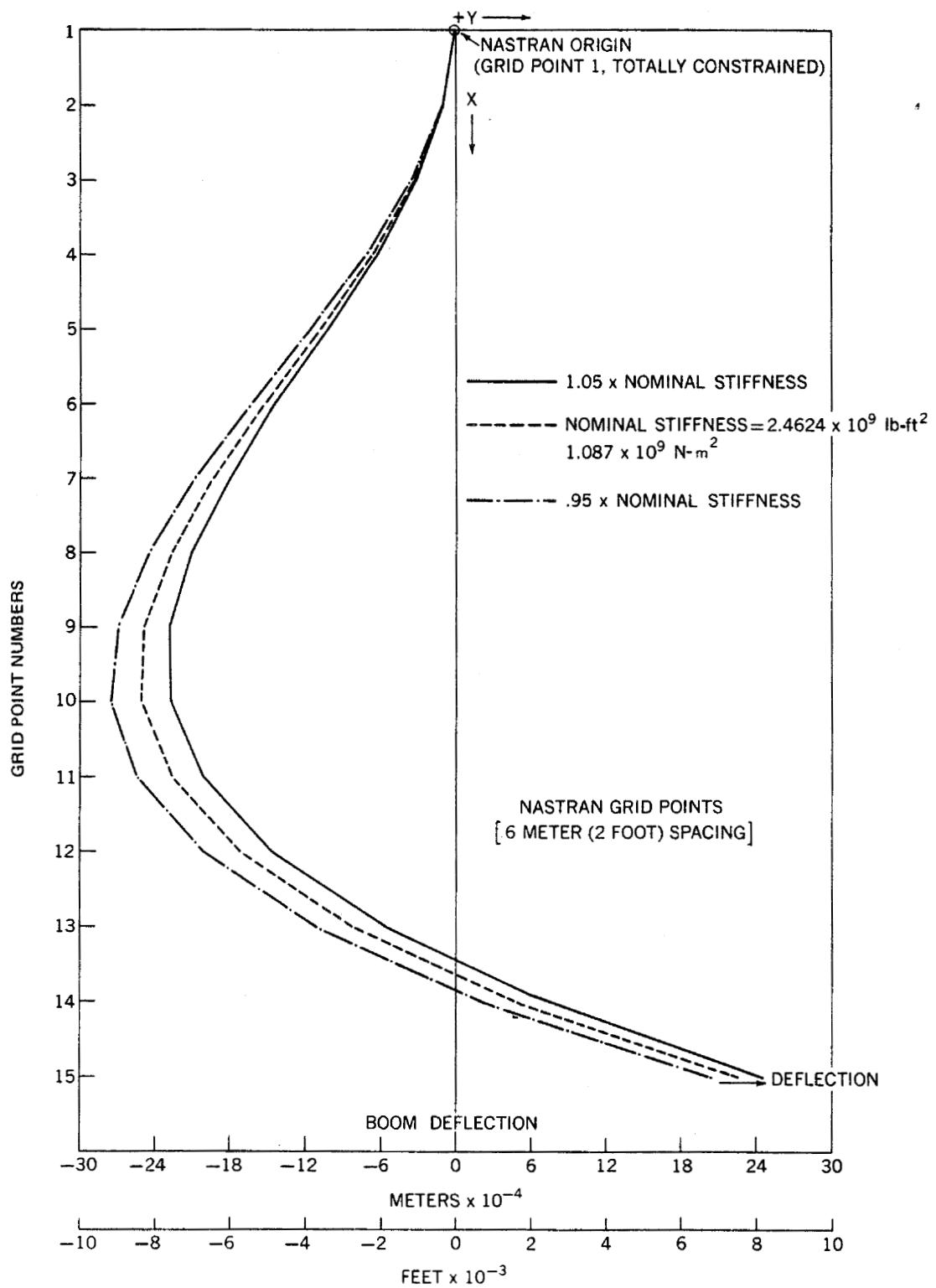


Figure 3. Computer Deflection Curves.

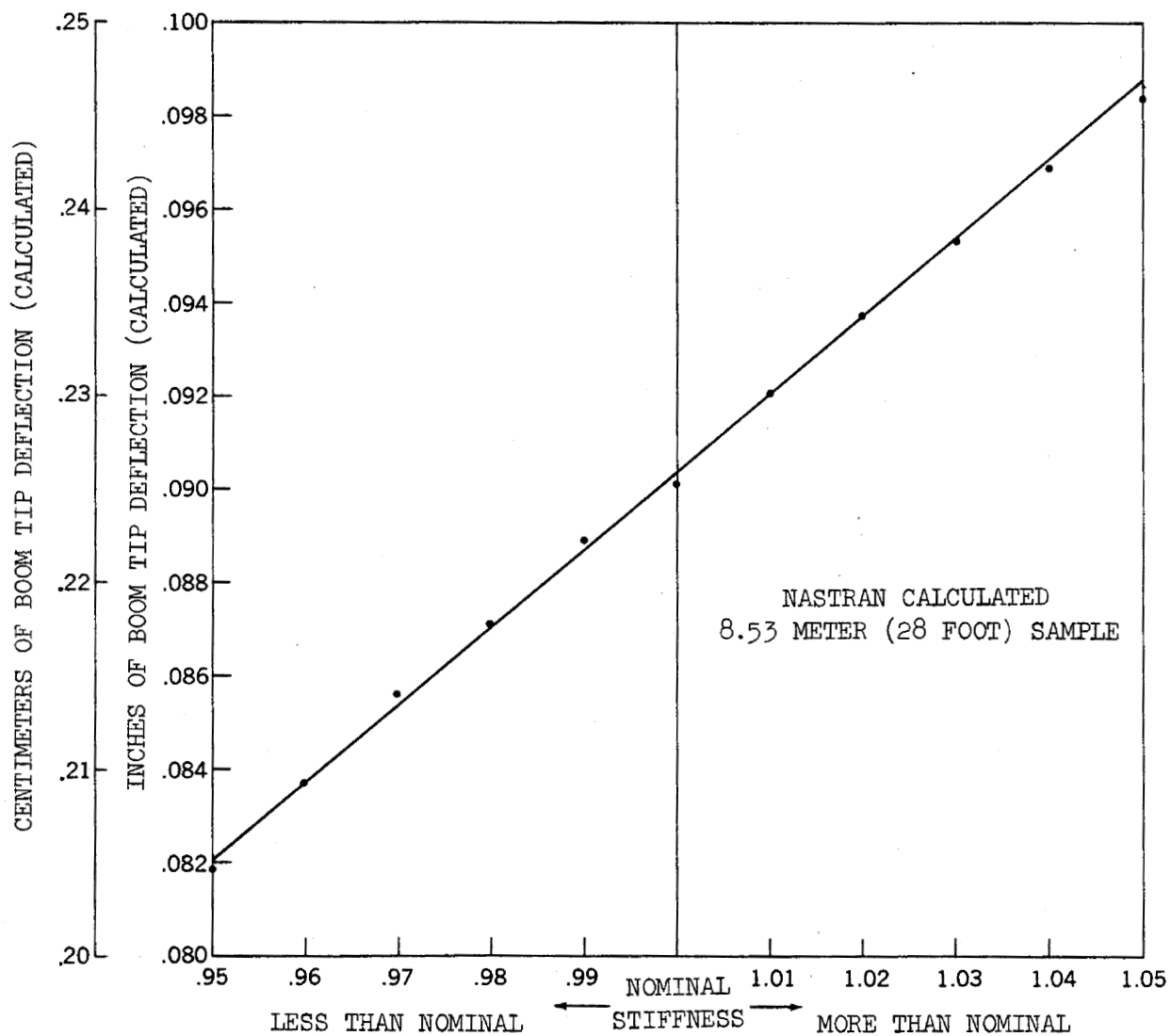


Figure 4. Boom Tip Deflection VS Stiffness.

SKYLAB I NASTRAN STRESS ANALYSIS MODELS

By William S. Viall

Teledyne Brown Engineering
Huntsville, Alabama

SUMMARY

Apollo Telescope Mount (ATM) and Orbital Workshop Stage (OWS) stress analysis models are discussed relative to why and how NASTRAN was used. The models discussed are for Rigid Format (SOL 1, 0) type analyses of space frames, stiffened cylinders, complex stiffened bulkheads, and simple panels with complex loading.

The discussions show that NASTRAN has many features that simplify rigid format static analyses. These features include grid-point sequencing, multiple coordinate systems, user master files, restart, bar-offset vectors, sufficient element catalog, and boundary condition options.

The quality and timeliness of stress analyses performed on Skylab hardware at Marshall Space Flight Center (MSFC) would not be possible with the current program library except for NASTRAN.

INTRODUCTION

This paper discusses some of the Skylab I flight hardware stress analysis models and states how and why NASTRAN was used in their analyses. The discussions briefly describe the hardware and models used, but no attempt is made to cover the modeling details, NASTRAN input, NASTRAN output, or quality of analysis. Reasons for using NASTRAN in lieu of other displacement method programs are stated; these reasons include both operational and analytical considerations. Operational considerations include ease of manipulating models, loads, and sequencing within NASTRAN, while analytical considerations include element selection, boundary conditions, and modeling geometry.

The plots included for the models discussed show general configuration, complexity, and boundary conditions.

Models considered for the Apollo Telescope Mount are:

- ATM Rack Model
- ATM Canister Sun End Bulkhead Models
- ATM Cable Tray Model
- ATM Components Test Panel Models.

Models considered for the Orbital Workshop Stage are:

- Tank Wall Edge-Weld Model
- Tank Wall Center-Weld Model.

The models discussed in this paper are limited to static analysis using the NASTRAN rigid format SOL 1, 0. The hardware configuration includes many types of structures such as space frame, skin stringer, torque box, honeycomb panels, and complex stiffened bulkheads.

APOLLO TELESCOPE MOUNT RACK MODEL

The ATM Rack (Figure 1) is an octagonal space frame with shear panels. The primary structure is the upper and lower octagonal rings and the eight vertical beams connecting the rings. During flight and some handling conditions the rack is supported by four sets of four-bar outriggers that intersect at nodes 13, 14, 15, and 16. During transportation the rack is supported by the Solar Array Support Ring which is below the lower ring. The Solar Array Support Ring is attached to the vertical beam extension below the lower ring and is braced to the lower ring by diagonal bracing. Two intercostals are located in each of the four outrigger bays and attach to the vertical beams. Four diagonal braces are located in the non-outrigger bays, and they attach to the upper and lower rings at alternate vertical beam attach points. Equipment panels that act as shear panels are located in each of the eight vertical bays and either fill, or partially fill, these bays. These panels are either attached to the flanges or to the webs of the vertical beams, as well as to the intercostals. Gyro support structure is located in three of the four outrigger bays in the upper half of the vertical bay.

The rack was designed for flight and orbital loads. Evaluation of orbital loads showed them to be non-critical, so they have since been excluded.

The flight design loads were:

1. Saturn IB lift-off with 95 percent ground wind (10 cases)
2. Saturn V lift-off with 95 percent ground wind (1 case)

3. Saturn V maximum acceleration (10 cases)
4. Saturn V separation and cutoff (1 case)
5. S-II separation and cutoff (not critical)
6. Saturn V max $q-\alpha$ (not critical).

Additional loads applied to the rack were transportation (4 cases), handling and erection (5 cases), and test (11 cases). These load conditions were not to impact the design, but they had to be considered during analysis.

A total of 42 different load cases was applied to the rack model; 31 of these cases (all except for test load cases) were run with the rack dead load times some load factor. To simplify reanalysis when the loads (dead load and load factors) changed, six unit load cases were defined:

- Three one-G loads in three mutually perpendicular directions
- Three one- α loads in three mutually perpendicular directions.

The ATM Rack model has been run in a multitude of configurations with respect to boundary conditions. For the flight cases the rack was supported at each outrigger by three bars that simulated the spring rates of the support structure, and for the transportation cases the rack was rigidly supported at the Solar Array Support Ring. For the handling and erection cases the rack was placed in the proper orientation, and the handling and erection equipment was modeled and added to the rack model.

The ATM Rack model has been developed by continually refining the latest model to suit the current analysis requirements. All the structural components cited above are included plus the simulated solar panels support frames in the folded position, simulated ATM canister and canister support structure, simulated gyros, and handling equipment for handling load cases only.

The current rack model runs in 29.6 min with 28 load cases and has 245 nodes, 590 bars, 28 rods, 20 triangles, 8 shear panels, and 16 quadrilaterals.

- The addition and scalar multiplier capability of the LOAD card allowed the use of six unit loadings from which loads for any combination of load direction and load factors could be obtained.
- The User Master File (UMF) capability allows the major portion of the bulk data deck (3000 cards) to remain at the computer facility on tape, so only a small UMF modification and case control deck was required.

- The restart capability of NASTRAN allows storage of inverted stiffness matrices for each type boundary condition. This saved 20 min per run and permitted timely recycling of analysis for revision to the loading conditions. The recycling required approximately 1 min per load case.
- The ATM Rack load paths do not all intersect at member centroids. The offset vector allows the inclusion of these eccentricities without the use of additional nodes. Approximately 60 bars were offset which resulted in a saving of 120 nodes.
- Analysis of the ATM Rack for handling loads with handling fixtures included in the model showed that the first set of fixtures was unstable. Modifications to the fixtures still produced a mathematically unstable stiffness matrix but the use of SUPPORT boundary constraints provided the necessary constraints to the fixtures which acted as a mechanism.
- The grid sequencing allowed optimization of run time and continual updating and refining of the model.
- Material allowable input and Margin of Safety calculations considerably reduced the engineering man hours required for the complete analysis.
- The multiple coordinate system capability allowed the rack-to-handling fixture and rack-to-simulated solar array panel orientations to be varied to define the highest stress levels. The capability also allowed this structure to be modeled in its own coordinate system.

The ATM Rack test results for transportation load cases agreed well with the analysis results. At the time this paper was written the flight tests were in progress and preliminary data evaluations indicate that analysis stresses are slightly higher than test data. The analytical displacements were much lower than predicted, since the outrigger support structure used for the test is much softer than that used in the model.

APOLLO TELESCOPE MOUNT CANISTER SUN END BULKHEAD MODELS

The ATM Sun End Bulkhead is a machined, integrally stiffened, circular aluminum bulkhead that acts as a mounting surface for electronic packages while in a low pressure environment. A stiffened fiber glass sun shield is attached to the aluminum bulkhead by fiber glass support posts which are

2 in. long and are bonded to both the bulkhead and sun shield with Epon Epoxy bond. The bulkhead is attached to the experiment package canister which is a longitudinally stiffened circular cylinder. The bulkhead design is based on the following three load conditions:

1. Ground Purge ultimate pressure (0.625 psi)
2. Flight lift-off acceleration loads (-4.7 G)
3. Flight cutoff acceleration loads (3.5 G).

Since the fiber glass sun shield was not available at the time the tests were scheduled, a structural qualification test was performed on an experiment package without the sun shield attached to the bulkhead. The tests structurally qualified the bulkhead, but deformations of the bulkhead indicate that the sun shield support posts might become overstressed at the bonded joints.

Two models were planned for the analysis. The first model was the full aluminum bulkhead with test loads. The results of this model were compared with test data. The second model was the same as the first model with the full sun shield added and with design loads applied. This model was too large for optimum turnaround time, so a third model was used which was one-half the second model with appropriate boundary conditions applied to the cut section. All three models had a portion of the longitudinal stiffened canister included to provide proper bulkhead boundary conditions.

The basic description of the three models follows:

1. Full Bulkhead Model (Figure 2). This model was supported at the lower end of the simulated canister. Figure 2 shows the vertical stiffeners but omits the vertical panels for clarity. The supports were applied in the plane of nodes 234, 239, 243, 247, 251, 255, 260, and 264. Figure 3 shows a top view of the bulkhead model. The three design conditions stated above were applied to this model. This model runs in 16.0 min for 3 load cases and has 267 nodes, 383 bars, 469 triangles, and 67 quadrilaterals.
2. Full Bulkhead Model with Sun Shield (Figure 4). This model has 475 nodes, 563 bars, 668 triangles, and 155 quadrilaterals. It was not run because of the long anticipated run time.
3. Bulkhead with Sun Shield Half Model. This model has the three load conditions stated above and 245 nodes, 300 bars, 297 triangles, and 80 quadrilaterals. At the time this paper was being prepared it had not been run.

NASTRAN was used to analyze the canister bulkhead for the following reasons:

- The grid sequencing capability of NASTRAN allowed the development of the bulkhead model followed by the addition of the sun shield with the final model optimized for run time.
- Material allowable input and Margin of Safety calculation capabilities reduced the amount of hand stress analysis required to perform the total analysis of the bulkhead.
- Bar-offset vectors allow all eccentric stiffeners to be properly located and their effect on bending of the bulkhead properly included in the analysis.
- The complex stress patterns inherent in the bulkhead caused by the cutouts, stiffeners, and normal loads are better approximated with the plate-bending capabilities of the NASTRAN elements.

The stress and deflection results of the canister Sun End Bulkhead analysis were very close to test results for the model without the sun shield. At the time this paper was written the results of the one-half bulkhead with sun shield attached were not available for comment.

APOLLO TELESCOPE MOUNT CABLE TRAY MODEL

The ATM Cable Tray (Figure 5) is a stringer-stiffened, torque-box type structure that supports all cable and wiring running from the ATM Rack to the experiment canister. The cable tray design is based on four flight and four transportation load conditions which are combinations of vibration and dynamic load factors. The Cable Tray is supported by hinges on both sides of the forked end and is fixed to a rotating drum at the other end with a hinge in the plane of the tray.

The cable tray NASTRAN model consists of 170 nodes with 66 bars, 10 triangles, and 100 quadrilaterals. The model runs on the UNIVAC 1108 in 9.0 min for 8 load cases. The matrix has a B equal to 158, a C equal to 0, and decomposes in 146 sec.

The cable tray is loaded so that it experiences high bending and torsional loads. The boundary conditions and loading are such that the tray exhibits large differential displacements.

NASTRAN was used to analyze the cable tray for the following reasons:

- Displacements had to be determined to define clearance problems, and NASTRAN would allow the application of accurate boundary

conditions on the cable tray and drum and a gross simulation of the very stiff drum with multipoint constraints.

- The high redundancy of stringer-stiffened, torque-box construction and the odd cable tray configuration required that plate bending of the box panels be considered to determine displacements accurately.
- Load distribution at discontinuities in the cable tray load paths were more realistic with plate-bending and bar-stiffener elements than with the standard shear panel modeling techniques used for analysis of torque boxes.
- Load distribution at discontinuities in the cable tray load paths were more realistic with plate-bending and bar-stiffener elements than with the standard shear panel modeling techniques used for analysis of torque boxes.

The NASTRAN cable tray stress and stiffness analysis proved to be valid during the cable tray structural test program.

APOLLO TELESCOPE MOUNT COMPONENTS TEST PANEL MODELS

The ATM Equipment Panels are either honeycomb sandwich or sheet stringer panel type structures that carry equipment packages, power supplies, and electronic "black boxes" in support of the ATM experiments. The panels are supported by the ATM Rack vertical beam webs and flanges. The panel attachments are continuous supports along three edges.

Basic flight, transportation, and erection and handling loads analyses were performed on these panels using the ATM Rack Model, but test loads analyses and predictions were performed on separate and more detailed models. Accurate data predictions and definition of all possible high stress points for the test loads were necessary, since the panels were attached to the 4-S ATM hardware and panel failure during the panel tests would have caused considerable delay in the total ATM test program.

Three component panels were modeled:

1. The Honeycomb Quarter Panel Model (Figure 6) was supported along the sides and upper edge. It was loaded at the load fixture attach points with the test load that simulates the worst combination of vibration and dynamic load factors defined by previous analyses. The model runs on the UNIVAC 1108 in 9.5 min for 1 load case and has 281 nodes, 27 triangles, and 208 quadrilaterals.

2. The Honeycomb Full Panel Model (Figure 7) was supported along the sides and upper edge. The model runs in 9.0 min for 1 load case and has 292 nodes, 61 triangles, and 214 quadrilateral panels.
3. The Skin-stringer Full Panel Model was supported along the sides and upper edge. The model has 273 nodes, 54 triangles, and 162 quadrilateral panels.

NASTRAN was used to analyze the components test panels for the following reasons:

- The components test panels had to be modeled with considerable detail to provide a fine stress pattern for the test loads. The resulting models were the optimum size to obtain quick turnaround through the MSFC computer facility.
- The CQUAD1 element available in the NASTRAN element library is an absolute idealization of the honeycomb panels.
- The plate-bending capability of the CQUAD1 element was necessary since the major test panel loads were out of plane.

The NASTRAN analyses used on these panels have been used to predict strain gage and displacement data for the test loads. At the time this paper was being prepared the Components Panel Tests had not been performed, and correlation with test data was not possible.

ORBITAL WORKSHOP STAGE TANK WALL

The Orbital Workshop Stage (OWS) tank wall is an integrally milled, 45° waffle-stiffened tank of 660.4 cm (260 in.) diameter. It is an S-IVB stage with the following structural modifications: addition of two floors, two scientific airlocks, an astronaut window, and an access door. The floors are suspended by a truncated cone that attaches at the upper end to the wall at the stiffener intersections and at the lower end to the outside floor ring. The floors are an isogrid beam system with isogrid grating attached.

The scientific airlocks are used to pass experiments through the tank wall; they have a 21.29 cm (8.38 in.) by 21.29 cm (8.38 in.) opening.

The astronaut window is a double-paned window with a diameter of 45.72 cm (18 in.). The window fits into a frame which, in turn, fits into a hole with a 46.53 cm (18.32 in.) diameter in the tank wall.

The access door is a 145.14 cm (57.14 in.) by 103.23 cm (40.64 in.) opening with semicircles at top and bottom; the semicircles have a diameter

of 103.23 cm (40.64 in.). The access door bolts to a frame which fits in a 146.41 cm (57.64 in.) by 104.50 cm (41.14 in.) hole in the tank wall.

The OWS tank is composed of 7 similar 682.50 cm (268.7 in.) by 296.42 cm (116.7 in.) panels rolled to a 330.20 cm (130.0 in.) radius and welded longitudinally along the long edges to form the circular tank. The panels vary structurally for the four holes specified above. The forward and aft ends of the tank are welded to Y-rings which are also attached to bulkheads and skirts.

The OWS tank design conditions are max $q-\alpha$ and ground wind load cases. At max $q-\alpha$ the tank is pressurized, has axial, shear, and bending moment loads applied to the top of the tank, and tank gravitational dead loads. For the ground wind load case, the access door is removed, and the tank is unpressurized, has axial, shear, and bending moments applied to the top of the tank, and the tank dead loads are in a 1-G environment.

The floor loads portion of the OWS tank dead loads are not uniformly distributed around the circumference. The two design conditions must be satisfied at any point around the circumference of the tank.

Two general types of models were developed for this analysis. The first type of model, called the Edge-Weld Model (Figure 8), is a model of one-seventh of the tank with one-half of the welds on the edges of the model. This basic Edge-Weld Model has 600 nodes, 801 bars, 180 triangles, 411 quadrilaterals, and runs in 58 min for 4 load cases. This model was placed on a User Master File (UMF) and modified for the three panels with tank wall penetrations. These three models are the scientific airlock model, the astronaut window model, and the access door with scientific airlock model.

The second type model, called the Center-Weld Model (Figure 9) is a model of one-seventh of the tank with the weld located at the center of the model. The basic Center-Weld Model has 536 nodes, 801 bars, 222 triangles, 349 quadrilaterals, and runs in 52 min with three load cases. This model was also placed on a UMF and modified for the four panels with tank wall penetrations. These models are the right side astronaut window model, left side astronaut window model, right side access door model, and left side access door model.

The models were developed in cylindrical coordinate systems with the positive z-axis being in the forward direction at the centerline of the panel curvature.

The tank wall cross section consists of the integrally milled, internally stiffened aluminum skin with insulation tiles in the pockets that also cover the stiffening. These insulation tiles are covered with one or more layers of fiber glass liner. The internal surface is a very thin layer of gold liner. This composite section is bonded together. The individual pocket panels are modeled as plates, and each discrete stiffener is modeled as an offset bar. One of the models was used to determine the plate and fiber glass liner combined axial and bending stiffness. This combined stiffness did not affect the stresses so only the aluminum skin was used for the panel properties.

Boundary conditions for the max $q-\alpha$ loading were radial and meridional rotation and tangential displacement constraints applied to the longitudinal edges of the models. The top edge has the radial displacement and radial and tangential rotations fixed. The bottom edge has an imposed radial displacement and tangential rotation as well as being fixed in all other directions.

The boundary conditions for the ground wind load case are the same as max $q-\alpha$, except the imposed deformations at the bottom edge are removed.

The bottom edge imposed radial displacements and tangential rotations were obtained from another program that analyzes shells of revolution. The top edge in reality should have boundary conditions similar to the bottom edge, but these were not applied since the top is the least stressed portion of the cylinder.

The unsymmetric loading caused by the varying floor loads means that the side boundary conditions are not totally correct; therefore, the stresses in bars and panels along the edge of all models are not correct. For this reason overlapping models were used in the analysis and only the stresses and deformation in the center one-half of the models were used.

NASTRAN was used for the analysis of the OWS tank wall for the following reasons:

- The OWS tank wall analysis required that stresses be determined for each pocket and compared with local buckling stress of the pockets and general instability buckling stress of the total tank. This was obtained by separating the loads in the skin and stringers by modeling each stringer discretely. This analysis could not be performed without considerable hand analysis if the offset vector capability of NASTRAN were not available.

- Bulk data for all variations of each type model were stored on the same UMF. These bulk data included unit loads for pressure body loads, and shell gravitational loads. The variable floor loads were also included for each separate model. The LOAD card permitted the combination of these unit load and special loads for any combination of pressure and G loads.
- The GRAV card capability allowed a simulated value to be used to include the change in vehicle bending moment in the longitudinal direction. This simulated G value was combined with the gravitation load factor to obtain a total G value.
- The models for the flight-tank configuration are being changed over to the test tank configuration by changing the properties on 18 PBAR, PTRIA2, and PQUAD2 cards per model. This modification is simpler for NASTRAN than for other programs available.

The results of the flight tank analysis showed that the tank was not overstressed. The results also showed where the critical high stress points were, and test instrumentation was defined from this analysis. Currently, the test tank models and test loads are being run to predict the test data for approximately 1000 channels of data for 9 test conditions and 2 load points per test condition.

CONCLUDING REMARKS

This survey of some of the analyses performed on Skylab I hardware shows that NASTRAN has the capability to analyze many different types of structure by utilizing the Rigid Format SOL 1, 0 static analysis.

The examples presented indicate that considerable detail and versatility of analysis is available, thereby reducing both engineering man hours and computer run time while producing a better product.

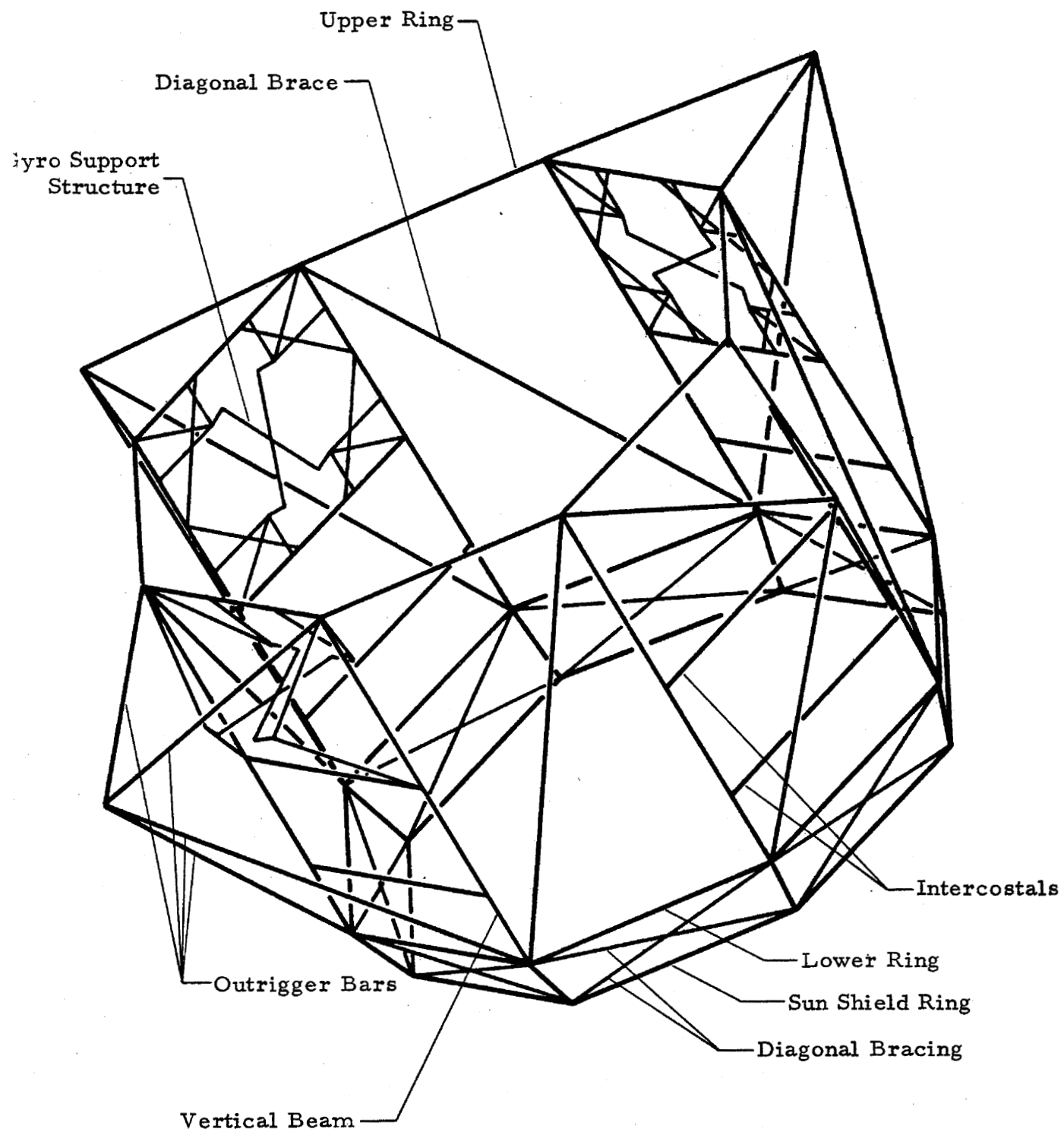


FIGURE 1. ATM RACK

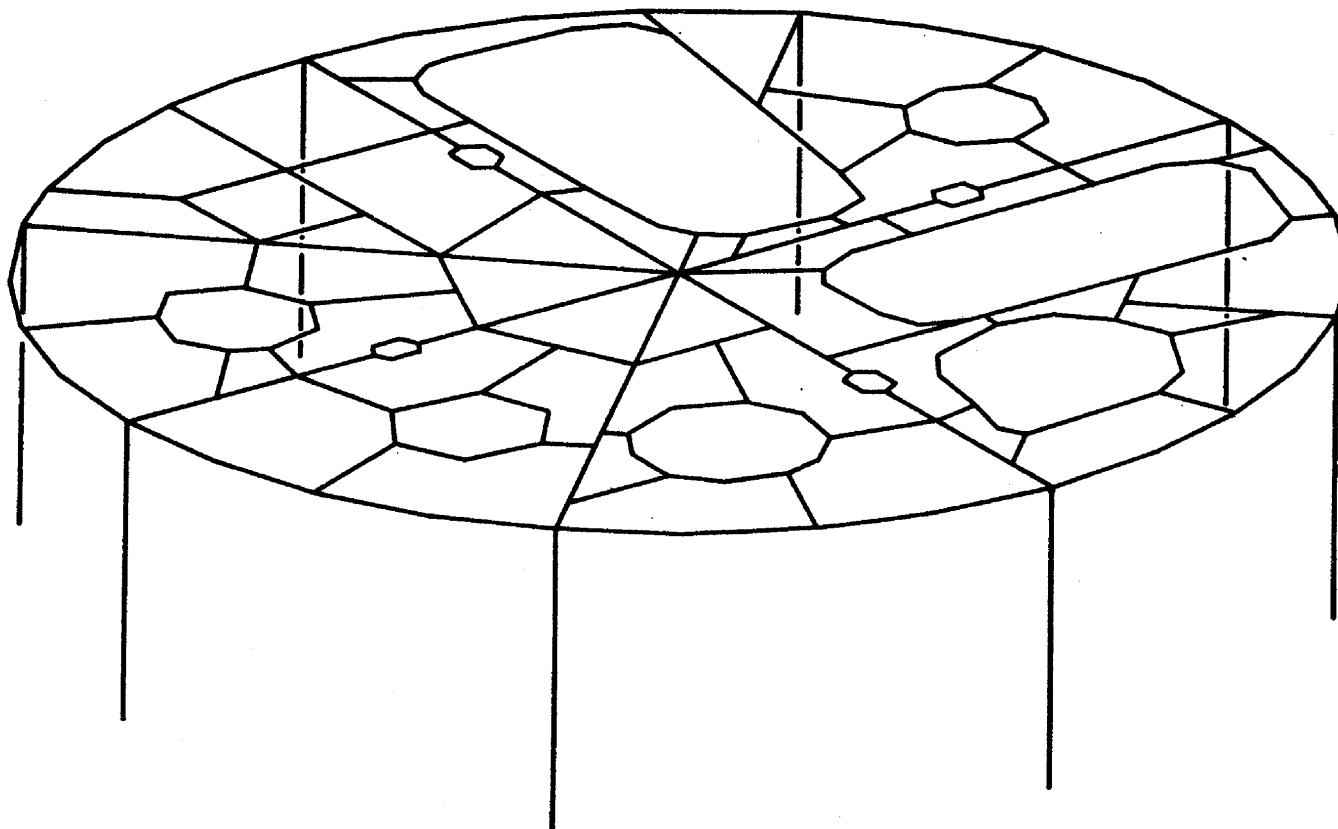


FIGURE 2. ATM SUN END BULKHEAD

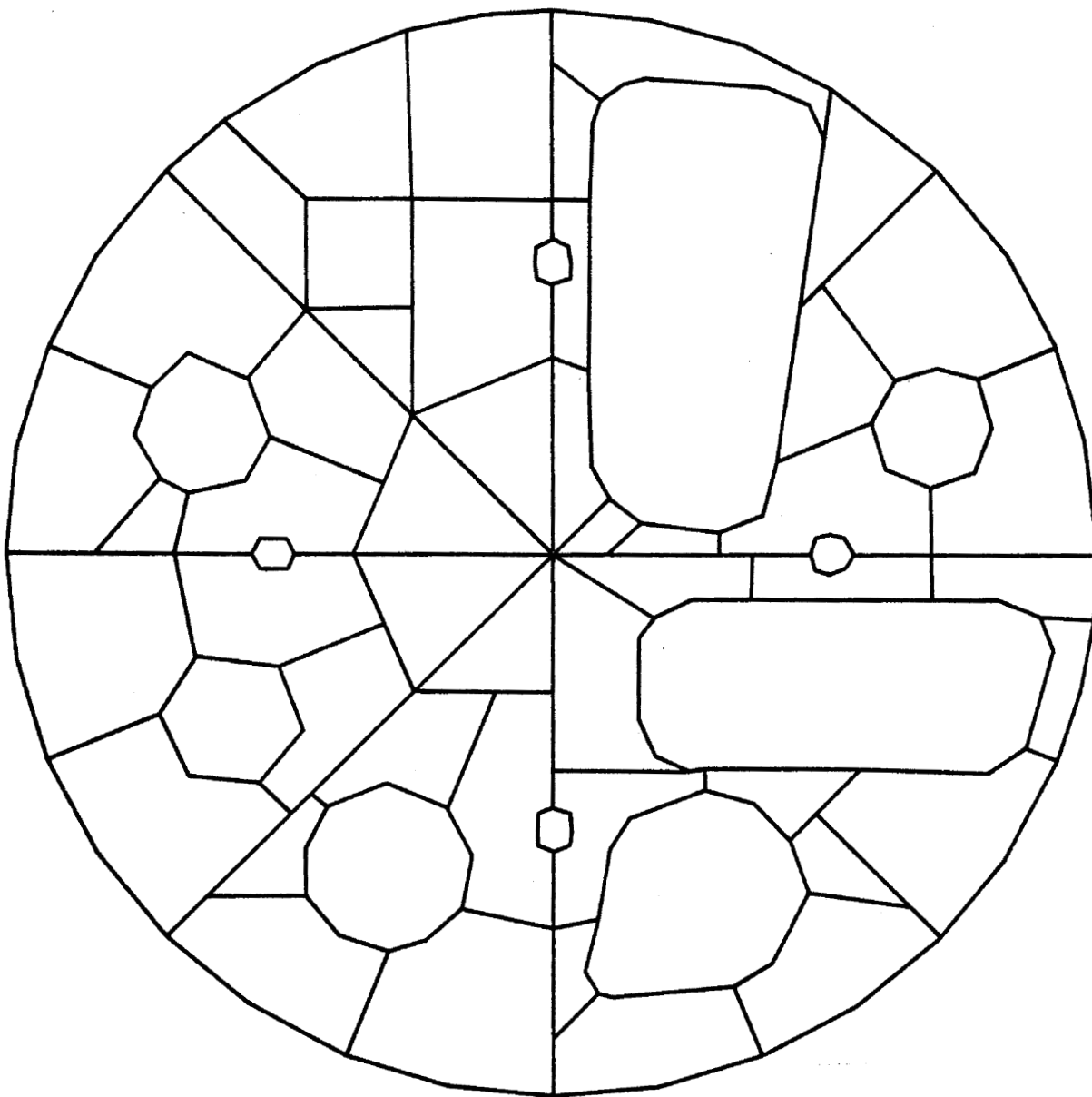


FIGURE 3. ATM SUN END BULKHEAD--TOP VIEW

NOT REPRODUCIBLE

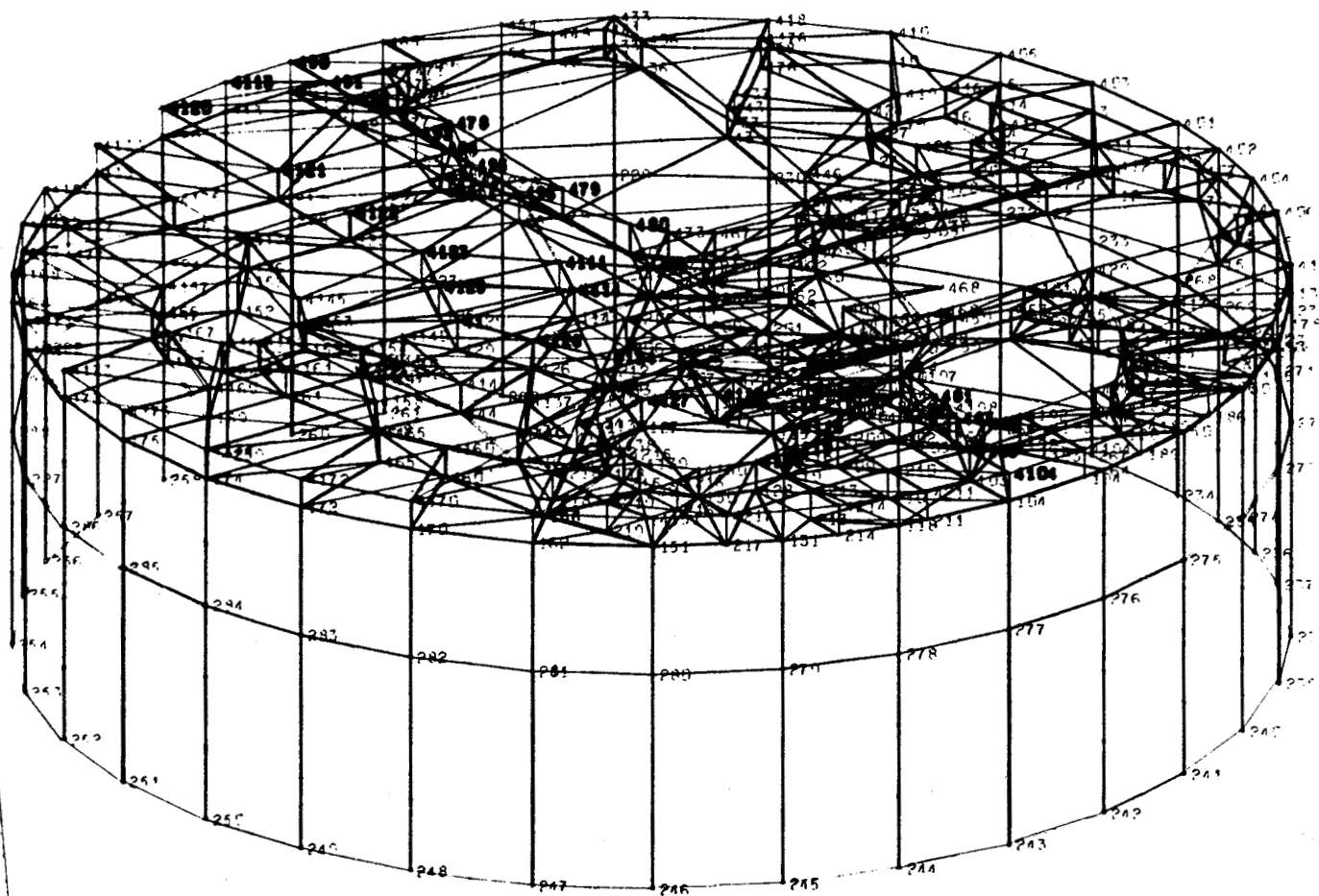


FIGURE 4. ATM SUN END BULKHEAD WITH SUN SHIELD

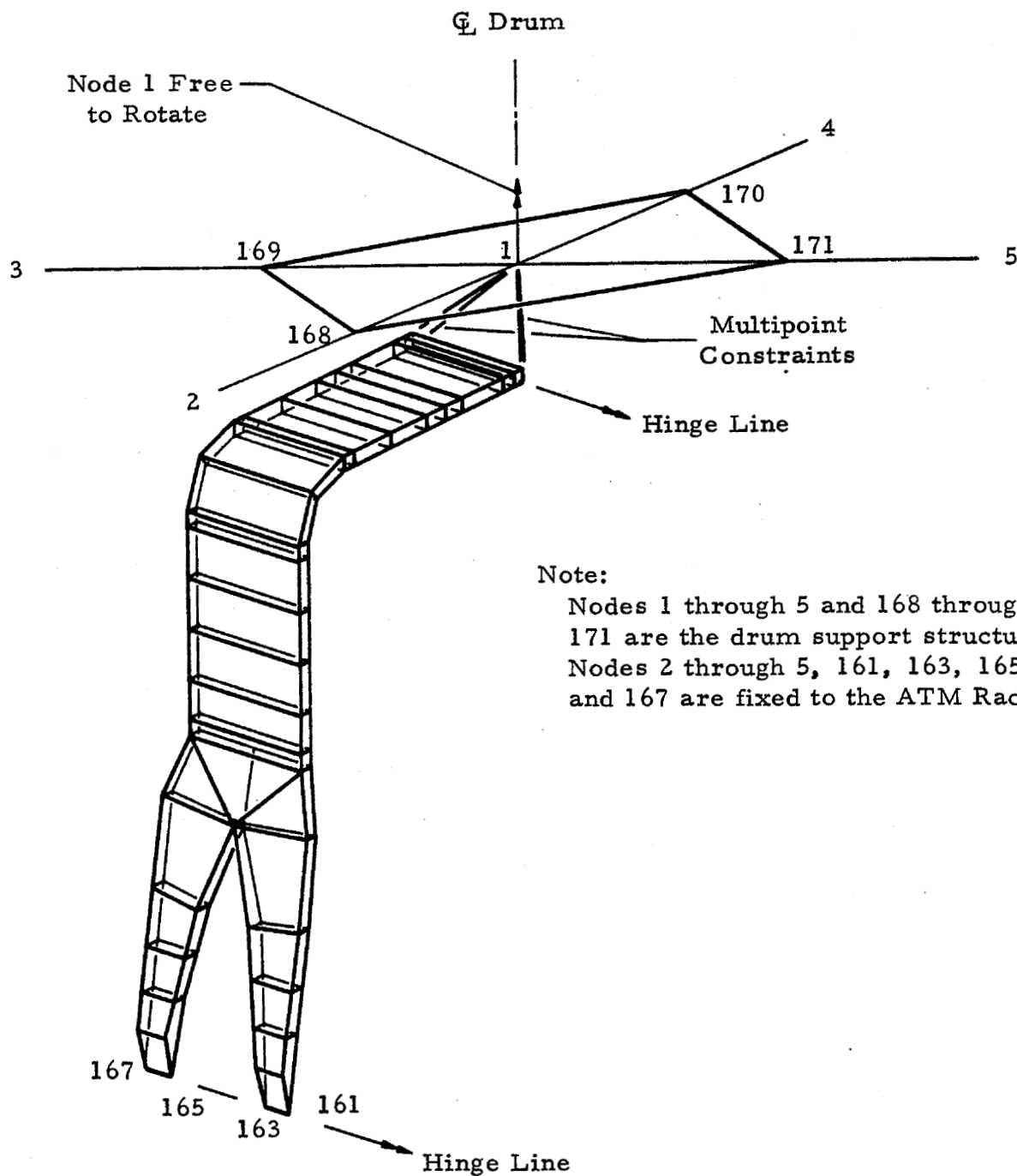


FIGURE 5. ATM CABLE TRAY

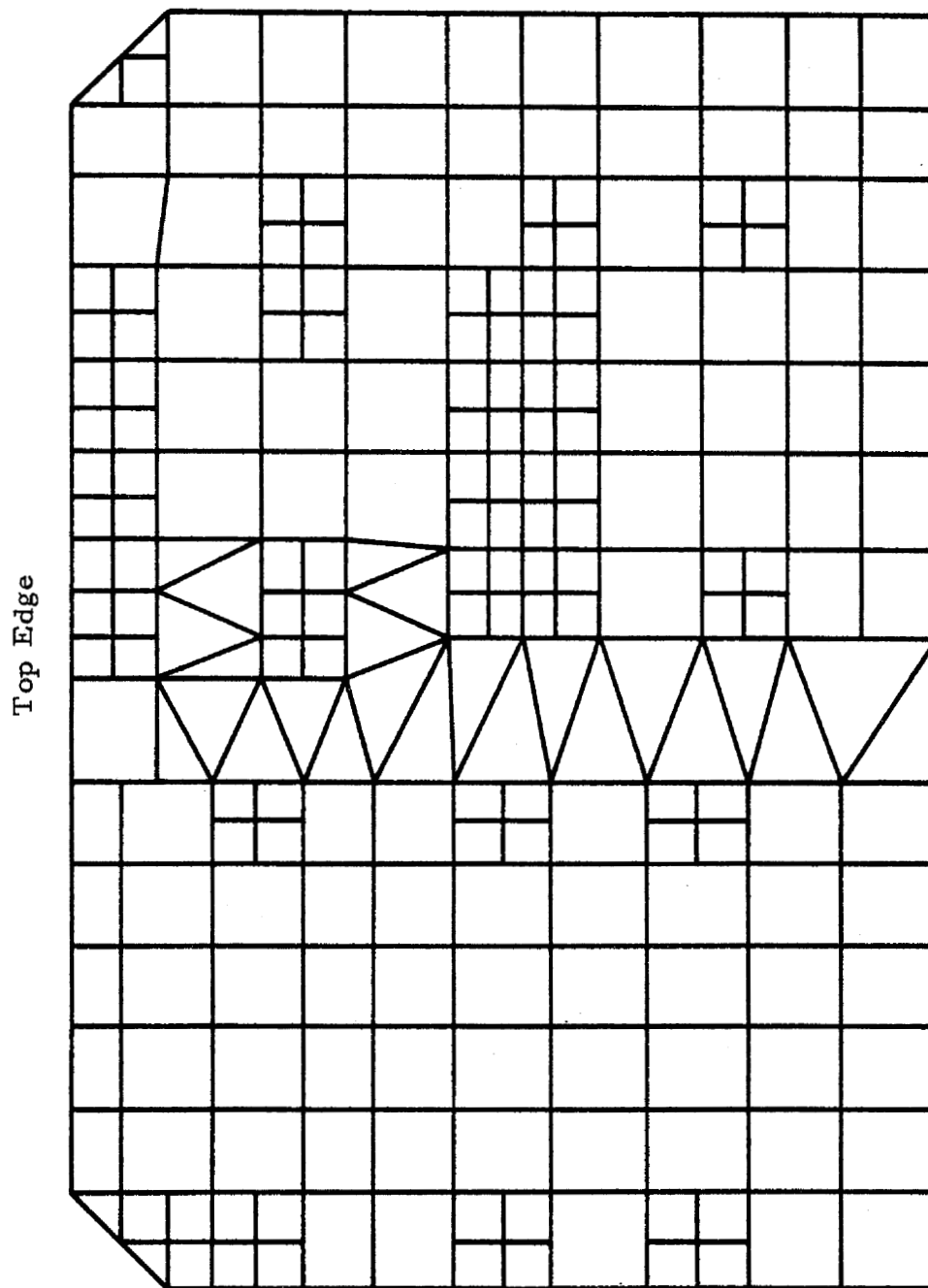


FIGURE 6. ATM HONEYCOMB QUARTER PANEL

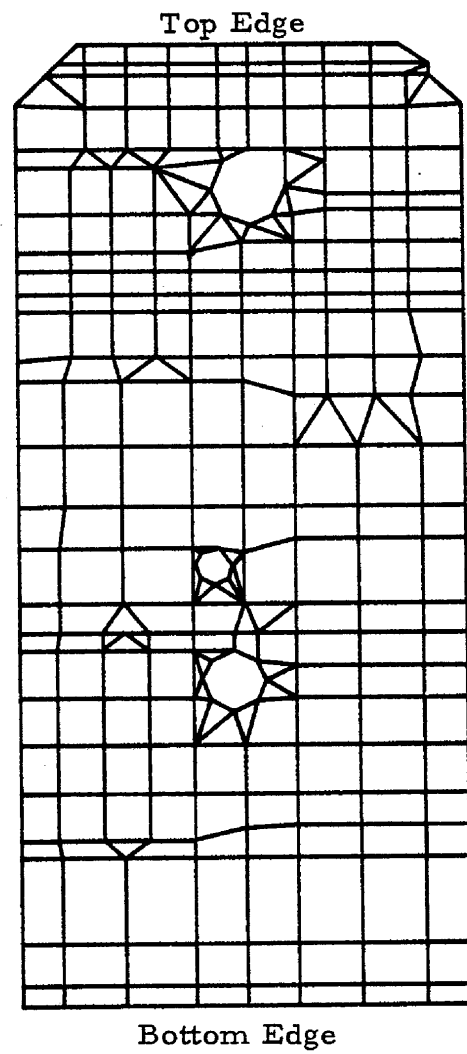


FIGURE 7. ATM HONEYCOMB FULL PANEL

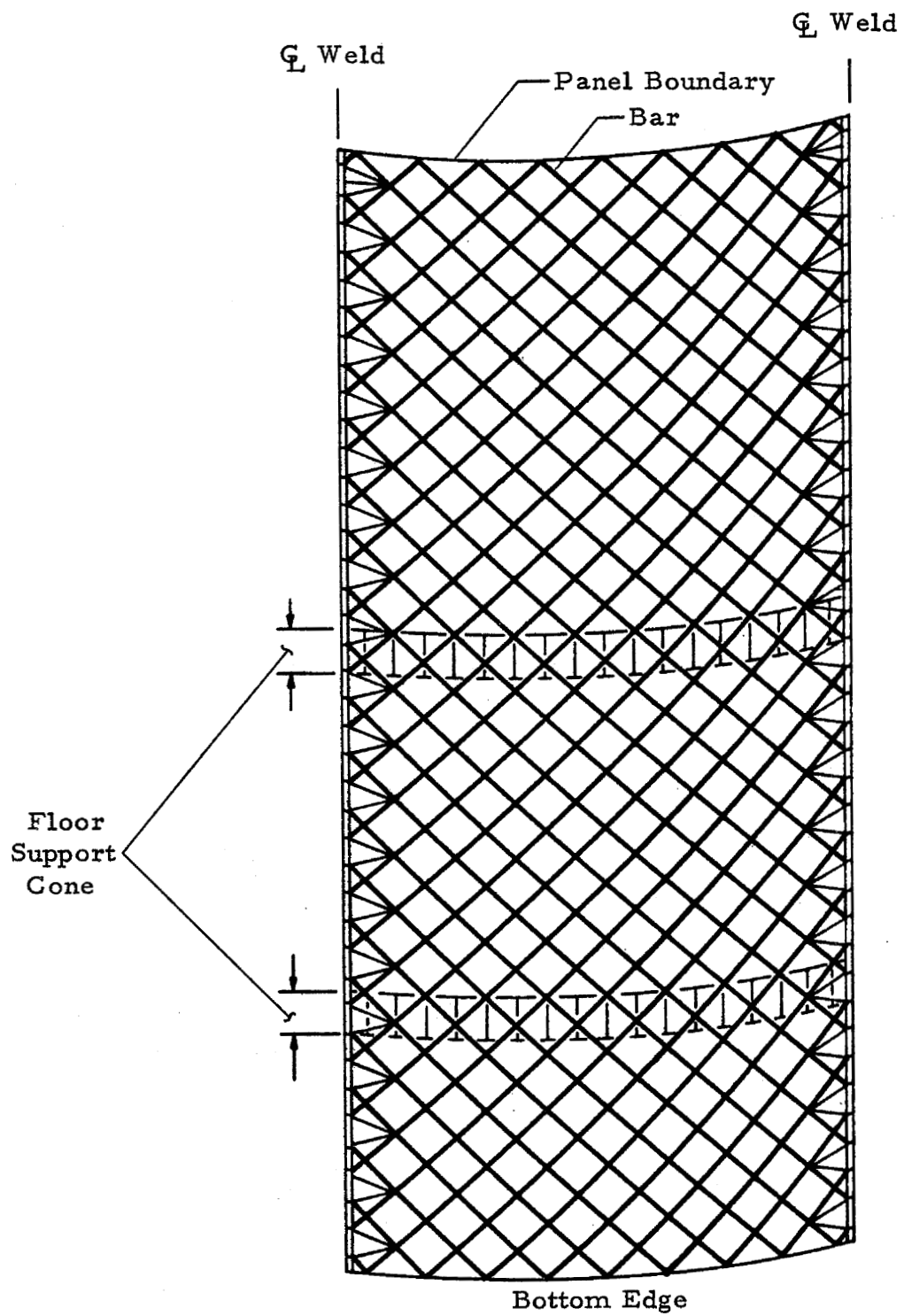


FIGURE 8. OWS EDGE-WELD MODEL

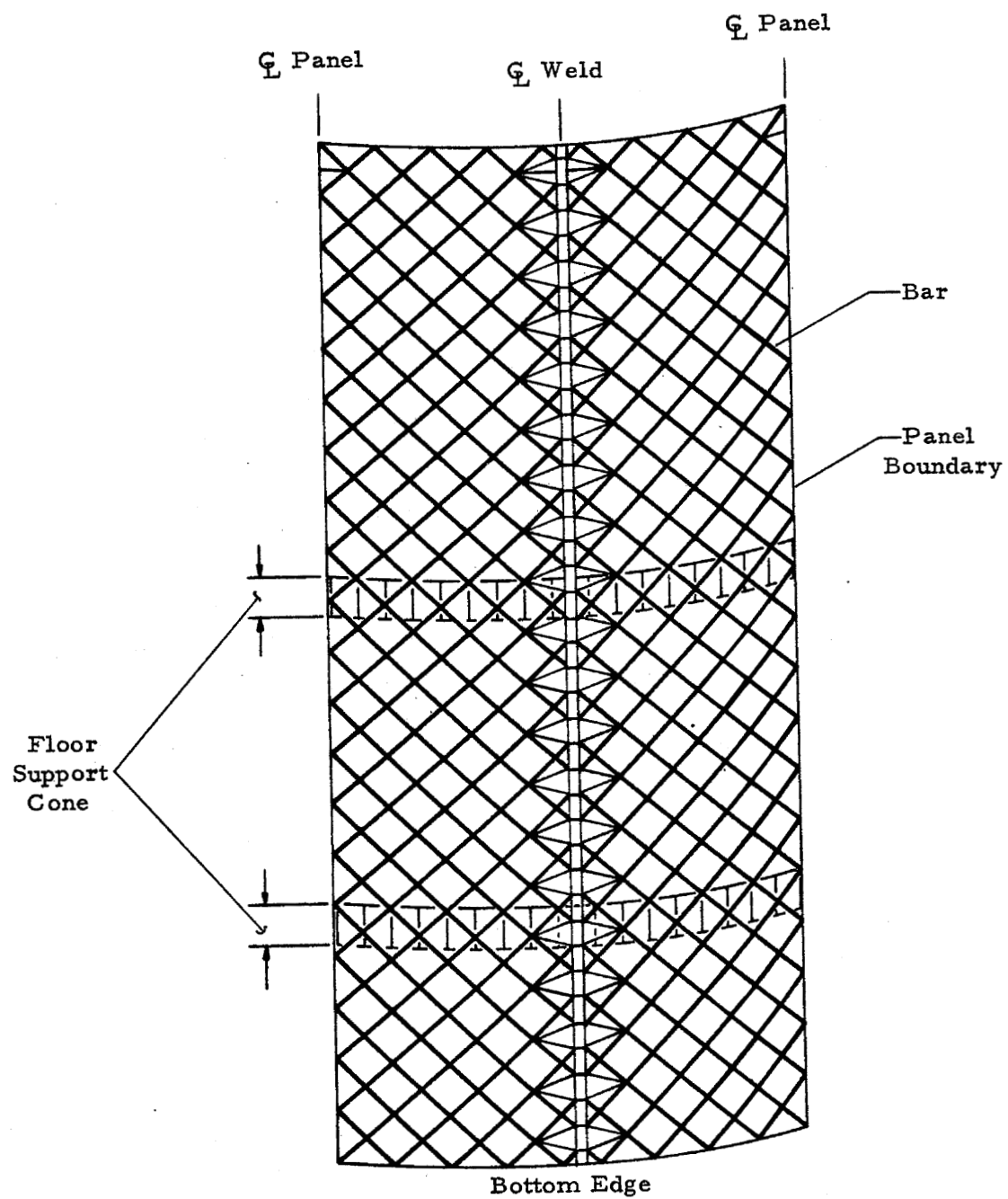


FIGURE 9. CENTER-WELD MODEL

SOME ASPECTS OF NASTRAN SOLUTION ACCURACY

by Gernot W. Haggemacher, Lockheed-California Company

Introduction

Various aspects of the accuracy of a NASTRAN solution for static and structural stability analysis have been explored by a series of specific examples, and the results have been evaluated. The following problems were investigated, using examples for which closed-form solutions were available.

1. Numerical accuracy of the static solution using the example of a cantilever beam.
2. Accuracy of column buckling.
3. Hydrostatic buckling of an arch.
4. Plate buckling in compression.
5. Accuracy of membrane and plate element elastic properties.

INVESTIGATION OF NASTRAN SOLUTION CAPABILITIES

Several investigations were made in 1970 on the adequacy, accuracy, and limitations of NASTRAN static analysis solutions. The principal results are discussed below.

Limitation of Solution Accuracy

In the displacement method the accuracy of the internal forces demands a very high numerical accuracy in the displacements. The present NASTRAN on the IBM 360-91 uses double precision arithmetic to determine displacement, but only single precision when deriving internal forces. The single precision accuracy of the CDC 6600 system is about twice that of the IBM 360-91. To explore the effect of this numerical precision, a simple cantilever beam, shown in Figure 1, consisting of caps, stiffeners, and shear panels, was used.

This beam was analyzed for a range of span to depth ratios (b/a), varying the number of spanwise fields from 50 to 1000 to observe the behavior of numerical accuracy. Examples were run on the in-house IBM 360-91 system, as well as on a CDC 6600 system through the courtesy of the MacNeal-Schwendler Corp. The digital accuracy available in these two machines is shown on Table 1. The deterioration of the solution accuracy with the increase in beam span is shown in Table 2. It illustrates that the solution of the displacements can be very satisfactory, while the corresponding stresses deteriorate earlier. At $b/a = 100$ the shear flow in the tip panel becomes erratic, and is useless above $b/a = 200$ for the IBM 360-91, while the result on the CDC 6600 is correct up to $b/a = 1000$. This is due to insufficient numerical accuracy of the IBM 360-91 single precision in the calculation of element strains from the very high tip deflections of the large-span beam.

Static Stability

The capability of NASTRAN rigid format 5 to perform static stability analyses (bifurcation type) has been investigated by a series of tests. Using problems for which theoretical closed-form solutions exist permits the determination of the accuracy of the numerical analysis and gives a good indication of how related problems, for which no theoretical solution exists, can be solved. The conclusions drawn from these buckling analyses apply similarly to the corresponding beam-column type solutions.

- (1) Column buckling. Comparisons of NASTRAN results with those of the classical Euler Column Theory

$$P_{CR} = \pi^2 \frac{EI}{l^2}$$

were made, using BAR elements to represent the column. The errors were below 0.1 percent when using five (5) or more BAR elements per half-wave of the buckling mode. This capability, however, does not include torsion-bending failure of open sections.

- (2) Stability of circular arch under hydrostatic pressure. The results of a NASTRAN analysis were compared with the closed-form solution

$$q_{crit} = 3 \frac{EI}{R^3}$$

in which q_{crit} = critical pressure of the arch in lb/inch,
R = radius of the arch, E = elastic modulus, and
I = moment of inertia of the cross section.

The results obtained from rigid format 5 were wrong. The reason for this error was that the current version of rigid format 5 of NASTRAN can only analyze the stability of structures under conservative load systems.

That is, the direction of the load vectors is invariant during buckling. This restriction that the load vectors remain invariant during buckling excludes such load situations as hydrostatic pressure, and would cause considerable error if this rigid format is used as it is. A solution to this type of problem was adapted to the NASTRAN stability analysis by using auxiliary matrix instructions (Appendix). The numerical solutions obtained with this modified procedure compared very well with the theoretical values; the error was only 0.2 percent when using 20 BAR elements per half-wave length of the buckling mode.

- (3) Plate buckling. Various types of plate compression problems were solved with NASTRAN and are summarized in Table 3.

Buckling loads calculated by these methods should, preferably, be consistently higher than theoretical values, by not more than 5 to 10 percent in the case of crude representation. The tabulated results show that the analyses of relatively long plates ran into serious trouble. This led to a detailed investigation of plate element stiffness. The following restrictions must be observed in the application of NASTRAN version 11.1.3 to plate problems:

- a) The use of NASTRAN QUAD plate elements must be restricted to side ratios between 1:1 and 1:1.5.
- b) Do not use the TWIST element.
- c) Plate-buckling networks must have a nearly square mesh.

The structural models as shown in Table 3 have various combinations of simply supported and free boundaries. The constraints which were imposed at the grid points to represent the various types of boundary conditions are shown in Figure 2. The "theoretical solution σ_{TH} " as listed in

Table 3 is the buckling stress evaluated from the appropriate one of the following equations:

- a) Square plate, simply supported along all four edges

$$\sigma_{TH} = \frac{4\pi^2 D}{b^2}$$

- b) Rectangular plate, simply supported along both compressed ends and one side, with the remaining side free

$$\sigma_{TH} = \left[\frac{6(1 - \nu)}{\pi^2} + \frac{b^2}{a^2} \right] \frac{\pi^2 D}{b^2 t}$$

- c) Column, simply supported at both ends

$$\sigma_{TH} = \frac{\pi^2 E b t^3}{12 a^2}$$

- d) Flange of angle, simply supported at compressed ends

$$\sigma_{TH} = \left[\frac{6(1 - \nu)}{\pi^2} + \frac{b^2}{a^2} \right] \frac{\pi^2 D}{b^2 t}$$

In these equations, D represents the flexural rigidity of the plate $\frac{Et^3}{12(1 - \nu^2)}$, a = length of the plate, b = width of the plate, t = plate thickness, ν = Poisson's ratio, and E = elastic modulus.

Quadrilateral and Triangular Plate Elements

When the plate element QUAD2 was used to investigate plate buckling problems, some of the results were much too high. This touched off a series of investigations into the details of the behavior of this element. Since all QUAD elements are built up from simple superposition of the TRIA element, these elements may have similar troubles. Thus a series of single-element test structures were set up to evaluate the plate flexibility variation with the plate aspect ratio. In Figure 3 the basic one-element model is shown supported as a

cantilever at grid points 1 and 4. These test structures were loaded by various simple unit loads at the free end, and the displacements at these grid points were compared. Six different values of aspect ratio a/b were evaluated: 1, 2, 4, 8, 16, and 32.

Some of the important findings presented in Figures 4 through 10 are the following:

- (1) The free-end displacements for some of the load conditions (Figures 4 through 6) increase monotonically as given by the theory. For others (Figures 7 through 10), the consistency breaks down rapidly for aspect ratios above 1.0; that is, the element becomes too rigid with increased length.
- (2) The plate-bending portion of the QUAD element (which is the same as the QDPLT element) behaves well for bending and transverse load (Figures 5 and 6) but deteriorates rapidly for torsion and twist (Figures 7 and 10).
- (3) The membrane portion of the QUAD element is correct over the whole range for constant axial load (Figure 4) but too rigid for an in-plane force-couple (Figures 8 and 9).
- (4) This irregular behavior of the QUAD2 element demonstrates that QUAD2 & QDPLT cannot be used above $a/b = 1.5$ and that QUAD2 & QDMEM contain an extremely rigid in-plane bending capability which is wrong.

Appendix. Set of DMAP Alters for Hydrostatic Buckling

The general equilibrium equation, including differential (or geometrical) stiffness, for problems such as hydrostatic buckling of an arch, can be given by the equation

$$([K] - \lambda([K_G] + [K_{GL}]))\{u\} = 0 \quad (A1)$$

where

- $[K]$ = Elastic Stiffness Matrix
- $[K_G]$ = Differential Stiffness Matrix for internal (element) forces, defined and used in NASTRAN rigid format 4 and 5
- $[K_{GL}]$ = Differential Stiffness Matrix for external, nodal loads; not defined in NASTRAN

At this place it is not possible to explore all ramifications of $[K_{GL}]$. It is a non-symmetrical matrix, hence also the combination

$$[K_{GN}] = [K_G] + [K_{GL}] \quad (A2)$$

Let the problem of the arch under hydrostatic pressure be formed in a cylindrical coordinate system (as a global system), see Figure 11, that is in terms of radial and tangential displacements. The hydrostatic pressure forces are always normal to the surface; hence they are not invariant during buckling, but change direction. The net effect is that the rows corresponding to the tangential degrees of freedom of the combined differential stiffness matrix $[K_{GN}]$ are zero; the other rows remain as in $[K_G]$.

This can easily be accomplished by a diagonal boolean matrix $[A]$, conveniently input as a DMIG, with (0) in all tangential D.O.F. The combined matrix is then given by the equation

$$[K_{GN}] = [A][K_G] \quad (A3)$$

With this matrix [A] the rigid format 5 is then ALTERed as follows:

ALTER 10⁴

\$ NEXT ROUTINE CONVERTS MATRIX KG FOR HYDROSTATIC STABILITY

MTRXIN,,MATPOOL,EQEXIN,SIL,/A,,/V,N,LUSET/V,N,NL/C,N,O/C,N,O \$

MPYAD A,KDGG,/KDGA/C,N,O/C,N,1/C,N,1/C,N,2 \$

EQUIV KDGA,KDGG/MPCF2 \$

ENDALTER

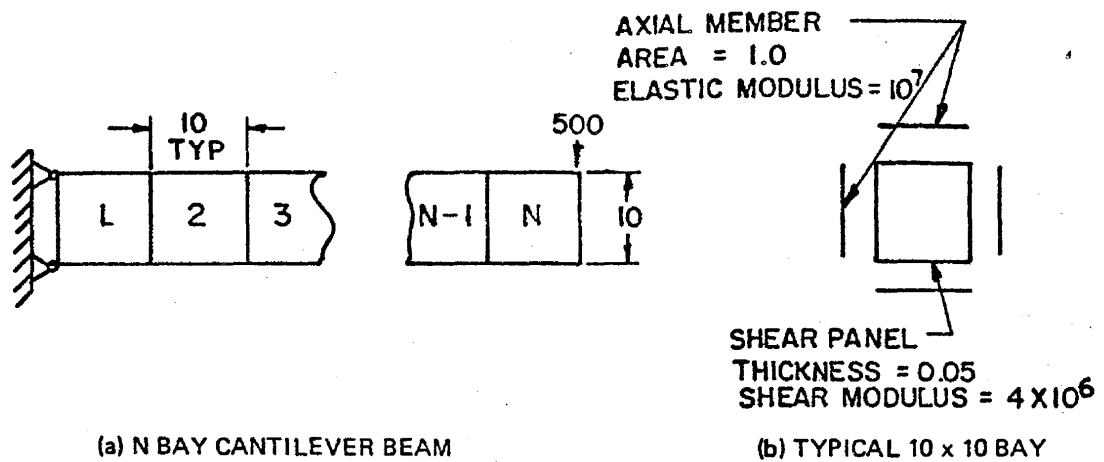


FIGURE 1. STRUCTURAL MODEL FOR NUMERICAL ACCURACY STUDY

TABLE 1. COMPUTER WORD LENGTH VS ACCURACY

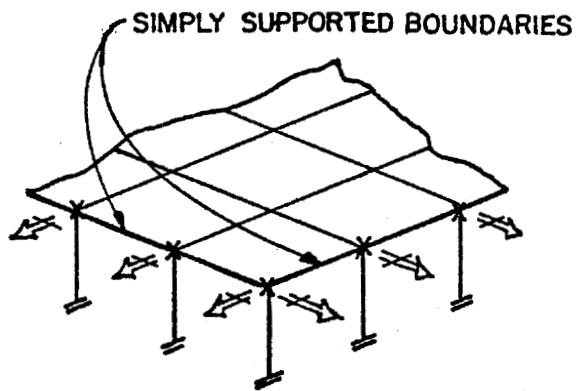
COMPUTER	IBM 360-91		CDC 6600	
	SINGLE	DOUBLE	SINGLE	DOUBLE
WORD LENGTH BINARY BITS	32	64	60	120
SIGNIFICANT FIGURES	6+	13+	14+	28+

TABLE 2. DEFLECTIONS AND STRESSES OF CANTILEVER BEAMS

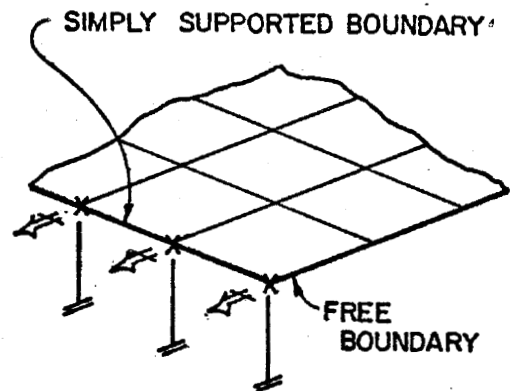
b/a	DEFLECTION AT FREE END			SHEAR STRESS OF PANEL AT FREE END		
	THEORETICAL	NASTRAN SOLUTION		THEORETICAL	NASTRAN SOLUTION	
		IBM 360-91	CDC 6600		IBM 360-91	CDC 6600
50	41.666	41.78745	41.78745	1,000.0	1,006.0	1,000.0
100	333.33	333.5747	NOT RUN	1,000.0	1,024.0	NOT RUN
150	1,125.0	1,125.362	NOT RUN	1,000.0	992.0	NOT RUN
200	2,666.6	2,667.150	2,667.150	1,000.0	1,024.0	1,000.0
500	41,666.6	41,668.23	41,667.87	1,000.0	8,192.0	1,000.0
1000	333,333.3	333,393.2	333,335.7	1,000.0	45,056.0	1,000.001

STRUCTURAL MODEL NOTES: (1) TYPICAL THICKNESS OF PLATES = 0.05 (2) X INDICATES SIMPLY SUPPORTED NODES	PROPERTIES OF PLATE ELEMENTS	NASTRAN RUN NO.	ASPECT RATIO OF ELEMENT	NASTRAN SOLUTION σ_N	THEORETICAL SOLUTION σ_{TH}	% ERROR $= \frac{\sigma_N - \sigma_{TH}}{\sigma_{TH}}$
	$E = 10 \times 10^6$ $G = 4 \times 10^6$	M50A	2" x 2" L/S = 1.0	1354.6	1370.8	-1.2%
	$E = 10 \times 10^6$ $G = 4 \times 10^6$	M51A	2" x 2" L/S = 1.0	516.5	499	3.5%
	$E = 10 \times 10^6$ $G = 4 \times 10^6$	M52A	2" x 4" L/S = 2.0	251.6	242	4.0%
	$E = 10 \times 10^6$ $G = 4 \times 10^6$	M53A	2" x 8" L/S = 4.0	247.25	177.7	39.1%
	$E = 10 \times 10^6$ $G = 4 \times 10^6$	M54	1" x 16" L/S = 16.0	6116.92	630.4	870.3%
	$E = 10.5 \times 10^6$ $G = 4 \times 10^6$	M41	0.4" x 6.4" L/S = 16.0	23.15	21.08	9.8%
	$E = 10.5 \times 10^6$ $G = 4 \times 10^6$	M20	0.4" x 0.8" L/S = 2.0	8358	8439	-1.0%
		M21	0.4" x 6.4" L/S = 16.0	45370	6968	551.1%

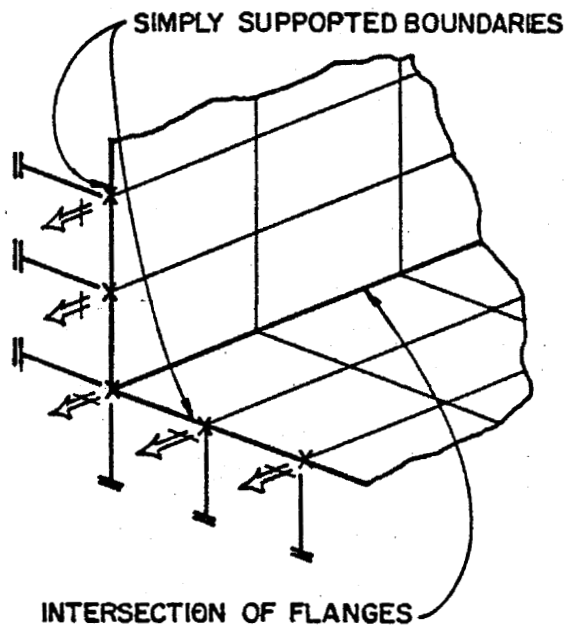
TABLE 3. BUCKLING STRESSES EVALUATED WITH NASTRAN PROGRAM



(a) BOTH ADJACENT BOUNDARIES
SIMPLY SUPPORTED



(b) ONE BOUNDARY SIMPLY SUPPORTED,
THE OTHER ONE FREE



(c) BOUNDARIES OF ANGLE COLUMN,
NEAR THE INTERSECTION OF FLANGES

NOTES:

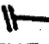

- (1)  INDICATES CONSTRAINT OF THE DISPLACEMENT IN THE DIRECTION OF THE LINE.
- (2)  INDICATES CONSTRAINT OF THE ROTATION ON THE PLANE WHICH IS PERPENDICULAR TO THE VECTOR.
- (3) EVERY GRID POINT IS CONSTRAINED, SO THAT IT CAN NOT ROTATE ON THE PLANE WHICH IS PARALLEL TO THE PLATE

FIGURE 2. BOUNDARY CONSTRAINTS OF THE STRUCTURAL MODELS IN TABLE 3

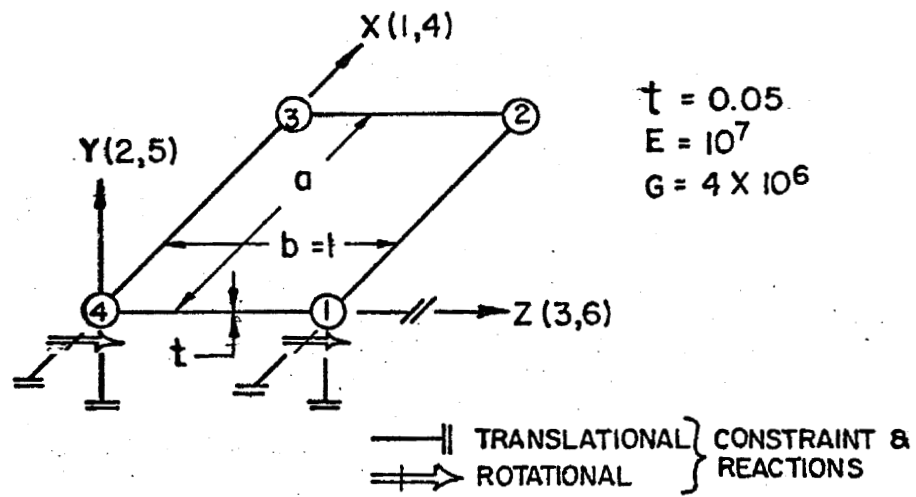


FIGURE 3. STRUCTURAL MODEL FOR THE INVESTIGATION OF QUAD2

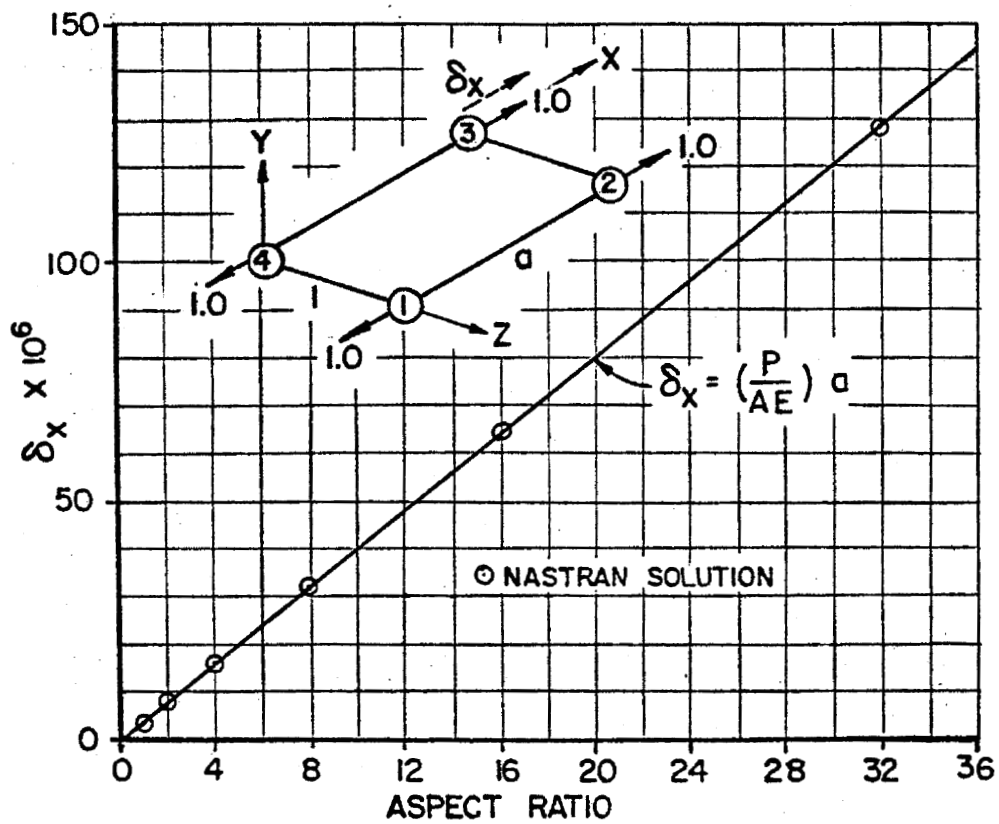


FIGURE 4. QUAD2 SINGLE ELEMENT LOAD-DISPLACEMENT CHARACTERISTICS

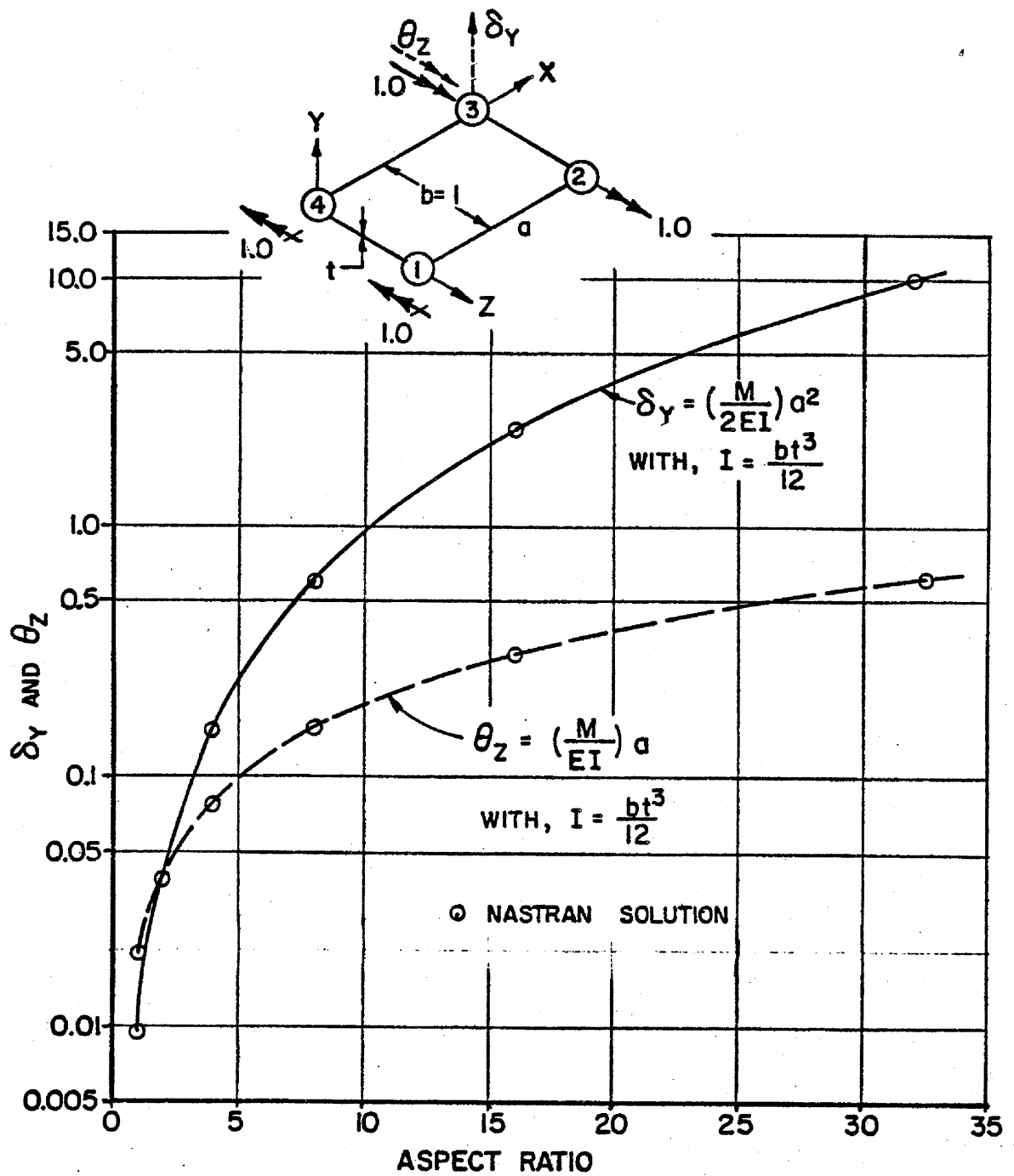


FIGURE 5. QUAD2 SINGLE ELEMENT LOAD-DISPLACEMENT CHARACTERISTICS

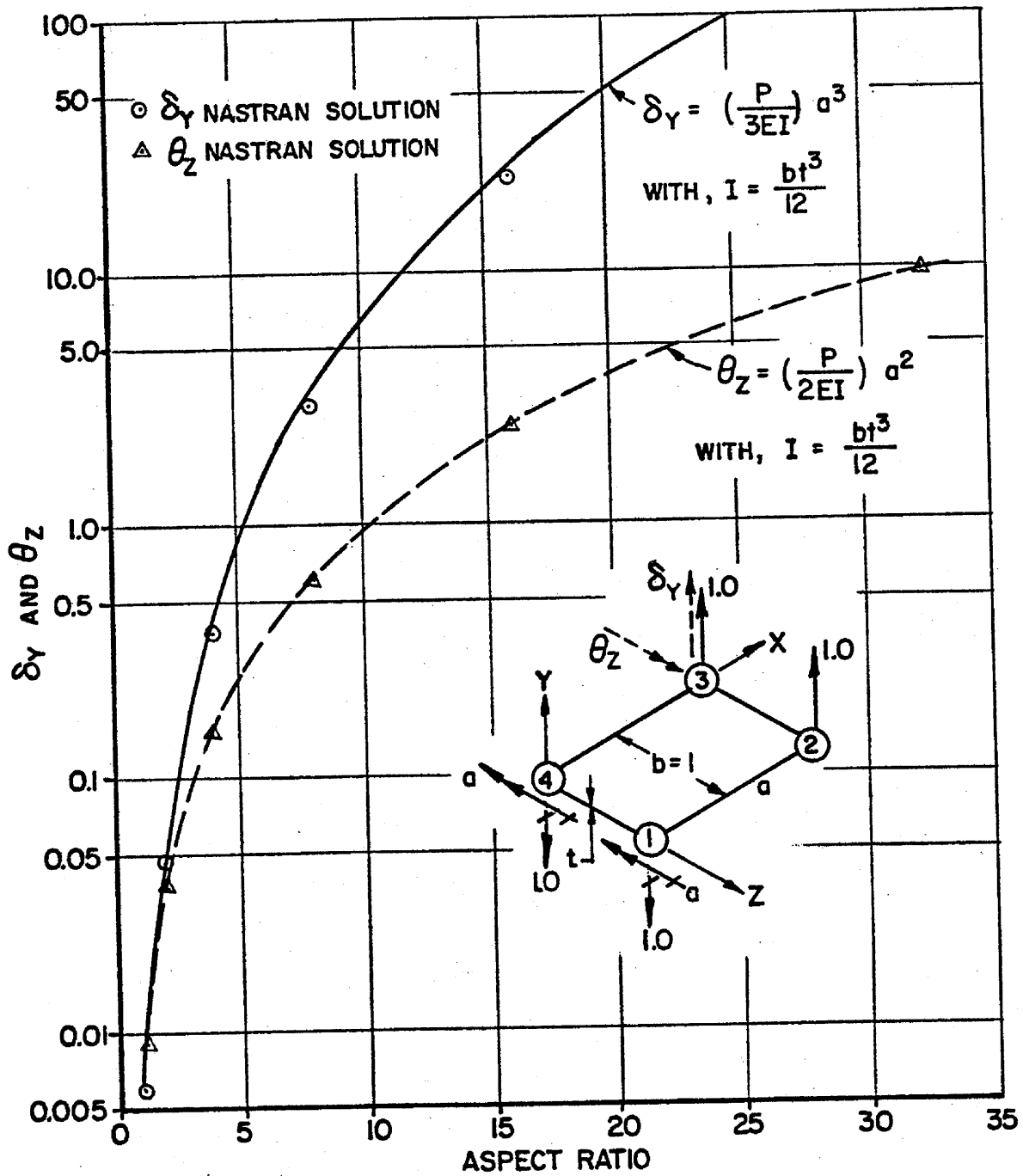


FIGURE 6. QUAD2 SINGLE ELEMENT LOAD-DISPLACEMENT CHARACTERISTICS

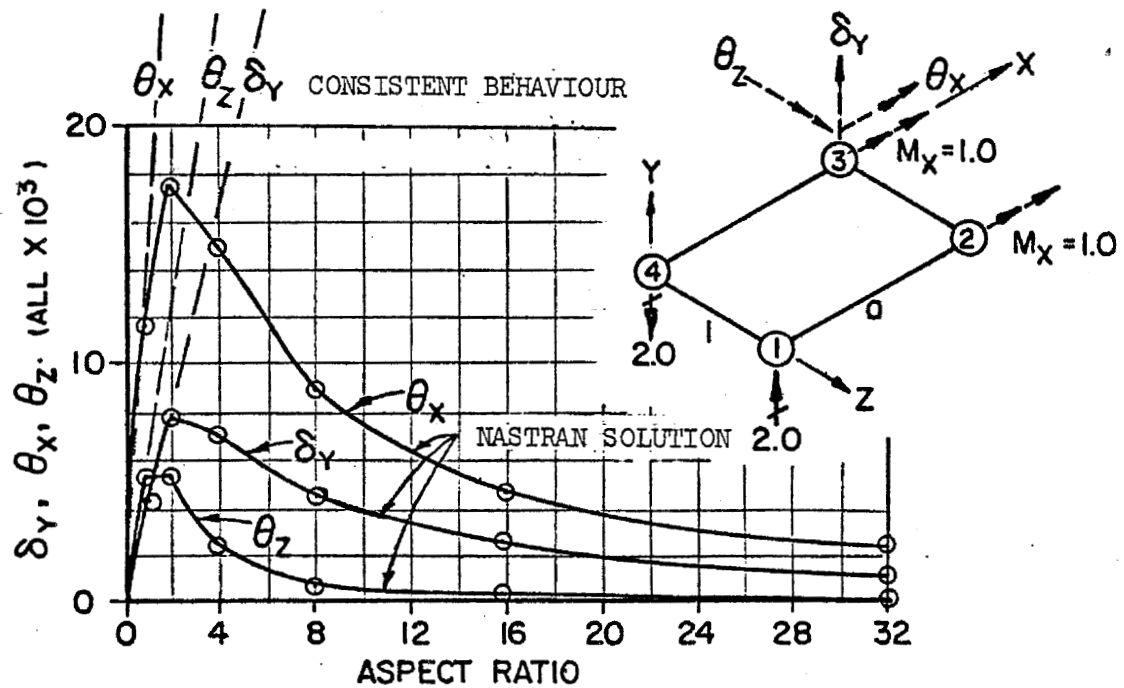


FIGURE 7. QUAD2 SINGLE ELEMENT LOAD-DISPLACEMENT CHARACTERISTICS

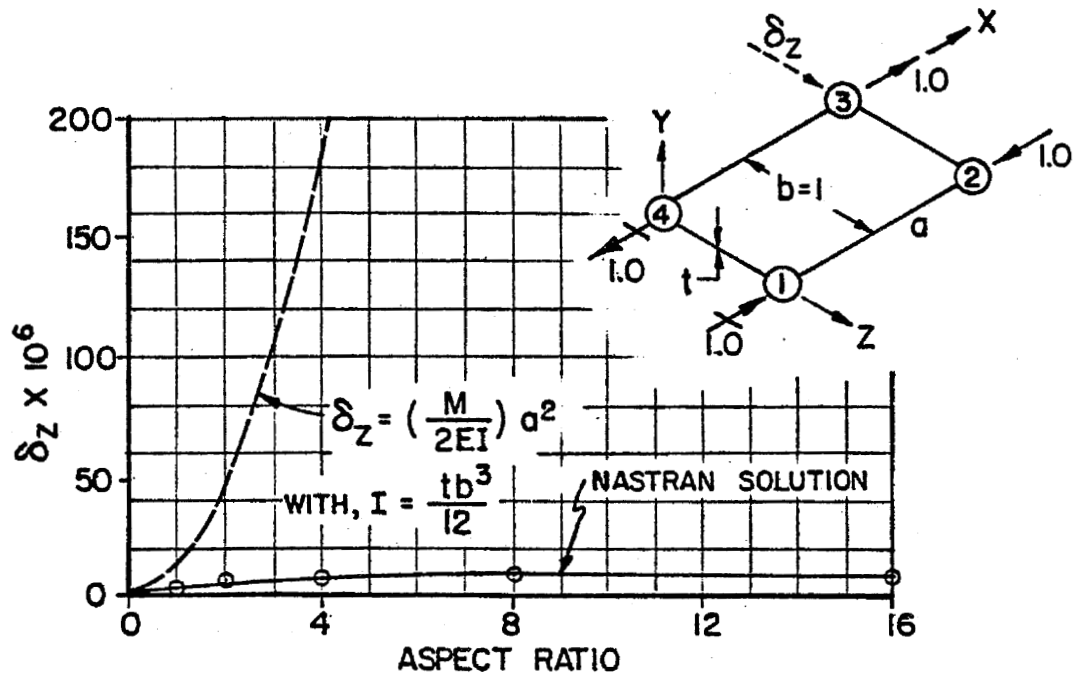


FIGURE 8. QUAD2 SINGLE ELEMENT LOAD-DISPLACEMENT CHARACTERISTICS

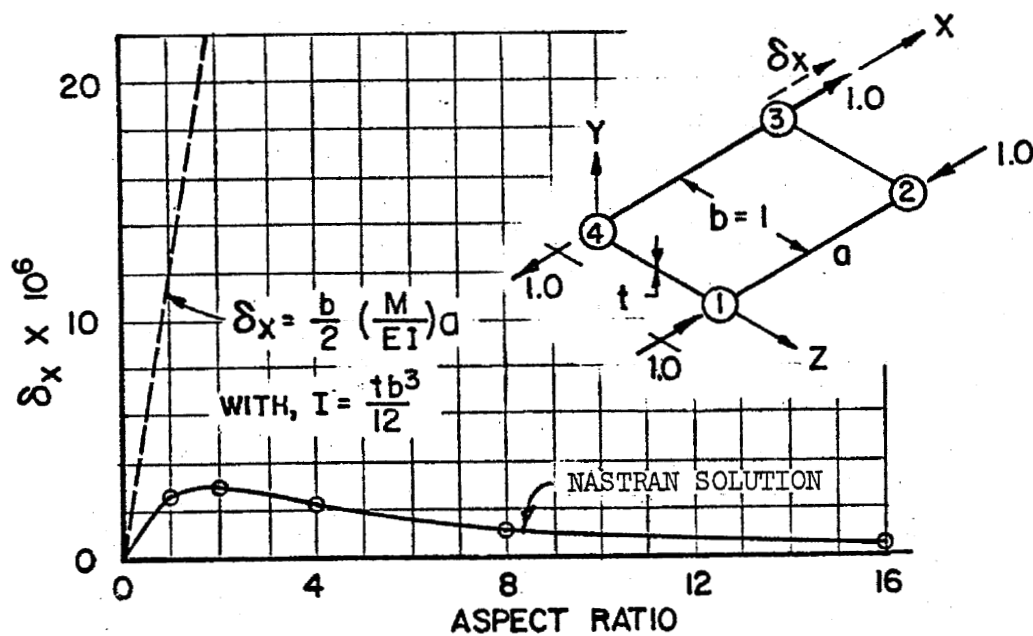


FIGURE 9. QUAD2 SINGLE ELEMENT LOAD-DISPLACEMENT CHARACTERISTICS

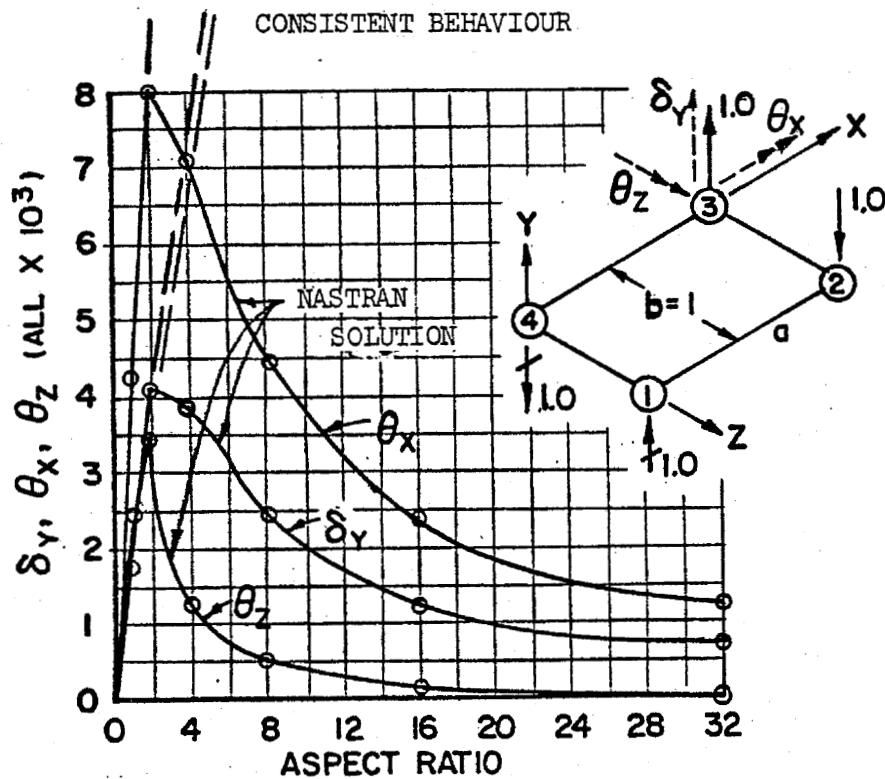


FIGURE 10. QUAD2 SINGLE ELEMENT LOAD-DISPLACEMENT CHARACTERISTICS

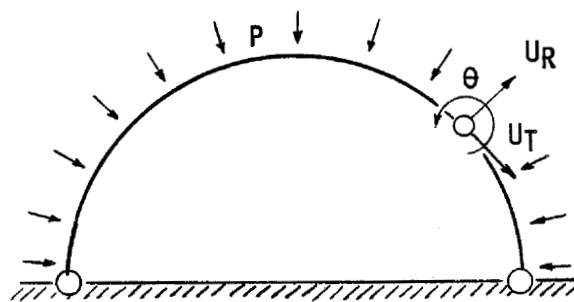


FIGURE 11. ARCH UNDER HYDROSTATIC PRESSURE

A NASTRAN BUCKLING ANALYSIS OF A LARGE STIFFENED CYLINDRICAL SHELL WITH A CUTOUT

By Richard H. Broliar

Teledyne Brown Engineering
Huntsville, Alabama

SUMMARY

A buckling analysis of the Skylab Workshop (SWS) cylinder window region is presented. The Skylab Workshop is a waffle-stiffened cylinder 6.81 m (268 in.) long with a radius of 3.30 m (130 in.). The circular cutout in the cylinder for the window is 45.7 cm (18.0 in.) in diameter. The criterion used in deciding how large a portion of the cylinder to model and what degree of grid refinement to use is explained. Test cases are presented which show that NASTRAN has the capability to handle cylindrical panel buckling problems if a sufficiently fine grid point pattern is used. The problems encountered in obtaining eigenvalues for large matrices (up to 2200 degrees of freedom) are discussed, and the importance of restraint of rotation about the radial axis at each grid point is explained.

INTRODUCTION

The crew compartment of the SWS is a waffle-stiffened cylinder 6.81 m (268 in.) long with a radius of 3.30 cm (130 in.). It was manufactured by modifying a tank of the Saturn V S-IVB stage. A window 45.7 cm (18 in.) in diameter was cut in the cylindrical wall of the waffle-stiffened tank. Figure 1 shows the window region of the tank. The window is designed to be non-load bearing. The basic wall of the SWS is shown in Figure 2. It is insulated with polyurethane foam which is covered on the inside with a fiber glass and metal foil liner.

The SWS cylindrical wall is subjected to axial compressive loads during ground wind prior to launch and during boost to orbit. The load distribution in the window region is nonuniform, since the load is being sheared around the cutout. This makes the window region a difficult area to analyze for buckling.

Preceding page blank

Initial buckling analyses of this region were made using the static analysis portion of NASTRAN to determine the average stress level at each individual waffle pocket, including the adjacent stiffeners. The bending stiffness of each pocket area around the window was then increased until the area showed a positive margin for buckling. In analyzing the pocket for buckling, the pocket and its adjacent stiffeners were imagined to be part of an entire cylinder with identical properties which was subjected to the same stress level that the individual pocket area experienced. The shell bending stiffness was increased where necessary by locally increasing the thickness of the fiber glass liner. Although this type analysis approach has been used successfully in the past for analyzing cylindrical walls and bulkheads, it is quite subjective and could be unconservative.

Therefore, it was decided that, if possible, NASTRAN should be used to make a more exact buckling analysis. In making this decision it was felt that this would be a good problem to use to see how well NASTRAN performed for curved shell buckling problems.

NASTRAN CYLINDRICAL PANEL BUCKLING TEST CASES

Before using NASTRAN for the Skylab problem, it was necessary to determine if the results obtained would be valid. To do this two groups of test cases were analyzed.

The first group was composed of cylindrical panels 34.11 cm (13.43 in.) wide and 170.6 cm (67.175 in.) long. The second group was composed of cylindrical panels 20.7° wide and 102.4 cm (40.3 in.) long and cylindrical panels about 40° wide and 2.39 m (94.0 in.) long. The panels in both groups had a radius of 3.30 m (130.0 in.), and all were loaded in axial compression. The minimum buckling load for all of the models examined was found by using an eigenvalue starting point considerably below the lowest possible eigenvalue.

Axisymmetric Buckling Cases

Figure 3 shows the four NASTRAN models of the panels in the first group. These curved panels were modeled using the flat quadrilateral and triangular NASTRAN elements. These models and all those discussed later were modeled in a cylindrical coordinate system, and all of the global degrees of freedom were in cylindrical coordinates. The models were simply supported at the top and bottom and loaded in axial compression. So that only axisymmetric motion would be allowed, all of the grid points were constrained for tangential displacement, rotation about a radial axis, and rotation about a longitudinal axis. The first cases analyzed in this group

were monocoque cylinders, identical to those shown in Figure 3, only without the stiffening ribs. These cylinders had skin thicknesses of 0.312 cm (0.123 in.), 0.749 cm (0.295 in.), and 1.14 cm (0.45 in.).

The skin thickness of 0.749 cm (0.295 in.) was chosen so that this monocoque cylinder would have the same buckling half-wave length in the longitudinal direction as the waffle-stiffened shell which will be discussed later.

Table I, Cases 1 through 12, shows the shell geometry and buckling results for these three skin thicknesses and four grid patterns. The results are compared with those calculated for the axisymmetric mode using the computer program given in Reference 1. As can be seen, the results improve markedly with increased grid refinement. These axisymmetric monocoque results are also shown in a different form in Figure 4. The data is plotted in this manner to show the good correlation between the eigenvalue accuracy and the number of grid points per half-wave. Interestingly, the results are almost independent of skin thickness for the cases examined.

A plot such as Figure 4 is useful for estimating the required degree of grid refinement needed to get results of the accuracy desired. To do this, one must first know approximately what the buckling half-wave length is in the longitudinal direction.

A waffle-stiffened cylinder with a skin thickness of 0.312 cm (0.123 in.) was also analyzed as a part of the first group. This cylinder was analyzed for axisymmetric buckling, again using the four grid patterns shown in Figure 3. The shell geometry and buckling results for the four grid patterns are shown in Table I, Cases 13 through 16. The results are compared with those calculated for the axisymmetric mode using a computer program based on the theory given in Reference 2. These results are also plotted in Figure 4.

Notice how the stiffened shell converges to the correct result more rapidly and with less grid points per half-wave than the monocoque cases. This improvement appears to be directly caused by the presence of the beam elements. The differential stiffness derivation assumptions of the NASTRAN beam element are considerably more refined than those of the NASTRAN plate element. Thus, the presence of the beam elements causes a more rapid convergence to the correct buckling load.

Cases 1 through 16 show that accurate results can be obtained for axisymmetric buckling of monocoque and waffle-stiffened cylindrical shells if a sufficiently fine grid pattern is used.

Non-Axisymmetric Buckling Cases

The second group to be analyzed contained wider cylindrical panels. These panels were simply supported on all four sides so they would buckle in non-axisymmetric modes.

Figures 5 and 6 show the two grid patterns used to analyze a 20.7°-wide cylindrical panel. This panel was first analyzed as a monocoque shell without the stiffeners shown in Figures 5 and 6. The two skin thicknesses examined were 0.749 cm (0.295 in.) and 1.14 cm (0.45 in.). The skin thickness of 0.312 cm (0.123 in.) was not analyzed because there would not have been sufficient grid points per half-wave for the two grid patterns being used. All of the interior grid points in each model were free for all six degrees of freedom. It did not appear necessary to restrain rotation about the radial axis, as would be necessary for a flat panel, because the four quadrilateral elements meeting at a grid point were not co-planar. Since these panels met at a slight angle at the grid point, they produced a stiffness for rotation about the radial axis. The grid points at the top boundary of the model were restrained for radial displacement, tangential displacement, rotation about a radial axis, and rotation about a longitudinal axis. The bottom grid points were restrained the same as the top, with the addition of restraint for longitudinal displacement. The side grid points were restrained for radial displacement, tangential displacement, rotation about a radial axis, and rotation about a tangential axis.

Table I, Cases 17 to 20, gives the results for these monocoque panels. These results are compared with buckling loads calculated using the computer program in Reference 1. In obtaining the buckling load from the computer program in Reference 1, only mode shapes that would give an integer number of half-waves across the panel were considered, i. e., nine or a multiple of nine circumferential full waves for a complete cylinder. The four points show no major trend other than an improvement in the eigenvalue with increased grid refinement. Also, the results are not as good as those obtained for the same skin thicknesses for axisymmetric buckling.

A waffle-stiffened cylinder with a skin thickness of 0.312 cm (0.123 in.) was also analyzed, using the two grid patterns shown in Figures 5 and 6. The results for this cylinder are shown in Table I, Cases 21 and 22. Interestingly, the accuracy of the eigenvalues was as good or better than those obtained for axisymmetric buckling of the same cylinder with the same size grid. This is just the opposite of the monocoque results. Again, this shows the marked effect of the beam elements.

As a part of this second group, a larger stiffened model was also analyzed using the two grid patterns shown in Figures 7 and 8. This model caused some unexpected difficulties. The 1P grid gave a buckling load below the correct value, whereas all preceding cases had given buckling loads above the correct value. In addition, a detailed examination of the results showed the eigenvector (buckling mode shape) to have large tangential displacements and large rotations about the radial axis. The 4P grid model had 2227 degrees of freedom and a semiband width of 168. It took 3 1/2 hr of Central Processing Unit (CPU) time for a single buckling decomposition. This was on a UNIVAC 1108 with 65,000 words of core. It appeared that in running this model the computer would very likely go down during the time spent in the Real Eigenvalue Analysis-Displacement (READ) Module. Therefore, NASTRAN was modified to print out each iteration in determining the eigenvalue and to leave READ after the first eigenvalue was obtained. All the program output was printed on tape as it was obtained, so that it would not be lost if a machine failure occurred. The eigenvalue and eigenvector were finally obtained after 7 3/4 hr of CPU time and 28 1/2 hr of wall clock time. Unfortunately, these results showed the same low eigenvalue and unusual eigenvector as the 1P grid model.

After a thorough review, it was concluded that the strange results, which only appeared for this large model, were probably caused by the low grid point stiffness for rotation about the radial axis. A study was initiated to determine if the correct results could be obtained by restraining all grid points for rotation about the radial axis.

The study showed that restraining the rotation about the radial axis increased the buckling load for the 1P and 4P 20.7°-wide models less than two percent. This small change was desirable since these small models were already giving reasonable results. Restraining the rotation about the radial axis produced a dramatic improvement in the eigenvector and a significant improvement in the eigenvalue for the large models.

Table I, Case 23, shows the results obtained for the 1P 41.4°-wide model. Before running the 4P 40°-wide model, it was changed from quadrilateral to triangular elements. The quadrilateral model grid points had been sequenced in horizontal rows so that its matrix had the minimum possible bandwidth with no active columns. Changing from quadrilateral elements to triangular elements reduced the vertical coupling in the model from two rows to one row. This change reduced the semiband width of the matrix by 50 percent and reduced the CPU time required to run the model by 78 percent. Figure 9 shows the triangular element model. The results for this model with the rotational restraint are given in Case 24 of Table I. The skin moment of inertia in this model includes the bending stiffness of the fiber glass liner.

Restraining the rotation about the radial axis corrected the problems in the eigenvector for both models and brought the eigenvalues into a reasonable range. For some currently unexplainable reason, the eigenvalues for both these large models were not as close as those obtained for the 20.7°-wide models, but the buckling results and run times obtained for the 4P triangular model meant that the SWS window model could be run successfully. The conclusion of the study on restraint of rotation about the radial axis was that all future cylindrical panel models should be run with this restraint.

SWS WINDOW ANALYSIS

All of the large models were sized so that a quarter segment of the SWS window could be placed in the lower corner of the model. Figure 10 shows the SWS window model. The shaded area around the window is where the fiber glass liner was increased in thickness to raise the buckling capability. Around the edge of the window is a ring which is relatively stiff for any motion normal to the shell. Both the structure and loading are symmetric about the right side and bottom of the model. A complete window was not modeled because it was felt that accurate results could be obtained with a quarter segment. Also, a complete model would have four times the number of degrees of freedom, double the semiband width, and an unacceptably long run time.

The model length was sized to allow at least three buckling half-waves above the region with the increased stiffness and to allow a uniform load to be applied at the top. The model width was sized so that the effect of the load shearing around the window would die out and so that the boundary condition along the left edge would not appreciably affect the buckling load.

The window model was simply supported along the top edge and left side. Ideally, to obtain all possible buckling modes with a quarter segment model that would be obtainable from a complete model, the quarter segment model should have a symmetric boundary condition along the bottom and right side for the static analysis. This static analysis would be used to determine the loads on each element. These element loads would be used to calculate the differential stiffness matrix. Then the stiffness and differential stiffness matrices would be supported for four buckling boundary conditions. The four buckling boundary conditions are the four possible combinations of symmetric and antisymmetric boundary conditions along the bottom and right side. Unfortunately, this dual boundary condition capability--one boundary condition for the static analysis and a second for the buckling analysis--is not currently available in NASTRAN. Therefore, for the problem at hand, a compromise was made, and the four buckling boundary conditions were used for the complete analysis.

The results of the buckling analysis of the window model for the four boundary conditions were good from an engineering standpoint but were rather unexciting from a research standpoint. All four boundary conditions showed the buckling radial displacements to be occurring in the basic shell at the top of the model. For all four cases the radial displacements attenuated upon entering the area of increased stiffness around the window. Also, all four boundary conditions gave buckling loads within one percent of each other. The conclusion of the analysis was that the increase in bending stiffness was sufficient to prevent buckling around the window. Also, the buckling capability of the basic shell adjacent to the area of increased stiffness was not lowered.

SIMILAR BUCKLING ANALYSES IN PROGRESS

The SWS has a second major cutout in its cylindrical wall: the access door shown in Figure 11. As mentioned previously, the SWS is subjected to axial compressive loads during ground wind prior to launch and during boost to orbit. The access door is removed for the first condition and installed for the second condition. Figure 12 shows the access door model. The buckling analysis of this model for door-in and door-out conditions is currently in progress.

IMPROVEMENTS TO NASTRAN'S BUCKLING CAPABILITY

As previously mentioned, the assumptions used for the NASTRAN plate derivation are somewhat crude. To compensate for this shortcoming, fine grids and longer run times are required to get accurate results. A second item that causes run times to be longer than necessary for most problems is the use of an unsymmetric decomposition routine in the READ module. For the 4P 40°-wide quadrilateral element model the unsymmetric decomposition routine, which is used in the buckling analysis, took 23 times as long as the symmetric decomposition routine used for the static analysis. This is unfortunate since the eigenvalue can be determined using a symmetric decomposition. Also, the dual boundary condition is not available at present in NASTRAN. To facilitate the solution of the remaining Skylab buckling problems and future buckling problems, Marshall Space Flight Center (MSFC) currently has a contract with the Mac Neal-Schwendler Corporation. Their contract task is:

- to develop an improved plate element for buckling
- to incorporate this plate element into the MSFC version of NASTRAN
- to incorporate the dual boundary condition option into NASTRAN
- to provide a READ module with a symmetric decomposition routine for NASTRAN.

This contract should be completed this fall, and it is the author's understanding from talking with the NASA Contracting Officer's Representative for this contract that the improvements to NASTRAN from the contract will be made available to the NASTRAN Systems Management Office.

CONCLUDING REMARKS

Test cases have been presented which show that NASTRAN has the capability to handle cylindrical panel buckling problems if a sufficiently fine grid point pattern is used. A good correlation has been shown between eigenvalue accuracy and grid points per half-wave for axisymmetric buckling of monocoque and stiffened cylindrical panels. The importance of restraint of rotation about the radial axis at each grid point has been shown for cylindrical panels buckling in non-axisymmetric modes.

REFERENCES

1. Dickson, J.N., and Broliar, R.H.: The General Instability of Eccentrically Stiffened Cylindrical Shells Under Axial Compression and Lateral Pressure. NASA CR-1280, January 1969.
2. Meyer, R.R.: Buckling of 45° Eccentric-Stiffened Waffle Cylinders. Journal of the Royal Aeronautical Society, July 1967.

TABLE I. NASTRAN CYLINDRICAL PANEL TEST RESULTS

Case	Model*	Skin Thickness, cm (in.)	Skin Area Moment of Inertia per Unit Width, cm ⁴ /cm (in ⁴ /in.)	Stiffener Height, d, cm (in.)	Stiffener Width, w, cm (in.)	Stiffener Spacing, a, cm (in.)	NASTRAN Buckling Load, N/cm (lb/in.)	Buckling Load from Reference, N/cm (lb/in.)	Percent Error in Buckling Load**	Number of Longitudinal Half-waves from Reference	Matrix Degrees of Freedom	Matrix Semiband Width	Buckling Decomposition Time, CPU sec
1	1P	0.312 (0.123)	0.00254 (0.000155)	—	—	—	4,037 (2,305)	1,308 (747)	208	10	45	12	1
2	4P	0.312 (0.123)	0.00254 (0.000155)	—	—	—	1,637 (935)	1,308 (747)	25.2	10	150	18	4
3	9P	0.312 (0.123)	0.00254 (0.000155)	—	—	—	1,436 (820)	1,308 (747)	9.8	10	315	24	11
4	16P	0.312 (0.123)	0.00254 (0.000155)	—	—	—	1,390 (794)	1,308 (747)	6.3	10	540	30	25
5	1P	0.749 (0.295)	0.0350 (0.00214)	—	—	—	10,606 (6,056)	7,515 (4,291)	41.1	6	45	12	1
6	4P	0.749 (0.295)	0.0350 (0.00214)	—	—	—	8,275 (4,725)	7,515 (4,291)	10.1	6	150	18	4
7	9P	0.749 (0.295)	0.0350 (0.00214)	—	—	—	7,793 (4,450)	7,515 (4,291)	3.7	6	315	24	11
8	16P	0.749 (0.295)	0.0350 (0.00214)	—	—	—	7,669 (4,379)	7,515 (4,291)	2.0	6	540	30	25
9	1P	1.14 (0.45)	0.123 (0.00759)	—	—	—	22,761 (12,997)	17,388 (9,929)	30.9	5	45	12	1
10	4P	1.14 (0.45)	0.123 (0.00759)	—	—	—	18,647 (10,648)	17,388 (9,929)	7.2	5	150	18	4
11	9P	1.14 (0.45)	0.123 (0.00759)	—	—	—	17,919 (10,232)	17,388 (9,929)	3.1	5	315	24	11
12	16P	1.14 (0.45)	0.123 (0.00759)	—	—	—	17,710 (10,113)	17,388 (9,929)	1.85	5	540	30	25
13	1P	0.312 (0.123)	0.00254 (0.000155)	1.59 (0.627)	0.366 (0.144)	24.13 (9.5)	3,723 (2,126)	2,800 (1,599)	33.0	6	45	12	1
14	4P	0.312 (0.123)	0.00254 (0.000155)	1.59 (0.627)	0.366 (0.144)	24.13 (9.5)	2,909 (1,661)	2,800 (1,599)	3.9	6	150	18	4
15	9P	0.312 (0.123)	0.00254 (0.000155)	1.59 (0.627)	0.366 (0.144)	24.13 (9.5)	2,847 (1,626)	2,800 (1,599)	1.7	6	315	24	11
16	16P	0.312 (0.123)	0.00254 (0.000155)	1.59 (0.627)	0.366 (0.144)	24.13 (9.5)	2,825 (1,613)	2,800 (1,599)	0.9	6	540	30	25
17	1P 20, 7*	0.749 (0.295)	0.0350 (0.00214)	—	—	—	12,091 (6,904)	7,469 (4,265)	61.9	2	111	38	4
18	4P 20, 7*	0.749 (0.295)	0.0350 (0.00214)	—	—	—	8,854 (5,056)	7,469 (4,265)	18.6	2	472	71	55
19	1P 20, 7*	1.14 (0.45)	0.123 (0.00759)	—	—	—	26,973 (15,402)	17,539 (10,015)	53.8	3	111	38	4
20	4P 20, 7*	1.14 (0.45)	0.123 (0.00759)	—	—	—	19,947 (11,390)	17,539 (10,015)	13.7	3	472	71	55
21	1P 20, 7*	0.312 (0.123)	0.00254 (0.000155)	1.59 (0.627)	0.366 (0.144)	24.13 (9.5)	3,716 (2,122)	3,243 (1,852)	14.6	4	111	38	4
22	4P 20, 7*	0.312 (0.123)	0.00254 (0.000155)	1.59 (0.627)	0.366 (0.144)	24.13 (9.5)	3,371 (1,925)	3,243 (1,852)	3.9	4	472	71	55
23	1P 41, 4*	0.312 (0.123)	0.00254 (0.000155)	1.59 (0.627)	0.366 (0.144)	24.13 (9.5)	3,772 (2,154)	2,905 (1,659)	29.8	9	469	73	82
24	4P 40*	0.340 (0.134)	0.0113 (0.000692)	1.905 (0.750)	0.254 (0.100)	24.13 (9.5)	4,347 (2,482)	3,874 (2,212)	12.2	8	1904	80	459

*Cases 1 through 16 are axisymmetric.

**Percent Error = $\frac{(\text{NASTRAN Buckling Load} - \text{Reference Buckling Load})}{\text{Reference Buckling Load}} \times 100$.

Note:

- The original calculations for this table were made in the U.S. Customary System.
- Young's Modulus = 10,500,000 psi

NOT REPRODUCIBLE

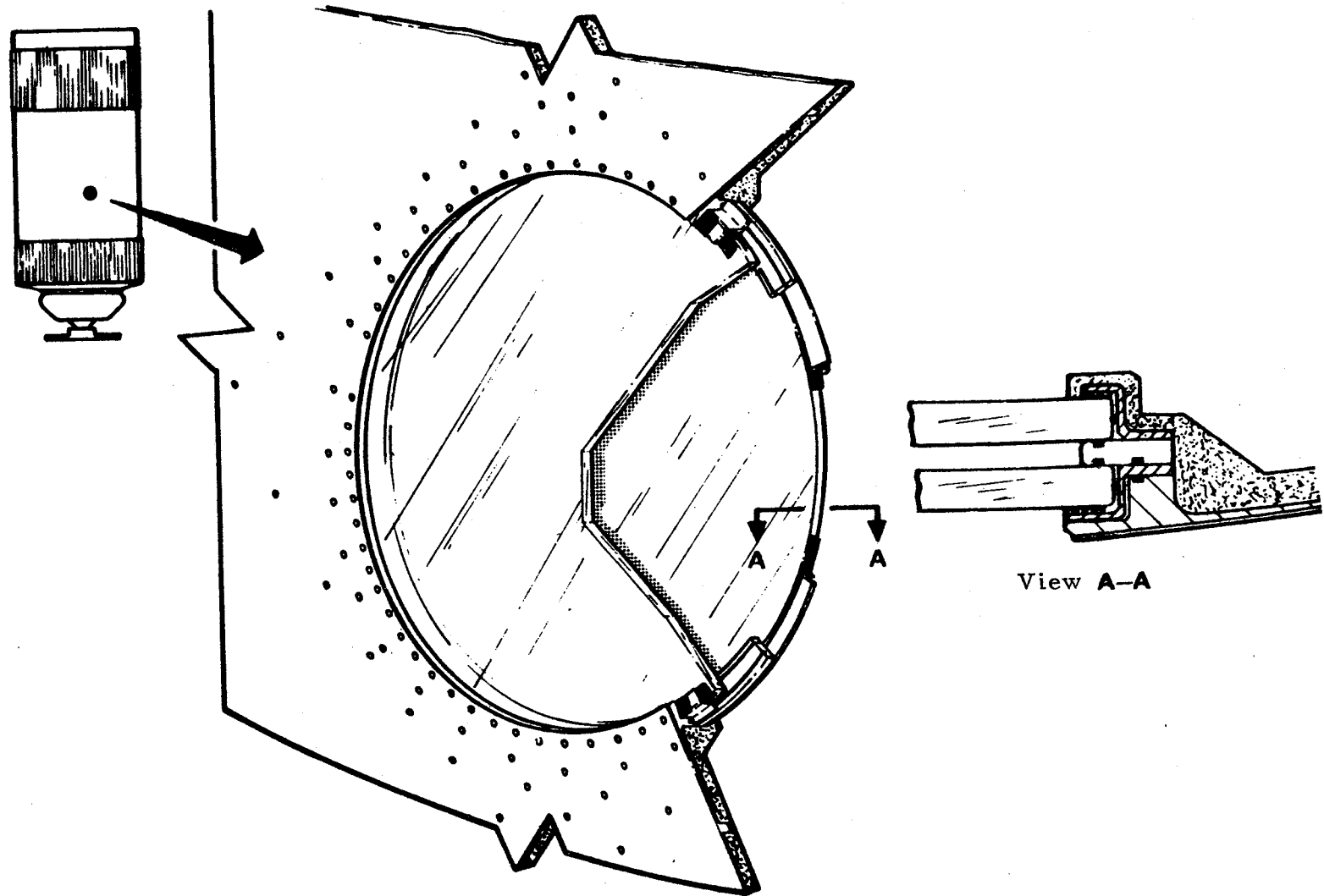


FIGURE 1. SKYLAB WORKSHOP WINDOW

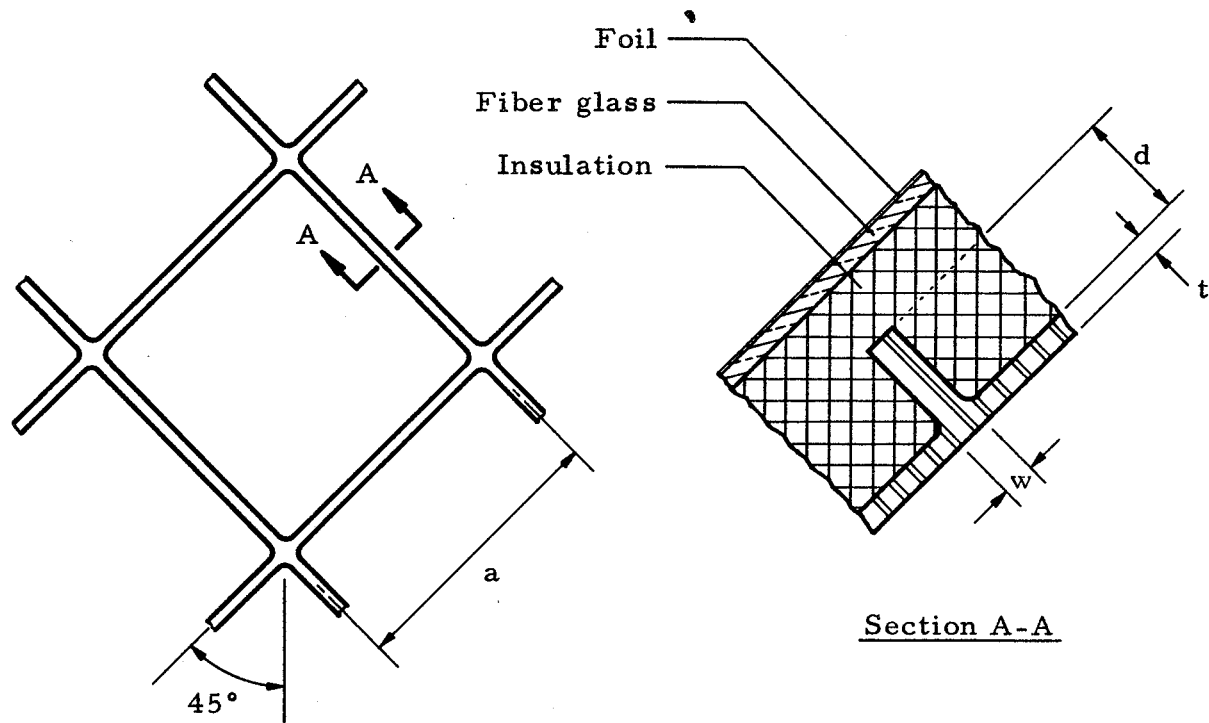


FIGURE 2. SKYLAB CYLINDER WALL

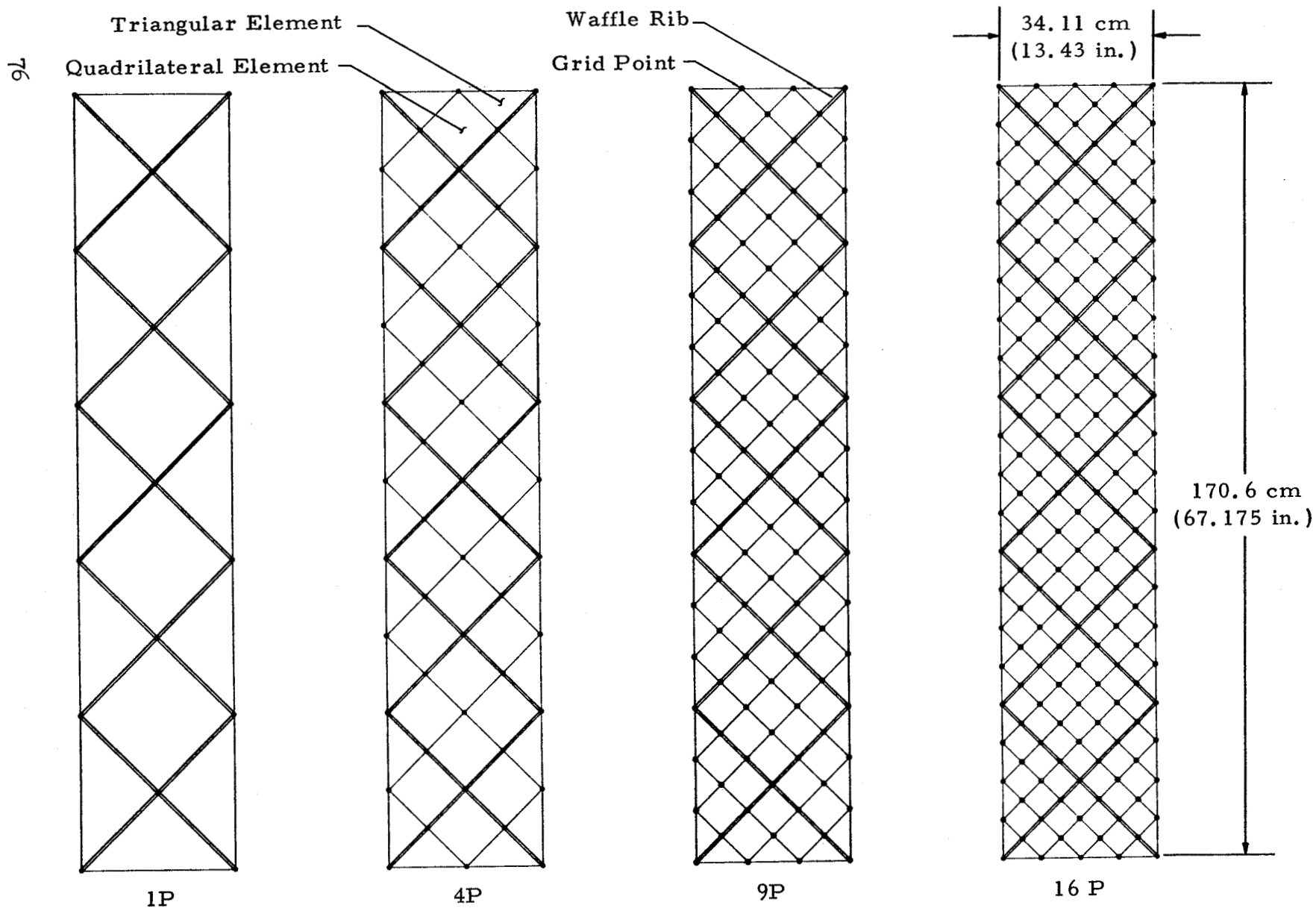


FIGURE 3. AXISYMMETRIC MODELS

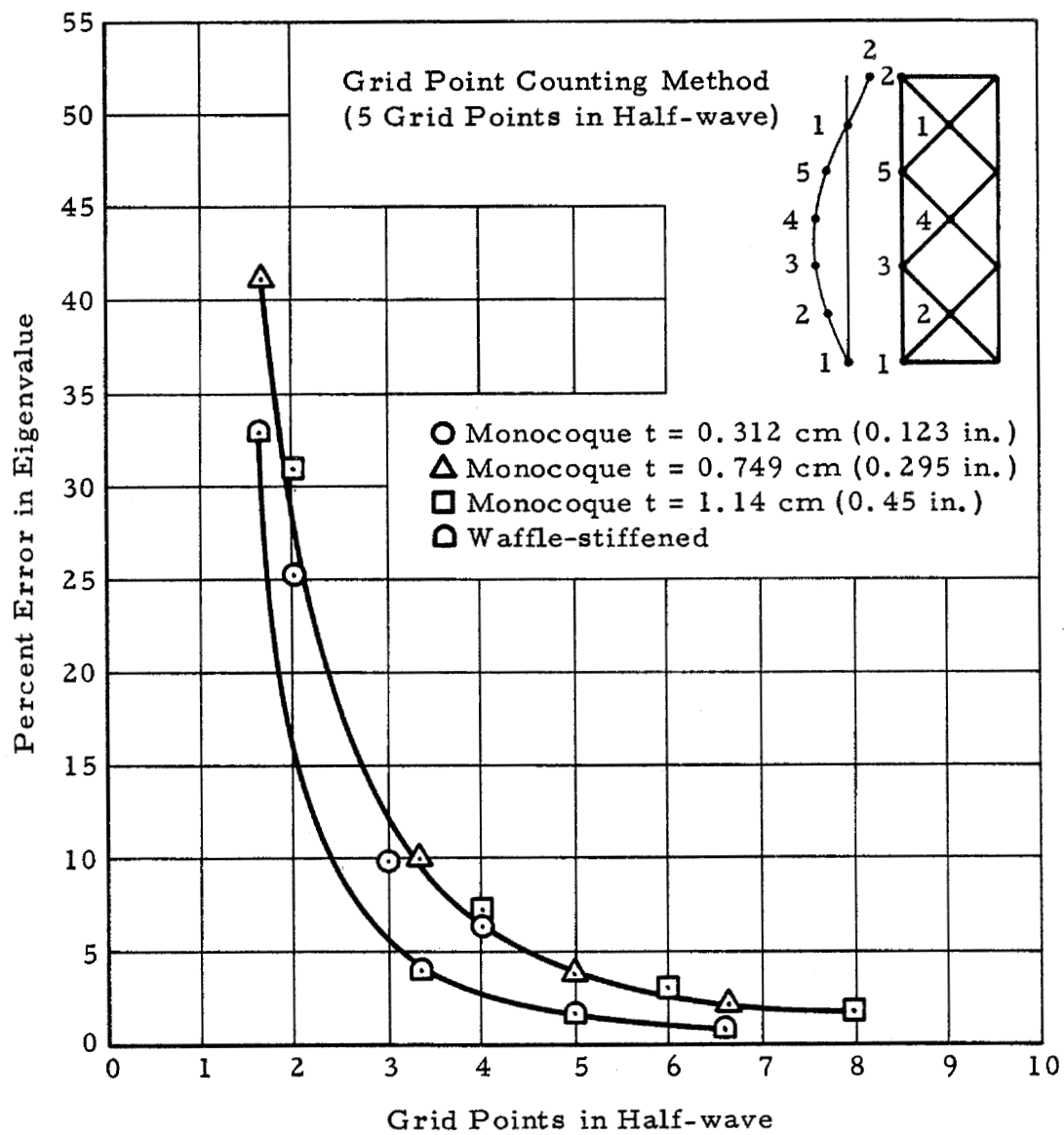


FIGURE 4. EIGENVALUE ACCURACY AS A FUNCTION OF GRID POINTS IN HALF-WAVE FOR AXISYMMETRIC BUCKLING

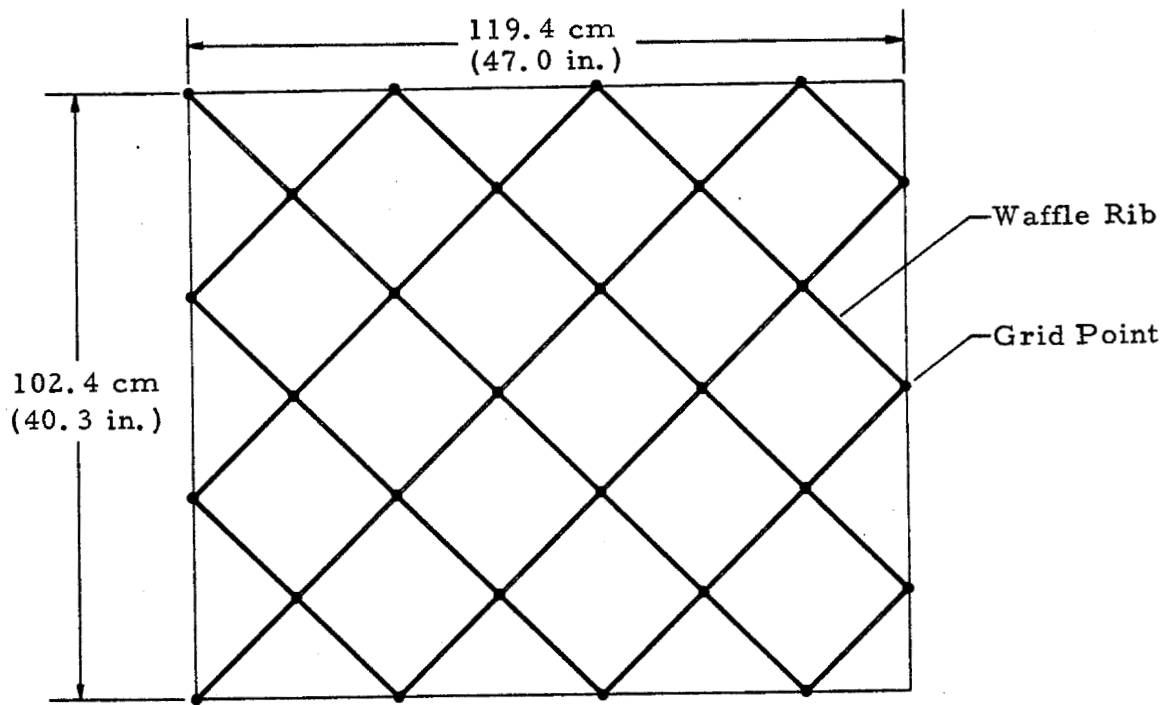


FIGURE 5. 1P 20.7°-WIDE CYLINDRICAL PANEL MODEL

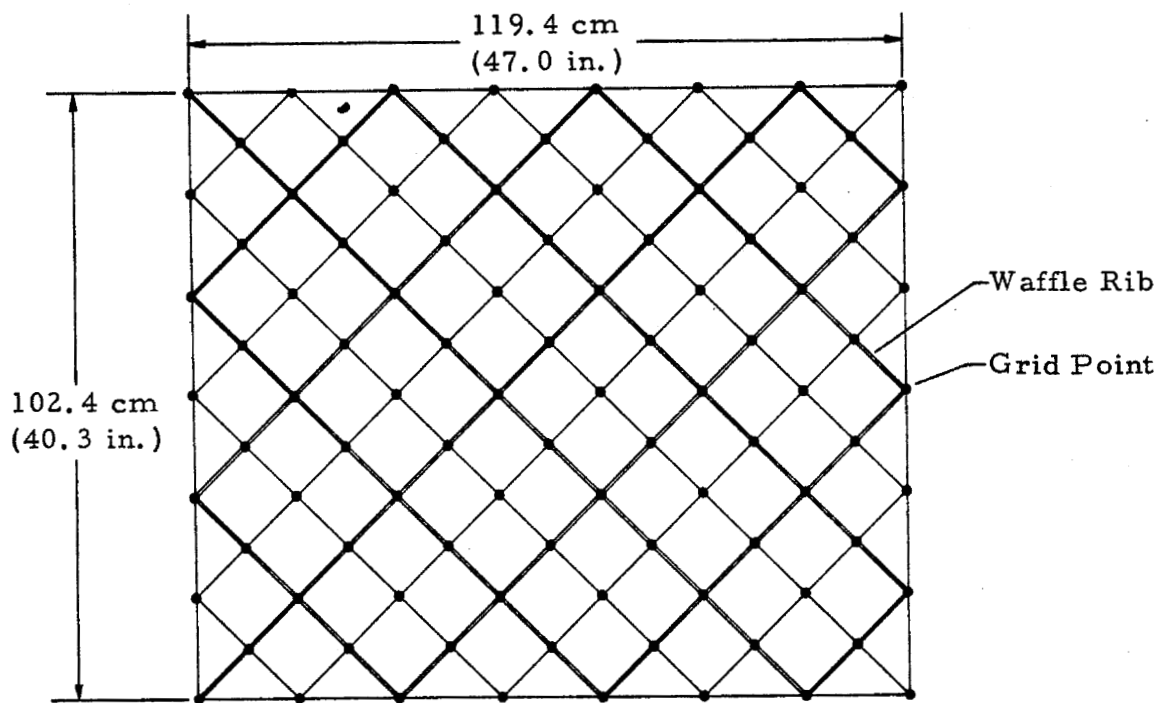


FIGURE 6. 4P 20.7°-WIDE CYLINDRICAL PANEL MODEL

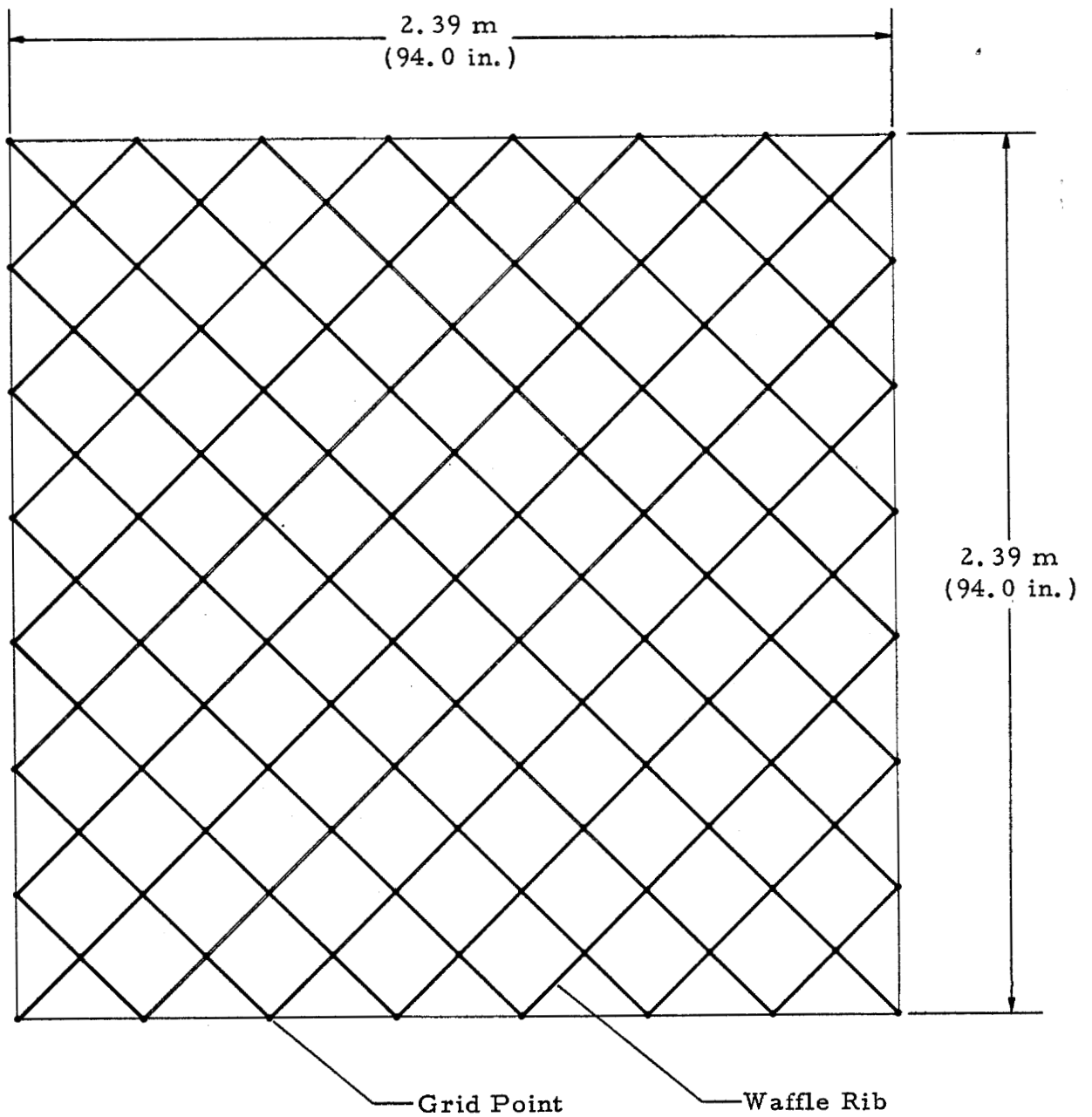


FIGURE 7. 1P 41.4°-WIDE CYLINDRICAL PANEL MODEL

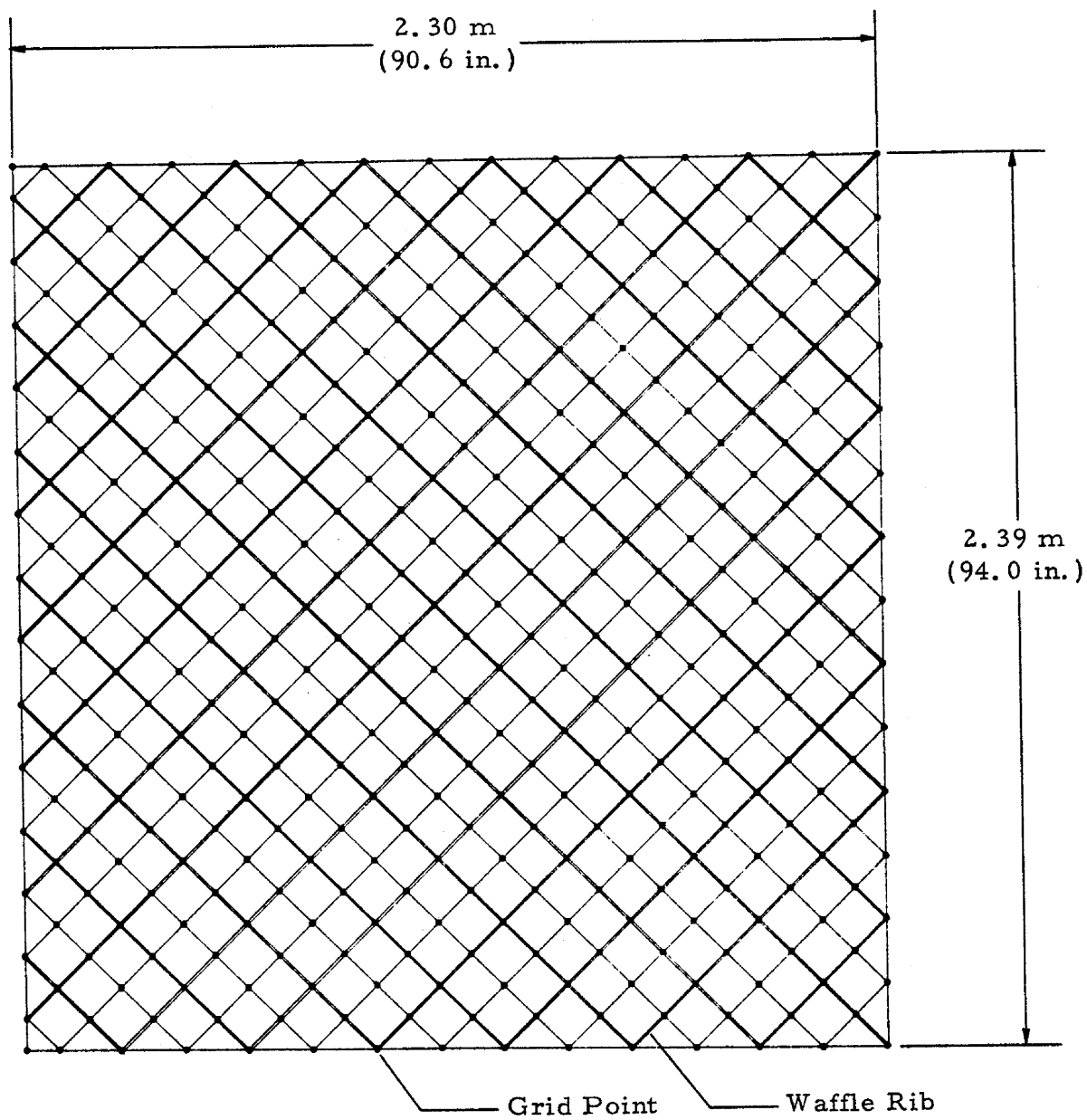


FIGURE 8. 4P 40°-WIDE QUADRILATERAL ELEMENT
CYLINDRICAL PANEL MODEL

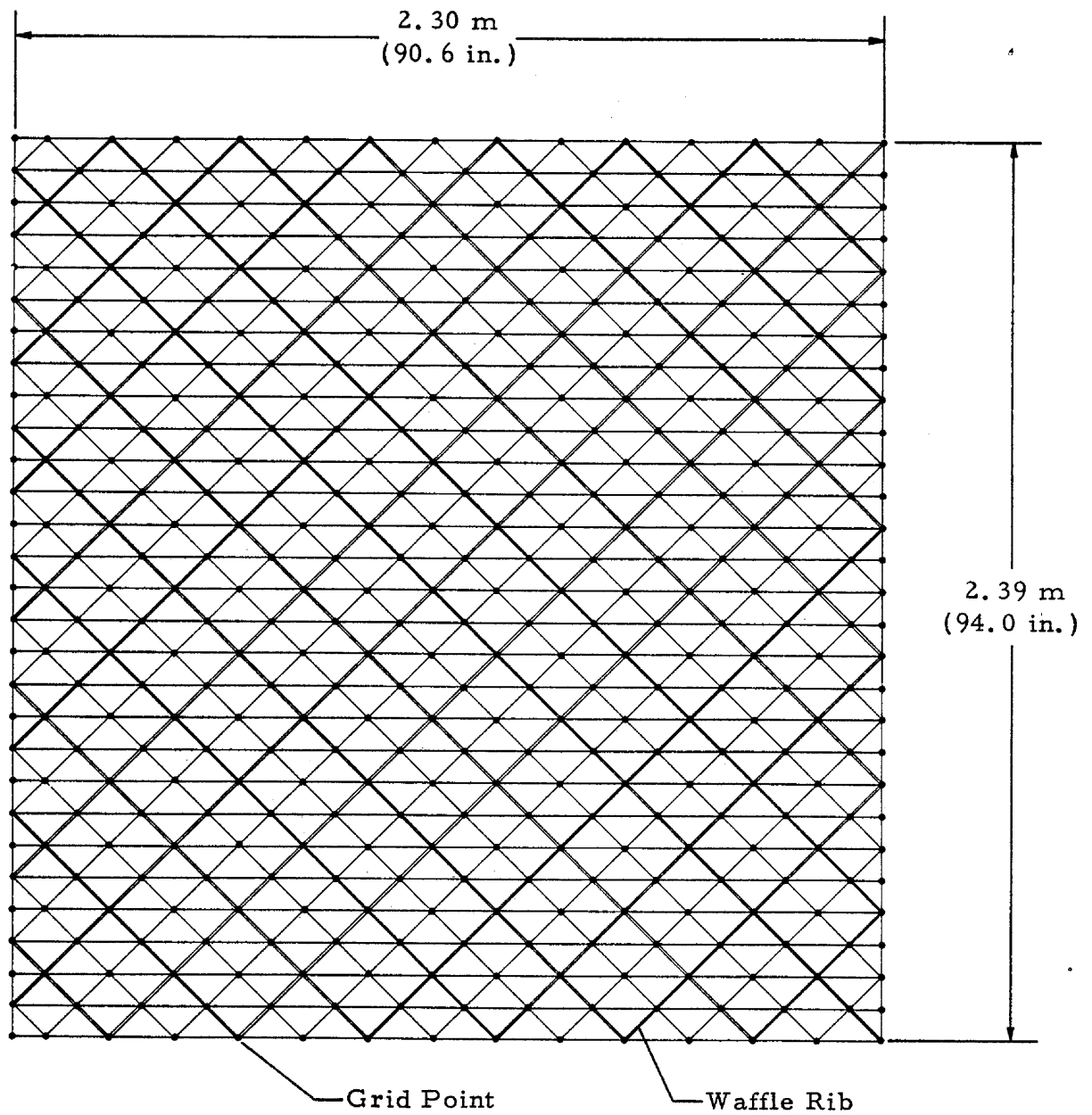


FIGURE 9. 40°-WIDE TRIANGULAR ELEMENT
CYLINDRICAL PANEL MODEL

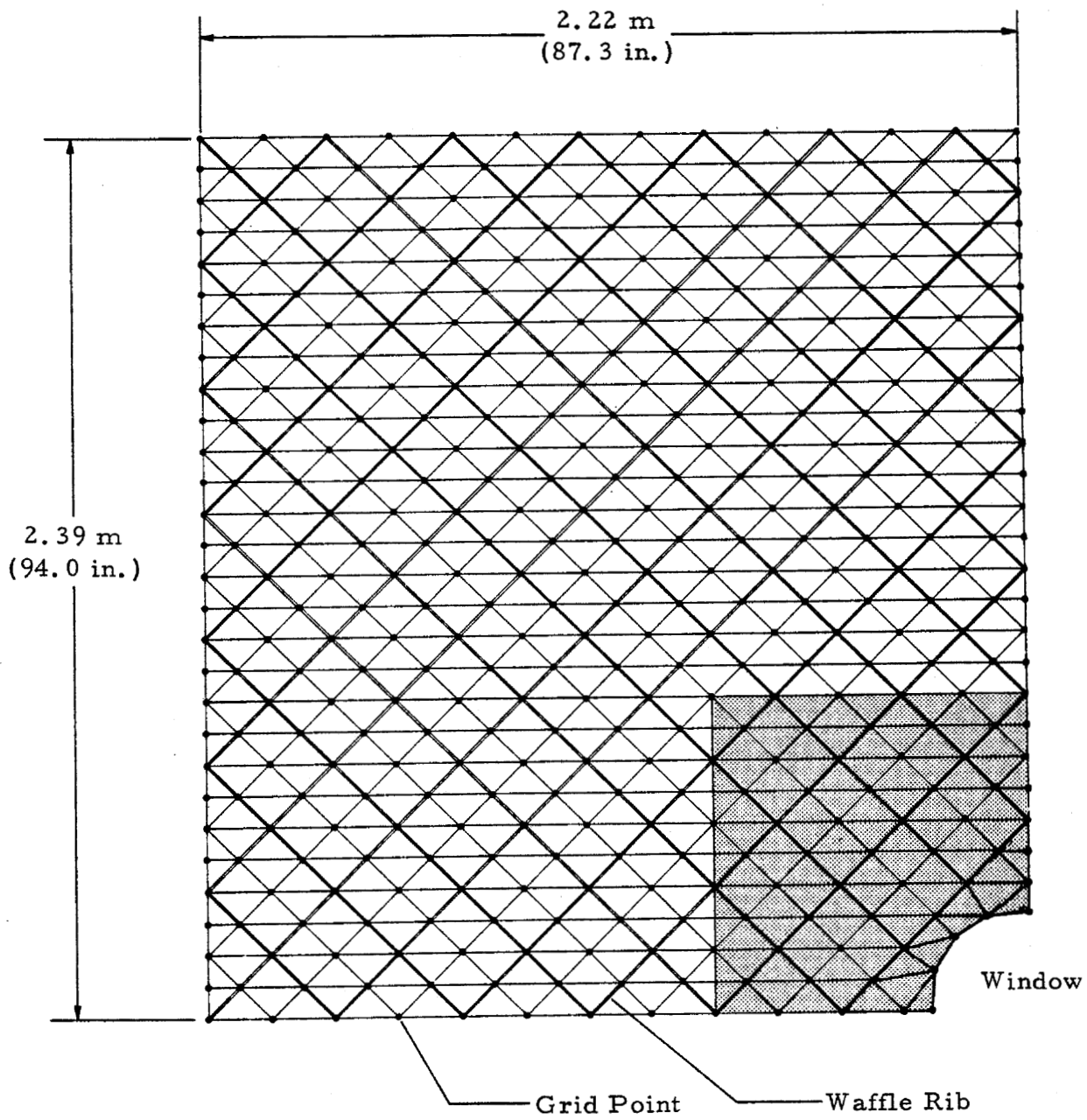


FIGURE 10. SKYLAB WORKSHOP WINDOW MODEL

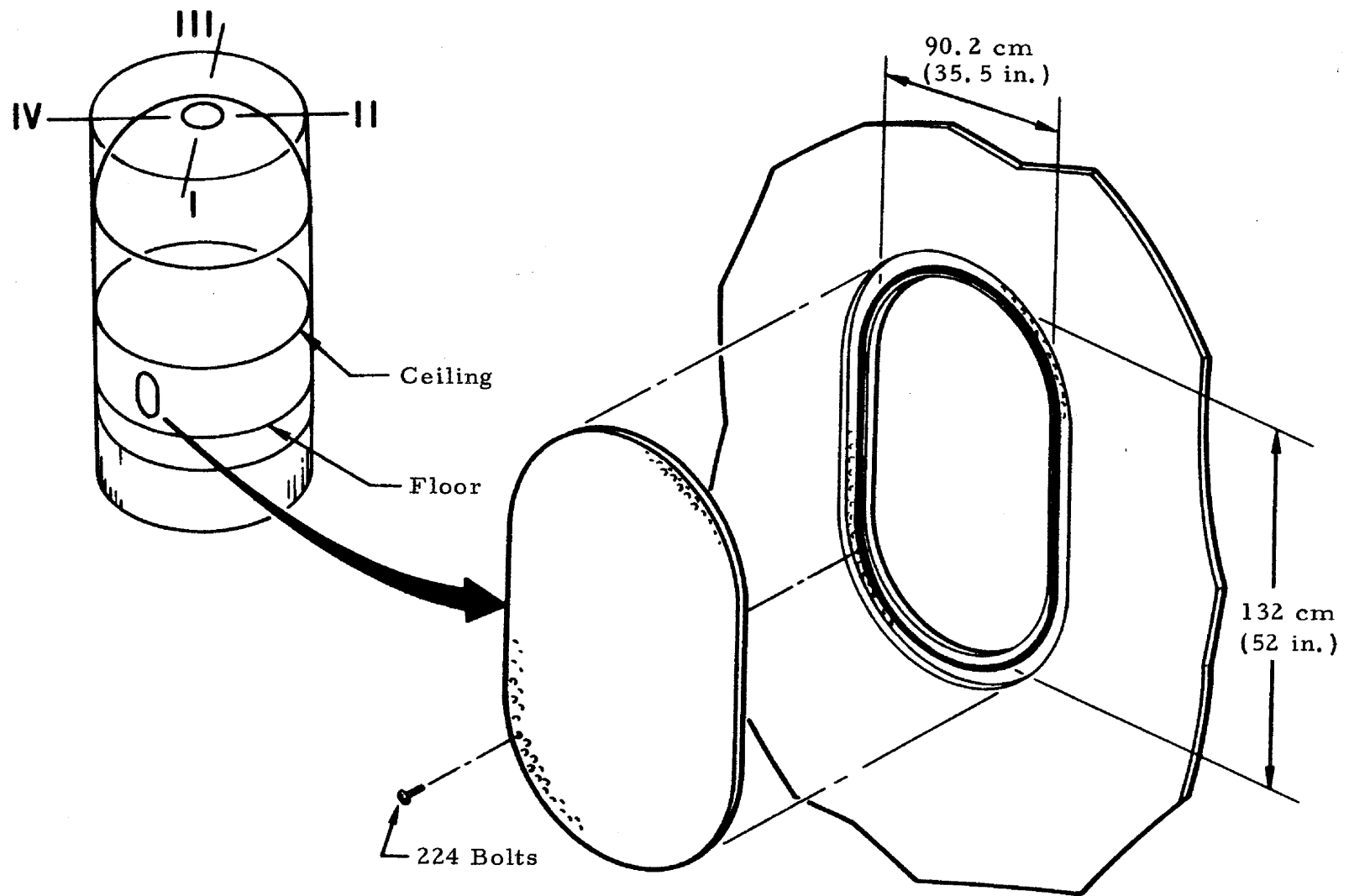


FIGURE 11. SKYLAB WORKSHOP ACCESS DOOR

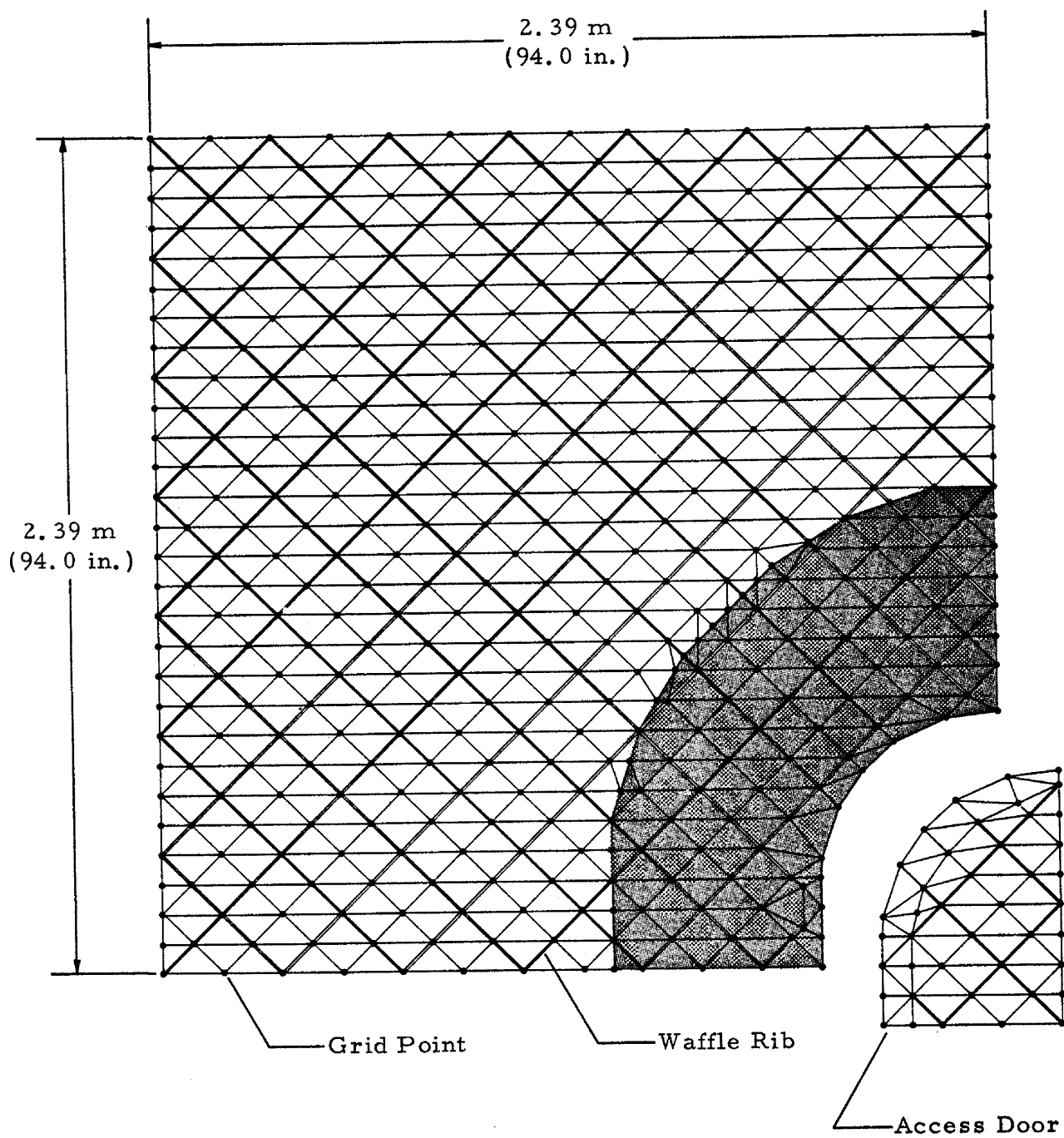


FIGURE 12. SKYLAB WORKSHOP ACCESS DOOR MODEL

NASTRAN DIFFERENTIAL STIFFNESS ANALYSIS
OF AN AIRCRAFT CANOPY

By Robert D. Bennett

Vought Aeronautics Company
A Division of LTV Aerospace Corporation

SUMMARY

Comparisons of internal member loads and stresses as generated by the NASTRAN Differential Stiffness and Static Analysis methods are presented for a tandem side opening canopy. A description of the structure analyzed and the load condition for which it is analyzed are included along with several computer and hand generated plots. The comparisons of the two methods show a general decrease in the internal member loads obtained by the Differential Stiffness method of analysis over the Static method of analysis.

INTRODUCTION

The magnitude of the design operating stresses in a canopy structure must be reliably known to insure both minimum weight and structural integrity. Minimum weight is required since the canopy ejection thruster size increases as the canopy weight increases. And, when pilot ejection through the canopy glass is required, the glass thickness must be as thin as possible. Determination of the stresses is complicated by the wide variation in material properties over the service temperature range. The complex shape of a canopy and the varying external pressures acting on a canopy structure also make the method of analysis difficult. The advent of structural analysis finite element computer programs has greatly eased the task of obtaining internal member loads in complex structures and has increased the accuracy of the solutions. However, to avoid unwarranted conservatism in the design of a canopy the geometric non-linearity of the structure should be taken into account. Since the stresses in a canopy glass are directly proportional to the radius of curvature of the glass cross-section, any great changes in shape during loading will greatly alter the stresses in the glass and in the frames and side rails of the structure. Through the simultaneous consideration of large non-linear motions and the applied loads, NASTRAN generates a Differential Stiffness solution based on the linear terms in the equations of motion of an elastic body. (Refer to the NASTRAN Theoretical Manual, ref. 1). Comparisons between the NASTRAN Differential Stiffness Analysis and the Static Analysis of a tandem side opening canopy show significant reductions in member loads when the differential stiffness theory is applied to the solution.

SYMBOLS

E	Young's modulus of elasticity
G	Shear modulus of elasticity
μ	Poisson's ratio
A	Cross-sectional area
I_1	Moment of inertia about axis 1-1
I_2	Moment of inertia about axis 2-2
J	Torsional moment of inertia

DESCRIPTION OF THE STRUCTURE

The structure described is a tandem side opening canopy which was analyzed during a recent company sponsored design program. The canopy consists of two pieces of stretched acrylic 0.25 inches thick, three frames, and two side rails. The frames are located at each end and at the center of the curved acrylic. The side rails are located at the bottom edges of the canopy acrylic and provide support for the frames and for the acrylic. Both the frames and the side rails are constructed of 7075-T6 aluminum alloy in this application. This canopy is designed to open to the pilot's right and is supported by four hinges on the right side rail. When in the closed position, the left hand side rail is latched at four points for side and vertical loads. Two shear pins, also located on the left side rail, extend into fuselage framing members and provide fore and aft restraint for the left side of the canopy. A left side view of the canopy structure is given in Figure 1. Figure 2 includes a top view of the structure and the properties of the stretched acrylic. The side rail cross-section is presented in Figure 3 along with the section properties. Figure 4 includes the cross-section and properties for the forward, mid and aft frames.

EXTERNAL LOADING

The external loading applied to the canopy is a symmetrical flight condition with an internal cabin pressure of 5.0 psi. The combined aerodynamic and internal pressure distribution is plotted over the top view of the canopy in Figure 5. During the actual design phase, five separate load conditions were investigated. The most critical load case was an unsymmetrical flight condition. However, to accomplish the objective of this paper the simpler of the load cases will suffice. To apply the

selected load condition to the equivalent structural model, the pressure distribution of Figure 5 was plotted on a plan form view of the canopy acrylic. The pressure acting at the centroid of each finite element representing the acrylic was determined and applied to the element.

NASTRAN FINITE ELEMENT MODEL

The finite element model representative of the canopy structure consists of 384 triangular bending plates and 203 six degree of freedom beams. The finite element plates represent the canopy acrylic and are located at the center plane of the acrylic. The finite element beams represent the side rails and the frames. The side rail elements are located at the shear center of the actual structural side rail. This is done so that the reactions along the canopy side rails will be in a proper location. The frame elements are located at the bending center of each frame. The finite elements representing the side rails and the frames are tied to the elements representing the acrylic by short beams. These beams do not exist in the actual structure and are used only to transfer loads from the acrylic to the frames and side rails. A stiffness of twice that of the side rails was used for the beams. The geometry of the structure is defined by 360 grid points yielding a total of 2118 degrees of freedom. There are actually two coordinate systems used to define the structure. The XYZ coordinate system shown in Figure 6 is used to define all the grid points except those at which the external reactions are located. The reaction points are defined by the coordinate system X' Y' Z' which is rotated 10.5° (counterclockwise when viewed from the left) about the Y axis of the XYZ coordinate system. The rotation places the X' axis in the plane formed by the canopy side rails and makes the Z' axis perpendicular to the rails. The external reactions thus obtained are either in the plane of the side rails or perpendicular to the plane and represent the actual structural reactions between the canopy and the fuselage. The canopy to fuselage tie points occur at 10 discrete points along the side rails. Referring to Figure 6, the reaction points 1, 2, 3 and 4 lie along the left side rail and are Y' and Z' reacted. Tie points 1 through 4 represent the canopy latch points. Tie points 5 and 6 are also located on the left side rail and are reacted through scalar springs in the X' direction. The springs represent the stiffness of the shear pins. Reaction points 7, 8, 9 and 10 are located on the right side beam and represent the hinges of the canopy. These points are reacted in the X' Y' and Z' directions.

Computer generated plots showing the top, side and end views of all the finite elements in the model are included in Figure 7, 8 and 9. Figure 10 is an orthographic three dimensional plot showing the canopy acrylic separated from the side rails, frames and standoffs.

COMPARISONS OF THE SOLUTIONS

Referring to Figure 11 through 18 the following comparisons between NASTRAN generated solutions (with and without differential stiffness) for internal member loads and stresses are presented.

Acrylic Longitudinal Stresses

From Figure 11, it is seen that the longitudinal stresses at the center plane of the acrylic are reduced by the application of differential stiffness theory. The maximum reduction occurs between the front and mid frames along longitudinal cut B. The 65% reduction in the static solution stress is accompanied by an 85% reduction in the displacement. (Fig. 12)

Acrylic Hoop Stresses

Figure 13 indicates only small changes in the acrylic hoop stresses. From a typical cross-section deflection plot (Fig. 14) it is seen that the cross-section is near circular to start with and when loaded, only small changes in curvature are created. From membrane theory, the hoop stress is directly proportional to the radius of curvature. Therefore, only small changes in stress are expected when the initial section is near circular and near uniform loading on the section is present. The hoop stresses in the acrylic are distributed to the side rails and act as a running load on a continuous beam. Since there is little change in the hoop stresses it is also expected that the reactions along the side rails will change proportionally. Figures 15 and 16 bear out this expectation.

Side Beam Loads

A noticeable effect occurs when the geometric non-linearity of the canopy is considered. The mid-frame effectiveness in supporting the side rails for vertical loading increases. From the vertical deflection plots in Figure 15 it is seen that the mid-frame creates an inflection point between the two mid supports when differential stiffness theory is used. The bending moments in the side rail just above the vertical reactions increase and the mid span moments decrease when differential stiffness is accounted for. The maximum increase is 122% over the linear solution at the front support. The maximum decrease occurs at mid span between the front support and the second support. The decrease is 66% over the linear solution. Figure 16 indicates only minor differences between the linear and non-linear solutions for the torsion and side loadings.

Mid-Frame Member Loads

The axial load in the mid-frame just above the side rail to mid-frame joint increases 900% from the linear solution to the non-linear solution. This increase in axial load indicates that the mid-frame is more effective in constraining the vertical motion of the side rails when differential stiffness theory is applied to the structure.

CONCLUDING REMARKS

The comparisons made between NASTRAN generated solutions with and without differential stiffness for the canopy structure have lead to the following conclusions:

The changes in geometry of a canopy cross-section greatly effect the internal member loads within the structure. In order to obtain correct design operating stresses within a canopy, deformations of the canopy under loading must be accounted for. The NASTRAN Static Analysis with differential stiffness offers a practical means for calculation of the design operating stresses.

The initial cross-section of the canopy influences the amount of difference between a linear and non-linear solution. These differences are reduced as the section approaches a circular shape.

REFERENCES

1. MacNeal, Richard H., "The NASTRAN Theoretical Manual," NASA SP-221, 1969.

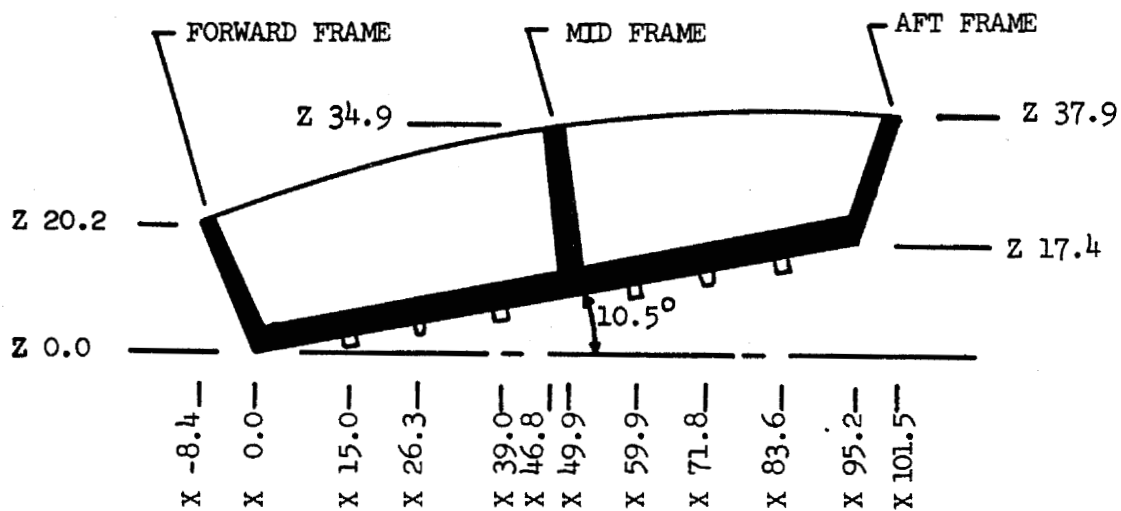


Figure 1. - Left Side View of the Canopy Structure

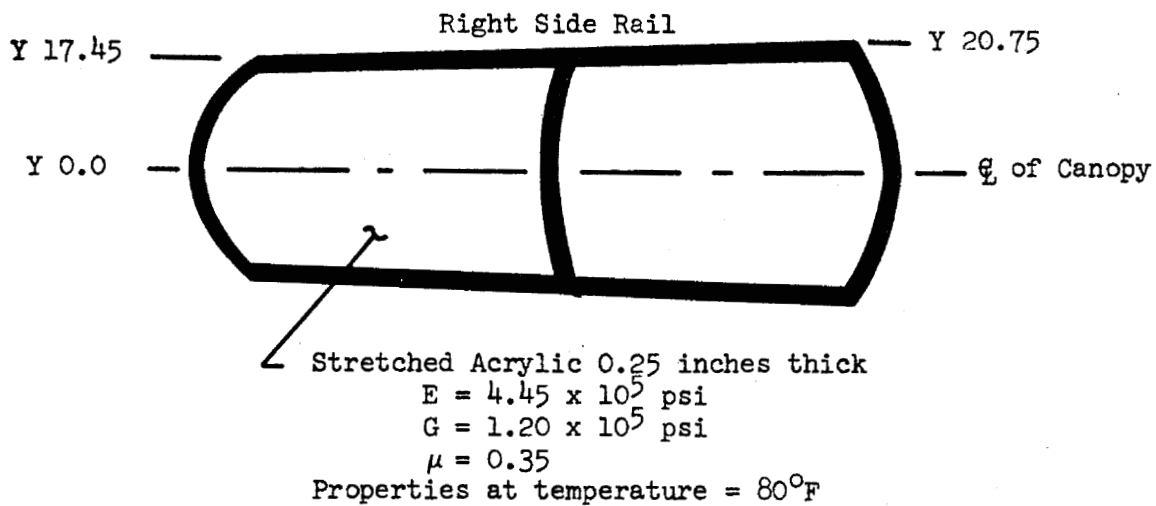
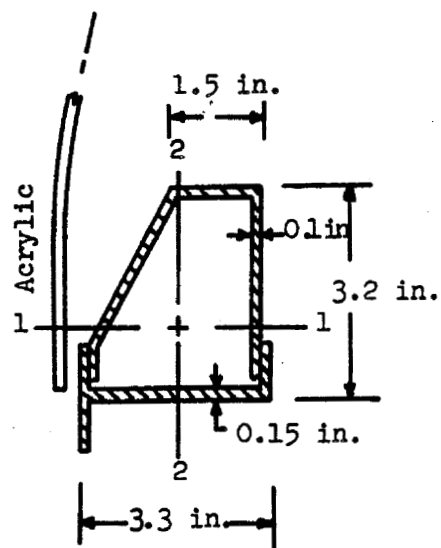


Figure 2. - Top View of Canopy Structure



7075-T6 ALUMINUM
SECTION PROPERTIES
AT ROOM TEMPERATURE

$$E = 10.3 \times 10^6 \text{ psi}$$

$$G = 3.9 \times 10^6 \text{ psi}$$

$$\mu = 0.33$$

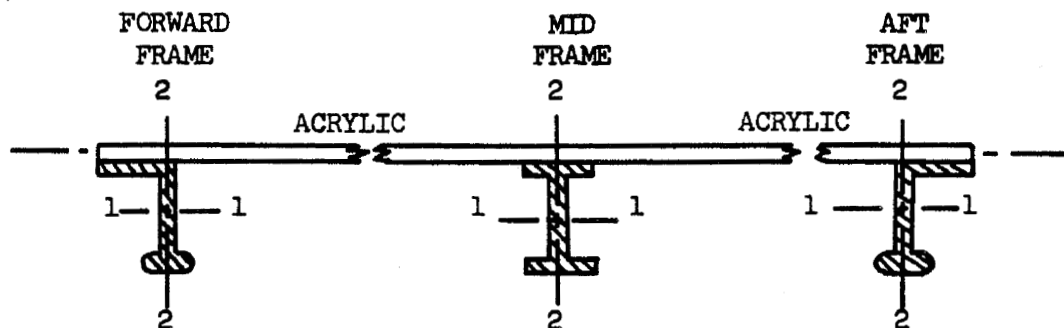
$$A = 1.42 \text{ in.}^2$$

$$I_1 = 2.39 \text{ in.}^4$$

$$I_2 = 1.80 \text{ in.}^4$$

$$J = 2.10 \text{ in.}^4$$

Figure 3. - Side Rail Cross Section and Section Properties



7075-T6 ALUMINUM
SECTION PROPERTIES AT ROOM TEMPERATURE

$$E = 10.30 \times 10^6 \text{ psi}$$

$$A = 0.58 \text{ in.}^2$$

$$I_1 = 0.25 \text{ in.}^4$$

$$I_2 = 0.0422 \text{ in.}^4$$

$$J = 0.0013 \text{ in.}^4$$

$$G = 3.90 \times 10^6 \text{ psi}$$

$$A = 1.16 \text{ in.}^2$$

$$I_1 = 0.50 \text{ in.}^4$$

$$I_2 = 0.08 \text{ in.}^4$$

$$J = 0.0013 \text{ in.}^4$$

$$\mu = 0.33$$

$$A = 0.58 \text{ in.}^2$$

$$I_1 = 0.25 \text{ in.}^4$$

$$I_2 = 0.0422 \text{ in.}^4$$

$$J = 0.0013 \text{ in.}^4$$

Figure 4. - Forward, Mid and Aft Frame Cross Sections
and Section Properties

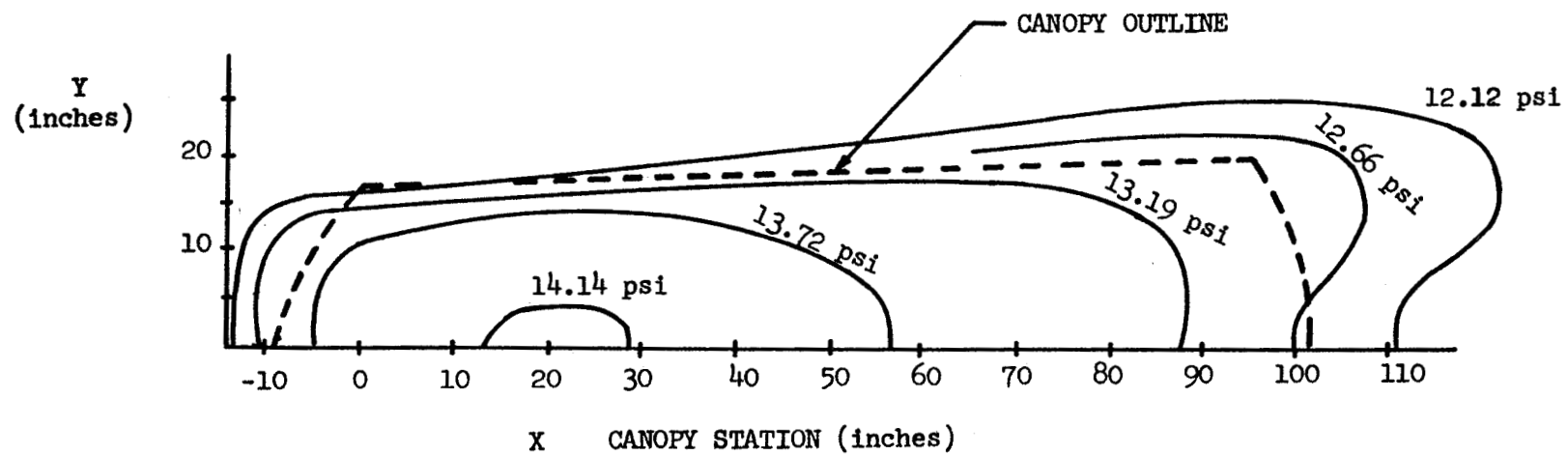


Figure 5. - Net Canopy Pressure Distribution

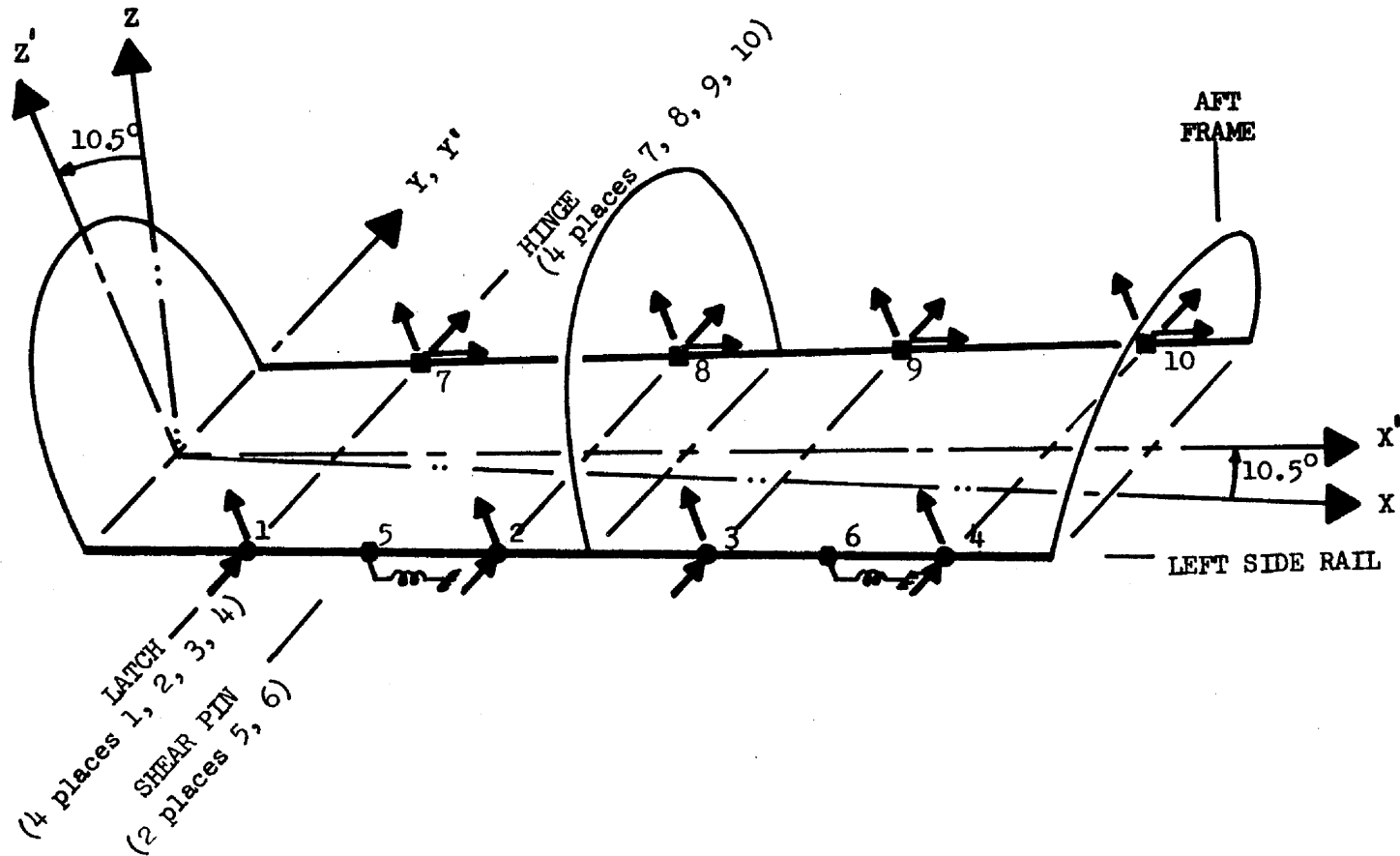


Figure 6. - Finite Element Model Coordinate Systems and Reactions

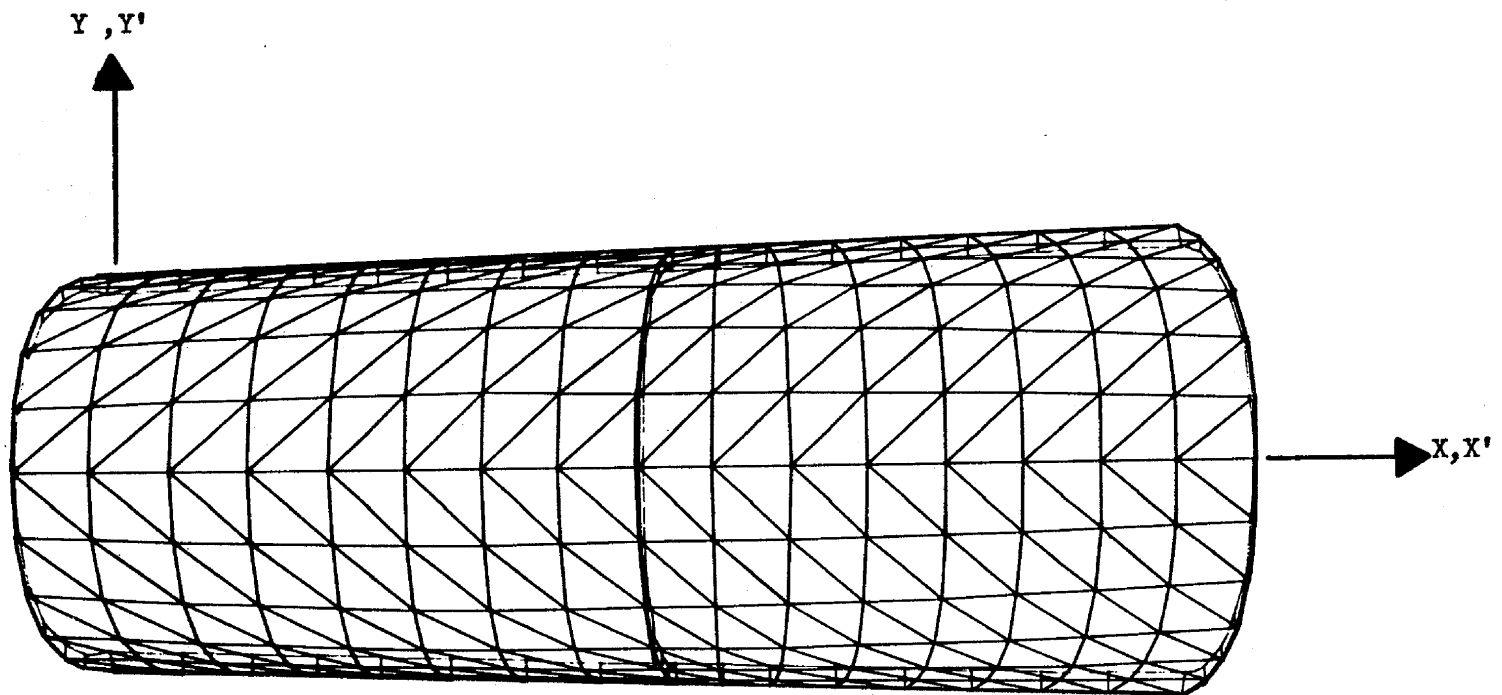


Figure 7.- Top View of the Canopy Model

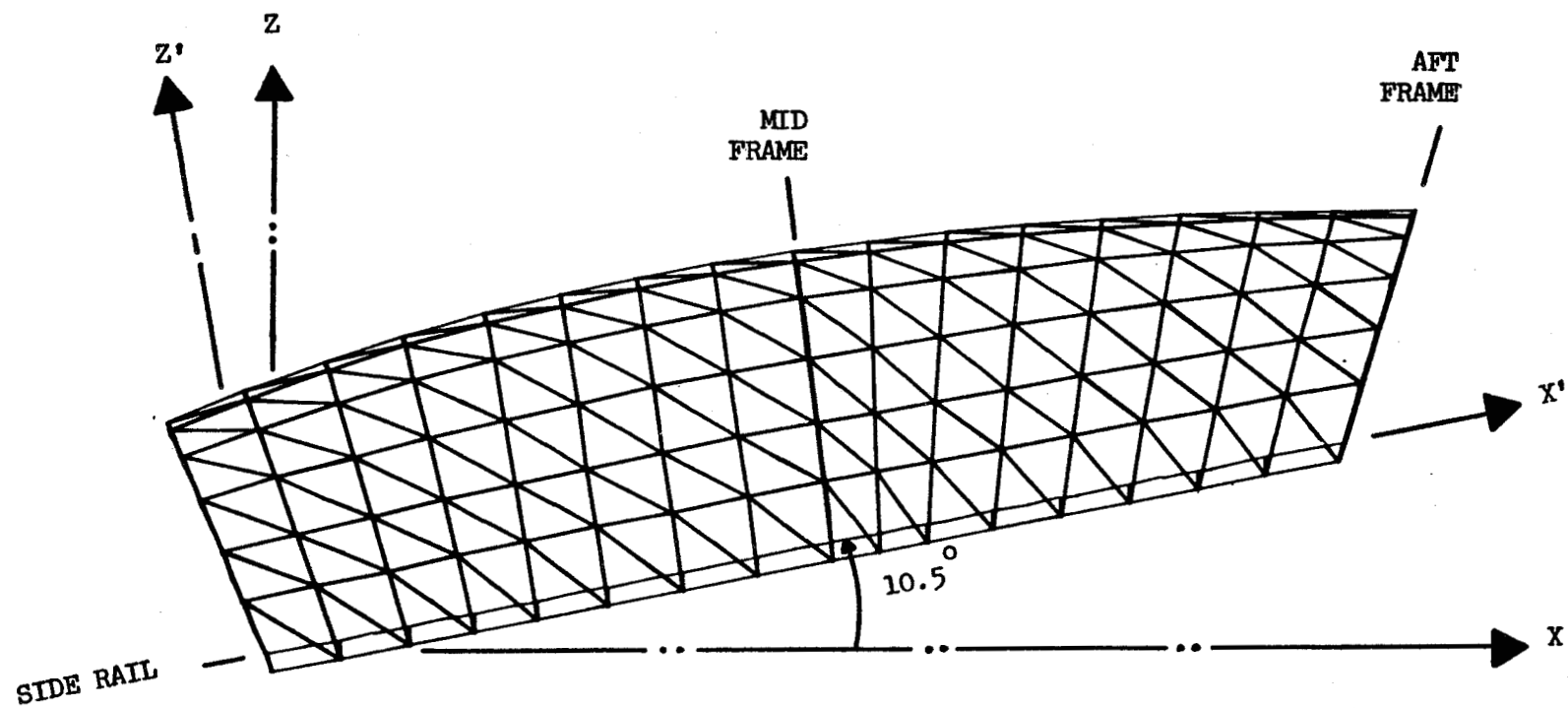


Figure 8.- Side View of the Canopy Model

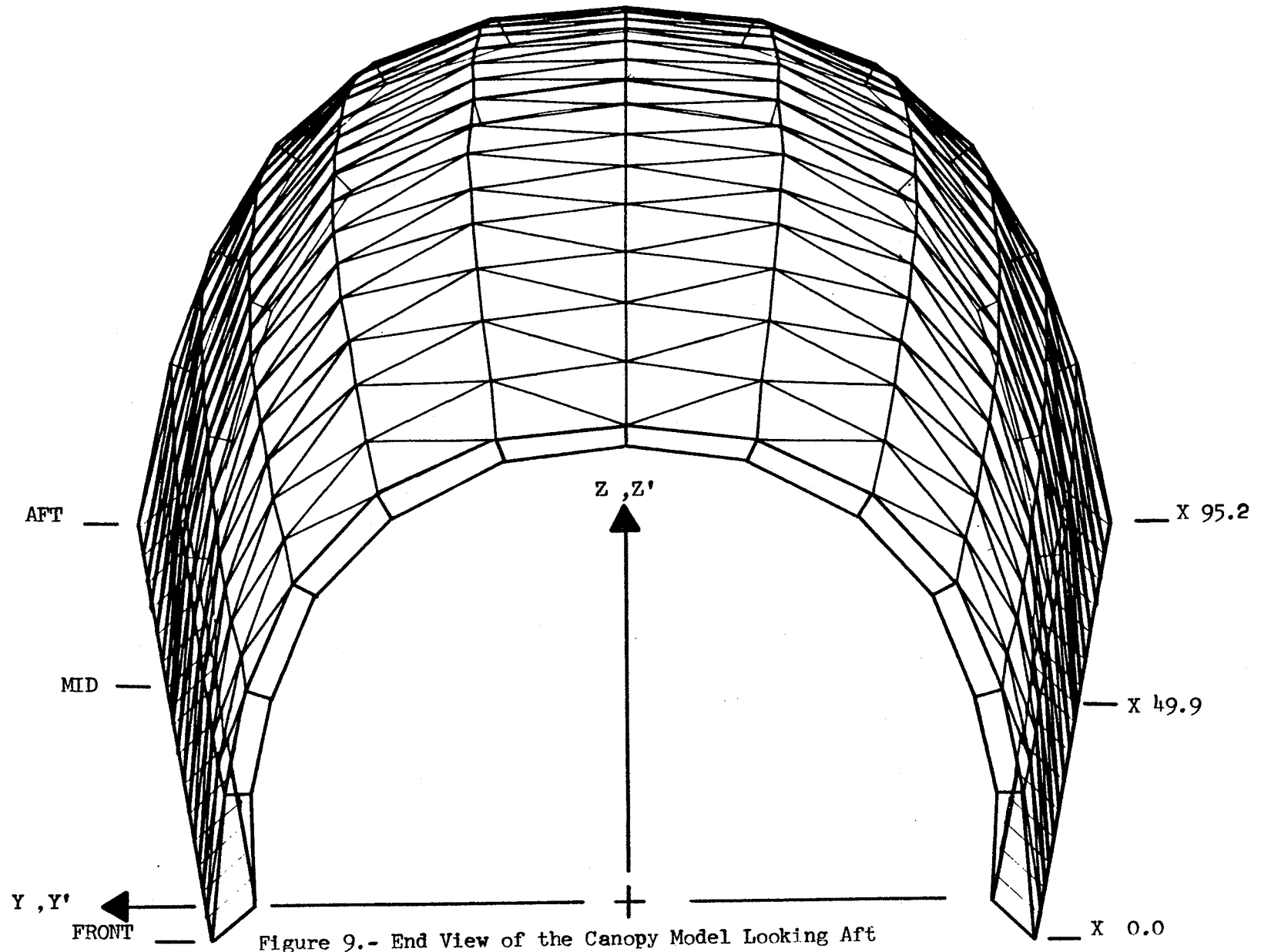


Figure 9.- End View of the Canopy Model Looking Aft

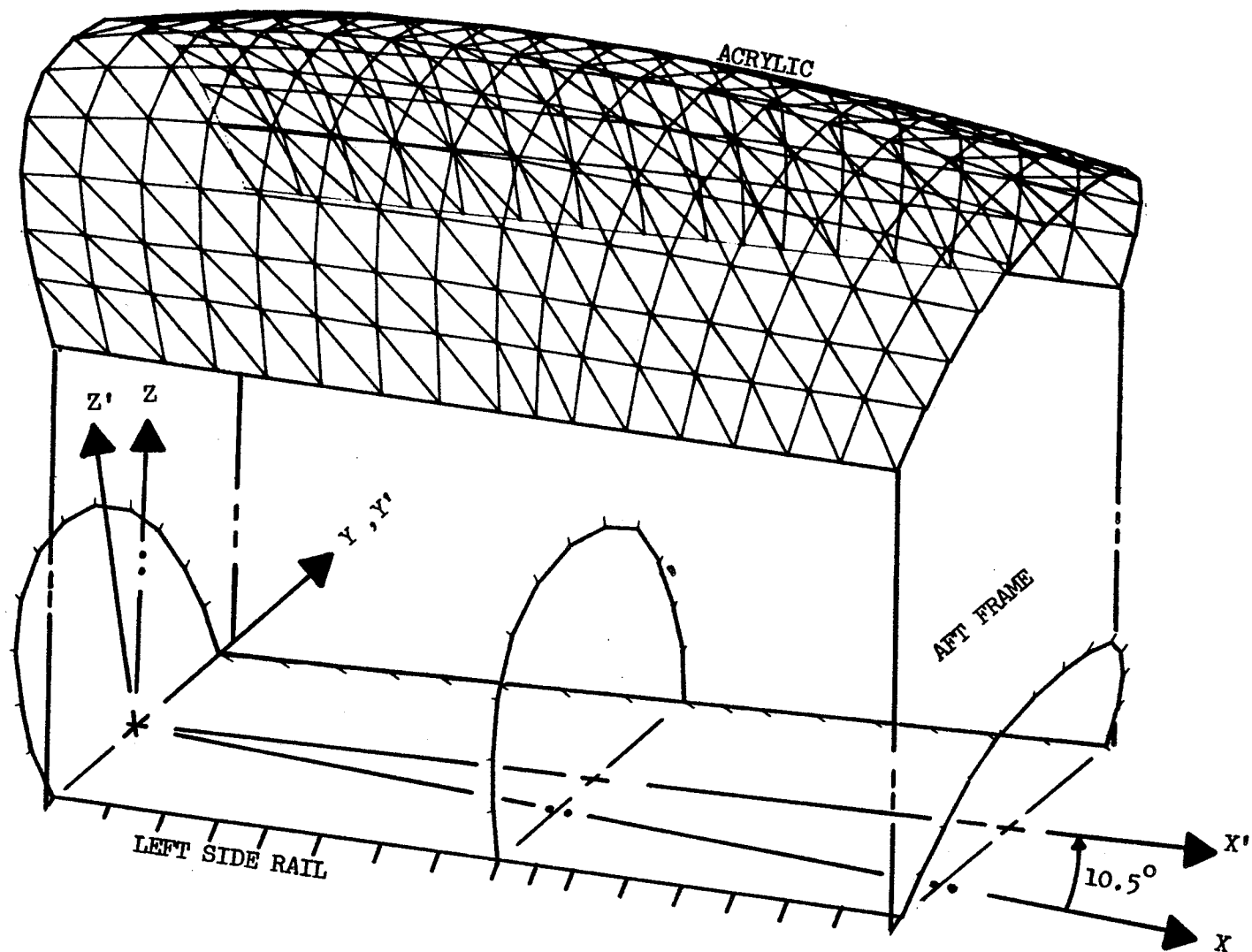
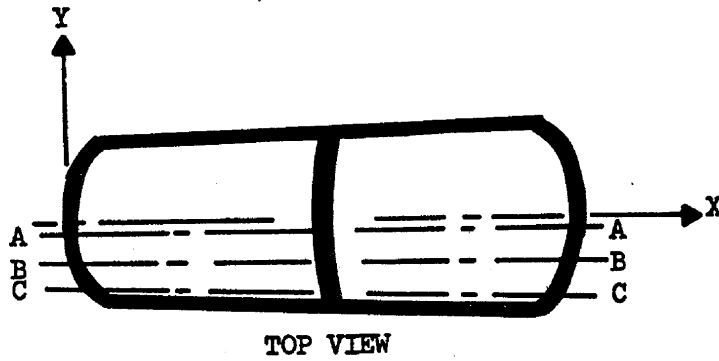
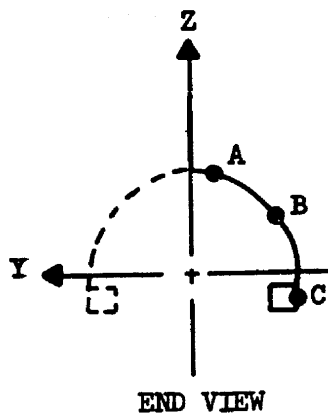
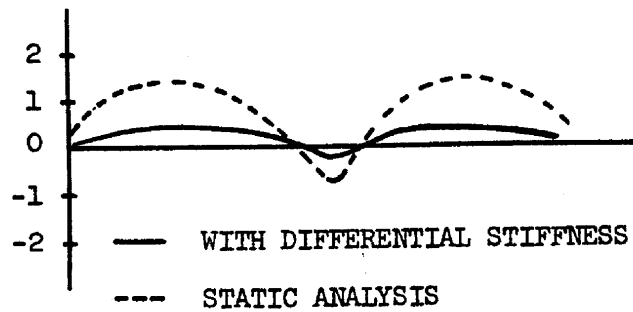


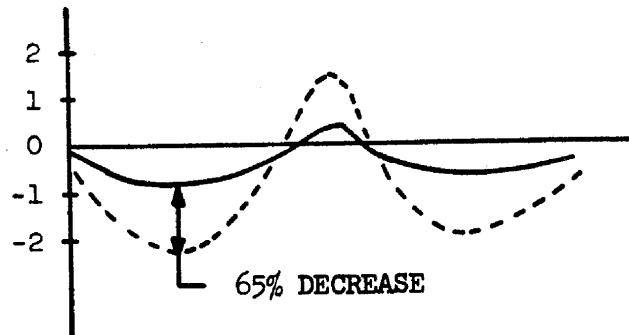
Figure 10.- Exploded 3 Dimensional View of the Canopy Model



STRESS ALONG LINE A
 ($\times 10^{-3}$ psi)
 (+) TENSION



STRESS ALONG LINE B
 ($\times 10^{-3}$ psi)



STRESS ALONG LINE C
 ($\times 10^{-3}$ psi)

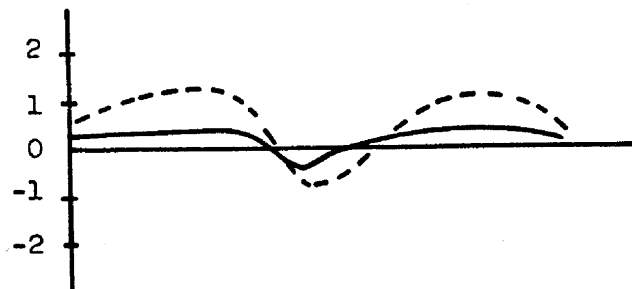
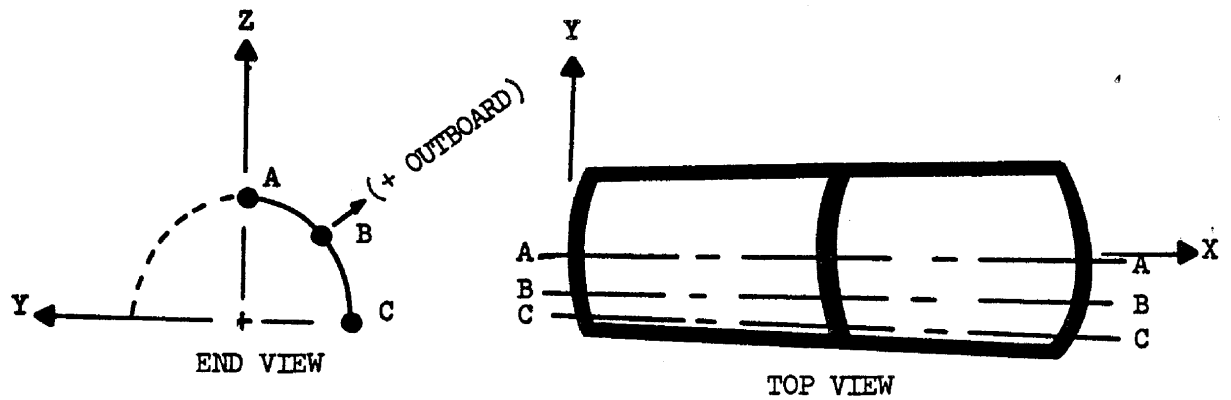
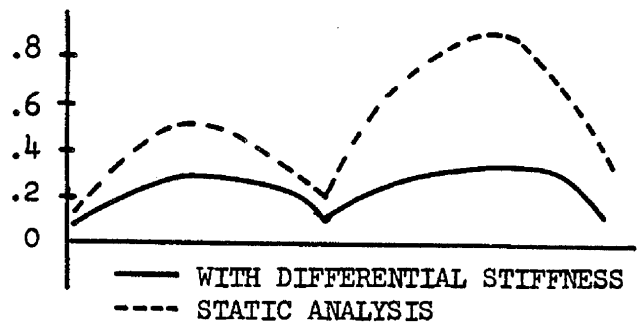


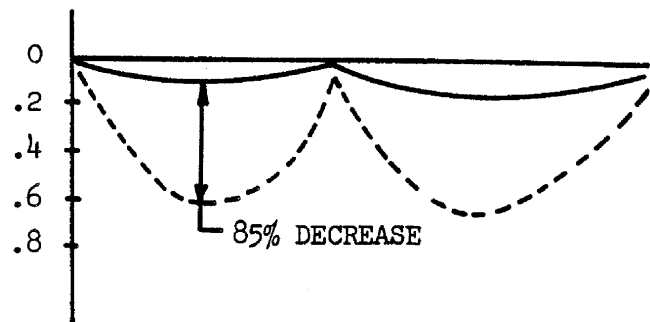
Figure 11. - Acrylic Longitudinal Stresses
 at Centroid



DEFLECTIONS ALONG
LINE A
(inches)
(+) OUTBOARD



DEFLECTIONS ALONG
LINE B
(inches)



DEFLECTIONS ALONG
LINE C
(inches)

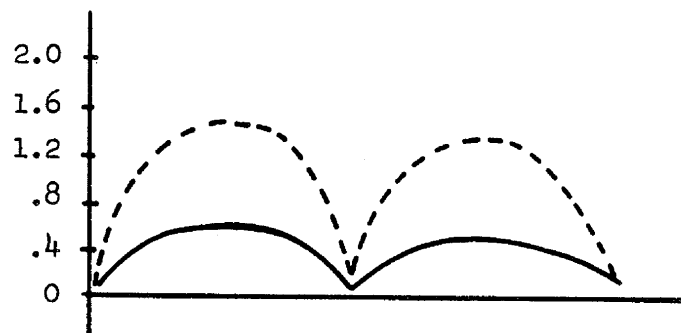
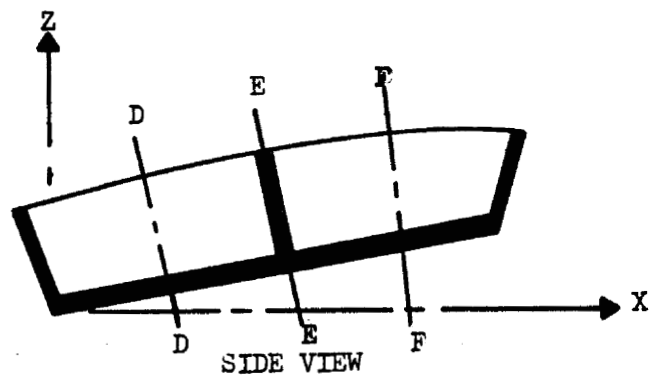
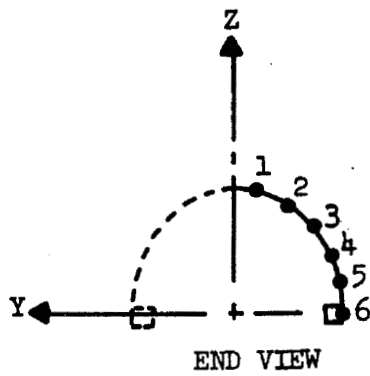
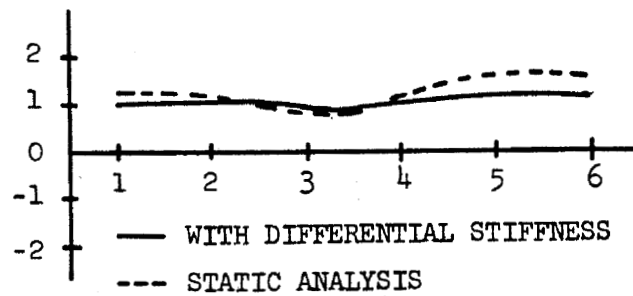


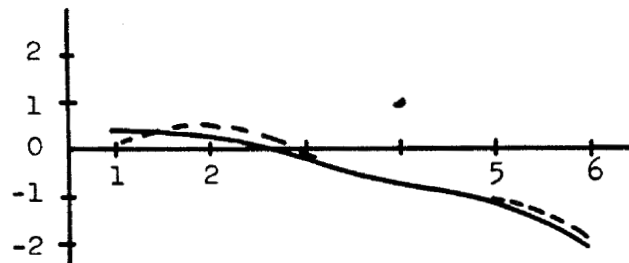
Figure 12. - Acrylic Longitudinal Deflections
for the Differential Stiffness Analysis



STRESS ALONG CUT D
($\times 10^{-3}$ psi)
(+) TENSION



STRESS ALONG CUT E
($\times 10^{-3}$ psi)



STRESS ALONG CUT F
($\times 10^{-3}$ psi)

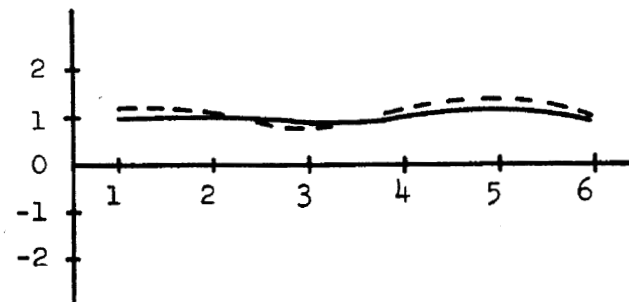


Figure 13. - Acrylic Hoop Stresses

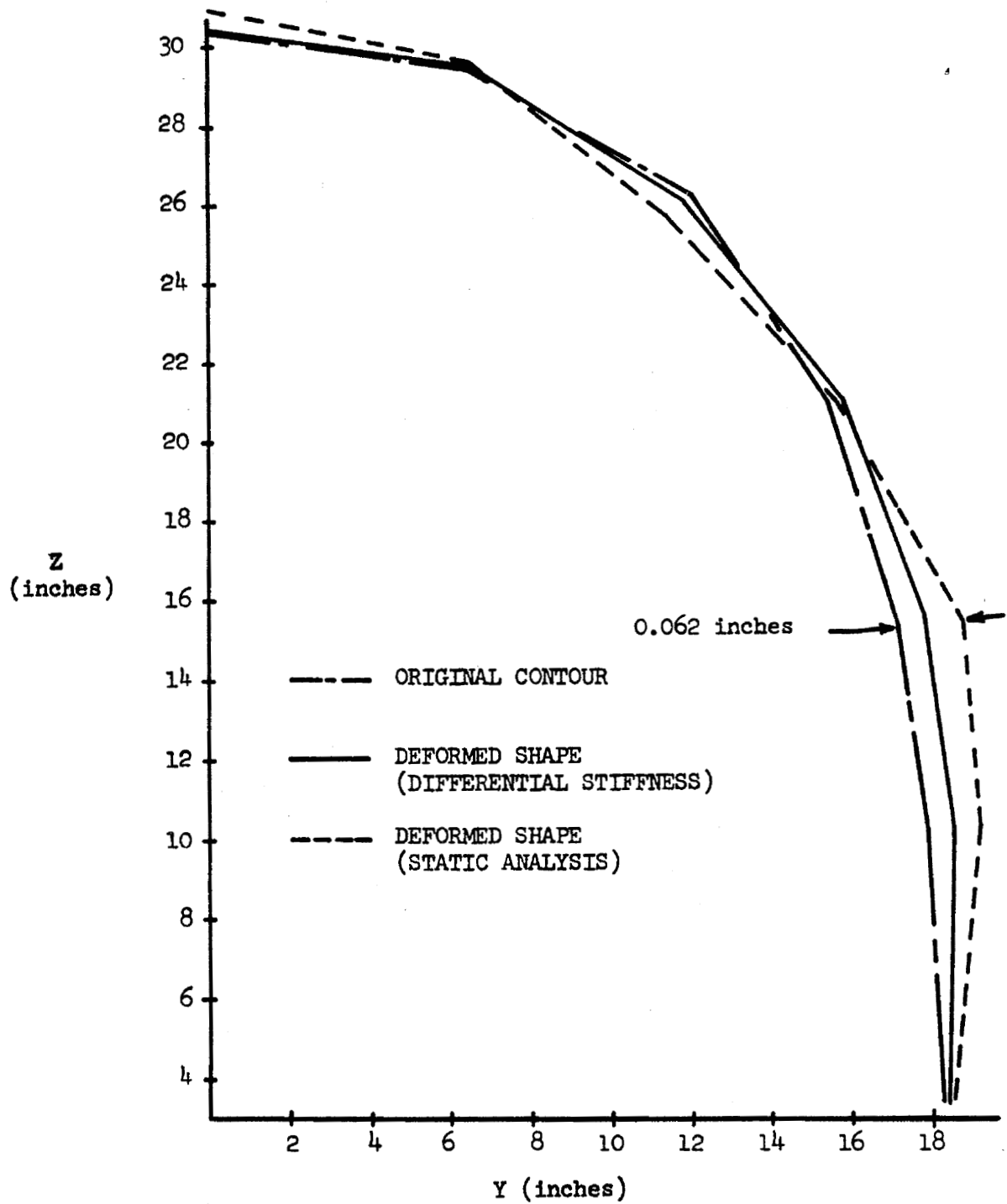


Figure 14. - Deflection of Acrylic Along Cut D

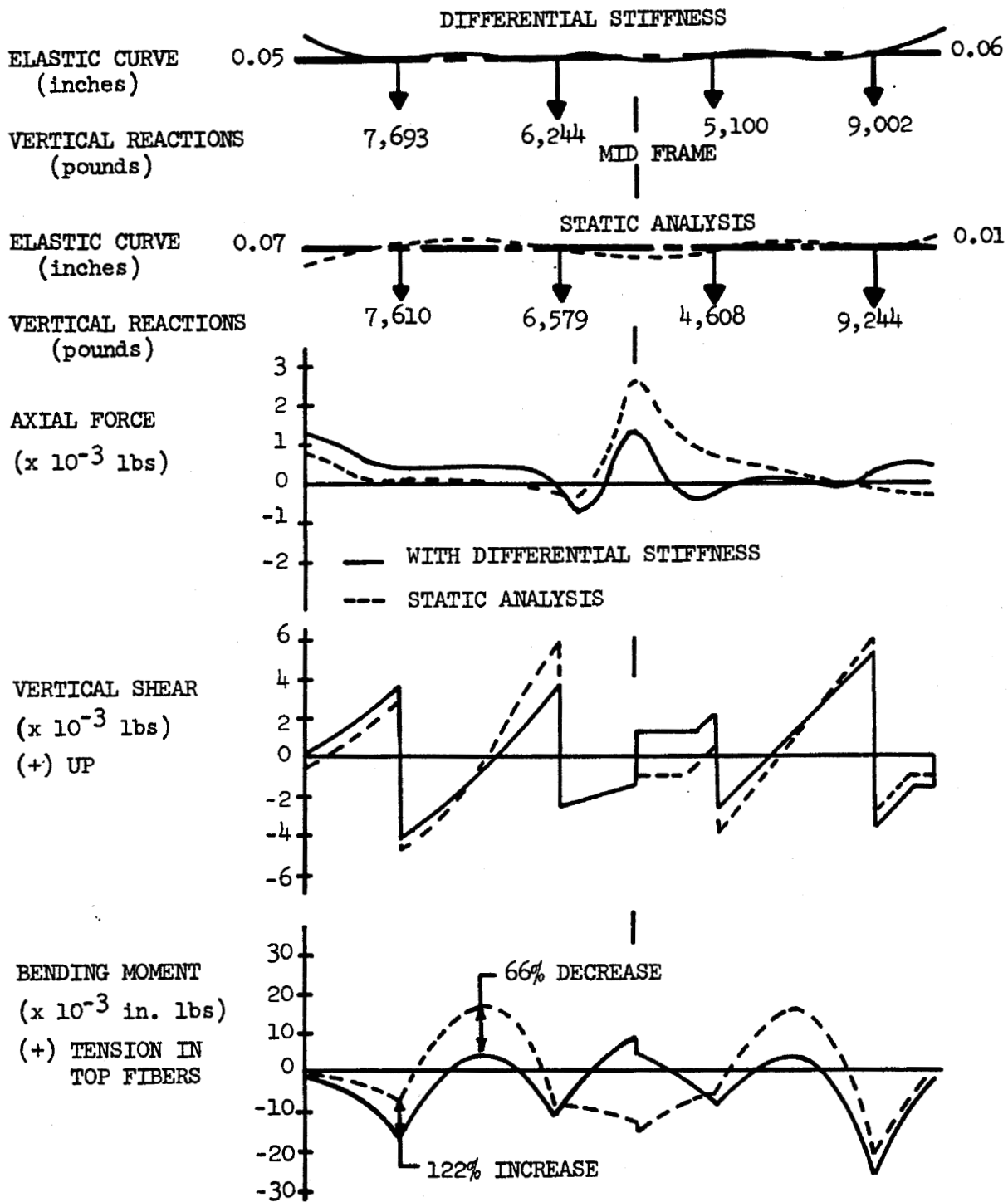


Figure 15. - Side Rail Vertical Loading and Axial Loading

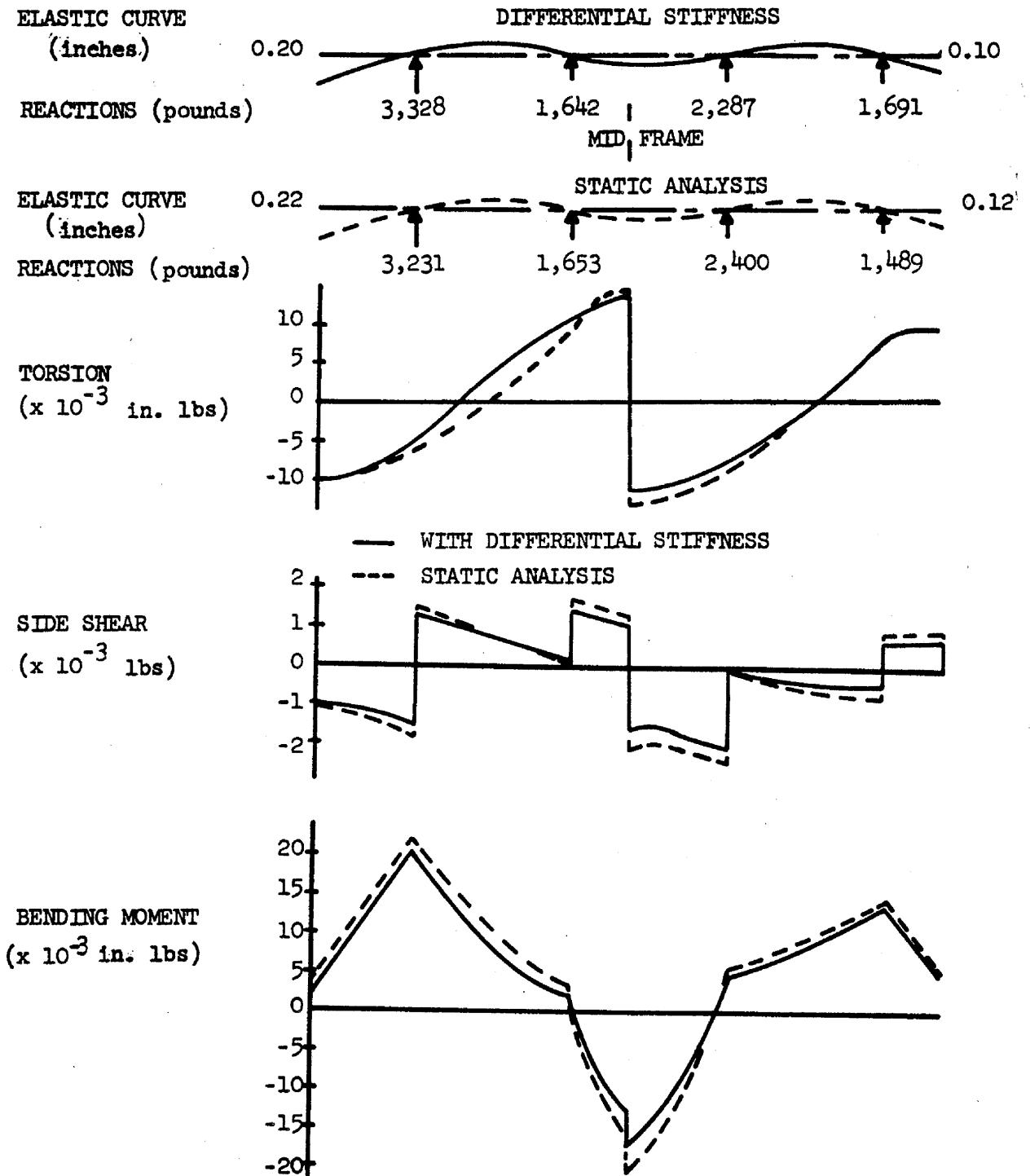


Figure 16. - Side Rail Side and Torsional Loadings

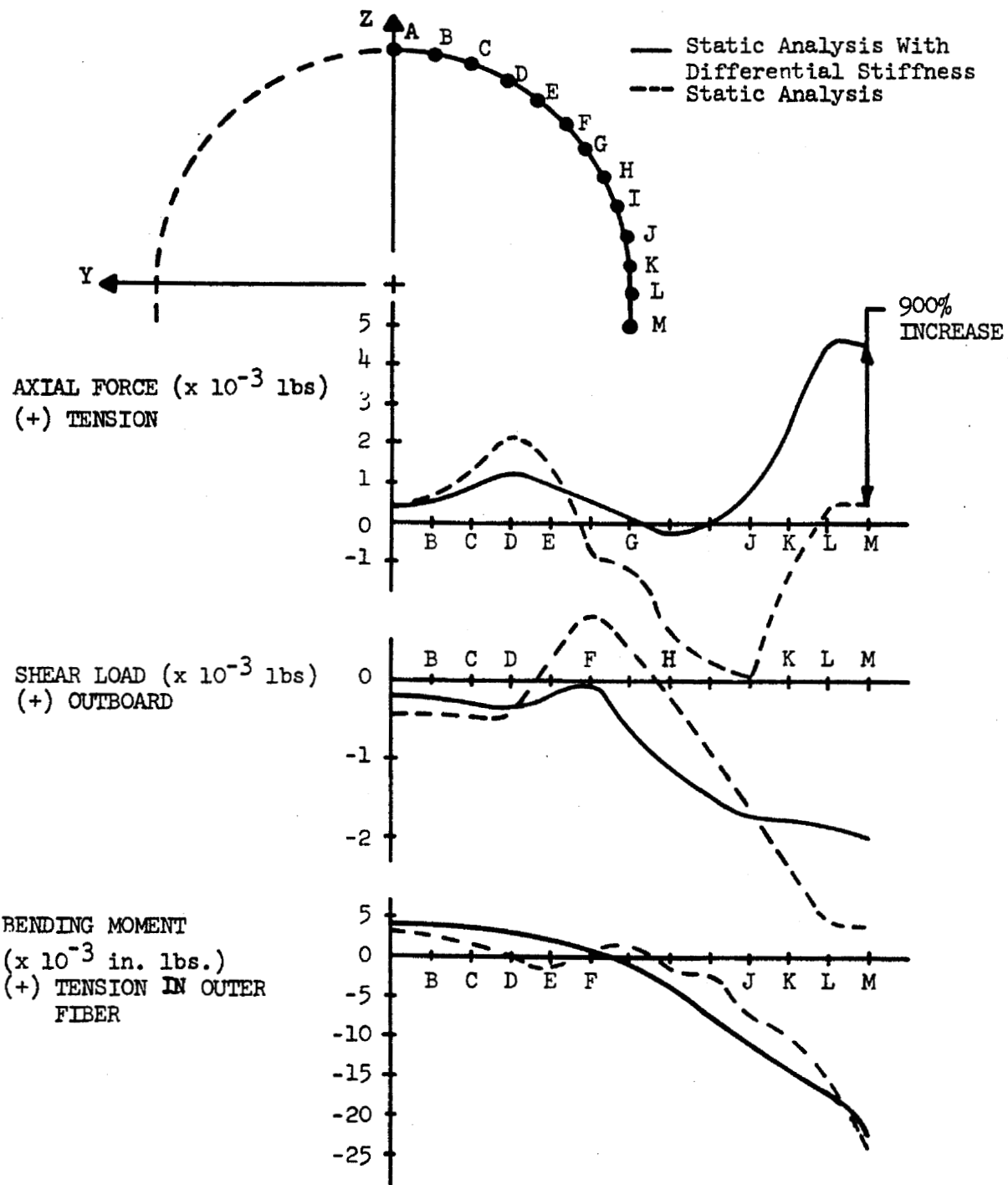


Figure 17. - Mid Frame Member Loads

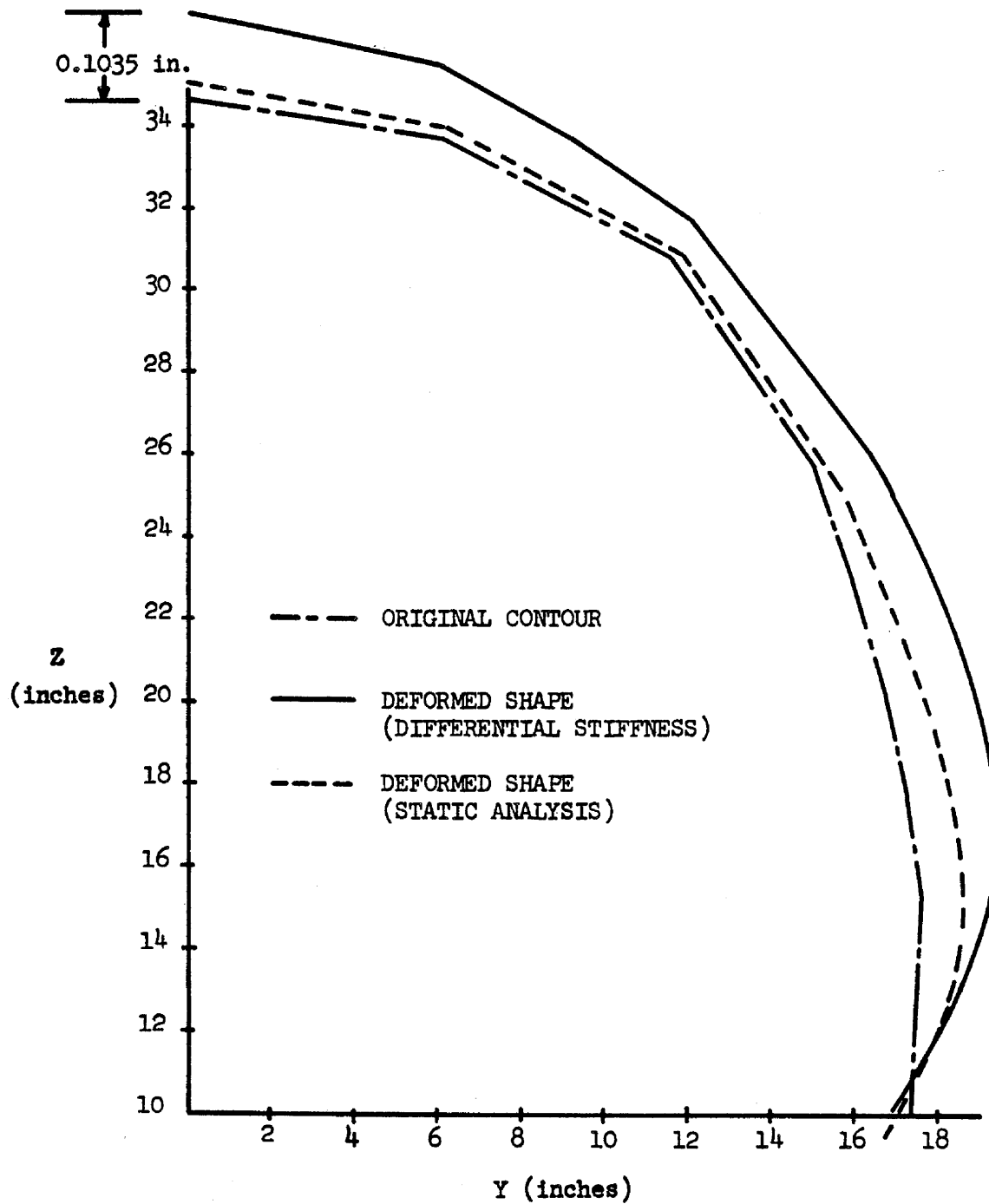


Figure 18. - Mid Frame Deflections

APPLICATION OF SMALL AND LARGE DISPLACEMENT
THEORY TO A LARGE FLEXIBLE SOLAR ARRAY AND
COMPARISON WITH STATIC TEST RESULTS

Ronald P. Schmitz

Sperry Rand Corporation
Space Support Division
Huntsville, Alabama

ABSTRACT

The NASTRAN program was used to perform a structural analysis of the Apollo Telescope Mount (ATM) Solar Array Wing. A high fidelity model containing 8286 DOF was used for the launch (cinched) and orbital (deployed) configurations. Extensive use was made of the multi-point constraint feature of NASTRAN to obtain proper load paths for the launch configuration and of the local coordinate feature to define subassemblies within the global coordinate system. Changes in configuration from deployed to cinched were obtained by rotating and translating the local coordinate systems. Static and Differential Stiffness Solutions (Formats 1 and 4) were obtained. Comparisons were made between these results and static load tests performed at NASA Marshall Space Flight Center.

INTRODUCTION

This paper discusses the application of the large displacement theory (Differential Stiffness Format) of NASTRAN to the structural analysis of the Apollo Telescope Mount (ATM) Solar Array. Two dimensional (2D) and three dimensional (3D) finite element models were developed for analysis. The results are compared with test data, and a discussion of the results is included.

The analyses were performed by the Engineering Analysis Department of the Sperry Rand Space Support Division and sponsored by NASA Marshall Space Flight Center (MSFC), Astrionics Laboratory, under contract NAS8-20055. The tests were performed by MSFC Test Laboratory. The test results were reprinted in References 1 and 2. The results of a small displacement theory analysis (Format 1) using the 3D model were reported in Reference 3.

NOMENCLATURE

δ	Displacement	m
DOF	Degree-of-Freedom	-
E	Modulus of Elasticity	N/m ²
G	Modulus of Rigidity	N/m ²
GP	Grid Point	

Preceding page blank

K	Stiffness	kg/m
M	Bending Moment	N-m
ρ	Density	kg/m ³

Subscripts

c	Core
f	Facing
g	Total DOF Subset
i	Constrained DOF Subset
x	radial
y	lateral
z	out-of-plane

DESCRIPTION OF SOLAR ARRAY

The Solar Array consists of four solar wings deployed in a cruciform configuration, Figure 1, with a total span of approximately 30 meters (without antenna). Each wing consists of five panels to which are mounted the solar cell modules, Figure 2. The module substrate is an aluminum honeycomb structure 1.27 x 51. x 62.5 cm in size. Twenty modules are mounted on each panel, except for the inboard panel, which contains ten modules. The panel area adjacent to the ATM Rack is void of modules for thermal control purposes. The panels, hinged together, are deployed from the launch configuration (cinched), Figure 3, using a scissors deployment scheme. Communication antennas are mounted at the tips of two adjacent wings and are deployed with the wing assemblies. The electric energy converted by the solar cells is used to power the ATM experiments and to recharge the battery system. The total area of the exposed solar cells is approximately 98.5 square meters.

LOAD CRITERIA

A static equivalent out-of-plane load of $\pm 0.2g$ was used to simulate the dynamic response of the deployed wing during the Command Module/SKYLAB docking maneuver.

FINITE ELEMENT MODELS

Two finite element models were developed for analysis of the ATM Solar Array. The first was a 2D model which was used for preliminary investigations of the static and dynamic characteristics of the wing. The second model was a large detailed 3D model of the array. This model was used for detailed stress analysis of the array in both the cinched and deployed configurations.

Two dimensional Model-

The 2D finite element model of the ATM Solar Array (Wing) is shown in Figure 4. It consists of 21 grid points and 20 bar elements. This model represents the bending, axial and shear stiffness of the outboard beam and scissor.

The model has 62 degrees of freedom (DOF) and a very narrow bandwidth, resulting in in-core decomposition and static solutions. The validity of the model is based upon the assumption that, for out-of-plane loads, the wing behaves as a cantilever beam and the panel side rails and the scissor members react the loads. Since the model does not contain in-plane stiffness elements, only out-of-plane loads were examined with this model.

Three dimensional Model-

The three dimensional (3D) finite element model of the deployed Wing (Figure 5) contains 1443 finite elements composed of bar, rod and quadrilateral plates, and 1381 grid points. The complete assembled stiffness matrix, K_{gg} , has 8286 DOF. There are 754 DOF constrained through boundary conditions and constraint equations (SPC's and MPC's), leaving 7532 DOF in the analysis stiffness matrix, K_{ll} .

Figure 6 illustrates the detailed model of a typical panel and scissor substructure. Among the many NASTRAN modeling features used to develop this model were:

- Each panel and scissor gridpoints were defined in separate local coordinate systems (11 total).
- All loads were applied in the basic coordinate system and all displacements were recovered in the local coordinate systems (1, 2, etc.).
- Multipoint constraint equations were used to attach the scissor to the supporting structure (Mounting Structure).
- Hinge connections between each panel, between each scissor and between scissor and panels, were modeled using the pin release feature of the bar elements.

The honeycomb modules were coarsely modeled using four CQUAD2 elements for each module. The following properties were used:

Facing,

$$\begin{aligned} E_f &= 6.8946 \times 10^{10} \text{ N/m}^2 & (10^7 \text{ lb/in}^2) \\ G_f &= 2.62 \times 10^{10} \text{ N/m}^2 & (3.8 \times 10^6 \text{ lb/in}^2) \\ \rho_f &= 10,308. \text{ kg/m}^3 & (0.3724 \text{ lb/in}^3) \quad (80 \text{ light weight modules}) \\ \rho_f &= 13458. \text{ kg/m}^3 & (0.4862 \text{ lb/in}^3) \quad (10 \text{ heavy weight modules}) \end{aligned}$$

Core,

$$\begin{aligned} E_c &= 6.8946 \times 10^{10} \text{ N/m}^2 & (10^7 \text{ lb/in}^2) \\ G_c &= 1.2738 \times 10^8 \text{ N/m}^2 & (18,475 \text{ lb/in}^2) \\ \rho_c &= 0.0 \end{aligned}$$

A complete discussion of this model may be found in Reference 3.

DISCUSSION OF RESULTS

The typical 2D and 3D deformed and undeformed geometry, as plotted by NASTRAN, is shown in Figure 7. The deformed shape for the linear and large displacement theories are compared in Figure 8. Figure 8 contains the results for the 2D, 3D models and static test data. Poor agreement was obtained using the 3D model for both theories, whereas, the 2D model gave acceptable results for both. Several characteristics of the model and actual wing are apparent from the displacement results:

- The fixity which occurs at the 2nd and 4th hinges, during +Z loads, is apparent from the continuity of slope at these hinges; while a large discontinuity occurs at both the 1st and 3rd hinges where no fixity exist.
- The change in tip deflection from linear to large displacement theory, was -11 percent for the 2D model and -6 percent for the 3D model. In the case of the 2D model this change was approximately the same as the accuracy of the test data, +6 percent. It is inconclusive, based upon the displacement results alone, whether large displacement theory is necessary.

- The 3D model is too flexible for out-of-plane loads. The tip deflection was 44 percent greater than test. Studies to determine the source of the increased flexibility are currently being performed.
- Due to the large displacement hysteresis observed during the test, the displacements are not the best criteria for comparing test and theory.

The scissor moment diagrams for the linear and large displacement theories are compared in Figure 9. Figure 9 contains the results for the 2D and 3D models and test data. The panel moment diagrams are shown in the same figure. The moment at the intersection of a panel and scissor is statically determinant and the total moment at any intersection is equal to the sum of the scissor moment and panel moment (Figure 10). From the test data, super-imposed on Figure 9, it is shown that a large fraction (33 percent) of the total moment is carried by the panels. The large displacement theory predicted 17 percent of the moment in the panels, while the linear displacement theory predicted only 0.2 percent.

CONCLUSIONS

As acknowledged by the NASTRAN authors, Reference 4, the Differential Stiffness format does not account for changes in the load distribution resulting from geometry changes. In the problem discussed in this paper the radial displacements of the wing, due to large rigid body movement, were not predicted by the large displacement theory. The movement inboard due to the large out-of-plane motion is not accounted for, and the reduction in the scissor and panel bending moments resulting from the geometry change were not calculated. This inaccuracy along with known errors in the test data accounts for the difference between test and large displacement theory results of the 2D model. The errors in the 3D model are more serious and additional study as to the source is currently being performed.

The most significant result of this study was the prediction of large bending moments in the panel by the large displacement theory, which were not predicted by the linear theory.

REFERENCES

1. Greer, A.T., "Results of ATM Solar Wing (Development Model) Deployment Tests", NASA, MSFC, S&E-ASTN-TF-10-71, March 1, 1971.
2. Vaught, E.W., "ATM Solar Array Docking Loads Test Evaluation," Sperry Space Support Division, Sperry Rand Corp., SP-209-0519, August 1971
3. "Structural Analysis of ATM Solar Array Assembly", Bahos, D.G., ed., Sperry Space Support Division, Sperry Rand Corp., SP-209-0491, May 28, 1971.
4. "The NASTRAN Theoretical Manual," MacNeal, R.H., ed., NASA SP-221, October 1969.

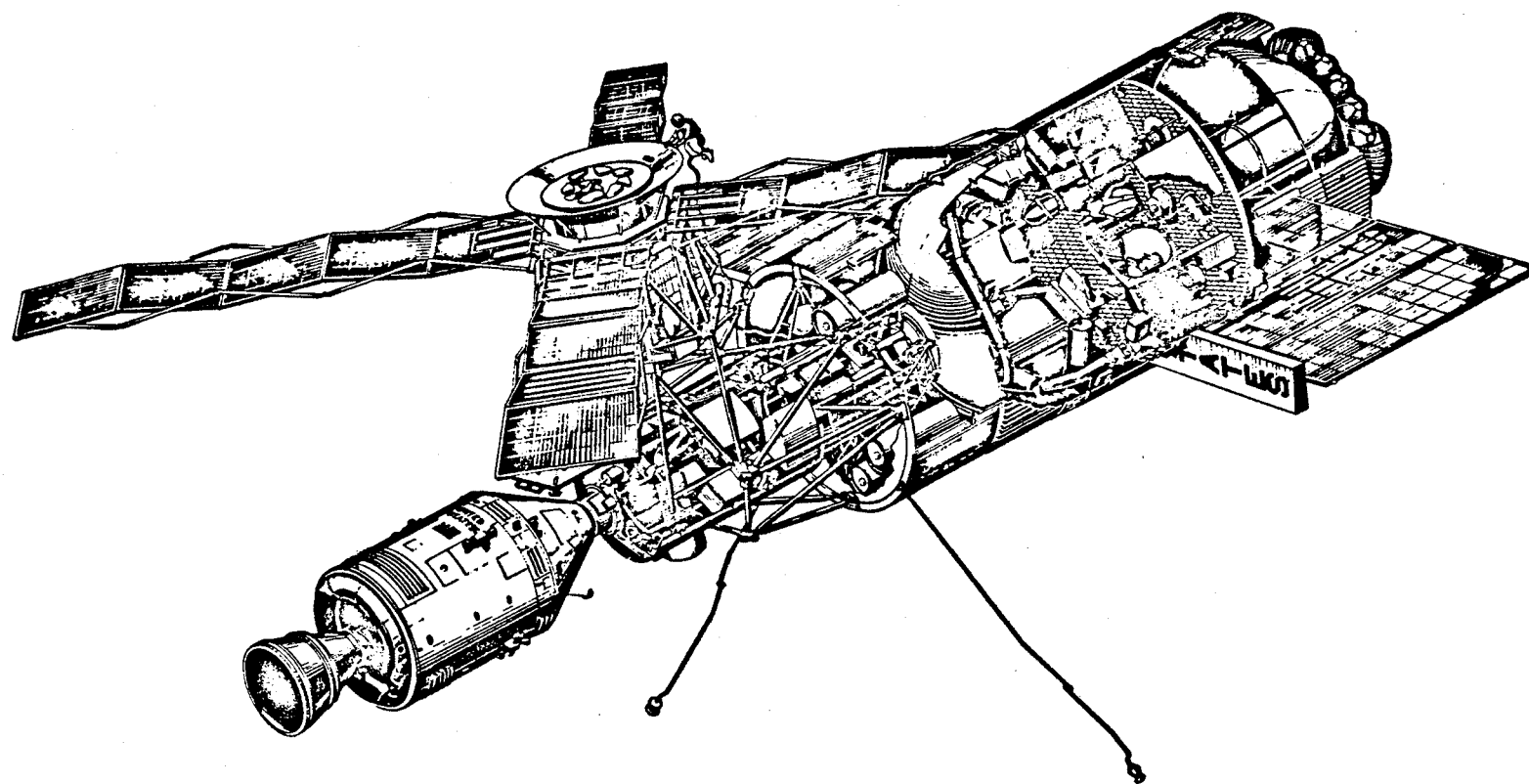


Figure 1. - Skylab configuration.

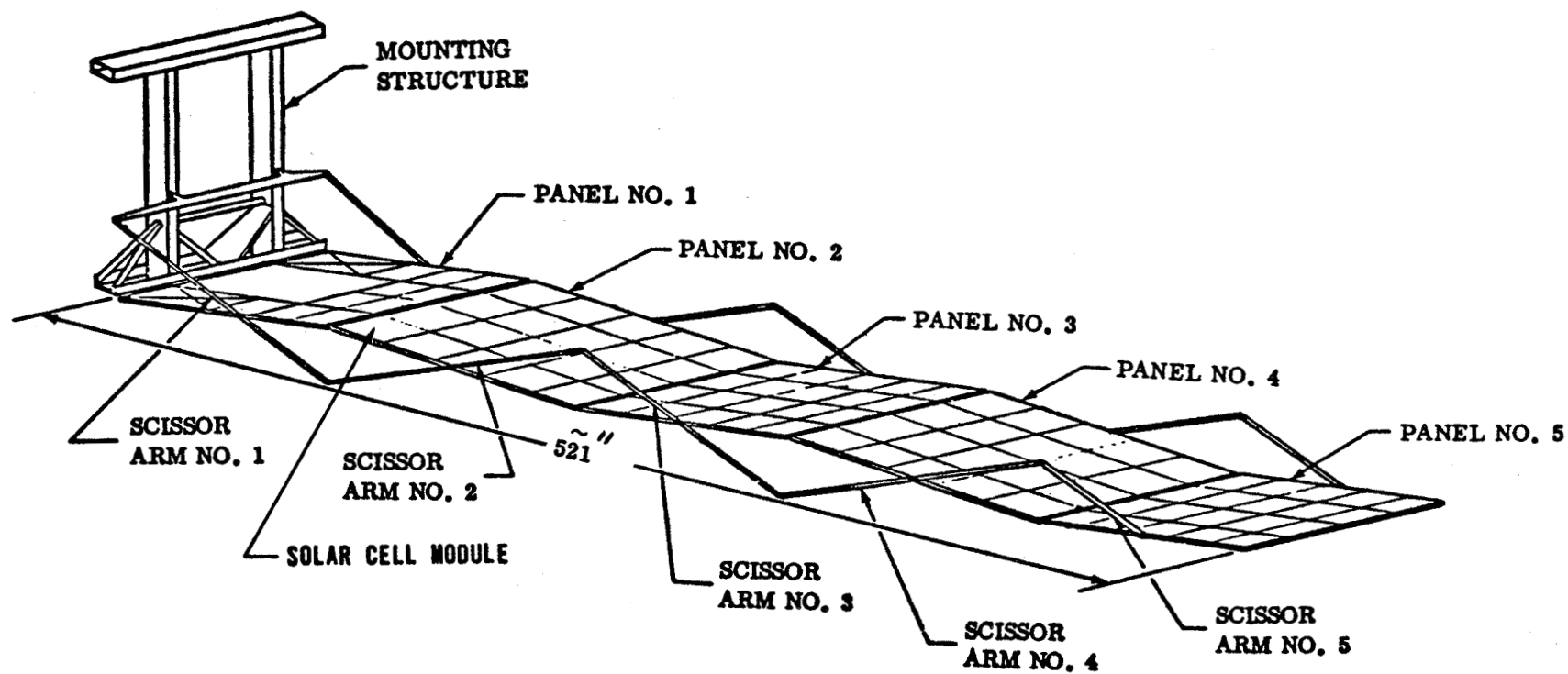


Figure 2. - ATM solar array configuration - deployed position.

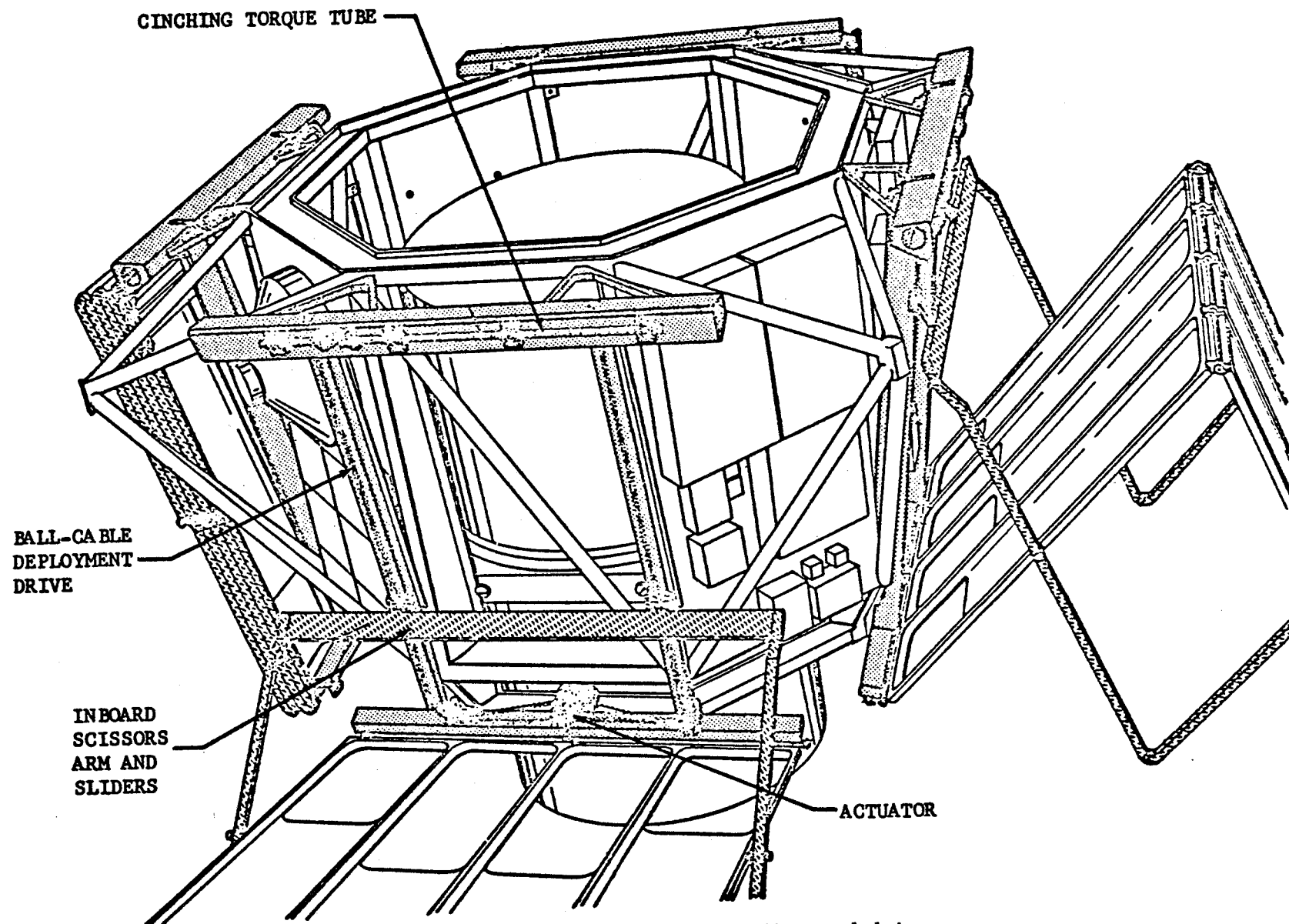


Figure 3. - Deployment actuation and drive.

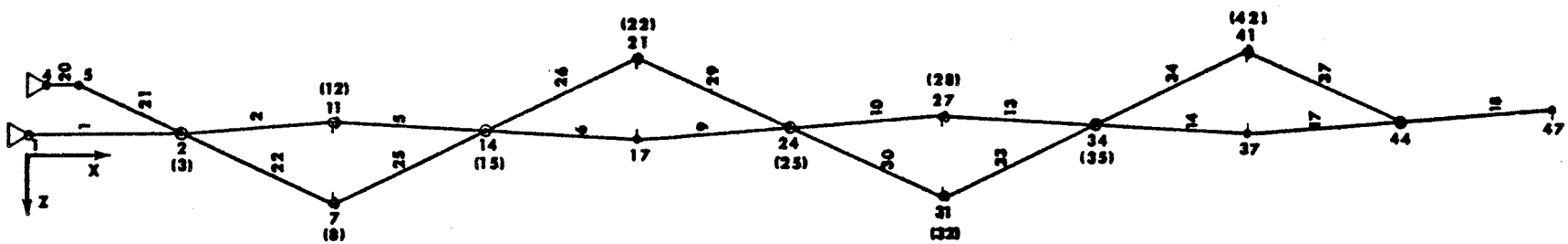


Figure 4. - Two dimensional finite element model of deployed wing.

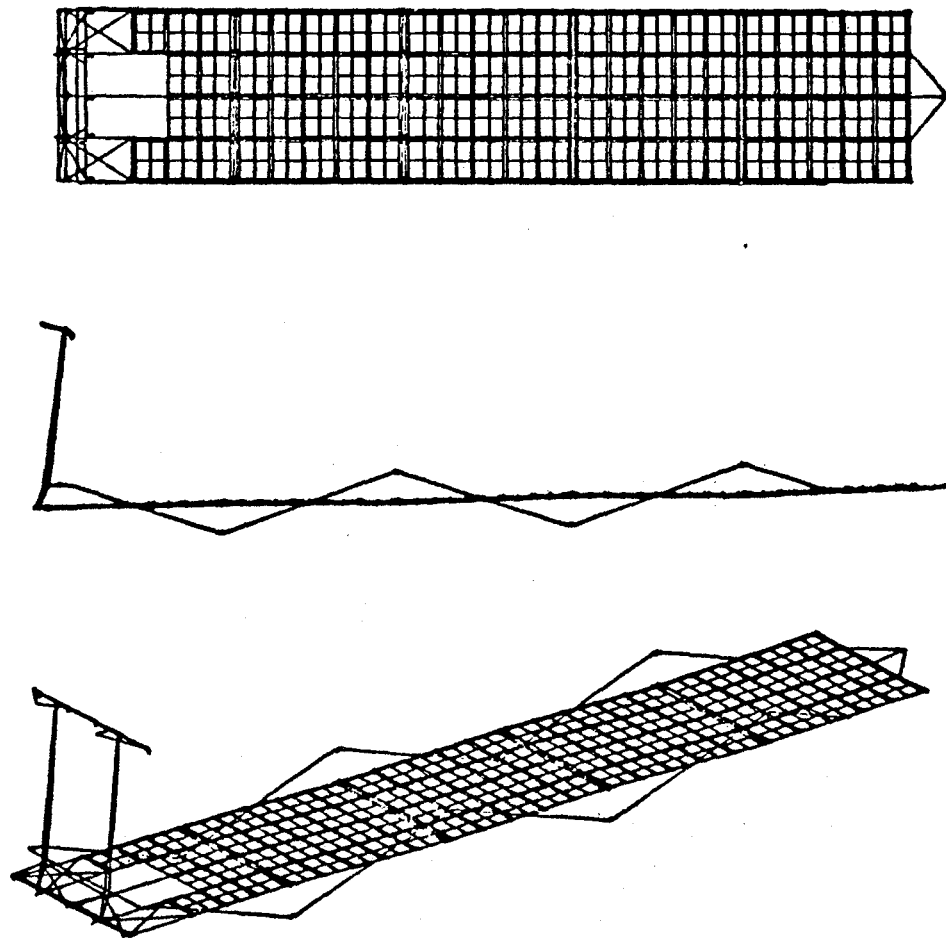


Figure 5. - Finite element model of deployed wing and mounting structure.

NOT REPRODUCIBLE

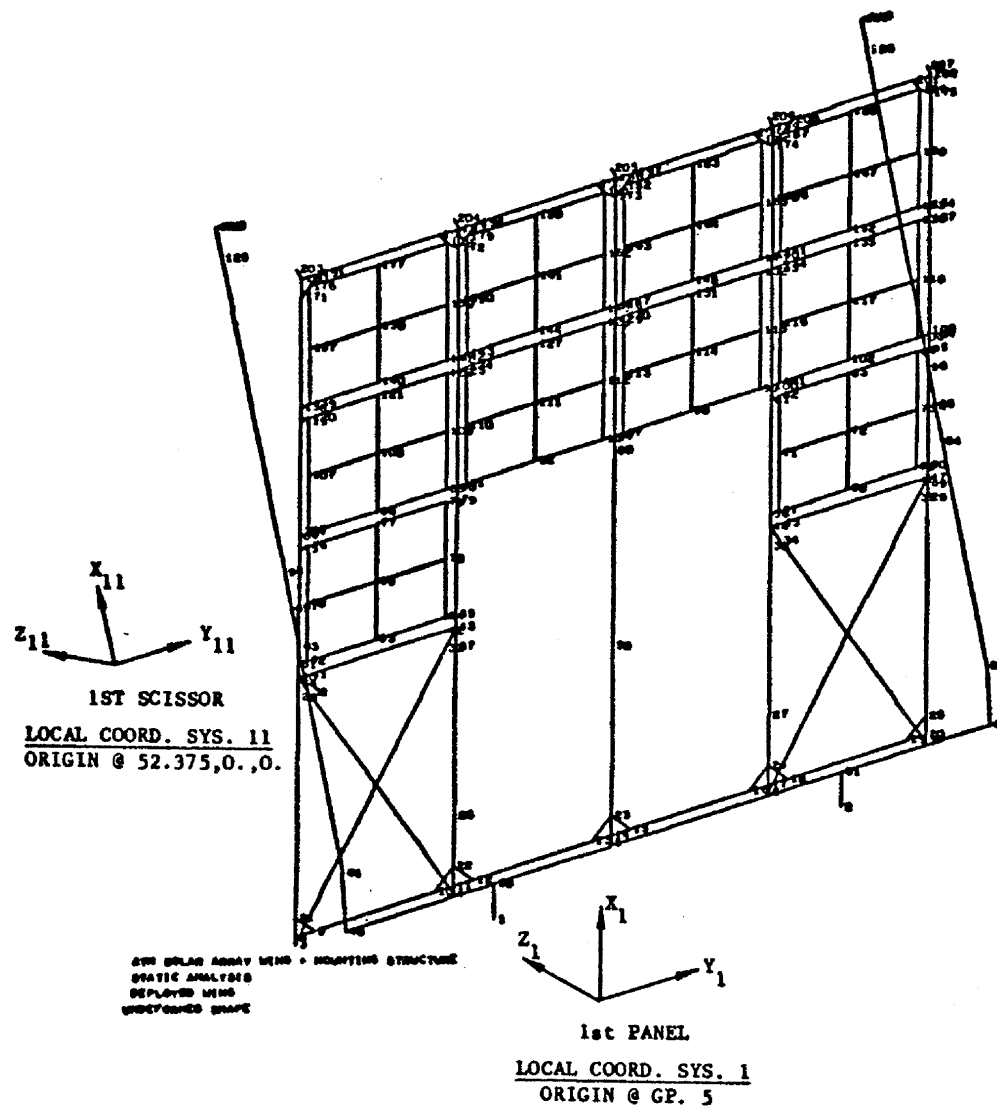


Figure 6. - First panel and scissor arm model with grid point numbers.

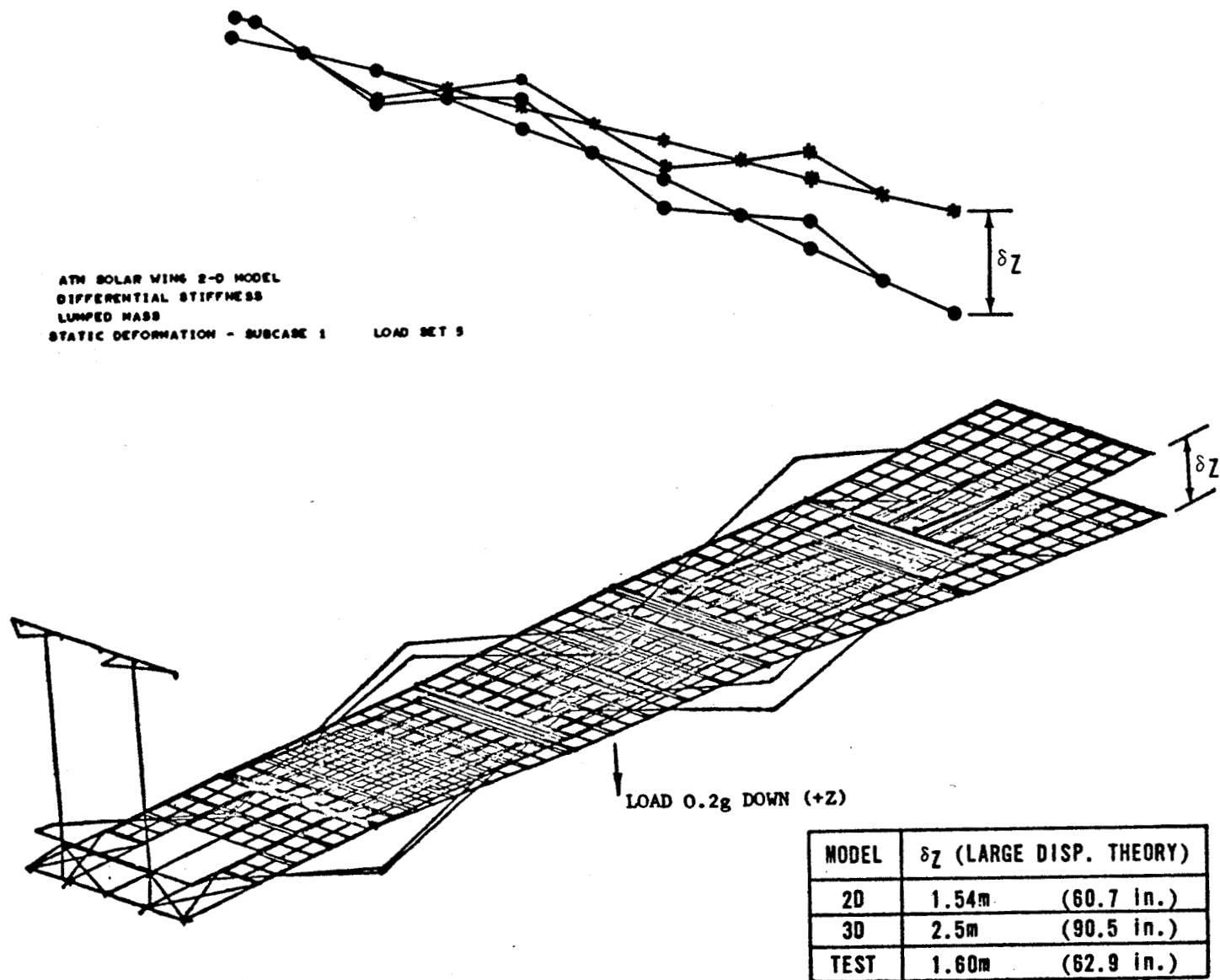


Figure 7. - 3D deployed wing, undeformed and deformed shape for 0.2g docking.

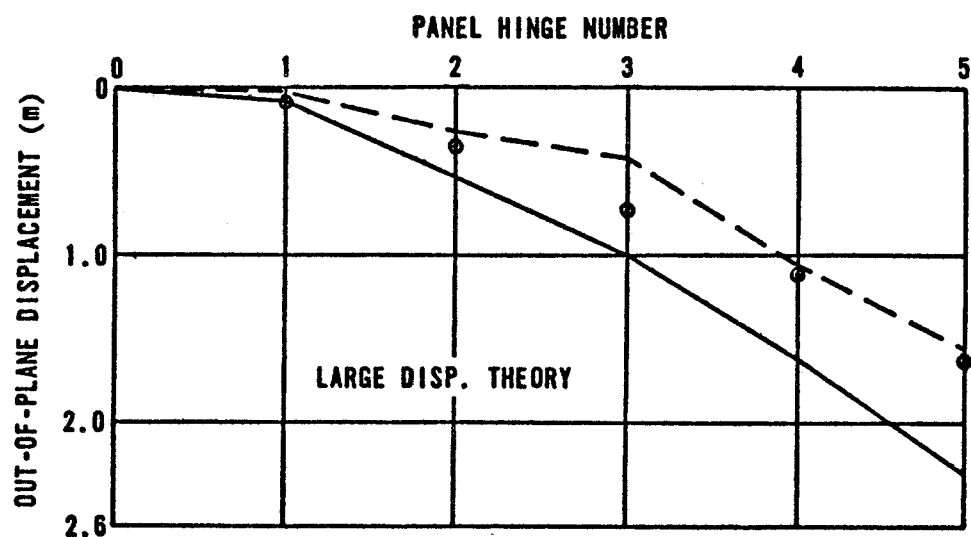
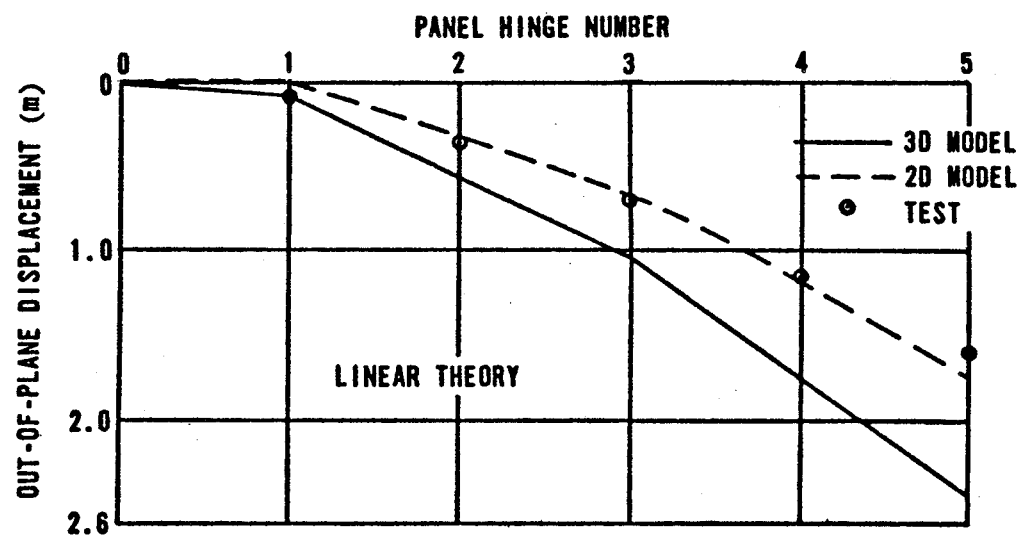


Figure 8. - ATM wing panel displacement for 0.2g docking load.

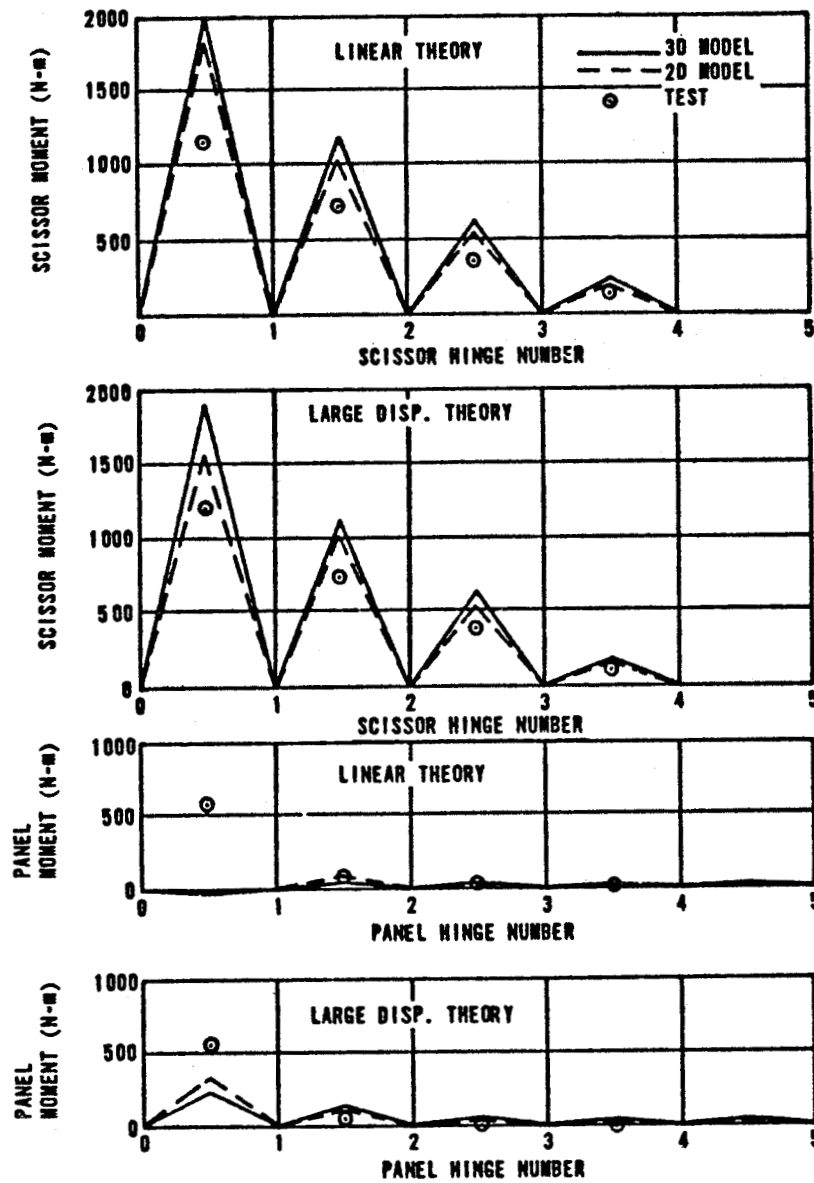


Figure 9. - Scissor and panel moment diagrams for 0.2g docking load.

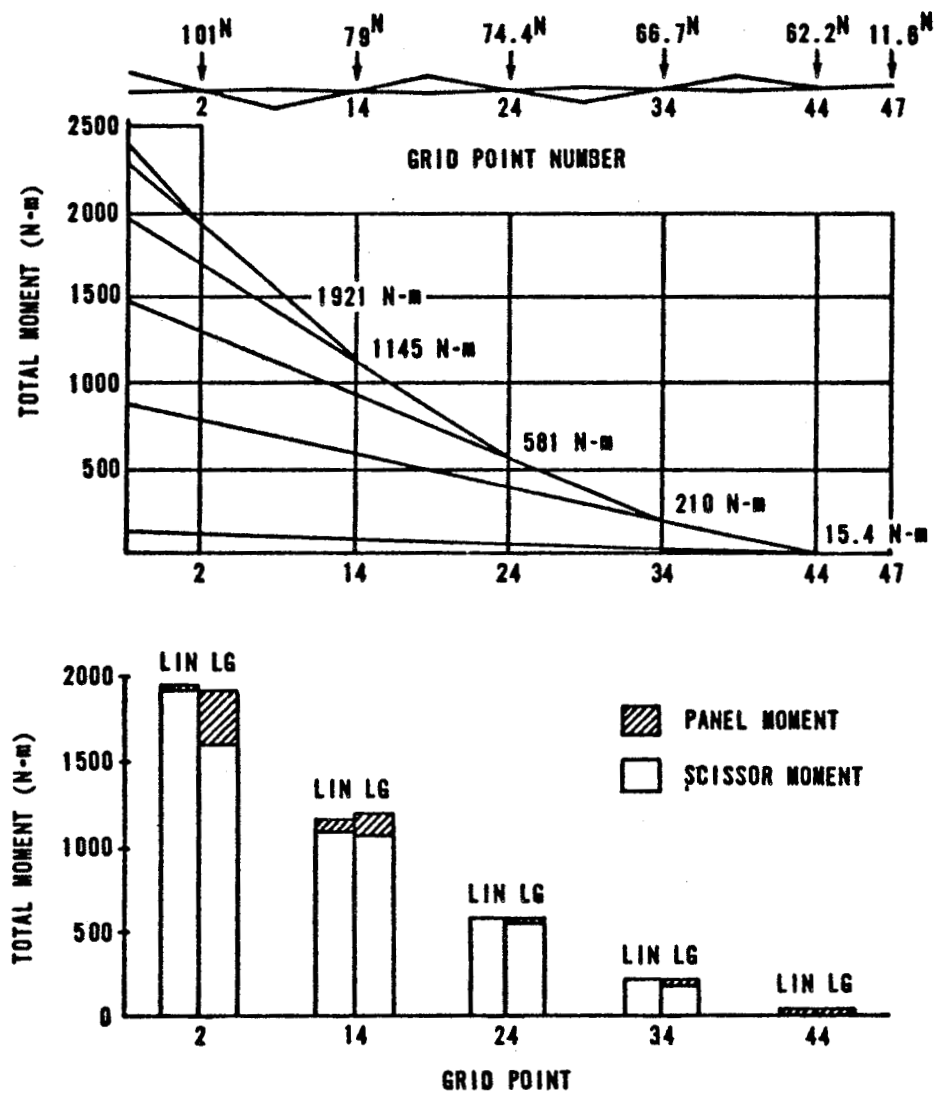


Figure 10. - 2D model applied load and total moment at scissor-panel intersection.

STATIC ANALYSIS OF THE 64-m (210-ft) ANTENNA REFLECTOR STRUCTURE*

By M. Smoot Katow

Jet Propulsion Laboratory

SUMMARY

Progressing from a space frame analysis (STAIR) using only prismatic bars connected at frictionless pin joints and one quadrant of input data, the structural model of the 64-m-diameter reflector structure was upgraded with the use of the NASTRAN program. Bars with bending resistance (CBARS) and plates (CQDMEM, CTRMEM and CSHEAR) were added at appropriate locations. The deflection results computed for the gravity loading case are closely correlated to field measured values and operational RF tests. Expansion of the input data to 1/2 structure permitted studies of minor structural modifications which, if implemented, should result in lower deformations from gravity loads. Procedures used to check for correct input data are noted.

INTRODUCTION

The NASA/JPL (National Aeronautics and Space Administration/Jet Propulsion Laboratory) Deep Space Instrumentation Facility (DSIF) 64-m-diameter antenna system with an azimuth-elevation axes type mount (figs. 1 and 2) commenced operation in April, 1966, at Goldstone, California. In June, 1963, the Rohr Corporation was awarded the contract to accomplish the final design, fabrication and erection.

Determining with precision the distortions of the paraboloidal reflective surface supported by the reflector structure under the environmental loads is a prime requisite in correctly predicting the radio-observing efficiency of the antenna system (ref. 1). The discussion in this paper will be limited to the calculation of distortions from gravity loading only. Specifically, these distortions are caused by the gravity loading that results from an elevation angle change from the 45° surface setting angle to the zenith look angle. At 45° , the surface panels are adjusted or set to fit the design paraboloid.

* This paper presents the results of one phase of research carried out at the Jet Propulsion Laboratory, California Institute of Technology, under Contract No. NAS 7-100, sponsored by the National Aeronautics and Space Administration.

Preceding page blank

The calculation that results in precise distortion numbers requires rigorous mathematical models (matrices) of structures. Their solutions require the use of electronic computers. In reference 2, the results from one system of matrix interpretive routine (STAIR, ref. 3) applied to the 64-m reflector structure are reported. The solutions were based on a one-quadrant structural model truss using bar members with pin-jointed connections. In this report, the structural model is upgraded by using a true 1/2 section comprised of some bars with bending stiffness where appropriate; plates, where used, are mathematically modeled. This analysis used the NASTRAN program (ref. 4). It is shown by comparisons to field data that predictions of gravity loading distortions can be made precisely with the use of NASTRAN.

One requisite to precise answers is accurate input data that describes the structure correctly. Also, the data must satisfy the key punching formats required by NASTRAN. To prevent obvious wasteful computing time, NASTRAN internally provides a large number of data checking algorithms. However, due to the existing computer costing formulas applicable to the 1108 Exec 8, this checking can result in excessive costs that are principally the result of multiplying the largest amount of core used by the CPU time. Suggestions made by others that the dry-run checking of input data may be economical is seconded. Some algorithms developed for dry-run checking of STAIR and SAMIS input data are suggested for possible use in checking NASTRAN input data.

SYMBOLS

RMS	root-mean-square sense of the RF pathlength errors
RF	radio frequency waves
SC4020	Stromberg-Carlson Photo Plotting Machine

64-m REFLECTOR STRUCTURE ANALYSIS HISTORY

It was in the later months of 1961 that the 64-m antenna project developed a need for a large structural analysis program suitable for engineering use.

At JPL, our Spacecraft Design Section had a need for rigorous mathematical models and their solutions to satisfy exotic requirements. The section's main interest was the analysis of the vibrational forces on a spacecraft during the launch operations. This need resulted in the development of the JPL/STIF-EIG program (ref. 5) by the middle of 1961. Later, the SAMIS program (ref. 6) was developed for structures larger than the maximum size of 130 degrees-of-freedom of STIF-EIG.

These JPL developed programs could not satisfy the static analysis requirements of the 64-m reflector structure because a large matrix solution

was necessary with the resultant prohibitively long computing time. The wavefront concept was not developed at this time. An algorithm for effectively decreasing the matrix size before the decomposition was needed to analyze large antenna structures.

In late 1958, Lincoln Laboratory commissioned the Civil Engineering Department of the Massachusetts Institute of Technology to develop the STAIR program (ref. 3). Although limited to analysis using bar members with pin joints, the problem inherent in a large matrix solution was avoided with the use of a solution algorithm that required the division of the structure into smaller units, which resulted in smaller matrices to invert. By provisions for reducing matrix sizes and the addition of matrices with further reduction of the summed matrix, it was possible to solve large structures that included some bar members with large bandwidth.

PIN-JOINTED/ONE-QUADRANT STRUCTURAL MODEL

The distortion results for the 64-m reflector structure under the gravity loading case of interest are reported in reference 2. The analysis program used was STAIR, where the bar members are limited to pin-jointed ends. The quantity of input data converted to the sizes of the dimension statements in the load generating portion of STAIR was close to the limits of the 7094 core capacity. Larger data would have necessitated supplemental computer runs with subsequent data processing definitely not desirable.

The computations proceeded with one quadrant of input data and restraints at the symmetry planes as developed by complying with the conditions noted by Newell (ref. 7). Even with one quadrant of input data modeling all the members, there were 750 GRIDs and 2565 CONRODs (using NASTRAN terminology). When FORCE cards were included, the total card count reached almost 6000 cards at times. For three loading conditions, the 7094 computing time started at 90 minutes initially, which was reduced to 55 minutes after some time studies resulted in more efficient use of the chain subroutine with the 7094 computer.

The principal difficulties in STAIR analysis were (1) the satisfying of the many rules of arranging the many structural units and (2), common with all computing programs, the generation of correct input data. When Lincoln Laboratory added a dry run checking program, this program was expanded at JPL to generate the loading program data. Further expansion resulted in a SC4020 structural plotting capability with viewing angles limited normal to the three planes of the coordinate system.

To predict matrix singularities caused by planar joints (since the member joints are frictionless), STAIR initially included a vector analysis algorithm for spotting planar joints of the internal nodes of each unit only. This checking scheme was expanded to check the complete structure with the effects of constraints included (see Appendix). Also, it was possible to count and output the number of bars connected to each node, and this information proved to be enlightening at times where symmetrical structures were checked.

Although the planar condition at each node can be checked as determined by the connecting bars, the frame can still be unstable, and the whole structure can exist in a "flying" condition by not being tied to "ground." For checking matrix singularities caused by instabilities at the nodes, we are suggesting that it may be possible to check for bending stiffnesses at the nodes for frames using CBARS.

For large structures, we found that it was easier to check the individual "tree" (BAR) in a "forest" (STRUCTURE) by sequencing the bar node numbers, first with respect to the first node against the second node, then sequencing with the first node followed by a sequenced second node for bars with the same first node numbers. In this way, undesirable wrong bars and duplicate bars can be spotted.

Further checks in a dry-run program can be made by computing and printing the gravity generated load vectors and the center of gravity, particularly helpful with symmetrical structures. (NASTRAN provides this with parameter GRDPNT and OLOAD cards.) Furthermore, the true bandwidth of the nodes can be easily computed by sequencing, renumbering, and differencing algorithms.

With the availability of the SEQGP cards in NASTRAN, the bandwidth as well as conversion to active column node numbers may be changed to suit. R. Levy of JPL has converted bandwidth re-numbering routines to produce SEQGP cards directly by computer analysis.

As input data were being prepared for the one-quadrant data for the first time, some apprehension as to the answers arose so it was decided to analyze the 1/4 reflector structure alone, for accuracy checking, without the elevation wheel assembly. To do this, the structure was revised to be symmetric about the 45-degree line or plane and the structure was computed for a Z direction gravity loading with only one Z support at C as shown on figure 3. Symmetric constraints were used at the YZ and XZ planes. As you can see, the symmetry of the deflection results, which also include the NASTRAN solution, shows that the deflection answers are precise enough for engineering use. It should be noted that several trials were needed to obtain this symmetry as this type of structure with the constraints and the single support is very sensitive to a slight lack of symmetry.

NASTRAN 1/2-REFLECTOR ANALYSIS

Our interest in upgrading the structural model from 1/4 to 1/2 reflector had continued because of (1) the discrepancies in performance as predicted and as resolved by RF operating tests using radio stars in February 1968 (fig. 4 and ref. 8) and (2) the desire to improve the gravity loading distortion by rearrangement of some truss members that could only be checked with a 1/2-structural model. The 1/2-model input data using pin-jointed members were generated and some test runs were made during the development of NASTRAN when the NASA contractors were using the computers located at JPL.

The plan view of the structure is shown on figure 5 with the elevation cross-sectional view on figure 6. Since the short rib trusses between the main rib trusses at the outer edges served as frames for supporting the surface panels, they were removed and replaced with equivalent weights or FORCE cards. To distinguish the nodes that serve to connect the reflector structure to the elevation wheel assembly, these nodes were shown as enlarged "dots" on figures 5 and 6. These nodes plus the elevation wheel nodes were then numbered with large GRID numbers. Hence, the stiffness matrix values for these large numbers place them in the active column spaces.

As shown in Table 1, the model was upgraded starting with analysis using just pin-jointed bar members (CONROD) to finally a structural model with bars with bending resistance (CBAR) and plates (CSHEAR, CTRMEM, CQDMEM).

The pin-jointed input data totaled a little less than 8000 cards or 4 boxes; these were transferred to the User's Master Tape by the NASA contractor for their use and then transferred to us. With their use an unknown number of times plus our use of at least 20 times in a span totaling 3 years, the one User's Master Tape has remained usable. On the other hand, some NASTRAN executable tapes have become unreadable in 6 months.

By using the REPCASE card, the displacement of the top nodes of the reflector structure were requested for punched card output. These data then became input to the best fitting RMS program (ref. 9) that computes the RMS of the pathlength errors and outputs contour level plots using the SC4020 plotter controlled by tapes generated by the RMS plotting subroutines in the 1108.

Using the method described in reference 2 to compute the RMS surface distortion at various elevation angles with the surface panel set to nominal paraboloid at 45 degrees elevation, the computed values for the one-quadrant STAIR and the 1/2-reflector NASTRAN analyses are shown on figure 6 for every 15 degrees. Overlaid are the RMS results as determined from radio measurements (ref. 8) showing the mean and standard deviation limits that include only the measurement scatter. The 64-m antenna configuration used the mono-cone RF set-up for these test values.

As figure 4 shows, predictions of the RMS surface distortion based on matrix analysis using NASTRAN with the upgraded structural model are closely correlated to the measured values using the field theodolite and to the values based on radio-observed measurements.

When the 64-m antenna was reconfigured with the Tri-Cone RF feed system in January 1970, as shown in figure 1, the field measurements were re-made for the first time since the antenna was placed into operation. An improved technique was used for the theodolite measurements. Figure 7 shows the comparisons between the computed, using the improved model, and the field measured values. The sharp imaging of the contour levels outlines are apparent.

64-m STRUCTURE UP-GRADE

With the availability of the 1/2-reflector model, it was possible to study a rearrangement of the connections between the reflector structure and the elevation wheel assembly. The existing knee bars shown dotted in figure 8 were removed and replaced with new reaction bars that, at first glance, appear to destroy symmetry. However, the new reaction bars are loaded only by the anti-symmetric force component as in the horizon look-gravity loading case. In the symmetric loading case, these bars provide only balancing forces.

The improvements for full loading of the antisymmetric gravity component resulted in a reduction distortion by a factor of 3.5; the symmetric loading distortion also decreases slightly (ref. 10).

CONCLUSIONS

It can be concluded that truss-type reflector structures can be precisely analyzed for distortions resulting from gravity force, and for wind forces and temperature loading if the forces and temperatures can be accurately described; this analysis can be performed by the NASTRAN structural computing program within reasonable cost and time.

A separate dry-run program for checking input data should be useful for 1108 Exec 8 operation in reducing computer costs since the cost computing algorithm, at present, penalizes programs that occupy large amounts of working core space.

REFERENCES

1. Ruze, J.: Antenna Tolerance Theory — A Review, Proceedings of the IEEE, Vol. 54, No. 4, pp. 633-640, April 1966.
2. Katow, M. S.: Techniques Used to Evaluate the Performance of the NASA/JPL 210-Foot Reflector Structure Under Environmental Loads; in Structures Technology for Large Radio and Radar Telescope Systems. Edited by J. W. Mar and H. Liebowitz. The M.I.T. Press, Cambridge, Massachusetts and London, 1969.
3. STAIR (Structural Analysis Interpretive Routine) Instruction Manual, Lincoln Manual No. 48. Lincoln Laboratory, Massachusetts Institute of Technology, March 1962.
4. NASA General Purpose Structural Analysis Program (NASTRAN), Computer Software Management and Information Center (COSMIC), Computer Center, University of Georgia, Athens, Ga.

5. Wada, B.: Stiffness Matrix Structural Analysis, (STIF-ELG), Technical Report No. 32-774. Jet Propulsion Laboratory, Pasadena, Calif., Oct. 31, 1965.
6. Melosh, R. J., Diether, P. A., Brennan, M.: Structural Analysis and Matrix Interpretive System (SAMIS) Program Report. Technical Memorandum No. 33-307, Jet Propulsion Laboratory, Pasadena, Calif., Dec. 15, 1966.
7. Newell, J. S.: The Use of Symmetric and Anti-Symmetric Loadings, J. Aeronaut. Sci., 1939.
8. Bathker, D. A.: Radio Frequency Performance of a 210-Foot Ground Antenna: X-Band. Technical Report 32-1417, Jet Propulsion Laboratory, Pasadena, Calif., Dec. 15, 1969.
9. Katow, M. S., and Schmele, L. W.: Antenna Structures: Evaluation Techniques of Reflector Distortions in Supporting Research and Advanced Development, Space Programs Summary 37-40, Vol. IV, pp. 176-184. Jet Propulsion Laboratory, Pasadena, Calif., Aug. 31, 1966.
10. Katow, M. S., 210-Ft-Diam Antenna Reflector Upgrade Study - Phase I, in Supporting Research and Advanced Development, Space Programs Summary 37-62, Vol. II, pp. 109-113, Jet Propulsion Laboratory, Pasadena, Calif.

APPENDIX

PLANAR JOINT CHECKING ALGORITHM (STAIR)

When the normalized direction vector for a bar is computed, the cross-product with the vector of a second bar at the same joint if equal to zero or close to it will signify a co-linear bar. A flag can be set at a node where two bars intersect. The dot product of the vector of the next bar, at this node, with the existing cross-product if not equal to zero or close to it will signify a node with three bars not in a plane. Some margin above zero for the products will be required for practical parallel tests. Because direction vectors of constraints are known, they should also be included in the checks.

Table 1. - NASTRAN 1/2-reflector analysis data*

Input card	Pin-jointed, number	CBARS and plates added, number
GRID**	951	783
GRID Δ	----	163
CONROD	3596	2516
CBAR	----	271
CQDMEM	----	172
CSHEAR	----	52
CTRMEM	----	20
<u>Other data</u>		
CPU-time/secs	1200	2220
DCOMP ^t -time/secs	531	1069
Degrees/Freedom	2853	3327
Bandwidth-B	120	97
Active column-C	38	90
Active column-R	119	96
CPU-time/secs	1320	2195
<p>* Number of loading conditions = 2 with GRAV and FORCE cards computer = 1108 Exec 8</p> <p>** = nodes with 3 degrees of freedom</p> <p>Δ = nodes with 6 degrees of freedom</p> <p>t = decomposition time</p>		

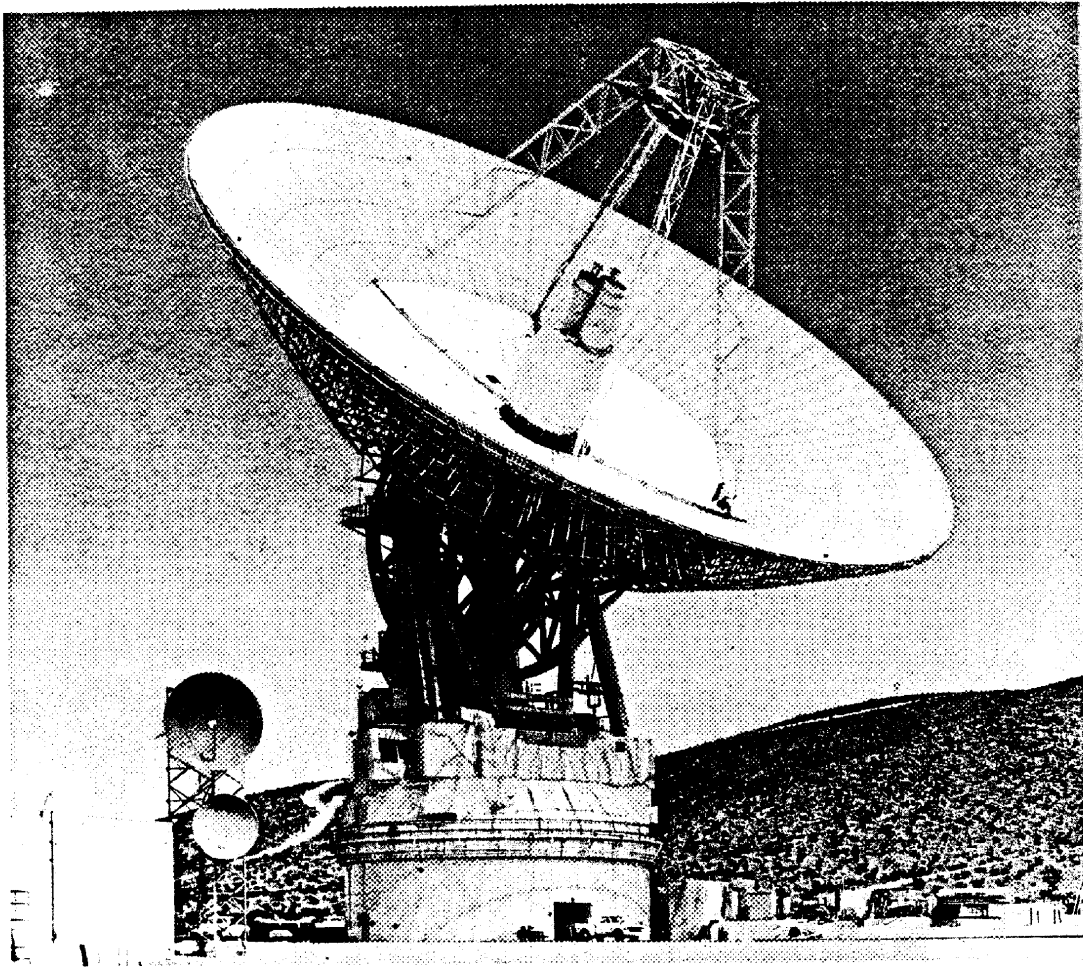


Figure 1. - Full view of 64-m antenna

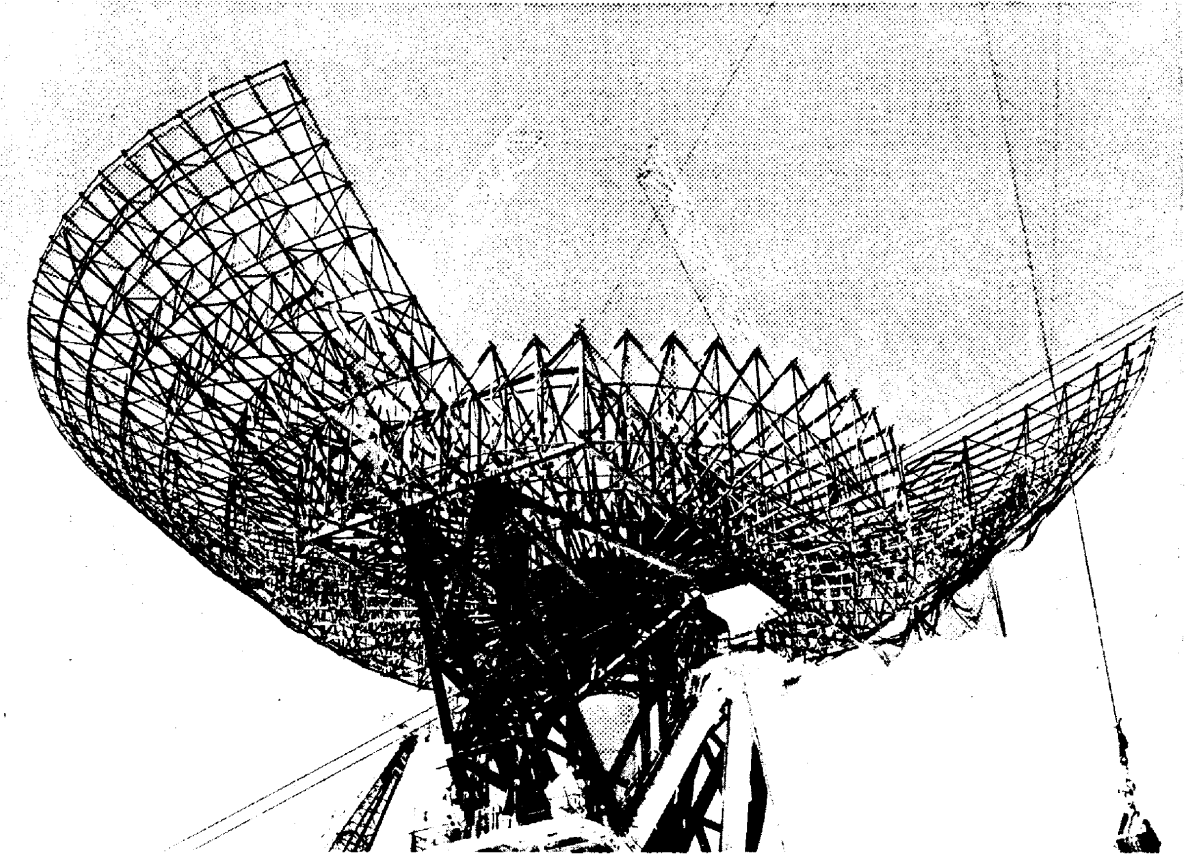


Figure 2. - Underview under construction

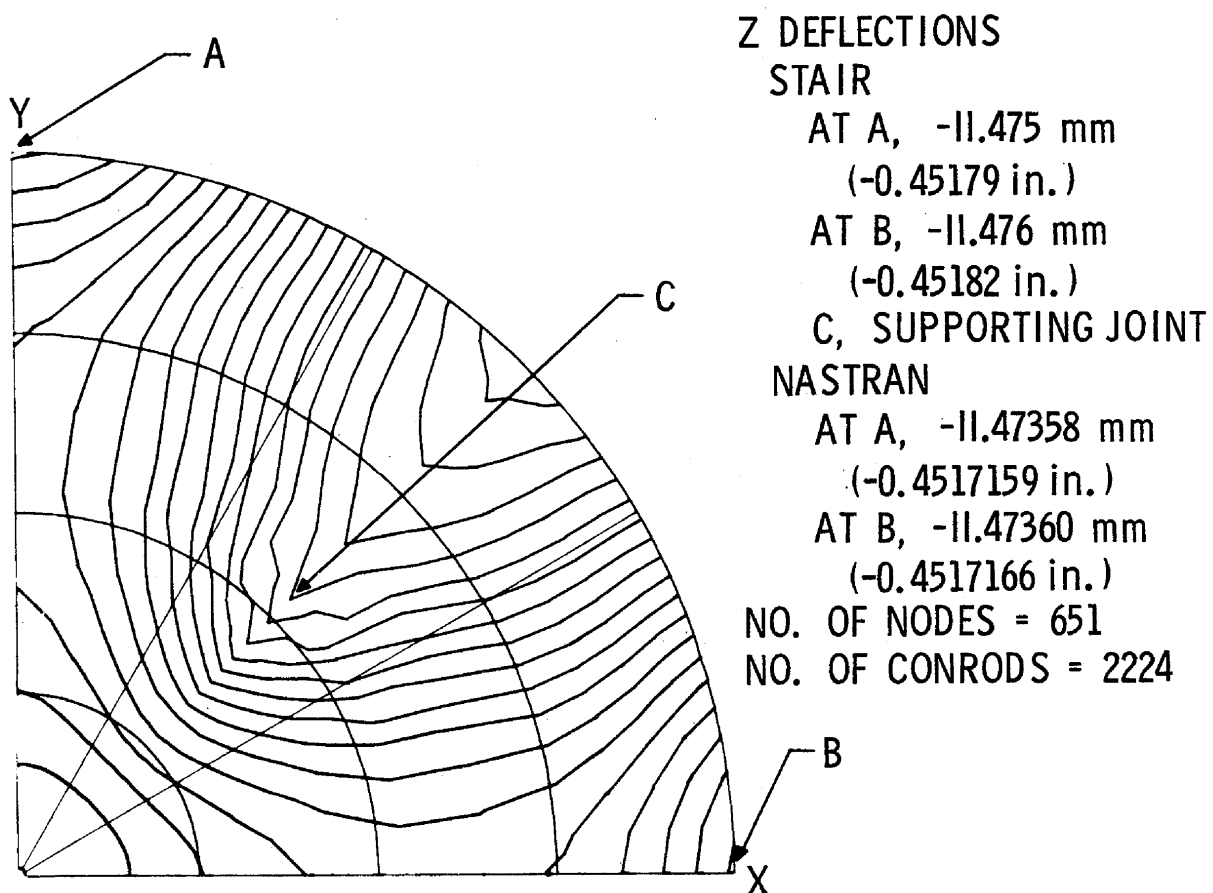


Figure 3.- Contour map of 1/4-symmetric deflection

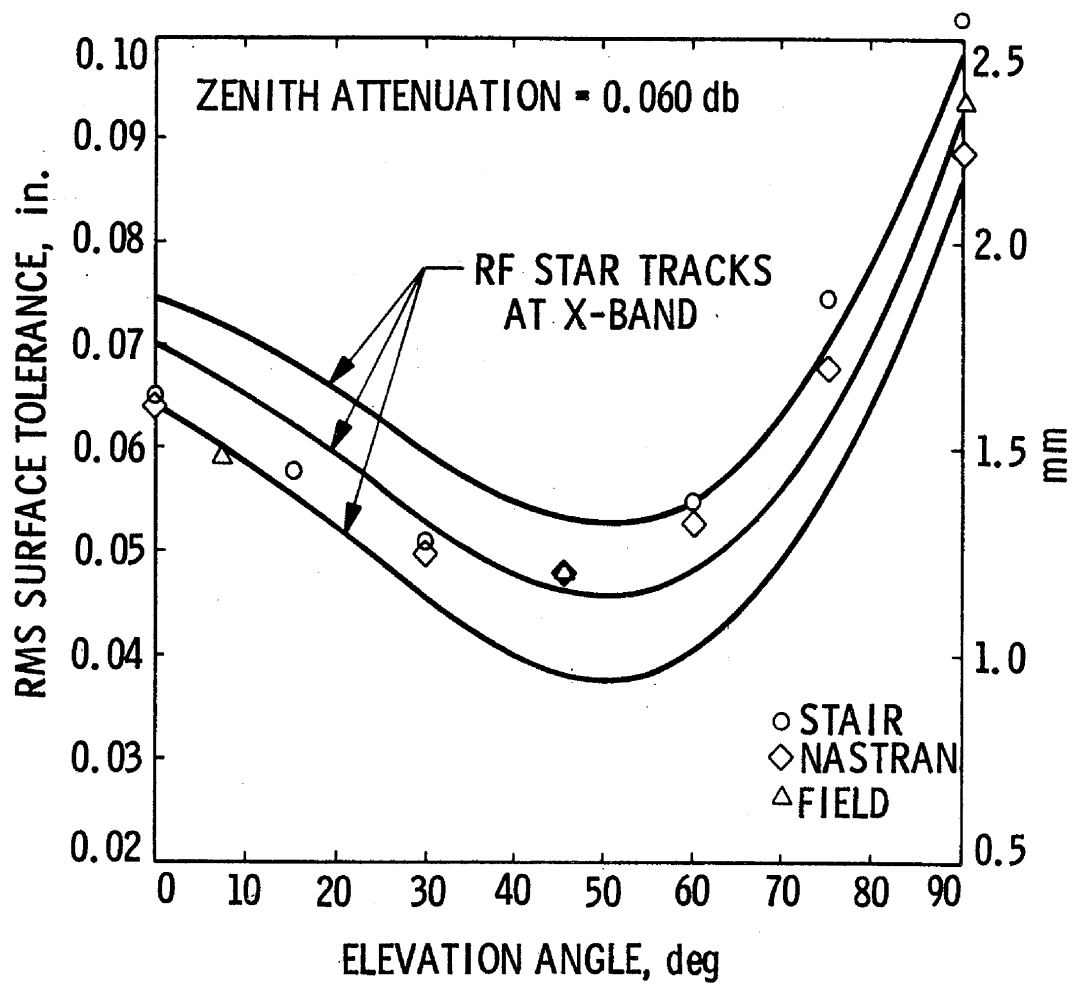


Figure 4.- RMS vs elevation angle

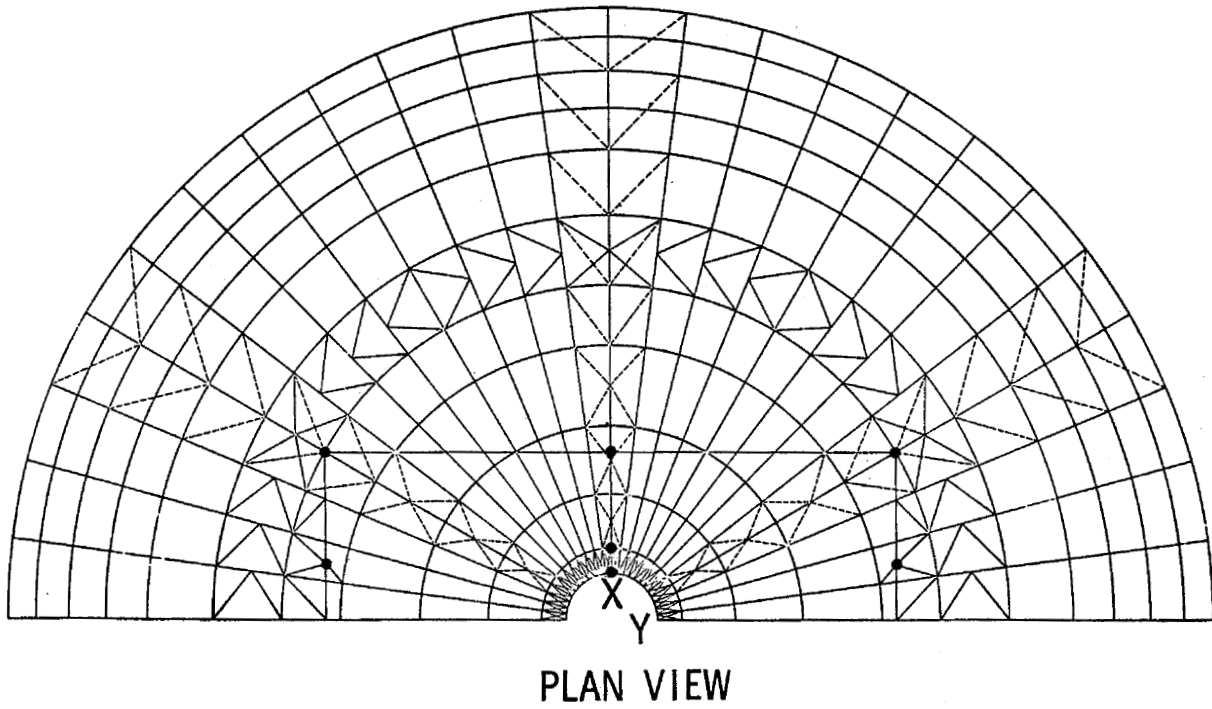


Figure 5.- Top view of 1/2-reflector structure

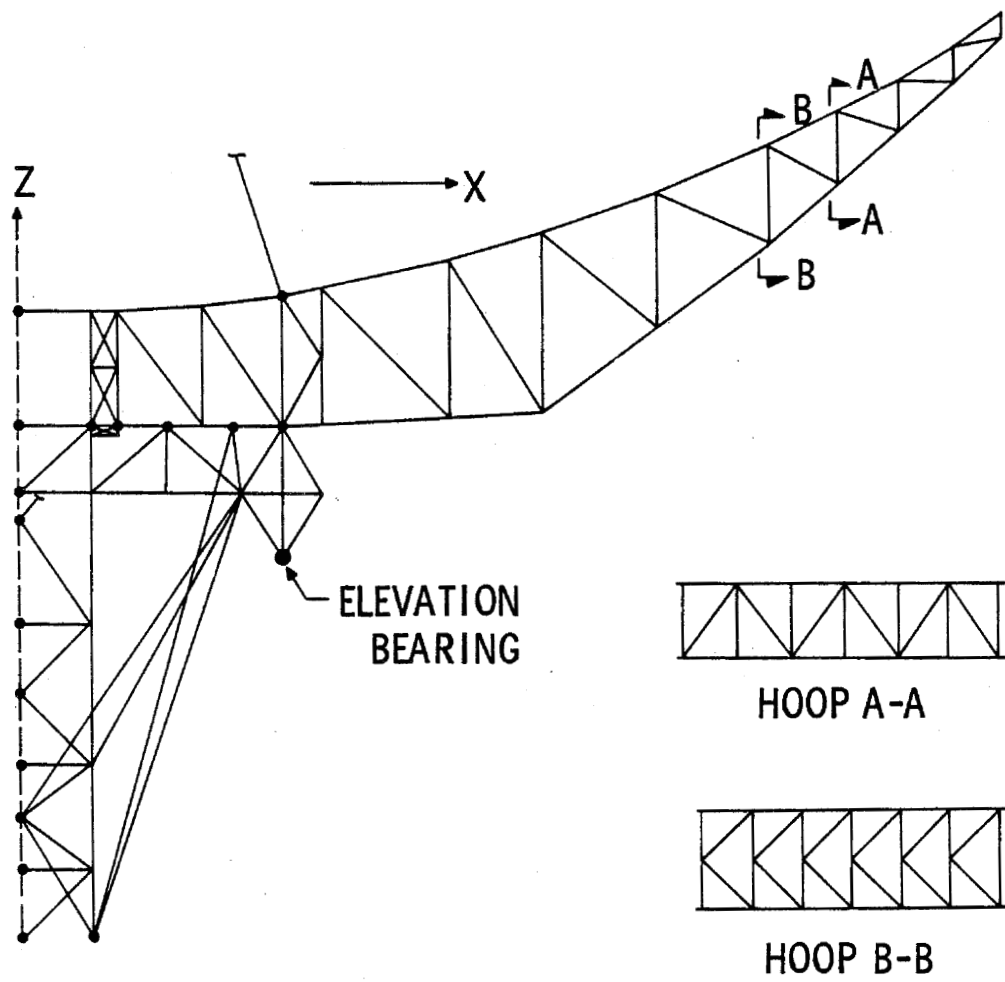


Figure 6.- Cross section

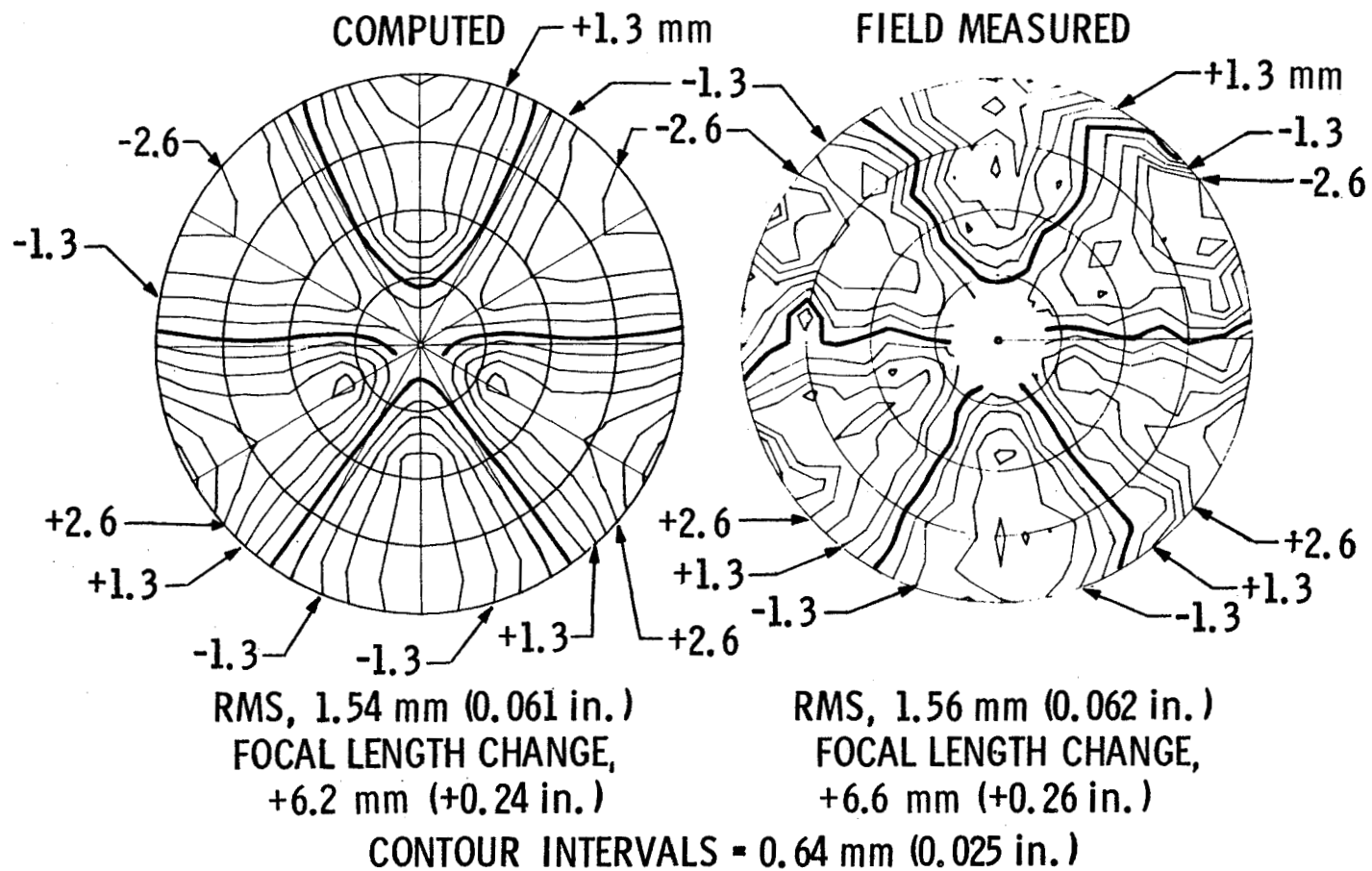


Figure 7. - 64-m antenna, tricone configured, gravity loading distortions after paraboloid best fit; zenith look-zero set at 45° elevation

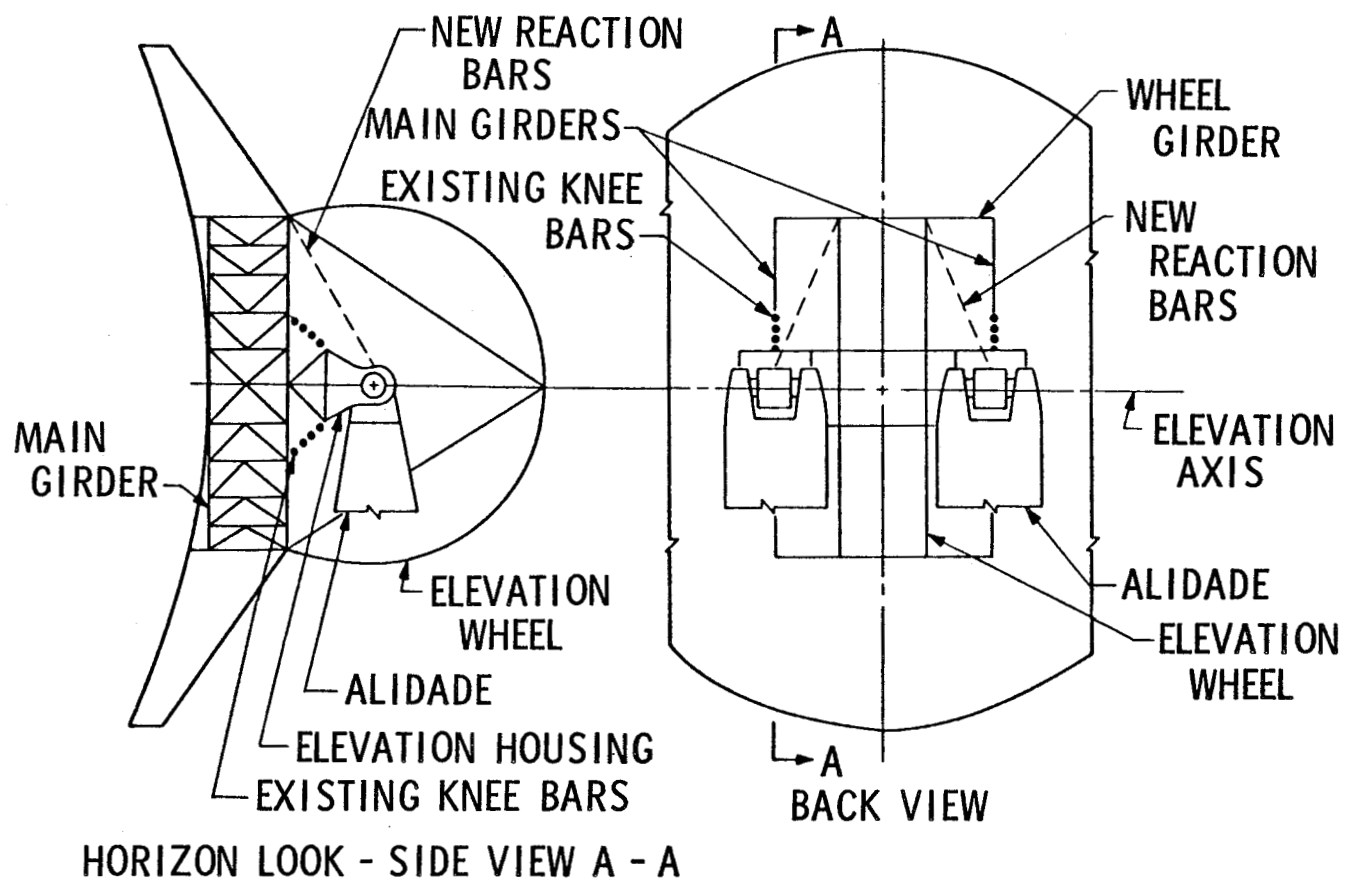


Figure 8. - 64-m revised back-up

NASTRAN-GAP: AN INTEGRATED APPROACH TO THE
ANALYSIS OF RADIATION PATTERNS OF DISTORTED REFLECTORS

By William L. Cook

Communications Satellite Corporation

SUMMARY

The COMSAT General Antenna Package (GAP), when used in conjunction with the NASTRAN Structural Analysis Program, provides the capability for directly determining the effects of structural distortions on reflecting antenna patterns.

An important feature of the GAP program is that the data format for coordinate systems, element definitions, grid point locations and displacements is identical to that of the NASTRAN program, thereby eliminating the necessity for data conversion and minimizing the ambiguity which often arises in the description of a program in two distinct engineering disciplines.

The analysis procedures in GAP are specifically designed to accommodate finite element data in an efficient manner. In particular, a displacement function is assumed for each surface element which is completely analogous to that used in the finite element derivation.

To demonstrate the capabilities of NASTRAN-GAP as an analysis tool, the radiation pattern from a parabolic reflector is calculated for both gravity and thermal loads.

INTRODUCTION

The difficulties of transferring information between two distinct engineering disciplines are readily apparent when attempting to trace radiation fields through reflecting antennas whose deflections are determined by means of a finite element program. For example, due to the size and complexity of the

Preceding page blank

data involved, any conversion is prone to errors and misinterpretations. But more importantly, the techniques commonly used in tracing the radiation field fail to take advantage of the special properties of finite element output data (e.g., the specification of grid point rotations and the capability for handling faceted surfaces). As a consequence, such techniques require the conversion of finite element data to a more tractable form, with a resulting loss in accuracy.

In order to create an efficient general purpose antenna analysis capability, it was recognized that these problems had to be overcome. Therefore, when work was begun on the COMSAT General Antenna Package in August 1970, the NASTRAN data format was adopted as the medium of communication between the two programs.

Capabilities of the GAP program include calculation of currents on each reflector, the radiation field at any point in the system, and far-field radiation patterns and gain, as well as the generation of correcting subreflectors. A broad range of user options and convenience features is provided.

The fields in the vicinity of the reflecting surfaces are found by means of a ray trace procedure in which the second derivatives of the wavefront are calculated for each ray. This information is used in determining both the divergence factor associated with each ray, and the second derivatives of the phase which are required by the wavefront integration scheme, a fast and accurate technique for determining the far-field pattern.

PROGRAM CAPABILITIES

The General Antenna Package provides the capability for tracing a radiation field (either transmitted or received) through a reflecting antenna system. In the case of transmission, the far-field radiation pattern may be determined, along with associated measures of antenna performance. User options include the calculation of the field on a specified aperture plane and the current distribution over any reflecting surface. An additional capability is provided for the generation of correcting subreflectors.

The input format is designed for maximum flexibility and convenience to the user. For example, up to twenty arbitrary coordinate systems (either rectangular, cylindrical or spherical) may be defined by the user for specifying radiation fields or reflecting surfaces.

The data are divided into three sections: A Control Deck, a Bulk Data Deck and a Deformation Deck. Bulk Data cards defining coordinate systems, grid points and element connections are identical to those in the NASTRAN deck, while the Deformation Deck consists of the NASTRAN punched output defining the grid point displacements.

Each radiation field in the vicinity of the antenna is represented by a collection of rays. There is no restriction on the number of rays defining a radiation field. Each ray is defined by its point of origin, direction, amplitude, associated area, phase, cumulative path length, and the second derivatives of the wavefront. When polarization is considered, the field components in two mutually perpendicular directions are also included.

Each reflecting surface is defined by specifying the coefficients of a polynomial equation, of which several types are provided. Alternately, the surface may be defined by an array of grid points connected by discrete triangular or quadrilateral elements, each of which corresponds to a finite element used in the structural analysis. The details of this formulation are discussed in the following section.

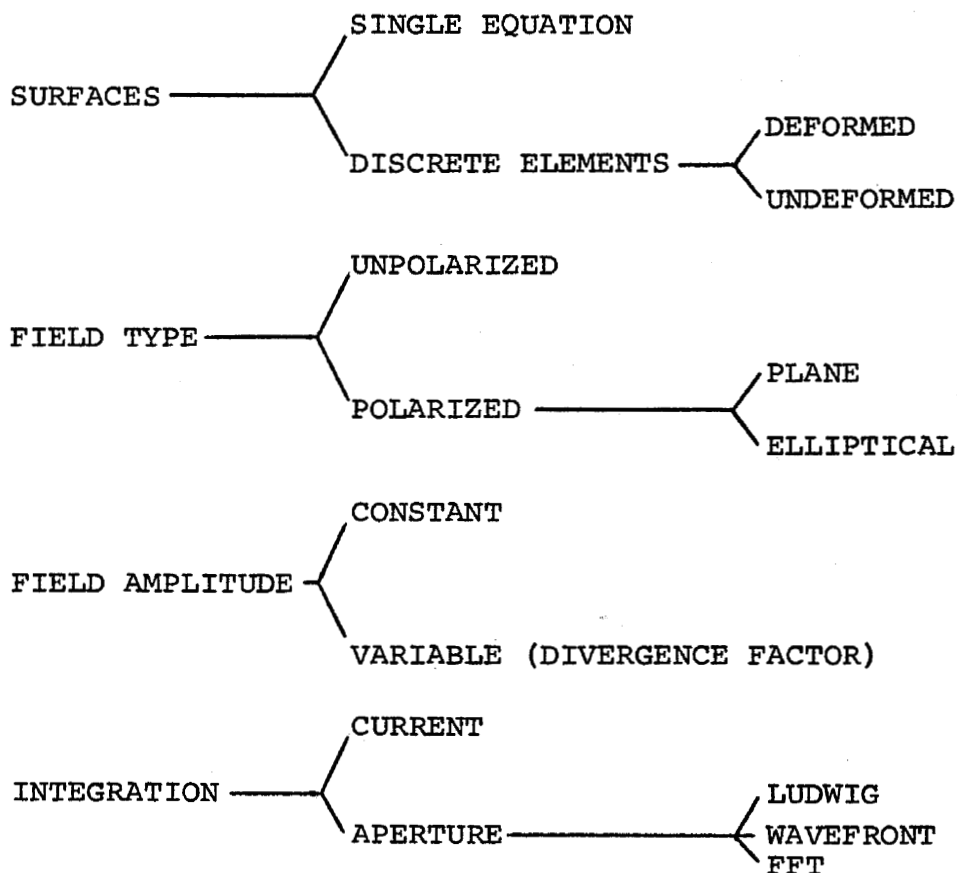
Given a description of the reflecting antenna system and the radiation field at any point in the system, the field at any subsequent point may be determined. This process involves finding, for each ray in the field, its point of intersection with the succeeding surface and then updating the ray origin, path length, amplitude and associated area accordingly. (The latter two items are functions of the divergence factor, which is in turn a function of both the distance traveled and the wavefront derivatives at the previous surface.) Now, knowing the first and second derivatives of both the incident wavefront and the reflecting surface, the corresponding derivatives of the reflected wavefront may be found. These quantities determine both the direction of the reflected ray and the curvature of the reflected wavefront.

At the user's option, the far-field radiation pattern of a transmitting antenna may be found by integration over the aperture field or over the current on the primary reflector. Several alternate aperture plane integration schemes are provided. The wavefront method involves a simple summation of the effects of each ray in the aperture field. The accuracy of this method relies on the fact that all first and second derivatives of the wavefront (and hence the phase) have been previously computed.

Two additional methods are available for determining the far field; the first is based on the Fast Fourier Transform and the second on a technique developed by Ludwig (reference 1).

Calculated field and current information may be output in printed tabular form, plotted in contour form or as cuts through specified planes, or else stored on cards or disk for subsequent restart.

The principal options available to the user are summarized in the following table:



DISCRETE ELEMENTS

The discrete element formulation is designed to accommodate deformed surfaces analyzed by finite element structural analysis programs (specifically the NASTRAN program), surfaces defined in terms of measured data, and surfaces composed of many segments, each represented by a separate equation. This latter category includes the special case of faceted surfaces composed of a large number of flat plates.

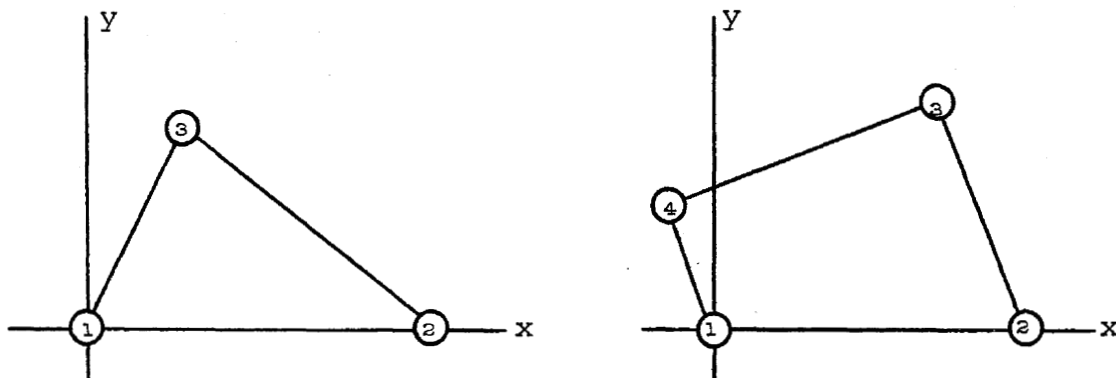
In the discrete element approach, the surface is defined by giving the locations of grid points in arbitrary coordinate systems, and by defining triangular or rectangular surface elements connecting those points. Each surface element is defined by listing the three or four grid points to which it is connected and by selecting the equation defining the surface over that triangular or quadrilateral region.

The ray trace procedure for surfaces composed of discrete elements differs from that for smooth surfaces in the following respects:

- 1) For each ray in the field, a search is made through the element list to determine which element the ray intersects.
- 2) Each element points to an equation describing the reflecting surface over the element. In the "undeformed" mode of analysis, the ray trace is performed in the usual manner, using the equation associated with the intersected element as the surface equation. In the "deformed" mode, the grid point displacements specified in the Deformation Deck are used to find a polynomial approximation to the deformed element surface.

The mathematical details involved in finding the intersected element and in approximating the deformed surface are shown below. Other aspects of the ray trace have been discussed briefly in the previous section and are not of concern here.

For each element defining the reflecting surface, an "element" coordinate system (x, y, z) is defined, such that the first grid point lies at the origin, the second lies along the positive x axis, and the third lies in the x - y plane.



The element coordinate systems for both triangular and quadrilateral elements are shown in the diagram above. In the undeformed mode, the original grid point locations are used; in the deformed mode, the grid point locations are incremented by the translations prescribed in the Deformation Deck.

The incident ray is then converted from the basic system to the element system, and the intersection of the ray with the x-y plane is determined. This point is denoted (x_a, y_a) . It now remains to determine whether (x_a, y_a) lies within the boundaries of the element, a straight-forward process which will not be belabored here. If the ray does not intersect the element, the next element in the list is selected and the process is repeated.

For quadrilateral elements, one additional step is required. Each quadrilateral may be considered to contain two triangular regions, bounded by grid points 1 - 2 - 3 and 1 - 3 - 4, respectively. The triangular region in which (x_a, y_a) lies is treated as a triangular element in the remainder of the analysis.

In the deformed element coordinate system, the deformed surface is approximated by the polynomial

$$z = a_0 + a_1x + a_2y + a_3x^2 + a_4xy + a_5y^2 + a_6x^3 + a_7(x^2y + xy^2) + a_8y^3 \quad (1)$$

Notice in equation (1) that the coefficients of the x^2y and xy^2 terms have been made equal. Some assumption of this kind was necessary, since the coefficients are evaluated in terms of nine displacement components (three at each corner) and, hence, cannot exceed nine in number. It should be

emphasized that an expansion of this type was chosen quite arbitrarily, and that alternate representations may well yield more accurate results.

The coefficients may be evaluated in terms of the values of z , $\partial z/\partial x$ and $\partial z/\partial y$ at each corner point, which are obtained by transforming the undeformed surface equation to the deformed element system, and adding in the effects of the grid point rotations in the x - y plane. We define,

$$\begin{aligned} z_i &= z(x_i, y_i) \\ z_{xi} &= \partial z(x_i, y_i)/\partial x \quad i = 1, 2, 3 \\ z_{yi} &= \partial z(x_i, y_i)/\partial y \end{aligned} \quad (2)$$

where i indicates the grid point number as in the diagram above. Notice that $x_1 = y_1 = y_2 = 0$, because of the manner in which the element coordinate system was defined. By differentiating equation (1) with respect to x and y ,

$$\begin{aligned} z_x &= a_1 + 2a_3x + a_4y + 3a_6x^2 + a_7(2xy + y^2) \\ z_y &= a_2 + a_4x + 2a_5y + a_7(x^2 + 2xy) + 3a_8y^2 \end{aligned} \quad (3)$$

and by evaluating equations (1) and (3) at each corner point, the following values of the coefficients are obtained:

$$\begin{aligned} a_0 &= z_1 \\ a_1 &= z_{x_1} \\ a_2 &= z_{y_1} \\ a_3 &= \frac{1}{x_2^2} (z_2 - z_1 - z_{x_1}x_2 - a_6x_2^3) \\ a_6 &= \frac{1}{x_2^2} \left[z_{x_2} - z_{x_1} - \frac{2}{x_2} (z_2 - z_1 - z_{x_1}x_2) \right] \\ a_7 &= \frac{z_{x_3} - z_{x_1} - 2a_3x_3 - y_3(z_{y_2} - z_{y_1})/x_2 - 3a_6x_3^2}{(-y_3x_2 + 2x_3y_3 + y_3^2)} \\ a_4 &= \frac{1}{x_2} (z_{y_2} - z_{y_1} - a_7x_2^2) \end{aligned} \quad (4)$$

$$a_8 = \frac{2}{y_3^3} \left[-z_3 + z_1 + z_{x_1}x_3 + z_{y_1}y_3 + a_3x_3^2 + a_4x_3y_3 \right. \\ \left. + \frac{y_3}{2}(z_{y_3} - z_{y_1} - a_4x_3 - a_7(x_3^2 + 2x_3y_3)) \right. \\ \left. + a_6x_3^3 + a_7(x_3^2y_3 + x_3y_3^2) \right] \\ a_5 = \frac{1}{2y_3} \left[z_{y_3} - z_{y_1} - a_4x_3 - a_7(x_3^2 + 2x_3y_3) - 3a_8y_3^2 \right]$$

We now wish to approximate the surface equation at point (x_a, y_a) . To do so, we will need an expression for the second derivatives of the surface; hence, from equation (3),

$$\begin{aligned} z_{xx} &= 2a_3 + 6a_6x + 2a_7y \\ z_{xy} &= a_4 + 2a_7(x + y) \\ z_{yy} &= 2a_5 + 2a_7x + 6a_8y \end{aligned} \quad (5)$$

Now, a Taylor series expansion about the point (x_a, y_a) gives,

$$\begin{aligned} z \approx z_a + (x - x_a)z_{xa} + (y - y_a)z_{ya} + \frac{1}{2}(x - x_a)^2 z_{xxa} \\ + (x - x_a)(y - y_a)z_{xya} + \frac{1}{2}(y - y_a)^2 z_{yya} \end{aligned} \quad (6)$$

or expressed in an equivalent form:

$$\begin{aligned} b_0 + b_1x + b_2y + b_3z + b_4x^2 + b_5y^2 \\ + b_6z^2 + b_7xy + b_8yz + b_9zx = 0 \end{aligned} \quad (7)$$

where,

$$\begin{aligned} b_0 &= z_a - x_az_{xa} - y_az_{ya} + \frac{1}{2}x_a^2 z_{xxa} \\ &\quad + x_ay_az_{xya} + \frac{1}{2}y_a^2 z_{yya} \\ b_1 &= z_{xa} - x_az_{xxa} - y_az_{xya} \\ b_2 &= z_{ya} - y_az_{yya} - x_az_{xya} \end{aligned}$$

$$b_3 = -1$$

$$b_4 = \frac{1}{2}z_{xxa}$$

$$b_5 = \frac{1}{2}z_{yya}$$

$$b_6 = 0$$

$$b_7 = z_{xya}$$

$$b_8 = 0$$

$$b_9 = 0$$

Now, equation (7) approximates the deformed surface in the vicinity of point (x_a, y_a) , which is the point where the incident ray intersects the plane through the three corner points of the element. This equation may be used to determine the point where the ray strikes the deformed surface as well as the properties of the reflected ray.

The approximation of equation (1) by equation (7) was occasioned solely by the availability of software for handling second order polynomials. More accurate results would doubtless be obtained by the direct solution of equation (1).

EXAMPLE: PARABOLIC REFLECTOR WITH DISTORTIONS

This example demonstrates the manner in which a distorted reflecting surface is handled by the General Antenna Package when the surface deformations are determined analytically by NASTRAN. No attempt has been made to compare the results with theoretical or experimental data. A comparison between GAP results and experimental measurements for an actual antenna may be found in reference 2.

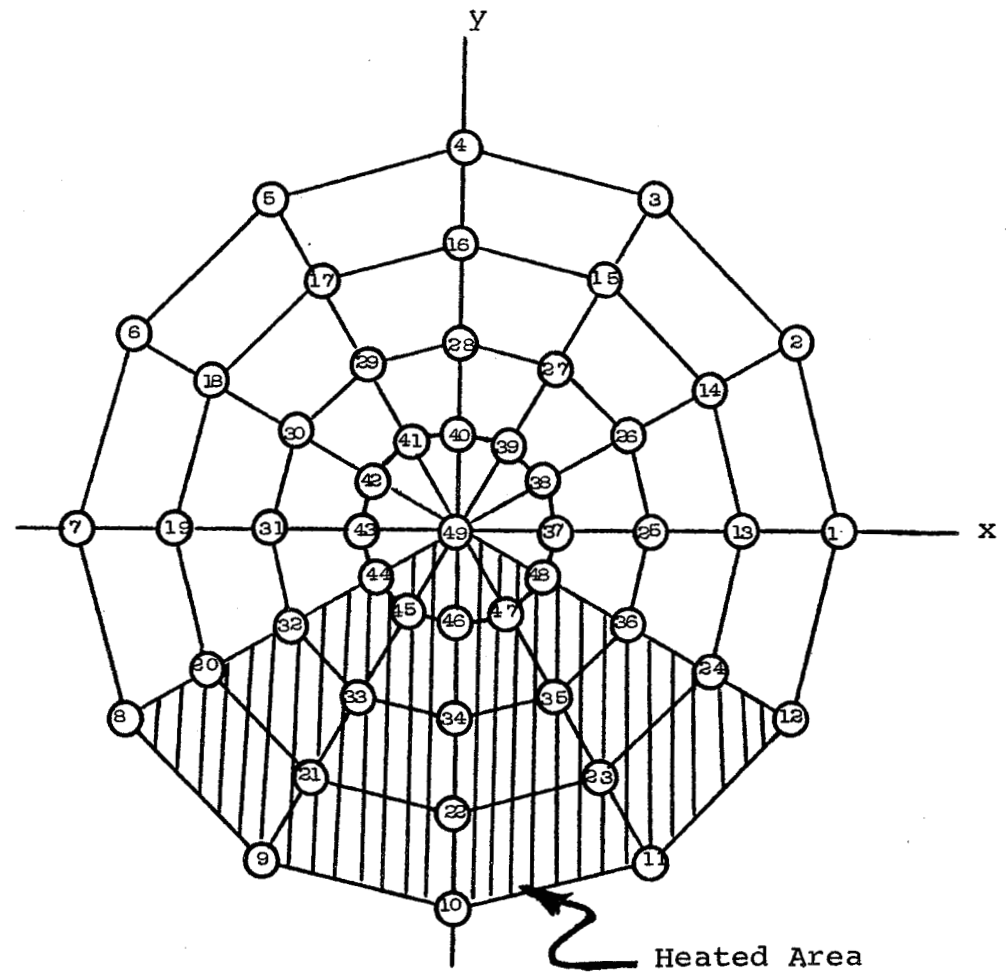
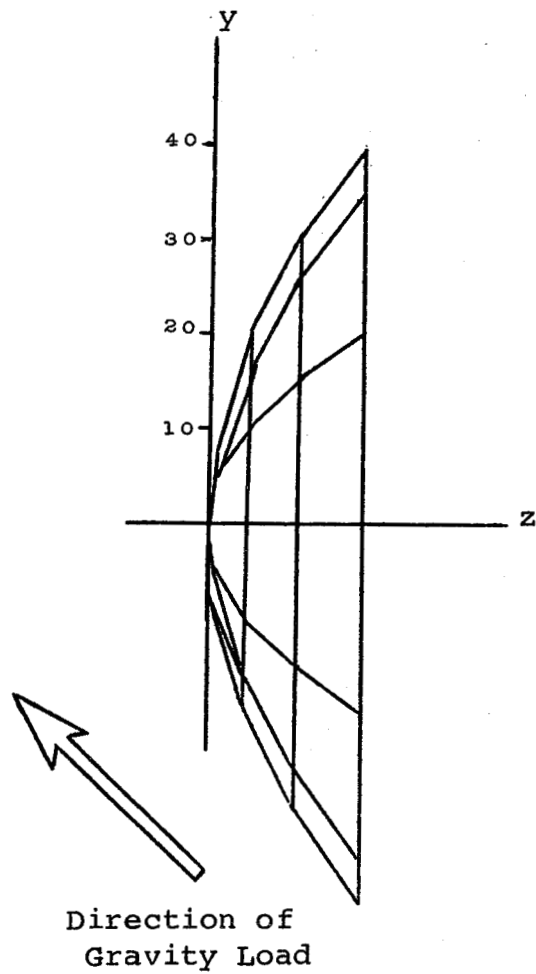
In this example, we wish to find the characteristics of a radiation field reflected from a deformed parabolic reflector, knowing the structural properties of the antenna and the nature of the applied load. We will examine two cases of particular interest: distortions due to a gravity load on the structure, and those due to a known temperature distribution.

The finite element model of the reflector is shown on the following page; in the interests of simplicity, the support structure has not been modeled, and is represented only by the constraints at grid points 40, 44 and 48. The direction of the gravity load is at 45° to the y axis, as shown on the left of the diagram. Thermal distortions are to be calculated for the simple temperature distribution indicated on the right-hand view; the shaded portion of the surface is 20° F warmer than the non-shaded portion.

The NASTRAN input data for this problem are listed below. All grid point and element data were generated by the AXIS program.* The gravity load applied to the structure is automatically calculated by NASTRAN based on the geometry and density of the material, and on the direction of the gravity vector. The TEMP Bulk Data cards define the temperature distribution over the surface. An ambient temperature is assumed for all grid points not specified.

* Cook, W. L., "Automated Input Data Preparation for NASTRAN," NASA Goddard Report X-321-69-231, April, 1969.

FINITE ELEMENT MODEL OF PARABOLIC DISH



NASTRAN Input Data

```

NASTRAN BUFFSIZE#259
ID USER,PROB1
TIME 6
APP DISPLACEMENT
SOL 1,0
CEND
TITLE# PARABOLIC DISH
SPC#2
OUTPUT
DISPLACEMENT%PRINT,PUNCH#ALL
SUBCASE 1
SUBTITLE# GRAVITY LOAD
LOAD#1
SUBCASE 2
SUBTITLE# THERMAL LOAD
TEMP%LOAD#2
BEGIN BULK
MAT1 1231.00E 07 3.00E-011.00E-011.20E-05
SPC1 2 123 40 44 48
GRAV 1 0 1.0 0.0 0.0 -1.0
TEMPD 2 0.0
TEMP 2 8 20.0 9 20.0 10 20.0
TEMP 2 11 20.0 12 20.0 20 20.0
TEMP 2 21 20.0 22 20.0 23 20.0
TEMP 2 24 20.0 32 20.0 33 20.0
TEMP 2 34 20.0 35 20.0 36 20.0
TEMP 2 44 20.0 45 20.0 46 20.0
TEMP 2 47 20.0 48 20.0 49 20.0
PQUAD2 1 123 0.1000
PQUAD2 2 123 0.1000
PQUAD2 3 123 0.1000
PTRIA2 5 123 0.1000
CORD2C 10 0 0.0 0.0 0.0 0.0 1.0 1.0 &222
&222 1.0 0.0 0.0
GRID 1 10 40.000 0.0 16.000 0
GRID 2 10 40.000 30.000 16.000 0
GRID 3 10 40.000 60.000 16.000 0
GRID 4 10 40.000 90.000 16.000 0
GRID 5 10 40.000 120.000 16.000 0
GRID 6 10 40.000 150.000 16.000 0
GRID 7 10 40.000 180.000 16.000 0
GRID 8 10 40.000 210.000 16.000 0
GRID 9 10 40.000 240.000 16.000 0
GRID 10 10 40.000 270.000 16.000 0
GRID 11 10 40.000 300.000 16.000 0
GRID 12 10 40.000 330.000 16.000 0
GRID 13 10 30.000 0.0 9.000 0
GRID 14 10 30.000 30.000 9.000 0
GRID 15 10 30.000 60.000 9.000 0
GRID 16 10 30.000 90.000 9.000 0
GRID 17 10 30.000 120.000 9.000 0
GRID 18 10 30.000 150.000 9.000 0
GRID 19 10 30.000 180.000 9.000 0
GRID 20 10 30.000 210.000 9.000 0
GRID 21 10 30.000 240.000 9.000 0
GRID 22 10 30.000 270.000 9.000 0

```

GRID	23	10	30.000	300.000	9.000	0
GRID	24	10	30.000	330.000	9.000	0
GRID	25	10	20.000	0.0	4.000	0
GRID	26	10	20.000	30.000	4.000	0
GRID	27	10	20.000	60.000	4.000	0
GRID	28	10	20.000	90.000	4.000	0
GRID	29	10	20.000	120.000	4.000	0
GRID	30	10	20.000	150.000	4.000	0
GRID	31	10	20.000	180.000	4.000	0
GRID	32	10	20.000	210.000	4.000	0
GRID	33	10	20.000	240.000	4.000	0
GRID	34	10	20.000	270.000	4.000	0
GRID	35	10	20.000	300.000	4.000	0
GRID	36	10	20.000	330.000	4.000	0
GRID	37	10	10.000	0.0	1.000	0
GRID	38	10	10.000	30.000	1.000	0
GRID	39	10	10.000	60.000	1.000	0
GRID	40	10	10.000	90.000	1.000	0
GRID	41	10	10.000	120.000	1.000	0
GRID	42	10	10.000	150.000	1.000	0
GRID	43	10	10.000	180.000	1.000	0
GRID	44	10	10.000	210.000	1.000	0
GRID	45	10	10.000	240.000	1.000	0
GRID	46	10	10.000	270.000	1.000	0
GRID	47	10	10.000	300.000	1.000	0
GRID	48	10	10.000	330.000	1.000	0
GRID	49	10	0.0	0.0	0.0	0
CQUAD2	1	1	1	2	14	13
CQUAD2	2	1	2	3	15	14
CQUAD2	3	1	3	4	16	15
CQUAD2	4	1	4	5	17	16
CQUAD2	5	1	5	6	18	17
CQUAD2	6	1	6	7	19	18
CQUAD2	7	1	7	8	20	19
CQUAD2	8	1	8	9	21	20
CQUAD2	9	1	9	10	22	21
CQUAD2	10	1	10	11	23	22
CQUAD2	11	1	11	12	24	23
CQUAD2	12	1	12	1	13	24
CQUAD2	13	2	13	14	26	25
CQUAD2	14	2	14	15	27	26
CQUAD2	15	2	15	16	28	27
CQUAD2	16	2	16	17	29	28
CQUAD2	17	2	17	18	30	29
CQUAD2	18	2	18	19	31	30
CQUAD2	19	2	19	20	32	31
CQUAD2	20	2	20	21	33	32
CQUAD2	21	2	21	22	34	33
CQUAD2	22	2	22	23	35	34
CQUAD2	23	2	23	24	36	35
CQUAD2	24	2	24	13	25	36
CQUAD2	25	3	25	26	38	37
CQUAD2	26	3	26	27	39	38
CQUAD2	27	3	27	28	40	39
CQUAD2	28	3	28	29	41	40
CQUAD2	29	3	29	30	42	41
CQUAD2	30	3	30	31	43	42
CQUAD2	31	3	31	32	44	43
CQUAD2	32	3	32	33	45	44
CQUAD2	33	3	33	34	46	45
CQUAD2	34	3	34	35	47	46
CQUAD2	35	3	35	36	48	47
CQUAD2	36	3	36	25	37	48
CTRIA2	37	5	37	38	49	

CTRIA2	38	5	38	39	49
CTRIA2	39	5	39	40	49
CTRIA2	40	5	40	41	49
CTRIA2	41	5	41	42	49
CTRIA2	42	5	42	43	49
CTRIA2	43	5	43	44	49
CTRIA2	44	5	44	45	49
CTRIA2	45	5	45	46	49
CTRIA2	46	5	46	47	49
CTRIA2	47	5	47	48	49
CTRIA2	48	5	48	37	49
ENDDATA					

Output from the NASTRAN program includes a punched deck containing the three translations and three rotations of each grid point in the structural model. This deck becomes the Deformation Deck in the GAP input data.

In addition, all Bulk Data Cards containing grid point, element and coordinate system information may be included directly in the GAP Bulk Data Deck.

Both types of data are included in the GAP input listing below, which is for the thermal case only. Additional information required by GAP includes the specification of a feed field (see the TABLE card in the Bulk Data Deck) and the equation of the undeformed surface -- in this case, a parabola of the form,

$$-100.0z + 1.0x^2 + 1.0y^2 = 0$$

The coefficients of this equation are defined on the EQN card in the Bulk Data Deck.

The "deformed" mode of analysis has been selected, indicating that the grid point displacements in the Deformation Deck are to be used to modify the surface equation over each element.

GAP Input Data

```

TITLE= DEFORMED PARABOLIC DISH
AMPLITUDE=CONSTANT      POLARIZATION=NO      MODE=DEFORMED
APERTURE=30  IFIELD=1    SURFACE 1=4        METHOD(APERTURE)=7
OUTPUT FARFIELD          OUTPUT(CPLOT) FARFIELD POWER
BEGIN BULK
PARAM 1.0      1.0      1.0      1.0
CURD2S* 30      0      0.0      0.0      0.0      17.677669529600 *
*      17.677669529600 0.0      -1.0      -1.0
&      1.0      0.0      0.0
CURD2R 40      0      0.0      0.0      0.0      0.0      1.0      1.0
&      1.0      0.0      0.0
EQN      12      1      40      10      -1.0      40.0      -360.0      360.0
&      0.0      16.0      0.0      0.0      0.0      -100.0      1.0      1.0
INTEG      7      2      31      8      -3.0      3.0      0.0      157.5
&      0      0      0      0      -50.0      50.0      -50.0      50.0
LIST      4      1      48      12
CURD2C 10      0      0.0      0.0      0.0      0.0      1.0      1.0      &222
&222      1.0      0.0      0.0
GRID      1      10      40.000      0.0      16.000      0
GRID      2      10      40.000      30.000      16.000      0
GRID      3      10      40.000      60.000      16.000      0
GRID      4      10      40.000      90.000      16.000      0
GRID      5      10      40.000      120.000      16.000      0
GRID      6      10      40.000      150.000      16.000      0
GRID      7      10      40.000      180.000      16.000      0
GRID      8      10      40.000      210.000      16.000      0
GRID      9      10      40.000      240.000      16.000      0
GRID      10      10      40.000      270.000      16.000      0
GRID      11      10      40.000      300.000      16.000      0
GRID      12      10      40.000      330.000      16.000      0
GRID      13      10      30.000      0.0      9.000      0
GRID      14      10      30.000      30.000      9.000      0
GRID      15      10      30.000      60.000      9.000      0
GRID      16      10      30.000      90.000      9.000      0
GRID      17      10      30.000      120.000      9.000      0
GRID      18      10      30.000      150.000      9.000      0
GRID      19      10      30.000      180.000      9.000      0
GRID      20      10      30.000      210.000      9.000      0
GRID      21      10      30.000      240.000      9.000      0
GRID      22      10      30.000      270.000      9.000      0
GRID      23      10      30.000      300.000      9.000      0
GRID      24      10      30.000      330.000      9.000      0
GRID      25      10      20.000      0.0      4.000      0
GRID      26      10      20.000      30.000      4.000      0
GRID      27      10      20.000      60.000      4.000      0
GRID      28      10      20.000      90.000      4.000      0
GRID      29      10      20.000      120.000      4.000      0
GRID      30      10      20.000      150.000      4.000      0
GRID      31      10      20.000      180.000      4.000      0
GRID      32      10      20.000      210.000      4.000      0
GRID      33      10      20.000      240.000      4.000      0
GRID      34      10      20.000      270.000      4.000      0
GRID      35      10      20.000      300.000      4.000      0
GRID      36      10      20.000      330.000      4.000      0
GRID      37      10      10.000      0.0      1.000      0
GRID      38      10      10.000      30.000      1.000      0
GRID      39      10      10.000      60.000      1.000      0

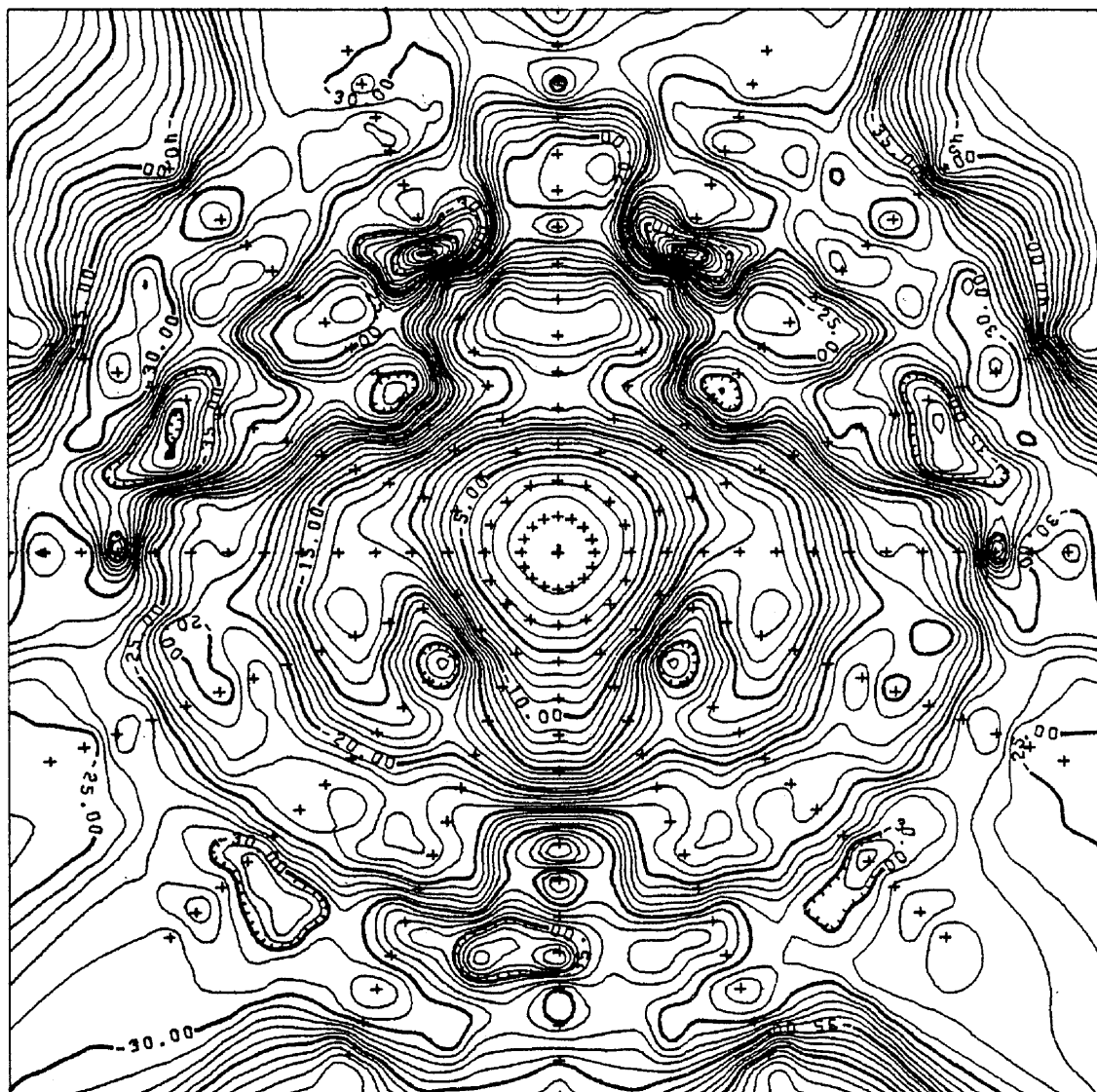
```

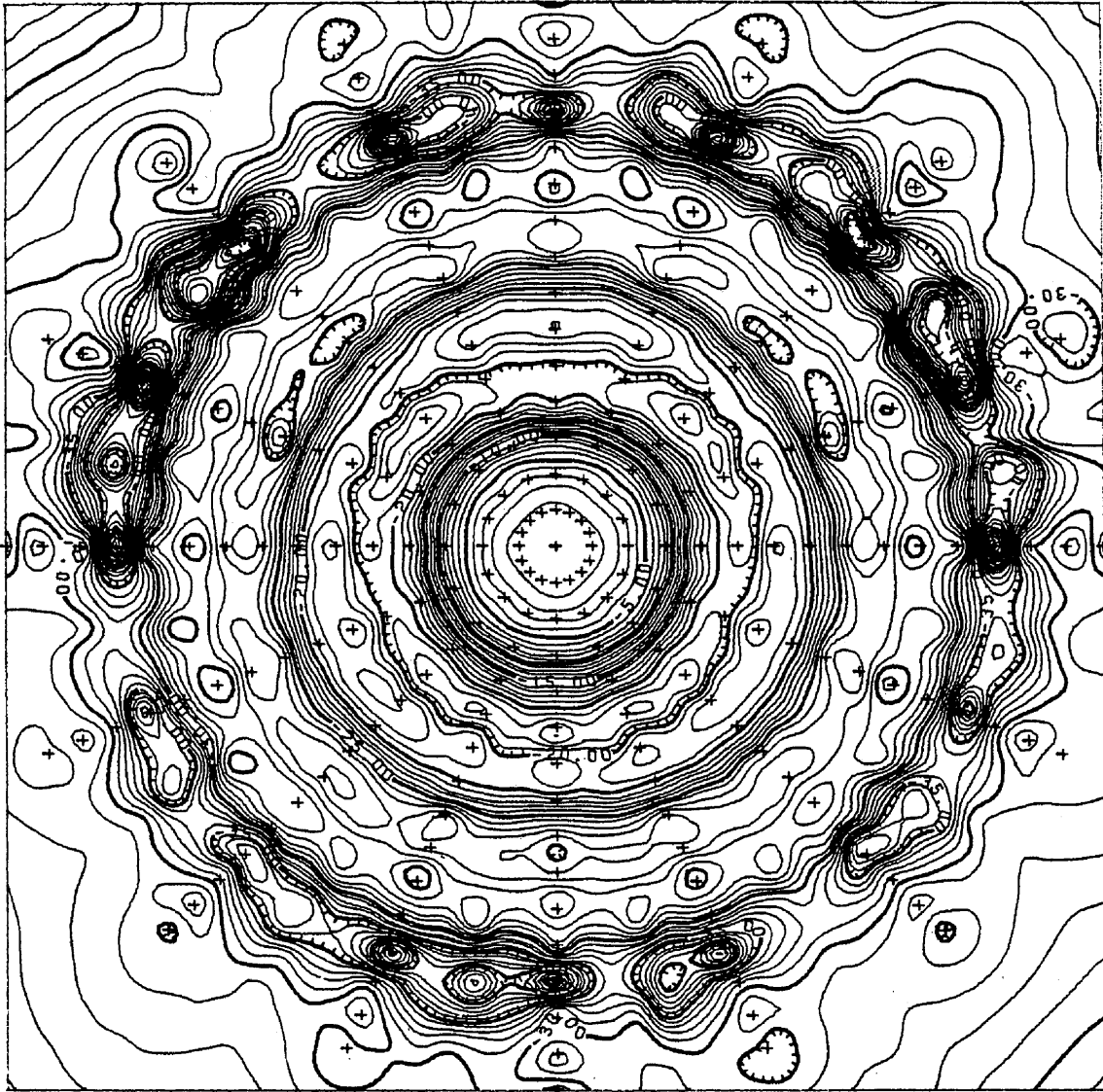
GRID	40	10	10.000	90.000	1.000	0		
GRID	41	10	10.000	120.000	1.000	0		
GRID	42	10	10.000	150.000	1.000	0		
GRID	43	10	10.000	180.000	1.000	0		
GRID	44	10	10.000	210.000	1.000	0		
GRID	45	10	10.000	240.000	1.000	0		
GRID	46	10	10.000	270.000	1.000	0		
GRID	47	10	10.000	300.000	1.000	0		
GRID	48	10	10.000	330.000	1.000	0		
GRID	49	10	0.0	0.0	0.0	0		
CQUAD2	1	1	1	2	14	13		
CQUAD2	2	1	2	3	15	14		
CQUAD2	3	1	3	4	16	15		
CQUAD2	4	1	4	5	17	16		
CQUAD2	5	1	5	6	18	17		
CQUAD2	6	1	6	7	19	18		
CQUAD2	7	1	7	8	20	19		
CQUAD2	8	1	8	9	21	20		
CQUAD2	9	1	9	10	22	21		
CQUAD2	10	1	10	11	23	22		
CQUAD2	11	1	11	12	24	23		
CQUAD2	12	1	12	1	13	24		
CQUAD2	13	2	13	14	26	25		
CQUAD2	14	2	14	15	27	26		
CQUAD2	15	2	15	16	28	27		
CQUAD2	16	2	16	17	29	28		
CQUAD2	17	2	17	18	30	29		
CQUAD2	18	2	18	19	31	30		
CQUAD2	19	2	19	20	32	31		
CQUAD2	20	2	20	21	33	32		
CQUAD2	21	2	21	22	34	33		
CQUAD2	22	2	22	23	35	34		
CQUAD2	23	2	23	24	36	35		
CQUAD2	24	2	24	13	25	36		
CQUAD2	25	3	25	26	38	37		
CQUAD2	26	3	26	27	39	38		
CQUAD2	27	3	27	28	40	39		
CQUAD2	28	3	28	29	41	40		
CQUAD2	29	3	29	30	42	41		
CQUAD2	30	3	30	31	43	42		
CQUAD2	31	3	31	32	44	43		
CQUAD2	32	3	32	33	45	44		
CQUAD2	33	3	33	34	46	45		
CQUAD2	34	3	34	35	47	46		
CQUAD2	35	3	35	36	48	47		
CQUAD2	36	3	36	25	37	48		
CTRIA2	37	5	37	38	49			
CTRIA2	38	5	38	39	49			
CTRIA2	39	5	39	40	49			
CTRIA2	40	5	40	41	49			
CTRIA2	41	5	41	42	49			
CTRIA2	42	5	42	43	49			
CTRIA2	43	5	43	44	49			
CTRIA2	44	5	44	45	49			
CTRIA2	45	5	45	46	49			
CTRIA2	46	5	46	47	49			
CTRIA2	47	5	47	48	49			
CTRIA2	48	5	48	37	49			
TABLE	1	30	1			0.02632		
E	0.0	0.0	0.0	1.0000	0.0	0.0	1.0000	0.0
E	0.0	0.0	0.0	1.0000	10.0000	0.0	1.0000	0.0
E	0.0	0.0	0.0	1.0000	10.0000	60.0000	1.0000	0.0
E	0.0	0.0	0.0	1.0000	10.0000	120.0000	1.0000	0.0
E	0.0	0.0	0.0	1.0000	10.0000	180.0000	1.0000	0.0

E	0.0	0.0	0.0	1.0000	10.0000	240.0000	1.0000	0.0
E	0.0	0.0	0.0	1.0000	10.0000	300.0000	1.0000	0.0
E	0.0	0.0	0.0	1.0000	20.0000	0.0	1.0000	0.0
E	0.0	0.0	0.0	1.0000	20.0000	30.0000	1.0000	0.0
E	0.0	0.0	0.0	1.0000	20.0000	60.0000	1.0000	0.0
E	0.0	0.0	0.0	1.0000	20.0000	90.0000	1.0000	0.0
E	0.0	0.0	0.0	1.0000	20.0000	120.0000	1.0000	0.0
E	0.0	0.0	0.0	1.0000	20.0000	150.0000	1.0000	0.0
E	0.0	0.0	0.0	1.0000	20.0000	180.0000	1.0000	0.0
E	0.0	0.0	0.0	1.0000	20.0000	210.0000	1.0000	0.0
E	0.0	0.0	0.0	1.0000	20.0000	240.0000	1.0000	0.0
E	0.0	0.0	0.0	1.0000	20.0000	270.0000	1.0000	0.0
E	0.0	0.0	0.0	1.0000	20.0000	300.0000	1.0000	0.0
E	0.0	0.0	0.0	1.0000	20.0000	330.0000	1.0000	0.0
E	0.0	0.0	0.0	1.0000	30.0000	0.0	1.0000	0.0
E	0.0	0.0	0.0	1.0000	30.0000	20.0000	1.0000	0.0
E	0.0	0.0	0.0	1.0000	30.0000	40.0000	1.0000	0.0
E	0.0	0.0	0.0	1.0000	30.0000	60.0000	1.0000	0.0
E	0.0	0.0	0.0	1.0000	30.0000	80.0000	1.0000	0.0
E	0.0	0.0	0.0	1.0000	30.0000	100.0000	1.0000	0.0
E	0.0	0.0	0.0	1.0000	30.0000	120.0000	1.0000	0.0
E	0.0	0.0	0.0	1.0000	30.0000	140.0000	1.0000	0.0
E	0.0	0.0	0.0	1.0000	30.0000	160.0000	1.0000	0.0
E	0.0	0.0	0.0	1.0000	30.0000	180.0000	1.0000	0.0
E	0.0	0.0	0.0	1.0000	30.0000	200.0000	1.0000	0.0
E	0.0	0.0	0.0	1.0000	30.0000	220.0000	1.0000	0.0
E	0.0	0.0	0.0	1.0000	30.0000	240.0000	1.0000	0.0
E	0.0	0.0	0.0	1.0000	30.0000	260.0000	1.0000	0.0
E	0.0	0.0	0.0	1.0000	30.0000	280.0000	1.0000	0.0
E	0.0	0.0	0.0	1.0000	30.0000	300.0000	1.0000	0.0
E	0.0	0.0	0.0	1.0000	30.0000	320.0000	1.0000	0.0
E	0.0	0.0	0.0	1.0000	30.0000	340.0000	1.0000	0.0
E	0.0	0.0	0.0	1.0000	40.0000	0.0	1.0000	0.0
E	0.0	0.0	0.0	1.0000	40.0000	10.0000	1.0000	0.0
E	0.0	0.0	0.0	1.0000	70.0000	285.8818	1.0000	0.0
E	0.0	0.0	0.0	1.0000	70.0000	296.4700	1.0000	0.0
E	0.0	0.0	0.0	1.0000	70.0000	307.0581	1.0000	0.0
E	0.0	0.0	0.0	1.0000	70.0000	317.6462	1.0000	0.0
E	0.0	0.0	0.0	1.0000	70.0000	328.2344	1.0000	0.0
E	0.0	0.0	0.0	1.0000	70.0000	338.8225	1.0000	0.0
E	0.0	0.0	0.0	1.0000	70.0000	349.4106	1.0000	0.0
ENDDATA								
-CONT-	1	G	-5.244812E-02	8.087635E-02	6.712717E-02			
-CONT-	2	G	-6.136972E-03	-5.575199E-03	1.104371E-03			
-CONT-	3	G	5.461220E-03	2.102917E-03	-3.354439E-02			
-CONT-	4	G	-4.848152E-03	-1.221903E-03	-1.489533E-03			
-CONT-	5	G	5.548466E-03	-1.318223E-02	-4.894407E-02			
-CONT-	6	G	-9.468717E-04	2.787626E-03	-1.519163E-03			
-CONT-	7	G	4.341153E-06	-6.345801E-03	-1.285914E-02			
-CONT-	8	G	3.782567E-04	6.665578E-07	-2.310222E-07			
-CONT-	9	G	-5.537350E-03	-1.316979E-02	-4.891899E-02			
-CONT-	10	G	-9.463490E-04	-2.786353E-03	1.518435E-03			
-CONT-	11	G	-5.448520E-03	2.118179E-03	-3.351427E-02			
-CONT-	12	G	-4.846938E-03	1.222401E-03	1.488583E-03			
-CONT-	13	G	5.244941E-02	8.087373E-02	6.713521E-02			
-CONT-	14	G	-6.135184E-03	5.574726E-03	-1.104952E-03			
-CONT-	15	G	7.262576E-02	1.017146E-01	8.397597E-02			
-CONT-	16	G	2.377849E-04	5.234983E-03	-8.206122E-03			
-CONT-	17	G	1.204326E-02	-8.974415E-02	-1.180302E-02			
-CONT-	18	G	8.195251E-03	2.106631E-03	-9.902306E-03			

	10	G	-2.960979E-06	-2.346913E-01	-6.604952E-02
-CONT-			1.083894E-02	-1.380762E-07	4.659697E-07
	11	G	-1.205062E-02	-8.972514E-02	-1.179475E-02
-CONT-			8.194841E-03	-2.107216E-03	9.903379E-03
	12	G	-7.263517E-02	1.017390E-01	8.398575E-02
-CONT-			2.366803E-04	-5.235758E-03	8.206557E-03
	13	G	-2.235898E-02	4.487815E-02	4.113846E-02
-CONT-			-3.094773E-03	-3.965825E-03	1.591355E-03
	14	G	-1.261065E-03	4.531831E-03	-7.059664E-03
-CONT-			-3.553450E-03	-1.022575E-03	-4.586026E-04
	15	G	1.401783E-03	-8.667372E-03	-2.401502E-02
-CONT-			-1.458688E-03	1.277847E-03	-3.088771E-04
	16	G	1.932342E-06	-6.657936E-03	-1.463335E-02
-CONT-			-2.670371E-05	5.049630E-07	-3.083256E-07
	17	G	-1.396861E-03	-8.658871E-03	-2.400097E-02
-CONT-			-1.458215E-03	-1.276911E-03	3.082694E-04
	18	G	1.266427E-03	4.541930E-03	-7.043384E-03
-CONT-			-3.552434E-03	1.023044E-03	4.579283E-04
	19	G	2.235969E-02	4.487806E-02	4.114283E-02
-CONT-			-3.093539E-03	3.965538E-03	-1.591763E-03
	20	G	2.454369E-02	4.300341E-02	4.117417E-02
-CONT-			5.598962E-04	4.276142E-03	-6.069619E-03
	21	G	2.590725E-03	-5.217077E-02	-1.530483E-02
-CONT-			5.774569E-03	1.613263E-03	-5.884990E-03
	22	G	-1.228893E-06	-1.196120E-01	-4.871749E-02
-CONT-			8.173604E-03	-2.246384E-07	3.650484E-07
	23	G	-2.593907E-03	-5.216019E-02	-1.529920E-02
-CONT-			5.774166E-03	-1.613670E-03	5.885750E-03
	24	G	-2.454748E-02	4.301555E-02	4.118017E-02
-CONT-			5.589365E-04	-4.276633E-03	6.069981E-03
	25	G	-6.147318E-03	1.966989E-02	1.898186E-02
-CONT-			-9.455173E-04	-2.843787E-03	1.217852E-03
	26	G	-1.416126E-03	4.684739E-03	2.337953E-03
-CONT-			-2.060431E-03	-9.149585E-04	2.700379E-04
	27	G	1.582625E-04	-3.838856E-03	-8.391727E-03
-CONT-			-1.152505E-03	4.988115E-04	3.739002E-04
	28	G	5.808650E-07	-4.547849E-03	-8.323602E-03
-CONT-			-1.244558E-03	3.423963E-07	-2.571190E-07
	29	G	-1.567858E-04	-3.834217E-03	-8.385442E-03
-CONT-			-1.152151E-03	-4.981656E-04	-3.743588E-04
	30	G	1.417671E-03	4.690167E-03	2.345125E-03
-CONT-			-2.059709E-03	9.153388E-04	-2.703653E-03
			147552E-03	1.967074E-02	1.898300E-03
			1.05E-04	2.843570E-03	-1.20E-03
				1.097286E-02	1.026904E-03
-CONT-	41	G	-2.485274E-04	-4.274079E-04	-2.808420E-04
	42	G	-2.646311E-04	1.718452E-03	8.442234E-04
-CONT-			-3.930575E-04	7.188318E-04	-9.481898E-04
	43	G	-6.781306E-05	3.764889E-03	2.928829E-03
-CONT-			-1.884632E-04	1.407725E-03	-1.197956E-03
	44	G	0.0	0.0	0.0
-CONT-			1.380401E-03	1.783945E-03	-1.786510E-03
	45	G	-8.523203E-04	-1.327321E-02	-9.775095E-03
-CONT-			2.623323E-03	1.175613E-03	-1.557995E-03
	46	G	-7.011329E-08	-1.914869E-02	-1.418656E-02
-CONT-			2.453898E-03	-1.490800E-07	7.237526E-08
	47	G	8.521762E-04	-1.327243E-02	-9.774450E-03
-CONT-			2.622999E-03	-1.175615E-03	1.558173E-03
	48	G	0.0	0.0	0.0
-CONT-			1.380087E-03	-1.783992E-03	1.786543E-03
	49	G	-5.827917E-08	-6.957762E-03	-7.683665E-03
-CONT-			1.055290E-03	5.520297E-08	-6.391639E-08
END					

Contour plots of power (in decibels) in the far field are included below; the first for thermal distortions and the second for deformations due to gravity. A similar plot for an undeformed parabola would show rings of concentric circles.





REFERENCES

- 1) Ludwig, A. C., "Computation of Radiation Patterns Involving Numerical Double Integration," IEEE Transactions on Antennas and Propagation, November, 1968.
- 2) Hyde, G., Korvin, W., and Price, R., "A Fixed Multiple Beam Toroidal Reflector Antenna Operating at Frequencies Above 12 GHz," IEEE International Conference on Communications, 1971, Conference Record, p. 27-11.

D

ANALYSIS OF A HOT ELEVON STRUCTURE

By H. W. Bergmann
North American Rockwell Space Division

and

James C. Robinson and Howard M. Adelman
NASA Langley Research Center

SUMMARY

The analysis of hot structures by the finite element method poses the problem of adequate structural modeling within the scope of existing computer programs for severe thermal gradients and also modeling provisions for thermal expansion. The paper describes an approach to the modeling and the subsequent analysis of a hot elevon test article. Solutions were obtained by the ASKA and the NASTRAN programs to evaluate some of their performance characteristics.

INTRODUCTION

The thermal environment of the Space Shuttle missions requires the design of major structural components either as thermally protected structures or as hot structures. From a series of trade and feasibility studies at the North American Rockwell Space Division, a particular design concept for a hot structure has evolved with sufficient potential to warrant its validation within the Space Shuttle Phase B Structural Test Program. For test purposes, the design concept has been applied to a section of the orbiter elevon.

In order to determine potential weaknesses of the design concept prior to the test, the structural response of the test article to mechanical and thermal loads was analyzed by the finite element displacement method. For comparison of performance characteristics of computer programs, solutions were obtained for essentially similar structural models with approximately the same number of degrees of freedom by both the ASKA program (ref. 1) operated on an IBM 360/85 and by the NASTRAN program (ref. 2) operated on a CDC 6600.

HOT ELEVON STRUCTURE

Test Article

The test article is 200 cm wide and 225 cm long and varies in depth linearly from 90 cm at the front to 50 cm at the rear. The overall configuration of the test article is shown in figure 1.

Preceding page blank

The structure consists basically of three ribs, a front and a rear spar, and sandwich-type top and bottom cover panels. The spars and ribs have corrugated webs and welded-on caps. The cover panels are connected to the spar and rib caps by riveting one flange of a Z-section to the edge of the inside face sheet, and the other flange of the Z-section to the rib or spar cap. The outside face sheet bears against, but is not fastened to, the caps. Details of this connection are included in figure 2.

The bending stiffness of the elevon is developed primarily by the rib and spar caps which are spliced at their intersections. Torsional stiffness is provided largely by the box-beam action of the rib and spar webs and the inside face sheets of the cover panels. The continuous connection to the caps and the stiffening effect of the core promote full utilization of the shear stiffness of the inside face sheets.

The ribs and spars and all Z-sections are made of René 41. The sandwich panel at the top as the elevon is mounted on the wing has 6Al-4V titanium face sheets and 3Al-2.5V titanium core. The bottom sandwich panel or hot surface consists of René 41 face sheets and Inconel 625 core.

The external supports of the structure are provided through fittings at the top and bottom cap of the center rib, and through a support at the rear of the center rib to prevent sideways.

The design concept reduces thermal stresses by holding temperature differences in adjacent parts of the structure to a minimum and by allowing unconstrained thermal deformations where temperature differences cannot be avoided. The thin outside face sheets, in particular, experience more severe thermal strains than the adjacent rib caps, but will deform more or less freely by virtue of their floating attachment and by the presence of the expansion slots indicated in figure 1.

Thermal strain compatibility between the inside face sheets of the panels and the more massive rib and spar caps is approached by spreading out the material in the cap configuration and by choosing the core depth such that the cap and inside face sheet temperatures increase at comparable rates. The fact that the cap temperatures rise slowly because of the heat sink property of the caps, and that the inside face sheet temperatures tend to lag because of the shielding effect of the outside face sheet, is of prime importance since the most severe temperature differences occur when the temperatures in caps and face sheets are still low, and the allowable stress levels accordingly high. The flexibility of the Z-sections adds to the relief of the thermal stresses in the face sheets. Thermal stresses in rib and spar webs are alleviated by the use of corrugations.

Analytical Model

The modeling of the structure was guided by the need to depict adequately the critical aspects of the design concept with a reasonable expenditure of time and effort. Accordingly, the hot René side of the structure was modeled

in considerable detail to investigate, in particular, the thermal-stress-relieving effect of the expansion slots, the attachment of the sandwich panels to the rib and spar caps, the flexing of the Z-sections, and the interaction between the Z-sections and the caps. The similarly constructed but much cooler titanium side, and the corrugated rib and spar webs, were conceived as support structures for the hot side. Their idealization was attempted in relatively coarse form as a series of membrane plates with flange members along their edges to represent the lumped rib and spar caps.

Figure 2 shows typical cross sections of the actual structure and figure 3, the idealized counterparts. Following standard practices, the face sheets of the sandwich panel were represented by quadrilateral membrane elements. The modeling of the core, lumped into a series of plates of equivalent thickness, as well as that of the corrugated webs, poses a more intricate problem. The individual elements must be capable of assuming curved shapes, such as that associated with pure bending, without exhibiting normal or shear stresses. This requirement precludes the use of quadrilateral membrane elements composed of constant-strain triangles, and, hence, quadrilateral membrane elements with linear stressfields were used in ASKA and rods and quadrilateral shear panels in NASTRAN. The bending stiffness of the idealized corrugated webs is simulated by suppressing the cap rotations about the intersections of caps and webs. In the modeling of the structure, no direct advantage of symmetry was taken. For simplification, however, the model was extended over only one of the two bays of the structure, but the complete center rib was included. For the analytical studies and the idealization shown in figure 3, the hot surface is the upper surface.

Boundary Conditions

The external supports of the structure require that, at the front end of the center rib, those translational degrees of the rib caps which do not interfere with free thermal expansion, be suppressed. Therefore, the upper cap in figure 1 is constrained against translation in all three directions and the lower cap is constrained against displacement in the plane normal to the stiffener connecting the upper and lower caps. At the rear end of the center spar, only the translation normal to the web is constrained to avoid sideway under load.

Loading Conditions

The loading conditions are thermal and mechanical and were applied without change of the boundary conditions. In loading case 1, the model was subjected to the temperature field indicated in figure 3. The cross section shown is typical for both the transverse and longitudinal direction. In loading case 2, the outside face sheet temperature of the panel was raised 222 K relative to the rest of the structure. Loading case 3 simulated a uniformly distributed pressure load on the panel. In loading case 4, a single concentrated load was applied at the rear end of the center rib; and in loading

case 5, a torsional moment was applied through two concentrated forces acting at the front and rear end of the outside rib.

The analysis was directed primarily at the response of the structure under loading condition 1. For economic reasons, the material properties were adjusted to these temperatures and maintained for all other loading conditions.

ANALYSIS BY THE ASKA PROGRAM

The analytical model consisted of (1) a sandwich panel with a slotted outside face sheet, (2) a frame combining the Z-sections and the rib and spar caps, and (3) a box assembly representing the rib and spar webs and the bottom side of the structure. The three parts were analyzed separately as substructures and subsequently reassembled as a hyperstructure.

Finite Element Model

Sandwich panel.- For the representation of both the face sheets and the lumped core, quadrilateral membrane elements with linear strain fields were chosen. The fineness of the nodal point grid was largely dictated by the aspect ratio limitation of the orthotropic core elements which retained good accuracy up to an element length-width ratio of 8. Pertinent details and a CRT plot of the modeled sandwich panel are shown in figure 4.

Frame assembly.- The frame assembly was modeled by triangular plate bending elements with cubic displacement fields for bending, and linear displacement fields for membrane deformations. The elements account for temperature differences through their thickness. In accordance with figure 3, only a portion of the caps was modeled as a plate, and the other portion lumped into a set of flange elements. The Z-section was simplified into an angle which is rigidly connected to the bottom of the cap. Figure 5 contains a CRT plot and other details of the modeled frame assembly.

Box assembly.- In close analogy to the sandwich core representation, the modeling of the corrugated rib and spar webs requires elements which can accommodate the extensional flexibility of such structures. Because of their taper and the varying temperature between the top and bottom caps, the modeling of the corrugated webs leads to additional problems which are most readily overcome by the use of linear-strain type quadrilaterals with orthotropic properties. These elements accept linear temperature variations between corner points and probably give reasonable accuracy even with relatively few nodal points. All of the rib and spar caps at the bottom side, including the Z-sections, were lumped into flange elements. By the nature of the attachment of the bottom sandwich panel, the inside face sheet as the major load-carrying component of the bottom panel, is represented by quadrilateral membrane elements. A CRT plot of the box assembly is shown in figure 6.

Hyperstructure. - In the subsequent joining process, the webs of the box were connected to the frame along the center line of the rib and spar caps, and the bottom face sheet of the sandwich panel to the horizontal leg of the frame angles. In both instances, membrane elements are tied to plate elements by declaring only the translations as common degrees of freedom. The top face sheet is not connected to the rib and spar caps. The structural stiffness matrix of the hyperstructure is of order 360 and almost fully populated.

Results

All ASKA computations were performed on the North American Rockwell Space Division's IBM 360/85 system in double-precision arithmetic. The maximum core requirement did not exceed 296,000 bytes.

Preceding the analysis of the composite model, a series of test runs was performed for the sandwich plate substructure to assess some of its characteristics.

In run 1, a temperature difference of 222 K between the face sheets of a nonslotted panel was imposed in the absence of any boundary constraints. The center deflection of the panel as determined by ASKA was 7.70 cm, which compares well with the value from the exact solution of 7.73 cm. Virtually no normal or shear stresses occurred in any of the elements. The solution involved a stiffness matrix of order 1,150 with semibandwidth of 129, and required a total of 155 CP seconds. In run 2, the analysis was repeated after providing knife-edge supports along the four edges of the panel. Even though the order of the stiffness matrix was reduced to 1,094, the solution required 164 CP seconds. Run 3 was performed after slotting the outside face sheet of the panel as indicated in figure 1. The additional nodal points were deliberately numbered such that the semibandwidth of the resulting stiffness matrix of order 1,292 increased to 1,205. The CP time for this case increased to 288 CP seconds. In run 4, finally, the semibandwidth was reduced to 174 through an internal renumbering routine and the solution obtained in 210 CP seconds.

The solution of the composite model was performed with restart provisions after the reduction of each of the substructures. The complete solution, including stress printout for all loading conditions, was obtained in 1,185 CP seconds. Figure 7 shows a summary of the CP requirements for the major processor steps.

The accuracy of the solution was tested against external equilibrium checks for loading conditions 4 and 5. In loading condition 4, the horizontal reactions at the front end of the center rib were found to deviate from the values required for equilibrium by 2.7 percent. In loading condition 5, the horizontal reactions were calculated with 0.9 percent deviation and the shear reaction with 0.2 percent deviation.

Figure 8 shows typical deflections of the analytical model under loading conditions 4 and 5, and the deflections calculated for the sandwich plate for

loading condition 2 are depicted in figure 9. The numbers in parentheses were obtained from NASTRAN; the results obtained from ASKA will be compared to the results obtained from NASTRAN in a subsequent section.

ANALYSIS BY NASTRAN

Finite Element Representation

The finite element representation used in the NASTRAN analysis is based on that of the ASKA analysis. Substructuring capability was not available in NASTRAN; consequently, the complete structure was analyzed in a single pass. However, for purposes of comparison with the ASKA model, the NASTRAN idealization of each of the three components will be discussed separately.

Sandwich panel.- The model of the sandwich panel is similar to that of figure 4. The grid spacing is exactly twice as fine as that of figure 4 because the ASKA element is a linear strain element, whereas the NASTRAN element is a constant strain element, which requires a finer grid for comparable accuracy. The face sheets are represented by constant strain quadrilateral membrane elements, and the core is represented by quadrilateral shear elements and rod elements. The latter elements provided the stiffness against vertical deformation of the core. The representation consists of 352 membrane elements, 426 shear elements, and 258 rod elements.

Frame assembly.- The frame assembly is modeled by triangular plate elements having both flexural and membrane stiffness, and by rod elements. This representation is identical to that used in the ASKA model (fig. 5). The plate element (CTRIA2) has first-order polynomials for the in-plane components of displacement and a third-order polynomial for the normal component. Temperature differences through the element are not accounted for. The frame representation contains 548 plate elements and 33 rod elements.

Box assembly.- The webs of the box assembly are modeled by a combination of shear elements for the vertical shear members and rod elements for the remaining vertical members. This representation consists of 38 shear elements and 38 rod elements. The bottom surface of the box assembly is modeled by 60 quadrilateral membrane elements and 33 rod elements.

Hyperstructure.- The components are joined by assigning the same grid point number to points which are attached. Boundary conditions are specified by use of single point constraints. After application of the constraints, the number of degrees of freedom in the structural model was 3179.

Results

All NASTRAN computations were performed on the Langley Research Center CDC 6600 computing system using a core allocation of 49152 (140,000 octal) 60-bit words. Two versions of NASTRAN were used. Level 12.1.0 is completely

in double precision and level 11.1.2, a nonstandard CDC 6600 version, uses single precision arithmetic, except in the stiffness matrix generation, where double precision is used.

A test run, similar to run 1 described in the ASKA discussion, was made with NASTRAN for a temperature difference of 222 K across the unslotted sandwich panel. The center deflection obtained by NASTRAN was 7.87 cm. This compared well with the prediction by ASKA of 7.70 cm and the exact solution of 7.73 cm. The finite element model had 1234 degrees of freedom and the solution required 360 central processor (CP) seconds using level 11.1.2 and 440 CP seconds using level 12.1.0.

The solution of the complete elevon model was performed in one pass. The results for the reaction forces were checked by a simple static force balance on a desk calculator and were correct to at least five significant figures. Some results of the NASTRAN analysis are shown (in parentheses) along with the ASKA results in figures 8 and 9.

Some deformations of the elevon for load case 5 shown in figure 8(b) agree reasonably well with the ASKA results at the rib and spar intersections, but appear to differ appreciably at the ends of the ribs. The deformations of the upper surface of the sandwich panel for load case 2 are shown in figure 9. In this case, the difference between the ASKA and NASTRAN results at the point of maximum deformation is about 12 percent. The reasons for the difference between the two solutions had not been determined at the time of publication of this paper, but it is felt that some difference existed in the models as a result of converting the input data from ASKA to NASTRAN.

The total computer central processor time required for the analysis of the complete elevon structure using NASTRAN level 11.1.2 was 2,276 seconds. The time required for each of the major steps is shown in figure 10. The total time of 1868 CP seconds (exclusive of the 408 seconds required for plotting) is roughly half again as much as the 1185 seconds required for the ASKA solution. The two analyses were run on different computers, which certainly has some influence on a direct time comparison. However, it appears that for the problem studied herein, ASKA was appreciably faster, perhaps because of its substructuring capability. It is, therefore, felt that this capability would be a desirable addition to NASTRAN.

CONCLUDING REMARKS

A static analysis was performed by both the ASKA computer program and NASTRAN to determine the deformation of a space shuttle hot elevon test article under thermal and mechanical loads. Detailed comparisons were made between running times of the two programs and also between results predicted by the two programs.

In general, the results from the two programs are in reasonably good agreement (with differences on the order of 12 percent), although some greater

discrepancies were noted. At publication time, the reasons for the differences have not been ascertained. It is felt, however, that small undetected errors may have accrued in the process of converting the input data from the ASKA format to that of NASTRAN.

The results of this study suggest that the substructuring capability of ASKA is helpful in reducing run time which justifies the current NASA plans to include this capability in NASTRAN.

REFERENCES

1. Schrem, E.; and Roy, J. R.: An Automatic System for Kinematic Analysis, ASKA Part 1. IUTAM Colloquium on High Speed Computing of Elastic Structures, University of Liege, Belgium, August 23-28, 1970.
2. Butler, Thomas C.; and Michel, Douglas: NASTRAN, A Summary of the Function and Capabilities of the NASA Structural Analysis Computer System. NASA SP-260, 1971.

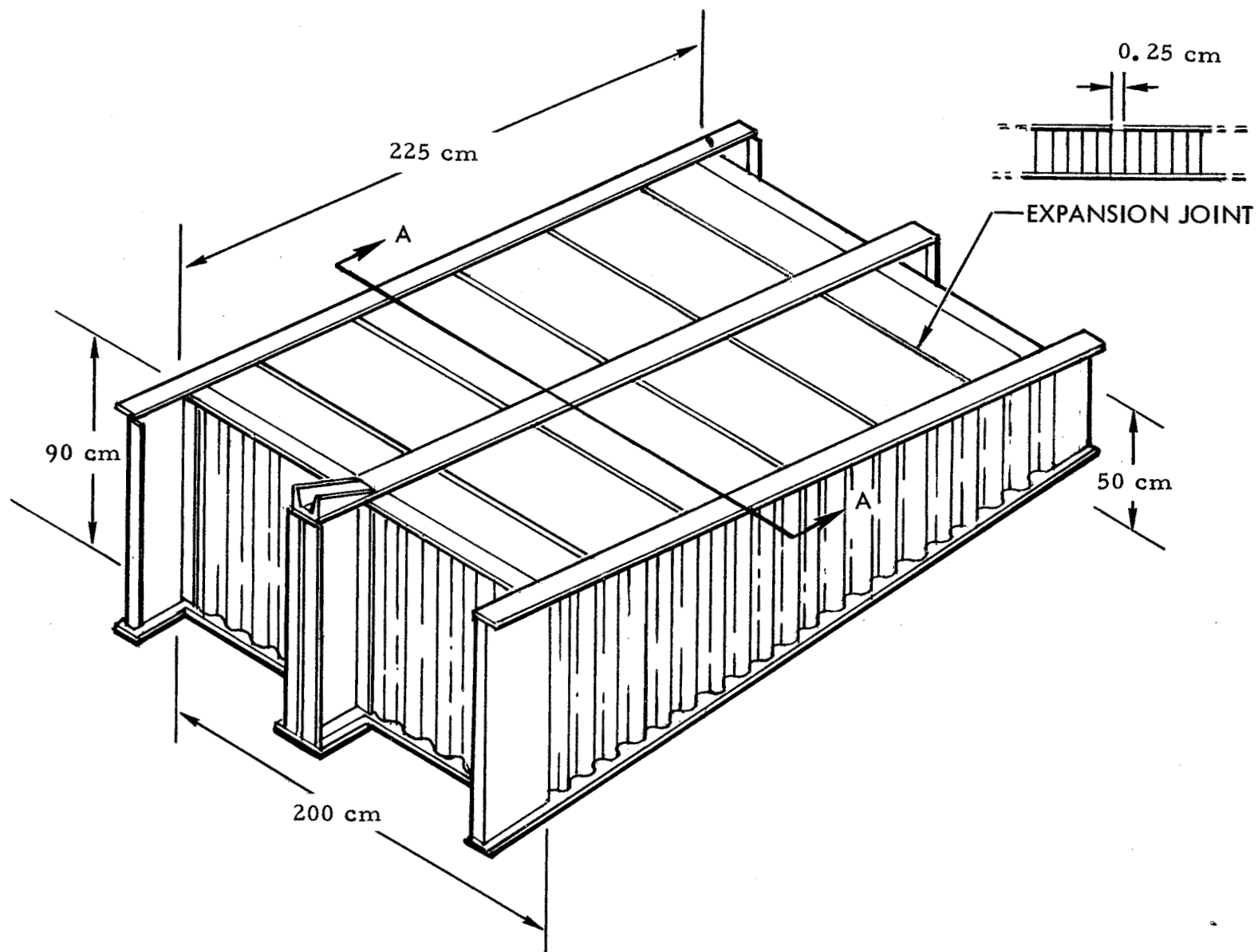


Figure 1.- Test article for hot elevator structure.

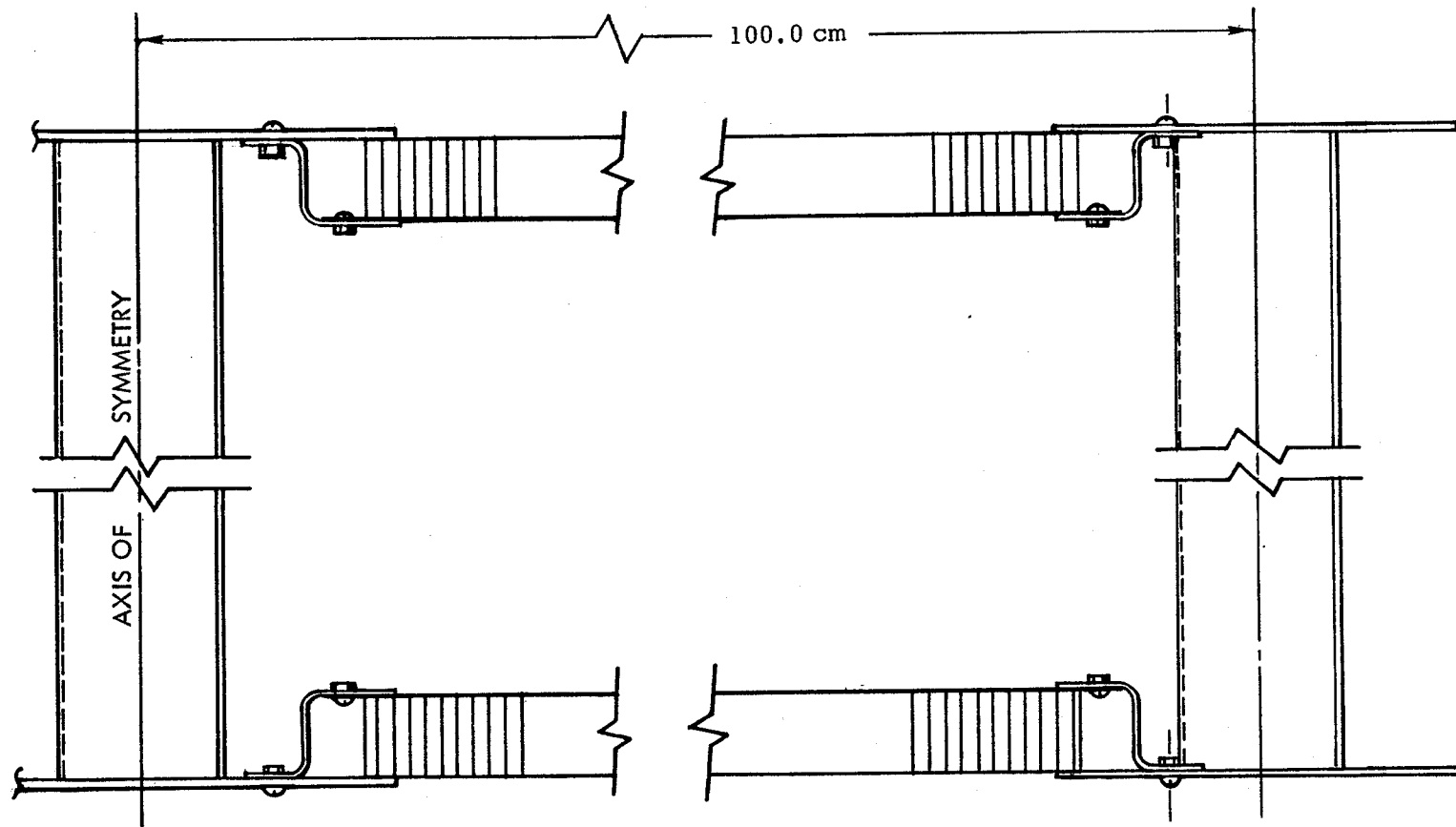


Figure 2.- Section A-A of test article.

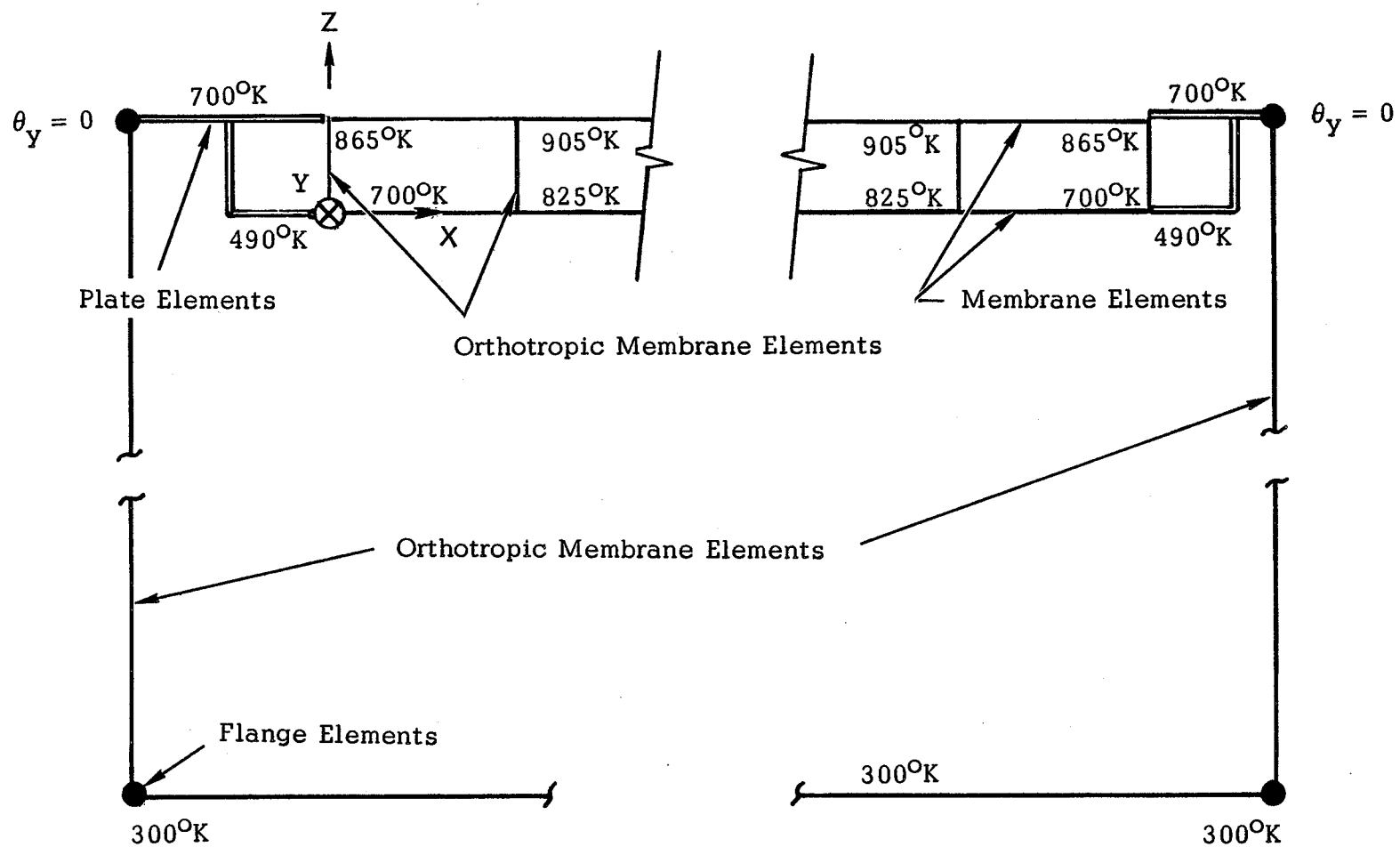


Figure 3.- Analytical model at section A-A.

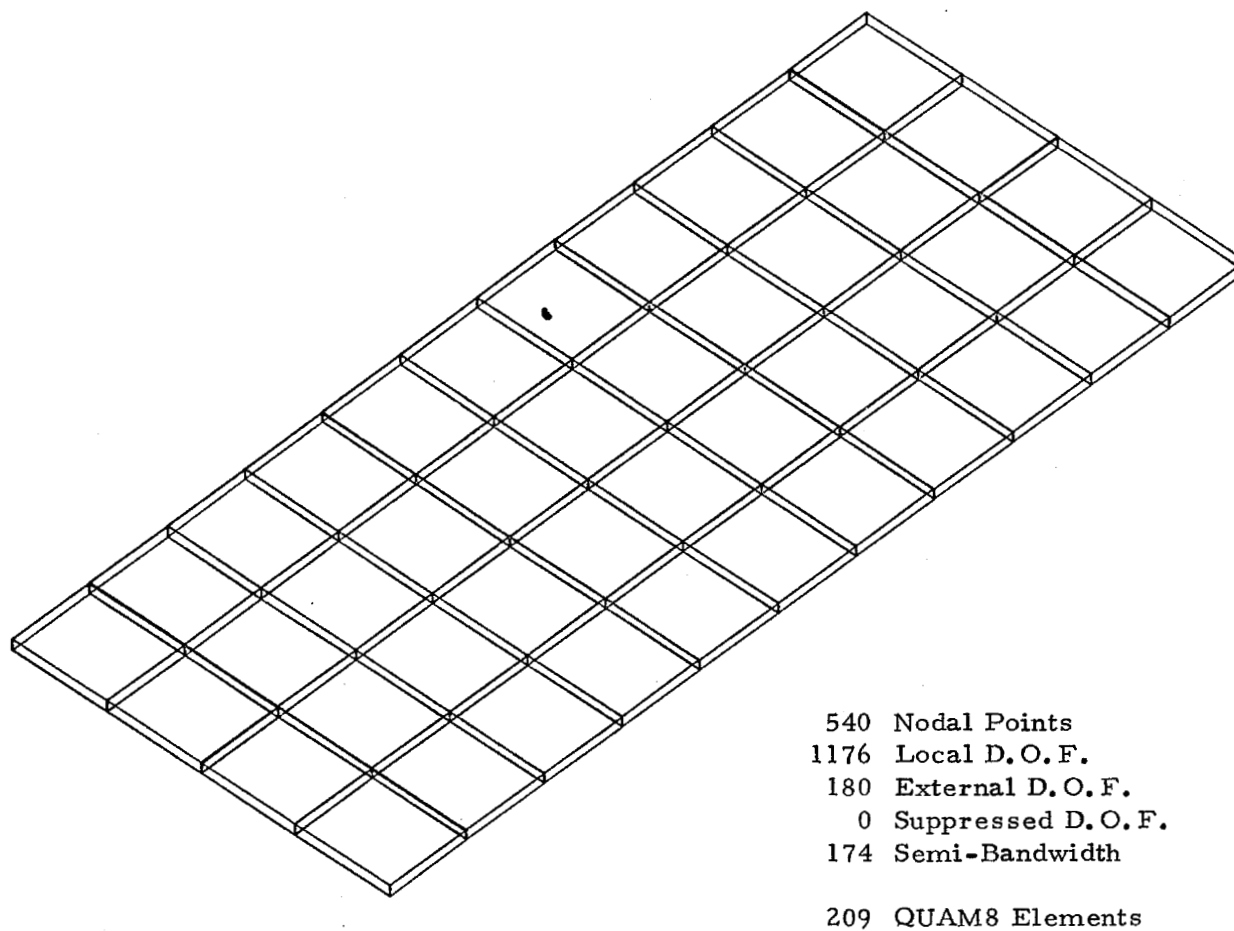
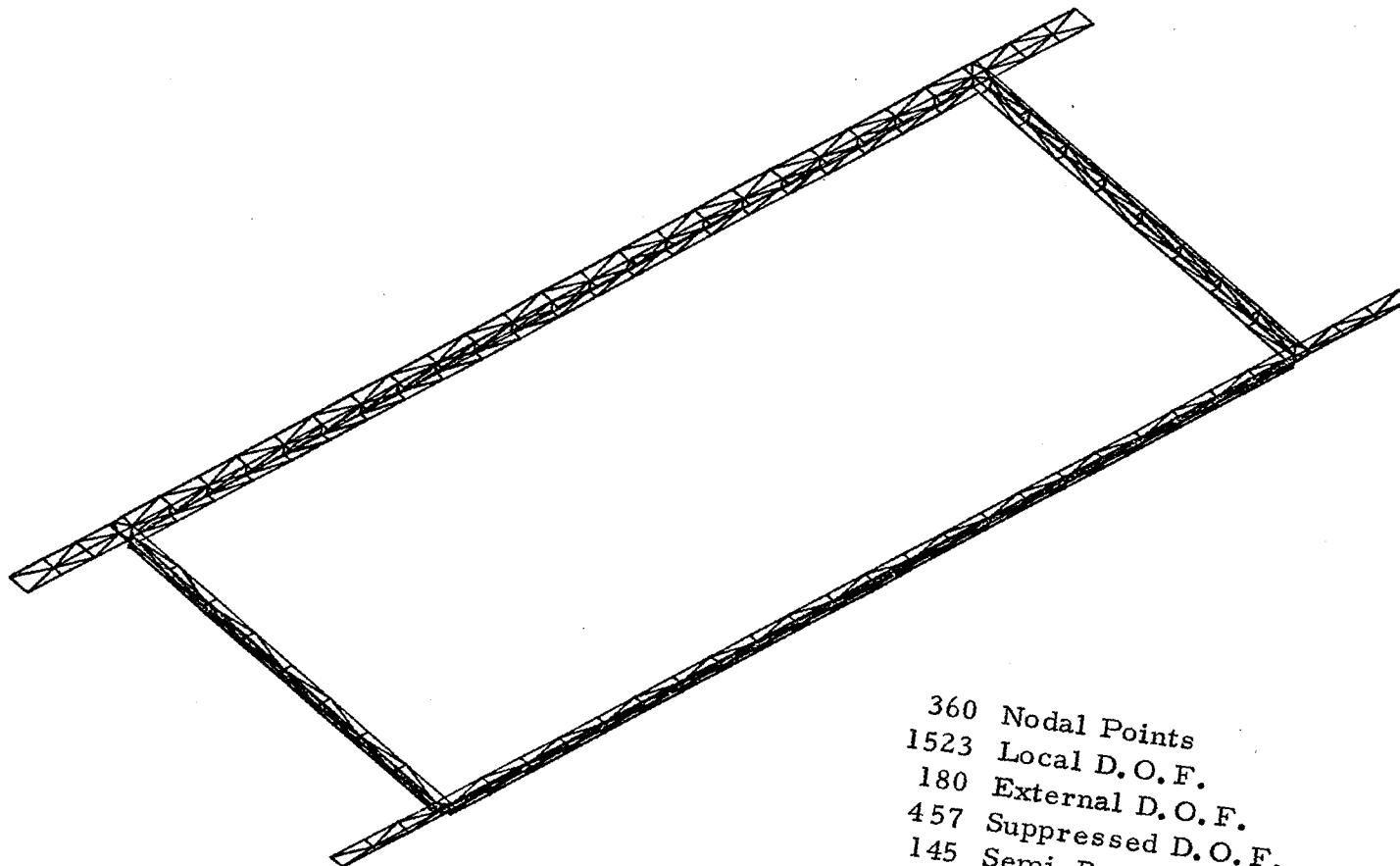


Figure 4.- Characteristics of substructure 1 - Sandwich Panel.



360 Nodal Points
1523 Local D.O.F.
180 External D.O.F.
457 Suppressed D.O.F.
145 Semi-Bandwidth
548 TRIB3 Elements
80 FLA2 Elements

Figure 5.- Characteristics of substructure 2 - Frame Assembly.

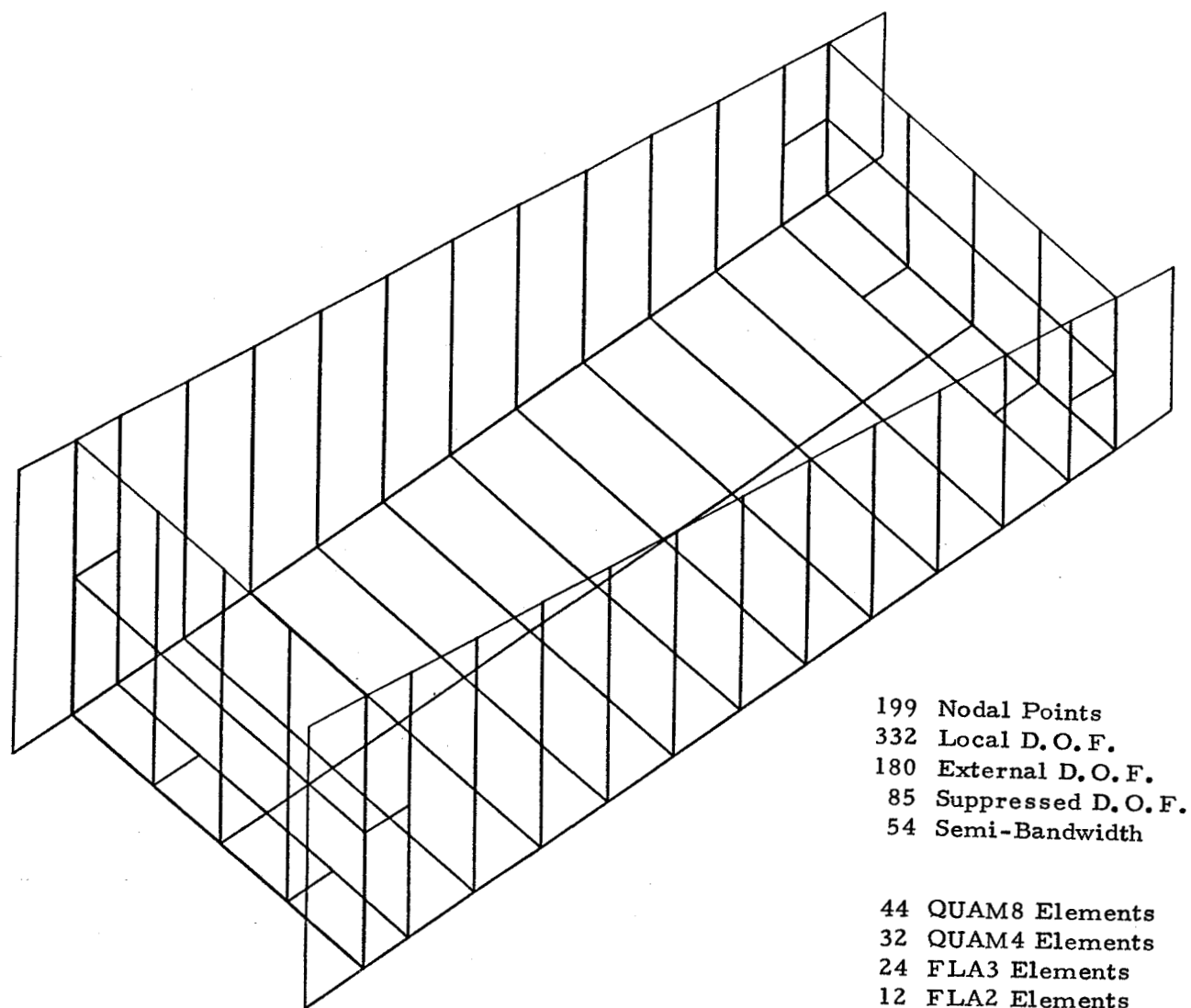
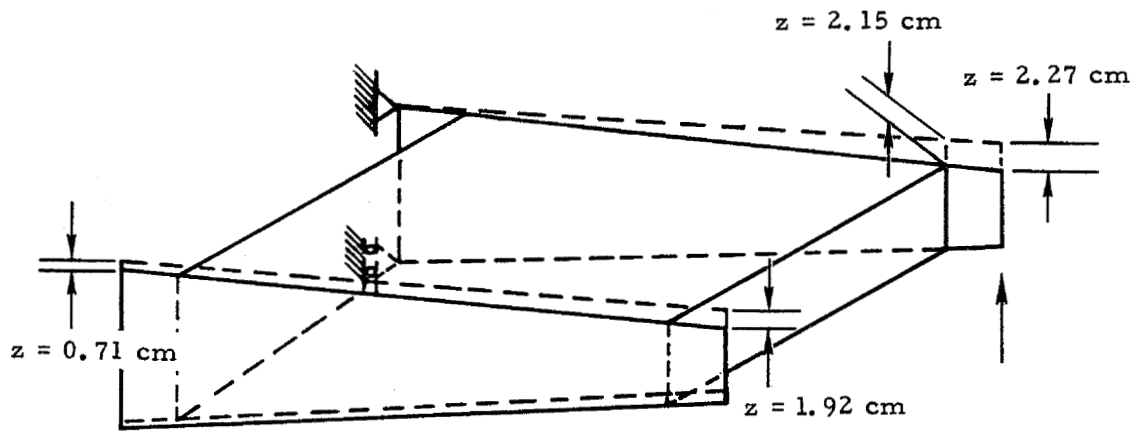


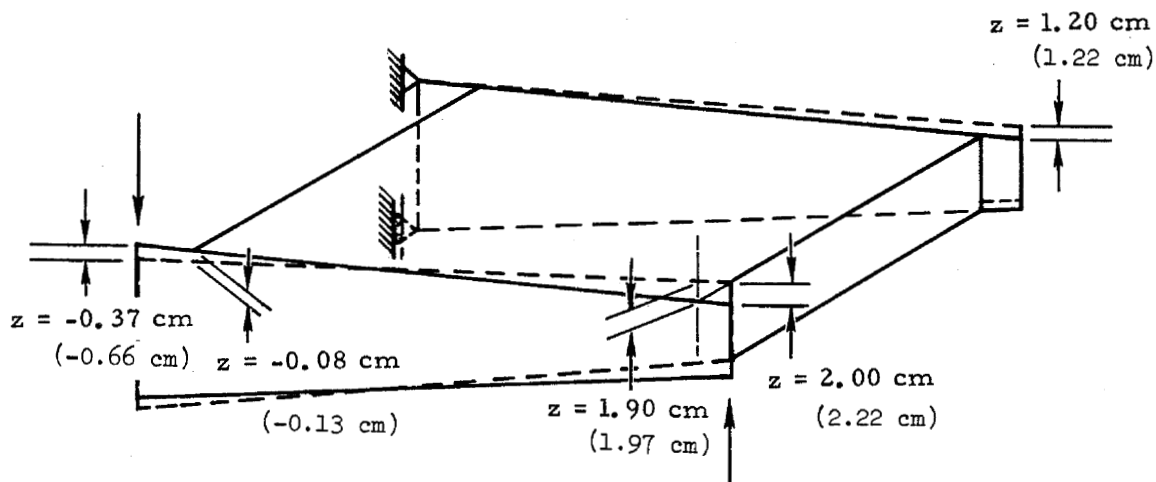
Figure 6.- Characteristics of substructure 3 - Box Assembly.

PROCESSOR STEP		CP TIME (SEC)			
		SUBSTRUCTURE NO. 1	SUBSTRUCTURE NO. 2	SUBSTRUCTURE NO. 3	HYPER- STRUCTURE
SK	ELEMENTAL STIFFN MATRICES	13	51	6	
BK	STRUCTURAL STIFFN MATRIX	39	87	10	
BR	LOAD MATRIX	17	15	8	
TRIA	TRIANGULARIZATION	36	26	2	
BTLC	INVERSE TRANSFORMATION	73	119	10	
SKM	REDUCTION OF STIFFN MATRIX	41	169	13	
SAV	SAVE DATA	18	31	5	
BKM	HYPERSTRUCT STIFFN MATRIX				39
TRIA	TRIANGULARIZATION OF BKM				38
SOLV	HYPERSTRUCT DISPLACEMENTS				6
SRLC	SUBSTRUCTURE DISPLACEMENTS	16	22	3	
ST	ELEMENTAL STRESSES	15	30	6	
BRR	EQUILIBRIUM CHECK	20	46	8	
REAC	REACTIONS	1	3	2	

Figure 7.- Computation time for major processor steps for ASKA.

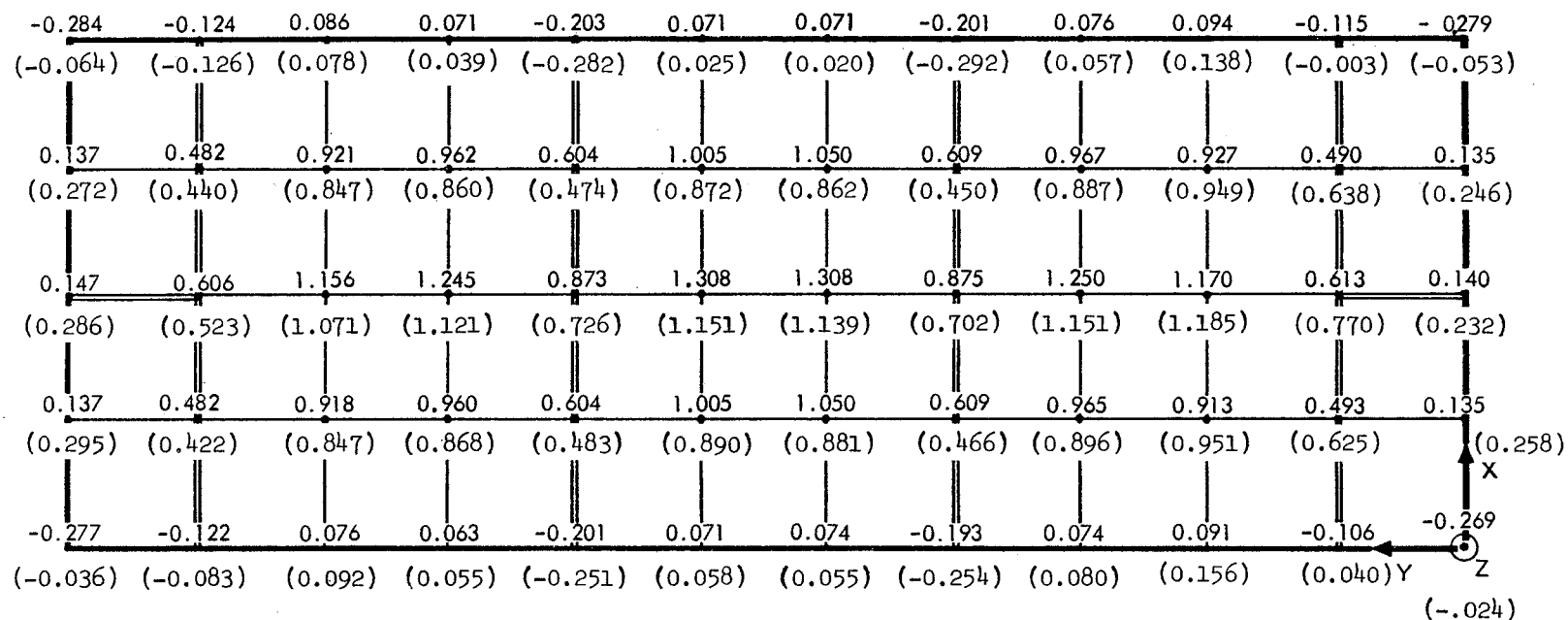


(a) Loading condition 4.



(b) Loading condition 5.

Figure 8.- Calculated deflections obtained from ASKA and NASTRAN. Quantities in parentheses were obtained from NASTRAN.



Loading condition 2

Figure 9.- Normal (Z) displacements of slotted sandwich panel calculated from ASKA and NASTRAN for loading condition 2. Displacements are in centimeters. Quantities in parentheses were obtained from NASTRAN.

PROCESSOR STEP		CP TIME (SEC)
		LEVEL 11.1.2
SEMI	NASTRAN PREFACE	117
	UNDEFORMED STRUCTURE PLOT	51
TAI	TABLE ASSEMBLER	30
SMA	STRUCTURAL MATRIX ASSEMBLER	481
SCEI	CONSTRAINT ELIMINATOR	50
RBMG	DECOMPOSITION	623
SSG1	LOAD MATRIX	153
SSG3	DISPLACEMENTS (INDEPENDENT)	180
SDR1	DISPLACEMENTS (DEPENDENT)	34
SDR2	ELEMENTAL STRESSES	135
PLOT	DEFORMED STRUCTURE PLOT	357

Figure 10.- Computation time for major processor steps for NASTRAN.

NASTRAN MODELING STUDIES IN THE NORMAL-MODE METHOD AND NORMAL-MODE SYNTHESIS

By Roy Leon Courtney

NASA Goddard Space Flight Center

SUMMARY

The results of finite-element and analytic solutions of the normal modes of a uniform beam under various end conditions are compared. The normal modes of a single component are synthesized to represent different single-component and multi-component structures. The results are compared for accuracy with the analytic structural solutions. Guidelines for finite-element structural modeling are developed which determine the minimum number of elements required to obtain specified levels of accuracy in normal-mode analysis and synthesis. The finite-element modeling studies are implemented on NASA's NASTRAN structural analysis computer program. Modeling techniques that represent a part of a structure by its normal modes in a computer structural analysis are presented.

INTRODUCTION

Problem Statement

The normal-mode method of structural analysis has been developed into a powerful tool in the analysis of large and complex aerospace structures. The value of this method lies in the fact that the simultaneous differential equations of motion which describe the linear dynamic characteristic of a structure are decoupled into independent differential equations when the displacements are expressed in terms of the normal modes. A normal or natural mode of vibration occurs when each point in the structure executes harmonic motion about a point of static equilibrium, with every point passing through its equilibrium position at the same instant and reaching its maximum displacement at the same instant. The form of the displacement of a structure is known as the normal-mode shape, and the frequency of the harmonic motion is known as the normal-mode frequency. Additionally, normal-mode shapes and frequencies are used to compute the modal properties of generalized mass, stiffness, and structural damping associated with the modes. NASA has prepared a general review and useful

bibliography of normal-mode analysis (Reference 1). Application of this method of analysis to space vehicles and a bibliography of both analytical and applied references are presented in References 2, 3, and 4.

There are basically two numerical methods of approach to the problem of determining the normal modes of structural systems: An exact problem formulation solved approximately and an approximate formulation solved exactly. For certain simple systems the exact solution for normal modes can be obtained by analytical methods. For complex structures, an approximate model of the problem defined by finite elements can be solved for an exact solution by using digital computers.

The technique of normal-mode synthesis is a process whereby the dynamic characteristics of the several components of the system are calculated separately and then brought together to evaluate the dynamic characteristics of the entire system, thereby increasing computer efficiency. Another major advantage of the normal-mode-synthesis technique is that the modal data may come from such diverse sources as analytic solutions, finite-element analyses, and vibration tests designed to determine normal modes. Thus, one structural analysis using modal synthesis can incorporate the representation of individual substructures analyzed by completely different techniques by separate engineering groups that may never have conferred about the complete structure.

The concept of modal synthesis is founded on the principle that a substructure is completely (or adequately) represented by its primary modes; if this is true, then the connections of these substructures at their interfaces can be described in terms of the modal quantities of the components. A set of equations can be written with coordinates in terms of normal-mode shapes and modal factors of the components. Solving these equations for the amplitude factors and multiplying by the component modes yields system modes.

Several investigators have developed complete methods of analysis by substructures; these methods incorporate the concept of normal-mode synthesis. Gladwell (Reference 5) developed the branch mode method of vibration analysis, which involves the imposition of a sequence of constraints on the system so that in each constrained system or branch only a few adjoining components vibrate in modes, called branch modes. These branch modes and appropriate rigid-body modes are used in a Rayleigh-Ritz analysis of the complete system. Craig and Bampton (Reference 6) extended the branch mode method to systems having highly redundant substructure boundaries.

Hurty (References 7 and 8) presented the method of component-mode synthesis in which the vibration modes of the composite structure are synthesized from generalized coordinates that are defined by a finite number of displacement modes for each component structure. These displacement modes are generated in three categories: Rigid-body, "constraint" modes, and "normal" modes.

MacNeal (Reference 9) devised a general solution to the problem of representing a part of a structure by its vibration modes when some or all of its connection points to the rest of the structure are restrained during measurement or calculation of substructure modes. This procedure is incorporated in the present study.

In this report the basis of normal-mode analysis and normal-mode synthesis is presented and modeling studies using finite elements and modal synthesis for structural problems are evolved, performed

on NASTRAN* (Reference 10), and compared to known analytic solutions for accuracy. The purpose of these studies is threefold:

- (1) To compare the results of the normal-mode solutions of structural problems analyzed by finite-element and other methods for accuracy.
- (2) To develop guidelines for efficient finite-element modeling so that required accuracies will result from the analysis.
- (3) To investigate modeling techniques in representing a part of a structure by its normal modes as implemented on a structural-analysis computer program.

METHOD OF ANALYSIS

Normal-Mode Analysis

In the normal-mode or modal method of dynamic problem formulation, the vibration modes of the structure in a selected frequency range are used as the degrees of freedom. Thus the number of degrees of freedom is reduced while the accuracy in the selected frequency range is maintained. In the direct method, the degrees of freedom are simply the displacements at connection points between substructures.

The advantage of the normal-mode method lies in the fact that the differential equations of motion of the structure are decoupled when the displacements are expressed in terms of the normal modes. Thus, a structure with n degrees of freedom may be expressed by n independent differential equations rather than by a system of n simultaneous differential equations.

The modal method of dynamic problem formulation is important in maximization of computational efficiency in certain types of problems. This method will usually be more efficient in problems where a small fraction of the modes are sufficient to produce the desired accuracy in the range of interest and where the stiffness matrix used in the direct method is not well banded. For problems without dynamic coupling, i.e., for problems in which the matrices of the modal formulation are diagonal, the modal method will frequently be more efficient, even though a large fraction of the modes are needed (Reference 10).

Eigenvalue Analysis

Eigenvalue analysis yields structural vibration modes from the symmetric mass and stiffness matrices, $[M_{aa}]$ and $[K_{aa}]$, generated by static analysis. The eigenvectors and eigenvalues produced by this analysis may be used to generate modal coordinates for further dynamic analysis.

The general form of the eigenvalue problem for vibration modes is

$$[K_{aa} - \lambda M_{aa}]\{u_a\} = 0, \quad (1)$$

*Nasa STRuctural ANalysis.

where $\{u_a\}$ is the displacement vector and the eigenvalues $\lambda_i = \omega_i^2$ are the squares of the natural frequencies. The results of the calculation are the eigenvalues and corresponding eigenvectors, $\{\phi_{ai}\}$, normalized so that the largest element of each eigenvector is unity.

The eigenvalue extraction method used in the present analysis is called the inverse power method with shifts, a particularly effective method of analysis for problems formulated by the displacement approach when only a fraction of all of the eigenvalues are required. Section 10.4 of Reference 10 gives a complete description of the theory and application of this method as implemented in NASTRAN.

Normal-Mode Synthesis

The normal-mode synthesis technique in structural analysis permits part of a structure to be described by its orthogonal vibration modes. In some instances structural information may not be available in other forms. Thus, normal-mode information derived from diverse sources, including vibration tests and other analyses such as energy methods and finite elements, may be combined in one structural analysis. Normal-mode synthesis has been found useful in many practical situations (Reference 2).

Section 14.1 of Reference 10 develops the modeling technique utilized in the present study, whereby a part of a structure is represented by its vibrational modes. This development is summarized below.

Description of part of a structure by vibration modes requires knowledge of how the connection points between parts of the structure were supported when the vibration modes were measured or computed. Three cases are distinguished:

- (1) All connection coordinates free.
- (2) All connection coordinates restrained.
- (3) Some connection coordinates free and some restrained.

The first condition is usually employed in vibration tests or analyses of large parts. Often it is not possible to achieve effectively unrestrained test conditions; however, unrestrained conditions can be obtained from calculated modes. For Case 1, the required data are the vibration mode frequencies, ω_i , the mode shapes of eigenvectors, $\{\phi_i\}$, and the mass distribution of the part, expressed by the mass matrix $[M_p]$. The eigenvectors need not be normalized in any particular manner. Let the degrees of freedom at the points of connection to the remainder of the structure be designated by the vector $\{u_c\}$. Then the motions of these points are related to the modal coordinates, $\{\xi_i\}$, of the part by

$$\{u_c\} = [\phi_{ci}]\{\xi_i\}. \quad (2)$$

The columns of $[\phi_{ci}]$ are the eigenvectors, $\{\phi_i\}$, abbreviated to include only the degrees of freedom at the connection points, $\{u_c\}$. The usual approximation of including only a finite number of eigenvectors in $[\phi_{ci}]$ produces an idealized model for the part that is too stiff. Specification of the part is completed

by calculation of the generalized mass, m_i , stiffness, k_i , and damping, b_i , associated with each modal coordinate, ξ_i , as follows:

$$m_i = \{\phi_i\}^T [M_p] \{\phi_i\}, \quad (3)$$

$$k_i = \omega_i^2 m_i, \quad (4)$$

and

$$b_i = g_i m_i \omega_i, \quad (5)$$

where g_i is a damping factor for the i th mode. Frequently g_i will not be accurately known.

The equation of motion for the generalized coordinate, ξ_i , is

$$(m_i p^2 + b_i p + k_i) \xi_i = \{\phi_{ci}\}^T \{f_c\}, \quad (6)$$

where p is the differential operator, $\{f_c\}$ is the vector of forces applied to the substructure at the connection points, and $\{\phi_{ci}\}$ is the eigenvector $\{\phi_i\}$ abbreviated to include only the degrees of freedom at connection points.

Equations (2) through (6) contain all of the information required to describe the part. In the construction of the idealized model, each of the rows of Equation (2) is regarded as an equation of constraint between a constrained degree of freedom, u_c , and the generalized coordinates, $\{\xi_i\}$. The generalized mass, stiffness, and damping elements connected to ξ_i are m_i , k_i , and b_i , respectively. Figure 1 illustrates the interconnection of the elements in diagrammatic form.

The derivation of an idealized model for Cases 2 and 3, in which some or all of the connection points are restrained during measurement or calculation of the substructure modes, is considerably more involved. A general solution devised by MacNeal (References 9 and 10) is developed in Section 14.1 of Reference 10.

MODELING STUDIES

Normal-Mode

Description

The structural problem chosen to compare the accuracy of solutions obtained by different methods is the determination of the normal modes of vibration of a constant-property beam with various end conditions. Vibration transverse to the axis of the beam is considered in only one plane. Damping and axial vibration are neglected.

The analytic method for the determination of the natural frequencies and modes of vibration of a beam and a detailed derivation of the corresponding characteristic functions are given in standard texts (References 11 and 12) on structural dynamics. Young and Felgar (Reference 13) tabulated the solution of the characteristic functions of this problem, with vibrations governed by the well known differential equation

$$EI \frac{\partial^4 y}{\partial x^4} - \rho \frac{\partial^2 y}{\partial t^2} = 0, \quad (7)$$

where x and y are the coordinates parallel and perpendicular, respectively, to the longitudinal axis of the beam; t is time; E is the modulus of elasticity; I is the moment of inertia; and ρ is the mass per unit length of the beam. Each of the functions for a given beam satisfies the differential equation

$$\frac{d^4 \phi_n}{dx^4} = \beta_n^4 \phi_n \quad (8)$$

and also satisfies the boundary conditions corresponding to the end conditions of the beam. In Equation (8) β_n is the characteristic number and $\phi_n(x)$ is the characteristic function for each type of beam. The natural circular frequency of the n th mode of vibration of the beam, ω_n , is given by

$$\omega_n = \beta_n^2 \sqrt{\frac{EI}{\rho}} = (\beta_n l)^2 \sqrt{\frac{EI}{\rho l^4}}, \quad (9)$$

where l is the length of the beam. These results are assumed to be the "known" solution to which the finite-element results are compared for accuracy.

The specific element used in the present modeling study is identified in NASTRAN by the mnemonic, CBAR, denoting the "connection, bar" element (Figure 2) that undergoes extension, torsion, bending in two perpendicular planes, and the associated shears. Section 5.2 of Reference 10 presents the detailed analytic description of this finite element.

The uniform beam is represented by four different finite-element models consisting of 5, 10, 20, and 40 elements, respectively, to ascertain the effect of the number of elements upon the accuracy of results. For ease in correlation of finite-element and differential equation results, beam properties were chosen to reduce to 1 the value of the terms within the radical in the second expression for ω in Equation (9). Figure 3 shows the four beam models. Thus, the natural frequency in radians per second of the n th mode resulting from the eigenvalue analysis of the finite-element formulation is directly comparable to the term $(\beta_n l)^2$ of Equation (9) as tabulated in Reference 13 for various beam types.

Free, supported, and clamped beam end conditions are combined to obtain six different types of beams: (1) Free-free, (2) free-supported, (3) free-clamped, (4) supported-supported, (5) supported-clamped, and (6) clamped-clamped.

Implementation

The normal-mode modeling study is implemented on the NASTRAN computer program, Release 11.1, which is operational on the IBM System 360/95 at Goddard Space Flight Center. NASTRAN embodies a lumped-element approach, whereby the distributed physical properties of a structure are represented by a model consisting of a finite number of idealized substructures or elements that are interconnected at a finite number of grid points, to which loads are applied. All inputs and outputs pertain to the idealized structural model.

The structural problem is defined by encoding the coordinate-system definition (CORD2R)*,

*NASTRAN mnemonics.

grid-point definition (GRID), element connections (CBAR), element property and materials (PBAR, MAT1), and method of eigenvalue extraction (EIGR), as prescribed by Reference 14.

The problem thus defined undergoes eigenvalue analysis using the inverse power method with shifts, which computes the following for each of the modes analyzed: eigenvalue, eigenvector normalized to the maximum displacement, natural frequency in radians per second and cycles per second, generalized stiffness, and generalized mass.

Normal-Mode Synthesis

General

The results of the normal-mode analysis provide a basis for solution of the following problems by synthesis of the normal modes of the constituent parts, i.e., by representing a part of a structure by its vibration modes. The eigenvectors and generalized properties of the first i modes of the beam with free-free end conditions are used in the application of the theory developed earlier for normal-mode synthesis.

Single-Component Structure

The structural problem chosen to demonstrate the synthesis of normal modes and to investigate the accuracy of the technique is the determination of the normal modes of a uniform cantilevered beam, i.e., a beam with fixed-free end conditions. The beam consists of a single component modeled by the modal properties of a beam with free-free end conditions. The first i free-free normal modes are selected to model the beam, where i must include the first two modes that are rigid-body modes. The generalized stiffness given by Equation (4) is zero for rigid-body modes since the natural frequency is zero. The various values of i selected include the two rigid-body modes plus arbitrarily selected flexible modes. The source of the modal information is the four finite-element models used in the normal-mode analysis, which consisted of 5, 10, 20, and 40 elements, respectively. Thus, for example, in the 10-element model the first i modes were used, where $i = 3, 5, 6, 9$, and 11. The following section presents the numerical results and compares them to known solutions for the modes of the cantilevered beam.

Implementation of the normal-mode synthesis on the NASTRAN program requires the declaration of the following for each mode used to model the structural part: (1) Scalar point (SPOINT), which is a point in vector space at which one degree of freedom is defined, (2) scalar mass (CMASS4) and stiffness connection (CELAS4) elements whose values are the generalized mass and stiffness, and (3) the coefficients of the matrix $[\phi_{ci}]$ of Equation (2), the columns of which are the eigenvectors of the i th mode, truncated to include only the degrees of freedom at the connection points. The scalar points become the generalized coordinates and degrees of freedom for the analysis. The relationship given by Equation (2) is declared in NASTRAN by a multipoint constraint equation (MPC).

Simulation of restrained end conditions of the beam is most easily accomplished by the connection of a spring (CELAS2) of very large spring constant, e.g., 10^{12} N/m (10^{10} lb/in.), at the connec-

tion points between ground and the restrained degrees of freedom. Figure 4 shows a representation of the model used for normal-mode synthesis of a single cantilevered beam.

Multiple-Component Structures

The modeling techniques described for a single-component structure are extended to structures with multiple components. In each problem formulation, the required modal information for each substructure is identical to that required in the preceding structure. Boundary conditions of the multiple-substructure problem are handled in the same manner as the end conditions of a single-element cantilever beam. Connections between adjoining substructures are made by declaring a scalar spring element (CELAS2) with a very large spring constant between appropriate translational and rotational degrees of freedom.

Structural normal modes are obtained by the normal-mode-synthesis technique as applied to the following structures, each divided into more than one substructure: (1) Three beams in series, cantilevered, (2) three beams in parallel, cantilevered, and (3) three beams in a portal arch. Figure 5 shows sketches of these structures. The next section presents the comparison of the results of the modeling study and the known solution as given by Equation (9) for the first and second structures and by a 120-finite-element model for the third structure.

ANALYSIS OF MODELING STUDIES

Normal-Mode Analysis

Values and units for the parameters required for the finite-element models described in the previous section are chosen as follows:

Modulus of elasticity	$E = 6.9 \times 10^{11} \text{ N/m}^2 (10^8 \text{ lb/in.}^2).$
Poisson's ratio	$\nu = 0.3.$
Mass per unit length	$\rho = 6.9 \times 10^3 \text{ N-sec}^2/\text{m}^2 (1.0 \text{ lb-sec}^2/\text{in.}^2).$
Area moments of inertia	$I_{1,2} = 41.6 \text{ cm}^4 (1.0 \text{ in.}^4).$
Cross-sectional area	$A = 6.5 \text{ cm}^2 (1.0 \text{ in.}^2).$
Torsional constant	$J = 41.6 \text{ cm}^4 (1.0 \text{ in.}^4).$
Length	$l = 254 \text{ cm} (100 \text{ in.}).$

Thus, the four models of the uniform beam consist of 5, 10, 20, and 40 bar elements, whose elemental lengths are 50.8, 25.4, 12.7, and 6.4 cm (20, 10, 5, and 2.5 in), respectively (Figure 3). As previously stated, this choice of parameter values permits direct comparison of the results of the eigenvalue analysis with those tabulated in Reference 13.

The complete matrix of problems studied consists of the four finite-element models solved for each of the six end conditions: (1) Free-free, (2) free-supported, (3) free-clamped, (4) supported-supported, (5) supported-clamped, and (6) clamped-clamped. Table 1 lists the numerical results of the eigenvalue analysis for the free-free end condition; Reference 15 records the numerical results for the remaining five conditions. Recorded data include—

- (1) Mode number, $i = 1, 2, 3, \dots, 20$.
- (2) Natural circular frequency of the i th mode of vibration of the beam in radians per second for the known solution given in Reference 13.
- (3) Accuracy, A , defined as the ratio of the finite-element solution to the known solution. This definition of accuracy shall be maintained throughout the analysis of results.

In general, if n is the number of unrestrained, independent degrees of freedom of the problem, then n normal modes exist. For example, six grid points are required to model the 5-element beam. For the free-free type beam, $n = 6$. These consist of two rigid-body modes and four flexible modes. Supporting one end of the beam reduces n by one and results in one rigid-body mode and four flexible modes. Clamping one end prohibits rigid-body motion. In Table 1, only flexible modes are recorded.

Table 1—Uniform beam with free-free end conditions.

Mode number	Frequency of known solution (rad/sec)	Accuracy, A			
		$N = 5$	$N = 10$	$N = 20$	$N = 40$
1	22.373	0.893	0.970	0.992	0.998
2	61.673	.838	.951	.987	.997
3	120.90	.796	.933	.982	.995
4	199.86	.734	.916	.977	.994
5	298.56		.900	.972	.993
6	416.99		.883	.967	.992
7	555.16		.857	.962	.990
8	713.08		.815	.957	.989
9	890.73		.743	.951	.988
10	1088.1			.945	.986
11	1305.3			.939	.985
12	1542.1			.930	.983
13	1798.7			.919	.982
14	2075.1			.905	.980
15	2371.2			.886	.979
16	2687.0			.860	.977
17	3022.6			.826	.975
18	3377.9			.783	.973
19	3752.9			.730	.971
20	4147.7				.969

Figure 6, a representative of the data recorded for the six end conditions, shows the normal-mode results for modes 1, 2, 3, 4, 5, 9, and 15 of the free-free type of beam. The coordinates of the figure are the number of finite elements in the model, N , versus the accuracy, A , of modal frequency, defined above. In general, accuracy approaches 1.0 asymptotically from below as the number of elements increases. The plot passes through the origin, since zero finite elements result in zero accuracy. This relationship is expressed by

$$N = \tan [Af(i, c)] , \quad (10)$$

where N is the number of elements in the model, $f(i, c)$ is a function of the mode number, i , and c is an angular constant.

Equation (10) can be used to estimate the number of finite elements required to model the beam for selected values of mode number, i , desired minimum accuracy, A , and beam end conditions. For example, for the beam with free-free end conditions, when

$$N > i + 2 , \quad (11)$$

these parameters determined by curve-fitting the empirical data are defined as

$$\begin{aligned} f(i, c) &= c + i \\ \text{and} \quad c &= 87.7 \text{ deg} . \end{aligned} \quad (12)$$

For $A = 0.90$ and $i = 2$, Equation (10) yields $N = 6.1$; when rounded to the next highest integer, $N = 7$. This estimate is verified by Figure 6.

A comparison of accuracies for both mode numbers and finite-element models as recorded in Table 1 reveals a general trend in the accuracy of the finite-element solution. For a specific mode number or for a specific number of finite elements in the beam model, a reduction in the degrees of freedom at the ends of the beam results in increased accuracy of the solution. This observation is explained by the fact that a decrease in freedom of the structure at the boundary requires a given number of elements to describe less complex displacements in the eigenvector, i.e., less difference in the end displacements of individual elements. Therefore, Equations (10), (11), and (12), when applied to beams with increased end fixity, represent overestimates of the minimum number of elements that will yield specified accuracies in the eigenvalue solution.

Normal-Mode Synthesis

Single-Component Structure

Numerical results of the single-component problem discussed earlier are shown in Figure 6. They correspond to the 5-, 10-, 20-, and 40-element beam models, respectively, used as sources of the substructure normal modes. The normal modes are computed for free-free end conditions. The first i modes are used to model the substructure. Data shown in Figure 6 include the number of normal modes, i , used to synthesize the model, the known solution, and the accuracy, A , of the modal fre-

quency defined as the ratio of the synthesized result to the known solution, as in the normal-mode analysis.

Representative data are shown in Figure 7a, which plots i versus A for the first, second, third, and fifth modal frequencies of the uniform cantilevered beam. Curves are included for the normal-mode source beams consisting of 5, 10, 20, and 40 elements.

Figure 7b shows the effect of varying i to represent a substructure in a plot of i versus A for modal data for the normal-mode source model consisting of 20 finite elements.

The following generalizations are drawn from the plotted data for this structure modeled by component modes:

- (1) There is nearly constant accuracy in modal frequency for the $i - 2$ modes where the first i normal modes are used to represent the substructure.

- (2) Accuracy of modes i and $i - 1$ are extremely poor, i.e., inaccurate by more than an order of magnitude.

- (3) For the minimum number of synthesized normal modes used to model the substructure, best accuracy for a specific normal mode, i' , of the structure is obtained when $i = i' + 2$. Thus, for a specific i' , a nontruncated set of normal modes represents a substructure more accurately than does a truncated set of modes.

Multiple-Component Structures

The several problems described in the earlier section exercise the normal-mode-synthesis technique for structures with more than one separable substructure.

Each structure is composed of three uniform beams previously discussed and analyzed by the normal-mode method. Each component beam is represented by the first 12 normal modes, i.e., two rigid-body modes and 10 flexible modes evaluated by the 40-element beam analysis for free-free end conditions. The 40-element source beam produces the most accurate results, therefore it is used to minimize error in the component modes. Stiffness connection elements (CELAS2), i.e., springs with very large spring constants, are used to couple the degrees of freedom of the substructures that are unrestrained when their normal modes are computed. Similarly, these fictitious springs provide the means to fix boundary conditions by connecting the appropriate degrees of freedom to ground.

The first structure studied is a cantilevered beam whose length is $3l$, composed of three uniform segments, each l in length, in series (see Figure 5). Substitution of $3l$ for l in Equation (9) yields the known solution for modal frequency. Reference 15 presents the known solutions and the accuracy, A , of normal-mode-synthesis results as a function of the number of modes, i , used to model each component; Figure 8 shows these data plotted as i versus A for representative normal modes of the complete structure. The curves approach an accuracy of 1.0 asymptotically from above as the number of normal modes synthesized for the substructures increases. The accuracy of the synthesized-structure modal frequency varies over a narrow range of values for modes numbered from 1 to nearly $2i$. For example, when seven modes are used to model each substructure, accuracy of the modal frequency

varies between 1.07 and 1.16 for all the structural modes numbered from 1 to 15. The model frequencies are inaccurate by an order of magnitude for structural modes greater than $2i$. As i increases, the range of values for A narrows and approaches 1.0. Reasonable engineering accuracy, e.g., within 10 percent, is obtained by use of a moderate number of component modes in the model. For example, 10-percent accuracy is obtained in the first mode when $i = 6$ and in the second mode when $i = 7$. When $i = 12$, all of the first 20 modes of the structure are computed with less than 10-percent error.

For the second structure, three parallel beams are fixed at one end and connected at the other. Table 2 gives data similar to that for the preceding structure. The known solution is the same as that for the single cantilevered beam, since the 3's cancel in the numerator and denominator of the term within the radical of Equation (9). Connections between components are made by the technique discussed for the previous structure. Normal-mode synthesis yields three computed modes corresponding to each mode of a single cantilevered beam. In the first synthesized mode all three parallel beams move in the same characteristic mode. In each of the other two synthesized modes, two beams move in the same cantilevered mode, while the third parallel beam takes a different mode shape. Good accuracy in modal frequency is obtained for structural modes in which each of the three components are characterized by the same substructure mode. This problem formulation demonstrates the ability of

Table 2—Normal-mode synthesis of three parallel beams fixed at one end and mutually connected at their other ends. Each component beam is modeled by the first 12 free-free modes computed from a 40-finite-element source beam.

Mode number of single cantilever beam	Frequency of known solution (rad/sec)	Mode number of three parallel beams	Computed natural Frequency (rad/sec)	Accuracy, A
1	3.5160	1	3.760	1.069
2	22.034	2	23.60	1.070
	none	2a	26.01	
	none	2b	26.01	
3	61.697	3	66.18	1.073
	none	3a	70.82	
	none	3b	70.82	
4	120.90	4	129.9	1.075
	none	4a	142.3	
	none	4b	142.3	
5	199.86	5	215.2	1.077
	none	5a	231.9	
	none	5b	231.9	
6	298.56	6	322.3	1.080
	none	6a	357.1	
	none	6b	357.1	

Table 3—Normal-mode synthesis of a three-beam portal frame, each component of which is modeled by the first 12 free-free modes computed from a 40-finite element source beam. Known solutions are the eigenvalue results of a finite-element model of the portal frame in which 40 bar elements represent each beam.

Portal frame mode number	Mode	Frequency of known solution (rad/sec)	Accuracy, <i>A</i>
1	antisymmetric	3.2035	1.532
1	symmetric	12.620	0.573
2	antisymmetric	20.621	0.989
2	symmetric	22.275	1.037
3	antisymmetric	44.794	0.875
3	symmetric	54.953	1.004

the synthesis technique to determine modes of the complete structure, which cannot be obtained from a simple combination of modes of the substructures.

The third structure is a three-member portal frame chosen to demonstrate the interconnection between substructures. Here the fictitious springs connect the appropriate degrees of freedom (see Figure 5). Rotations at the ends of adjoining beams are connected to maintain continuity of displacement between substructures. Transverse displacements at the top of the two vertical-support beams are connected, since longitudinal extension of the horizontal beam is neglected. Table 3 tabulates the following data for this structure: The known solution for normal modes, the mode number and type with respect to symmetry, and the accuracy, *A*, of the normal-mode-synthesis technique. The results of a finite-element, normal-mode analysis are assumed to be the known solutions. This model consists of 40 bar elements for each of the three constituent beams. Accuracy is poor for the first symmetric and antisymmetric modes, i.e., approximately 55-percent error. However, accuracy improves with higher mode numbers.

CONCLUSIONS

In this report, the bases in finite-element analysis of the normal-mode method and the normal-mode-synthesis technique were presented and their features, applications, and implementation with NASTRAN were discussed. A normal-mode modeling study of a uniform beam resulted in guidelines for prediction of accuracy in analysis compared to a known solution for the problem. Modal data from this modeling study were used to represent substructures in a modeling study of the normal-mode synthesis. One single-component structure and three multiple-component structures demonstrated normal-mode synthesis and its modeling techniques as implemented on NASTRAN.

The limited examples treated in the present study are intended to investigate accuracy obtained by the analyses and to demonstrate the application of these techniques on NASTRAN. Accuracy

guidelines can be applied judiciously to similar structures, e.g., tapered beams. Though normal modes may be synthesized from many diverse sources, the analyst should be cautioned to use extreme care in dynamic partitioning techniques, especially when truncating the modes used to represent a substructure.

The selection of an adequate number of finite elements needed to model a structure yields good accuracy in the solution obtained by normal-mode analysis. The synthesis of components represented by their normal modes yields more accurate results for the entire structure when the component modes are characteristic of the modal contribution of the substructure than when these modes are not characteristic of the modal contributions. Further study of the reason for the less accurate results may lead to a better understanding of the general applications and limitations of normal-mode synthesis.

REFERENCES

1. Archer, J. S.: Natural Vibration Model Analysis. NASA SP-8012, September 1968.
2. Paddock, G. B.: Dynamic Stability of Space Vehicles, Vol. I—Lateral Vibration Modes. NASA CR-935, November 1967.
3. Staley, J. A.: Dynamic Stability of Space Vehicles, Vol. II—Determination of Longitudinal Vibration Modes. NASA CR-936, November 1967.
4. Gieseke, R., et al.: Dynamic Stability of Space Vehicles, Vol. III—Torsional Vibration Modes. NASA CR-937, November 1967.
5. Gladwell, G. M. L.: Branch Mode Analysis of Vibrating Systems. *J. Sound Vibration* Vol. I, 1964, pp. 41-59.
6. Craig, R. R., and Bampton, M. C. C.: Coupling of Substructures for Dynamic Analyses. *AIAA Journal*, Vol. 6, No. 7, July 1968, pp. 1313-1319.
7. Hurty, W. C.: Dynamic Analysis of Structural Systems by Component Mode Synthesis. Jet Propulsion Laboratory, California Institute of Technology TR 32-350, January 1964.
8. Hurty, W. C.: Dynamic Analysis of Structural Systems Using Component Modes. *AIAA Journal* Vol. 3, No. 4, April 1965, pp. 678-685.
9. MacNeal, R. H.: Vibration of Composite Systems. Office of Scientific Research Report OSR TN-55-120, October 1954.
10. The NASTRAN Theoretical Manual. MacNeal, R. H., ed., NASA SP-221, October 1969.
11. Timoshenko, S.: Vibration Problems in Engineering. 2nd ed., New York: D. Van Nostrand Co., 1937.
12. Hurty, W. C., and Rubinstein, M. F.: Dynamics of Structures. Englewood Cliffs, New Jersey: Prentice-Hall, Inc., 1964.

13. Young, D., and Felgar, R. P., Jr.: Tables of Characteristic Functions Representing Normal Modes of Vibration of a Beam. Austin, Texas: University of Texas Press, July 1949.
14. The NASTRAN User's Manual, McCormick, C. W., ed., NASA SP-222, October 1969.
15. Courtney, Roy Leon: Finite-Element Modeling Studies in the Normal-Mode Method and Normal-Mode Synthesis. NASA TN D-6326, May 1971.

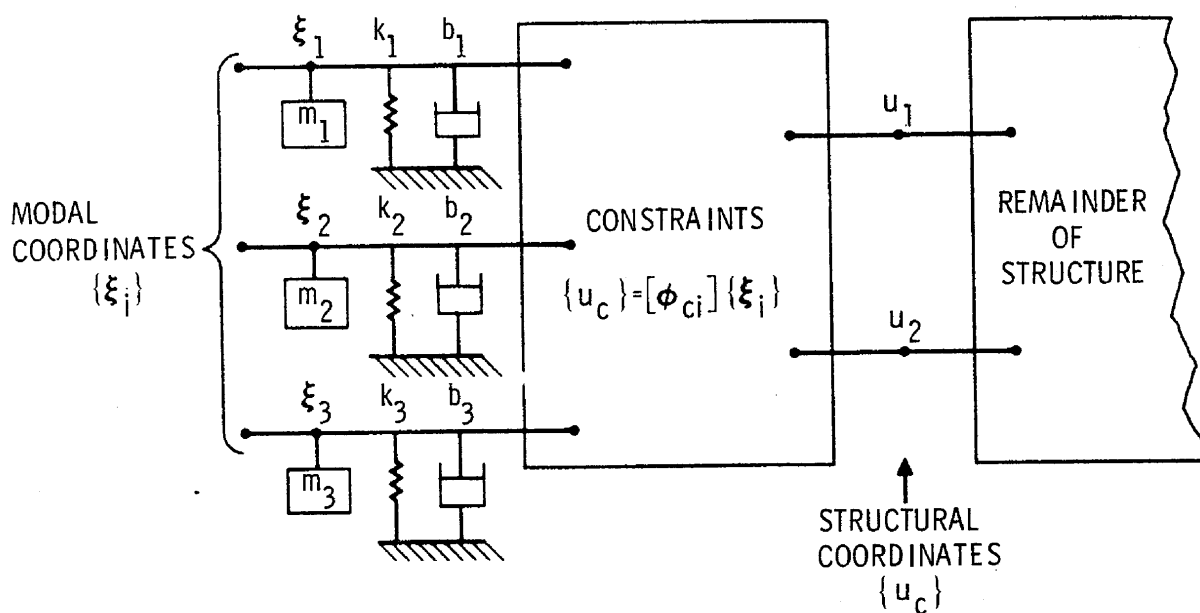
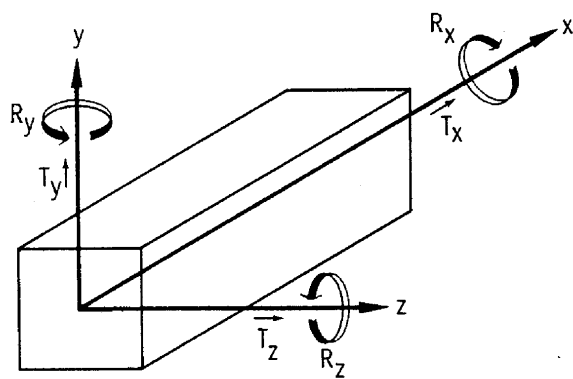


Figure 1.—Representation of a part of a structure by its vibration modes, Case 1: All connection points are free while the modes are calculated.



R = Rotation
T = Translation

Figure 2.—Bar element.

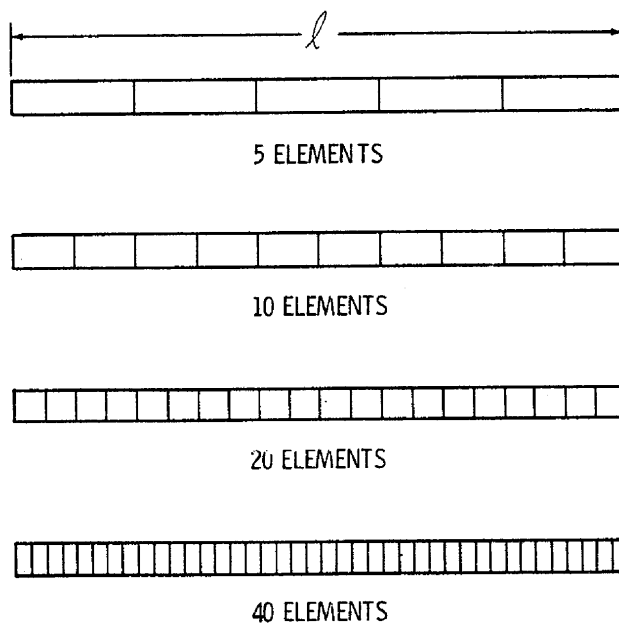


Figure 3.—Four finite-element models of a beam.

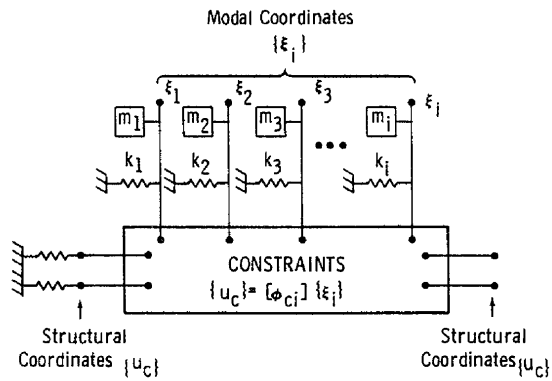


Figure 4.—Representation of the model for normal-mode synthesis of a single cantilevered beam.

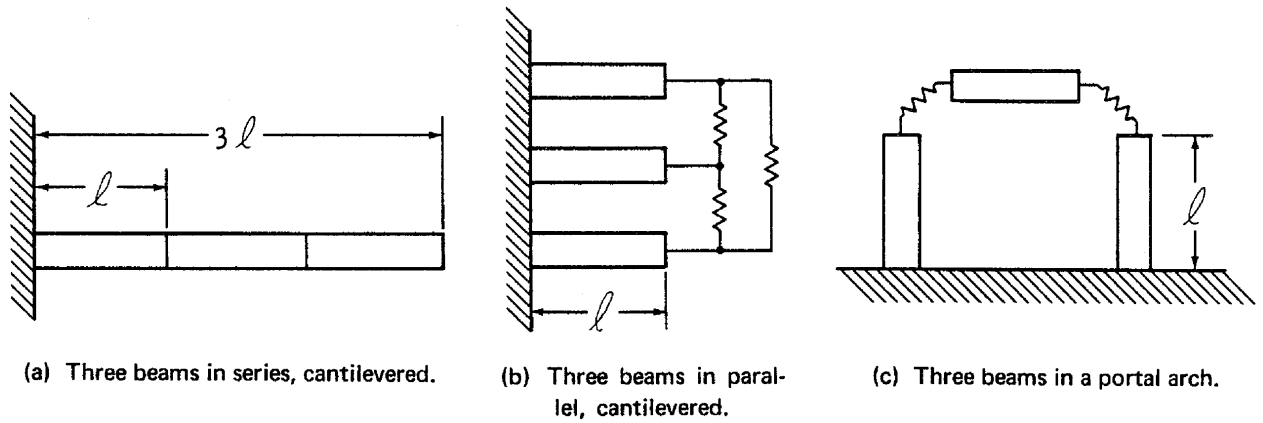


Figure 5.—Multiple-component structures modeled by normal-mode synthesis.

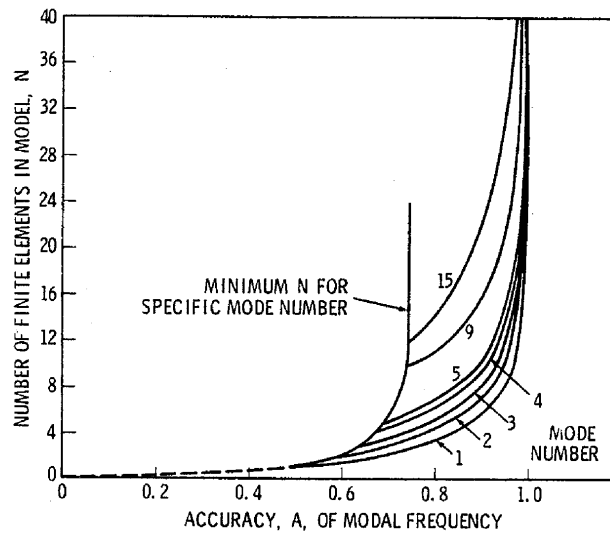
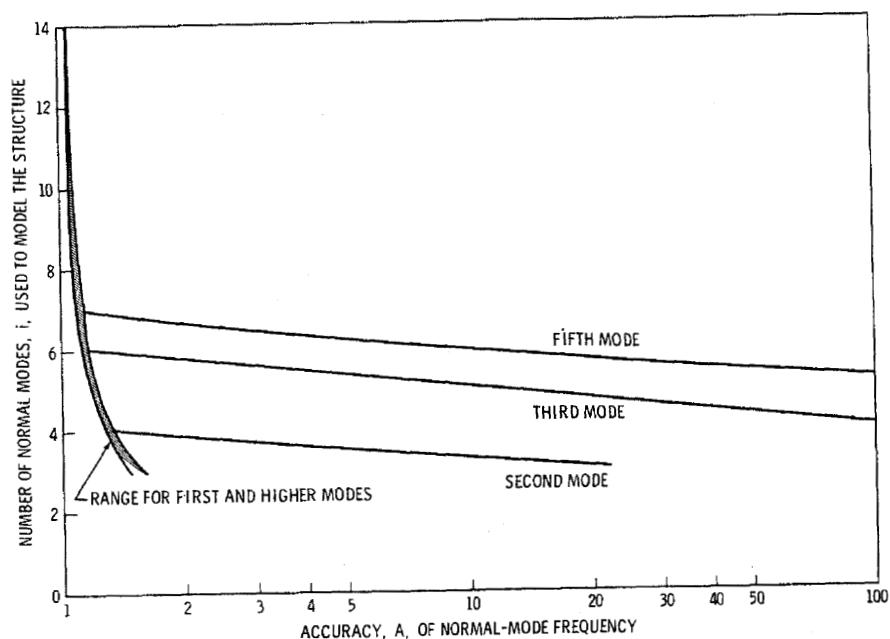
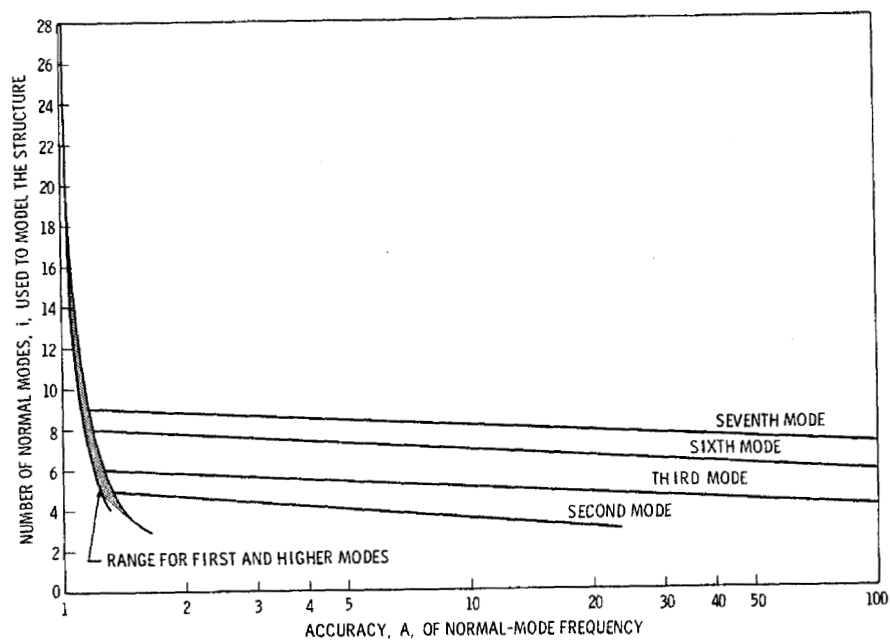


Figure 6.—Results of normal-mode analysis of a beam with free-free end conditions.



(a) Cantilevered beam modeled by free-free modes computed from source beams containing 5, 10, 20, and 40 elements (Tables B1 through B4 of Reference 15).



(b) Cantilevered beam modeled by free-free modes computed from a 20-element source beam (Table B3 of Reference 15).

Figure 7.—Results of normal-mode synthesis of a single-component structure.

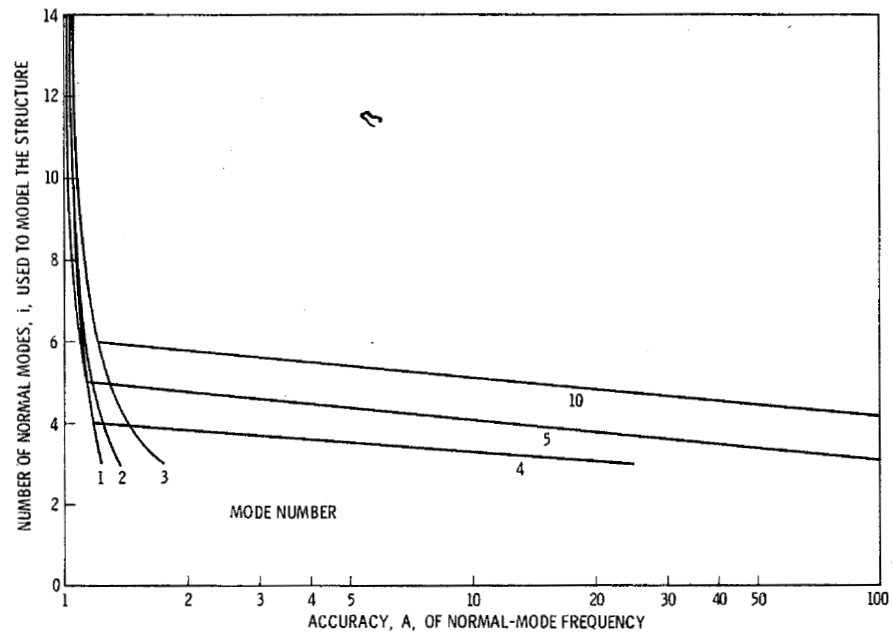


Figure 8.—Results of normal-mode synthesis of a multiple-component structure, three uniform beams in parallel, cantilevered.

Preceding page blank

GUYAN REDUCTION SOLUTIONS
RECYCLED FOR IMPROVED ACCURACY*

By Roy Levy

Jet Propulsion Laboratory, Pasadena, California

ABSTRACT

The accuracy of conventional solutions of the eigenvalue problem by means of the Guyan reduction method is examined for analytical models of several practical structures. Evaluations are made of eigenvalue accuracy with respect to the relative numbers of retained indicator degrees of freedom. When a relatively small number of indicator degrees of freedom are employed, solutions are likely to be inaccurate unless prior knowledge of the mode shapes is used in selecting these degrees of freedom.

One improvement for recovering the lowest modes is to supplement the indicator displacements with static loading displacement functions. A further, and more powerful remedy is to perform iterative repetitions of the solution procedure by extending Stodola's method of matrix iteration, which operates with one eigenvector at a time, to a block iteration operating on a group of vectors simultaneously. This de-emphasizes the need for a judicious selection of indicators, since it is shown that an arbitrary selection of n indicators will eventually produce solutions that converge to n exact modal solutions. Great improvements in accuracy can be achieved with only a few iterative cycles and relatively small numbers of retained degrees of freedom. This method is effective when only a few valid modal solutions are required and the order of the matrix is so large that the computational time without reduction would ordinarily be prohibitive.

CONVENTIONAL CONDENSATION METHODS

Procedures to condense the order of the eigenvalue problem solution for structural analysis are frequently used for computational efficiency and economy. As an example, the well known Guyan reduction (ref. 1) procedure, which is incorporated within NASTRAN, is particularly attractive whenever the order of the system of equations to be solved is large and the solution is

*This paper presents the results of one phase of research carried out at the Jet Propulsion Laboratory, California Institute of Technology, under Contract No. NAS 7-100, sponsored by the National Aeronautics and Space Administration.

required for only a relatively small number of natural frequencies and corresponding mode shapes. Equivalent conventional procedures are described in references 2 and 3.

With a discrete idealization of the structure, the order of the eigenvalue solution needs to be only as large as the number of degrees of freedom with non-zero entries in the mass matrix. The number of elastic degrees of freedom is given by the order of the stiffness or flexibility matrix, and is equal to or greater than the mass degrees of freedom. Therefore, because the size of the eigenvalue problem depends upon the size of the mass matrix, condensation procedures have been referred to as mass matrix reduction methods. Although specific descriptions and details of implementations vary, conventional approaches to condensation could often be considered as Rayleigh-Ritz approximation techniques (ref. 4). These are employed in solving the following homogeneous system of N equations for the unknown displacements $\{X\}$:

$$[M] \{\ddot{X}\} + [K] \{X\} = \{0\} \quad (1)$$

where $[M]$ is the mass matrix and $[K]$ is the stiffness matrix. The solution furnishes the eigenvectors and the corresponding eigenvalues, which are measures of the modal natural frequencies.

A reduction in the order of the system from N to L ($L < N$) can be effected by the transformation

$$\{X\} = [\gamma] \{\xi\} \quad (2)$$

where $[\gamma]$ is an assumed transformation matrix of order $N \times L$ and $\{\xi\}$ is a set of generalized coordinates associated with the transformation. This reduces the order of the problem to L , and the equations to be solved are

$$[M] \{\ddot{\xi}\} + [K] \{\xi\} = 0 \quad (3)$$

where

$$[M] = [\gamma]^t [M] [\gamma] \quad (3a)$$

and

$$[K] = [\gamma]^t [K] [\gamma] \quad (3b)$$

The solution to equation (3) produces the eigenvalues and the modal matrix of eigenvectors $[\phi]$ associated with the set of generalized coordinates. The set of L eigenvectors of order N for the original system can be recovered from

$$[X] = [\gamma][\phi] \quad (4)$$

The transformation matrix, which is the key to the procedure, can be considered as a set of L N -component vectors, with each vector equivalent to an assumed displacement function. The approximation of the solution depends upon how closely the assumed displacement functions (or linear combinations of them) agree with the actual eigenvectors. Whenever a displacement function is the true eigenvector, the resulting solution for the corresponding mode will be exact. Nevertheless, it is one of the advantages of the Rayleigh-Ritz method that the approximations of the solution tend to be less severe than the approximations of the assumed functions. On the other hand, there is no assurance that gross inaccuracies will not occur as a result of unfavorable choices for the transformation matrix.

A simple way to generate a set of displacement functions for the transformation matrix is to make a selection of a set of L "indicator" degrees of freedom, and then to develop static displacement vectors consistent with either unit displacements (ref. 1) or unit loads (refs. 2 and 3) at each indicator. Whether displacements or loads should be used to generate the displacement functions is theoretically immaterial; the logical choice depends upon convenience of execution for the available software. Consequently, the major requirement in proceeding with a condensed solution is the selection of suitable indicator degrees of freedom. Unfortunately, only a minute amount of guidance is available to assist in the selection, and even this guidance is of questionable value. Possible guidelines are the following:

1. Select the degrees of freedom that have the largest entries in the mass matrix.
2. Select the degrees of freedom that have the largest movements (components of the eigenvector) in the modes of interest.

The first guideline can be defended in the limiting case: when the magnitude of one particular mass is overwhelming with respect to the sums of the magnitudes of the remaining masses, the system is then essentially equivalent to one uncoupled degree of freedom for each elastic degree of freedom at the predominant mass. There is no clear defense for this guideline in the very practical and common case in which there is no single mass that predominates.

The second guideline allows the solution to develop good approximations to the true eigenvectors by means of linear combinations of the

indicator-generated displacement functions. The principle is clearly sound, but successful application depends upon knowing part of the answer in advance. In the case of regular classical structures, such as beams or strings, the true mode shapes are well known and the application is clear. However, for practical structures of irregular geometry and properties, identification of the important degrees of freedom approaches guesswork. Therefore, success can depend upon chance.

ACCURACY TESTS OF CONVENTIONAL METHOD

The accuracy of condensed solutions was assessed for the analytical models of two structures used in the field of radar antennas. These particular models are of interest because they represent practical illustrations of irregular structures, and depart considerably from classical examples.

The first model is of an experimental structure built to simulate a 30-deg sector of a 26-m-diameter reflector. Its framing is shown in figure 1. The structure mass is about 2400 kg and consists of structural steel tees and angles. The reflecting surface comprises an additional 360 kg of non-structural panels supported on the top chords of the trusses. Joint connections were idealized as pinned, with the exception of a few cases in which relatively stiff members were continuous across the joints. The mass matrix for the full model represents 190 translational degrees of freedom. The order of the stiffness matrix is slightly larger because of a few rotational degrees of freedom.

The second model is of the pedestal that provides the support and driving mechanism for the polar wheel of a 26-m-diameter reflector. Figure 2 shows a view of the framework. Bearings on the polar shaft support the polar wheel; the polar drive is by pinions at the drive skid. The mass of the framing members — steel angles, tees, pipes, and wide-flange beams — is about 42,000 kg. Additional concentrations, which total 18,000 kg, are distributed to joints in the vicinity of the drive skid and at the upper and lower bearings of the polar shaft. The mass matrix for the full model has 165 translational degrees of freedom. The stiffness matrix, with rotations included, contains 195 degrees of freedom.

The orders of both of these models were so small that it was feasible to solve the eigenvalue problems without condensation. After this, the solution accuracy for the first four frequencies and mode shapes was tracked through successive condensation solutions with diminishing numbers of indicator degrees of freedom. These indicators were originally chosen as carefully as would be expected in ordinary practice, and with reference to the guidelines stated previously.

Figures 3 and 4 show the errors in frequency plotted against the percent of degrees of freedom retained. This percentage is for the ratio of the number of indicator degrees of freedom to the order of the uncondensed mass matrix. Quick comparisons of mode shapes were also made for the cases

represented in these figures by examining the eigenvector components with the largest magnitudes. It was found, in general, that the eigenvector errors were considerably larger than the frequency errors. In some instances, the mode shapes from condensed solutions with small frequency errors were found to be unrelated to the mode shapes from the full solution. Usually, if frequencies were in error by more than about 3 to 5%, the mode shapes were no better than poor; frequency errors greater than 10 to 15% were accompanied by mode shapes that were rated from very poor to completely unrelated to the full-solution mode shapes.

According to a conventional rule of thumb, the ratio of the number of degrees of freedom in the model to the number of accurate modes in the solution is between two and three. Therefore, according to this rule, the first four modes should be reproduced for either of these two models by retaining less than 10% of the full number of degrees of freedom. From another standpoint, it would not seem reasonable to consider condensation procedures to be highly effective unless accurate solutions for several modes could be obtained consistently with at least an order of magnitude reduction in the solution size. With these anticipations in mind, the results presented in figures 3 and 4, which show large errors for retentions greater than 10%, were highly disappointing.

However, the procedure was not abandoned at this point; instead, an entirely different approach was used for selection of the indicator degrees of freedom. This was an after-the-fact selection, in which the mode shapes from the uncondensed solutions were inspected to select the degrees of freedom that actually had the largest motions. Trial-and-error changes were also made in the retained set of indicators, as the number of indicators in the set was being reduced, in an attempt to identify and retain certain key degrees of freedom that apparently controlled solution validity.

The results of the modified selection of indicators, shown in figures 5 and 6, are a substantial improvement. For both models, the first four modes have been recovered with the order of the condensed eigenvalue problem solution (as given by the number of indicators) equal to less than 10% of the order of the uncondensed mass matrix.

EVALUATION OF RESULTS OF CONVENTIONAL METHOD

The success achieved for the modified selection confirms the theoretical validity of the conventional method but is of little practical help to the analyst. Although it was found that a selection of indicator degrees of freedom that included the degrees of freedom with the largest modal displacements tended to produce a substantial improvement in the validity of the solution, to make such a selection would require either clairvoyance or prior knowledge. By examination of the degrees of freedom that were eventually retained in the successful sets of indicators, it was also found neither necessary nor sufficient to choose degrees of freedom with the largest entries in the mass matrix.

Another unfortunate property of the conventional method is the failure to converge toward improved accuracy. Addition of indicators to a poorly chosen set would sometimes closely reproduce the current inaccurate solution. The danger here is that the consistency of the results could be misinterpreted as evidence of accuracy. Accuracy appears to depend upon the choice of a set of indicators (not necessarily a large set) that contains key but elusive degrees of freedom. In some instances, the omission or addition of a single key indicator triggered the loss or recovery of a complete mode.

One more difficulty of the conventional method is that success or failure may be model-dependent. Better success was observed here in original selections for the reflector model than for the pedestal model. One reason for the difference may be the separation of the natural modes. It seems that the best results are obtained for analytical models in which the modes have the widest frequency separation.

MODIFICATIONS FOR CONVENTIONAL METHOD

Two modifications to the conventional method are effective in increasing reliability and removing some of the dependence upon the analyst's intuition or prior knowledge. The first consists of augmenting the indicator-derived displacement functions with up to six additional "static loading" displacement vectors. The second involves improving accuracy by iterative recycling of the Rayleigh-Ritz procedure.

Iterative solutions within a reduced space have been proposed previously. Jennings and Orr (ref. 5) described a simultaneous iteration method that employs an orthogonal set of trial vectors, and they also indicate an extension that can be used for solutions of unconstrained structures. Ojalvo and Newman (ref. 6) proposed a reduced-space solution employing a recursion algorithm to generate sequences of trial vectors. Whetstone and Jones (ref. 7) used an initial Rayleigh-Ritz method based upon a selection of static force and rigid-body displacement vectors as the starting point for a reduced-space Stodola method solution that generates orthogonal eigenvectors one at a time. More recently, Dong, Wolf, and Peterson* employed iterative repetitions of the Rayleigh-Ritz method. The iterative Rayleigh-Ritz method, which is possibly the simplest of all to implement within existing analysis systems, is examined here with respect to accuracy and economy for practical applications. Additional displacement functions for the first modification can be developed within the context of a standard matrix interpretive analysis formulation such as the SAMIS program. The recycling modification, which also appears to have more potential, has been readily incorporated within both the SAMIS and NASTRAN programs.

*In an article to be published in the Int. J. Numer. Meth. Eng.

Augmented Displacement Function Modification

The additional displacement functions are developed by first determining the six rigid-body displacements of the structure for independent unit motions (three translations and three rotations) of the foundation. A loading matrix is derived by post-multiplying the mass matrix by the $N \times 6$ matrix of rigid-body displacements. That is, let $[\rho]$ be the set of rigid-body displacements and let $[P]$ be the loading matrix; then

$$[P] = [M][\rho] \quad (5)$$

This loading is applied to the structure, and the corresponding displacements are added to the displacements constructed from the indicators. The resulting set of displacement functions becomes the transformation used in the condensed solution. Thus, let $[\gamma_R]$ be the additional static-loading displacement functions, and let $[\gamma_I]$ be the displacement functions generated by indicators; then $[\gamma_R]$ is found from the solution of

$$[K][\gamma_R] = [P] \quad (6)$$

and

$$[\gamma] = [\gamma_I | \gamma_R] \quad (7)$$

From this point on, the solution proceeds in the conventional way (see eq. 2). The order of the condensed eigenvalue problem is now $L + 6$. If L is small, the increase can be readily accommodated in the solution; if L is large, the increase is relatively small. Therefore, the increase in the size of the solution and the computation time caused by the additional functions is not significant. In a limited number of evaluations of the relative accuracy improvement, it appears that the rigid-body translations have a larger influence than the rigid-body foundation rotations. Hence, the effort in generating program input to define foundation rotations may not be worthwhile.

The added displacement functions constructed from the rigid-body translations are proportional to the displacements that result from loading the structure with its own weight applied sequentially in the directions of the foundation motions. In fact, the suggested additional displacement functions were motivated by typically successful applications of Rayleigh's method in recovering first-mode frequencies with the assumption of a single static self-weight loading displacement function. Therefore, the modification will ordinarily ensure the recovery of the fundamental frequency, and thereby remove at least one defect that has occasionally been noted in the conventional method.

Recycling Modification

The recycling modification is applied after an initial solution using indicator functions (optionally augmented by the static loading functions). The initial mode shapes for the full N degrees of freedom are recovered as in equation (4) and are then applied as in equation (5) (in place of the rigid-body displacements) to generate new loading vectors; e. g.,

$$[X^0] = [\gamma^0] [\phi^0] \quad (8)$$

$$[P^1] = [M] [X^0] \quad (9)$$

After this, the transformation matrix for the first additional cycle is constructed by solving

$$[K] [\gamma^1] = [P^1] \quad (10)$$

The eigenvalue problem solution is then regenerated according to equation (3). This procedure can be repeated iteratively until convergence to within a specified criterion is achieved. Equations (8), (9), and (10) are applicable with incremented superscripts at each subsequent cycle. A schematic of the NASTRAN program adjustments to incorporate this modification is shown in Appendix A. A mathematical proof of eventual cyclic convergence need not be supplied; it is only necessary to consider this as an extension of Stodola's procedure of matrix iteration (ref. 4), for which convergence is readily established (ref. 8). That is, instead of iterating on one trial modal vector at a time, the present modification is an extension to a block iteration that operates upon several vectors simultaneously. Here, the eigenvalue problem is solved repeatedly in a greatly reduced space, which is in contrast to the classical uncondensed solution procedures that perform only one solution of the problem in the full space of the original mass matrix. Therefore, to achieve solution economy, the emphasis is now placed upon efficient performance of the operations leading to the formation of equation (3) rather than upon the procedures used in obtaining solutions to this equation.

RESULTS AND DISCUSSION OF MODIFICATIONS

The effects of the modifications to the procedures for the pedestal model are shown in figure 7. Three curves are included for each mode: curve A is for reference — to show the accuracy for the conventional initial solution with indicator functions only; curve B shows the accuracy for the first modification — that is, six static-loading functions have been added to the indicator functions of curve A; curve C represents the accuracy obtained with the addition of only one new iteration cycle and starting with the mode shapes associated with the points of curve B. It can be seen in comparison with the conventional solution that solutions with the six new displacement functions are often several times more accurate, and that solutions from

the iteration cycle are typically more accurate by more than one order of magnitude.

Most of the indicators selected for the curves of figure 7 were from the after-the-fact selection, and consisted of a relatively small set. In a few cases, the addition of one iteration to the initial solution for larger sets of indicators produced excellent accuracy for relatively larger numbers of natural modes. In some of these examples, the particular set of indicators had produced invalid results on the initial cycle.

Two 5-cycle tests were performed for this model: the first was for six indicator functions with no static-loading functions; the second was for six static-loading functions with no indicator functions. Both tests revealed the four lowest frequencies with less than 0.6% error and with mode shapes rated between excellent (first mode) and fair (fourth mode). The indicator functions did not produce the first mode until the third cycle (50 and 10% errors at first and second cycles, respectively). The static-loading functions produced the first-mode frequency with less than 0.1% error at the second cycle, starting from 2.0% at the first cycle. At each cycle, in both of these cases, the errors in frequency diminished monotonically for all six of the modes.

Most of the iterative solution tests that have been made so far have been for analytical models of less than 200 degrees of freedom. For these models, the Givens method in NASTRAN rapidly provided the solutions for all modes of the uncondensed models. Hence, for these relatively small models, there were no large gains in computation times to be achieved through iterative procedures. However, for larger models, the Givens method becomes impractical, and the solution is best obtained in NASTRAN via the Inverse Power method. If the problem size is large enough, the computation time required to find a few modes becomes substantial. It would then be more economical to solve the eigenvalue problem using the Givens method within a reduced space to perform a few iterative cycles.

In one example, an Inverse Power method solution was obtained without condensation for an analytical model of an antenna reflector that contained about 1300 degrees of freedom. Only the first modal solution was generated, which required about 32 min of computation time (Univac 1108-Exec 8 computer) in the eigenvalue solution phase. After this, a Guyan reduction solution was performed with 29 indicator degrees of freedom and continued through five additional iteration cycles. The initial solution was completed after 15 min, the first iteration required 13 min, and each of the four subsequent iteration cycles took 8 min. The changes in modal frequencies at each cycle diminish approximately according to a geometric progression. This relationship was used to extrapolate the modal frequencies at convergence. Figure 8a shows the numbers of natural frequencies obtained cyclically with respect to limiting percentages of variation from the extrapolated convergent frequencies. Figure 8b indicates the estimated computer time saved if the same number of modes that were obtained with less than 0.05% variation from the convergent frequencies had been derived by the Inverse Power method on the uncondensed model. The Inverse Power method

time was estimated as 32 min for the first mode and 24 min for each additional mode. Since the first mode from the initial Guyan reduction had a variation of 1.6% and the remaining modes had higher variations, the corresponding computation time at the zero'th cycle on the figure is represented as a loss.

CONCLUSION

The two new modifications tend to make results of condensed eigenvalue solutions considerably more reliable and accurate by removing some of the emphasis on the difficult and subjective choice of the indicator degrees of freedom. The modification that consists of adding the new static-loading displacement functions will usually add very little to the solution time. The cycling modification will require significant additional solution time for each cycle; (of the same order as for one cycle of the conventional method).

Iterative cycling provides the analyst with several approaches. He can select L indicators (possibly at random) and, with a sufficient number of cycles, be assured of recovering the first L natural modes to within some specified convergence criterion. Alternatively, a selection of a multiple of L indicators should be capable of producing the same L modes with a smaller number of iteration cycles. It has been found that the time for each iteration cycle tends to be proportional to the number of displacement functions employed; therefore another possibility for improving solution efficiency is to consider truncating the set of displacement functions used for the later cycles. Finding the best ways to exploit these opportunities requires additional tests. Nevertheless, until these are provided, it is clear that one additional cycle in itself is very useful, even if only to establish the validity of a conventional condensed solution.

REFERENCES

1. Guyan, R.J.: Reduction of Stiffness and Mass Matrices. AIAA J., vol. 3, no. 2, 1965, p. 380.
2. Kaufman, S., and Hall, D.B.: Reduction of Mass and Loading Matrices. AIAA J., vol. 6, no. 3, 1968, pp. 550-551.
3. Ramsden, R.N., and Stoker, R.J.: Mass Condensation: A Semi-automatic Method for Reducing the Size of Vibration Problems. Int. J. Numer. Meth. Eng. vol. 1, 1969, pp. 333-349.
4. Bisplinghoff, R.L., Ashley, H., and Halfman, R.L.: Aeroelasticity. 1st ed., Addison-Wesley, Redding, Massachusetts, 1957.
5. Jennings, A., and Orr, D.R.L.: Application of the Simultaneous Iteration Method to Undamped Vibration Problems. Int. J. Numer. Meth. Eng., vol. 3, 1971, pp. 13-24.

6. Ojalvo, I.U., and Newman, M.: Vibration Modes of Large Structures by an Automatic Matrix-Reduction Method. AIAA J., vol. 8, no. 7, 1970, pp. 1234-1239.
7. Whetstone, W.D., and Jones, C.E.: Vibrational Characteristics of Linear Space Frames. Proc. ASCE: J. Struct. Div., vol. 95, no. ST 10, 1969, pp. 2077-2091.
8. Hurty, W.C., and Rubinstein, M.F.: Dynamics of Structures. 1st ed., Prentice-Hall, Englewood Cliffs, New Jersey, 1964.

APPENDIX A

Schematic of NASTRAN Rigid Format No. 3 Modifications for Recycled Eigenvalue Solutions

$$\text{DMAP 70 } [K_{ff}] = \left[\begin{array}{c|c} \bar{K}_{aa} & K_{ao} \\ \hline K_{oa} & K_{oo} \end{array} \right] \text{ and } [M_{ff}] = \left[\begin{array}{c|c} \bar{M}_{aa} & M_{ao} \\ \hline M_{oa} & M_{oo} \end{array} \right]$$

$$\text{SOLVE: } [K_{ff}] \begin{bmatrix} I_{aa} \\ G_o \end{bmatrix} = \begin{bmatrix} K_{aa} \\ \text{NULL} \end{bmatrix}, \text{ FOR } G_o \text{ AND } K_{aa}$$

$$\text{LET: } \begin{bmatrix} \gamma^o \end{bmatrix} = \begin{bmatrix} I_{aa} \\ G_o \end{bmatrix}$$

$$\text{FIND: } [M_{aa}^o] = [\gamma^o]^T [M_{ff}] [\gamma^o]$$

$$(\text{EQ. 3a, b}) [K_{aa}^o] = [\gamma^o]^T [K_{ff}] [\gamma^o]$$

DMAP 87 (EQ. 3) SOLVE EIGENVALUE PROBLEM
FOR EIGENVALUES AND EIGENVECTORS, $[\phi_a^o]$

DMAP 93 (EQ. 8) RECOVER $[X^o] = [\gamma^o] [\phi_a^o]$

EXISTING DMAP INSTRUCTIONS

BEGIN ITERATIONS

i = 1

$$(\text{EQ. 9}) \text{ FIND: } [P^i] = [M_{ff}] [X^{i-1}]$$

$$(\text{EQ. 10}) \text{ SOLVE: } [K_{ff}] [\gamma^i] = [P^i], \text{ FOR } [\gamma^i]$$

(SAVE DECOMPOSITION OF K_{ff} WHEN $i = 1$.)

$$(\text{EQ. 3a, b}) \text{ FIND: } [M_{aa}^i] = [\gamma^i]^T [M_{ff}] [\gamma^i]$$

$$[K_{aa}^i] = [\gamma^i]^T [P^i]$$

(EQ. 3) SOLVE EIGENVALUE PROBLEM, GIVEN $[M_{aa}^i]$ AND
 $[K_{aa}^i]$ FOR EIGENVALUES AND EIGENVECTORS, $[\phi_a^i]$

$$\text{RECOVER: } [X^i] = [\gamma^i] [\phi_a^i]$$

NEW DMAP AFTER PACKAGE

i = i + 1

NO

i > i_{max} ?

YES

RESUME RIGID FORMAT

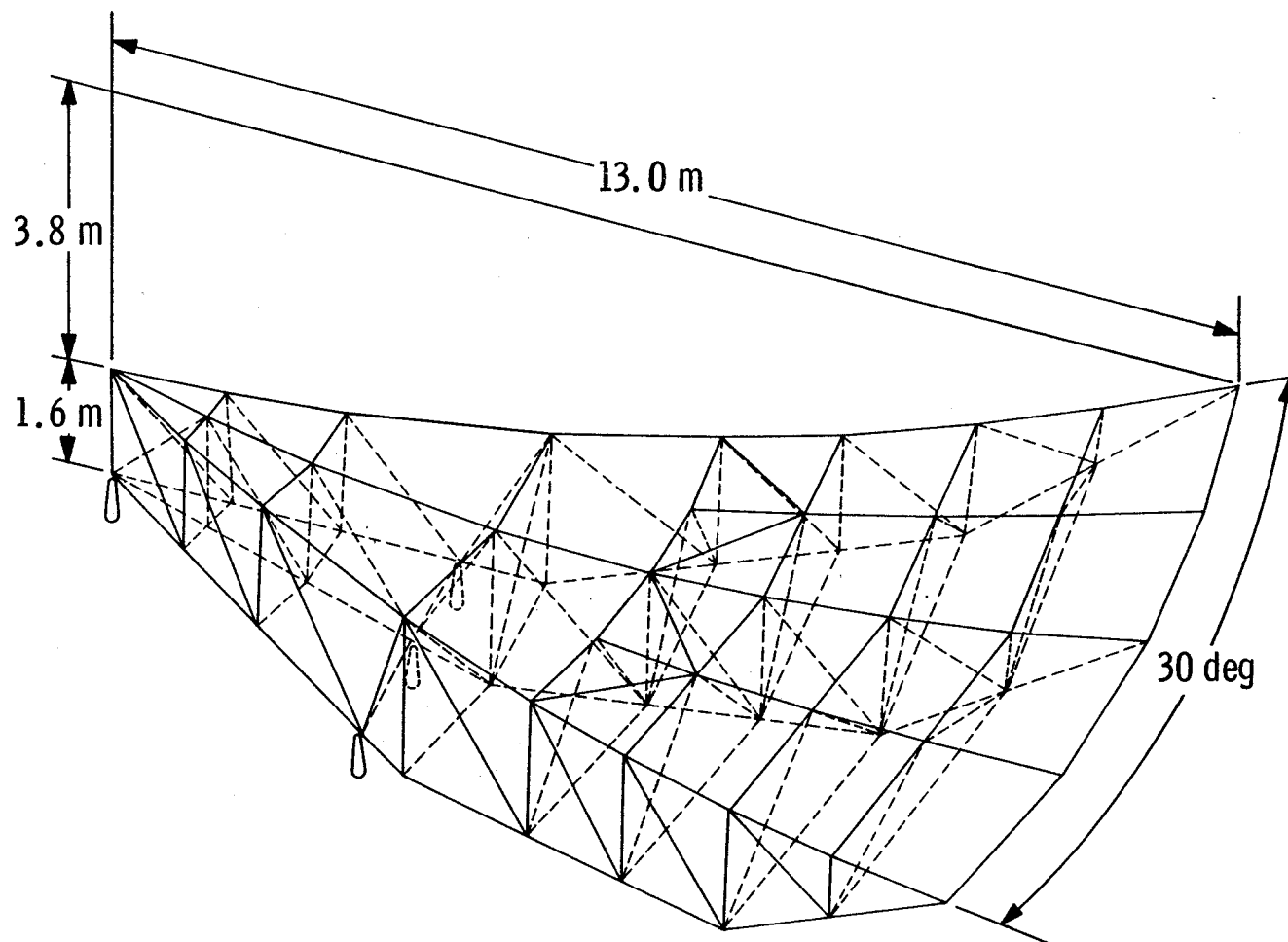


Figure 1. - Thirty-degree reflector sector structure

PEDESTAL STRUCTURE

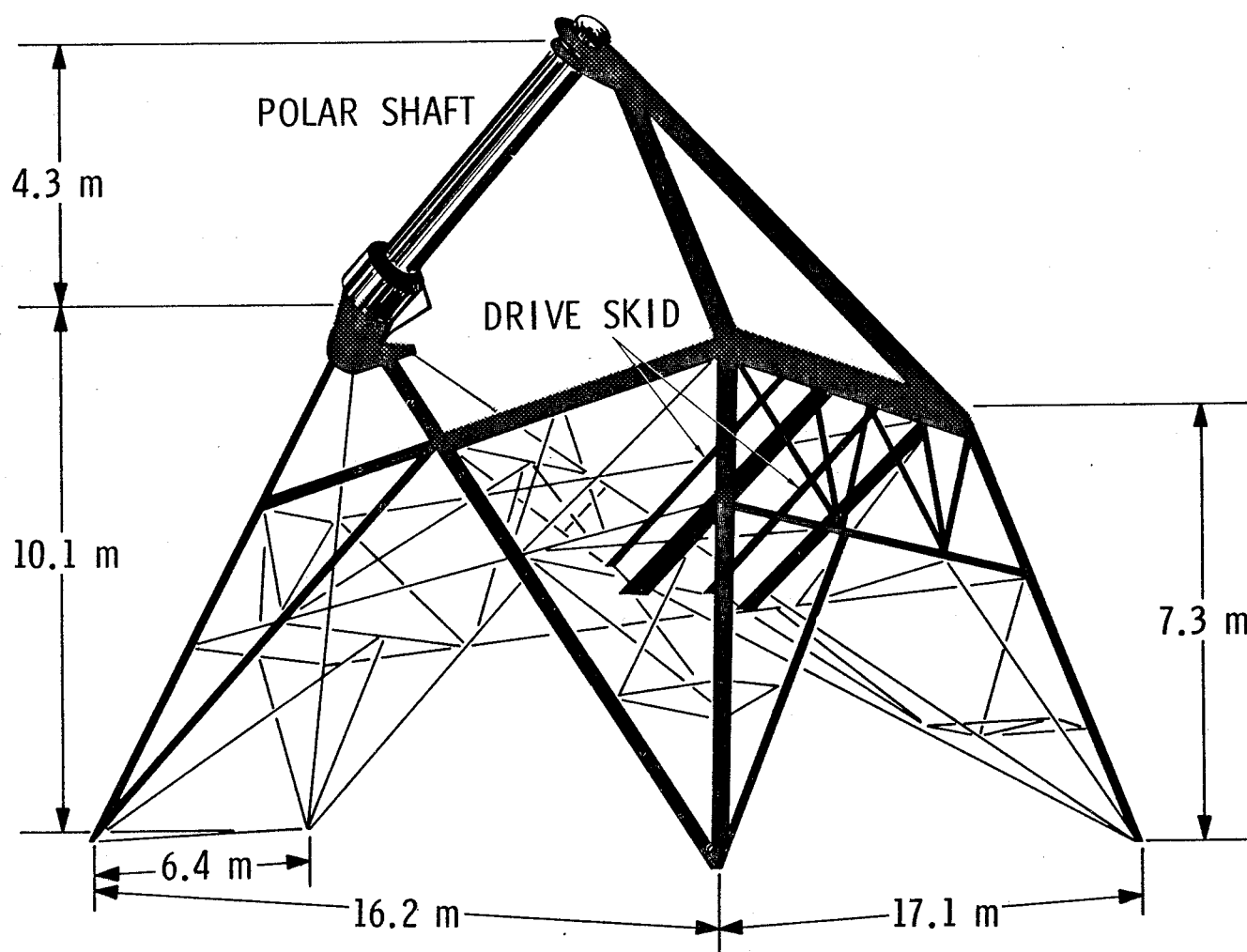


Figure 2. - Pedestal structure

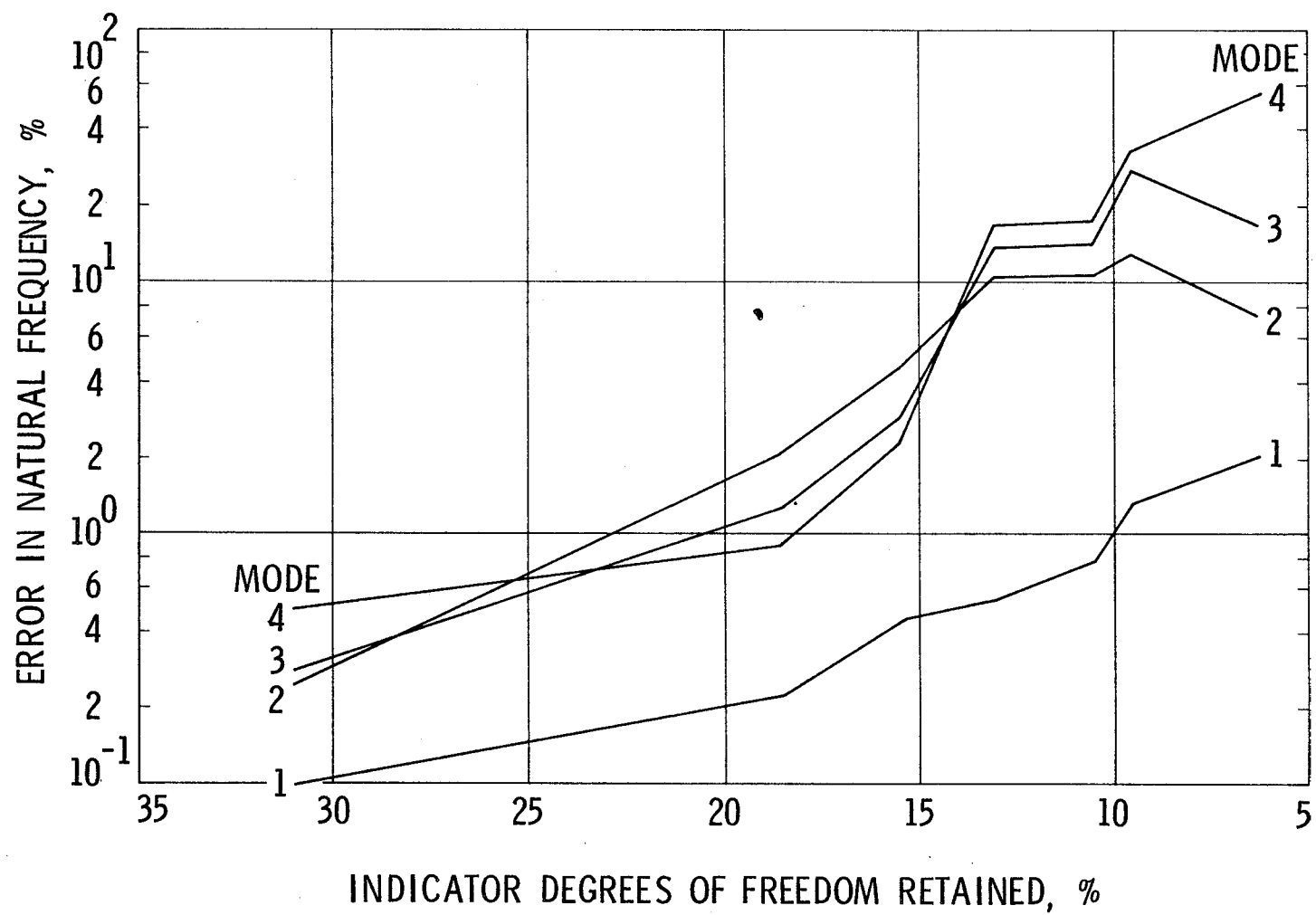


Figure 3. - Accuracy of condensed solution for reflector sector structure:
original indicator selections

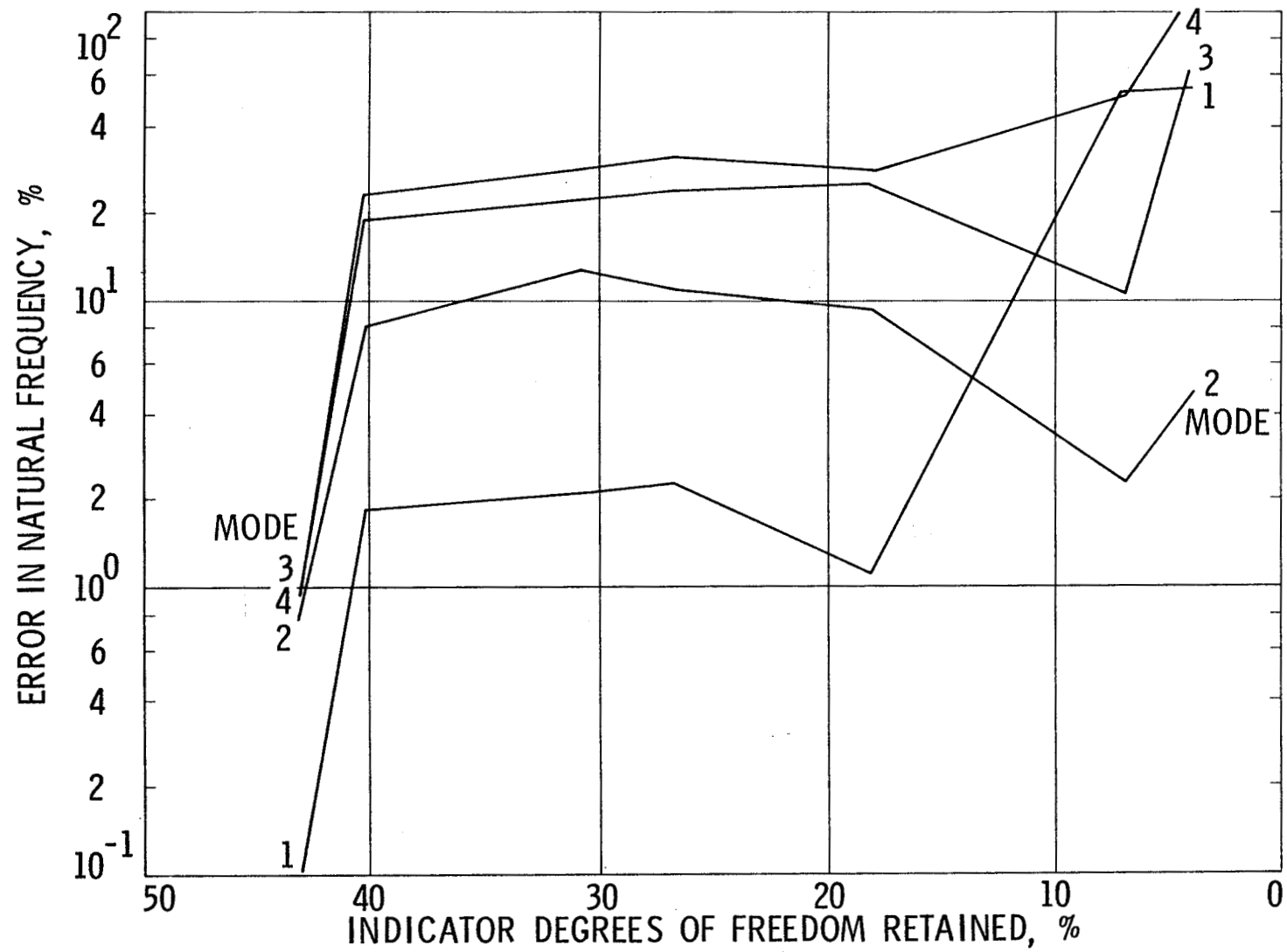


Figure 4. - Accuracy of condensed solution for pedestal structure:
original indicator selections

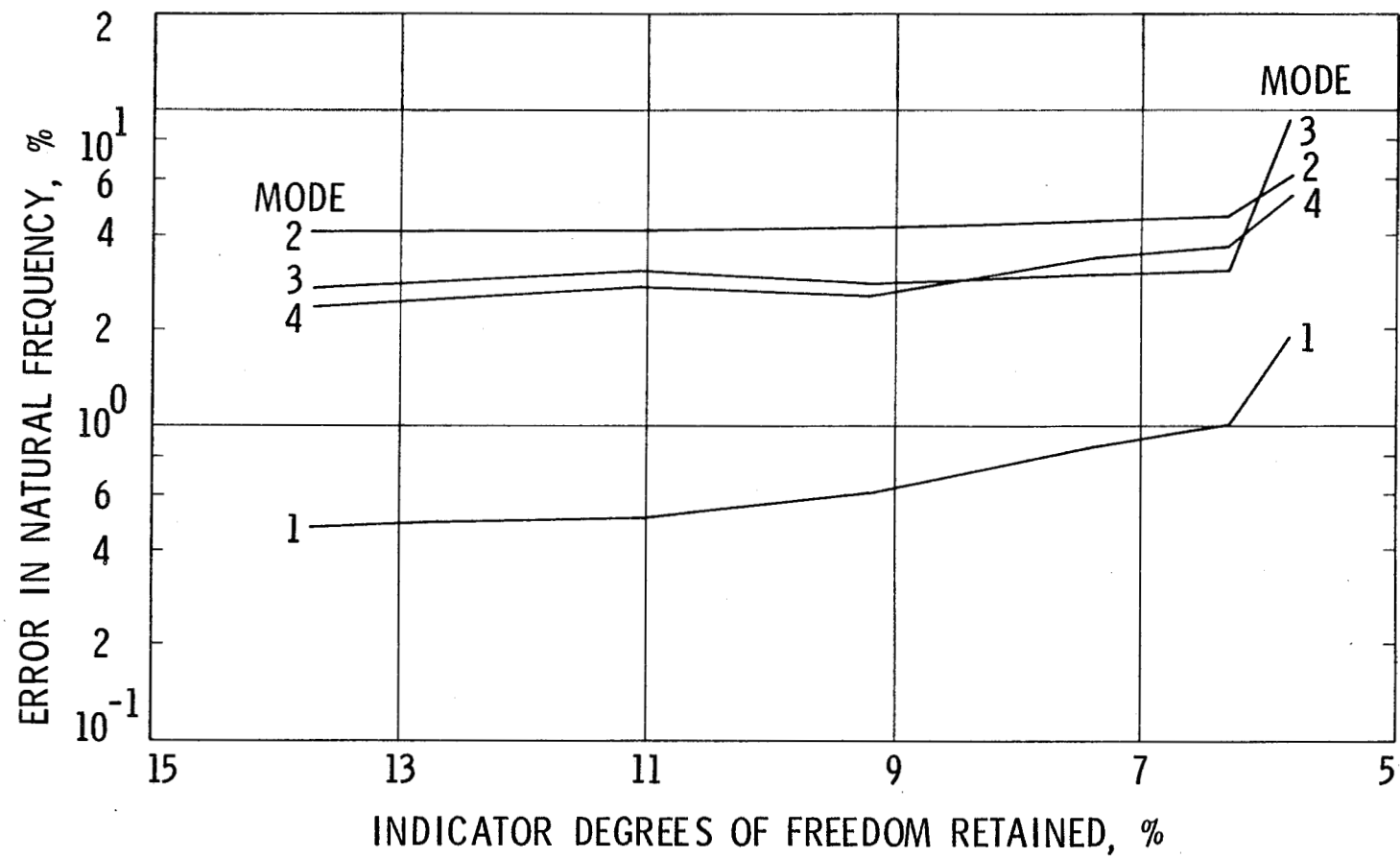


Figure 5. - Accuracy of condensed solution for reflector sector structure:
after-the-fact indicator selections

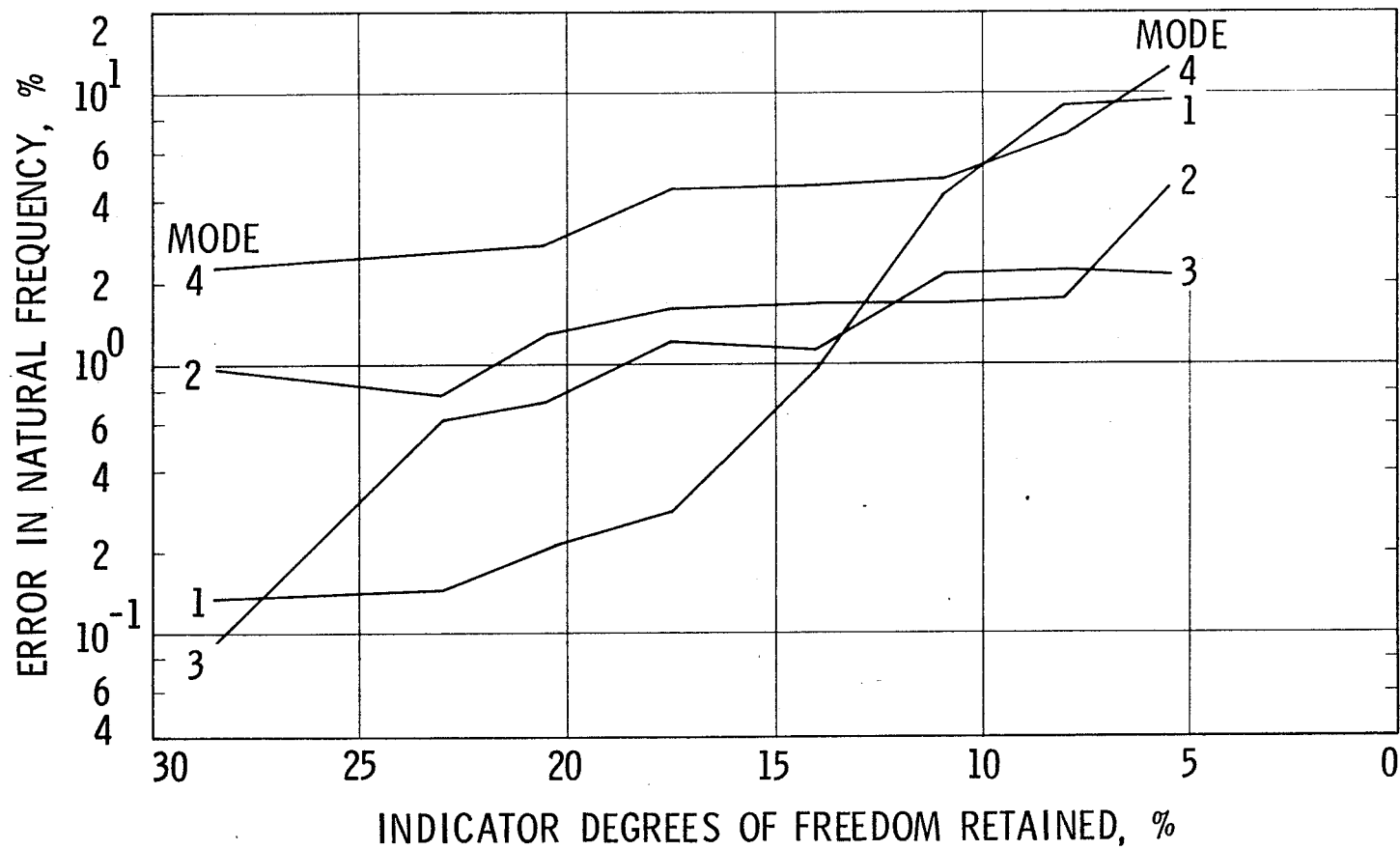


Figure 6. - Accuracy of condensed solution for pedestal structure:
after-the-fact indicator selections

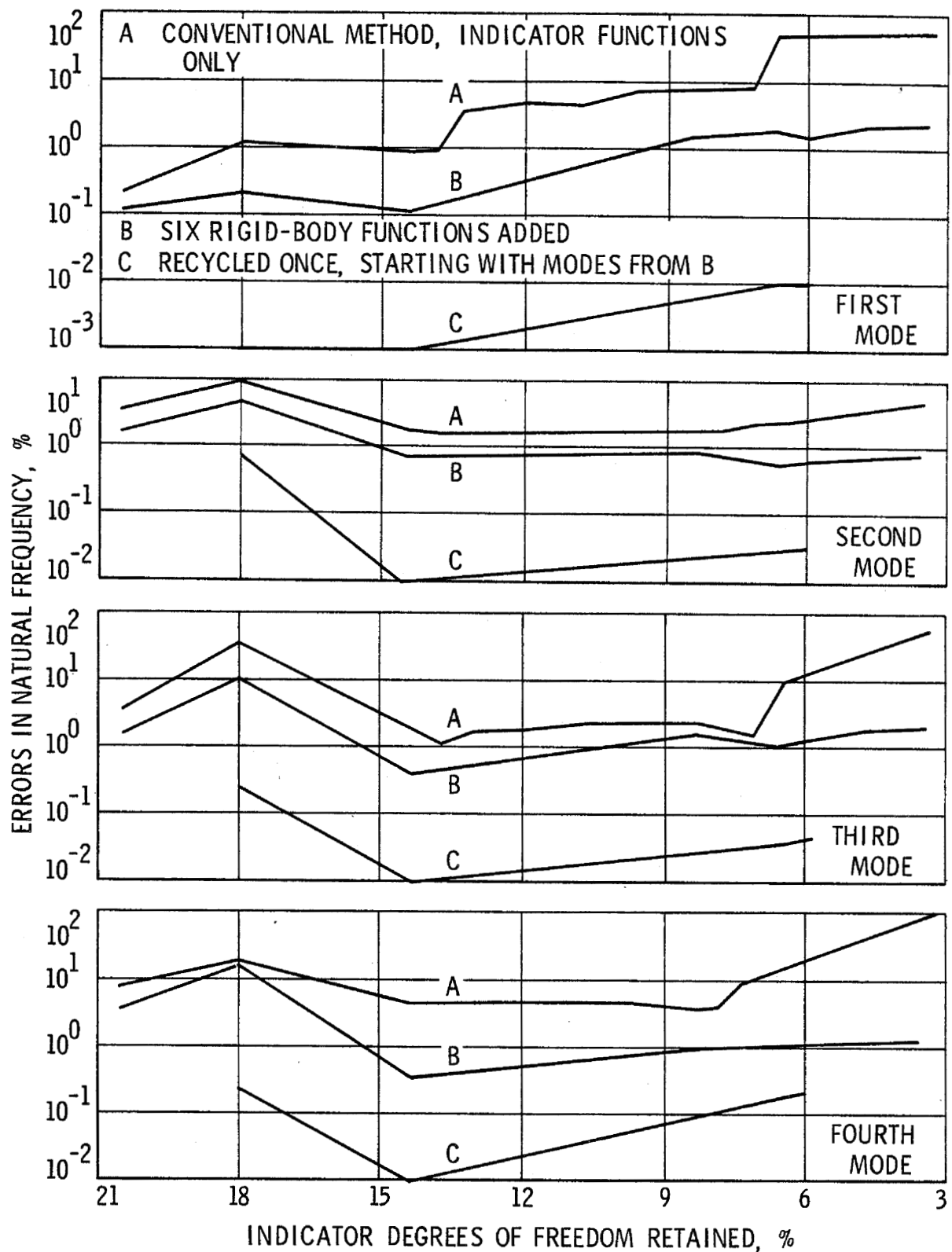


Figure 7. - Improvement of pedestal structure solution accuracy

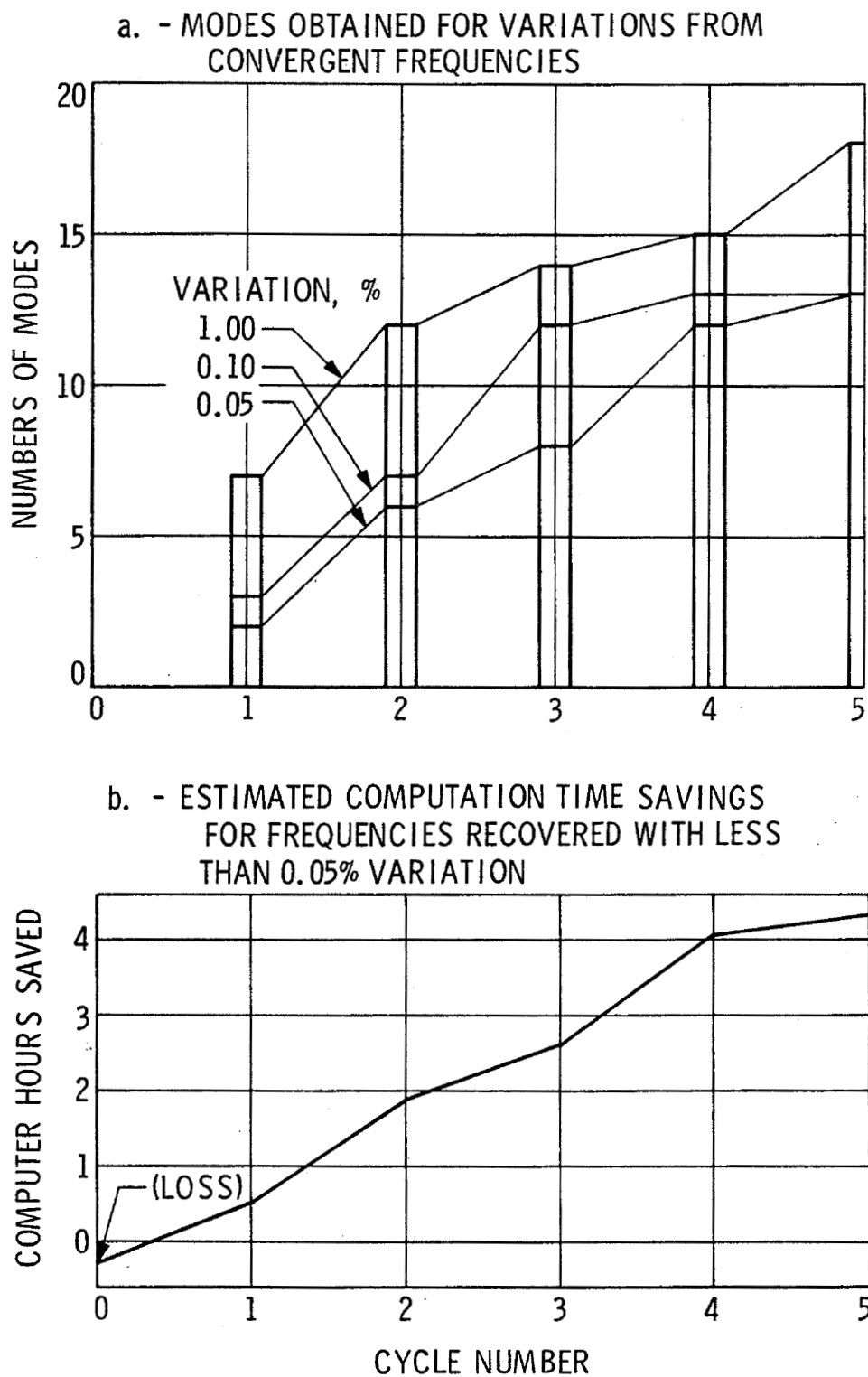


Figure 8. - Recycled solutions for antenna reflector

MODAL ANALYSIS OF THE MATED SPACE SHUTTLE CONFIGURATION

R. K. Gieseke
Senior Dynamics Engineer

Convair Aerospace Division of General Dynamics
San Diego, California

SUMMARY

The development of analytical dynamic models for the Space Shuttle system is traced from simplified early versions through current models of complex representation. The sequence of models also displays changes in design that have occurred during configuration definition and development activities. Alterations to the analytical models for accuracy of representation and improved graphical display are explained. A discussion is included that examines the program characteristics of NASTRAN, particularly as it operates within the environment of the computer monitor system and influences the analysis procedure.

INTRODUCTION

Space Shuttle is a substantial departure from currently employed concepts of space launch vehicles. Not only does it represent a change in operational technique — a fully reusable system rather than a totally expendable one — and open the door to a meaningful manned earth orbit program, it also presents new and challenging technical problems.

The shuttle concept of operations provides for a booster vehicle providing power to lift the system to high altitude and an orbiter vehicle to complete the mission of carrying men and supplies to an earth-orbiting destination. The two vehicles are mated in piggyback fashion during the boost phase. At an optimum point in the trajectory, the orbiter is separated from the booster and, under its own power, continues into orbit, carrying the payload. The booster begins a cruiseback phase, and once back in the lower atmosphere, uses jet engines to effect a powered horizontal landing. The orbiter, when it returns from its mission, re-enters the atmosphere and lands in a similar fashion. Following a period of refurbishment, booster and orbiter vehicles are ready for another earth-to-orbit mission.

Several variations of Space Shuttle configurations, representing different operational concepts, currently exist and are being examined. The discussion that follows reviews the history of modal analysis via NASTRAN for the Space Shuttle during recent configuration definition and development activities, beginning with unsophisticated beam system representations and progressing through successive levels of complex structural modeling.

Since the work reported here has been done by a potential booster vehicle contractor, emphasis is placed on the booster portion of the Space Shuttle system. Thus, while both vehicles are included in the studies, booster behavior is the principal area of interest.

EARLY ANALYTICAL MODELS

In the initial stages of development of a program such as Space Shuttle, mission requirements and vehicle configurations tend to change rapidly. Structural analysis during this period is generally limited to gross design factors; dynamic considerations more often than not are defined only as load factors, often based solely on judgment and simple hand calculations.

When all but a few candidate configurations have been eliminated, structural analysis of some greater depth may begin. Structural dynamics models for this phase are generally quite simple, since significant design changes are inevitable and the effort required to achieve extreme accuracy cannot be justified.

The first Space Shuttle analytical model constructed for use with NASTRAN simulated an orbiter mated to a V-tail configured booster. An artist's rendition of this booster design is shown in figure 1. Estimates of EI, AE, and GJ distributions along the lengths of the fuselage, wings, and tail provided approximate section properties for uniform beam segments (NASTRAN's BAR elements) used to represent these components of the booster vehicle. Elastic characteristics of the orbiter were not available at the time of this study; consequently, a rigid orbiter simulation was used. The model takes advantage of the symmetry of both vehicles in the pitch plane and represents the left side of the mated configuration only (figure 2).

At the time of this analysis, the arrangement of the booster-orbiter attachment linkages and their elastic properties was not firmly defined. Consequently, spring rates were assigned to the links so as to give the desired minimum 2.0 Hz frequency of response for rigid vehicles. Representation of the attachment links (figure 3) in the NASTRAN model was by scalar springs (ELASi).

Connection of the various components was achieved through the use of dependency equations, or, in NASTRAN terminology, equations of multipoint constraint (MPC). The BAR elements representing the booster fuselage were located along the booster fuselage centerline. Wing and tail roots were located at the periphery of the fuselage cross-section, one fuselage radius away from the fuselage BAR segments. Additional grid points were located on the fuselage center line at the same fuselage station as the neutral axes of the wing and tail at their respective roots. Rigid links were introduced into the model connecting booster fuselage elements to wing and tail roots. These rigid links permitted the motions of wing and tail root grid points to be defined in terms of the fuselage grid points adjacent.

The ends of the booster-orbiter attachment springs were likewise located at a geometric offset from both vehicle center lines. Dependency equations were employed here also, expressing motions at the spring ends as functions of the motions of points on booster and orbiter center lines. For the booster, these points were in the transverse plane of the spring ends; for the orbiter, the center of gravity was used as the reference grid point. (Since the orbiter was rigid, there can be only one independent grid point in the model.)

For graphical display purposes, plot elements (PLOT) were included to show the fictitious rigid connection links between components and the attachment springs. The rigid orbiter center line was also displayed through the use of plot elements connecting grid points at nose and tail. These points were rigidly connected to the orbiter center of gravity by multipoint constraint equations.

This first Space Shuttle model contained 34 grid points, but the various constraints imposed on it reduced the number of degrees of freedom of the eigenvalue problem to about 100 for a given symmetry boundary condition. Since no coordinate elimination procedures (OMIT cards) were employed, the stiffness matrix remained reasonably well banded, with a semi-bandwidth of 30 to 40. Modal data was extracted with a minimum of effort and expense.

When the V-tail concept was replaced with a conventional vertical tail version (figure 4), the modal model was accordingly revised (figure 5). This change provided an opportunity to introduce certain changes in modeling concept.

The first area of model improvement was the introduction of a new representation of longitudinal behavior for the booster fuselage. Earlier studies (ref. 1) have developed a spring-mass analogy to account for the interaction of fluids and their tanks under longitudinal excitation. The presence of large amounts of propellants in the booster fuselage invalidates any simulation of longitudinal behavior based on structural characteristics alone, hence the necessity for a distinct

fluid-tank longitudinal model (figure 6). Models such as this have been shown to give good approximation to the first longitudinal mode of fluids in elastic tanks.

The fluid-tank model was incorporated into the Space Shuttle model by (1) defining the new booster fuselage longitudinal description using scalar points and scalar springs; (2) constraining all longitudinal degrees of freedom in the booster fuselage beam representation; and (3) rewriting all pertinent multipoint constraint equations, substituting the appropriate scalar degree of freedom in the new model for the previously used fuselage longitudinal degree of freedom.

Secondly, with the earlier model, it was impossible to display wing and tail torsional responses. To overcome this deficiency, grid points were added to the model on the leading and trailing edges of wing and tail surfaces directly in line with the existing grid points located on the neutral axes of those components. The aerodynamic surfaces were still idealized as beams, so these new grid points were not used for any elasticity or mass definition. However, by assuming that the cross-sections of the surfaces remained rigid when deforming, the motions of the edge points could be defined (through the use of MPC equations) in terms of the motions of the corresponding points on the neutral axes. Plot elements connecting the edge points permitted the neutral plane of the aerodynamic surfaces to be displayed in the structure plots, and more accurate evaluation of the character of the modal distortions was possible.

The eigenvalue problem resulting from this simulation is not significantly larger than that of the first described model, although, with the addition of grid points on the edges of the aerodynamic surfaces, the initial order of the problem (NASTRAN's g-size) is increased by over 200. At the moderate cost involved in handling the additional dependent degrees of freedom, a much more meaningful display of modal distortions is achieved (figure 7).

Analysis of the model just described revealed that the configuration had a fundamental elastic mode under antisymmetric boundary conditions of 0.82 Hz. At this frequency, coupling of structural responses with nonstructural dynamic effects such as slosh or rigid body control frequencies, becomes possible. The mode shape associated with this frequency indicated that the two vehicles were yawing in opposition with very little bending. The potential energy of the mode shape was found to be concentrated in the attachment springs and in torsional distortion of the booster fuselage. Since neither orbiter flexibility nor booster fuselage local flexibilities had been included in the model, the actual frequency for the design would be substantially lower than that calculated, and adverse coupling problems would be a near certainty.

FUSELAGE MODEL REFINEMENT

To accurately evaluate the effectiveness of the fuselage structural redesign initiated to raise the fundamental antisymmetric frequency, a detailed structural model of the booster fuselage was developed for the next configuration in the sequence, a delta wing version (figure 8). In anticipation that this model would later be incorporated into a complete system dynamic model, NASTRAN was chosen to be the analytical tool to be used in the loads analysis to take advantage of its capacity for both static and dynamic studies. The portion of the booster fuselage modeled as a stiffened cylinder included the region from the forward orbiter attach point to the leading wing spar, some 1-1/3 diameters aft of the rear orbiter attach point. This region incorporates the intertank structure plus the forward portion of the LH₂ tank (figure 9). Major strength frames such as those supporting the attachment fittings were modeled directly, using six BAR elements of different section properties, each representing a 30-degree segment of a half-frame. Other stiffening frames were modeled in a similar manner after first combining several into one equivalent frame. Longitudinal stiffeners at 30 degrees around the fuselage circumference were given section properties to duplicate the axial load carrying capacity of the actual stiffeners plus the effective

skin areas. Rectangular shear panels completed the fuselage model. The orbiter attachment links (which, by this time, had been designed) were represented by axial load carrying (ROD) elements. By fixing the aft-most frame and applying loads to the orbiter side of the attachment links, a detailed stress analysis was carried out. This model provided a good evaluation of the flexibility of the booster fuselage local structure supporting the orbiter attachment links as well as the links themselves. As design changes have been made, the model has been revised and used to evaluate the effect of such changes on the flexibilities of the region.

To use this cylindrical model for evaluation of modal properties of the mated configuration required both integration of the model into the simulation of the rest of the structure and adding mass information in an effective manner.

The remainder of the booster fuselage, both fore and aft, was still defined only in terms of stiffness and mass versus fuselage station; the beam simulation approach previously employed was again used for these regions. The problem of compatibility between the beam representation and the detailed skin-frame model is accomplished by defining grid points located at the intersection of the planes of the first and last frame modeled, and the fuselage center line. The adjacent beam elements connect directly to these grid points.

Figure 10 shows a cross-section of a frame of the fuselage model. Displacement coordinates are shown to be in a cylindrical system (direction 1 is radial; 2 is tangential; 3 is normal) for exterior grid points 1 through 7 and rectangular for the center grid point, 0. Rotation about a coordinate direction, i , is identified as component $i + 3$. Let $u_i(j)$ represent motion component i for grid point j . Then a set of compatibility expressions can be written as

$$u_1(0) = (u_3(1) + u_3(7))/2 \quad (1)$$

$$u_2(0) = (-u_1(1) + u_2(7))/2 \quad (2)$$

$$u_3(0) = (u_1(1) - u_1(7))/2 \quad (3)$$

$$u_4(0) = (u_2(1) + u_2(7))/2r \quad (4)$$

$$u_5(0) = (u_1(1) - u_1(7))/2r \quad (5)$$

$$u_6(0) = u_3(4)/r \quad (6)$$

To reduce the size of the modal problem as far as practical, mass distribution in the fuselage, including propellants, was defined in terms of fuselage station. Concentrated masses were assigned to fictitious grid points located on the fuselage center line at each frame of the model. Application of the compatibility equations (1) through (6) at each frame related these masses to the elasticity of the fuselage structure.

The delta wing design of this new configuration does not lend itself to simple beam simulation of aerodynamic surfaces. Efforts were made to incorporate flexible aerodynamic surfaces into the dynamic model, but for reasons that will be discussed below, attempts to do so were unsuccessful. The critical concern at the time was the frequency of the lowest elastic mode. Previous work had suggested that for the lowest modes, little strain energy would be found in the aerodynamic surfaces. Consequently, it was decided to proceed with the analysis using rigid representation of the aerodynamic surfaces.

Orbiter stiffness and mass distributions versus longitudinal station were obtained and a flexible beam model made for it. The assembled dynamic model is shown in figure 11. The unrestrained

size of the system (g-size) is 750. Application of boundary constraints and dependency equations (SPC and MPC cards) reduced this order to 501. All remaining degrees of freedom without mass properties were removed by static condensation procedures (OMIT cards), leaving an eigenvalue problem size of 58. The fundamental antisymmetric mode obtained (figure 12) had a frequency of 0.9 Hz or 0.08 Hz more than the earlier, simplified model. The additional flexibility contained in the new model due to the local structure effects is compensated for by increased stiffness due to redesign, hence the negligible change in frequency.

The wing and tail of the booster generate large loads that are reacted into the fuselage immediately aft of the region modeled in detail. The transformation from cylinder to beam representation used in this study was inadequate to transmit these loads properly and excessive model distortions resulted in this region. If the stiffened cylinder form of representation for the booster fuselage were extended further aft, the proper paths for loads from the aerodynamic surfaces could be developed and more representative modal displacements would result.

The model described above is inadequate if higher modes of the structure are to be obtained, since rigid aerodynamic surfaces were used. As the frequency approaches that of the aerodynamic surfaces alone, their contribution becomes more significant and an elastic representation becomes a necessity.

MODELING OF FLEXIBLE AERODYNAMIC SURFACES

The design of the aerodynamic surfaces -- wing, tail, and canard -- of the Space Shuttle booster was assigned to the engineering staff at the Fort Worth operation of Convair Aerospace. An analytical model of each surface was prepared and analyzed at that facility using a computer program other than NASTRAN. The elastic characteristics of the three components were transmitted to the San Diego operation of Convair Aerospace in the form of an unrestrained stiffness matrix on cards. Concentrated weight distributions and geometric data were supplied in printed form. These latter two classes of data were easily reformatted into NASTRAN form, the weight data as CONM2 cards and the geometric data as GRID cards.

The procedure chosen to enter the elasticity information for the aerodynamic surfaces into the NASTRAN simulation was to use DMIG cards to input the stiffness matrices directly, then add them to the stiffness matrix generated by NASTRAN for the remainder of the structure. Once the matrix additions are accomplished, the analysis continues in the normal manner.

The stiffness matrices for the canard, wing, and tail are respectively of order 42, 98, and 42, and essentially full due to earlier static condensations. Using small field form exclusively, some 7,000 card images are required to enter the data. The limitation of eight characters per field where exponential form is necessary degrades the accuracy of the data to a degree that adequate description of the characteristics of the aerodynamic surfaces could not be achieved in this fashion. One possible remedy is the use of large field format for the DMIG cards, but this was rejected as a solution due to the cost and hazards associated with processing 14,000 bulk data cards.

The technique currently being implemented for introducing the elasticity of the aerodynamic surfaces involves the use of the general element (GENEL). Using static condensation techniques, the degrees of freedom in each stiffness matrix have been reduced to a number more appropriate to the task of obtaining total vehicle modes. The mass matrices have also been reduced using the same Guyan techniques as in NASTRAN. For the canard, wing, and tail, these reduced orders are 5, 40, and 10 respectively. Inversion of the stiffness matrices, after determinate constraints are applied, produces the flexibility matrix required for the general element definition. Use of the general element enables the elastic properties of the aerodynamic surfaces to be entered into the analysis by using only 300 cards. And, as the theoretical discussion of the general element points out, for

the same number of significant digits, the flexibility matrix contains more accuracy since the rigid body components have been removed.

The modal amplitude at all grid points on the aerodynamic surfaces can be recovered if the grid points are included in the initial description of the system. The deleted degrees of freedom are indicated as fixed on the GRID card, so that the eigenvector resulting from the eigenvalue operation will indicate zero amplitudes for these elements.

The condensation process has performed the following operation

$$[K_{red}] = [K_{rr}] - [K_{rd}][K_{dd}]^{-1} [K_{dr}] \quad (7)$$

where

$[K_{red}]$ is the condensed stiffness matrix and $[K_{rr}]$, $[K_{rd}]$, $[K_{dd}]$, and $[K_{dr}]$ are partitions of the original matrix with subscripts r and d indicating retained and deleted degrees of freedom, respectively. Defining

$$[G] = [K_{dd}]^{-1} [K_{dr}] \quad (8)$$

from the theory upon which the condensation is based

$$[u_d] = [G] \{u_r\} \quad (9)$$

where $\{u_d\}$ is the vector of deleted degrees of freedom and $\{u_r\}$ is the vector of degrees of freedom retained.

The g-size eigenvector matrix produced by modules READ and SDR1 can be partitioned into nonsurface degrees of freedom, surface degrees of freedom retained, and surface degrees of freedom deleted.

$$\{\bar{\phi}\} = \begin{Bmatrix} \phi \\ \text{---} \\ \phi_r \\ \text{---} \\ \phi_d \end{Bmatrix} = \begin{Bmatrix} \phi \\ \text{---} \\ \phi_r \\ \text{---} \\ 0 \end{Bmatrix} \quad (10)$$

If the recovery matrix, $[G]$, is entered into the analysis via DMIG cards, it will be given an order equal to the g-size, with zero fill where appropriate. Thus, it can modify the eigenvector matrix via matrix algebra to obtain the modal amplitude of the deleted surface degrees of freedom.

$$\begin{Bmatrix} 0 \\ \text{---} \\ 0 \\ \text{---} \\ \phi_d \end{Bmatrix} = \begin{bmatrix} 0 & 0 & 0 \\ \text{---} & \text{---} & \text{---} \\ 0 & 0 & 0 \\ \text{---} & \text{---} & \text{---} \\ 0 & G & 0 \end{bmatrix} \begin{Bmatrix} \phi \\ \text{---} \\ \phi_r \\ \text{---} \\ 0 \end{Bmatrix} \quad (11)$$

The final eigenvector, including all coordinates on the aerodynamic surfaces, is

$$\{\bar{\phi}\} = \begin{Bmatrix} \phi \\ \text{---} \\ \phi_r \\ \text{---} \\ 0 \end{Bmatrix} + \begin{Bmatrix} 0 \\ \text{---} \\ 0 \\ \text{---} \\ \phi_d \end{Bmatrix} \quad (12)$$

This procedure will be applied to the current Space Shuttle model, shown in figure 13. This model with flexible booster aerodynamic surfaces and detailed modeling of the entire booster fuselage, is expected to yield much useful information about the dynamic characteristics of the Space Shuttle vehicle.

PROGRAM-ORIENTED CONSIDERATIONS

All analytical investigations are idealizations of reality, influenced among other things by the nature of the analysis tools available. The characteristics of NASTRAN, particularly when situated in the environment of the Computer Laboratory at the San Diego operation of Convair Aerospace, have influenced the analyses just described in several significant ways.

The current configuration of the Scientific Data Processing Laboratory at the San Diego facility consists of a CDC 6400 system that includes a central processor of 65,00010 - sixty-bit word capacity. It currently uses the SCOPE 3.2 monitor system. About 140,0008 words at core storage are available to the batch job user. To restate the size of available core in terms that may be more meaningful to NASTRAN users, for this facility the matrix decomposition routines of NASTRAN are limited to semiband widths of 140 to 160 for symmetric decomposition and 70 to 80 for unsymmetric decomposition if spill logic is to be avoided.

NASTRAN has not been constructed to operate most effectively in such a confining environment and consequently, comparisons with other programs are often unfavorable. The planned single precision option will substantially improve NASTRAN's performance on CDC computers, both in terms of speed of operation and in practical problem size. Further, the use of a symmetric matrix decomposition procedure for normal mode extraction would further enhance its attractiveness to structural dynamicists.

A computer user cost algorithm that assigns progressively higher scaling factors to larger field length jobs has forced users to experiment with minimum field length requests when using NASTRAN. For the size and character of problems being analyzed, experience has shown that nearly all functional modules can operate at a field length of 120,0008 cells or less. One regularly used module that needs more memory is the Structural Matrix Assembler, phase 1 (SMA1), which normally requires an additional 10,0008 cells. Operations involving matrix decomposition have field length requirements more directly dependent on the order of the matrices involved. To reduce the cost of a NASTRAN analysis, the execution of the sequence of functional modules may be arbitrarily broken into three or more segments of different field lengths. For example, modal analysis problems have been solved in three separate passes: first, at a field length of 130,0008 cells, to get past SMA1; the second, at a field length of 120,0008 cells, to continue the analysis to the eigenvalue module, READ; and lastly, at a field length of 140,0008 cells, the execution of the READ module, which involves an unsymmetric matrix decomposition, and final output of eigenfunctions. Plotting, if desired, is acquired in a fourth run, at 120,0008 cells of core storage.

But by far the most difficult problem associated with using NASTRAN is the fact that it has not been possible to access the source code. The CDC version of NASTRAN was coded for the standards of the Langley Research Center CDC facility, which has a unique version of the CDC RUN compiler. As a consequence, NASTRAN source code cannot be compiled using the standard RUN compiler or the San Diego operation RUN compiler. Further, no correction or modifications can be made and when a program error is found, the only recourse is to redefine the solution process so that the error is not encountered. All potential resolutions to this problem have thus far been judged unacceptable or have encountered difficulties in implementation. A source code based on standard RUN compiler FORTRAN for future versions of NASTRAN would substantially improve the task of program maintenance at the various CDC installations having the program.

REFERENCES

1. Rose, R.G., Staley, J.A., and Simson, A.K.: A Study of System-Coupled Longitudinal Instabilities in Liquid Rockets — Part I, Analytical Model. AFRPL-TR-65-163, Sept. 1965.

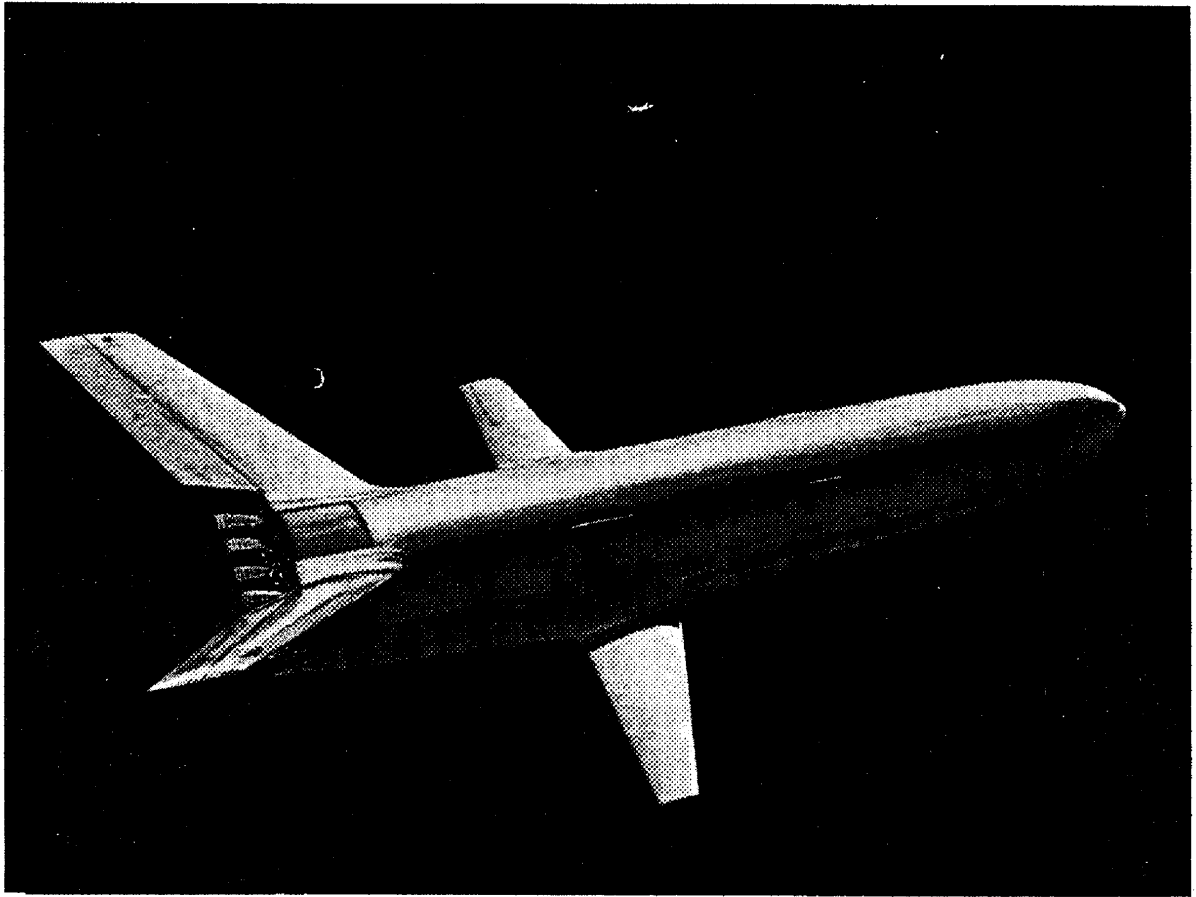


Figure 1.- V-tail configuration.

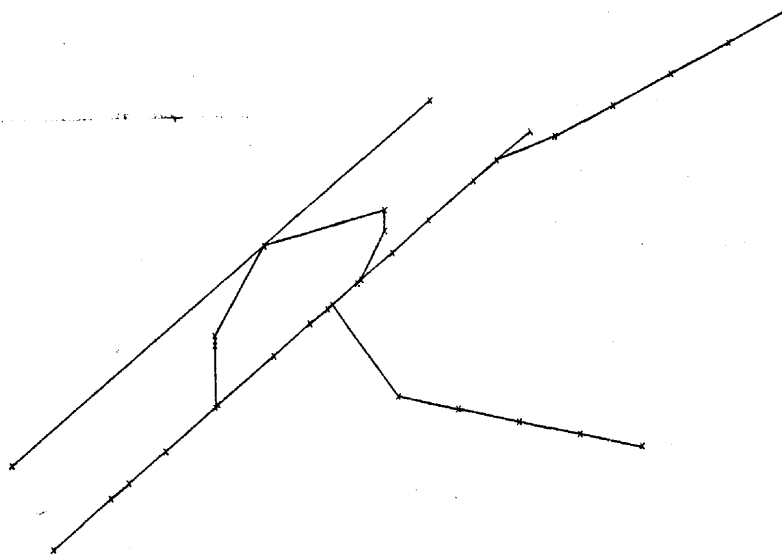


Figure 2.- V-tail version dynamic model.

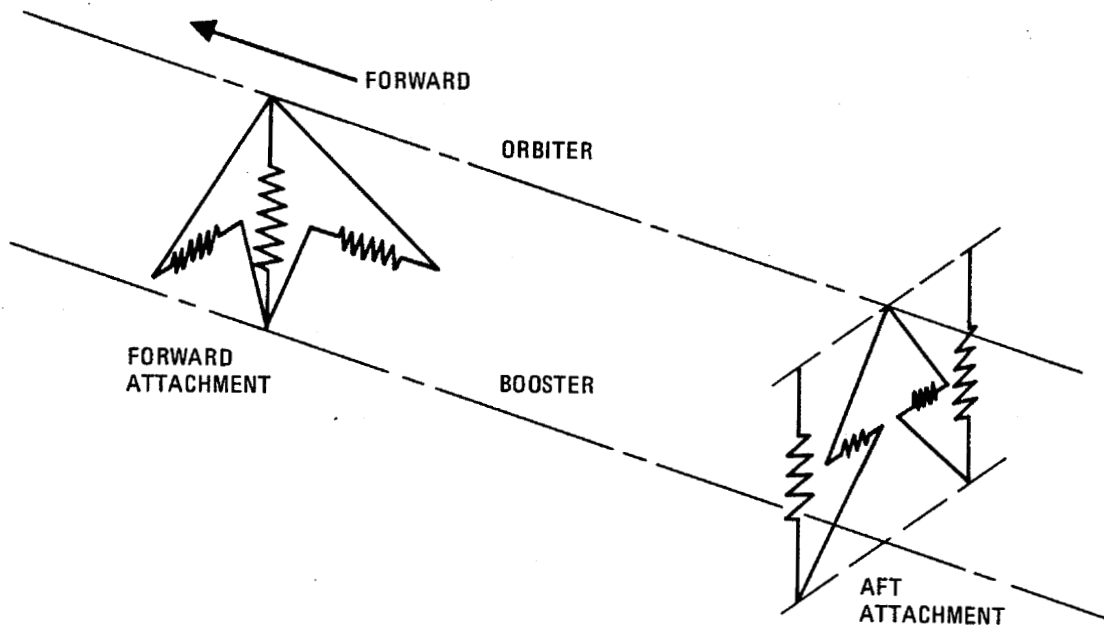


Figure 3.- Attachment link model.

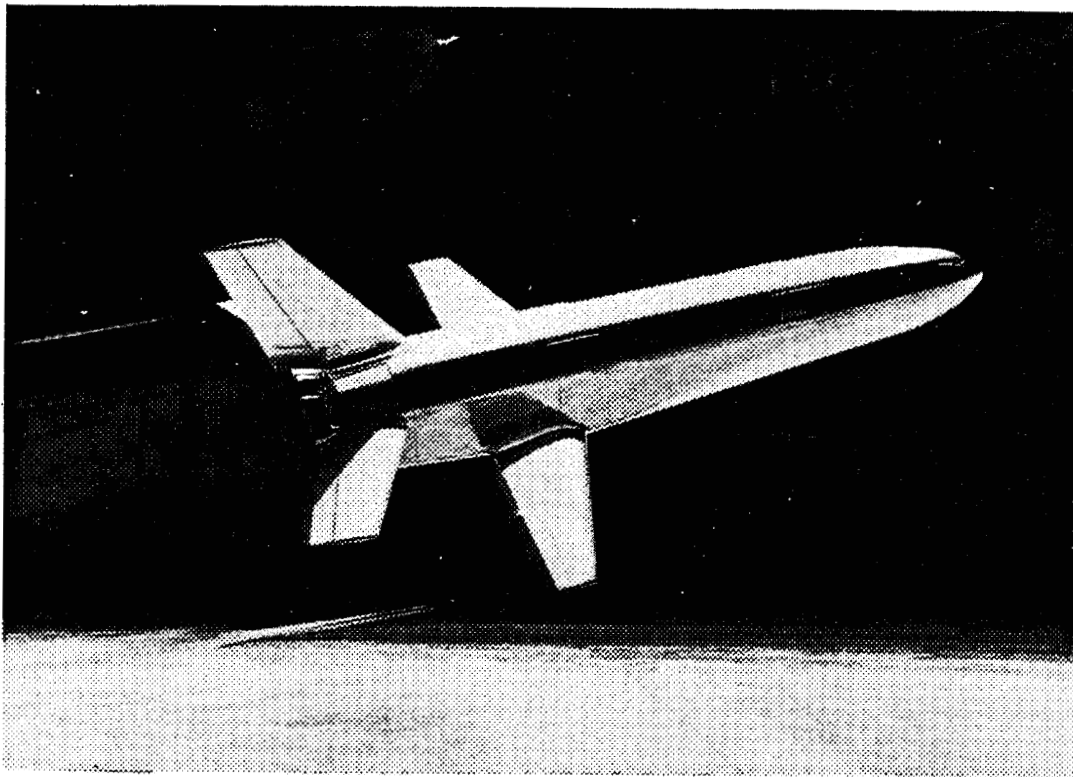


Figure 4.- Vertical tail configuration.

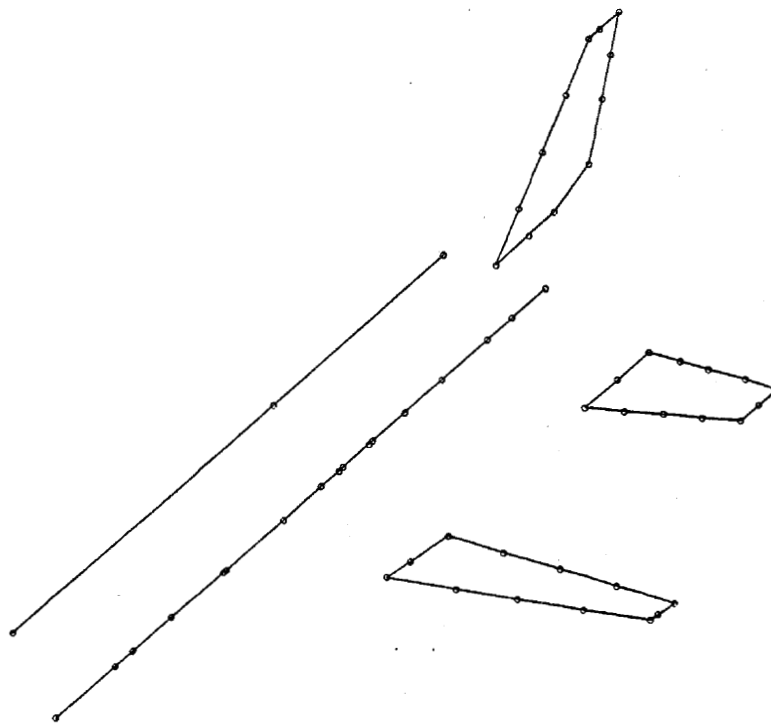


Figure 5.- Vertical tail version dynamic model.

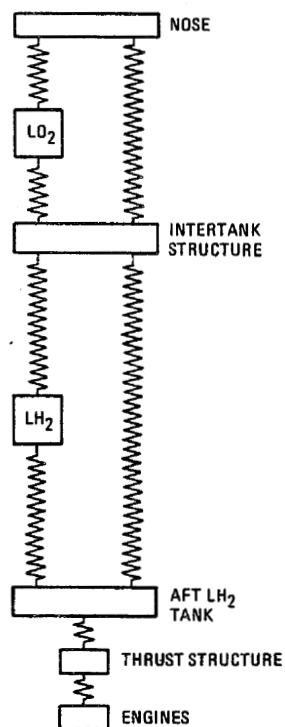


Figure 6.- Fluid-tank longitudinal model.

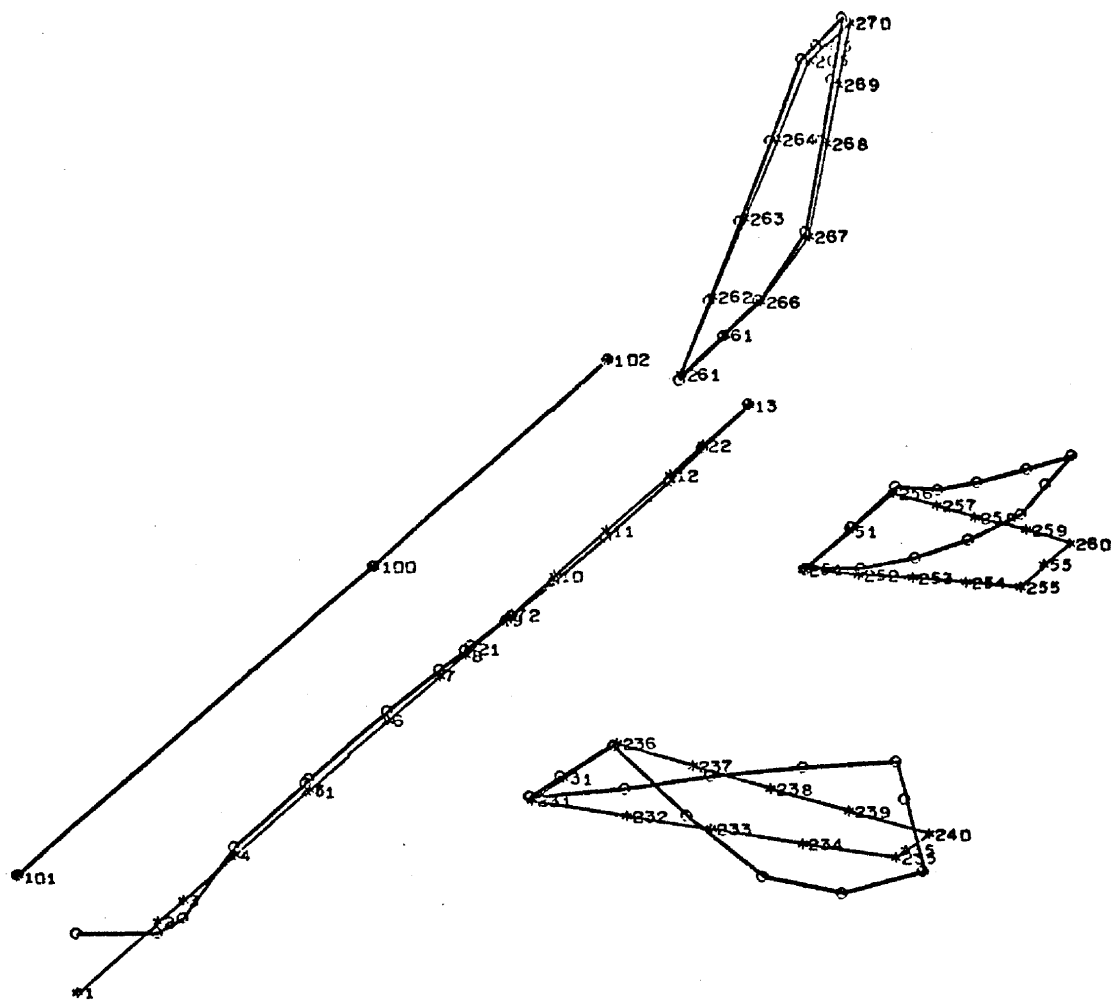


Figure 7.- Wing torsion vibration mode shape.

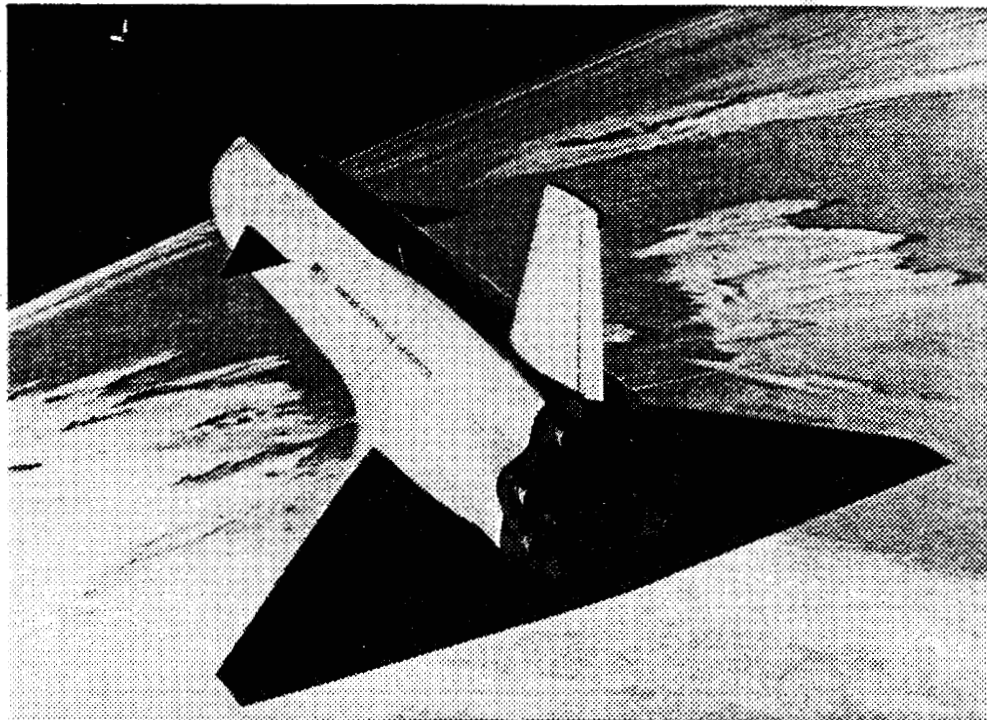


Figure 8.- Delta wing configuration.

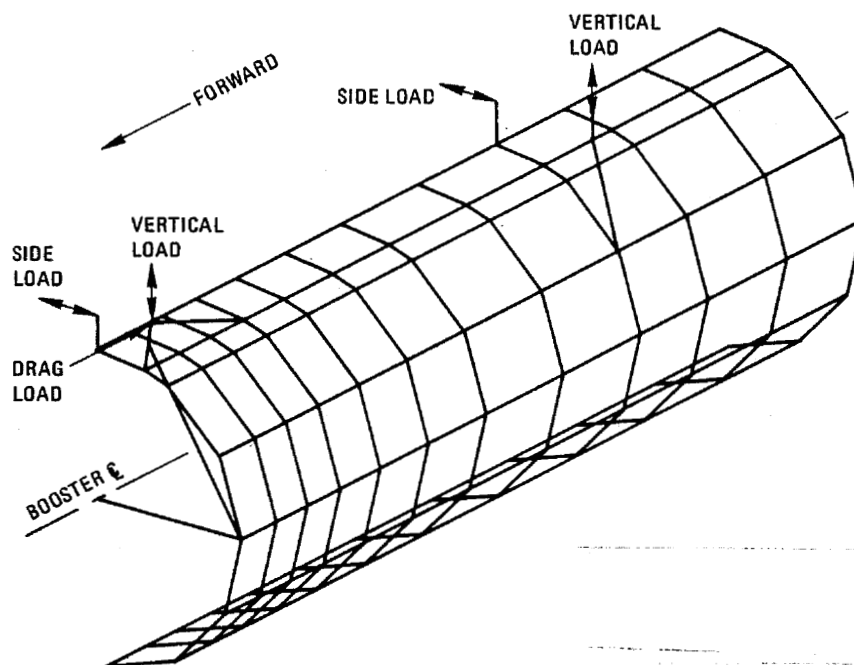


Figure 9.- Booster fuselage stress model.

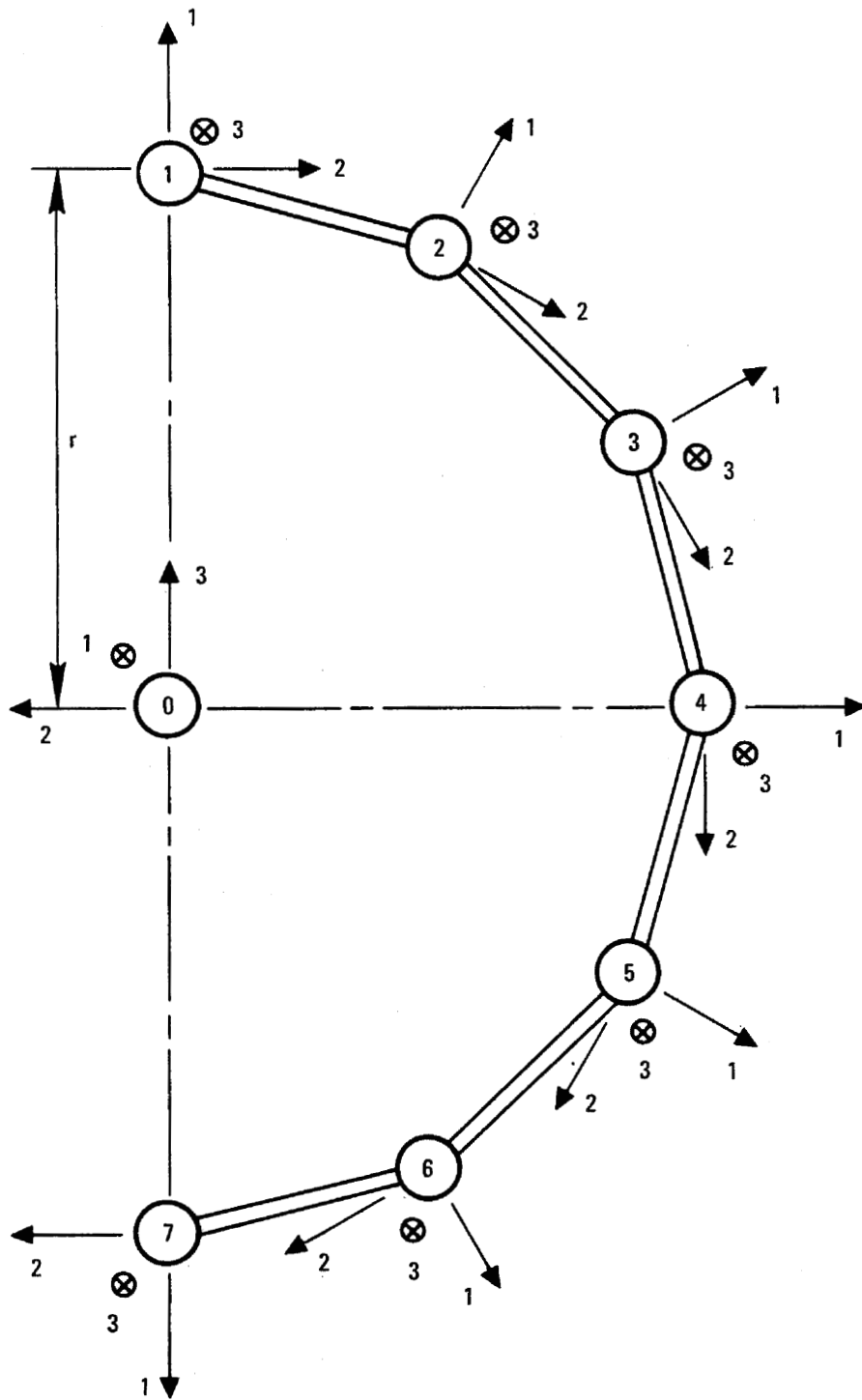


Figure 10.- Fuselage model cross-section.

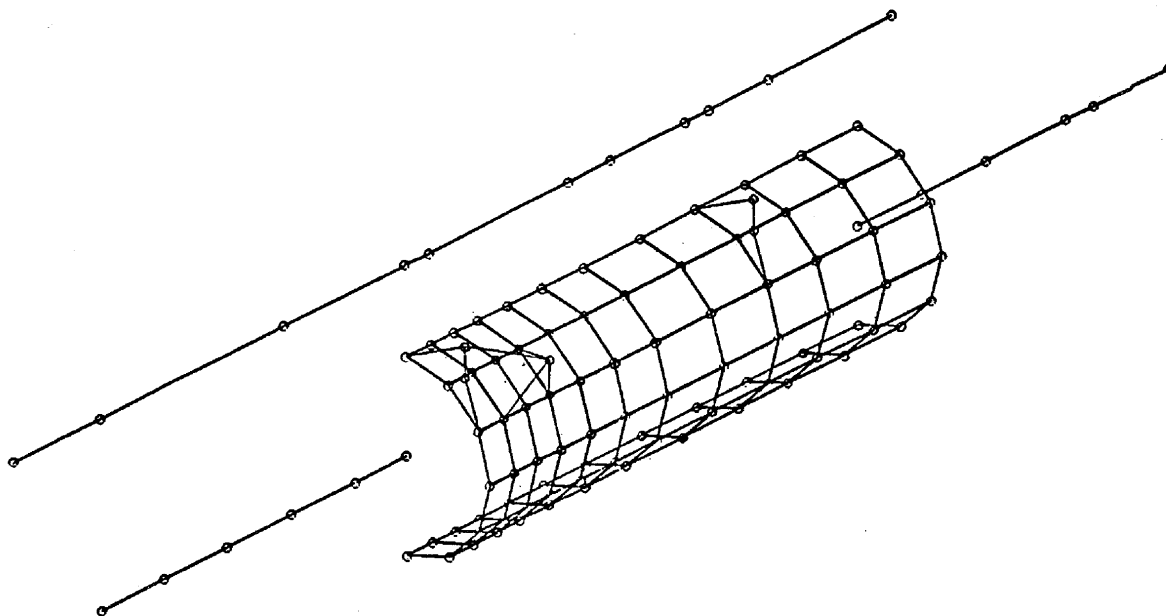


Figure 11.- Delta wing version dynamic model with detailed fuselage.

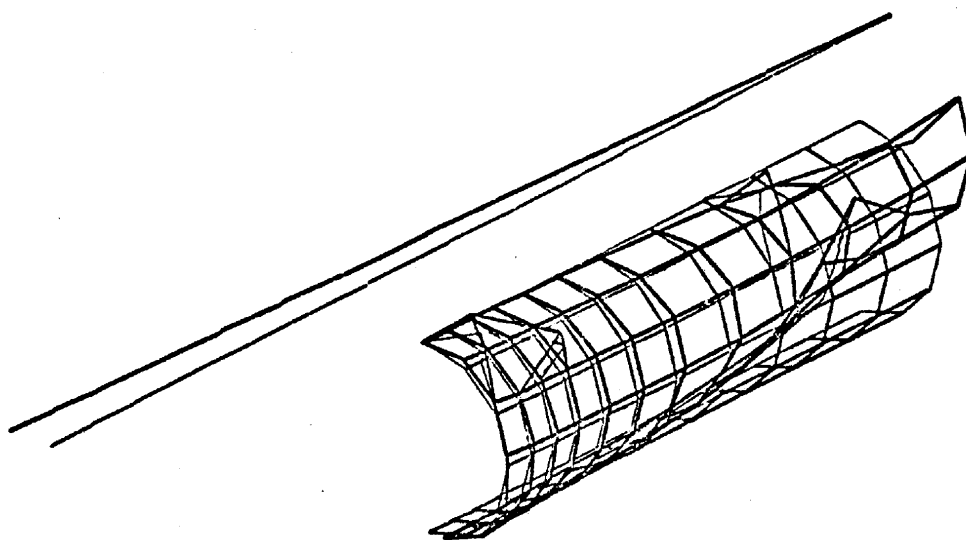


Figure 12.- Fundamental antisymmetric vibration mode shape.

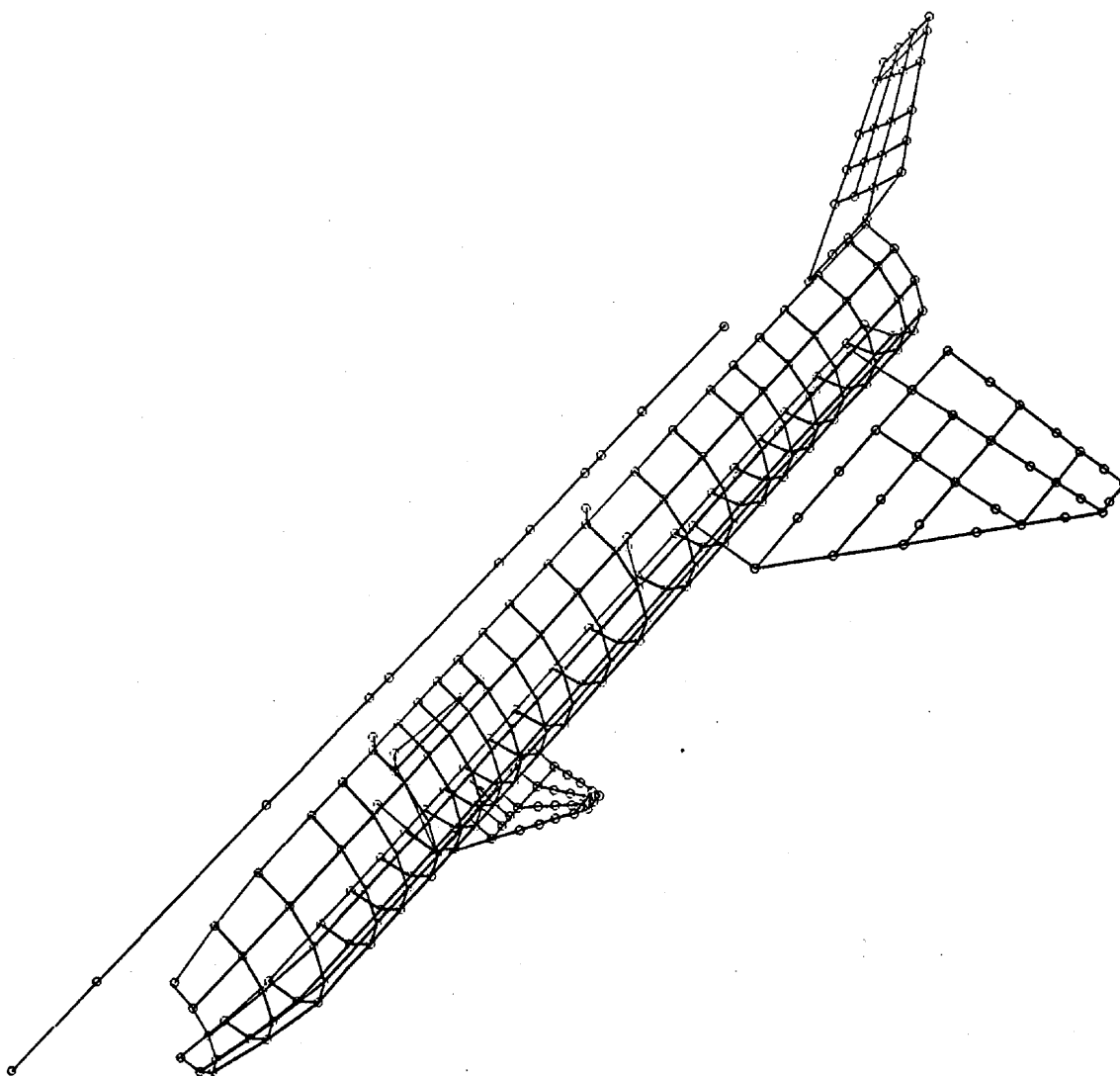


Figure 13.- Detailed dynamic model for delta wing version.

NORMAL MODE ANALYSIS OF THE RADIO ASTRONOMY EXPLORER
(RAE) BOOMS AND SPACECRAFT

by

Dr. K. N. Jabbour

NASA Goddard Space Flight Center

SUMMARY

In this paper, the problem of determining the normal modes of RAE booms and spacecraft for in-flight configuration is analyzed. The solution is based on the use of a finite element model of the booms and spacecraft along with NASTRAN's normal mode analysis. The inverse power method of eigenvalue extraction was utilized.

The results are presented as a summary of real eigenvalues and plots of the six rigid body mode shapes, the eight first mode shapes, and the eight second mode shapes.

The study showed that considerable care must be exercised when using NASTRAN in the solution of complex problems.

INTRODUCTION

The objective of the RAE satellite project is to measure the intensity of radio signals from celestial sources. To achieve this objective the spacecraft employed a pair of long "V" antennas back to back, thus forming a large "X" with central hub of instrumentation at the juncture of the antennas (fig. 1). The antennas (or the booms) are tubular structures which were deployed from the central body once the spacecraft was in 6000 km circular orbit. Gravity-gradient attitude stabilization was used so that one set will always point toward the earth.

The problem of determining the in-flight boom shape is an important one because the interpretation of the experimental data requires an accurate knowledge of the antenna pattern at the time of observation (see refs. 1 to 7). The booms in orbit are under the influence of gravitational, inertial, and solar pressure forces and thermal bending.

The purpose of this study is to generate a NASTRAN model to determine the normal modes of RAE booms in a field free of gravitational, inertial, and thermal forces.

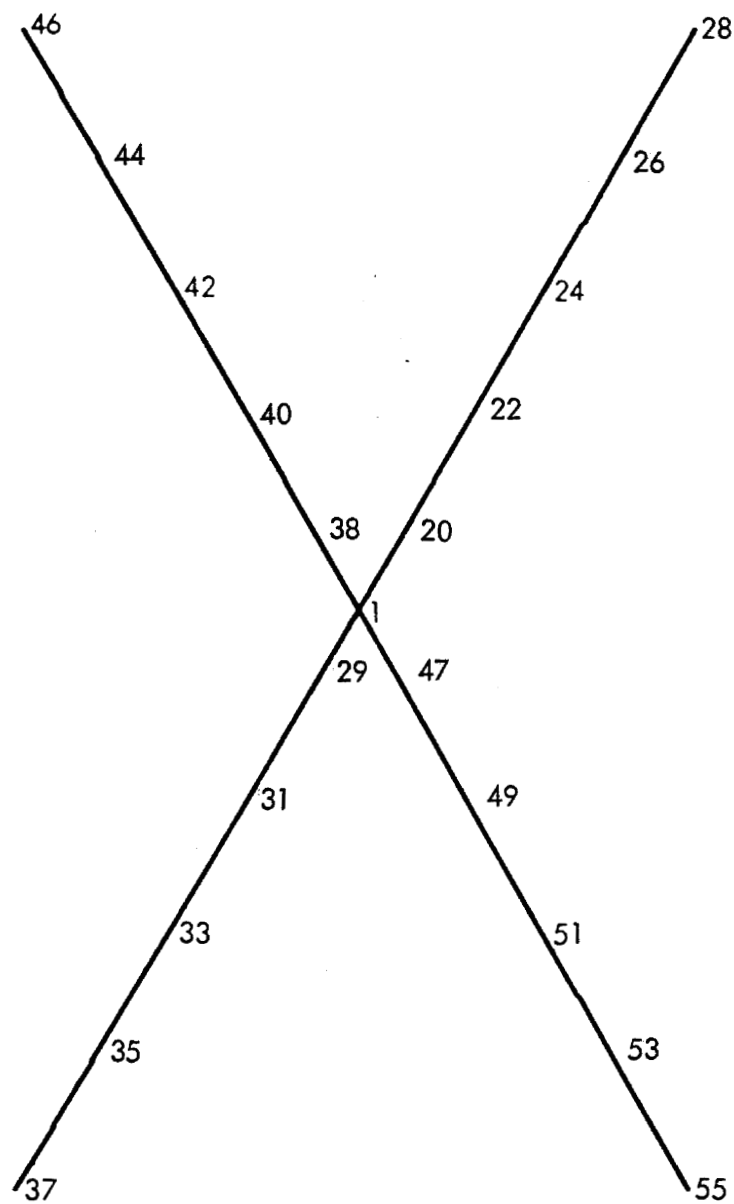


Figure 1. RAE booms geometry.

COMPUTER SIMULATION

The RAE booms were modeled using CBAR elements with coordinate systems parallel to the booms. Multipoint constraint (MPC) cards were used to express the inextensibility of the booms in the longitudinal direction. CONM2 and SUPORT cards were used to model the central hub and its fictitious support. Figure 1 shows the finite element model for RAE booms and spacecraft.

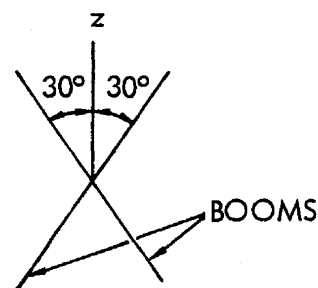
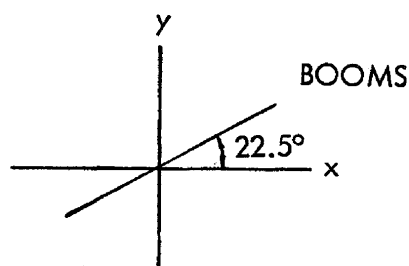
A reasonable and accurate way of modeling the booms necessitated the use of 37 grid points having 144 degrees of freedom. The computer time required for a nominal run was between 8 and 12 minutes using an IBM 360/95. The plots shown in figures 2 to 5 were generated using a Stromberg-Carlson 4020 plotter.

The parameters involved in this study, as used in the bulk data, are:

1. Tube diameter = 0.58 inch
2. Weight = 0.017 lb/ft
3. Effective Stiffness, $EI = 2000 \text{ lb-in}^2$
4. Length = 450 to 750 feet
5. "V" angle = 60°
6. Central Hub Weight = 425.73 lb
7. Central Hub Inertias:

$$\begin{aligned}I_{xx} &= 81,046.56 \text{ slug-in}^2 \\I_{yy} &= 931.5276 \text{ slug-in}^2 \\I_{zz} &= 81,761.04 \text{ slug-in}^2 \\I_{xy} &= 3,924.336 \text{ slug-in}^2\end{aligned}$$

x, y, and z axes are defined as shown below:



COMPUTER RESULTS

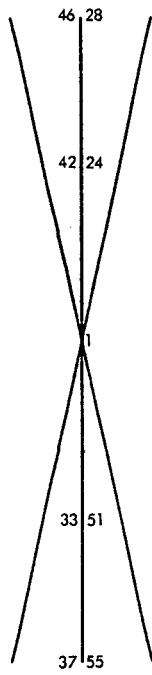
The following table summarizes the RAE booms real eigenvalues, frequencies, and periods for 450' length. Figures 2 to 5 give plots of the booms mode shapes.

Mode No.	Mode Shape	Eigenvalue	Cycles, Hz.	Period, Min.
1	Rigid Body	0.0	0.0	
2		0.0	0.0	
3		0.0	0.0	
4		0.0	0.0	
5		0.0	0.0	
6		0.0	0.0	
7	First	7.834167E-06	4.454681E-04	37.414
8		7.835346E-06	4.455014E-04	37.411
9		7.916286E-06	4.477967E-04	37.219
10		8.083241E-06	4.524940E-04	36.833
11		8.168096E-06	4.548628E-04	36.641
12		2.457935E-05	7.890512E-04	21.122
13		5.291584E-05	1.157745E-03	14.396
14		1.461759E-04	1.924234E-03	8.661
15	Second	2.993210E-04	2.753524E-03	6.053
16		2.993350E-04	2.753588E-03	6.052
17		3.002940E-04	2.757995E-03	6.043
18		3.022924E-04	2.767157E-03	6.023
19		3.033204E-04	2.771858E-03	6.013
20		3.179533E-04	2.837931E-03	5.873
21		3.632512E-04	3.033358E-03	5.494
22		1.462397E-03	6.086290E-03	2.738

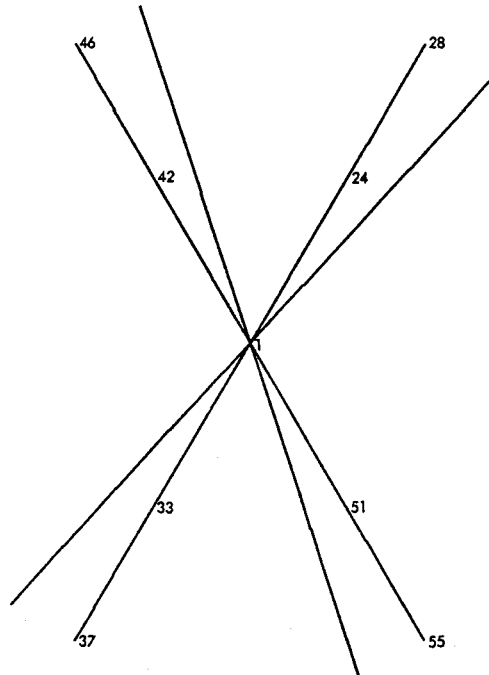
SENSITIVITY AND COMPARISON OF RESULTS

Parameter variation studies have been performed in order to establish the stability of the eigenvalues and the frequencies. The following observations are made, based on these studies:

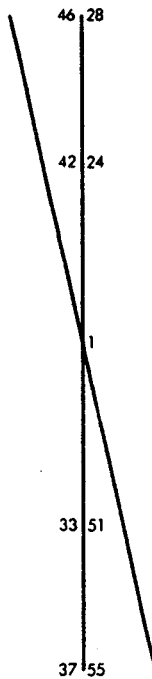
1. The eigenvalues are relatively insensitive to a reasonable variation of the central hub inertias.
2. Varying the number of grid points has a small effect on the eigenvalues and frequencies.



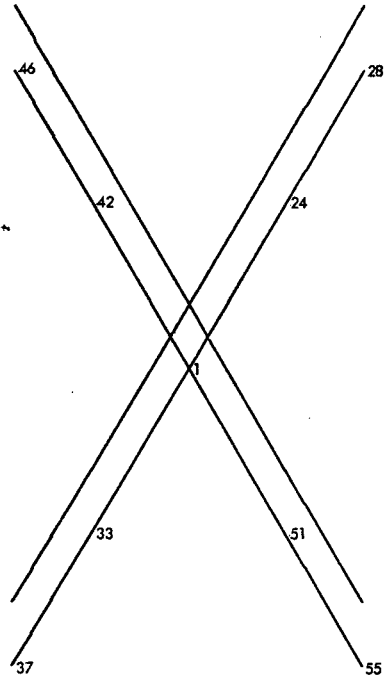
(a) Mode 1 Eigenvalue = 0.



(b) Mode 2 Eigenvalue = 0.



(c) Mode 3 Eigenvalue = 0.



(d) Mode 4 Eigenvalue = 0.

Figure 2. RAE booms rigid body modes.

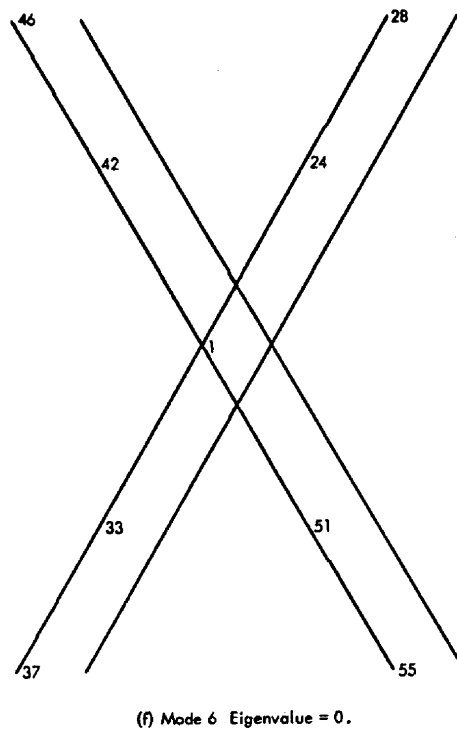
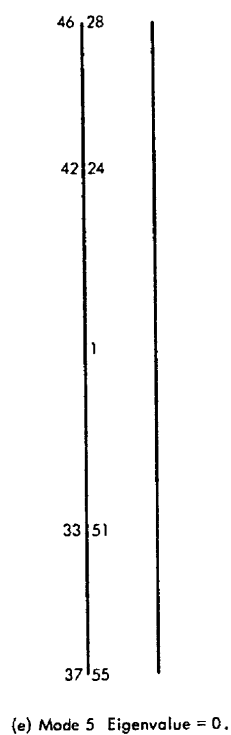
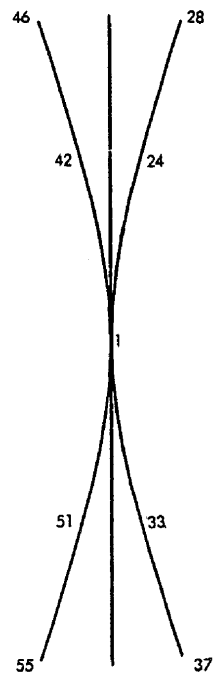
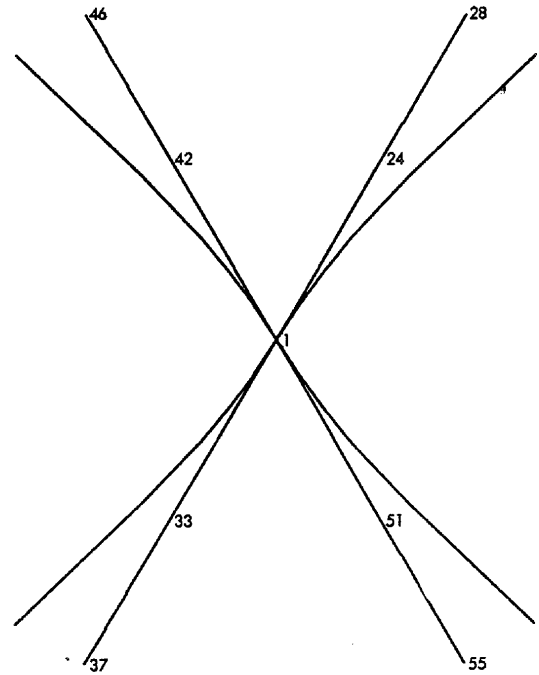


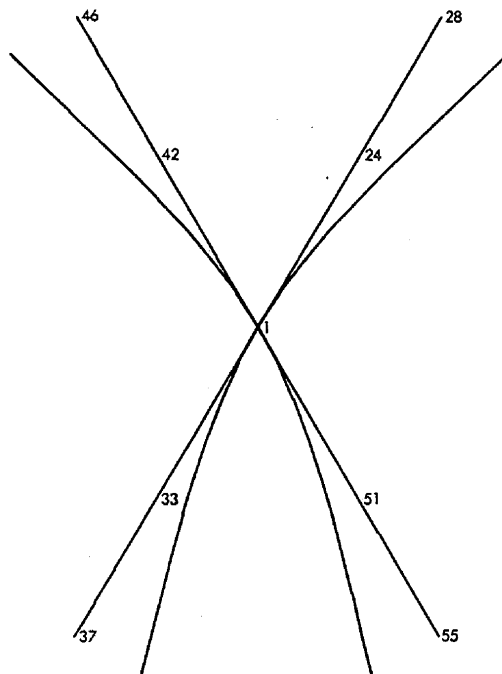
Figure 2 (continued). RAE booms rigid body modes.



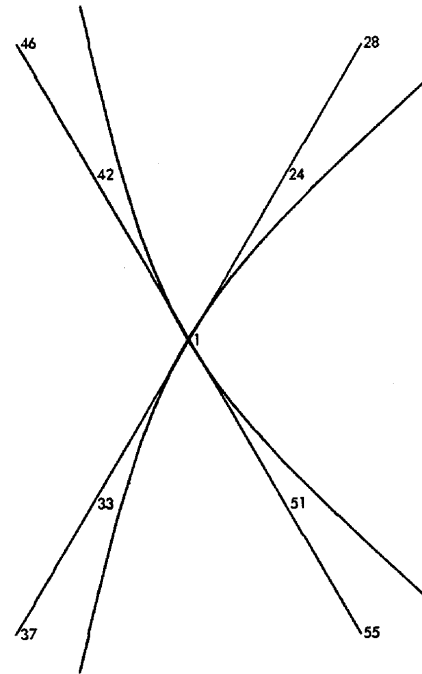
(a) Mode 7 Eigenvalue = 7.8341664×10^{-6}



(b) Mode 8 Eigenvalue = 7.8353456×10^{-6}



(c) Mode 9 Eigenvalue = 7.9162848×10^{-6}

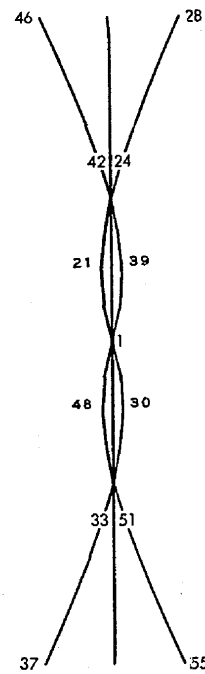


(d) Mode 10 Eigenvalue = 8.0832400×10^{-6}

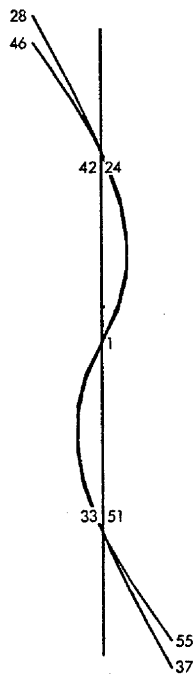
Figure 3. RAE booms first mode shapes.



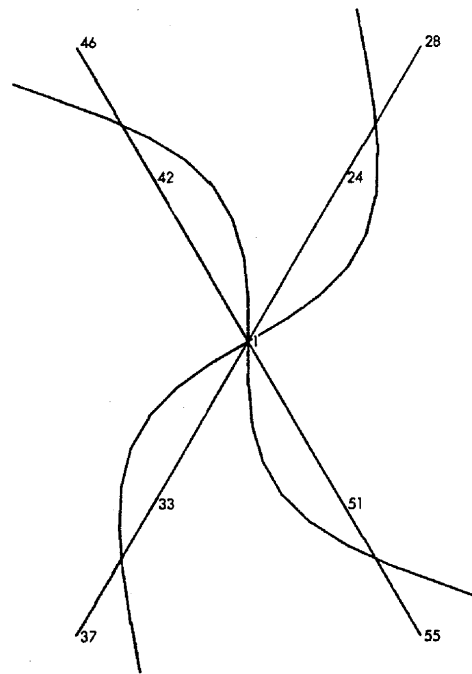
(e) Mode 11 Eigenvalue = 8.1680960×10^{-6}



(f) Mode 12 Eigenvalue = 2.4579344×10^{-5}

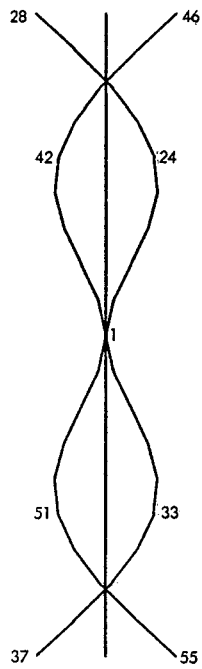


(g) Mode 13 Eigenvalue = 5.2915840×10^{-5}

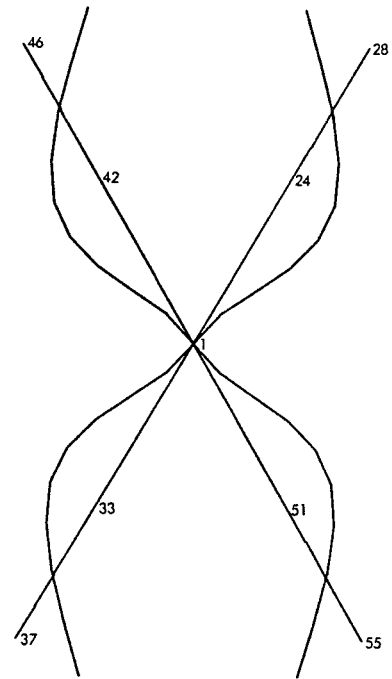


(h) Mode 14 Eigenvalue = 0.0001461758

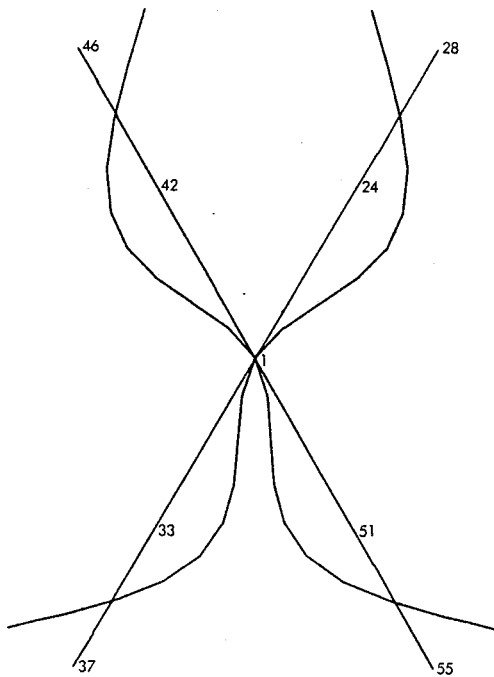
Figure 3 (continued). RAE booms first mode shapes.



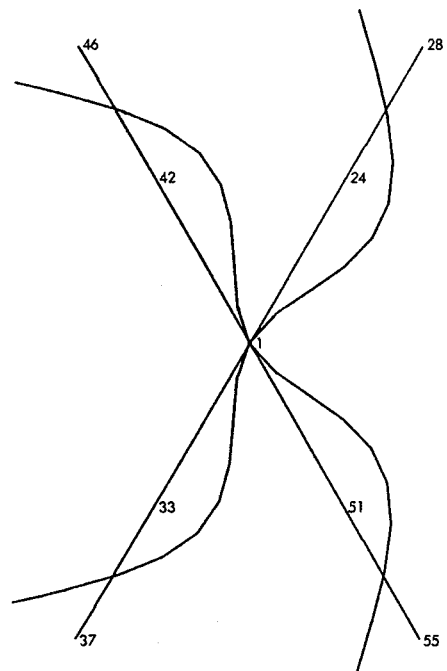
(a) Mode 15 Eigenvalue = 0.0002993209



(b) Mode 16 Eigenvalue = 0.0002993348



(c) Mode 17 Eigenvalue = 0.0003002939

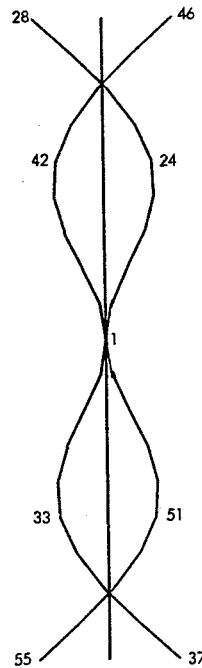


(d) Mode 18 Eigenvalue = 0.0003022923

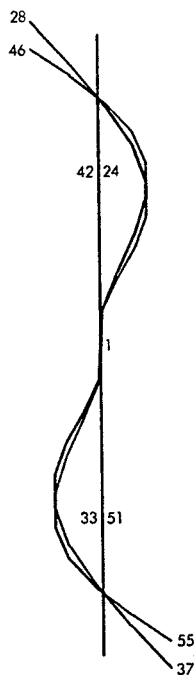
Figure 4. RAE booms second mode shapes.



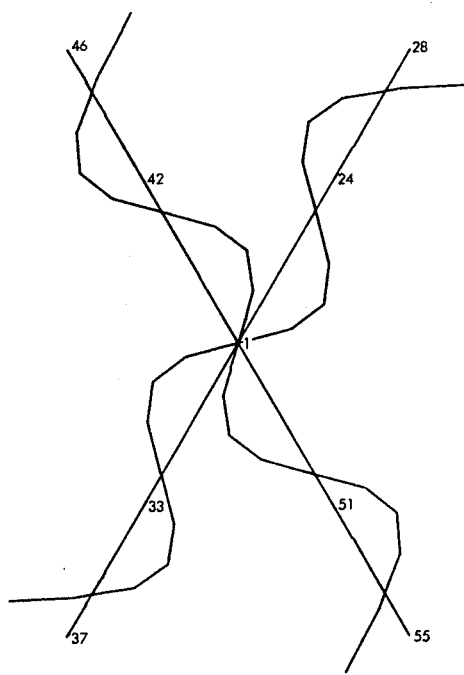
(e) Mode 19 Eigenvalue = 0.0003033203



(f) Mode 20 Eigenvalue = 0.0003179532

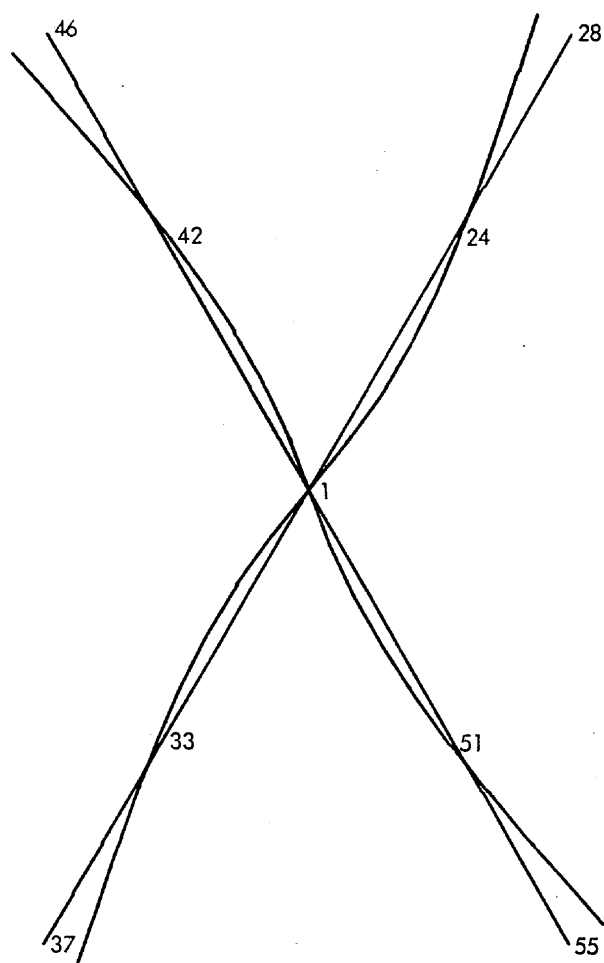


(g) Mode 21 Eigenvalue = 0.0003632510

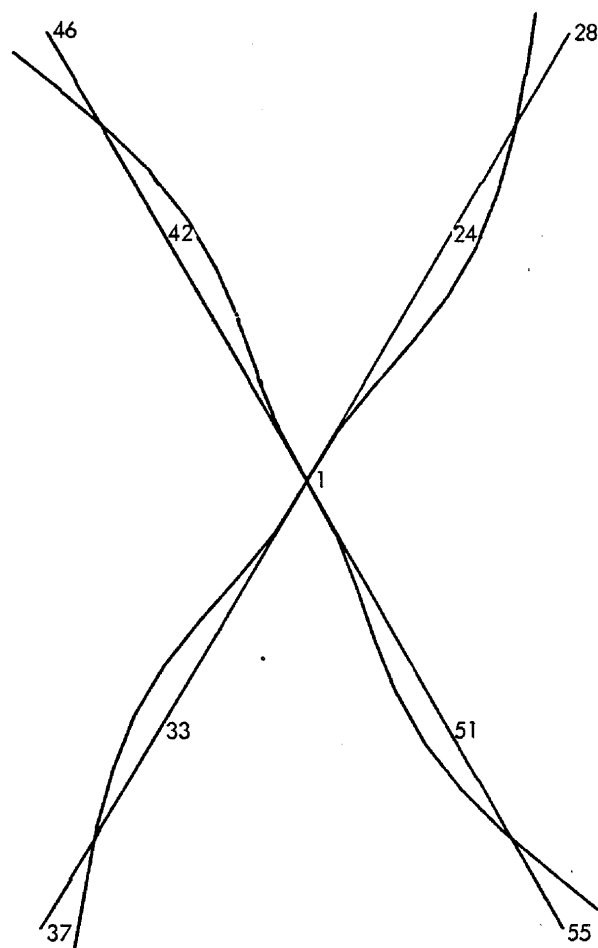


(h) Mode 22 Eigenvalue = 0.0014623971

Figure 4 (continued). RAE booms second mode shapes.



(a) Mode 13-A Eigenvalue = 5.2915840×10^{-5}



(b) Mode 21-A Eigenvalue = 0.0003632510

Figure 5. Additional views of RAE booms mode shapes.

The comparison between the results of this study and the results obtained in reference 1 are not conclusive because the assumptions used in both analyses are different. However, a check was made using the same boom stiffness and mass. The results compared well for the first six modes where the maximum difference was less than 7.2%. Greater discrepancy was found in modes 13 and 14. No second modes were obtained in reference 1.

FUTURE RESEARCH

This study was initiated to test NASTRAN's capabilities to extract closely spaced eigenvalues of small magnitude. The work was concluded with success, although some difficulties were encountered in the early runs. Since then, it is felt that additional work should be initiated to complete this study through the inclusion of gravitational, inertial, and thermal effects. The extension of this work will yield more meaningful results which can be easily compared with some of the results in references 1 to 7.

CONCLUSIONS

The first computer runs for the RAE booms and spacecraft normal mode analysis were performed between August and November 1969. Therefore, some of the difficulties which were encountered at that time may have been resolved now. Some of these were:

1. Difficulty of interpreting some of the NASTRAN messages concerning the reasons for termination of the eigenvalue analysis.
2. Non-uniformity in the computer time required for similar runs. At least one run required about 43 minutes while other runs of a very similar deck (eigenvalue search region is slightly different) required about 13 minutes. Moreover, the matrix decomposition time estimate, given by NASTRAN, varied between 119 seconds and 34 seconds.
3. Difficulty in judging the need for multipoint constraints.

It should be noted that the runs performed recently were consistent in the decomposition time estimate and the required computer time. However, this study showed that considerable care must be exercised when using NASTRAN in the solution of complex problems. It is recommended that the results be checked, whenever possible, using different model and/or independent analysis.

REFERENCES

1. Keat, J. E.: Proposed Technique for Deployment of RAE Booms From 450' to 750'. Westinghouse Electric Corporation, DSC #7280, April 1968.
2. AVCO Corporation: Investigation of the Dynamic Characteristics of a V Antenna for the RAE Satellite, NASA CR-962, March 1968.
3. AVCO Missiles, Space and Electronics Group, Space Systems Division: Interim Report for the Investigation of the Dynamic Characteristics of a V Antenna for the RAE Satellite, AVSSD-0103-67-RR, October 1966.
4. Farrell, J. L., Newton, J. K., and Connelly, J. J.: Digital Program for Dynamics of Non-Rigid Gravity Gradient Satellites, NASA CR-1119, August 1968.
5. Newton, J. K., and Farrell, J. L.: Eigenfrequencies of a Flexible Gravity Gradient Satellite, Westinghouse Electric Corporation, DSC-6439, April 1967.
6. Farrell, J. L., and Newton, J. K.: Continuous and Discrete RAE Structural Models, Jour. of Spacecraft and Rockets, Vol. 6, No. 4, April 1969, pp. 414-423.
7. Flatley, T. W.: Equilibrium Shape of an Array of Long Elastic Structural Members in Circular Orbit, NASA TN D-3173, March 1966.

STATIC AND DYNAMIC ANALYSIS, F-14A

BORON HORIZONTAL STABILIZER

By S. L. Huang and H. Rubin

Naval Air Development Center

SUMMARY

A static stress analysis and a dynamic modal analysis of the horizontal stabilizer of the F-14A aircraft has been conducted at the Naval Air Development Center employing the NASTRAN program. The structural model contains 1518 elements including bars, rods, shear panels and orthotropic and isotropic membrane elements with 1357 degrees of freedom. Static deflection and stresses, including thermal stresses, under maximum load at room and at elevated temperatures are calculated and results are in good agreement with experimental data. Through application of "Guyan Reduction" the number of degrees of freedom used in the dynamic analysis is reduced to 137. The frequencies and mode shapes for the first two modes are obtained.

NOMENCLATURE

E	Modulus of elasticity in tension and compression
G	Modulus of elasticity in shear
ν	Poisson's ratio
x,y,z	Laminate material coordinates
σ_x, σ_y	Normal components of stress parallel to x- and y-axes
σ_{xy}	Shear component of stress in x,y coordinates

Preceding page blank

INTRODUCTION

The horizontal stabilizer is an all movable surface pivoting about a shaft integral with the fuselage. Surface actuation is by hydraulic actuator mounted within the fuselage and acting on the stabilizer horn fitting. The entire assembly is depicted schematically in figure 1. The stabilizer is composed of four major structural parts: the main panel, leading edge, trailing edge and tip. The main load carrying component is the main panel assembly; the other three components resist aerodynamic pressure and transfer it to the main panel. The leading edge, trailing edge and tip assemblies are of full depth aluminum honeycomb core with aluminum skins. The main panel is of sandwich construction with aluminum honeycomb core and boron-epoxy composite cover skins. Composite skins are structurally optimized with laminates of various constructions, orientations and thicknesses tailored to local strength requirements. Titanium is used for root and intermediate ribs, forward and rear closure beams, and intercostal pivot-bearing-support beams. The skins in the pivot area are titanium to enable fastening to the titanium substructure. The boron skins are attached to the titanium by means of bonded splice joints.

STRUCTURAL IDEALIZATION

The idealized structural model is shown in figure 2. It is a NASTRAN computer-drawn plot showing the geometry, the individual elements and the interconnection of the model. The model includes the main panel but excludes the leading and trailing edges and the wing tip. The honeycomb core has been compressed into discrete spar and rib shear panels of equivalent shear stiffness and rods of equivalent compressive stiffness. The metallic skins are represented by isotropic quadrilateral membrane elements, and the boron-epoxy laminated skins are represented by orthotropic triangular membrane elements. There are additional rod elements to represent axial load carrying material along the ribs and beams. The pivot shaft is represented by bar elements which carry axial and shear loads as well as bending moments. The end of the pivot shaft supported by the fuselage is assumed to be fixed. The bearings are simulated by radial rods connected to the shaft. Free bearing rotation is simulated by eliminating the connections between the rotational motions of the bars and rods at the connecting grid points.

The structural model consists of 673 membrane elements, 444 shear panels, 399 rods and two bars for a total of 1518 elements interconnected at 453 grid points. The total number of degrees of freedom is 1357.

STATIC ANALYSIS

Static Load

The idealized structure was analyzed for the critical loading condition, maximum bending. Results were obtained at room temperature and at 422°K. The distributed aerodynamic load was replaced with concentrated forces acting at the grid points. These concentrated forces were computed from static test loads and are statically equivalent to the static test loads. Since the wing tip and the leading and trailing edges are absent from the idealized structure, test loads applied to these parts were replaced with statically equivalent loads acting at adjacent grid points. To react to the applied loads and provide static equilibrium the idealized structure is supported by a cantilever beam (the pivot shaft) passing through the two bearings. The stabilizer is constrained from rotation by a pin-ended rod connecting the pivot horn to a fixed point.

Problems Encountered and Solutions

The major problems encountered while running the static analysis using rigid format 1 of NASTRAN version 11.1 included:

1. Lefthanded coordinate system which is not compatible with NASTRAN.
2. Meaningless results for shear panels with two sides parallel and the other two nearly parallel.
3. Isotropic quadrilateral membrane element with all three material properties E, G and ν independent of each other gives meaningless results.
4. Erroneous NASTRAN calculated stiffness and stresses for orthotropic quadrilateral membrane element resulted from incorrect transformation of local material properties.
5. Error in transforming coefficients of thermal expansion to local coordinates.
6. Total number of different orthotropic materials exceeded the number permitted in the program.

Following actions were taken to resolve the above problems:

1. Switch to righthanded coordinate system.
2. Reassign one of the nearly parallel sides of the shear panel as the side connecting local element grid points G1 and G2.

3. Avoid the use of isotropic quadrilateral membrane element with all three material properties independent.
4. Employ orthotropic triangular membrane element instead of orthotropic quadrilateral element.
5. Adjust input values for coefficients of thermal expansion such that upon the erroneous coordinate transformation the results yield correct values for the coefficients of thermal expansion in the particular local coordinates.
6. Keep the total number of orthotropic materials to less than 100.

NASTRAN Results and Comparison with Test

The structural model for the F-14A horizontal stabilizer was statically analyzed for the loading condition described above using NASTRAN program version 11.1 on an IBM 360/65 computer. A typical run takes 24 minutes in CPU time.

In this analysis the following numerical data were output:

Displacements at all grid points

Stresses for all elements

Element forces

A computer drawn pictorial representation of the stabilizer deformation at room temperature under the prescribed loading is presented in figure 3. It shows superimposed orthographic views of both the deformed and the undeformed structural model. To provide a clear separation between the two views, the displacements of the stabilizer are deliberately exaggerated (approximately 50% larger than actual size). Numerical values of the vertical components of the displacements (displacements normal to the planform of the stabilizer) at selected points are tabulated in Table I. Also shown are the comparable test deflection reported by the contractor.

In general, the correlation between the NASTRAN calculated deflections and the test results are reasonably good.

Figures 4 and 5 are plots of laminate skin stresses at room temperature along two chordwise sections R-8 and R-13, respectively. Physical locations of these sections are shown in figure 2. Test stresses calculated from experimental measurements are presented for comparison. There is good agreement for the dominant stress (normal stress in the direction of laminate material axis). In general, NASTRAN stresses are slightly higher than the experimental data. Internal forces and moments have been calculated for

the NASTRAN stresses along section R-8. These were checked for static equilibrium with the externally applied forces and found to be in close agreement. On the other hand, internal forces and moments estimated from measured stresses are lower than the externally imposed forces and moments.

Skin stresses at elevated temperature are different from their corresponding values at room temperature, as a result of differences of thermal expansion coefficients of the various structural materials including the differences between the various laminate constructions. Since no valid experimental results are available for comparison, the trend and the magnitude of the changes in stresses from room to elevated temperature were carefully examined on the basis of the thermal elastic properties of the entire structure and found to be correct.

DYNAMIC ANALYSIS

Reduction of Stiffness and Mass Matrices

In a dynamic analysis of a structure fewer grid points are needed to describe the inertia properties of the structure than those needed to describe the elastic properties in the static analysis of the same structure for a comparable degree of accuracy. Carrying out a dynamic analysis with more grid points or degrees of freedom than is needed will result in increased computational time and cost with little gain in accuracy.

Rather than construct a new structural model for dynamic analysis, the model used in the static analysis was employed in the following dynamic analysis with the degrees of freedom reduced by the application of Guyan Reduction, a procedure incorporated in NASTRAN. This procedure is essentially a rational redistribution of the inertia properties of the stabilizer to a set of selected grid points uniformly distributed over one surface of the structure. With only one degree of freedom at each grid point retained, namely the displacement component normal to the stabilizer planform, the resulting number of degrees of freedom in the dynamic analysis is 137.

Problems Encountered and Solutions

NASTRAN rigid format 3 with inverse power method is used to obtain the first few natural frequencies and mode shapes of the stabilizer.

As described in the static test, the stabilizer is considered to be supported by the pivot shaft, and constrained from rotation by a control rod connecting the pivot horn to a fixed point. Unlike in the static analysis, problems encountered in the dynamic analysis are few and relatively straightforward. These include:

1. Insufficient file storage even though three (3) disc packs from an IBM 2314 unit were provided.

2. Error occurred during a restart run. The NASTRAN program attempted to partition out rigid body supports, a procedure which is not called for in this particular computer run of the rigid format.

The first problem was solved by storing several data blocks on tapes and revising the procedure library such that unused data storage allocations are released. The second problem was circumvented by using appropriate ALTER statements to jump over DMAP statements between 73 and 81 where the unwanted matrix partition is executed.

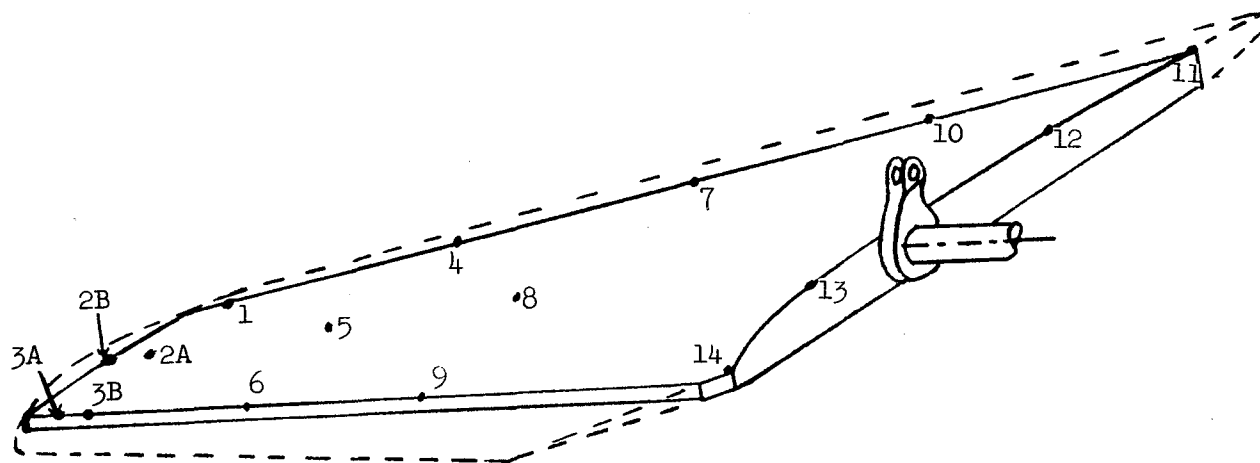
NASTRAN Results and Comparison with Test

Two normal modes of vibrations, one bending and one torsional, were obtained using a cold start plus two restarts. The total CPU time used was 150 minutes of which 104 minutes were required for the stiffness and mass matrices reduction. The natural frequencies associated with the two modes are 21.4 and 39.2 Hz for the bending and the torsional modes of vibrations, respectively. Mode shapes are depicted in figures 6 and 7. Experimental mode shapes are in general agreement with the corresponding NASTRAN calculated results. The corresponding natural frequencies determined experimentally are 15.5 and 35.4 Hz. The large discrepancy in natural frequency between the NASTRAN calculated and the experimentally determined bending vibration is primarily attributed to the difference in the bending stiffness of the pivot shaft including its boundary support between the structure model analyzed and the experimental test set-up.

CONCLUDING REMARKS

The application of NASTRAN to solve static and dynamic problems of complicated structures is convenient and powerful. There are, however, many pitfalls and errors. Hence, results from NASTRAN must be scrutinized very carefully whenever a new application is undertaken. In view of the substantial computational effort required in reducing the stiffness and mass matrices with Guyan Reduction it may be advantageous in some instances to construct a new structural model with fewer grid points for dynamic analysis.

TABLE I.- COMPARISON OF NASTRAN AND TEST VERTICAL DEFLECTIONS



Point	Vertical deflection, cm				Point	Vertical deflection, cm			
	R.T.		422° K			R.T.		422° K	
	Test	NASTRAN	Test	NASTRAN		Test	NASTRAN	Test	NASTRAN
1	38.1	37.72	35.8	40.41	7	9.02	5.74	8.6	5.94
2A	41.7	40.89	----	43.89	8	14.5	11.00	15.0	11.48
2B	----	48.84	52.1	52.63	9	20.6	16.74	20.6	17.40
3A	45.7	45.11	----	48.44	10	-2.51	-3.30	-4.14	-3.38
3B	----	43.26	48.8	46.38	11	-7.80	-9.86	-9.65	-10.06
4	20.3	18.64	24.9	19.61	12	-3.35	-3.99	-4.11	-4.09
5	28.4	23.32	29.5	24.66	13	4.95	3.96	4.98	4.01
6	31.8	28.30	34.5	29.92	14	9.78	8.71	10.77	8.86

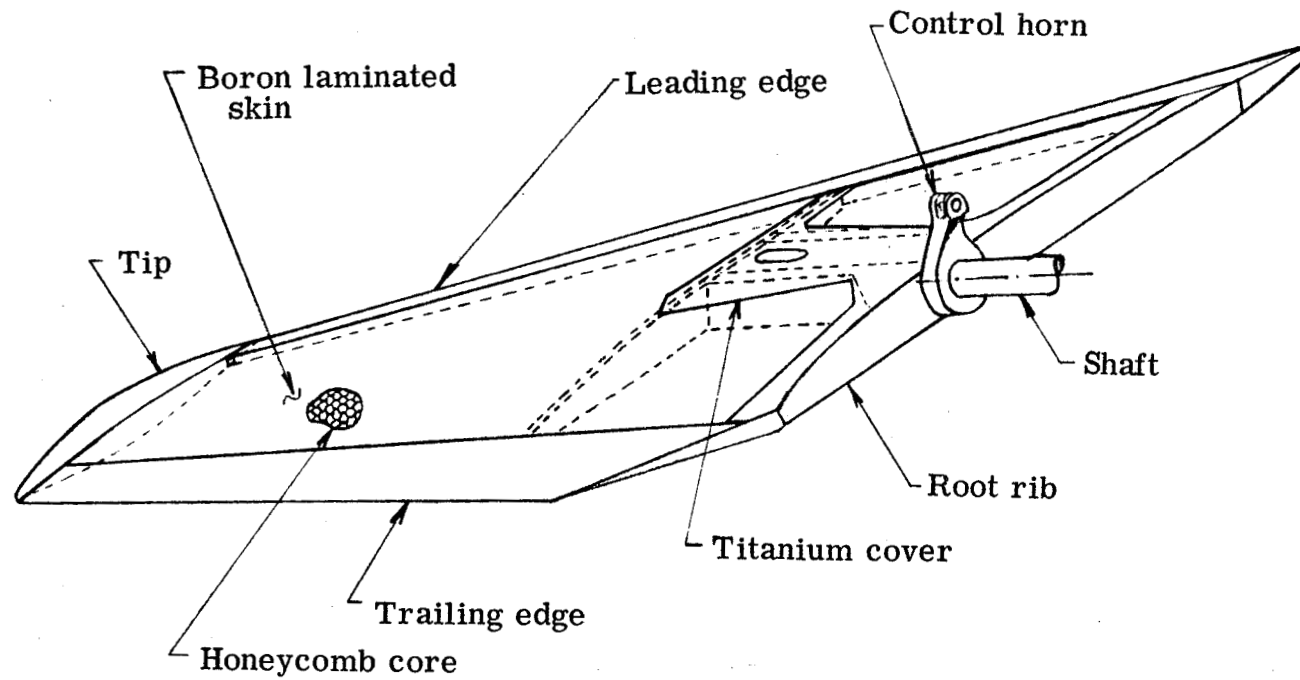


Figure 1.- General structural arrangement, F-14A horizontal stabilizer.

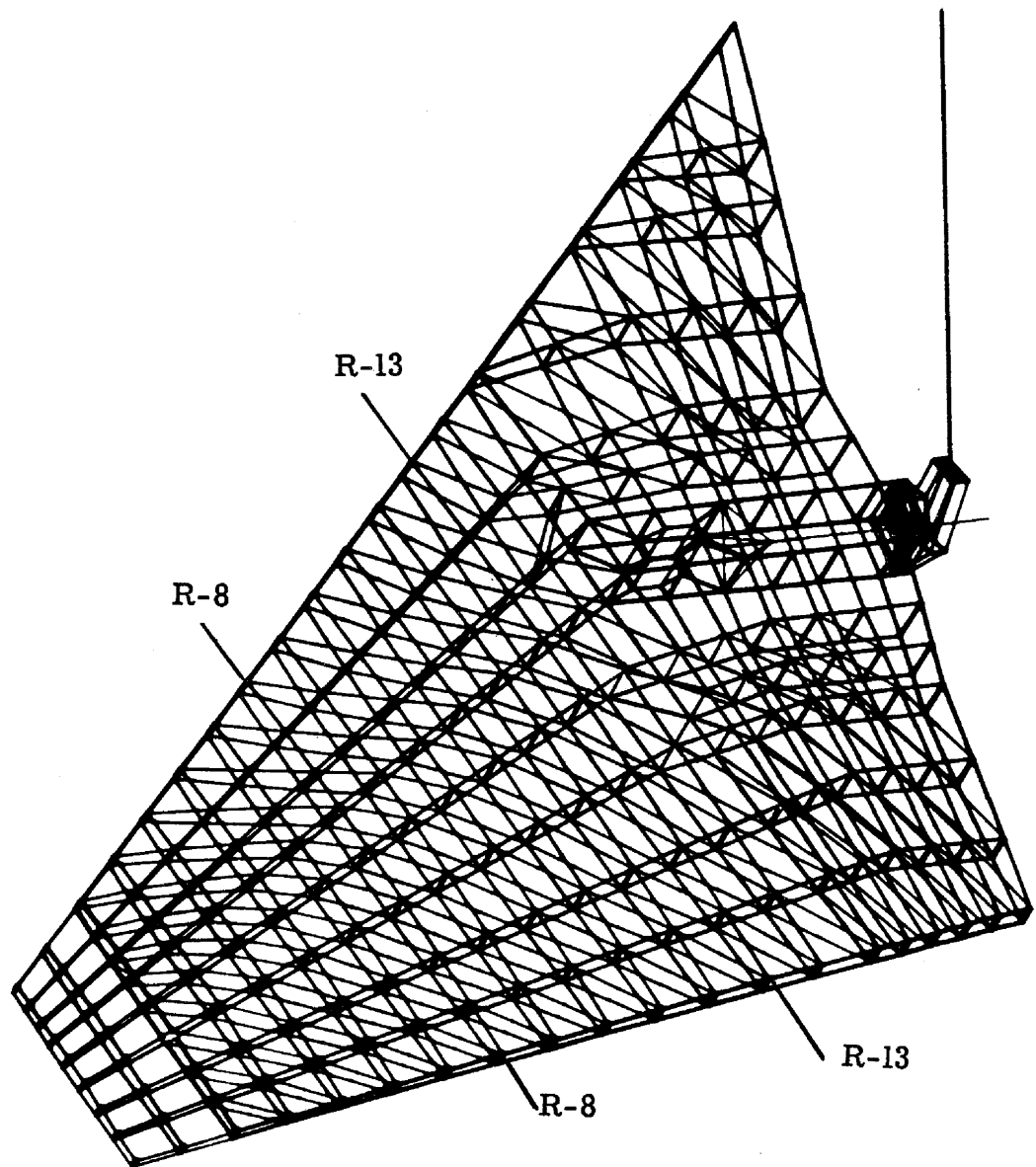


Figure 2.- Finite element structural model.

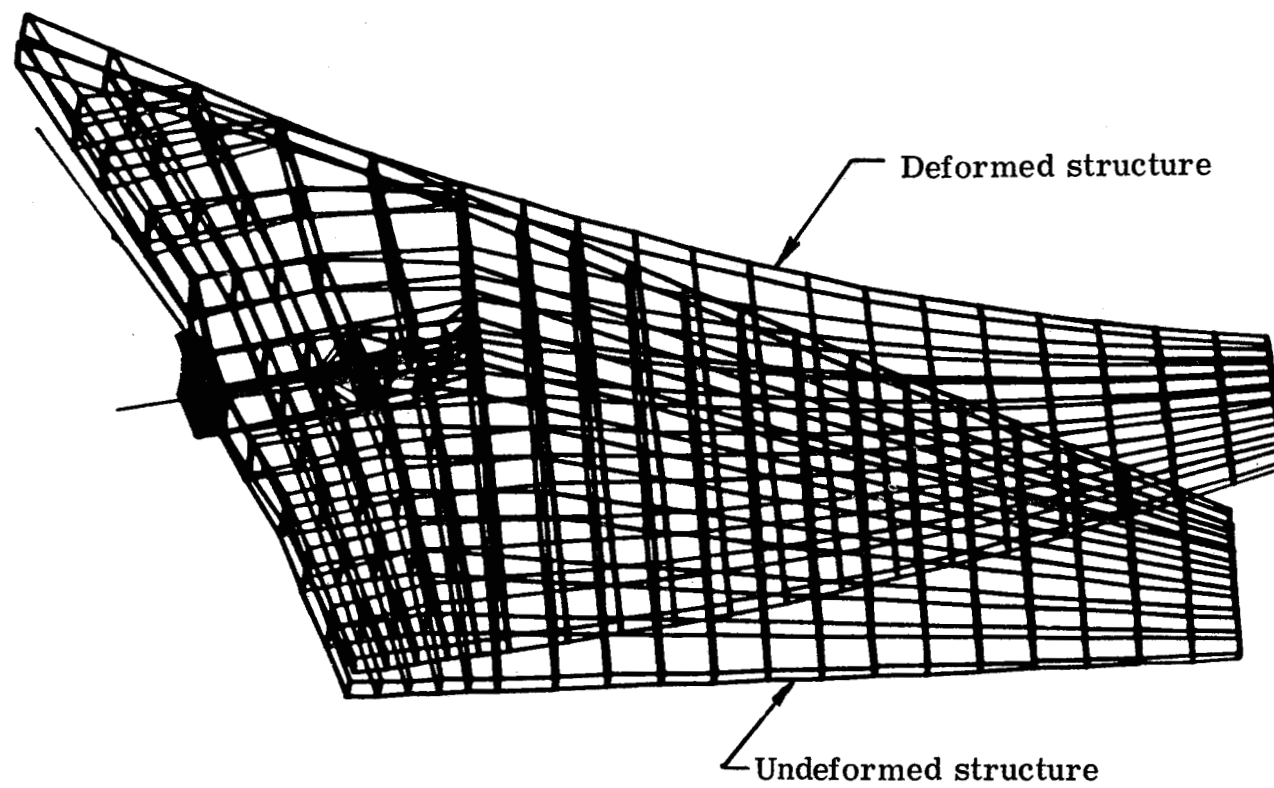


Figure 3.- Deformed and undeformed structural model.

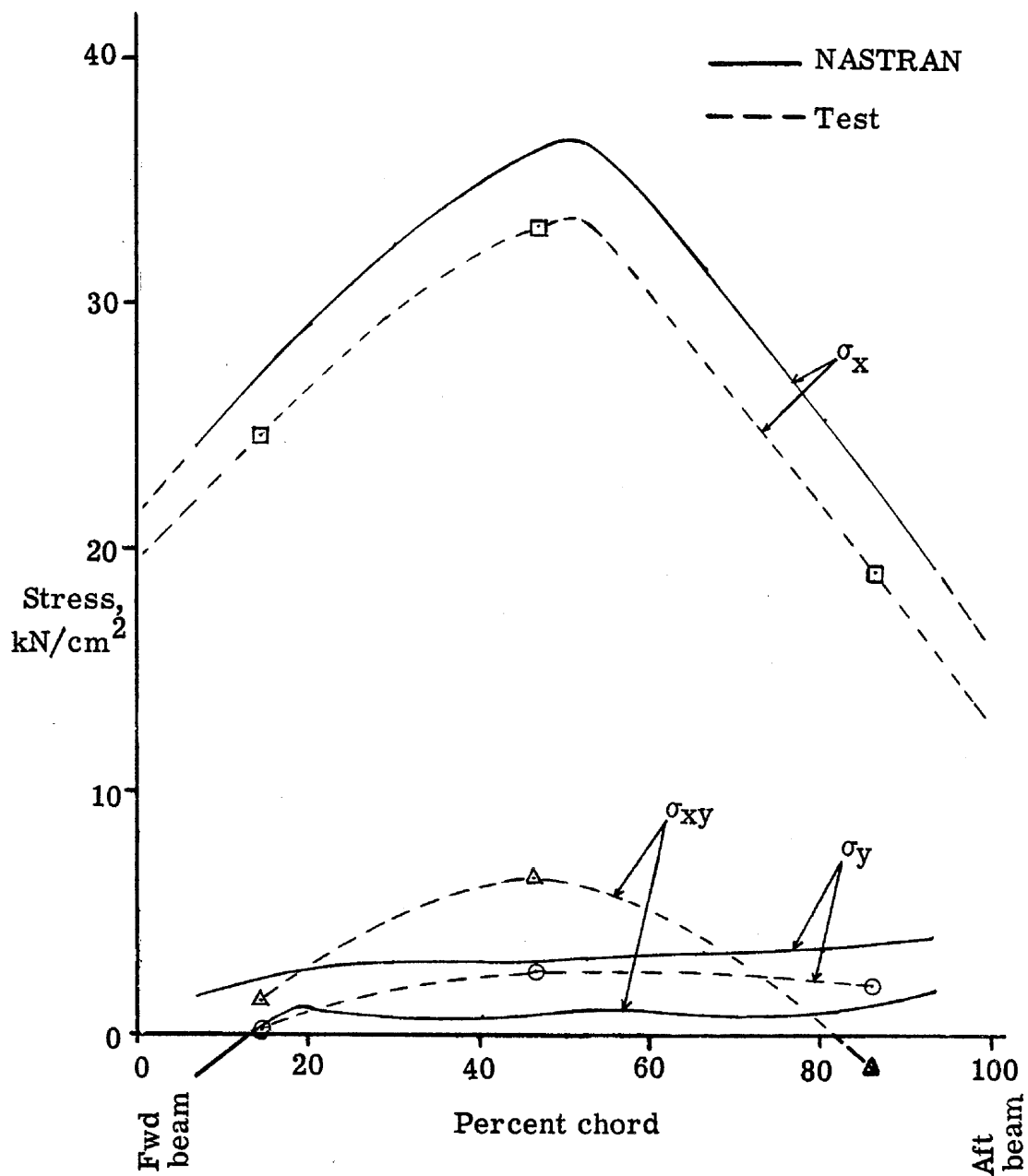


Figure 4.- Comparison of NASTRAN and test laminate stress along section R-8, R.T.

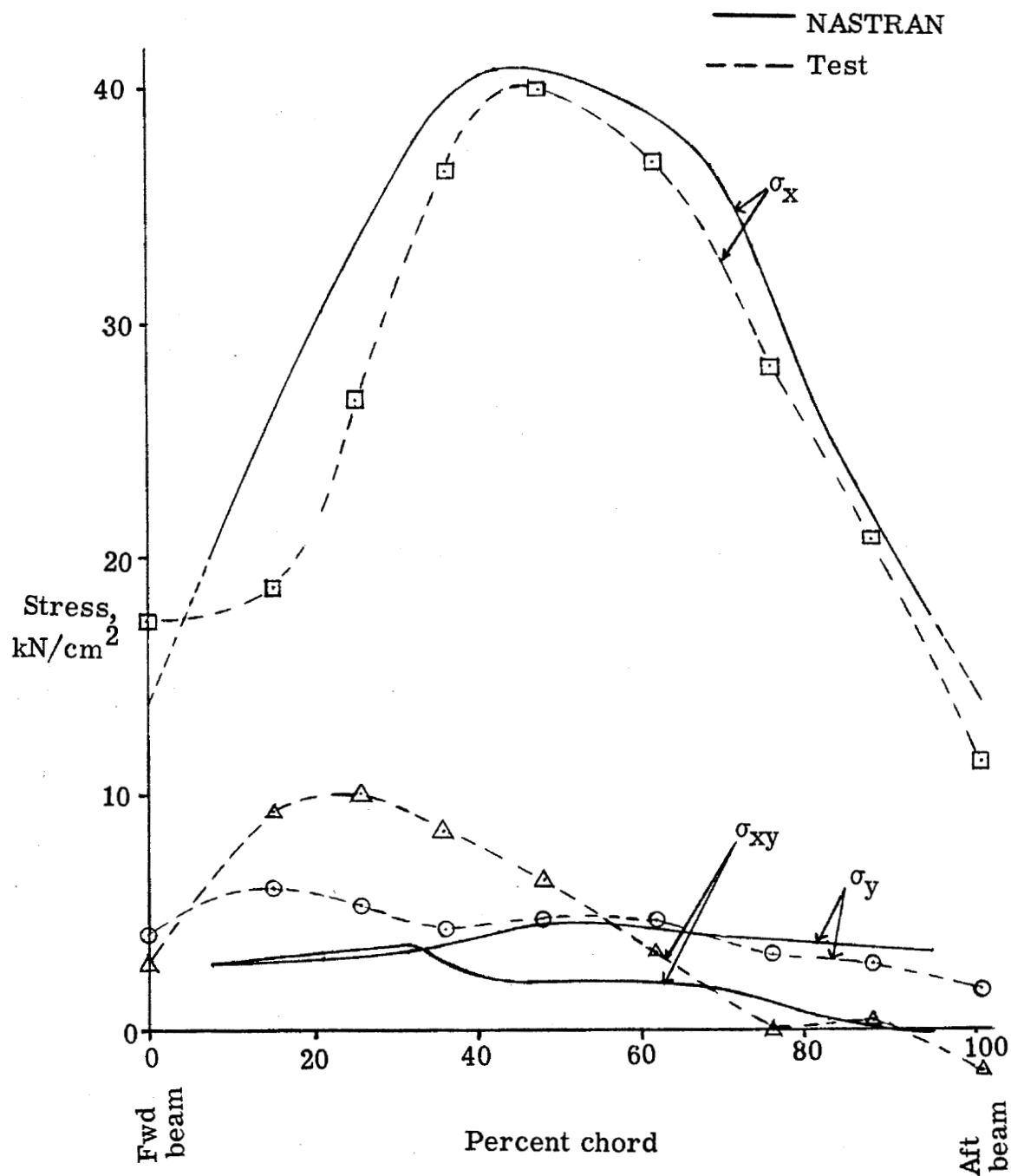


Figure 5.- Comparison of NASTRAN and test laminate stress along section R-13, R.T.

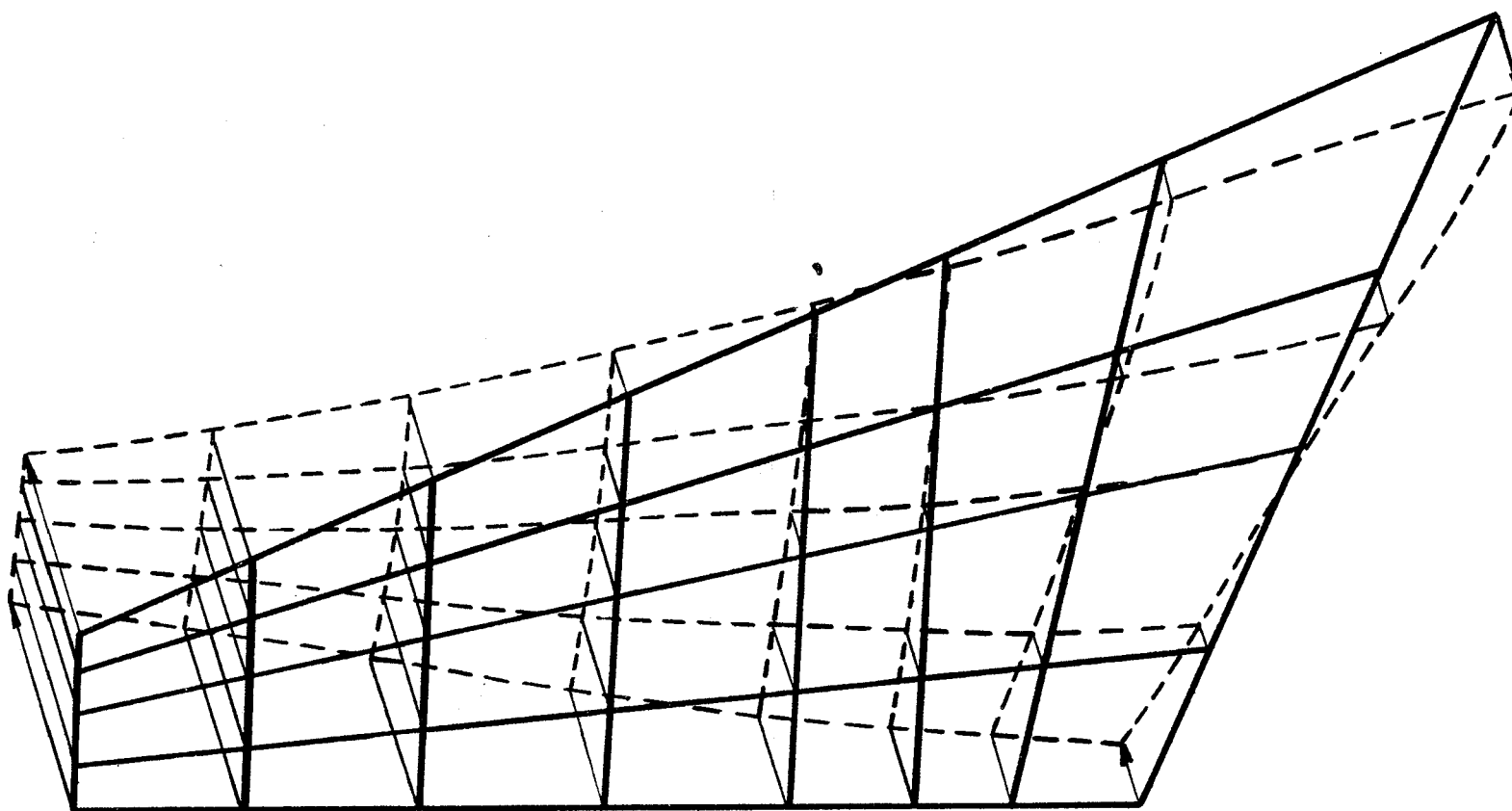


Figure 6.- First bending mode shape. $f = 21.4$ Hz.

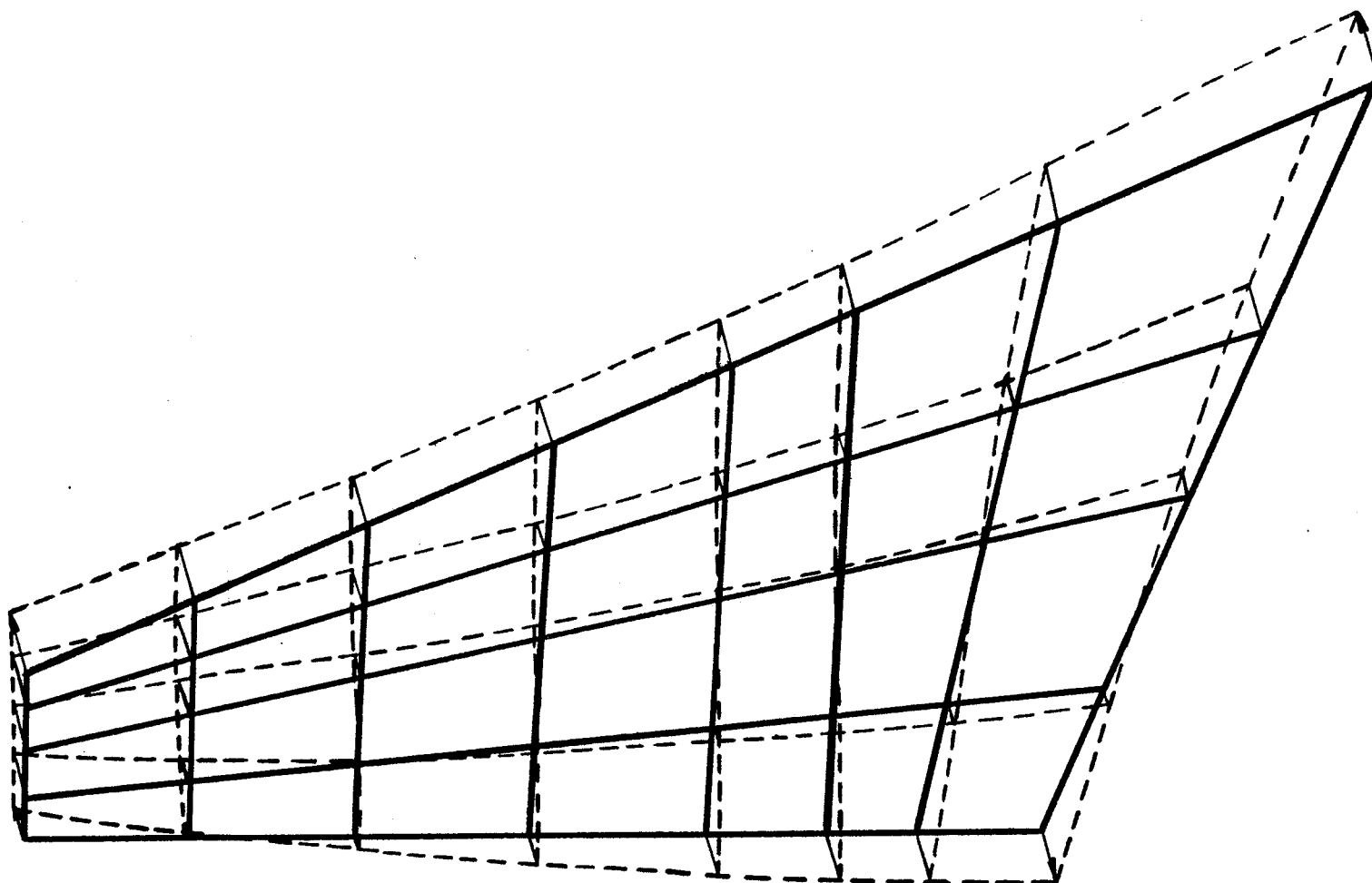


Figure 7.- Torsional mode shape. $f = 39.2$ Hz.

ADAPTATION OF NASTRAN TO THE ANALYSIS OF THE VIKING SPACE VEHICLE

By Thomas C. Jones and Larry D. Pinson
NASA Langley Research Center

SUMMARY

A normal mode analysis of the complete Viking launch vehicle (stage 1-shutdown configuration) using a modification of NASTRAN version (11.1.0) on the CDC 6600 computer system is presented. The operational and logistics problems discussed in this paper are typical of those encountered in the use of NASTRAN for any large problem. The vehicle is divided into three basic substructures which are modeled and checked separately, then joined to yield a complete, unreduced model of the system. Eigenvalues are extracted using the inverse power method. The results of this study demonstrate the broad versatility of NASTRAN for simultaneously modeling structures by direct matrix input, general elements, and rigid links along with the standard library of finite elements. It also indicates the large computer time requirements of NASTRAN for extracting roots of large order matrices.

INTRODUCTION

Assembly of a complete finite element model of the Viking launch vehicle and spacecraft system yields a relatively large composite model (greater than 900 elastic degrees of freedom and 500 dynamic degrees of freedom). Eigenvalue analyses of such large models with unreduced dynamic degrees of freedom have traditionally led to excessive computer run times and core storage requirements. Hence, a modal synthesis (substructuring) procedure (reference 1) was adopted by the Viking project as the baseline approach for modal analyses.

Modal synthesis does not offer the degree of accuracy, the visibility of the overall model definition, nor the ease of model changes afforded by a direct use of the complete, unreduced model. A direct approach was selected for the work being performed at the Langley Research Center (LRC) in support of the Viking project. This decision was based partially on the availability of the NASTRAN program (refs. 2, 3, and 4) which was formulated for treating large systems such as the Viking space vehicle. The objective of using the direct approach was to provide a means for accurately and easily performing dynamics studies requiring parametric model changes and to provide a backup for modal synthesis. The configuration analyzed was the Titan/Centaur/Viking space vehicle at stage 1 shutdown.

The purpose of this paper is to present the LRC experience gained during this investigation on the application of NASTRAN to the eigenvalue analysis of the Viking space vehicle. Particular emphasis is given to the flexibility of

NASTRAN in synthesizing a composite structural model from substructure models which were generated independently.

It was known at the outset that for large problems, the current version of NASTRAN (11.1.0) would require excessive computation times on the Control Data Corp. (CDC) 6600 computers at LRC. The primary reason is that NASTRAN was written in double precision to yield 14-16 digits of accuracy. On the CDC 6000 series computers single precision gives about 14 digits of accuracy. The NASTRAN double precision code, thus, imposes unnecessarily large arithmetic computation times and storage requirements upon the CDC system. Further, the NASTRAN code uses an unsymmetric decomposition in the inverse power method of eigenvalue extraction. This also produces a penalty for symmetric eigenvalue problems because of unnecessary computations and storage requirements.

Because of the characteristics of the CDC computer, conversions were made in NASTRAN to utilize single precision arithmetic operations in the multiply-add (MPYAD) routine, the equation solution (FBS) routine, and the symmetric decomposition routine (SDCOMP). In addition, symmetric decomposition was added to the inverse power method for root extraction. A complete account of the modifications and their effects on storage and run times is given in reference 5. The output and input for the modified version of NASTRAN (11.1.2) used in the present study is identical to that of the standard version (11.1.0).

Although none of the concepts used in this analysis are new, it is believed that several of the adaptations are of general interest. The features of NASTRAN used in the modeling of the structure are discussed along with the problems encountered.

SYSTEM DESCRIPTION

In this section, a description of the physical system analyzed is given along with a description of the finite element models used to represent the system.

System Components

The Viking Space Vehicle at stage 1 shutdown is composed of the booster and the Viking spacecraft as shown in figure 1. The booster consists of the Titan III-D first and second stages, the Centaur D-1T, and the shroud. The booster weighs approximately 609 kN (137,000 lb) and is 48.13 m (157.9 ft) long, including the length of the shroud.

The Viking spacecraft consists of the Centaur-Truss Adaptor, Viking Transition Adaptor, Viking Spacecraft Adaptor, Orbiter Bus, Viking Lander Capsule Adaptor, and the Viking Lander. This assemblage weighs approximately 32 kN (7200 lb) and is 5.786 m (227.8 in.) in length, including all adaptor sections.

Substructure Finite Element Models

For the purpose of this NASTRAN analysis the Viking Space Vehicle was divided into three substructures. Referring to figure 1, the Viking Lander is considered as one of the substructures. Another substructure, the Viking Orbiter, constitutes the remainder of the Viking spacecraft. The third substructure, the booster, is considered to be made up of the expended Titan first-stage, the Titan second-stage (fully loaded with fuel and oxidizer), the Centaur, and the shroud.

Lander model.- The finite element dynamic model of the Viking Lander was generated from an existing "Martin-Denver Space Frame Program" finite element model. Of the three substructures comprising the Viking Space Vehicle, the Martin Marietta Corp. (MMC) lander model lent itself to the most straightforward adaptation to NASTRAN. This model is made up of 73 grid points, 42 massless rods, 87 massless bars, 111 concentrated translational masses, and 21 inertias.

Orbiter model.- The finite element dynamic model of the Viking Orbiter was generated from an existing Jet Propulsion Laboratory (JPL) "Structural Analysis and Matrix Interpretive System" (SAMIS), (references 6 and 7), finite element model. The JPL model consists of 180 grid points, 106 massless rods, 57 massless bars, 109 rigid links, and read-in mass and stiffness matrices. The read-in stiffness matrices were used to represent the torsional stiffness of the packing between the bus rings, and the combined stiffness of the Transition and Centaur Truss Adaptors. The total mass of the elastic Orbiter and rigid Lander was represented by a read-in mass matrix.

The SAMIS technique for rigidly linking two points is through the use of "SAMIS substitute grid points." Since this technique is not available in NASTRAN, multipoint constraints (discussed in a subsequent section) were used as a replacement.

Booster.- The NASTRAN finite element dynamic model of the booster was generated from two sources -- a finite element model developed by MMC and basic data (AE, EI, GJ). Grid points were located on the booster centerline and were connected with general elements or, where possible, with bar elements. Structural mass was lumped at the grid points and each geometric grid point was allowed six degrees of freedom (d.o.f.). The basic structural model is illustrated in figure 2. Since the shroud encapsulates both the payload and the Centaur stage, the centerlines of both these components coincide. In figure 2 the shroud model is shown offset from the centerline for clarity.

In addition to the basic structural model shown, spring-mass systems were attached to the geometric grid points in order to represent branch components such as engines and sloshing liquids. The nonsloshing portion of liquid in propellant tanks was distributed to the geometric grid points as though it were structural mass while the sloshing portion of liquid was attached to the appropriate geometric grid point through a spring. These masses were presumed to act in pitch and yaw. Longitudinally, a different spring-mass system was used to represent the liquid. In this direction the entire liquid mass within a tank was lumped and springs were attached between that mass and grid points

at both ends of the tank. The engines were attached at appropriate geometric grid points in pitch, yaw, and roll by use of a six-by-six mass matrix. In the longitudinal direction, engines were attached to these grid points through springs.

The resulting model of the booster consists of 49 grid points, 13 general elements, 35 bar elements, 23 scalar springs, 75 scalar (1 d.o.f.) masses and 63 concentrated (6 d.o.f.) masses. Various combinations of scalar and concentrated mass were used to define the total mass at the grid points.

NASTRAN MODELING PROCEDURES AND INNOVATIONS

The formulation of the composite Viking Space Vehicle was divided into two phases. The first phase consisted of defining, in terms of NASTRAN input, acceptable models representing each of three substructures. Secondly, these models were combined into one model representing the composite space vehicle. Both phases included the use of global and secondary coordinate systems, multipoint constraint relations, read-in matrices, general elements, and bulk data logistics strategy.

Selection of Global Coordinate System

The three right-handed rectangular coordinate systems used in this analysis are shown in figure 3. These are the same coordinate systems used by the contractors in the development of the substructural models. The system describing the Orbiter was chosen as the global and displacement coordinate system. This selection eliminates the requirement for transforming the "read-in" stiffness and mass matrices associated with the Orbiter.

Bulk Data Logistics

The combined model of the Viking Space Vehicle was described by 4447 bulk data cards. This volume of input data increases the likelihood of errors and the logistics of bulk data handling can become, at best, time consuming. Many of these logistics problems were eliminated by the methods discussed in the following sections.

Element numbering.- A reduction of the overall modeling complexity was achieved by breaking the model down into three substructures which could be modeled and checked out independently. Unique blocks of numbers were assigned to each portion of the structure to label the elements.

The existing grid point sequencing of each substructure started with grid point one. Since each grid point must have a unique number, a block of numbers from 1 to 10,000 was assigned to the booster and shroud; 10,001 to 20,000 to the orbiter; and numbers greater than 20,000 to the lander. By adding 10,000 and 20,000 to the existing grid point labels for the Orbiter and Lander,

respectively, the initial grid point labeling of all three substructures was preserved as the three right-hand digits. Large gaps existed in the grid point numbering, however, this did not create any problem because of the dual internal-external grid point labeling system of NASTRAN.

In addition to a unique numbering system for grid points, all bulk data cards (material, property, mass, continuation identifications, etc.) were given unique identifications using a similar block numbering scheme.

Substructure orientated bulk data cards.- There are certain bulk data cards which can be used to supply repetitive input. One such card is the "BAROR" card which allows all bar elements indicated to have the orientation specified on this card. Another bulk data card, the "WTMASS" parameter, scales all mass entries by the multiplier indicated. Both devices can effectively be used to define a complete structure. However, these features were avoided in the modeling of substructures because they were not applicable to each substructure of the composite model.

Multipoint Constraint Relations

Extensive use was made of the multipoint constraint (MPC) relationship in the substructure model of the Orbiter and in the composite structural model. Both the use and method of formulation are discussed in the following sections.

Use of multipoint constraint relations.- The use of multipoint constraint relations in the formulation of the analytical model served two functions. The first use consisted of defining rigid links to represent portions of structure. This procedure was used extensively to model solar panels, links between elastic grid points and mass entries (figure 4-a), and structural offsets (figure 4-b).

The second use consisted of providing a means of joining the substructural models together. The juncture at the Viking Orbiter/Lander interface is made at three locations. The MPC relationships were written with coefficients obtained by redefining the juncture coordinates of the Lander in the displacement coordinate systems. This procedure is always used to obtain coefficients for MPC relationships when joining structures with grids not defined in the displacement coordinate system. It should be emphasized that this procedure is not discussed in the NASTRAN manuals.

The juncture of the Orbiter to the booster model was different since the booster is essentially a stick model. Points at the base of the Centaur Truss Adaptor were rigidly linked to a point along the centerline of the booster. This point was, in turn, rigidly linked to the elastic grid representing the top of the Centaur.

Formulation of multipoint constraint relations.- To facilitate the use of MPC's in the representation of rigid links and to minimize input errors, a computer program was written. Input to this program was in the form of NASTRAN bulk data grid cards and a list of both the independent and dependent grid

points. The program output provides punched MPC bulk data cards for direct use in NASTRAN.

The computer generated MPC equations are linear and are of the general form

$$\sum A_n u_n = 0, \quad (1)$$

where A_n is the coordinate coefficient of the displacement u_n . The independent coordinate is always written in terms of the dependent coordinate.

A rigid link joining two points in space can be described by a set of six linear equations involving coordinates of the related points -- three translation equations and three rotation equations.

Figure 5 shows two points in space, A and B. These two points are linked together rigidly with point "A" chosen to be dependent on the motion of point "B." The translation of "A" in terms of "B" is expressed by,

$$\begin{aligned} u_{x_A} - u_{x_B} + u_{\theta_{y_B}} (Z_B - Z_A) - u_{\theta_{z_B}} (Y_B - Y_A) &= 0 \\ u_{y_A} - u_{y_B} + u_{\theta_{z_B}} (X_B - X_A) - u_{\theta_{x_B}} (Z_B - Z_A) &= 0 \\ u_{z_A} - u_{z_B} + u_{\theta_{x_B}} (Y_B - Y_A) - u_{\theta_{y_B}} (X_B - X_A) &= 0 \end{aligned} \quad (2)$$

and the rotation of "A" in terms of "B" is expressed by,

$$\begin{aligned} u_{\theta_{x_A}} - u_{\theta_{x_B}} &= 0 \\ u_{\theta_{y_A}} - u_{\theta_{y_B}} &= 0 \\ u_{\theta_{z_A}} - u_{\theta_{z_B}} &= 0 \end{aligned} \quad (3)$$

where the X, Y, Z refer to the coordinates of the indicated point; u_x , u_y , u_z denote the translational displacement in the X, Y, Z directions; u_{θ_x} , u_{θ_y} , u_{θ_z} denote the rotational displacement about the X, Y, Z axes, respectively.

For the composite model 109 grid points were rigidly linked in this fashion in all six directions, and 22 grids were linked rigidly in five directions. This results in a reduction of 764 independent degrees of freedom.

Read-In Matrices

NASTRAN rigid format 3 (normal mode analysis) does not provide for matrices to be "read-in" directly. A part of the data describing the Viking Orbiter structure was supplied as stiffness and mass matrices. A DMAP alteration allowing direct matrix input was therefore made and is shown in the example below.

```

ALTER 26,29
MTRXIN, ,MATPOOL,EQEXIN,SIL,/STIF,WTR1,/V,N,LUSET/V,N,NOM1/V,N,NOM2/
      C,N,0 $
SMA1  CSTM,MPT,ECPT,GPCT,DIT/KGGY,,GPST/V,N,NOGENL/V,N,NOK4GG $
ADD   KGGY,STIF/KGGX/C,N,(1.0,0.0)/C,N,(1.0,0.0) $
CHKPNT KGGX,GPST $
SMA2  CSTM,MPT,ECPT,GPCT,DIT/MGG1,/V,Y,WTMASS=1.0/V,N,NOMGG/
      V,N,NOBGG/V,Y,COUPBAR=-1 $
SAVE  NOMGG $
ADD   MGG1,WTR1/MGG/C,N,(1.0,0.0)/C,N,(1.0,0.0) $
ENDALTER

```

The stiffness matrix to be "read-in" is labeled "STIF" and the mass matrix "WTR1." Both of these matrices are coded on "DMIG" and are "read-in" through the instruction entitled "MTRXIN." The output from the stiffness matrix generator is relabeled KGGY rather than KGGX in order to avoid relabeling of the stiffness matrix several times later in the DMAP sequence. KGGY is then added to STIF, the read-in stiffness, with the resulting summation being the same size of KGGY. Since neither KGGY or STIF is to be scaled the real portion of the matrix multiplier is unity. The output from this module is then checkpointed. A similar procedure is followed in the addition of the internally generated mass matrix "MGG1" and the read-in mass matrix WTR1.

The two read-in stiffness matrices describing the Orbiter model were combined and read-in as a single matrix having 1809 nonzero terms. The read-in mass matrix had 196 nonzero elements. Input of the nonzero matrix elements to nine significant figures (including signs and decimals) was accomplished using the large field DMIG bulk data cards. A total of 2206 bulk data cards were required.

General Element

In order to compare the NASTRAN booster model with the existing MMC model it was desirable to maintain the same grid points. General elements were, therefore, used to replace the nonuniform bar elements in the MMC model. This approach eliminated the need for placing additional grid points at each location corresponding to a change in the properties of the cross section.

Flexibility matrices for the general elements were generated by using NASTRAN rigid format 1 (static analysis). Each variable-property beam was modeled as a series of stepped uniform beams cantilevered between the MMC grid points. The flexibility matrices for all the general elements were generated in a single run by coding the data for all the cantilever substructures as though they were one structure. Four subsets of unit loads were simultaneously applied to all substructures, yielding four solution vectors. Only four subsets were needed instead of six because of pitch-yaw symmetry. Each solution vector, therefore, contained one column of the flexibility matrix for each cantilever substructure.

RESULTS AND DISCUSSION

Significant results of the analysis are presented and discussed in this section. Data which support the eigenvalue correlation between contractor analyses and NASTRAN results are examined. In addition, eigenvalue data are presented for the composite model along with selected structural plots for both the undeformed and modally deformed models. Finally, operational problems encountered in the analysis are discussed along with methods for alleviation.

Substructure Eigenvalue Correlation

The basis for establishing confidence in substructure modeling is the comparison of eigenvalues obtained from contractor finite element analyses with those eigenvalues calculated with NASTRAN. The modal synthesis approach used by the MMC employed cantilevered modes for both the Lander and the Orbiter (with an attached rigid Lander). Further, free-free modes were employed for the booster (with an attached rigid spacecraft). These same conditions were duplicated in the eigenvalue analyses of the NASTRAN substructure models so that the comparison would be direct. The results obtained for each substructure model are discussed in the following subsections.

Lander model.— The cantilevered model of the Viking Lander contains 402 elastic degrees of freedom and 132 dynamic degrees of freedom, i.e., degrees of freedom with mass. The 270 degrees of freedom associated with the massless coordinates were eliminated by the Guyan reduction method leaving a total system of order 132.

All eigenvalues and associated eigenvectors for the first 40 modes were computed using the Givens method. A tabulation of the first 28 frequencies

calculated by MMC and by LRC using NASTRAN is given in table I. Note the excellent overall agreement between the frequencies with maximum deviation of approximately 4.6 percent for the 16th mode based on the MMC value. In general, the NASTRAN results gave slightly higher frequencies with exact agreement to two place accuracy for seven of the 28 modes given. This close agreement supports the validity of the NASTRAN model.

Orbiter model.- The Givens method of root extraction was also used in the NASTRAN formulation to compute all eigenvalues and the first 25 eigenvectors for the cantilevered Viking Orbiter. The system was represented by 148 dynamic d.o.f. and 219 elastic d.o.f. The original system of equations had 764 dependent coordinates eliminated by the MPC equations and 71 massless coordinates eliminated by the Guyan reduction.

Shown in table II is a comparison of the frequencies from the NASTRAN analysis with those obtained from the JPL SAMIS analysis. Again, very good agreement is indicated by the frequency comparisons with the exception of the first two frequencies. These frequencies are associated with localized solar panel motions and do not represent major structural modes. This correlation for the Orbiter substructure model validates the procedure for DMAP alterations discussed in a previous section entitled "Read-In Matrices." In addition, the validity of the MPC representation of rigid links is verified.

Booster model.- The free-free model of the Viking booster has 310 elastic d.o.f. and 236 dynamic d.o.f. The inverse power method was used to extract the first 35 eigenvalues and the associated eigenvectors.

A comparison between the natural frequencies generated using NASTRAN and those generated by MMC using modal synthesis is shown in table III. Good agreement is indicated except for two double frequencies which were not predicted by NASTRAN. These correspond to two lateral modes. Discussions with the contractor and comparison of mode shapes indicates that the discrepancy is due to different methods of treatment of the liquid propellants in the second-stage. This correlation tends to verify the modeling of the nonuniform bar elements with general elements. These results are also indicative of the accuracy of the modal approach used by MMC.

Plotting.- Structural plots, both undeformed and modally deformed proved to be very useful in the development of accurate mathematical models. Initially, plots were made of each substructure and of the composite structure in order to verify geometry. Figure 6 illustrates the undeformed computer plot for the combined Viking Orbiter and Lander model. From this view and several others, the complete geometry was checked.

An important finding was observed from a plot of the first major longitudinal mode of this structure as shown on figure 7. Note that excessive deformations are exhibited by the Bioshield separation ring in the upper area of the Lander. This plot resulted in a MMC revision in the modeling of that part of the structure to eliminate the unrealistic elastic deformation.

Composite Structure Eigenvalues

The complete NASTRAN model of the Viking Space Vehicle was synthesized from the substructure models representing the Orbiter, Lander, and Booster. These components were merged by using MPC relationships and coordinate transformations. The combined model is represented by 931 elastic d.o.f. and 516 dynamic d.o.f. Eigenvalues for 45 modes (all less than 16 Hz) were calculated using the inverse power method and are listed in table IV. No comparative data is available for the exact configuration analyzed. However, some measure of confidence in the results is obtained by correlating the frequencies of the composite model with those of the substructure. For example, the first eight roots of table IV (all below 2 Hz) agree very closely with the eight roots (four double roots) of table III. This good agreement is due to the near rigid body behavior of the spacecraft below 2 Hz. In addition, the ninth root of table IV, which is associated with localized panel motion on the Orbiter is the same as the fundamental Orbiter root given in table II.

The Givens method was not used for the eigenvalue analysis of the composite model since its size exceeded the storage capacity of the LRC computers. In addition, a Guyan reduction was not used to reduce the size of the problem to its dynamic d.o.f. since run times increased when this procedure was attempted.

Operational Problems

Several NASTRAN problems were encountered which dealt with either program errors, or large computing times. These problems are discussed in this section along with possible measures for avoiding such problems.

Run time requirements.- Perhaps the most significant problem encountered in the course of this study is the long times required by NASTRAN to compute eigenvalues and eigenvectors. Using the modified version of NASTRAN (11.1.2) and approximately 40 percent of the CDC 6600 digital computers storage, the central processing time (cpu) was in excess of three minutes for each root extracted. Practically, this situation allowed only a few eigenvalues and eigenvectors to be computed since approximately 27.3 hours (cpu) would be required to find all the roots. It is noted that large time requirements are inherent in the tracking method for root extraction rather than in the NASTRAN system. Therefore, in order to reduce time requirements, a substantial reduction in the size of the matrices representing the model would be required.

Checkpoint dictionary omissions.- A checkpoint dictionary problem has been detected which is associated with secondary restarts. Not all tables and matrices are transferred from the old problem tape to the new problem tape. Neither are all the required tables which are not transferred, regenerated without specific DMAP alterations. This presents problems in such areas as plotting. For example, if plots are to be made from secondary restart tapes, the DMAP instruction "Geometry Processor 2," might be reexecuted to develop the "Element Connection Table." A check can be made from the checkpoint

dictionary listing prior to reexecution, to determine if needed information is on the old problem tape. In the event a needed table does not appear in the checkpoint dictionary, it can be regenerated by "alterating out" the DMAP statement which generated the table initially and replacing it with the statement which was eliminated.

Implementation of the General Element

It was found that errors were present in certain modes of operation involving use of the general element. Incorrect results are generated when the rigid body matrix is input directly. However, when NASTRAN is allowed to generate its own rigid body matrix correct results are obtained. Also, NASTRAN would not execute if the number of general elements used was even. As a consequence when the Titan model, with an odd number of general elements (11), was combined with the shroud (3 general elements) and Centaur models (the Centaur model had no general elements), the resulting booster model with an even number of general elements would not execute. To circumvent this problem, one general element was approximated with a series of three bar elements at the top of the shroud. The resulting booster model with an odd number of general elements (13) executed correctly.

CONCLUDING REMARKS

Experience gained with the application of NASTRAN to the Viking Space Vehicle in the stage 1 shutdown configuration has been presented. The more important aspects of this study are presented.

Computing time associated with eigenvalue extraction for the composite model (approximately 900 elastic d.o.f.) made computation of more than a few roots impractical. Even with the speed improvements incorporated into NASTRAN version (11.1.2), the direct eigenvalue analysis of large unreduced structural problems is not a practical approach. Use of the Guyan reduction to eliminate only the massless d.o.f. did not alleviate this time problem. However, a reduction in computing time might be achieved by a larger reduction to 200-300 dynamic d.o.f. This reduction procedure is the only alternative presently available in NASTRAN to modal synthesis.

The modeling flexibility of NASTRAN was demonstrated by use of adaptations in the program of several rather specialized features found in other finite element programs. In the present application, the ability to incorporate scalar masses, scalar springs, flexibility coefficients, direct input matrices, and rigid links was exercised. The ability to represent several portions of a structure in different coordinate systems is found to be an extremely useful feature.

Plotting of the undeformed model, in the highly versatile manner allowed by the program, provides a check on the geometric representation. In addition, the modally deformed plots provide a qualitative evaluation of the physical properties of the elements comprising the model.

REFERENCES

1. Hruda, Richard F.: Modal Coupling Program and Report. Report No. ED-2002-1256, Martin Marietta Corporation, February 10, 1971.
2. MacNeal, Richard H.: The NASTRAN Theoretical Manual. NASA SP-221, August 1969.
3. McCormick, Caleb W.: The NASTRAN User's Manual. NASA SP-222, September 1970.
4. Douglas, Frank J.: The NASTRAN Programmer's Manual. NASA SP-223, October 1969.
5. McCormick, C. W.: Modification to CDC Version of NASTRAN Level 11.1. Report No. 114-1, MacNeal-Schwendler Corporation, February 1, 1971.
6. Melosh, R. J.; and Christiansen, H. N.: Structural Analysis and Matrix Interpretive System (SAMIS) Program: Technical Report. Technical Memorandum No. 33-311, Jet Propulsion Laboratory, November 1, 1966.
7. Lang, T. E.: Structural Analysis and Matrix Interpretive System (SAMIS) User Report. Technical Memorandum No. 33-305, Jet Propulsion Laboratory, March 1, 1967.

TABLE I

COMPARISON OF VIKING LANDER FREQUENCIES (Hz)
COMPUTED BY THE MARTIN MARIETTA
CORPORATION (MMC) AND BY THE
NASTRAN PROGRAM

MMC	NASTRAN
10.94	10.99
12.35	12.43
12.40	12.50
12.61	12.68
12.69	12.74
12.°	12.94
14. J2	14.02
14.73	14.74
14.85	14.85
15.44	15.44
15.46	15.46
15.55	15.55
16.83	16.86
16.93	16.92
22.72	22.77
25.84	27.03
27.05	27.13
30.12	30.11
31.12	30.12
31.16	31.16
32.78	32.99
44.17	44.14
46.44	46.19
46.57	46.50
49.96	49.95
50.34	50.29
52.01	51.96
55.30	54.70

TABLE II

COMPARISON OF VIKING ORBITER FREQUENCIES (Hz)
COMPUTED BY JPL USING SAMIS AND BY THE
NASTRAN PROGRAM

<u>JPL (SAMIS)</u>	<u>NASA (NASTRAN)</u>
2.30	2.17
2.99	2.88
4.28	4.27
4.45	4.45
5.65	5.65
5.69	5.69
6.89	6.89
7.04	7.04
7.47	7.47
8.39	8.36
10.61	10.49
12.17	12.27
12.32	12.30
13.17	13.08
13.21	13.59
13.96	14.02
14.44	14.33
15.31	15.58
15.92	16.10
17.70	17.60
20.12	19.96
21.44	22.18
22.54	23.11
24.12	24.35
25.19	25.16

TABLE III

COMPARISON OF VIKING BOOSTER FREQUENCIES (Hz)
COMPUTED BY THE MARTIN MARIETTA
CORPORATION (MMC) AND BY THE
NASTRAN PROGRAM

NASTRAN	MMC
1.34*	1.36*
1.43*	1.43*
1.48*	1.48*
1.73*	1.75*
2.56*	2.57*
5.93*	5.93*
6.84	6.85
9.71*	9.04*
	11.4*
	13.9*
13.9	14.1
15.1*	16.1*
15.8*	18.1*
17.1	18.1
21.9	21.9
22.2	22.9
25.4*	26.2*
27.2*	28.4
26.8	29.2
28.1	31.5

*lateral frequencies are double roots corresponding to pitch
and yaw directions

TABLE IV

COMPOSITE VIKING SPACE VEHICLE FREQUENCIES (Hz)

$f_1 = 1.34$	$f_{23} = 9.38$
$f_2 = 1.34$	$f_{24} = 9.53$
$f_3 = 1.42$	$f_{25} = 10.06$
$f_4 = 1.43$	$f_{26} = 10.24$
$f_5 = 1.48$	$f_{27} = 11.36$
$f_6 = 1.48$	$f_{28} = 11.45$
$f_7 = 1.73$	$f_{29} = 11.93$
$f_8 = 1.73$	$f_{30} = 12.26$
$f_9 = 2.16$	$f_{31} = 13.00$
$f_{10} = 2.40$	$f_{32} = 13.26$
$f_{11} = 2.43$	$f_{33} = 13.48$
$f_{12} = 2.93$	$f_{34} = 13.50$
$f_{13} = 4.17$	$f_{35} = 13.62$
$f_{14} = 4.60$	$f_{36} = 13.81$
$f_{15} = 5.19$	$f_{37} = 14.23$
$f_{16} = 5.65$	$f_{38} = 14.43$
$f_{17} = 5.73$	$f_{39} = 14.55$
$f_{18} = 5.91$	$f_{40} = 14.73$
$f_{19} = 6.84$	$f_{41} = 15.24$
$f_{20} = 6.98$	$f_{42} = 15.41$
$f_{21} = 7.05$	$f_{43} = 15.44$
$f_{22} = 8.19$	$f_{44} = 15.71$
	$f_{45} = 15.83$

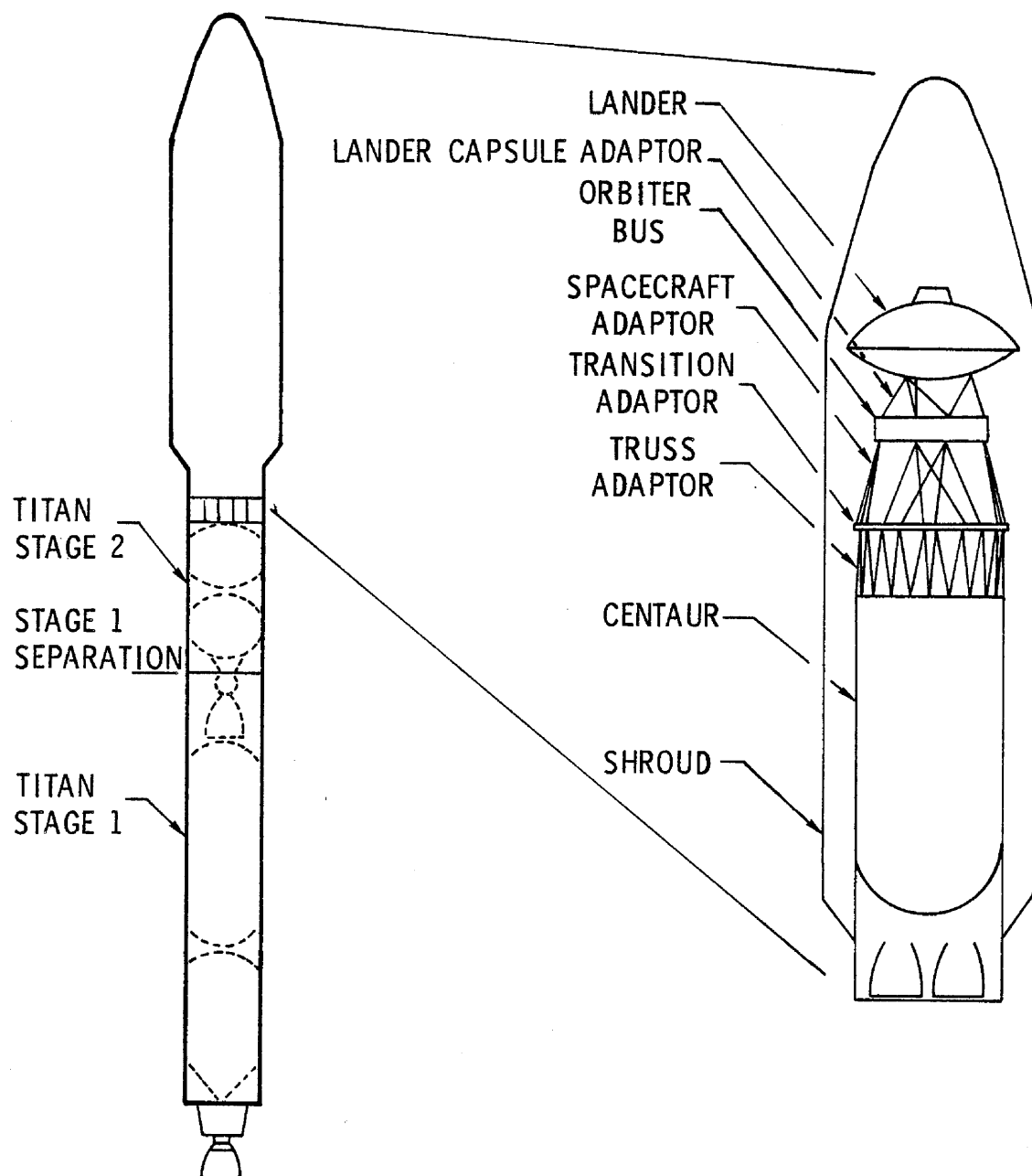


Figure 1.- Viking Space Vehicle - Stage 1 Configuration.

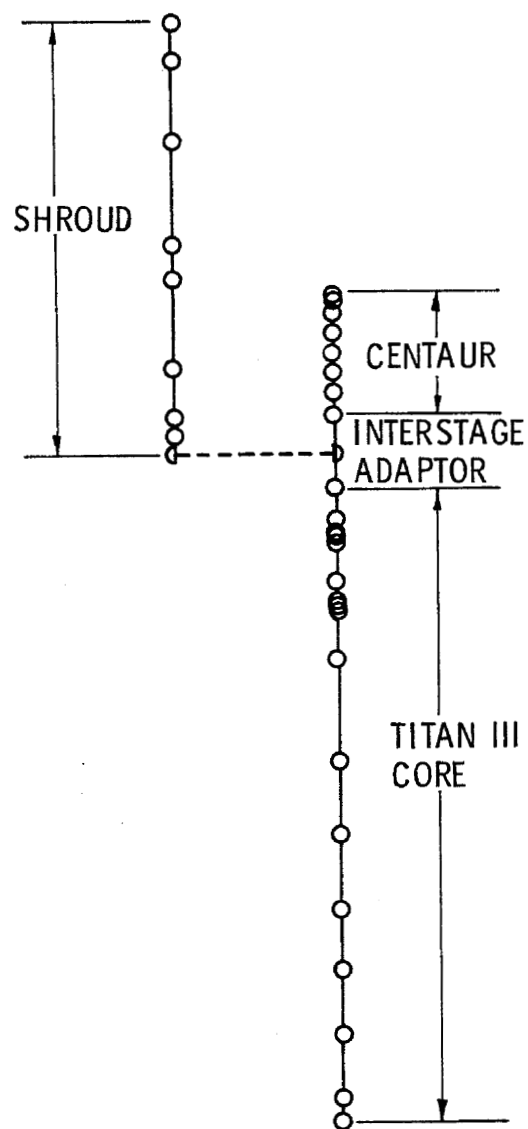


Figure 2. - Finite element model of booster - Viking Space Vehicle.

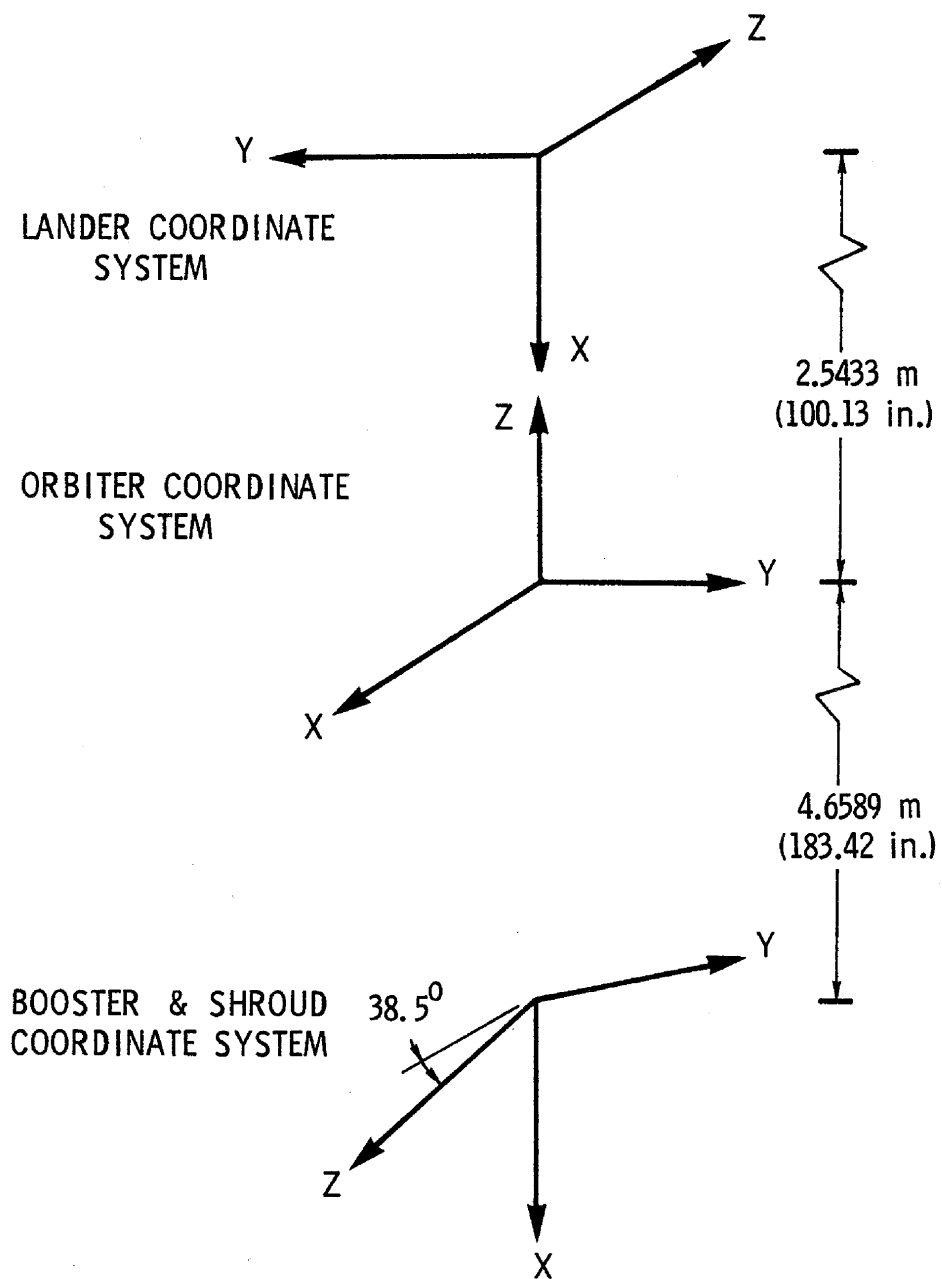
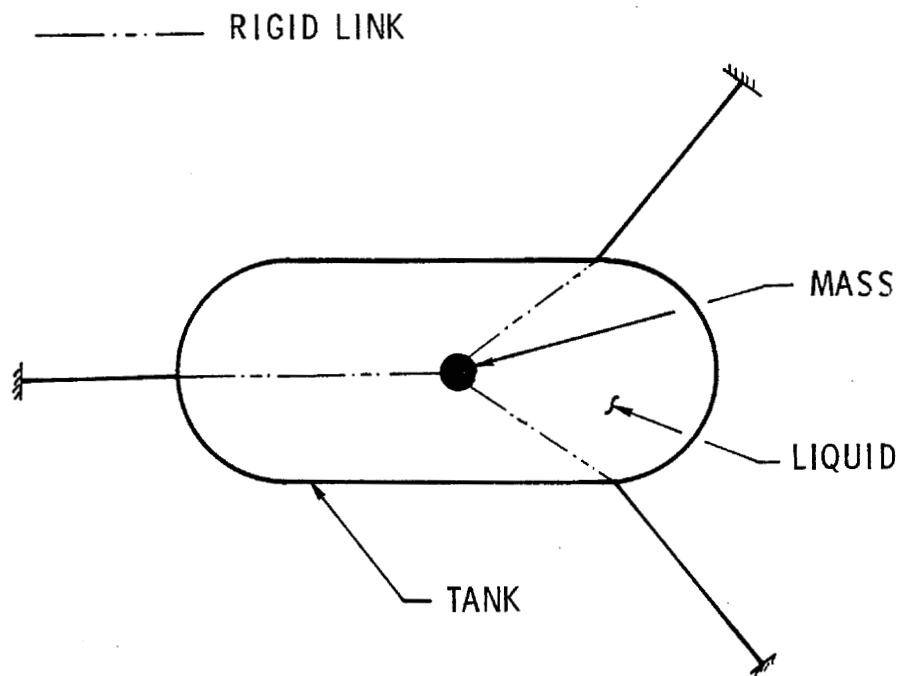
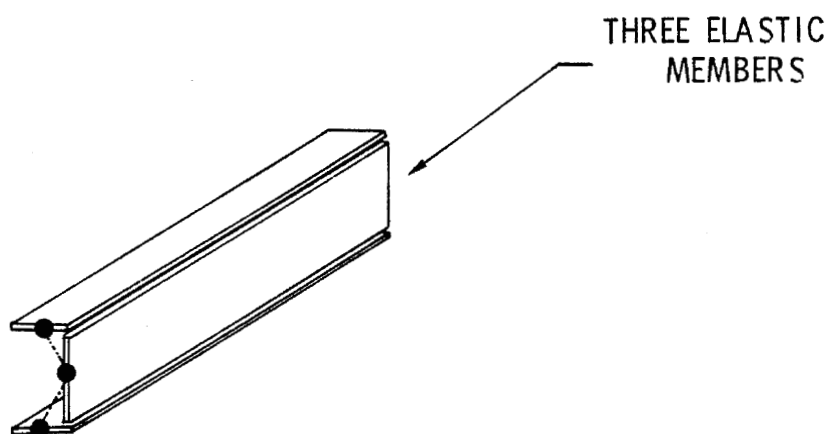


Figure 3. - Viking Space Vehicle coordinate systems.



(a) Link between elastic gridpoint and mass.



(a) Structural offsets.

Figure 4. - Uses of multipoint constraints.

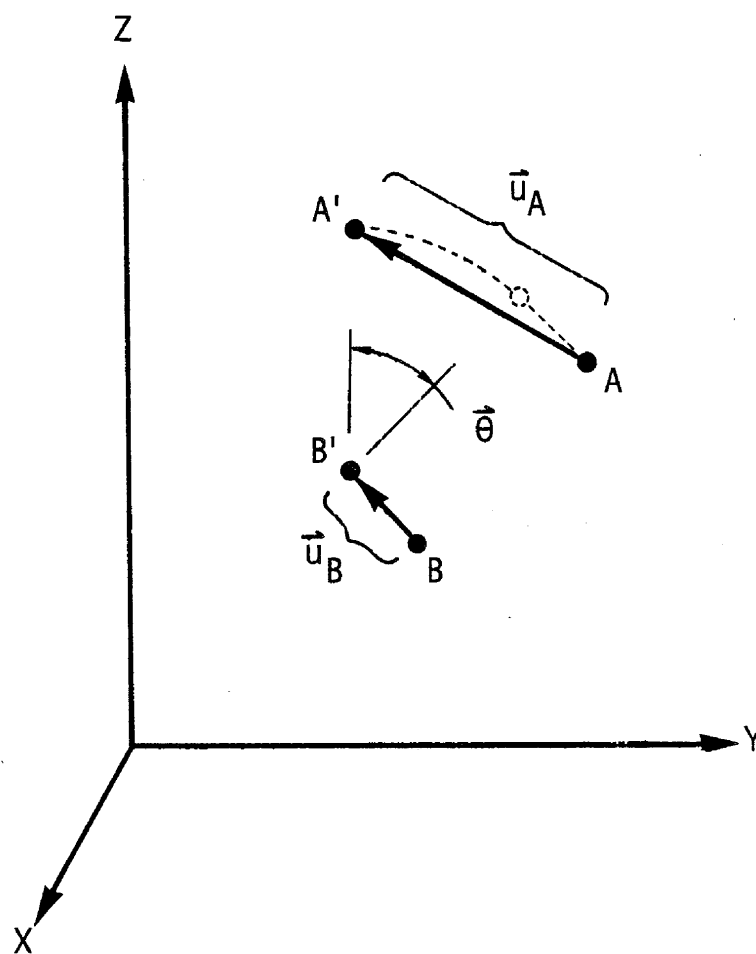


Figure 5. - Dependent displacement of two rigidly linked gridpoints.

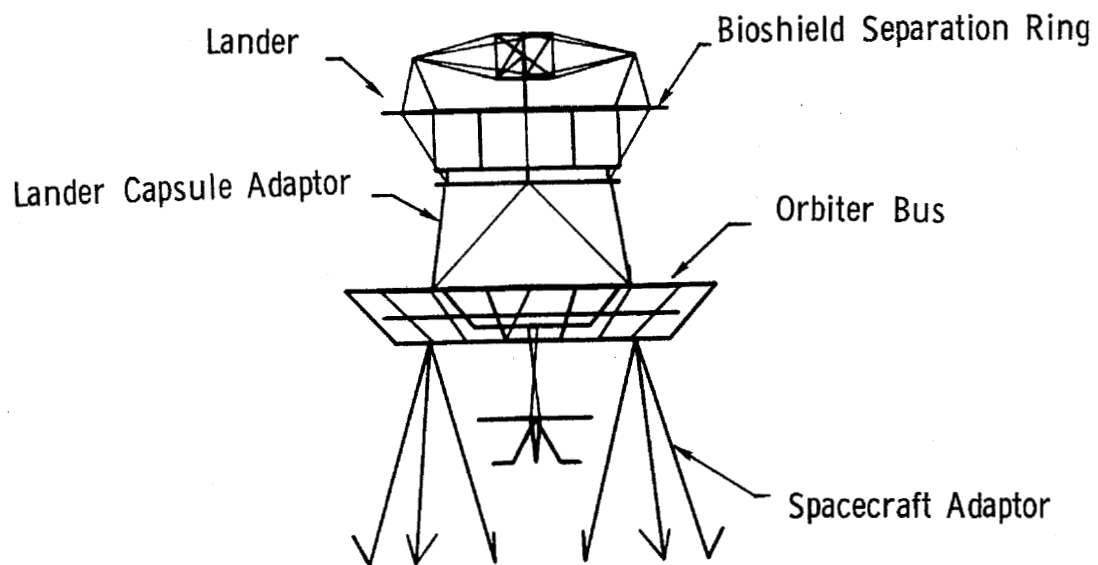


Figure 6. - Underformed structural plot - Orbiter and Lander.

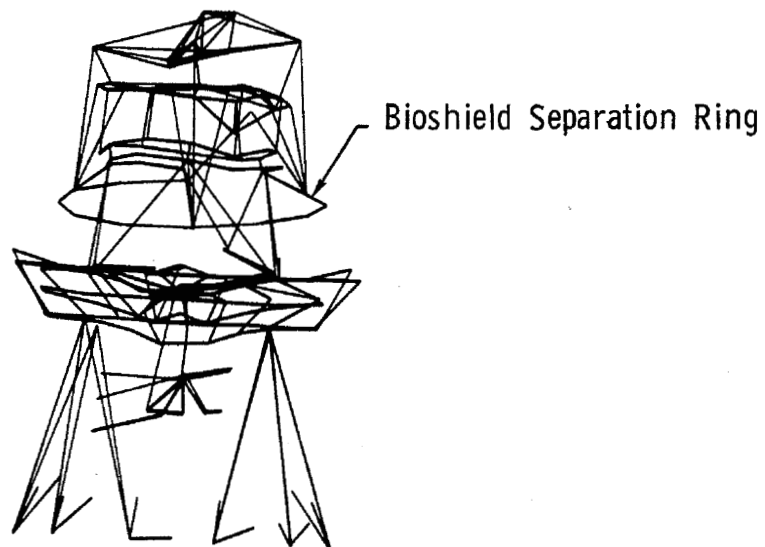


Figure 7. - Modally deformed structural plot - Orbiter and Lander, cantilevered frequency of 17.6 Hz.

ACOUSTIC ANALYSIS OF SOLID ROCKET MOTOR CAVITIES

BY A FINITE ELEMENT METHOD

By David N. Herting, Jerrard A. Joseph, Loren R. Kuusinen,
and Richard H. MacNeal

The MacNeal-Schwendler Corporation

SUMMARY

This paper describes an approach to the solution of acoustic modes in a cavity containing both axisymmetric regions and evenly spaced radial slots. A finite element approach is used with degrees of freedom taken as the harmonic coefficients in a Fourier expansion of the pressure. If the assumptions are made that the radial slots are evenly spaced around the circumference and that the circumferential pressure gradient within each slot is negligible, the equations for the harmonic coefficients become uncoupled. Formulas are derived by which the finite element stiffness and mass matrices may be computed. In addition, special terms are derived to account for rapid expansion of the flow in the opening between the slots and the circular cavity. Results are given for three operational solid rocket motors having four, six, and twelve radial slots respectively. Comparisons with other analytic results and with experimental results are given where these data are available.

INTRODUCTION

Throughout engineering history the different disciplines of applied mechanics have borrowed formulations and methods from each other in a cross pollinization process known as the mathematical analog. In particular, structural dynamicists have freely used the methods of electrical circuit analysis to formulate their equations and they have employed electric analog computers [1] to solve their problems. With the advent of the digital computer, the methods used in structural analysis have been improved to the point where a very sophisticated capability now exists in structural analysis computer programs. It is therefore, appropriate to consider using that capability for the solutions of analogous problems in other disciplines, including electromagnetics, fluid dynamics, and heat transfer.

The subject of this paper is the solution of acoustic problems using finite element methods adopted from structural analysis. The NASTRAN (NASA STRuctural ANalysis) program [2] has been modified to solve acoustic problems by substituting pressure for displacement, and fluid particle accelerations for the components of internal structural force. The NASTRAN program is basically a system for solving matrix equations of high order. It uses mass, damping, and stiffness matrices in its solutions. When a fluid is analyzed instead of a structure, its properties produce analogous matrices having different physical meaning, but with the same form. Thus NASTRAN

provides the capability to solve linear fluid problems with hundreds or thousands of degrees of freedom including statics (potential flow), normal modes, frequency response, and transient response. The modifications of NASTRAN that provide the capability are documented in additions to the NASTRAN Manuals, [2], [3], and [4], and in an applications report, [5], which gives detailed instructions for using the new acoustic capability.

Although the fluid models presented in this paper are restricted to a locally homogeneous compressible fluid having small motions, the capability is present to expand the sophistication of the solution to include additional effects, such as those caused by solid particles suspended in the fluid, and by finite ambient flow velocity (Mach Number effect).

The immediate motivation for the work described in the paper was the need for a better means to calculate the vibration mode frequencies and mode shapes of the interior cavities of solid propellant rocket motors. The cavities in functional rocket motors generally have complex shapes that include a number of symmetrically placed slots (or fins) cut into the propellant, whose purpose is to increase the area of the burning surface. The acoustic analysis of these cavities could be modelled with three dimensional finite elements that fill the entire cavity. Since solution costs increase roughly as the cube of the number of finite elements, there is good reason to use symmetry properties to reduce problem size.

The approach that will be described reduces the problem from three to two dimensions by means of assumptions regarding the variation of the pressure in the circumferential direction. Within the central axisymmetric

core of the cavity the pressure is expanded in a finite Fourier series with respect to the circumferential coordinate, having a number of terms equal to the number of slots. The pressure in the slotted region is also expanded in a Fourier series but within each slot the pressure gradient in the circumferential direction is assumed to be zero. With this assumption, and with appropriate approximations to the boundary conditions at the interface between the central cavity and the slots, the Fourier pressure coefficients become uncoupled from each other. They are, of course, functions of the (r,z) coordinates in a radial plane. The solution for each coefficient may, accordingly, be accomplished with two dimensional finite elements.

The reduction from three to two dimensions is beneficial because it reduces complexity and solution cost. It also introduces the concept that the vibration modes may be separated into groups according to the number of waves (n) in the circumferential direction. Due to the assumption of zero circumferential pressure gradient in the slots, the approach is more accurate for n small than for n large and also more accurate for narrow slots than for wide slots. No meaningful information at all is produced for n larger than half the number of slots. Thus the approach has limited application. It has, however, been tested by solving a variety of realistic problems and comparing solutions with experimental results from cold flow models. These solutions will be presented after the theory has been described in greater detail.

THEORY

Acoustic vibrations are governed by the wave equation, which can be stated in terms of the pressure fluctuation p as

$$\nabla \cdot \left(\frac{1}{\rho} \nabla p \right) = \frac{1}{B} \frac{\partial^2 p}{\partial t^2} \quad (1)$$

where ρ is the density of the fluid and B is its bulk modulus. Note that in the form given, ρ and B may vary with position in the fluid. Fluid particle acceleration, $\ddot{\vec{u}}$, is related to the pressure by

$$\ddot{\vec{u}} = - \frac{1}{\rho} \nabla p \quad (2)$$

The variational form of Equation (1) in terms of the total energy, H , is

$$\delta H = \delta \int_V \left[\frac{1}{2B} \dot{p}^2 + \frac{1}{2\rho} (\nabla p \cdot \nabla p) \right] dV - \int_S \delta p \frac{1}{\rho} \nabla p \cdot d\vec{S} = 0 \quad (3)$$

The volume integral in Equation (3) is the energy stored in the fluid and the surface integral is the energy flow through the boundary. In order to establish an analogy between the acoustic problem and the structural analysis computer program, p is "identified" as a structural displacement. The volume integral in Equation (3) is then recognized as the sum of a "kinetic" energy

$$T = \frac{1}{2} \int_V \frac{1}{B} \dot{p}^2 dV \quad (4)$$

and a "potential" energy

$$U = \frac{1}{2} \int_V \frac{1}{\rho} (\nabla p \cdot \nabla p) dV \quad (5)$$

wherein $\frac{1}{\rho}$ is analogous to a mass density and $\frac{1}{\rho}$ is analogous to a stiffness. We observe from Equation (2) that the fluid particle acceleration assumes the role of an internal force.

In the finite element method of solution, a set of variables, p_i , equal to the values of p at specific points, is chosen to be the degrees of freedom, and the volume is divided into subregions, called elements, with vertices defined by the points where p_i is defined. The internal pressure field for each element depends only on the pressures at the vertices of the element. A "stiffness" matrix $[K]$ is formed from the potential energy by the equation

$$K_{ij} = \frac{\partial^2 U}{\partial p_i \partial p_j} \quad (6)$$

and a "mass" matrix $[M]$ is formed from the kinetic energy by the equation

$$M_{ij} = \frac{\partial^2 T}{\partial \dot{p}_i \partial \dot{p}_j} \quad (7)$$

The stiffness and mass matrices are formed separately for each element. The set of simultaneous equations describing the pressures at discrete points, obtained by merging the matrices for the individual elements, may then be written as

$$[M_{ij}]\{\ddot{p}_j\} + [K_{ij}]\{p_j\} = \{I_i\} , \quad (8)$$

where $\{p_j\}$ is the vector of pressures at grid points and $\{I_i\}$ is a vector of "generalized forces". $\{I_i\}$ is null except at the boundaries, where it represents the surface integral of particle acceleration normal to the surface.

A useful side benefit of the formulation expressed in Equation (8) is that the incompressible potential flow problem may also be solved. The velocity potential function, ϕ , is related to the pressure by

$$\rho \dot{\phi} = p . \quad (9)$$

The mass flow rate, Q_i , into the fluid at any point, is the integral of the volume acceleration, i.e.,

$$\dot{Q}_i = I_i . \quad (10)$$

Substituting Equations (9) and (10) into Equation (8) and integrating with respect to time, results in the equation for the potential field,

$$[K_{ij}]\{\rho \phi_j\} = \{Q_i\} . \quad (11)$$

$\{Q_i\}$ is zero at impermeable boundaries.

AXISYMMETRIC REGION

Returning to the acoustic problem, it is seen that the mathematical model for the compressible fluid consists of a gridwork of points at which pressures are calculated, and a set of "fluid elements" which are connected to the grid points and which fill the space occupied by the fluid. The model is analogous to a finite element structural model. The pressure is analogous to displacement and the pressure gradient is analogous to strain.

Consider the application to an axisymmetric fluid region, such that the pressure distribution can be expanded in a Fourier series in the circumferential direction. The equivalent structural model is defined by a set of fluid grid points in a plane that includes the axis of symmetry. Each axisymmetric fluid element occupies the interior of a circular ring that is concentric with the axis of symmetry and whose cross-section is a polygon. Triangular and quadrilateral cross-sectional shapes will be considered.

The Fourier series expansion of the pressure within any fluid element is

$$p(r, \phi, z) = p^0 + \sum_{n=1}^N P^n \cos n\phi + \sum_{n=1}^N P^{n*} \sin n\phi . \quad (12)$$

The coefficients P^0 , P^n and P^{n*} are functions of position in a radial plane containing the axis of symmetry. They are expanded in truncated power series of the radial and axial coordinates as follows

$$P^n(r, z) = q_0^n + q_1^n r + q_2^n z + \dots \quad n \geq 0 , \quad (13)$$

$$P^{n*}(r, z) = q_0^{n*} + q_1^{n*} r + q_2^{n*} z + \dots \quad n \geq 1 . \quad (14)$$

The number of terms in each series is equal to the number of grid points to which the element is connected. The coefficients q_j^n and q_j^{n*} will be called the generalized coordinates of the element. They are selected to make the values of P^n and P^{n*} match the values of the pressure coefficients at the connected grid points. Thus, if P_i^n is the value of P^n at the i^{th} grid point,

$$\{q_j^n\} = [H_{qp}^n] \{P_i^n\} \quad , \quad (15)$$

$$\{q_j^{n*}\} = [H_{qp}^n] \{P_i^{n*}\} \quad , \quad (16)$$

where $[H_{qp}^n]$ is a matrix of constant coefficients. Note that the matrices for the starred and unstarred coefficients are identical. Since $[H_{qp}^n]$ is evaluated from its inverse, it must be a square matrix, and the number of generalized coordinates for each harmonic coefficient must be equal to the number of grid points to which the element is attached.

The gradient of the pressure, ∇p , is the vector

$$\nabla p = \frac{\partial p}{\partial r} \vec{e}_r + \frac{1}{r} \frac{\partial p}{\partial \phi} \vec{e}_\phi + \frac{\partial p}{\partial z} \vec{e}_z \quad . \quad (17)$$

where \vec{e}_r , \vec{e}_ϕ and \vec{e}_z are unit vectors. Hence, using Equation 1,

$$\begin{aligned} \nabla p = & \left[\frac{\partial p^0}{\partial r} + \sum_{n=1}^N \left(\frac{\partial P^n}{\partial r} \cos n\phi + \frac{\partial P^{n*}}{\partial r} \sin n\phi \right) \right] \vec{e}_r \\ & + \left[\sum_{n=1}^N \frac{n}{r} (-P^n \sin n\phi + P^{n*} \cos n\phi) \right] \vec{e}_\phi \\ & + \left[\frac{\partial p^0}{\partial z} + \sum_{n=1}^N \left(\frac{\partial P^n}{\partial z} \cos n\phi + \frac{\partial P^{n*}}{\partial z} \sin n\phi \right) \right] \vec{e}_z \quad . \end{aligned} \quad (18)$$

The integral over the volume in Equation 5 consists of separate integrals over the angle, ϕ , and over the cross-sectional area, A . Thus

$$U = \frac{1}{2} \int_A \left[\int_{\phi} \frac{1}{\rho} \nabla p \cdot \nabla p r d\phi \right] dA, \quad (19)$$

where $dA = dr dz$. The inner integration results in zero values for all products of different harmonics and all sine-cosine products. The potential energy expression, after applying the inner integration, is

$$\begin{aligned} U = & \int \frac{\pi r}{\rho} \left[\left(\frac{\partial p^0}{\partial r} \right)^2 + \left(\frac{\partial p^0}{\partial z} \right)^2 \right] dA \\ & + \sum_{n=1}^N \int \frac{\pi r}{2\rho} \left[\left(\frac{\partial p^n}{\partial r} \right)^2 + \left(\frac{\partial p^n}{\partial z} \right)^2 + \frac{n^2}{r^2} (p^n)^2 \right] dA \\ & + \sum_{n=1}^N \int \frac{\pi r}{2\rho} \left[\left(\frac{\partial p^{n*}}{\partial r} \right)^2 + \left(\frac{\partial p^{n*}}{\partial z} \right)^2 + \frac{n^2}{r^2} (p^{n*})^2 \right] dA. \end{aligned} \quad (20)$$

Note that the harmonics, n , are uncoupled, and that the starred and unstarred terms are uncoupled.

The pressure coefficients P^0 , P^n and P^{n*} , which vary throughout the element, may be evaluated in terms of the generalized coordinates q_j^0 , q_j^n and q_j^{n*} by means of Equations (13) and (14). Making this substitution in Equation 20, the stiffness matrix referred to the generalized coordinates may then be computed from

$$K_{ij}^{nq} = \frac{\partial^2 U}{\partial q_i^n \partial q_j^n}. \quad (21)$$

Using Equation (15), which expresses a linear relationship between the pressure coefficients at grid points and the generalized coordinates, the stiffness matrix referred to the pressure coefficients at grid points is

$$[K_{ij}^n] = [H_{qp}^n]^T [K_{ij}^{nq}] [H_{qp}^n] \quad (22)$$

The stiffness matrix for the starred pressure coefficients is identically the same.

The equivalent mass matrix is derived in a similar manner. The "kinetic" energy, Equation (4), is first expanded in terms of the harmonic pressure coefficients. When the integration with respect to ϕ is carried out, the result is

$$T = T_o + \sum_{n=1}^N T_n + \sum_{n=1}^N T_n^* \quad (23)$$

where

$$\left. \begin{aligned} T_o &= \int_A \frac{\pi r}{B} (\dot{p}^o)^2 dA \\ T_n &= \int_A \frac{\pi r}{2B} (\dot{p}^n)^2 dA \\ T_n^* &= \int_A \frac{\pi r}{2B} (\dot{p}^{n*})^2 dA \end{aligned} \right\} \quad (24)$$

The relationship between pressure coefficients at internal points and at grid points has the form

$$\dot{p}^n = \sum_j f_j^n(r, z) \dot{p}_j^n \quad n \geq 0, \quad (25)$$

$$\dot{p}^{n*} = \sum_j f_j^n(r, z) \dot{p}_j^{n*} \quad n \geq 1,$$

where $f_j^n(r, z)$ are functions of the shape of the element.

The terms in the mass matrix, referred to pressure coefficients at the fluid grid points, are, from Equation (7),

$$M_{ij}^n = \frac{\partial^2 T_n}{\partial \dot{p}_i^n \partial \dot{p}_j^n} = \frac{\pi}{B} \int_A f_i^n f_j^n r \, dA \quad n \geq 1. \quad (26)$$

where it is assumed that B is constant over the cross-section, A , of the element. The result for $n = 0$ is twice as large. The mass matrices for the starred terms are identical to those for the unstarred terms.

The calculations of matrix terms indicated by Equations (22) and (26) are straightforward, even if somewhat tedious. The details of the derivation and the results are described in the NASTRAN Theoretical Manual, Ref [2], Section 16.1.4. The cross-sectional element shapes included in NASTRAN are a triangle, a quadrilateral constructed from four overlapping triangles, and a special trapezoidal element adjacent to the axis of symmetry.

SLOT REGION

A slot region is defined as a series of narrow, evenly spaced cavities with their midplanes passing through the axis of the fluid. If the pressure gradient in the circumferential direction is ignored, the pressure in the j^{th} slot can be described by a finite Fourier series:

$$p_j = p^0(r,z) + \sum_{n=1}^N p^n(r,z) \cos n\phi_j + \sum_{n=1}^{N^*} p^{n^*}(r,z) \sin n\phi_j \quad (27)$$

The slots are placed at angles

$$\phi_j = \frac{2\pi j}{M} \quad j = 0, 1, 2, \dots, M-1 \quad (28)$$

where M is the total number of slots. The total number of terms in the series, $1+N+N^*$, must equal M in order to provide a unique decomposition of an arbitrary pressure distribution into Fourier components. If M is an odd number

$$N = N^* = \frac{M-1}{2} \quad (29)$$

If M is an even number

$$\left. \begin{aligned} N &= \frac{M}{2} \\ N^* &= \frac{M}{2} - 1 \end{aligned} \right\} \quad (30)$$

The equation for generalized potential energy is the same as Equation (19) except that the integration over ϕ is carried out as follows

$$\int_0^{2\pi} f(\phi) r d\phi = \sum_{j=0}^{M-1} w f(\phi_j) \quad (31)$$

where $f(\phi)$ is any function and w is the slot width, assumed to be equal for all slots.

Substituting Equation 31 into Equation 19 results in the following expression for the potential energy

$$U = \frac{1}{2} \int_A \left(\frac{w}{\rho} \sum_{j=0}^{M-1} \nabla p(\phi_j) \cdot \nabla p(\phi_j) \right) dA \quad (32)$$

where $dA = dr dz$.

Ignoring the gradient in the ϕ direction, the equation for the pressure gradient is

$$\begin{aligned} \nabla p = & \left[\frac{\partial p^0}{\partial r} + \sum_{n=1}^{k \leq \frac{M}{2}} \left(\frac{\partial p^n}{\partial r} \cos n\phi + \frac{\partial p^{n*}}{\partial r} \sin n\phi \right) \right] \vec{e}_r \\ & + \left[\frac{\partial p^0}{\partial z} + \sum_{n=1}^{k \leq \frac{M}{2}} \left(\frac{\partial p^n}{\partial z} \cos n\phi + \frac{\partial p^{n*}}{\partial z} \sin n\phi \right) \right] \vec{e}_z \end{aligned} \quad (33)$$

where $k = M/2$ for M even and $k = (M-1)/2$ for M odd. Substituting Equation (33) into Equation (32) results in a rather involved expression. The cross product terms between different harmonics will however, disappear, which may be shown as follows.

Since $\phi = 0$ is a plane of symmetry,

$$\sum_{j=0}^{M-1} \cos \frac{2\pi m j}{M} \sin \frac{2\pi n j}{M} = 0 \quad \text{for all } m, n \quad (34)$$

Define the coefficients:

$$R_{mn} = \sum_{j=0}^{M-1} \cos \frac{2\pi m j}{M} \cos \frac{2\pi n j}{M} = \frac{1}{2} \sum_{j=0}^{M-1} \left[\cos \left(\frac{2\pi j}{M} (m-n) \right) + \cos \left(\frac{2\pi j}{M} (m+n) \right) \right]$$

$$S_{mn} = \sum_{j=0}^{M-1} \sin \frac{2\pi m j}{M} \sin \frac{2\pi n j}{M} = \frac{1}{2} \sum_{j=0}^{M-1} \left[\cos \left(\frac{2\pi j}{M} (m-n) \right) - \cos \left(\frac{2\pi j}{M} (m+n) \right) \right] \quad (35)$$

The only conditions under which the sums of the cosine terms give a nonzero result occur when $(m+n)/M = 0$ or 1 , or when $(m-n)/M = 0$ or 1 . Since $n \leq M/2$ and $m \leq M/2$ the latter condition can occur only if $n = m$, and the former condition can occur only if $m = n = 0$ or if $m = n = M/2$. Thus all of the cross product terms ($m \neq n$) disappear. In addition

$$\left. \begin{aligned} R_{mm} &= S_{mm} = \frac{M}{2} && \text{for } m \neq 0, \frac{M}{2} \\ R_{00} &= R_{\frac{M}{2}, \frac{M}{2}} = M \\ S_{00} &= S_{\frac{M}{2}, \frac{M}{2}} = 0 \end{aligned} \right\} \quad (36)$$

Since the cross product terms disappear, the potential energy may be written

$$U = U^0 + \sum_{n=1}^{k < \frac{M}{2}} (U^n + U^{n*}) + U^{\frac{M}{2}} \quad (37)$$

where

$$\begin{aligned}
 U^n &= \frac{M}{4} \int_A \frac{w}{\rho} (\nabla_2 P^n) \cdot (\nabla_2 P^n) dA & 0 < n < \frac{M}{2} \\
 U^{n*} &= \frac{M}{4} \int_A \frac{w}{\rho} (\nabla_2 P^{n*}) \cdot (\nabla_2 P^{n*}) dA & 0 < n^* < \frac{M}{2} \\
 U^0 &= \frac{M}{2} \int_A \frac{w}{\rho} (\nabla_2 P^0) \cdot (\nabla_2 P^0) dA \\
 U^{\frac{M}{2}} &= \frac{M}{2} \int_A \frac{w}{\rho} (\nabla_2 P^{M/2}) \cdot (\nabla_2 P^{M/2}) dA
 \end{aligned} \tag{38}$$

∇_2 is the two dimensional gradient operator

$$\nabla_2 = \vec{e}_r \frac{\partial}{\partial r} + \vec{e}_z \frac{\partial}{\partial z} \tag{39}$$

In an analysis of the vibration modes of the cavity, the results for the sine coefficients, P^{n*} , will be identical to the results for the cosine coefficients, and they are, therefore, of no further interest. Each distinct cosine coefficient, $0 \leq n \leq M/2$, produces a distinct set of vibration modes.

The kinetic energy may be analyzed in the same manner as the potential energy. From Equation (4), and integration in the circumferential direction,

$$\left. \begin{aligned}
 T^n &= \frac{M}{4} \int_A \frac{w}{B} (\dot{p}^n)^2 dA & 0 < n < \frac{M}{2} \\
 T^0 &= \frac{M}{2} \int_A \frac{w}{B} (\dot{p}^0)^2 dA \\
 T^{\frac{M}{2}} &= \frac{M}{2} \int_A \frac{w}{B} (\dot{p}^{M/2})^2 dA
 \end{aligned} \right\} \quad (40)$$

Stiffness and mass matrices for the slot region are formed from the potential and kinetic energies in a manner analogous to that for the axisymmetric region. The NASTRAN Theoretical Manual, Ref [2], Section 16.2.2, contains derivations for a triangular element and for a quadrilateral element constructed from four overlapping triangles. The slot width, w , which is specified at grid points, is assumed to vary linearly with position over each triangular element. The slot elements can be used by themselves to solve two dimensional potential problems.

INTERCONNECTION OF THE SLOT REGION AND THE AXISYMMETRIC REGION

In the central cavity, it is assumed that the pressure

$$p_c = p_c^n(r, z) \cos n\phi \quad (41)$$

It is also assumed, in the slot region, that in the m^{th} slot,

$$p_{s,m} = p_s^n(r, z) \cos n\phi_m \quad (42)$$

where ϕ_m is the azimuth angle at the midplane of the m^{th} slot, see Figure 1.

A question then arises as to how the pressure at the mouth of the slot is related to the pressure in the cylindrical region. We might, for example, assume that the pressure in the mouth of the m^{th} slot, $p_{s,m}$, is equal to the pressure in the cylindrical region evaluated at $\phi = \phi_m$, the midpoint of the slot. A better assumption, particularly for wide slots, is that $p_{s,m}$ is equal to the average pressure in the cylindrical region, averaged over the slot width. Thus, using Equation (41), the pressure in the width of the m^{th} slot is

$$\begin{aligned} p_{s,m} &= p_c^n(r_o, z) \frac{1}{w_o} \int_{\phi_m - \frac{w_o}{2r_o}}^{\phi_m + \frac{w_o}{2r_o}} \cos n\phi \cdot r_o \, d\phi \\ &= p_c^n(r_o, z) \cos n\phi_m \cdot \frac{\sin \frac{nw_o}{2r_o}}{\frac{nw_o}{2r_o}} \\ &= p_{c,m} \cdot \frac{\sin \frac{nw_o}{2r_o}}{\frac{nw_o}{2r_o}} = p_{c,m}^\alpha \end{aligned} \quad (43)$$

Note that the ratio $p_{s,m}/p_{c,m}$ is independent of m so that upon substituting Equation (41) and (42) into Equation (43)

$$\frac{p_s^n(r_o, z)}{p_c^n(r_o, z)} = \alpha \quad (44)$$

The factor $nw_o/2r_o$ achieves a maximum value of $\pi/2$ for $n = M/2$ (the highest mode index) and $w_o = 2\pi r_o/M$, i.e., if the slots occupy the entire circumference. Table 1 shows how the ratio of p_s^n to p_c^n depends on $nw_o/2r_o$.

Table 1 Slot Correction Factor

$\frac{nw}{2r_o}$	0	.2	.4	.6	.8	1.0	$\pi/2$
$\frac{p_s^n}{p_c^n} = \alpha$	1.0	.995	.975	.942	.898	.840	.636

Note that the effect becomes significant for $nw_o/2r_o > 0.5$, i.e., when each slot covers greater than a twelfth of a wave length.

The rapid expansion of the flow upon entering the central cavity produces a pressure drop that should be accounted for. It may be shown [6] that the effect of an abrupt change in the diameter of a pipe is to add a coupling impedance that is equivalent to a short additional length of pipe. Our problem is a little different in that the slot is long (in the z direction) compared to its width. Smythe [7], has solved the analogous problem for the added resistance of a conducting strip whose width suddenly changes from w_1 to w_2 . His solution, expressed in terms of an added effective length, l_e , of the strip is

$$\ell_e = \frac{w_1}{2\pi} \left[\left(\beta + \frac{1}{\beta} \right) \log_e \frac{\beta+1}{\beta-1} + 2 \log_e \frac{(\beta+1)(\beta-1)}{4\beta} \right] \quad (45)$$

where $\beta = w_2/w_1$. Equation (45) is plotted in Figure 2. The bracketed expression has a logarithmic singularity as $\beta \rightarrow \infty$, but it is seen that $\ell_e / \sqrt{w_1 w_2}$ remains finite (in fact approaches zero) as $\beta \rightarrow \infty$. By way of comparison, the effective length of a round pipe of diameter w_1 approaches $4w_1/3\pi = .42w_1$ as $\beta \rightarrow \infty$.

The "stiffness" of the added length is

$$K_e = \frac{w_1 t}{\rho \ell_e} \quad (46)$$

where ρ is the density of the fluid and t is the transverse dimension of the slot.

The two effects described above may be combined to define a stiffness matrix that couples P_s^n and P_c^n . They are represented schematically in Figure 3. The equation for the constraint shown in Figure 3 is

$$\bar{P}_s^n = P_c^n \cdot \alpha \quad (47)$$

The scalar spring constant K_e is given by Equation (46). The equation of constraint and the scalar spring produce a "stiffness" matrix as follows

$$\begin{Bmatrix} I_s \\ I_c \end{Bmatrix} = \begin{bmatrix} K_e & -K_e \alpha \\ -K_e \alpha & K_e \alpha^2 \end{bmatrix} \begin{Bmatrix} P_s^n \\ P_c^n \end{Bmatrix} \quad (48)$$

COMPLETE FINITE ELEMENT MODEL

The complete finite element model for a typical solid propellant motor cavity is shown in Figure 4. Note that axisymmetric tubular rings that have no direct connection to the central cavity may be attached to the slot region. The entire cross section is covered with triangular and quadrilateral finite elements connected to grid points at which the pressure is defined. Along boundaries between the slot region and axisymmetric cavities, two degrees of freedom are defined and interconnected by the stiffness matrix given in Equation (48).

The input data to the computer consists of the locations and identifications of the grid points, the identification of the finite elements and their connections to grid points, and the physical properties, ρ , B , and slot width w , all of which may vary with position.

No special procedures are required to account for the boundary conditions at rigid surfaces, which is an important aspect of the finite element method. At nozzles and at other boundaries where the normal velocity depends on the pressure, the relationship between velocity and pressure may be represented by lumped impedance elements, see, for example, Ref. [8].

The complete analysis of a problem requires a solution for each set of terms in the Fourier series of pressure about the circumference. Each case, which is selected by the input value, n , produces a solution for one harmonic in the Fourier series. The longitudinal and axisymmetric "breathing" modes will result from $n = 0$. Simple lateral modes will result from $n = 1$. Larger values of n will result in more complicated modes. The meaningful range for a structure with slots is $n \leq \frac{M}{2}$ where M is the number of slots.

SOLVED PROBLEMS

In order to prove the validity of the theory and the correctness of the implementation, a series of problems were solved with the modified version of NASTRAN. These included a relatively simple test problem used to assess the accuracy of the assumptions for the radial slots, and three realistic rocket motor cavities, with four, six, and twelve slots respectively.

The test problem is illustrated in Figure 5; it consists of a central cavity and four slots. The pressure distribution was assumed to be independent of the location along the z axis and only lateral modes ($n = 1$) were considered. The problem was solved with three different methods: Method 1 used the theory described in preceding sections including the slot-cavity interconnection matrix. Fifteen finite elements were located in a radial line, including nine in the slot region. Method 2 used the same data except that the interconnection stiffness matrix was replaced by a rigid connection. In Method 3, one-quarter of the cross section normal to the z axis was cut up into 94 two dimensional elements, see Figure 6. The pressure along the y axis was set equal to zero in order to provide the proper boundary condition for lateral modes.

The lowest mode shapes and frequencies obtained with the three methods are compared in Figure 7. The difference in frequency between Methods 1 and 2 indicates that the slot-cavity correction matrix has a modest effect (5%). The comparison between Methods 1 and 3 validates the approach used in Method 1 for cavities with cross sections similar in shape to the test problem. No firm conclusions can be drawn regarding the magnitude of the error in Method 1, because Method 3 is also an approximate method which is known to give frequencies that are too high.

The first of the actual solid rocket motor cavities to be analyzed is the Minuteman III, Stage III, shown in Figure 8, together with the finite element model used in its analysis. As may be seen, it consists of six slots and a long slender central cavity of irregular shape. The finite element model contains approximately 130 grid points. This motor cavity had previously been analyzed [9] with a finite element model based on an electrical network analogy [10]. In addition, vibration modes were measured in a cold-flow model. Vibration mode frequencies for two different harmonic orders ($n = 0$ and $n = 1$) and for cavity dimensions corresponding to two different burn times ($t = 0$ and $t = 3$ sec.) are compared in Table 2. It is seen that all results are in excellent agreement. Pressure distributions for two of the modes are presented in Figure 9.

The second rocket motor cavity is the Minuteman II, Stage III, shown in Figure 10. The cavity includes four conical nozzle ports with attached constant width slots, and a central cavity. The treatment of the relatively bulbous nozzle ports as variable width slots constitutes a fairly severe strain on the assumption of zero circumferential pressure gradient. The entrance to the nozzle port is assumed closed in order to match available experimental measurements on a cold flow model. This assumption could be replaced by an assumption of zero pressure or by an impedance relationship between pressure and normal velocity. The configuration shown in Figure 10 also assumes that a two inch layer of propellant has burned away from the surface of the cavity.

Table 2. Natural Frequencies for the Third Stage, Minuteman III, Motor Cavity

Burn Time (sec.)	Harmonic (n)	Mode	Frequency, Hz		
			Ref. [10]	This Paper	Experimental
0.0	0	1	105.3	105.2	
		2	208.8	212.9	
		3	310.6	316.7	
		4	374.7	380.5	
		5	454.9	455.2	
	1	1	275.5	275.8	
		2	354.4	360.6	
		3	615.3	641.9	
3.0	0	1	90.2	90.1	93.
		2	196.0	199.5	200.
		3	305.9	310.4	312.
		4	386.5	388.0	388.
		5	453.1	449.1	466.
		6	503.6	512.8	518.
	1	1	239.2	238.9	239.0
		2	314.2	316.1	324.0
		3	539.2	541.6	
		4		567.4	

Vibration mode frequencies are presented in Table 3 for two different burn depths and are compared with the available cold flow model experimental data. Acceptable agreement is obtained except for one mode, which suggests that the experiment missed one of a pair of close roots. It is interesting to observe that not all modes decrease in frequency as the propellant is burned away. Figure 11 shows computed pressure distributions for the lowest longitudinal ($n = 0$) and lateral ($n = 1$) modes for two inches of propellant burn.

Table 3. Natural Frequencies for the Third Stage Minuteman II Motor Cavity

Harmonic (n)	Mode	Frequency (Hertz)			
		2" Burn		5" Burn	
		NASTRAN	Experimental	NASTRAN	Experimental
0	1	578.4	557	517.7	507
	2	982.9	939	911.7	882
	3	1,406.0		1,364.7	1340
	4	1,535.5	1432	1,621.7	1545
	5	2,007.6	1928	1,909.8	1842
	6	2,084.8			
1	1	771.4		858.7	
	2	1,449.4		1,266.9	
	3	2,004.3		1,729.1	
	4	2,294.0		1,998.0	
	5			2,290.9	
	6			2,493.7	

The third rocket motor cavity is the second stage of the Poseidon shown in Figure 12. It has twelve radial slots and the finite element model has 85 grid points. The frequencies for the axisymmetric modes ($n = 0$) and the lateral modes ($n = 1$) are listed in Table 4 for cavity dimensions corresponding to two different depths of propellant burn. Again it is seen that not all of the frequencies decrease as the cavity becomes larger. Confirming experimental data were not available for this cavity. Mode shapes for the six lowest axisymmetric modes with zero propellant burn are plotted in Figure 13.

Table 4. Natural Frequencies for the Second Stage Poseidon Motor Cavity

Harmonic (n)	Mode	Frequency (Hertz)			
		0 Burn		3" Burn	
		NASTRAN	Experimental	NASTRAN	Experimental
0	1	388.1	398	324.0	322
	2	645.0	645	678.3	689
	3	962.0	962	1039.2	1051
	4	1422.0	1422	1430.8	1425
	5	1769.0	1728	1830.9	1831
	6	2010.8	2130	1994.4	
1	1	835.1		737.8	
	2	1313.4	1216	833.9	868
	3	1659.1	1620	1344.0	1349
	4	1832.8	1798	1558.2	1552
	5	2105.7		1812.5	
	6	2236.8		2130.1	2094

REFERENCES

1. MacNeal, R. H. Electric Circuit Analogies for Elastic Structures, Wiley, N. Y., 1962.
2. "The NASTRAN Theoretical Manual", NASA SP-221, Sept 1970.
3. "The NASTRAN User's Manual" NASA SP-222, Sept. 1970.
4. "The NASTRAN Programmer's Manual" NASA SP-223, Sept. 1970.
5. Herting, D. N. "Application Manual for NASTRAN Acoustic Cavity Analysis", MacNeal-Schwendler Corp. Report No. MS 116-2, May 1971.
6. Rschevkin, S. N. The Theory of Sound, The MacMillan Co., N. Y. 1963, p 218.
7. Smythe, W. R. Static and Dynamic Electricity, McGraw-Hill, N. Y. 1939, pp 230 - 233.
8. Morse, P. M. Vibration and Sound, McGraw-Hill, 1948, p 274.
9. Joseph, J. A. "An Acoustical Analysis of a Gas Cavity", MacNeal-Schwendler Report MS 92-1, March 19, 1970.
10. MacNeal, R. H., "An Asymmetrical Finite Difference Network", Q. of Applied Math, Vol. XI No. 3, Oct. 1953.

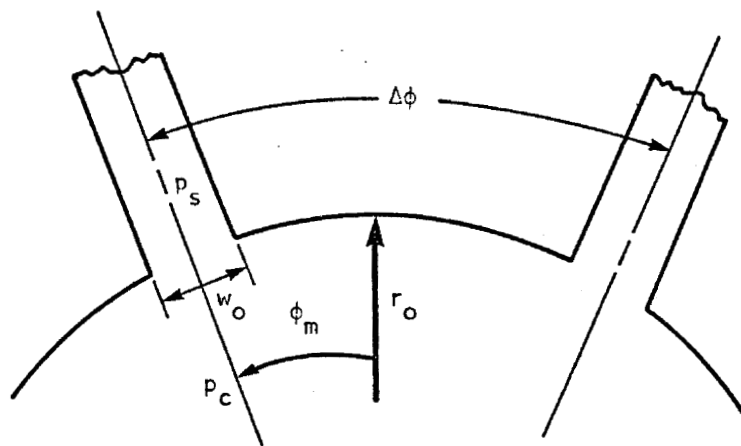


Figure 1. Interface Between Slots and Central Cavity

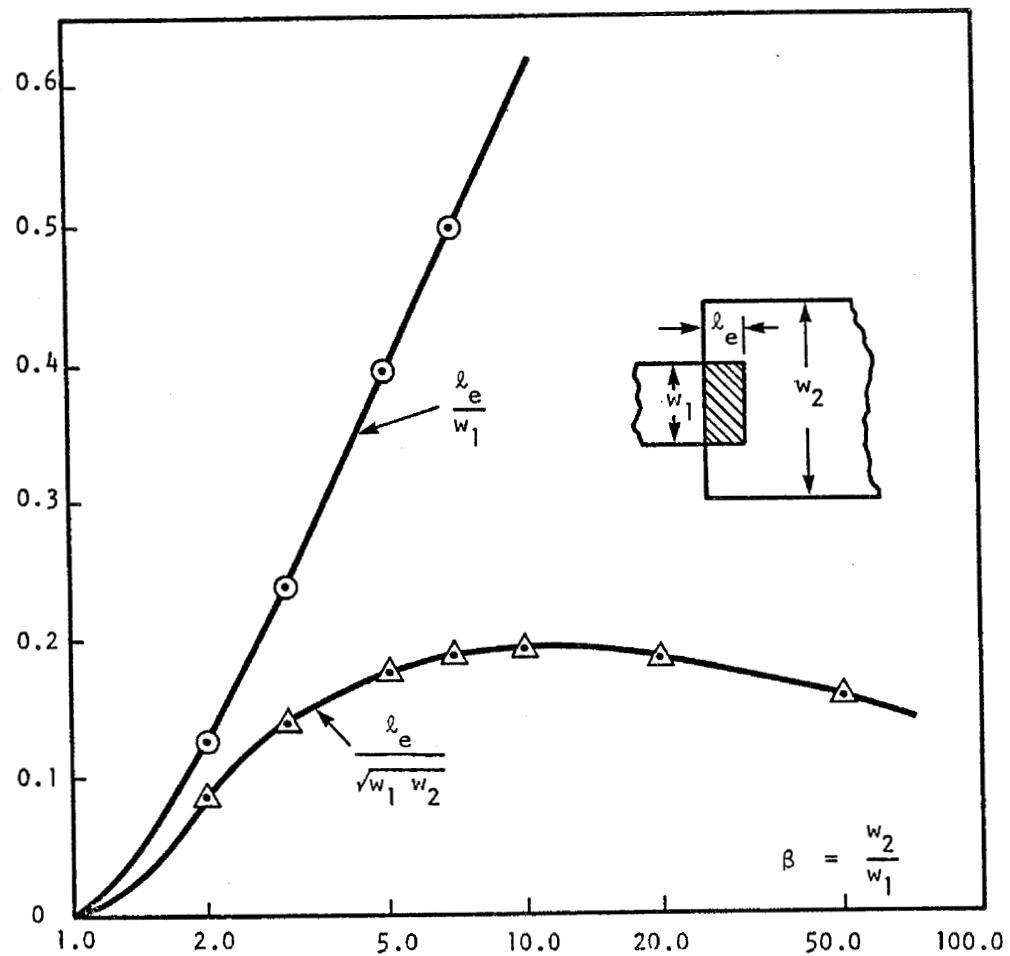


Figure 2. Effective Length of the Abrupt Change in the Width of a Strip

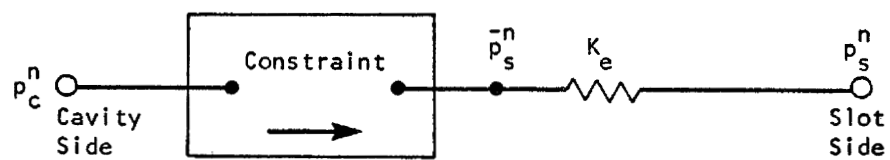


Figure 3. Finite Element Model for Slot-Cavity Interconnection

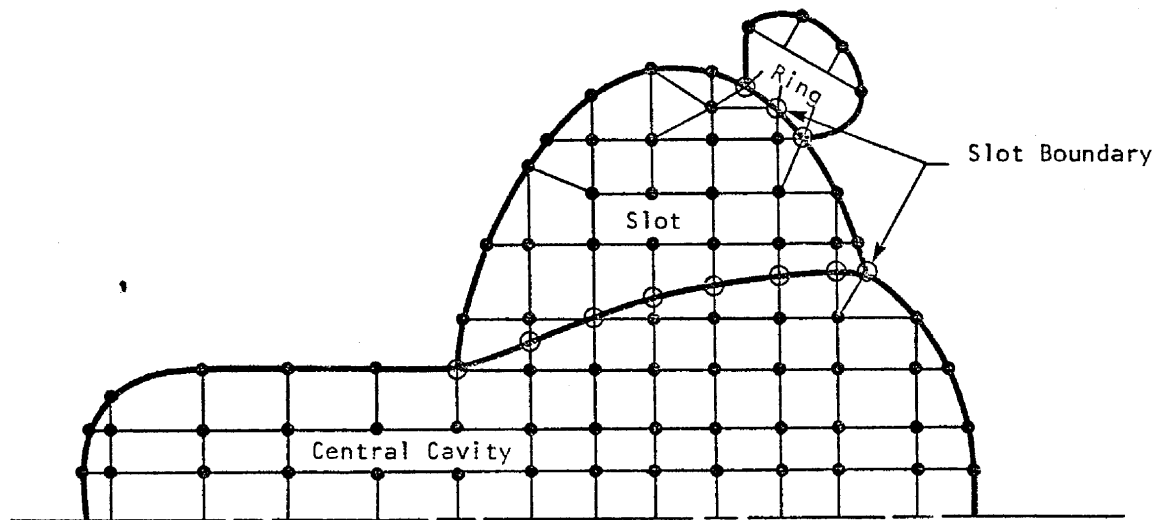


Figure 4. Finite Element Model of Acoustic Cavity

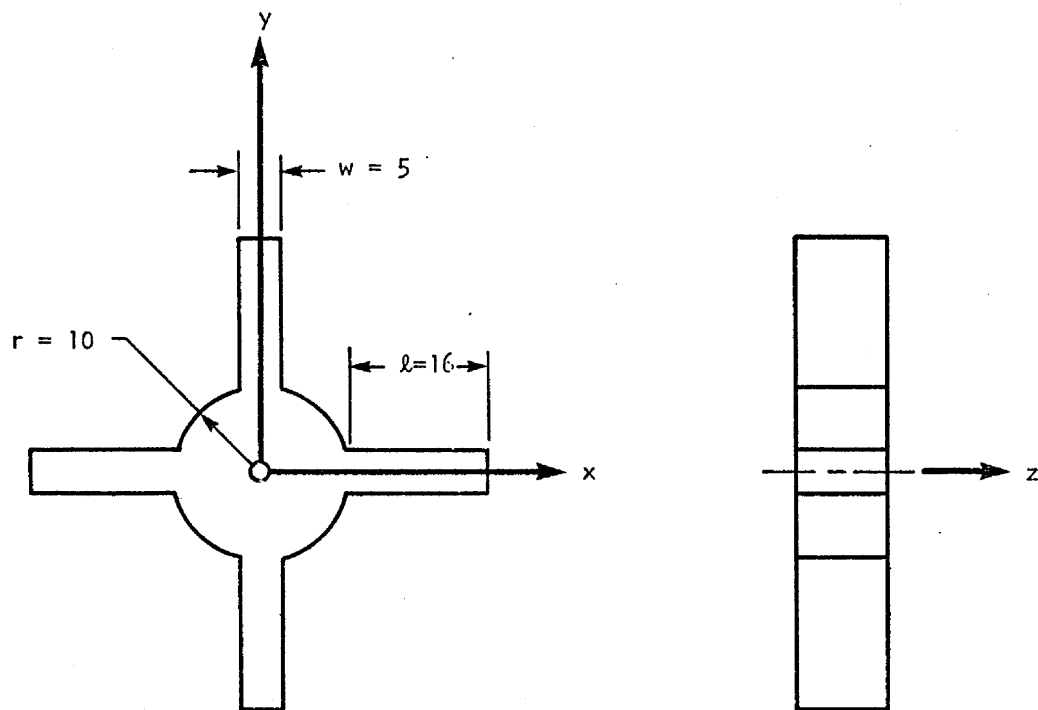


Figure 5. Test Problem

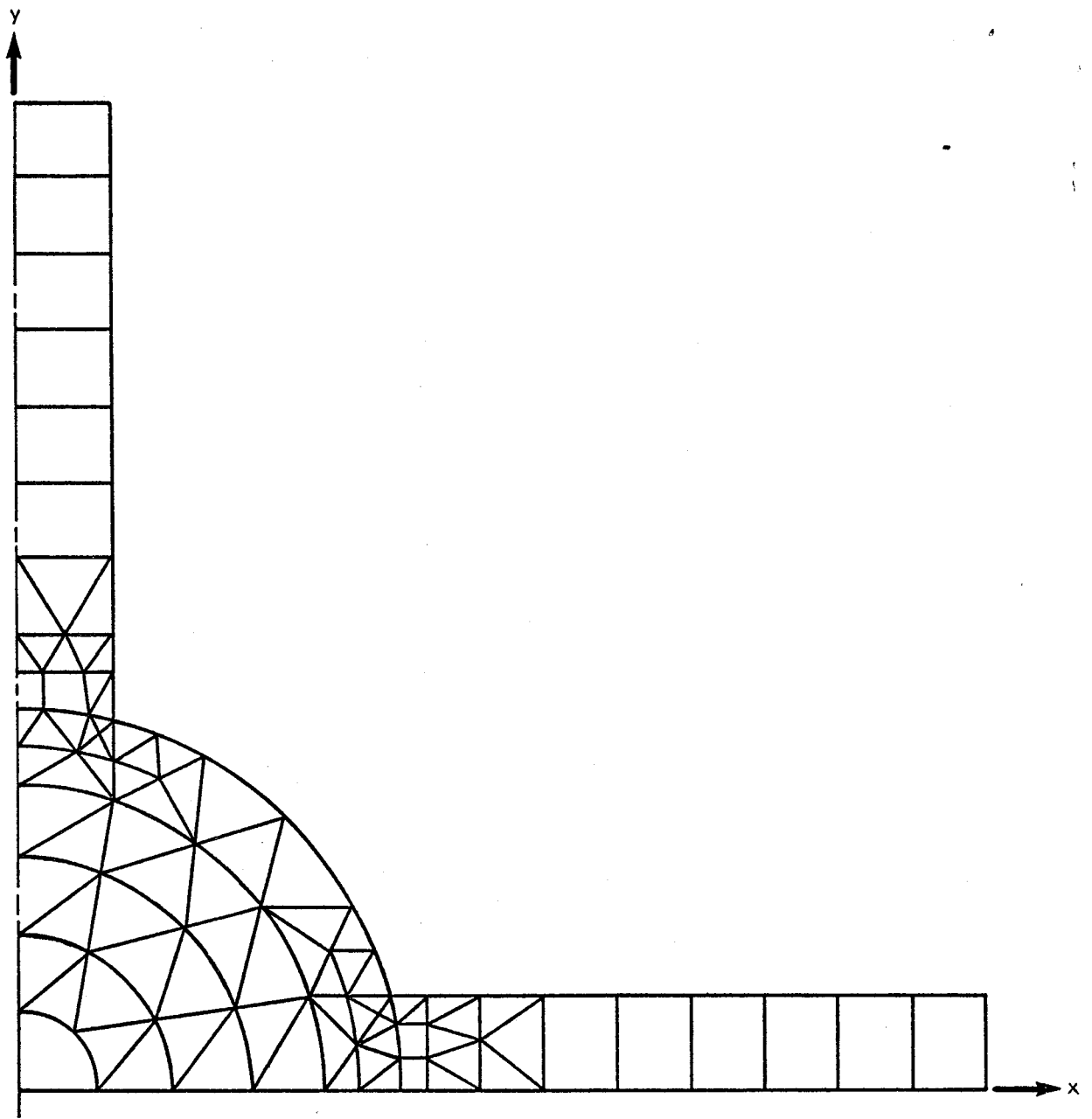


Figure 6. Two Dimensional Finite Element Model of Test Problem

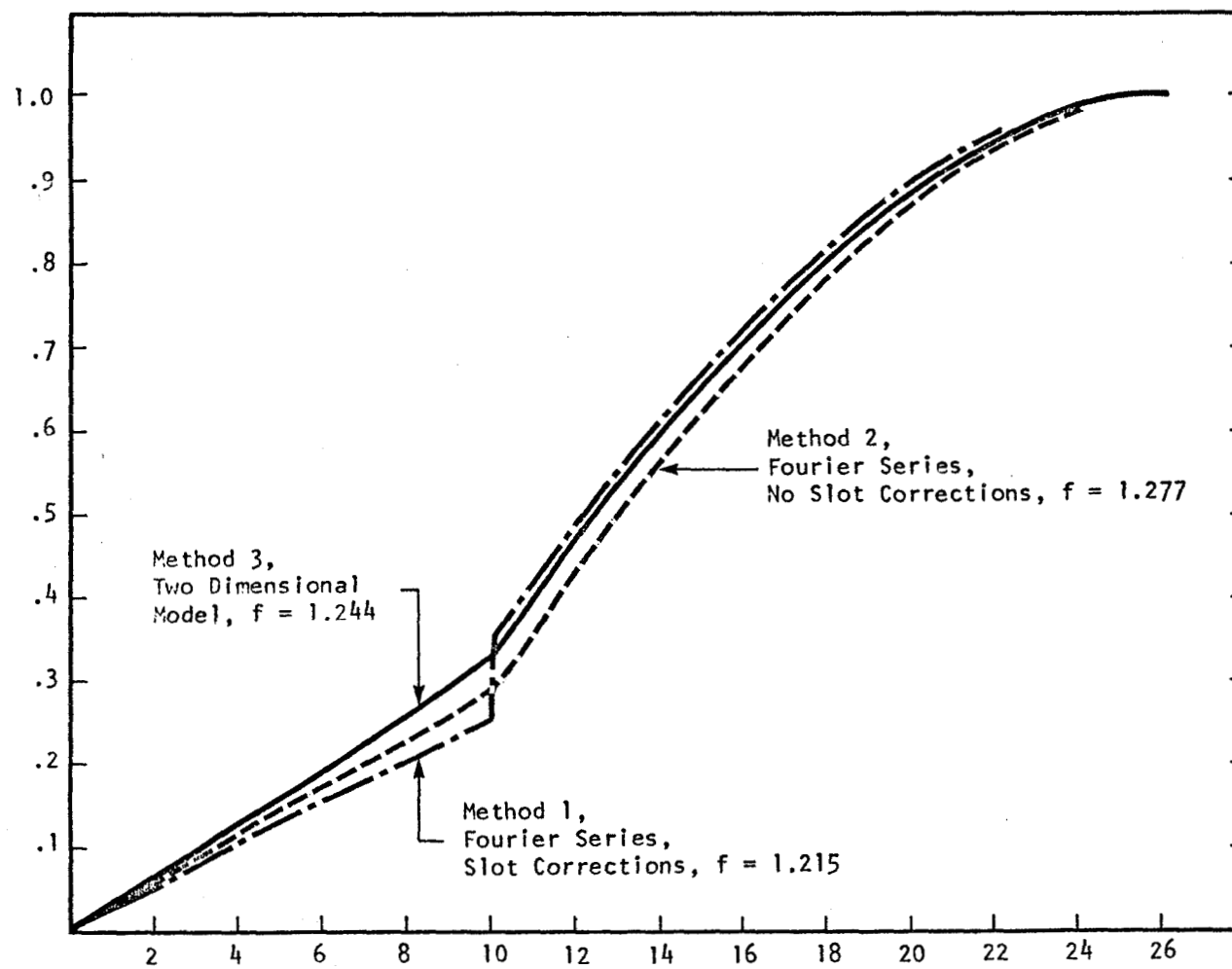


Figure 7. Pressure Distribution along X-Axis for the Lowest Mode of the Test Problem

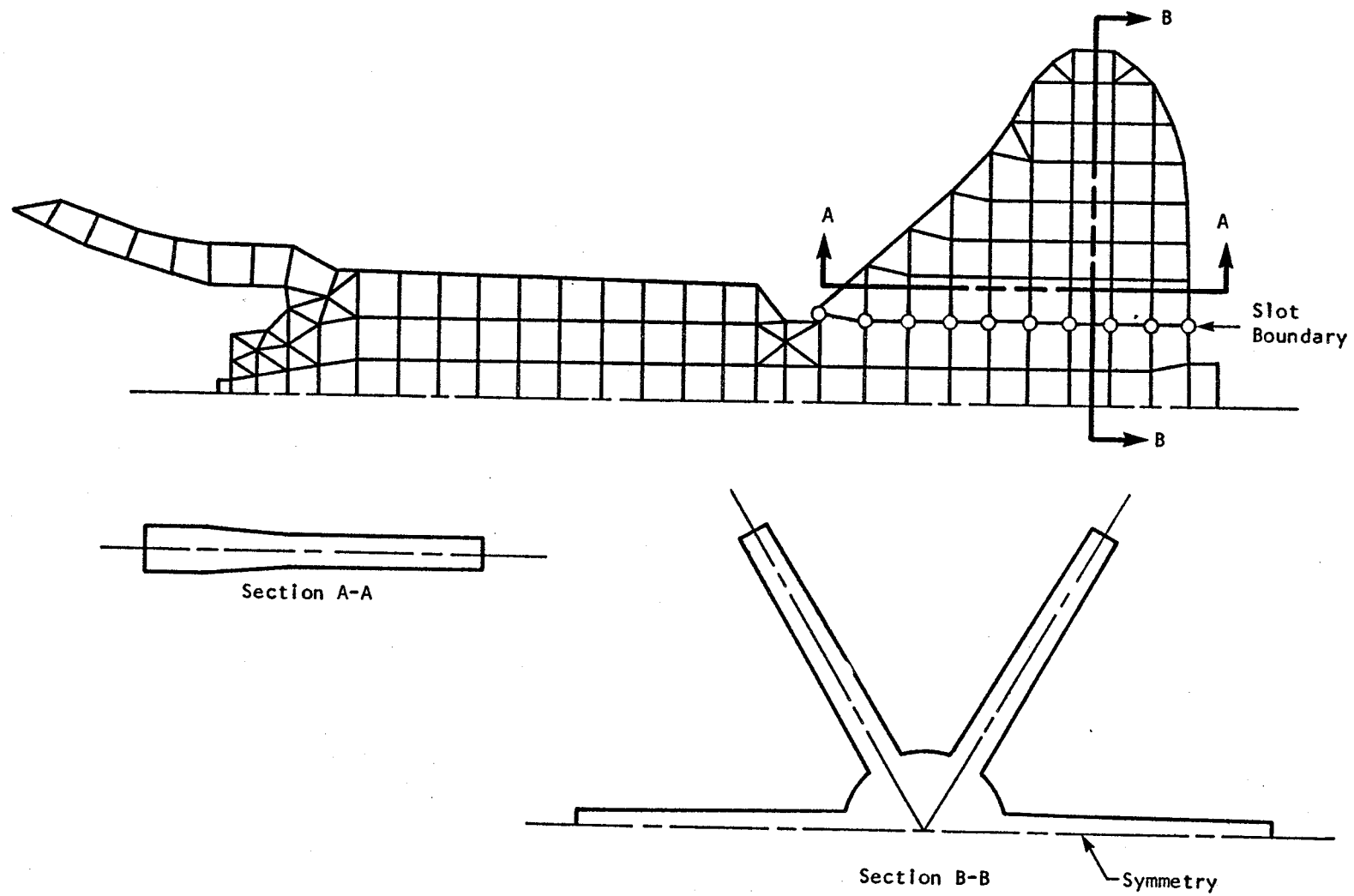
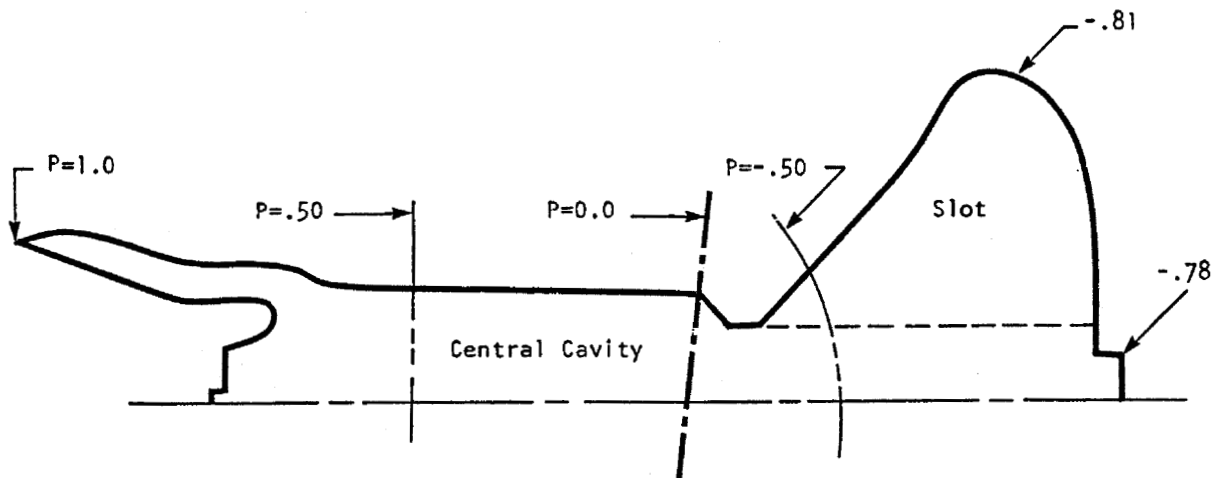
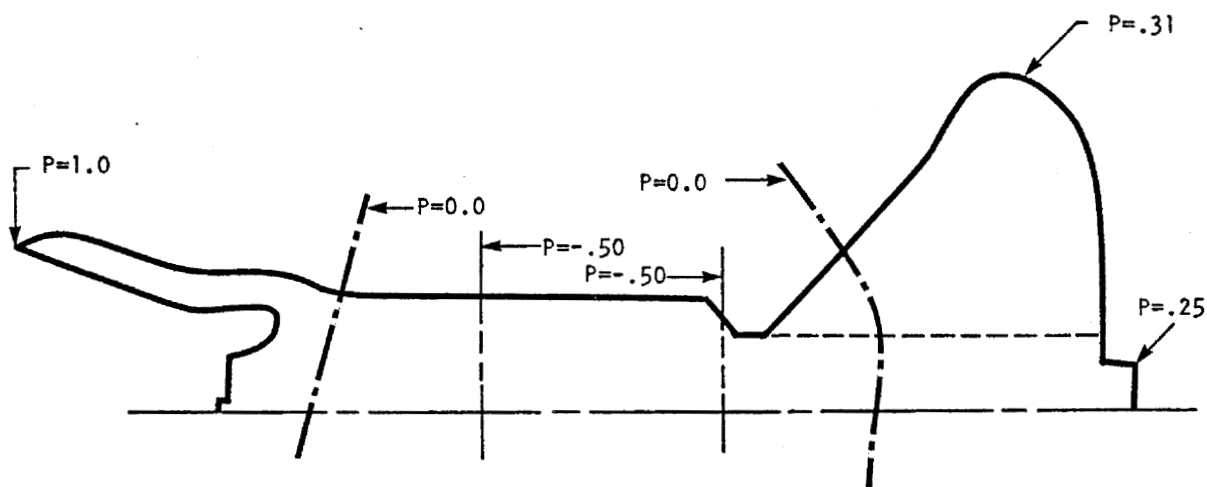


Figure 8. Minuteman III, Stage III, Rocket Motor



Mode 1 $f = 90.1 \text{ Hz}$, $n = 0$



Mode 2 $f = 199.5 \text{ Hz}$, $n = 0$

Figure 9. Minuteman III, Stage III, Mode Shapes for First Two Modes,
 $n = 0$, $t = 3.0 \text{ sec.}$

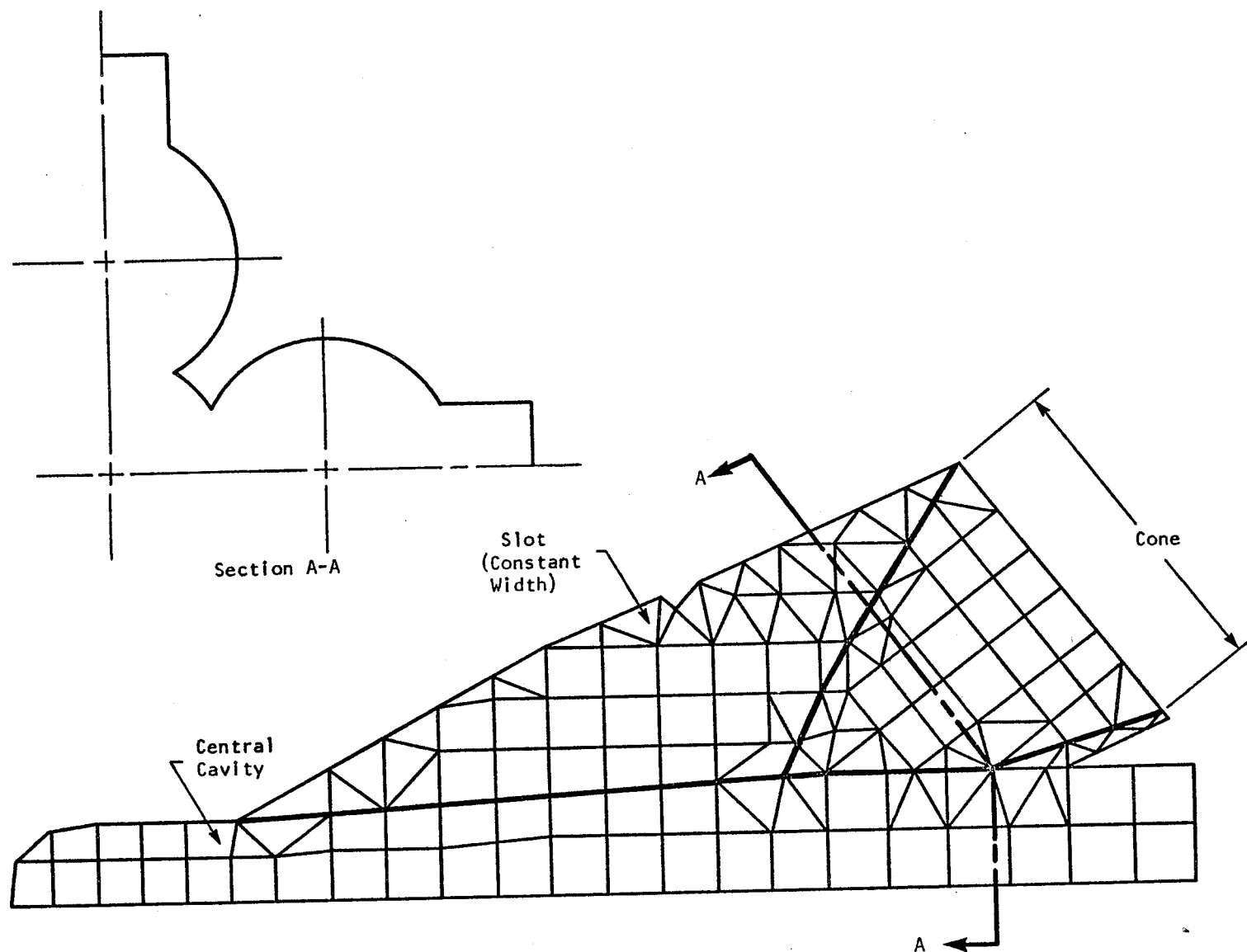
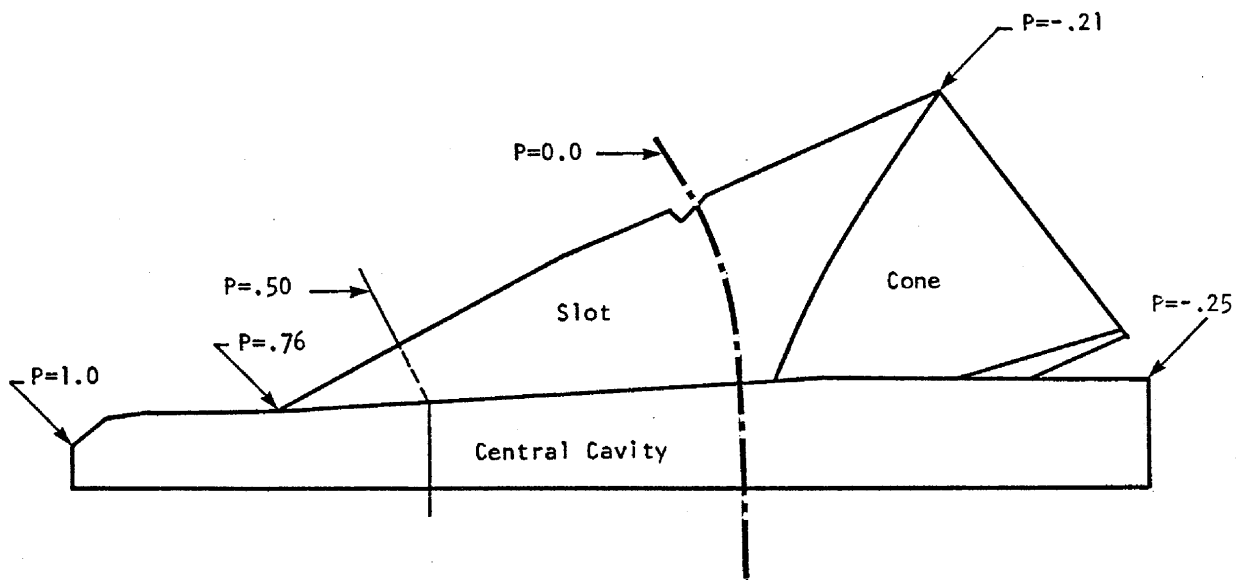
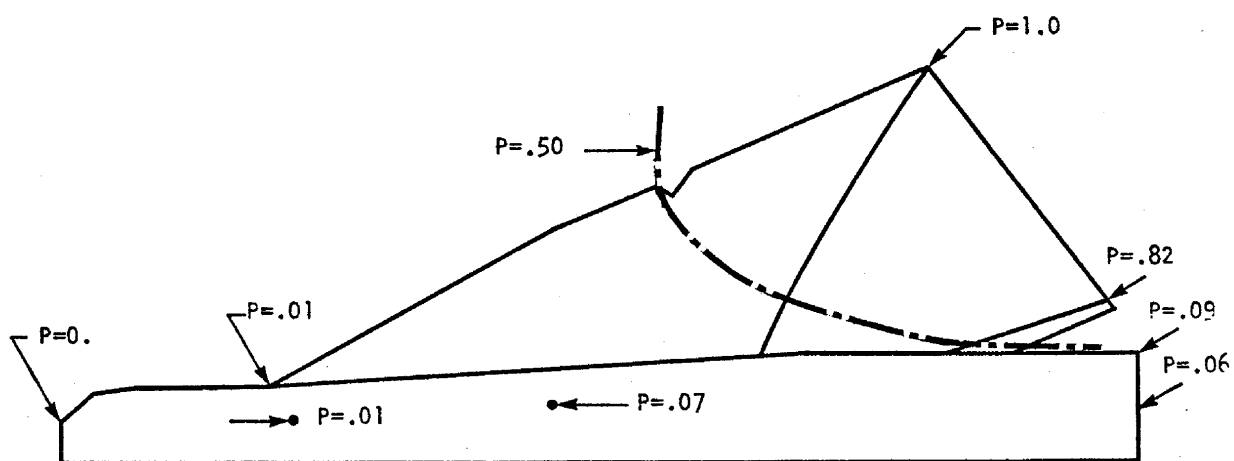


Figure 10. Minuteman II, Stage III, Rocket Motor



$f = 578.4 \text{ Hz}, n = 0$



$f = 777.4 \text{ Hz}, n = 1$

Figure 11. Minuteman II, Stage III, Mode Shapes for Lowest Modes,

2" Burn, $n = 0$ and $n = 1$

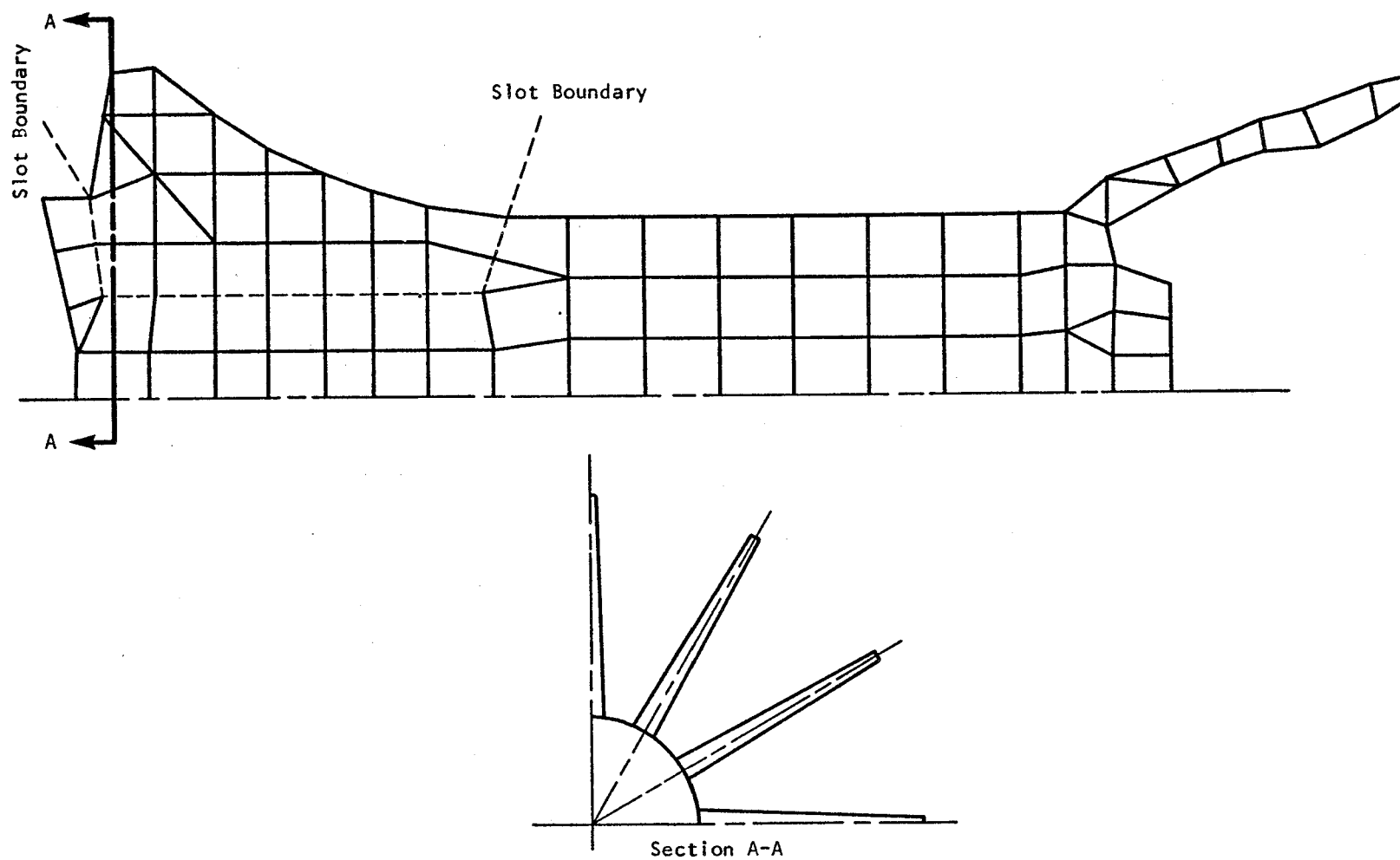
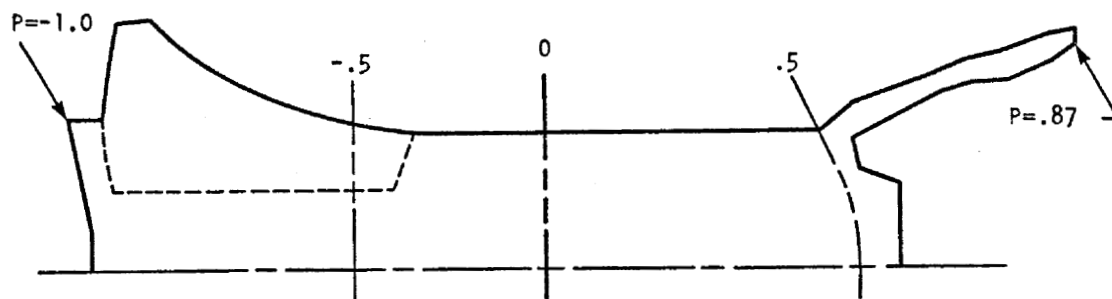
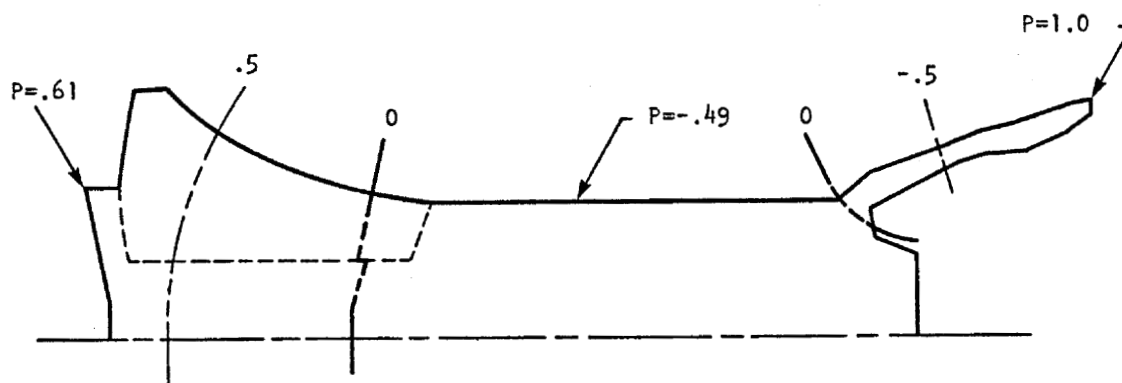


Figure 12. Second Stage Poseidon Rocket Motor

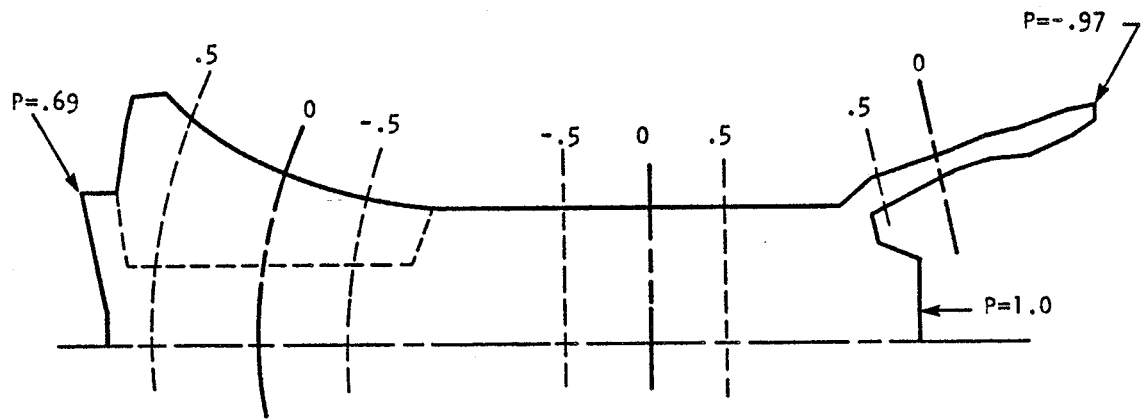


a) Mode 1. $f = 388.1$ Hz

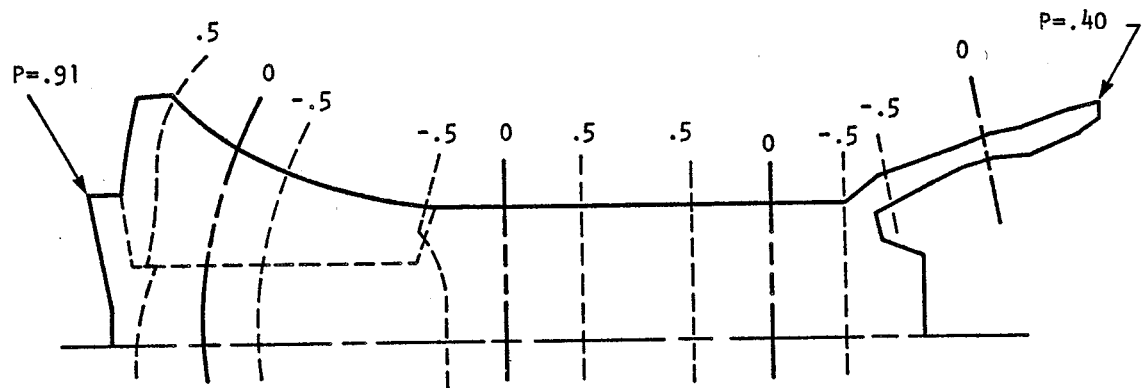


b) Mode 2. $f = 645.0$ Hz

Figure 13. Second Stage Poseidon Mode Shapes, $n = 0$, $t = 0.0$ sec.



c) Mode 3. $f = 962.0$ Hz



d) Mode 4. $f = 1,422.0$ Hz

Figure 13. (Continued)

PRACTICAL ANALYSIS OF PLATE VIBRATIONS

USING NASTRAN

Robert R. Clary
NASA Langley Research Center

SUMMARY

This paper discusses the successful application of the NASA structural analysis (NASTRAN) computer program for calculating the vibration characteristics of a variety of plate configurations. Calculated natural frequencies and nodal patterns are generally in good agreement with measured data for (1) research filamentary composite material plates, (2) wing flutter models fabricated with metal reinforced with composite material, and (3) a metal plate supported on an elastic boundary.

INTRODUCTION

Application of new design concepts and materials to structural plates which are employed in modern aircraft, spacecraft, and propulsion systems requires the analysis of the vibration characteristics of a wide variety of plate configurations. These plates may be constructed with isotropic or orthotropic materials and may involve combinations of dissimilar materials. Boundaries may be free, fixed, or elastically restrained, and there may be internal supports.

In an effort to determine the effectiveness of the NASTRAN program for calculating structural vibration characteristics of plates, NASTRAN has been applied to a number of different plate configurations. This paper presents some results from three of these studies summarized as follows:

1. Composite material plates.- An analytical and experimental study was made on a series of filamentary composite material plates with all layers having the same filament orientation. Natural frequencies and mode shapes were obtained as the filament orientation was varied from along the longest dimension of the plate to transverse to the longest dimension of the plate. This study is discussed in detail in reference 1.
2. Laminated wing models.- Analytical and experimental results have been obtained for a series of metal wing models reinforced with filamentary composite material and for a series of bare aluminum wing models. The filament orientation was varied from along the wing chord to along the wing span. These models were fabricated for a program being conducted by Dr. Paul Cooper to determine flutter characteristics of composite material wing models.

3. Metal plate with a variable elastic boundary.- The influence of an elastic boundary condition on the vibration characteristics of a metal plate was investigated using classical theory under a University Grant. These results are presented in references 2 and 3. Results were obtained using the NASTRAN program and compared with results from the classical theory.

EXPERIMENTAL AND ANALYTICAL MODELS

Unidirectional Composite Material Plates

The unidirectional composite material plates are illustrated in figure 1. The plates were built up from layers of prepreg tape consisting of an epoxy matrix reinforced with boron filaments. The tape was oriented so that all filaments of each plate lie at the same angle with respect to the long axis of the plate. The filament angle θ was varied from 0° to 90° and the number of layers, n , was varied from 6 to 24. This type of lay-up results in a highly orthotropic plate where Young's modulus in the direction of the filaments is eight times that in the direction transverse to the filaments. Each plate was 46.2 cm long and 7 cm wide. Tests were conducted with the plates having simulated free boundary conditions.

The plates were represented mathematically as an assembly of quadrilateral plate (CQDPLT) elements (fig. 1) having consistent mass matrices (PARAM = COUPMASS). In the analytical formulation underlying the NASTRAN elements, it is assumed that the element material is homogeneous. The orthotropic material properties of each element were described by the material property matrix (MAT2 CARD). Material properties were taken from experimental data published in the literature. The mathematical model had 165 elements and 204 grid points. The in-plane rotations and displacements were constrained to be zero. The resulting model had 612 degrees of freedom. The inverse power method of eigenvalue extraction was used to obtain the first 9 to 10 natural frequencies and mode shapes. A rough approximation of the frequency range of interest was obtained in advance using beam theory. The program computed all modes in the specified range in one pass and gave three very good rigid body modes (near zero eigenvalues). This required approximately 2500 seconds of central processing time (CPU) and a total time of approximately 6700 seconds on the CDC 6600 computer.

Reinforced-Aluminum Wing Flutter Models

A sketch of the reinforced plate models is shown in figure 2. Each plate was tested with its root clamped in a massive backstop to simulate a fixed boundary condition. The plates were constructed with six layers of boron/epoxy placed on each side of an aluminum plate. The boron/epoxy was laid up in a symmetric manner about the aluminum core with the filament angle of the layers alternating between $+\theta$ and $-\theta$. Plates were constructed with filament angles of 0° , $\pm 45^\circ$, and 90° . Each plate was 106.7 cm wide at the root and 80.5 cm long. An aluminum plate to be used as a control specimen and having the same planform dimensions and a thickness of 0.64 cm was also tested and analyzed.

The plates were represented mathematically as an assembly of quadrilateral plate (CQDPLT) elements, and triangular plate (CTRPLT) elements having consistent mass matrices (PARAM = COUPMASS). It may be of interest to note the special way in which the stiffnesses of these elements were put into NASTRAN. As stated previously, in the analytical formulation underlying the NASTRAN elements it is assumed that the element material is homogeneous. Thus it is not possible to input directly the properties of each layer of a laminated structure. For a homogeneous material, the plate flexural rigidities are obtained internally in NASTRAN by multiplying the material modulus matrix by the inertia. For these laminated plates, the flexural rigidities were calculated externally using laminated plate theory. The rigidities were input to NASTRAN in place of the material modulus matrix and the inertia was input as unity. It should be noted that this procedure does not provide a means for obtaining stresses in each layer directly from NASTRAN as would be desired for detailed stress analysis of laminated structures. There exists a need for special elements if NASTRAN is to be used efficiently for complete analysis of laminates.

The mathematical model had 48 elements and 58 grid points. The in-plane rotations and displacements were constrained to be zero. The resulting model had 174 degrees of freedom. The Givens' method of eigenvalue extraction was used to obtain all the natural frequencies and the first 11 mode shapes. As a point of interest, it is noted that it was not necessary to OMIT the rotational degrees of freedom because consistent mass matrices were used. When lumped masses are used, zero inertias are associated with the rotations and OMITs are required if the NASTRAN Givens' procedure is to succeed. The time for the eigenvalue solution was approximately 330 seconds of central processing time and the total time was approximately 1270 seconds.

Isotropic Plate With Elastic Restraints at Boundary

A sketch of the plate with three edges simply supported and one edge elastically restrained is presented in figure 3. The plate is 76.2 cm long, 38.1 cm wide, and 0.32 cm thick. Three edges were simply supported and there were elastic restraints at the other edge. The plate was represented mathematically for NASTRAN as an assembly of quadrilateral plate (CQDPLT) elements having consistent mass matrices. The mathematical model had 225 elements and 256 grid points. The in-plane rotations and displacements were constrained to be zero. The resulting model had 768 degrees of freedom. The elastic restraints were represented as 16 springs (CELAS2 CARD) evenly spaced along one edge. The inverse power method of eigenvalue extraction was used to obtain the first five natural frequencies and mode shapes. The frequency range of interest was obtained in advance from results published in reference 3. The program computed all modes in the specified range in one pass. This required approximately 1600 seconds of central processing time and the total time was approximately 4200 seconds.

PRESENTATION AND DISCUSSION OF RESULTS

Unidirectional Composite Material Plates

Measured and calculated nodal patterns were classified as either beam type or plate type. Typical patterns for the first and second beam-type and plate-type modes are presented in figure 4. In all cases, the nodal patterns were highly dependent on the filament angle θ (see ref. 1). For the beam-type modes, the slope of the node lines varied as much as 45° as the filament angle was varied. For the plate-type modes the nodal patterns varied from a combination of straight lines intersecting each other to curved lines sloping away from each other. In all cases, there was very good agreement between the measured nodal patterns and those calculated by NASTRAN.

The natural frequencies were also highly dependent on the filament angle as shown for the beam-type modes in figure 5 and the plate-type modes in figure 6. These data are for plates having 24 layers of composite material but similar data were obtained for plates with 6 and 12 layers. The natural frequencies of the first four beam-type modes decreased significantly (approximately 60 percent) as the filament angle increased from 0° to 60° . There was little change in frequency with a further increase in filament angle up to 90° . In general, there was good agreement between the measured and calculated frequencies for the beam-type modes.

The natural frequencies of the first two plate-type modes increased by approximately 90 percent as the filament angle increased from 0° to 30° and decreased with a further increase in filament angle. In general, there was good agreement between the measured and calculated frequencies. However, it should be pointed out that for the plates having 6 and 12 layers with a filament angle of 0° the agreement was not quite so good.

Reinforced-Aluminum Wing Flutter Models

The first wing model studied was the aluminum control panel. The measured and calculated natural frequencies and nodal patterns are presented in figure 7. There is very good agreement between the measured and calculated data. The maximum error between the calculated and measured frequencies of the first 10 modes is 8.3 percent. Only one set of patterns is presented since there were no discernible differences between the measured and calculated nodal patterns.

Results for the aluminum panels reinforced with boron/epoxy material are shown for filament angles of 0° , $\pm 45^\circ$, and 90° in figure 8. In cases where there were no discernible differences between the measured and calculated nodal patterns only one set of patterns is presented. For the panel with $\theta = 90^\circ$ (fig. 8(a)), there is good agreement between the measured and calculated frequencies. All of the calculated frequencies are higher than those measured. The average error for the first 10 modes is 6.3 percent. The calculated nodal patterns are in very good agreement with the measured nodal

patterns for the first six modes. For the higher modes, there are some differences between the calculated and measured node lines but, in general, the overall patterns are very similar.

For the panel with $\theta = \pm 45^\circ$ (fig. 8(b)), the calculated frequencies are in very good agreement with the measured frequencies. The average error for the first 10 modes is only 5.2 percent. The calculated nodal patterns are generally in very good agreement with the measured patterns; with some differences in the second, seventh, ninth, and tenth modes.

For the panel with $\theta = 0^\circ$ (fig. 8(c)) the calculated frequencies show only fair agreement with the measured frequencies. The average error for the first 10 modes is 11.1 percent. For the third mode the error is 27.4 percent. There are also significant differences between the calculated and measured nodal patterns but, in general, the overall patterns are similar. The reason for these discrepancies has not been determined at this writing. However, it should be noted that for some of the unidirectional composite material plates having a filament angle of 0° similar discrepancies were present.

Plate With Elastic Restraints at Boundary

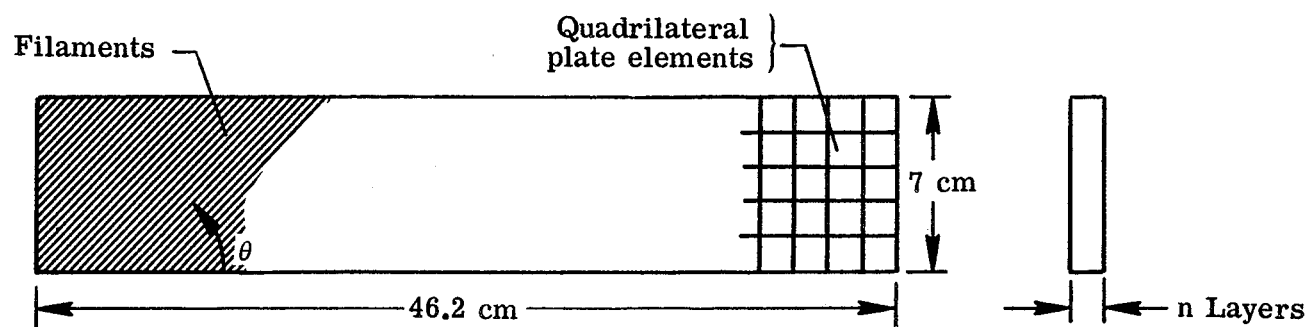
Effects of the elastic edge restraints on the natural frequencies of the first three modes of the plate are shown in figure 9. When the elastic edge restraint is zero, the edge is free; as the restraint is increased, the boundary condition approaches a simply supported condition. The natural frequencies calculated using the NASTRAN program are in very good agreement with those predicted with the closed-form solution using classical plate theory.

CONCLUDING REMARKS

Comparison of results obtained with the NASTRAN computer program with results from experiments and classical theory showed NASTRAN to be very effective in calculating the vibration characteristics of isotropic and orthotropic plates with free, fixed, and elastically restrained edges. Good results were also obtained for plates laminated with dissimilar materials. However, there exists a need for special elements to improve the effectiveness of NASTRAN in analyzing laminated structures.

REFERENCES

1. Clary, Robert R.: Vibration Characteristics of Unidirectional Filamentary Composite Material Panels. Paper presented at Second ASTM Conference on Composite Materials: Testing and Design (Anaheim, California), April 1971.
2. Egle, D. M.: The Influence of Changing End Conditions on the Resonant Response of Beams and Plates. NASA CR-1736, 1971.
3. Henry, F. D.; and Egle, D. M.: The Effect of an Elastic Edge Restraint on the Forced Vibration of a Rectangular Plate. Paper presented at the Fifth Southeastern Conference on Theoretical and Applied Mechanics (Raleigh-Durham, North Carolina), April 1970.



$\theta = 0^\circ, 10^\circ, 30^\circ, 45^\circ, 60^\circ, 90^\circ$
 $n = 6, 12, 24$

165 Elements
 204 Grid points
 612 Degrees of freedom
 2500 CPU Seconds

Figure 1.- Description of unidirectional boron/epoxy plates.

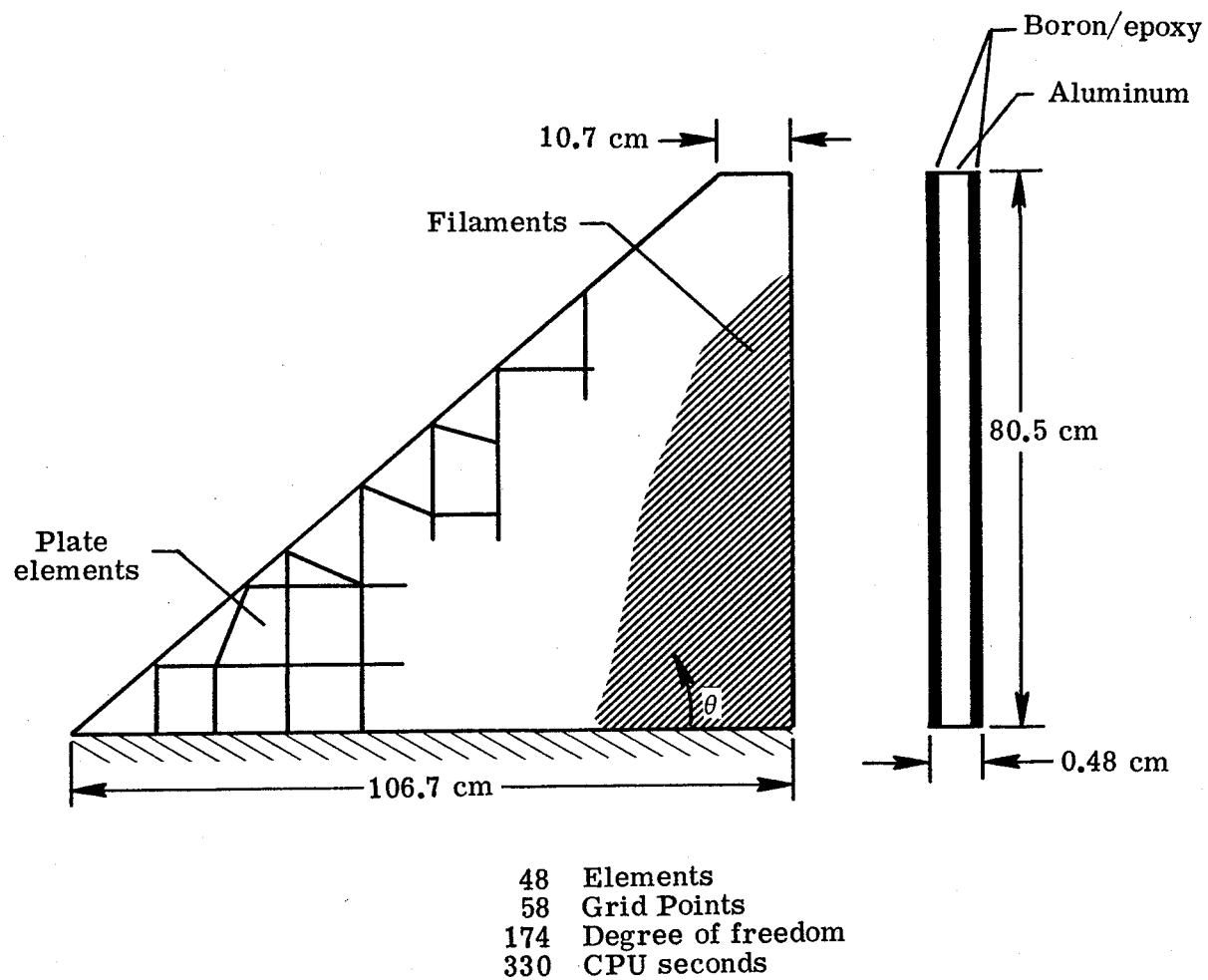


Figure 2.- Description of reinforced-aluminum wing flutter model.

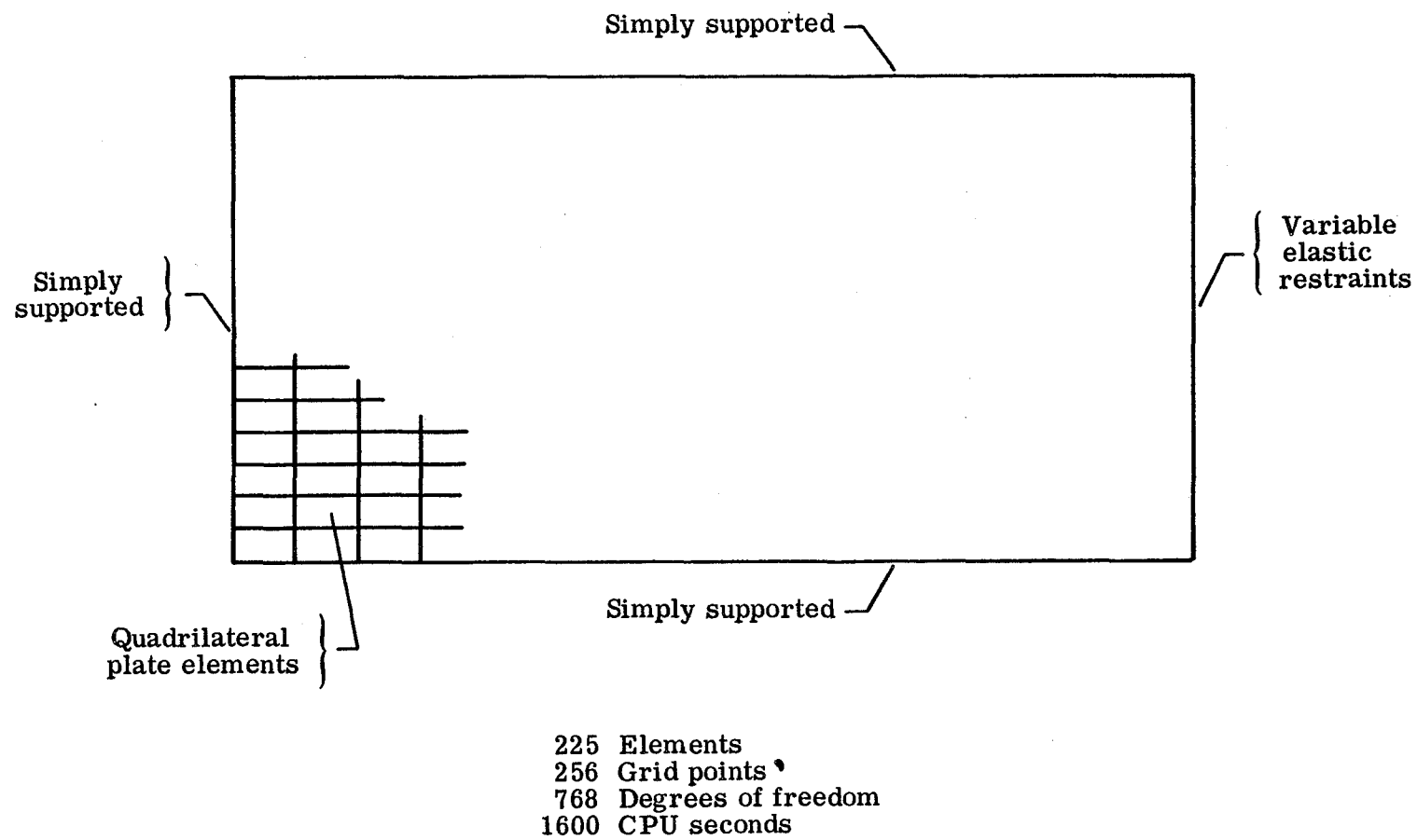


Figure 3.- Description of the plate with variable elastic restraints along one edge.

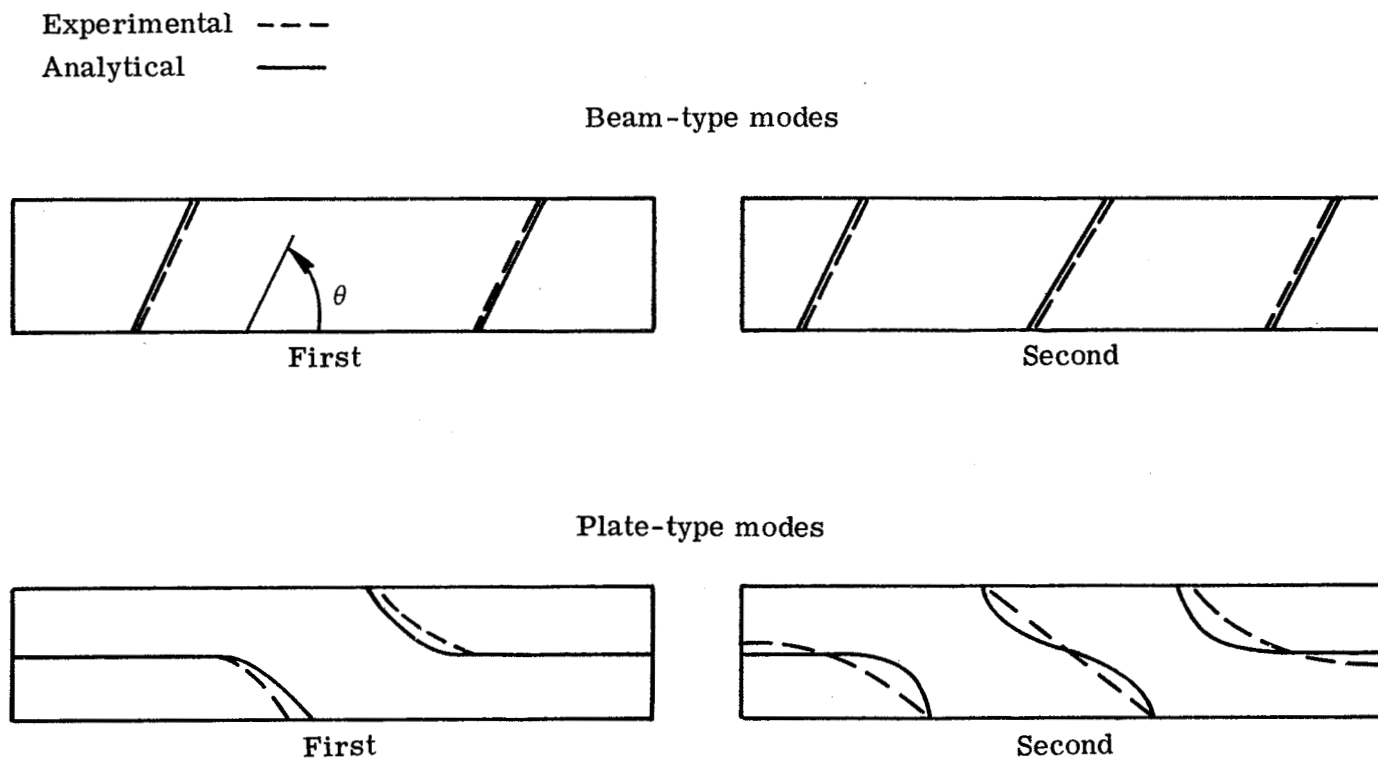


Figure 4.- Typical nodal patterns of the unidirectional composite material plates.

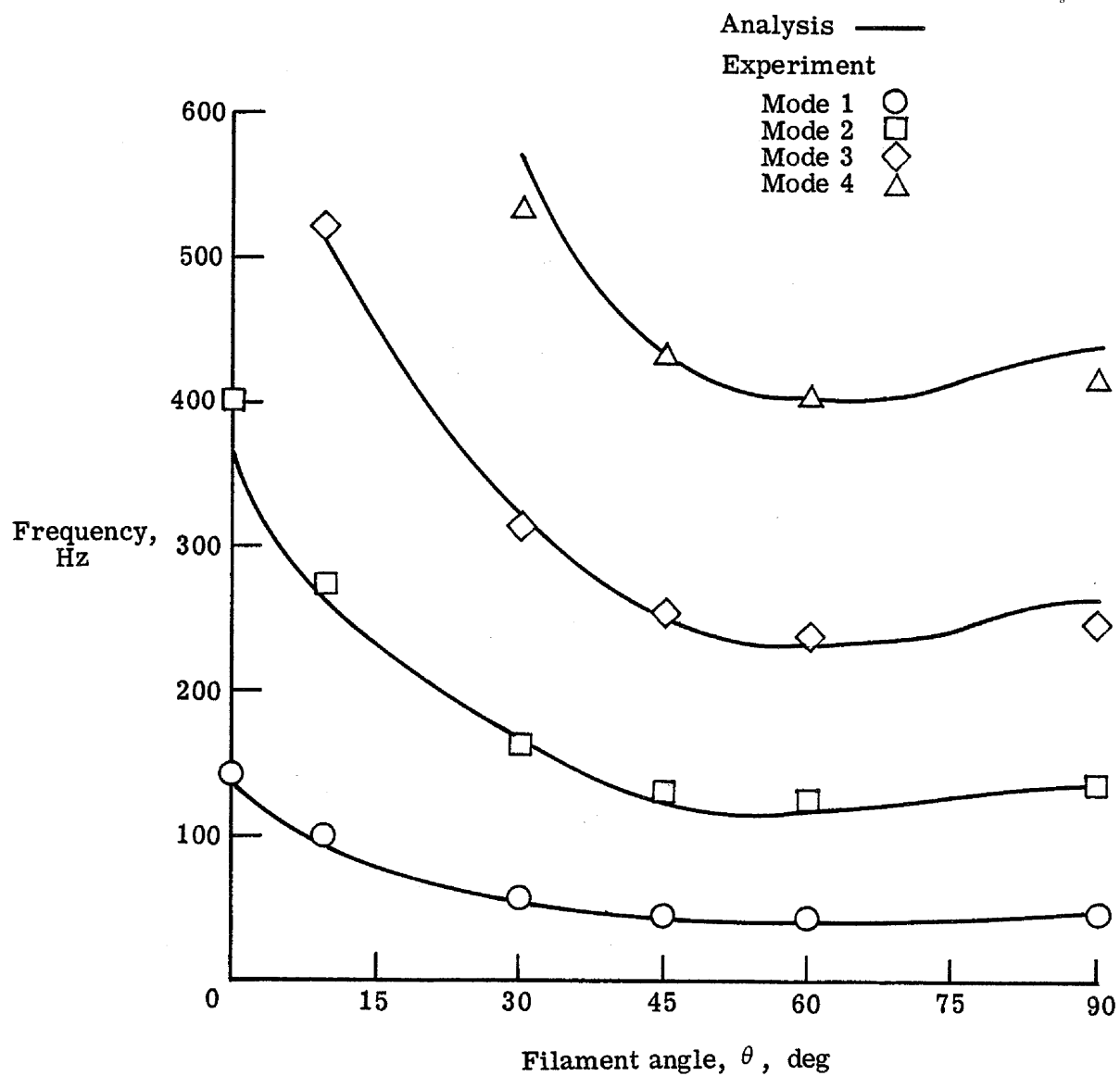


Figure 5.- Variation of the natural frequencies of the first four beam-type modes of unidirectional composite material plates.

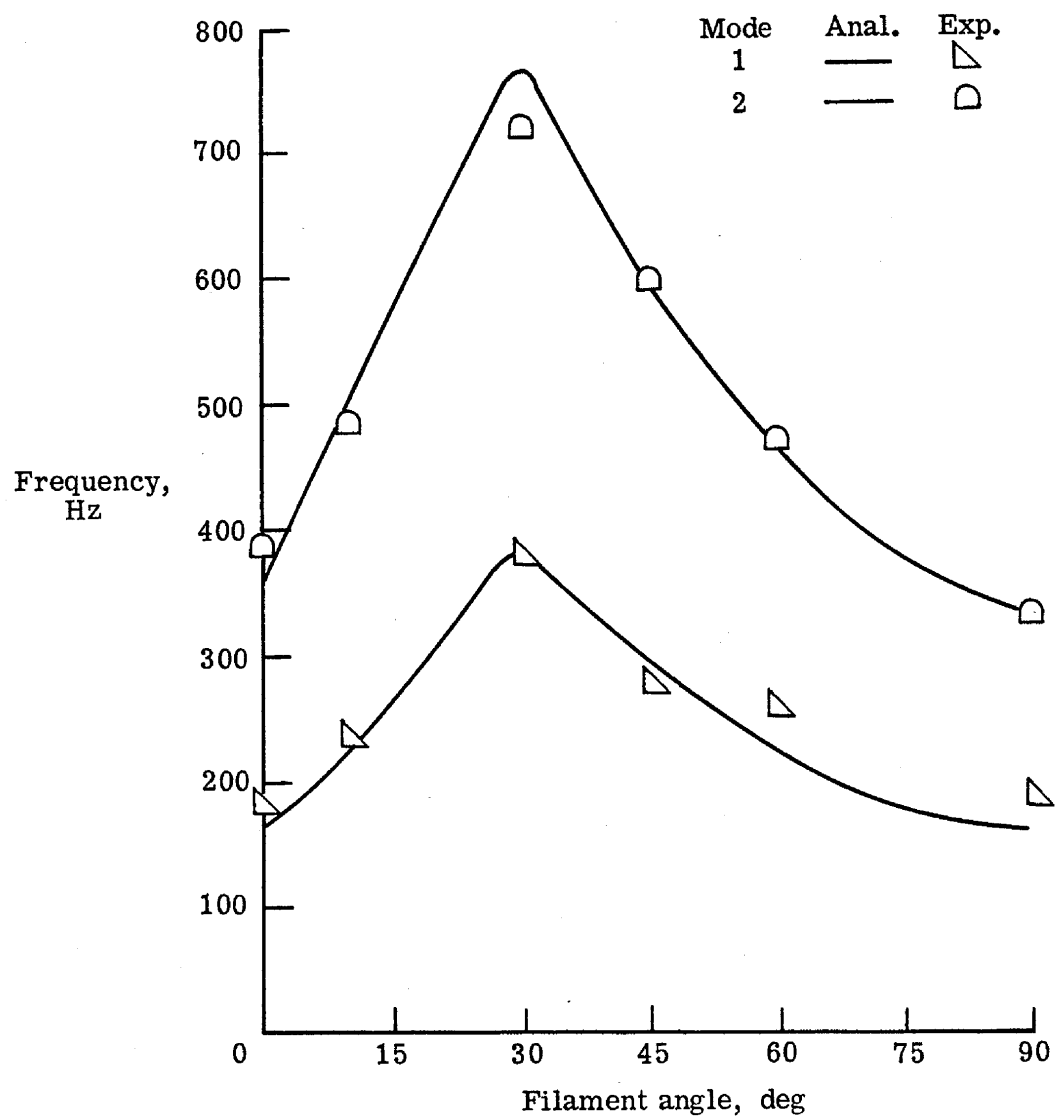
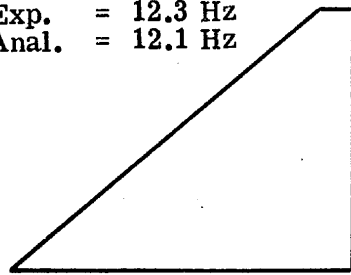
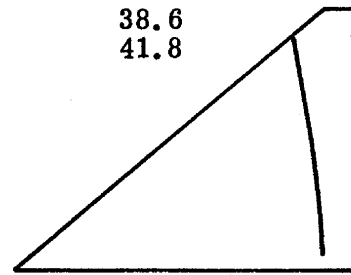


Figure 6.- Variation of the natural frequencies of the first two plate-type modes of unidirectional composite material plates.

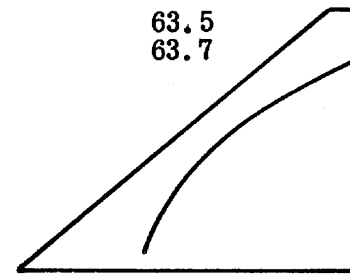
Exp. = 12.3 Hz
Anal. = 12.1 Hz



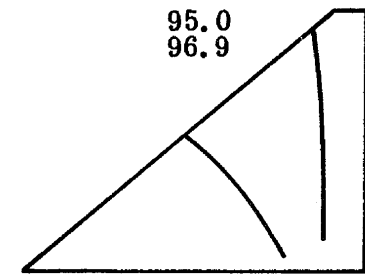
Mode no. 1



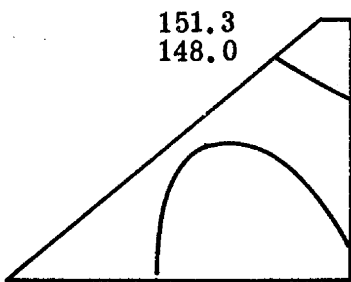
2



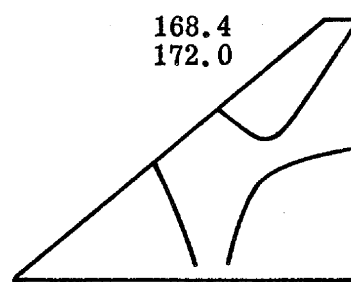
3



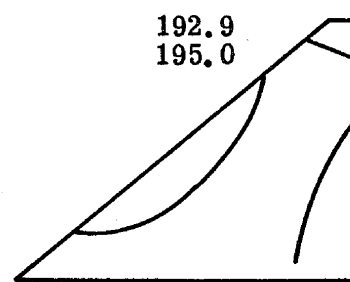
4



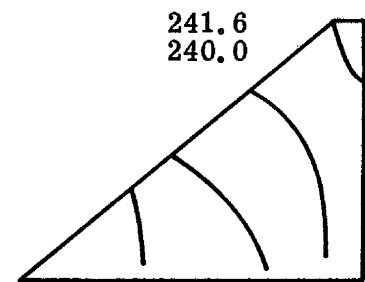
5



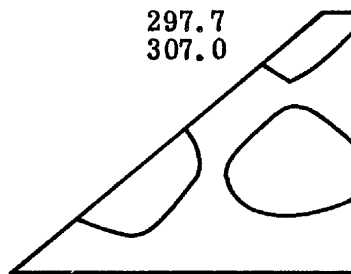
6



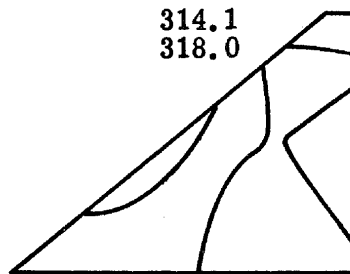
7



8



9

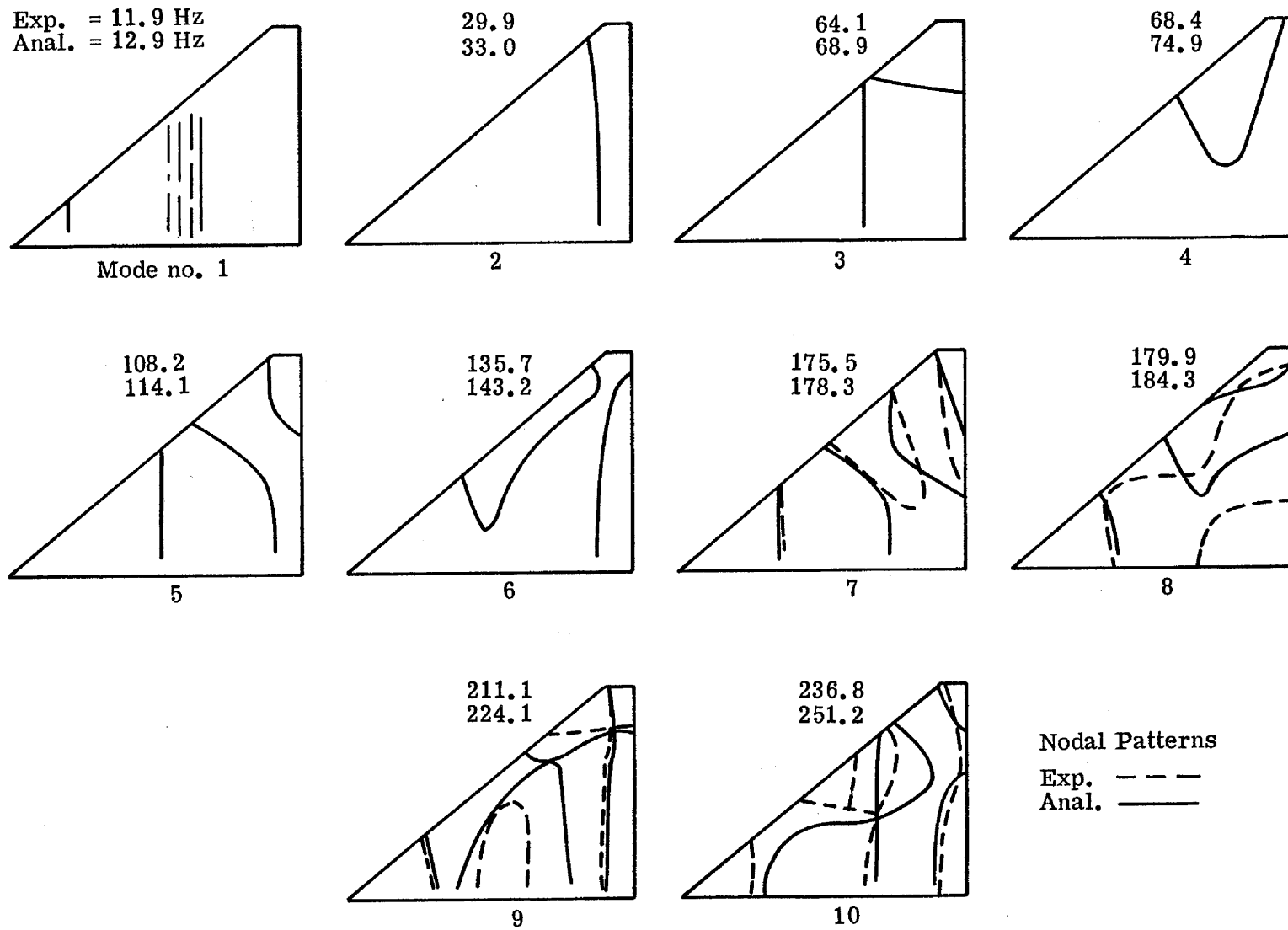


10

Nodal patterns

Exp. —
Anal. —

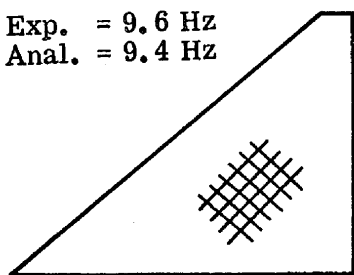
Figure 7.- Natural frequencies and nodal patterns of aluminum wing model.



(a) $\theta = 90^\circ$.

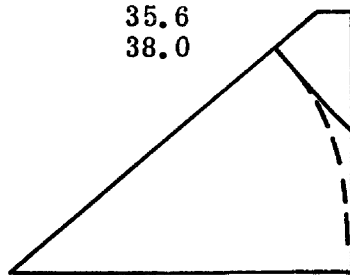
Figure 8.- Natural frequencies and nodal patterns of reinforced-aluminum panels.

Exp. = 9.6 Hz
Anal. = 9.4 Hz



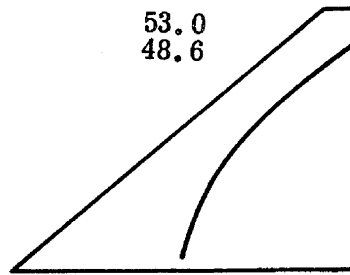
Mode no. 1

35.6
38.0



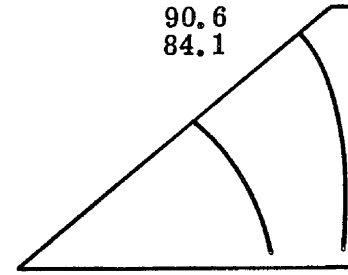
2

53.0
48.6



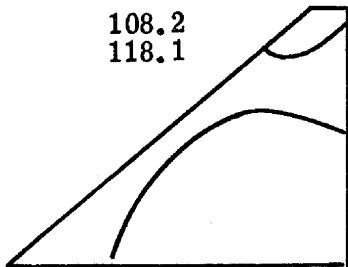
3

90.6
84.1



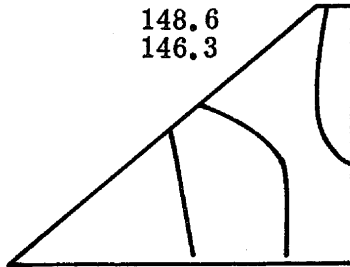
4

108.2
118.1



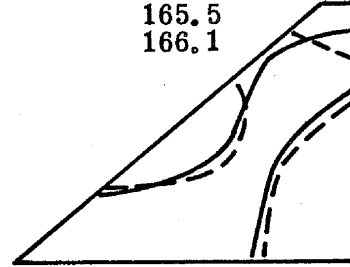
5

148.6
146.3



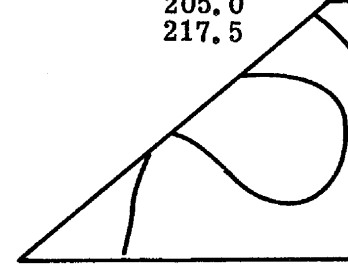
6

165.5
166.1



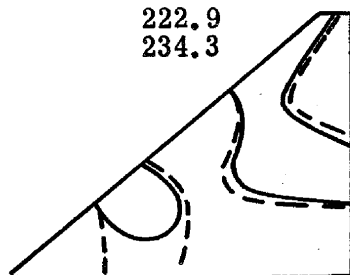
7

205.0
217.5



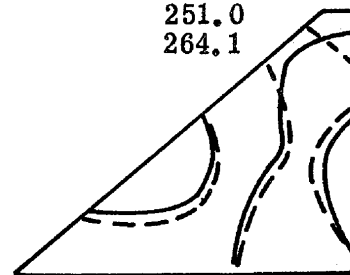
8

222.9
234.3



9

251.0
264.1



10

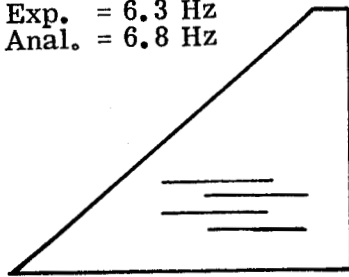
Nodal Patterns

Exp. ---
Anal. ———

(b) $\theta = \pm 45^\circ$.

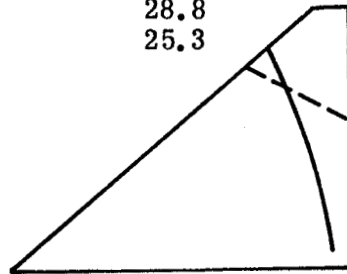
Figure 8.- Continued.

Exp. = 6.3 Hz
Anal. = 6.8 Hz



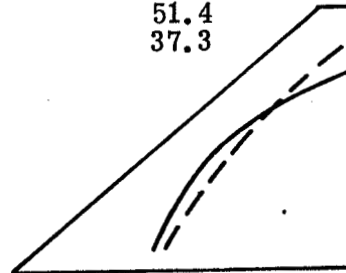
Mode no. 1

28.8
25.3



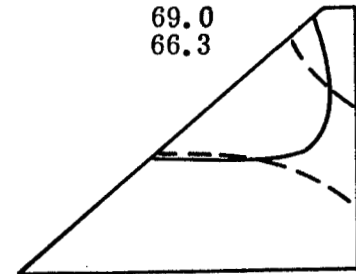
2

51.4
37.3



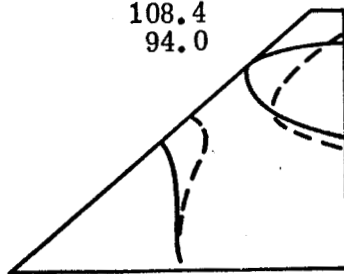
3

69.0
66.3



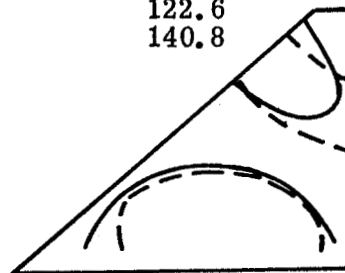
4

108.4
94.0



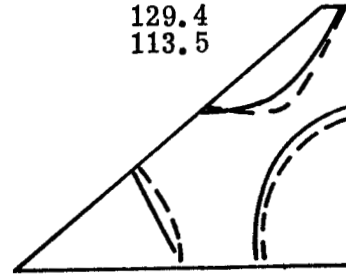
5

122.6
140.8



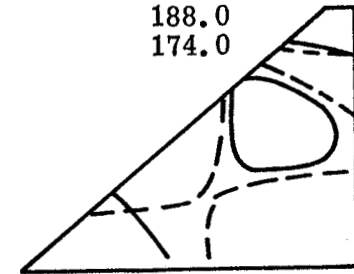
6

129.4
113.5



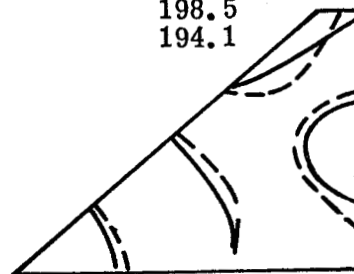
7

188.0
174.0



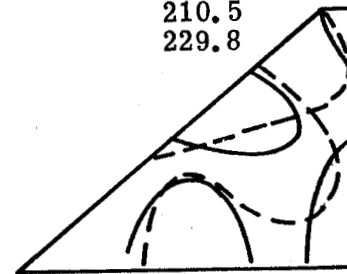
8

198.5
194.1



9

210.5
229.8



10

Nodal Patterns

Exp. ---
Anal. —

(c) $\theta = 0^\circ$.

Figure 8.- Concluded.

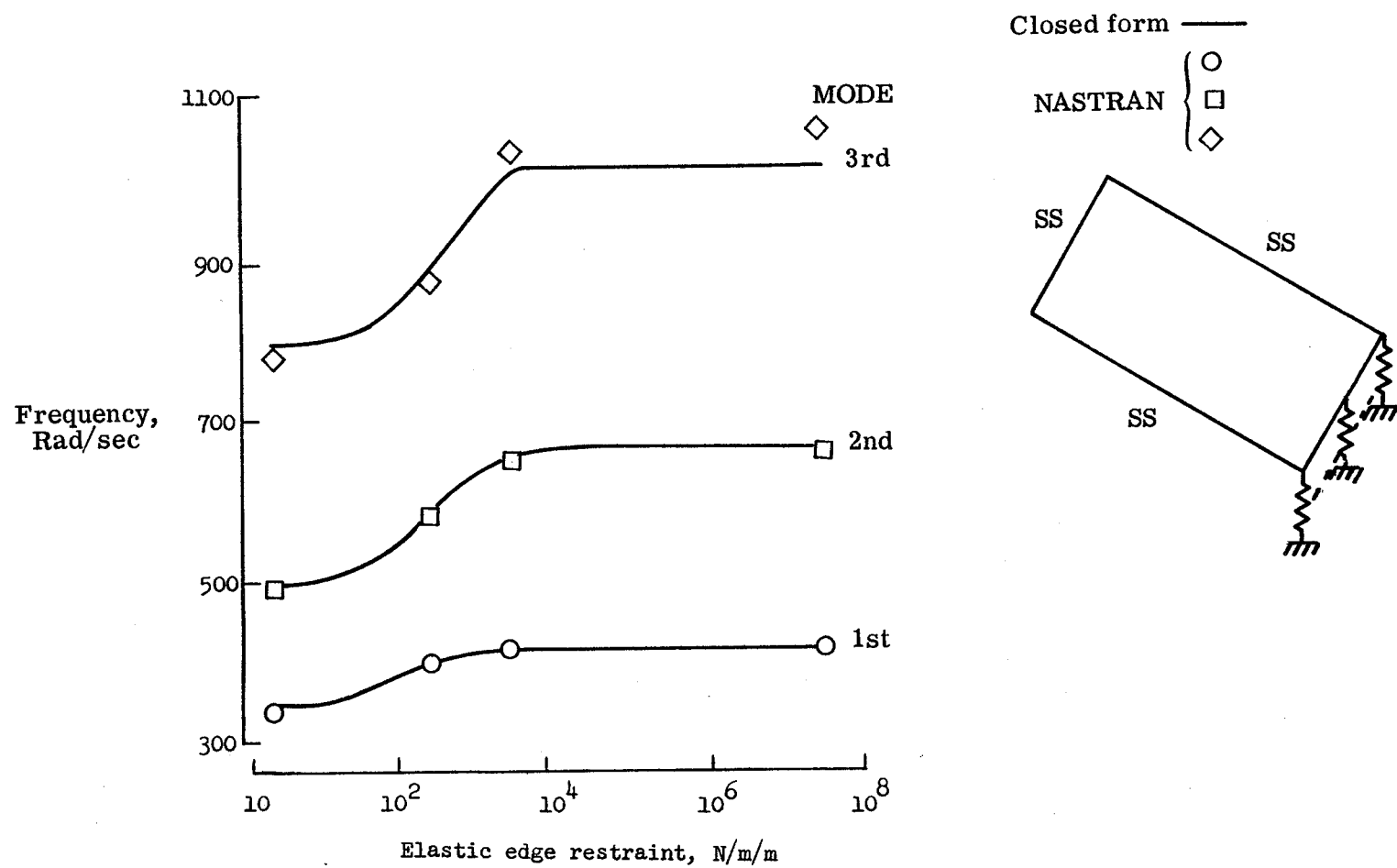


Figure 9.- Effects of elastic edge restraints on natural frequencies of metal plate.

MODAL ANALYSIS OF A NINE-BAY SKIN-STRINGER PANEL

By Robert E. Grandle and Carl E. Rucker
NASA Langley Research Center

SUMMARY

Results obtained using a NASTRAN normal mode analysis of a nine-bay skin-stringer panel 68.58 cm (27 inches) by 93.98 cm (37 inches) of typical aircraft construction are presented.

The aluminum panel was made up of a plate, Z section stringers, and channel section frames and was assumed to have fully fixed edges. Stress and mode shape data for the lower order modes obtained from a NASTRAN analysis of a 266-grid-point division of the panel are presented and compared with experimental data.

INTRODUCTION

As part of Langley's research on the response and fatigue of aircraft structures due to acoustic loading, programs are underway to determine the effectiveness of varying the substructure to control the response and sonic fatigue of skin-stringer type structures. In these programs, analytical methods to evaluate response due to incremental changes in structural design are very useful. Among analytical methods used in these programs are NASTRAN and a special-purpose finite-element program. The finite-element program was developed by the Lockheed-Georgia Company as part of an analytical/experimental study conducted under contract to the Langley Research Center. This study was made on a typical aircraft type structural panel and the NASTRAN program was applied to obtain modes and stresses for this panel design.

This paper describes the nine-bay skin panel used in the study and presents the results obtained from the experiments, the special-purpose analysis, and the NASTRAN analysis. Presented are comparisons of the modal frequencies and stress values obtained from NASTRAN with those obtained from the experiment. Also, the modal frequencies obtained from the NASTRAN are compared with those from the special-purpose program.

DESCRIPTION OF PANEL STRUCTURE

A flat aluminum skin-stringer panel constructed from channels and Z stringers bonded to the plate was used as the test structure. The panel was 93.98 cm (37 inches) by 68.58 cm (27 inches), as shown in figure 1. The skin thickness was 0.081 cm (0.032 inch), the channel thickness 0.122 cm (0.048 inch), and the Z stiffener thickness 0.1016 cm (0.040 inch). The stiffeners, whose

dimensions are shown in figure 2, were bonded to the face plate using a structural adhesive. The substructure stiffeners consisted of two 93.98 cm long channel frames and two 68.58 cm long Z section stringers framing a 25.40 cm (10 inches) by 38.10 cm (15 inches) center bay.

The stiffeners introduced some asymmetry into the structure because the cross sections of each pair "faced" in the same directional sense, rather than being oriented symmetrically about lines of midlength and midwidth.

EXPERIMENTAL TESTS

The experimental tests were performed in the facilities of Lockheed-Georgia. The panel was supported around the perimeter by a steel frame and attached by two rows of machine screws, spaced at 2.54 cm (1 inch) to approximate fixed edge conditions.

A photograph of the test panel is shown in figure 3, which indicates strain-gage locations and panel attachment points to the test fixture. The strain gages located in the center of the panel had a grid length of 0.9525 cm (0.375 inch), the others had a 0.47625 cm (0.1875 inch) grid length. From these strain gages, stresses were determined using the acoustic excitation arrangement of six speakers as shown in figure 4. The speakers in this system can be phased independently. The modes in this paper were determined by two phase conditions shown in the lower part of the figure. All of the modes, except the 127-Hz mode, were determined using the in-phase arrangement indicated in the lower left of the figure. The 127-Hz mode used the configuration in the lower right of figure 4. All NASTRAN results corresponded to an in-phase type excitation.

ANALYTICAL SOLUTIONS

Finite-Element Solution

The special-purpose finite-element program is based on a displacement method and uses modeling of the stiffness and consistent mass matrices for thin-walled open section beams. This method involves modification of a rectangular plate bending element to include a fundamental interior mode for the element as a generalized coordinate. This program, which has not been published, was developed by Mr. Fred Rudder of Lockheed-Georgia Company.

NASTRAN Solution

NASTRAN modeling of the panel consisted of a simple division of the panel into 5.08 cm (2.0 inch) square elements. In order to accomplish this division, 1.27 cm (0.5 inch) of the panel perimeter, which has no effect on the experiment or analytical response properties, was neglected. The panel was divided into

234 CQUAD2 elements with a corresponding 266 grid points as shown in figure 5. The stiffeners were modeled with CBAR elements which were also 5.08 cm long and attached to the nearest grid point. The Z stringers were modeled with 13 elements each and the channels with 18 elements each. The inertia properties of the Z, and channel stiffeners were input for the inertial properties of the CBAR elements. The rotational inertia was input as zero and no attempt was made in this model to align the principal axis of the CBAR elements with the actual principal axis of the stiffeners. Therefore, rotational coupling of the stiffeners was deleted in this model.

The panel was oriented in the x-y plane of a rectangular coordinate system with the lower left corner of the plate (grid point 1) as the origin. In order to approximate the clamped edge conditions of the panel, all external grid points were fully fixed and all perimeter CQUAD2 elements of figure 5 were given the properties of steel to simulate the support. The panel was analyzed by using the rigid format 3 normal modes analysis. The problem was run with the inverse-power method for solution of the eigenvalues using the standard double-precision arithmetic, and also using single-precision arithmetic of level 11.1.2 which shortened the solution times. During some runs, only the rotation about the Z axis was constrained for the interior grid points while for other runs the in-plane X and the Y translation components were constrained as well. The inverse-power method was employed using coupled mass and generalized mass normalization. Solution times, grid point degrees of freedom, and modal frequencies are listed in Table I. From this table it can be seen that for the same constraints, the decomposition times and total CPU (central processor unit) time is much less using single-precision arithmetic for the same number of modes. The constraining of three degrees of freedom instead of one had a similar effect on the run times for the same number of modes. This reduction in the number of degrees of freedom resulted in less than a 1-percent change in modal frequency and little change in mode shapes and stress ratios. The modes were plotted by using the NASTRAN structure plotting routine in order to determine which modes were of interest for acoustic fatigue and response determinations. The quadrilateral and bar elements were plotted separately to allow them to be examined in better perspective. The default view angle was used and the time required to generate the plot tape in a restart for seven modes and 14 plots was 148 seconds CPU time and a total time of 1081 seconds (sum of CPU and PPU times). Lockheed reported only four modes from their experimental work and all of these are compared to NASTRAN modes which were obtained at comparable mode numbers and shapes.

COMPARISON OF RESULTS

A frequency comparison is shown in figure 6 from the three studies used for these four modes. The four mode shapes defined during the experiments are presented in figures 7, 9, 11, and 13, as formulated by the NASTRAN structure plotter. Outer fiber bending stresses for CQUAD2 element obtained from NASTRAN are compared with experimentally determined stresses in normalized form in figures 8, 10, 12, and 14. The undeformed locations of the stringer are also shown. The stresses were normalized for each mode to the maximum interior

stress within each set of data (experimental set and NASTRAN set). Normal stress ratios are plotted corresponding to the strain-gage measurement directions.

The first panel mode was found at 63.906 Hz by NASTRAN and is shown in figure 7. This mode is basically that of a single panel in which most of the deflection occurs in the center bay. NASTRAN stress distributions are compared with experimental distributions for the first mode in figure 8, and are seen to be in generally good agreement. Figure 9 shows the second panel mode, and figure 10 the corresponding stress distribution at 81.949 Hz. Agreement between the two methods is not quite as good as for the first mode although the frequencies correspond almost precisely. Two conditions which may account for these differences may be lack of rotational coupling in the stiffeners and the larger size of the quadrilateral element relative to the strain gage. The third panel mode from the NASTRAN analysis is presented in figure 11 at 94.129 Hz. The third experimental mode compared is at 110 Hz, and a comparison of the calculated with measured stresses is shown in figure 12 and is noted also to result in poor agreement. There is a wide variance in the frequency for this third mode among the three methods used and the reasons for this are probably due, again, to the lack of rotational coupling in our model as well as a slight alteration of the modal participation or coupling between panel bays in the experimental case. The first stiffener mode (the fourth panel mode) is so termed because it is the lowest frequency mode that has appreciably large motion of the stiffeners. Its NASTRAN calculated frequency is 125.539 Hz. The first stiffener mode is shown in figure 13 at 125.539 Hz. Panel and bar modal deflections are shown separately in figure 13. The agreement evident in the stresses for this mode are shown in figure 14, and was not expected since the experiment was conducted using the out-of-phase acoustic excitation discussed previously and illustrated in figure 4. The stringer influence prevented the panel from being excited, experimentally, with the in-phase excitation; but apparently the stiffener influence improved the data for this case as the in-phase motion of the stiffeners has an effect on the panels.

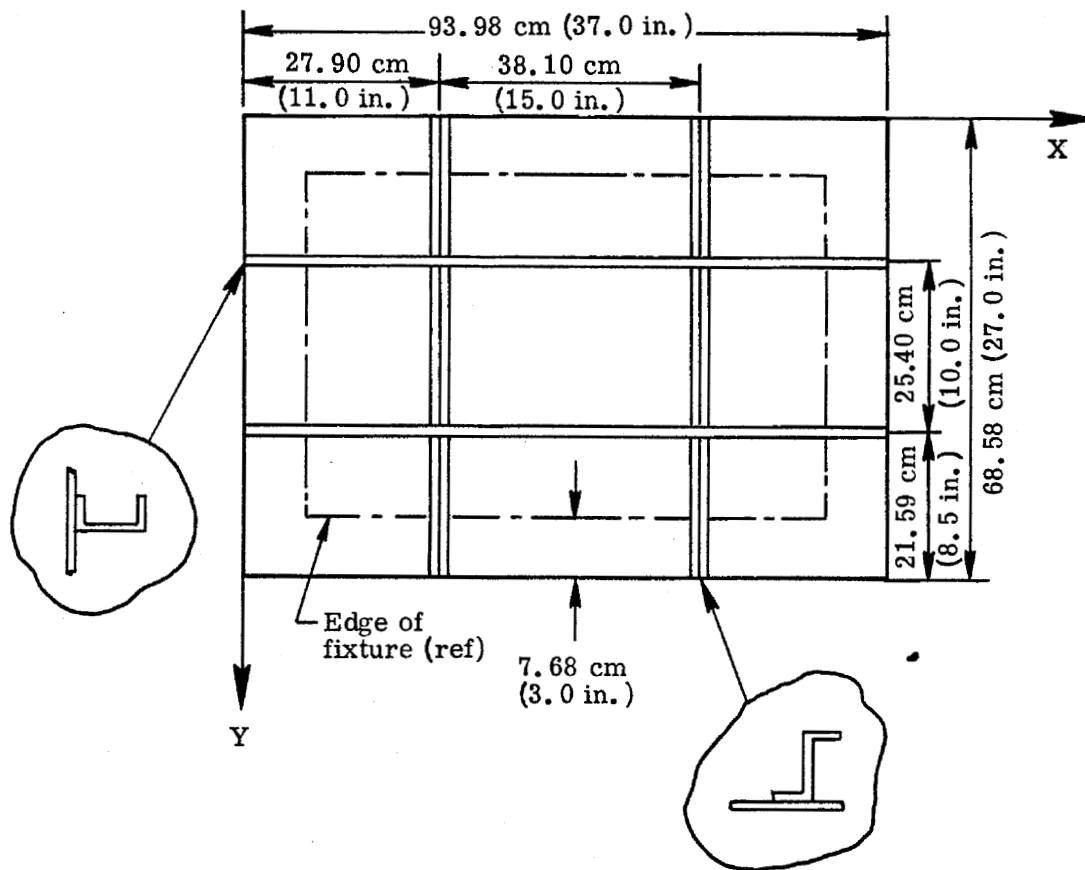
CONCLUDING REMARKS

The results presented in this paper are judged satisfactory even though the NASTRAN and experimental results were determined separately without opportunity for refinement through repeating experiments.

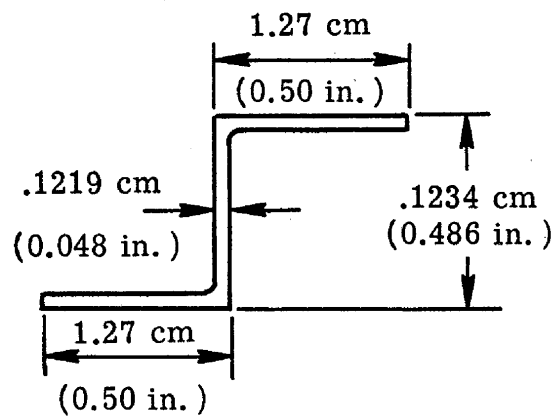
NASTRAN was found to be a good, but slightly unwieldy, analytical tool for evaluating response and stress due to incremental changes in structural design of skin-stringer panels. For this type of problem, it was found that computer running time was reduced significantly by decreasing the number of degrees of freedom per grid point without an appreciable loss in accuracy of the results. Also, the time was further reduced by the use of level 11.1.2, where single-precision arithmetic is used without noticeable change in the results, if the problem is run on a computer with at least a 60-bit word.

TABLE I
COMPARATIVE NASTRAN RUN DATA

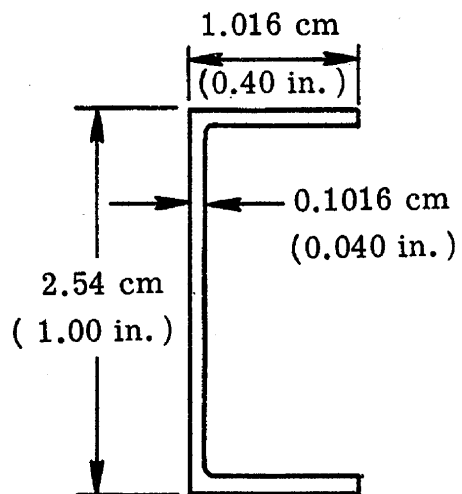
Precision	Degrees of freedom per interior grid point	Number of eigenvalues	Time in seconds per decomposition	Total CPU time (sec)	Total time seconds	Bandwidth	Start points	No. of triangular decomposition	No. of vector iterations	Frequency (Hz)
Single	3	7	19	1928	4787	46	2	10	101	103.85 to 126.24
Single	5	2	50	1132	3212	72	2	3	21	63.90 to 81.95
Single	5	5	50	2188	5688	72	1	6	52	94.12 to 104.20
Double	3	1	97	583	1872	46	1	2	12	81.99



1.- Skin-stringer panel overall dimensions.

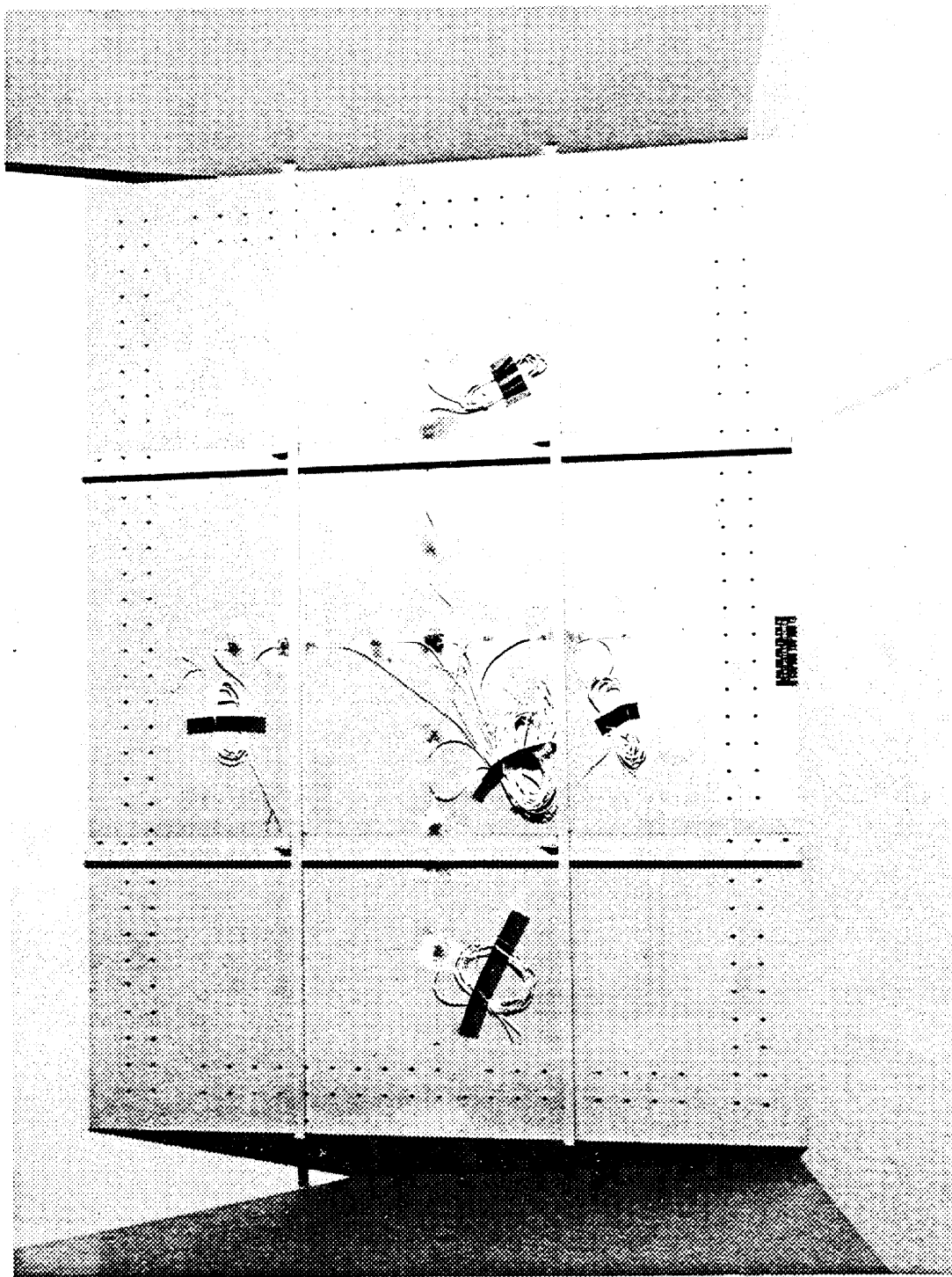


7075-T6
Aluminum
extrusion

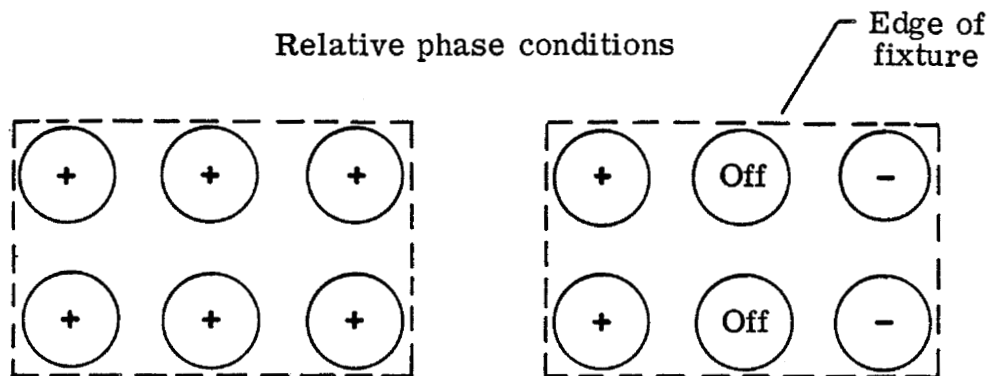
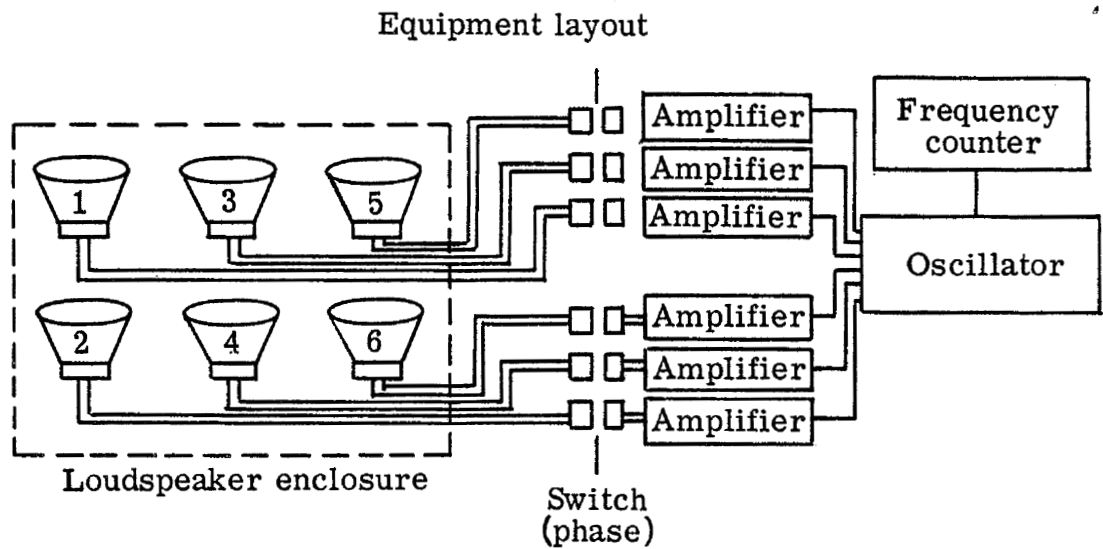


7075-T6
Aluminum
extrusion

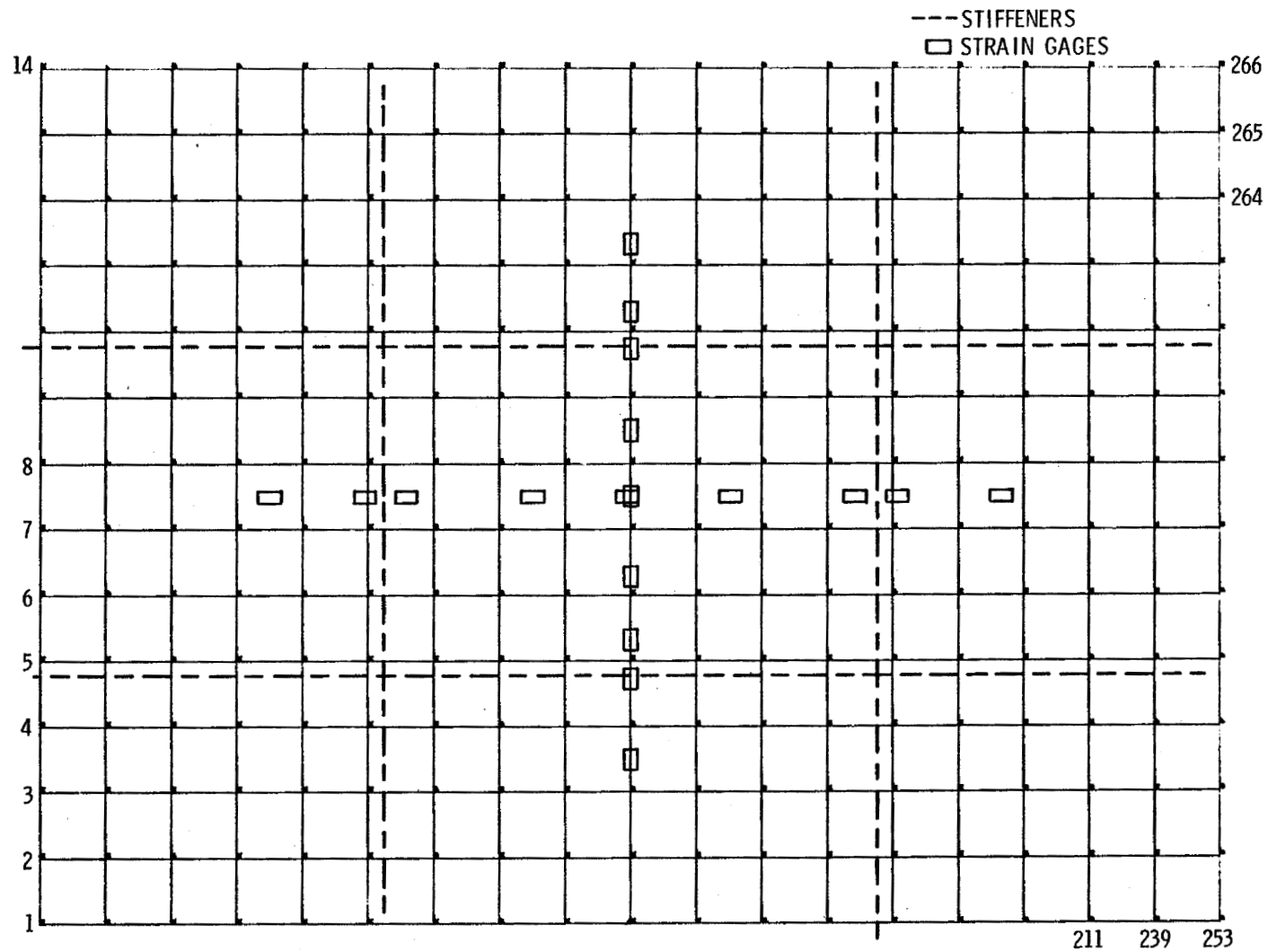
2.- Panel stiffener dimensions.



3.- Substructure view of skin-stringer panel.



4.- Acoustic excitation diagram for experimental tests.



5.- NASTRAN model showing grid points, CBAR elements, and relationship of strain gages to elements.

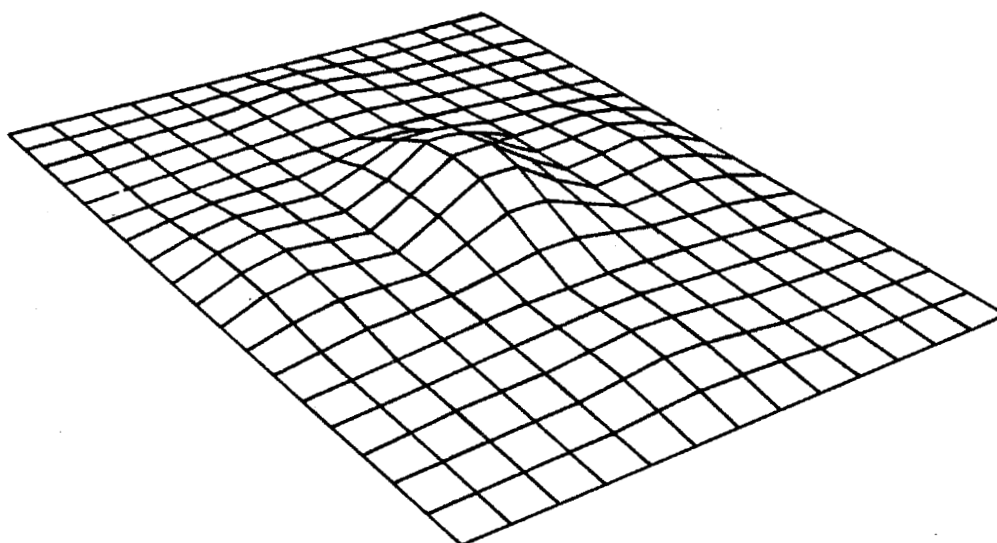
FREQUENCY COMPARISON

Hz

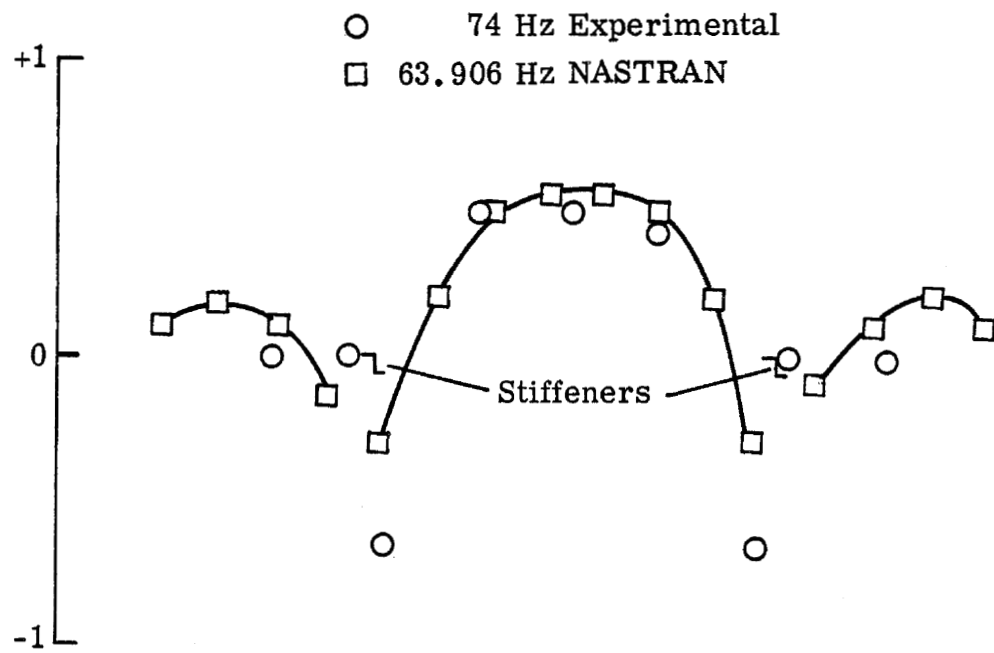
Panel Mode Number	Lockheed Experimental	Lockheed Analytical	NASTRAN
1	74	82	63.906
2	82	87	81.949
3	110	88	94.129
4 *	126	-	125.539

* Out of phase excitation used

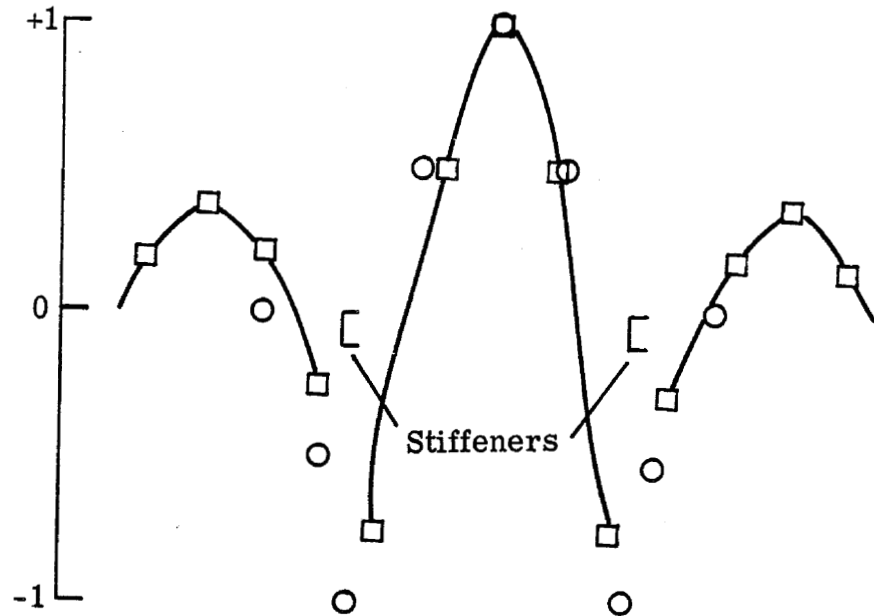
Figure 6. - Comparison of Lockheed and NASTRAN analytical results with experimental frequencies.



7.- NASTRAN first panel mode shape at 63.906 Hz.

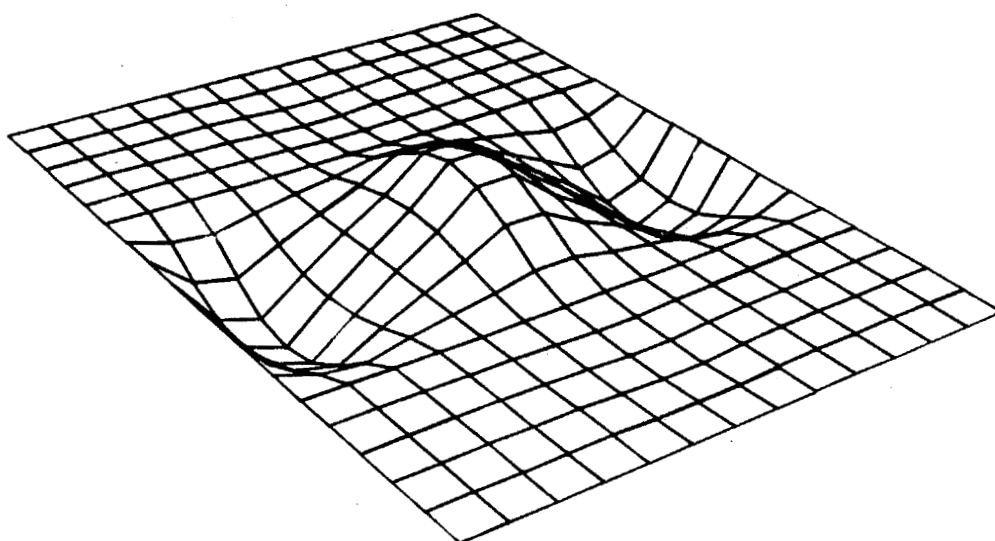


Normal stress distribution across panel length

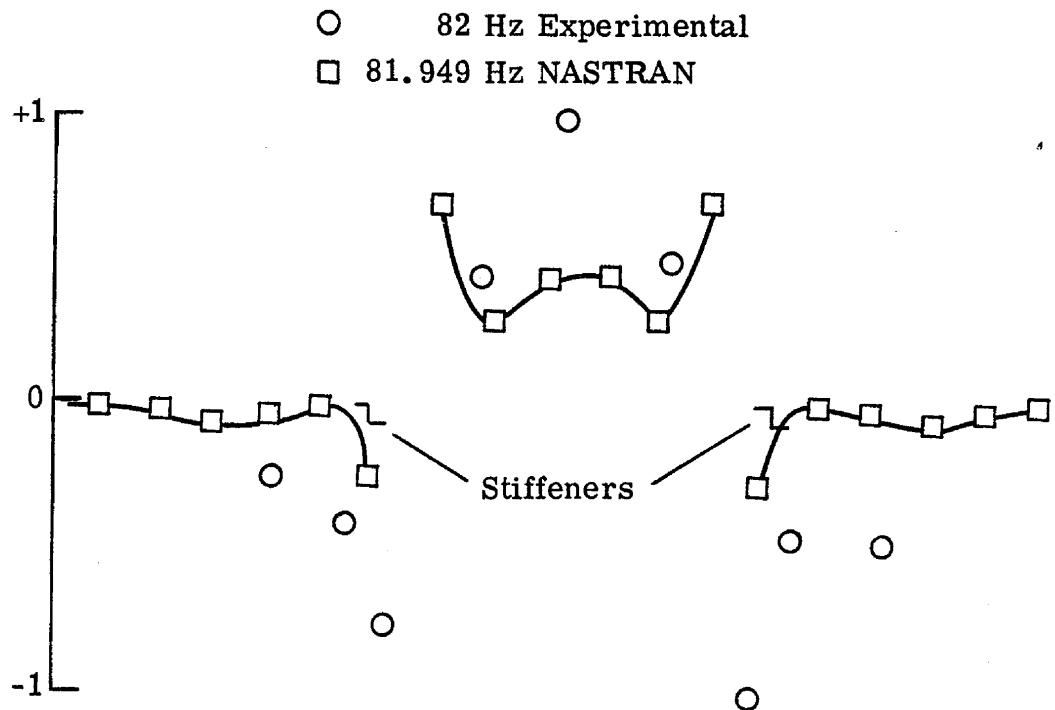


Normal stress distribution across panel width

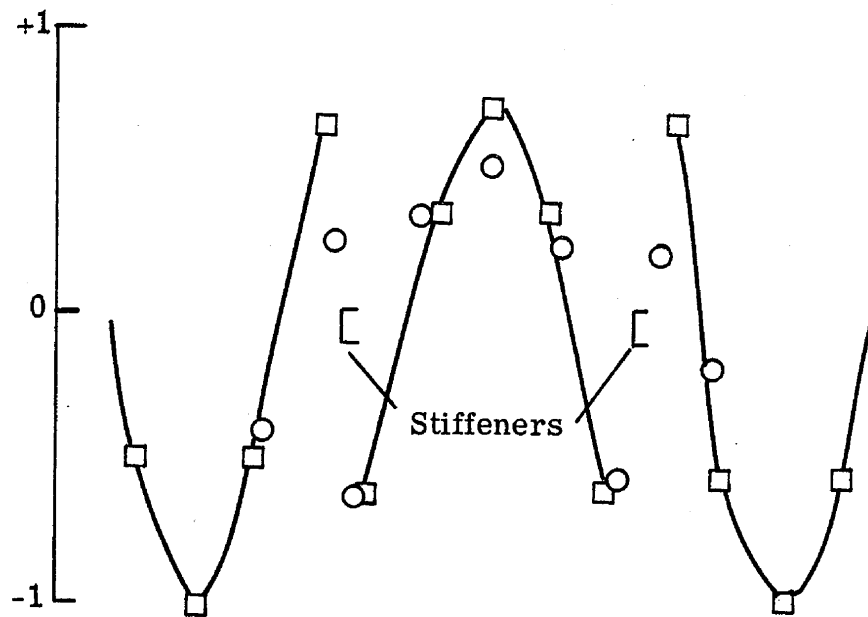
8.- Ratio of stress response for first panel mode experiment and NASTRAN analysis.



9.- NASTRAN second panel mode at 81.949 Hz.

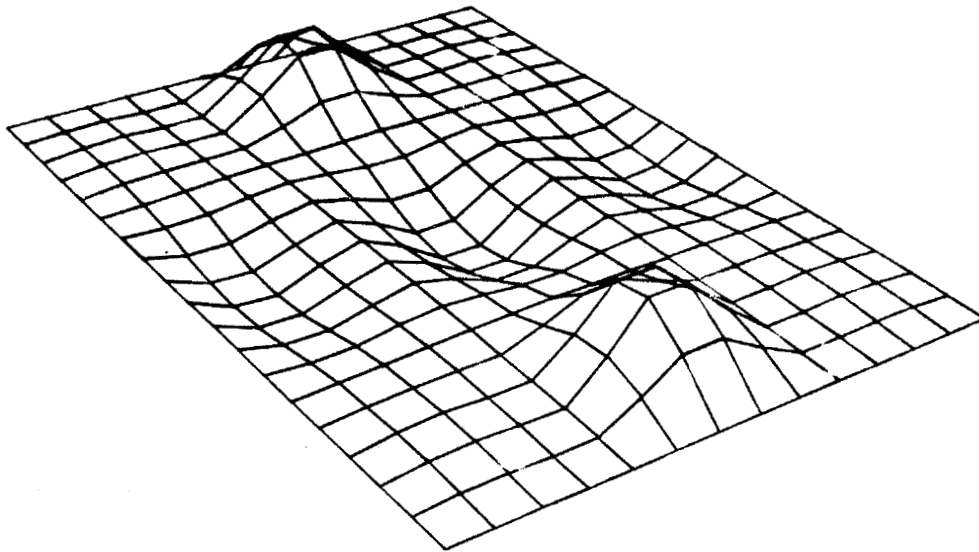


Normal stress distribution across panel length

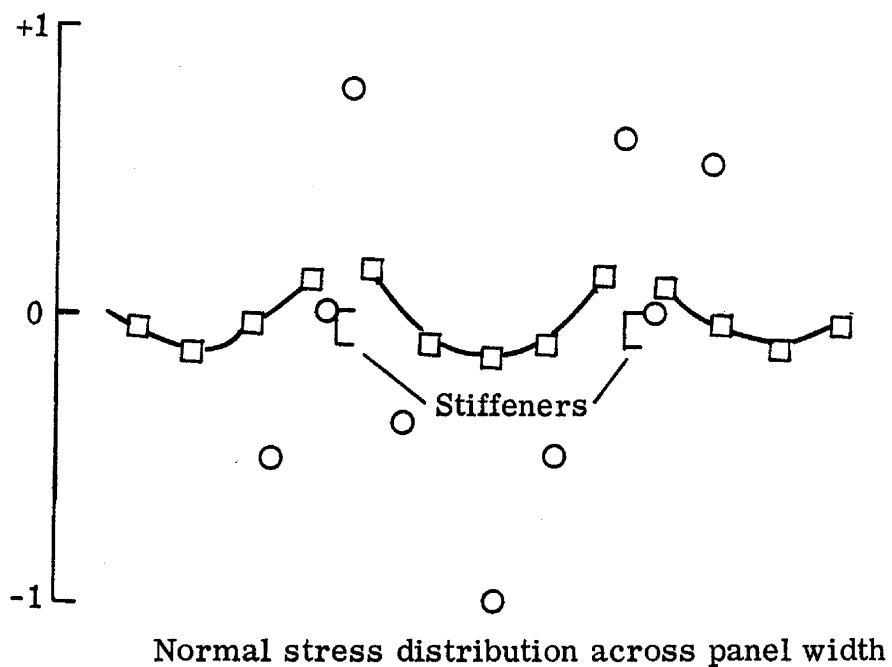
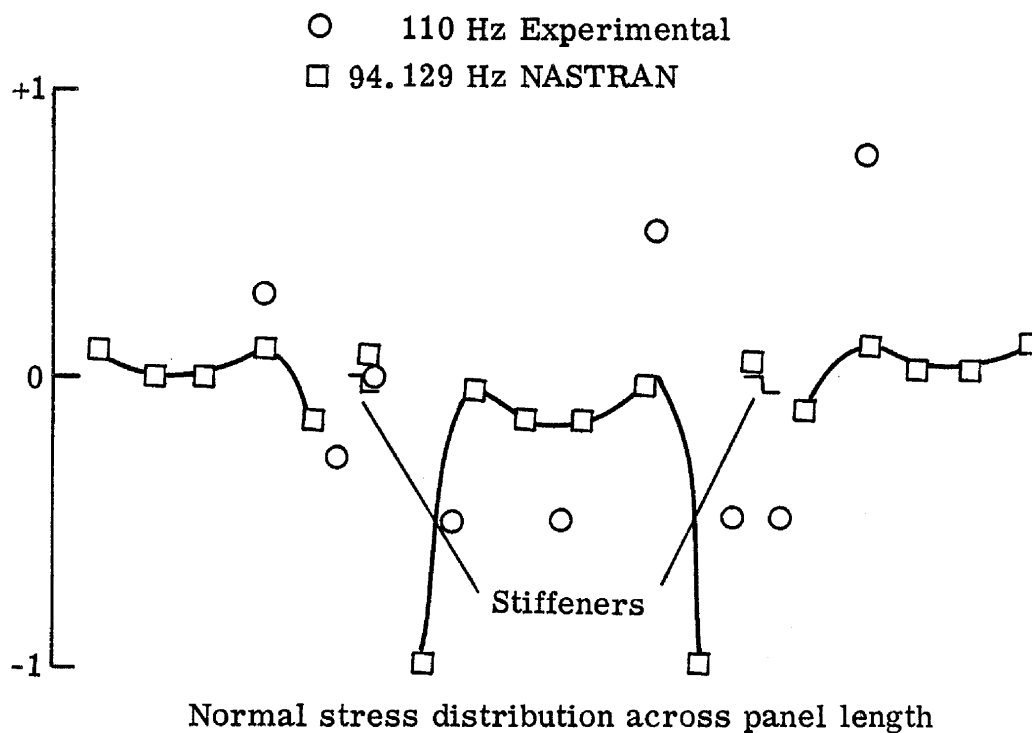


Normal stress distribution across panel width

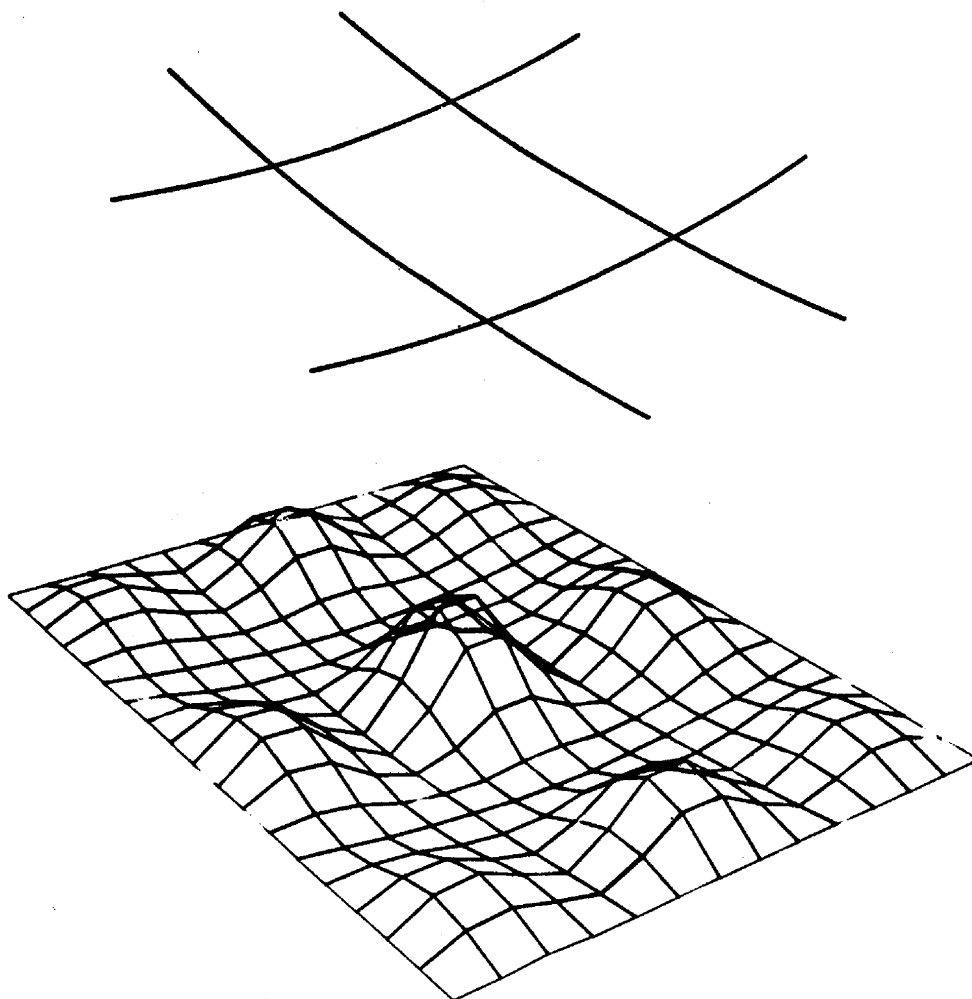
10.- Ratio of stress response for second panel mode from experiment and NASTRAN analysis.



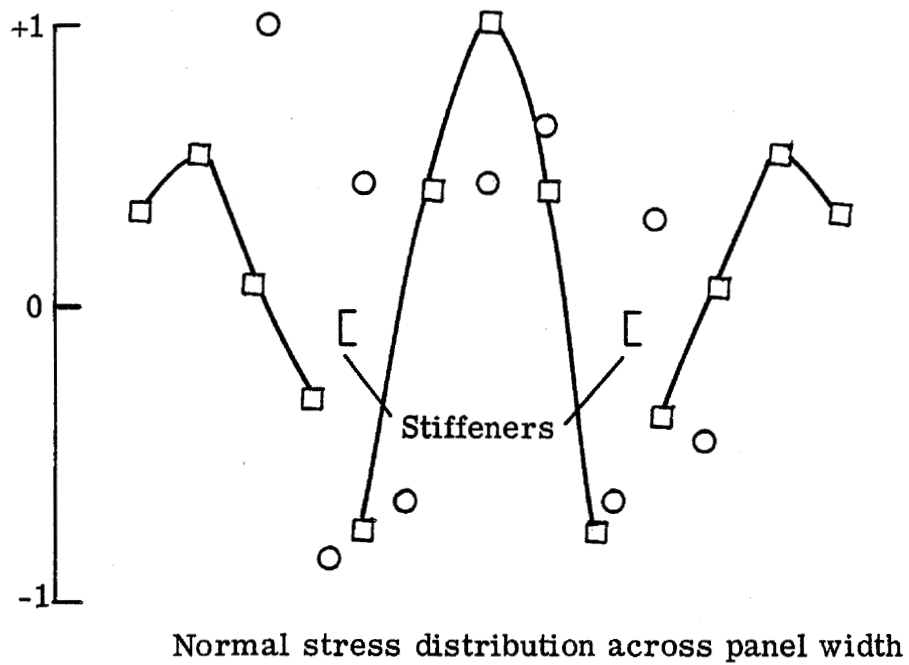
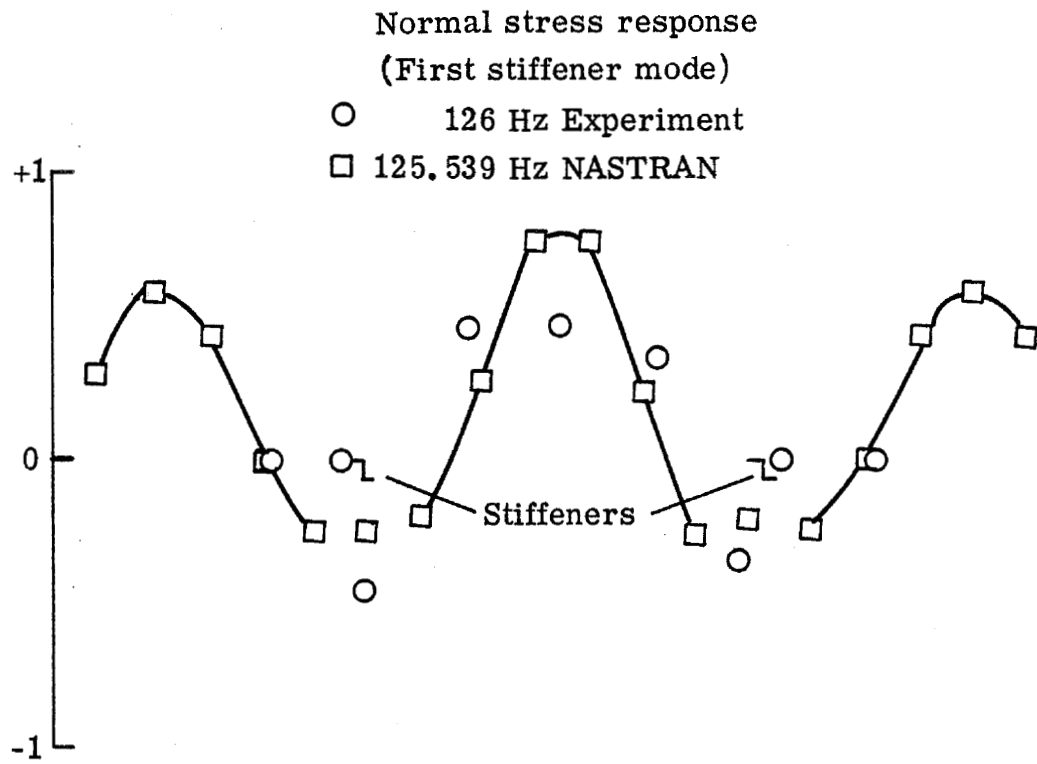
11.- NASTRAN third panel mode at 94.129 Hz.



12.- Ratio of stress response for third panel mode from experiment and NASTRAN analysis.



13.- Stiffener deflection and fourth panel mode corresponding to panel mode at 125.539 Hz.



14.- Ratio of panel stress response for fourth panel mode from experiment and NASTRAN analysis.

STRUCTURAL DYNAMIC ANALYSIS OF ELECTRONIC
ASSEMBLIES USING NASTRAN RESTART/FORMAT CHANGE
CAPABILITY

By Ronald P. Schmitz

Sperry Rand Corporation
Space Support Division
Huntsville, Alabama

ABSTRACT

This paper deals with the application of the NASTRAN program to structural dynamic response of electronic packaging and support structure. The structure modeled and analyzed was the Experiment Support System Assembly (ESS) of the SKYLAB Orbital Workshop. The analysis used three rigid formats: Eigenvalue Analysis (Format 3), Frequency Response (Format 11) and Static Analysis (Format 1). The same model was used for each analysis using NASTRAN's checkpoint/restart/format change capability. Geometry plotting and xy plotting were used to illustrate the mode shapes and acceleration response.

INTRODUCTION

This paper illustrates a technique used to analyze electronic assemblies and supporting structure subjected to random vibration loads using the NASTRAN program, Reference 1. In addition, NASTRAN's Checkpoint/Restart/Format change capability (Reference 2) is illustrated and an overview is given to the full analysis.

The Experiment Support System (ESS) of the Skylab Orbital Workshop (OWS), shown in Figure 1, was used to illustrate the technique. The original analysis was performed for NASA, MSFC Astrionics Laboratory under Contract NAS8-20055 by the Engineering Analysis Section, Sperry Rand Space Support Division. The effort was initiated in September 1969 and completed December 1970. During this period various design concepts were evaluated. Results of the analysis for the final design was contained in Sperry Report SP-211-0463 (Reference 3).

The ESS provides, in a single package, control of the OWS biomedical experiments. Located within the ESS Enclosure are all of the biomedical electronic control and display subassemblies. These subassemblies include:

- Primary Power Supply
- Secondary Power Supply
- Distributor
- Vector Cardiogram (VCG)
- Experiment Control Panel
- Speaker
- Cable Harness
- Meter Panel
- Blood Pressure Measuring System (BPMS)
- Power Panel
- Cabin Pressure
- Gas Interface

Figure 2 illustrates the control panel of the ESS Enclosure and the relative location of each subassembly.

NOMENCLATURE

<u>Symbol</u>	<u>Definition</u>	<u>Units</u>
A	Steady State Acceleration	g
DOF	Degrees of Freedom	
f	Frequency	Hz
g	Peak Sine Acceleration	g
\overline{G}	Static Equivalent Acceleration	g
G_{rms}	RMS Acceleration of Random Vibration	g
H	Transmissibility ($\frac{out}{in}$)	-
K	Structural Stiffness	N/m
M	Structural or Lumped Mass	kg

Q	Transmissibility ($\frac{\text{out}}{\text{in}}$)	-
PSD	Power Spectral Density, Acceleration	g^2/Hz
S	Acceleration Power Spectral Density (PSD)	g^2/Hz
t	Time	s
ω	Frequency	rad/s
\ddot{U}	Acceleration	m/s^2
X	Translation in X Direction	m
Y	Translation in Y Direction	m
Z	Translation in Z Direction	m

Subscripts

g	Total DOF subset
in	Input
rms	Root Mean Square
ss	Steady State
vd	Vehicle Dynamics
n	natural

LOAD CRITERIA

Although the ESS does not operate during launch, it must withstand launch and boost accelerations and vibrations, reaching orbit undamaged structurally and functionally. These loads include a maximum boost acceleration of + 4.7g, Vehicle Dynamics of 3.6g from 3 to 60 hertz in the flight axis and 6.2 g_{rms} composite lift-off random vibration in the lateral axes. The complete vibration criteria is shown in Table I. For preliminary design analysis these loads may be combined with each other depending upon the period of flight being examined and the frequency regime in which the structure is responsive. The general equation for defining a combined "static equivalent" load is,

$$\bar{G} = S_{ss} + Qg_{vd} + G_{rms} \quad (1)$$

where A_{ss} = steady state acceleration (g)

Q = transmissibility between loaded and excited grid point

g_{vd} = peak sine acceleration (g)

$$G_{rms} = \sigma \sqrt{\pi / 2 f_n Q \text{ PSD}_{in}} \quad (g_{rms}) \quad (2)$$

If no structural resonances occur below 60 hertz, Vehicle Dynamic criteria may be ignored, likewise maximum steady state acceleration occurs during burnout of the 1st stage (4.7g) and is not combined with lift-off random vibration.

DISCUSSION OF ANALYSIS

The complete structure associated with the ESS includes the side rails, the ESS Enclosure and the electronic subassemblies (Figure 3). The dynamic loads are transmitted from the OWS floor and ceiling through the side rail and ESS Enclosure into the subassemblies. To analyze the subassemblies in detail it is necessary to predict the amplification and/or isolation of the input load resulting from the intermediate structure.

To develop working finite element modes which are accurate yet sufficiently small to permit efficient use of computer time and analysis techniques within NASTRAN, it was necessary to substructure the ESS. Inspection of the structure reveals three "levels" of structures with sufficiently different stiffness that they may be uncoupled and modeled independently. They are:

- Side Rail
- ESS Enclosure
- Electronic Subassemblies

Finite Element Models

Side Rail. A NASTRAN finite element model of the Side Rail (ESS enclosure support structure) was developed to predict the amplification of loads between the floor/ceiling and the ESS Enclosure. The model consists of 69 grid points connected by 107 bar and 45 shear panel elements. The stiffness of the ESS Enclosure was modeled as a rigid body using constraint equations to transfer load through the enclosure

structure. The weight of the enclosure was distributed as lumped masses at each attach point.

Omit coordinates were used to obtain a dynamic model containing 66 degrees of freedom (DOF). The analysis set, K_{aa} , includes each boundary grid point where the ESS Enclosure is attached and mass concentrated. The model was used only for frequency response analysis. The checkpoint/restart capability was used, however, to obtain a complete set of acceleration responses for the three loading cases (1 g in the x, y, and z directions). This model is shown in Figure 4.

ESS Enclosure. A NASTRAN finite element model of the ESS Enclosure, shown in Figures 5 thru 7, was developed for static and dynamic analyses. The model consists of 178 grid points connected by 270 bar, 26 triangular plate, and 90 quadrilateral elements. The model resulted in a total structural stiffness matrix, K_{gg} , with 1068 DOF which was used for static analysis. This matrix was further reduced to 72 dynamic DOF for normal mode and frequency response analyses, see Figure 8.

Each electronic subassembly was modeled as a rigid body using rigid, massless bar elements connecting the concentrated mass of the subassembly from its c.g. to the attached points on the ESS Enclosure.

ESS Electronic Subassemblies. The primary power supply (PS) was included in this paper as representative of the other assemblies. It illustrates the prediction of the vibration environment and the calculation of stresses on the lowest "level" structure. A NASTRAN finite element model of the PS, shown in Figure 9, was developed for static and dynamic analyses. The model consists of 154 grid points connected by 156 plate elements. The model resulted in a total structural stiffness matrix, K_{gg} , with 924 DOF, which was used for static analysis. The matrix was further reduced to 39 dynamic DOF for normal mode and frequency response analysis (Figure 9).

Overview of Analysis

An overview of the complete analysis follows:

1. A frequency response analysis of the Side Rail structure was performed using 1g base excitation, for each of the three axes (three subcases). The results are summarized in Table II.
2. A normal mode analysis of the ESS Enclosure was performed. Typical mode shapes are illustrated in Figures 10 thru 13.
3. The response frequencies of the two structures were compared. The side rails were found to have a low first resonant frequency (44 hertz) compared with the enclosure (245.5 hertz). The assumption that the

ESS Enclosure can be treated as a rigid body supported by a flexible side rail structure was confirmed.

4. A Restart/Format change was made on the enclosure model from normal mode to static. The static equivalent loads (GRAV loads) were calculated using the gains and resonant frequencies calculated for the side rail model. Equation (1) was used to calculate these loads; the results are also included in Table II.
5. A Restart/Format change was then made on the enclosure model from normal mode to frequency response. The frequency response analysis was performed using lg base excitation for each of the three axes (three subcases). The response for each electronic subassembly is summarized in Table III. A typical acceleration response plot of the PS node is contained in Figure 14, for x-axis excitation. The random response at each of the electronic subassemblies was calculated in the same computer run. A typical acceleration PSD plot for the PS is shown in Figure 15.
6. A normal mode analysis of the PS was performed. Typical mode shapes are illustrated in Figure 16 thru 18.
7. The resonant frequencies of the PS were compared with those of the enclosure. The lowest frequency was found to be 542 hertz, thus confirming the rigid body assumption used in the enclosure model.
8. A Restart/Format change was made on the PS model from normal mode to static. The static equivalent loads (GRAV loads) were calculated using the gains and resonant frequencies calculated from the side rail and ESS Enclosure models. Since the resonant frequencies of the power supply were all above the Vehicle Dynamic criteria defined in Table I, only the random criteria is of interest. The resulting static equivalent loads are summarized in Table IV.
9. A Restart/Format change was then made on the PS model from normal modes to frequency response. The frequency response analysis was performed using lg base excitation, for each of the three axes (three subcases). The acceleration response and phase for a grid point associated with a critical electronic component is shown in Figure 19.
10. A detailed stress analysis was performed on all structural components of the ESS Enclosure and PS using the element forces and stresses predicted by the static solutions.

Application of Special NASTRAN Features

Rigid Body Simulation

Substructures which are relatively stiff compared with their supporting structure were modeled as rigid bodies. In the model of the side rail, the ESS Enclosure was modeled using multi-point constraint equations. These equations enforced displacements between attach points. The weight of the enclosure was distributed as lumped masses at each attach point.

The electronic subassemblies located within the ESS Enclosure were simulated as rigid bodies within the enclosure model by lumping the mass of each subassembly at its c.g. and then attaching this lumped mass to the enclosure subassembly interface using massless rigid bar elements (stiffness $\approx 100 \times$ ESS Enclosure frame stiffness). Figure 8 illustrates the finite element model of the Enclosure structure and the bar elements used to represent the subassemblies.

Base Acceleration Excitation

Since NASTRAN is limited to applied forces in the frequency response format, seismic masses (approximately $10^5 \times$ weight of the structure) are attached at each excited grid point. A force is then applied, equal to the seismic mass, which results in a 1g sinusoidal acceleration at these grid points. The use of very large masses and forces reduces to a negligible amount the feedback to the excited grid points from the resonating structure.

Checkpoint/Restart/Format Change

Three rigid formats were used in this analysis, Formats 1, 3, and 11. Unfortunately the use of base excitation precludes using the same geometry and constraint bulk data for all three formats. This minimizes the benefit of the Restart/Format change feature of NASTRAN unless care is taken to checkpoint the proper model.

When using base excitation, the normal mode format should be the first format checkpointed. The boundary condition will be a free-free structure, where the single point constraints are not specified in the case control deck and SUPORT's are used to remove the rigid body modes. The seismic masses are included in the model during this checkpoint run. All bulk data cards necessary for the static and frequency response restarts may be included at this time.

When the restart is made for the static analysis the SUPORT and OMIT cards are deleted from the bulk data and the SPC card added to the case control deck. This will effectively ground out all seismic masses used for the frequency response analysis. The GRAV cards are added to the bulk data and LOAD cards to the case control deck. The change from SUPORT to SPC constraints requires a new decomposition for the static Restart, however, the reactions may be recovered, and are not available using SUPORT constraints. The time lost due to geometry changes in this format restart is more than compensated for in the restart of the frequency response format.

When restarting the frequency response format from the normal mode format, no changes are required to the geometry or constraint bulk data. Therefore, the problem will restart at the module DPD and skip over modules SMP1 (Guyan reduction) and READ (real eigenvalue extraction) saving a significant amount of time, see Figure 20.

Subsequent restarts of the frequency response format are normally required to obtain acceleration and random response plots for multiple subcases. The first frequency response analysis should be checkpointed. Subsequent restarts for new print and plot output normally take very little time (typically less than 3 minutes on the Univac 1108).

A restart of the normal mode analysis is often required to obtain all of the modes of interest. In addition, a good check on the accuracy of the model is obtained by calculating the lowest natural frequency of the structure without the use of OMIT cards and compare this result with the result obtained using OMIT cards. Changes can then be made, if necessary, to the OMIT set before the time consuming frequency response analysis is performed.

Random Analysis

A unit input acceleration is required for random analysis to satisfy the condition that the output acceleration be equal to the magnification factor, $H(\omega)$. The output PSD (S_j) then can be solved from the following equation

$$S_j = H_{ja}^2(\omega) S_a$$

for acceleration PSD the units of this equation become,

$$\frac{(\text{m/sec}^2)^2}{\text{hertz}} = \left[\frac{(\text{m/sec}^2)}{g} \right]^2 \frac{g^2}{\text{hertz}} \quad \text{or} \quad \frac{(\text{in/sec}^2)^2}{\text{hertz}} = \left[\frac{(\text{in/sec}^2)}{g} \right]^2 \frac{g^2}{\text{hertz}}$$

Run Time Summary

A summary of the total run times and significant time spent in specific modules are illustrated in Figure 20 for the ESS Enclosure model.

The accumulated cpu time (Univac 1108, NASTRAN Level 12.1.002 MSFC) is plotted as a function of DMAP instruction number, and where large times are accumulated in one module the name of the module is given. Gaps in the curves indicate DMAP instructions which were skipped during restart/format change (Formats 1 and 11).

Bandwidth, DOF and run time comparisons are contained in Table V, for the symmetric decomposition (SDCO), matrix reduction (SMP1) and eigenvalue extraction (READ) of the three finite element models discussed in this paper.

REFERENCES

1. "The NASTRAN Theoretical Manual," MacNeal, R. H., ed., NASA SP-221, October 1969.
2. "The NASTRAN User's Manual," McCormick, C. W., ed., NASA SP-222, September 1970.
3. Loafman, J. W., Schmitz, R. P., Vaught, E. W., "Structural Dynamic Analysis of Experiment Support System Enclosure, Power Supply and Distributor", Sperry Space Support Division, Sperry Rand Corp., SP-211-0463, February 15, 1971.

TABLE 1. ESS VIBRATION CRITERIA AT OWS FLOOR AND CEILING

1. Vehicle Dynamics Criteria

Flight Axis (3-60 Hz @ 3 oct/min)

3	-	7 Hz @ 0.43 Inches D. A. Disp.
7	-	14 Hz @ 1.1 G's peak
14	-	25 Hz @ 0.11 Inches D. A. Disp.
25	-	60 Hz @ 3.6 G's peak

Lateral Axes (2-20 Hz @ 3 oct/min)

2	-	4 Hz @ 0.34 Inches D. A. Disp.
4	-	7 Hz @ 0.28 G's peak
7	-	20 Hz @ 0.08 G's peak

2. Sinusoidal Evaluation Criteria (20-2000 Hz @ 1 oct/min)

20	-	100 Hz @ 0.0020 Inches D. A. Disp.
100	-	2000 Hz @ 1.0 G's peak

3. Lift-Off Random Vibration Criteria (1 min/axis)

Flight Axis		Lateral axes	
	2 Hz @ 0.0065 g^2/Hz^*	2	- 10 Hz @ 0.010 g^2/Hz^*
2	- 5 Hz @ +6 dB/oct*	10	- 20 Hz @ +10 dB/oct*
5	- 20 Hz @ 0.10 g^2/Hz^*	20	- 100 Hz @ 0.10 g^2/Hz
20	- 30 Hz @ 0.10 g^2/Hz	100	- 2000 Hz @ -3 dB/oct
30	- 1000 Hz @ -3 dB/oct		2000 Hz @ 0.0050 g^2/Hz
1000	- 2000 Hz @ 0.0030 g^2/Hz		

Composite = 4.1 Grms

Composite = 6.2 Grms

4. Boost Random Vibration Criteria (2 min/axis)

Flight Axis		Lateral Axes	
	2 Hz @ 0.0017 g^2/Hz^*	2	- 10 Hz @ 0.0025 g^2/Hz^*
2	- 5 Hz @ +6 dB/oct*	10	- 20 Hz @ +10 dB/oct*
5	- 20 Hz @ 0.025 g^2/Hz^*	20	- 100 Hz @ 0.025 g^2/Hz
20	- 30 Hz @ 0.025 g^2/Hz	100	- 2000 Hz @ -3 dB/oct
30	- 1000 Hz @ -3 dB/oct		2000 Hz @ 0.0012 g^2/Hz
1000	- 2000 Hz @ 0.00070 g^2/Hz		

Composite = 1.9 Grms

Composite = 3.1 Grms

*Design criteria only - no test required

5. Shock Criteria

No shock test required

TABLE II. ESS SIDE RAIL MODEL FREQUENCY RESPONSE RESULTS AND ENCLOSURE STATIC EQUIVALENT LOADS

EXCITATION DIRECTION	SIDE RAIL RESONANT FREQUENCY (HERTZ)	SIDE RAIL GAIN Q	RANDOM ACCEL. PSD _{in} (g ² /Hz)	STEADY STATE ACCELERATION A _{ss}	STATIC EQUIPMENT LOAD ON ENCLOSURE G**
X	209	8.54	.014	4.7	18.49
Y	67	5.19*	0.1	0.0	14.05
Z	44	5.5*	0.1	0.0	13.58

* $Q_{AVE.} = \frac{Q_{TOP} + Q_{BOTTOM}}{2}$ AVERAGE GAIN THROUGHOUT ESS ENCLOSURE

** SEE EQUATION (2)

TABLE III. ESS ENCLOSURE MODEL FREQUENCY RESPONSE RESULTS

SUBASSEMBLY		VCG (GP 151)	METER PANEL (GP 156)	BMS (GP 157)	SECONDARY POWER SUPPLY (GP 162)		PRIMARY POWER SUPPLY (GP 163)			DISTRIBUTOR (GP 164)	
EXCITATION DIRECTION X	FREQ	727.9	727.9	672.3	209.	489.4	209.	489.4	788.0	209.	489.4
	U _x	22.2	23.05	17.57	10.26	23.37	10.97	32.91	30.68	12.95	70.71
	GAIN	2.26	2.35	1.79	1.05	2.38	1.1	3.35	3.13	1.32	7.20
Y	FREQ	239.5	239.5	239.5	67.	239.5	67.	239.5		67.	417.5
	U _y	33.01	69.31	73.99	9.81	31.71	9.81	23.86		9.81	86.99
	GAIN				1.0		1.0			1.0	
Z	FREQ	621.	621.	621.	44	621.	44.	621.	853.	44.	621.
	U _z	65.64	88.20	63.04	9.81	26.04	9.81	61.54	29.09	9.81	35.64
	GAIN	5.77	8.98	6.42	1.0	2.65	1.0	6.27	2.96	1.0	3.63

TABLE IV. ESS POWER SUPPLY MODEL STATIC EQUIVALENT LOAD SUMMARY

EXCITATION DIRECTION	CRITICAL FREQUENCY* (Hertz)	Q_{SR}	Q_{ENCL}	Q_{TOTAL}	PSD_{IN} (g^2/Hz)	PSD_{OUT} (g^2/Hz)	\bar{G}^{**} (g)
X (FLIGHT)	209.	8.	1.1	8.8	.014	1.08	13.99
Y	67.	5.19	1.0	5.19	0.1	2.69	14.05
Z	44.	5.5	1.0	5.5	0.09	2.72	13.58

* AT RESONANT FREQUENCIES OF THE ENCLOSURE, THE SIDE RAIL ARE ISOLATING, $Q_{SR} < 1.0$.

** SEE EQUATION (2)

TABLE V. SUMMARY OF MATRIX DECOMPOSITION

MODEL	DOF	B	C	R	t_{test}	t_{actual}
SIDE RAIL	414	51	14	50	22	16.1
ENCLOSURE	912	46	83	45	300.	180.2
POWER SUPPLY	861	101	0	100	66.	56.5

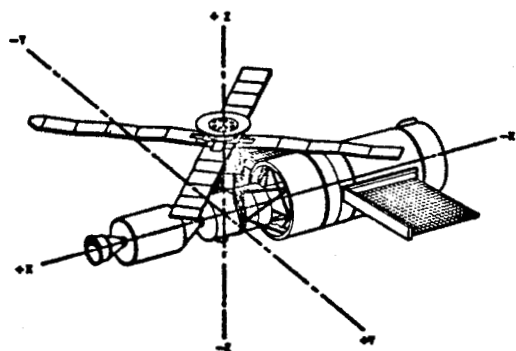
SUMMARY OF MATRIX REDUCTION (SMP1)

MODEL	K_{NN} (DOF)	K_{AA} (DOF)	t_{test} (DECOMP)	t_{actual} (SMP1)
SIDE RAIL	414	66	22.	207.2
ENCLOSURE	1044	72	257.	906.
POWER SUPPLY	861	39	66.	284.1

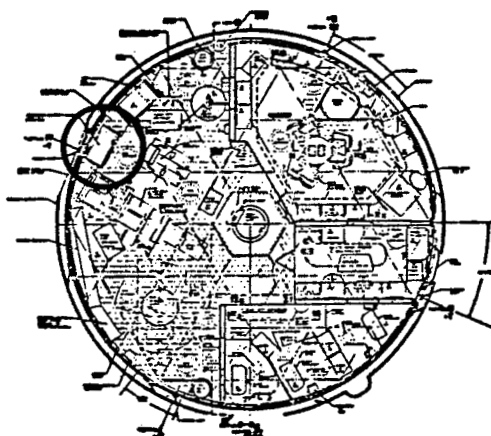
SUMMARY OF EIGENVALUE EXTRACTION (READ)

MODEL	K_{AA}	K_{LL}	B	C	R	B	C	DECOMP TIME		t/ROOT
								t_{test}	t_{actual}	
SIDE RAIL	66	-	66	0	65	65	0	11.	8.6	60.1
ENCLOSURE	72	52	38	35	71	34	37	10.	15.1	66.8
POWER SUPPLY	39	-	21	19	38	18	20	2.	3.2	19.5

FIGURE 1. SKYLAB ORBITAL WORKSHOP



SKYLAB ORBITAL WORKSHOP CLUSTER



ORBITAL WORKSHOP FLOOR PLAN

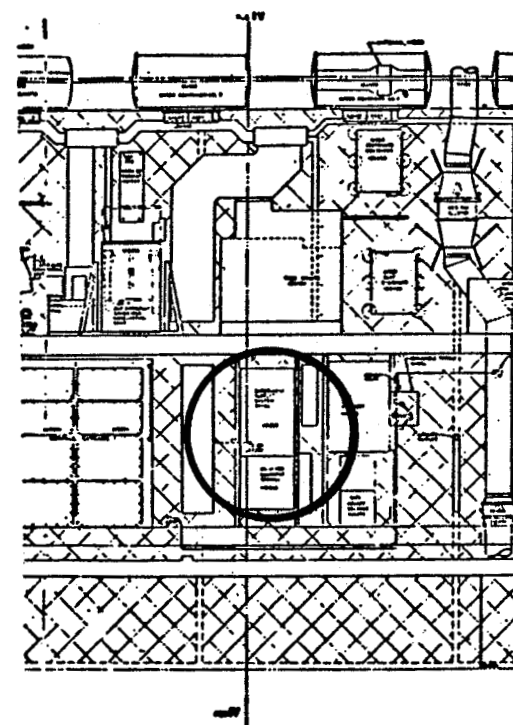
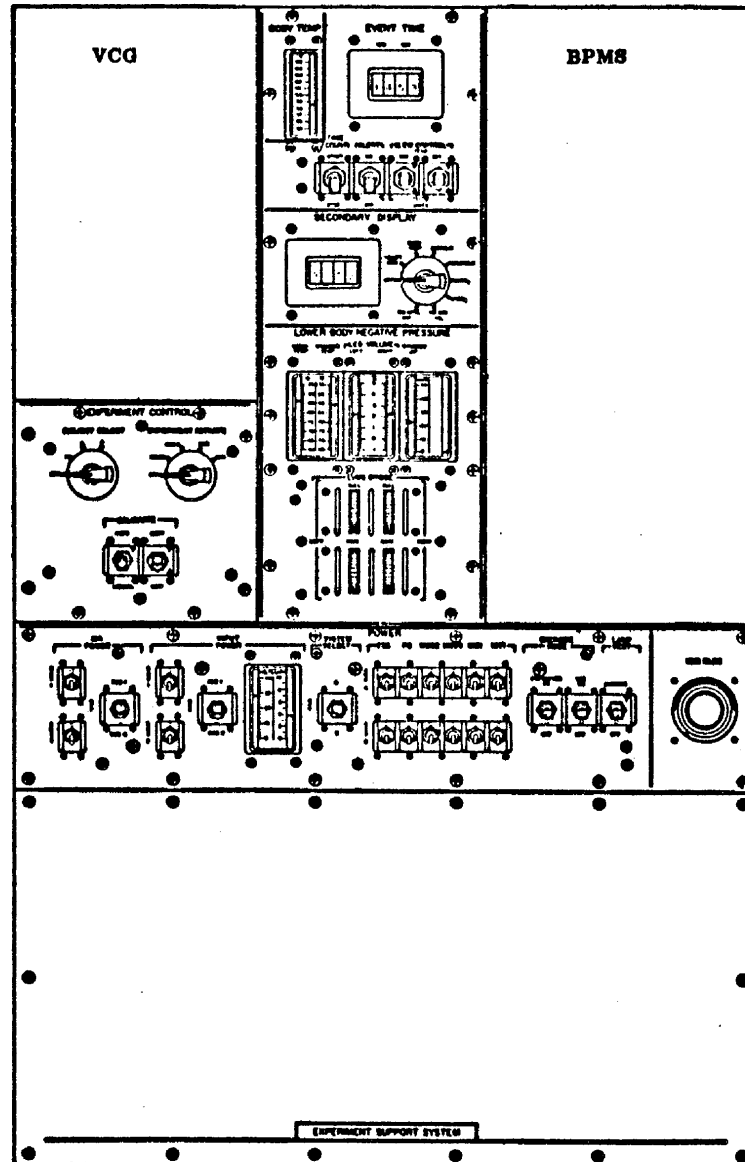
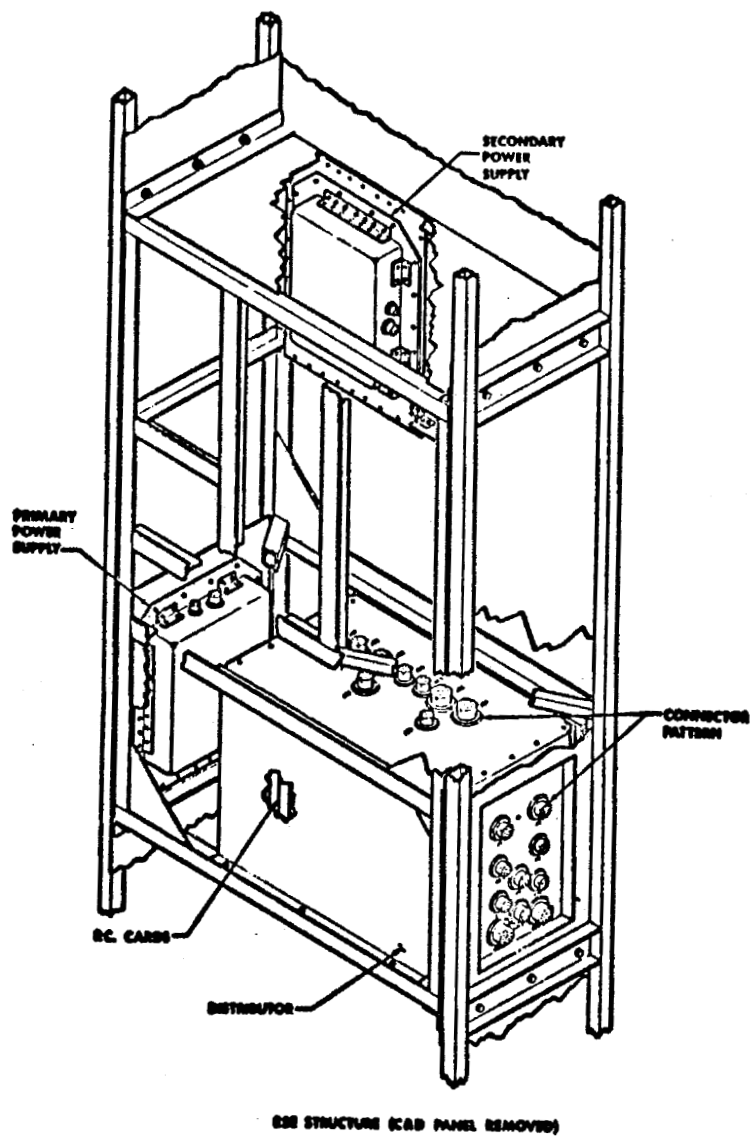
ORBITAL WORKSHOP ELEVATION SHOWING
LOCATION OF EXPERIMENT SUPPORT SYSTEM

FIGURE 2. ESS CONTROL PANEL



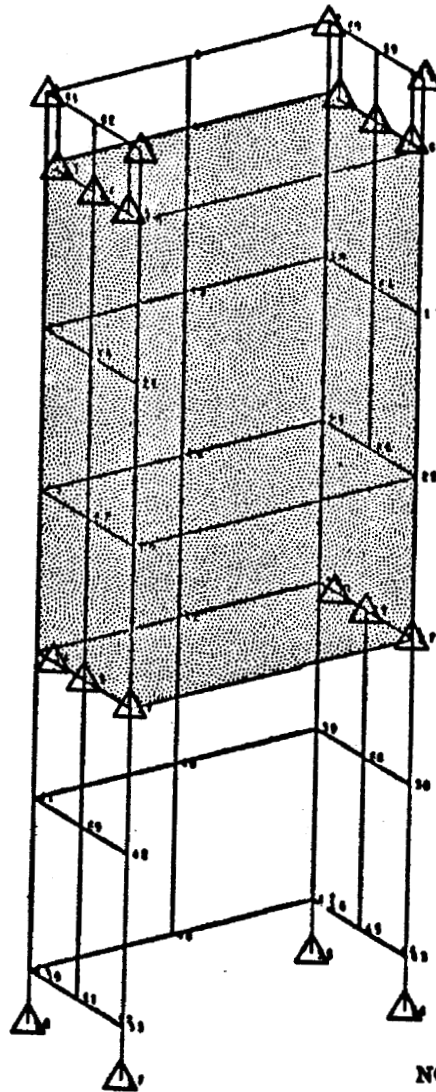
NOT REPRODUCIBLE

FIGURE 3. ESS SIDE RAILS, ENCLOSURE AND ELECTRONIC ASSEMBLIES



NOT REPRODUCIBLE

FIGURE 4. ESS SIDE RAIL MODEL WITH DYNAMIC COORDINATES



ESS SIDE RAILS
FREQUENCY RESPONSE ANALYSIS
MADE OF TOP ENCLOSURE ONLY
UNDEFORMED SHAPE

NOTE: ESS MODELED AS A
RIGID BOX WEIGHING
182.5 LBS. (SHADED
AREA).

△ DYNAMIC COORDINATE

NOT REPRODUCIBLE

FIGURE 5. ESS FINITE ELEMENT MODEL OF FRAME

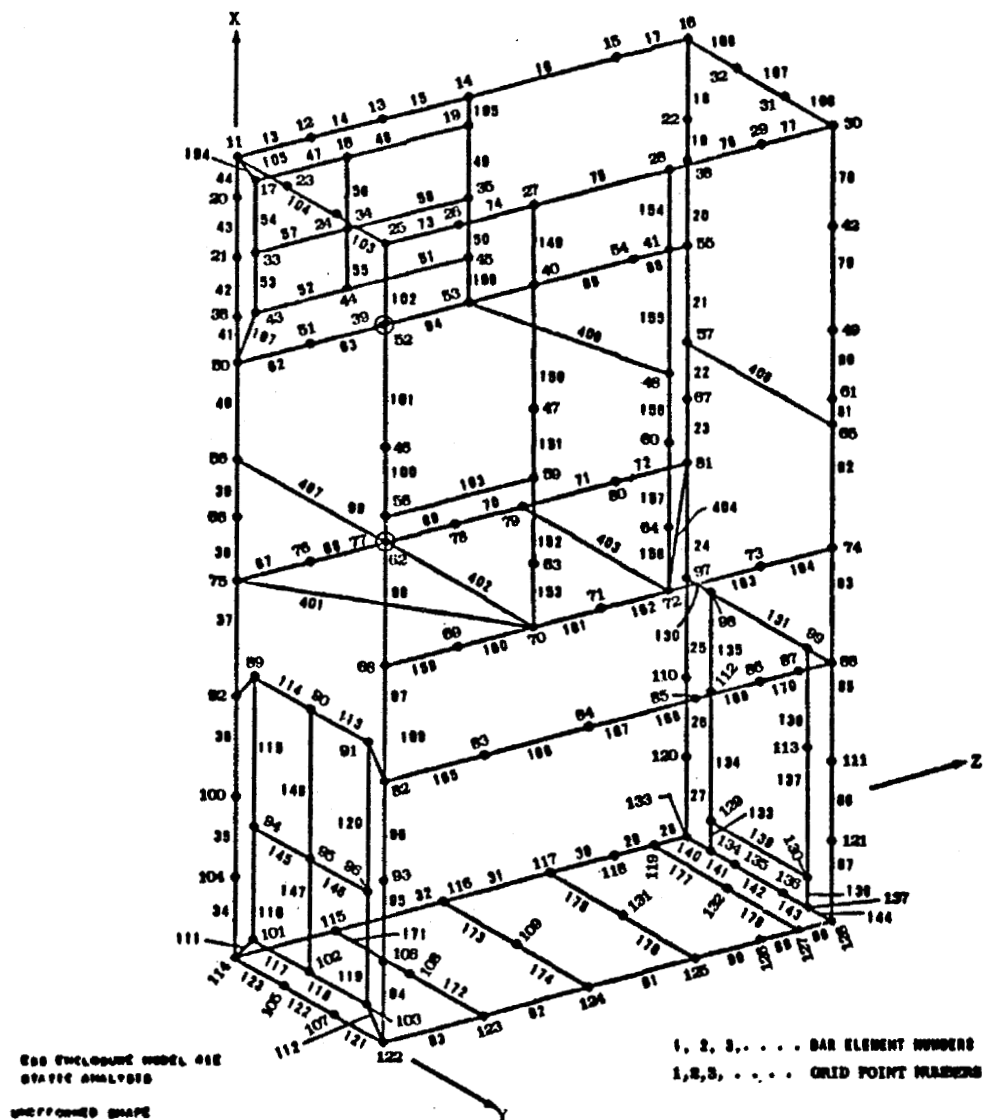
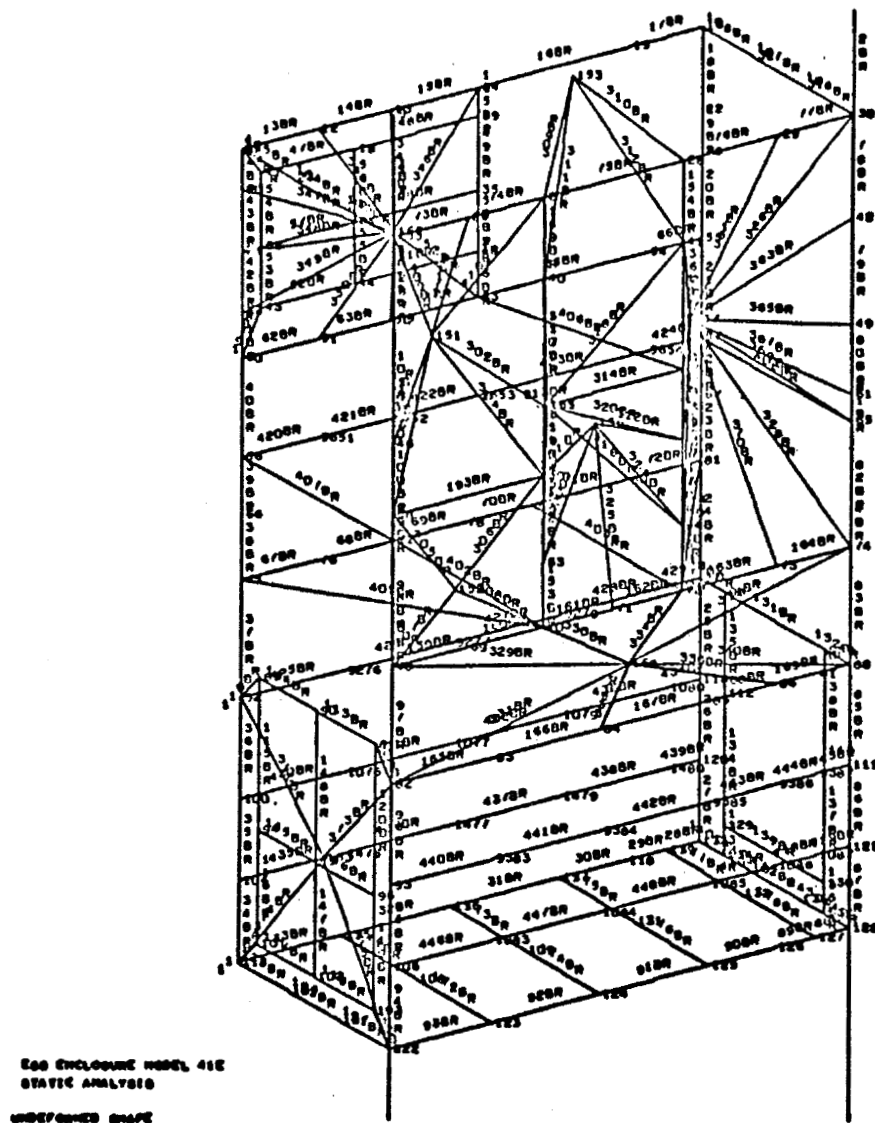
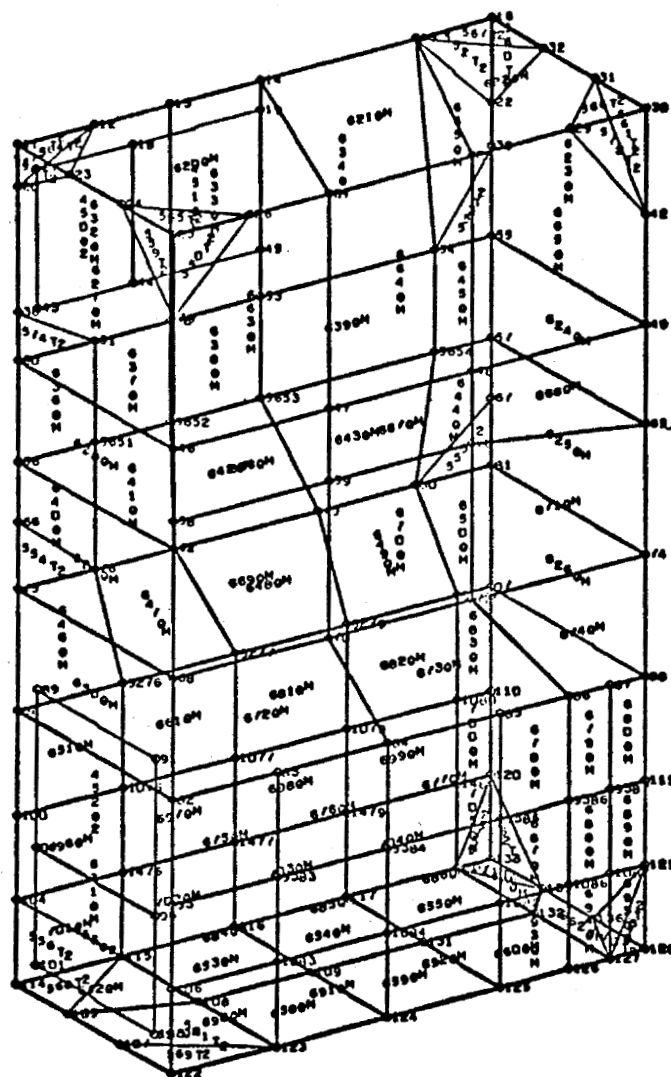


FIGURE 6. ESS FINITE ELEMENT MODEL OF BAR ELEMENTS



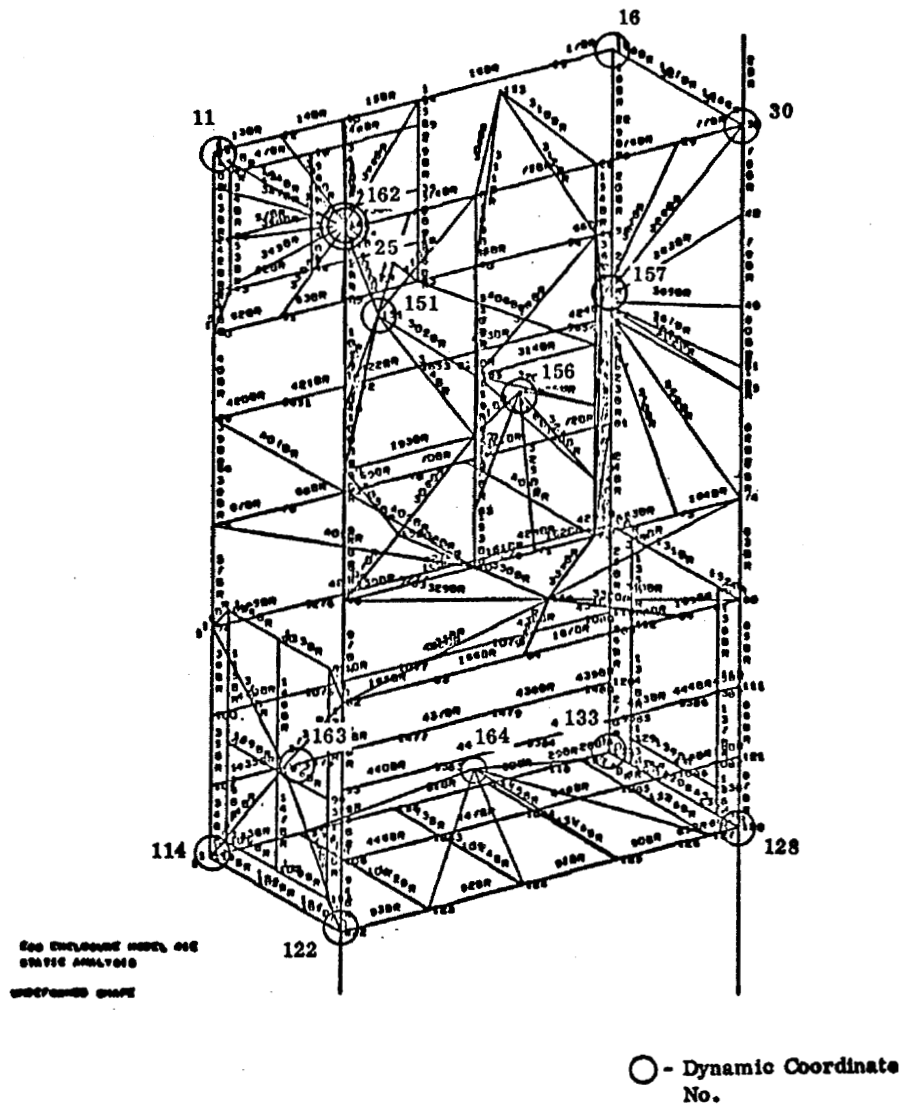
NOT REPRODUCIBLE

FIGURE 7. ESS FINITE ELEMENT MODEL OF PLATE ELEMENTS



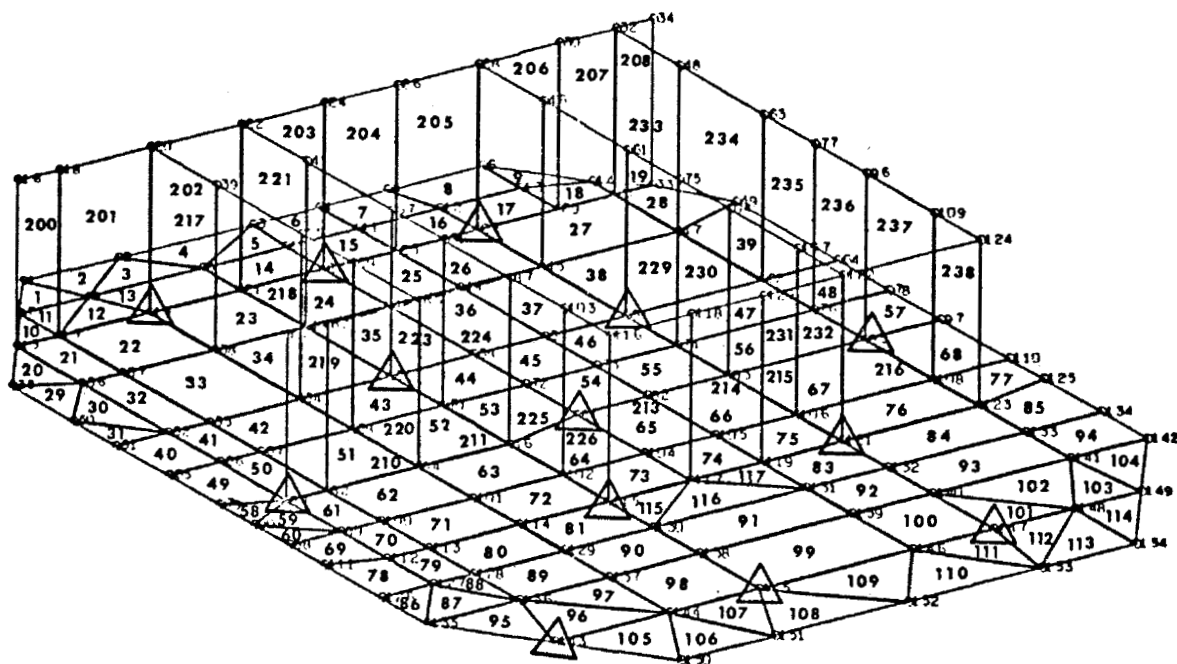
ESS ENCLOSURE MODEL 012
 STATIC ANALYSIS
 UNDEFORMED SHAPE

FIGURE 8. ESS DYNAMIC COORDINATES OF FINITE ELEMENT MODEL



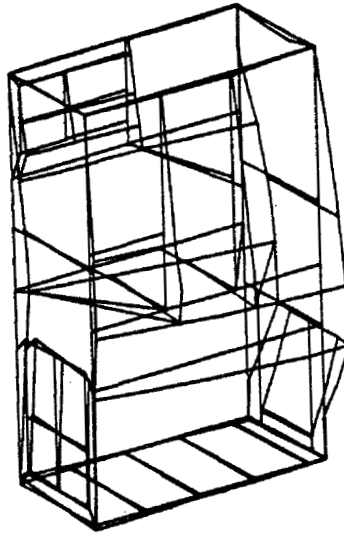
NOT REPRODUCIBLE

FIGURE 9. POWER SUPPLY FINITE ELEMENT MODEL WITH DYNAMIC COORDINATES



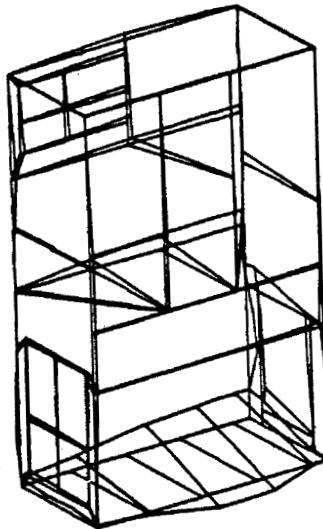
△ DYNAMIC COORDINATES

POWER SUPPLY BASE (ESS)
EIGENVALUE PROBLEM
UNDEFORMED SHAPE



ESS ENCLOSURE MODEL 407
MODAL MODE ANALYSIS
MODE 1 DEFORMATION - DISCRETE 1 MODE 21 EIGENVALUE = 2379630.7000

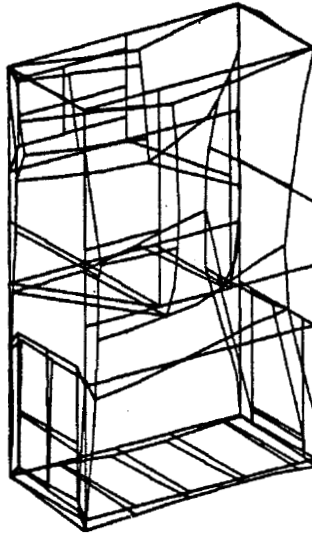
FIGURE 10. ESS ENCLOSURE MODE SHAPE FOR $f_1 = 245.5$ Hz



ESS ENCLOSURE MODEL 407
MODAL MODE ANALYSIS
MODE 2 DEFORMATION - DISCRETE 1 MODE 22 EIGENVALUE = 7426791.5000

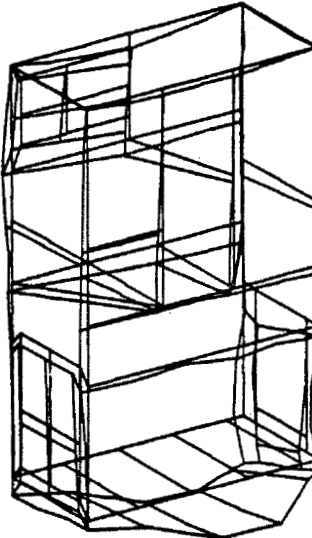
FIGURE 11. ESS ENCLOSURE MODE SHAPE FOR $f_2 = 433.7$ Hz

NOT REPRODUCIBLE



ESS ENCLOSURE MODEL 40P
NORMAL MODE ANALYSIS
MODAL DEFORMATION - SUBCASE 1 MODE 25 EIGENVALUE = 9410006.0000

FIGURE 12. ESS ENCLOSURE MODE SHAPE FOR $f_3 = 488.5$ Hz



ESS ENCLOSURE MODEL 40P
NORMAL MODE ANALYSIS
MODAL DEFORMATION - SUBCASE 1 MODE 26 EIGENVALUE = 9690191.0000

FIGURE 13. ESS ENCLOSURE MODE SHAPE FOR $f_4 = 499.7$ Hz

FIGURE 14. ESS ENCLOSURE, PS NO. 1 ACCELERATION RESPONSE TO 1g-X-AXIS EXCITATION

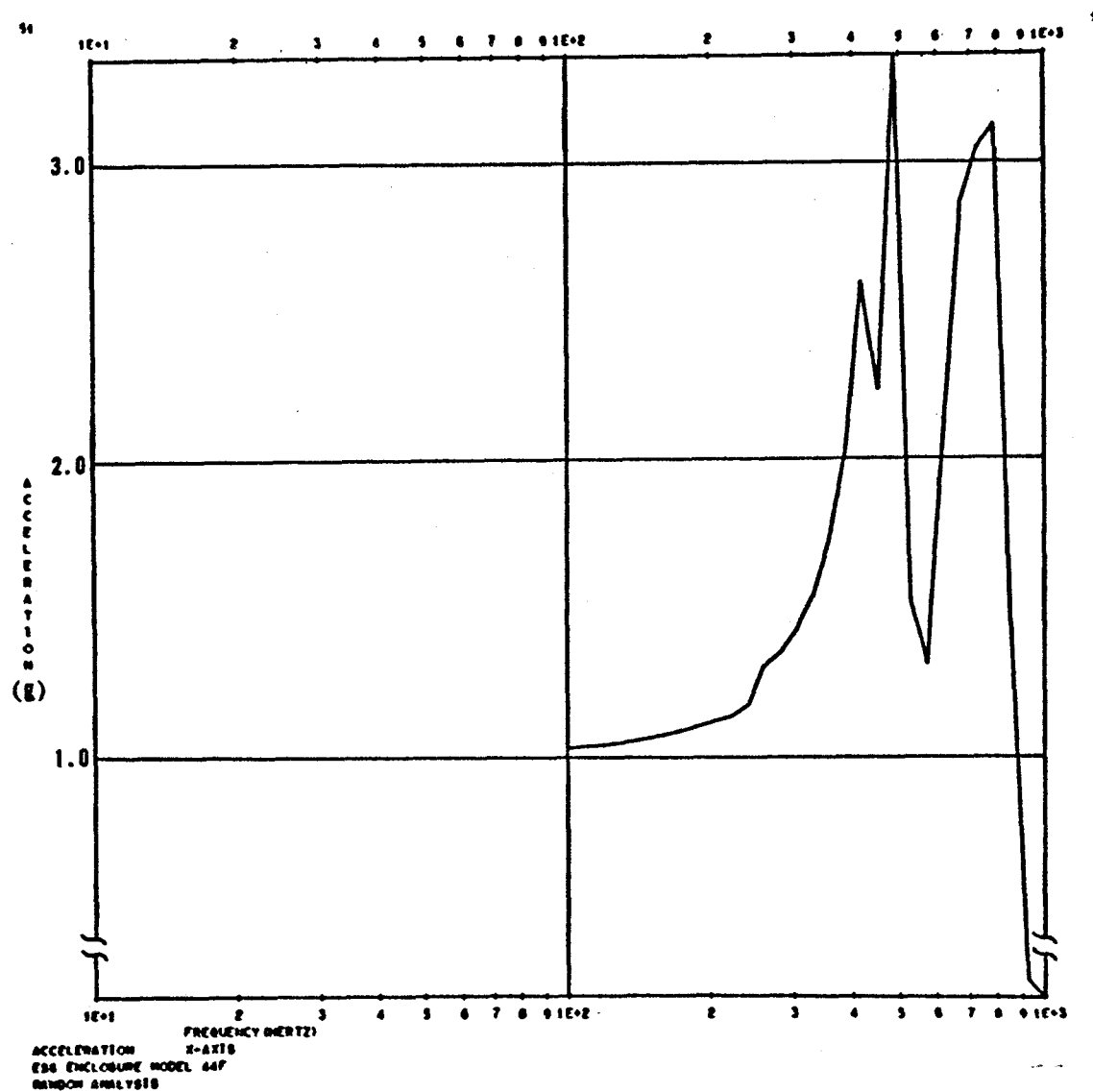
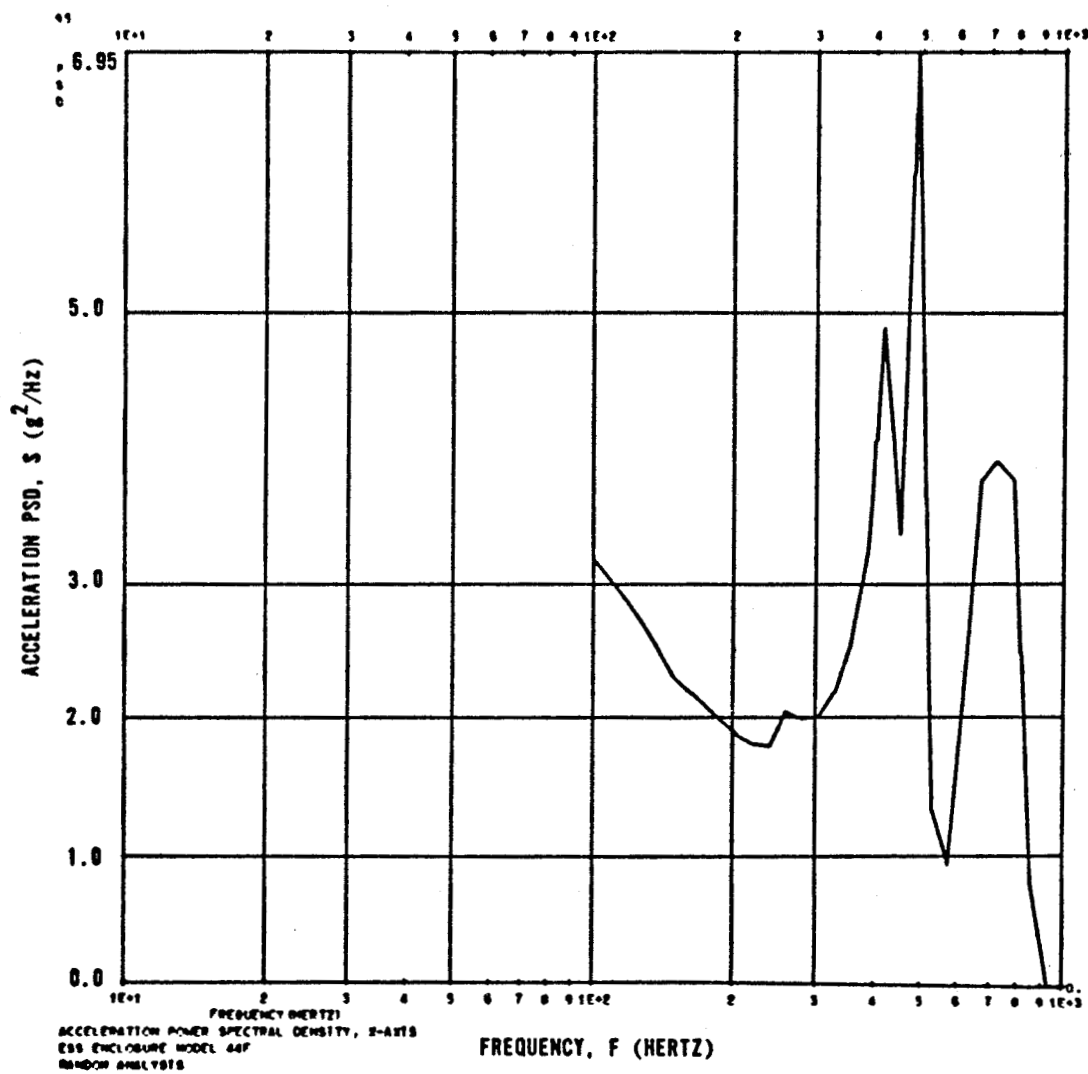
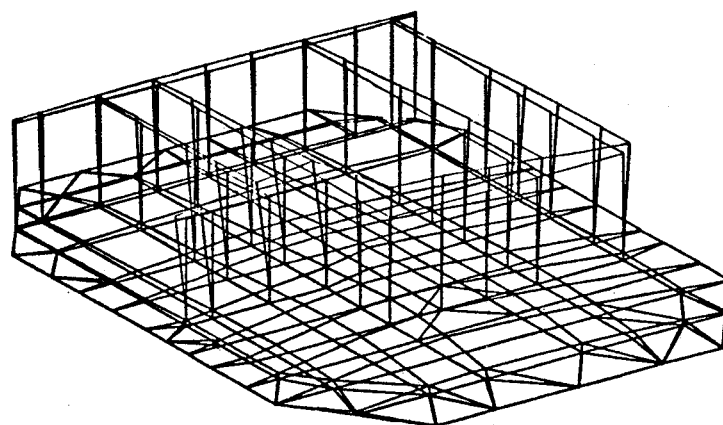


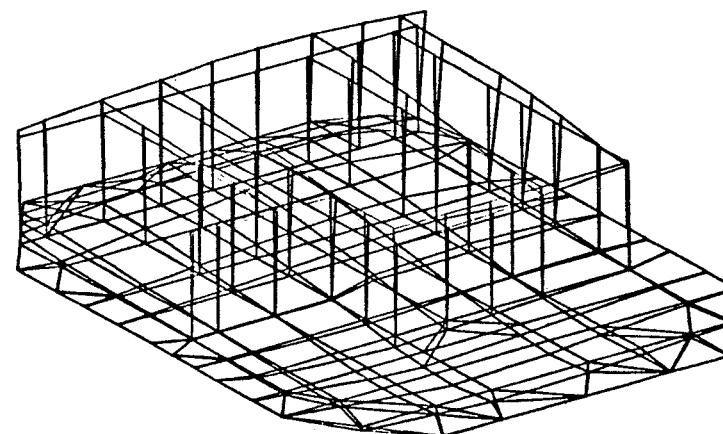
FIGURE 15. ESS ENCLOSURE, PS NO. 1 ACCELERATION PSD RESPONSE FOR HI
RANDOM VIBRATION CRITERIA (FLIGHT AXIS)





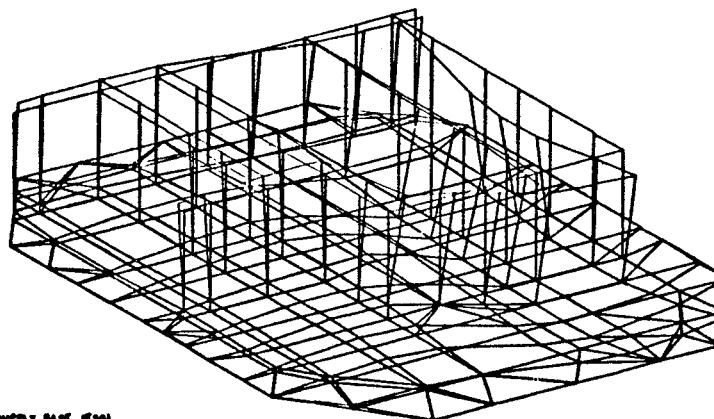
POWER SUPPLY BASE (E88)
 EI DEVALUE PROBLEM
 MODAL DEFORMATION - SUBCASE 1 NODE 1 EI DEVALUE = 11.041019.000

FIGURE 16. POWER SUPPLY MODE SHAPE FOR $f_1 = 542$ Hz



POWER SUPPLY BASE (E88)
 EI DEVALUE PROBLEM
 MODAL DEFORMATION - SUBCASE 1 NODE 2 EI DEVALUE = 652.72126.000

FIGURE 17. POWER SUPPLY MODE SHAPE FOR $f_2 = 1295$ Hz



POWER SUPPLY BASE (E88)
 EI DEVALUE PROBLEM
 MODAL DEFORMATION - SUBCASE 1 NODE 3 EI DEVALUE = 1010.000.000

FIGURE 18. POWER SUPPLY MODE SHAPE FOR $f_3 = 1600$ Hz

NOT REPRODUCIBLE

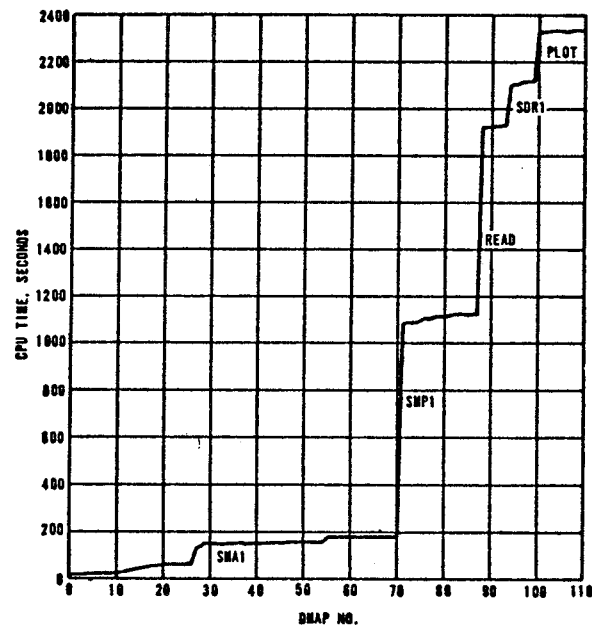
The figure consists of two vertically stacked plots sharing a common x-axis representing Frequency in Hertz (Hz). The x-axis is logarithmic, with major ticks at 1E+1, 2, 3, 5, 7, 1E+2, 2, 3, 5, 7, 1E+3, 2, 3, 5, 7, and 1E+4.

The top plot displays Acceleration in g (grams) on the y-axis, ranging from 0 to 3.0. The curve shows a sharp resonance peak at approximately 7 Hz, reaching an acceleration of about 3.0 g. There are smaller peaks around 3 Hz and 10 Hz.

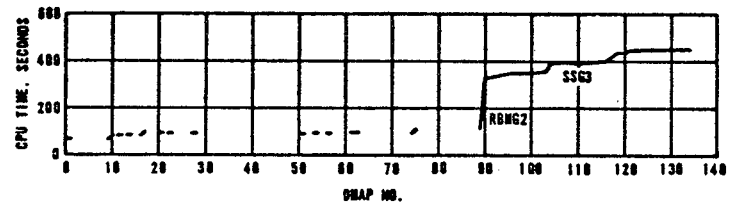
The bottom plot displays Phase in degrees (deg.) on the y-axis, ranging from 0.0 to 360.0. The phase curve shows a sharp drop at approximately 7 Hz, indicating a resonance point. The phase starts around 300 degrees at low frequencies, drops to a minimum near 0 degrees at the resonance frequency, and then rises back towards 360 degrees at higher frequencies.

390

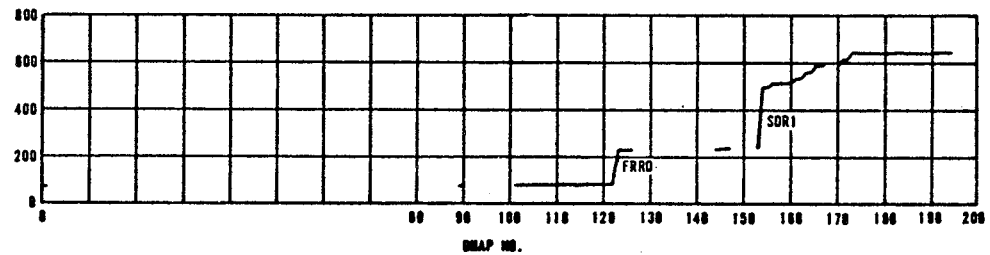
FIGURE 20. RUN TIME SUMMARY FOR CHECKPOINT/RESTART/FORMAT
CHANGE OF FORMATS 1, 3 AND 11



FORMAT 3 CHKPNT



FORMAT 1 CHKPNT/RESTART/FORMAT CHANGE



FORMAT 11 CHKPNT/RESTART/FORMAT CHANGE

THE RESPONSE OF SHELLS TO
DISTRIBUTED RANDOM LOADS USING NASTRAN

By Gary K. Jones

Goddard Space Flight Center

SUMMARY

The performance of the NASTRAN modal random response analysis, rigid format 11, was investigated using a hypothetical stiffened cylindrical shell excited by a simulated turbulent boundary layer pressure field. The cylindrical shell (2.54 meters in diameter, 3.353 meters in length) was simply supported at both ends. In order to assess the effect of the model detail on the results, two models were developed. One model had 360 degrees of freedom and the other 720 degrees of freedom. The real part of the forcing function (co-spectral density) was represented by an exponentially decaying cosine function and the imaginary part of the forcing function (quad-spectral density) was represented by an exponentially decaying sine function. Problems associated with NASTRAN operations were encountered, but to a large extent, were successfully resolved. Only the random response (displacement spectral density) obtained for the 360 d.o.f. model is presented in this paper. No response data for the complex model (720 d.o.f.) is presented inasmuch as this portion of the investigation is still in progress.

INTRODUCTION

The analytical prediction of the structural response of aerospace vehicles to random forces is of key concern to aerospace engineers. The designer must assess the structural effects of the random input forces in an effort to achieve an adequate structural design. The task of determining analytically the structural response to distributed random forces is in general quite involved and time consuming.

The purpose of this paper is to describe the use of NASTRAN in determining the dynamic response of a cylindrical shell excited by a simulated turbulent boundary layer pressure field. One result of this effort is an assessment of how well the modal random response portion of NASTRAN performs. Although all dimensions, loads and results are expressed in SI units in the paper, the calculations were performed using English units.

DESCRIPTION OF THE PROBLEM

The hypothetical structural system used in this analysis was a 2.54 meter diameter, 3.353 meter long shell that was simply supported at both edges. The shell structure was assumed to be constructed of aluminum honeycomb (.0254 meter thick core with .002 meter face sheets), together with integral longitudinal and circumferential stiffeners (.0254 meter square, .002 meter thick wall, aluminum tubing). The longitudinal stiffeners were spaced every 36 degrees around the cylinder and the circumferential ring stiffeners were axially spaced .559 meters apart.

The random forcing function was selected so as to approximate, at least in form, a turbulent boundary layer loading function (Ref. 1). For a given pair of grid points u and v , the spectral density (PSD) of the loading function was defined as:

$$\text{PSD}_{u,v}(\xi, \eta, f) = \begin{cases} 0. N^2/\text{Hz} & f < 100 \text{ Hz}, f > 300 \text{ Hz} \\ .317 [\cos 3.94\eta - i \sin 3.94\eta] e^{-0.05\xi - .984|\eta|} & 100 \text{ Hz} \leq f \leq 300 \text{ Hz} \end{cases}$$

f = frequency, Hz

$i = \sqrt{-1}$

ξ = circumferential distance between grid points u and v , degrees (less than 180 degrees)

η = axial distance between grid points u and v, meters

Note that for the case $u = v$ we have $\xi = 0$, $\eta = 0$ and the function is real valued:

$$\text{PSD}_{u,v}(0,0,f) = \begin{cases} 0.0 \text{ N}^2/\text{Hz} & f < 100 \text{ Hz}, \quad f > 300 \text{ Hz} \\ .317 \text{ N}^2/\text{Hz} & 100 \text{ Hz} \leq f \leq 300 \text{ Hz} \end{cases}$$

For the case $u \neq v$ the function is complex. The real part (co-spectral density) was represented by a decaying cosine function and the imaginary part (quad-spectral density) by a decaying sine function. Note that in matrix formulation the loading function leads to a hermitian spectral density matrix which is required by the physics of the problem. The structural damping constant was assumed to be .02 (i.e. $Q = 50$) for this investigation.

NASTRAN ANALYSIS

The NASTRAN analysis flow diagram is illustrated in Figure 1. The analysis was performed in four steps.

1. Finite element models of the shell structure were developed.
2. Modal analyses (rigid format 3) were performed using NASTRAN and a restart tape and deck were generated.
3. A computer program was written to generate a NASTRAN input tape that contained the NASTRAN executive deck, case control deck, and required random input deck.
4. Using as input the tapes generated in the previous step and the NASTRAN restart tapes from the modal analyses, the NASTRAN random response analyses (rigid format 11) were performed. Note that the normal NASTRAN JCL had been modified so as to accept tape input rather than cards.

Two NASTRAN finite element models (Figure 2 and 3) of the same axisymmetric shell structure were developed in order to assess the effect of the model detail on the results. The small model (model 1) consisted of 70 grid points, 360 degrees

of freedom, 100 CBAR structural elements and 60 CQUAD1 structural elements. The large model (model 2) had 140 grid points, 720 degrees of freedom, 140 CBAR structural elements, and 120 CQUAD1 structural elements. Note that the grid pattern in model 1 follows the stiffener pattern in the shell, and that the model 2 grid pattern has twice the number of circumferential grid points as has model 1. The edge grid points in both models were constrained so as to simulate a simply supported condition. Due to the symmetry of the input force field and the structure, the response at 3 grid points (2, 3 and 4) for model 1 and at 6 grid points (2, 3, 4, 9, 10 and 11) for model 2 were sufficient to define the response of the entire structure.

The modal analysis (step 2) was accomplished with little difficulty and the results summarized in Table 1. Shell model 1 was found to have 12 modes in the frequency range of interest (100 - 300 Hz); however, due to the axisymmetric character of the structure only 7 distinct modes were obtained. Shell model 2 was found to have 20 modal frequencies and 10 distinct modes in the 100 - 300 Hz band. As can be seen from Table 1, there was a considerable difference in the modal frequencies obtained from the analyses of the two models. While the modes of the complex model (720 d.o.f.) more accurately reflect the dynamic properties of the shell; either modal set may be used with equal validity in determining NASTRAN's ability to calculate random response.

An auxiliary Fortran program (step 3) was written by the author that would:

- Generate the random input loads for all the unconstrained grid points from the basic equation of the loading spectral density.
- Generate a digital tape having the appropriate case control, executive control and random loading cards necessary to execute NASTRAN rigid format 11.

The requirement for this program was due to the large number of random loading cards used as input into NASTRAN. The model 1 NASTRAN deck contained 1275 random loading cards (RANDPS) and the model 2 deck contained 5050 random loading cards.

Step 4 in the analyses, the NASTRAN modal random response (rigid format 11), makes use of modal data to derive a dynamic transfer function for a set of input frequencies and then using the input random loads to calculate the structural response at those frequencies.

While steps 1, 2 and 3 were performed with little difficulty, considerable difficulty was encountered in performing the random analyses (step 4). To enumerate the problems with NASTRAN in the sequence that they occurred:

- The first computer runs with rigid format 11 were made to determine the response of model 1 at 49 frequencies using level 11.1 NASTRAN. The result in all cases was an OCO error occurring in the matrix multiplication routine (MPYAD). The OCO, which is an IBM System 360 error code, indicates an imprecise interrupt which can be due to a variety of program errors.
- Later runs, using level 12.0 NASTRAN to solve the same problem, yielded a B-37 error in the SDR2 module. The B-37 which also is an IBM System 360 error code, indicates that not enough peripheral (disk) storage space was available to execute the desired operation.
- Reducing the number of frequencies from 49 to 14 for the model 1 analyses resulted in wrong values of random response being given by the program. This problem was traced to an error in the "method 2" routine in the MPYAD module in NASTRAN. By reducing the number of frequencies to 9 or less, apparently correct answers were obtained inasmuch as this change caused the "method 1" routine in MPYAD to be used.

In spite of these difficulties, the random response of model 1 was obtained using NASTRAN. The analysis of the random response of model 2 has encountered problems similar to, but more severe than those of model 1.

To be specific, for the model 2 analysis, it appears that a maximum of only 3 frequencies can be input per computer run if one is to avoid using the "method 2" routine in the MPYAD module. At this stage in the investigation, the random response of model 2 has been obtained for only a few frequencies.

Presented in Table 2 are the computer run times for the various size rigid format 11 analyses. Note that it is most efficient from the computer-run-time point of view to input as many frequencies as possible per run; however, as long as the "method 2" routine of the MPYAD module gives the wrong answers, the analyst is severely limited in the number of frequencies that can be input in any one computer run.

DISCUSSION OF THE RESULTS OF THE ANALYSES

The random response (i.e. displacement spectral density) of shell model 1 (360 d.o.f.) obtained using NASTRAN is presented in Figure 4. Due to the problems mentioned in a previous section, the analysis of the complex shell model (model 2, 720 d.o.f.) has not yet been completed, thus no data for this configuration will be presented even though the output spectra at a few frequencies have been determined.

No experimental data or closed form solutions were available to check the results obtained for the shell response, however, checks with relatively crude hand calculations indicated that the NASTRAN calculated response seemed reasonable. With one exception, the responses at the 3 grid points were quite similar. At grid point 4, there apparently was no response for modes in the frequency range of 258 - 260 Hz. This peculiarity was attributed to the fact that these modes have node points at grid point 4.

The effect on the response spectral density of the quad-part of the input loading spectral density was numerically assessed by setting this part of the input equal to zero for one computer run. Comparison of the response spectrum for the zero-quad run and non-zero-quad runs indicates that the input quad spectral density had little effect (~1%) on the output displacement spectral density.

CONCLUSIONS

Based upon this investigation, the following conclusions were reached:

- The use of NASTRAN to determine structural response to distributed random force fields is practicable, provided

level 12.0 NASTRAN is used and the use of "method 2" in the MPYAD module is avoided.

- The capability of NASTRAN to analyze large structural response problems would be considerably enhanced if the "method 2" routine in the MPYAD module is debugged.
- An effort should be made to determine the feasibility of including in NASTRAN an automated scheme to generate the required random input data. If this feature could be implemented, the analyst's task would be significantly reduced.

REFERENCE

1. Jacobs, L. D., Lagerquist, D. R., and Gloyna, Fred L.: Response of Complex Structures to Turbulent Boundary Layers. Journal of Aircraft, May-June 1970, pp. 210-219

n	m	Model 1 360 d.o.f.	Model 2 720 d.o.f.
4	1	154.4, 154.4 Hz	130.7, 130.7 Hz
3	1	149.8, 149.8 Hz	131.4, 131.4 Hz
5	1	170.2 Hz -	160.7, 167.4 Hz
2	1	187.5, 187.5 Hz	175.8, 175.8 Hz
4	2	258.4, 258.4 Hz	214.5, 214.5 Hz
6	1	- -	217.3, 217.3 Hz
5	2	259.2 Hz -	219. , 228.5 Hz
3	2	- -	243.7, 243.7 Hz
6	2	- -	259.9, 259.9 Hz
1	1	280.4, 280.4 Hz	276.8, 276.8 Hz

n number of circumferential waves
m number of axial half waves

MODAL FREQUENCIES

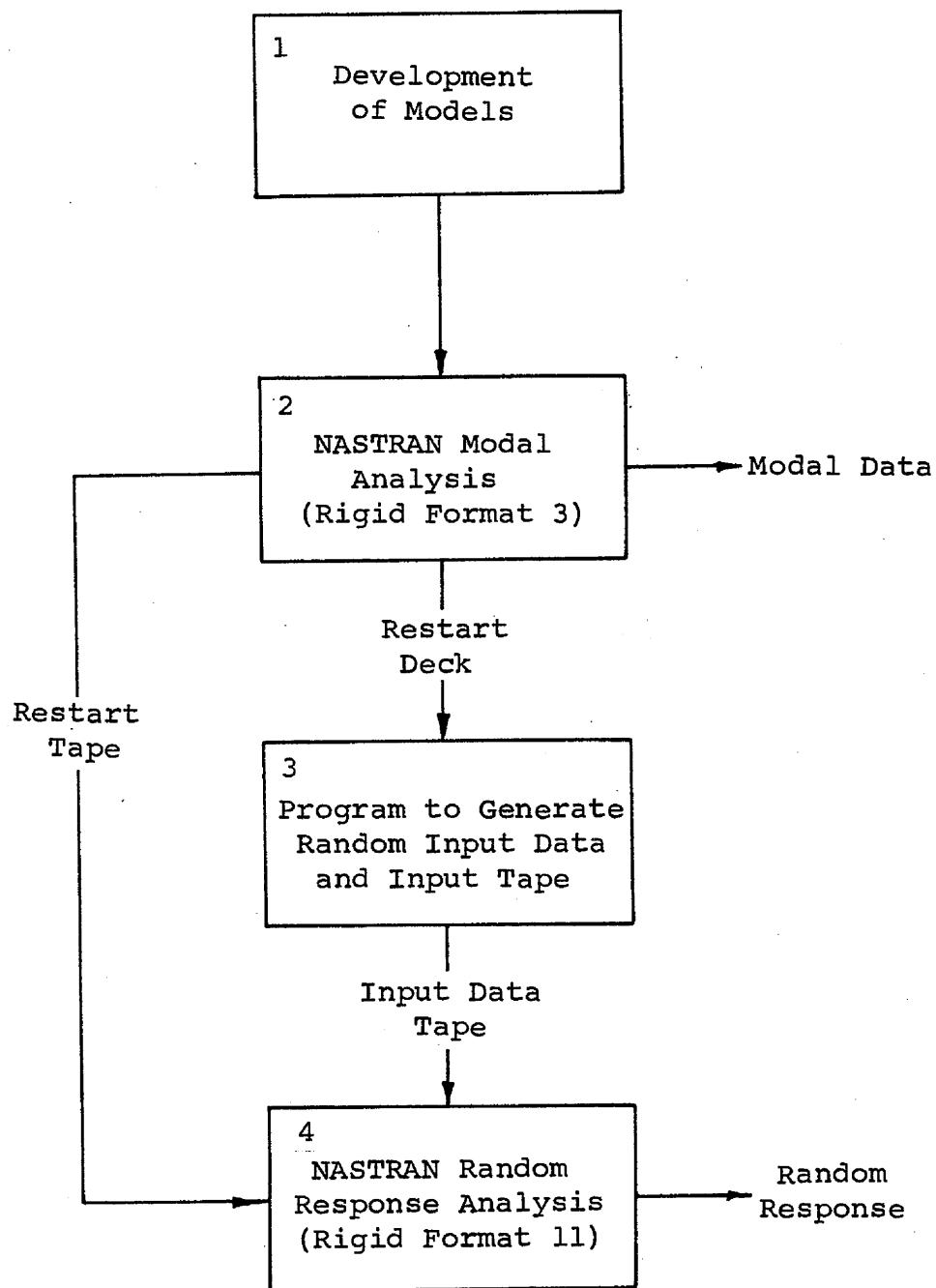
TABLE 1

Item	Computer Time (Min)	Computer Time Per Frequency (Min)
Model 1 360 d.o.f. 7 Freq.	10.6	1.51
Model 1 360 d.o.f. 9 Freq.	12.5	1.39
Model 1 360 d.o.f.* 14 Freq.	16.6	1.19
Model 2 720 d.o.f. 2 Freq.	15.4	7.70

*Gave wrong answers.

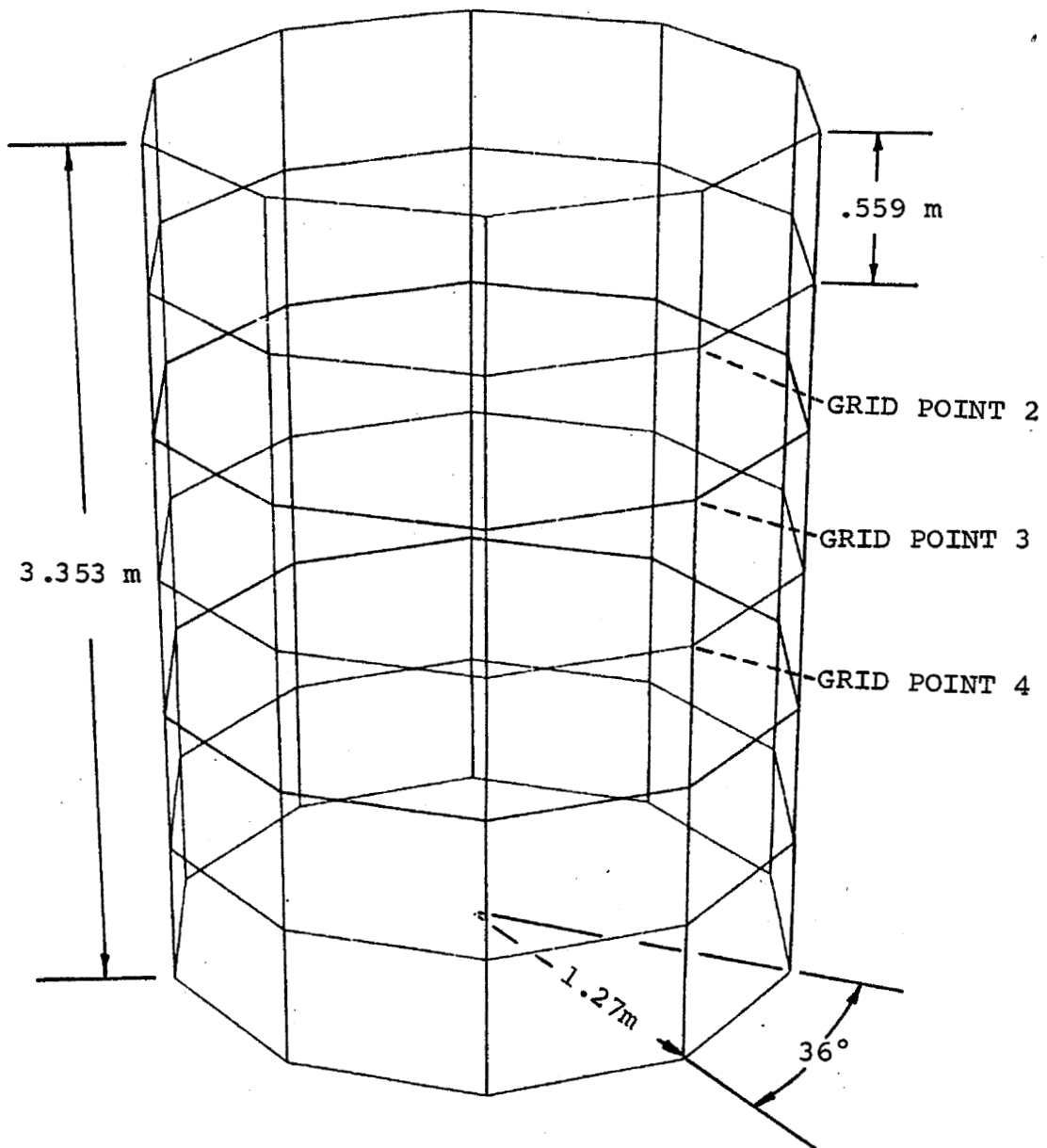
COMPUTER RUN TIMES

TABLE 2



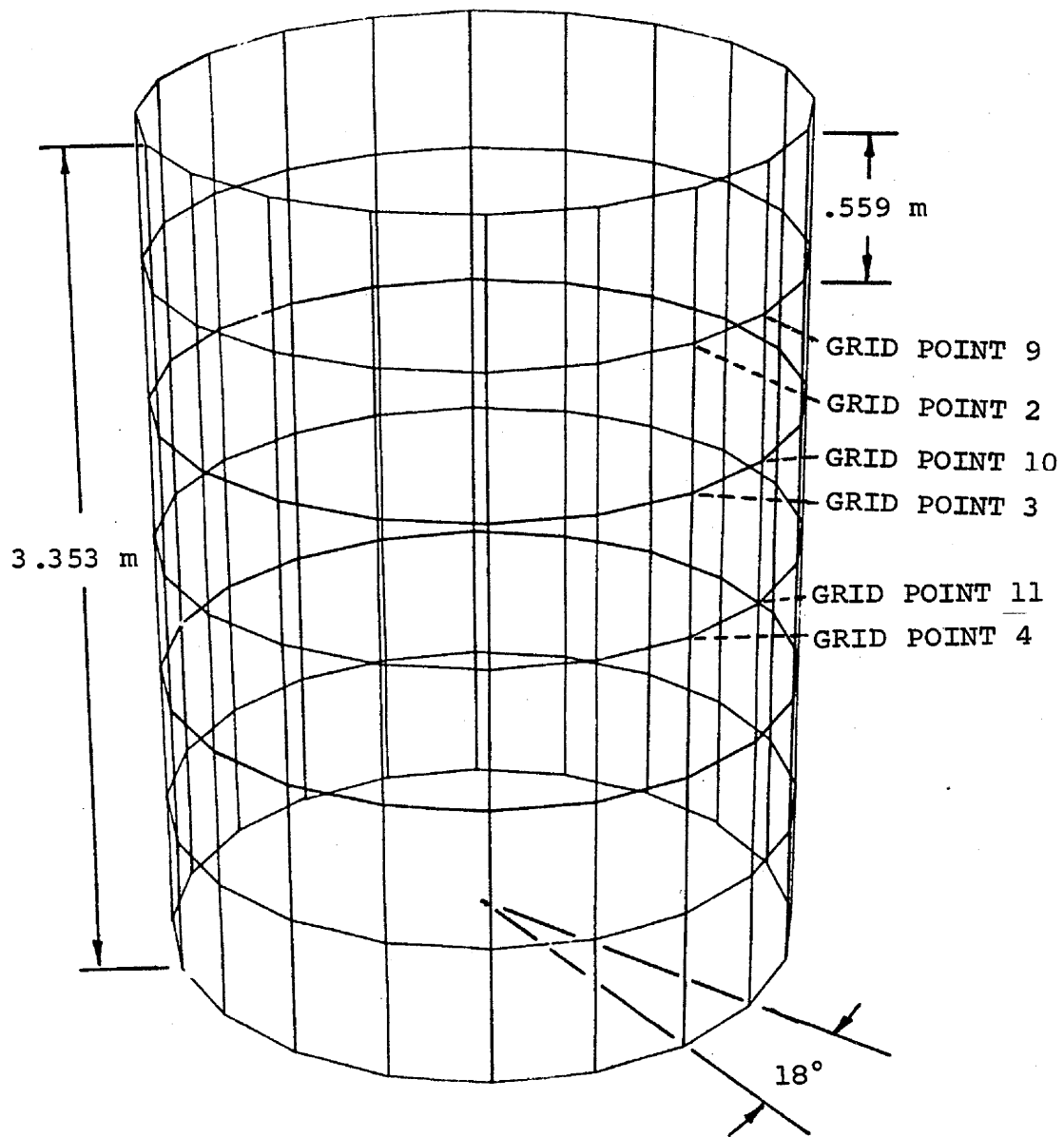
ANALYSIS FLOW DIAGRAM

FIGURE 1



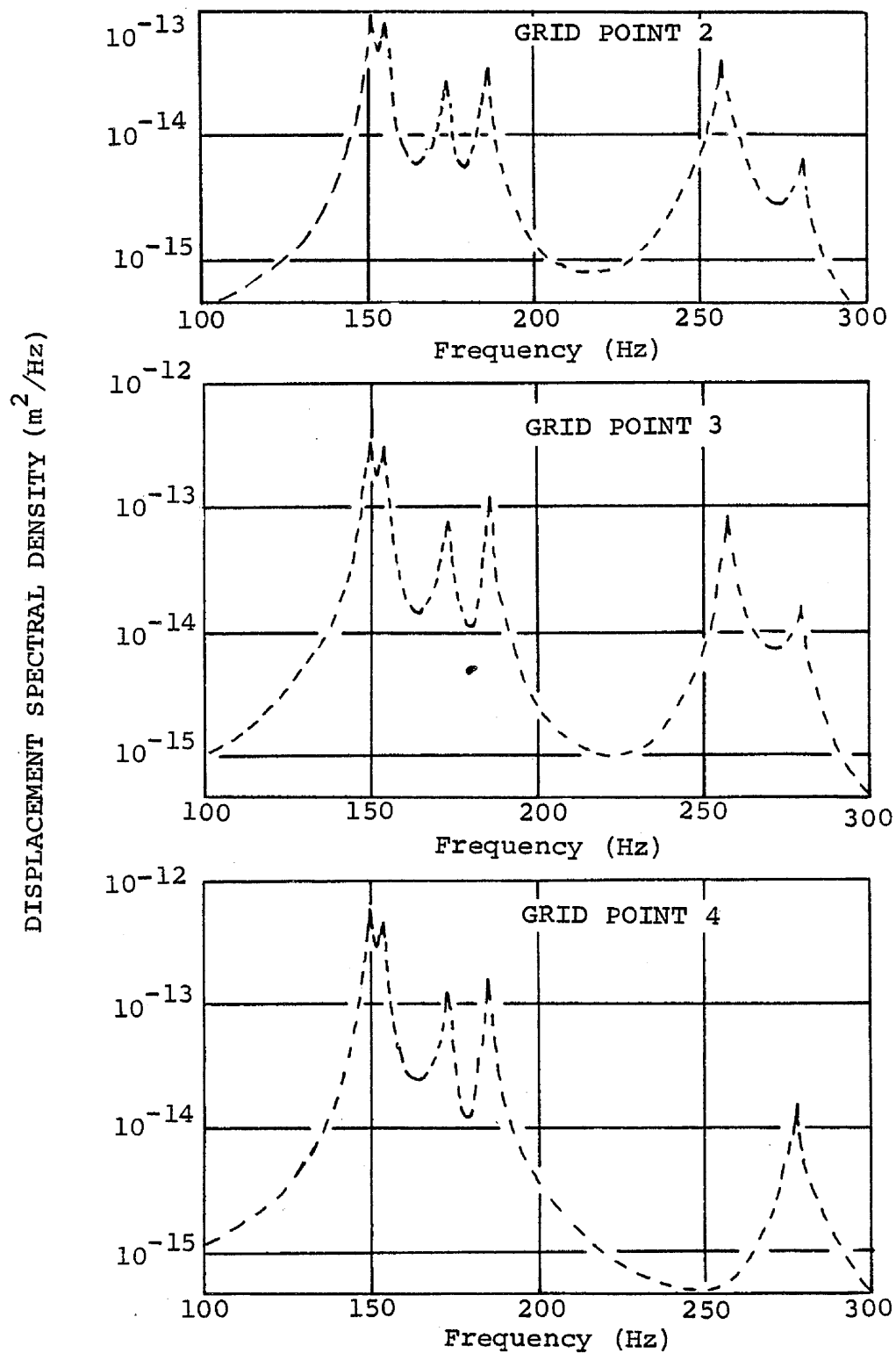
SHELL MODEL 1

FIGURE 2



SHELL MODEL 2

FIGURE 3



SHELL MODEL 1 DISPLACEMENT SPECTRAL DENSITY
FIGURE 4

APPLICATIONS OF NASTRAN TO COUPLED STRUCTURAL AND HYDRODYNAMIC
RESPONSES IN AIRCRAFT HYDRAULIC SYSTEMS

By James T. Howlett
NASA Langley Research Center

SUMMARY

This paper demonstrates that the NASTRAN computer program can be used to analyze the coupled fluid and structural responses of multibranch pipes as occur in aircraft hydraulic systems. The techniques used to model hydraulic lines with NASTRAN are explained. Example problems are presented which demonstrate the validity of the analytical model for a simple standpipe system and which demonstrate that the technique is promising as a basis for detailed dynamic analysis of hydraulic systems of actual aircraft.

INTRODUCTION

Modern high-performance aircraft require increasingly efficient hydraulic systems in order to perform effectively. These hydraulic systems operate at much higher static pressures than in the past and the piping and other associated equipment is usually designed to obtain minimum weight. These conditions of high operating pressures and minimum weight, together with pressure ripples and surges introduced by pumps and other items of equipment, produce coupled fluid-structural vibrations which must be considered in the design of the hydraulic system. Although much work, both experimental and analytical, has been done on hydraulic systems (for example refs. 1 to 5), previous workers in the field have largely neglected the coupled fluid and structural vibrations. Some research has been done in this area (refs. 2 to 4, for example), but present capabilities fall far short of the necessary ability to accurately predict coupled responses in practical situations.

This paper presents the initial results of a research effort to develop analytical procedures for predicting the coupled fluid-structural responses of aircraft hydraulic systems. The NASTRAN computer program has been an important part of this effort. The bar elements in NASTRAN have been used to develop an analytical model of a piping system filled with fluid. This analytical model includes the coupled interactions between the motion of the fluid and the motion of the pipes, as well as the effects of joints where several sections of pipe are joined. The flexibility of NASTRAN in allowing the user to specify multi-point constraints is an essential ingredient of the analytical approach. The paper presents a structural analogy which is the basis for the analytical model, describes the implementation of this analytical model on the NASTRAN computer program and then concludes with some examples which demonstrate the validity of the approach and indicate how the method can be applied to the analysis of hydraulic systems on realistic aircraft.

Preceding page blank

SYMBOLS

A	cross-sectional area
B	bulk modulus of fluid
c	speed of sound in fluid
E	Young's modulus
p	pressure
u	axial displacement of pipe
ξ	axial displacement of fluid
ρ	density
Subscripts:	
1,2,3,4	stations in standpipe configuration

ANALYTICAL MODEL

The purpose of this section is to explain the techniques used to model hydraulic lines with NASTRAN. The analogy between the motion of a column of fluid and the longitudinal motion of a bar is developed and the implementation of this structural analog on the NASTRAN computer program is described.

Structural Analogy

An idealized section of hydraulic system line is shown in figure 1, where solid lines are used to represent the pipe and dashed lines are used to represent the fluid inside the pipe. The equation of motion satisfied by the column of fluid inside the pipe is the classic one-dimensional wave equation

$$\frac{\partial^2 \xi}{\partial t^2} = c^2 \frac{\partial^2 \xi}{\partial x^2} \quad (1)$$

where ξ = longitudinal displacement of fluid

x = longitudinal distance along pipe

$$c = \sqrt{\frac{B}{\rho}}$$

B = bulk modulus of fluid

ρ = fluid density

Equation (1) is the same equation as that for longitudinal motion of a bar where

c is the speed of sound in the bar or $\sqrt{\frac{E}{\rho}}$, E is Young's modulus and ρ

is the material density of the bar. This structural analogy is used to represent the fluid inside the pipe. Thus the coupled fluid-pipe system is represented as a bar within a bar. The fluid bar is considered to have axial stiffness only, whereas the pipe is considered to have both axial and bending stiffness. For the fluid bar, the value of the bulk modulus B is used in place of Young's modulus E and the fluid density ρ is used in place of the material density.

In the axial direction, the pipe and the fluid are uncoupled, except for capped ends, bends in the pipe, or points at which two or more different pipes are joined. In the lateral direction, the fluid is constrained to move with the pipe so that the mass of the fluid does affect the bending motion of the pipe.

Fluid pressure is analogous to stress in a bar. The following table summarizes and compares end conditions for some cases of interest.

TABLE 1.- END CONDITIONS ON FLUIDS AND PIPES

Bar	Fluid
Free end: stress = $-E \frac{\partial u}{\partial x} = 0$	Open end: pressure = $-B \frac{\partial \xi}{\partial x} = 0$
Clamped end: $u = 0$	Capped end of rigid pipe: $\xi = 0$
	Capped end of elastic pipe: $\xi = u$

At joints in the piping system the structural analogy breaks down to some extent, and special equations of constraint must be written to describe the coupling between the various parts of the system. The sections of pipe are joined with the standard structural constraints. The fluid in any section of pipe moves with the pipe laterally as discussed above. The equations of constraint for the fluid are equality of pressures at the joint and the conservation of mass in the joint. If conservation of mass is imposed at the joint and the principle of minimum energy is used to obtain the equations of motion, then the equality of pressures emerges as a natural boundary condition. Thus the equality of pressures at the joint need not be specified as an additional constraint and only the conservation of mass is required. In the present analysis, the joint is assumed to be a small section in which the constrained fluid at any instant of time is incompressible. This assumption implies that the conservation of mass in the joint becomes conservation of volume. The volume of fluid flowing into the joint must equal the volume of fluid flowing out of the joint.

Consider, for example, the configuration shown in figure 2. Let A_L and A_R be the cross-sectional area of the fluid in the left and right-hand pipes,

respectively. Similarly, let u_l, ξ_l and u_r, ξ_r be the axial displacements of the pipe and fluid of the left and right-hand sections at the joint. Assume that u_l, ξ_l are positive coming into the joint and u_r, ξ_r are positive going out of the joint. The equation for conservation of volume at the joint is

$$A_l (\xi_l - u_l) = A_r (\xi_r - u_r)$$

or

$$A_l \xi_l - A_l u_l - A_r \xi_r + A_r u_r = 0 \quad (2)$$

For the special case of a rigid pipe the motion of the pipe does not enter into the problem and the constraint at the joint which corresponds to equation (2) is

$$A_l \xi_l - A_r \xi_r = 0 \quad (3)$$

Equation (2) is readily generalized for the case where several pipes come together at a joint.

NASTRAN Model

The analytical representation of the interaction of fluid-pipe motion as described previously is accomplished with NASTRAN by using CBAR elements. A straight section of pipe filled with fluid is shown in figure 3, together with a finite element breakdown and the associated NASTRAN grid points. As indicated in figure 3, the same finite element breakdown is used for both the fluid and the pipe. Distinct grid points are used for fluid elements and pipe elements, although the grid points for the pipe elements are at the same physical locations as the grid points for the fluid elements.

Consider, first, the NASTRAN representation for the fluid. Each fluid element is represented by a CBAR element, with the bulk modulus of the fluid being input to the program in place of Young's modulus and the fluid density input in place of the density of the structural material. In order to give these fluid elements zero bending stiffness, the moments of inertia are input as zero. The fluid elements in a straight section of pipe are joined the same way as structural elements are joined; that is, a common grid point is used at the juncture between elements.

The pipe is represented in NASTRAN in the standard way. It is important to remember that the grid points for the pipe are distinct from the grid points for the fluid although they have the same physical locations.

The fluid and pipe are coupled by using multipoint constraints. Except for the displacement in the axial direction, the fluid grid points are

constrained to have the same displacements as the pipe grid points. In the axial direction, the fluid and pipe are uncoupled, except at capped ends and joints. At a capped end, the fluid displacement is equated to the pipe displacement (see Table 1). At each joint, equations of constraint expressing the conservation of volume are imposed (see, for example, equation (2)). It should be noted that this method of modeling joints requires that a distinct grid point must be used for each end of each column of fluid entering the joint. In order to simplify bookkeeping, a separate grid point is also used for the end of each pipe entering the joint. Then the following three conditions are imposed by the use of the NASTRAN multipoint constraint feature:

1. Conservation of volume at the joint
2. Equality of lateral motions of fluid and pipes at the joint
3. Desired compatibility between the structural elements entering the joint

APPLICATIONS

Standpipe System

To demonstrate the validity of the approach which has been described, a simple standpipe system was analyzed (fig. 4). The structure is steel pipe with 2.54 cm outside diameter and a wall thickness of 0.305 cm. One end of the horizontal pipe is open; the other end of the horizontal pipe and also the upper end of the vertical pipe are capped. The open end of the horizontal pipe is clamped and the downstream end is restrained from moving vertically at a point 0.203 m from the capped end. The fluid in the pipe is water and the speed of sound in water is taken to be 1478 m/s. The system is viewed as six separate parts which are joined as previously described. Each of the three fluid columns and each of the three pipes is represented by 10 CBAR elements in NASTRAN. The fluid is forced at the open end of the main pipe with a harmonically oscillating pressure of amplitude 6900 N/m². The system was analyzed first considering the pipes to be rigid. Frequency response results were computed using rigid format 8 and the pressure ratios p_2/p_1 , p_3/p_1 , and p_4/p_1 are compared in Table 2 to exact values obtained by using the equations presented in reference 4. The NASTRAN values have been faired to obtain the pressure at the ends of the elements since NASTRAN outputs the average axial stress (pressure) in an element. As the table indicates, the agreement is quite good.

Pressure distributions throughout the system with rigid pipes, computed at a frequency of 485 Hz, are shown by the solid curves in figure 5. For convenience, the three sections of pipe are shown separated in the figure. The forcing frequency, 485 Hz, is of particular interest because it is the first organ pipe frequency of the standpipe. As is well known for the case of a rigid structure, the pressure in the main line downstream of the standpipe should be zero at this frequency. As shown by the solid curves in figure 5, this phenomenon is predicted by the present analysis.

TABLE 2.- COMPARISON OF PRESSURE RATIOS PREDICTED BY NASTRAN TO THOSE PREDICTED BY EXACT THEORY FOR THE CASE OF A STANDPIPE

f, Hz	P ₂ /P ₁		P ₃ /P ₁		P ₄ /P ₁	
	NASTRAN	Exact	NASTRAN	Exact	NASTRAN	Exact
375	-0.26	-0.26	-0.38	-0.38	-0.76	-0.76
400	-.21	-.21	-.32	-.32	-.77	-.76
450	-.1	-.1	-.18	-.18	-.9	-.89
485	0	0	0	0	-1.16	-1.16
500	.07	.07	.14	.14	-1.39	-1.38
550	1.28	1.27	3.35	3.39	-6.03	-6.04

Figure 5 also shows results for the pressure distribution when the pipes are considered to be elastic. The distribution is slightly different than that for a rigid structure, as shown by the dotted curves. For instance, the pressure in the main line downstream of the standpipe, although relatively small, is no longer precisely zero. The overall pressure distributions are not much different for the two cases. However, there definitely is coupling between the motion of the fluid and the motion of the structure. The effect of this coupling is shown in figure 6, which presents a plot of the lateral displacement of the structure along the various lengths of pipe. As indicated in the figure, the structure does undergo bending deformation due to axial forcing of the fluid at the open end of the pipe. If the frequency of the forcing function happened to be near a natural frequency of the system, the structure would oscillate at large amplitudes. This demonstrates the importance of considering the coupled fluid and structural motion of hydraulic systems.

Realistic Airplane Hydraulic System

Figure 7 shows a sketch of the pressure distributions predicted by the analysis for a large segment of the hydraulic system on an actual developmental fighter airplane. Although the system was modeled in three dimensions, the piping is shown straightened and flattened out for clarity of presentation. The structure is assumed to be rigid and 277 elements were used to model the fluid in NASTRAN. The sections indicated as filter module (FM) and pressure module (PM) were actually rather complicated components of the hydraulic system but were modeled as short sections of pipe with diameters much larger than those of the main line. The analytical model includes approximately 14 m of pipe with a total of six different diameters. The ends of the pipe are assumed to be capped at the positions indicated as direct lift control (DLC) and high lift gear box (HLGB). The forcing function is a harmonically oscillating pressure at a frequency of 700 Hz having an amplitude of 6900 N/m² at the pump outlet.

One limitation of this method is the large size of the problem when the complete hydraulic system is analyzed. In the present case, for example, only a rigid structure is considered and the problem has 277 degrees of freedom. If the elasticity of the structure is included, the size of the problem increases by about a factor of 6, and the analysis would become expensive. One possible method of avoiding this difficulty is to consider only part of the structure as elastic, although such a procedure has some obvious drawbacks and should be used with care. Another technique which could be very useful in solving coupled fluid-structural problems is the use of substructuring. The present method is well adapted to substructuring because of the small number of degrees of freedom at the joints. Incorporation of substructuring capability into NASTRAN could provide an efficient way to analyze aircraft hydraulic systems.

This example does demonstrate the potential of the method for analyzing the effects of pressure ripples on large sections of hydraulic lines of actual aircraft. As figure 7 shows, at a frequency of 700 Hz the large volume of fluid in the filter module significantly attenuates the pressure downstream, except in the short line leading to the direct lift control. The pressure module further attenuates the downstream pressure. This attenuation of pressure by a large volume of fluid is in qualitative agreement with well-known classical results.

CONCLUDING REMARKS

This paper has demonstrated that the NASTRAN computer program can be used to analyze the coupled fluid and structural responses of multibranch pipes as occur in aircraft hydraulic systems. The multipoint constraint feature of NASTRAN is an important part of the analytical approach. Example problems have been presented which demonstrate the validity of the analytical model for the case of a simple standpipe system and which demonstrate that the technique is promising as a basis for detailed dynamic analysis of hydraulic systems of actual aircraft. Much work remains to be done, both analytically and experimentally, to develop techniques for using the approach to model parts of hydraulic systems other than the lines — such as pumps, manifolds, filters, valves, and structural joints.

REFERENCES

1. Davis, Don D., Jr.; Stokes, George M.; Moore, Dewey; and Stevens, George L., Jr.: Theoretical and Experimental Investigation of Mufflers With Comments on Engine-Exhaust Muffler Design. NACA Report 1192, 1954.
2. Regetz, John D., Jr.: An Experimental Determination of the Dynamic Response of a Long Hydraulic Line. NASA TN D-576, 1960.

3. Blade, Robert J.; Lewis, William; and Goodykoontz, Jack H.: Study of a Sinusoidally Perturbed Flow in a Line Including a 90° Elbow With Flexible Supports. NASA TN D-1216, 1962.
4. D'Souza, A. F.; and Oldenburger, R.: Dynamic Response of Fluid Lines. J. Basic Engineering, Trans. ASME Series D., Vol. 86, September 1964, pp. 589-598.
5. Lewis, William; Blade, Robert J.; and Dorsch, Robert G.: Study of the Effect of a Closed-End Side Branch on Sinusoidally Perturbed Flow of Liquid in a Line. NASA TN D-1876, 1963.

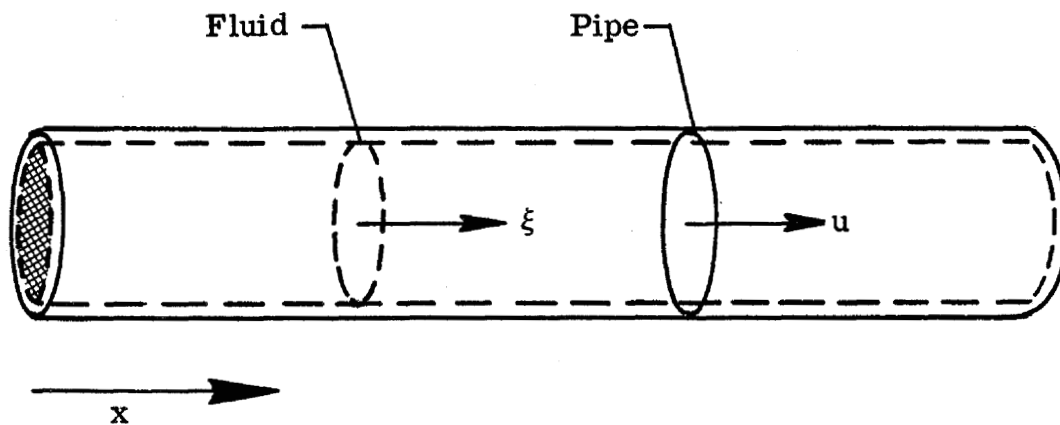


Figure 1.- Idealized section of a hydraulic line.

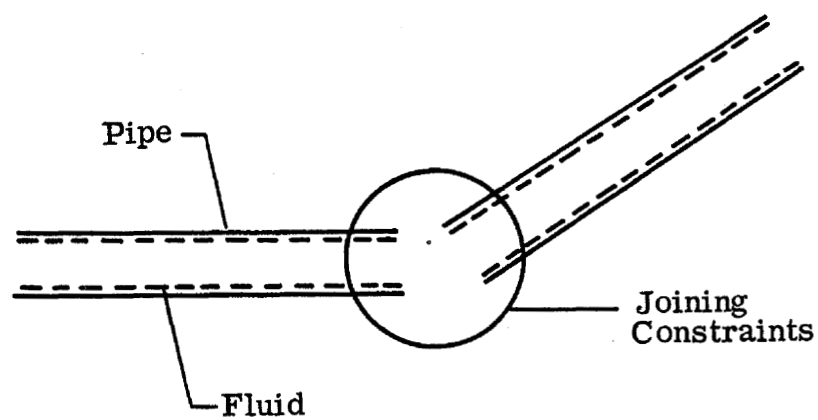


Figure 2.- Analytical model of fluid-structure interactions.

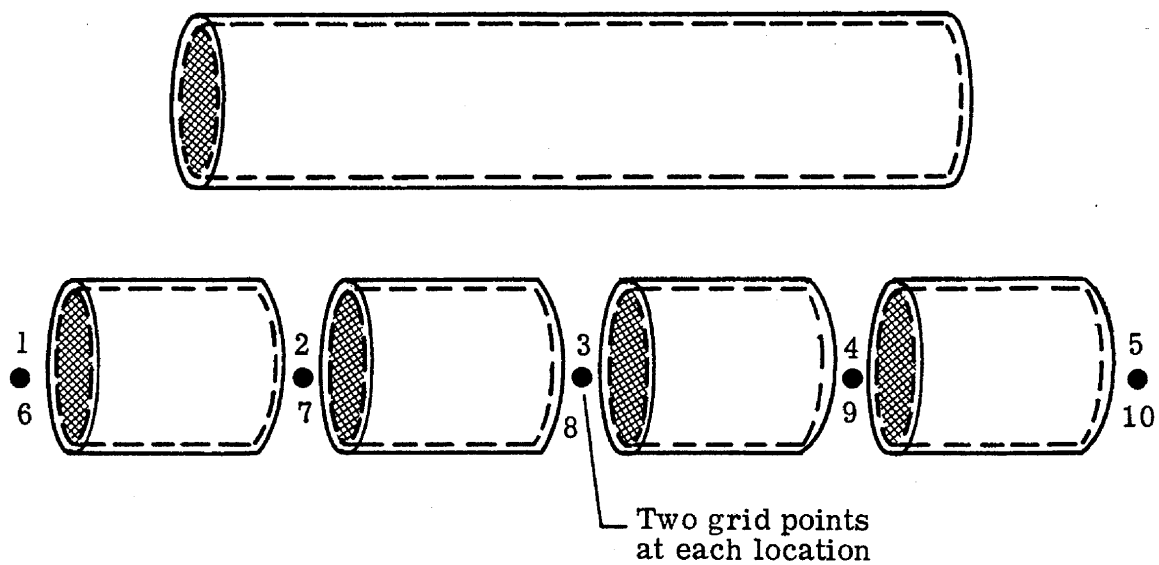


Figure 3.- NASTRAN model of fluid in a straight pipe.

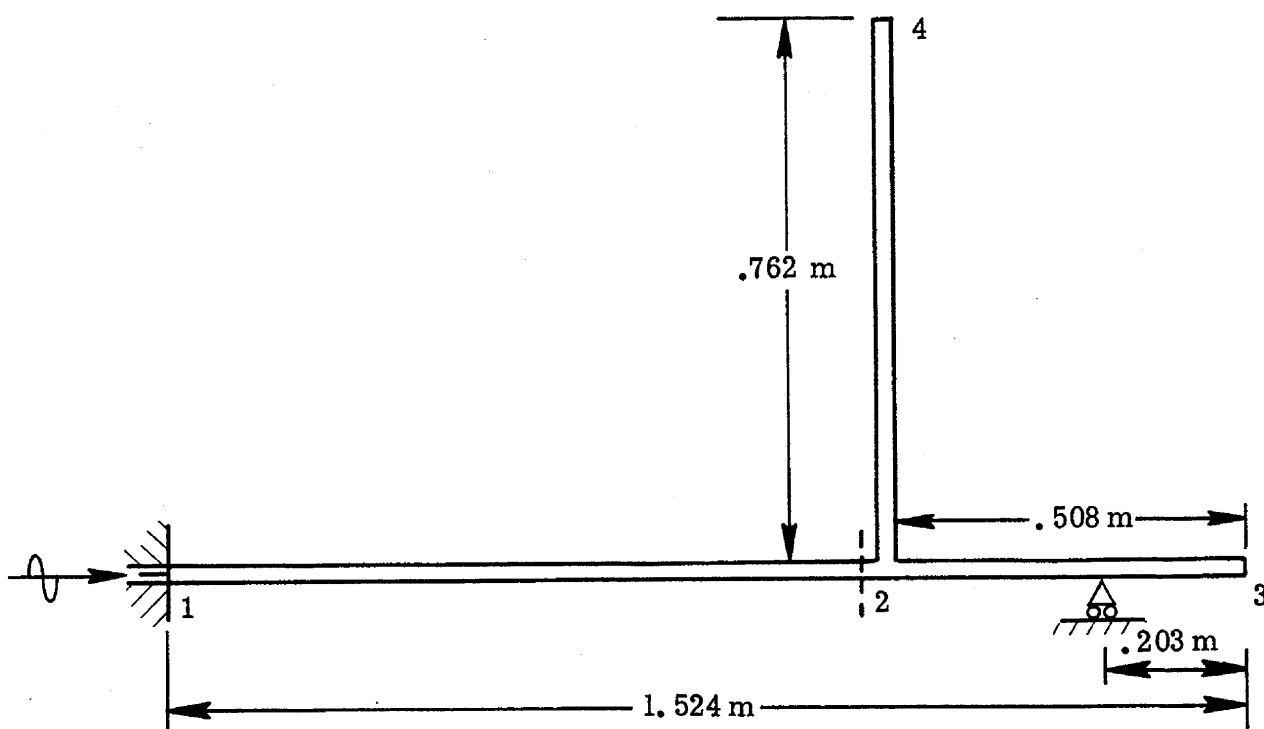


Figure 4.- Standpipe configuration analyzed.

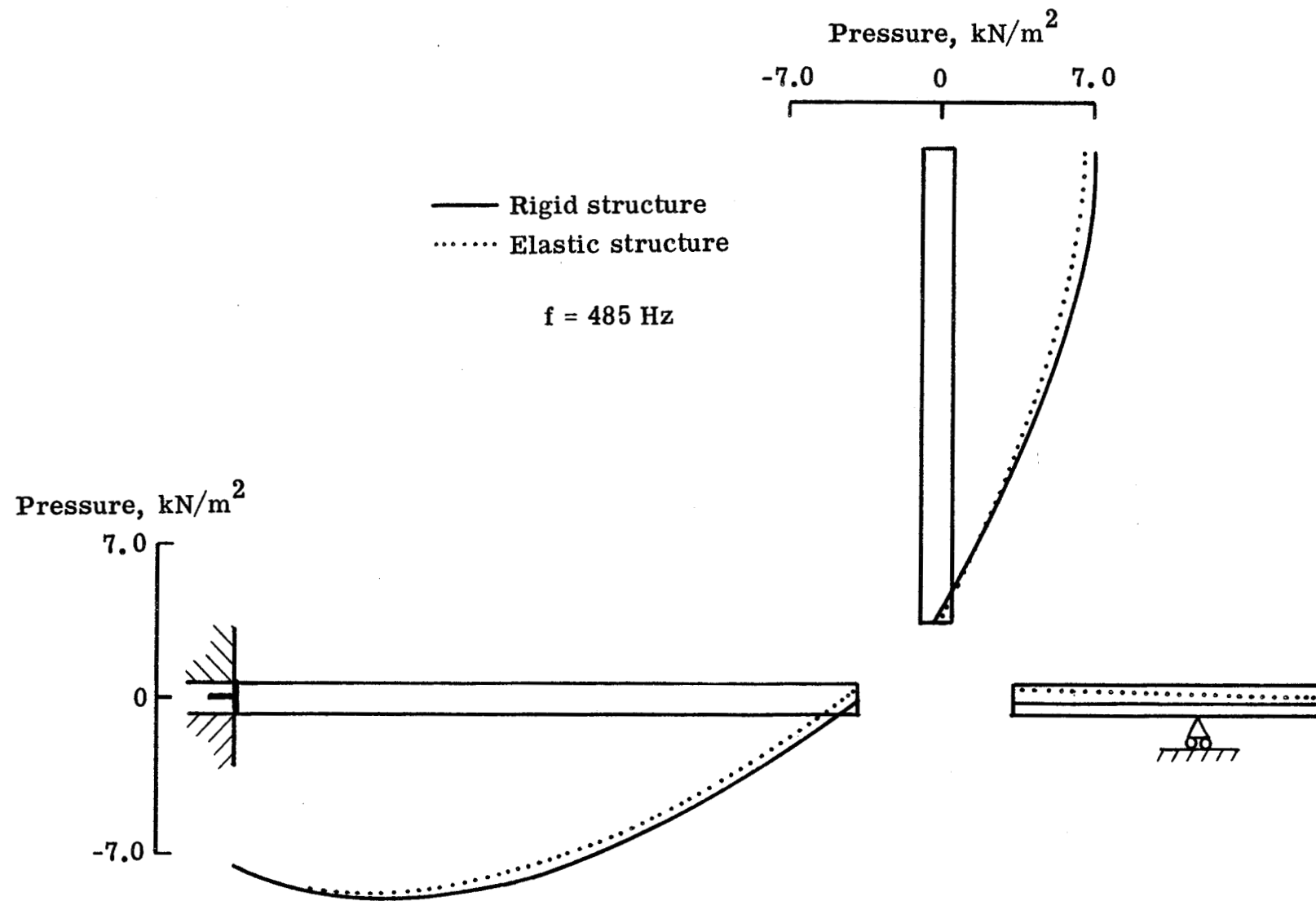


Figure 5.- Simulation of effect of standpipe.

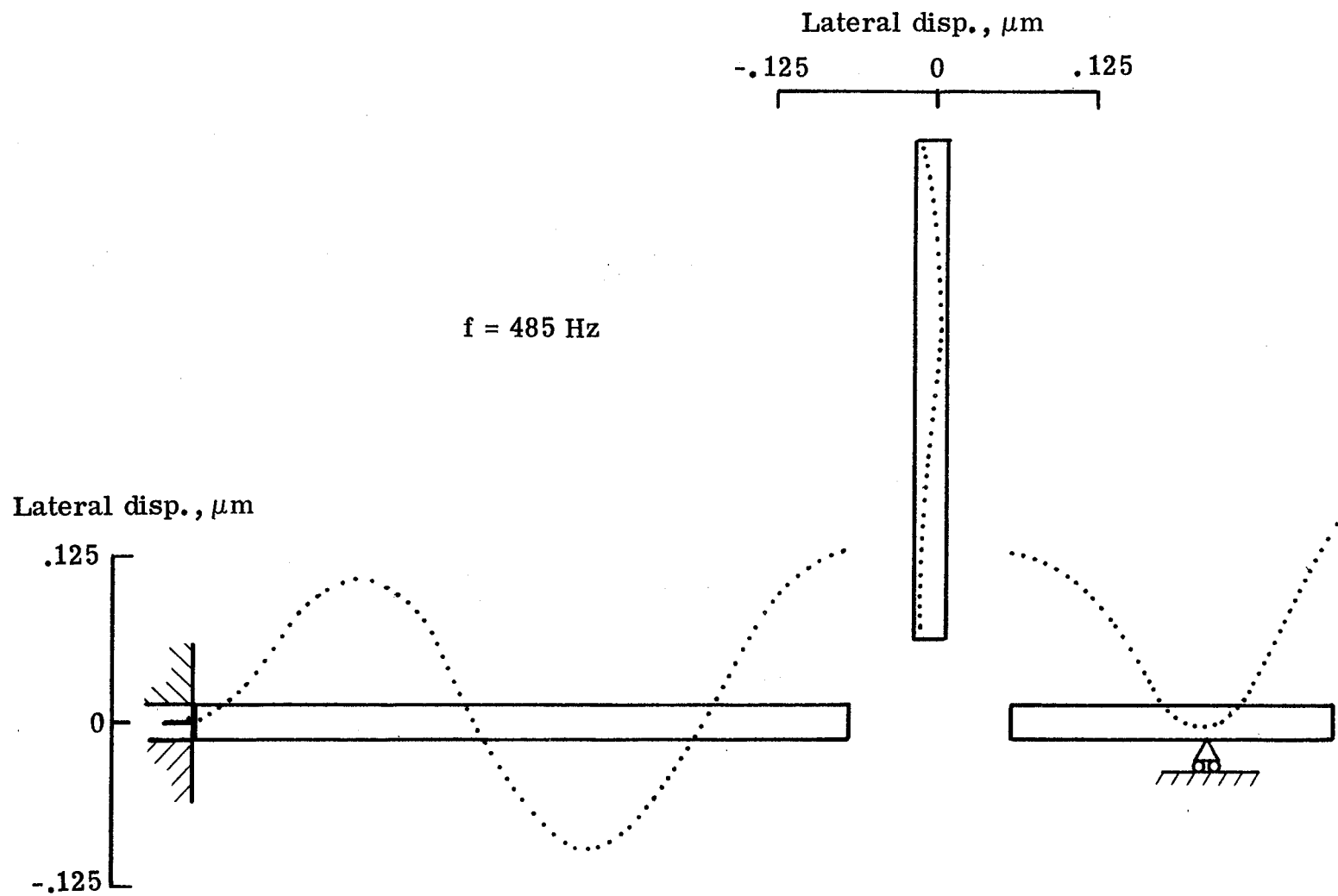


Figure 6.- Lateral response of standpipe structure.

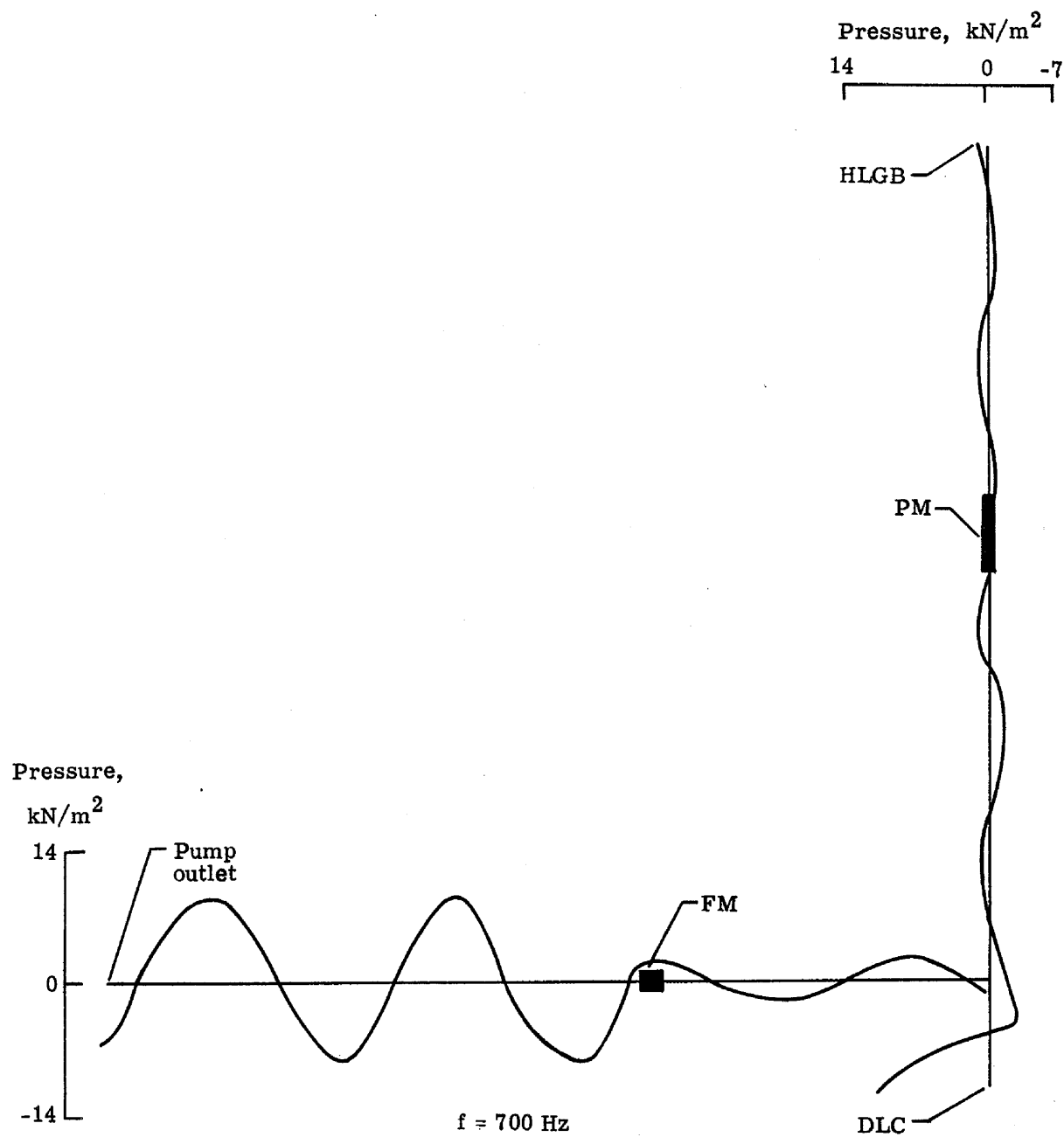


Figure 7.- Sketch of pressure distribution predicted for a section of an aircraft hydraulic system.

N71-36277

Application of NASTRAN to a Space Shuttle Dynamics Model

by E. A. Thornton

Old Dominion University

SUMMARY

A NASTRAN analysis of the normal modes of a 1/15 scale space shuttle dynamics model is described. Fuselage and wing components were analyzed first in a free-free condition and then assembled to give the complete model. The finite element idealization employed bar elements, concentrated masses, general elements and modeled rigid connections using multipoint equations of constraint. A Guyan reduction was used, and the eigenvalue problem for the complete model was solved using the Givens method.

INTRODUCTION

The determination of the dynamic characteristics of a spacecraft structure is always an important step in the development of the overall spacecraft system. This is particularly true for the space shuttle since a new concept in space vehicle design is being used. The space shuttle will be comprised of a parallel arrangement of the launch vehicle and space vehicle during the launch phase. This arrangement raises the possibility of dynamic effects not previously encountered.

To initiate dynamic studies of the space shuttle, Langley Research Center (LRC) designed and procured a 1/15 scale model of proposed straight wing and delta wing configurations of the shuttle. The vibration characteristics of this model are being analytically and experimentally investigated.

During an 11 week period at Langley Research Center in the summer of 1970, the author, under the NASA-ASEE Summer Faculty Fellowship program, was involved in NASTRAN computations to establish pre-test frequencies and mode shapes for the straight wing configuration of this model. Some of the results of this work and some preliminary experimental results were presented at the NASA Space Shuttle Technology Conference held at LRC in March, 1971, (reference 1).

Preceding page blank

The present paper describes the NASTRAN analysis of the natural frequencies and mode shapes of the delta wing configuration of this model.

DESCRIPTION OF MODEL

The space shuttle dynamics model is a parallel beam-type structure that is dynamically representative of the stiffness and mass properties of an early Manned Spacecraft Center configuration of the shuttle. The model is shown schematically in Figure 1. Scaled simulated propellant masses can be varied on the booster and orbiter to simulate desired flight times. An important feature of the model are two elastic interfaces joining the booster and orbiter. These were designed with removable spring leaves which permit varying the nominal spring constants in the pitch and yaw planes. Four nominal sets of spring leaves were designed.

The booster fuselage spar was fabricated from thin walled, tapered aluminum cylindrical sections reinforced by internal bulkheads. The orbiter fuselage spar is similar except that over a major portion of its length the diameter is constant. Each fuselage component has foam ballast weight holders used to support lead weights which simulate the propellant. The orbiter fuselage includes a lead nose mass to simulate the payload.

Each wing has three spars which were designed to give the proper bending stiffness distribution for the wing. The wings are clamped to the fuselages at three locations through mounting brackets welded to each spar. Outboard of the mounting bracket, each spar cross section tapers linearly from the fuselage to the wing tip. The three spars are connected by forward-aft members which are generally angle bars except at the wing tips where flat bars were used.

NASTRAN IDEALIZATION

In this section the NASTRAN idealization of the model will be described first. Then two methods of representing the elastic interfaces will be described. Finally, a description of the method of representing the fuselage-wing interfaces will be discussed.

Fuselage Components

The booster fuselage was idealized by an assembly of ten concentrated masses and nine beam elements. The concentrated masses were represented in NASTRAN using the bulk data card CONM2, and the beam elements were represented by CBAR elements. The idealization of the booster fuselage is shown in Figure 2.

Since the CBAR beam element is uniform, the cross-sectional properties used were average values based on the diameter at the mid-point of each element.

Added weights 2 and 4, (See Figure 1) being distributed over relatively short lengths, were represented as concentrated masses at grid points 5 and 8, respectively. Added weights 1 and 3 were distributed uniformly over elements 2 and 3 and modeled as non-structural mass (NSM). Concentrated masses were used to model local distributions of mass, such as reinforcing bulkheads. The mass moment of inertia I_{xx} about the roll axis of the fuselage was represented by concentrations at each grid point.

The orbiter fuselage was idealized in a manner similar to the booster fuselage. Seven beam elements and eight concentrated masses were used. The idealization of the orbiter fuselage is also shown in Figure 2. The two added weights of this component were distributed over their supporting beam elements and modeled as NSM. The payload was modeled as a concentrated mass.

Wing Components

The booster delta wing is shown schematically in Figure 3. The wing was idealized using 55 CBAR elements. For the spars which are tapered the average properties of the elements were used. The lower half of the fuselage mounting brackets (not shown) which are welded to the wing spars were represented as concentrated masses. The bending stiffnesses of these brackets were neglected.

The orbiter delta wing is shown schematically in Figure 4. The wing was idealized using 29 CBAR elements. As for the booster wing, average values were used for the tapered portions. Equal concentrated masses were located at grid points 1-9 to

represent the fuselage mounting brackets (not shown).

Elastic Interface

The elastic interfaces were idealized in two ways. In the first idealization the interface was represented using simple linear springs with the nominal spring constants in the pitch and yaw planes. These were input as bulk data through the use of the CELAS2 card.

In the second representation of the elastic interfaces the general structural element GENEL was used. The element describes the elastic interface through a six by six flexibility matrix [Z] and a six by six rigid body transformation matrix [S], (See references 2 and 3).

For the four nominal cases of the elastic interface stiffnesses, the flexibility matrix [Z] was calculated external to NASTRAN making use of a FORTRAN program. For one nominal case of the interfaces, experimental data for the flexibility coefficients was used as input to the general element.

Fuselage-Wing Interfaces

Each fuselage-wing interface was assumed to be rigid. These rigid connections were modeled by writing equations of constraint between the displacement components at the grid points of interest. These equations were written in the form of multipoint equations of constraint

$$\sum_j A_j u_j = 0$$

where A_j are coefficients determined from geometry and u_j are the displacement components. The coefficients of the constraint equations were input as bulk data using MPC cards.

The wings were attached to the fuselage by assuming a rigid connection between six grid points at the outboard edges of the mounting brackets on the wing spars and the nearest grid points on the fuselage. Thus the wings were "cantilevered" from the fuselage with the cantilever points below and outboard of the fuselage centerline.

For the booster fuselage-wing interface grid points 6, 8, 9 on the booster fuselage were connected to grid points 34-39 on the booster wing. A total of 36 equations of constraint were written for the booster fuselage-wing interface. The orbiter fuselage-wing interface was modeled in a similar way. For this interface, 36 equations of constraint were also written.

RESULTS

In this section the results of the analysis will be presented and discussed beginning first with frequencies and mode shapes of each component. Then the results for the elastically connected fuselages will be described. Finally the frequencies and mode shapes for the complete model will be described.

Component Modes

Fuselages

The booster fuselage has 60 degrees of freedom (DOF) with all displacements permitted; the orbiter has 54 DOF permitting all displacements. The consistent mass matrix option was specified, and the eigenvalue problems were solved by the inverse power method. The natural frequencies of the booster and orbiter fuselages are tabulated in Table I. For comparison, some preliminary experimental data obtained at LRC are also listed.

Table I

Natural frequencies of booster and orbiter fuselages.

	Mode	Booster fuselage		Orbiter fuselage	
		f_a , Hz	f_e , Hz	f_a , Hz	f_e , Hz
Bending	1	36.8	36.3 ^a , 36.8 ^b	103.5	103.4 ^a , 102.7 ^b
	2	117.2	95.2 ^a , 98.8 ^b	229.7	205 ^a , 201 ^b
	3	198.7	181.9 ^a , 177.3 ^b	460.3	
Torsion	1	114.3	88.9		
	2	243.4	161.8		
Axial	1	240.2			

^aPitch excitation

^bYaw excitation

The experimental frequencies tend to confirm the predicted values particularly in the lower modes. The agreement becomes poorer in the higher modes. Better agreement with the experimental values for the higher modes could possibly be found by including the rotatory inertia of the added weights and by further subdivision of the fuselages using more beam elements. Because of the reasonable agreement of the lower modes these steps were not pursued.

Wings

In a free-free condition with all grid points having 6 displacement components the booster delta wing has 198 DOF, and the orbiter delta has 162 DOF. To reduce the size of the eigenvalue problems the lumped mass option was selected for each wing, and the rotational displacement components were deleted from the eigenvalue problem through the use of the bulk data card OMIT1. This reduced the size of the eigenvalue problems for the booster and orbiter wings to 99 and 81 DOF, respectively. Both of these eigenvalue problems were solved using the Givens method. The predicted frequencies of the first ten modes are compared with preliminary experimental data in Table II.

Table II

Frequencies of free-free booster and orbiter wings.

Mode	Booster wing		Orbiter wing	
	f_a , Hz	f_e , Hz	f_a , Hz	f_e , Hz
1	24.6	26.4	26.3	
2	26.4	24.8	29.3	
3	27.3	26.4	31.0	28.5, 32.2
4	28.0	26.0	61.3	
5	49.4		63.2	66.9
6	54.4	60.4	67.5	74.5
7	65.0		69.1	
8	69.4		73.4	
9	69.6	73.8		100.7
10	96.1			112.5

The experimental frequencies show reasonable agreement with the predicted values; however, a number of the theoretical modes were not detected in the vibration tests. This may be due to a number of reasons including the fact that some of the frequencies

tend to be very closely spaced.

The NASTRAN structural plotter was used to generate mode shape plots for the wing components. The first three modes of the booster wing viewed in this manner are shown in Figure 5. In the plots, each wing is viewed from an aft position at an angle of 23° above the plane of the wings.

Elastically Connected Fuselages

The frequencies of the elastically connected fuselages were first calculated with scalar springs with axial and roll displacements prohibited. A consistent mass matrix was selected, and the inverse power method was used to solve the eigenvalue problem. Frequencies for the elastically connected fuselages were also calculated using the general element to represent each elastic interface by its theoretical flexibility matrix. The lumped mass approach was taken and rotational components of displacement in the XZ and YZ planes were omitted. Each grid point was thus permitted to have all three translational components of displacement and a rotational component of displacement about the X axis. The resulting eigenvalue problem involved 72 DOF and was solved by the Givens method. The frequencies were also calculated with this approach using the experimentally determined flexibility matrix. These results are compared with the frequencies for the nominal spring constants and the theoretical flexibility matrix in Table III. Experimental frequencies are also given for comparison.

As Table III indicates, the scalar spring idealization of the interface predicts the frequencies of the pitch and yaw modes to be identical. The pitch frequencies for the first four modes were predicted fairly well, but the yaw modes and the combined pitch-axial modes were poorly predicted. The agreement between the frequencies predicted by the flexibility matrix representations of the interface and the experimental frequencies is generally good. The only significant error occurs for the combined pitch-axial mode. The reason for the large difference for this mode is not known.

Complete Model

The final representation of the complete model was obtained by joining the wings to the fuselages with the equations of constraint. With 6 DOF permitted at all grid points the complete model possessed 432 DOF after the multipoint constraints were imposed. To reduce the degrees of freedom the lumped

Table III Comparison of frequencies for elastically connected fuselages.

Nominal Interface Scalar springs ^a		Theoretical Flexibility Matrix ^b		Experimental Flexibility Matrix ^b		Measured Frequencies ^c	
f_a , Hz	Motion	f_a , Hz	Motion	f_a , Hz	Motion	f_e , Hz	Motion
10.7	Pitch	11.2	Pitch	11.3	Pitch	11.3	Pitch
10.7	Yaw	17.4	Yaw	16.3	Yaw		
25.9	Pitch	25.0	Pitch	25.1	Pitch	26.5	Pitch
25.9	Yaw	34.4	Yaw	33.5	Yaw		
36.3	Pitch	37.4	Pitch	37.3	Pitch	38.1	Pitch
36.3	Yaw	40.1	Yaw	38.5	Yaw		
93.8	Pitch	75.2	Pitch-axial	64.3	Pitch-axial	55.6	Pitch-axial
93.8	Yaw	96.2	Yaw	88.4	Roll		
110.5	Pitch	104.9	Pitch	95.5	Yaw		
110.5	Yaw	110.4	Roll-yaw	102.6	Pitch	91.7	Pitch
191.0	Pitch	113.1	Yaw	112.9	Pitch		
191.0	Yaw	118.7	Pitch	116.7	Pitch	98.6, 101.9	Pitch
		131.9	Roll	123.9	Roll		

^a Inverse power method with consistent mass matrix.

^b Givens method with lumped mass matrix.

^c Pitch excitation only.

mass approach was taken. All rotational coordinates on the wings were omitted as well as rotations in the XZ and YZ planes on the fuselage except at wing attachment points. Roll rotations were permitted on both fuselages. The Givens method was used to solve the final matrix eigenvalue problem with 246 DOF. The total computational time (CPU) on an LRC CDC 6600 computer was 2924 seconds to calculate all eigenvalues and twenty-five eigenvectors.

For the elastic interface considered, there were forty modes predicted with frequencies less than 200 Hz. Of the first thirty-two modes, eight modes involved coupled motions between the fuselages, and twenty-four modes involved uncoupled wing vibrations. Computer plots of the mode shapes were used to classify the modes according to their predominant motion. The plotter view of the undeformed model is shown in Figure 6. Since the wings were attached to the fuselages by constraint equations, no element connections are shown between the fuselages and wings in Figure 6b. The general element representation of the interfaces is also not shown by the plotter. Two typical modes are shown in Figure 7.

Correlations with experimental data are currently being made at LRC. NASTRAN predicted the first mode experimental frequency of 10.9 Hz correctly; however, a comparison of the mode shapes for the higher modes will be necessary before any definite conclusions can be reached.

CONCLUDING REMARKS

A NASTRAN normal mode analysis of a space shuttle dynamics model has been made proceeding from free-free component analyses to an analysis of the complete model. Agreement with experimental vibration results was generally good for the components. Correlation with the test data for the complete model has not yet been completed but the lower modes appear to be in agreement.

The results of the study showed NASTRAN to be an effective analysis method for the model. Computational times generally tended to be long on the LRC CDC 6600 computer. The program, however, was relatively convenient to use because of its thorough documentation. The structural plotter was particularly easy to program and proved to be a valuable asset in obtaining a visual representation of the comparatively complex modes of the model.

REFERENCES

1. Leadbetter, S. A. and Kiefling, L. A., "Recent Studies of Space Shuttle Multibody Dynamics", NASA Space Shuttle Technology Conference, NASA TM X-2274, Vol. III, pp. 3-25, (April 1971).
2. McCormick, C. W., Editor, "The NASTRAN User's Manual", NASA SP-222, September 1970.
3. MacNeal, R. H., Editor, "The NASTRAN Theoretical Manual", NASA SP-221, September 1970.

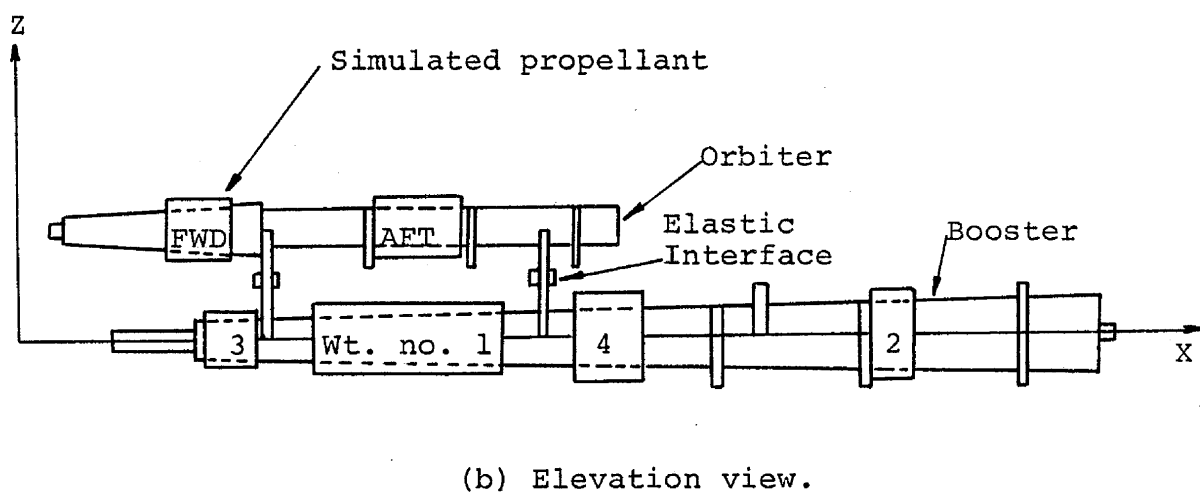
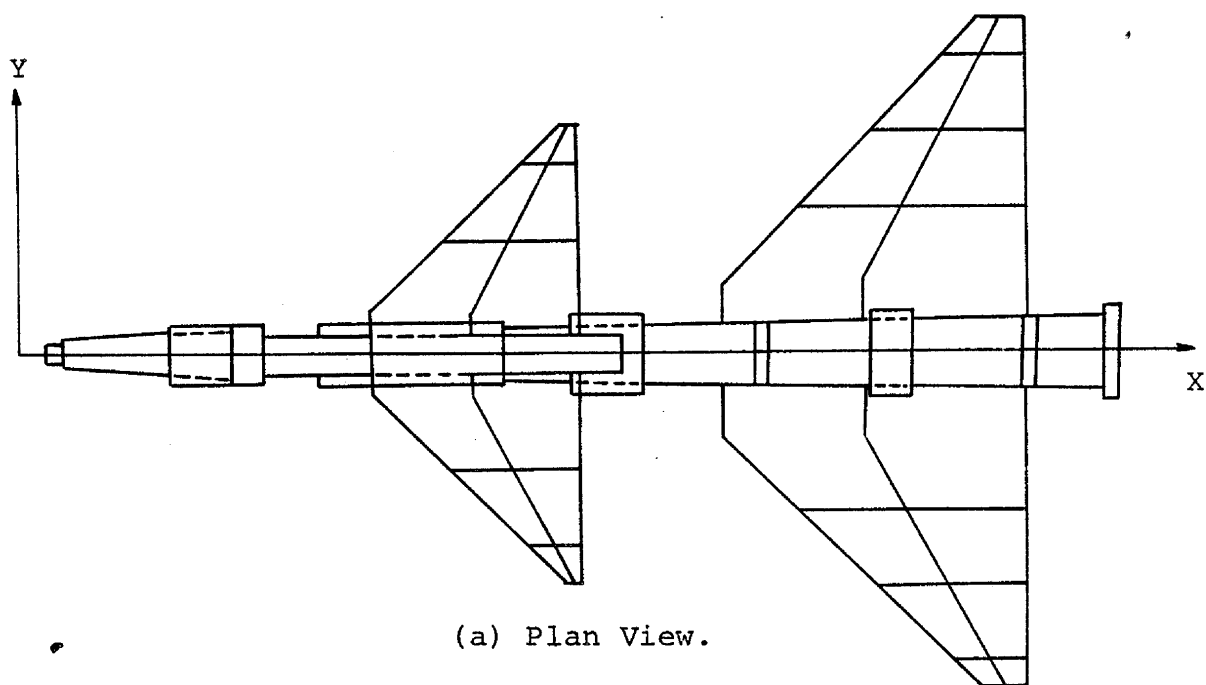
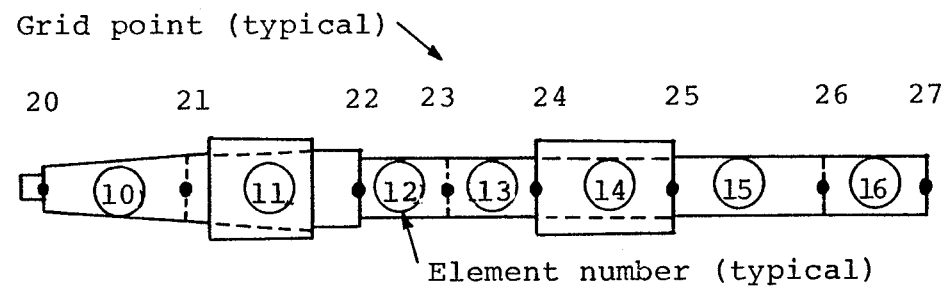
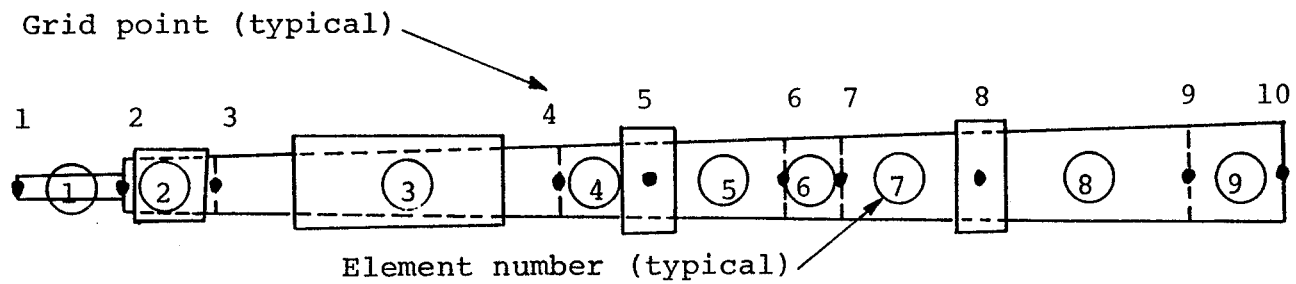


Figure 1 - Schematic of 1/15 scale space shuttle model.



(a) Orbiter fuselage.



(b) Booster fuselage.

Figure 2 - Schematic of booster and orbiter fuselages.

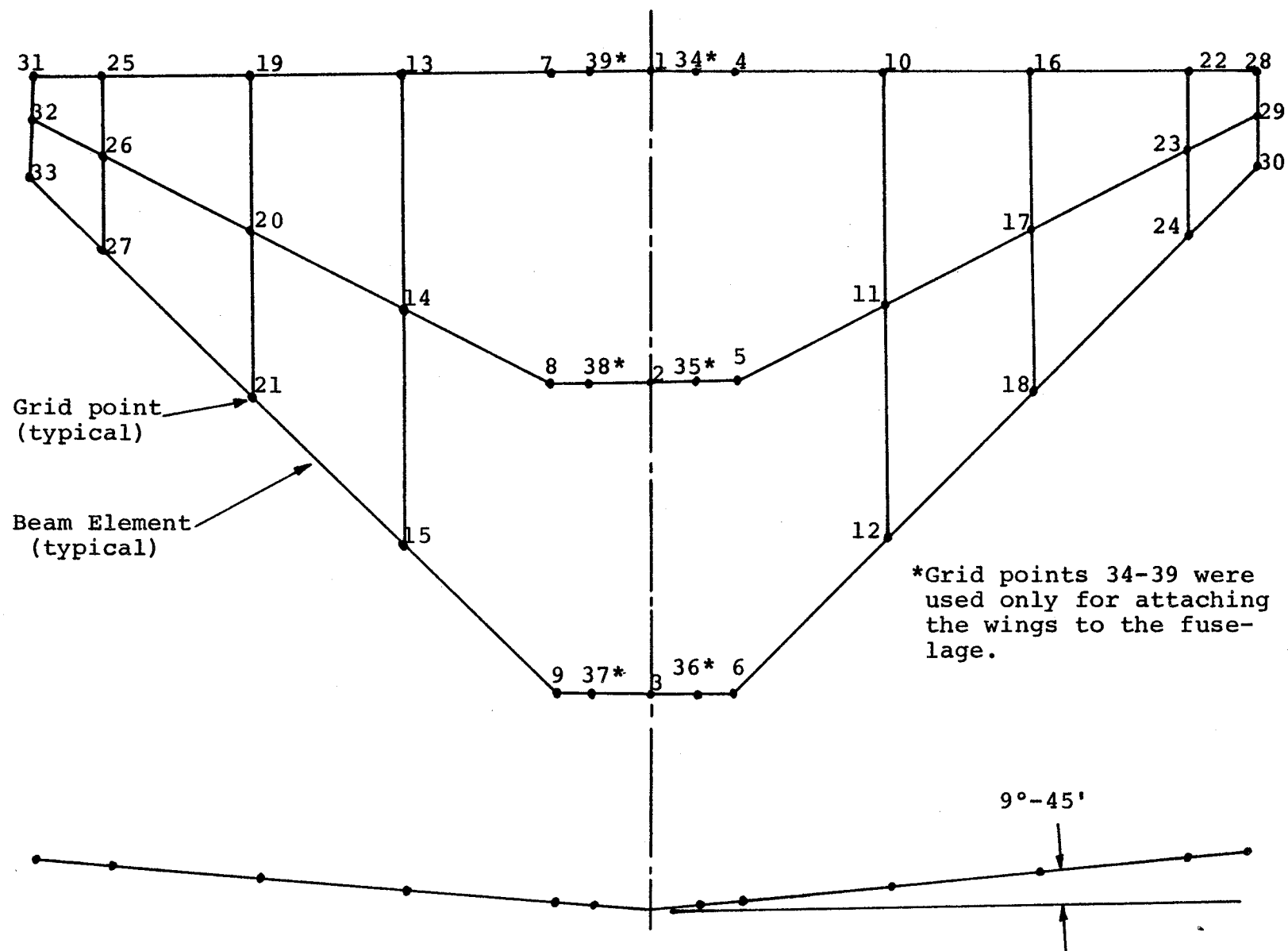


Figure 3 - Schematic of booster delta wing.

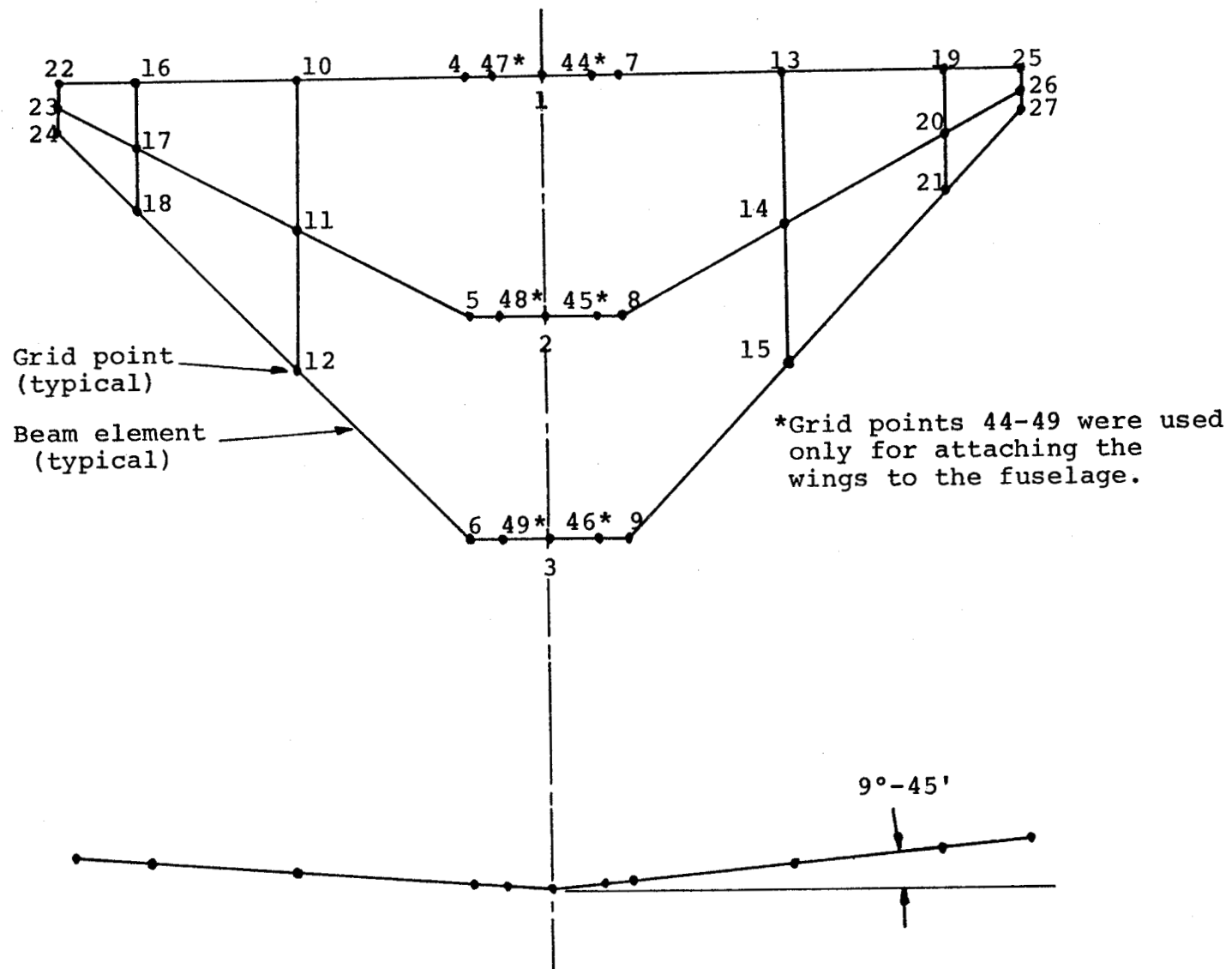
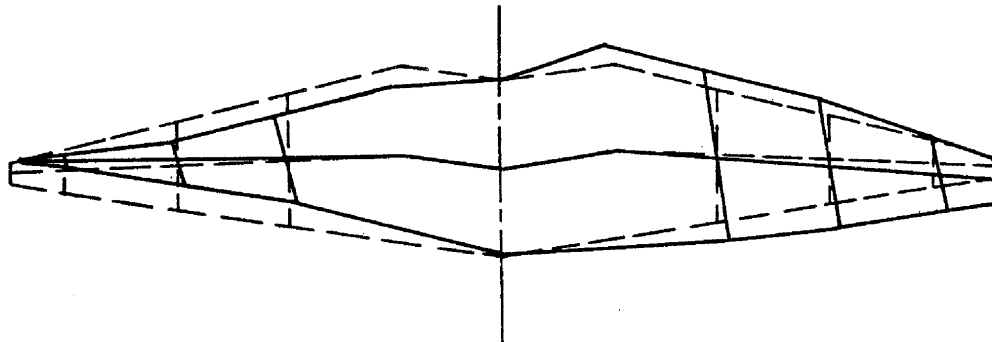
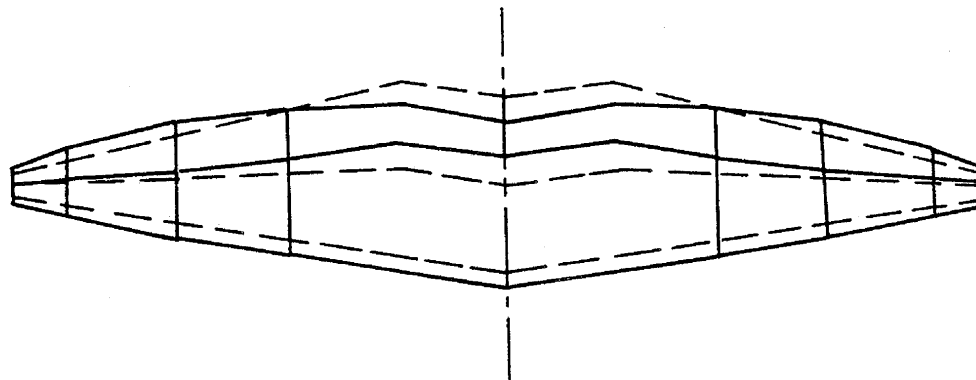


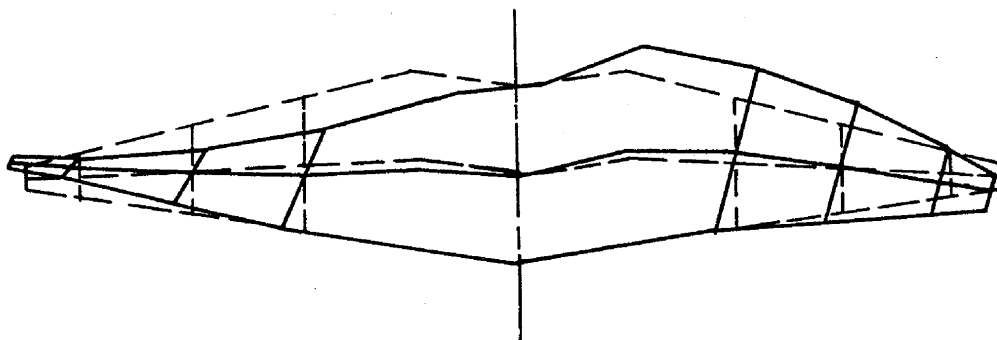
Figure 4 - Schematic of orbiter delta wing.



(a) Mode 1, $f_a = 24.6$ Hz, $f_e = 26.4$ Hz.

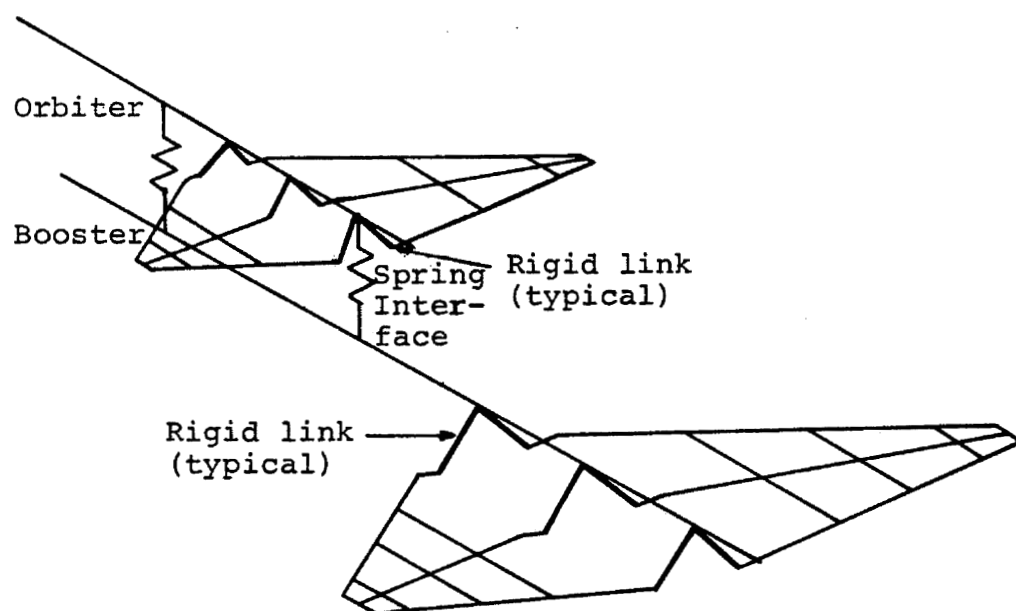


(b) Mode 2, $f_a = 26.4$ Hz, $f_e = 24.8$ Hz.

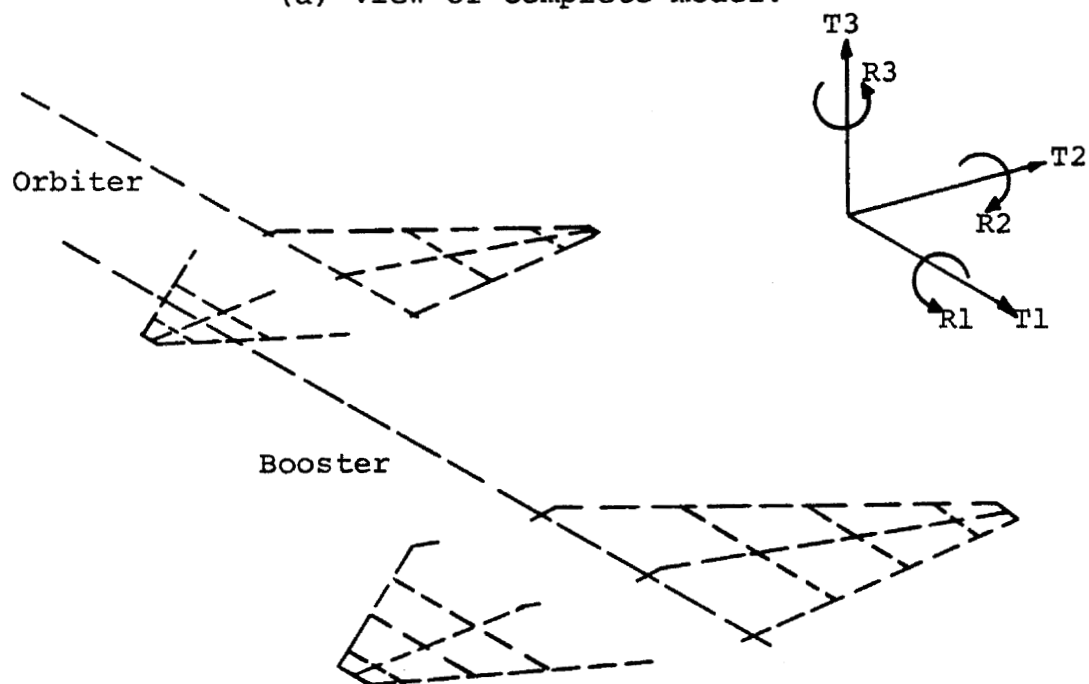


(c) Mode 3, $f_a = 27.3$ Hz, $f_e = 26.4$ Hz.

Figure 5 - Mode shapes of booster delta wing.

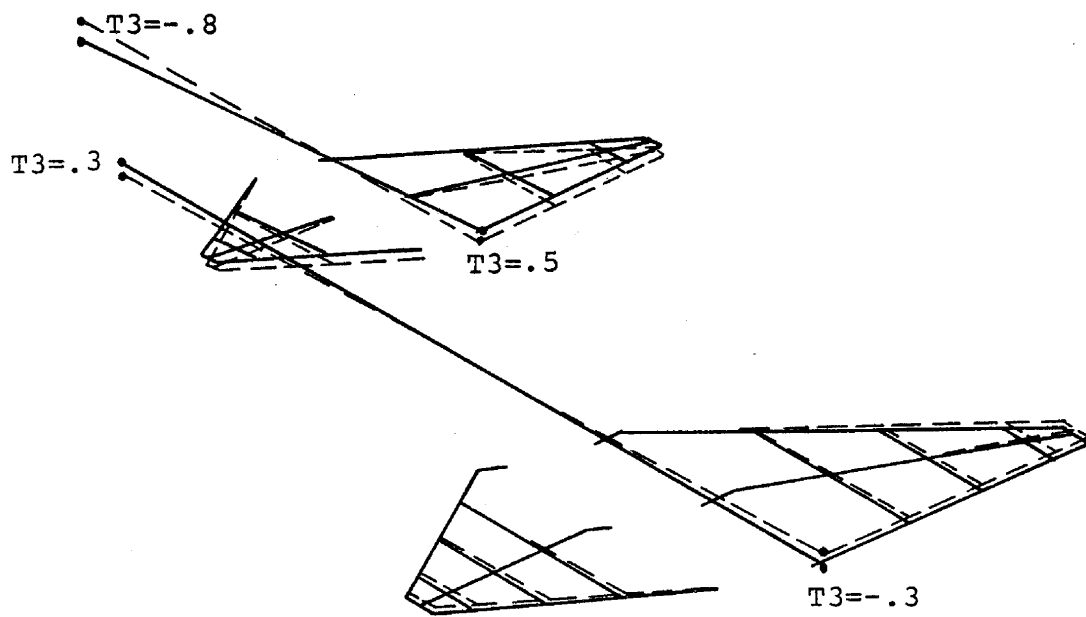


(a) View of complete model.

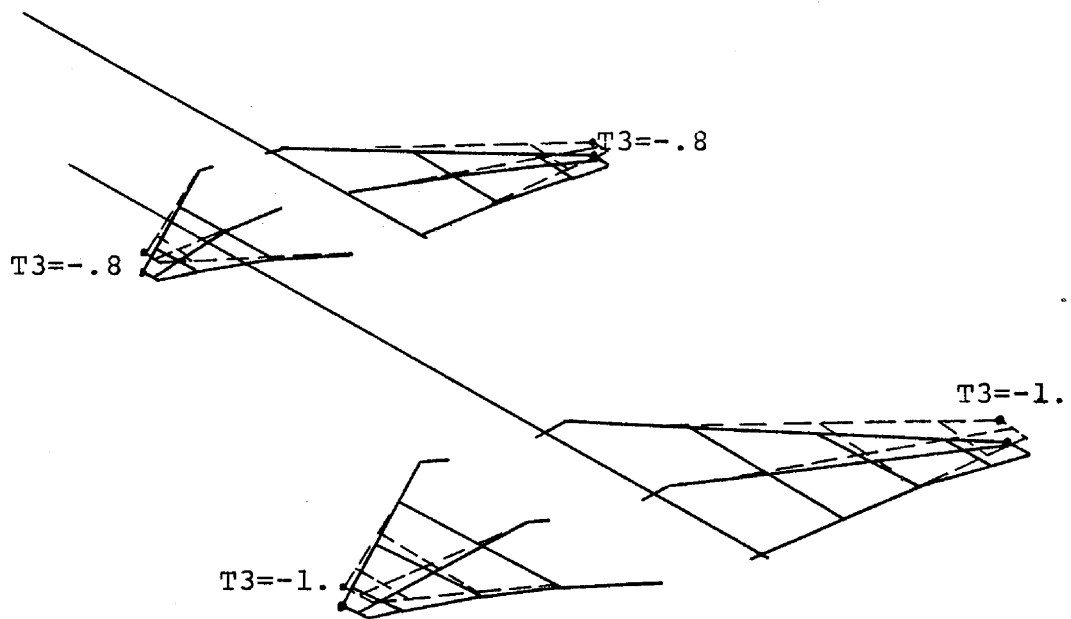


(b) Plotter view of undeformed model.

Figure 6 - Plotter orientation for model mode shape plots.



(a) Mode 1, 10.9 Hz.



(b) Mode 6, 30.9 Hz.

Figure 7 - Mode shapes of complete model.

Preceding page blank

COMPLEX EIGENVALUE SOLUTION TO A SPINNING SKYLAB PROBLEM

Jayant S. Patel
Principal Engineer
Teledyne-Brown Engineering Company, Inc.
Huntsville, Alabama

S. M. Seltzer
Sr. Research Engineer, Astrionics Laboratory
George C. Marshall Space Flight Center
Marshall Space Flight Center, Alabama

INTRODUCTION

In 1970, NASA's Marshall Space Flight Center initiated a study to determine the possibility of spinning the Skylab (this nation's first manned orbiting space station). The purpose of the spin would be to provide an artificial gravity environment to assess and compare the physiological and mental ramifications of prolonged zero-gravity and artificial-gravity environments. Several study teams were formed at the Marshall Space Flight Center. The co-authors of this paper comprise a portion of one of the study teams that have been designated to conduct this study until conclusive results have been obtained. It is anticipated that the results of the study would be appropriate not only for Skylab but also for analysis of future spacecraft, particularly those that are combined of several connected bodies with attached flexible appendages (such as Skylab).

In spinning the Skylab, it would be necessary to spin the vehicle about a principal axis of intermediate moment of inertia in order to keep the solar panels pointed nominally toward the sun. Since it was hoped that passive stability could be achieved, it became necessary to consider deploying masses either on cables or extendable booms so that the principal axis of maximum moment of inertia could point in the same direction as the normal to solar panels.

To study the stability of motion of a spinning Skylab, the method of hybrid coordinates developed by Dr. P. W. Likins (ref. 1) of the University

Acknowledgment: The assistance and advice of Mr. D. W. Justice, Aerospace Engineer, Dr. John Glaese, Aerospace Engineer, Dr. Gerhard Schweitzer, NASA Postdoctoral Research Associate, and Dr. Bernard Asner, Aerospace Technologist, of the George C. Marshall Space Flight Center, along with Messrs. Archie Jordan and Tommy Franklin, members of the Programming Staff of Computer Sciences Corp., in developing the material described in this paper is greatly appreciated.

of California, Los Angeles, is used. The first part of the method consists of obtaining the eigenvalues and eigenvectors of a spinning flexible structure. In the second part of the method, the equations of motion of the entire vehicle and the remaining rigid bodies are written. In this paper attention is focused only on the first part of the method.

EQUATIONS OF MOTION

The equations of motion of a spinning structure are briefly derived here to show how they differ from those of a non-spinning structure. The direct use of the Newton-Euler equations give

$$\begin{aligned}\underline{F}^s &= m^s \underline{A}^s \\ \underline{T}^s &= \frac{d}{dt} \underline{H}^s\end{aligned}\quad (1)$$

for the s^{th} rigid body of a flexible appendage; where m^s is the mass, \underline{A}^s is the absolute translational acceleration vector. \underline{F}^s and \underline{T}^s are the sum of the external and connection force and torque vectors, respectively. \underline{H}^s is the angular momentum vector and i denotes differentiation in the inertial frame of reference.

For a rigid body of an appendage spinning nominally in the steady state with an angular velocity $\underline{\omega}$ (fig. 1), the expression for acceleration is written as

$$\begin{aligned}\underline{A}^s &= \frac{b_d^2}{dt^2} (\underline{c} + \underline{u}^s) + 2\underline{\omega} \times \frac{b_d}{dt} (\underline{c} + \underline{u}^s) + \underline{\omega} \times (\underline{\omega} \times (\underline{c} + \underline{u}^s)) + \underline{\omega} \times (\underline{\omega} \times \underline{r}^s) \\ &+ \frac{d}{dt} \underline{\omega} \times (\underline{c} + \underline{u}^s + \underline{r}^s) + \frac{d}{dt} \underline{R}\end{aligned}\quad (2)$$

$$\begin{aligned}\underline{T}^s &= \frac{d}{dt} (\underline{I}^s \cdot \underline{\omega}^s) = \frac{d}{dt} (\underline{I}^s \cdot (\underline{\omega} + \underline{\beta}^s)) \\ &= \underline{I}^s \cdot \left[\frac{d}{dt} \underline{\omega} + \frac{b_d^2}{dt^2} \underline{\beta}^s + \underline{\omega} \times \frac{b_d}{dt} \underline{\beta}^s \right] \\ &+ \underline{\omega} \times \underline{I}^s \cdot \underline{\omega} + \underline{\omega} \times \underline{I}^s \cdot \frac{b_d}{dt} \underline{\beta}^s + \frac{b_d}{dt} \underline{\beta}^s \times \underline{I}^s \cdot \underline{\omega}\end{aligned}\quad (3)$$

where \underline{c} is a vector representing the location of the mass center at time 't' with respect to its steady state position. \underline{u}^s and $\underline{\beta}^s$ are vectors representing the displacement and small rotation, respectively, of the s^{th} rigid body from its steady state configuration. \underline{r}^s is a vector representing the location of the s^{th} rigid body of the appendage in its steady state configuration measured from the steady state mass center location. \underline{I}^s is the inertia diadic of the s^{th} rigid body. Superscript b denotes differentiation in the reference frame b imbedded in the rigid body with the origin at the steady state mass center location.

For zero spin ($\omega = 0$), eq. (2) and (3) reduce to the familiar form

$$\underline{A}^s = \frac{i d^3}{dt^2} (\underline{R} + \underline{c} + \underline{r}^s + \underline{u}^s) \quad (2-a)$$

and

$$\underline{T}^s = \underline{I}^s \cdot \frac{i d^2}{dt^2} \underline{\beta}^s \quad (3-a)$$

In matrix notation the second term on the right hand side of eq. (2), which is due to coriolis acceleration, gives rise to a skew-symmetric matrix; whereas, the third term, which is due to the centripetal acceleration, yields a symmetric matrix. The fourth term represents a steady state centripetal acceleration which describes the steady state configuration and stretching forces which, in turn, gives rise to the second order geometric stiffness matrix. In the absence of angular acceleration, the fifth term vanishes. If rotational dynamics are the primary concern, the effect of translation of the orbit is disregarded and the last term also vanishes. The fourth term on the right hand side of eq. (3) represents the steady state rotation, and the last two terms will cancel each other if the inertia matrix is diagonal with all the terms having the same magnitude.

Conservation of linear momentum provides the relation

$$\underline{c} = - \frac{1}{M} \sum_{s=1}^p m^s \underline{u}^s \quad (4)$$

where M is the cumulative mass of all appendages and the central rigid body, and p is the total number of masses representing all of the appendages.

The set of equations of motion of all of the rigid bodies representing the appendages is obtained by substituting eq. (4) into eq. (2) and writing the resulting eq. (2) and (3), for all rigid bodies in matrix form:

$$[M'] \{\ddot{u}\} + [G'] \{\dot{u}\} + [K'' + K_e + K_g] \{u\} = \{F\} \quad (5)$$

The use of eq. (4) eliminates the remaining translational rigid body degrees-of-freedom. As a result the mass matrix M' is a symmetric non-diagonal matrix, G' is in general a fully populated skew-symmetric matrix of coriolis acceleration terms. K' is a fully populated symmetric matrix of centrifugal acceleration terms. K_e and K_g are elastic and geometric (differential) stiffness matrices, respectively, (and are obtained from the NASTRAN Program) and {u} is the vector of generalized displacements. In the absence of spin, matrices G, K' and K_g will be identically zero, and the eigenvalue problem reduces to the standard eigenvalue problem of a free-free structure.

Matrices M', G', and K' have the following properties:

$$\begin{aligned} [M'] &= [M] [T] \\ [G'] &= [G] [T] \\ [K'] &= [K''] [T] \end{aligned} \quad (6)$$

where

$$[G] = \begin{bmatrix} [G]^1 & 0 & & & \\ 0 & [G]^2 & & & \\ & & \ddots & & \\ & & & 0 & \\ & & & 0 & [G]^P \end{bmatrix}$$

$$[K'''] = \begin{bmatrix} [K''']^1 & 0 & & & \\ 0 & [K''']^2 & & & \\ & & \ddots & & \\ & & & 0 & \\ & & & 0 & [K''']^P \end{bmatrix}$$

$$[G]^i = \begin{bmatrix} 0 & -2m_1\omega_3 & 2m_1\omega_2 & 0 & 0 & 0 \\ 2m_1\omega_3 & 0 & -2m_1\omega_1 & 0 & 0 & 0 \\ -2m_1\omega_2 & 2m_1\omega_1 & 0 & 0 & 0 & 0 \\ 0 & 0 & 0 & 0 & -I_1\omega_3 & I_1\omega_2 \\ 0 & 0 & 0 & I_1\omega_3 & 0 & -I_1\omega_1 \\ 0 & 0 & 0 & -I_1\omega_2 & I_1\omega_1 & 0 \end{bmatrix}$$

$$[K''']^i = \begin{bmatrix} -m_1(\omega_2^2 + \omega_3^2) & m_1\omega_1\omega_3 & m_1\omega_1\omega_2 & 0 & 0 & 0 \\ m_1\omega_1\omega_3 & -m_1(\omega_1^2 + \omega_3^2) & m_1\omega_2\omega_3 & 0 & 0 & 0 \\ m_1\omega_1\omega_2 & m_1\omega_2\omega_3 & -m_1(\omega_1^2 + \omega_2^2) & 0 & 0 & 0 \\ 0 & 0 & 0 & 0 & 0 & 0 \\ 0 & 0 & 0 & 0 & 0 & 0 \\ 0 & 0 & 0 & 0 & 0 & 0 \end{bmatrix}$$

$$[T]^{-1} = \begin{bmatrix} [E - S_+ \mu^1] \frac{1}{S_0} & 0 & \frac{1}{S_0} [\mu^2] & 0 \\ 0 & [E] & 0 & 0 \\ \frac{1}{S_0} [\mu^1] & 0 & [E - S_+ \mu^2] \frac{1}{S_0} & 0 \\ 0 & 0 & 0 & [E] \\ & & & \ddots \\ & & & & [E - S_+ \mu^p] \frac{1}{S_0} & 0 \\ & & & & 0 & [E] \end{bmatrix}$$

$$[E] = \begin{bmatrix} 1 & 0 & 0 \\ 0 & 1 & 0 \\ 0 & 0 & 1 \end{bmatrix} \quad [S] = \begin{bmatrix} S_1 & 0 & 0 \\ 0 & S_1 & 0 \\ 0 & 0 & S_1 \end{bmatrix}$$

$$[\mu^i] = \begin{bmatrix} \mu_i & 0 & 0 \\ 0 & \mu_i & 0 \\ 0 & 0 & \mu_i \end{bmatrix} \quad S_0 = 1 - \sum_{k=1}^p \mu_k \quad S_1 = 1 - S_0$$

$$\mu_i = \frac{m_i}{M_0 + \sum_{k=1}^p m_k}$$

443

Matrices $[G]$, $[K''']$, $[T]$ and $[T]^{-1}$ are the square matrices of the dimension $6p \times 6p$. Rows and columns corresponding to the degrees-of-freedom which are constrained to be zero should be removed.

Relations (6) afford a transformation.

$$\{y\} = [T] \{u\} \quad (7)$$

Substitution of eq. (7) into eq. (5) provides a transformed set of equations of motion

$$[M]\{\ddot{y}\} + [G]\{\dot{y}\} + [K''' + (K_e + K_g)T^{-1}]\{y\} = \{F\} \quad (8)$$

where $\{y\}$ is the vector representing the displacement of masses with respect to the center of mass of the system.

Transformation

Set of eq. (8) is being used because it has the advantage of requiring less computer storage core than eq. (5) and because it uses a NASTRAN generated mass matrix. However, this approach has the disadvantage that the matrix $[K_e + K_g][T]^{-1}$ is non-symmetric. The eigenvectors of eq. (8) are obtained and transformed by eq. (7) to yield the eigenvectors of eq. (5).

Since it is not possible to uncouple either the set of eq. (5) or the set of eq. (8), they are reduced to the state space formulation in several steps. This leads to the uncoupled set of eq. (10) which are amenable to truncation. The first step is to write the state space equation,

$$A\dot{q} + Bq = L \quad (9)$$

where

$$A = \begin{bmatrix} M' & 0 \\ 0 & K' \end{bmatrix}, \quad B = \begin{bmatrix} G' & K' \\ -K' & 0 \end{bmatrix}, \quad L = \begin{Bmatrix} F \\ 0 \end{Bmatrix}$$

$$K' = K'' + K_e + K_g, \quad \{q\} = \begin{Bmatrix} \dot{u} \\ u \end{Bmatrix}$$

The eigenvectors of eq. (9) are constructed from those of eq. (8).

Let $\bar{\Phi}_i$ be the i^{th} eigenvector of eq. (9) and $\bar{\Phi}'_i$ be the i^{th} eigenvector of the adjoint of eq. (9). Using the transformation $q = \bar{\Phi}z$ and premultiplying eq. (9) by the matrix $\bar{\Phi}'^T$, one finally obtains a set of uncoupled equations

$$A^D \dot{z} + B^D z = \bar{\Phi}'^T L \quad (10)$$

where A^D and B^D are diagonal matrices defined by $A^D = \bar{\Phi}'^T A \bar{\Phi}$, $B^D = \bar{\Phi}'^T B \bar{\Phi}$, $\bar{\Phi} = [\bar{\Phi}_1 | \bar{\Phi}_2 | \dots | \bar{\Phi}_n]$, $\bar{\Phi}' = [\bar{\Phi}'_1 | \bar{\Phi}'_2 | \dots | \bar{\Phi}'_n]$ where n denotes the number of eigenvectors retained after truncation.

The elements of the eigenvectors of the spinning structure are complex which shows that in its normal mode, lumped masses vibrate not only with different amplitudes but with different phase angles, as against the case of a non-spinning structure in which lumped masses vibrate with different amplitudes, but they are either in-phase or out-of-the-phase by 180° .

COMPUTER PROGRAM

Since none of the rigid formats of NASTRAN can solve this problem, a sequence of DMAP statements is written and used with dummy DMAP modules for construction and operation of the matrices $[G]$, $[K]$, $[T]$, and $[T]^{-1}$ which are not available in NASTRAN.

These matrices are generated by considering all six degrees-of-freedom of each of the node points where mass is located and then removing the rows and columns corresponding to the constrained degrees-of-freedom as shown on GRID and SPC cards. To obtain the eigenvalues and eigenvectors, eq. (8) are programmed. However, with only a minor change in DMAP instruction, eq. (5) can be programmed as an alternate approach.

Example

The eigenvalue problem associated with solar panels attached to the Skylab Apollo Telescope Mount and Orbital Workshop is idealized into a 102 degrees-of-freedom system and solved. So that the results can be more easily studied, eigenvalues of an L-beam with six-lumped masses and 36 degrees-of-freedom shown in fig. 2 are illustrated here.

The results are tabulated in Table No. 1. Also, to show the effect of retaining the geometric stiffness matrix, two cases for each spin rate are shown. The results show that it is important to retain the geometric stiffness matrix. The lowest natural frequency corresponds to the vibrations of the masses in the plane of rotation. It is this frequency which is substantially affected by the spin rate, even with a relatively slow spin rate which is less than the fundamental natural frequency. The second natural frequency corresponds to the vibrations in the vertical plane. The last column shows the case where the spin velocity is higher than the first two natural frequencies.

CONCLUSION

The effect of rotation on the structural and dynamical behavior of a spinning body with flexible appendages can be significant, as shown by example. To adequately include this effect in a digital simulation requires a complex eigenvalue solution to a fairly high order system. The feasibility of such an approach is indicated in the paper.

REFERENCE

1. Likins, P. W.: Dynamics and Control of Flexible Space Vehicles. NASA TR-32-1329, Revision 1, Jan. 1970.

TABLE 1: EIGENVALUES FOR ROTATING L-BEAM

Eigenvalues (rad./ sec.)Case		Spin in rad./sec.									
		(0.0)	(0.314159)	(0.628318)	(1.570795)	(3.14159)	(4.712385)	(6.28318)	(9.42477)	(10)	(12.56636)
ω_1	A	11.211634	11.122227	11.014938	10.719895	10.298015	9.9117894	9.5184119	8.4956303	8.2524514	6.8684777
	B	11.213511	11.120531	10.998942	10.605564	9.8331139	8.9033124	7.7947030	4.6870204	3.860928	12.407949
ω_2	A	11.256337	11.354685	11.470914	11.864305	12.615366	13.495101	14.474969	16.706492	17.135632	19.181195
	B	11.256425	11.349406	11.45669	11.742783	12.136161	12.422253	12.608214	12.708346	12.679737	27.09166
ω_3	A	31.113625	31.113625	31.113625	31.131506	31.154177	31.240005	31.440269	32.355766	32.61325	34.043714
	B	31.125567	31.125567	31.096958	31.011130	30.753647	30.353117	29.83815	28.593647	28.336163	44.943848
ω_4	A	39.231777	39.231777	39.26754	39.41059	39.822787	40.50941	41.396297	43.627821	44.085509	46.288484
	B	39.250602	39.250602	39.279211	39.36503	39.736959	40.309145	41.024377	42.826761	43.198682	112.23286
ω_5	A	112.93888	112.93888	112.93888	113.1534	113.83408	114.86492	116.46704	120.70121	121.61671	126.30863
	B	112.91949	112.91949	112.91949	112.91949	112.86227	112.80505	112.74783	112.51896	112.51896	138.21009
ω_6	A	138.18741	138.18741	138.18741	138.2589	138.55340	139.12558	139.81221	141.75764	142.21539	144.50413
	B	138.21009	138.21009	138.21009	138.21009	138.21009	138.21009	138.21009	138.21009	138.21009	279.5393

Case A - Geometric stiffness matrix retained.

Case B - Geometric stiffness matrix neglected.

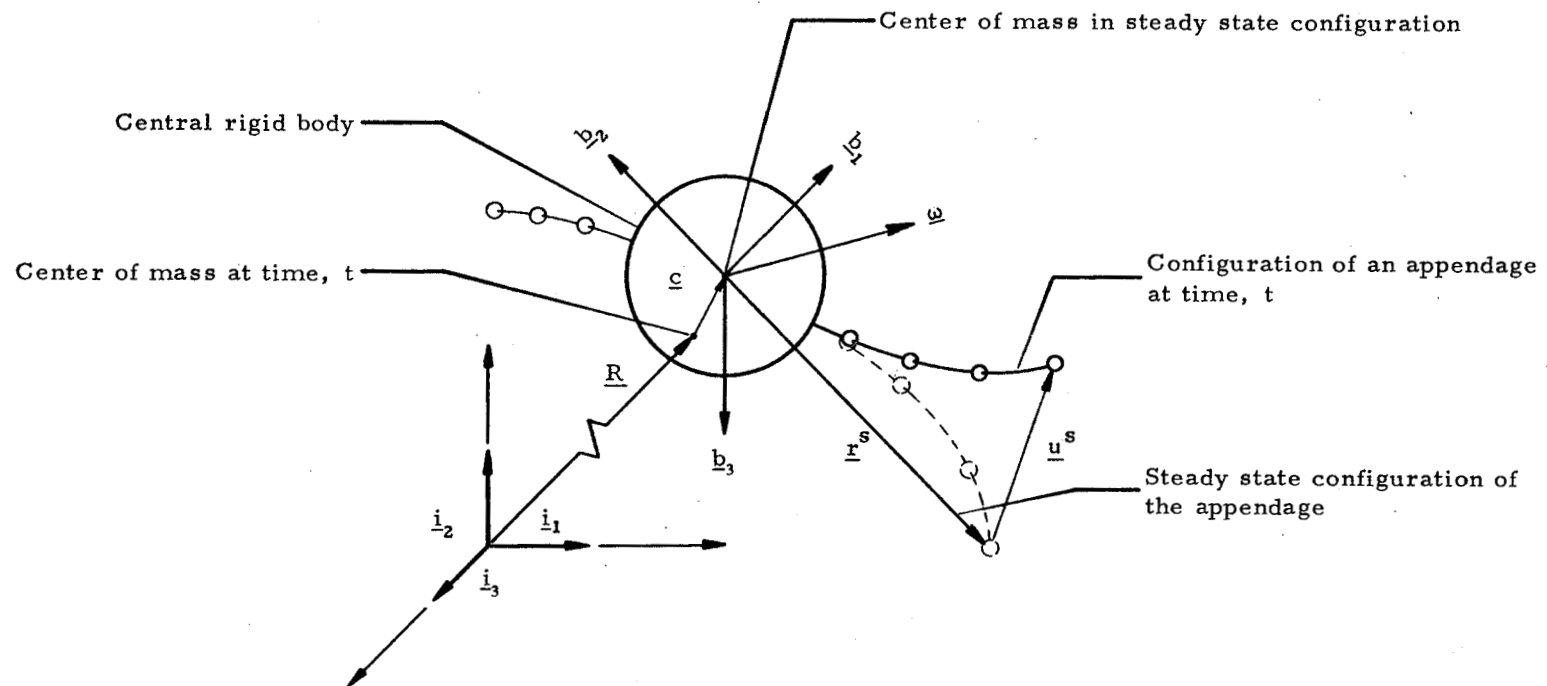


FIGURE 1. GEOMETRY OF SPINNING FLEXIBLE APPENDAGE AND CENTRAL BODY

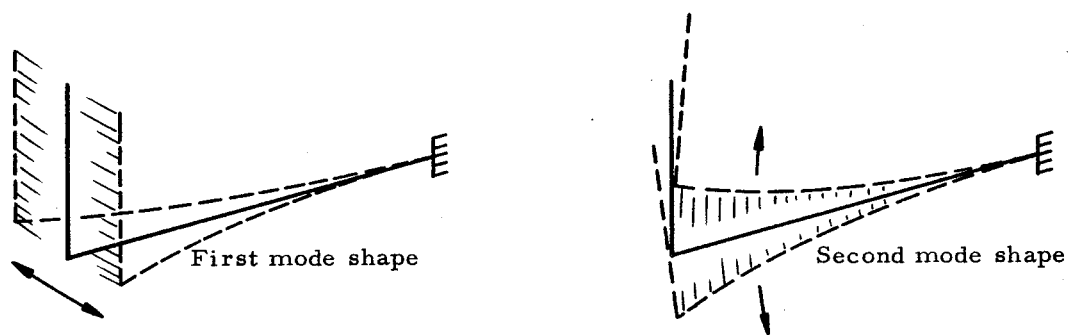
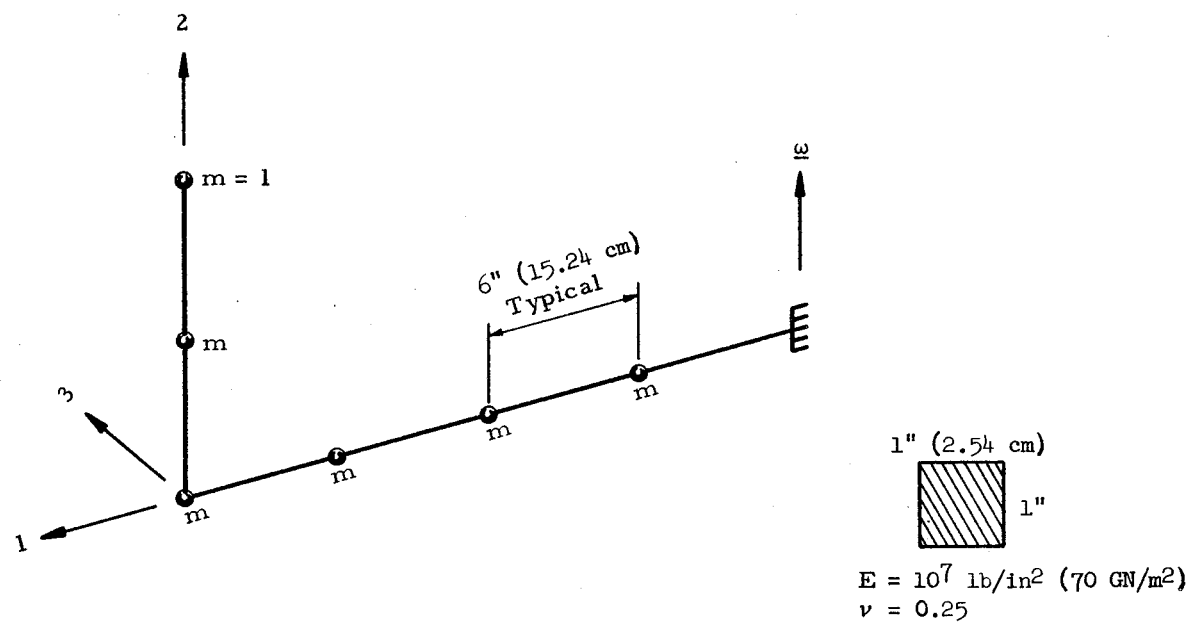


FIGURE 2. SPINNING CANTILEVER L-BEAM

Preceding page blank

APPLICATION OF NASTRAN TO THE ANALYSIS OF A
SPACE SHUTTLE ORBITER STRUCTURE

By Gary L. Giles
NASA Langley Research Center

and

John H. Dutton
McDonnell Douglas Corporation, St. Louis, Missouri

SUMMARY

An analytical study of a space shuttle orbiter structure is being made at NASA Langley Research Center using NASTRAN as the analysis program. The analysis starts with a finite element model with over 3000 joint degrees of freedom, which was developed by the McDonnell Douglas Corporation (St. Louis) during its Phase B studies of the orbiter. The model has structural members sized using the fully stressed design procedure in the Automated Structural Design (ASD) program. To date, conversion to the NASTRAN format of the topological ASD input data for the complete vehicle and conversion of eight wing loading conditions has been completed. In addition, a structural analysis of the orbiter wing has been completed. The effort required to convert the data is discussed, and basic differences in the two finite element programs are described. Also, the performances of the NASTRAN and ASD programs are compared in terms of calculated quantities such as stresses and displacements, and in computational times required for a single analysis cycle of the orbiter wing structure.

INTRODUCTION

Calculations for an entire shuttle orbiter under a variety of loading conditions are being made at the Langley Research Center on the Langley CDC 6600 computer system using the NASTRAN program (ref. 1) as the analysis tool. The calculations are being made to gain experience in the analysis of a large complex structure with realistic loading conditions. The particular structure was chosen for analysis because it has previously been analyzed by the McDonnell Douglas Corporation and its finite element model was available.

The finite element model, which had over 3000 joint degrees of freedom, was developed during Phase B studies of the orbiter. A fully stressed design of this model was obtained by McDonnell Douglas using the Automated Structural Design (ASD) program described in reference 2. Their calculations were made on an IBM 360/85 computer system. The purpose of the present paper is to report on the initial phase of the study and to discuss results obtained to date.

DESCRIPTION OF FINITE ELEMENT MODEL

Principal structural components of the space shuttle orbiter considered in this study are shown schematically in figure 1. The finite element structural model (fig. 2) of this vehicle was developed by the McDonnell Douglas Corporation. The model is symmetrical about the centerline of the vehicle so it was necessary to represent only half of the model in the analysis. The half-model contains 1388 joints and 3154 joint degrees of freedom. Rods, bars, and shear panels are the finite elements used to represent the structural members. A total of 2636 rods, 27 bars, and 1355 shear panels are included in the model. Approximately five man-months were needed to generate the topological definition of the model (i.e., joint locations and specification of finite elements connecting the joints). Alternate structural arrangements were tried until proper load paths were established during this period of time. Sizes of the elements were then determined using the fully stressed design procedure in the ASD program.

The model consists of eight discrete modules which are assembled into a single structure (fig. 3). The eight modules are: (1) main wing box, (2) forward wing, (3) nose, (4) main propellant tanks, (5) crew compartment, (6) upper fuselage, (7) aft fuselage, and (8) vertical tail. This method of defining the structure permits the assignment of a particular module to the group responsible for its design.

Although the data are prepared in many smaller sets, the assembled structure is analyzed by the ASD program in a single computer run, as is done in the 12.1 version of NASTRAN. Thus, substructuring was not used in the analysis and the use of modules merely provided a convenient method of book-keeping for the voluminous quantities of input and output data generated in the analysis of a large structure. However, the complete model can be divided into several modules which can be analyzed alone, replaced by modified or alternative configurations, or changed to improve detailed definition in an area of particular interest, without affecting the overall model.

Conversion of the topological ASD input data to the NASTRAN format produced a bulk data deck containing 19,143 cards. In addition, eight load conditions which act only on the wing (modules 1 and 2, fig. 3) have also been converted. However, input data for five external loading conditions (concentrated forces and pressures) and two thermal conditions for the complete vehicle have not yet been converted.

COMPARISON OF ASD AND NASTRAN PROGRAM FEATURES

Any comparison of two computer programs is generally rather nebulous. The original purpose of the programs, types of analyses they will perform, types of finite elements available, maximum size of problem, computer systems on which the programs are operational, ease of use, etc., can vary widely and can have a significant impact on the quantity that is being compared, usually computational time for a given problem. Since NASTRAN is a widely used general purpose structural analysis program and its features are well known and documented, it is inevitable that it will be compared with other programs. The comparisons presented in this paper will tend to emphasize the desirable features of the ASD program with the thought that such comparisons might provide guidance in the continuing future development of the NASTRAN program. Incorporation of such features must, of course, be weighed against compromising the original purpose of the NASTRAN program.

The Automated Structural Design (ASD) program uses a "combined" method of analysis rather than either of the traditional force or displacement methods; NASTRAN uses the displacement method. In the combined method, all of the equilibrium and compatibility equations are combined into a single set of simultaneous equations which are solved in a single operation for all forces or stresses and displacements. The apparent disadvantage of solving the resulting large set of equations (twice the order of the force or displacement method) has been resolved by the development of an efficient bookkeeping system which handles only the non-zero elements of the matrix during the analysis. This procedure is not affected appreciably by the "band-width" of the matrix, a very desirable feature that makes the modular arrangement of the structural model feasible. Some penalty in computational time will be involved when using NASTRAN to analyze the model in this study because running time of version 12.1 of NASTRAN is band-width dependent.

NASTRAN was designed to be open-ended in the size of problem it can handle; ASD can accommodate large problems also, the only limitation being a maximum of 65,535 degrees of freedom for the structure. Thus, either program can handle the size problems being run currently in industry.

The version of the ASD program described in reference 2 is limited to static analysis but also includes a fully-stressed element resizing procedure. Iterations of analysis and resizing can be made until the desired tolerance on member sizes from consecutive iterations is obtained. The capability for member resizing is a desirable feature for a finite element program, particularly for use in preliminary design. A recommendation that this feature be incorporated into the NASTRAN program cannot be made at this time, however, since it is not clear whether improved versions of NASTRAN will be economically competitive with existing programs in such design applications (refs. 2 to 4).

Rods, bars, and shear panels are the only finite elements available in ASD and were thus the elements used to define the model considered in the present study. The ASD rod and bar members can be either single-segment as in NASTRAN or double-segment. The double-segment member has a node at the center and can have different cross-sectional areas for the two segments. Either all single-segment or all double-segment rods and bars can be used in a given structure, but not both types. The shear panels must correspond to the types of rod and bar members in a given structure. When shear panels are used with a double-segment member a connection is made to the rods or bars at the center of each side of the panel.

The orbiter structure (fig. 2) was modeled with double-segment members, and since NASTRAN does not contain such finite elements, the areas of the two segments in a member were averaged and converted to a rod or bar element of constant area along its length. Hence, the finite element representation of the structure as analyzed by ASD is not the same as the one analyzed by NASTRAN. This modeling difference will affect the numerical results obtained in this study.

It is often desirable to isolate portions of a complex finite element structural idealization in order to examine these smaller segments in greater detail. Plots or printed output can be assessed for the selected portion of the structure without being confused with the remainder of the structure. This can be done in NASTRAN by specifying a SET of grid points and/or elements that define that portion of the model to be considered. The ASD program has a similar capability and in addition allows the user to specify sectioning planes which cut through and isolate portions of a structure to be plotted. For example, sectioning planes could be defined on each side of a fuselage frame so that a plot of the single frame would result. Incorporation of this capability into NASTRAN, with an option to generate internally SET definitions from sectioning plane specifications, would greatly reduce the burden on the analyst of preparing SET cards.

CONVERSION OF ASD INPUT DATA TO NASTRAN FORMAT

In the present study, computer routines were written to convert the ASD input data to the NASTRAN format. In this section of the paper, some of the difficulties encountered with the conversion are indicated, and procedures to circumvent these difficulties are described.

In the ASD data, the grid points or joints in each individual module of the structure are numbered sequentially starting with the number 1. Direct conversion of grid points would have resulted in more than one grid point with the same number. Since NASTRAN does not require sequential grid numbering, it was possible to convert the points to unique numbers by using the scheme
 $(\text{NASTRAN grid number}) = (\text{ASD module number}) \times 100,000 + \text{ASD grid number}.$

A similar procedure was used for the element connection, element property, and material type identification numbers. Such a numbering procedure is useful in general finite element analyses as an aid in bookkeeping of large amounts of data.

The wing modules (1) and (2) were defined in a different coordinate system than the other modules. All modules were assigned a different coordinate system number and the modules were made compatible using the NASTRAN bulk data card CORD1R. A similar method of defining various parts of the same structure in different coordinate systems is included in the ASD program and was used to produce the module definition plot shown in figure 3. The eight modules are automatically connected by the ASD program; multipoint constraints (MPC bulk data cards) were used to connect the modules for the NASTRAN input deck.

The principal difficulty encountered during the conversion of the data was that of incorporating structural constraints which are internally determined by the ASD program. The ASD program assigns degrees of freedom to each grid point after investigating the geometry of the rod and bar elements at the grid point. If all rod and bar members intersecting at a grid point lie in a plane, constraints prohibiting displacement of that grid point out of the plane are automatically generated. These constraints, which remove singularities in the stiffness matrix, must be supplied as input data to the NASTRAN program since it does not automatically provide any constraints of this type. To generate these constraints, procedures were incorporated in the conversion routines which (1) determined all the rods or bars connected at each grid point, (2) calculated the volume of the largest parallelepiped that would be constructed between unit vectors colinear with any three members at the joint, and (3) if the volume was less than a small specified value (zero volume would indicate all members were exactly in the same plane) generated a multipoint constraint which would restrict displacement out of that plane.

The relatively large number (19,143) of cards generated by the conversion of data were put on a NASTRAN users master file (UMF) to minimize the handling of such a large bulk data deck. Since the modules were converted one at a time, poor ordering of the cards resulted and, hence, a computer time of 20 central processor (CPU) minutes and 50 peripheral processor (PPU) minutes on a CDC 6600 were required to generate the UMF. Experience using the UMF with this data, which was grouped in modules, indicated the desirability of being able to call and execute bulk data from several problem decks assigned to the same or different users master files. This would allow division of a large data deck into smaller decks, thus facilitating bookkeeping procedures. Also, a bulk data printout could be requested using ECHO selected portions of the data, rather than the complete deck with the corresponding large amount of printed output.

NUMERICAL RESULTS

A NASTRAN analysis of the entire orbiter had not been made at the time of the preparation of this paper since all external loading conditions have not been converted to the NASTRAN format. A structural analysis has been made by McDonnell Douglas using the ASD program for eight design conditions considering both symmetrical and antisymmetrical loads applied to half the structure having the appropriate boundary conditions. The results were combined to obtain the asymmetrical behavior of the complete vehicle. The computer time required for an analysis-resize-analysis cycle was 21.6 CPU minutes and 80.6 PPU minutes. A NASTRAN analysis for the same conditions will be performed during a later phase of the study to obtain comparative computational time.

An analysis of the wing has been completed using both ASD and NASTRAN. The finite element model contained 255 grid points and 759 degrees of freedom. The wing was supported along the root rib of the 3-bay main wing box (module 1) and at the intersection of the leading edge spar and the root rib of the forward wing section (module 2). The loadings considered in the analysis corresponded to a 2.5g subsonic pullup maneuver, vertical ascent max α q loading, engine thrust, main gear landing, main gear braking, turning, taxiing, and hoisting. These eight load cases were applied to the wing and deflections and internal stresses were determined.

The normal displacements obtained with ASD and NASTRAN for the orbiter wing along the rear spar and tip rib are compared in figures 4 and 5 for the 2.5g subsonic pullup maneuver. The solid curves correspond to ASD results and the symbols to NASTRAN results. Excellent agreement between results is obtained even with the differences in modeling mentioned earlier in the discussion of the differences between the ASD and NASTRAN programs. Note that the scale in figure 5 has been exaggerated for clarity. The maximum difference found between displacement values obtained by these two programs was 2 percent.

Spar cap axial stresses on the upper surface at the wing root are shown in figure 6 for the 2.5g subsonic pullup case. The ASD rod and bar elements are connected at their midpoints to the adjacent shear panels. Thus, the stresses in the two segments of a rod can have different values. These two values were averaged to compare the stress data with the NASTRAN stresses, which are constant along the length of the rod or bar. The agreement is poor for some of the spars. These spars are probably in regions where considerable stress redistribution is occurring, and a significant amount of load is being transferred at the midpoint connections of the rod and shear panels. A more realistic comparison would be obtained if the total load being transferred across a particular section of the models were calculated; it is anticipated that such results would be in considerably better agreement.

The ASD program required approximately 0.8 minutes of CPU and 2.0 minutes of PPU time on an IBM 360/85 computer for a single analysis with all eight loading conditions, while NASTRAN used 9.4 minutes CPU and 13.7 PPU time on a CDC 6600 computer.

Since the model was generated for the ASD program, which is band-width independent, some penalty of computational time is undoubtedly encountered in the NASTRAN computation over what would be required if a numbering scheme which gives minimum band-width had been used. However, even with this factor accounted for, it is expected that the ASD program, which has been tailored for efficient use during preliminary design, would still be significantly faster than the NASTRAN program for solution of this problem.

CONCLUDING REMARKS

The NASTRAN program is being used to analyze a space shuttle orbiter finite element model which was developed by the McDonnell Douglas Corporation. User experience and numerical results obtained during the initial phase of this study were described. The structural members of the model were sized by McDonnell Douglas using the fully stressed design procedure in the Automated Structural Design (ASD) program. The effort required to convert the input data for the ASD program to the format required for the NASTRAN program was discussed, basic differences in the two finite element programs were described, and desirable features of each program were indicated.

Stresses and displacements from an analysis of the orbiter wing structure were obtained for eight loading conditions. Results for one loading condition were compared with ASD results at selected locations on the wing. Excellent agreement was obtained between wing displacements calculated with the NASTRAN program and with the ASD program; agreement between wing root spar cap stresses obtained from the two programs was not as good, but the difference can be attributed to the use of double-segment finite elements in the ASD analysis, which are not available in NASTRAN. The computational time required for the NASTRAN analysis of the wing structure using a CDC 6600 computing system was more than a factor of 10 greater than that required by the ASD program on an IBM 360/85 computing system.

REFERENCES

1. Butler, Thomas G.; and Michel, Douglas: NASTRAN, A Summary of the Functions and Capabilities of the NASA Structural Analysis Computer System. NASA SP-260, 1971.
2. Eshleman, A. L., Jr.; and Anderson, G. E.: User's Manual, Automated Structural Design Computer Program. McDonnell Douglas Corporation Document DAC-33447, June 1970.
3. Dwyer, Walter J.; Emerton, Robert K.; and Ojalvo, Irving U.: An Automated Procedure for the Optimization of Practical Aerospace Structures. AFFDL-TR-70-118, Wright-Patterson AFB, Ohio, April 1971.
4. Whetstone, W. D.: User's Manual for the December 1969 Version of SNAP/FSD. LMSC/HREC D 162100, January 1970.

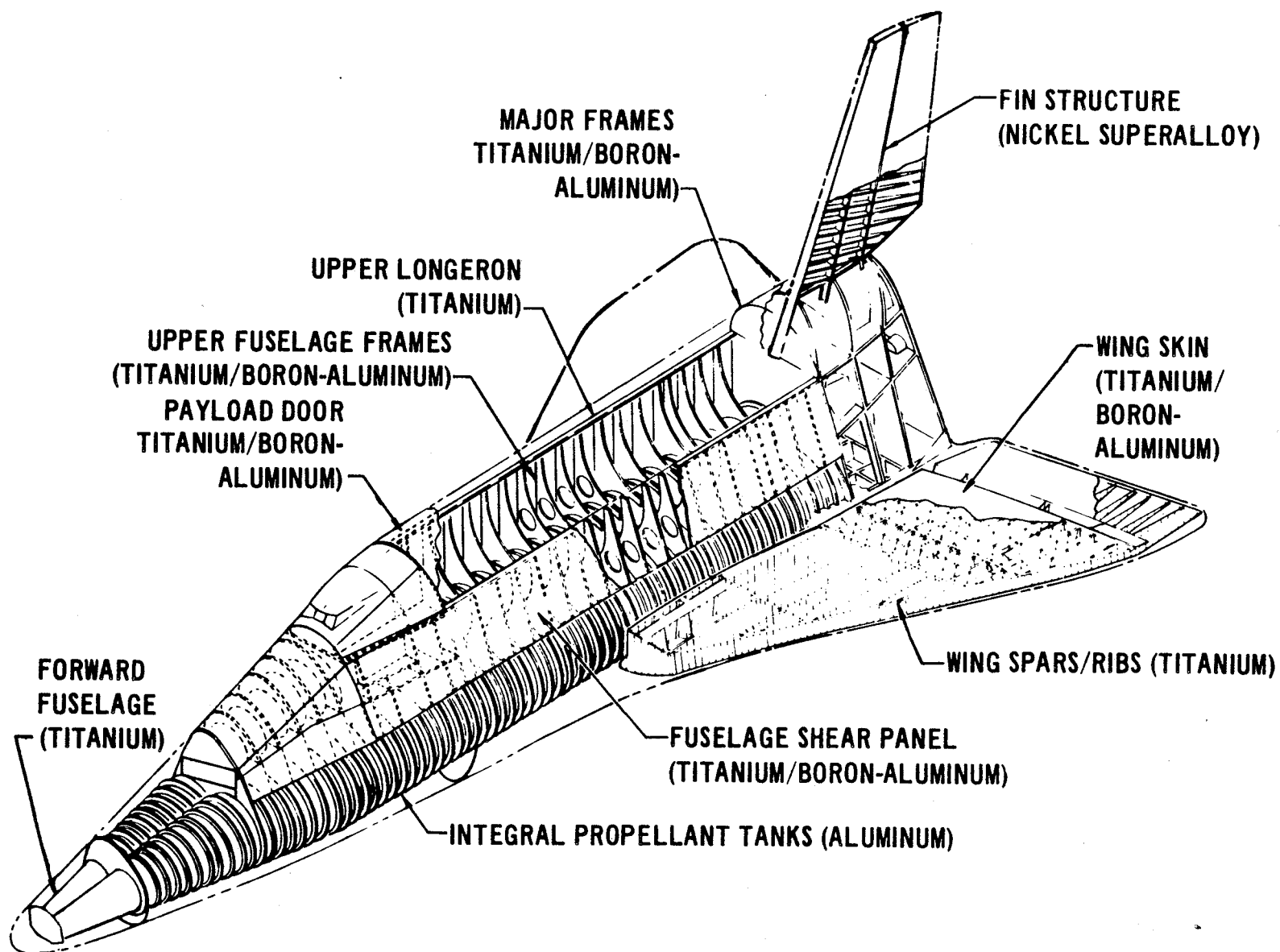


Figure 1.- Structural definition of space shuttle orbiter configuration developed by McDonnell Douglas Corporation during Phase B studies.

NODES	2776
BARS	5326
PANELS	2710
JT.DEG. OF FREEDOM	6308

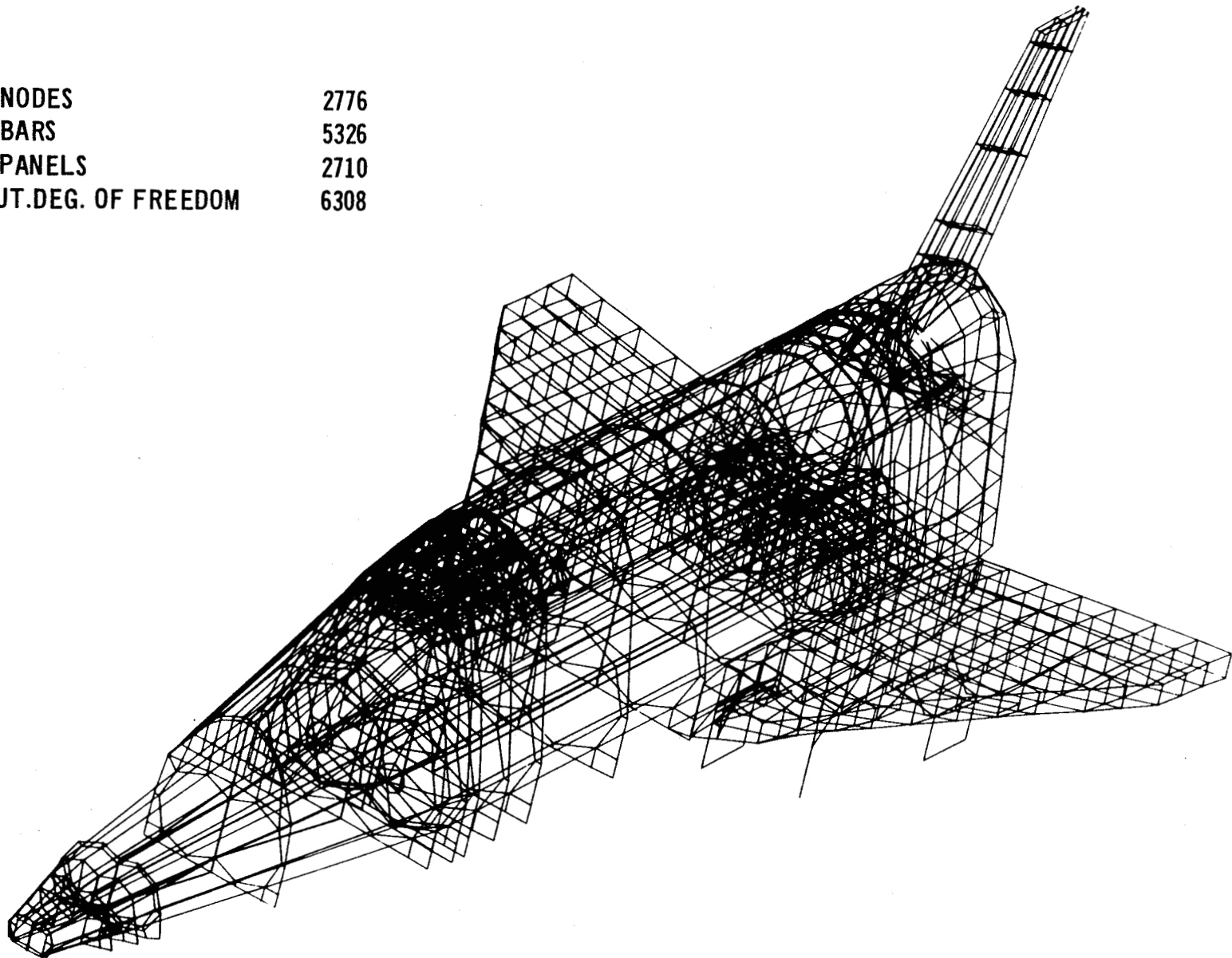


Figure 2.- Finite element model of shuttle orbiter configuration.

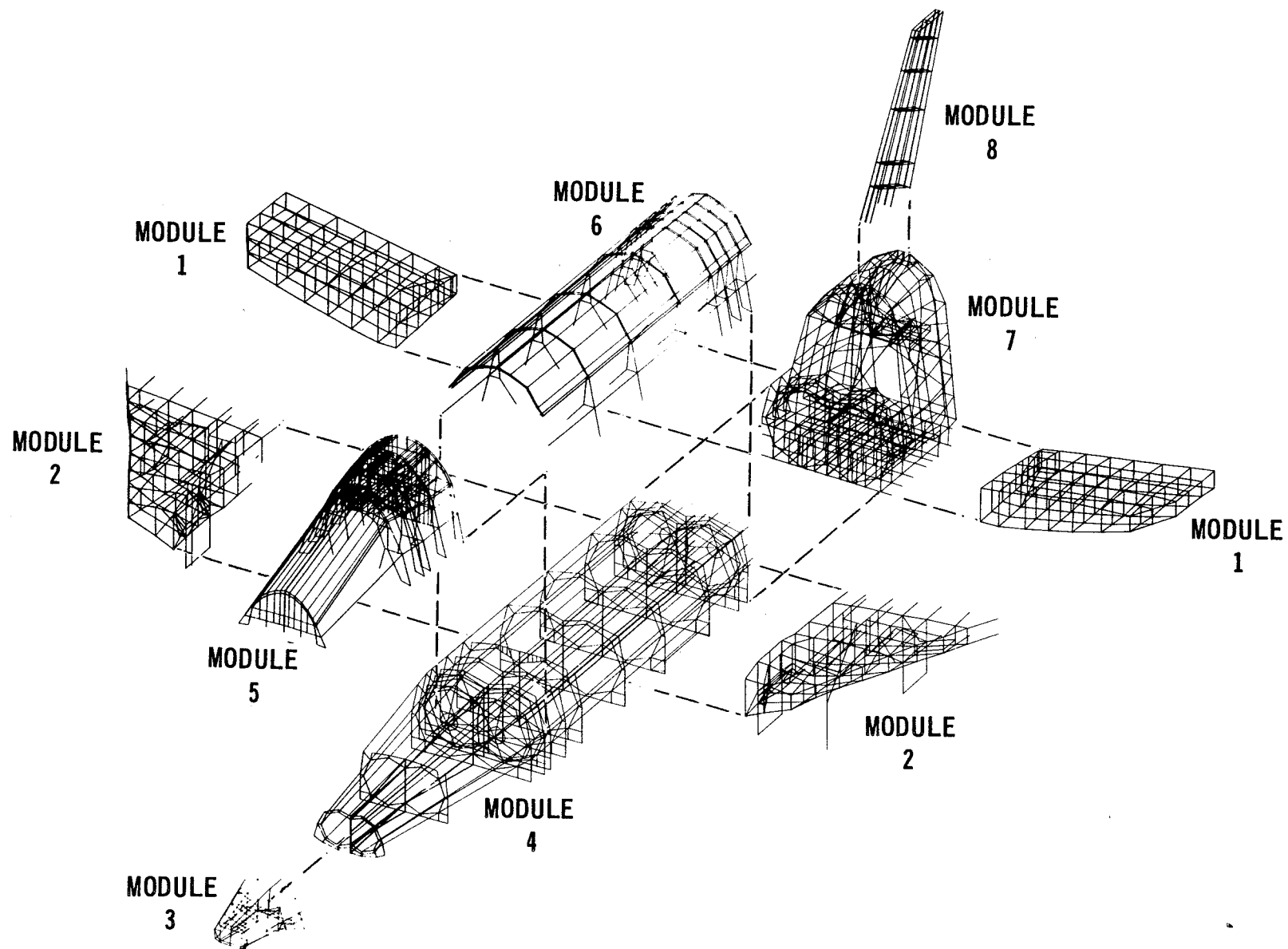


Figure 3.- Module definition for finite element model.

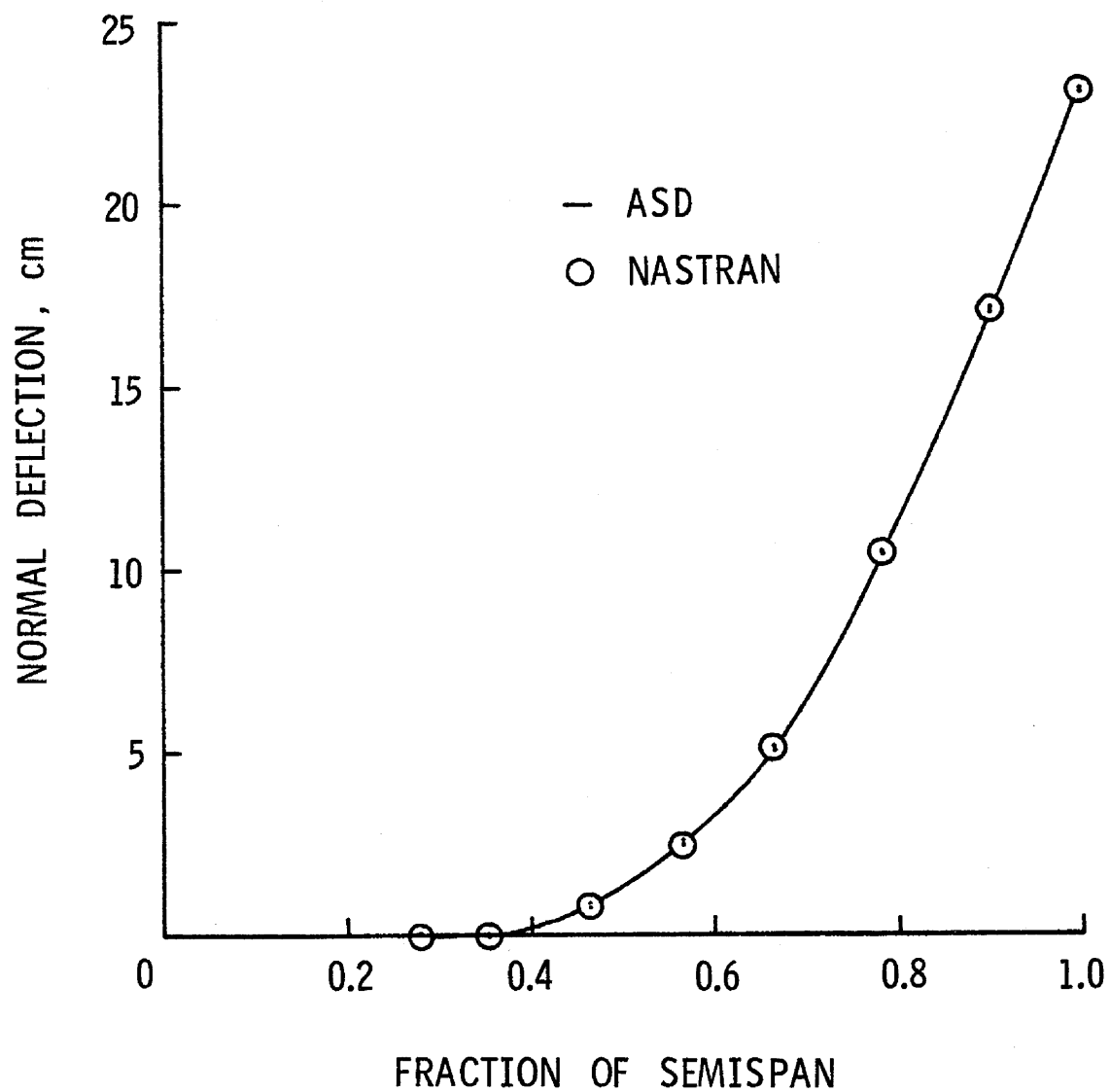


Figure 4.- Normal displacements of orbiter wing along rear spar obtained from an analysis of the wing. Wing loading corresponds to 2.5g subsonic pullup.

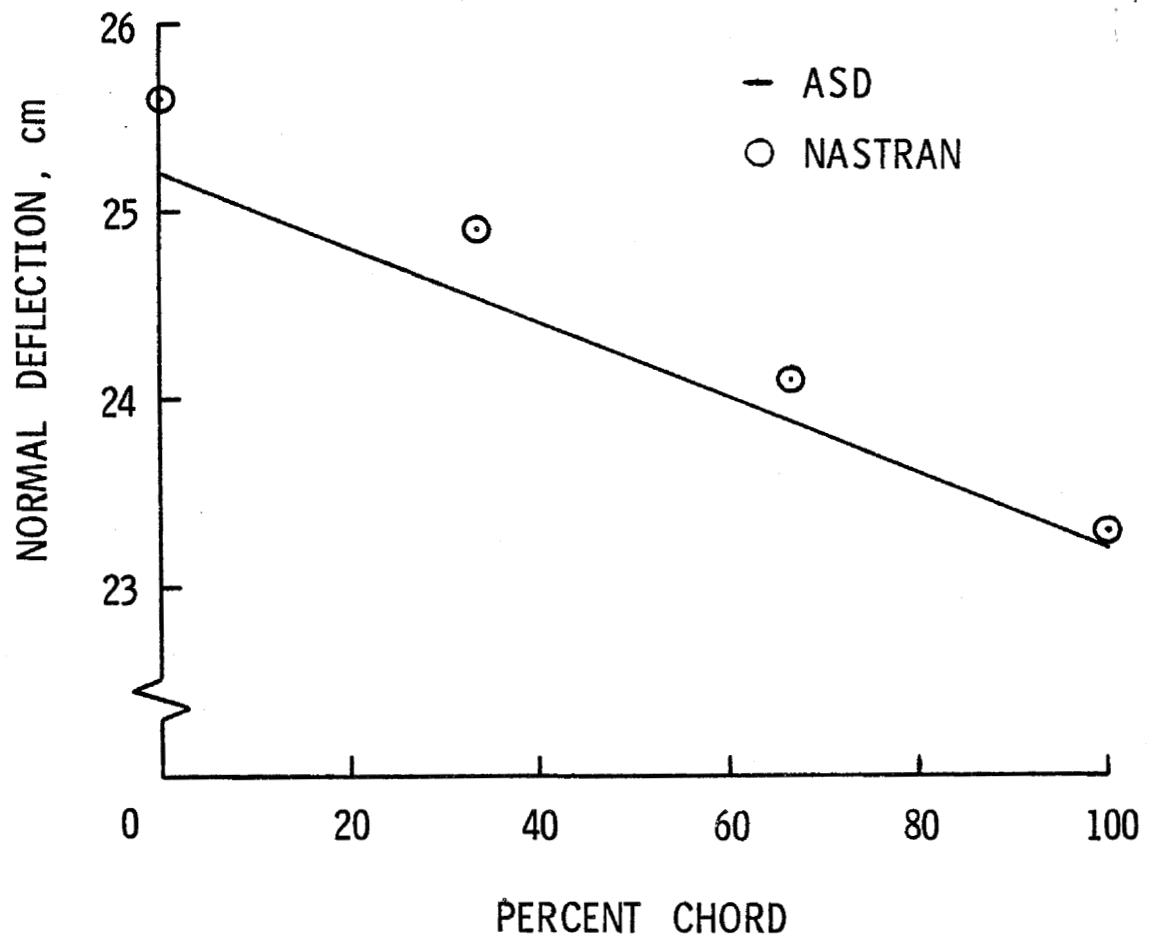
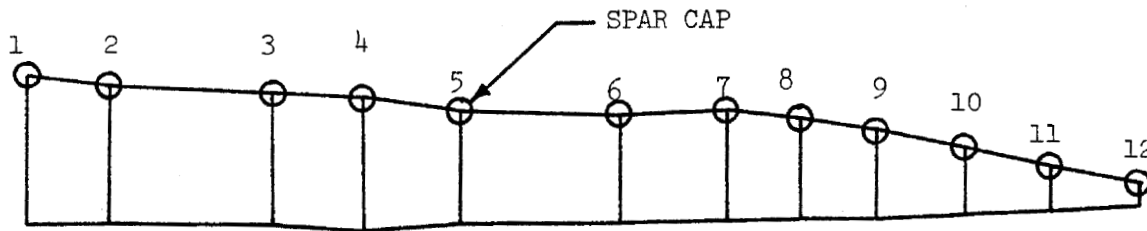


Figure 5.- Normal displacements of orbiter wing along tip rib obtained from an analysis of the wing. Wing loading corresponds to 2.5g subsonic pullup.



FINITE ELEMENT MODEL OF WING ROOT RIB

SPAR CAP. NO.	AXIAL STRESS, MN/m ²	
	NASTRAN	ASD
1	25.7	25.3
2	-14.8	-15.3
3	-100.2	-85.4
4	-89.3	-71.5
5	+6.4	-16.2
6	-51.9	-33.9
7	-1472.7	-1303.4
8	-637.8	-246.8
9	-574.2	-558.1
10	-266.1	-129.8
11	-175.4	-165.6
12	-182.5	-262.7

Figure 6.- Spar cap axial stresses at the wing root obtained from an analysis of the wing. Wing loading corresponds to 2.5g subsonic pullup.

NASTRAN AS ANALYSIS TOOL IN A STRUCTURAL DESIGN OPTIMIZATION PROCESS

By J. E. Sobieszczanski* and D. D. Loendorf**

ABSTRACT

The use of NASTRAN as the analysis tool in a structural design process is described. A section of an aircraft fuselage type structure with rings, stringers and skin idealized by 408 finite elements and 858 degrees of freedom was optimized in an analysis - evaluation - redesign closed cycle.

NASTRAN was employed in the "analysis step", with the "evaluation" and "redesign" steps supported by separate programs, and data transfer was carried out by hand. This procedure proved to be workable with turn-around time for one redesign cycle requiring one day. Approximately five redesign cycles were needed to converge to an optimized design.

INTRODUCTION

The success of any structural design procedure hinges upon the efficiency of the analysis tool used for the repetitive computation of stresses and deflections following each structural modification. Many standard computer programs exist for structural synthesis, yet they are often not readily available to engineers who may need to occasionally perform structural optimization. Furthermore, substantial time is often required to learn to use them efficiently. For some users, NASTRAN may be the only comprehensive structural analysis tool available to be used in a design process. A procedure found useful in such cases is reported in the present paper wherein NASTRAN has been used in a structural design mode supported by a small programmable desk top calculator.

* Aerospace Engineer, NASA, Langley Research Center

** Aerospace Engineer, Langley Directorate, U.S. Army Air Mobility R & D Laboratory.

AUTOMATED DESIGN PROCEDURE

Basic Objective

The subject of the design is a cantilevered cylindrical shell simulating the aft section of an aircraft fuselage. The shell shown in Fig. 1 is stiffened by rings, stringers and floor members and carries a load uniformly distributed along the floor to approximate a cargo load in a pull-up maneuver.

The objective of the design process is to reduce the weight of the shell by repeated application of the fully stressed design (FSD) procedure to stringers and skin panels in presence of reinforcing rings of different in-plane bending stiffnesses. Considering ring bending stiffness as a variable parameter an investigation of the following phenomena was carried out:

- influence of the ring bending stiffness on the bending stress distribution across the fuselage section.
- influence of the ring bending stiffness on the behavior of FSD as an iterative method.
- distribution of the stringer cross-sectional areas and panel thicknesses generated by FSD for different ring stiffnesses.
- relationship between the minimum weight resulting from FSD and the ring bending stiffness.

Computational Procedure

The design procedure consisted of an initialization and the arrangement of the following three steps in a repetitive sequence:

1. the use of NASTRAN for stress and deflection analysis
2. the use of a FSD method to correct stringer areas and skin thicknesses
3. the use of a ring sizing program to select the lightest possible ring section for a given moment of inertia, and internal forces.

An initial design consisting of assumed cross-sectional areas for stringers, cross-sectional areas and moments of inertia for rings and thicknesses for skin was chosen and the information flow proceeded as shown in Figure 2.

Input for NASTRAN was generated automatically, using a specially written program (block 2, Fig. 2), and placed on tape for subsequent reading by NASTRAN. NASTRAN (block 3, Fig. 2) analysis was performed using a finite-element model of the fuselage as shown in Figure 3. The stringers were modeled by ROD elements (tension/compression), the rings were idealized as polygonal frameworks

using CBAR elements (tension/compression and bending) and the skin was approximated by the CQDMEM elements (membrane state of stress)*. To insure that a reasonable mesh size was used around the circumference, convergency experiments were carried out by varying the angle α (Fig. 3) from 30° to 15° to 7.5° . An $\alpha = 30^\circ$ was chosen as a compromise between the desire to keep NASTRAN execution time at a minimum yet retain accuracy requirements. Therefore the fuselage model used contained 156 RODS, 132 BARS and 120 CQDMEMS with 858 unknown degrees of freedom. In view of symmetry of the load and structure, the above figures were reduced approximately one-half in the actual computation.

The FSD method (block 4, Fig. 2) used to design the ROD and CQDMEM elements was as follows:

$$\begin{bmatrix} \text{new stringer} \\ \text{cross-section} \\ \text{area} \end{bmatrix} = \begin{bmatrix} \text{old stringer} \\ \text{cross section} \\ \text{area} \end{bmatrix} \times \begin{bmatrix} \text{stress in old stringer} \\ \text{allowable stress} \end{bmatrix}$$

$$\begin{bmatrix} \text{new thickness} \\ \text{of a membrane} \\ \text{plate} \end{bmatrix} = \begin{bmatrix} \text{old thickness} \\ \text{of a membrane} \\ \text{plate} \end{bmatrix} \times \begin{bmatrix} \text{equivalent stress} \\ \text{in old plate} \\ \text{allowable stress} \end{bmatrix}$$

The equivalent stress in CQDMEM elements was computed according to the Huber-von Mises formula. Ring spacing was selected, based on Shanley's criterion (ref. 2). The ring cross-sections were assumed to be of the channel type, constant in circumferential direction. They were dimensioned by the ring sizing program (block 5, Fig. 2) which performed a constrained minimization (ref. 3) of the ring cross-section area in a way so as to make its moment of inertia equal to the given value while accounting for: buckling of the free flange, yielding, minimum gage for thickness and minimum flange width. The internal forces for stress constraint evaluations were available at this stage from NASTRAN analysis in step 1. Torsional stability of the ring cross-section was assumed to be provided by stringers which in the real structure intersect the ring in relatively close spacing. The ring spacing, shown in Figure 3, remained unchanged for all experiments, as the Shanley criterion was satisfied by a large margin for all values of the cross-sectional moment of inertia. The flow of computations shown in Fig. 2 was executed for several ring cross-sectional moments of inertia.

*For detailed description of the finite elements see NASTRAN manual (ref. 1).

To conclude the description of the flow chart (Fig. 2) components, one has to mention that block 6 represents engineering judgment rather than an automatic cut-off criterion.

The computational power used in blocks 2, 3 and 5 was supplied by a CDC 6600 computer while the FSD structural modifications block 4, were made using a Hewlett-Packard 9100 B programmable desk top calculator. All data transfer was done manually except for the transfer from block 2 to block 3 which occurred via tape within the CDC computer.

COMPUTER EXPERIMENTS AND RESULTS

The numerical experiments have been carried out adopting the load intensity and shell dimensions shown in Fig. 1, 3 respectively as representative of the numerical values which occur in the design of transport aircraft. The structure was assumed to be all-aluminum alloy with an allowable stress of $19.61 \times 10^4 \text{ kN/m}^2$ (2000 kgf/cm^2).

Influence of Ring Stiffness On Stress Distribution Across Fuselage

The influence of the ring in-plane bending stiffness on the bending stress distribution over the fuselage cross-section was investigated by assuming uniform stringer cross-section areas (5.2 cm^2) and membrane plate thickness (0.1 cm) throughout. A single NASTRAN analysis (blocks 1, 2, 3 in Fig. 2) was carried out for each of the ring moments of inertia; low, medium and high corresponding to 1.3, 65, 650 cm^4 respectively. The low end of this range of values is characteristic of a typical transport fuselage design.

Figure 4 shows stresses in stringers in the root bay obtained from this experiment. It is clear that an increase in the ring bending stiffness causes the stress distribution to approach that of elementary beam theory. Conversely, a loss of stress occurs in comparison with that theory near the extreme cross-section fiber for low stiffness ring. This loss has an obvious adverse effect on the structural efficiency in bending.

Influence Of Ring Stiffness On FSD Behavior

Having demonstrated the above relationship, attention was focused on the FSD behavior in the presence of varying ring bending stiffness. This was motivated by the fact that FSD is currently being frequently used as a tool in the structural design of fuselages. In this experiment, the computation illustrated by the flowchart in Fig. 2 (all blocks) was repeated for the following five values of the ring cross-sectional moment of inertia: 1.3, 25, 65, 200, 650 cm^4 . Figure 5 illustrates how the typical stringer area and plate thickness varied over five FSD iterations. Figure 5 also shows the stress being asymptotically driven toward the allowable.

One may note the so-called abnormal behavior of FSD in the 4th iteration for the membrane plate in presence of the medium and high ring stiffnesses. The thickness increased in this iteration, but so did the effective stress. This occurs when the increased element stiffness attracts more force than may be offset by the increment of the cross-sectional dimensions, resulting in larger stresses in the element. This phenomenon usually signals ill-behavior of the FSD and is one of the shortcomings of that method. However, in this particular case this abnormality was weak, barely discernible on the graph, and therefore did not destroy FSD convergency. Figure 5 also shows that stringer and plate dimensions converge to different asymptotical values for different ring stiffnesses.

Distribution Of Material For Different Ring Stiffnesses

Figure 6 shows the stringer areas and the plate thicknesses as they resulted after five iterations of FSD in the presence of rings of low and high in-plane bending stiffnesses. The stringer/plate material distribution is distinctly different for the two cases. For high ring bending stiffness, the largest stringer is the one most distant from the neutral axis, while, the loss of stress in that stringer for low ring bending stiffness, illustrated in Fig. 4, causes the material to shift toward the neutral axis for such a low stiffness ring and as a result stringer No. 2 becomes the largest.

As one may expect, the former distribution is more efficient than the latter (more material away from neutral axis) and, indeed, the total weight of stringers and plates for high ring stiffness amounts to 83% of the corresponding weight for the low ring stiffness.

This result suggests that increasing the ring stiffnesses has a beneficial effect on the structural efficiency of the stringer/plate assembly in bending. The ring stiffness increase, however, carries a certain weight penalty which has to be balanced with the stringer/plate weight reduction. This trade-off situation indicates a possibility of the existence of an optimal ring stiffness.

Relationship Between Minimum Weight And Ring Stiffness

The trade-off between stringer/plate weight and ring weight, determined from the ring sizing program (block 5, Fig. 2), is shown in Figure 7. This trade off is consistent for all ring stiffnesses since the ring sizing program produces the lightest possible ring for given set of constraints while, on the other hand, the stringer/plate weight is pseudo-optimized by FSD. The reduction of stringer/plate weight, curve 1, and the increase of ring weight, curve 2, are both due to an increase in the ring stiffness. The total weight of the fuselage vs. the ring stiffness is shown by curve 3, which is the sum of curves 1 and 2. For this particular fuselage example, curve 3 shows a distinct minimum in the vicinity of a ring bending stiffness equal to 25 cm^4 . For this case, a total reduction in fuselage section weight of approximately 9% may be realized or traded for about 7% to 10% of payload increase when considering the structural weight to payload ratio.

The experiments described heretofore were based on a single load condition illustrated in Fig. 1. Two additional load conditions were analyzed without FSD application, to preliminary assess their effects on the above findings. They were: internal pressure and tail vertical load. It was found for the internal pressure (0.75 atm) case that stresses are negligible compared to those generated by the load shown in Fig. 1. The tail load case analysis resulted in fuselage bending stresses which conformed to the elementary beam theory regardless of the ring stiffnesses, due to the reinforced diaphragm that closes the tail end of the fuselage. Thus the ring optimality problem in the sense defined in this paper cannot be posed for this loading case.

This statement may be elaborated upon as follows. The essential difference between the tail load and the load distributed as shown in Fig. 1 is that the former does not have the gradient of the shear force on the fuselage cross-section in the longitudinal direction which is present in the latter and necessary for the ring stiffness effects to appear. This may be explained as follows. The stress distribution in the fuselage for the low ring stiffness appears to be similar to shear-lag in a torsion box. This shear-lag phenomenon in a torsion box is due to panel deformations in shear only, while in the fuselage, it is amplified by in-plane bending deformation of the rings. This in-plane bending will occur only when there exists a longitudinal gradient of the shear force on the fuselage cross-section. In the present case, this gradient was due to the concentrated floor loads along the length of the fuselage section.

CONCLUSIONS

The following conclusions result from the above experiments. The in-plane bending stiffness influences the stress distribution over the fuselage cross-section when the loading case is such that a gradient of shear force on the fuselage cross-section exists in the longitudinal direction. For rings with low bending stiffness, there is a loss of stress in the fibers most distant from the neutral axis.

Increase of the ring stiffness increases the ring weight and decreases the stringer/plate weight which results in the existence of a minimum in the total weight function. A total weight reduction of up to 9% has been demonstrated by selecting an optimal ring stiffness. The optimal ring stiffness was found to be considerably larger than the one required for overall stability of the stiffened shell according to Shanley's criterion.

Numerical experiments such as those described in this paper undoubtedly require a fast, reliable and convenient-to-use program to carry out repetitive structural analysis. NASTRAN turned out to be such a tool, with the convenience of its input - output formats helpful in assembling other auxiliary programs around it.

Computation times for one passage through the flow chart (Fig. 2) were:

- NASTRAN analysis 106 CPU sec. 825 PPU sec.
- Hewlett-Packard "on the machine time" 5 min.
- Manual data transfer 10 min.
- Turn around 1 day.

The conclusion is that the speed, reliability, and operational convenience offered by NASTRAN encourages its incorporation as a "black box" into computer program systems created specifically for a given purpose and that good practical results may be achieved in very realistic calendar time even without a "hands off" interface between NASTRAN and its companion programs.

Another resulting suggestion is that the potential of such NASTRAN centered computer program systems would gain enormously had there been a way to fully integrate NASTRAN with other programs into a repetitive loop.

REFERENCES

1. McNeal, R. H.: The NASTRAN Theoretical Manual NASA SP-221. NASA, OTU, Sept. 1970, chapter 5.
2. Shanley, R. F.: Weight-Strength Analysis of Aircraft Structures. McGraw-Hill, N.Y., 1952, pp. 65-72.
3. Fox, R. L.: Optimization Methods for Engineering Design. Addison-Wesley Publ. Co., Reading, Mass., 1971, chapter 4.

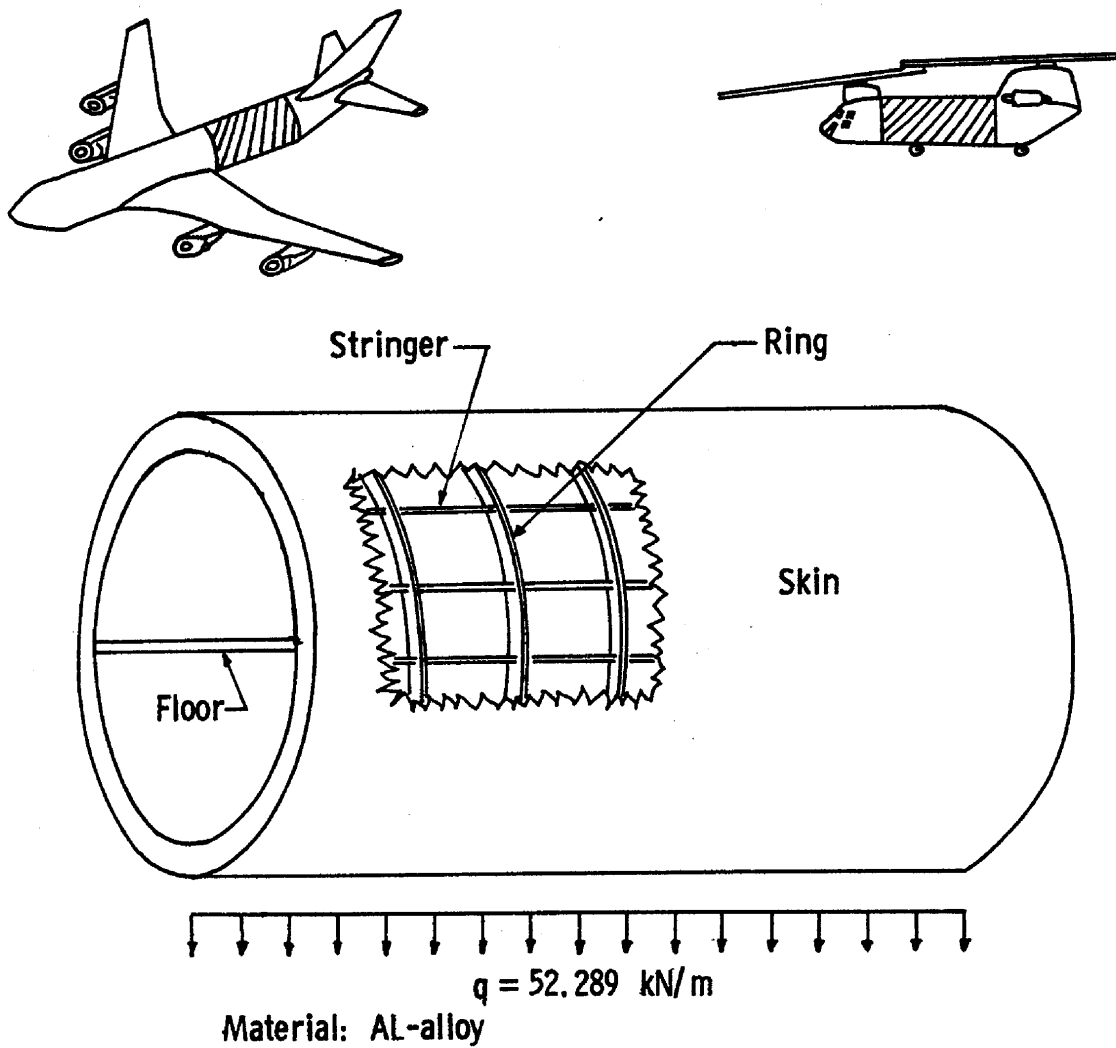


Figure 1. Section of an aircraft fuselage with a uniformly distributed load

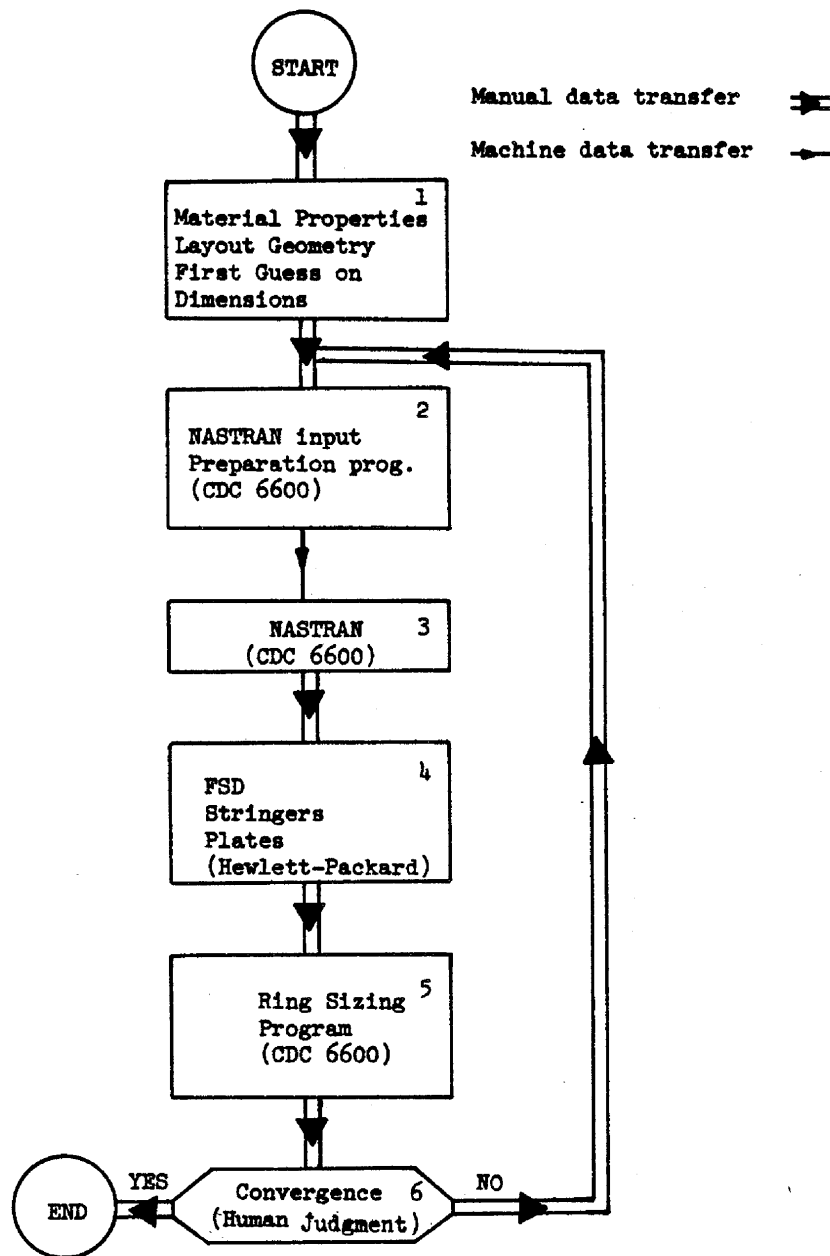


Figure 2. Flowchart of the redesign process

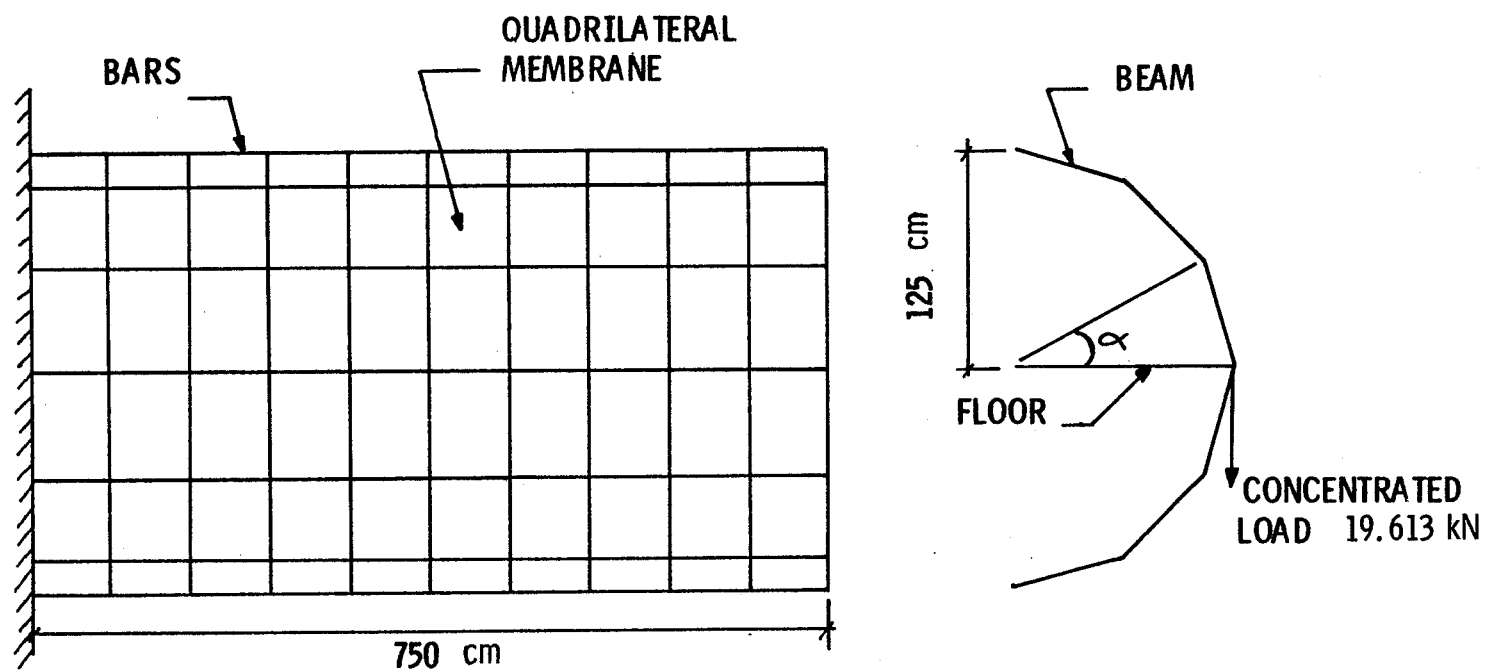


Figure 3. Idealized finite element model of the fuselage section

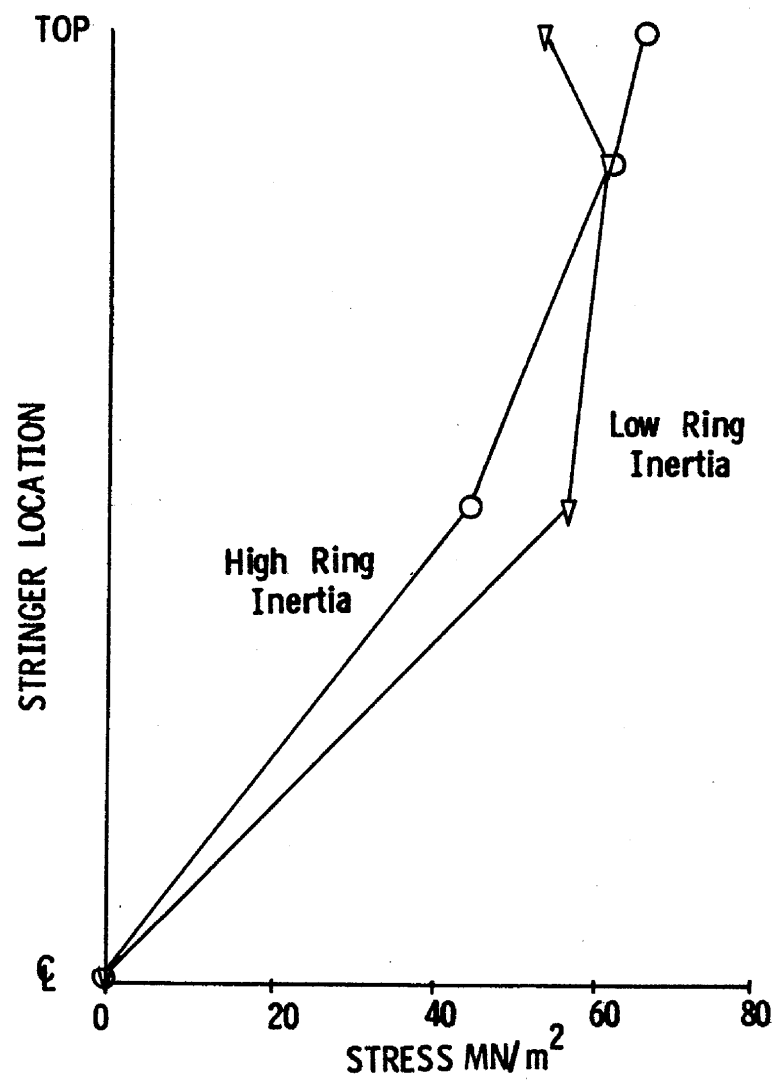


Figure 4. Bending stress distribution in the stringers over the fuselage cross-section for different ring stiffnesses

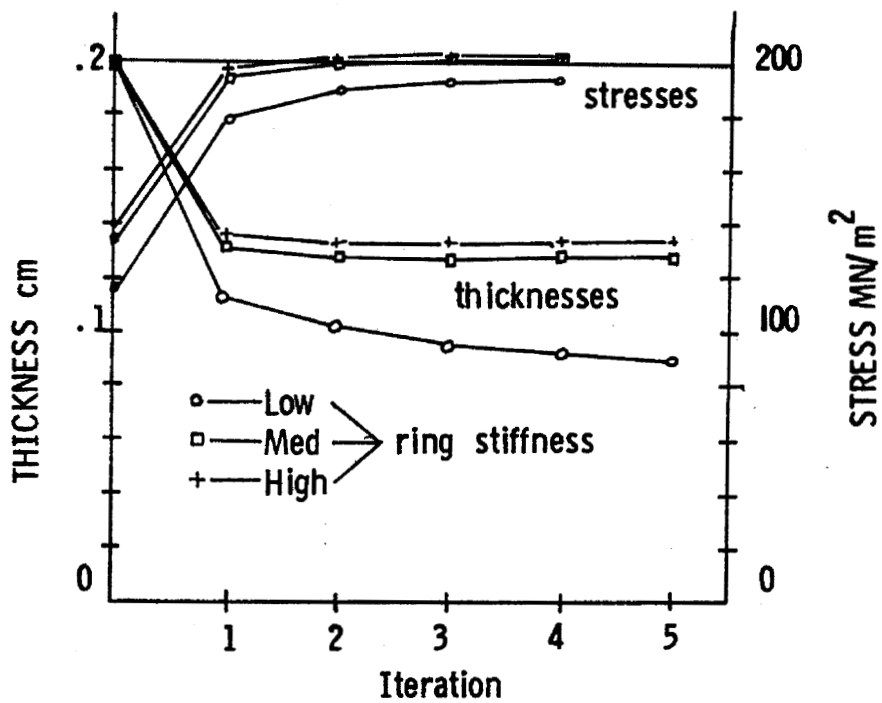
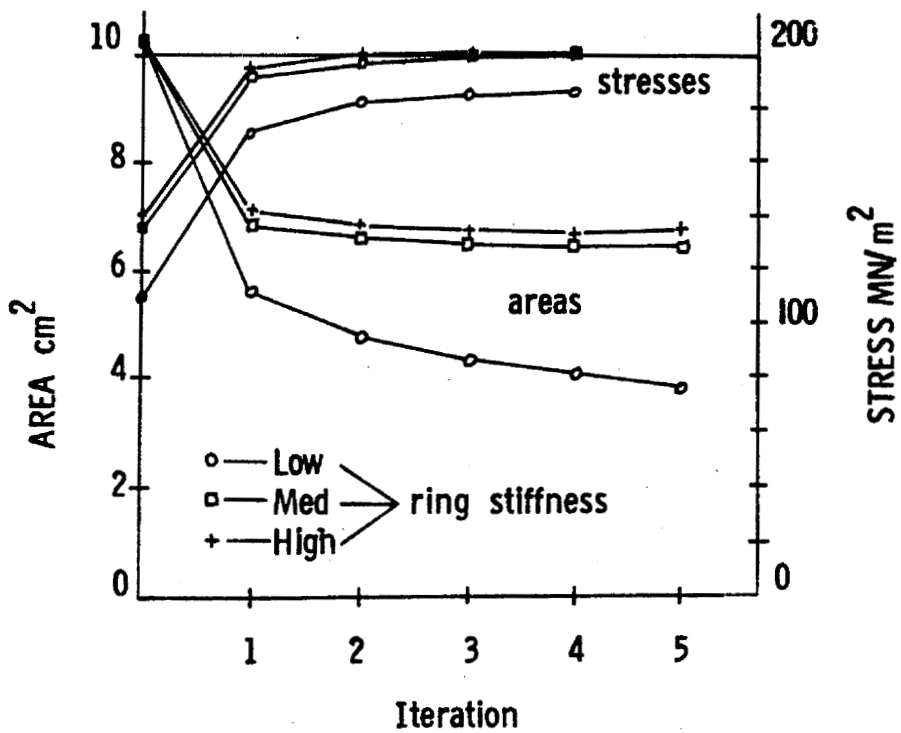


Figure 5. History of five FSD iterations for different ring stiffnesses

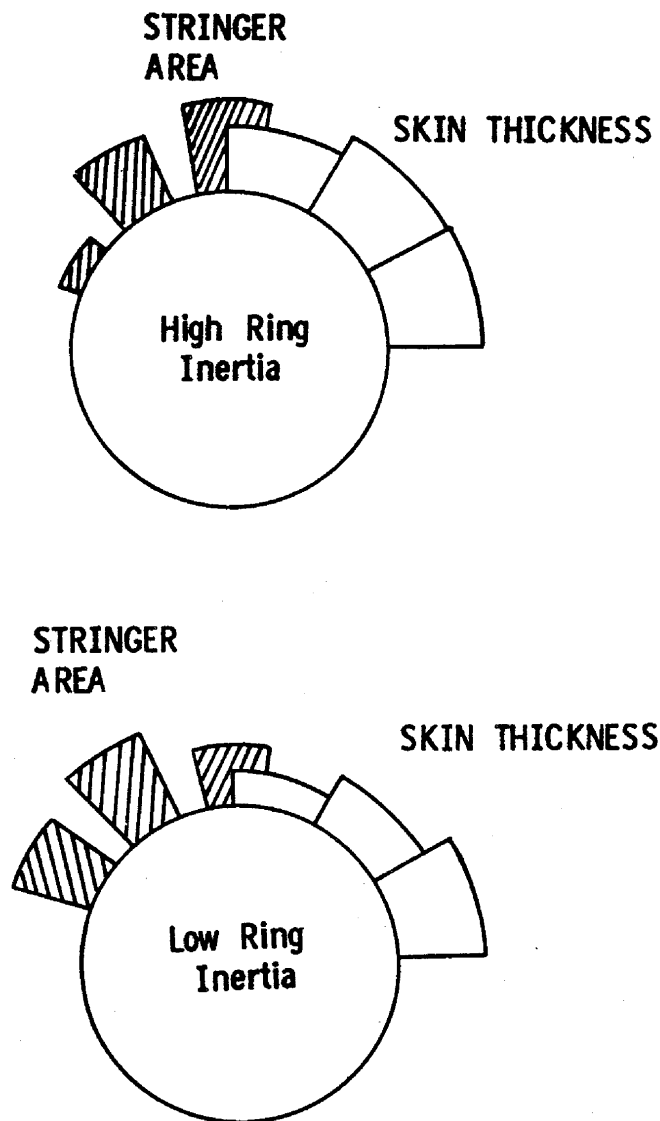


Figure 6. Stringer area and plate thickness distribution after FSD for low and high ring bending stiffnesses

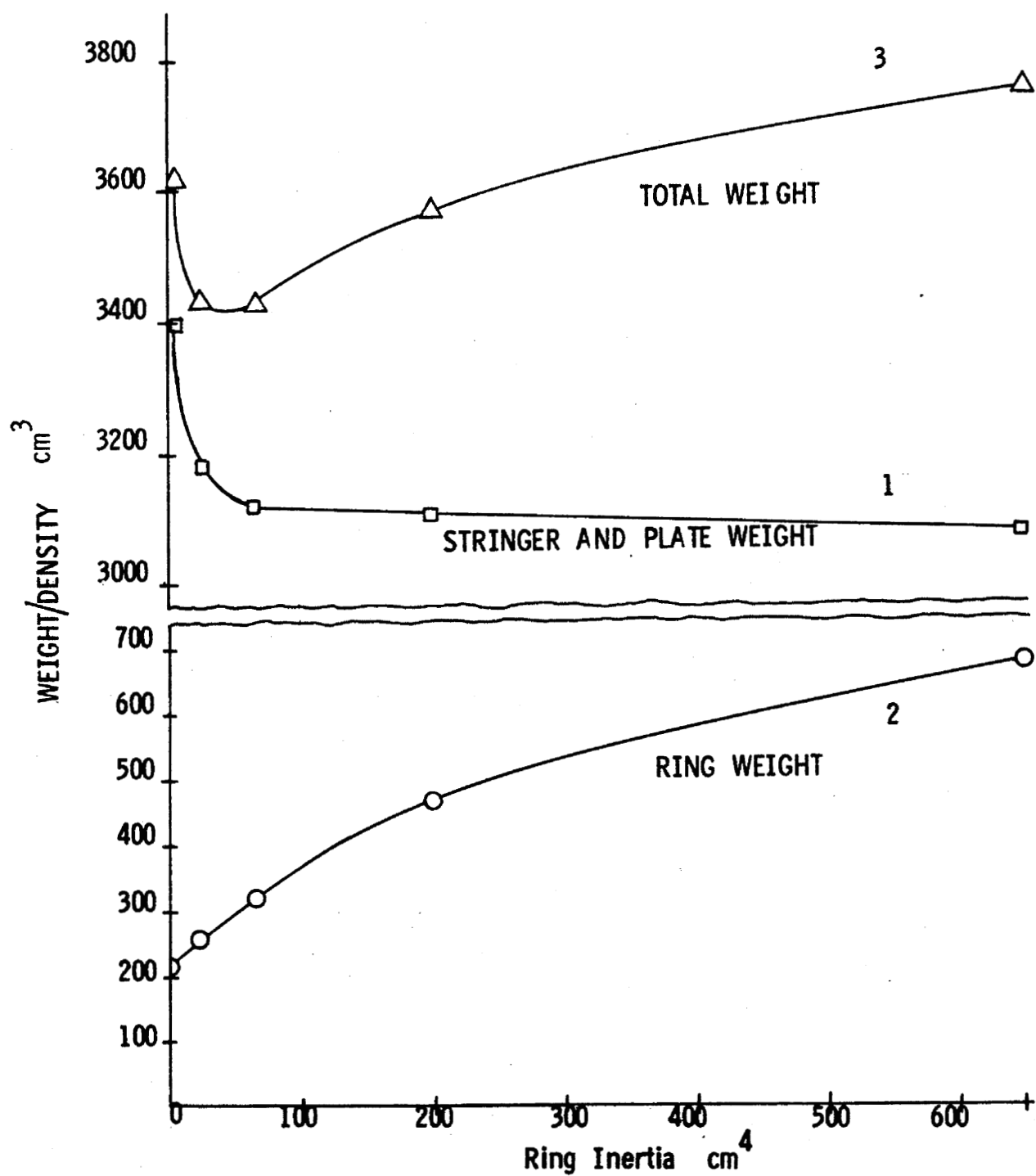


Figure 7. Trade off between ring weight and stringer/plate weight resulting in optimal ring stiffness

STRUCTURAL ANALYSIS AND DESIGN OPTIMIZATION OF SPACECRAFT USING NASTRAN

By Roy L. Courtney

NASA Goddard Space Flight Center

SUMMARY

The practical application of NASTRAN in the structural analysis and design optimization of spacecraft structures includes the statement of design objectives, definition of loading conditions, creation of NASTRAN models capable of meeting the design objectives, and evaluation of numerical results to achieve the final design. Two approaches to modeling spacecraft structures are suggested. Specific examples of load definition, NASTRAN-modeling techniques, and methods of interpreting results are drawn from the analyses of several spacecraft under study and design at Goddard Space Flight Center (GSFC). These examples show that NASTRAN can be of practical use in designing an optimum structure in the initial phase of a spacecraft program.

INTRODUCTION

Structural analysis and design optimization of spacecraft begins with conceptual layout drawings representing the configuration that best satisfies the systems requirements as defined by the members of the design team. The general arrangement of significant components and primary structure should be identified. Structural details such as material selection, cross-section design, and arrangement of secondary structure are the subjects for analysis and optimization.

Early introduction of NASA's NASTRAN program into the design process provides a strong analytic basis for evaluation of options, knowledge of structural behavior, and implementation of specific design objectives.

DESIGN OBJECTIVES

A clear statement of the objectives for a specific design aids the structural analyst using NASTRAN in developing the best mathematical models of the problem to obtain the desired results. The degree of planning and of modeling detail is a function of the purpose for studying the structure.

Design objectives can range from merely establishing the adequacy of an existing design to requiring that the current configuration be evolved to one having minimum weight, minimum deflections, and evenly distributed loading for all significant static and dynamic loads.

Each objective suggests very different approaches. For example, the analyst may choose to demonstrate design adequacy of a spacecraft concept by verifying only certain critical structural members by hand calculations or coarse-grid math models.

Requiring an optimum spacecraft design suggests that the analyst must create both a family of math models of the entire structure to demonstrate efficient load paths, and a series of models of significant components to compare design alternatives, deflections, stresses, and loads.

Associated with defining design objectives is establishment of acceptance criteria for evaluating analytic results of NASTRAN models, such as acceptable stress levels of materials, maximum deflection limits for critical-alignment components, and the desired structural behavior under load. Application of appropriate acceptance criteria to analytic results guides the analyst to an acceptable design.

DESIGN LOADS

Design loads used in the initial evaluation of spacecraft concepts are defined by a combination of dynamic launch-environment loads including acceleration, vibration, and spin. To permit these loads to be applied statically to the primary structure of the spacecraft, its lowest resonant frequencies in both thrust and lateral directions are assumed initially to be at least a factor of two above those of the launch vehicle. This assumption is verified by frequency analysis of the NASTRAN model of the spacecraft. If spacecraft and launch-vehicle resonant frequencies coincide, several approaches are available:

- (1) Modifications to the structure may be required to change the spacecraft resonance or to withstand increased loads.

- (2) The math-model results justify a coupled dynamic analysis of spacecraft and launch vehicle, which may result in a notching of the vibration spectrum of the launch environment.

Table 1 summarizes a set of static design loads that are typical of a Delta launch vehicle with a spin-stabilized third stage. These worst-case loads are based upon a 2-sigma (2σ) range of measured-flight loads multiplied by a 1.5 factor of safety for design.

Increased symmetry in the environmental loads relaxes the requirement for complete NASTRAN modeling. The model must be adequate to react only to the most general load to be applied. For example, conditions 1 and 2 in Table 1 are axially symmetric with respect to the thrust and an arbitrary lateral axis.

Consider a spacecraft symmetric about its thrust axis during launch, a frequent configuration for spin-stabilized spacecraft; then, a NASTRAN model needs to include only half of the spacecraft divided by its plane of symmetry. Use of the proper boundary conditions at the cut plane simulates the symmetric reactions of the omitted half. The axial load of condition 3 in Table 1 could be applied to the NASTRAN model of the smallest segment of symmetric geometry, e. g., a one-eighth segment of a structure with eight symmetric compartments.

Table 1—Typical design loads for the Delta launch vehicle.

Load Condition	Source	Axis	Load (g)	Spin (rpm)
1	Lift-off	Thrust	3.0	0
		Any lateral	3.5	
2	First and second stage	Thrust	15.8	0
		Any lateral	3.0	
3	Third stage	Thrust	17.4	90

CREATING THE NASTRAN MODEL

Approaches

The major problem in using NASTRAN to solve structural problems is the creation of a math model that sufficiently represents the structure to obtain accurate results while reducing the size of the problem to run efficiently on general-purpose computers. Practical experience has shown that complex NASTRAN problems requiring large amounts of core and long time requests receive low priority on the computer, causing

long dead times in the analysis. All modeling techniques should be directed toward creating an individual problem to achieve the design objectives while running efficiently with minimum core and time requests on nondedicated machines.

Two approaches used to answer specific design questions have been developed for structural analysis of spacecraft: (1) creation of a family of NASTRAN models of the entire spacecraft with components differing between problems in arrangement and properties, and (2) development of NASTRAN models of individual structural components.

In the former the scope and complexity of the problem require structural features to be coarsely modeled with few elements and interconnections. Gross effects of loads on the structure, such as load path and total deflection, are compared for successive concepts to arrive at a final, evenly loaded configuration. Figure 1 shows as an example the half-spacecraft NASTRAN model of the Planetary Explorer spacecraft recommended in its Phase A study. * A GSFC document** describes in detail the development of this concept-evaluation model.

For the second approach individual structural components can be modeled with adequate elements and connections yielding detailed values for local stress and deflection, thus permitting evaluation of subtle structural changes in a single component. Loads can be defined by the spacecraft design loads or derived from the results of the coarse model of the entire spacecraft. Figure 2 shows the NASTRAN model of one-twelfth of the main platform for the Planetary Explorer consisting of 243 CQUAD2 elements.† This segment of the platform, represented by only two CQUAD2 elements in the half-spacecraft model (Figure 1), was used to determine an arrangement of platform-support struts to minimize midspan deflection and to investigate the structural impact of imbedding heat pipes in the core of the sandwich-material platform. Twelve platform-support struts were recommended for the entire platform. Addition of three circumferential heat pipes reduced deflection of the unsupported midspan by a factor of two compared to the platform without heat pipes.

Modeling Techniques

Coordinate Systems

Convenient coordinate reference systems for the spacecraft are generally established at its interface with the launch vehicle, where input loads are defined and

* Marcotte, Paul G., dir.: Planetary Explorer, Phase A Report and Universal Bus Description. NASA GSFC internal report, May 1971.

** Hewitt, Dennis R.: Planetary Explorer Structural Concept Evaluation Model Using NASTRAN. NASA GSFC document X-762-71-181, April 1971.

† NASTRAN mnemonic for input cards and defined in Reference 1.

resultants are required. Definition of reference systems at interfaces of components supplied by various contractors can simplify exchange of structural data and models. Additional coordinate axes can easily describe symmetric geometry, e.g., use of a cylindrical coordinate system only to define the truncated conical section of a spacecraft centerstructure.

GRID-Point Patterns

GRID points (the connection points of structural elements) are arranged in patterns to suit the purpose of the model. Coarse spacing permits load-path analysis, whereas fine spacing accommodates modeling of structural details. Solution accuracy is directly related to the fineness of GRID arrangement. Regions of a structure for which detailed results are desired may be finely modeled, and regions of less interest more coarsely represented.

The pattern of GRID points for surfaces modeled by plate elements should strive for square quadrilaterals and equilateral triangles. The ratio of height to base should never exceed 3:1, because basic assumptions used to develop these elements are violated at higher ratios.

By preassigning different blocks of numbers for GRID-point identification to each component of a spacecraft, the unmodified bulk-data decks of individual problems can be merged to create a model of the entire structure, thus averting much of the tedious job of developing the bulk-data deck.

Proper sequencing of GRID-point identification numbers by initial assignment or resequencing with the SEQGP card minimizes computer storage and time requirements. The decomposition of the coupled structural stiffness matrix, described in Reference 2, is simplified by reducing the bandwidth of coupled degrees of freedom and eliminating or greatly reducing the number of off-diagonal terms. In the NASTRAN model the analyst strives to minimize the following:

- (1) The number of GRID points, each having six degrees of freedom, between successive sets of similar geometry.
- (2) The incidence of connections between sets of similar geometry to a common GRID point.

A typical scheme for GRID-point sequencing of a similar set of structural geometry (Figure 3) begins with GRID-point numbers at the top of the structure, continues downward through significant connections of structural members, and ends at the point of connection between adjacent sets of similar geometry. The initial bandwidth for this model is the number of degrees of freedom per GRID point multiplied by the number of GRID points in a set of similar geometry plus one, i.e., $6 \times (18 + 1) = 114$. This grid pattern repeated at 13 stations at 15-degree intervals about the centerline forms

the half-spacecraft model shown in Figure 1. The connection between GRID points 10 and 500 represents the off-diagonal term that is treated as an active column in the decomposition of the coupled-structure stiffness matrix.

Element Selection

The structural analyst decides upon the desired behavior of each component and selects the appropriate NASTRAN finite element to implement that design. If a long and slender structural member transmits only torsion, tension, and compression, the CTUBE element should be chosen rather than the more general CBAR element, which includes bending.

The following points have been very useful in the practical modeling of spacecraft:

- (1) Triangular plate elements provide the required transition between regions coarsely and finely modeled by quadrilateral elements.
- (2) Lumped-mass elements (CMASS) conveniently represent undefined or ill-defined components for which weight and mass properties are assumed or known.
- (3) Multipoint constraint (MPC) equations should be used to connect certain concentrated mass elements to the rest of the structure; however, these are complex and tedious to implement. A practical alternative is to provide the desired connection by fictitious CBAR elements with properties of high stiffness relative to the rest of the structure, and no mass. A rigid connection is provided without adding weighted elements to the structure. This technique was used to connect the solid propellant motor to the center structure for the Planetary Explorer model, GRID points 500 and 10, respectively (Figure 3).
- (4) Use of NASTRAN utility programs described elsewhere* to generate coordinate, geometry, connection, and property cards for certain restricted geometrical shapes greatly reduces the tedious job of bulk-data encoding.

Property and Material Definition

Property and material characteristics must be defined consistently with mass units, or with weight units used with the appropriate value for the parameter WTMASS defined on the PARAM card.

* Cook, William L.: Automated Input Data Preparation for NASTRAN. NASA GSFC document X-321-69-237, April 1969.

Boundary Conditions and Single-Point Constraints (SPC)

When spacecraft symmetry permits the modeling of a segment of the entire structure, care must be exercised to constrain to zero the appropriate degrees of freedom along the cut plane to represent balanced reaction by adjacent segments for loads acting parallel with the cut plane. Figure 4 shows that degrees of freedom 2, 4, and 6 in a cylindrical coordinate system are balanced and therefore set equal to zero for GRID points along the cut plane of the hemicylinder.

A major source of NASTRAN-job failures for a new model is GRID-point singularities arising from unconnected degrees of freedom. Degrees of freedom connected to elements for which no stiffness exist are conveniently set equal to zero by SPC cards, e.g., rotation in the plane of a plate element is not permitted.

EVALUATING THE NASTRAN RESULTS

Numerical Results

Several approaches can be taken in evaluating the numeric results of a successful NASTRAN job. For the math model of the entire spacecraft that has been modeled relatively coarsely, specific results should be compared between several NASTRAN models representing structural alternatives to discern trends and effects caused by the modification in structure. The significant observation is the change in value of a particular parameter between configurations, not its absolute value, since its source is a relatively coarse model.

In the numeric results of a fine-grid math model of a structural component, primary emphasis is placed upon the absolute value of a parameter, e.g., stress and deflection. The criteria of acceptance defined by the analyst is applied directly to the numeric results to determine the value of the analyzed design. The designer verifies that the spacecraft-design criteria have been met, e.g., stress or deflection limits have not been exceeded while ensuring that the member is contributing efficiently to an overall lightweight design.

One problem the structural analyst has is the volume of numeric results computed by NASTRAN. Additional evaluation techniques are required to communicate NASTRAN results to other members of the spacecraft-design team for decision upon the final recommended configuration.

NASTRAN Graphics

Structure and xy-plotting generated by NASTRAN are extremely useful aids in interpreting analytic results. Principal uses of structure plotting in spacecraft design include—

(1) Identifying modeling errors of geometry definition, element connection, boundary specification, and omission of elements, as shown in Figure 5 for a spacecraft configuration.

(2) Visualizing relative displacements of complex models under combined loads.

NASTRAN structure plotting capability used alone and in conjunction with a shadowing computer program, reported in Reference 3, provides a valuable tool in several nonstructural analyses required in spacecraft design. The desired spacecraft configuration is modeled only by geometry definition and PLOTTEL elements, which merely connect two points graphically when plotted. Varying the projection angles of the model creates a series of plots that are analyzed to optimize the configuration. Thermal, power, and attitude control systems are aided, respectively, through depicting shadowing of one component by another, projected solar-array area, and center of pressure. Alternate configurations are compared by modifying geometric definition of the spacecraft model. A NASTRAN model (Figure 6) consisting of only PLOTTEL elements was used to evaluate solar-array configurations for the Small Applications Technology Satellite study.

User Graphics

Occasionally the user must create special graphic displays to augment those of NASTRAN for comparison of numeric results and communication with other members of the spacecraft-design group. A sketch (Figure 7) of the structural configuration with loading, deflection, and forces for one of many configurations studied provided a concise basis for evolving an optimum configuration for the Planetary Explorer study.

RECOMMENDATIONS

To aid the analyst, the following additions to the capabilities of NASTRAN are recommended for implementation:

(1) Provision for automated multipoint-constraint (MPC) equations calculated from the initial configuration of specified degrees of freedom.

(2) An option for a diagnostic computer run of the complete structural problem without execution of time-consuming mathematics.

CONCLUDING REMARKS

Typical conclusions from NASTRAN analysis of spacecraft structures include the following:

(1) A recommended structural arrangement for optimal loading and efficient structural components evolved through concept-evaluation models of the entire spacecraft.

(2) Specific values of engineering-design parameters (e.g., stress and deflection) for selected structures determined through models of individual components.

NASTRAN has been an important practical tool in the structural design and analysis of spacecraft during the initial phase of certain spacecraft programs at GSFC. To ensure efficient design of spacecraft structures, the use of NASTRAN on current and future NASA programs should be encouraged and required.

REFERENCES

1. The NASTRAN User's Manual. C. W. McCormick, ed., NASA SP-222, October 1969.
2. The NASTRAN Theoretical Manual. R. H. MacNeal, ed., NASA SP-221, October 1969.
3. Skladany, Joseph T., and Rochkind, Allen B.: Determination of Net Thermal Energy Incident on a Satellite. Paper 67-HT-56, ASME-AIChE Heat Transfer Conference, August 1967. Available from UNITED Engineering Center, 345 East 47th Street, New York, N. Y.

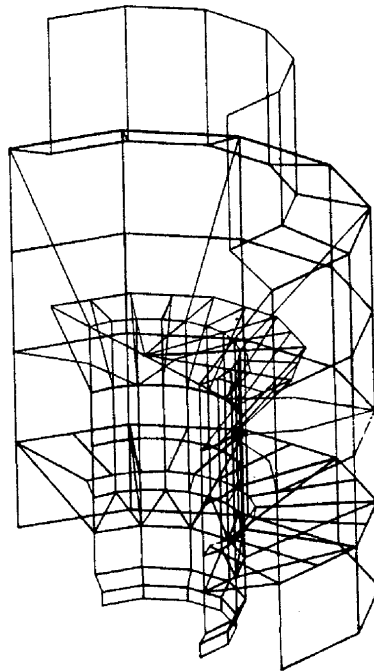


Figure 1.—NASTRAN model of one-half of the Planetary Explorer spacecraft.

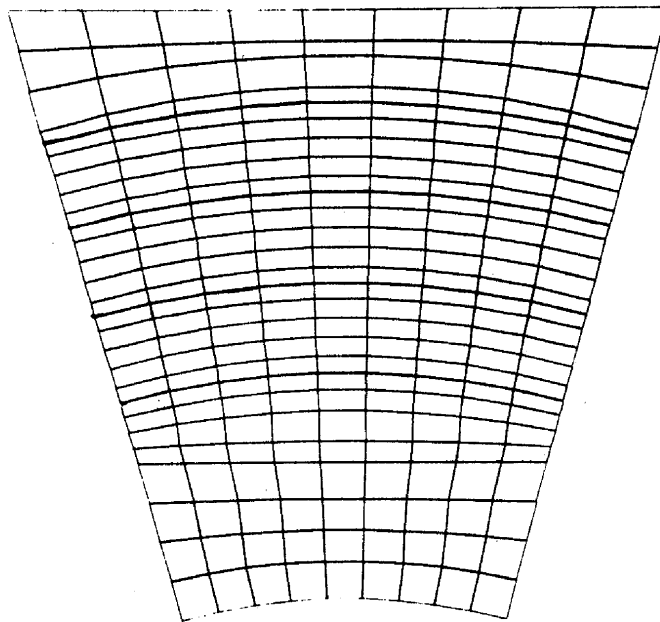


Figure 2.—NASTRAN model of one-twelfth of the platform for the Planetary Explorer spacecraft.

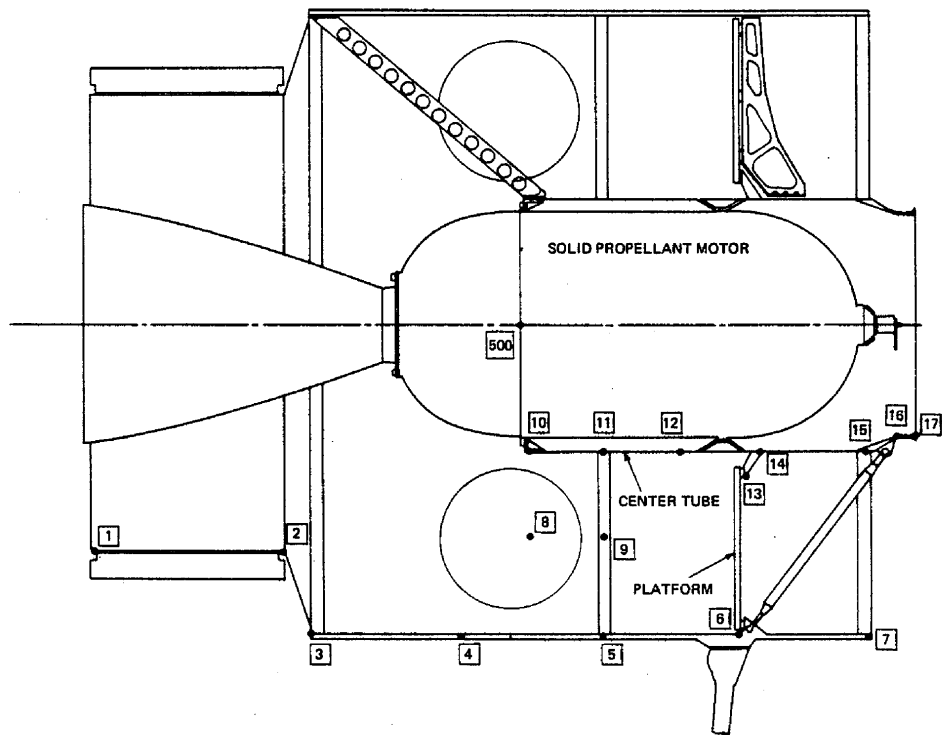


Figure 3.—Typical sequencing of GRID points for NASTRAN modeling of spacecraft structures.

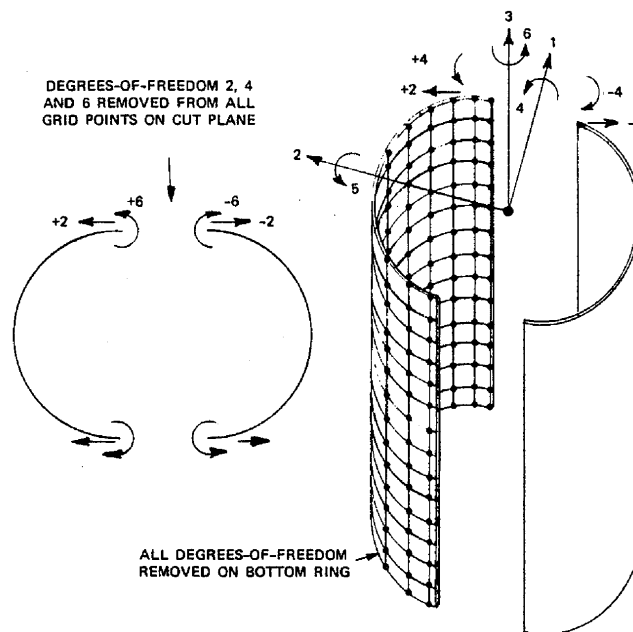


Figure 4.—Balanced degrees of freedom for GRID points on the cut plane of a NASTRAN model.

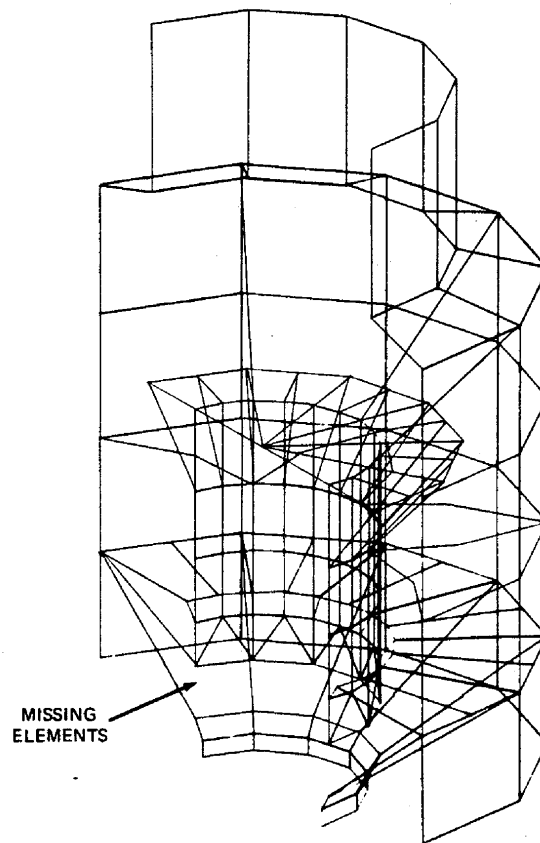


Figure 5.—Identification of modeling errors through the NASTRAN structural plots.

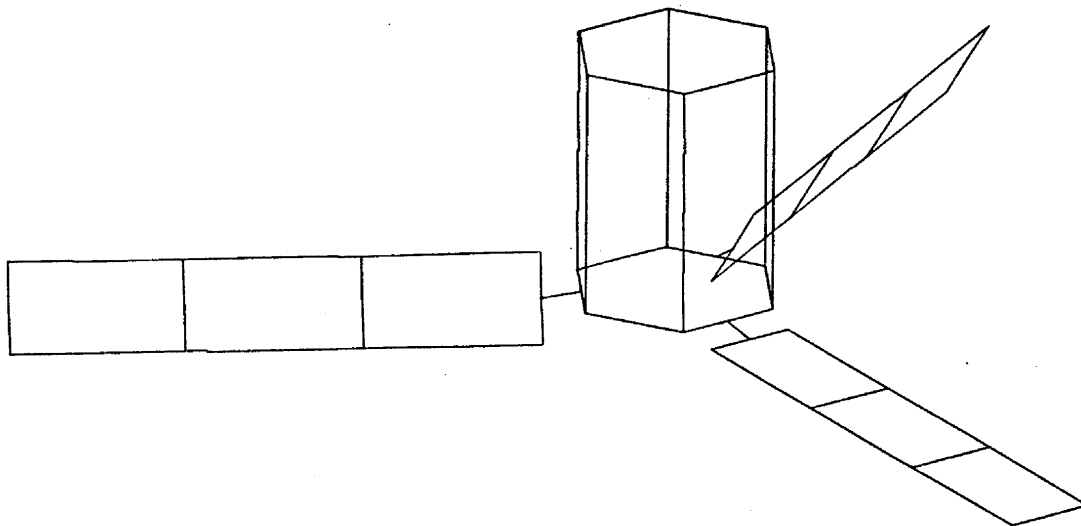


Figure 6.—NASTRAN structural plot used for configuration analyses of the Small Applications Technology Satellite.

THE USE OF NASTRAN IN THE ANALYSIS
OF LARGE COMPLEX AIRFRAME STRUCTURES -
MODELING TECHNIQUES AND ORGANIZATION

By Gernot W. Haggemacher, Lockheed California Company

CONTENTS

INTRODUCTION

1. ANALYSIS, PURPOSE, AND STRUCTURAL MODEL DESCRIPTION
2. DATA ORGANIZATION
3. SELECTED STRUCTURAL PROBLEMS
4. OBSERVATIONS ON THE USE OF NASTRAN FOR LARGE AIRCRAFT STRUCTURES

INTRODUCTION

This report presents a brief evaluation of the NASTRAN system based predominantly on a large airframe analysis performed for NASA AMES. In addition to this analysis NASTRAN has been used in the past two years for a variety of airframe structure analyses in support of projects.

The NASTRAN system has been found to be very versatile, fairly easy to use when following the rigid format, with many outstanding features.

Preceding page blank

Within the scope and purpose of this paper, it is hardly avoidable that the discussion can only point out selected features which were particularly helpful. Apart from this it is felt that an emphasis on problems, difficulties and errors encountered in this work will be more helpful in the further development of the system.

These applications were made in a production environment which includes the use of unskilled help as well as skilled personnel with no finite element experience. The effort was directed by a small staff with more than ten years background in the field, which include the SST, L1011, and S3A operations and the use of other program systems. This forms the background on which this use of the system was measured.

Partly NASTRAN fulfilled and improved on many of our advanced requirements; in other parts it does not have capabilities which we were used to; thirdly, and naturally, it still falls short of our pipe dreams.

1. ANALYSIS, PURPOSE, AND STRUCTURAL MODEL DESCRIPTION

The YF12 structural model analysis which is the main source for this paper was performed under contract to NASA AMES, with three purposes in mind:

- a) The principal purpose of the work was to provide a detailed structural model for internal load-stress analysis, as well as for dynamic (model) analysis, to support an extensive test and flight test program.
- b) A second purpose is to use this analysis for an evaluation of the practical aspects of using NASTRAN for a large and complex airframe analysis, and of the problems which may arise from using the same detailed model for dynamic analysis. (Modal and flutter analysis.)
- c) A third purpose was to make such modifications to NASTRAN as would either be necessary to accomplish the purpose or add considerably to the efficiency of the analysis. This aspect is discussed in a separate presentation.

The analysis model was developed in close cooperation between NASA AMES and the Lockheed California Company. It was deliberately designed to be somewhat more elaborate than what might be considered adequate for this type of aircraft to more properly serve the purpose. Indeed the complexity of the model was doubtless very instrumental in pointing out certain strong and weak points of the NASTRAN system.

The statistics of the model and a general view of the airplane it represents are shown in figure 1. The model may be considered rather elaborate for this type of craft and construction. The number of freedoms and elements used for the analysis of modern airliners may however easily exceed those of the present model.

A top view of the total airplane model is shown in figure 2. It is a symmetrical half-structure, with proper boundary constraints for symmetrical and anti-symmetrical conditions at the symmetry plane. The detail includes all wing beams, wing ribs, nacelle frames and major fuselage frames. Secondary fuselage frames (2 for each main frame) are omitted. Additional chordwise wing caps, without ribs, are used to represent chordwise stiffness of the wing surface structure. Elements used are exclusively:

- ROD - elements for longerons, beam caps and chordwise surface caps
- SHEAR - panels for skin and bulkhead shear
- BAR - elements for frames and selected longerons

On the fuselage and nacelle all principal longerons are represented by Rod elements. To adequately define the circumferential contour of the shell, additional points with longitudinally connecting rods and surface Shear panels are used. These secondary rods represent only a nominal axial stiffness of the fuselage and nacelle skin to adequately subdivide the shell shear panels.

The fuselage frames do not coincide with the wing-beams; note the exception of the two beams bounding the main gear well.

The wing-beam nacelle-frame joint fittings are modeled very closely as trusses, the remainder of the nacelle frame is modeled by bar elements with offsets to represent the rather deep frames. The transition from the truss to the BAR's is made by MPC equations.

A very large number of MPC equations were used for a variety of problems; more of this later. Membrane elements were not used for two main reasons.

- a) The wing surface of the aircraft is designed for chordwise and shear-stiffness, very low spanwise stiffness and approximately zero Poisson's ratio.
- b) Triangular and quadrilateral constant strain membrane panels are not sufficiently accurate in a widely spaced, non-square mesh arrangement.

Figure 3 shows a complete wing-beam nacelle-frame model assembly as plotted by NASTRAN. Detailed plots of this nature were used extensively with great success for checkout. Overall plots of everything are very impressive but of limited practical use. Model beams consist of an inner pair of RODS for main caps, and an outer pair presenting the (rather low) spanwise skin effectiveness. Plots of the outer wing and the aft fuselage are shown in figures 4 and 5.

2. DATA ORGANIZATION

For an analysis project of this size, and with a large number of people involved in the data preparation phase, a tight organization of data preparation and checking is a key to success.

To achieve this an elaborate data numbering system was set up ab initio which proved a great help in organization, checking and cross referencing of the data. The NASTRAN BULK DATA ID system made it possible to completely integrate the NASTRAN identification into this reference system.

A number of standard tabular forms were established for GRID-PS, SPC, MPC, and CBAR inertias and pin flags, to aid in the organization, bookkeeping, cross referencing and data checking. For a large structure such as this, the property identification must be identical to the connection identification. Approximately 15 different materials were used, and 6 coordinate systems for different parts of the aircraft.

All data identification numbers include a key which identifies the structural part and the model-fuselage station where it belongs. That same key is used for model drawing numbers and paragraph and page number for all back-up data and calculations.

3. DISCUSSION OF SELECTED STRUCTURAL PROBLEMS

This section discusses the representation of some particular structural problems using NASTRAN program features, other than the more or less routine use of structural elements.

3.1 MULTIPOINT CONSTRAINTS

The NASTRAN Multipoint Constraint Equation (MPC) is a very versatile and necessary tool. The equation

$$[C_d] \{u_d\} + [C_i] \{u_i\} = 0 \quad (3.1-1)$$

relates the dependent nodal displacement $\{u_d\}$ to the independent displacements $\{u_i\}$

Such relations are needed in many places to express "rigid connections".

Usually it is most convenient to visualize the relation directly in terms of displacements (equation 3.1-1).

There are situations where determination of $[C_d]$ and $[C_i]$ in terms of nodal displacements runs into difficulties. Another relation than 3.1-1 may be helpful.

Let $[C] = -[C_d]^{-1} [C_i]$ (3.1-2)

then $\{u_d\} = [C] \{u_i\}$ (3.1-3)

Corresponding to the transformation of displacements (equation -1 or -3), the transformation of the applied nodal forces is performed according to the following equation:

$$\{\bar{P}_i\} = \{P_i\} + [C]^T \{P_d\} = \{P_i\} + \{P_{id}\} \quad (3.1-4)$$

In many cases the matrix $[C]^T$ in equation (3.1-4) is easy to form on the basis of equilibrium considerations, replacing the load applied in a dependent freedom, $\{P_d\}$, by a set of loads $\{P_{id}\}$ in the independent freedoms, which are in equilibrium.

$$\{P_{id}\} = [C]^T \{P_d\} \quad (3.1-5)$$

The matrix $[C]$ established by equation (3.1-5) is then used to write the NASTRAN MPC equation as in equation (3.1-3).

An example of the latter type is the relation of the displacement of the engine CG, as dependent freedoms, to the displacement of the connection nodes. The relation (3.1-5) is easy to form in terms of reaction at the engine mounts due to unit loads (and moments) at the engine CG. See figure 6.

3.2 ACTUATOR SETS

Another practical example of the use of MPC equations are sets of actuators. A set of actuators for one control surface, operating on a central pressure source p cannot be represented by independent ROD elements. The YF model contains three actuators for the inboard elevon, six for the outboard. (See figure 7.)

All actuator forces of a system of n actuators are linearly dependent upon a single variable, the basic pressure p ; they are rarely exactly parallel.

The actuator forces are:

$$\{F_{Ai}\} = \{A_i\} \times [p] \quad (3.2-1)$$

where $\{A_i\}$ are the piston areas

$[p]$ is the system pressure

The forces acting on the structural points j from the actuator system $\{F_{jA}\}$ are related to the actuator forces $\{F_{Ai}\}$ by the transformation matrix $[E_{ji}]$ (c, n)

The actuator nodal forces are therefore

$$\{F_{jA}\} = [E_{ji}] \{F_{Ai}\} = [E_{ji}] \{A_i\} p \quad (3.2-2)$$

Corresponding to the single pressure variable p (lb /in²) a displacement variable u_p (in³) is defined which represents the complete system (volumetric) displacement resulting from hydraulic fluid compressibility and all hardware deflection as a function of the pressure. The systems deflection is

$$u_p = (D_H + \sum_i A_i^2 \frac{lR_i}{EA_R} + D_c) \times p = D_p \times p \quad (3.2-3)$$

where D_H The change in fluid volume for unit pressure

D_c Container flexibility for unit pressure

$(A_i^2 \frac{lR_i}{EA_{Ri}})$ Actuator hardware flexibility related to the pressure

D_p Is the systems flexibility in $\text{in}^3/\text{lb /in}^2$

A_{Ri} Piston rod area of the actuator

A_i Actuator piston area on which the pressure works.

The systems spring constant is

$$[K_p] = [D_p^{-1}] \quad (3.2-4)$$

Let

$$[T_A] = [E_{ji}] \{A_i\} \quad (3.2-5)$$

then equation (2)

$$\{F_{jA}\} = [T_A] \{P_A\} \quad (3.2-6)$$

is the force transformation, giving the actuator end forces $\{F_{jA}\}$ in terms of pressure P and hence

$$\{u_p\} = [T_A^T] \{u_i\} \quad (3.2-7)$$

is the displacement transformation or

$$\{u_p\} - [T_A^T] \{u_i\} = 0 \quad (3.2-8)$$

Equation -8 corresponds to a multipoint constraint condition of standard MPC format, relating the displacement freedom $\{u_p\}$ of the actuator pressure system to the displacement $\{u_i\}$ at the actuator end-point, at the control surface and the wing trailing edge.

The procedure requires the following NASTRAN data for a complete actuator system.

1. A scalar point (SPOINT) S
2. A scalar element (CELAS4) from the SPOINT to ground, spring constant $[K_p]$ (equation 3.2-4) reflecting the complete systems volumetric displacement. The force read-out is the pressure p .
3. One MPC equation relating the dependent displacement of the SPOINT to the independent displacements of all actuator endpoints (equation 3.2-8). The matrix $[T_A]$ can easily be obtained from the considerations of equations 3.2-2 and -6.

3.3 TWIST PANELS

A few twist-panels were needed to represent torsion boxes. In the present case, as well as to represent torsion boxes in a CBAR gridwork, the NASTRAN CTWIST is not applicable, since it is expressed in terms of moment vectors at the corners. What is needed is a torsion element leading to nodal forces as shown in figure 8.

This was accomplished (for two elements required only) by the same principle as shown in 3.2, expressing by equation 3.2-2 the nodal forces due to the torsion moment, and the scalar element to represent the torsional stiffness.

4. OBSERVATIONS ON THE USE OF NASTRAN FOR LARGE AIRCRAFT STRUCTURES

The preparation of the YF12 model and data have led to a number of observations which are critical of the system in its present form. Some of them appear to be serious necessities for the large scale aircraft use and demand solution more urgently than others which can be classified more as luxuries. Their present status costs manpower and delays; weighing them must determine the urgency with which we are to attack the solution of these problems. And while for many of these problems the theoretical solutions are available to us, it would go far beyond the scope of this report to enter into their discussion.

- . The observations are based on large aircraft analysis, such as the one shown, as well as on a project environment and a large number of participants (non-expert). (See fig. 1.)
- . Most of the criticisms involve inconsistencies, inconveniences, cost in manpower; few are lack of capabilities.
- . Criticism does not necessarily imply that the NASTRAN programmer disregarded certain requirements or misjudged necessities, but rather that within the framework and budgeting of the NASTRAN release a certain level has been achieved which leaves room for many significant improvements and "conveniences". Even at the present time some may already be worked on by NASA or the maintenance contractor, some are worked on at our company.

4.1 ELEMENTS

A detailed critique of the NASTRAN element library is not within the scope and purpose of this presentation. We would however like to make the following general comment concerning the element library system.

The wider the intended and actual user community of NASTRAN, the more difficult, if not impossible, will it be for NASA to keep abreast with all product requirements for finite elements. Also, as a central issuing agency NASA will likely be very deliberate before officially introducing new elements. For the individual user the capability to react with special elements to a given situation can acquire an urgency entirely different than NASA's or may have special element requirements of limited use for others.

In the opinion of the author it is urgent to review the NASTRAN element handling system with the goal to drastically simplify exchange or addition of new element types, not only for the purpose of element checkout, but for productive use. Suggestions are

- . A standard NASA issued element library similar to the present.
- . Exchangeable library packages for specialized users.
- . Users element package, with all elements controlled by the user without NASA approval.

All elements should be usable together, where technically feasible.

4.2 CHECKING FEATURES

The NASTRAN input data diagnostic is in most aspects very satisfactory.

Some rather time- consuming problems were discovered:

1. Multipoint constraint equations. The diagnostic does not discover if a degree of freedom is used twice in the same equation, or the same D.O.F. is dependent in two MPC equations. The equation apparently is written incorrectly and the problem terminates during MPC equation reduction, without specific indications.
2. A major problem arises from the gridpoint singularity checking procedure. It is unfortunately quite inadequate, misleading, and thus requires a high degree of experience to be evaluated because it often gives an entirely wrong message.
 - a) The check does not take into account stabilization by MPC equation.
 - b) Only single point singularities (instabilities), relative to all other points being fixed, can be discovered, but not multilinkage instabilities.
 - c) It frequently gives a singularity message for freedoms which are elastically perfectly stable.

3. Singularity of the complete K matrix is only discovered and located, if the singularity resulted in an absolute "zero" of the pivot element. It should be possible to store the values of the pivot elements in the process of reduction, and calculate the values

$$\{S\} = \frac{\{KP\}}{\{KD\}}$$

Where

$\{KP\}$ is a column vector of all pivot values coming up during reduction.

$\{KD\}$ is a column vector of all values on the diagonal of the unreduced K Matrix

$\{S\}$ an element by element division of the values in $\{KP\}$ by the values in $\{KD\}$.

The values in $\{S\}$ will provide valuable information on details of the "behaviour" of the K Matrix, and on the location of singularities which result in very small pivot values.

4. The use of the NASTRAN Plot package for systematic pictorials of parts of the structure is a very valuable aid in checking the correct shape and element connections of the model structure. The only drawback is the inability to provide titles identifying each plot.
5. The BALANCE OF EXTERNAL LOADS

The correct balance of an external load condition applied by means of the various NASTRAN BULK DATA cannot presently be checked through the program except at the end of a run from the values in the static supports. It should be made possible to check the sum of all load components, and the resultant location, using the BULK INPUT for LOADS and GRIDPOINT COORDINATES only, before investing in a complete solution.

4.3 BULK DATA USE

- 4.3.1 The philosophy of the NASTRAN data set appears to be that all load and constraint information needed to analyze the structural model under a great variety of loading, constraint, and thermal environment, is provided for on BULK DATA cards with proper SET identification.

The rigid format, EXEC & CASE control cards then provide the means of specifying the load and constraint condition for which provisions were made in the BULK data. These features avoid a considerable amount of error-prone data card shuffling.

- 4.3.2 An unfortunate exception to this principle is the SUPORT card, which is used to define fictitious supports, needed for static analysis with inertia relief. Only one card is provided for in the BULK data; it has no identification and cannot be called for in CASE control.

Therefore, it is not possible to make an inertia relief analysis for different constraint conditions, such as symmetric and anti-symmetric, from the same BULK deck (and thus from the same UMF tape) because it is necessary to exchange the SUPORT card to replace fictitious supports for a symmetric freebody by those for an anti-symmetric freebody.

- 4.3.3 For large number of load conditions as occur frequently for project airframe analysis, the present CASE control system and stress recovery and output system practically excludes the use of NASTRAN for the production analysis of the mass of flight maneuver, gust and ground conditions involved in a complex aircraft system.

- a) It is presently not possible to analyze more than 20 conditions in one run.
- b) A SUBCASE definition in CASE control is required for each non-zero load column in the load matrix $\{P\}$
- c) Output space is wasted in cases of displacement vectors (loads) zero, which causes a full set of output of zero's.

These items are important under production environment of computer-mechanized design load formulation.

It should become an operational option that without any individual CASE control the displacement vector and stress output is produced for every non-zero column (and only for those) of an input load matrix.

- 4.3.4 The unique NASTRAN BULK DATA identification system permits the data ID numbering to be well integrated into an all encompassing identification system of model drawings, worksheets, backup data and cross references.

The possibility to group the input data into Subject-logical blocks is disturbed by the alphabetic order of the sorted "Echo", whereas the first letters of the card-code have not been used to group related data.

COORD system cards amidst the CONNECTION cards, Scalar Points not with GRID points, BAROR-card not with CBAR's etc. This renders checking the "Sorted Echo" somewhat awkward.

4.4 MULTIPLE COORDINATE SYSTEMS

- 4.4.1 The capability of inputting gridpoint coordinates in a multitude of different coordinate systems proved to be a great advantage for gridpoint coordinate input on the complex structure of the YF12, making it possible to use directly drawing measurements. The fuselage is in the basic system, the wing is rotated about the y axis, the elevons are measured relative to the hinge lines, the nacelle relative to the engine CL, the rudder relative to its middle plane, rotated about the engine CL. A total of seven coordinate systems were used for input, avoiding at that level a lot of work and errors.

- . Analogous however, any MPC, SPC, CBAR-OFFSET would be most easily established, and input in the system used for the coordinates. Unfortunately NASTRAN requires input for above items in the global system which is chosen for deflection output requirements, usually one standard coordinating system for the whole airplane.

This requires large amount of manual transformation for MPC and OFFSET data, which are prone to errors. SPC, by its nature, is logically applied in the global system if nodal displacements are specified.

For the large number of MPC and CBAR OFFSETS used in the present analysis, these proved to be the single largest headache in data preparation, errors and checking.

An MPC generator of considerable flexibility will considerably reduce work and errors.

- . Bending element offset, the majority would most conveniently and logically be specified in the local element system (particularly for shell frames and rings). An additional optional CBAR element formula would be helpful.
- . In connection with the remarks above, experience has shown that the single precision for the coordinate transformations is on the IBM 360 system only marginally satisfactory. For coordinates of the order of 2540 cm (1000 in.) or more (Fuselage Stations), six digit accuracy results in some SPC and MPC leakage which is detrimental to checking reliability.

4.5 TEMPERATURE

Specification of temperature at nodal points is "wrong" input from two points of view:

- a) Temperature is in the material and thus in the element, not at the node. It is difficult to get realistic input on a model under these circumstances.
- b) In thermal-finite element analyses the necessary input is directly produced from element data (not nodal data).

4.6 ALTERS AND DMAP

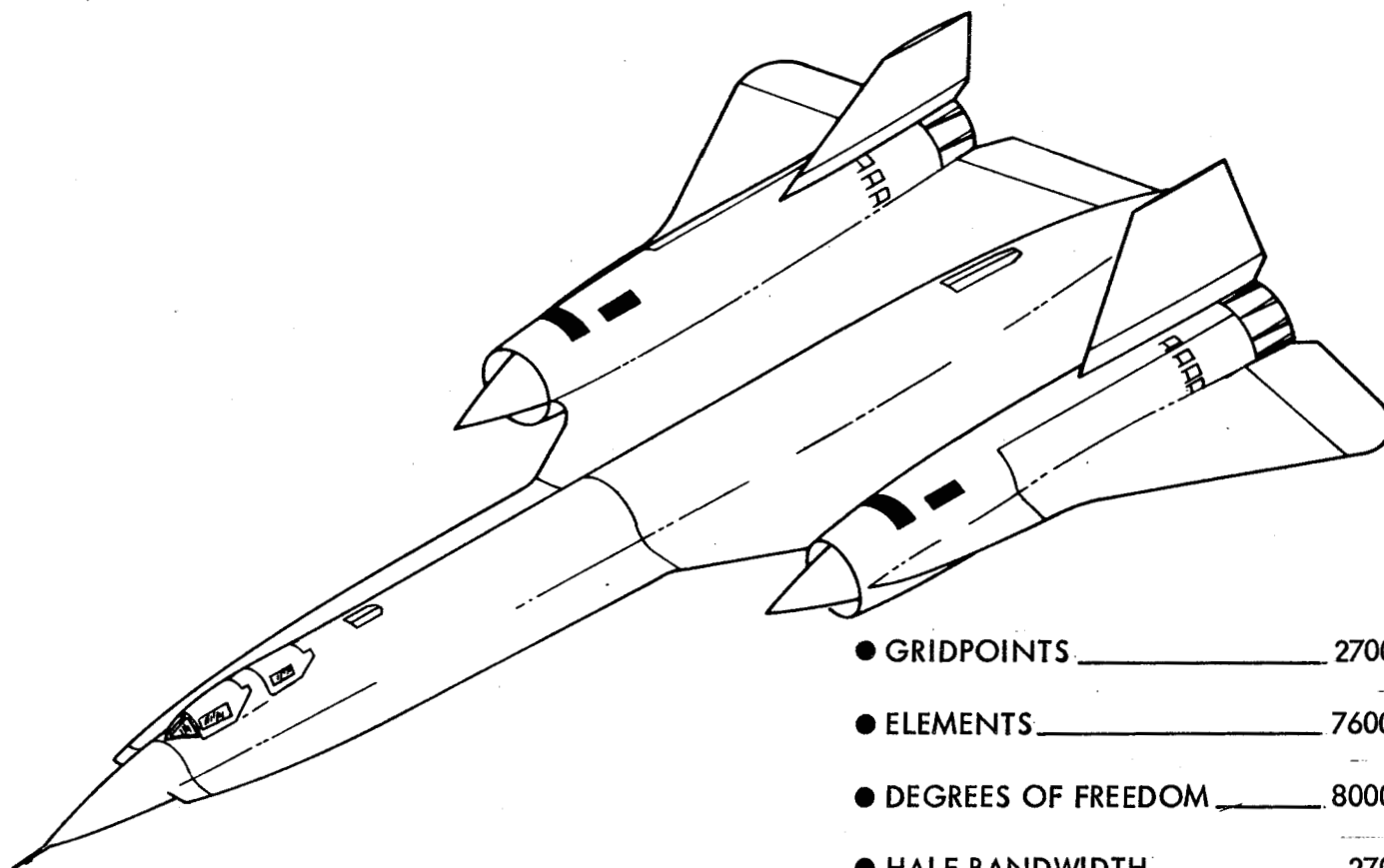
The NASTRAN rigid formats are great convenience for a large number of routine work, so is the ALTER capability to interrupt and reenter a rigid format string, a well designed feature, which is an absolute necessity for any of the more complex operations. The DMAP Modules and DMI Matrix input can be used for operation sequence inserted into a rigid format in this fashion. The DMAP system has however some major drawbacks:

1. The modules available for matrix operations and particularly manipulations are rather limited.
2. The format of DMAP instructions is rather cumbersome compared to other matrix algebra instructions.
3. The direct matrix input card format, although quite general, uses a large number of cards, and is quite inconvenient for sparse matrices.

CONCLUSION

The analysis of the YF12 structure and the corresponding evaluation of NASTRAN has been the result of very satisfying teamwork, and a stimulating cooperation with the NASA AMES and EDWARDS personnel involved with the contract.

It was quite impossible within this report to touch on all interesting experiences with the analysis system. The critical part of this review is intended as a constructive contribution by a team which is concerned with an intensive pursuit of the further development of the NASTRAN system as a practical tool for large scale aircraft analyses.



- GRIDPOINTS _____ 2700
- ELEMENTS _____ 7600
- DEGREES OF FREEDOM _____ 8000
- HALF BANDWIDTH _____ 270
- BULK DATA CARDS _____ 18,000

FIGURE 1 NASTRAN MODEL STATISTICS YF-12

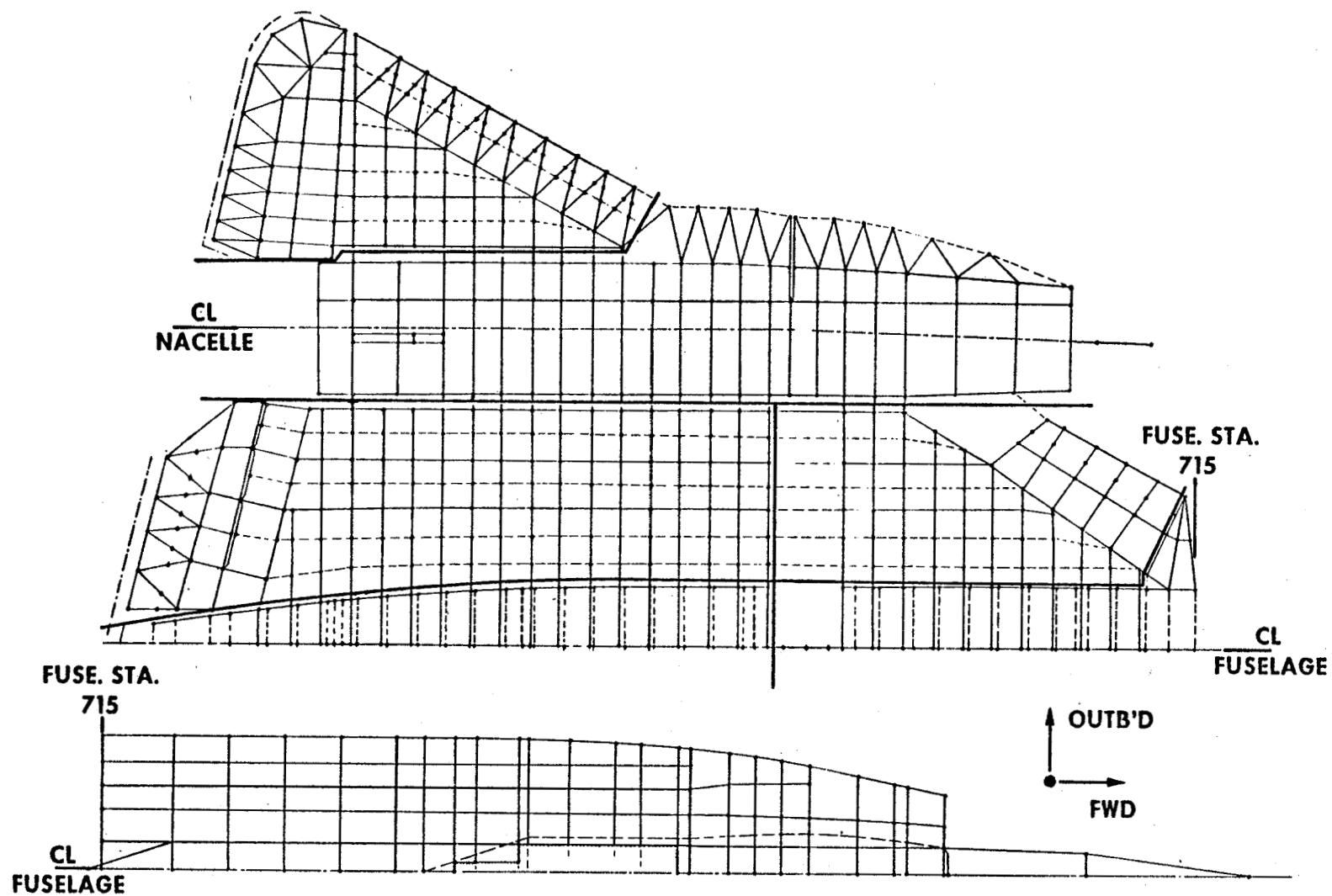


FIGURE 2 NASTRAN MODEL PLANFORM AND SUBSTRUCTURE DIVISION YF-12

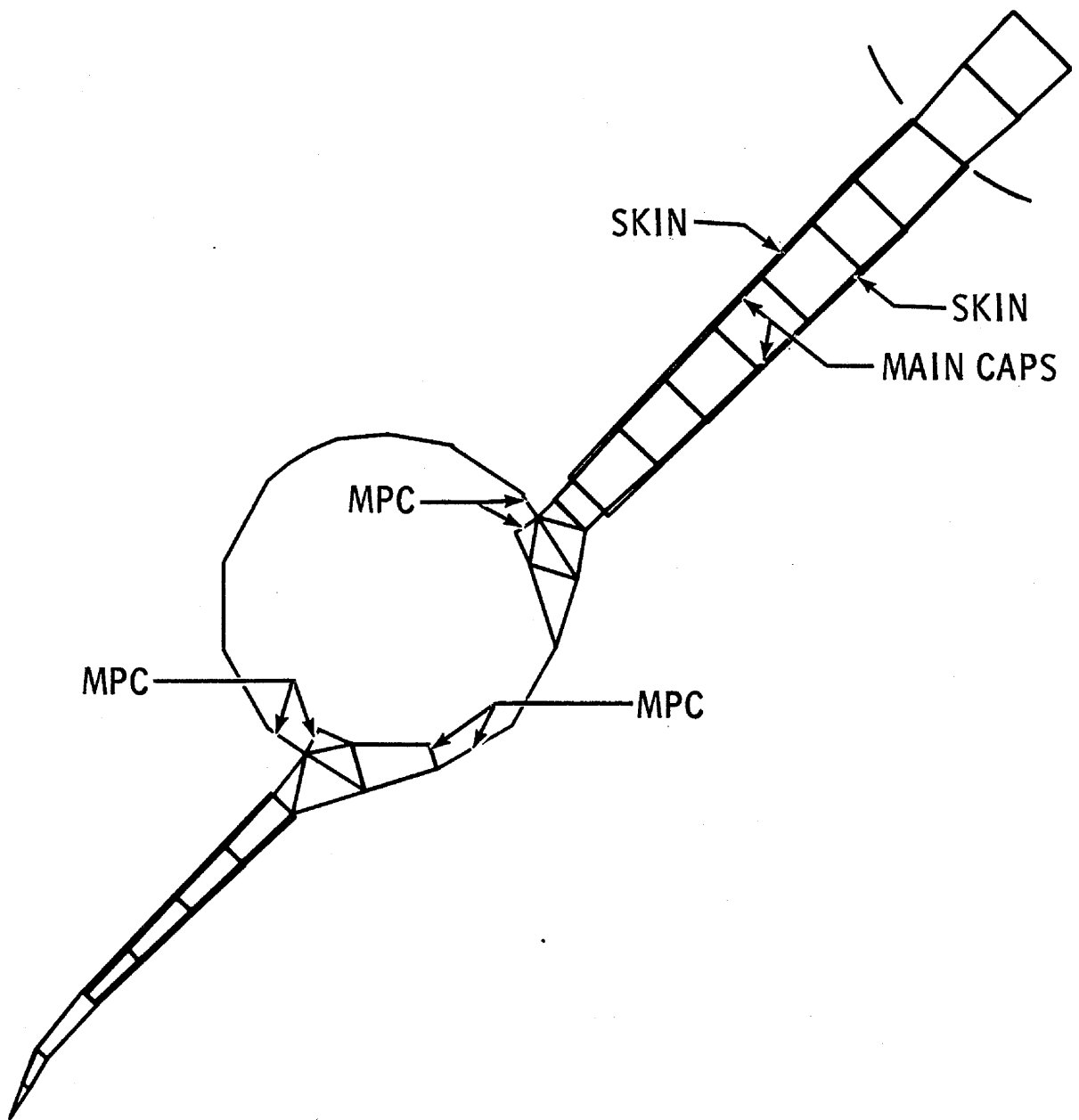


FIGURE 3 COMPLETE WING BEAM STATION NASTRAN PLOT

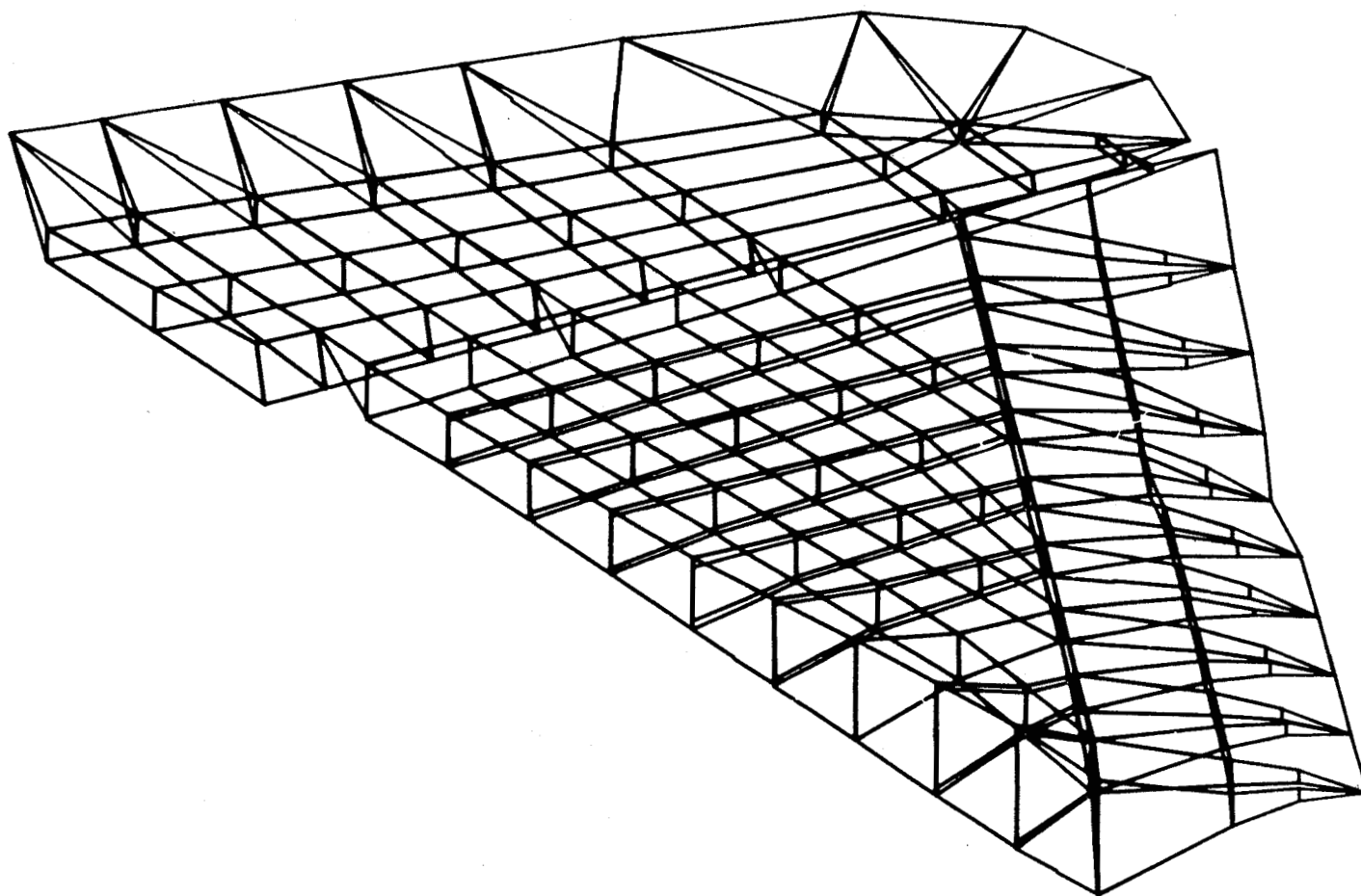


FIGURE 4 OUTER WING YF 12 NASTRAN ISOMETRIC MODEL PLOT

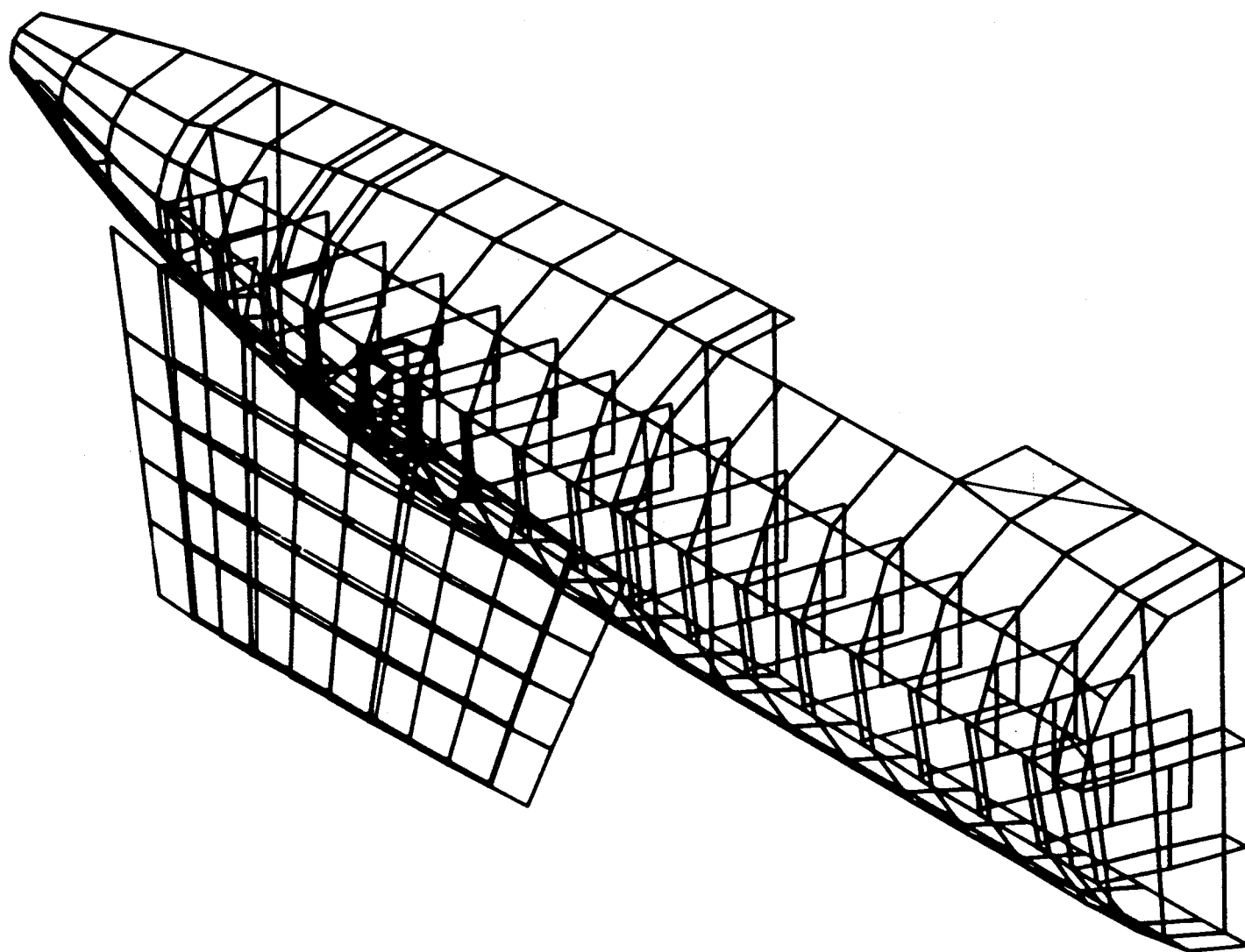


FIGURE 5 AFT FUSELAGE YF 12 NASTRAN STRUCTURE MODEL PLOT

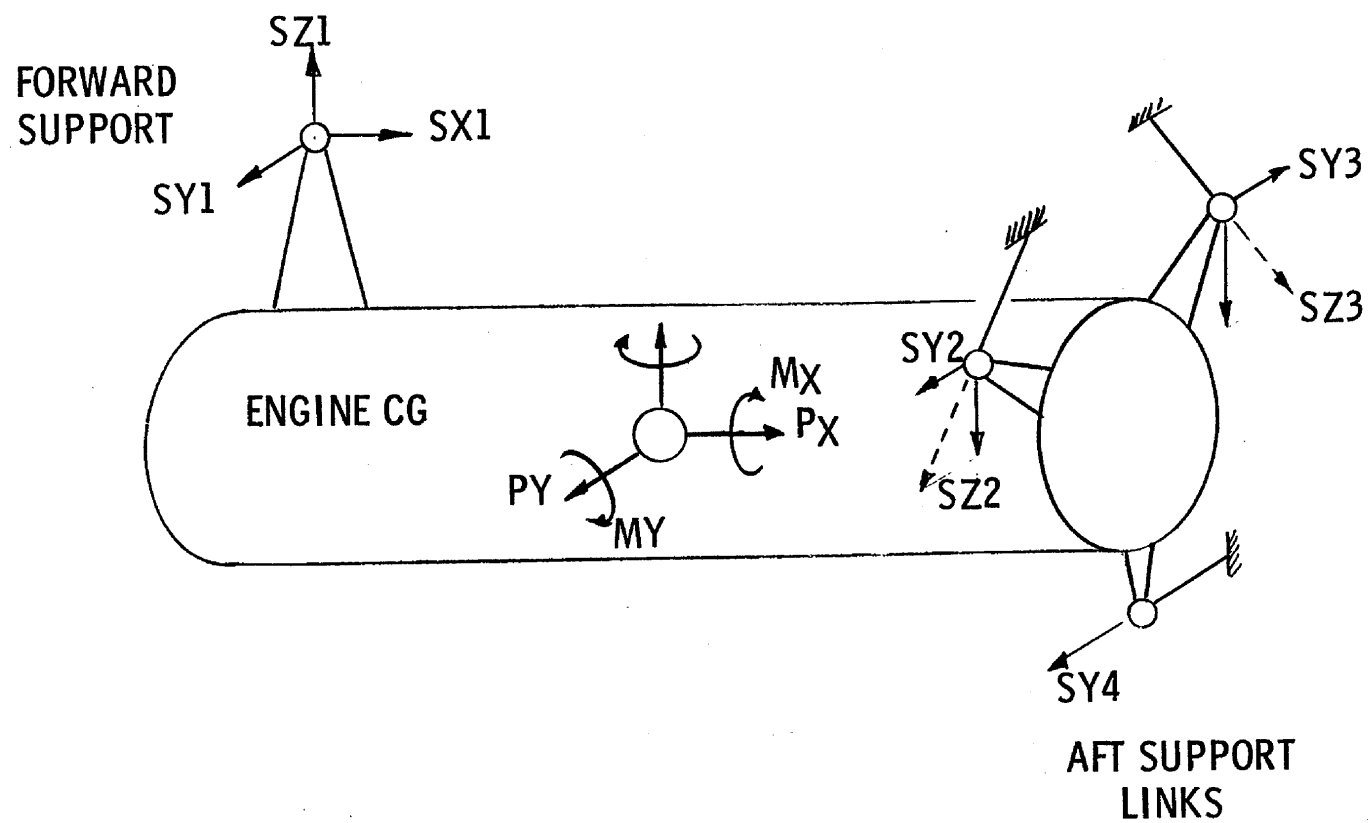


FIGURE 6 ENGINE SUPPORT SYSTEM

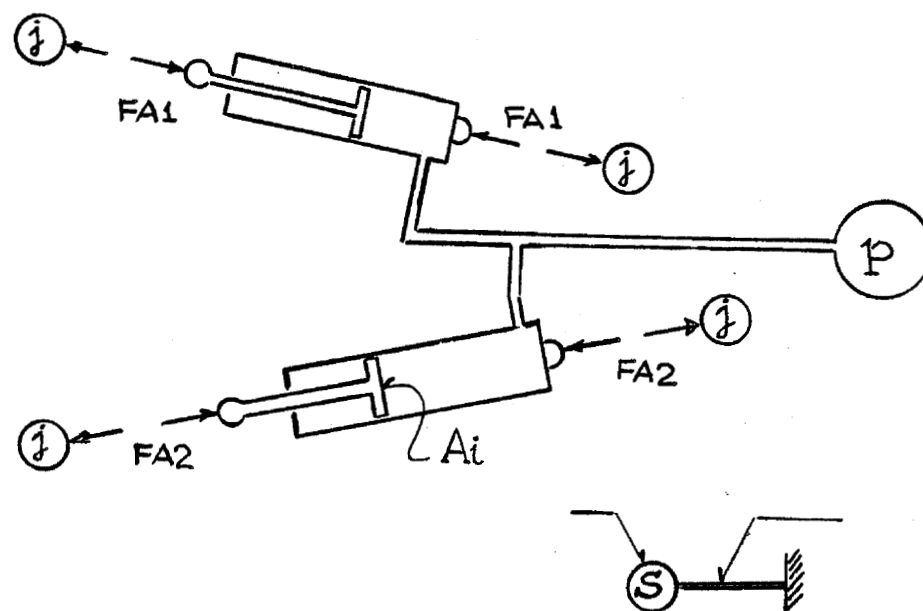


FIGURE 7 SYSTEM OF ACTUATORS

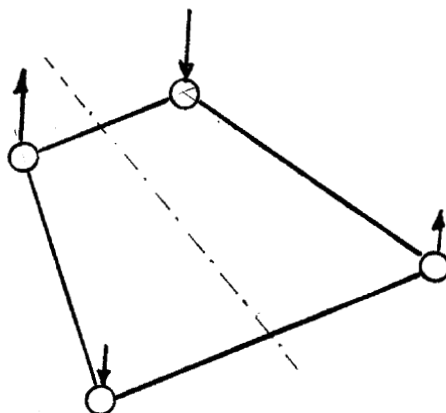


FIGURE 8 TWIST PANEL

NASTRAN DOCUMENTATION FROM AN HISTORICAL VIEWPOINT

By Frank J. Douglas

Computer Sciences Corporation

SUMMARY

This paper traces the background of NASTRAN documentation (i.e., the steps that preceded the big push at final documentation) and analyzes the management and technical approaches to the documentation process. The management approach to NASTRAN documentation is reviewed to consider how the whole effort might be improved if we were doing it again; and the technical approach is discussed with emphasis on specifications and standards. Some lessons learned from the documentation experience and the difficulty of putting these lessons into practice are then described. The maintenance of NASTRAN documentation is reviewed with respect to the two updates already made, and we conclude that because of proper planning the maintenance of NASTRAN documentation is off to a solid start. The paper ends with some thoughts on automated aids to documentation and some suggestions for the future. The Appendix provides a list of the style and format specifications used in NASTRAN documentation.

BACKGROUND

In a seminar on automated documentation at Goddard Space Flight Center (GSFC), organized by Mr. Darrin Gridley about a year ago, it was remarked that software documentation can be generally divided into two types. In Type 1 documentation, top level specifications are developed which describe in detail what the program is going to do (requirements analysis) and approval is obtained from the powers-that-be that this is the desired approach. The design is then broken up into successively smaller segments, until the parts of the design are small enough that they can be assigned for coding. A document describing the design is generated before any code is written. In such a situation, the program documentation is almost automatically generated prior to the writing of the program itself.

Type 2 documentation, on the other hand, arises when a computer programmer looks at a problem, considers what the program is supposed to accomplish, writes the program, checks it out, and satisfies himself that the program does substantially what it is supposed to do. At that point, he customarily turns his back and starts to walk away, whereupon his supervisor shouts, "Stop, wait a moment; you haven't finished yet--you haven't *documented*!" "Oh, that's right," he says, and proceeds to pull together such notes as he can lay his hands on, supplement them with a couple of general writeups to cover the more glaring omissions that he may note in the resulting sheaf of papers, and then toss them all onto his boss's desk with the air of one who has shown remarkable

Preceding page blank

patience to do such a job at all and should not be pushed too far. Noting this, his supervisor usually doesn't complain too much. For one thing, he hasn't looked the document over carefully enough to criticize it (even if he has the qualifications to judge). For another, he has already assigned the programmer to another crash program; and anyway, in many cases, the programmer has already left to join another organization. In today's depressed programmer market, especially in the aerospace industry, the prima donna attitude of the Type 2 documenter and that "another organization" are becoming things of the past- -but slowly, very slowly.

The NASTRAN documentation effort can be pointed out as an example of substantially Type 1 documentation. Its beginnings were especially solid.

In January 1966, Computer Sciences Corporation (CSC) was awarded a contract for the program definition stage of what was then called the General Purpose Structural Analysis (GPSA) Program. This definition stage consisted of the development of program requirements by NASA and the generation of preliminary program designs by two teams of contractors, one of which was headed by CSC. The preliminary designs, documented in the form of Technical Evaluation Reports, were completed in April 1966.

In June 1966, GSFC awarded the development contract, NAS5-10049, to the team headed by CSC, with the MacNeal-Schwendler Corporation the principal subcontractor. A document-as-you-go (Type 1) policy was initiated, with two main document types- -the Mathematical Specification (MS) and the Functional Module Mathematical Specification (FMMS). In an MS, the analyst lays the groundwork and then derives, in mathematical or logical terms, the necessary raw material that will eventually find its way into the programming system. In an FMMS, the raw material of an MS is developed to the "medium rare" point, so that a programmer can use it as a design and coding specification.

In general, the writer of an MS was not required to be knowledgeable about the software architecture. The FMMS writer, on the other hand, had to understand the analysis as well as its implementation in the system. The FMMS contained a definition of the inputs to the module (or algorithm if the specification spanned less than a module) and of the outputs, as well as a detailed discussion of the method, equations, logic, and restrictions.

MS's were eventually used in large part as the raw data for the Theoretical Manual (TM); and FMMS's were heavily used as the raw data for the Programmer's Manual (PM). The data for the User's Manual (UM) was gathered from various sources, including the static training course manuals, Input Data Card Format documents, Output File Specifications documents, and Program and Data Flow documents.

In addition to the MS's and the other allied design documents, a variety of other materials were used in development of the manuals. In addition to the source code, these were:

- The rigid formats, evolved over the period of contractual performance, which described all data blocks and the modules from which they were output. They provided data for Section 2 of the PM and, of course, constitute much of Section 3 of the UM.

- The descriptions of utility routines such as GINO and the packing routines. These became the basis for the subroutine descriptions that make up Section 3 of the PM.
- A glossary of terms which was maintained on IBM cards as the project developed and which formed the basis of the NASTRAN Dictionary in Section 7 of the UM.

MANAGEMENT AND TECHNICAL APPROACH

Management Approach

In the fall of 1968, a schedule of incremental deliveries, on a section-by-section basis, was established for both the Preliminary Version and the Final Version of the three NASTRAN manuals. At this time, I was appointed NASTRAN Documentation Manager, in which capacity I was responsible for the quality and timely delivery of all three manuals. Additionally I was appointed Editor of the Programmer's Manual. Dr. Richard H. MacNeal and Professor C. W. McCormick of MacNeal-Schwendler Corporation were appointed Editors of the Theoretical Manual and User's Manual, respectively. Figure 1 shows the organization of the documentation effort.

The writers for the three manuals (the programmers and analysts who had designed and developed the system) spanned the three corporations in the NASTRAN consortium at that time: Computer Sciences Corporation, the MacNeal-Schwendler Corporation, and Bell Aerospace Company. This was matrix organization at its wildest and wooliest- editors were screaming at editors, editors at writers, and writers at editors. Yes, Virginia, matrix organization implies teamwork through conflict (Reference 1).

Because of the very tight schedules imposed on the documentation staff, we sometimes went without such luxuries as typed drafts. Our biggest problem was Type 2 documentation symptom number 1- we started too late. We began so late, in fact, that, in order to have a chance at making the delivery schedules, we decided to eliminate the normal cycle through the technical publications organization and handle those functions ourselves, to the extent we could, in parallel with the actual writing of the manuals. The TM and the UM would be done at the MacNeal-Schwendler facility in Pasadena; the PM would be done at CSC's facility in El Segundo, thirty miles away.

Because of my two-hat role as Documentation Manager and Editor of the Programmer's Manual, as well as the very tight schedule, one role had to dominate; and the Editor of the Programmer's Manual won out. One might think that this would have caused many incompatibilities among the manuals. These incompatibilities, however, were kept to a minimum for two reasons: the unifying internal design document, MS-47, (Reference 2)- see Technical Approach; and the unflinching dedication to NASTRAN documentation excellence on the part of Tom Butler, GSFC's NASTRAN Project Manager, and his staff. On the whole, therefore, the manuals were much more compatible than might have been expected; for example, one of the more conspicuous incompatibilities between the PM on the one hand, and the TM and the UM on the other, is the use of the word

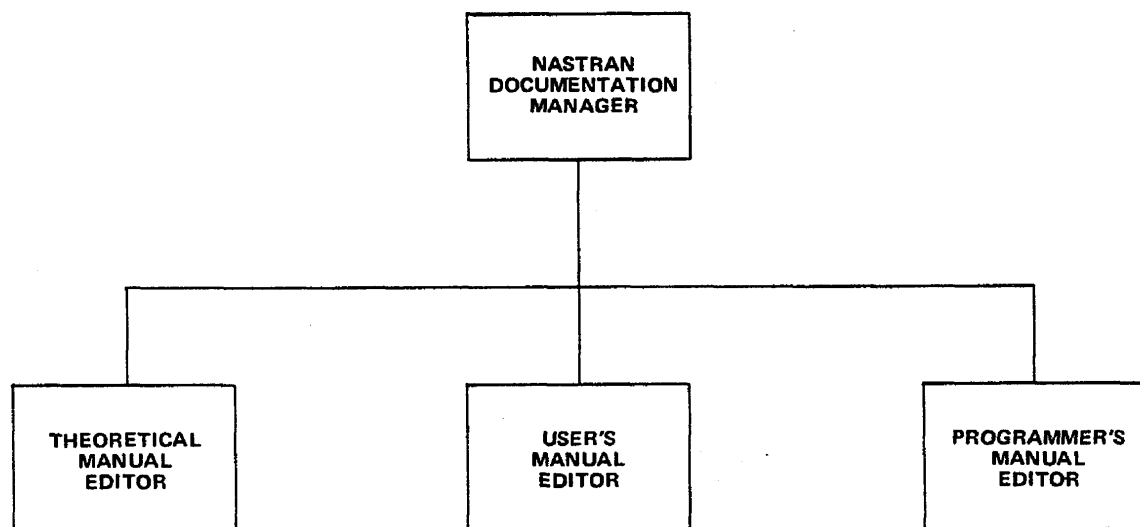


Figure 1. NASTRAN Documentation Organization

"section" in the text when cross-referencing (e.g., "see Section 4.1.3"). The PM (incorrectly) uses a lower case "s" for section; the TM and the UM correctly use "Section."

I think, in retrospect, that it was a big mistake to have no professional writers assigned to the NASTRAN documentation team. In fact, if I had to do it all over again, I'd opt for three editors, each supported by a full-time technical writer. Leading my organization would be a part-time documentation manager, assisted by a part-time technical writing supervisor, who would insure compatibility of style across all three manuals.

Review Cycle

For the PM, the sequence of events that led up to publishing the Preliminary Version of the manual was:

1. The Editor developed major section outlines (sometimes these were annotated).
2. The Editor developed writing assignments and schedules.
3. Technical Staff personnel submitted handwritten material which was edited by the PM Editor.
4. The material was typed and Xeroxed (no proofreading was done by the typist).
5. The Editor proofed and performed a light re-edit of the Xeroxed copy.
6. The Editor returned a copy to the author for further proofing and changes.
7. The author returned his copy to the Editor, who in turn reviewed it and gave it to the typist for corrections.

When a major section was completed, five Xerox copies were sent to Tom Butler at the NASTRAN Project Office at GSFC for a two-week review. Tom and the Project Office staff reviewed each section microscopically and conducted round-table discussions. After the review was completed, Tom Butler sent the Editor written comments which usually consisted of general comments embodied in a letter and specific comments annotated on one of the copies. Most often the comments could be implemented by mortising the original typescripts.

When there were serious disagreements between the Editor and Tom Butler, a phone call followed by a written confirmation usually settled them. The thoroughness and dedication of the GSFC review team were the necessary cohesive forces that eliminated the majority of inconsistencies in the Preliminary Versions of the Manuals.

It's interesting to note that although the writers and reviewers were separated by 3000 miles, an average of one phone call per week, of duration of from one to two hours, provided, in most cases,

adequate time for clarifications, explanations and, in some instances, negotiations. For isolated cases, disagreements were settled in meetings between Tom Butler and the Editor when they happened to be in the same place. However, disagreements never caused travel.

Technical Approach

Specifications for NASTRAN manuals were set during a six-month period of correspondence between Professor McCormick, Project Manager for the MacNeal-Schwendler Corporation and later Editor of the User's Manual, and Tom Butler. These specifications were published as an internal design document, MS-47 (Reference 2). They are presented in the first part of the Appendix of this paper, so that those who wish to update the manuals to reflect their own enhancements may conform to a single, well defined format. The first 29 items in the Appendix are, with some light editing, the contents of MS-47. Items 30 through 41 are additional specifications that either evolved over the period of documentation or were tacit assumptions from the outset.

Although the MS-47 format specifications were indispensable, standards for the typing of mathematical expressions and for flowchart symbols were lacking. Correct typing of mathematical expressions is a difficult task; some of the principal roadblocks in achieving this are:

- A set of procedures for doing this specialized work is usually lacking.
- There are great variations in writers' notations (how many ways are there to write the Greek letter "alpha"?).
- Many typists have an ingrained prejudice against typing mathematical expressions.
- Many managers are unwilling to pay the price for quality mathematical typing.

A good standard for mathematical typing is Reference 3. Even this reference, however, doesn't mention one of my pet peeves about the matrix notation in Section 3 of the User's Manual- namely, that the transpose operator, like the inverse operator, should be placed outside ($[A]^T$) rather than inside ($[A^T]$) the matrix brackets. Why did I allow this notation to remain? The answer is simple: to change it would have meant an increase in cost and a slippage in schedule that could not be tolerated.

No standards for flowchart symbols were imposed on NASTRAN manuals. Writers and editors alike relied on what they recalled from past experience; and the subject of standards, as I recall, was never brought up.

In some recent work of mine for GSFC, in which I am leading an effort to produce a Quality Assurance Handbook for the Telemetry Computation Branch of GSFC's Information Processing Division, I recommended the adoption of the American National Standards Institute's (ANSI) standard X3.5 for flowchart symbols (Reference 4). An excellent tutorial by Ned Chapin in the use

of this standard is given in Reference 5, and I recommend it to anyone interested in software documentation standards.

LESSONS LEARNED

Managing the NASTRAN documentation effort taught me many lessons; among the most important are:

- Professional technical writing guidance and support are needed.
- Proofreaders independent of the author, the editor, and the typist are needed.
- Closer liaison among editors is needed. Better still would be either (a) a documentation manager who doesn't have day-to-day editorial responsibility; (b) a centralized production shop of typists and proofreaders; or (c) both (a) and (b).
- There should be early agreement on format and subject matter.
- Standards must be firmed up early. These include a dictionary, a style guide, standards for mathematical expressions and flowchart symbols, and technical dictionaries or glossaries.
- Modularity of documentation is essential.
- Programming (especially coding) standards should be integrated with documentation standards.

These points are further discussed below.

The primary lesson I learned was: let the technical publications people do their thing. Because of the service orientation of such an organization, the range of capabilities can be quite extensive, and this variance can be used to advantage. In other words, a set philosophy vis-a-vis the technical publications department isn't necessary; the manager can select those services that he needs or can afford.

I think that the degree to which a project manager uses a publications organization will depend heavily upon his attitude (and, of course, that of his customer) towards the written word. If he believes it is extremely important to his effort (as I do), he is best advised to lean heavily on the publications department, even if some of his authors are frustrated junior Hemingways. I mean this from an editorial or technical writing point of view and not necessarily from an organizational point of view, although I don't exclude the latter.

My experience has shown that proofreading cannot be accomplished adequately by the person who typed the document; and to have the author do proofreading of his own is both inadequate and wasteful- -he can be doing something else. A junior editor should be assigned to this function.

As indicated previously, I fulfilled two roles. A better allocation of manpower would have been to keep the functional boxes in Figure 1 unchanged but to have different persons in each box. An additional aid to uniformity would have been a typing and proofreading team centrally located and dedicated to NASTRAN documentation in general, rather than geographically spread out with typists dedicated to only one manual.

Early agreement on format is necessary so that the impact of nonstandard items (e.g., typewriters, oversized mats) can be absorbed in the schedule. I was very fortunate to have MS-47 at my disposal in plenty of time before writing and final typing began. However, we did not have an early agreement on the contents of the manuals. This would have been much more of a problem if we had not had the MS's, FMMS's, and other functional specifications.

My votes for standards go to: *The American Heritage Dictionary of the English Language*, the GPO *Style Manual, A Guide to the Typing of Mathematical Notation* (Reference 3), the ANSI X3.5 *Standard Flowchart Symbols* (Reference 4) and *Datamation's "ADP Glossary"* (Reference 6).

Documentation that will change often, as will NASTRAN's, must be designed modularly. I think the manuals serve as good examples of modular documentation. A specific example is Section 2.3 of the PM. There, the functional organization of grouping data blocks output from a module, along with the technique of starting a new page for each module, allows the document to be updated easily and in such a way as to preserve the current format.

Coding standards can be established so that the code not only is self-documenting but also fits into documentation standards. The only way to implement this idea is to design the documentation at the same time one designs the system.

PUTTING THE LESSONS LEARNED INTO PRACTICE

Most of the lessons learned from my NASTRAN documentation experience point up the fact that quality documentation costs money, and lots of it. Reference 7, *Manned Space Flight Center Documentation Cost Guide*, lists ten types of documents (handbooks, procedures, tech manuals, etc.) with costs per page for each type. Costs include both preparation and production costs. These (total) costs range from a minimum of \$35 per page for a "normal" procedure to a maximum of \$315 per page for a "complex" specification. The cost guide, which serves as a reference point for evaluating the estimated cost of technical or management data of various types, does not define what constitutes each type of manual. However, intuitively categorizing the NASTRAN manuals as halfway between handbooks (\$92 per page minimum, \$171 per page maximum) and tech manuals (\$141 per page minimum, \$233 per page maximum), and the degree of complexity as halfway between "normal" and "complex", then the cost of NASTRAN manuals should have been

somewhere around \$159 per page. Although I have no statistics to back it up (I didn't have access to the NASTRAN accounting records, and even if I did, time spent developing preliminary specifications such as the MS's was not segregated from other tasks), I believe we did NASTRAN documentation for less than this average price tag. I like to think it was done for less, not because of inferior quality, but because of superior talent.

MAINTENANCE

Proper maintenance of the manuals requires an intimate knowledge of both the manuals and the system. Therefore, an integrated approach to NASTRAN maintenance is absolutely necessary; that is, corrections to the system must be reflected in the manuals concurrently. I think the publication of manual updates concurrent with the release of a new level of the system is a most necessary postulate for orderly dissemination of NASTRAN. Experience has shown us that this is the case.

The manuals have been updated twice, and the update procedure worked out as part of MS-47 has worked well. The original issue of the manuals was in October 1969 and corresponded to the so-called Phase I system. The six Phase II items were documented as manual updates dated January 1, 1970, and March 1, 1970. These updates, along with document maintenance items completed under CSC's first NASTRAN maintenance task under Contract NAS 5-11723, were published in September 1970 as part of level 12.0, the general release level.

Under a second, recently completed NASTRAN maintenance task, also under NAS 5-11723, CSC produced over 1000 pages of changes and additions to the NASTRAN manuals. These included: the changes due to the MacNeal-Schwendler effort to develop and implement hydroelastic and thermal bending capability (NAS 5-11780); incorporation, as Section 6.8 of the PM, of the (NAS 5-10049) Fourteenth Quarterly Report which described the programming interfaces necessary to add structural elements; addition to the PM of a new section, numbered 7 and entitled Support Programs (7.1 is an introduction, 7.2 gives programming details for the CDC 6000 Linkage Editor and Segment Loader, and 7.3 describes the source conversion program that generates a CDC 6000 source tape from a UNIVAC 1108 source tape); and a list of effective pages for each of the manuals.

THE FUTURE

One of the most interesting facts that struck me when reflecting on my NASTRAN documentation experience was the difference between what we documented and how we documented it. The NASTRAN system is one of the largest scientific batch processing (as opposed to real-time) systems known. The bulk of its code is machine independent, and the system runs on the three third-generation computers most widely used for scientific applications. In contrast to the system, the documentation exists on camera-ready typescripts (mats)- a production process that has

changed little since World War II. Intuitively one feels that there must be a better way to update the manuals- -automation naturally immediately comes to mind.

One tool that shortens the composing cycle for documents is IBM's Magnetic Tape Selectric Typewriter (MTST) system. The MacNeal-Schwendler Corporation began using an MTST system to place the Preliminary Version of the User's Manual on tape so that changes precipitated by the GSFC Project Office review could be incorporated easily. The use of the MTST system was discontinued early, however, because the number and types of changes requested by GSFC were such that, in order to save valuable calendar time, mortising the Preliminary Version mats was chosen over the alternative of updating tapes and playing them back onto new mats.

Since the format and style of the NASTRAN manuals are less fluid now than they were when the MTST experiment was tried, it can perhaps be tried again, or better still, simulated and compared with other automated aids to documentation that are available.

UNIVAC has two automatic documentation systems that operate under Exec 8: the DOC processor and UNADS, the UNIVAC Automatic Documentation System. I have seen only one example of a document produced by the DOC processor and one example produced by UNADS (which is the documentation of UNADS itself). There is no comparison; the UNADS document won hands down. A nice feature of UNADS is that it allows the user to construct an index automatically.

An overall index would be a welcome addition to each of the three manuals. Other additions I'd like to see in the manuals over the months to come:

- An index in Section 2.3 (Case Control Deck) of the UM that would list, in alphabetical order, each case control card mnemonic along with the alternative spelling, if any, and the functional group (e.g., applied loads, constraint selections, etc.) to which the card belongs.
- An index in Section 2.4 (Bulk Data Deck) of the UM that would list, in alphabetical order, each bulk data card and the functional group (e.g., element definition, coordinate system definition, static load) to which it belongs.
- A complete description in Section 5 of the PM of how to generate the absolute NASTRAN elements from the source tapes available from COSMIC.
- Transformation of Section 4.87 of the PM into a section of its own- -say, Section 8.
- A table (in matrix form) in Section 4.87 of the Programmer's Manual which shows all elements versus capability (e.g., stiffness, lumped mass, coupled mass, output of complex stresses).

APPENDIX

Specifications for NASTRAN Manuals

1. Original image area will be 8-1/4 x 10-3/4 inches plus page number.
2. Final size will be 80 percent of original size.
3. Manuals will be printed on both sides of 8-1/2 x 11 inch paper and punched for standard three-ring loose-leaf binders.
4. Text will be typed on a 12-pitch IBM Selectric using LETTER GOTHIC ball number 005. Carbon ribbon will be used.
5. Mathematical symbols and Greek characters will be typed using SYMBOL 10 ball number 061.
6. Double-spacing will be used except where groups of a few single-spaced lines separated by double-spacing for the groups is more desirable for clarity or appearance.
7. Paragraphs, including indented paragraphs, will be separated by 2-1/2 spaces.
8. Section and subsection titles will be separated from the text and from each other by triple-spaces.
9. Major section (e.g., 10.) and major subsection (e.g., 10.4) titles will be typed with uppercase letters.
10. Minor subsection titles (e.g., 10.4.2 and 10.4.2.4) will be typed with lowercase letters, initial capitals, and underlined.
11. Major sections such as

10. EIGENVALUE EXTRACTION METHODS

will be provided with a thumb-tab divider.

12. Major subsections will be identified with a decimal classification and two numbers, as follows:

10.4 THE INVERSE POWER METHOD WITH SHIFTS

13. Minor subsections will be identified with a decimal classification and three numbers as follows:

10.4.2 Theory for Real Eigenvalue Analysis

14. When necessary, minor subsections may be further subdivided and identified with four numbers. Titles will be typed with lowercase letters and initial capitals as follows:

10.4.2.4 Sweeping Previously Found Eigenvalues

15. Major subsections and bulk data card descriptions will begin at the top of a righthand page. Other units such as module descriptions or similar items may begin at the top of a page where clarity or convenience of use is thereby improved. In the case of large major subsections, minor subsections may begin at the top of the next page.

16. Page numbers will be centered at the bottom of each page.

17. Pages will be identified by a major subsection identification number and a dash number, as follows:

2.1-1
2.1-2
2.1-3

18. Pages inserted at a later date between pages of the original issue will be identified by letters and date of issue as follows:

2.1-2	Original page
2.1-2a (9/1/71)	Added page
2.1-2b (9/1/71)	Added page
2.1-3	Original page

19. Pages changed after the original issue will be identified in the usual manner followed by the date of the change, as follows:

3.1-2	Original page
3.1-3 (10/8/71)	Revised page
3.1-4	Original page

20. Running headings, in capitals, will be centered at the top of each page. The major section name will be used on the lefthand or even-numbered page, and the major subsection name will be used on the righthand or odd-numbered page.

21. References will be listed at the end of each major section and will be numbered consecutively beginning with 1 for the first reference in each major section.

22. Equations will be numbered consecutively beginning with 1 for the first equation in each major subsection. When major subsections contain many equations (more than 50), equation numbers may begin with 1 for the first equation in each minor subsection. References to

equations outside a major subsection must refer to both the equation number and the major subsection number.

23. Tables and figures will be numbered consecutively beginning with 1 for the first table or figure in each major subsection. References to tables and figures outside a major subsection must refer to both the table or figure number and the major subsection number.
24. The words Reference, Table, Figure, and Equation will be spelled out with initial capitals when used either in the text or in a caption. The associated Arabic numeral will not be enclosed in parentheses.
25. Equations will be centered on the line and separated from the text with triple-spaces. Equations will be punctuated as part of the text and be identified at the righthand margin with an Arabic numeral in parentheses.
26. Table titles will be typed in lowercase with initial capitals and a period at the end:

Table 3. This Is an Example of a Table Title.

Single-line titles will be centered over the table, and multiple-line titles will be left-justified with the last line centered.

27. Figure captions will be typed in lowercase except for the first word with a period at the end:

Figure 4. This is an example of a figure caption.

Single-line captions will be centered under the figure, and multiple-line captions will be left-justified with the last line centered.

28. A description of the complete NASTRAN documentation along with important historical facts will appear in the Preface of the Theoretical Manual.
29. Preliminary manuals will be full-size Xerox copies on 8-1/2 x 11 inch paper with "perfect" binding.

Additional Specifications for NASTRAN Manuals

30. As a general rule, material should not be repeated in more than one place. A good example of this rule's application is Section 4.87 of the Programmer's Manual. The material here is not repeated in the Theoretical Manual, as one might logically think it would be.
31. *Webster's Third New International Dictionary* notwithstanding, the word "data," according to NASA headquarters, is plural in all contexts.

32. The only permissible way to change the camera-ready manuscripts is by mortising. In particular, erasures and opaque white paint are not acceptable.
33. The transpose operator for a matrix should be placed outside the brackets (e.g., $[A]^T$ is the correct form, and $[A^T]$ is an incorrect form). The same rule applies to the inverse operator (e.g., $[A]^{-1}$ is the correct form).
34. References to other sections of the manuals should use an uppercase "S" in the word "Section" (e.g., "see Section 5.3") for the Theoretical and User's Manuals, and a lowercase "s" in the word "section" (e.g., "see section 5.3") for the Programmer's Manual. The lowercase "s" in the Programmer's Manual, although incorrect, is advocated for consistency within the PM.
35. Data block names, module names, bulk data card types, all entry point names, and FORTRAN variable names will be capital letters with the letter O slashed.
36. The names of the three card decks necessary to run a problem under the NASTRAN system will be consistently called: Executive Control Deck, Case Control Deck, and Bulk Data Deck, with initial capitals as shown.
37. All subscripts for matrices will be lowercase letters, e.g., $[K_{gg}]$, $[K_{fs}]$.
38. The following often-used acronyms and terms are always capitalized:

NASTRAN, FORTRAN, GINO, DMAP, FIAT, FIST, OSCAR, SORT1, SORT2

The NASTRAN Dictionary, Section 7 of the UM, defines capitalization rules for NASTRAN terms.

39. When a group of equations appears in succession without text between them, center the longest equation and line-up the equal signs of the remaining equations with the equal sign of the longest equation.
40. All minus and plus signs in equations shall have one space before and after. There shall be two spaces before and after all equal signs in equations. There shall be no spaces between parenthetical expressions.

Example:

$$[A][B] + [D] = [C]. \quad (1)$$

41. The following words will be initially capitalized wherever they appear:

Reference, Table, Figure, Equation, Piecewise Linear Analysis, Preface, New Problem Tape, Old Problem Tape, Problem Tape, Executive Control Deck, Case Control Deck, Bulk Data Deck, Rigid Format (PM only), Data Pool File, Executive System.

REFERENCES

1. Business Week: Teamwork Through Conflict. March 20, 1971.
2. McCormick, C. W.: Specifications for NASTRAN Manuals. MS-47, November 1968 (developed under Contract NAS5-10049).
3. Stewart, Dorothy G. : A Guide To The Typing of Mathematical Notation. The Rand Corporation, P-3090, November 1964 (AD-613 942).
4. American National Standards Institute: Standard Flowchart Symbols and Their Use in Information Processing, X3.5-1970, 1970.
5. Chapin, Ned: Flowcharting With the ANSI Standard: A Tutorial. Computing Surveys, Vol. 2, No. 2, June 1970, pp. 119-146.
6. Datamation: ADP Glossary.
7. National Aeronautics and Space Administration: Manned Space Flight Center Documentation Cost Guide. June 1969.

DATA MANAGEMENT REQUIREMENTS FOR LARGE PROBLEMS

by Stanley D. Hansen and Dr. Harald B. Hansteen

The Boeing Company

Renton, Washington

SUMMARY

During the last five years Boeing Commercial Airplane Division has heavily utilized very large capacity finite element computer programs in production analyses of the 747 and SST airframes. This experience has led to the development of programs to assist the using engineer in preparation and interpretation of finite element data and to the development of algorithms with high capacity and efficiency to handle the data processing requirements. It is believed that what has been learned is generally applicable to large finite element problems and that any computer code, such as NASTRAN, must eventually be configured to provide or interface with the requirements described in this paper.

ACKNOWLEDGEMENTS

The information presented in this paper is the result of experience accumulated by members of the Boeing Commercial Airplane Division Structures Staff of which the authors have only been a part. It should be mentioned that the original development of the region and set algebra commands was the work of Mr. Steve Komjathy of the SST engineering staff.

Preceding page blank

INTRODUCTION

It soon becomes obvious to any user of finite element computer codes that the data associated with the analysis is extremely voluminous. The finite element analysis Boeing performed on the SST airframe serves to illustrate this point. The division of aircraft by substructures is shown in Figure 1. The wing-body intersection was analyzed as a single elastic structure because of the redundant attachment between wing and body. This required an interaction procedure to couple the seven substructures forming the idealization of the wing-body region. Size characteristics for these seven substructures are given in Figure 2. Each substructure required an average of 60,000 input items to describe grid point loading. This totals to approximately two million input items for all substructures. There were twelve internal load values computed for each beam element and fifteen for each plate element. Symmetrical half structure was used requiring that both a symmetrical and antisymmetrical boundary condition be processed. There were forty generalized unit load conditions in the solution. These conditions were expanded to two hundred conditions by superposition. The combined output for these seven substructures contained over 100 million stress values. Cab, forward body, aft body and empennage sections were also analyzed. Hence, the total volume of stress and displacement items available for the airframe in a single analysis was in the order of hundreds of millions.

The statistics given above may seem exaggerated to the user who has never applied finite elements to large structures. However, considerably more data than that described is generated to complete the airframe design. For example, geometry, section properties and loads are updated and stresses and deflections recomputed for each succeeding configuration of the airframe. In addition, flutter and dynamic analyses are made using response data generated from the finite element stiffness models.

Computer codes are now available with capabilities, capacities and efficiencies adequate for the analysis of any size structure Boeing is now producing or contemplating. Indeed, the present ability to produce stresses and deflections has far exceeded the engineers' ability to assimilate them without the assistance of the computer. Computer code for generating data, plotting, data checking and generating of reports has, in the past, been looked upon as a luxury. In fact, they are an absolute necessity if the engineer is to

effectively utilize the finite element method in analyzing problems of the size and complexity of the SST airframe.

A finite element capability may be viewed from two distinct vantage points. First is the finite element theory and computer code. In just one decade theory and codes have developed from a few severely limited mistrusted programs to the high capacity, highly efficient and universally accepted structural analysis capability of today. Third generation computers, efficient matrix arithmetic algorithms and substructuring technology have given capacities that are essentially limited only by economics. However, the development of theory and computer code is of interest to the production analysis and design engineer only to the extent the code is reliable and to the extent he understands the theory and the preparation and interpretation of data. The application of finite element capability on production aircraft has brought pressure for the development of computer codes to assist in the preparation and interpretation of data. It has also brought a change in the administration of the analysis work. The massive amounts of data and the unforgiving nature of the computer have produced a requirement for assembly line like production and control methods. Also, unlike hand analysis methods where answers are forthcoming almost on demand depending on how much the engineer is willing to assume, the finite element programs do not yield any answers until they yield all answers. Hence the second vantage point is that of the production engineer and his management.

Management and the production engineer have learned that substructuring is a necessary tactic for:

- (1) Division of structural analysis responsibility between contractors
- (2) Division of the structure according to group responsibility
- (3) Division of the analysis by major structural assembly components
- (4) Iterating a single substructure for configuration and design studies while using contiguous substructures as boundary conditions
- (5) Refining the grid of a subregion for a more detailed analysis while using the response of the entire region as boundary conditions for the subregion

(6) Computer code and hardware capacity and reliability considerations

(7) Improved bandwidth or equation conditioning.

Only the last two are associated with the computer. Substructuring has the added advantage of allowing parallel preparation and processing of data and of permitting communication of technical information between contractors in a precise and mutually understood form.

The subject is much too broad to cover in a single presentation. Rather, some comments on data generation, checking and interpretation are given followed by a formulation for substructure analysis and a discussion on some associated matrix arithmetic algorithms.

DATA PREPARATION AND INTERPRETATION COMPUTER CODES

Data Generation

Geometry and element generation schemes depend upon the regularity of the structure. Code for automated generation of total data sets is desirable and necessary for analysis of solids because of extensive repetitiveness and because the three dimensional arrangement makes it difficult for the engineer to visualize the grid points and elements. Automated generation of total data sets also serves well in space structures that have perfect (or near perfect) symmetry. Many structures, however, appear regular but, in fact, are highly irregular structurally. Aircraft, for example, appear regular for aerodynamic reasons. In actuality, the supporting airframe is grossly irregular because of access and lightening holes, equipment installations and the like. For this type of structure, it is effective to provide repeat factors and short segment generators in the bulk data language. For example, statements of the type

```
RØD1  1  3  5.6/  
*+3   1  2  2  .2/
```

expand to

```
RØD1  1  3  5.6/  
RØD2  3  5  5.8/  
RØD3  5  7  6.0/  
RØD4  7  9  6.2/
```

by successively adding the factors in the second statement to those in the first statement. The * and + identify the statement type and give the direction of the increment. Many other statements are easily developed. These data statements can easily be interpreted and expanded as they are read, resulting in a fully expanded data set.

The advantages of these statements are:

- (1) they reduce volume
- (2) the reduction in data volume reduces the incidence of error
- (3) data errors extend over a larger number of statements when expanded and are therefore more detectable.
- (4) they are easily included in the bulk data statements.

Very large analysis tasks, such as the SST airframe, typically require that many engineers access essentially the same input data. If each engineer researches or computes his own, the arbitrary choices that inevitably present themselves result in some differences in the same data produced by different engineers. In this instance, it is advantageous to create master files of

data including the entire airframe. Such a master dimension file was available for geometry data on the SST. Section property data could similarly be provided and updated for succeeding design iterations. The use of master data files ensures that the entire engineering group is accessing identical information. Hence, load and stress groups and groups modeling interfacing substructures would use compatible data.

Another useful concept is substructure extraction. This concept has been applied in two ways:

- (1) Substructure Division - In this procedure the data for the entire structure is prepared and checked as a single data set. A computer code is then used to divide the set into consistent substructure data sets complete with correspondence tables necessary for interaction and backsubstitution. The extraction process eliminates errors in coordinates at substructure interfaces. It also provides a ready means of redefining substructures.
- (2) Analysis of a Subregion - In this procedure, a data subset is extracted from the substructure data set after the substructure analysis has been completed. Hence the data subset is extracted complete with deflection boundary conditions. If the deflections for every freedom computed in the larger substructure are applied as specified deflections at every freedom in the data subset, reactions are obtained around the boundary of the subregion resulting in an equilibrium freebody. This is a surprisingly efficient procedure for obtaining freebodies. The efficiency is obtained because the reactions are computed by a direct matrix multiplication without having to solve a system of equations.

Loads generation computer codes essentially convert loads originally computed for airloads panels, cargo, pressure, etc., to a statically equivalent set of grid point loads. The volume of loads data nearly always exceeds the volume of grid point and element data. Airframe loads are computed for a balanced aircraft (all load conditions sum to zero). Hence a loads generation computer code is essential for redistributing the loads and maintaining the force balance.

Data Checking

The volume of data in large structures works against hand checking because of the hypnotizing effect that page after page of tabular data has upon the human mind. Computer code can be generated to assist. However, in a complete sense, data checking is beyond the capability of the computer because it does not have access to the total set of information used to create the data, nor is the computer able to exercise judgement. Hence, difficult as it is, the only complete check is an item-by-item review by someone using the familiar red and blue pencil.

To be effective in assisting the checking process, several different capabilities should be available. Some of those used at Boeing are:

- (1) Format check - Computer code is used to report data items that are incorrectly formatted.
- (2) Geometry and element connectivity check - Plotting is the only effective method of detecting errors of this type. The selection of view and scale is critical to remove hidden lines and to bring the smallest allowable error within the resolution of the plot.
- (3) Consistency check - Computer code is used to detect such items as duplicate grid point identifiers, re-entrant corners in quadrilateral plates, warped quadrilateral plates, unacceptable definitions of beam principal planes, radii shorter than one half the distance between curved beam end points, and the like. Computer code is also used to check coordinate matching across substructure interfaces.
- (4) Accuracy check - Errors are detected by placing bounds on the data item. For example, Young's modulus for most metals is greater than one million lb/in² and less than 50 million lb/in². Values outside this range can be detected and a warning message printed. Errors within the bounds are more difficult to check and generally yield only to an item-by-item hand check.

The form in which data errors detected by computer code are presented to the user is important. It is poor practice to print an error number referencing a fuller description in a manual. It is much better to (1) print a descriptive statement that is accurate and complete and (2) print the precise card image or location in which the error occurs.

Ideally, data checking code should locate all errors in a single pass. This is not possible if the error is such that the data checking code becomes lost. Good recovery can be provided, however, if the data is divided by readily identifiable header cards or delimiters that the data checking code can search for in the event it becomes lost.

Data Updating

Large volumes of data cannot be managed by hand in card deck form. Simple activities such as reading the card decks into the computer or correcting data by inserting new cards have an intolerable error probability. A better procedure is to place the data on magnetic tape or permanent disk files. This requires an updated program with the following capabilities:

- (1) Sorting - Large data sets are necessarily keyed for sorting. This requirement stems from creating the data in separate sets and then merging them into a single complete data set.

- (2) Update Functions - Update functions are based on sorting keys. Sorting keys may be simple ascending numbers in columns 73-80; a composite number in columns 73-80 based upon grid point, element, loadcase and card function; or the grid point, element and loadcase identifiers themselves. A workable set of update functions includes DELETE, CORRECT, REPLACE, INSERT.

The result of the update operation is a new master data tape containing updated card images. The old master data tape is preserved unaltered.

Interactive Data Checking and Updating

If a computer with permanent files and time sharing is available, considerable engineering flowtime can be saved by error checking and correcting from an interactive terminal. A simple text CRT terminal is adequate and can be located in the engineering work areas because of its silent operation. Working copies of updated files can be obtained by batch printing from the terminal. As data is read, the checking program detects errors and displays a descriptive message along with the offending card image. The correction is made directly from the terminal keyboard. Data updates may be made directly by paging to the appropriate location and using the update commands.

Processing Checks

Except for the basic truth that the finite element input data must be processed to obtain deflections, stresses, etc., the processing of data is of no interest to the engineer. His interests lie simply in the translation of structure into coded data and the interpretation of results.

Beyond answers, the engineer requires two things from the processing stage. First, if the processing fails because of data errors (such as equation dependency) not detectable in the initial data checking, the engineer needs to know the exact location of the error in the data. Traditional conditioning numbers giving overall evaluation of the stability of an equation set have little practical value. Equations of the order of many thousands are being routinely solved. The detection of specific dependencies in such large sets and the association of these dependencies with the original finite element data is a practical necessity in the production environment. Boeing has successfully implemented an algorithm that detects digit loss on an equation-by-equation basis. The offending equation is specifically identified with the corresponding grid point and freedom. This check has proven invaluable to production engineers in locating conditioning problems stemming from dependencies or near dependencies.

The second item required by the engineer is an equilibrium check of loads and reactions. Although there are limitations to the validity of this check, its existence at least gives the engineer the assurance that the loads have been carried through the structure to the support points. Thus he has more than faith and hope to support the accuracy of the solution.

Postprocessing

The task of analyzing and interpreting the data output from the processing stage is formidable even for small structures. For structures of the size being discussed here, most of the value of the analysis is lost without the assistance of the computer in extracting, manipulating and displaying pertinent data. Plot programs that show deflections, stress contours, bending moment curves and the like are invaluable. However, the great volume of data available in comparison with the relatively small amount of data required by each engineer makes the continual massaging of the total data set inefficient. Boeing is currently developing a postprocessing computer code in an attempt to cope with this problem.

The postprocessor is designed to accept data generated by other programs and to manipulate, interpret and display this data as directed by user-defined instructions through the control program. The postprocessor is provided with a read interface for each program the postprocessor interfaces. Other than at the read interface, data stored on postprocessor files is independent of the data source.

Extraction

The extract capability allows the user to extract those specific items of data from the finite element output that are of interest to him. Especially designed accessing and mapping routines are used to locate and extract data items in an economically efficient manner from large volumes of data. The extract capability immediately reduces the volume of data to that particular subset needed by the user. All types of data may be extracted and placed on the postprocessor files including data from different finite element processors, different substructures, coordinates, deflections, stiffness properties, internal loads, etc. All data items placed on the postprocessor files are identified in postprocessor dictionaries and may be accessed singly or in groups using the dictionary entries.

Report

This module allows the engineer to print tabular reports by naming items to be printed and giving their location on the page. The report module allows the insertion of titles, page headings, page footings and column headings.

Plot

This module allows the engineer to plot data stored on postprocessor files.

Superposition

This module allows the engineer to scale and combine data.

Special Functions

These include modules to calculate $M_c/I + P/A$, transform coordinate systems, determine maximum or critical conditions, computer margins of safety, dump buckled plate loads into adjacent frames, etc.

Region Commands

The region commands are a method of extracting data groups from specific geometric regions of the structure rather than naming the data item by item. Some typical commands and their result are as follows:

name/PLANE N1 N2 N3 BY width/INCLUDE string/EXCLUDE string/

This command identifies a region identified by "name" consisting of a plane defined by grid points N1, N2 and N3 with a thickness of "width". The plane extends to infinity. All grid points lying within this region will be extracted. Grid points outside the plane may be included or those inside excluded from the set using the INCLUDE and EXCLUDE commands. A "string" is given in the form N1 THRU N2 BY N3 where N1 is the beginning identifier, N2 is the ending identifier and N3 is the step size. The statement may be of the form N1 THRU N2 BY N3 or N1 THRU N2 or N1. Any number of statements may be included in the string, separated by commas as:

N1 THRU N2 BY N3, N1 THRU N2, N1, N1, N1 THRU N2, etc.

Other region commands are of the form:

name/ CYLINDER N1 TO N2 BY radius/ INCLUDE string/EXCLUDE string/

defining a circular cylinder with end points and centerline defined by grid points N1 and N2 and radius as specified.

name/TUBE N1 TO N2 BY string/INCLUDE string/EXCLUDE string/

defining an irregular cylinder the same as the circular cylinder except the outside boundary is defined by a string of grid points projected parallel to the tube centerline defined by N1 and N2.

name/LIST string/

defining a list of grid points making up the set. Specific data is extracted from the regions by commands such as the following:

FETCH name BEAMINLD MX1 MX2 FX1 FX2

resulting in beam internal loads MX1, MX2, FX1, FX2 being extracted for all beams with the region previously defined as "name".

Set Algebra

Sets of data extracted by the region commands may be combined using set algebra instructions of the form

J U K (union of sets J and K)

J I K (intersection of sets J and K)

C J (complement of J)

The commands may be combined as

(J U K) (C (M I N) U J)

Instructions are interpreted left to right and from innermost to outermost pairs of parentheses. Typically, data is divided into many small sets on the postprocessor files. Set algebra commands allow the user to combine sets in a variety of ways.

Summary of Observations

Thus it is seen that large finite element problems create the need for a range of data handling computer programs to ensure that the management of the data is accurate, reliable and efficient.

Substructuring has also been shown to be a necessary tactic for the processing of large finite element problems. Central to the effectiveness of a substructuring technique is the efficiency of the formulation and the supporting matrix arithmetic/storage algorithms.

SUBSTRUCTURING

General

The analysis of structures by the finite element method involves the generation and solution of (large) systems of linear equations. These equations represent equilibrium conditions at the nodes of the structure, and are expressed in terms of the nodal displacement - force relations. Whether a structure is analyzed by a substructure technique or a total structure approach, the system of equations to be solved is essentially the same provided an identical element idealization has been made. The actual difference between the two approaches is expressed by the sequence in which the equations are generated and solved. In the total structure approach generation of all the equations is completed before a solution is carried out. In the substructure analysis several subsets of the complete system of equations are first established independently. A partial solution is performed on each subset by eliminating equations which do not couple with equations in other subsets. The remaining equations are then combined and a final solution is carried through.

The results of the two approaches would be identical if computations were to be carried out with infinite accuracy. However, since computers can only perform finite precision arithmetic, the two solutions will in fact differ somewhat. The discrepancies in the results will in the majority of cases be outside the range of practical importance.

Method

The substructure analysis consists of the following four major phases:

Idealization -- The structure is divided into a number of substructures which in turn are being idealized by a finite element representation. In each substructure there will be some grid points which connect to other substructures; these grid points are referred to as "interact" grid points. Other grid points will be unique to one substructure. These grid points are called "internal" grid points.

Reduction -- The equilibrium equations for each substructure are independently formed and a partial solution is carried through with respect to the displacement components at the internal grid points. The reduced system of equations represent modified equilibrium relations for the interact grid points.

Interaction -- The total structure is connected by enforcing continuity conditions along the substructure interfaces, and by adding the equilibrium equations for the interact grid points. A solution for the displacements at these grid points is then carried out.

Backsubstitution -- In the backsubstitution phase the displacements at the internal grid points of a substructure are computed. When all displacements are known, the element stresses may be calculated.

Formulation

The basic systems of equations for a substructure may be expressed by the following matrix relations:

$$\begin{bmatrix} K_{oo} & K_{oa} & K_{os} \\ T & & \\ K_{os} & K_{oa} & K_{as} \\ T & & \\ K_{os} & K_{as} & K_{ss} \end{bmatrix} \begin{Bmatrix} U_o \\ U_a \\ U_s \end{Bmatrix} = \begin{Bmatrix} P_o \\ P_a \\ P_s \end{Bmatrix} \quad (1)$$

A more compact form for the same relations is:

$$KU = P \quad (2)$$

In the above equations the following notation has been used:

- K - The stiffness matrix of the structure
- U - The vector of grid point displacements
- P - The vector of grid point loads
- U_o - The set of displacements at the internal grid points.

U_a - The set of displacements at interact grid points

U_s - The set of displacements which have a prescribed value

A partial solution of equation (1) is carried through with respect to the U_o displacements. From the first matrix equation one obtains:

$$U_o = K_{oo}^{-1} (P_o - K_{oa} U_a - K_{os} U_s) \quad (3)$$

Substituting this expression into the second matrix equation the reduced system of equations may be written:

$$\bar{K}_{aa} U_a = \bar{P}_a \quad (4)$$

in which

$$\bar{K}_{aa} = K_{aa} - K_{oa}^T K_{oo}^{-1} K_{oa} \quad (5)$$

$$\bar{P}_a = P_a - K_{oa}^T K_{oo}^{-1} P_o - (K_{as} - K_{oa}^T K_{oo}^{-1} K_{os}) U_s \quad (6)$$

\bar{K}_{aa} and \bar{P}_a are the reduced stiffness matrix and the reduced load matrix, respectively. Both matrices are formed in the reduction phase of the substructuring process. Equation (3) is used in the backsubstitution phase to recover displacements at internal grid points.

Equations (3), (5), and (6) may be modified by introducing the following notation:

L_o - The lower triangular matrix obtained by performing a Cholesky decomposition on K_{oo}

thus

$$K_{oo} = L_o L_o^T \quad (7)$$

and further

$$C_{oa} = L_o^{-1} K_{oa} \quad (8)$$

$$C_{os} = L_o^{-1} K_{os} \quad (9)$$

$$H_o = L_o^{-1} P_o \quad (10)$$

With this notation equations (3), (5), and (6) become:

$$U_o = (L_o^T)^{-1} (H_o - C_{oa} U_a - C_{os} U_s) \quad (11)$$

$$\bar{K}_{aa} = K_{aa} - C_{oa}^T C_{oa} \quad (12)$$

$$\bar{P}_a = P_a - C_{oa}^T H_o - (K_{as} - C_{oa}^T C_{os}) U_s \quad (13)$$

Equations (7) through (13) together with the generation and solution of the interacted system of equations represent the basic steps which must be performed in a substructure analysis.

Efficiency

The substructuring technique is almost by definition related to the analysis of computationally large structures. The economy of a computer program will therefore be closely related to the efficiency with which matrix transformations are carried out. Some of the basic considerations which should be taken into account in the design of the program are discussed below.

The matrix C_{oa} of equation (8) should be formed by doing a forward substitute pass on the system of equations $L_o C_{oa} = K_{oa}$, rather than by inverting the L_o matrix. The C_{os} and H_o matrices of equations (9) and (10) are formed similarly. Furthermore, a matrix A which is expressed by the transformation $A = (L_o^T)^{-1} B$ should be computed by performing a backward substitution pass on the system $L_o^T A = B$ (Equation (11)).

The reduced stiffness matrix K_{aa} of a substructure should be formed according to equation (12) in which the symmetry of the triple product $K_{oa}^T K_{oo}^{-1} K_{oa}$ has been taken into account. The alternative way of processing where a matrix G_o is first computed as $G_o = (L_o L_o^T)^{-1} K_{oa}$ and then premultiplied by K_{ao}^T adds a backward substitute pass to the required transformations.

Advantage should be taken of the considerable sparseness inherent in the structural stiffness matrix K , both with respect to incore processing and secondary storage requirements. These considerations are probably well incorporated in most linear equation algorithms of contemporary structure programs. However, as the substructuring approach requires several large matrix multiply operations, similar sparse techniques should be made available in these algorithms.

The problem is complicated because the sparseness of the product matrices may vary from a population ratio of a few percent up to one hundred percent. Basing the strategy of a matrix multiplication on a sparse technique when the product matrices are essentially full may be as costly as the case of the reverse relationship. Algorithms covering both possibilities should be provided.

The matrices of Equations (7) - (13) will generally be large and must be located on secondary storage devices such as disks or magnetic tapes. Transformations on the matrices are carried out in a piece-wise manner by bringing relatively small subpartitions of the matrices into the central unit of the computer at the same time. This strategy may require recycling of matrices through the central memory area a large number of times. For this reason the requirement of an efficient data transfer strategy becomes a major concern.

The primary goal of this strategy should be to minimize the total amount of data that has to be transferred. In the case of matrix multiplications substantial benefits can be obtained by studying the storage format of the product matrices (row-wise or column-wise representation), and the relative sizes of the subpartitions of the product matrices and the result matrix. Other factors that should be considered are overlapped transfer on separate storage units and overlapping of incore processing and data transfer.

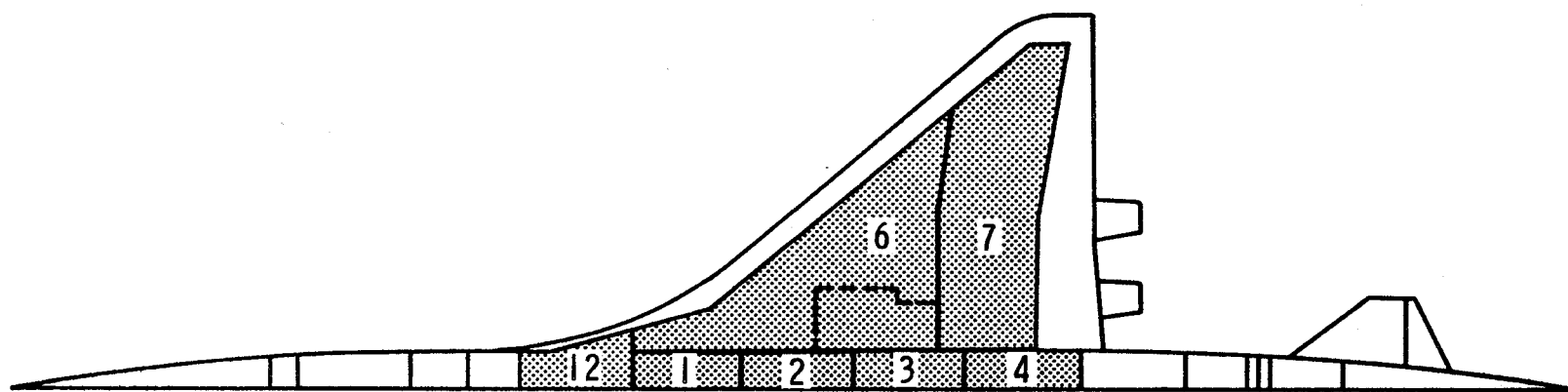


Figure 1. S ST Wing-body intersection analysis substructuring.

Substructure	Description	Nodes	Loadcases	Beams	Plates	Interact Freeds	Total Freeds
12	Body	846	40	1771	940	807	5076
1	Body	780	40	1569	924	884	4680
2	Body	809	40	1450	822	779	4854
3	Body	706	40	1314	736	699	4236
4	Body	802	40	1365	806	688	4812
6	Wing Box	951	40	1403	1420	525	2853
7	Wing Trailing Edge	<u>1045</u>	<u>40</u>	<u>1694</u>	<u>1836</u>	<u>246</u>	<u>3135</u>
Total		5936	40	10566	7484	2560*	29646

* Several freedoms at substructure interfaces contribute to a single interaction freedom

Figure 2. SST Wing-body interaction analysis.

N71-36285

NASA TECHNOLOGY TRANSFER:

THE COMPUTER SOFTWARE DISSEMINATION PROGRAM

By Joseph M. Carlson
Technology Utilization Office
NASA Headquarters

The National Aeronautics and Space Administration established in 1962 a formal program to transfer the results of its research and development activities to applications in non-aerospace sectors of the economy. The program is institutionally operated by the Technology Utilization Office at NASA Headquarters and by TU Officers within each of the NASA Field Centers. When the program got underway, and technological developments began to be reported by NASA employees and contractors, it became clear that one particular kind of technological product was developing which should be handled a slightly different way than other R&D work sponsored by NASA. Accordingly in 1966, NASA established a focal point to evaluate and disseminate its computer programs. The Computer Software Management and Information Center (COSMIC) is operated for NASA by the University of Georgia at Athens, Georgia.

COSMIC is interesting because it is the only element of the Technology Utilization Program which combines the functions of evaluation and dissemination of new technology; traditionally these functions have been separated because the capability to do the two tasks generally does not reside within the same organization. Generally when new technological developments are reported by NASA scientists and engineers as well as contractor employees, they are evaluated according to criteria including novelty, significance, technical adequacy, and potential for non-aerospace application. In general, the same criteria hold true for our evaluation of computer software. Over the years, our evaluation techniques and procedures have become more specific and refined as our experience grew; and as a better understanding of documentation requirements and evaluation procedures developed within the data processing industry and in the multiplicity of standards groups in existence. The requirements for complete and thorough documentation are probably more demanding for our purposes than in any other kind of function, since every program disseminated by COSMIC must be capable of third party use; i.e. by people who may have no knowledge of the specific nature of the R&D program which necessitated the original software development. Other criteria for computer program acceptance in the COSMIC inventory have also changed over time: one of the obvious changes is that since the inventory has now grown to a level where we have over 900 programs available for dissemination, we now receive programs which are substantially identical to items already in the inventory, and must make a judgment as to whether a new software submission has enough unique features to merit its inclusion.

The COSMIC program has evolved into a successful dissemination activity which currently provides a significant number of programs to users who are able to benefit from the existing investment in the Nation's space program. In calendar year 1970, COSMIC disseminated over 2500 software packages. Traditionally, our software dissemination has been limited to the public and private sector organizations in the United States. However, we have just completed negotiations for our first international exchange of software on a quid pro quo basis. NASA programs, of course, have always been available to foreign organizations engaged in joint research projects with NASA, however this is the first instance where the exchange has taken place based on purely economic and technical considerations, i.e. the trading of programs judged to have approximately equal value and utility. This exchange involves two NASA programs, which were traded for two programs developed by the Tokyo Research Laboratory of the Japanese firm, Hitachi Ltd. The two NASA programs are now being transmitted to Japan, and we will soon be receiving the Japanese programs in return. The exchange process in this case was long and rather laborious negotiation of successive steps to determine continuing mutual interest, but we look forward to further exchanges, many of which are now in the early stages of negotiation, with a somewhat simplified exchange procedure. Thus, we will now have a situation where two Japanese programs, previously unavailable in the U.S., will be available to U.S. users at no more than the cost of reproduction of the program and documentation, in exchange for two NASA programs which have already been publicly available in the United States for several years.

As many of you know, COSMIC programs are announced to potential users through the Computer Program Abstracts Journal which is published on a quarterly basis by NASA. When programs are received and evaluated by COSMIC, abstracts and technical descriptions of machine and language requirements, program size and price, are prepared by COSMIC and forwarded to our printing and composition facility for inclusion in CPA Journal. The Department of Defense joined NASA in the COSMIC effort in 1968, and after some initial delay, their programs are now beginning to flow into the Center, and are also announced in the Journal.

We feel that there is clear evidence that users in the American public and private sectors have already gained significant economic and technical benefits from the public availability of this software, originally developed in response to NASA mission requirements. One of the best examples which illustrates this point is the public availability of NASTRAN. Since many of you have now had some experience in developing NASTRAN applications, I am sure you can attest to the significance of having available to you, a program for which the original development cost has been estimated at over \$3,000,000. As new applications of NASTRAN continue to be developed, whether here at Langley under the guidance of the NASTRAN Systems Management Office, or in industrial or other governmental applications, we will do what we can to help in the exchange of information about useful applications, to continue to make the most of this opportunity to capitalize on an existing investment in research and development. I hope that many of you will continue to take an interest in NASA technological developments, and will investigate other programs, as well as NASTRAN, which we are making publicly available on a continuing basis through the Technology Utilization Program.

NASTRAN EXPERIENCES OF FORT WORTH OPERATION,
CONVAIR AEROSPACE DIVISION OF GENERAL DYNAMICS

by Merle Allen
Project Structures Engineer
Convair Aerospace Division, General Dynamics

SUMMARY

The preliminary and updated versions of NASTRAN have been acquired and implemented on the facility's IBM-360 computing system. After implementation of the preliminary version (level 8.1.0), a series of small exploratory problems were solved to determine the procedure's accuracy, usability, and economy. Seven of the rigid formats and DMAP were used. Structure and x-y plots were obtained. The results indicate that NASTRAN is easy to use and is accurate. It is not economical for small problems because it is both general purpose and programmed for large problems.

Following the high degree of success realized with the small problems, the procedure was released for general internal use. NASTRAN familiarization courses were prepared and taught in-plant by this writer. Two significant F-111 problems, consisting of buckling of the wing carry-through box cover plates and canopy normal modes, were analyzed.

The updated version (level 12.0.0) was acquired in December 1970 and implemented on an IBM 360/65/65/50 at a cost of 40 programming manhours and 1.0 computer hour. It is currently being used in a NASA study on Advanced Transport Technology.

INTRODUCTION

Both the preliminary and updated versions of NASTRAN have been acquired and implemented on the Convair Aerospace Division, Fort Worth Operation's IBM-360 computing system. The preliminary version implemented was level 8.1.0; the updated version was 12.0.0. Acquisition was from the Computer Software Management and Information Center (COSMIC), a National Aeronautics and Space

Administration (NASA) sponsored non-profit facility located at the University of Georgia.

Implementation of the preliminary version was completed 5 May 1970. It was accomplished by members of the company's professional programming staff for a cost of 180 programming manhours and 3 IBM-360 computer hours. Approximately half the computer time was used to solve some of the sample problems obtained with the procedure. Most of the implementation cost was incurred because of two difficulties encountered; these are discussed below.

The updated version was acquired 21 December 1970, and its implementation was finalized 12 March 1971. Again, the task was accomplished by company programmers and the costs were 40 manhours and 1 computer hour.

Because of their large size, both versions of NASTRAN have been loaded onto (and operate from) a reserved disk pack (IBM 2316).

Two significant operational problems were encountered during the implementation of the preliminary version. The first involved the input data, which require IBM 7090 graphics. The keypunch personnel normally punch IBM 360 graphics and use equipment designed for that purpose. When IBM 7090 graphics are required (only four characters are different from the IBM 360), the same equipment is used and a special switch is depressed to obtain the IBM 7090 characters whenever they are encountered. Because the keypunch personnel rely on their memory to obtain the IBM 7090 characters, numerous errors were made, which led to NASTRAN aborts.

This first difficulty was circumvented by coding a small procedure that reads the input data in either IBM 360 graphics, 7090 graphics or a mixture of both and converts it to IBM 7090 graphics wherever required. It acts as a front step to NASTRAN and executes automatically with it whenever NASTRAN is used. Hence, the input data may now be keypunched in IBM 360 graphics.

The second difficulty involved the magnetic tapes which NASTRAN produces for the Stromberg Carlson 4020 plotter. NASTRAN produces a 7-track tape; the Fort Worth Operation plotter requires a 9-track tape. This problem was resolved by coding a small procedure which operates independently and converts the NASTRAN-produced 7-track tape to the 9-track used in plotting. It possesses the disadvantage of requiring an extra computer run; presently, it

is being used on an interim basis since it is planned that NASTRAN will be modified at a future date.

PRELIMINARY EVALUATION

Following the implementation of the preliminary version (level 8.1.0), NASTRAN was used to solve a series of small exploratory type problems. This approach was taken because of the limited budget and time available and the necessity of validating certain facets of the procedure before releasing it for general internal use. The problems were thus tailored toward the objective of validating:

1. that the implementation was successful
2. that those finite elements and modules most likely to be used in aircraft type analysis were operational and accurate
3. that the problems could be solved without undue user difficulty.

Both static and dynamic problem types were solved. The static problems consisted primarily of performing a stress analysis on a cantilevered beam, a wing spar, and an anisotropic membrane, all under mechanical loads or predeformed; solving for internal loads of a pressure-loaded isotropic plate; performing a column buckling analysis; and solving for stresses of a skin-stringer arrangement, loaded thermally. In all cases, answers were made available for comparison with NASTRAN, either through solution on a desk calculator or by other finite-element procedures. Multiple load conditions were used in some cases.

The finite-element types used included the bar, rod, shear panel, quadrilateral and triangular membranes, the triangular homogeneous plate encompassing both membrane and bending, the quadrilateral bending homogeneous plate, and the quadrilateral nonhomogeneous element encompassing both membrane and bending degrees of freedom.

The results indicate the existence of two procedure errors. First, solutions were not obtained (in one computer pass) for all load conditions when a load condition change included changes in

the boundary conditions. Solutions were obtained in one computer pass for all load conditions prior to the first change in boundary conditions. Restarts were then made to obtain solutions for subsequent load cases. This situation was reported to NASA for correction.

Second, the anisotropic-membrane problem was first idealized by use of the quadrilateral membrane element. This element yielded incorrect loads and stresses. However, this error had already been catalogued by COSMIC so that its use in a problem of this type was inadvertant. A switch in elements to the triangular membrane yielded accurate results.

The dynamic problems solved consisted of calculation of natural modes of vibration and associated frequencies and frequency and transient response. Natural (normal) modes were calculated for a fixed beam, a free beam, and a composite plate through use of rigid format 3. DMAP was used to calculate normal modes and frequencies for a structure, where the stiffness and mass matrices had been calculated in procedures foreign to NASTRAN. Both the determinant and inverse-power methods were used. Resulting modes were plotted successfully through use of the SHAPE and VECTOR functions, but superposition of the two was not successful. Natural-frequency calculations were compared against results obtained with closed-form solutions for the beams and against test for the plate. Accuracies were well within engineering requirements in all cases.

The subject of both the frequency and transient response analyses was a simple beam. In each case, both the model and direct approaches were used. For the frequency-response problem, the load type was discrete. The distribution of load along the beam span was arranged to have the same shape as that of the first mode; hence, only the first mode contributed to the response. The load magnitude varied linearly with frequency. A solution to this problem was manually obtained on a desk calculator and the NASTRAN modal and direct results were compared against it. Results showed the NASTRAN solutions to be correct; however, the answers were printed in magnitude and phase-angle format (per user instructions) and were mislabeled "Real/Imaginary" in accordance with the COSMIC catalogued discrepancy. Split-frame x-y type plots were obtained, but the data plotted was incorrect after having been correctly printed. Plot requests were for magnitude on the upper frame and phase angle on the lower, both plotted versus frequency.

Transient response results were not obtained by other means for comparison with NASTRAN. However, the modal and direct results compared closely and appeared reasonable. Displacements, velocities, accelerations, and element loads were plotted versus time in NASTRAN. The plots were correct.

FAMILIARIZATION AND APPLICATION

Following the high degree of success realized with the small exploratory-type problems, the preliminary version was released for general use. A NASTRAN familiarization course was prepared for structural analysts and was taught in-plant after normal working hours by this author. The course was given twice so that all the interested personnel were accommodated. Each course spanned seven weeks, with classes held twice weekly. Class duration was one hour, for a 14-hour-lecture course. Thirty-two analysts completed the course.

NASTRAN has now been utilized in analyzing the F-111 airplane in two significant problem areas. The first consisted of a static stress and buckling analysis of the upper and lower cover panels on the wing carry-through box structure. In the lower-panel problem, 150 elements and 150 joints (639 degrees of freedom) were used. It executed in 1888 central processing unit (CPU) seconds. In the upper-panel problems, 250 elements and 138 joints (602 degrees of freedom) were used. It executed in 1895 CPU seconds. The NASTRAN results compare closely with results previously obtained by other means, with NASTRAN yielding slightly higher buckling loads. Lower cover results were about 3 percent different; upper-cover results were less than 10 percent different, the exact amount being dependent on the boundary conditions used.

The second F-111 problem for which NASTRAN was utilized consisted of obtaining the natural modes for an updated-type canopy preparatory to a flutter analysis. In this problem, 118 elements and 75 grids (135-size dynamic matrix) were used. The CPU time for the first three modes (obtained by the Inverse Power Method) was 1354 seconds. A restart was then made for additional modes and frequencies. No other results were available for comparison. The flutter analysis, which used the modes, indicated a stable structure, without cockpit pressurization; subsequent flight flutter tests confirmed the analysis.

At this writing, NASTRAN (level 12.0.0) is being used in a NASA study of Advanced Transport Technology.

CONCLUSIONS

The following conclusions are predicated on the results of the small exploratory problems and the F-111 applications to date:

1. By virtue of the 12 rigid formats and DMAP, the versatility of NASTRAN far exceeds that of other existing procedures.
2. It is surprisingly easy to use for so large and complex a procedure. The numerous usability features (such as the diagnostics, restart, tailoring of the printed output, and plotting) make it easier to obtain solutions, interpret results, and present data.
3. Engineering accuracy requirements are satisfied for those modules and finite elements exercised, with some exceptions as noted.
4. Computer run-time requirements (on a single computer-pass basis) are not competitive for small problems but should be competitive for large problems. Utilizing the rather extensive restart capabilities of NASTRAN could easily make it more economical for moderate-sized problems, relative to other finite-element procedures.

A SPECIAL NASTRAN PROGRAM FOR INPUT CHECKING AND
UNDEFORMED STRUCTURE PLOTTING

By Willianna W. Smith

NASA Langley Research Center

INTRODUCTION

The NASTRAN computer program, which has become a very frequently used tool for structural analysis, requires a vast amount of data preparation for its input. Errors in data occur which the user must find and correct before he can get a successful computer run. Extensive diagnostics are provided within the NASTRAN program, but due to the impact of the large field length (amount of central memory) required for execution on the multiprogramming/multiprocessing mode of computer operation, turn-around time can be rather lengthy. This, of course, causes the user considerable delay in the completion of his analysis. This paper describes a program for the CDC 6000 computer which helps the user debug his input cards more rapidly; the ideas are applicable to other NASTRAN computers.

REQUIREMENTS

An investigation was launched to determine the possibility of providing the user, in a considerably smaller package than the regular NASTRAN program, the capabilities of having his input data deck checked and a plot of the undeformed structure produced.

Because of the queuing priorities for operating systems built around multiprogramming techniques and the hardware requirements for execution (core, disk storage, etc.), a maximum of 28,672 words (70K octal) of central memory was chosen as a desirable field length to attain. A program of this size would not only allow for more rapid access to the computer, but would permit job submittals through remote terminal facilities.

In addition, the program was to be generated from the current level (12.0) of NASTRAN in such a way that it could be easily updated for future levels, if necessary.

PROGRAM AREAS INVESTIGATED

A DMAP sequence to accomplish the input data analysis and plotting is illustrated in the NASTRAN User's Manual, page 5.4-3 and requires execution of the following NASTRAN modules:

A. Executive Preface Modules

1. Executive Control Section Analysis (XCSA)
2. Input File Processor, Part 1 (IFP1)
3. Executive Bulk Data Sort (XSORT)
4. Input File Processor (IFP)
5. Input File Processor 3 (IFP3)

B. Functional Modules

1. Geometry Processor - Phase 1 (GP1)
2. Geometry Processor - Phase 2 (GP2)
3. Plot Set Definition Processor (PLTSET)
4. Structural Plotter (PLOT)

C. Executive DMAP Modules

1. SAVE
2. Set Values (SETVAL)

D. Output Module

1. Print Message (PRTMSG)

Link 1 and Link 2 of the regular NASTRAN program contain all modules involved but 32,768 (100K octal) words of core are needed to load the routines - this is exclusive of buffers and work area necessary for execution.

In an effort to reduce core requirements, subroutine descriptions were scrutinized to determine which, if any, could be excluded from the overlay structure. Open core requirements for the various modules were reviewed and SYSTEM parameters defining the length of buffers and indexes were examined as possible areas for increasing available core.

ALTERATIONS AND ADDITIONS TO THE REGULAR NASTRAN PROGRAM

Based on the preliminary findings, the decision was reached that the desired goal could be accomplished and construction of the necessary overlay structure was begun.

The Special NASTRAN program has as its basis Links 0, 1, and 2 of the regular NASTRAN program. All modules not required for the DMAP sequence have been removed and subroutines dealing with checkpointing, restarting and xy-plotting have been eliminated from the links.

After the required object decks and control cards for the overlay structure (see figs. 1.0, 1.1, 1.2, and 1.3) were processed by the Linkage Editor, computer runs were made using an arbitrary existing rigid format - statements not needed having been eliminated with ALTER cards - and the NASTRAN card for changing system parameters at execution time. Parameters varied were MAXFIL (maximum number of files to be added to FIAT), NBRMST (length of master index), NBRSUB (length of subindex) and SYSBUF (number of words in a GINO buffer).

When the desired results were obtained efforts were directed towards making all alterations invisible to the user. The following changes were made at the source level and new object decks produced.

1. Input and output buffer length set to 201 (octal) on program card of the Fortran program NASTRAN.
2. Punch file declaration removed from program card of the Fortran program NASTRAN.
3. In the principal Block Data program for NASTRAN; MAXFIL reduced from 32 to 18, NBRMST reduced from 62 to 10, NBRSUB reduced from 126 to 50 and NBRCBU reduced from 530 to 30.
4. Length of a GINO buffer, defined in subroutine BTSTRP, reduced from 1166 to 140.
5. DMAP sequence made into Displacement Rigid Format 18 containing 15 DMAP instructions. This required writing subroutine LD50 (fig. 2.0) to create the DMAP and Decision Records for the Executive Table XCSA.

All other existing LDi routines RENAMED LD50 - at the SUBSYS level - so the user does not have to change his solution number in order to use the special program.

CAPABILITIES OF THE SPECIAL NASTRAN PROGRAM

1. Analyzes all input data cards.
2. Provides a plot of the undeformed structure, if so directed by the proper structural plotter control cards.
3. Executable in 28,672 (70K octal) words of central memory.

LIMITATIONS OF THE SPECIAL NASTRAN PROGRAM

1. Displacement Approach must be used.
2. Does not contain checkpoint or restart capabilities.
3. Plotter output restricted to the DD 80 B microfilm plotter.
4. No punch output available.

CONCLUDING REMARKS

The Special NASTRAN program, in meeting the intended goal of input checking and undeformed structure plotting within 28,672 words of core, accepts as its input the data deck of a regular NASTRAN run. This allows the analyst to utilize both programs without intermediate changes in his data cards.

LINKEDIT LET,OUTFILE=NAST(T),PARAM(4)=20, PARAM(5)=50,	
PARAM(6)=6000,PARAM(2)=1200	
LIBRARY NASTOBJ	
LINK 0	SPLK0001
RENAME SYSTEM = SYSTEM.	SPLK0002
RENAME PEXIT = LINK20.	SPLK0003
RENAME MSGWRT = LINK20.	SPLK0004
RENAME GINOIO = IO6600	SPLK0005
RENAME XBACKSP= XBKREC \$ COULD BE REMOVED POSSIBLY	SPLK0006
RENAME RWUNLD = RETURN	SPLK0007
RENAME XREAD(IO6600)=READX	SPLK0008
RENAME XWRITE(IO6600)=WRITEX	SPLK0009
INSERT SYSTEM, XNSTRN	SPLK0010
INCLUDE NASTOBJ(BLKDATA(TIME))	SPLK0011
INCLUDE NASTOBJ(NASTRAN, BLKDATA(GINO66),CCNMSG)	SPLK0012
INCLUDE NASTOBJ(IC6600,GINO,DUMP,RETURN,OPEN,BCKREC,CLOSE,EOF,FWOREC)	SPLK0013
INCLUDE NASTOBJ(READ,REWIND,SKPFIL,WRITE,XGINO,XEOT,TMTGO,WRTTRL,RDTRL)	SPLK0014
INCLUDE NASTOBJ(WRTTRLZ,MESAGE,FNAME)	SPLK0015
INCLUDE NASTOBJ(OPNCCR,WRTCOR)	SPLK0016
INCLUDE NASTOBJ(RDCCR,CPNCORZ,PRELOC,LOCATE,PRELOCZ,SSWITCH,GOPEN)	SPLK0017
INCLUDE NASTOBJ(FREAD,CLSTAB)	SPLK0018
ENTRY NASTRAN	SPLK0019
END	SPLK0020

Figure 1.0

LINK 1	SPLK1001
RENAME SETC = RETURN	SPLK1002
RENAME NTRAN=DUMP \$ 1108 DECK ONLY	SPLK1003
RENAME SEARCH=DUMP \$ NOT USED ON THE 6400/6600	SPLK1004
RENAME SYSTEM = SYSTEM. \$ RENAME THE CDC SYSTEM ROUTINE CALLS	SPLK1005
RENAME PEXIT = LINK20.	SPLK1006
RENAME XCR = XCRF	SPLK1007
RENAME LD01 = LD50	SPLK1008
RENAME LD02 = LD50	SPLK1009
RENAME LD03 = LD50	SPLK1010
RENAME LD04 = LD50	SPLK1011
RENAME LD05 = LD50	SPLK1012
RENAME LD06 = LD50	SPLK1013
RENAME LD07 = LD50	SPLK1014
RENAME LD08 = LD50	SPLK1015
RENAME LD09 = LD50	SPLK1016
RENAME LD10 = LD50	SPLK1017
RENAME LD11 = LD50	SPLK1018
RENAME LD12 = LD50	SPLK1019
RENAME LD45 = LD50	SPLK1020
RENAME LD46 = RETURN	SPLK1021
RENAME LD47 = RETURN	SPLK1022
RENAME LD48 = RETURN	SPLK1023
RENAME LD49 = RETURN	SPLK1024
RENAME LD51 = RETURN	SPLK1025
RENAME TTLPG = RETURN	SPLK1026
INCLUDE NASTOBJ(XSEM1,GNFIST,TAPBIT,PAGE,PAGE1,PAGE2,PAGEZZZ)	SPLK1027
INCLUDE NASTOBJ(BLKDATA(XSRTBD))	SPLK1028
OVERLAY A1	SPLK1029
INCLUDE NASTOBJ(MSGWRT,USRMSG)	SPLK1030
OVERLAY A1	SPLK1031
INCLUDE NASTOBJ(BTSTRP)	SPLK1032
INCLUDE NASTOBJ(ENDSYSZ,ENDSYS,BGNSYS)	SPLK1033
INSERT ZENDSYS	SPLK1034
OVERLAY A1	SPLK1035
INCLUDE NASTOBJ(BLKDATA(XSFA1),XCEI,XPOLCK,XFILPS)	SPLK1036
INCLUDE NASTOBJ(XPURGE)	SPLK1037
INCLUDE NASTOBJ(XSAVE)	SPLK1038
INCLUDE NASTOBJ(XPLECK,XPOLCKZ,XSFA,XCLEAN,XPUNP,XDPH,XSOSGN)	SPLK1039
INSERT XSFA1,ZXPOLCK	SPLK1040
OVERLAY ESFA	SPLK1041
INSERT ESFA	SPLK1042
OVERLAY A1	SPLK1043
INCLUDE NASTOBJ(BLKDATA(IFPX0),BLKDATA(IFPX1),BLKDATA(UMFZZZ),SEMINT)	SPLK1044
INSERT IFPX0,XOLDPT,IFPX1,UMFZZZ	SPLK1045
OVERLAY DD	SPLK1046
INCLUDE NASTOBJ(XRCARD)	SPLK1047
OVERLAY D	SPLK1048
INCLUDE NASTOBJ(GNFAT,XCSA,XRGDFM)	SPLK1049
INCLUDE NASTOBJ(XSBSET)	SPLK1050
OVERLAY E1	SPLK1051
INSERT XCSABF	SPLK1052
OVERLAY E1	SPLK1053
INCLUDE NASTOBJ(LD50)	SPLK1054
OVERLAY D	SPLK1055
INCLUDE NASTOBJ(SORT,BLKDATA(IFP1A),FNDPLT)	SPLK1056
INCLUDE NASTOBJ(IFP1,IFP1C,IFP1C,IFP1E,IFP1F,IFP1G,SWSRT)	SPLK1057
INSERT SETUP,IFP1A	SPLK1058
OVERLAY IFP1X	SPLK1059
INSERT IFP1X	SPLK1060

Figure 1.1

OVERLAY D	SPLK1061
INCLUDE NASTOBJ(XFADJ1,XRECPS,XFADJ,CROFLG,RPAGE,XBCDBI,EXTINT,INITCO)	SPLK1062
INCLUDE NASTOBJ(XPRETY,INTEXT,XRECP SZ,ISFT)	SPLK1063
INSERT ZXRECPS	SPLK1064
OVERLAY UMF	SPLK1065
INCLUDE NASTOBJ(XSCRT)	SPLK1066
OVERLAY ESORT	SPLK1067
INSERT ESORT	SPLK1068
OVERLAY UMF	SPLK1069
INCLUDE NASTOBJ(UMFECT)	SPLK1070
OVERLAY UMFXXX	SPLK1071
INSERT UMFXXX	SPLK1072
OVERLAY D	SPLK1073
INCLUDE NASTOBJ(BLKDATA(XGPI2),BLKDATA(XGPIC),XGPI,XGPIDG,XGPIMW,)	SPLK1074
INCLUDE NASTOBJ(XGPICGZ)	SPLK1075
INSERT XGPIC,XGPID,XGPI2,XGPI3,XGPI4,XGPI5,XGPI6,XGPI7,XGPI8,XGPI2X	SPLK1076
INSERT ZXGPIDG	SPLK1077
OVERLAY E	SPLK1078
INCLUDE NASTOBJ(BLKDATA(XLKSPC),XGPISB)	SPLK1079
INSERT XLKSPC	SPLK1080
OVERLAY E	SPLK1081
INCLUDE NASTOBJ(XOSGEN)	SPLK1082
INCLUDE NASTOBJ(XSCNDM)	SPLK1083
OVERLAY EE	SPLK1084
INCLUDE NASTOBJ(XPARAM)	SPLK1085
OVERLAY XGPI1	SPLK1086
INSERT XGPI1	SPLK1087
OVERLAY EE	SPLK1088
INCLUDE NASTOBJ(XIPFL)	SPLK1089
OVERLAY EE	SPLK1090
INCLUDE NASTOBJ(XLAKHD)	SPLK1091
OVERLAY E	SPLK1092
INCLUDE NASTOBJ(XFLORD,XFLDEF)	SPLK1093
OVERLAY E	SPLK1094
INCLUDE NASTOBJ(OSCCMP)	SPLK1095
OVERLAY DD	SPLK1096
INCLUDE NASTOBJ(RCARC,IFPPK,IFP)	SPLK1097
INCLUDE NASTOBJ(BLKDATA(IFPX2),BLKDATA(IFPX3),BLKDATA(IFPX4))	SPLK1098
INCLUDE NASTOBJ(BLKDATA(IFPX5),BLKDATA(IFPX6),BLKDATA(IFPX7))	SPLK1099
INSERT IFPX2,IFPX3,IFPX4,IFPX5,IFPX6,IFPX7	SPLK1100
OVERLAY DDD	SPLK1101
INCLUDE NASTOBJ(IFS2P)	SPLK1102
OVERLAY IFPXX	SPLK1103
INSERT IFPXX	SPLK1104
OVERLAY DDD	SPLK1105
INCLUDE NASTOBJ(IFS1P)	SPLK1106
OVERLAY DDD	SPLK1107
INCLUDE NASTOBJ(IFS3P)	SPLK1108
OVERLAY DDD	SPLK1109
INCLUDE NASTOBJ(IFS4P)	SPLK1110
OVERLAY DD	SPLK1111
INCLUDE NASTOBJ(BLKDATA(IFP3BD),IFP3,IFP3B)	SPLK1112
INSERT IFP3BD,IFP3LV	SPLK1113
OVERLAY IFP3ZZ	SPLK1114
INSERT IFP3ZZ	SPLK1115
ENTRY XSEM1	SPLK1116
END	SPLK1117

Figure 1.1 (Concluded)

LINK 2	SPLK2001
RENAME SETC = RETURN	SPLK2002
RENAME NTRAN=DUMP \$ 1108 DECK ONLY	SPLK2003
RENAME SEARCH=DUMP \$ ACT USED ON THE 6400/6600	SPLK2004
RENAME PEXIT = LINK20.	SPLK2005
RENAME BTSTRP = RETURN	SPLK2006
RENAME SYSTEM = SYSTEM.	SPLK2007
RENAME INPTT1 = RETURN	SPLK2008
RENAME INPTT2 = RETURN	SPLK2009
RENAME INPTT3 = RETURN	SPLK2010
RENAME INPTT4 = RETURN	SPLK2011
INCLUDE NASTOBJ(XSEM2,GNFIST,TAPBIT,PAGE,PAGE1,PAGE2,PAGEZZZ,INTLST)	SPLK2012
INCLUDE NASTOBJ(SETVAL,INTGPT,INTGPX,INTGPXZ,RDMODE,RDMCDX,RDMODXZ)	SPLK2013
INCLUDE NASTOBJ(RDMODY,RDWORD)	SPLK2014
OVERLAY A	SPLK2015
INCLUDE NASTOBJ(MSGWRT,LSRMSG)	SPLK2016
OVERLAY A	SPLK2017
INCLUDE NASTOBJ(ENDSYSZ,ENDSYS,BGNSYS)	SPLK2018
INSERT ZENDSYS	SPLK2019
OVERLAY A	SPLK2020
INCLUDE NASTOBJ(BLKDATA(XSFA1),XCEI,XPGLCK,XFILPS,QPARAM)	SPLK2021
INCLUDE NASTOBJ(XSAVE)	SPLK2022
INCLUDE NASTOBJ(XFILFS,XPLEQK,XPOLCKZ,XSFA,XSOSGN,XCLEAN,XPUNP,XDPH)	SPLK2023
INSERT XSFA1,ZXPCLCK	SPLK2024
OVERLAY ESFA	SPLK2025
INSERT ESFA	SPLK2026
OVERLAY A	SPLK2027
INCLUDE NASTOBJ(TABPT,TABPRT)	SPLK2028
OVERLAY TABPR	SPLK2029
INCLUDE NASTOBJ(MATPRN,MATDUM)	SPLK2030
OVERLAY TABPRX	SPLK2031
INSERT TABPRX	SPLK2032
OVERLAY TABPR	SPLK2033
INCLUDE NASTOBJ(PFTPRM)	SPLK2034
OVERLAY A	SPLK2035
INCLUDE NASTOBJ(BLKDATA(INPUTA,IUNION,INPUT)	SPLK2036
INSERT INPUTA	SPLK2037
OVERLAY INPUTX	SPLK2038
INSERT INPUTX	SPLK2039
OVERLAY A	SPLK2040
INCLUDE NASTOBJ(EJECT,WRTMSG,PRTMSG)	SPLK2041

Figure 1.2

OVERLAY	XXPMSG	SPLK2042
INSERT	XXPMSG	SPLK2043
OVERLAY	A	SPLK2044
INCLUDE	NASTOBJ(SORT,BLKDATA(GPTA1))	SPLK2045
INSERT	SETUP,GPTA1	SPLK2046
OVERLAY	GPX1	SPLK2047
INCLUDE	NASTOBJ(GP1)	SPLK2048
INSERT	GPA1	SPLK2049
OVERLAY	GPX1	SPLK2050
INCLUDE	NASTOBJ(GP2)	SPLK2051
INSERT	GPA2	SPLK2052
OVERLAY	A	SPLK2056
INCLUDE	NASTOBJ(BLKDATA(EDES),COMECT,CNSTRC,OPLTST,SETINP)	SPLK2057
INSERT	ECES,XXPSET	SPLK2058
OVERLAY	A	SPLK2059
INCLUDE	NASTOBJ(BLKDATA(CHAR94),AXIS,CRWCHR,IDPLOT,LINE,PLTSET,PRINT)	SPLK2060
INCLUDE	NASTOBJ(SCLOSE,SELCAM,SEOF,SGINOZZ,SKPFRM,SOPEN,STPLOT,SWRITE)	SPLK2061
INCLUDE	NASTOBJ(SYMBCL,TYPE,TYPINT,FNCPLT,DPLCT,DRAW)	SPLK2062
INCLUDE	NASTOBJ(ELELBL,FIND,FNDSET,GPTLBL,GPTSYM,HEAD)	SPLK2063
INCLUDE	NASTOBJ(MINMAX,PARAM,PERPEC,PLOT,PLTOPR,PROCES,SHAPE,WRTprt)	SPLK2064
INCLUDE	NASTOBJ(LINES,TYPE9,WPLT9)	SPLK2065
INSERT	CHAR94,CHRCRW,XXPARM,PLTCAT,SYMBLS,DRWDAT,RSTXXX	SPLK2066
OVERLAY	XXPLOT	SPLK2067
INSERT	XXPLCT	SPLK2068
ENTRY	XSEM2	SPLK2069
END		SPLK2070

Figure 1.2 (Concluded)

```

LINK 20
RENAME   SETC = RETURN
RENAME   SYSTEM = SYSTEM.
RENAME   EXIT(PEXIT) = PEXIT66
INCLUDE  NASTOBJ(PEXIT,MSGWRT,USRMSG,PAGE,PAGE1,PAGE2,PAGEZZZ,PEXIT66)
ENTRY    PEXIT
END

```

```

SPLK2001
SPLK2002
SPLK2003
SPLK2004
SPLK2005
SPLK2006
SPLK2007

```

Figure 1.3

```

SUBROUTINE LD50(SUBSET)
INTEGER RD(144)
DATA NPTP/4,NPTP/
INTEGER IS1(15)
DATA IS1/1,1,1,1,1,1,1,1,1,1,1,1,1,1,1/
DATA RD/
A4HBEGI, 4HN PR, 4HEFAC, 4HE - , 4HCEC, 4HKS I, 4HNPUT, 4H AND,
B4H PLO, 4HTS U, 4HNDEF, 4HCRME, 4HD ST, 4HRUCT, 4HURE , 4H$ ,
C4HGP1 , 4HGCOM, 4H1,GE, 4HCM2,, 4H/GPL, 4H,EQE, 4HXIN,, 4HGPD,
D4H,CST, 4HM,BG, 4HPDT,, 4HSIL/, 4HV,N,, 4HLUSE, 4HT/C,, 4HN,12,
E4H3/V,, 4HN,NO, 4HGPD, 4H $ , 4HSAVE, 4H LUS, 4HET $, 4HGP2 ,
F4HGCOM, 4H2,EQ, 4HEXIN, 4H/ECT, 4H $ , 4HPLTS, 4HET P, 4HCDB,,
G4HEQEX, 4HIN,E, 4HCT/P, 4HLTSE, 4HTX,P, 4HLP, 4HGP, 4HSETS,
Z4H,ELS, 4HETS ,
H4H/V,N, 4H,NSI, 4HL/V,, 4HN,JU, 4HMPPL, 4HOT $, 4HSAVE, 4H NSI,
I4HL,JU, 4HMPPL, 4HOT $, 4HPRTM, 4HSG P, 4HLTSE, 4HTX//, 4H $ ,
J4HSETV, 4HAL /, 4H/V,N, 4H,PLT, 4HFLG/, 4HC,N,, 4H1/V,, 4HN,PF,
K4HILE/, 4HC,N,, 4HO $ , 4HSAVE, 4H PLT, 4HFLG,, 4HPFIL, 4HE $ ,
L4HCCND, 4H P1,, 4HJUMP, 4HPLOT, 4H $ , 4HPLOT, 4H PLT, 4HPAR,,
M4HGPSE, 4HTS,E, 4HLSET, 4HS,CA, 4HSECC, 4H,BGP, 4HDT,E, 4HQEXI,
N4HN,SI, 4HL,,/, 4HPLOT, 4HX1/V, 4H,N,N, 4HSIL/, 4HV,N,, 4HLUSE,
O4HT/V,, 4HN,JU, 4HMPPL, 4HCT/V, 4H,N,P, 4HLTFL, 4HG/V,, 4HN,PF,
P4HILE , 4H$ , 4HSAVE, 4H JUM, 4HPPL, 4HT,PL, 4HTFLG, 4H,PFI,
Q4HLE $, 4HPRTM, 4HSG P, 4HLOTX, 4H1//$, 4HLABE, 4HL P1, 4H$ ,
R4HEND , 4H$ , 4H , 4H , 4H , 4H /
CALL WRITE (NPTP,RD,144,1)
CALL WRITE (NPTP,15,1,0)
CALL WRITE (NPTP,1,1,0)
CALL WRITE(NPTP,IS1,15,0)
CALL WRITE(NPTP,C,1,0)
CALL WRITE(NPTP,C,1,0)
RETURN
END

```

Figure 2.0

EXPERIENCES IN NASTRAN INSTALLATION AND TRAINING

By Caleb W. McCormick

The MacNeal-Schwendler Corporation

SUMMARY

The experiences of The MacNeal-Schwendler Corporation in NASTRAN installation and training are reviewed. Experiences in installation cover a wide variety of computers and a number of different operating systems. Training periods have varied from one or two days, directed at specific applications, up to two weeks or more covering both static and dynamic analysis.

INTRODUCTION

The MacNeal-Schwendler Corporation has participated in the installation and/or training in the use of NASTRAN for 35 different organizations. Included in the list of clients are seven NASA Centers, several aerospace organizations and other industrial users, primarily in turbine manufacturing and atomic power plant applications. Most of the clients own or lease their computers. However, several of the users have solved their problems on computers at commercial data centers. In these cases, access to the computer has been through the use of computer terminal facilities located some distance from the central processor.

NASTRAN has been operational at the CDC Cybernet Data Centers for several months. The data center operation makes NASTRAN available to many organizations that would otherwise not be able to use the program. Since, in general NASTRAN runs more efficiently on large computers and larger computers provide more computing power per dollar spent, it is usually much less costly to run problems on large computers, particularly the larger problems. Although individual users can rarely afford large computers, the data centers almost always use the largest computers available in conjunction with multiprogramming operating systems. The design of NASTRAN permits the user to request only that fraction of the available hardware that is needed for his particular problem. It is anticipated that the use of remote terminals and other data center services will increase substantially as NASTRAN becomes more widely used. Data centers can also serve as training centers for new NASTRAN users.

NASTRAN INSTALLATION

Installation Procedures

NASTRAN installation is defined as the transformation of a standard executable version of NASTRAN on a physical tape into an operating version for the user at a particular installation. The following three general tasks are associated with the installation operation:

1. Provide direct access storage for the program.
2. Check NASTRAN interfaces with resident operating system.
3. Provide operating system control cards for the user.

Some form of direct access residence must be provided for the executable version of NASTRAN. At some installations permanent space is provided on either disks or drums. In these cases, the first part of the installation merely involves the transfer of the executable NASTRAN from tape to direct access storage with the aid of the available operating system utilities. At other installations, permanent residence on direct access devices is not permitted. In these cases, the transfer of the executable NASTRAN from sequential to direct access storage must be performed for each execution. This transfer is a rather expensive operation, and for very small problems, may require as much computer time as the problem solution.

A preliminary check on possible conflicts between NASTRAN and the resident operating system can be made by discussing this question with the programmer responsible for maintaining the operating system at each installation. A final check is made by attempting to execute NASTRAN. These conflicts arise because of local variations in the standard operating systems. Fortunately, the number of interfaces between NASTRAN and the resident operating system is limited to a few well-defined areas. The interfaces that are most likely to give difficulty are associated with the dynamic use of main and secondary storage. One important interface is associated with the definition of the secondary storage files at the beginning of each NASTRAN execution. A related interface is associated with the use of the secondary storage files for intermediate results during problem solution. Another important interface is associated with the determination of the amount and location of main storage that has been assigned to NASTRAN by the resident operating system.

The operating system control cards are related to the definition of secondary storage files, requested amount of secondary storage, and definition of input streams. In many cases the operating system control cards are defined in a procedure library and the user needs only to execute this procedure and override any defaults that he wishes. Typical overrides are to request additional main storage and request physical tapes for one or more secondary storage files.

Due to the limited use of the Univac EXEC 8 operating system outside of NASA centers, The MacNeal-Schwendler Corporation has not had any experience with variations in this operating system. There have been some discussions relative to the modification of NASTRAN to run under the EXEC II operating system. However, this is a substantial task, and requires a number of modifications to the operating system, particularly the loader, and the development of new NASTRAN routines for transferring data between main and secondary storage.

IBM Installations

The MacNeal-Schwendler Corporation has used NASTRAN on the following models of the IBM 360/370 series: 50, 65, 75, 85, 91, 95, 155, and 195. Most of the operating systems have used the MVT (Multiprogramming with a Variable number of Tasks) job scheduler. A few of the smaller systems (models 50 and 65) have used the MFT (Multiprogramming with a Fixed number of Tasks) job scheduler. Although the single-task environment (PCP) was used on a model 50 during the development of NASTRAN, this form of job scheduler has not been encountered recently.

In addition to the various job schedulers, a number of different job supervisors have been encountered. These are operating systems that extend the capability of the basic OS/360 by controlling one or more computers that in turn are using any one of the job schedulers - MVT, MFT, or PCP. The IBM released job supervisor is called the Attached Support Processor (ASP). A number of other local job supervisors have been encountered such as HASP, LASP, and a special triplex system.

In all of these experiences with IBM hardware and operating systems, only modest difficulties have been encountered in the use of NASTRAN. Moreover, when difficulties have been encountered, the problem has usually been solved with the use of control cards at execution time, rather than by making coding changes in NASTRAN. Although there were some problems associated with early releases of NASTRAN and OS that required coding changes, no such difficulties have been encountered recently.

Direct access storage for the executable NASTRAN program is provided on the 2314 disk storage device. Approximately one-third of a disk pack is required for the NASTRAN program. At some installations, space is provided on permanently mounted packs, whereas other installations use private packs that are mounted on request for each NASTRAN execution. The executable load module is copied from a magnetic tape to the disk pack using standard system utility programs.

Differences in options that are used when a particular operating system is generated (SYSGEN) will affect the amount of space needed in the NASTRAN execution region for operating system routines. For example, at one installation one of the operating system routines was marked nonreentrant. Consequently, a fresh copy of the routine was loaded when any of the NASTRAN links (currently 13 in number) were loaded. Moreover, each new copy required

separate main memory space for storage. If insufficient space is provided for system routines, the operating system will terminate the job with an error message (80A) indicating this fact. Additional space can be provided for operating system routines by changing the value of SYSTEM(31) on the NASTRAN card at execution time.

One of the main tasks in adapting NASTRAN to a particular operating system and a particular hardware configuration is to design a procedure for the PRØCLIB to provide most of the necessary operating system control cards. The majority of these cards are associated with the definition of the secondary storage files. The buffer sizes for these files should be selected with due regard for the fact that larger buffers are more efficient, but require additional main memory space. The buffer size must not be greater than a single track on the 2314 disk pack, and for efficiency, an integral number of buffers should fit on a single track of the disk storage device. The initial allocations should be adjusted to fit the average size problem contemplated, with provision made for overrides at execution time for larger problems.

CDC Installation

The MacNeal-Schwendler Corporation has used NASTRAN on a number of different CDC 6000 series machines using local variations of the SCØPE 3 operating system. The main difficulties on these machines have been associated with the XBØØT routine and local variations in the operating system library routines. The XBØØT routine is the interface between the SCØPE loader and the NASTRAN loader. In many cases, minor modifications have been made to XBØØT to accommodate local variations in the SCØPE operating system. Based on these experiences, an executable version of NASTRAN can now be generated that will run on all operating systems that have been encountered for CDC 6000 series machines.

The NASTRAN executable program usually exists as a sequential file on tape. The first few records of the file contain an initial load program produced by the special NASTRAN linkage editor. The remainder of the file contains the NASTRAN executable program produced by the NASTRAN linkage editor. The NASTRAN program is initiated by executing an operating system control statement that causes the CDC loader to load the initial program and transfer control to XBØØT. The XBØØT program reads the remainder of the file, writes it on the disk in indexed form, reads the first part of the NASTRAN program into main memory, and transfers control to NASTRAN.

Some installations permit NASTRAN to remain on the disk in indexed form. In these cases, the execution of NASTRAN only requires a control statement pointing to the NASTRAN permanent file on the disk. At some of the CDC Data Centers, NASTRAN is kept in indexed form on mountable disk packs. In these cases, the user only needs to request a disk pack mount in order to have NASTRAN available in direct access form.

At the Langley Research Center, NASTRAN is resident on a data cell. The user requests the NASTRAN program by including a FETCH control statement in his data deck. This statement causes NASTRAN to be fetched from the data cell and placed on the disk in direct access form. Once NASTRAN is fetched it is allowed to remain in residence on the disk as long as the space is not needed for other programs in execution. If NASTRAN is already in residence on the disk, the operating system skips the fetch step and proceeds directly to the execution of NASTRAN.

Since only a few control cards are required to execute NASTRAN on the CDC 6000 series, no special catalog procedures are required. No control cards are needed to define the secondary storage files as these definitions are handled internally by the NASTRAN executive system. The secondary storage space is allocated by the operating system as needed during execution.

One of the troublesome variations in the SCOPE operating system is the manner in which the main memory field length is adjusted during execution. In many cases, a control card (RFL) is provided that permits the user to request a field length of his choice. In other cases, the field length is reduced to that needed for the first program loaded. This latter situation causes trouble because the dynamic use of main memory in NASTRAN does not permit the use of a dimension statement that includes the working space. Unless a control card (NØRFL) is provided to prevent this reduction, all main memory space beyond the code in the initial load program is returned to the operating system, and NASTRAN is unable to continue beyond the execution of the initial program. If the field length is reduced and a NØRFL control card is not present in the operating system, it is necessary to modify the initial load program in order to protect the main memory space.

NASTRAN TRAINING

User Training

User training is herein defined as preparing a person already experienced in finite element modeling to use NASTRAN for the analysis of structures subjected to static and dynamic loads. Basic training sessions have usually extended over a period of one week. The usual format has been classroom sessions in the morning and problem solution sessions in the afternoon. The actual experience of preparing a NASTRAN data deck and submitting problems for solution is an important part of the NASTRAN training. Shorter periods of training have been used, but most people find the more intensive training less desirable, unless they are experienced in the use of other finite element programs. In some cases, the basic training has extended over a two-week period. In these cases, it has been found desirable to conduct two sessions of one week each, separated by a period of about two weeks.

Many organizations find it desirable to supplement the basic training with some form of continuing assistance. This additional help is usually supplied on an on-call basis as needed for special problems. In some cases,

advanced training courses of up to one week duration have been conducted, covering such topics as techniques for the solution of very large problems and additional training in the use of direct matrix abstraction procedures (DMAP). Basic training courses usually emphasize the use of rigid formats with little or no discussion of matrix abstraction programming. There will be a continuing need for modest amounts of additional training when new capabilities are added to NASTRAN.

Many users have learned to use NASTRAN without the benefit of formal training. In most cases, these people were already experienced users of other finite element programs. Probably the biggest problem associated with self-help operations is the lack of a training manual. The User's Manual is organized as a reference manual, and as such it is difficult for untrained persons to use. Perhaps funds will someday be allocated for the preparation of a self-help training manual. It has even been suggested by some that a training movie would be a useful vehicle for NASTRAN training.

Programmer Training

Programmer training has varied from a few hours to several days or even longer when programmers have been given a complete working knowledge of NASTRAN. All programmer training has been conducted as on-the-job training, rather than formal classroom instruction. This approach has been found to be the most effective as usually only one or at most a few programmers are involved at any one time.

The minimum programmer training consists of a brief description of the NASTRAN program structure, along with instruction in the operation of NASTRAN on a particular hardware configuration with a particular operating system. This will include a discussion of the provision of direct access storage for the executable version of NASTRAN, and the development of a set of operating system control cards along with a cataloged procedure if desirable. The programmer is also instructed in variations of the operating system control cards that are required for checkpointing, restarting, plotting, use of tapes etc. Some instruction in the interpretation of NASTRAN error messages and possible difficulties with the particular operating system being used are included in the minimum programmer training. In open shop installations, the user is frequently responsible for the operation of NASTRAN, and hence, in these cases, the user is given the minimum programmer training.

The next level of programmer training is to learn the procedures for using the source and object libraries to make changes in NASTRAN and link edit a revised executable version. This level of training will permit the programmer to correct errors and make modifications to the program. Many installations will want to develop this operational capability in order to take advantage of known error corrections between standard CØSMIC releases of NASTRAN.

Only a few installations desire the highest level of programmer training. Complete training in the development of new NASTRAN code requires several weeks of on-the-job training. There is little need for this level of training unless an organization wishes to actively make contributions to the development of NASTRAN, either for their own use or as a contractor.

CONCLUDING REMARKS

Experiences gained in a wide variety of NASTRAN installations has made it possible to generate a single version of NASTRAN that will run on all known versions of a given operating system. User training of one week and programmer training of a few hours seems to be satisfactory for the usual NASTRAN operations. More extensive user training is required for the solution of large problems and more extensive programmer training is required if one wishes to do program development work with NASTRAN.

NASTRAN INSTALLATION: IMPLEMENTATION STEPS
AND POSSIBLE PROBLEMS ENCOUNTERED

By Howard E. Dielmann

Computer Sciences Corporation

SUMMARY

NASTRAN, from its inception, was designed to operate on several diverse computer systems. It is currently installed and operating on the CDC 6600, the IBM 360, and the UNIVAC 1108. This paper discusses the steps found by CSC to be necessary in installing NASTRAN on a computer system and the possible obstacles that might be encountered in undertaking NASTRAN installation. Reference is made to actual problems that arose during installation on the above machines. With a knowledge of what has happened to date in setting up NASTRAN, the future user will be better able to cope with and understand the implications of installing NASTRAN on his computer.

INTRODUCTION

The NASTRAN program had as its primary directive to design and develop NASTRAN in such a manner that it could be easily implemented on several different machines. These machines were the IBM 7094 under IBSYS, the UNIVAC 1108 under EXEC II and EXEC 8, the IBM 360 under OS, and the CDC 6600 under SCOPE. The problems associated with machine dependence were given considerable attention during the initial phases of NASTRAN's development. An attempt was made to utilize a subset of FORTRAN IV that was compatible with the specified machines (reference 1), and to avoid dependencies on machine characteristics such as 36-bit words or 6-bit characters. Despite the planning devoted to avoiding dependencies, many obstacles arose whenever NASTRAN was implemented on a computer system. These obstacles generally occurred because of the enormous size of NASTRAN,¹ its extreme and varied demands on the operating system, or the lack of capabilities of the particular operating system involved.

¹ NASTRAN consists of over 700 subroutines and comprises some 145,000 cards. The compiled object code contains approximately 900,000 words, and the absolute or executable program consists of over 1,800,000 words (IBM 360 statistics).

Early in the development of NASTRAN, the hardware capabilities and to some extent, the software capabilities of the second generation IBM 7094 and UNIVAC 1108 EXEC II were taxed excessively, and NASTRAN evolved into a third generation system. The third generation systems are better equipped to meet NASTRAN's hardware requirements, but no operating system to date has been able to sufficiently satisfy all of the software requirements of NASTRAN. These third generation operating systems are not designed to give to any one application program the total resources that NASTRAN requires (core, files, etc.) without limiting the execution of NASTRAN or affecting the operation of the computer system.

The intent of this paper is to identify both the steps and the obstacles that might be encountered in installing NASTRAN. The particular problems encountered in adapting NASTRAN to other computer systems cannot, of course, be addressed by this paper, since these will vary from one computer system to another.

However, a general observation can be made that will apply to the implementation of NASTRAN regardless of the particular computer system involved. The observation is this: that a comprehensive and flexible operating system greatly aids in the installation effort. Many of the obstacles we encountered in installing NASTRAN involved services related to the operating system, such as library editing, compiling, loading, and I/O control. If the proper facilities either were not available, or were insufficient, programs had to be written to provide these services. We therefore feel that the following features of an operating system are either necessary or desirable: (1) a source and object library editing capability, (2) a standard and efficient FORTRAN IV compiler, (3) a sophisticated loader capable of handling large overlays, (4) an extensive control language that allows multiple file definitions, dump specifications, etc., and (5) macro-level I/O calls.

This paper is presented in the general order of the steps employed in installing NASTRAN:

1. Hardware evaluation
2. Software implementation
 - a. Source language creation
 - b. FORTRAN compilation
 - c. Source and object library updating
 - d. Machine-dependent deck conversion
 - e. Absolute program creation

- f. NASTRAN execution
- g. Tailoring of NASTRAN to the computer system

HARDWARE EVALUATION

The initial question to be resolved when considering the installation of NASTRAN on a computer system is whether the hardware configuration will support NASTRAN. The primary requirement of NASTRAN is a large amount of core. NASTRAN can operate on as little as 45K words of core (UNIVAC 1108), but problem solving capability can be limited even with 65K words.² For large problems, at least 100K words should be available. The second question is whether sufficient auxiliary storage space is available. (This allocation can be provided through disk, drum, or other available storage devices.) A minimum of 30 files must be defined, each requiring a space allocation of 50K to 500K words.³ As problem size increases, so does the need for auxiliary storage. For convenient operation, the hardware should be configured with at least five tape drives available to NASTRAN. If only a minimum hardware configuration is available, NASTRAN will operate, but it will be limited as to the size of a problem that it can solve. Moreover, a problem run on a larger system will usually take considerably longer to run on a smaller configuration, since insufficient core storage may cause spill in matrix operations. Other hardware features such as the number and speed of I/O channels and the speed of the auxiliary storage devices will also affect the operating efficiency of NASTRAN.

SOFTWARE IMPLEMENTATION

Source Language Creation

When we began to code NASTRAN and create source decks, it soon became apparent that card decks were too bulky. IBM 7094 IBSYS provided a card to tape utility, and NASTRAN card image source tapes were used. Compilations were made from the tape and the tape was updated via a CSC-written update program as new or modified decks were added.

²For example, a 45K system should be able to solve a 175-order complex eigenvalue problem; a 65K system, a 900-order problem; and a 100K system, a 2,100-order problem.

³For example, a single 1,000 order double precision matrix that is 25 percent dense requires 500,000 words of storage.

When the first NASTRAN system was to be developed on the UNIVAC 1108 EXEC II, a corresponding source tape was needed. A utility program to convert the IBM 7094 tape to UNIVAC 1108 EXEC II format was written. Once converted, this tape was acceptable as input to the FORTRAN compiler. Eventually, corresponding programs were written to provide input source tapes to the UNIVAC 1108 EXEC 8, the IBM 360, and the CDC 6600.

The first step in putting NASTRAN on a computer is to obtain or create a source tape that can be used as input to the system's compiler. In all likelihood, this will require creating a program that converts a current UNIVAC 1108, IBM 360, or CDC 6600 source tape to the required format. However, some operating systems may already have the capability to handle this task (the RCA SPECTRA 7, for example, accepts IBM 360 tape) and eliminate this step.

FORTRAN Compilation

The next step, and supposedly the easiest, is the compilation of all of the source language decks. Surprisingly, however, this step has activated numerous problems in the past. This situation no doubt has been due to the large number of source decks (700 subroutines, 145,000 source statements) and the variety and complexity of the code involved; if any errors exist in the target computer's FORTRAN compiler, they usually show up while the NASTRAN subroutines are being compiled. These errors appear either as a compilation abort, extraneous error messages, or incorrectly generated object code. Incorrect code may occur when optimization of the object code is selected. If this occurs, the use of optimization should be avoided. If other compiler errors are identified, they can usually be circumvented by rewriting the FORTRAN code.⁴

Another and potentially more serious problem relates to the definition of standard FORTRAN. CSC in attempting to avoid this problem defined a subset of the ASA standard FORTRAN IV that was to be used. This meant that certain features available under one compiler could not be used unless those features were available on all compilers. As a result, octal or hexadecimal data statement, for example, could not be used. However, in spite of our efforts, it was impossible to define a subset that was compatible on the CDC 6600. That system's compiler required a different format for nonstandard returns and did not allow multiple entry points.

⁴For example, it was found that EXEC 8 failed to compile properly when a deck with one entry point contained nonstandard returns. An additional dummy entry point was inserted into decks having one entry point and nonstandard returns, and correct code was thereafter generated.

When it became necessary to implement NASTRAN on the CDC 6600, a program was written to convert the source decks to 6600 compiler format. This program, similar to the FORTRAN II to FORTRAN IV SIFT program, modifies the format of nonstandard returns and eliminates multiple entry points.

With a strong background in working with FORTRAN, and with data on the integrity of the FORTRAN compiler involved, the degree of difficulty in compiling NASTRAN can be measured. If a given compiler is known to have errors, it should be avoided - presuming, of course, that a choice of compilers is available. If optimization has caused problems in the past, it should not be used. If the FORTRAN IV language differs from the standard that NASTRAN has used, a SIFT-type program may have to be developed. Overall, however, with a competent system, this task should be a purely mechanical one, consisting of a string compilation of all decks.

Source and Object Library Updating

Inherent in the compilation of source language decks is the creation of an object library tape. In order to maintain library tapes, a source and object library edit and update program is necessary. In the case of the IBM 7094, a source and object library edit and update program did not exist, and such a program therefore had to be written. Although a third generation system generally has such a capability, the capability is sometimes cumbersome to use. (For example, the IBM 360 object tape has to be edited to provide control section names for input to the Linkage Editor.)

By using library edit features, changes to source programs can be made by simply specifying in an update deck the changes that are to be made to the library source program. When this deck is compiled, the source and object libraries are automatically updated.

A sophisticated library edit capability in a target system can greatly facilitate compilation and subsequent updates to the system. Desirable features of an edit program include the following: (1) an update option for inserting, deleting, or adding cards, (2) the capability of allowing source and object libraries to be maintained on random access devices, (3) the ability to automatically update the source and object libraries when a deck is recompiled, and (4) the capability of listing and identifying all decks by time and date compiled.

Machine-Dependent Deck Conversion

Once the FORTRAN decks have been compiled, the machine-dependent programs must be converted. These machine-dependent programs consist of several assembly language decks, some Data Block decks, and some FORTRAN decks.

Through a concerted effort, assembly language coding was kept to a minimum, since CSC considered it more important to provide easily convertible FORTRAN code than to obtain the increase in efficiency provided by assembly code. The few assembly language programs that do exist consist of function-type subroutines (AND, OR, LSHIFT, etc.) and operating system-type interface routines (CPU clock, time of day clock, console message, etc.). Of the assembly language subroutines, some can be simply converted (i.e., AND, OR, LSHIFT), while others must be implemented according to the interface with the system (i.e., reading the CPU clock). Generally, the operating system provides subroutines that return the time of day, that return the elapsed CPU time, and that send messages to the computer operator. Under these circumstances, the only change required in the NASTRAN decks is to code a routine that calls the system subroutine providing these capabilities.

During NASTRAN's development, block data programs that contained system parameters were defined. These parameters include machine characteristics, and various subroutines utilize this data. In installing NASTRAN, the system parameters must be modified to identify such characteristics as computer word size, number of bits per character, number of characters per word, timing information, etc. The application subroutines utilize this information to accomplish such tasks as extracting a character from a word, based on the character and word length definitions contained in the data base.

The third set of decks that must be changed are the machine-dependent FORTRAN decks. These decks generally handle some of the NASTRAN-operating system interfaces. One of these decks is GINOIO, which contains the physical I/O calls to the system output devices. Preferably, GINOIO should contain macro-level I/O calls, but can contain FORTRAN READ/WRITE calls, although such calls are extremely inefficient. A second deck that must be modified (and that may have to be in assembly language) is GNFIAT, which must identify and transmit to NASTRAN the number and name of all files allocated to the run. Several smaller decks that accomplish initialization and link switching must also be changed.

To accomplish the conversion of these machine-dependent programs usually requires persons knowledgeable in both the intricacies of NASTRAN and the internal aspects of the operating system.

Absolute Program Creation

One of the most difficult tasks required in installing NASTRAN is the creation of the overlays and the generation of the absolute (executable) elements, since no two loaders of third generation computers are even remotely similar. In addition to this problem, most loaders are not equipped to handle an overlay as large or as complex

as that of NASTRAN. Fairly early in the development of NASTRAN, we exceeded the capacity of the IBM 7094 loader, and subsequently exceeded a size limitation on the UNIVAC 1108 EXEC II due to fixed table sizes. However, even the third generation loaders have not been well equipped to handle the NASTRAN overlay.

NASTRAN is divided into 14 separate links, each with its own overlay tree structure. These links can be created independently and can be thought of as separate programs. Therefore, if a deck is changed in one link, only that link has to be regenerated. Communication between the links is handled via data contained on external storage. The EXEC 8 overlay loader handled the structuring of each link extremely well. Only those decks that defined origins had to be explicitly named, while all other subroutines were included automatically. However, EXEC 8 failed in providing a convenient mechanism for crossing between links. This was eventually solved by using external control cards to determine the link to be executed, calling the link in, and passing control to it. On the IBM 360, the linking concept is entirely different and consists of a super link occupying a region of its own. The functional links are loaded into a second region, with the super link program responsible for passing control between functional links.

In addition, the execution time loading characteristics between systems differ. The UNIVAC 1108 has a segment loader, which causes a segment of an overlay to be loaded only when the segment is explicitly called. The IBM 360, on the other hand, has a string loader, loading the segment called and all other segments between it and the main link. This caused problems; a job might run for example, on the IBM 360 but not the UNIVAC 1108 because the same segments were not loaded into core at the same time.

When we began the installation of NASTRAN on the CDC 6600, we encountered a loader with such limited capability that implementation was impossible. It was therefore necessary to write a loader to handle NASTRAN's requirements. A loader was written for the CDC 6600 (primarily in FORTRAN), and was patterned after the IBM 360 Linkage Editor/Loader.

The difficulty of establishing NASTRAN on a system depends on the capabilities of the system loader. If other large programs requiring overlays have been implemented successfully on the target computer, then NASTRAN can probably be installed. As mentioned earlier, if the operating system has a sophisticated loader capable of handling large overlays, the problems connected with NASTRAN installation will be minimal. If, however, the required loader capabilities do not exist, a new loader may have to be written. Since most third generation systems possess competent loaders, however, the likelihood of having to write a new loader is not great.

NASTRAN Execution

Once the absolute programs have all been created, NASTRAN is ready for execution. The control stream for executing NASTRAN must now be constructed by the user. NASTRAN requires a large number of separate I/O files (more than 30) with a significant amount of peripheral storage allocated to each file. These files are defined by means of the operating system's control language⁵ and are identified by FORTRAN logical unit numbers.⁶

The operating system's control language is also used to specify the location of absolute programs (i.e., if they are catalogued on permanent storage) or to cause the programs to be read from tape. If sufficient auxiliary storage is available, the NASTRAN absolutes should remain resident, rather than be reloaded from tape for each run. The control stream must also identify under what abnormal end conditions a dump is to be taken, what portions of main core storage are to be dumped, and with what format.

This, of course will not be the first time in implementing NASTRAN on the target computer that extensive use has been made of the operating system's control language. Throughout the initial stages of NASTRAN generation, the compilations and library edits required the use of many control language features. From our experience, we found that a control language should be sophisticated enough to perform the necessary tasks, but not so detailed that it becomes cumbersome to use and difficult to understand.

Tailoring of NASTRAN to the Computer System

At this point, NASTRAN should be operational on the target computer. However, the installation should not yet be considered complete. Ideally, NASTRAN should be tailored to the particular computer system. This customizing includes setting up standard procedures to reduce the effort required to operate NASTRAN and extend its flexibility.

Many things can be done to simplify the control stream required to execute NASTRAN. One of these, already mentioned, is to catalog the NASTRAN system on a permanent file that is available to all users. Another means might be to group the many control cards necessary to define the files into one data set that is callable by a single control card. It may be possible to include in this call a

⁵For example, on the IBM 360 DD cards are used to define the unit number, physical device (tape, disk, etc.,) and space allocation.

⁶For example, the integers 8, 9, 10, 11, etc.

parameter that defines the space allocation.⁷ It may also be possible to specify a region size on the run card, and therefore to provide a flexible NASTRAN system in terms of core and file size. By implementing the above suggestions, it is likely that the number of control cards needed can be reduced to as few as four or five.

Several changes can also be made to improve the run efficiency of NASTRAN. The NASTRAN buffer size can be tailored to fit the particular random access devices used. That is, buffer size can be set to correspond to half-track or full-track. Since data buffers should not cross track boundaries, such tailoring can improve the efficiency of the I/O and provide better utilization of auxiliary storage.

Machine timing characteristics such as internal arithmetic speed and I/O speed are stored in the data base, and are used to make logical decisions concerning the most efficient means of decomposing a matrix. Timing studies can be made to refine the data base times and thus to enable the decomposition routines to make proper decisions.

A longer range goal might include the conversion of some of the time-critical FORTRAN routines to assembly language, since conversion of these routines can lead to a substantial savings in machine time. Here, the I/O and PACK/UNPACK routines are good candidates for conversion. Also, if macro-level I/O was not used initially in GINOIO, it is well worth considering it at this point.

CONCLUDING REMARKS

The user who intends to install NASTRAN on a computer should now have a reasonable idea of the nature of the task before him. He also has an outline of the necessary steps to install NASTRAN. However, each computer is unique, and the problems as well as the solutions that he encounters in implementing NASTRAN may be distinctly different from those of the past.

Users about to install NASTRAN can reduce the magnitude of the installation effort if three resources are available: first, a capable and well checked out operating system; second, a person knowledgeable in the use and internal workings of that system; and third, a person experienced in the use and internal design of NASTRAN.

⁷On the IBM 360, for example, a PROC was set up to define the DD cards. A parameter included in the PROC defines the space allocation for each file.

REFERENCE

1. Second Quarterly Report for NASA General Purpose Structural Analysis Program (1 November 1966 - 1 January 1967) pp. 25-71, prepared by CSC for Goddard Space Flight Center, Greenbelt, Maryland.

AN EVALUATION OF CURRENT NASTRAN DISCRETE
ELEMENT MODELS FOR MONOCOQUE AND
SEMI-MONOCOQUE STRUCTURES*

By Edward L. Stanton
and William F. Bozich

McDonnell Douglas Astronautics Company
Huntington Beach, California

ABSTRACT

The current discrete element analysis models in NASTRAN, Levels 8.1.0 and 11.1.0, are evaluated for semi-monocoque and monocoque structures. Comparative results are presented with the FORMAT-III general-purpose code for a swept wing statics analysis and a Skylab substructure vibration analysis. Good agreement between Level 11.1.0 and FORMAT-III is demonstrated; however, a major error in Level 8.1.0 was discovered on the Skylab vibration problem. The computational performance of NASTRAN was superior to FORMAT, but the vibration rigid format was found to have several inefficiencies. Comparative results are also presented between Level 11.1.0 and STACUSS, SLADE, BOND, UNIVALVE, and another special-purpose code. Results for two of the structures analyzed, a cylindrical shell and an elliptic plate, indicate curved discrete elements are significantly more accurate than the plate elements in NASTRAN for the same number of degrees of freedom.

SYMBOLS

CPU	central processor unit
E	Young's modulus
G	plane stress material properties matrix
h	plate thickness
Hz	cycles per second
L	length
N	dimension of the stiffness matrix

*This work was performed under the sponsorship of the McDonnell Douglas Astronautics Company Independent Research and Development Program. Portions of the work reported were done under Contract NAS9-6555 (Skylab). One test problem was taken from work performed for the Air Force Space and Missile Systems Organization under Contract F04701-70-C-0159.

N/m^2	Newtons per square meter
PPU	peripheral processor unit
R	cylinder radius
SS	systems seconds - composite time charge
u, v, w	elastic displacements
μsec	microseconds
ν	Poisson's ratio

INTRODUCTION

An evaluation of most special-purpose structural analysis programs can be accomplished using closed-form solutions of academic problems with restricted geometry. A general-purpose program like NASTRAN, however, is more difficult to evaluate in that it must also be tested for complex built-up structural analysis problems. This can be accomplished using known experimental results or solutions from existing general-purpose programs like FORMAT that have been extensively tested for a variety of structures. The present paper evaluates current NASTRAN (Levels 8.1.0 and 11.1.0) discrete element models for semi-monocoque and monocoque structures using comparative results from FORMAT, special-purpose programs, and closed-form solutions. In particular, comparisons are provided for a multi-cell swept wing, a water bottle storage rack assembly on the Skylab vehicle, and two common structural shapes. The accuracy of the NASTRAN results are of primary interest, but the question of program efficiency also receives attention.

General-purpose code comparisons are made for semi-monocoque structures using NASTRAN rigid formats one (statics) and three (normal modes). In the case of the swept wing problem, only static results are available; however, these include both force method and displacement method solutions by FORMAT. The Skylab storage rack problem is analyzed for static deflections and natural modes using a reduced dynamic model (Guyan reduction option) for the symmetric modes and the unreduced model for anti-symmetric modes. The FORMAT solutions are obtained using the force method and a matrix condensation procedure equivalent to Guyan reduction. Modeling differences between the force method and displacement method idealizations of the storage rack structure are described. Special-purpose code comparisons are made for monocoque structures using NASTRAN rigid formats one (statics), three (normal modes), and nine (direct transient response). A simply supported cylinder under external pressure is analyzed using the CQUAD2 plate element. These results are compared with curved shell element solutions from the STACUSS and SLADE special-purpose codes. An orthotropic elliptic plate loaded by an external pressure is also analyzed using NASTRAN plate elements and the results compared with the Lekhnitskii

closed-form solution. Comparisons are also made with a new parametric discrete element code. The final problem considered is the transient response of an impulsively loaded free ring segment. The structure is modeled using beam elements and the response compared with results from the BOND and UNIVALVE ring codes. These data and data from the preceding problems provide detailed information on the current modeling capability of NASTRAN for monocoque and semi-monocoque structures.

GENERAL-PURPOSE CODE COMPARISONS FOR SEMI-MONOCOQUE STRUCTURES

General-purpose discrete element programs are designed primarily for the analysis of complex built-up structures. Irregular construction and geometry make it difficult, if not impossible, to analyze these structures by other methods and it was this capability in NASTRAN that was first to be evaluated at MDAC. A very large percentage of the total analysis cost for such structures is associated with development of the discrete element model from engineering drawings and a large percentage of this cost is associated with the generation of grid coordinate data. NASTRAN has no built-in capability in this area although user coded modules can be added to provide a basic capability such as that in FORMAT (see ref. 1, pp 91-92). Ideally the computer graphics used in the actual design (ref. 2) should be available to aid in the construction of the analysis model.

The NASTRAN Level 11.1.0 results, compared in this section with FORMAT-III results, were obtained on the CDC 6500 in double precision. The FORMAT-III results were obtained in single precision on the UNIVAC 1108 and the CDC 6500. This difference in computational precision did not significantly affect the accuracy comparisons, although it did increase the NASTRAN central processor unit (CPU) times.

Semi-monocoque Swept Wing

The swept wing problem is taken from the FORMAT User's Manual (ref. 1) and features many items common to built-up structure. These included oblique reactions, thermal loading, skewed element geometry, tapered sections, and multiple materials. The wing (see fig. 1) has a 0.5236-radian sweep angle, a multi-rib outer section, and a tapered root section. The two sections have a gap between them and are connected by the front and rear spar caps. The discrete element idealization of the front spar has bending stiffness in two planes outboard of node 33 (see figs. 2 through 4). The structure is basically aluminum with a number of steel stiffeners and is subjected to both mechanical and thermal load conditions. The NASTRAN and FORMAT displacement idealizations use similar elements although the element matrices are slightly different. The FORMAT force method model of the wing uses the same grid points but different plate and panel elements as described in reference 1. The first load condition is a 4,448-Newton lift force on the front spar wing tip (see fig. 1, vector 37) and the second load condition is a

temperature increment of 111.1°K at nodes 5, 6, 7 and 8 (see fig. 2). Comparative results for the mechanical load condition (see figs. 5 through 9) show good agreement with the largest differences occurring in the displacement directly under the load. The maximum displacement difference between NASTRAN and either FORMAT solution is 7 percent. The comparison of internal bar forces is actually better, as figure 7 demonstrates, with the maximum difference between NASTRAN and either FORMAT solution being 3.5 percent. Results from the thermal load condition (see figs. 10 through 13) show smaller differences than for the mechanical load condition. The computational performance of NASTRAN Level 11.1.0 was significantly better than that of FORMAT-III. The CDC 6500 NASTRAN solution for five load conditions required 171 CPU seconds, 364 PPU seconds, and 218 SS seconds. The PPU time includes 200 seconds required to copy NASTRAN from tape to disk which can be avoided by using permanent disk storage. This solution was in double precision, a waste of time and core on CDC 6000 series computers. The single-precision FORMAT displacement solution required 1320 seconds on the UNIVAC 1108 which executes FORMAT in very nearly the same time as the CDC 6500. The size of this problem is relatively small (N=232) and the majority of the CPU time is not spent solving the equilibrium equations. NASTRAN used only 21 seconds and FORMAT 60 seconds. The principal reason for the computational difference in this problem is the use of a pre-programmed rigid format by NASTRAN.

Skylab Storage Rack--Statics

The Skylab vehicle has a water bottle storage rack assembly (see figs. 14 and 15) consisting of 3 built-up frames, with 10 cylindrical water tanks distributed around the circumference between the 2 lower frames, 25 storage racks distributed around the upper frame, and a conical skirt connecting the assembly to the Skylab primary structure. The water containers hold 3044 kg of water, the contents of the storage cabinets has a mass of 1361 kg and the total mass of the structure is 6976 kg.

A NASTRAN idealization that uses one plane of symmetry was generated for half the structure (see fig. 16) using an earlier FORMAT-III idealization wherever possible. Some modeling differences occurred because the FORMAT-III force method shear panel has mid-side nodes and the associated bar (rod) element has mid-length reactions, while the NASTRAN shear panels have nodes at the corners. A summary of the FORMAT-III and NASTRAN idealization for half the structure is presented in table 1. Heavy use of bars and shear panels to represent bulkheads in the force method model is designed to keep the number of redundants small. This situation does not occur in the displacement method and membrane elements were used in the NASTRAN idealization of the bulkheads. The most serious deviation from the FORMAT-III modeling occurred in representing the conical skirt support for the storage rack assembly. The FORMAT-III idealization used direct input flexibility matrices at the support reactions to represent the conical skirt while in the NASTRAN model the vertical and tangential displacements were prescribed to be zero at the outer circumference of the lower ring frame. This modeling difference could have been removed using the general element feature in

NASTRAN; however, this was not done for budgetary reasons.

NASTRAN solutions for static unit loads were obtained and compared with existing force method results obtained from the FORMAT-III program. Figure 17 indicates good agreement between FORMAT-III and NASTRAN Level 11.1.0 for the upper ring frame and water container support structure, while at the lower ring frame the NASTRAN model is too stiff because of the modeling of the supports. The lack of correlation with Level 8.1.0 of NASTRAN, shown in figure 17, is due to an error which occurs in this early release for a special class of multipoint constraint equations. The swept wing problem for example also used multipoint constraint equations but no significant differences in the Level 8.1.0 and Level 11.1.0 results were observed. The computational performance of NASTRAN was again superior to FORMAT. The module times listed in table 2 indicate, surprisingly, that the multipoint constraint eliminator took longer than decomposition of the stiffness matrix. These results were obtained after renumbering the grid points using BANDIT (see ref. 3) to reduce the bandwidth of the stiffness matrix. Prior to renumbering, the semi-bandwidth was 289 with 26 active columns and the problem "spilled" badly. Excessive data transfer (i.e., spill) occurs on the CDC 6000 series when the sum squared of the semi-bandwidth and the number of active columns exceeds the working core storage available. NASTRAN estimated over 5000 CPU seconds to decompose the poorly sequenced matrix and terminated the run on its time-to-go check. Only 91.3 CPU seconds were used by BANDIT to save over 5000 CPU seconds. In general, bandwidth minimization will not always be the best strategy because of the active column feature; however, it is a good baseline strategy used often at MDAC.

Skylab Storage Rack--Vibration

NASTRAN solutions for the natural vibration characteristics were also obtained and compared with those obtained from the FORMAT-III program. The FORMAT-III model for structural and nonstructural mass consisted of concentrated (lumped) masses for 250 dynamic degrees of freedom in the complete structure. A matrix reduction procedure similar to "Guyan reduction" was used to condense the static discrete element model to these 250 degrees of freedom before computing vibration modes. The same mass idealization and dynamic degrees of freedom were used in the NASTRAN model except for the conical skirt modeling differences and the use of structural symmetry in the NASTRAN model. This resulted in a 115 degree of freedom model after Guyan reduction, since some of the degrees of freedom at the supports were restricted by the support conditions.

The NASTRAN results for the symmetric modes were computed for the reduced system using the Givens method. The lowest antisymmetric mode was obtained by inverse iteration for the unreduced system, with the mass restricted to 115 degrees of freedom, after applying antisymmetric boundary conditions at the plane of structural symmetry. The frequency comparisons between FORMAT-III and Level 11.1.0 given in table 3 for the first 10 structural modes, indicate that the NASTRAN results were consistently higher by from 3.6 to 7.8 percent which is in keeping with the too stiff boundary

conditions. The mode shapes for the complete FORMAT model were either symmetric (modes 1, 3, 5, 7, and 10) or antisymmetric to the precision of the printout, which was seven significant digits. The mode shapes agree very well away from the boundary (see figures 18 through 20) and in every case the degree of freedom having the maximum displacement was the same.

The computational performance of NASTRAN was only average. The problem used 40 minutes of CDC 6500 CPU time which is broken down for the major modules in table 4. The direct matrix reduction from 571 to 115 degrees of freedom required just under 20 minutes, which is not particularly efficient. In this problem, the omitted coordinates have no mass so that reduction of the mass matrix is trivial. Apparently NASTRAN did not detect this situation. Module SMP1 operates on both the stiffness and mass matrices simultaneously which can also cause inefficiencies on restart. Changes in mass data on a restart run, for example, will cause the stiffness matrix to be reduced all over again. Another inefficiency in SMP1 is the direct matrix reduction of the mass matrix. Sequential reduction such as that used in DYNAL (ref. 4) has reduced problems from 600 to 105 degrees of freedom in under 5 minutes of equivalent CDC 6500 time. The computational performance of inverse iteration (see table 4) on the unreduced problem could also be improved. A significant inefficiency in this routine is the use of an unsymmetric matrix decomposition for symmetric matrices. This not only increases the number of computations; it reduces by nearly one-half the size problem that can be solved without matrix spill. The vibration rigid format also ignores direct matrix input data without printing a warning message. This is not only an inconvenience it can be dangerous.

SPECIAL-PURPOSE CODE COMPARISONS FOR MONOCOQUE STRUCTURES

Special-purpose codes usually are restricted to a particular geometry which they represent exactly. General-purpose codes, in contrast, often approximate curved structures as a series of initially straight discrete elements. As a result special-purpose codes tend to be not only faster but more accurate for a given problem size. The analyst must weigh these advantages against the disadvantage of having to learn the operating characteristics of several different programs and having to maintain them. Comparative results are presented in this section that should assist the analyst in evaluating the relative merits of NASTRAN for certain structural shapes. These include circular shells, elliptic plates, and curved beams.

Simply Supported Cylinder

STACUSS and SLADE are recently developed special-purpose codes (refs. 5 and 6) that can analyze shells of revolution with cutouts using general curved shell discrete elements. At present NASTRAN must model general shell structures using flat plate elements and it is important to have estimates of the loss in accuracy, hence efficiency, incurred using NASTRAN for these

structures. To provide such data, a cylinder simply supported in w , with $u=v=0$ boundary conditions, is analyzed under a uniform pressure. The decay length for boundary effects is approximately $L/4$ so that shell bending is important in the solution. Using axial symmetry, a 10-degree strip of 10 curved elements model the structure in STACUSS and SLADE, while a double strip of 20 elements (20 degrees) is needed by NASTRAN to model the curvature effects. In general the number of elements can be the same, even for symmetry models. The STACUSS elements have the same number of degrees of freedom per node as the NASTRAN elements while the SLADE element has 16 additional u, v displacement degrees of freedom. This allows the influence of curved elements and high order elements to be separated. Results for meridional moment, meridional displacement, and normal displacement (see table 5) indicate that curved shell elements can improve the maximum moment prediction by 16 percent, the maximum meridional displacement by 10 percent, and the maximum normal displacement by 3 percent. These percentages are based on a reference shell-of-revolution discrete element solution using 50 elements over the length of the cylinder. The well-known Timoshenko solution has different u boundary conditions. The STACUSS and SLADE results agree very well indicating that higher order u, v displacement functions are not needed in this problem. If the applied load had a meridional or circumferential component, this conclusion might well change. The NASTRAN and SLADE solutions were obtained on the CDC 6500 and required 97 and 45 CPU seconds, respectively. The STACUSS solution was obtained on the IBM 360/65 and required 79 CPU seconds. In all cases the majority of the CPU time was spent generating the matrices for the problem. The time spent solving equilibrium equations was very small. Recalling that the NASTRAN model used twice as many elements as the SLADE or STACUSS models, there will be little computational difference, in general, even though there is an accuracy difference for the same grid. To summarize, the NASTRAN comparisons demonstrate that flat plate elements can yield static shell solutions with reasonable accuracy but available curved shell elements offer a significant improvement.

Orthotropic Elliptic Plate

Triangular and quadrilateral plate elements do not model the geometry efficiently in many plate problems. A simple example is a circular plate, or a plate with a circular hole, where a straight-sided bending element models the deformed geometry better than the undeformed. Discrete elements with variable edge geometry, called parametric or isoparametric elements, can improve solution accuracy for these problems in much the same way as curved shell elements improved the cylinder results. To estimate the potential improvement, an orthotropic elliptic plate was analyzed using NASTRAN and a parametric element code developed at MDAC. The plate is simply supported and loaded by a uniform pressure of 36.895 N/m^2 . A closed-form solution for this problem is available (see ref. 7) to establish accuracy. Comparative results between straight-sided NASTRAN elements and curved edge parametric elements are presented in table 6 for several grid refinements. The NASTRAN results for the 4×4 grid (see fig. 21) have converged to within 8 percent of the maximum displacement and 12 percent of the maximum stress. (The center-point element stresses were interpolated and extrapolated to obtain the grid

point stresses.) The parametric element results for the 2x2 grid have converged to within 5 percent of the maximum displacement and 6 percent of the maximum stress. These data demonstrate that straight-sided elements can require over four times as many variables for similar accuracy. The NASTRAN 4x4 grid solution also required more CPU time than any of the parametric element solutions. As with the curved shell element comparisons, the NASTRAN results are of acceptable accuracy but the curved-edge plate element results offer a significant improvement.

Dynamic Response of Curved Beam

The planar response of an impulsively loaded, free ring segment having a 0.8238 radian arc was computed using rigid format nine of NASTRAN. The ring segment had an outside radius of 12.7 cm, a thickness of 1.016 cm, and a width of 2.54 cm, a Young's modulus of 2.068×10^4 N/m² and a density of 1.64 gm/cm³ with an initial velocity of 4.79 m/sec. One-half the beam was modeled using 12 straight beam segments with the coupled mass formulation and no transverse shear. The linear elastic results for bending moment and axial force at the centerline were compared with solutions obtained from the MDAC BOND code (ref. 8) and the UNIVALVE code (ref. 9).

The BOND code is based on the general numerical method outlined in reference 10, and uses a lumped-parameter, spring-mass model to determine the dynamic elastic plastic response of soft-bonded layered rings. Only the linear elastic option is used for the present problem. A semicircular segment was modeled using 120 lumped masses in two rings connected by radial and tangential springs. To model the arc segment, all masses located in the outer ring and those in the inner ring beyond the actual arc segment were prescribed to be very small. The actual model for half the circular arc segment was thus represented by 8 of the 120 lumped masses. The BOND results are for a location 0.02618 radian from the centerline.

The UNIVALVE code computes the two-dimensional, large deflection response of arbitrary planar beams and rings using finite differences in space and time. The material may be elastic-plastic and exhibit strain hardening and rate sensitivity; however, these were not used in the present problem. The ring was modeled using both 12 and 24 mesh points along half the curved ring segment, and the results from the 12 point model were compared with NASTRAN.

A comparison of the axial force at the centerline (fig. 22) shows good agreement for all three analyses. A comparison of the centerline bending moment (fig. 23) indicates that the NASTRAN peak moment is 17 percent higher than the UNIVALVE solution, although there was good correlation in frequency. The NASTRAN peak moment was 5 percent greater than the BOND result, which had a slightly higher frequency. The use of a lumped mass idealization resulted in a 7 percent reduction in the NASTRAN peak moment which occurs at 45 μ sec.

When a low transverse shear modulus of $2.068 \times 10^3 \text{ N/m}^2$ was introduced, the NASTRAN results agreed closely with the UNIVALVE results. Table 7 lists the maximum force for the first 100 μsec , and summarizes the numerical integration run times. It is noted that the NASTRAN program employs an implicit integration scheme, while the BOND and UNIVALVE solutions employ an explicit scheme. In addition the number of degrees of freedom and time steps varied for the different solutions, which makes a meaningful comparison of solution times difficult.

The NASTRAN solution was run on the CDC 6500 with the transient response module TRD requiring 259 seconds to execute 500 time steps for the 37 degree of freedom model. The solution was obtained using a 1- μsec time step with the results printed out every fifth step. There was little change in the solution when the step size was reduced to 0.5 μsec .

The UNIVALVE program determines a mesh size for the time variable based on the mesh size for the space variable. A separate run was made with double the number of mesh points, with the solution changing by about 1 percent. A large number of time steps were required for the BOND program to insure solution stability. In summary, the NASTRAN results are of acceptable accuracy but the solution time is excessive in comparison to UNIVALVE. The time required by the transient response module in NASTRAN was only 26 percent of the time shown in table 7. This means implicit versus explicit integration was not the principal reason for the longer NASTRAN run time.

CONCLUSIONS

The general elements in NASTRAN, Level 11.1.0, were found to adequately model semi-monocoque and monocoque structures for linear static and dynamic analyses. However, the modeling efficiency of NASTRAN can be significantly improved with the addition of general curved shell elements and variable-geometry parametric discrete elements. This change should include modification of the matrix assembly modules to eliminate the present six degree of freedom per grid point restriction. These conclusions are based on comparisons with both force method and displacement method solutions using a variety of discrete elements. The early NASTRAN release, Level 8.1.0, was found to have a serious error in the multipoint constraint eliminator that is not present in Level 11.1.0. This error caused an erroneous solution of a Skylab component test case.

The computational performance of the static analysis rigid format was superior to FORMAT-III; however, NASTRAN Level 11.1.0 has no substructuring capability. The sparse matrix routines and the restart monitor performed well although multiple restarts occasionally produced missing files. The structural plot module is easy to use but needs a larger character set to make the title legible. The vibration rigid format, by comparison, was relatively inefficient, especially the Guyan reduction portion. The direct transient response rigid format was also relatively slow. In part, this is the

result of using double precision on the CDC 6500. A single precision option is definitely needed for CDC 6000 series computers. In conclusion, it should be noted that NASTRAN contains many features not reviewed in this paper.

ACKNOWLEDGMENTS

The authors are indebted to several colleagues at MDAC for providing the FORMAT and BOND results and to the Kaman Nuclear Corporation for providing the UNIVALVE results. In particular, the authors wish to thank Mr. T. Meagher and Mr. N. DeMuth of the Kaman Nuclear Corporation and Mr. T. E. Mack, Mr. J. M. Hector, Dr. D. J. McGovern, and Mr. H. L. Chane of MDAC.

REFERENCES

1. Pickard, J.: FORMAT-Fortran Matrix Abstraction Technique, Volume V. Engineering User and Technical Report. AFFDL-TR-66-207, Dec. 1968.
2. Eshleman, A. L. and Meriwether, H. D.: Graphic Applications to Aerospace Structural Design Problems. Douglas Paper No. 4650, Sept. 1967.
3. Everstine, G. C.: BANDIT - A Computer Program to Renumber NASTRAN Grid Points for Reduced Bandwidth. NSRDC Technical Note AML-6-70, Feb. 1970.
4. ICES DYNAL User's Manual. McDonnell Douglas Automation Report MDC N0040-021, 1970.
5. Kotanchik, J. J. and Berg, B. A.: STACUSS 1: A Discrete-Element Program for the Static Analysis of Single-Layer Curved Stiffened Shells Subjected to Mechanical and Thermal Loads. MIT Report ASRL TR-146-9, Dec. 1969.
6. Key, S. W. and Beisinger, Z. E.: SLADE - A Computer Program for the Static Analysis of Thin Shells. Sandia Report SC-RR-69-369, Nov. 1970.
7. Hearmon, R. F. S.: An Introduction to Applied Anisotropic Elasticity. Oxford University Press, 1961.
8. Chane, H. L.: Dynamic Elastic-Plastic Response of Soft Bonded Rings. McDonnell Douglas Astronautics Report DAC-63324, May 1970.

9. Kreig, R. D. and Duffey, T. A.: UNIVALVE II, A Code to Calculate the Large Deflection Dynamic Response of Beams, Rings, Plates and Cylinders. Sandia Report SC-RR-68-303, Oct. 1968.
10. Leech, J. W., Pian, T. H. H., Witmer, E.A., and Herrman, W.: Dynamic Response of Shells to Externally - Applied Dynamic Loads. MIT Report ASD-TDR-62-610, May 1962.

Table 1.--Skylab storage rack discrete
element model data

Model	FORMAT-III	NASTRAN
Grid Points	279	245
Axial Rod Elements	497	387
Bar Elements*	12	12
Shear Panels	193	138
Triangular Membranes	66	106
Quadrilateral Membranes	0	40
*Axial load plus bending in one plane		

Table 2.--NASTRAN computational performance
Skylab static analysis

Module	CPU sec*	Description
SEMI	46.922	NASTRAN preface
TAI	16.637	Table assembler
SMAI	101.327	Structural matrix assembler
MCE2	183.838	Multi-point constraint eliminator
RBMG	104.623	Decompose stiffness matrix
SSG3	31.599	Static solution generator
SDRI	15.163	Stress data recovery
*CDC 6500 central processor unit times		

Table 3. --Skylab storage rack frequency comparisons

Mode	FORMAT-III (Hz)	NASTRAN 11.1.0* (Hz)	Difference
1	12.618	13.580	7.6%
2	13.131	13.962	6.3%
3	14.918	16.067	7.7%
4	15.106	-	-
5	16.105	16.822	4.5%
6	16.343	-	-
7	17.686	18.325	3.6%
8	18.402	-	-
9	18.751	-	-
10	19.841	21.391	7.8%

*Only one antisymmetric mode was computed

Table 4. --NASTRAN computational performance--
Skylab vibration analyses

Module	CPU seconds	Description
SEMI	62.210 (59.728)*	NASTRAN preface
TAI	18.458 (18.313)	Table assembler
SMA1	102.147 (102.141)	Stiffness matrix generator
SMA2	17.536 (17.498)	Mass matrix generator
MCE2	225.239 (214.521)	Multi-point constraint eliminator
SCE1	21.940 (22.032)	Single point constraint eliminator
SMP1	1141.285 -	Matrix reduction (Guyan)
READ	563.743 (782.943)	Real eigenvalue analysis
SDR1	61.341 (9.715)	Stress data recovery

*Time for first antisymmetric mode using inverse iteration

Table 5. --Cylindrical shell comparisons

Meridional Moment (Newton-centimeters)				Meridional Displacement (meters) x 10 ⁻⁶				Normal Displacement (meters) x 10 ⁻⁶		
X/L	N*	ST*	SL*	X/L	N	ST	SL	N	ST	SL
0.025	-179.5	-256.8	-257.8	0.10	-1.454	-1.342	-1.319	-50.13	-53.56	-53.68
0.125	-227.2	-250.7	-251.6	0.20	-1.180	-0.9625	-0.9260	-60.29	-61.86	-61.94
0.225	-30.71	-19.57	-18.75	0.30	-0.7266	-0.5494	-0.5230	-59.01	-59.13	-59.10
0.325	-8.557	-15.84	-16.58	0.40	-0.3314	-0.2622	-0.2498	-58.22	-58.06	-58.02
0.425	-3.333	-3.323	-0.3648	0.50	0	0	0	-58.11	-58.01	-57.98

*N = NASTRAN, ST = STACUSS, SL = SLADE

$$E = 68.95 \times 10^9 \text{ N/m}^2 \quad \nu = 0.3 \quad L = 50.8 \text{ cm} \quad R = 25.4 \text{ cm} \quad \text{External pressure} = 68.95 \times 10^6 \text{ N/m}^2$$

Table 6. --Orthotropic elliptic plate comparisons

Grid	Dimension		Maximum Displacement (meters) $\times 10^{-2}$		Maximum Stress (Newtons/meter ²) $\times 10^6$		Maximum Shear Stress (Newtons/meter ²) $\times 10^6$		CPU Seconds	
	N*	P*	N	P	N	P	N	P	N	P
2x2	8	9	0.3470	0.2830	-18.93	-17.36	-7.598	-7.703	26	15
3x3	21	25	0.3178	0.2819	-24.27	-17.88	-9.894	-7.944	44	28
4x4	40	40	0.3030	0.2817	-20.55	-18.08	-8.715	-8.034	69	54
Exact Solution			0.2816		-18.35		-8.154			
*N - NASTRAN Elements , P - Parametric Elements										

Table 7--Curved beam comparisons

	NASTRAN	BOND*	UNIVALVE
Computer	CDC 6500	CDC 6500	CDC 6400
Degree of freedom	37	240	24
Number of times steps	100	1000	200
CPU seconds	206	269	7
Maximum axial force (Newtons)	-2692	-2731	-2749
Maximum bending moment (Newton-centimeters)	-201.3	-190.8	-162.7

*The BOND values are 0.02618 radian from the centerline

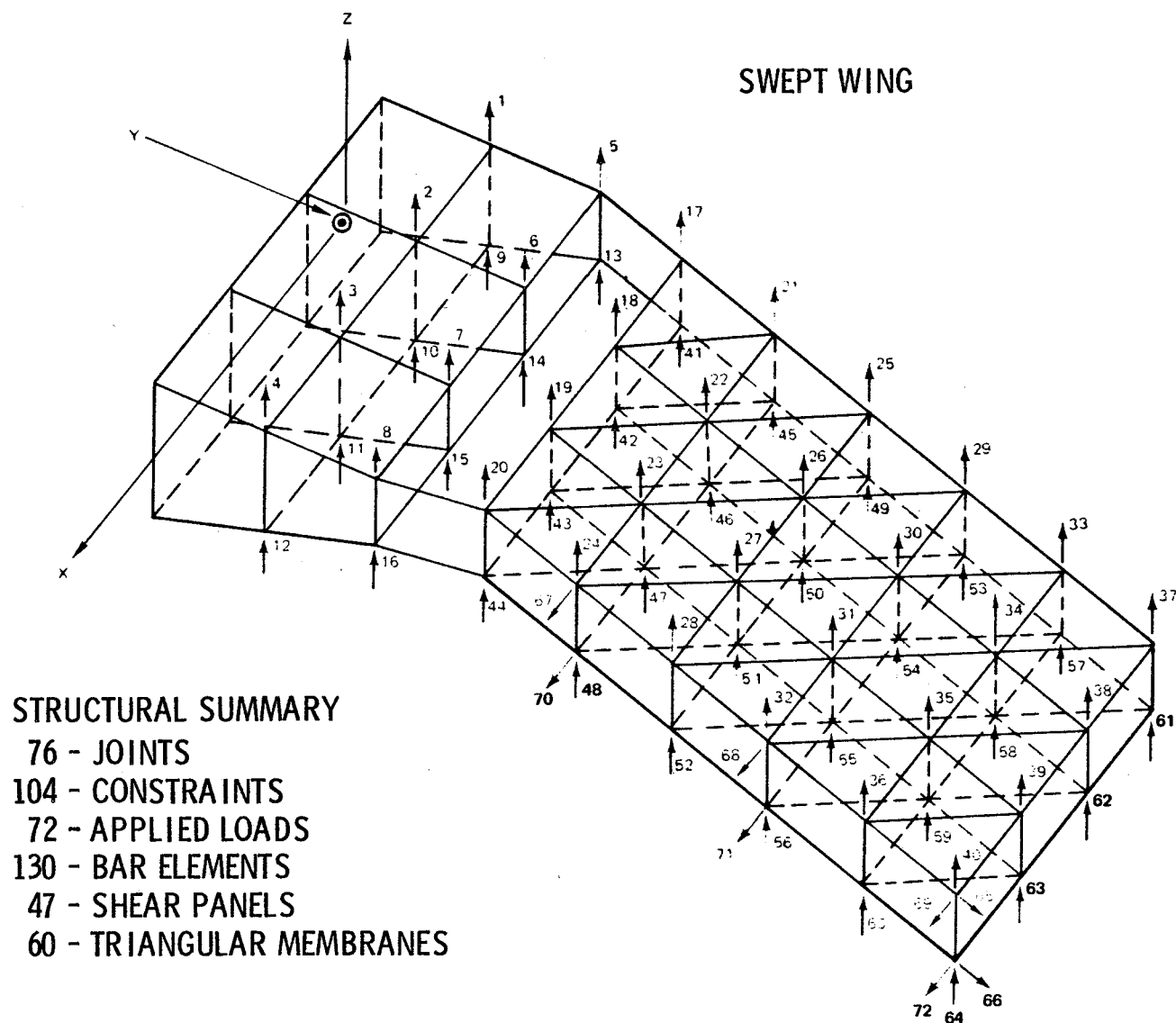


Figure 1.—Structural configuration and applied loads

Figure 2.—Idealization upper surface

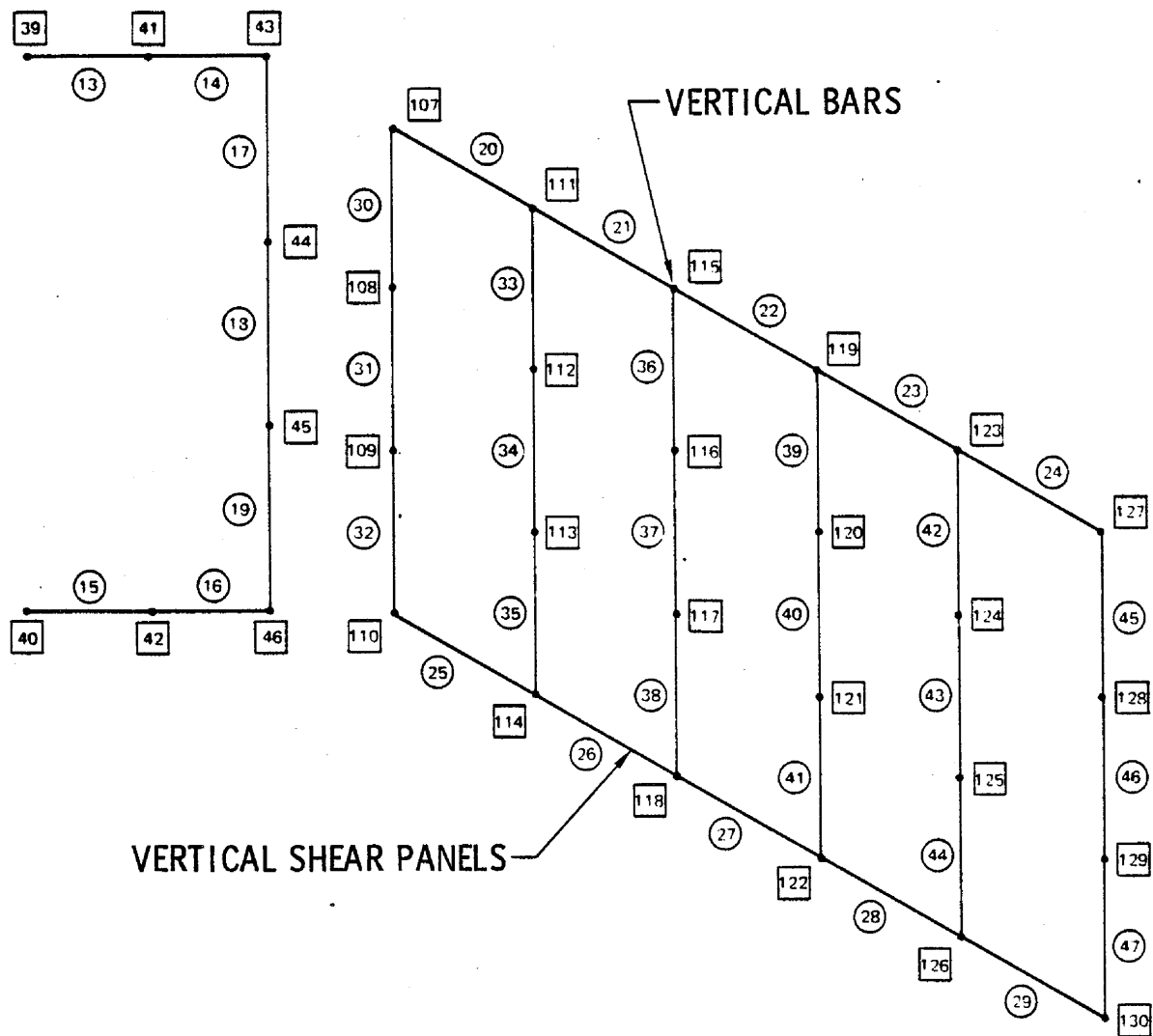


Figure 3.—Idealization middle plane swept wing vertical elements

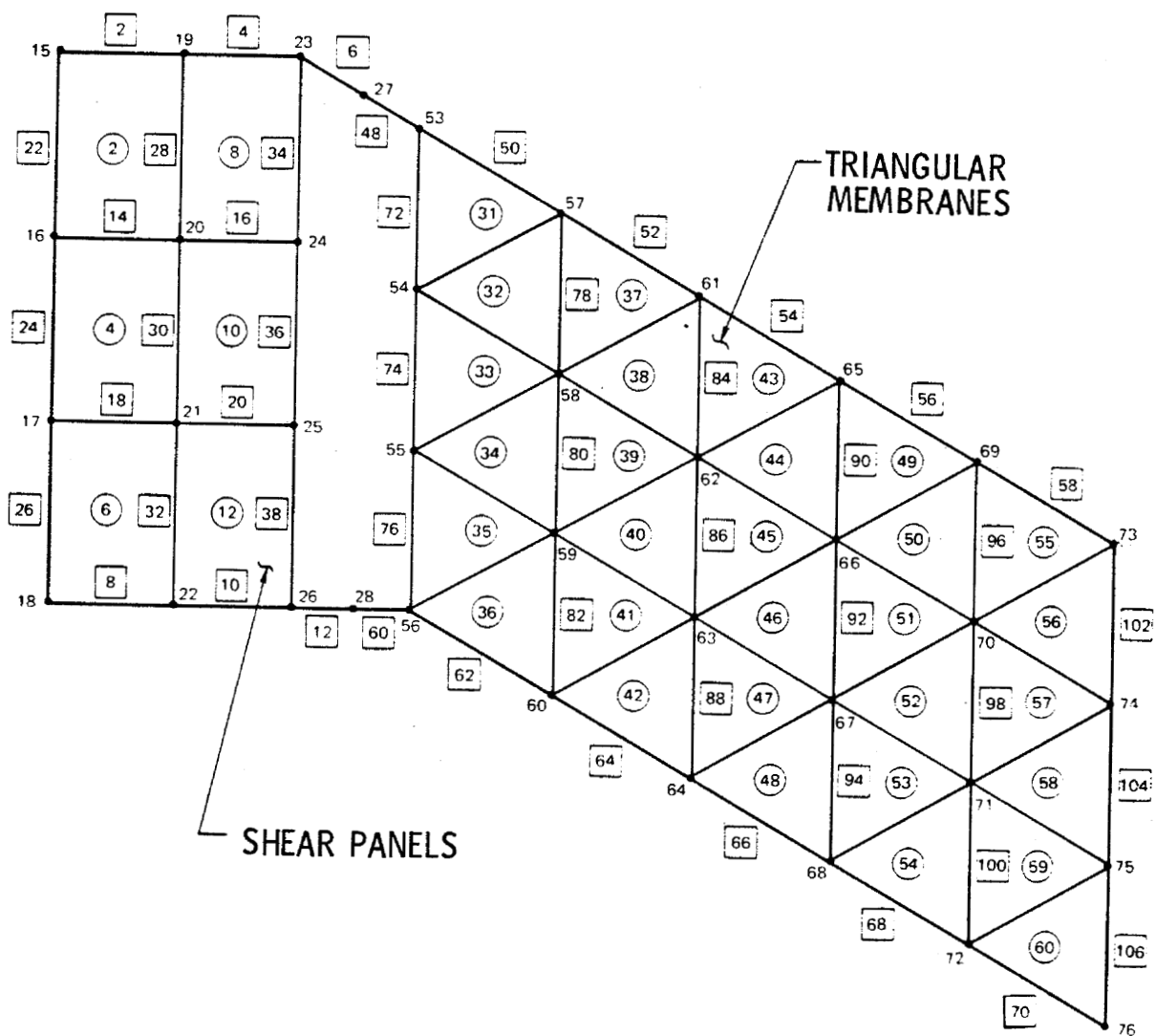


Figure 4.—Swept wing lower surface elements

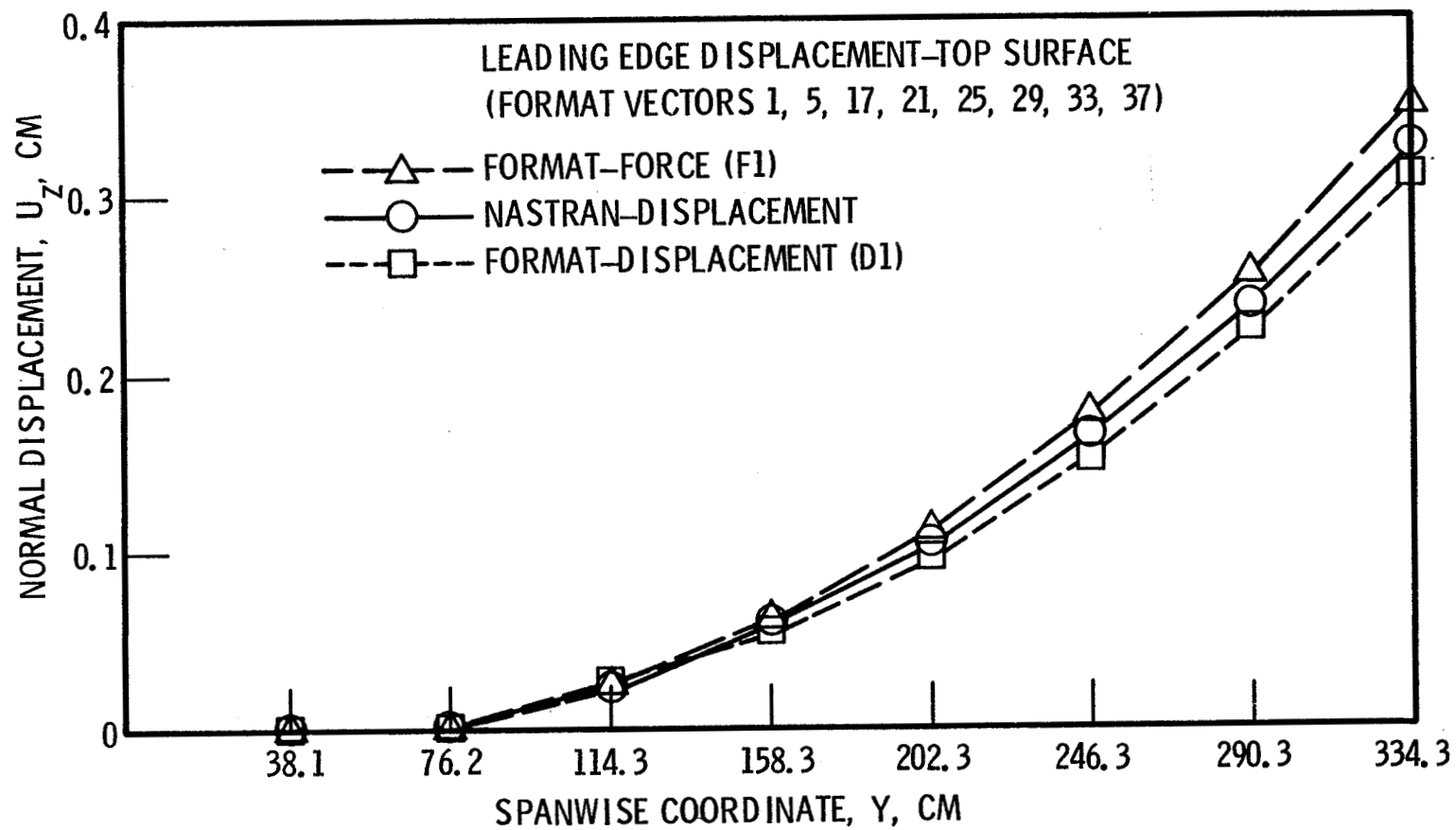


Figure 5.—Swept wing top surface leading edge displacement

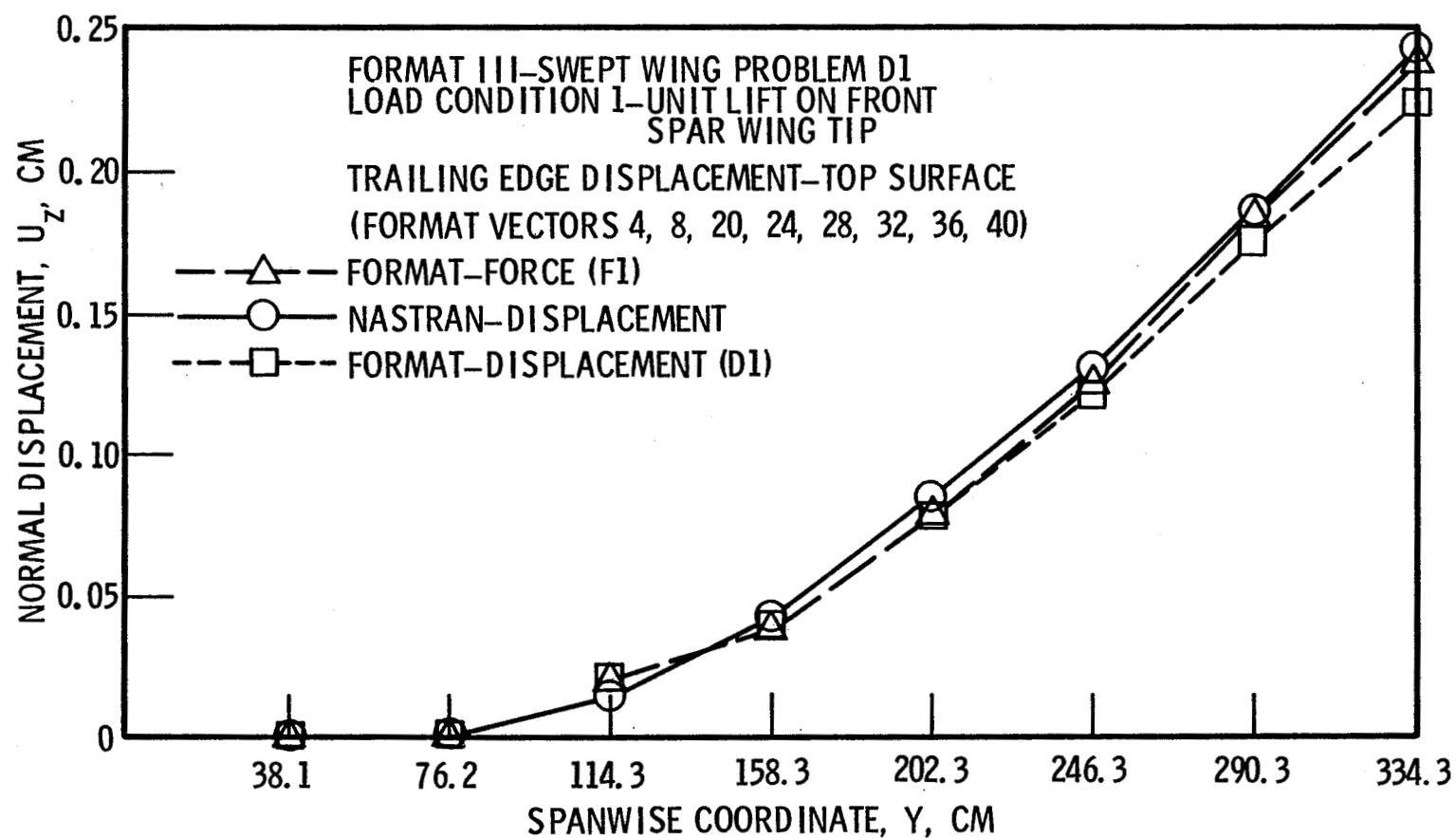


Figure 6.—Swept wing top surface trailing edge displacement

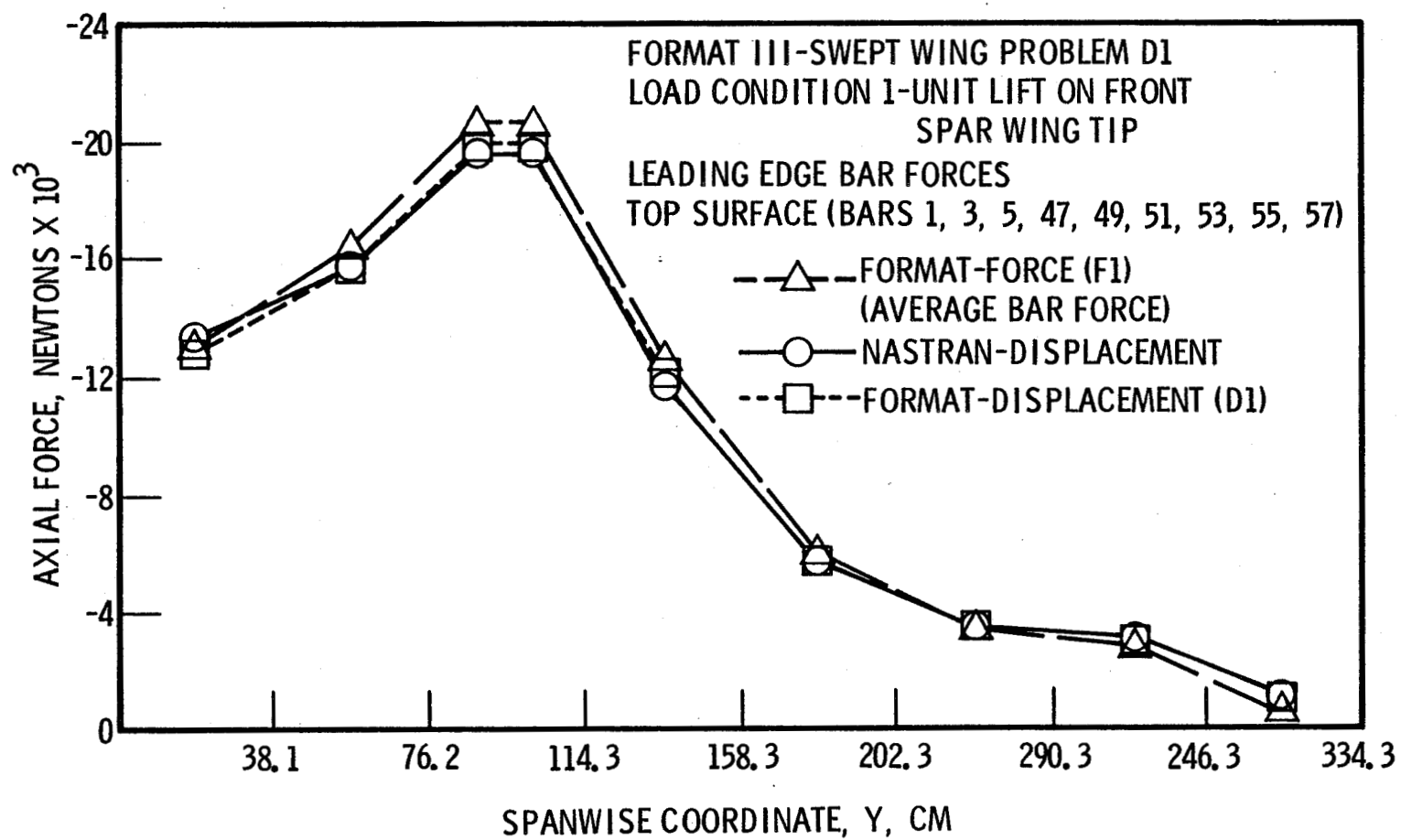


Figure 7.—Swept wing leading edge bar forces

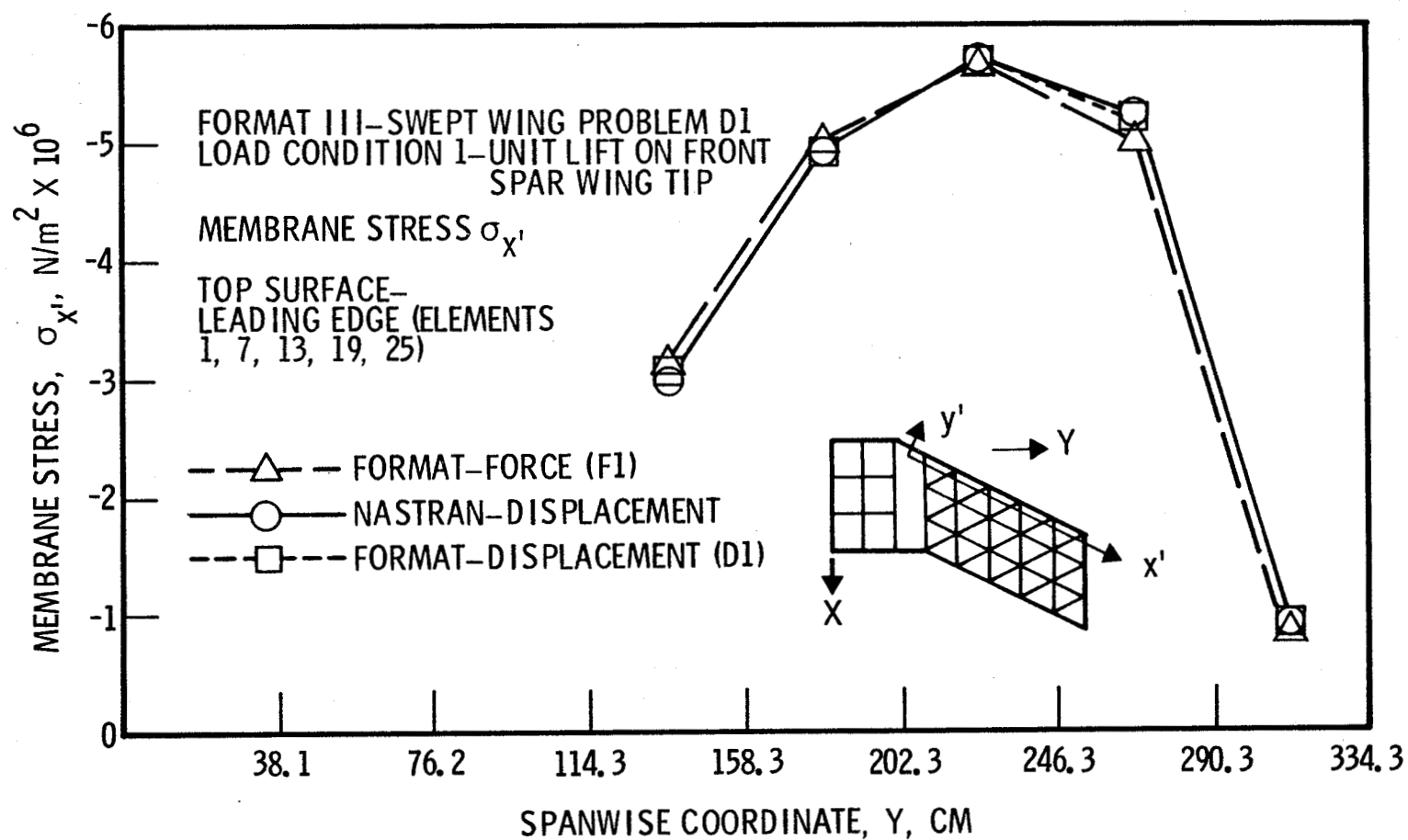


Figure 8.—Swept wing top surface membrane stress

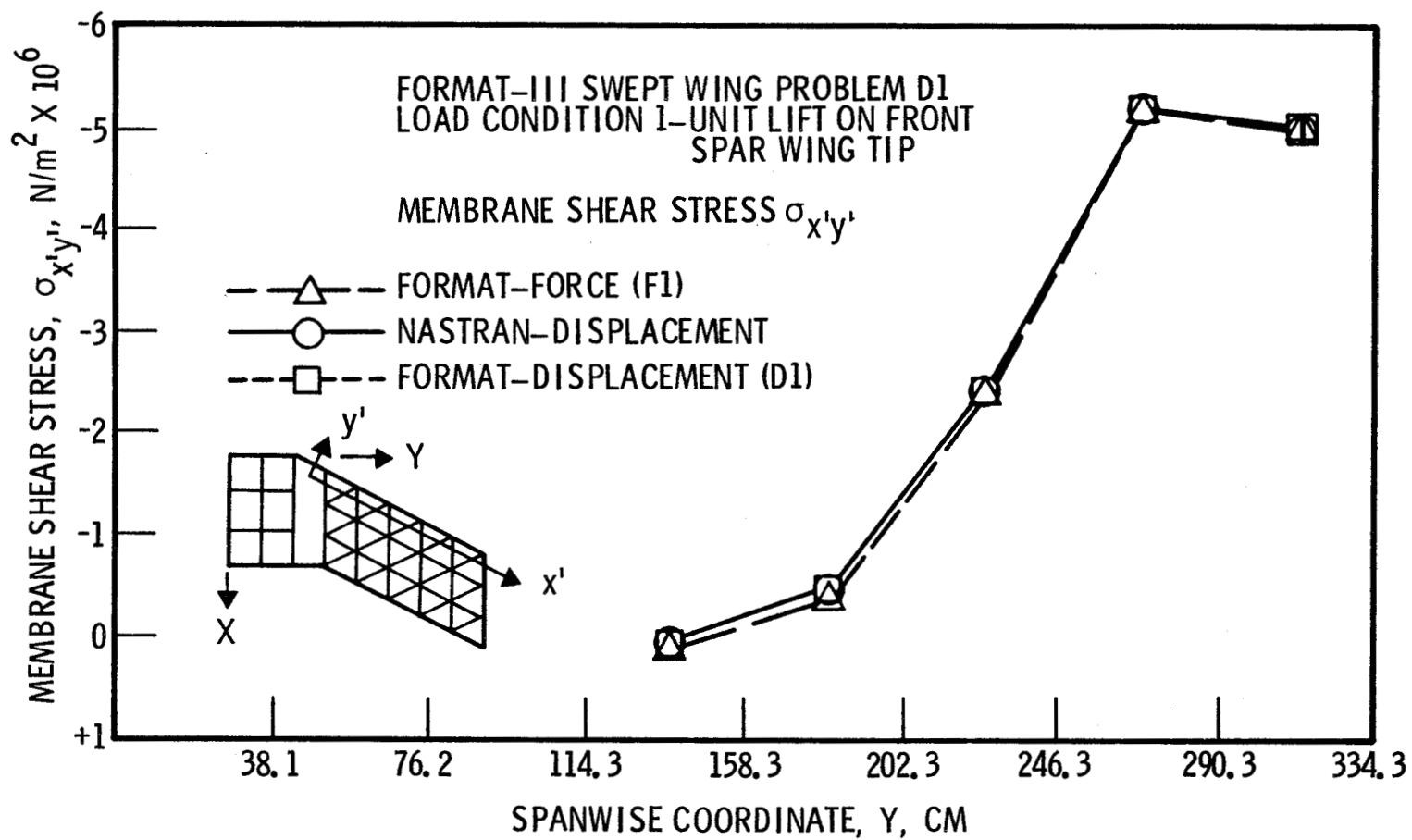


Figure 9.—Swept wing top surface shear stress

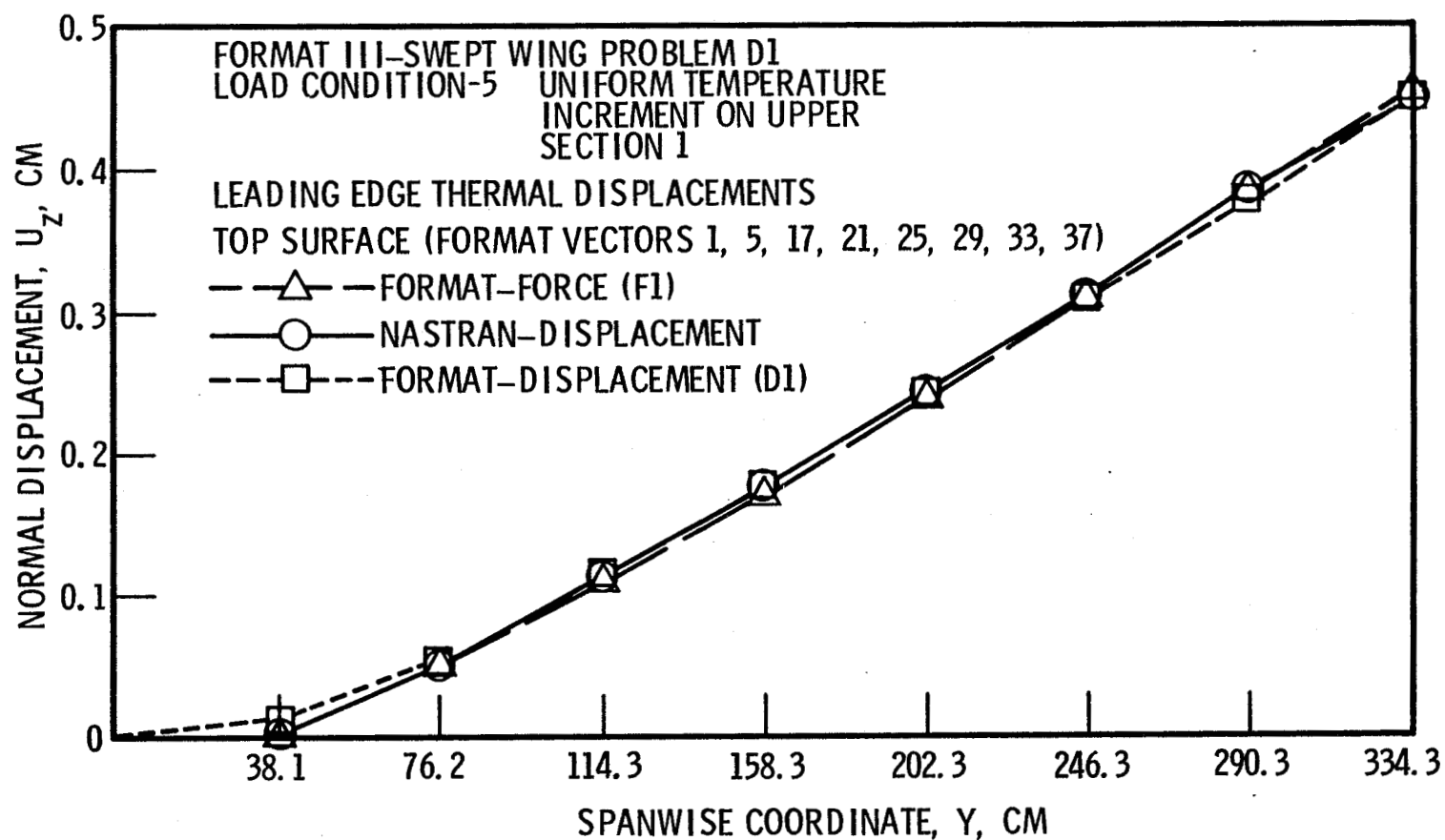


Figure 10.—Swept wing leading edge thermal displacements

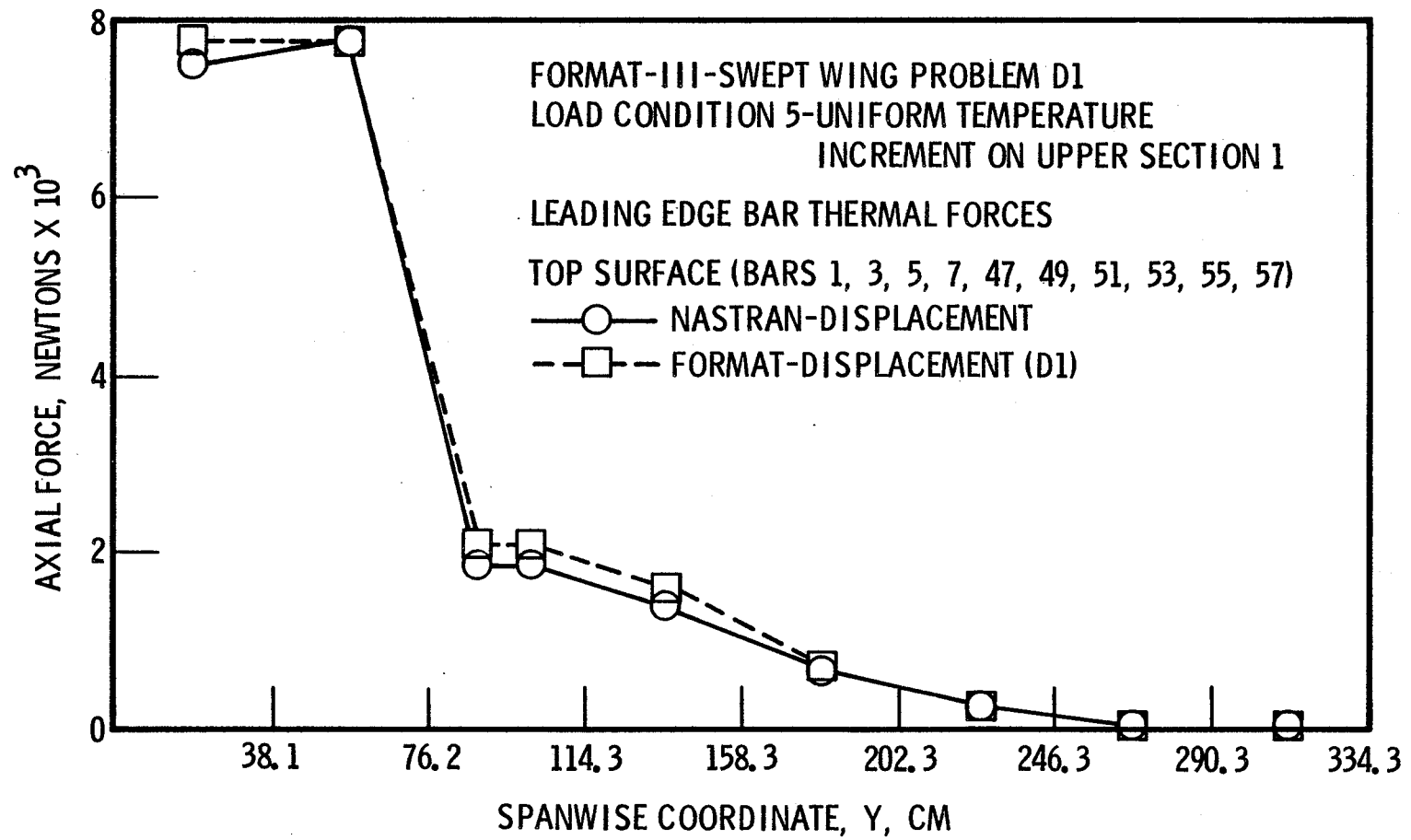


Figure 11.—Swept wing leading edge bar thermal forces

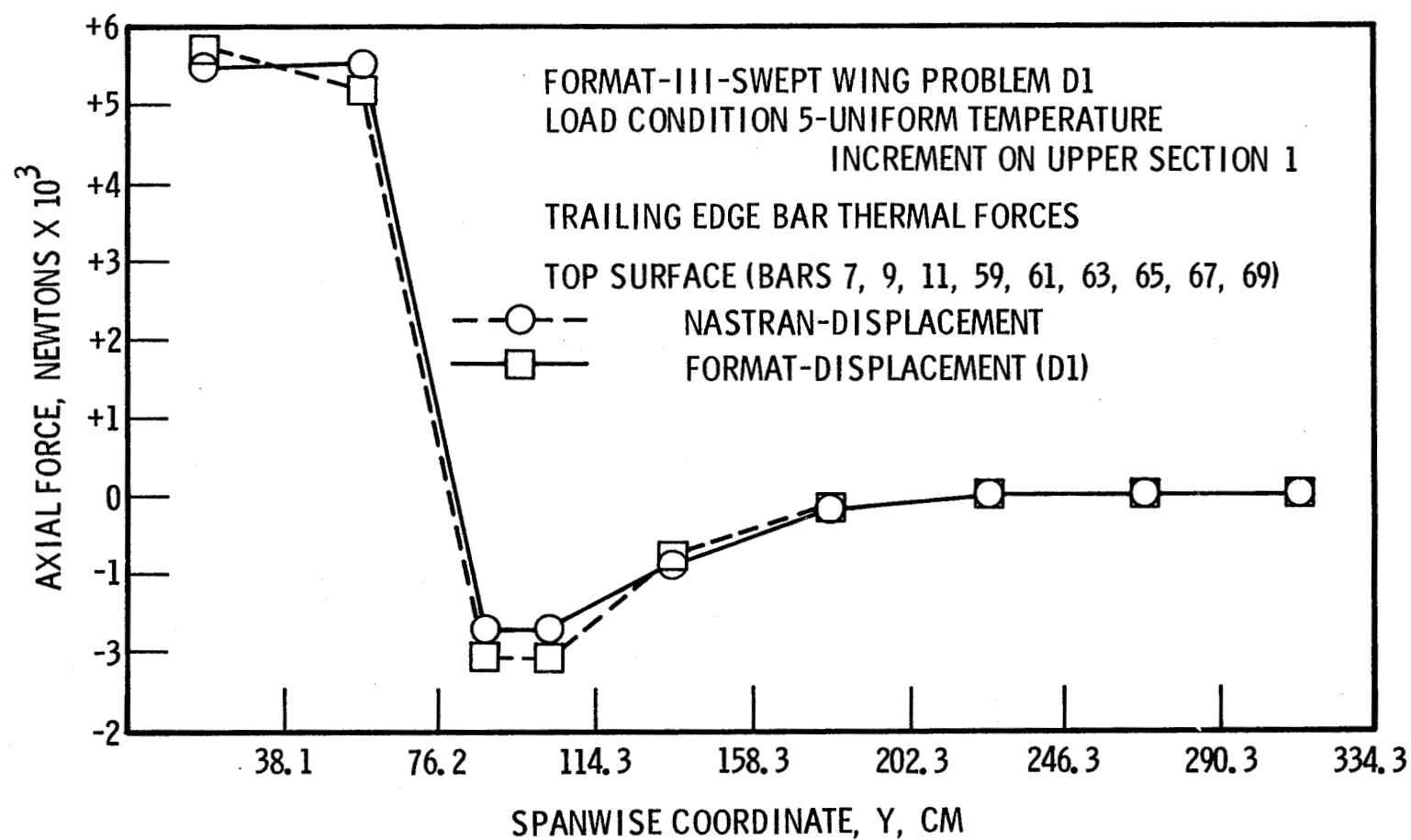


Figure 12.—Swept wing trailing edge bar thermal forces

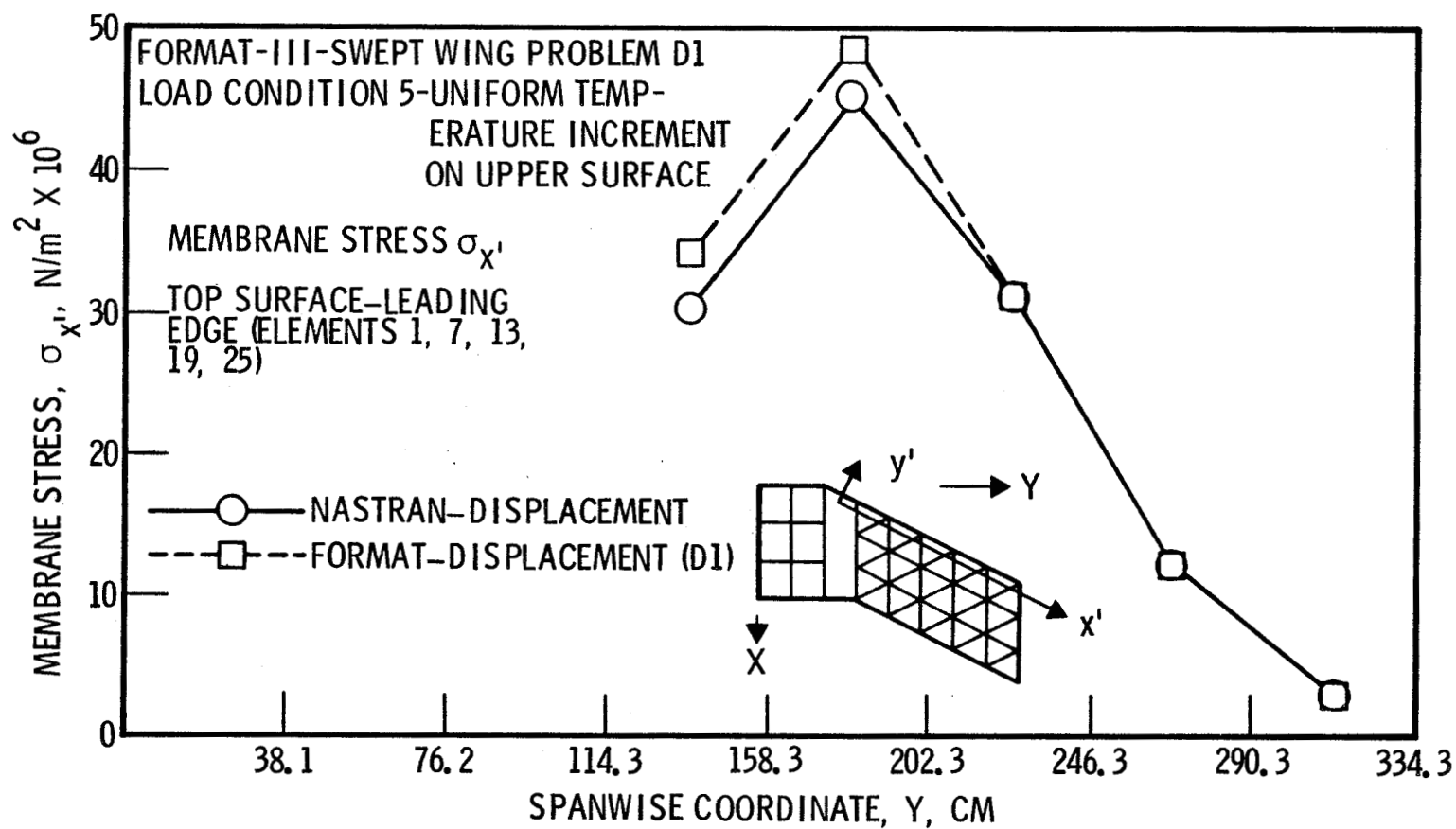
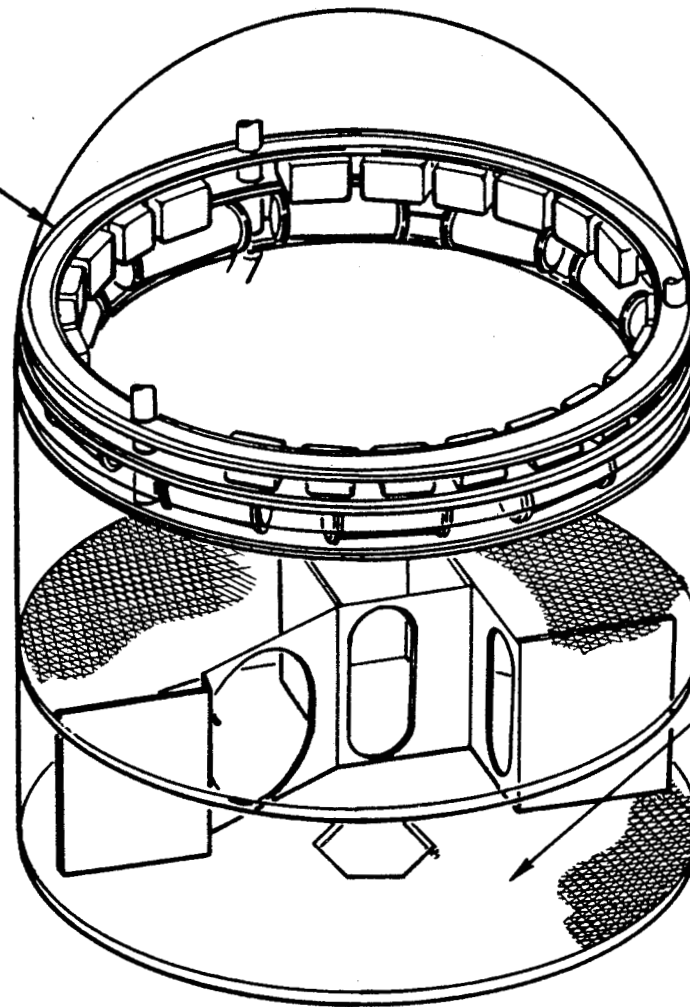


Figure 13.—Swept wing top surface membrane thermal stress

WATER CONTAINER
AND STOWAGE CABINET
SUPPORT STRUCTURE



CREW QUARTERS
STRUCTURE

Figure 14.—Orbital workshop habitation area structural arrangement

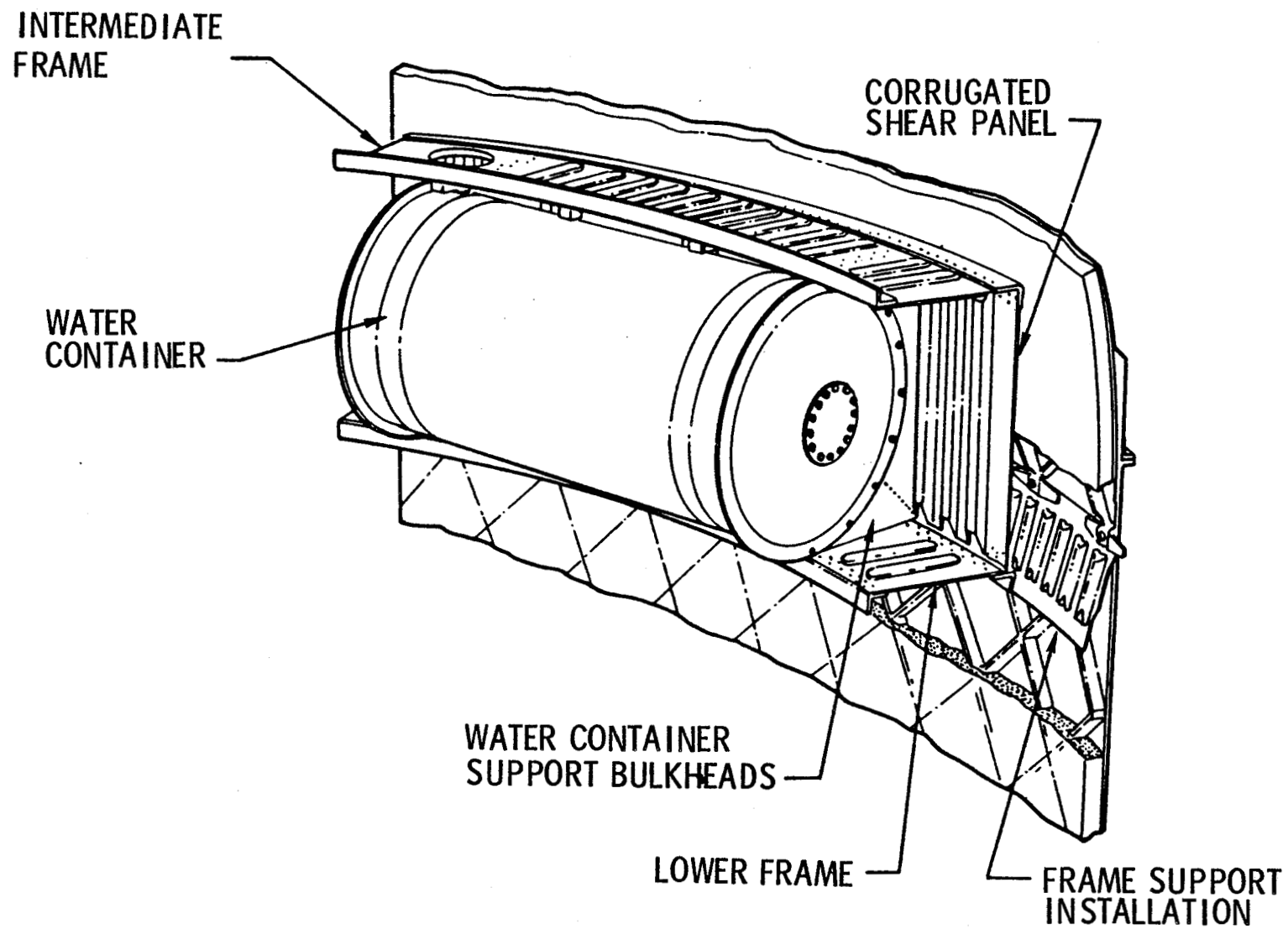


Figure 15.—Skylab water container segment

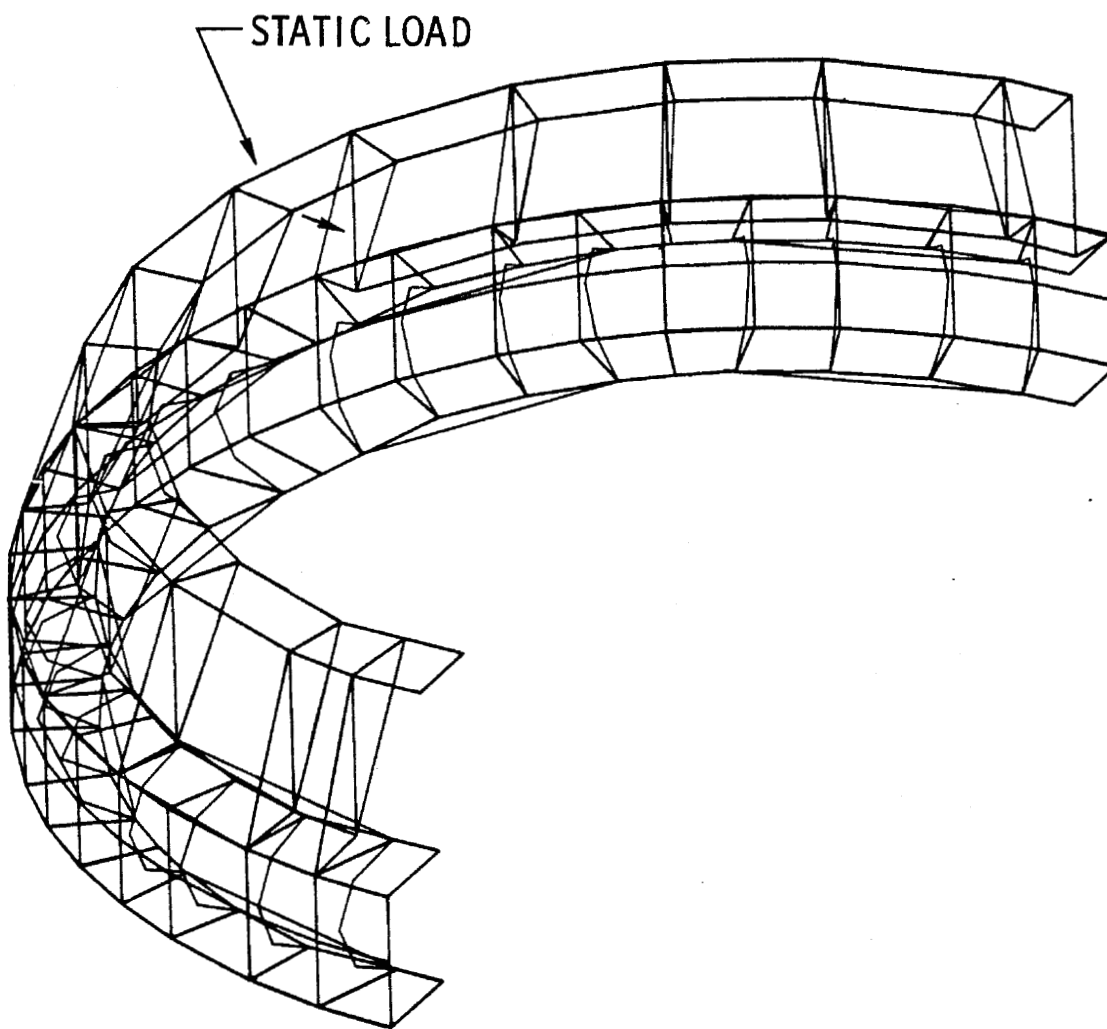


Figure 16.—NASTRAN model of Skylab water cabinet

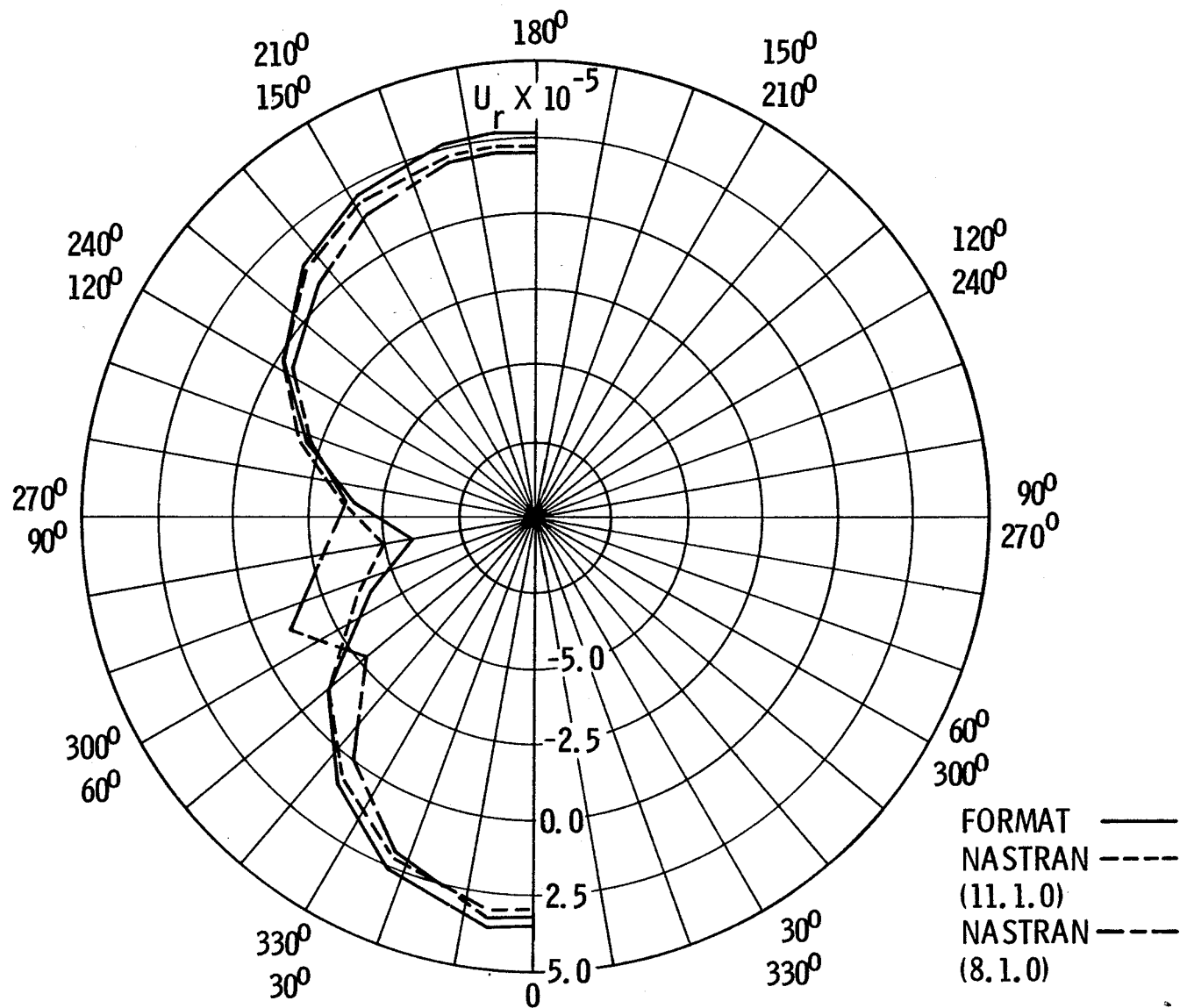


Figure 17.—Skylab problem radial displacement upper frame

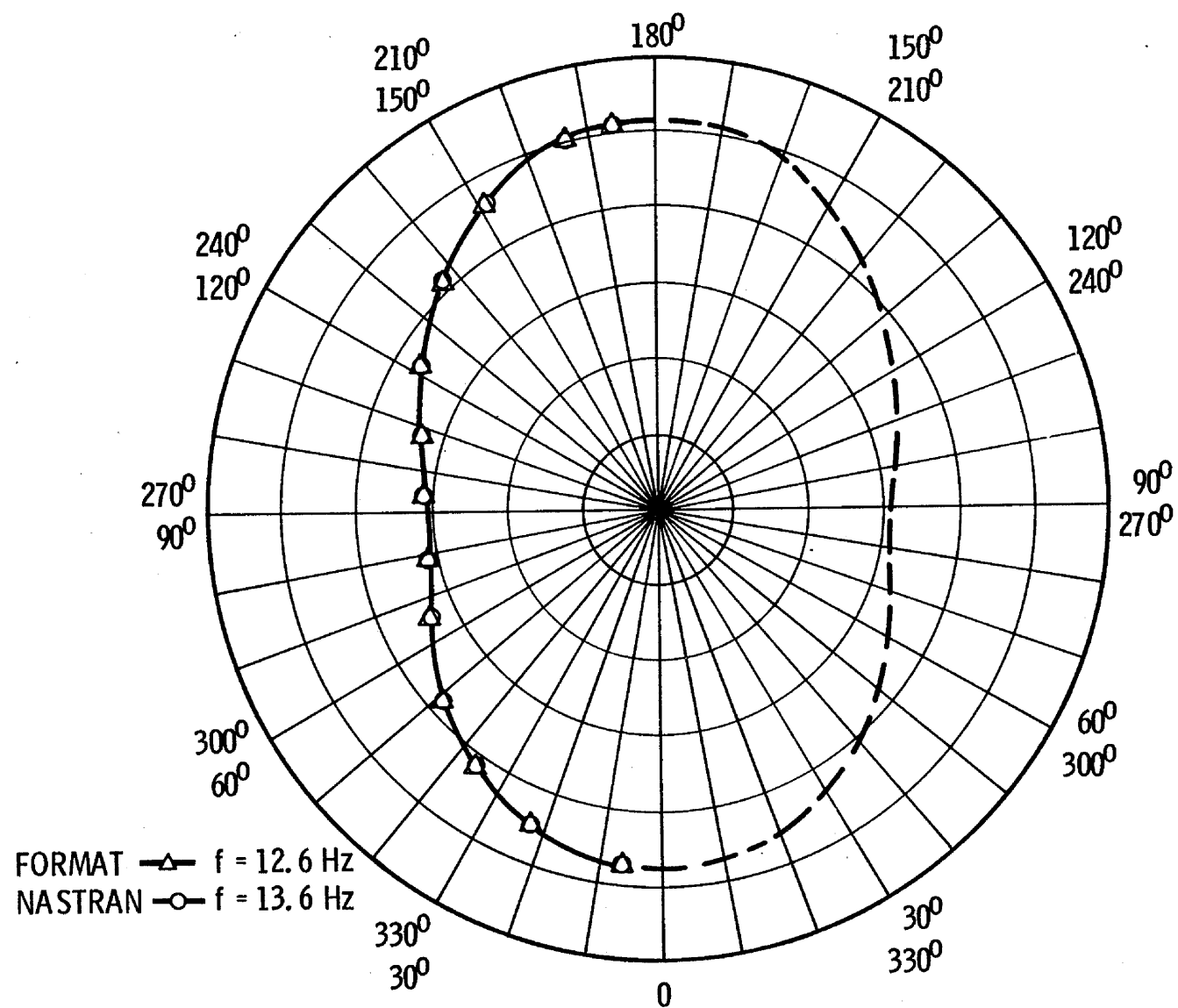


Figure 18.—First symmetric mode radial displacement upper frame

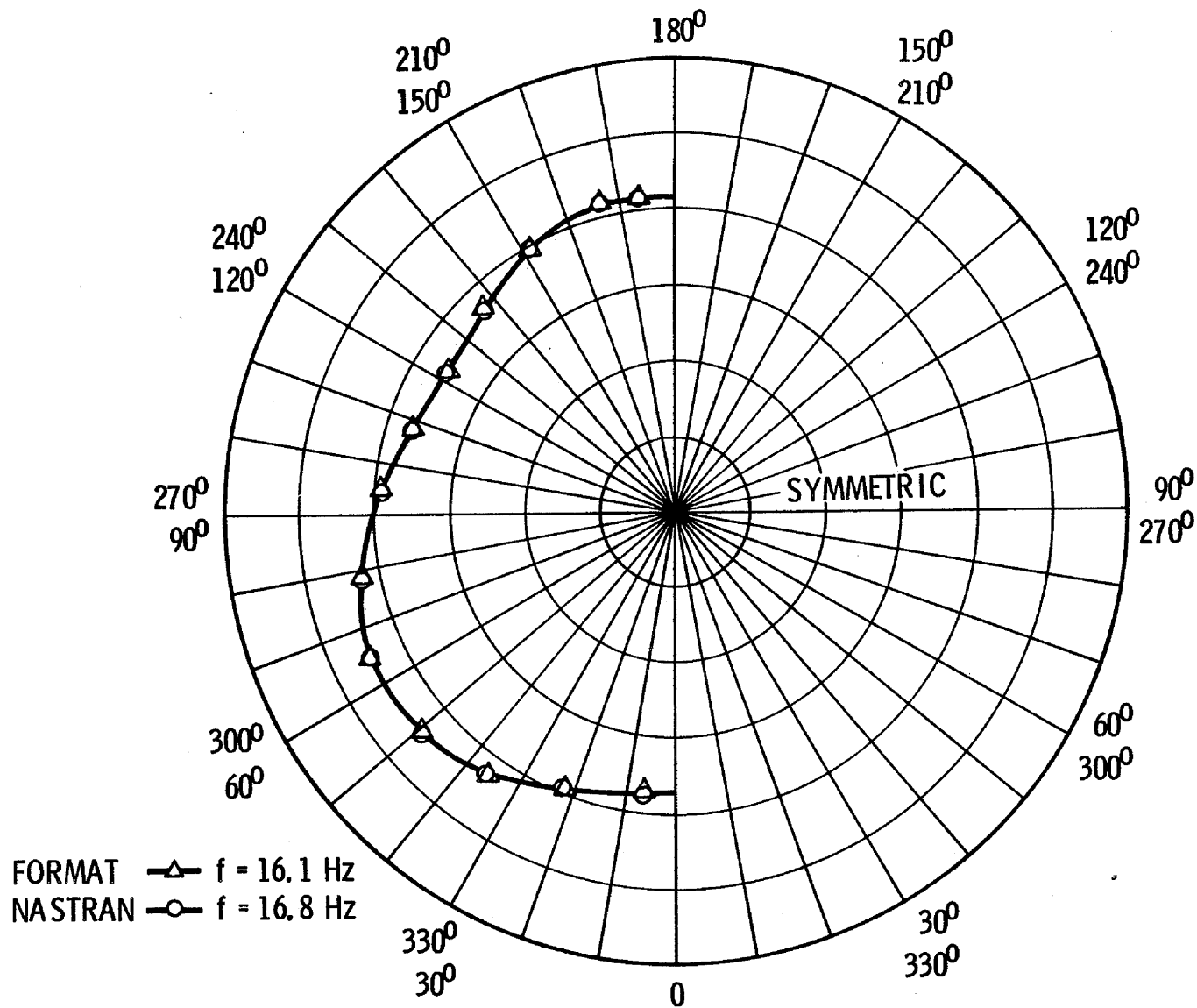


Figure 19.—Third symmetric mode radial displacement upper frame

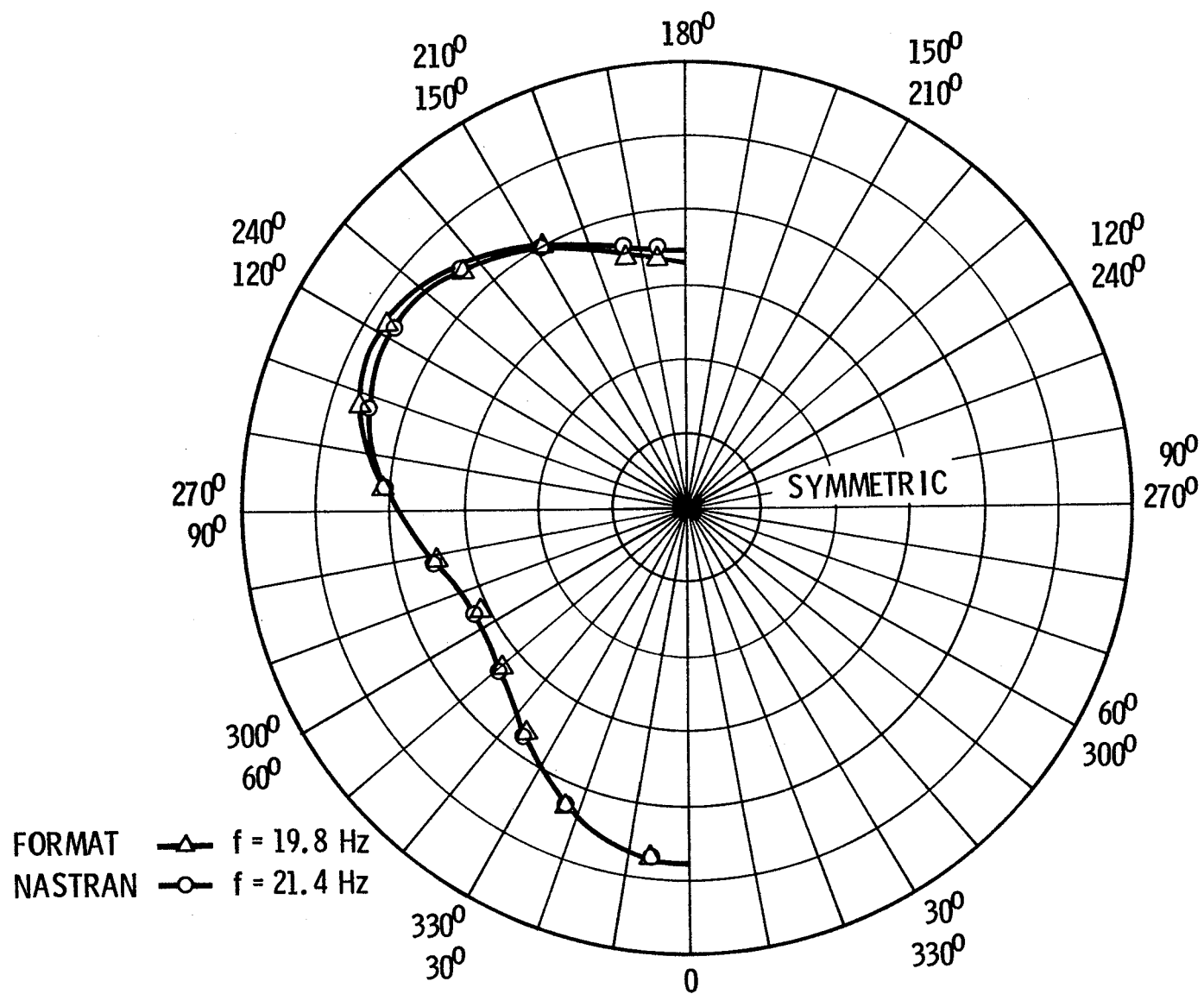


Figure 20.—Fifth symmetric mode radial displacement upper frame

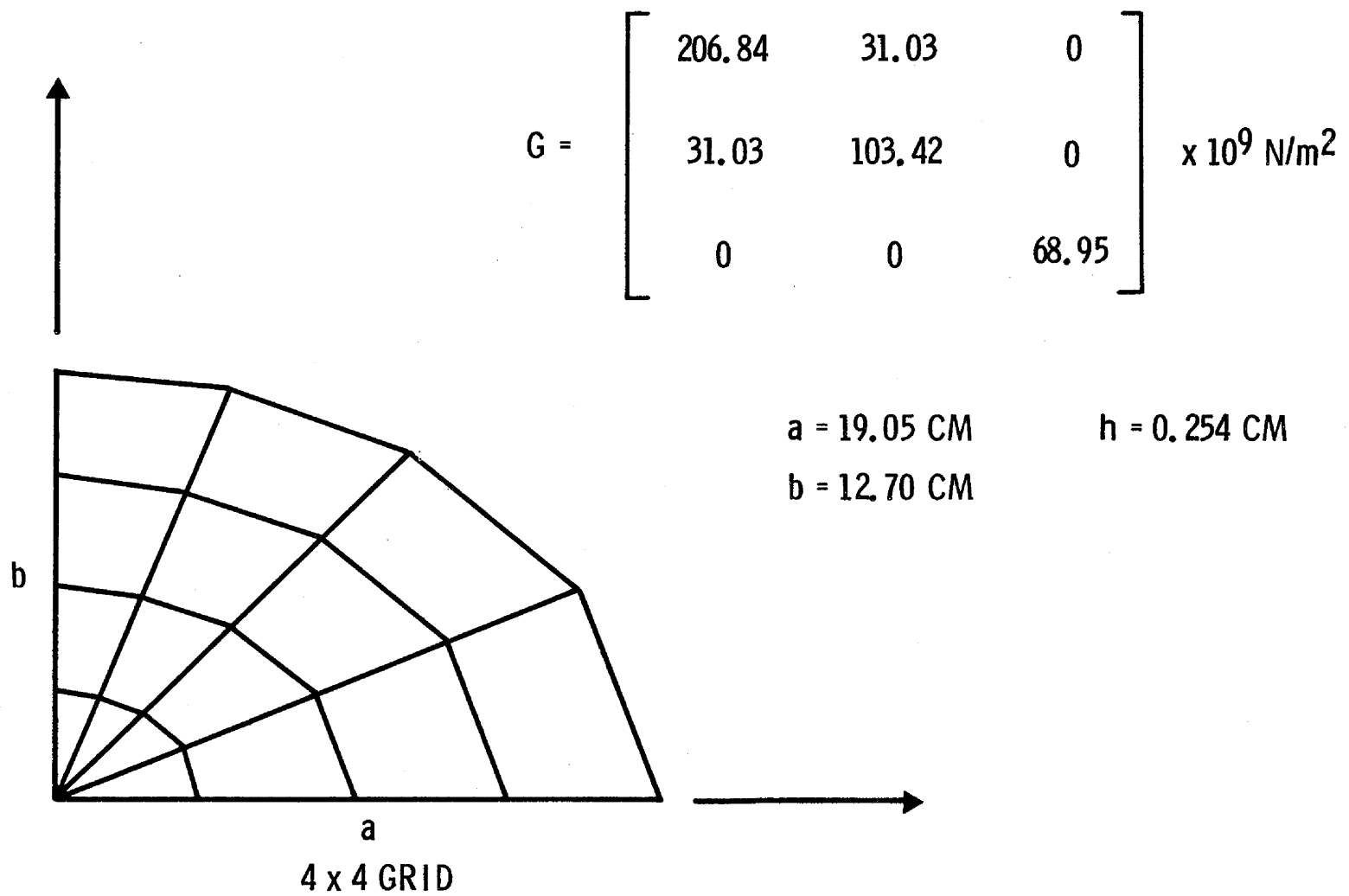


Figure 21.—Elliptic plate symmetry idealization

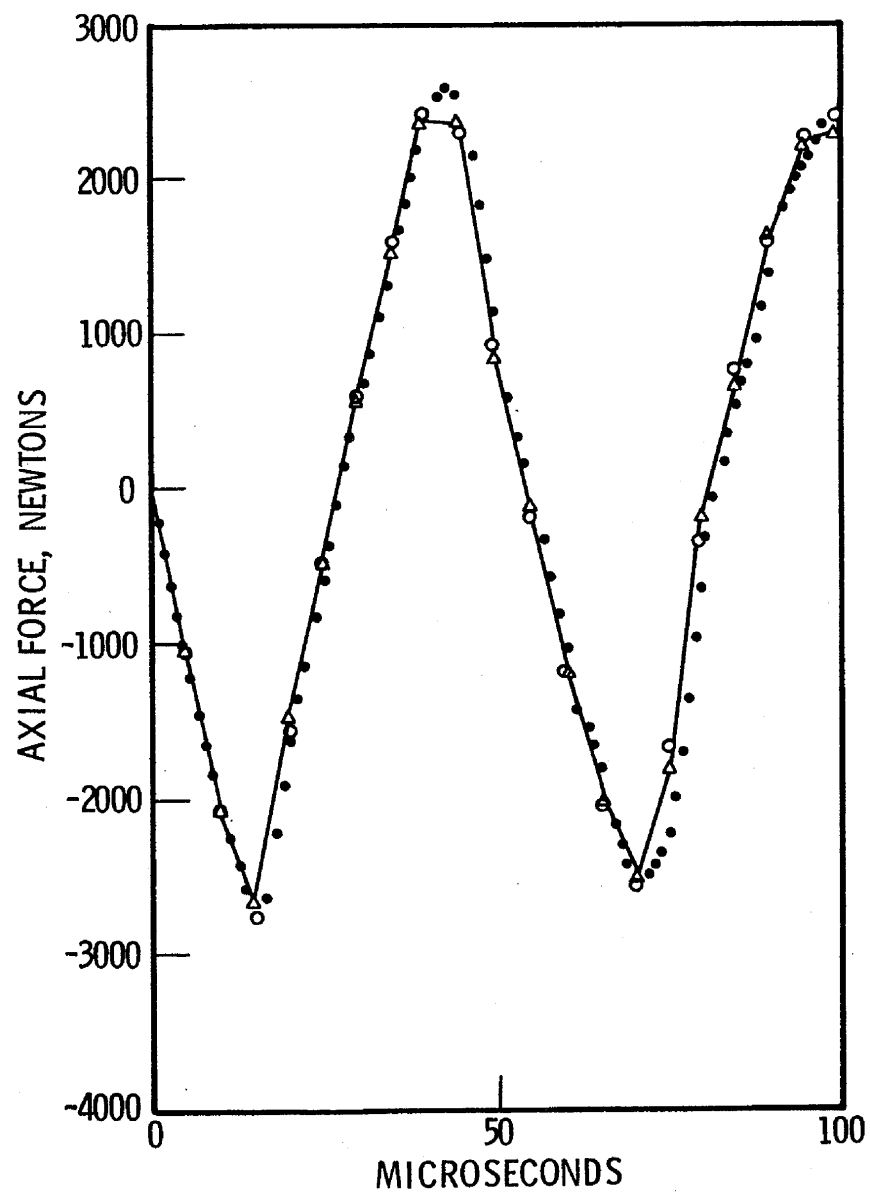
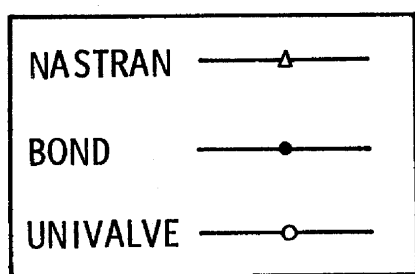


Figure 22.—Ring segment axial force comparisons

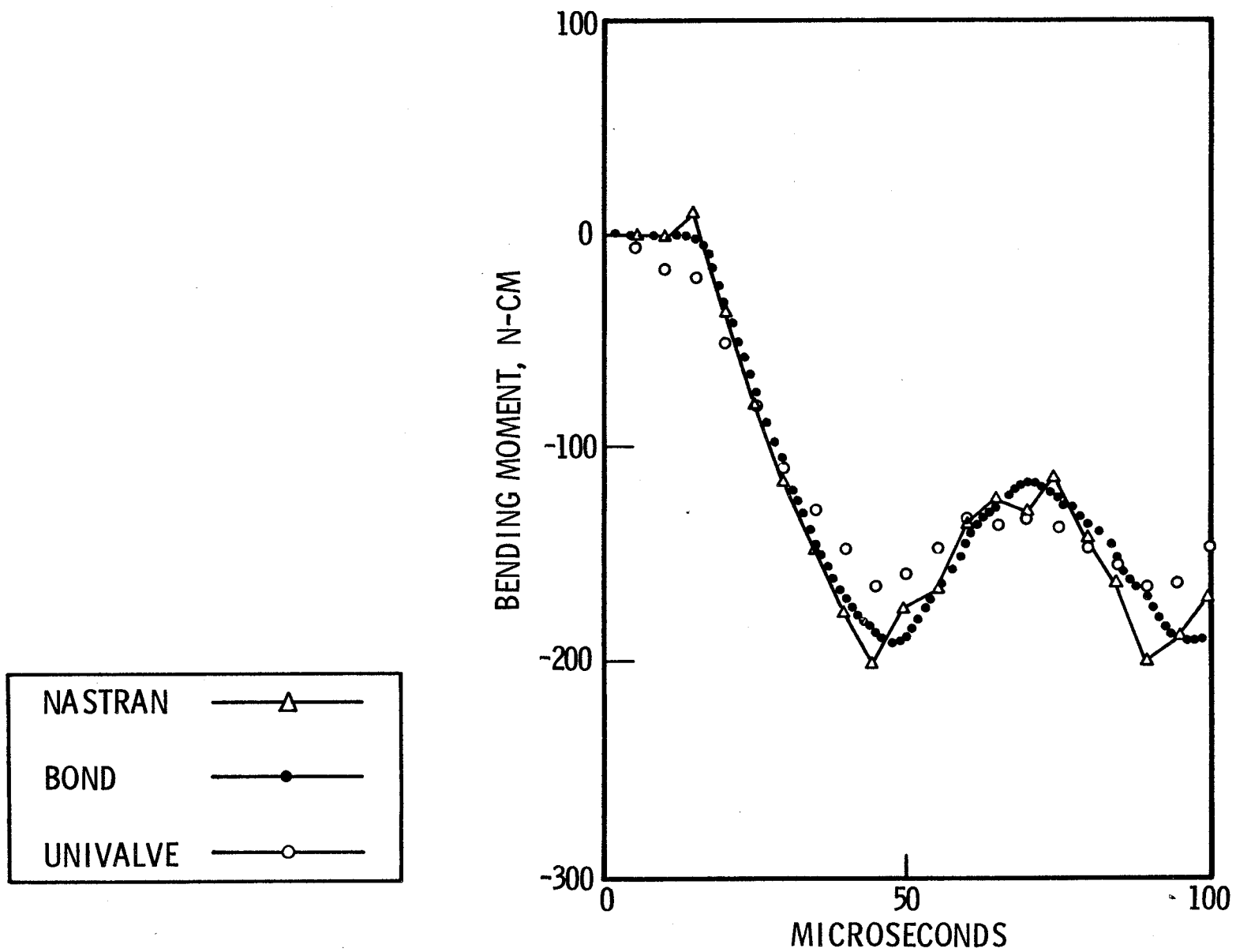


Figure 23.—Ring segment bending moment comparisons

SAVINGS IN NASTRAN DECOMPOSITION TIME BY SEQUENCING TO
REDUCE ACTIVE COLUMNS*

By R. Levy
Jet Propulsion Laboratory

S. Wall
Computer Sciences Corporation

SUMMARY

In large-capacity computer programs for structural analysis, computational efficiency is improved and core storage requirements are reduced by taking advantage of the typical sparseness in the stiffness matrix. In the past, the goal of reordering has been to minimize stiffness matrix bandwidth. An alternative reordering procedure has the goal of reducing matrix wavefront. When applied to the NASTRAN Program, this is equivalent to the reduction of the number of active columns for zero bandwidth. Comparisons are supplied that show the relative compactness that can be achieved for practical structural models with wavefront sequencing and with bandwidth sequencing. Examples show that wavefront sequencing can produce savings in the time required for subsequent decomposition of the stiffness matrix.

INTRODUCTION

Large-capacity computer programs for structural analysis operate most efficiently when the computational procedure is formulated to capitalize on the typical sparseness of the structural stiffness matrix. Sparseness is used to advantage by confining the computational operations to a compact region that is densely populated with nonzero coefficients and by omitting operations for the empty region in which the coefficients are zero. Consequently, it is often desirable to reorder a given stiffness matrix to make the region for computations as compact as possible and to make the empty region as large as possible. Traditionally, the compactness of the stiffness matrix has been measured by the matrix bandwidth, but an alternative equation-solving approach (ref. 1) performs the computations within the region delineated by the matrix wavefront. The wavefront approach is attractive because the maximum

* This paper presents the results of one phase of research carried out at the Jet Propulsion Laboratory, California Institute of Technology, under Contract No. NAS 7-100, sponsored by the National Aeronautics and Space Administration.

Preceding page blank

wavefront is often considerably less than the maximum bandwidth, and it can never be greater.

Efficiency and storage requirements of the NASTRAN stiffness matrix decomposition procedure depend upon both the bandwidth size and the number of active columns. Wavefront and active columns are related because the number of active columns is equal to the wavefront reduced by the number of columns within the bandwidth; when the bandwidth is zero, the wavefront equals the number of active columns. However, in NASTRAN the emphasis for efficiency is directed towards bandwidth processing rather than active column processing. Consequently, preprocessor programs have been used in the past to generate sequence cards that reduce the bandwidth of large-order stiffness matrices independently of possible reductions in active columns. Nevertheless, it will be shown subsequently that practical difficulties in obtaining NASTRAN solutions for structures that have been bandwidth-sequenced can sometimes be overcome by wavefront sequencing to reduce the number of active columns with no regard for bandwidth.

COMPARISONS OF BANDWIDTH AND WAVEFRONT SEQUENCING

Algorithms described in references 2, 3, and 4 have been designed to reorder nodes for bandwidth reduction. More recently, wavefront reduction approaches have been given in references 5 and 6. Resequencing procedures, either for bandwidth or wavefront reduction, do not ensure achievement of the optimal sequence. Results can be considered acceptable if there is an improvement from an initial sequencing in a local optimum sense rather than convergence to an absolute minimum in a global sense. For this reason, it is sometimes useful to perform resequencing several times, with each cycle starting from a different initial sequence. This provides the opportunity of selecting the most favorable of the several local minimums that will be developed from the various cycles.

In one test of wavefront resequencing for an analytical model with about 500 nodes, the initial sequencing had been developed by inspection and study of the connectivity. The maximum wavefront was 43. One resequencing computer cycle reduced the initial maximum wavefront to 30. In another test, the initial sequencing was scrambled at random, which produced a maximum wavefront of 92. One computer cycle reduced this to 40. Subsequently, as the result of the best of six additional computer cycles, the maximum wavefront was reduced to 27. In these, the starting node for each cycle was chosen at random.

Table 1 shows comparisons of resequencing tests to reduce either wavefront or bandwidth. These tests were performed for the analytical models of structural components used in ground-based radar antenna systems. The table shows that, after sequencing, the wavefront tends to be less than half the bandwidth, which can provide computational advantages in subsequent analysis.

DECOMPOSITION TIME COMPARISONS

We first used wavefront sequencing in NASTRAN when an eigenvalue solution was unable to proceed because of insufficient core. The problem contained 1300 unconstrained degrees of freedom and had been originally sequenced for bandwidth reduction. To process one column of the stiffness matrix for NASTRAN decomposition, the minimum core storage requirements considering only the predominant terms are given approximately by the following relations:

$$SS = C \cdot B + C^2/2$$

$$SU = 3 \cdot C \cdot B + C^2$$

where

SS is the storage for symmetrical decomposition (statics solution)

SU is the storage for unsymmetrical decomposition (eigenvalue solution)

B is the bandwidth

C is the number of active columns

The initial approach to find a remedy was to experiment with changes in the NASTRAN algorithm that attempts to allocate a favorable combination of B and C to be used for the decomposition. From this, the best result would have allowed a solution to proceed with B = 135 and C = 35, with 60 min as the estimated decomposition time.

However, before attempting the solution, we noticed the strong dependence of the formula for unsymmetrical decomposition upon the product of active columns and bandwidth. Therefore, an alternative remedy to reduce storage was to reduce this product term by forcing the bandwidth to be small while increasing the number of active columns. The objective was to produce a net decrease in the SU storage and to permit more efficient processing by allowing more of the matrix to remain in core, eliminating some of the expensive out-of-core spilling. Consequently, the problem was resequenced for wavefront reduction, leading to a successful execution with a bandwidth of 3 and 102 active columns. The actual decomposition time was less than 11 min.

Table 2 contains a summary of a few cases where the NASTRAN decomposition times have been determined for alternative types of sequencing. The statics problems show about 20% savings for wavefront sequencing; the eigenvalue problem saving is considerably greater.

CONCLUSION

Examples show savings in the NASTRAN decomposition times when use is made of wavefront sequencing, which reduces the number of active columns, rather than sequencing which reduces the bandwidth. It appears that the relative inefficiency in processing active columns by NASTRAN compared with processing bandwidth columns is more than offset by the relatively smaller numbers of active columns that can be achieved by sequencing.

REFERENCES

1. Melosh, R. J., and Bamford, R. M.: Efficient Solution of Load-Deflection Equations. *Journal of the Structural Division, ASCE*, vol. 95, no. ST4, Apr. 1969, pp. 661-676.
2. Rosen, R.: Matrix Bandwidth Minimization. *Proceedings of the 23rd National Conference of the ACM, Brandon/Systems Press, Inc.*, New Jersey, 1968, p. 585.
3. Akyuz, F. A., and Utku, S.: An Automatic Node-Relabeling Scheme for Bandwidth Minimization of Stiffness Matrices. *AIAA Journal*, vol. 6, no. 4, Apr. 1968, pp. 728-730.
4. Cuthill, E., and McKee, S.: Reducing the Bandwidth of Sparse Symmetric Matrices. *Applied Mathematics Laboratory Technical Note AML-40-69, Naval Ship Research and Development Center, Washington, D. C.*, June 1969.
5. King, I. R.: An Automatic Reordering Scheme for Simultaneous Equations Derived from Network Systems. *International Journal for Numerical Methods in Engineering*, vol. 2, 1970, pp. 523-533.
6. Levy, R.: Resequencing of the Structural Stiffness Matrix to Improve Computational Efficiency. *JPL Quarterly Technical Review*, vol. 1, no. 2, July 1971.

Table 1. - Nodal resequencing comparison

Component type	Total nodes	Initial nodes		Nodes after ^a resequencing	
		Bandwidth	Wavefront	Bandwidth ^a	Wavefront ^b
Antenna pedestal	56	40	20	23	11
Quadripod	66	41	18	16	8
Various reflector structures					
Coarse grid	83	73	30	24	12
Azimuth-elevation type	466	200	52	75	29
Polar type	506	---	92	--	28
^a Bandwidth sequencing by method of reference 2. ^b Wavefront sequencing by method of reference 6.					

Table 2. - NASTRAN stiffness matrix decomposition time

Component type	Problem type	Decomposition time for sequencing method, s	
		Bandwidth	Wavefront
Coarse grid reflector	Statics	10.4	7.5
Azimuth-elevation reflector	Statics	260.1	215.2
	Eigenvalue	3604.5	635.4

NEW ELEMENT DEFINITION CAPABILITY FOR NASTRAN

By Myles M. Hurwitz and Michael E. Golden

Naval Ship Research and Development Center

ABSTRACT

A major concern of NASTRAN users is the lack of sophisticated elements in the NASTRAN element library. Adding a structural element to NASTRAN requires detailed familiarity with various parts of the program. This paper describes a NASTRAN preprocessor, a new element definition capability, which an analyst may use to generate the NASTRAN tables and routines required for a new element. This preprocessor is written in the string-manipulation language SNOBOL.

INTRODUCTION

Although NASTRAN's system design is quite good, its present library of finite elements leaves something to be desired. The NASTRAN System Management Office here at Langley has taken steps to greatly improve the library of elements, but it would be very advantageous for an analyst to use his own special or experimental element in NASTRAN. However, implementing his element into NASTRAN is a task the analyst may not wish to undertake, since it requires detailed familiarity with NASTRAN internal structure, such as its variables, tables, routines, structure, and restrictions.

Therefore, we have written a NASTRAN preprocessor, a new element definition capability, with which an analyst may implement his own element into NASTRAN relatively easily. This preprocessor will take the user's input, given in symbolic form, and will generate the FORTRAN subroutines and BLOCK DATA subprograms which NASTRAN requires to use the new element. The preprocessor is written in the SNOBOL language and is, therefore, a SNOBOL program which generates FORTRAN routines. After the analyst inserts these generated routines into NASTRAN, the new element is ready for use.

Preceding page blank

DESCRIPTION OF THE PREPROCESSOR

Presently, the preprocessor is set up so that a new element may use the entire NASTRAN capability except the Differential Stiffness and Piecewise Linear Analysis Rigid Formats.

The input to the preprocessor is divided into sections which we call packets. The presently available data packets are

- Preliminary Data Packet
- Global Variable Packet
- Stiffness Matrix Packet
- Mass Matrix Packet
- Viscous Damping Matrix Packet
- Thermal Loading Vector Packet
- Stress Matrix Packet
- Stress and Force Calculation Packet
- Output Packet

Each packet except the Preliminary Data, Global Variable, and Output packets will cause the preprocessor to generate a FORTRAN subroutine which will calculate the appropriate quantity for the new element. For example, the user will specify in the Stiffness Matrix Packet, through matrix and scalar expressions, the method by which the stiffness matrix for his element should be calculated. The preprocessor will then generate the subroutine, conforming to NASTRAN's rules and restrictions, to perform these calculations. Naturally, if a particular quantity is not needed for the new element (a viscous damping matrix or thermal loading vector, for example), the packet corresponding to that quantity need not be specified.

The Global Variable Packet contains definitions of variables which may be used in several subsequent packets. The Preliminary Data and Output packets will cause the preprocessor to generate BLOCK DATA subprograms which contain updates to present NASTRAN tables.

Two examples will provide some idea of the capabilities of the preprocessor. If we wish to define the vector V_{12} as follows:

$$V_{12} = \begin{pmatrix} x_2 - x_1 \\ y_2 - y_1 \\ z_2 - z_1 \end{pmatrix}$$

then the preprocessor statement

V12, 3, 1, TERM

indicates that V_{12} is a 3x1 matrix and is to be defined term-by-term.

The statements

V12
1,1,X2-X1
2,1,Y2-Y1
3,1,Z2-Z1

provide the actual definition for V12. (Of course, X1,Y1,Z1,X2,Y2, and Z2 had to be defined previously. These variables could have been defined by the user, or they could be some of the many variables predefined by either the preprocessor or NASTRAN.)

As a second example, we might wish to define the matrix C by

$$C = A^T B$$

where A^T is the transpose of a previously defined matrix A, and B is a previously defined matrix.

If A is a 2x3 matrix and if B is also a 2x3 matrix, then the following two sets of statements will define C.

C, 3, 3, EQUA

and

C
TR(A)*B

Notice, then, that matrix as well as scalar operations are recognized by the preprocessor.

SAMPLE PROBLEM

As a sample problem we prepared the input required by the preprocessor to produce routines corresponding to the triangular membrane element presently in NASTRAN. All packets listed previously, except the Viscous Damping Matrix Packet, were used. All the FORTRAN subroutines and BLOCK DATA subprograms were generated in 11 minutes (CPU) on the CDC 6400 central processing unit of the CDC 6700 computer. Preliminary results indicate that the computer-generated routines are nearly as fast

as the handwritten routines. We expect more extensive comparisons, as well as more efficient routines, to be available later.

CONCLUDING REMARKS

We feel that the new element definition capability described in this paper is a good vehicle for augmenting NASTRAN's element library relatively easily. With it, the analyst need not involve himself with NASTRAN's internal structure, and yet he will have the NASTRAN system capability available for his own element. Work is continuing to produce a more efficient program, to produce more efficient generated routines, and to increase the preprocessor's capability.

VIBRATION STUDIES OF A FLAT PLATE AND A BUILT-UP WING

By James H. Starnes, Jr.
NASA Langley Research Center

SUMMARY

The natural vibration frequencies of a clamped flat plate and a built-up wing were computed by two different finite element computer programs and compared with existing experimental data. The results of this study indicate that by using a finite element program it is possible to obtain the accuracy desired for parametric design studies even for complex built-up structures. However, the differences in central processing unit execution times between the two programs revealed that it is economically feasible to develop automated design procedures or make parametric design studies involving many iterations only if computer programs tailored for very efficient operation are available.

INTRODUCTION

In the flutter analysis of aircraft wings, it is standard practice to use the natural vibration modes and frequencies as input data to aeroelasticity programs which determine a wing's flutter characteristics. As a result of the recent development of large finite element structural analysis computer programs, realistic complex wing structures can now be readily analyzed to obtain such data. However, in the development of automated design procedures involving many geometric and structural iterations during preliminary design, it is necessary that the finite element program used to provide the natural modes and frequencies not use excessive computer time and hence make the whole concept of automated design prohibitively expensive. To determine the feasibility of using existing programs as the analysis tools in automated design studies, finite element models of two representative structures were formulated and the first few natural frequencies of these structures were determined by the use of the NASA Structural Analysis (NASTRAN) finite element program summarized in reference 1. As the number of dynamic degrees of freedom and the complexity of the structure increased it was found that the central processing unit (CPU) execution times became prohibitively large for making parametric studies. Therefore, it was decided to determine if there was an available finite element program that could compute the natural frequencies of the structures in significantly shorter CPU times and, consequently, make parametric design studies economically feasible.

One logical candidate program was the dynamics version of the Structural Network Analysis (SNAP) finite element program (ref. 2), which was specifically tailored for very efficient operation. This version of SNAP has recently become available, and uses different programming techniques and solution strategies than NASTRAN.

The purpose of this paper is to compare natural frequencies and CPU times for SNAP and NASTRAN for a clamped flat plate and a free-free built-up wing. Since SNAP is not operational at the Langley Research Center at present, W. D. Whetstone of the Lockheed Missiles and Space Company, Huntsville, Alabama, provided the SNAP solutions by the use of Lockheed Huntsville's Univac 1108 Exec 8 computer system. The NASTRAN solutions were obtained from the Langley Research Center CDC 6600 computer system. The calculated results from the two computer programs were also compared with experimental results for the two types of structures.

DESCRIPTION OF THE MODELS

The models selected for this study represented two characteristic wing type structures. A simple two-dimensional topology and a straightforward dynamics problem are represented by a clamped flat plate. As an example of such a model, the 8.64 mm thick 45° delta magnesium plate with a 15.24 cm root chord studied experimentally in reference 3 was described by two grid point networks which were numbered to give the minimum bandwidth for the matrices associated with the finite element problem. The first network had 10 spanwise and 10 chordwise elements (10 by 10), and the second had 30 spanwise and 30 chordwise elements (30 by 30) as shown in figure 1. The structural elements were modeled with the combination bending and membrane plate elements of NASTRAN (CQUAD2 and CTRIA2) and the corresponding elements of SNAP. Although the structural model is simple enough conceptually, the dynamics problem becomes more demanding as the number of grid points increases. For the 10 by 10 network the model has 66 grid points and 165 dynamic degrees of freedom, while for the 30 by 30 network there are 496 grid points and 1395 dynamic degrees of freedom.

The second model selected for analysis was the free-free built-up wing studied experimentally in reference 4. This model represents a more complex topology than the flat plate, is representative of a realistic aircraft wing structure, and has the additional dynamic phenomenon of rigid body modes. The wing was manufactured to close tolerances and each component was carefully weighed and measured. It is felt that an accurate enough definition of this wing's geometry and mass distribution existed to establish this model as an acceptable standard for comparison with analytical results. A photograph of the final fabricated wing is shown in figure 2, and the details of the wing construction are shown in figure 3. This wing consists of ribs, spars, caps, cover panels, and external spanwise stringers. All components of the wing were made from 2024 aluminum alloy. The grid point network used to model the right half of the wing was selected so that the four node cover panel elements would be square, as shown in figure 4. The grid point network was numbered to provide minimum bandwidth matrices for the finite element problem. The finite element model used for the NASTRAN analysis consisted of membrane elements for the cover panels (CQDMEM and CTRMEM); shear panel elements for the ribs and spars (CSHEAR); and rod elements (CROD) for rib and spar caps, the external spanwise stringers, and the intersections of the ribs and spars. The corresponding elements were used for the SNAP model, however, it should be noted that there are some differences in the formulation of the membrane and shear finite

elements used in the two programs. The nonstructural masses (rivet heads) were applied to the rod elements. For the convenience of input preparation, two external spanwise stringers were lumped at each of the two spanwise grid lines between the spars. Also, the two ribs located 35.6 cm and 40.6 cm from the root chord (fig. 3) were lumped at 40.6 cm from the root chord. While the model did vary slightly from the actual wing geometry, the masses of the actual wing and the model were virtually the same (92.66 kg vs 92.92 kg). In an attempt to reduce the CPU execution times for the NASTRAN solution, the top and bottom grid points were tied together by multipoint constraints (MPC's) so that the depth distribution remained constant for the resulting wing. The NASTRAN model has 234 grid points, but because of the MPC's and constraints on the in-plane degrees of freedom introduced with OMIT cards it only had 117 dynamic degrees of freedom. The SNAP model was not constrained to have a depth distribution which remained constant and did have in-plane degrees of freedom. Therefore, the SNAP model had 650 dynamic degrees of freedom for its 234 grid points. Advantage was not taken of midplane symmetry in the SNAP model; if it had been, only 325 dynamic degrees of freedom would have been required.

DISCUSSION OF THE COMPUTER PROGRAMS

The finite element programs used in this study are based on different solution strategies and programming techniques. NASTRAN (refs. 5 and 6) is based on matrix solution techniques which are dependent upon matrix bandwidth and active matrix columns. It performs its matrix operations such as assembling initial matrices, applying multiple and single point constraints, and matrix decomposition in a sequential fashion, while storing data on peripheral equipment between each step. The desired natural frequencies for this study were determined by using NASTRAN's Inverse Power Method with Shifts option. The NASTRAN solutions were obtained by the use of the Langley Research Center CDC 6600 computer system using NASTRAN Level 11.1.2, a version of NASTRAN which has some CDC 6600 single precision operations.

SNAP is based on sparse matrix solution techniques and uses programming techniques which minimize secondary data storage requirements (refs. 7 and 8). The desired natural frequencies were determined by a matrix iteration technique which sweeps out the lower modes. The SNAP solutions were obtained from the Univac 1108 Exec 8 computer system at the Lockheed Missiles and Space Company, Huntsville, Alabama, by the use of the SNAP Dynamic Analysis Version V70E (ref. 2) which allows Univac 1108 double precision operations.

DISCUSSION OF RESULTS

The results of the analyses and experiments for the clamped 45° flat plate are presented in Table I which gives the natural frequencies, degrees of freedom, and the CPU times for the computer solutions. Based on these results it is possible to compare the first three natural vibration frequencies of the plate and the amount of CPU execution time required by each computer

program. The maximum difference (approximately 1.1 percent) between the corresponding computed results from the two computer programs occurs for the third frequency of the 10 by 10 grid point network model. The difference between the computed results of the 10 by 10 and 30 by 30 networks is a result of the finer structural modeling for the 30 by 30 network. To test for solution convergence, a 20 by 20 grid point network was analyzed by NASTRAN and the results were within approximately 0.5 percent of the 30 by 30 network solutions. Therefore, the 30 by 30 network results are considered to be the converged analytical solution. The discrepancy between the analytical and experimental results is attributed to the difficulty in providing a true clamped boundary condition for the experiment.

The results of the analyses and experiment of the built-up wing are presented in Table II which gives the natural frequencies, degrees of freedom, and the CPU times for the computer solutions. Again it is possible to compare the analytical and experimental results and the CPU execution times for the two analytical results. The results presented are the first four anti-symmetrical frequencies of the wing which are actually the second, fourth, sixth, and eighth natural frequencies. The differences in the analytical results from SNAP and NASTRAN for the two lower frequencies are attributed to the previously mentioned differences in the formulation of the membrane and shear finite elements of the two programs and in the number of in-plane degrees of freedom. The two lower analytical frequencies compare very well with the experimental results, while the two higher frequencies begin showing noticeable differences of the order of up to 7 percent. These differences are attributed to the approximations made in modeling the structure for the finite element solutions.

For both analytical models there was a one-to-one correlation between the structural components used in the modeling of the structures for the two finite element programs. The automatic grid point and element generating features of SNAP were not used. The most significant difference between the solutions provided by the two computer programs was the CPU execution times required to obtain the corresponding solutions. Even though the programs were run on different machines at different facilities, as was pointed out previously, the factor of 15 between the CPU execution times of the two programs for the 30 by 30 grid point network flat plate model cannot be attributed primarily to machine or system differences. Rather, the factor of 15 decrease in CPU execution time must be attributed to the differences in programming techniques and solution strategies of the two programs. It is also worth noting that the ratios of the CPU execution times for the two programs are not constant with problem size. As the number of degrees of freedom increases, the ratio of NASTRAN CPU time to SNAP CPU time increases (compare the ratio of 4 for the 10 by 10 network and the ratio of 15 for the 30 by 30 network of the clamped flat plate). It is noted that SNAP has been used in a number of applications (ref. 9) to compute the modes and frequencies of models which had 4000 to 8000 dynamic degrees of freedom and were substantially more topologically complex than the 30 by 30 flat plate model. Typical CPU times to get 5 to 10 modes for these large order models were on the order of 60 minutes. Although the CPU time for SNAP is less than the CPU time for NASTRAN for the built-up wing calculation, the difference would be even greater if the two models had had the same number of degrees of freedom.

Another difference in the two program solutions, which becomes very important when the size of the structural model becomes large, is the core and auxiliary storage unit requirements. For the largest problem considered in this study (the 30 by 30 flat plate) SNAP required approximately 0.75 million words of storage to solve the problem, while NASTRAN required approximately 3.25 million words to solve the same problem.

The results of this study suggest that parametric design studies involving the calculation of natural modes and frequencies of large complex structures are economically feasible only if use is made of large scale finite element computer programs specifically tailored for operating efficiency. In addition, the results indicate that use of sparse matrix solution techniques, such as employed in SNAP, can provide order of magnitude decreases in CPU time compared to programs, such as NASTRAN, which use more conventional matrix solution techniques, that are dependent on matrix bandwidth, and sequential matrix operations. Such reductions in computing time can greatly influence the selection of analysis tools for automated design procedures. Although work is currently underway to improve the operating efficiency of NASTRAN, it remains to be seen whether such improvements can significantly close the gap and make NASTRAN competitive with the highly efficient programs that now exist.

It must also be pointed out that CPU execution time is not the only factor influencing the cost of running a computer program. Peripheral processing unit (PPU) time will also contribute to computing costs, but since the method of computing PPU time varies from system to system a comparison of PPU times was not made.

It would have been more meaningful to have run the two different programs on the same machine, but unfortunately SNAP Dynamics is currently available only on the Univac 1108. Conversion of SNAP Dynamics to the CDC 6600 is currently in progress, and once this conversion has been completed, a true one-to-one comparison between NASTRAN and SNAP Dynamics for calculating natural modes and frequencies can be made.

CONCLUDING REMARKS

To explore the feasibility of using large finite element computer programs to develop automated design procedures or to make parametric design studies involving many iterations for aircraft structures, vibration calculations for two representative wing structures were made using two available finite element computer programs, NASTRAN and SNAP. These programs are based on different programing techniques and solution strategies. Results for the first few modes from the two computer analyses were compared with existing experimental data, and found to possess the accuracy desired for parametric design studies even for complex built-up structures.

The central processing unit (CPU) execution times for each of the computer programs were compared, and it was found that there were significant differences in the times required to find solutions for the two computer programs, with

NASTRAN requiring more time. Although the use of different computers and facilities could have had some effect on the differences in computing times between the two computer programs used in this study, the time differences are so large that other factors must be the primary cause. Therefore, the differences in CPU execution times between NASTRAN and SNAP observed in this study are attributed to the differences in the solution strategies and programing techniques between the two programs.

Based on the results of this study, it is concluded that parametric design studies involving the natural modes and frequencies of large structures are economically feasible only if use is made of large scale finite element computer programs tailored for very efficient operation. At this time, the use of NASTRAN for such studies would be severely restricted because of the high and probably prohibitive cost associated with the correspondingly high CPU execution time.

REFERENCES

1. Butler, Thomas G.; and Michel, Douglas: NASTRAN, A Summary of the Functions and Capabilities of the NASA Structural Analysis Computer System. NASA SP-260, 1971.
2. Whetstone, W. D.: Structural Network Analysis Program User's Manual, Dynamic Analysis Version V70E. IMSC-HREC D225101 (Contract NAS8-26352), Lockheed Missiles and Space Company, Huntsville, Alabama, May 1971.
3. Hanson, Perry W.; and Tuovila, W. J.: Experimentally Determined Natural Vibration Modes of Some Cantilever-Wing Flutter Models by Using an Acceleration Method. NACA TN 4010, 1957.
4. Kordes, Eldon E.; Kruszewski, Edwin T.; and Weidman, Deene J.: Experimental Influence Coefficients and Vibration Modes of a Built-up 45° Delta-Wing Specimen. NACA TN 3999, 1957.
5. MacNeal, Richard H., ed.: The NASTRAN Theoretical Manual. NASA SP-221, 1970.
6. McCormick, Caleb W., ed.: The NASTRAN User's Manual. NASA SP-222, 1970.
7. Whetstone, William D.; and Jones, Charles E.: Vibrational Characteristics of Linear Space Frames. J. Struct. Div., ASCE, October 1969.
8. Whetstone, W. D.: Computer Analysis of Large Linear Frames. J. Struct. Div., ASCE, November 1969.
9. Leimbach, K. R.; and Moore, R. A.: Vibrational Characteristics of a McDonnell Douglas Low Crossrange Space Shuttle Launch Configuration. IMSC-HREC D162974 (Contract NAS8-20082), Lockheed Missiles and Space Company, Huntsville, Alabama, March 1971.

TABLE I. - RESULTS FOR A 45° CLAMPED FLAT PLATE

	10 by 10		30 by 30		Experiment
	NASTRAN	SNAP	NASTRAN	SNAP	
f_1 (Hz)	55.6	55.5	55.9	55.9	50
f_2 (Hz)	205.5	205.4	210.8	210.8	184
f_3 (Hz)	283.2	280.1	292.1	291.7	258
CPU time (sec)	114	29	5559	365	
Dynamic degrees of freedom	165	165	1395	1395	

TABLE II. - RESULTS FOR THE FIRST FOUR ANTISYMMETRIC
FREQUENCIES OF A FREE-FREE BUILT-UP WING

	NASTRAN	SNAP	Experiment
f_1 (Hz)	53.1	54.5	52.2
f_2 (Hz)	91.7	93.7	91.7
f_3 (Hz)	136.0	136.0	131.1
f_4 (Hz)	181.2	181.8	169.2
CPU time (sec)	422	178	
Dynamic degrees of freedom	117	650	

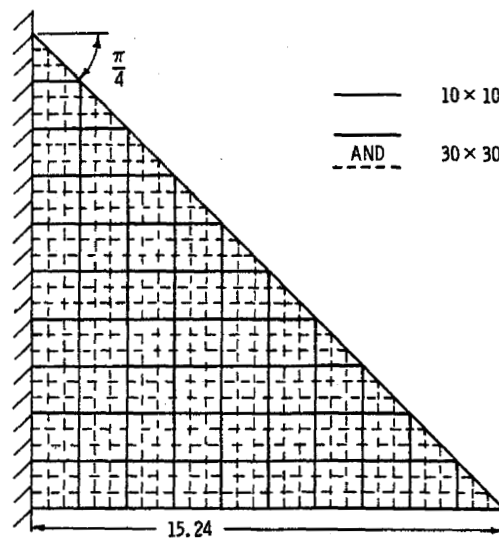


Figure 1.- 45° flat plate grid point networks.
Dimensions are in centimeters.

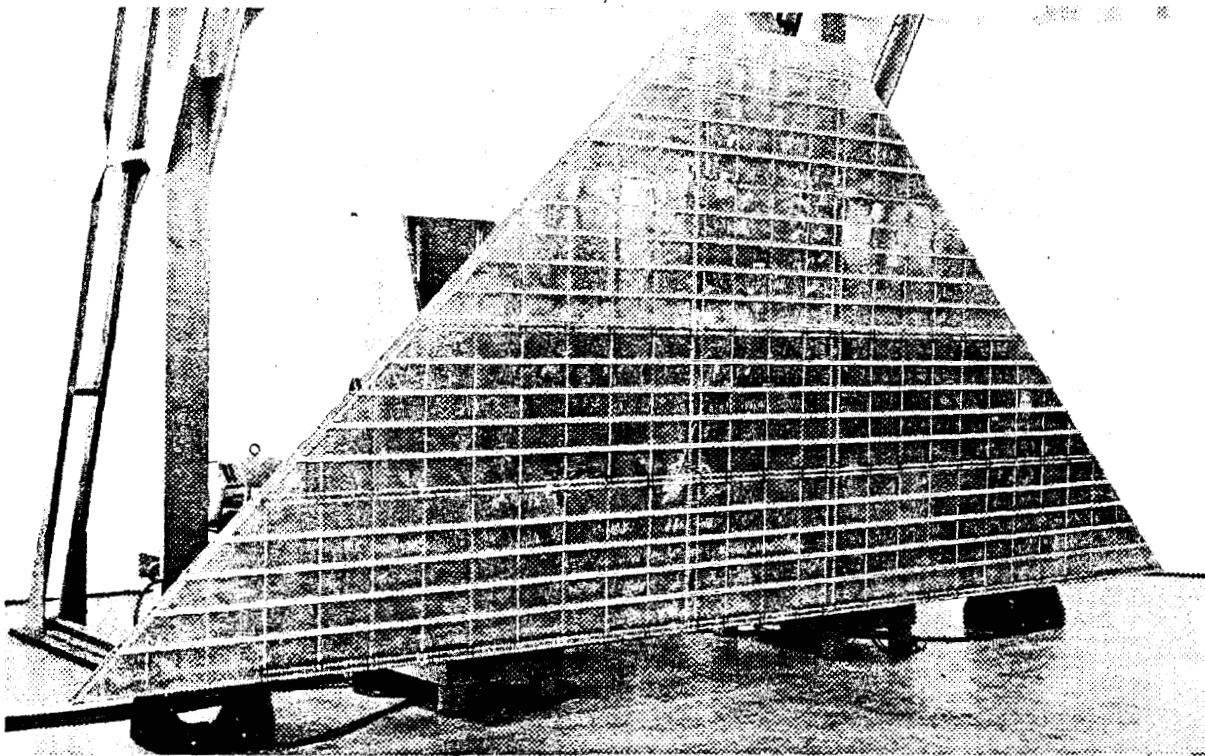
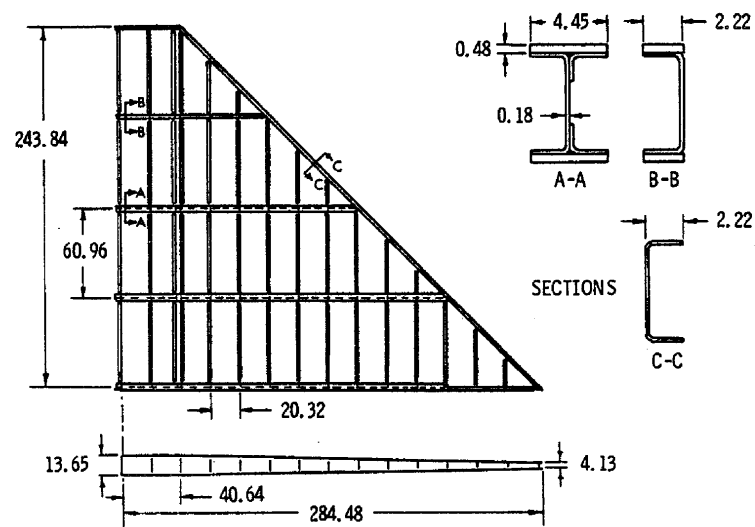
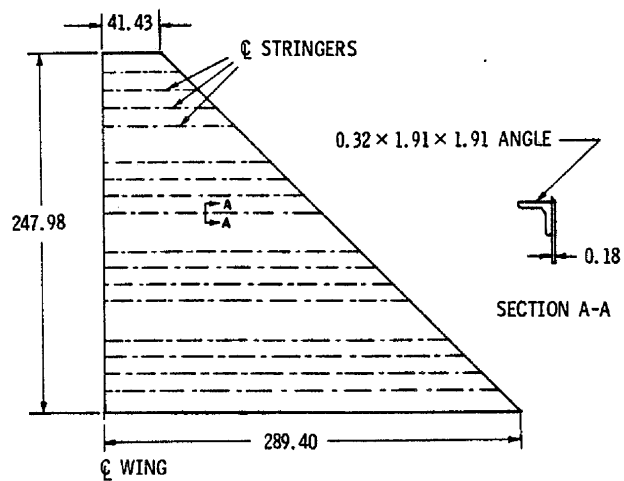


Figure 2.- Experimental built-up wing.



(a) Internal construction.



(b) Cover.

Figure 3.- Nominal dimensions of experimental built-up wing.
Dimensions are in centimeters.

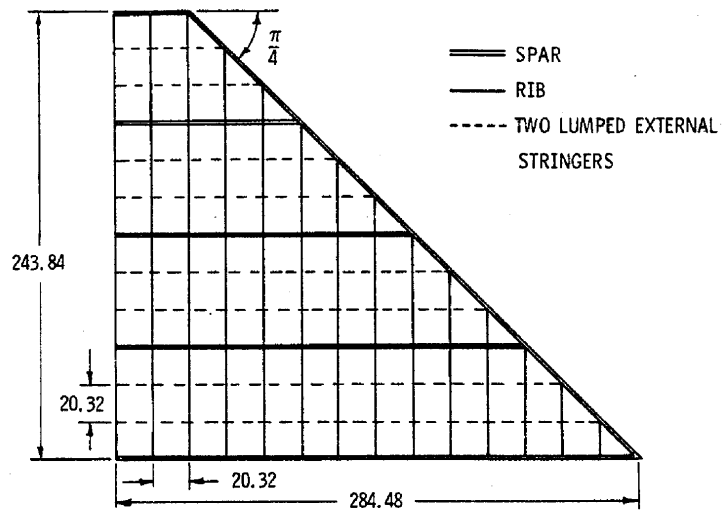


Figure 4.- Built-up wing grid point network and model planform. Dimensions are in centimeters.

PRODUCTION OF MOTION PICTURES OF A CONTINUOUSLY DEFORMING STRUCTURE USING NASTRAN

by Robert J. Reynolds

Convair Aerospace Division of General Dynamics
San Diego, California

SUMMARY

An in-house program (MIDAS IV) was recently developed to determine the transient response of an elastic structure under the influence of numerous complex boundary constraint conditions. With the aid of a small intermediate Fortran processor, the output from MIDAS IV was input to NASTRAN. Under the control of a user-developed DMAP set of instructions, NASTRAN produced SC-4020 output, suitable for 16mm projection, of the time-varying motion of a continuously deforming structure.

INTRODUCTION

A recent redesign effort required that a highly redundant, reliable nose fairing jettison technique be developed for the Atlas/Centaur launch vehicle. The costly nature of nose fairing jettison tests simulating the many possible off-nominal conditions that might exist during a flight dictated that analytic techniques be used to evaluate proposed jettison systems. The analysis would be required to simulate all possible conditions during a nominal jettison to develop structural loads and deflections. More importantly, the analysis would be used to predict whether or how a nose fairing would jettison if a constraint were momentarily imposed. The constraint devices were assumed to be the separation fittings holding the nose fairing halves to each other and the launch vehicle.

The planned jettison sequence consists of the time-sequenced firing of 16 separation fittings. In this operation, the two fairing halves are unlatched from the launch vehicle and each other. Two separation spring cartridges, located in the forward area of the nose fairing, then push against the released half fairings, allowing the fairings to rotate away from the launch vehicle. Their jettison trajectory is controlled by a hinge-release mechanism at the aft end of each fairing half. Figure 1 shows a typical nose fairing.

An analysis was performed to determine if it were possible to constrain one or more separation fittings so that by absorption of the potential energy stored in the separation spring cartridges, the constraint would be removed but insufficient energy or proper momentum vector would exist to jettison the nose fairing. Such an analysis required the description of the elastic behavior of a shell structure under the influence of time-dependent and deflection-dependent forcing functions.

Under the pressures of a high-priority investigation, it was necessary to select or develop an analysis tool that could accommodate rigid and elastic modes and time-dependent and deflection-dependent forcing functions with discontinuous boundary points. The tool would be required to handle the behavior of a separation fitting as it was time-released or as it broke in direct tension or bending — i.e., under a deflection-dependent behavior. Also, once a constrained fitting failed by violating a deflection criterion, a reduction of the controlling deflection should not re-engage the fitting.

Considering the many discontinuous parameters involved in the analysis, it was decided to use an in-house version of MIDAS, (Modified Integration Digital Analog Simulator, Ref. 1), known as MIDAS IV, to perform the basic analysis. As its name suggests, the program is a digital simulation of an analog computer and it readily provided the logic/switching capability and integration routines necessary to perform the transient analysis. To minimize the awkward matrix algebra aspect of the problem in such a simulation, the structure definition was limited to seven generalized coordinates for each fairing half: five rigid-body, one symmetric, and one antisymmetric. An evaluation of this abbreviated structural definition showed that for this analysis, the seven generalized coordinates per half could adequately describe the structural behavior. The analysis was more sensitive to the description of the boundary conditions than it was to extensive elastic definition. NASTRAN was considered for the basic analysis, but was set aside due to inexperience with the transient analysis modules of NASTRAN, lack of verification of the operational status of the nonlinear force capability, and uncertainty in the technique to handle complex logic/switching problems.

As might be imagined, many different constraint possibilities were suggested and analyzed. The above description is a considerable simplification of the jettison simulation. Typical MIDAS IV outputs involved monitoring more than 200 response functions; time-dependent printed and plotted output of those individual response functions were obtained. It soon became apparent that, while volumes of computer output were being generated and many very enlightening individual characteristics were being observed, an overall feel, or evaluation, of the influence of a particular set of constraints on the elastic vibrating structure was lacking. At this point, it was decided to generate motion pictures of the deforming elastic structure under the influence of the more plausible constraint conditions.

INTERFACING WITH NASTRAN

The Scientific Data Processing Laboratory at the San Diego operation of Convair Aerospace consists of a CDC 6400 operating under the SCOPE 3.2 monitor system with the core storage available for batch jobs being approximately 140000g words. The level 11.1.0 version of NASTRAN is operational on this facility. The comments and restrictions discussed should be considered in light of the NASTRAN version level and operating environment defined herein. The Stromberg Carlson SC-4020 is available offline and is used as an output device by both NASTRAN and in-house programs to generate 16mm and 35mm plots.

The task of generating the desired motion pictures consisted of four major steps:

1. Run the desired MIDAS IV simulation to generate time-dependent generalized coordinates on a recoverable storage device.
2. Run an intermediate processor to develop the elastic deformations of the structure from the available generalized coordinates as a function of time and output the information in a format suitable for NASTRAN.
3. Run NASTRAN to generate the time-varying deformed structure plots using as input the data from Step 2.
4. Convert the standard SC-4020 file output from NASTRAN to a form suitable for framing on 16mm film and process the data to film.

The MIDAS IV simulation-generated magnetic tape output of the time histories of user-selected response functions include, in this case, the generalized coordinates of the modes used to describe the behavior of the structure. With this file of data, an intermediate processor was developed to transform the generalized coordinates to spatial motion of selected nodes on the structure and output these

motions in a format suitable for NASTRAN. It was decided to introduce the data to NASTRAN using the DTI bulk data input card format. The selected DTI data block name would then be referenced in the appropriate DMAP instruction for plotting a deformed structure.

The original thought was to use the double-field input format due to uncertainties in the magnitude of the motion. At first glance, it was not apparent that any selected (Fortran) F field format in an eight-column wide field would be adequate to handle all motions from the nominal fairing jettison simulation to a highly constrained simulation, the maximum deformation ranging from approximately 254 cm (100 in.) to 1 cm (0.4 in.).

In developing the large-field (16 column wide) formatted data, an implicit restriction in NASTRAN was disclosed. A DTI NASTRAN logical record of data was formatted in 16-column fields. By chance, the data was punched in an odd number of physical cards. When this information was supplied to the NASTRAN input processor, unrelated fatal diagnostics occurred. The problem was that NASTRAN defines a logical card as one containing eight fields of data, which in large-field formats requires two physical cards. Thus, for the above case of an odd number of physical cards per logical record, the last physical card of the first logical record was only the first half of the last logical card and the input processor read the first physical card in the next logical record as the second half of the previous logical card. At this point, all input processing stopped because NASTRAN realized that continuation identifiers were inconsistent and data form was not correct. The moral is that logical records should contain integer multiples of eight fields of data in any combination of large- or small-field formats.

In spite of the pains taken to learn the above lesson, it was later decided to use the simpler small field format. The problem here was that the desire was to make a 200-frame film. For the size of structure considered, 20 physical cards of small-field formatted DTI data would be required per frame or a total of 4,000 cards of input – most being continuation cards. On the available computer facility, the NASTRAN input file processor required eight minutes of central processor time to digest a data deck of this bulk (approximately 50 GRID and PLOT cards were also processed). This processor time was attributed to the large number of continuation cards involved. Others at this facility have experienced similar time expenditures when inputting large logical records of DMI and DMIG cards. Thus, the thought of processing 8,000 large-field formatted data cards was dropped.

The intermediate processor between MIDAS IV and NASTRAN was thus configured to generate the small field DTI data and action was taken to minimize the Fortran F format problem. Since the DTI data would, in general, be quite voluminous, an additional feature was added to the processor to merge the data directly into a skeleton NASTRAN input data deck containing the desired Executive, Case Control, and other bulk data cards in a sorted manner. This disk or magnetic tape file of information would serve as the input to NASTRAN and alleviate punching large volumes of cards.

The second lesson learned was that the use of the "NASTRAN Card", described in Section 6.3.1 of the NASTRAN Programmer's Manual, to redefine the system input/output (I/O) files on this computer facility is ineffective. It was necessary to make modifications to the NASTRAN routine, XBOOT, a CDC version peculiar routine, so that I/O file redefinition was available to the user through the CDC control card causing execution of NASTRAN.

These difficulties overcome, it was now possible to acquire the desired execution of NASTRAN from the output of a user-developed processor.

The output for the SC-4020 plotter was designed to consist of some n frames of undeformed structure, followed by deformed structure plots. Input parameters to the intermediate processor dictated the sampling frequency of the data; these parameters were varied, depending upon the nature of analysis simulation and the desire to view different response frequencies. The DMAP set of instructions assembled to provide this output, along with a typical Case Control and abbreviated bulk

data setup, is shown in Table 1. The data block defining the transient motions is labelled RVEC. Isometrics of the idealized fairing are shown in Figure 2 in the closed and partially jettisoned positions – the latter corresponding to approximately the top-dead-center of rotation of each fairing half above the hinge axis. The structure's global coordinate system has been superimposed to interpret the Case Control and GRID cards.

The view for the motion picture production was selected to be the projection on the global x, y plane; i.e., a top view. In the analysis, the box structure representing the cylindrical portion of the fairing has a uniform cross-section, but for a top view, depth perception was desired. Since the perspective projection plot option is incorrect on this computer facility, the base of the box structure was arbitrarily drawn 16% smaller than the frame at the cone/cylinder intersection. This produces the tapered appearance of Figure 2. The benefits of this strategy are shown in Figure 3.

Experimentation was necessary to devise the proper form of DTI header information so that the data block could be interpreted in the context used in generating time-varying deformed structure plots.

The structure contained 26 nodes; thus, it was necessary to provide motion definition relative to the undeformed structure for 26 x 6 or 156 degrees of freedom. As is evident in Table 1, the rotation terms were ignored and arbitrarily set to zero. Other integer data in the 0 DTI record defined the form of the data provided. The remaining DTI records defined the nodal motion in a time-slice manner. Data contained in a typical DTI logical record is:

Subcase number	1
Transient response flag	3
Load set number	1
Time value	t
Row position of first element	1
Element type	1
3 unused integers	5989, 6036, 6065
156 data points of motion	real, single precision
End of column mark	16777215
End of logical record mark	ENDREC

The only peculiarity noted is that the number of nodes defined in set 1 had to be greater than 26; otherwise, the NASTRAN fatal error message 3003 appeared stating "Attempt to read past the end of a logical record in data set SIL (File 107) in Subroutine FREAD."

Having provided a suitable data input format to NASTRAN, it was then possible using the DMAP instructions shown in Table 1 to generate the desired SC 4020 plotted output. The Case Control cards shown in Table 1 are typical of those used to generate 20 frames of undeformed structure plots, one blank frame and 200 frames of deformed structure plots when the DTI data were input at 0.005-second intervals of analysis simulation. Typical computer running times were:

Input Processor (of approximately 4,000 cards)	500
20 Undeformed Structure Plots	20
200 Deformed Structure Plots	220
General NASTRAN Overhead	20
Total Central Processor (CP) Time	760
Total Peripheral Processor (PP) Time	360 sec.

The standard mode of operation was to submit as one batch job to the CDC 6400 a two-step setup, consisting of the execution of the intermediate processor, costing typically 20 CP seconds, generating a disk file of the NASTRAN input, followed by execution of NASTRAN with the appropriate input file redefinition via CDC control card.

With computer cost algorithms and efficient core utilization as primary motivations, it was found that the above described job would execute in the same CP and PP times at 120000g words of core storage as at 140000g.

SC-4020 TAPE PROCESSING

Execution of the above NASTRAN job produced about forty pages of printed output (if the bulk data echo were suppressed), containing informative messages from the plot module and a magnetic tape suitable for processing by the SC-4020. Standard output from the SC-4020 consists of 35mm film, which is processed to obtain paper copy. Since 16mm sprocketed film was desired, special handling by the SC-4020 operator was necessary. Two areas of difficulty occurred here.

The NASTRAN-generated magnetic tape included data directing film frame advance to the standard SC-4020 software for producing 35mm film. When this facility's standard movie program for generating 16mm film was loaded, the NASTRAN-provided frame advance information was incompatible and a minor software modification to the movie program was necessary.

The second difficulty involved the scaling algorithm used by NASTRAN in sizing the structure for plotting. Though user override is available, the default mode is to assume a square region for plotting. The structure is sized for plotting based on the MAXIMUM DEFORMATION information provided in the Case Control. For this application, it was desirable to have a continuous display of the same size structure throughout the film; thus, the same MAXIMUM DEFORMATION was used to scale both the undeformed and deformed structure plots. Since a nominal nose fairing simulation would include considerable rigid body motion, additional care was needed in scale selection to avoid having the deformed structure plotted off the frame. Unfortunately, a 16mm frame has a 4 wide by 3 high aspect ratio. To accommodate the film size, the top view of the structure was selected for plotting with the principal motion being along the horizontal direction. Then by proper positioning of the camera in the SC-4020, the operator was able to center the plotted data on the 16mm frame, thereby eliminating the loss of data due to off-frame projection during SC-4020 processing. A display comparing the 16mm film framing of a horizontal and vertical jettison is shown in Figure 3 as it was generated by NASTRAN.

RESULTS

The results of this exercise provided an output display of a continuously deforming structure. The typical reaction of engineering personnel to such a display was significant comprehension of the simulation results and a "but of course it behaves that way" exclaimer when many long hours studying individual responses produced more questions than answers. It was necessary only to generate a few motion pictures of the more plausible constraint conditions in the analysis to educate and inform the viewers of the scope of the problem being studied and the influence of selected boundary conditions. While it is difficult to evaluate the worth of the overall display in aiding analyst comprehension of the problem, it became apparent that one hour spent studying the details of the information provided in the motion picture was easily worth one or two days studying time-history plots of individual deflections. For larger and more detailed structures, the benefits would be even more dramatic.

CONCLUSIONS AND IMPROVEMENTS

This task provided the opportunity to establish an important communication link between in-house programs and NASTRAN. It defined the restrictions associated with large field bulk data input, revealed the obstacle to CDC users in redefining I/O files, disclosed the costly nature of large bulk data sets where many continuations are involved, and provided an important tool in understanding the transient response of a deforming structure.

To improve the efficiency in running NASTRAN in this mode it is apparent that more efficient means must be devised to input large blocks of bulk data where numerous continuation cards are involved. This may be achieved through modification to the NASTRAN input processor or by the user generating a properly configured user master file or old problem tape containing the desired information. Should the need for 16mm plots from NASTRAN become more common, it would also be desirable to modify the NASTRAN plot module to provide such capability as a user-requested option and avoid the need for special handling by the SC-4020 operator.

REFERENCE

1. "The SCI Continuous System Simulation Language (CSSL)", Simulation, Volume 9, No. 6, December 1967, pp. 281-303.

Table 1. Typical NASTRAN input deck listing for motion picture production with abbreviated bulk data deck (Continued).

```

$ END OF LEADER SETUP
PLOT TRANSIENT DEFORMATION TIME 0.000, 2.000,
MAXIMUM DEFORMATION 70.,
SET 1 ORIGIN 1 SHAPE
BEGIN BULK
DTI RVEC 0 6 156 2 1 156 0+00
+DU ENDFEC
DTI RVEC 1 3 1 0.0000 1 1+ 1
+ 15989 6036 6065 0.000 0.000 0.000 0.000 0.000+ 2
+ 2 0.000 0.000 0.000 0.000 0.000 0.000 0.000+ 3
+ 3 0.000 0.000 0.000 0.000 0.000 0.000 0.000+ 4
+ 4 0.000 0.000 0.000 0.000 0.000 0.000 0.000+ 5
+ 5 0.000 0.000 0.000 0.000 0.000 0.000 0.000+ 6
+ 6 0.000 0.000 0.000 0.000 0.000 0.000 0.000+ 7
+ 7 0.000 0.000 0.000 0.000 0.000 0.000 0.000+ 8
+ 8 0.000 0.000 0.000 0.000 0.000 0.000 0.000+ 9
+ 9 0.000 0.000 0.000 0.000 0.000 0.000 0.000+ 10
+ 10 0.000 0.000 0.000 0.000 0.000 0.000 0.000+ 11
+ 11 0.000 -0.000 -0.000 0.000 0.000 0.000 -0.000+ 12
+ 12 -0.000 0.000 0.000 0.000 0.000 0.000 0.000+ 13
+ 13 0.000 0.000 0.000 -0.000 -0.000 0.000 0.000+ 14
+ 14 0.000 -0.000 -0.000 0.000 0.000 0.000 -0.000+ 15
+ 15 -0.000 0.000 0.000 0.000 0.000 -0.000 0.000+ 16
+ 16 0.000 0.000 0.000 -0.000 -0.000 0.000 0.000+ 17
+ 17 0.000 -0.000 -0.000 0.000 0.000 0.000 -0.000+ 18
+ 18 -0.000 0.000 0.000 0.000 0.000 -0.000 0.000+ 19
+ 19 0.000 0.000 0.000 -0.000 -0.000 0.000 0.000+ 20
+ 20 0.000 -0.000 -0.000 0.000 0.000 0.000 0.00016777215+ 21
+ 21 ENDFEC
.
.
.
* INTERMEDIATE NASTRAN LOGICAL RECORDS 2 THROUGH (NREC - 1) HAVE BEEN REMOVED *
* FOR THIS DTI BULK DATA
.
.
.
DTI RVEC 6 1 3 1 .7025 1 1+ 106
+ 1065989 6036 6065 -.025 -2.546 -17.178 0.000 0.000+ 107
+ 107 0.000 -.086 -2.656 -17.169 0.000 0.000 -.190+ 108
+ 108 -26.389 -9.300 0.000 0.000 0.000 .017 -56.516 -9.291+ 109
+ 109 0.000 0.000 0.000 -.113 -102.902 -2.531 0.000 0.000+ 110
+ 110 0.000 -.113 -102.955 -2.536 0.000 0.000 0.000 -1.133+ 111
+ 111 -103.494 -6.407 0.000 0.000 0.000 0.000 -.032 .006+ 112
+ 112 0.000 0.000 0.000 0.000 -.142 .021 0.000 0.000+ 113
+ 113 0.000 -.023 -53.875 7.884 0.000 0.000 0.000 -.023+ 114
+ 114 -54.002 7.894 0.000 0.000 0.000 -.087 -102.148 2.630+ 115
+ 115 0.000 0.000 0.000 -.087 -102.201 2.630 0.000 0.000+ 116
+ 116 0.000 -.007 2.596 -17.218 0.000 0.000 0.000 .037+ 117
+ 117 2.626 -17.203 0.000 0.000 0.000 .116 56.561 -9.306+ 118
+ 118 0.000 0.000 0.000 -.034 56.594 -9.291 0.000 0.000+ 119
+ 119 0.000 .064 103.127 -2.502 0.000 0.000 0.000 .064+ 120
+ 120 103.139 -2.498 0.000 0.000 0.000 .059 102.564 1.379+ 121
+ 121 0.000 0.000 0.000 -0.000 .071 .005 0.000 0.000+ 122
+ 122 0.000 -0.000 .101 .020 0.000 0.000 0.000 .025+ 123
+ 123 54.036 7.917 0.000 0.000 0.000 .025 54.068 7.933+ 124
+ 124 0.000 0.000 0.000 .058 102.369 2.671 0.000 0.000+ 125
+ 125 0.000 .058 102.381 2.675 0.000 0.000 0.00016777215+ 126
+ 126 ENDFEC
GRID 1 50.0 60.0 0.00
GRID 2 -50.0 60.0 0.00
GRID 3 60.0 60.0 -188.
GRID 4 -60.0 60.0 -188.
GRID 5 10.0 60.0 -350.
GRID 6 -10.0 60.0 -350.
GRID 7 0.00 73.5 -350.
GRID 8 50.0 10.00 0.00
GRID 9 -50.0 10.00 0.00
GRID 10 60.0 0.00 -188.
GRID 11 -60.0 0.00 -188.
GRID 12 10.0 42.0 -350.
GRID 13 -10.0 42.0 -350.
GRID 14 -50.0 60.0 0.00
GRID 15 +50.0 60.0 0.00
GRID 16 -60.0 60.0 -188.
GRID 17 +60.0 60.0 -188.
GRID 18 -10.0 60.0 -350.
GRID 19 +10.0 60.0 -350.
GRID 20 0.00 73.5 -350.
GRID 21 -50.0 110.0 0.00
GRID 22 +50.0 110.0 0.00
GRID 23 -60.0 120.0 -188.
GRID 24 +60.0 120.0 -188.
GRID 25 -10.0 78.0 -350.
GRID 26 +10.0 78.0 -350.
GRID 101 00.0 00.0 0.00
PLOTTEL 1 1 8 2 8 9
PLOTTEL 3 9 2 4 3 10
PLOTTEL 5 10 11 6 11 4
PLOTTEL 7 5 12 8 12 13
PLOTTEL 9 13 6 10 6 7
PLOTTEL 11 7 5 12 1 3
PLOTTEL 13 8 10 14 9 11
PLOTTEL 15 2 4 16 3 5
PLOTTEL 17 10 12 18 11 13
PLOTTEL 19 4 6 20 14 21
PLOTTEL 21 21 22 22 22 15
PLOTTEL 23 16 23 24 23 24
PLOTTEL 25 24 17 26 18 25
PLOTTEL 27 25 20 28 26 19
PLOTTEL 29 19 26 30 20 18
PLOTTEL 31 14 16 32 21 23
PLOTTEL 33 22 24 34 15 17
PLOTTEL 35 16 18 36 23 25
PLOTTEL 37 24 26 38 17 19
ENDDATA

```

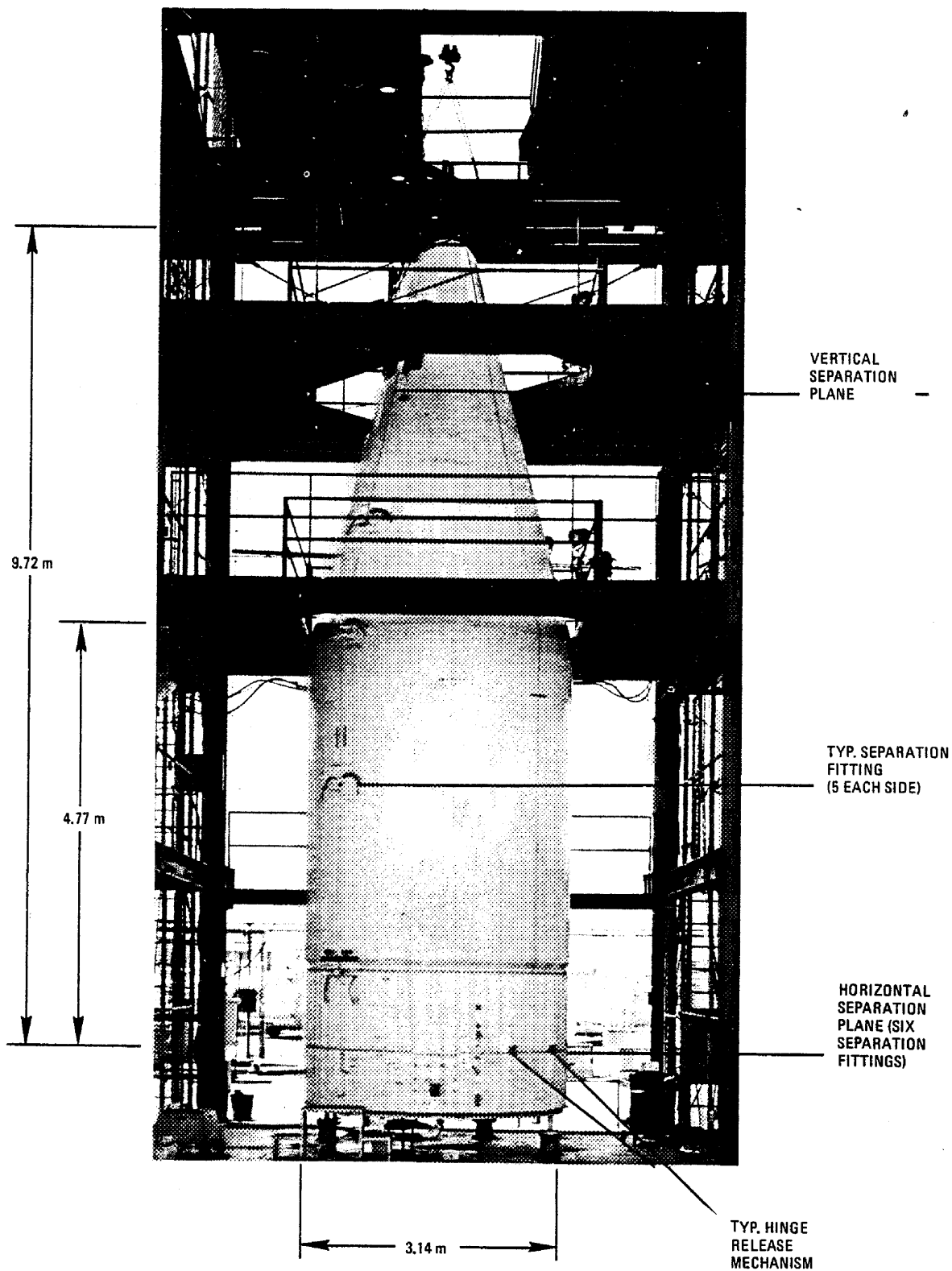


Figure 1. Typical OAO Atlas/Centaur nose fairing.

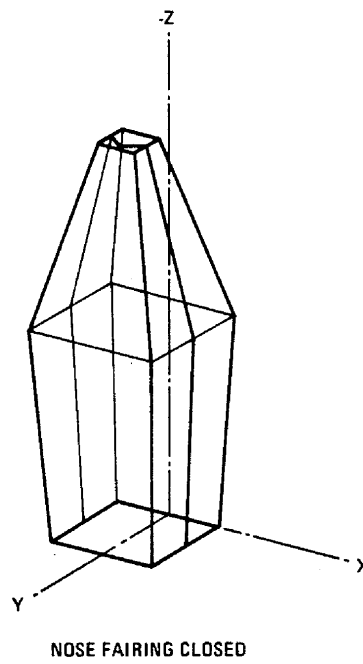
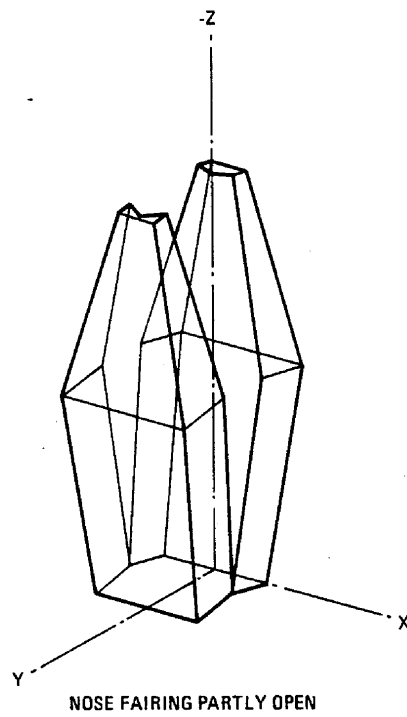


Figure 2. Nose fairing idealization for jettison simulation.

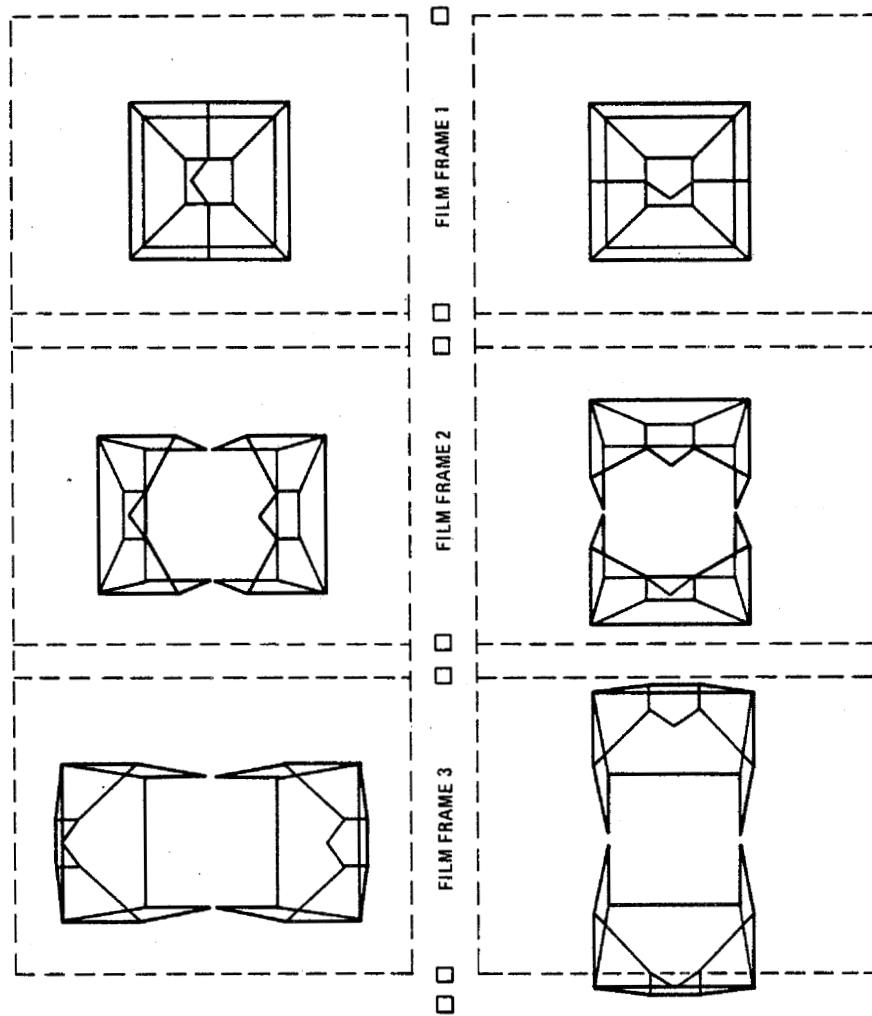


Figure 3. Framing comparison on a 16mm (4 x 3) film strip.

AN INTERACTIVE COMPUTER GRAPHICS PROGRAM FOR NASTRAN

By Michael Cronk
Convair Aerospace Division of General Dynamics

SUMMARY

Experience in developing and using interactive computer graphics programs has shown that they can be useful tools for checking finite-element models prior to structural analysis and for displaying the results of the analysis in a meaningful fashion. This paper describes such a program applied to NASTRAN that has resulted in cost savings in model checkout and increased flexibility in the use of NASTRAN. Shortcomings in using the NASTRAN structure plotter and advantages of an on-line interactive graphics program are discussed. Program features such as arbitrarily oriented three-dimensional views of beams, quadrilaterals, loads, constraints, and member sizes are described. Preliminary results are presented to indicate the flexibility of the interactive approach to model checkout. Future additions to the CDC 6400 program for reviewing analysis results are indicated.

INTRODUCTION

On-line interactive computer graphics consists of a cathode-ray tube (CRT) for displaying information, a light-sensing device called a "light pen" for communication, and a computer program that provides the information. The program first displays a list of instruction commands or options, called a "menu", from which the user makes a selection. The menu items or individual commands that cause program execution are called "light buttons." The program responds to user commands initiated by holding the light pen over a "display item" or light button on the CRT and depressing a switch on the pen. Upon receipt of the command the program displays further menus, performs calculations, displays plots and diagrams, etc., depending on the nature of the command and the type of program. In this fashion the user directs desired operations and responds to displayed information.

Interactive computer graphics offers several improvements over the normal digital mode of operation. Turnaround time is reduced by the ability to display "immediately" the results of computation, modify the data, and recompute. Several iterations of the submit job, compute, look at printout, correct data, and resubmit process can be compressed into one session at the display device. Judgment and insight to the problem

are enhanced by using the graphic display. Rapid comparison of various designs or analyses, often essential during preliminary design or "panic" redesign, are readily accomplished.

One application area for the first interactive computer graphics system at Convair Aerospace was the finite-element analysis of structures, for which a graphics program was prepared to interface a large analysis program. The analysis program handled up to 2,160 degrees of freedom, and the preparation and checkout of data decks was a large and costly task. The interactive graphics program was successful in significantly reducing the cost and time for checking out the model and for understanding the results, and it became operational about the time NASTRAN was acquired. The success of the original graphics program, plus the limitations of the NASTRAN structure plotter, soon led to developing a similar program for NASTRAN.

The structure plotter in NASTRAN has several disadvantages. The technique of representing three- and four-sided members by plotting their edges is confusing when cutouts are present or other elements are plotted. There is no provision for displaying member properties, material properties, or applied loads. A given set of NASTRAN plots may be unsatisfactory due to errors in the request or poor viewing angles. If a given view is incorrect, another submittal of the NASTRAN job is required, and this can be costly and time consuming. Interactive graphics does not have these limitations since the user immediately views the requested plot and can correct errors in the plot selection.

Several ground rules were defined at the start of developing NASTRAN graphics:

1. NASTRAN graphics should be compatible with NASTRAN as far as input data is concerned, allowing a NASTRAN user to take his complete data deck, including restart cards and old problem tape, and enter them in the graphics program without change.
2. The graphics program should be modular and easily expandable to meet additional requirements.
3. The graphics program process should be tutorial and relatively easy for a user to learn.

The graphics program has two primary functions. The first is to debug the structural model. This implies that the user should be able to display in a meaningful fashion as much of the information contained in the data deck as is feasible for a visual check for errors. This includes geometry and a representation of all NASTRAN connection cards at arbitrary orientations. This function is being enlarged to display member properties such as cross section area, moments of inertia, and thicknesses, to display vectors showing the applied loads, and to plot stress-strain curves and other tabular input data.

The second function of the program is to display analysis results. Deformed structure plots for statics, buckling, mode shapes and transient response constitute a minimum capability as an output device. This second function is being enlarged to display plots of internal loads on a portion of the structure, time histories of response functions, and the deformed structure at a selected time.

DESCRIPTION OF THE PROGRAM

The NASTRAN interactive graphics program consists of two parts. The first is a preprocessor composed primarily of selected NASTRAN modules from Links 0, 1, and 2. The function of the preprocessor is to read the user's data deck from cards and the old problem tape, and to generate a special file for use by the graphics program. The NASTRAN error-checking process during input has been left intact, allowing the user to obtain a printout containing the standard error checks associated with reading the executive and case control decks and the bulk data deck. Certain executive functions associated with restarting and DMAPing have been omitted. This allows running an untried data deck through the preprocessor for graphics before making an initial run on NASTRAN, without losing the error-checking capability of NASTRAN. It then allows using the graphics program to visually check the model. If results of a previous NASTRAN analysis are to be plotted, the preprocessor finds the appropriate data block on the old problem tape and stores it on the file used by the graphics program. The bulk data cards listed in Table 1 comprise the cards currently stored for graphics display. Others will be added as required.

The second part is the graphics program, beginning with a menu of options (Figure 1). From this menu the user selects with the light pen the first option he desires for his first plot. The program then displays information concerning the selected option and waits for further direction. When all the options for a given plot have been selected the user "picks" the PLOT lightbutton. The program then computes and displays the plot of the structure according to the selected options (Figure 2). As each plot is displayed it may be given a title by the user and stored. At a later time any combination of previously titled plots may be redisplayed. This is particularly useful for overlaying undeformed and deformed plots (Figure 3). To create another plot the user picks a button that returns the program to the menu of options.

Three options are used to select which kind of connection elements are to be displayed. "One-Dimensional Elements" asks the user to select from this list of one-dimensional elements: CBAR, CONROD, CROD, CTUBE, or PLOTEL. All elements of the selected types will be plotted. Similarly "Three-Sided Elements" offers a choice of CTRBSC, CTRIA1, CTRIA2, CTRMEN, or CTRPLT. "Four-Sided Elements" offers a choice of CSHEAR, CQUAD1, CQUAD2, CQDMEN, CQDPLT, or CTWIST. For all three of the

options, if a particular bulk data type is not present in the data, its name does not appear in the list. Figure 4 shows an aircraft bulkhead composed of CSHEAR and CONROD elements.

Since a given model may contain many grid points, and plots of the whole structure may become confusing, two options are available to limit the portion of the model from which the connection elements will be displayed. One option allows the user to select a set of predefined grid points, called a substructure, to be plotted. These substructures are defined by card input for the preprocessor program and can be used to define parts of the structure the user wishes to view separately, such as a rib, bulkhead, or wing. These substructures can also be defined from the CRT. The other option limits the portion of the model to be viewed by entering geometric limits on the model axis, thus defining a subspace. Elements that extend beyond this subspace are not plotted. Figure 5 is a geometric limitation of the model shown in Figure 2.

An option is available for the user to annotate the grid points with the grid ID or a symbol, and four line-style options are available for plot construction. Selection of the latter will result in the plot being constructed with solid, broken, dashed, or center lines. An undeformed plot can be constructed with solid lines and overlaid with a deformed plot drawn with dashed or broken lines for easier distinction (Figure 3). The model may be viewed at any arbitrary orientation. This orientation is initially defined by inputting the projected angles between the model basic system and a display tube, two-dimensional coordinate system. After the model has been displayed at the initial orientation, the user can rotate the model about any of the model axes through any arbitrary angle. This permits altering the viewing angles at will.

Magnification factors can also be input to stretch the model along any axis, for better visibility of members that might be hidden by other members.

Selecting the PLOT light button with the light pen results in a plot of the structure, in 5 to 10 seconds, conforming to options the user has selected. It takes from one to three minutes to select all the options required for a typical plot. The plots can be studied at the tube or photographed for later use.

Deformed plots are produced by first selecting the load set, mode number, or time increment for statics, modes or buckling, and transient response, respectively. The maximum desired deformation is input and the procedure continues as for any plot.

HARDWARE-SOFTWARE

The graphics program uses 20,000 words out of a 65,000 (60-bit) word central memory on a CDC 6400 computer operating under the Scope 3.2 operating system. The two 274 CRT display consoles are each driven by a CDC 1700 computer, which can handle

up to six CRT's. One of the 1700 computers also acts as a remote job entry terminal to the 6400. If two graphics programs are run concurrently, they time share the same central memory in the 6400 computer. Scientific batch work runs in the background. The program is written in Fortran IV using the CDC Interactive Graphics System (IGS).

FUTURE ADDITIONS TO THE PROGRAM

Expansion of the program in several areas is being considered, such as adapting an existing graphics program for general X-Y plotting. This would enable the user to produce plots of tabular input data, such as transient forces or material thermal dependencies for debugging purposes, and X-Y plots of NASTRAN output data such as transient response results. The user would be able to display time history plots and then the deformed structure plot for any particular time.

An additional debugging capability for input data also is desired. Such items as displays of applied loads, member properties, and material properties would be useful. Once items are displayed it is logical to desire to modify and add to the data at the display console and punch out update cards for the NASTRAN data deck. Software to do this could be written, as it was for a similar program at Convair Aerospace. The feasibility of implementing this capability is being studied.

The capability to display more results is of immediate interest. Plots of internal loads, for example, can be superimposed on views of portions of the structure—shears, axial loads, moments, etc. — and can be easily understood if presented properly.

Monitoring and control of automatic data generating programs can also be done with the display tube. The user can see that the data generated is correct; if not he can regenerate the data.

CONCLUSIONS

An interactive graphics program has been written for NASTRAN that produces undeformed and deformed plots of a structure without the limitations of the NASTRAN plotter. All the NASTRAN connection elements can be displayed. Plots can be saved and overlaid for comparison. The existing program is the first part of a program to review more thoroughly the NASTRAN input data and also to display much of the NASTRAN output. Use of this program will result in cost savings during model checkout and in greater insight to using NASTRAN to solve structural problems.

Table 1. NASTRAN bulk data cards used in NASTRAN Graphics Program.

GRID	CTUBE	CTRMEM	PTWIST
CORD1C	CSHEAR	CTRPLT	PTRBSC
CORD1R	CQUAD1	PBAR	PTRIA1
CORD1S	CQUAD2	PROD	PTRIA2
CORD2C	CQDMEM	PTUBE	PTRMEM
CORD2R	CQDPLT	PSHEAR	PTRPLT
CORD2S	CTWIST	PQUAD1	MAT1
CBAR	CTRBSC	PQUAD2	MAT2
CONROD	CTRIA1	PQDMEM	MAT3
CROD	CTRIA2	PQDPLT	PLOTEL

DISPLAY MODEL MENU

THIS IS THE MENU FOR DISPLAYING A VIEW OF THE MODEL.
PICK CHOICE FROM LIST TO LEFT OF WINDOW WITH THE LIGHTPEN AND
RESPOND TO INFORMATION IN WINDOW. WHEN ALL CHOICES THAT YOU DESIRE
FOR THIS PLOT HAVE BEEN MADE, PICK PLOT WITH THE LIGHT PEN. ALL
CHOICES CAN BE CANCELLED BY PICKING RETURN TO DISPLAY MODEL. A
LIST OF THE CHOICES YOU HAVE MADE WILL BE CREATED BELOW THE WINDOW.
IF GEOPLOT IS USED IT MUST BE USED BEFORE SCALING OR IT WILL BE IGNORED.
IF SUBSTRUCTURE IS USED IT MUST BE USED BEFORE SCALING OR IT WILL BE IGNORED.
DEFLECTIONS MUST BE PICKED BEFORE SCALING.

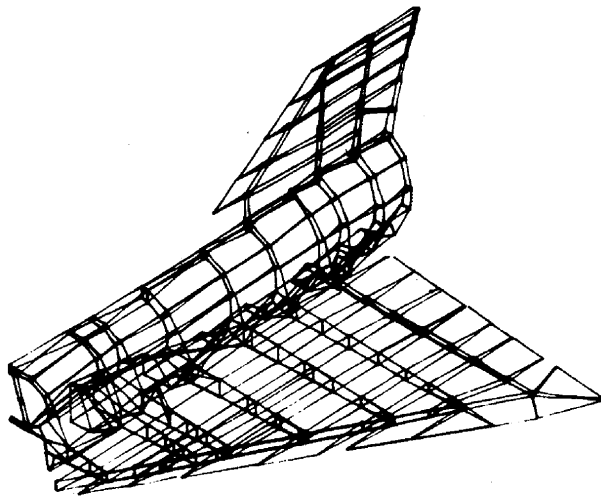
1. DISPLAY ONE DIMENSIONAL ELEMENTS
2. DISPLAY THREE SIDED ELEMENTS
3. DISPLAY FOUR SIDED ELEMENTS
4. DISPLAY SUBSTRUCTURE
5. DISPLAY GRID DEFLECTIONS
6. CHOOSE LINE STYLE FOR PLOT
7. GEOMETRIC LIMITATION
8. SCALE PLOT FOR LARGEST VIEW
9. SCALE PLOT FOR FURTHER ROTATION
ABOUT MODEL AXIS
10. ANNOTATE GRID POINTS
11. DISPLAY OLD PLOTS
12. DEFINE SUBSTRUCTURES
13. WRITE TIME (FOR DEBUG WORK)
14. DUPLICATE DATA BASE (FOR DEBUG WORK)

PLOT

RETURN TO MAIN MENU

RETURN TO DISPLAY MODEL

Figure 1. Menu of options for the program.



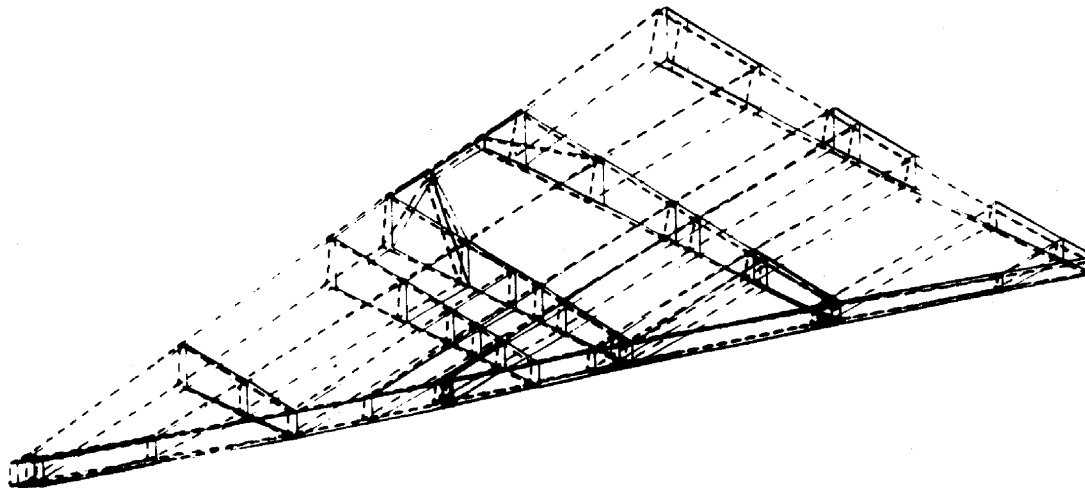
RETURN TO
MAIN MENU

RETURN TO
DISPLAY MODEL

TITLE AND SAVE
MODEL PICTURE

DISPLAY TITLES
FOR OVERLAY

Figure 2. Undeformed plot of F-106 model.



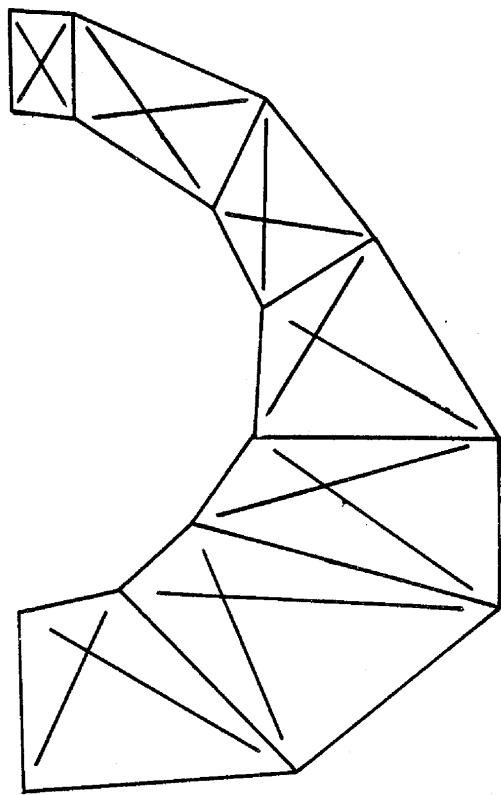
RETURN TO
MAIN MENU

RETURN TO
DISPLAY MODEL

TITLE AND SAVE
MODEL PICTURE

DISPLAY TITLES
FOR OVERLAY

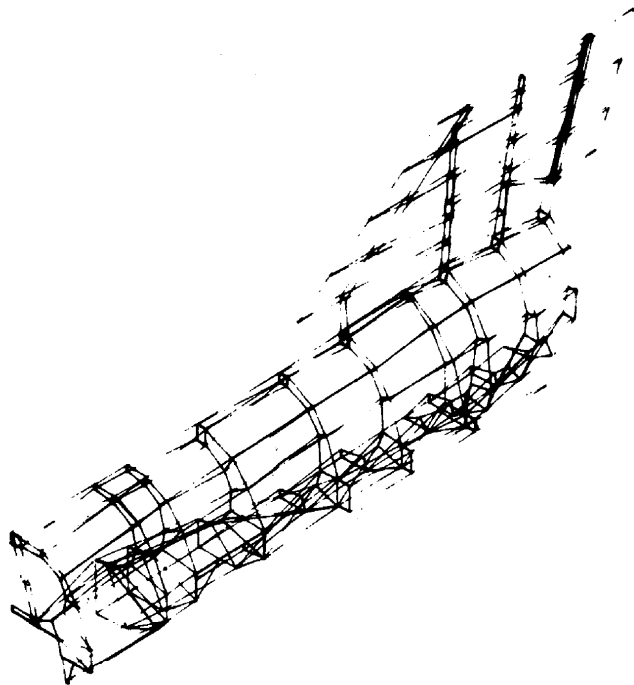
Figure 3. Deformed plot of F-106 model wing in dashed lines overlying undeformed plot.



RETURN TO
MAIN MENU
RETURN TO
DISPLAY MODEL
TITLE AND SAVE
MODEL PICTURE

DISPLAY TITLES
FOR OVERLAY

Figure 4. Plot of F-106 model fuselage frame showing CONROD and CSHEAR elements.



RETURN TO
MAIN MENU
RETURN TO
DISPLAY MODEL
TITLE AND SAVE
MODEL PICTURE

DISPLAY TITLES
FOR OVERLAY

Figure 5. Plot of F-106 model with wing removed by use of geometric limitation option.

NASTRAN USER INTERFACES - AUTOMATED

INPUT INNOVATIONS

By Malcolm W. Ice

Preceding page blank

Boeing Computer Services, Inc.

SUMMARY

The following features have been incorporated at Boeing to make the usage of NASTRAN easier and less susceptible to error: 1) automatic generation of finite element input, 2) BCD/EBCDIC input transparency, and 3) additional symbolic parameters in the NASTRAN user procedure.

INTRODUCTION

The NASTRAN user interface, i.e. the communication linkage between the user and NASTRAN, is a very important part of the NASTRAN system. Naturally the user must first correctly describe his problem to NASTRAN before he can expect NASTRAN to solve the problem. Therefore it is important that the user interface allow quick and convenient preparation of the problem with a minimum chance for input error. The features presented in this paper have been incorporated at Boeing to significantly improve the standard user interface for the IBM 360 version of NASTRAN. These features have significantly increased the usability of NASTRAN while reducing the chance of input error. They have also reduced the amount of training necessary for Boeing engineers to learn to use NASTRAN.

SAIL/NASTRAN LINKAGE

Several years ago a revolutionary finite element input capability was developed at Boeing. This capability, called SAIL (Structural Analysis Input Language), is a language used to describe basic finite element input data such as gridpoints, element connections, loads, etc. However, unlike the usual finite element input schemes, SAIL does not require the user to explicitly input each logical item of data (i.e. each gridpoint, structural element, load, etc.). Instead, simple straightforward techniques are available within SAIL for the user to describe algorithms to generate blocks of data. In this manner, the user can take advantage of patterns and sequences which may occur in his data. Usually structures can be described within SAIL using only a fraction of the cards that would otherwise be required if each item of data were explicitly input. It is not unusual for input card volume to be reduced by factors of four, ten, or even twenty.

SAIL Data Generation Techniques

While a detailed description of the SAIL input capability will not be given here (more information is given in reference 1), the three major data generating concepts employed by SAIL will be briefly described.

Incremental Indexing. This feature is perhaps the most powerful and useful of the SAIL data generating techniques. Looping and indexing techniques similar to the Fortran "DO" loop are applied to finite element input statements. To make use of the incremental indexing feature, statements to establish gridpoints, structural elements, loads, etc. are placed within loops such that they are "executed" a number of times, with each execution establishing a new item of input in the series being described. An example of this technique is given in Table 1 where the 65 gridpoints and 48 quadrilateral plates of the parabolic dish shown in figure 1 are input with only 18 SAIL statements.

Substructure Transformation. This technique involves considering a set of input data to be a logical group (a substructure). This set of data is then translated and rotated to form other sets of data (other substructures). Figure 2 illustrates some possible uses of substructure transformations.

External Data Generators. This concept is completely analogous to the concept of subroutines in Fortran programming. Here data generating subroutines are written using SAIL statements and are "called" from the main stream of data input to generate desired sets of data. For example, an external data generator could be written which generates a rectangular stiffened panel when called. The inputs to the generator, or "calling sequence", might be the panel dimensions, panel thickness, and coordinates locating one corner of the panel. The user could then build up a structure of stiffened panels by merely making several calls to the panel generator, supplying a correct set of inputs for each call.

The SAIL data generating techniques will probably be somewhat obscure from these very brief descriptions. However, the important thing is that most structures can utilize these data generating techniques to reduce input data volume. It should also be noted that data which is automatically generated will be uniformly correct - no isolated keypunch errors can occur.

Implementation of SAIL/NASTRAN

Naturally it was desired to utilize the SAIL input techniques for NASTRAN analyses. The implementation of the SAIL/NASTRAN linkage involved modifying SAIL such that NASTRAN Bulk Data cards could be produced from the basic finite element data stored within SAIL. While there was not a one-for-one correspondence between SAIL and NASTRAN for all possible input items, a basic set of data could easily be translated from the

SAIL format to the NASTRAN Bulk Data format. This set includes gridpoints, element connections, element property lists, material tables, loads, temperatures, and single point constraints.

To complete the implementation of the SAIL/NASTRAN linkage, additional job steps were added to the NASTRAN user procedure to accommodate the SAIL capability. The data flow was arranged so that the user supplies a standard NASTRAN deck consisting of Executive Control, Case Control, and Bulk Data. Optionally, he may supply SAIL input also. In this case, the Bulk Data which results from the SAIL input is appended to the set of Bulk Data supplied in the standard NASTRAN deck. This allows the user to use SAIL as applicable and to supply the remainder of the input via standard Bulk Data cards.

Advantages of SAIL/NASTRAN

One obvious advantage gained by establishing the SAIL/NASTRAN linkage is that the powerful data generating techniques of SAIL can be used to input NASTRAN data. Another advantage is that Boeing structural analysts can more easily learn to use NASTRAN because of their previous familiarity with SAIL. The final advantage, and a very important one, is that a structural problem which has been described with SAIL input can be solved by using Boeing's own structural analysis programs or by using NASTRAN. This allows backup problem solving capabilities and provides independent analyses for checking results.

The SAIL/NASTRAN linkage has also been valuable in acquainting Boeing engineers with the NASTRAN program. A typical engineer naturally prefers to use Boeing's own programs because he is much more familiar with them. However, occasionally during the course of analysis, a capability is required which does not exist in the Boeing program, but does exist in NASTRAN. The engineer is then quite ready to consider NASTRAN, especially since he does not have to re-program his input data. Soon he is familiar with NASTRAN and incorporates it into his repertory of structural analysis tools.

SAIL/NASTRAN Applications at Boeing

The following NASTRAN applications at Boeing have relied upon the SAIL/NASTRAN linkage for success.

NASTRAN Evaluation. Shortly after receiving the NASTRAN program, Boeing conducted an evaluation and familiarization study of NASTRAN. The SAIL/NASTRAN linkage allowed many "off the shelf" problems to be run on NASTRAN.

Buckling Check. A large deflection analysis of a three dimensional truss was conducted using Boeing's Advanced Structural Analyzer (ASTRA). The results of this analysis showed structural collapse at a much lower load than anticipated. A buckling analysis was then made with NASTRAN, using the same input deck that was used in the ASTRA analysis. The buckling load predicted by NASTRAN agreed with the collapse load determined by ASTRA.

Heat Shield Buckling. A buckling analysis was required for a heat shield on the Burner IIA missile. The shield was conical in shape, and the analysis was required as quickly as possible. The entire problem was coded within a few hours using SAIL, and the NASTRAN buckling results were obtained by the next day.

BCD/EBCDIC INPUT TRANSPARENCY

NASTRAN normally expects input data to be prepared using the BCD character set. The use of BCD characters on Boeing's IBM 360 installation (where the EBCDIC character set is standard) is inconvenient and increases the chance of keypunch error. Therefore a simple procedure was incorporated which eliminated the need for the NASTRAN user to distinguish between BCD and EBCDIC in preparing NASTRAN input.

A separate job step was added at the beginning of the NASTRAN procedure. This step executes a small, simple Fortran program which reads each card in the NASTRAN input deck, substitutes BCD characters for EBCDIC characters as necessary (only left and right parentheses, equal sign, and plus sign need be considered), and then writes the card into a data set which will become the input to NASTRAN.

This method of providing BCD/EBCDIC input transparency was very easy to incorporate and required no change to the NASTRAN program. The few additional seconds of computer time required to process the input deck are more than offset by the increased user convenience and input error reduction. Note also that the added step can easily be discarded when NASTRAN has its own BCD/EBCDIC transparency.

AUGMENTED NASTRAN USER PROC

The basic NASTRAN user procedure which is delivered with the 360 version of NASTRAN provides the user the ability to automatically obtain all the necessary JCL (Job Control Language) for making a NASTRAN run using no magnetic tapes. However, if the user wishes to make a NASTRAN run which requires tapes (e.g. a checkpoint run or a restart run), he must supply JCL to override the procedure and call for the proper tapes to be mounted.

Since the construction of error-free JCL statements tends to be difficult and confusing to the average engineer using NASTRAN at Boeing, the NASTRAN user procedure has been augmented with some additional symbolic parameters. These parameters allow the NASTRAN user to obtain JCL to mount tapes by merely coding keywords on the "EXEC NASTRAN" card. No other JCL is required. The augmented procedure makes NASTRAN much more convenient to use and practically eliminates the chance of a JCL error.

The complete list of parameters added to the user procedure includes:

T = tt. A parameter for specifying the CPU time limit of the NASTRAN step.

R = rrrK. A parameter for specifying the region size for the NASTRAN step.

NEWPROB=. A parameter to call for a tape to be mounted on the NASTRAN unit for writing a new problem tape.

OLDPROB=,OLDPTP=nnnnnn. Parameters to call for tape nnnnnn to be mounted as an old problem tape.

SC4020=. A parameter to call for a tape to be mounted for generation of SC4020 plots.

UMF=,UMFTP=nnnnnn. Parameters to call for tape nnnnnn to be mounted as a user master file.

NUMF=. A parameter to call for a tape to be mounted on the NASTRAN unit for writing a new User Master File.

To use these parameters, the user merely codes the applicable keywords, in any order, on the EXEC NASTRAN card. For example, suppose a check-point run is to be made. The EXEC card is:

```
// EXEC NASTRAN,NEWPROB=
```

The keyword "NEWPROB=" activates JCL to call for a tape to be mounted on the NASTRAN unit for the new problem tape. Likewise, if a restart run is being made to use a tape (serial number = 012345) which was generated on a previous checkpoint run, the EXEC card could be written as:

```
// EXEC NASTRAN,OLDPROB=,OLDPTP=012345
```

No additional JCL is required to mount the restart tape. If on the above restart run the user wished to specify a time limit and region size and create plots, he could code:

```
// EXEC NASTRAN,OLDPROB=,OLDPTP=012345,  
// T=15,R=560K,SC4020=
```


(Note: The EXEC card is continued in the normal manner of JCL continuation.)
Again no additional JCL is required.

The revisions required to incorporate these parameters into the NASTRAN procedure are shown in figure 3. These revisions are, of course, for the Boeing facility, but should require little modification for other 360 installations. JCL to incorporate the BCD/EBCDIC preprocessor discussed earlier is also shown in Figure 3, but the JCL necessary to implement the SAIL capability has been omitted.

CONCLUDING REMARKS

The features added to the NASTRAN user interface presented in this paper have all proven to be cost effective. The cost of implementing each item has been more than offset by the increased NASTRAN usability and the decreased input error potential. The NASTRAN program itself has not been modified at all. Instead, JCL has been modified and peripheral programs have been included in the NASTRAN system.

REFERENCES

1. Greene, Herness, Ice, Salus, and Strome, "ASTRA-Boeing's Advanced Structural Analyzer" published in "Structures Technology for Large Radio and Radar Telescope Systems", MIT Press, Mar and Liebowitz, editors.

SAIL Statements	Notes
COORDINATE SYSTEM = CYLINDRICAL	Set coordinate system to "cylindrical".
START LOOP 1 FOR I = 1,13	
START LOOP 2 FOR J = 1,5	
ID = (I-1)*5 + J	
R = (J-1)*6 + 3.0	Loops to generate thirteen groups of five nodes each. Note that the z-coordinate is calculated as a function of the radial coordinate, R.
Z = (10./729.)*R*R	
THETA = (I-1)*15	
N(ID) = (R,THETA,Z)	
END LOOP 2	
END LOOP 1	
ELEMENT TYPE = 204	Set element type to isotropic quadrilateral plate.
START LOOP 3 FOR I = 1,12	
START LOOP 4 FOR J = 1,4	
ID = (I-1)*5 + J	Loops to generate twelve groups of four quadrilaterals each. Assume that Table Entry 7 contains a list of thicknesses and a material ID for the plate elements.
S(ID) = N(ID), N(ID+1), N(ID+5), N(ID+6), T(7)	
END LOOP 4	
END LOOP 3	
T(7) = .25, .25, M(4)	Define Table Entry 7

Table 1 - SAIL Statements to Generate Input for the Parabolic Dish Shown in Figure 1.

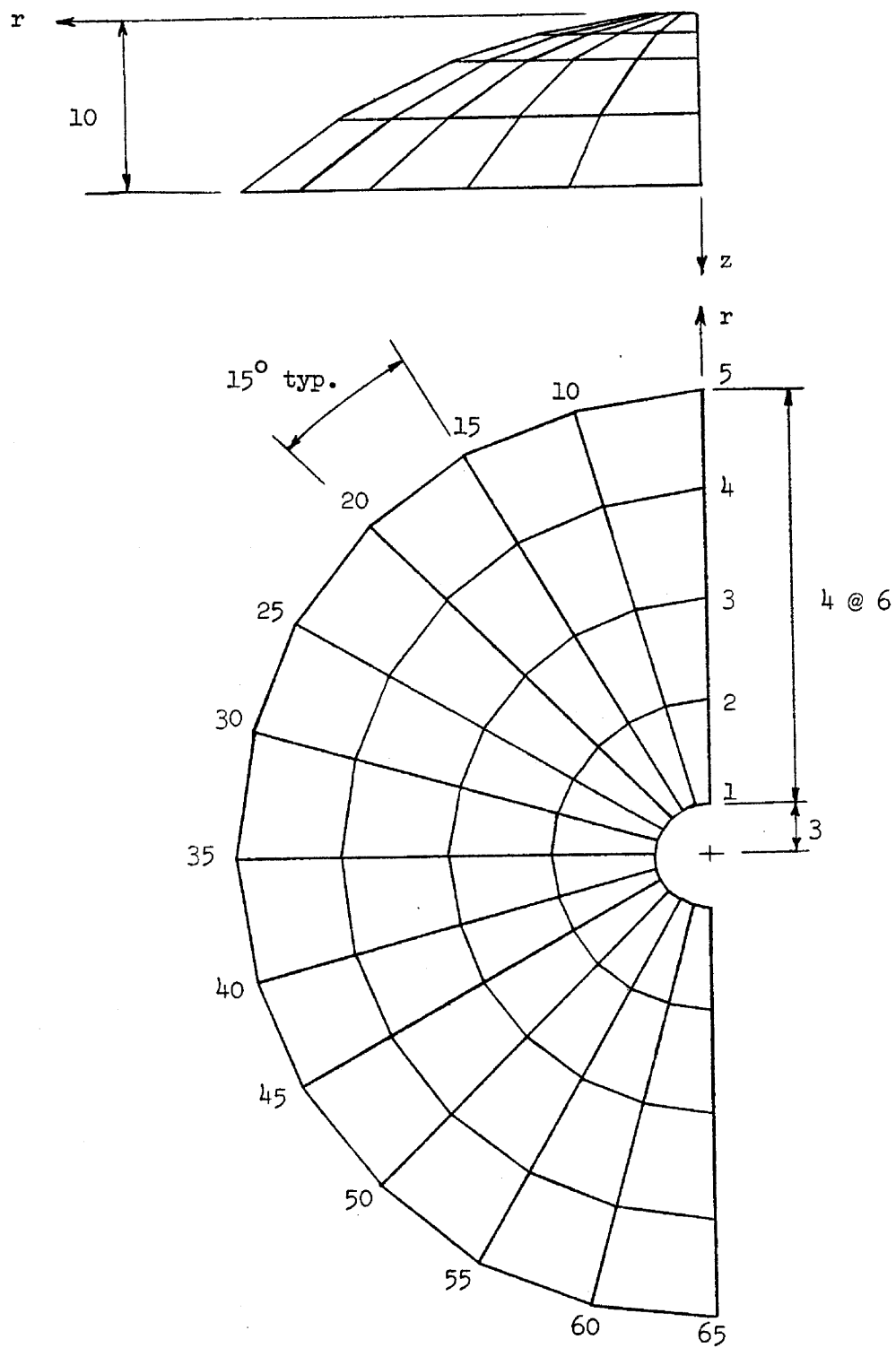
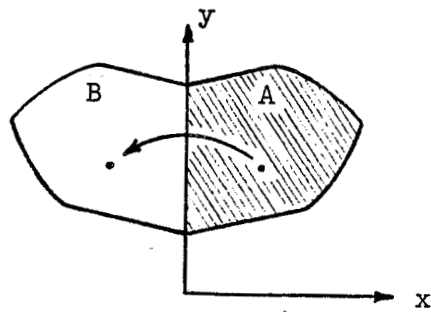
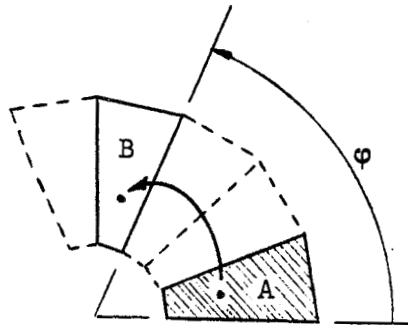


Figure 1 - Finite Element Model of a Parabolic Dish.



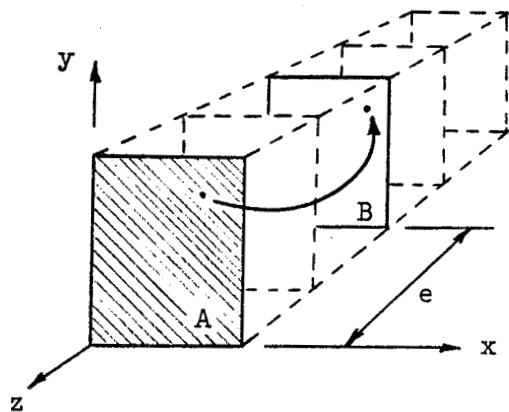
Symmetric Half:

$$\begin{Bmatrix} x \\ y \\ z \end{Bmatrix}_B = \begin{bmatrix} -1 & 0 & 0 \\ 0 & 1 & 0 \\ 0 & 0 & 1 \end{bmatrix} \begin{Bmatrix} x \\ y \\ z \end{Bmatrix}_A$$



Translation:

$$\begin{Bmatrix} r \\ \theta \\ z \end{Bmatrix}_B = \begin{Bmatrix} 0 \\ \phi \\ 0 \end{Bmatrix} + \begin{Bmatrix} r \\ \theta \\ z \end{Bmatrix}_A$$



Translation:

$$\begin{Bmatrix} x \\ y \\ z \end{Bmatrix}_B = \begin{Bmatrix} 0 \\ 0 \\ -e \end{Bmatrix} + \begin{Bmatrix} x \\ y \\ z \end{Bmatrix}_A$$

Figure 2 - Examples of Substructure Transformation.

```

//DEFAULT PROC PRINT=A,SP1=1,SP2=5,BLK1=7204,BLK2=7208,VCT=1,
//      R=350K,T=20,UMF='SYSDA,SPACE=(TRK,1) ',UMFTP=000000,
//      NUMF='SYSDA,SPACE=(TRK,1) ',NEWPROB='SYSDA,SPACE=(CYL,(1,2)) ',
//      OLDPROB='SYSDA,SPACE=(TRK,1) ',OLDPTP=000000,
//      SC4020='SYSDA,SPACE=(TRK,1) '
//INPUT EXEC PGM=PREPR,REGION=70K,TIME=3
//FT05F001 DD DDNAME=DECK
//FT06F001 DD SYSOUT=A
//FT02F001 DD UNIT=SYSDA,SPACE=(TRK,(20,40)),DSN=&&NSTNIN,DISP=(,PASS),
//          DCB=(RECFM=FB,LRECL=80,BLKSIZE=800)
//NS EXEC PGM=NASTRAN,REGION=&R,TIME=&T
//FT04F001 DD SYSOUT=&PRINT
//FT05F001 DD DSN=*.INPUT.FT02F001,DISP=(OLD,DELETE)
//          :
//          :
//FT11F001 DD DCB=(RECFM=VS,LRECL=&BLK1,BLKSIZE=&BLK2,BUFNO=1),          X
//          UNIT=&UMF.2400-3,VOL=SER=&UMFTP,DSN=XX&UMFTP,LABEL=(2,BLP),    X
//          DISP=(OLD,KEEP)
//FT12F001 DD DCB=*.FT11F001,UNIT=&NUMF.2400-3,DISP=(,KEEP),DSN=NEWUMF
//          :
//          :
//NPTP DD DCB=*.FT08F001,UNIT=&NEWPROB.2400-3,DSN=NEWPROB,DISP=(,KEEP)
//OPTP DD DCB=*.FT08F001,UNIT=&OLDPROB.2400-3,VOL=SER=&OLDPTP,          X
//          DSN=XX&OLDPTP,DISP=(OLD,KEEP),LABEL=(2,BLP)
//          :
//          :
//PLT2 DD DCB=(RECFM=U,BLKSIZE=720,BUFNO=1,DEN=2),          X
//          UNIT=&SC4020.2400-2,DISP=(,KEEP),LABEL=(,NL),DSN=SC4020

```

Figure 3 - Modifications to NASTRAN User Procedure.

PROCEDURE FOR EFFICIENTLY GENERATING, CHECKING, AND DISPLAYING NASTRAN
INPUT AND OUTPUT DATA FOR ANALYSIS OF AEROSPACE VEHICLE STRUCTURES

By Gary L. Giles
NASA Langley Research Center

and

Charles L. Blackburn
AVCO Aerostructures Div., Nashville, Tennessee

SUMMARY

Auxiliary computer routines which automatically generate input data for a wide variety of aerospace vehicles and graphically display output data in the form of contour plots have been developed for use with the NASTRAN analysis program. These routines offer a significant savings in man-hours required to develop a finite element model and to interpret the data resulting from an analysis.

The input data routines provide a capability for developing large reliable finite element models from a minimum amount of basic data pertaining to the external shape of the vehicle. For preliminary design studies, design changes can be accomplished with substantial time reductions by using such routines. In addition, the contour plots of the output data allow for rapid evaluation of the voluminous results obtained in such studies.

INTRODUCTION

The calendar time required for a finite element analysis results primarily from preparation of input data to describe the structural model. Weeks or months are often needed to prepare input for a structure containing a large number of elements, while the analysis can be performed in minutes or hours of computer time. A reduction of this input preparation time would expedite the time required for an overall design process and reduce the manpower costs required for each analysis. Furthermore, as pointed out in reference 1, the provision for automated data input is important for preliminary design in particular since excessive time for input preparation could negate the effectiveness of efficient analysis and design procedures.

An important aspect of data generation routines, especially when the finite element model contains a large number of nodes and elements, is the accuracy the automated routine provides in dimensioning the nodes, numbering the nodes

and elements, and connecting the elements at the correct nodes. Even the most careful finite element analyst has experienced difficulties with errors in such data when the input is hand generated. Another arduous task in finite element analysis is the evaluation of the multitude of results or output for the structural response of large aerospace vehicles. Since the evaluation of voluminous amounts of tabulated output data is very time consuming, the analyst tends to investigate only that data associated with areas of a structure believed to be critical, and actual critical locations may be overlooked.

Auxiliary computer routines which automatically generate the input data and graphically present the output data for the NASTRAN computer program are described in this paper. These routines were developed for use in preliminary design studies where many simplified but widely varying external shapes and internal structural configurations must be considered. Although the routines have been exercised primarily on space shuttle orbiter configurations, they are sufficiently general for application to a wide variety of aircraft configurations including hypersonic cruise vehicles and advanced technology transports. The input data generation routines require a minimum amount of user prepared data to generate a detailed finite element model. The basic input data required is geometric information which numerically describes an external shape. A fuselage, wing, and/or empennage structure can be automatically generated within this external shape.

To assist in data analysis and also to reduce the possibility of missing critical design areas, NASTRAN oriented computer routines have been developed for presenting the output in the form of contour plots. These contour plots are particularly useful for presenting stress distributions, deformation patterns, and vibration or buckling mode shapes. For structural optimization studies, the thickness variation of skins, panels, or plates can also be shown by such plots.

INPUT GENERATION

In order to perform a structural analysis of a complex aerospace vehicle, it is first necessary to construct a mathematical model of the vehicle structure from engineering drawings in a form amenable to the method of solution. For a NASTRAN analysis, the model is an idealized network of finite structural elements. A finite element model of any large structure, particularly a very complex configuration, may contain errors due to human judgment, mispunched data cards, or incorrectly transcribed data. The following discussion describes two input data generation routines which substantially reduce both the effort required to generate finite element models and the chances for input errors in the models.

Fuselage Input Data Generator

Although the fuselage input data generator was developed for fuselage type structures, it is applicable to virtually any type of stiffened shell structure. The structure is modeled as a series of stiffened shells referred to as fuselage segments. Since a complete fuselage is usually of considerable length with large cross-sectional dimensional variations, these segments allow the engineer to work with smaller and more uniform structural components. For example, it is common practice to reduce the fuselage into three segments: namely forward, mid, and aft fuselage sections.

Each segment of the fuselage model contains a prescribed number of equally spaced frames which can differ from segment to segment. The perimeter of the frames is dictated by the cross sectional dimensions of the fuselage external shape. The present routine approximates a given external shape with elliptical sections and straight lines. This approximation adequately represents the shape, requires minimum basic input data, and permits easy determination of the frame's grid point coordinates. Presently, the frames are structurally modeled with straight beam elements capable of withstanding axial, shear, and bending loads. Only minor modifications of the routine are required to implement a proposed generalization to permit representation of the frames as deep beam members modeled with shear web and cap (or rod) elements.

The number of grid points about the circumference of a frame is dictated by the number of longerons. The desired number of longerons (and hence frame grid points) is basic input data and is constant for all fuselage segments, but the spacing of the longerons (and hence the length of the frame elements) is determined within the program. To obtain an adequate geometric representation the spacing of the longerons is closer in the regions of maximum curvature of the frames and the spacing widens with decreasing curvature. Similarly, the straight beam elements used in the frame modeling are shortest in the areas of increased curvature, and they lengthen with decreasing curvature. The longerons are idealized as axially loaded rod elements of length equal to the frame spacing.

With the shape of the frames determined and the number of longerons and frames specified the mesh size or nodal network of the finite element model is readily determined for a particular fuselage segment. The location of each grid point within the overall fuselage structure is defined by a numbering scheme which identifies the segment, frame, and longeron position corresponding to the point. The coordinates of the grid points so determined by the routine are output on punched cards in the proper format for incorporation into the NASTRAN computer program.

To complete the finite element model the surface or skin of the fuselage is represented by plate membrane elements. The size of these elements is dictated by the mesh generated for the frames and longerons. Although the fuselage input data generator does not consider the offset of the rod and beam elements relative to the plate elements' midplane, it could be readily modified

to account for the offset by using features within the NASTRAN program. Finally, the connecting data for the entire set of structural elements is generated and punched on cards with a NASTRAN format.

The method described in reference 2 is used to define the external (aerodynamic) shape of an aerospace vehicle. A finite element structural model is generated inside this shape using the data generation routines. Figure 1 shows the external shape definition of one concept of a space shuttle orbiter configuration and the corresponding finite element model of a segment of the fuselage structure containing 1400 degrees of freedom. User prepared input was 70 cards to define the external shape of the fuselage, and 15 cards for the structural model description. The resulting NASTRAN input deck that was automatically generated and punched contained 1513 cards. The effort required to generate the model from engineering drawings using the methods of this paper was less than 4 man-hours.

Wing and Empennage Input Data Generator

As in the case of the fuselage data generator a simplified input option is desired for describing the structural arrangement of the wing within an external aerodynamic shape. Such a program would serve as input data generator for both wing and empennage structures (horizontal and vertical tail) since the structural arrangements of these components are similar. For the sake of brevity only the wing will be referred to in the description of this routine.

Figure 2 shows a structural arrangement for the wing and carry through structure corresponding to the shuttle orbiter external wing shape shown in figure 1. The numbered points indicate the corners of various substructures having quadrilateral (for example, 8, 11, 12, 9) and triangular (for example, 3, 7, 4) planforms which are used for describing the total wing planform. The corner point locations of the substructures are physically specified by values of percent chord and fraction of semispan. In general, these substructures include many finite elements used to represent the actual structural members corresponding to ribs, spar, and cover sheets.

For the particular configuration shown, certain interior spars intersect the leading edge spar, whereas all ribs are parallel to the orbiter centerline. The number of ribs and spars in a substructure are specified by the user utilizing a numbering scheme for the corner points. This numbering scheme is based on a five digit number in which the first two digits represent a particular rib, the second two digits represent a particular spar, and the fifth digit designates whether the corner point is on the upper or lower surface (1 for upper, 2 for lower). The ribs and spars are numbered consecutively from inboard to outboard and from leading to trailing edge, respectively. For example, corner point number 8 of figure 2 would be designated as 10071 corresponding to the intersection of the tenth rib and seventh spar on the upper surface. From the numbering scheme the program can determine the number of spars or ribs which intersect the sides of the substructure. These spars and ribs are then equally spaced along the sides and their grid points are calculated from the

physical dimensions of the corner points. The elevation or z-coordinate variation of the wing (indicating twist or camber) is determined from the external shape definition. The program yields this data in punched card form with a NASTRAN grid card format.

Having generated the nodal network for the wing, the routine automatically generates the appropriate NASTRAN element cards. The finite element model consists of plate membrane elements for the upper and lower wing skins and plate shear elements for the ribs and spars. Presently, the program does not account for cap members or vertical stiffeners attached to the ribs and spars. In order to maintain stability of the shear plate elements, a NASTRAN multi-point constraint card is generated to give equal vertical deflections for similar grid points on the upper and lower surfaces. To account for variations in thickness of the various elements, appropriate NASTRAN property cards are punched for each finite structural element.

For the structure shown in figure 2, which has 911 degrees of freedom, 30 basic data cards were required to describe the external shape and 38 cards were required to generate a NASTRAN input deck of 1577 cards. Less than 2 man-hours were required to generate the finite element model.

GRAPHIC OUTPUT

Although the NASTRAN program has a capability for making plots for both the undeformed and deformed structures, one must resort to the tabulated output to determine the magnitude of the displacements. It is sometimes difficult to visualize the node lines from such plots of higher order vibration and buckling modes. Furthermore, only the tabulated data for the stresses acting on each structural element is available in the NASTRAN output.

The interpretation of NASTRAN output data can be facilitated by presenting the data in the form of contour plots. Such plots make it possible for the knowledgeable design engineer to identify immediately the critical design areas, and they greatly facilitate evaluation of the large amounts of data generated in a typical NASTRAN analysis. The following discussion describes a routine for efficiently generating displacement and stress contour plots directly from NASTRAN punched input and output data for surfaces with irregular boundaries representative of current aircraft wing planforms.

Contour Plot Program

All NASTRAN output data are given with respect to a grid point or structural element. The locations of the grid points or elements are specified in the NASTRAN input data deck, and for the most general case the locations are described by three-dimensional coordinates. Therefore, to form contour plots for a particular surface or planform, only output data corresponding to grid points or elements on that surface or planform would be used. In the following discussion the grid point or centroid of the structural element will be called a

control point for convenience of description. Also, the NASTRAN output data such as stresses, displacements, and mode shapes will be referred to as the magnitude or elevation of the contour surface.

Since contour plots represent lines of constant elevation or magnitude of a surface with respect to a datum plane, it was first necessary to develop an analytical model that adequately described the contour surface. The model chosen was based on a series of connected triangular planes having coordinates at each vertex coincident with both the two dimensional control point coordinates and the magnitude of the contour variable. These triangular planes offer two distinct advantages: namely, (1) a simple analytical expression for describing the flat plane and (2) easily obtained coordinates of the plane using NASTRAN input and output data for triangular and/or quadrilateral plate elements. The quadrilateral elements are idealized as two triangular elements for development of the contour surface. Another advantage, due to the formulation of the problem, is the increased accuracy of the surface as the mesh size decreases to obtain a desired accuracy for the structural analysis.

With the contour surface idealized as a network of triangular plane segments, the contour lines can be developed in a straightforward manner using the following computation scheme. For a finite element analysis calculated displacements are associated with the actual grid points. Hence, for a certain triangular contour plane the maximum and minimum elevation (values of displacement) at the vertices (grid points) are determined from the NASTRAN data corresponding to the particular element. These maximum and minimum values and the specified contour interval are used to calculate the number of contour lines and their magnitude occurring in the triangular plane. Area coordinates are used to determine the intercepts of the contour lines with the edges of the triangular plane. By proper manipulation of the area coordinates the intercepts of the previously calculated contour lines with the edges of the triangular plane can be determined in terms of the datum plane coordinates. A contour line will have intercepts at two edges of the triangle, and the plot routine connects a straight line between these intercept points. This method is then generalized to calculate all the contour lines within a triangular plane for every triangular plane of the contour surface contained in a prescribed boundary.

The stress data resulting from a finite element analysis is associated with the elements rather than the actual grid points. For data reduction the stresses are assumed to be acting at the centroid of the element. In addition to the control points located at the elements centroid, other control points coinciding with the grid points are also used. The magnitude of the stress at a particular grid point is determined from a weighted average of the appropriate stress values associated with those elements connected at the grid point. This increase in the number of control points results in a finer mesh of triangular planes for describing the stress surface than for the displacements. These triangular planes are constructed in such a way that each interior element contains a weighted stress value at one of its vertices. For those triangular planes adjacent to the structure's boundary two vertices are based on weighted data; hence, near a boundary the contour lines are of questionable accuracy.

Illustrative Examples

To illustrate the potential value of these contour plots for numerically representing the deformed structural shape, a NASTRAN static and vibration analysis was performed for the space shuttle orbiter type wing shown in figure 2. The wing carry-thru structure was allowed to deflect only in a direction normal to the plane of the wing along the orbiter center line (line 1-2, fig. 2). The leading edge tip of the wing root (point 3, fig. 2) and the intersection of the wing and wing carry-thru (line 5-6, fig. 2) were constrained to have zero deflection normal to the plane of the wing. The displacement pattern for the wing static displacement under a uniform pressure distribution on the exposed wing box is presented in figure 3. Vibration mode shapes for the first six modes are presented in figures 4 to 9. These results show the relationship between two different methods of graphic output. The upper drawing in each figure is a contour plot of the displacement. The lower drawing in each figure is the corresponding NASTRAN oblique plot of the deformed structure. Note that even the complex shape of the sixth mode is well represented by the contour plot. The magnitudes of the contour labels have been scaled for ease of presentation and hence show only relative magnitudes. The contour charts make it possible to perform an immediate numerical evaluation of the NASTRAN displacement data. These contour plots present the essential data from approximately 90 pages of tabulated data. A planned revision of the program will emphasize the node lines (zero deflection) by dashed lines for contour plots of vibration or buckling modes.

A stress distribution based on the von Mises effective stress criterion is shown in figure 10 for the upper surface skin of the wing structure shown in figure 2. This stress contour plot represents 3 pages of tabulated data. Again, the magnitude of the contour lines have been scaled for ease of presentation. The contour chart readily identifies stress concentrations and regions of maximum stress. Since the membrane stress of a plate element is proportional to the element's thickness, a plot similar to figure 10 could be used for showing the thickness variation resulting from structural optimization studies.

CONCLUDING REMARKS

Auxiliary computer routines which automatically generate input data for a wide variety of aerospace vehicles and graphically display output data in the form of contour plots have been developed for use with the NASTRAN analysis program. These routines offer a significant savings in man-hours required to develop a finite element model and to interpret the data resulting from an analysis.

The input data routines provide a capability for developing large reliable finite element models from a minimum amount of basic data pertinent to the external shape of the vehicle. For preliminary design studies, design changes can be accomplished with substantial time reductions by using such routines. In addition, the contour plots of the output data allow for rapid evaluation of the voluminous results obtained in such studies.

REFERENCES

1. Giles, Gary L.: Procedure for Automating Aircraft Wing Structural Design. Journal of the Structural Division, ASCE, Vol. 97, No. ST1, Proc. Paper 7821, Jan. 1971, pp. 99-113.
2. Craidon, Charlotte B.: Description of a Digital Computer Program for Airplane Configuration Plots. NASA TM X-2074, 1970.

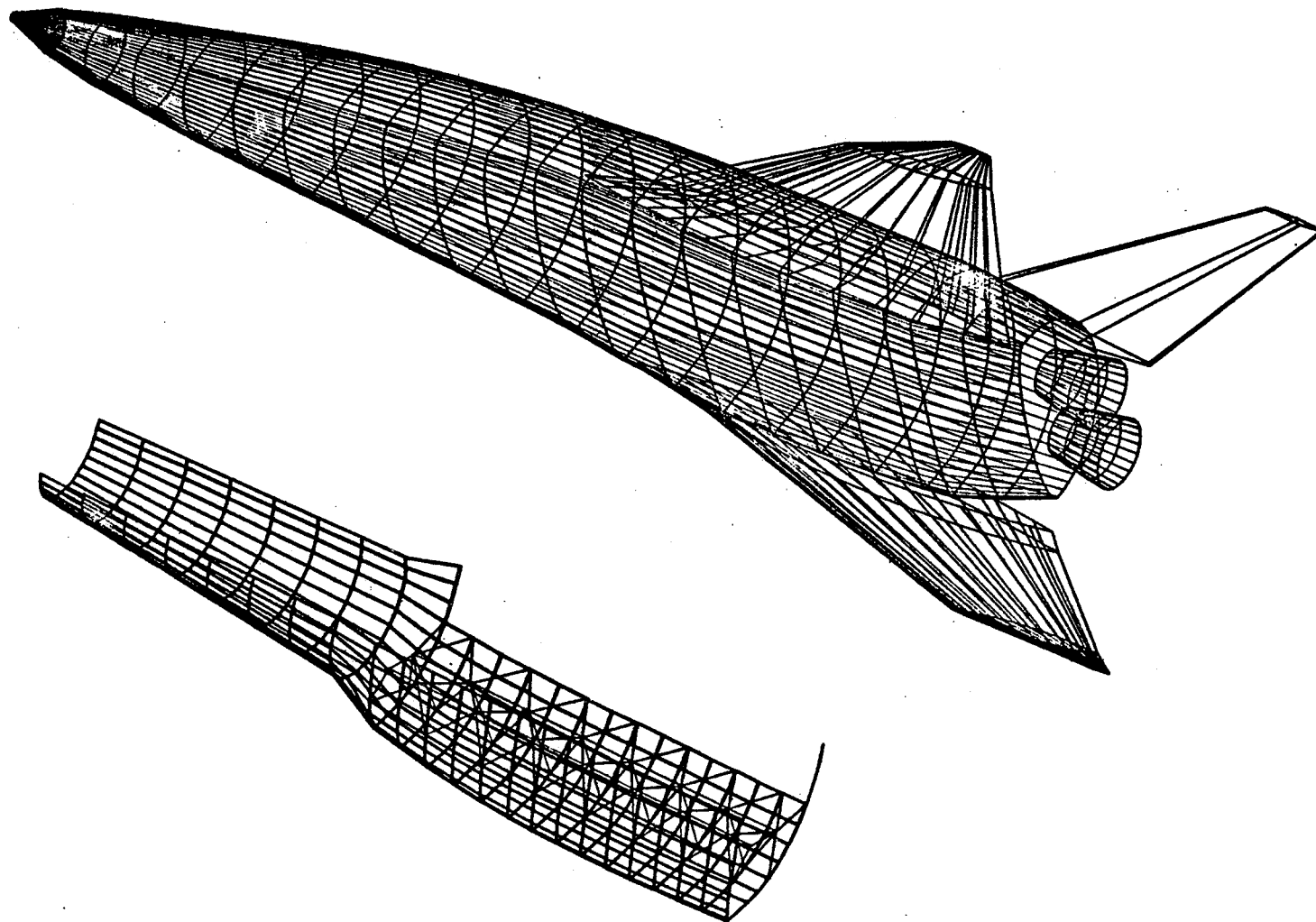


Figure 1.- Numerical external shape of space shuttle orbiter and the
finite element model for a segment of its fuselage structure.

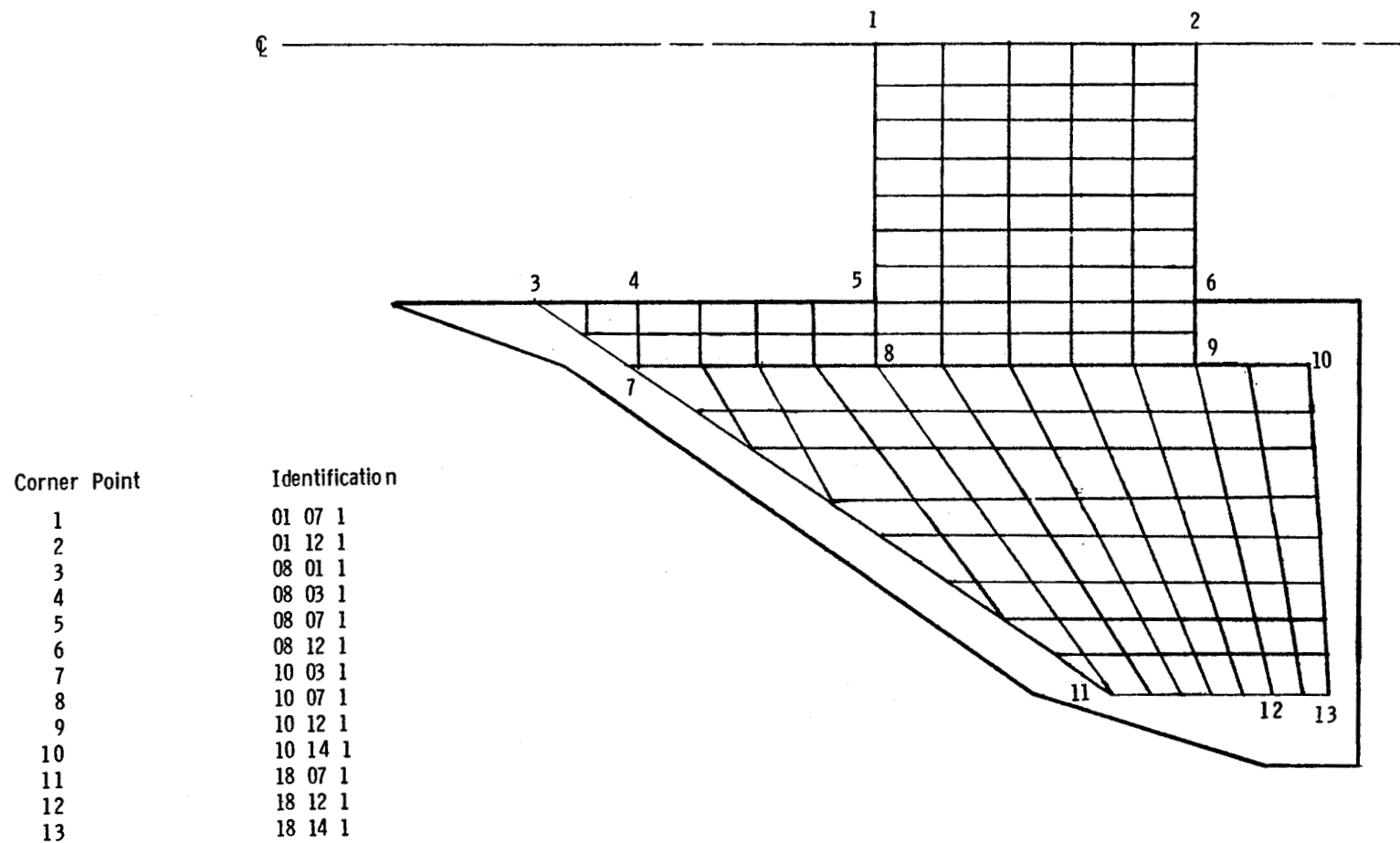
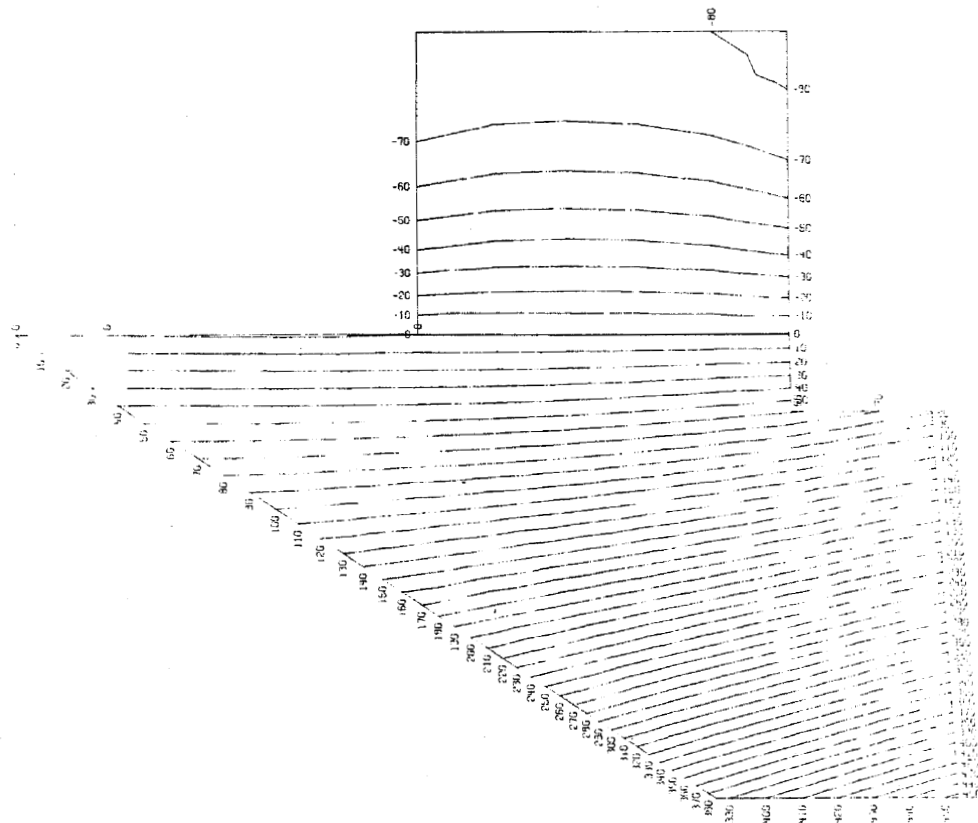
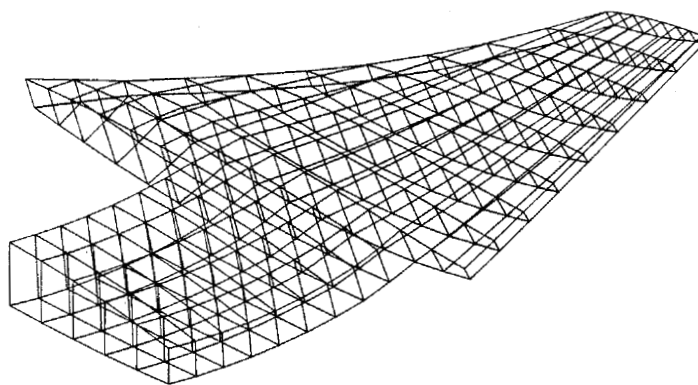


Figure 2.- Finite element model of a wing structure within the external shape of a space shuttle orbiter wing.

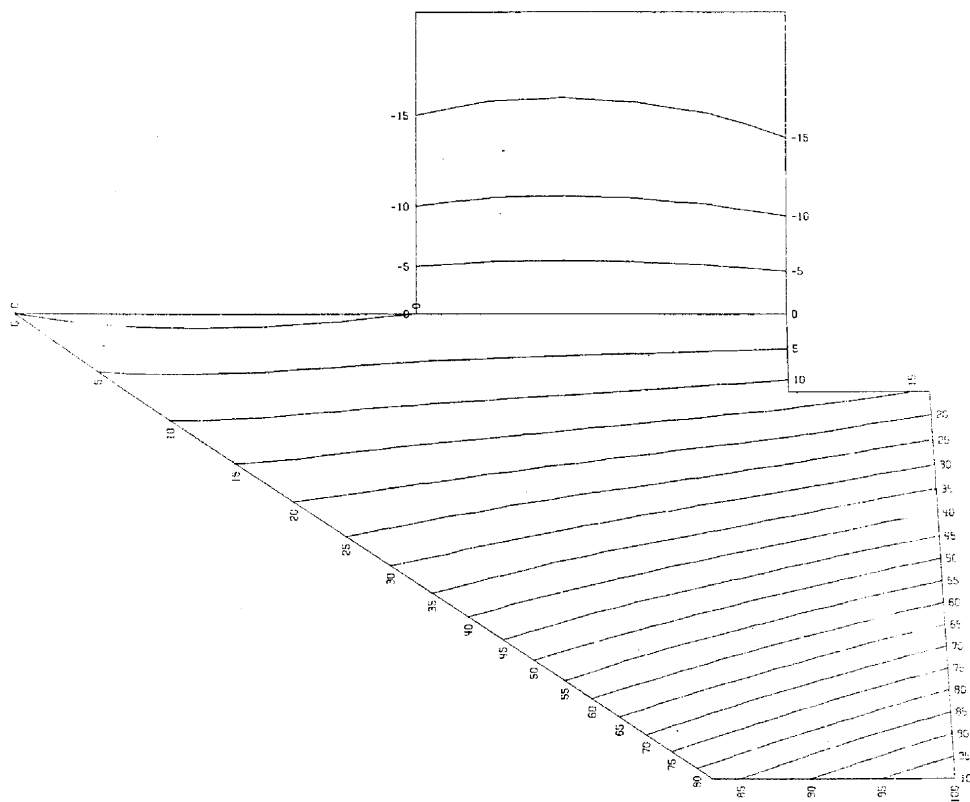


(a) Contour plot.

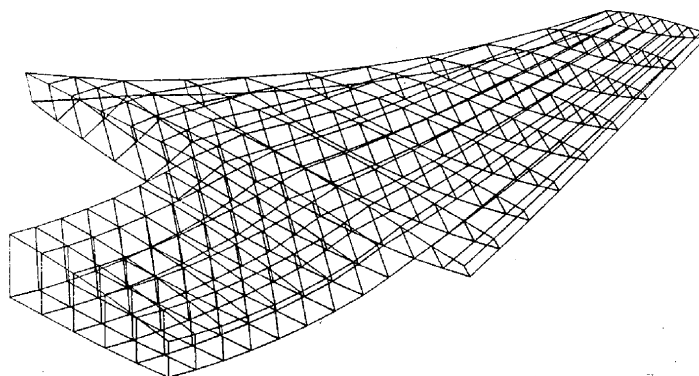


(b) NASTRAN plot.

Figure 3.- Static deflection of a space shuttle orbiter wing subjected to a uniform pressure loading.

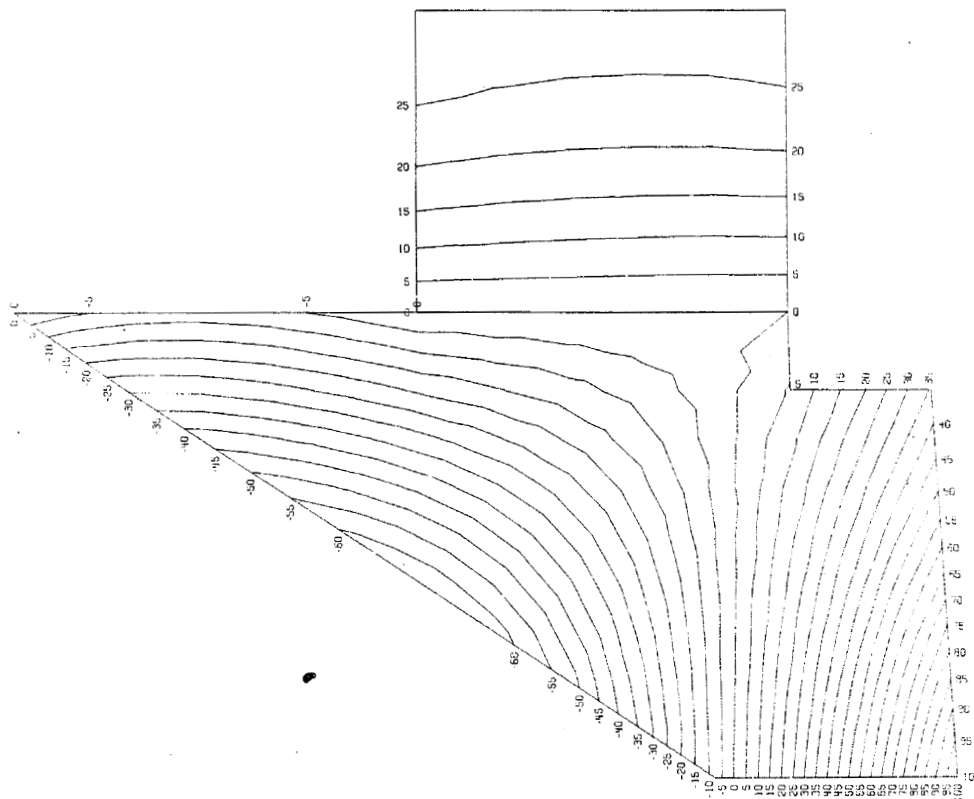


(a) Contour plot.

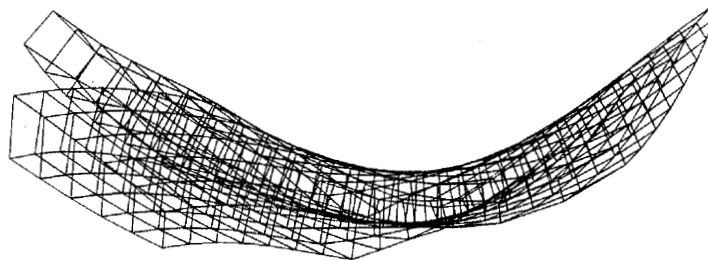


(b) NASTRAN plot.

Figure 4.- First vibration mode shape of a space shuttle orbiter wing.

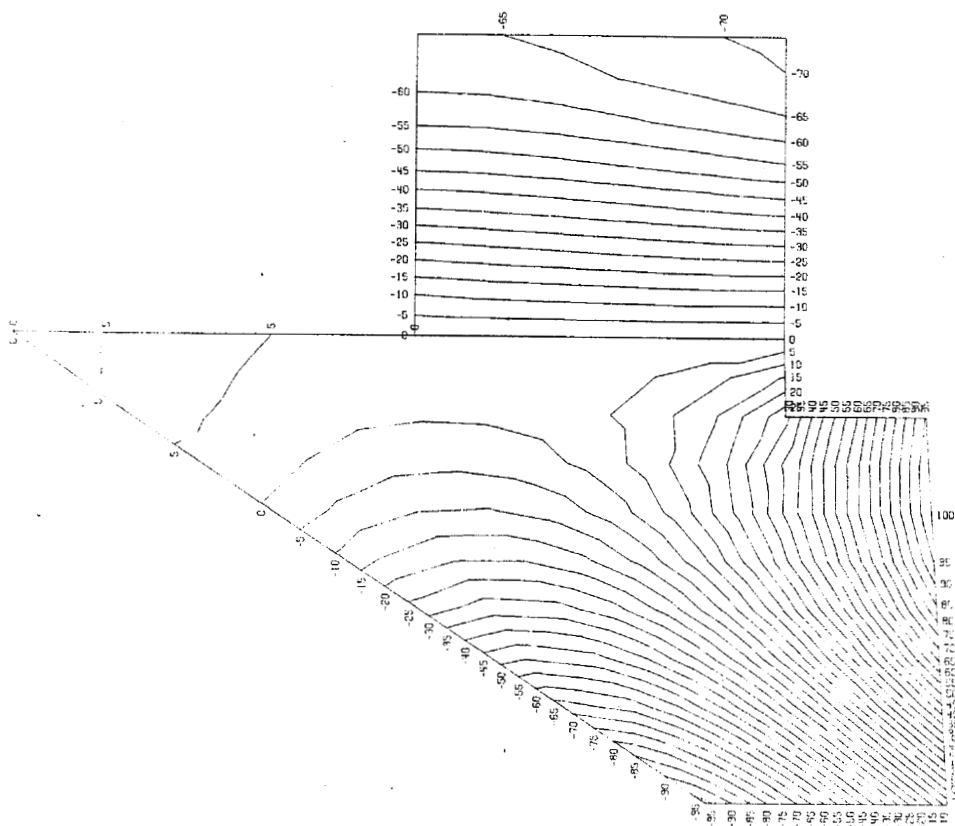


(a) Contour plot.

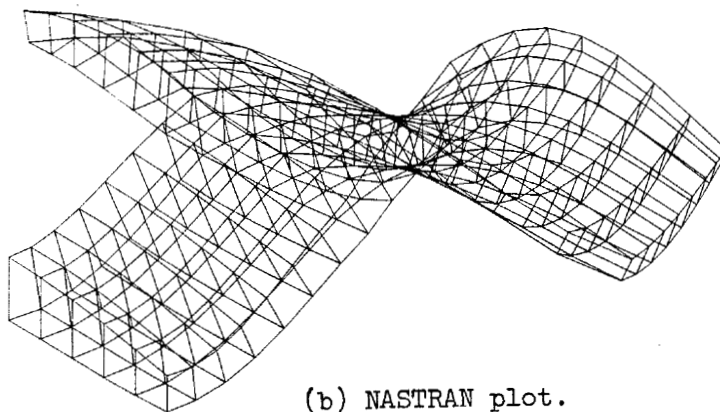


(b) NASTRAN plot.

Figure 5.- Second vibration mode shape of a space shuttle orbiter wing.

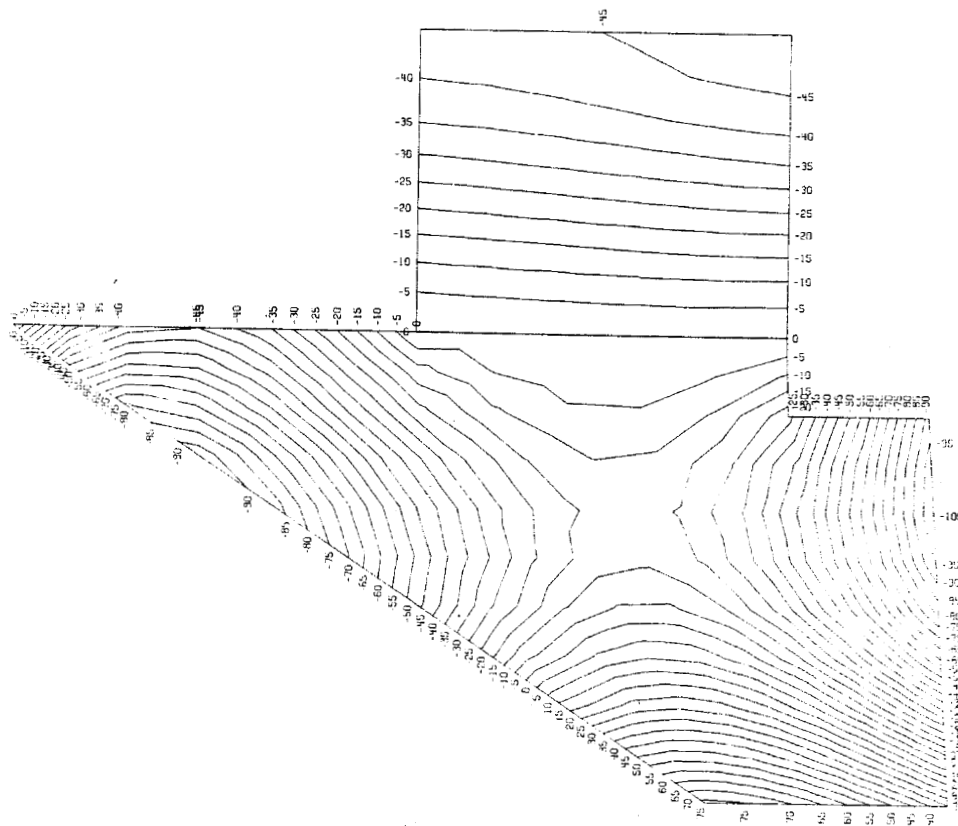


(a) Contour plot.

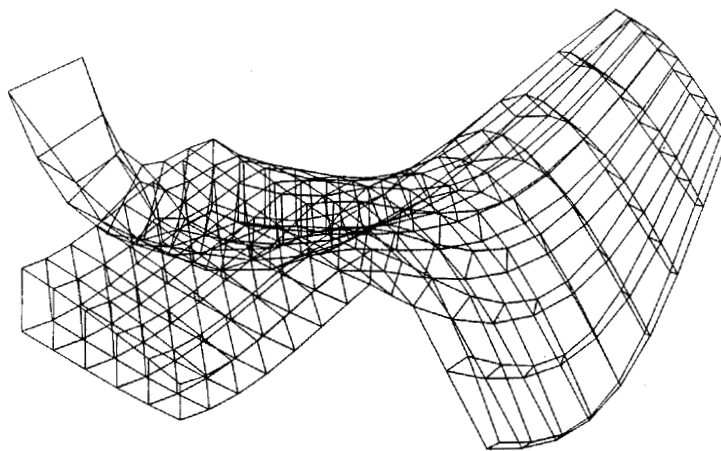


(b) NASTRAN plot.

Figure 6.- Third vibration mode shape of a space shuttle orbiter wing.

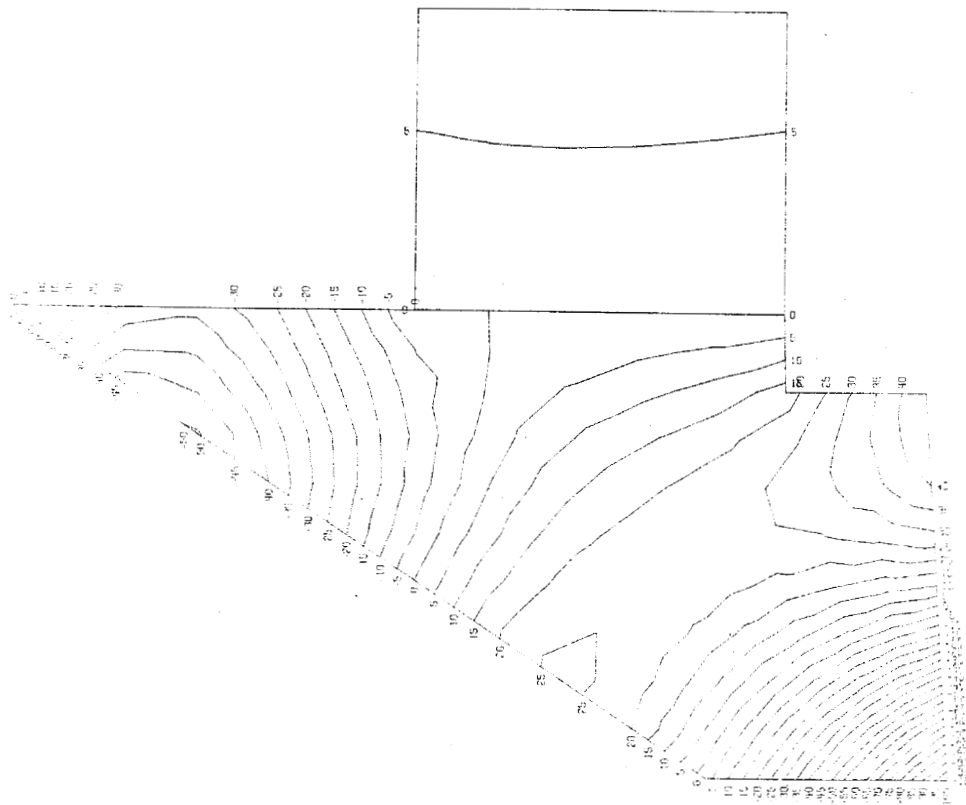


(a) Contour plot.

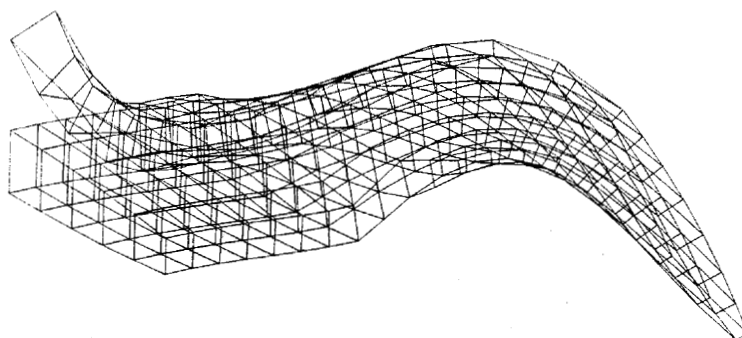


(b) NASTRAN plot.

Figure 7.- Fourth vibration mode shape of a space shuttle orbiter wing.

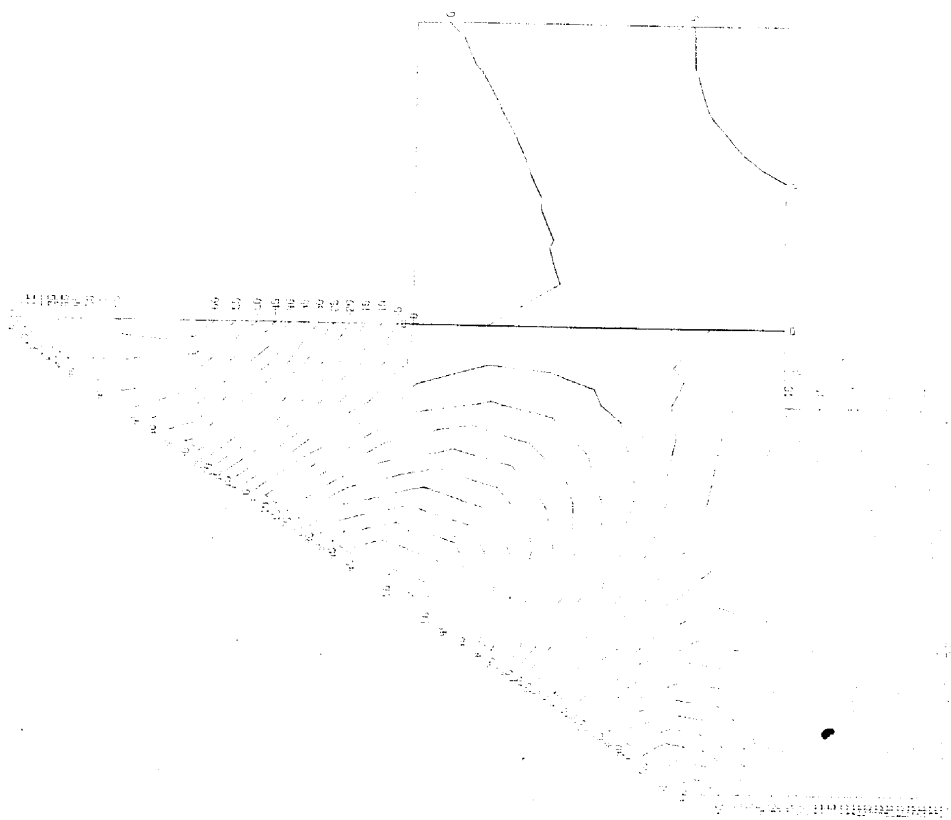


(a) Contour plot.

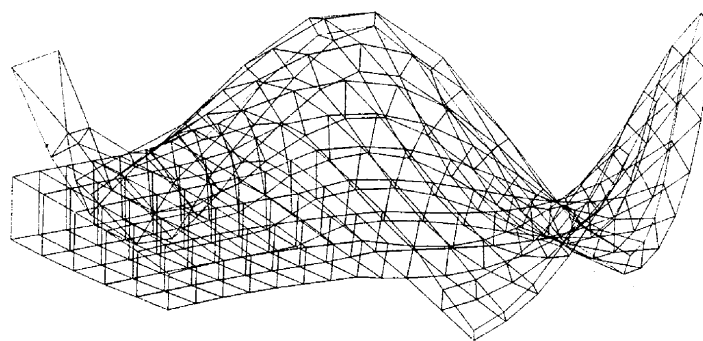


(b) NASTRAN plot.

Figure 8.- Fifth vibration mode shape of a space shuttle orbiter wing.



(a) Contour plot.



(b) NASTRAN plot.

Figure 9.- Sixth vibration mode shape of a space shuttle orbiter wing.

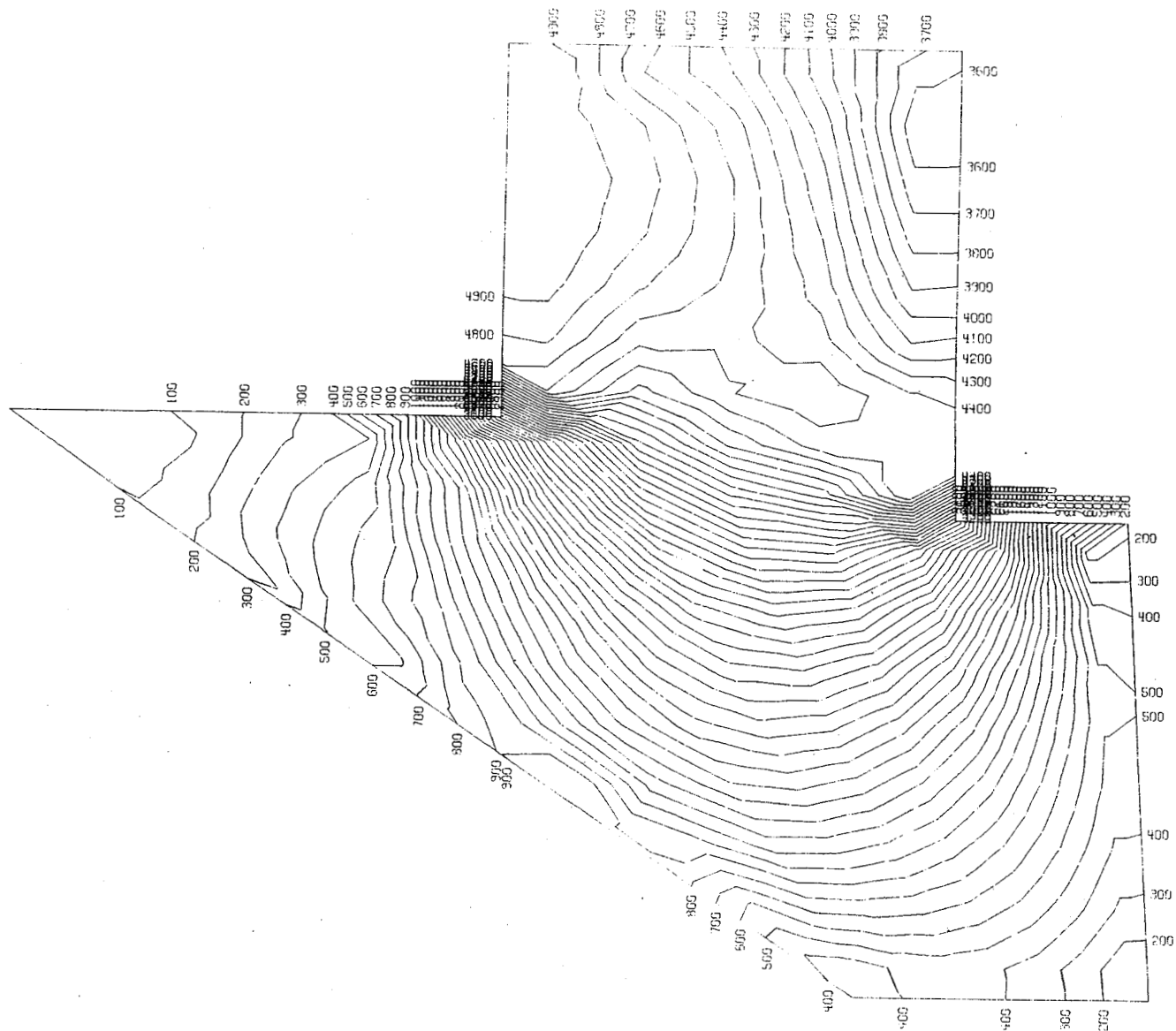


Figure 10.— Distribution of stress magnitude given by Von Mises' effective stress for a space shuttle orbiter wing subjected to a uniform pressure loading.

VEHICLE STRUCTURAL ANALYSIS -
PRE AND POST PROCESSOR DATA HANDLING

By T. Furuike and S. Yahata

North American Rockwell, Space Division

SUMMARY

Present finite element structural analysis capability has progressed to such a point that complex structures are described by tens of thousands of degrees of freedom. This places an increasing burden on the engineer in terms of quantity of data (both input and output). The nature of the design process requires the ability to update and change during the analysis. Pre processors, post processors and multiple level substructuring programs, in support of the general finite element program, partially fulfill these needs. The use of these auxiliary programs indicates a need for further developments to NASTRAN.

INTRODUCTION

The Shuttle Program is a good example of a large complex structural system consisting of multiple bodies, (namely the booster and orbiter vehicles), that requires the model-modal-loads-stress (MMLS) solution. It would take many tens of thousands of degrees of freedom with extremely wide, sparsely banded stiffness matrices to have a fairly detailed mathematical model of the vehicles. The NASTRAN (Refs. 1-3) program is a general purpose digital computer program for the analysis of large complex structures. There are many other existing structural analysis computer programs that are not as general as NASTRAN. Use of the NASTRAN program without aid of various pre and post processors is likely to lead to many human errors. The NASTRAN DMAP option to include auxiliary programs does exist. The data handling problem increases at a more rapid rate than the increase in degrees of freedom. The generation of satisfactory mathematical models will be assured with a greater degree of certainty with the aid of these auxiliary programs. Furthermore, the use of programs like NASTRAN without the availability of multiple level substructuring for analyzing the mated configuration will be costly in money and schedule time.

In order to help the engineer in performing structural analysis, an automated computer program logic to determine the model-modal-loads-stress (MMLS) solution is presented in Figure 1.

PRE PROCESSOR DATA HANDLING

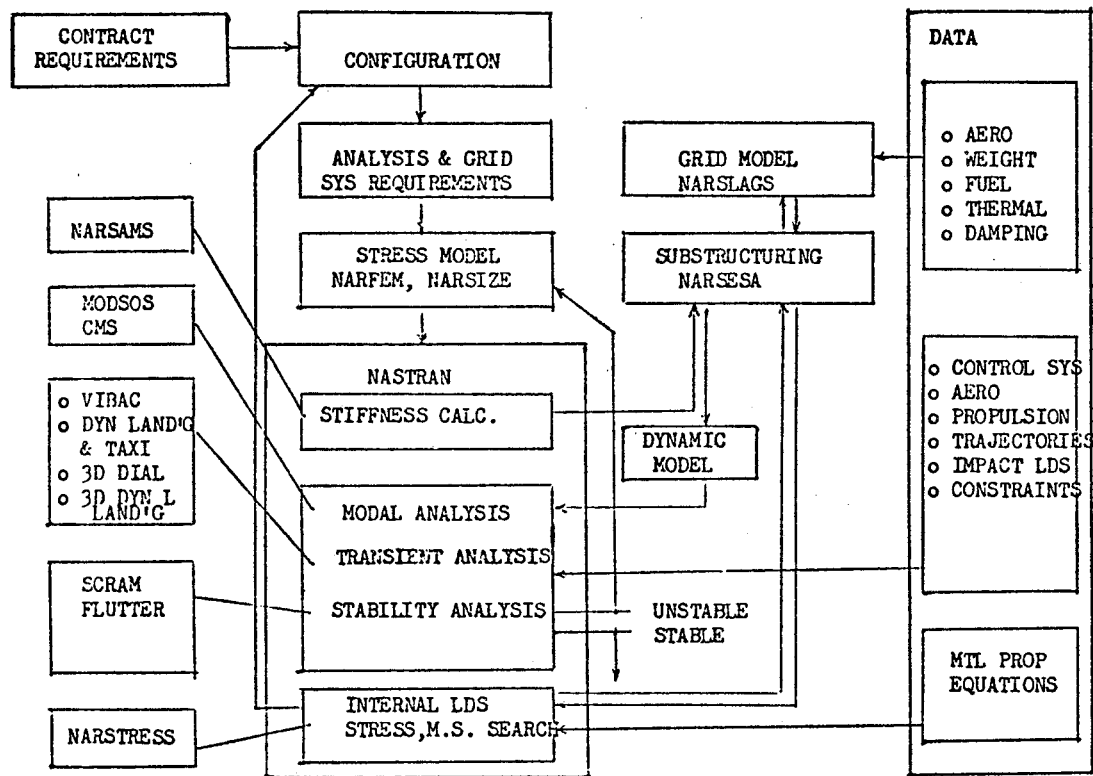
Finite Element Model

As the structure becomes large and complex, the need for pre processor data management becomes very important. Initially, an automated stress model is generated by the finite element modeling computer program called NARFEM (North American Rockwell Finite Element Model) (Ref. 4). The model generation provides for an accurate production detail model, assists manual check, reduces and eliminates many human errors and provides models compatible with preliminary and finalized design. The NARFEM program (see Figure 2) is an essential tool to obtain the necessary output data for a minimum amount of command input. These data may represent hundreds or thousands of input cards describing the finite element model (geometry, mesh topology, element description).

The topology need not be well ordered. The automated modeling generator reduces the data handling by using the following: (a) an internal numbering system to take advantage of any regularity even in highly irregular structures; (b) an internal computation of coordinates of many nodes from a minimum of geometric parameters; (c) mesh topology generation by taking advantage of the regularity of the internal numbering sequence; (d) simply controlled renumbering systems that convert topology to irregular actual patterns. In order to provide a visual check, the NARFEM program produces CRT plots of each model. The options provided include the capability of generating various line diagram representations of the mesh topology. For example the "beams only" plots can be separated from "triangular and quadrilateral elements only" in order to help the engineer check of missing elements.

The NARFEM program can read in existing modeling data which the user may wish to modify in order to study alternate design concepts on any portion of the original model. Figure 3 shows a typical structure in which the "erase" and "patch" features of NARFEM were applied to a detailed door model. Here the program performed the changes in the third quadrant and then rotated 90° to formulate the desired fourth quadrant. Figure 3 also illustrates a typical CRT plot of the automated node numbering of the door section.

Figure 1 - NR/SD SYSTEM (MODEL MODAL LOADS STRESS)



SUPPORT PROGRAMS

- 3D DIAL 3 DIMEN DYNAMIC INTERACTION OF AUTOPILOT WITH LOADS
- NARFEM GEOM-PROCESS
- NARSESA MULTIPLE LEVEL SUBSTRUCTURING
- NARSIZE ELEMENT SIZING
- NARSLAGS STRUCTURAL LOADS AND GRID
- VIBAC VIBRATION AND ACOUSTICS
- NARSTRESS STRESS SEARCH AND M.S.
- NARSAMS FINITE ELEMENT PROGRAM
- SCRAM STABILITY PROGRAM

NARFEM

(FINITE ELEMENT
MODELING SYSTEM)

AUTOMATICALLY GENERATES
DETAILED STRUCTURAL MODELS
for use in finite element
stiffness methods programs

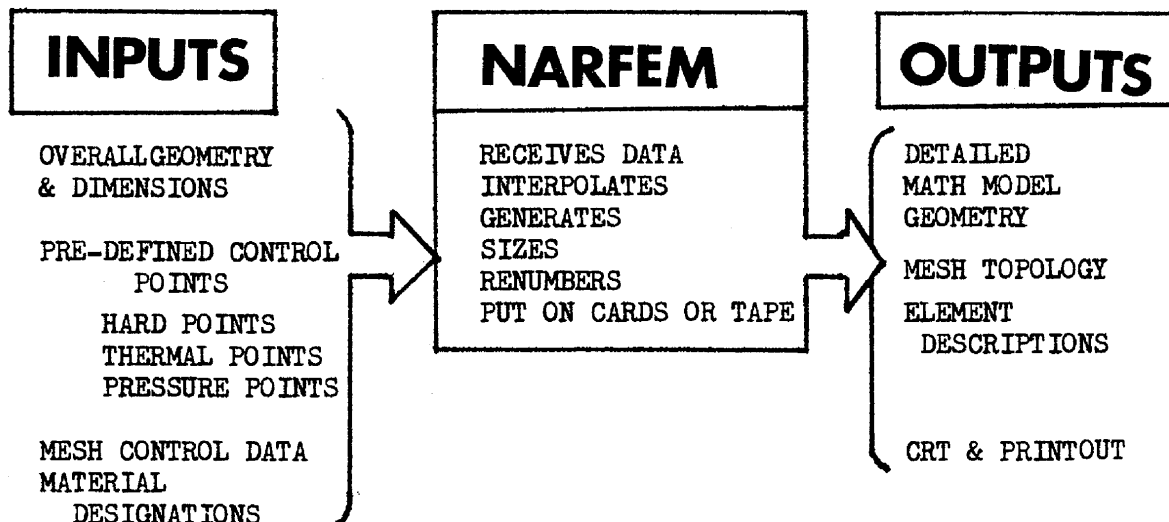


Figure 2 - FINITE ELEMENT MODELING SYSTEM

Figure 3 - "ERASE-REPLACE" FEATURE EXAMPLE ON A DETAIL DOOR MODEL.

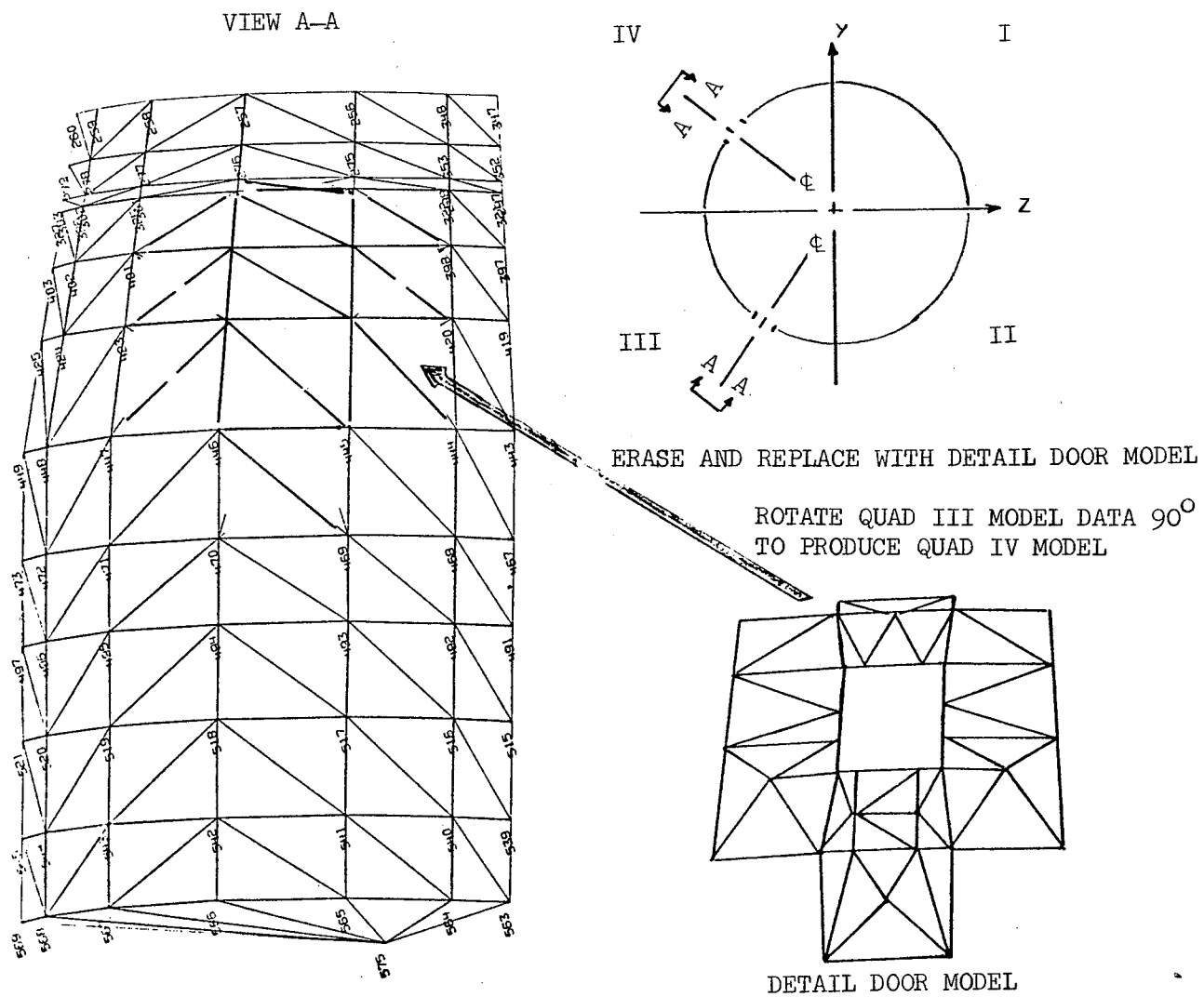


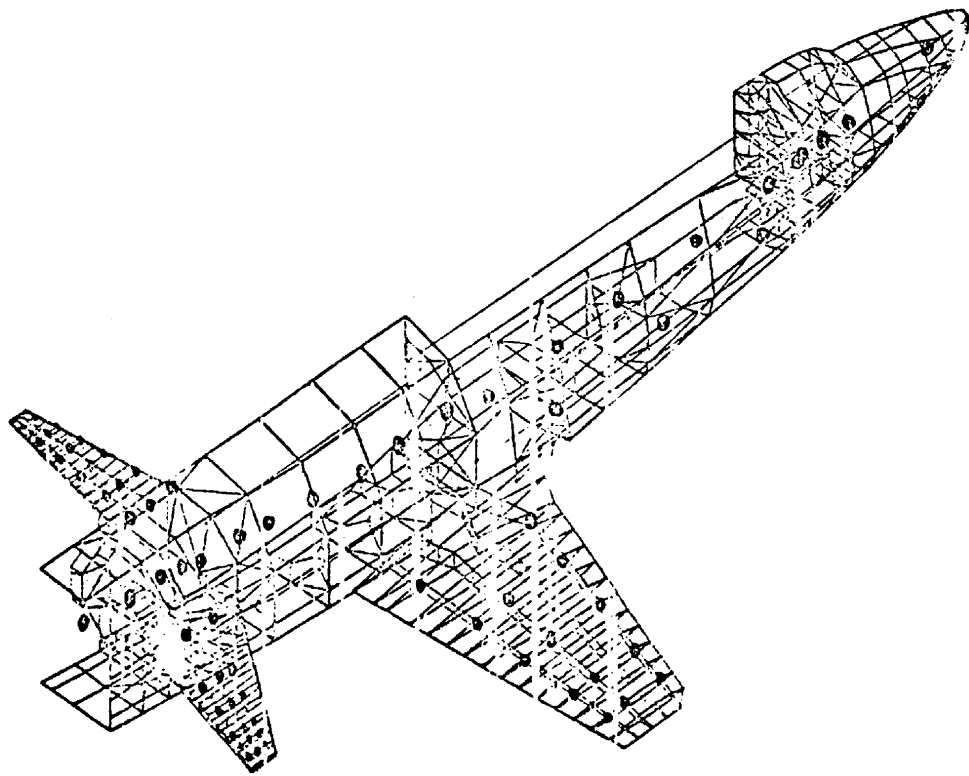
Figure 4 illustrates a rotated three dimensional view of the spacecraft orbiter model. Here only the symmetric half of the model is generated. The large dots shown in the figure indicate the points on the model which were retained for the dynamic model.

Print out review may reveal situations in which the nodes should be renumbered. NARFEM can renumber nodes and elements to reduce the unwanted wide banded matrices. The program can also remove any extraneous nodes or change the numbering order. The model generator provides punched card output which can be used as input to programs like NARSAMS (Ref. 5). The output information includes element description, coordinate or grid cards, etc. From these and other control cards the stiffness matrix in free-free or reduced state is generated.

The NARSLAGS program (North American Rockwell Structural Loads Analysis Grid System) will generate loads for the stress model from input data of selected points. Figure 5 shows a typical illustration of the aerodynamic input to create the loads idealization for the dynamic and stress models. In general the dynamic model requires fewer degrees of freedom than the stress model. The NARSLAGS program also generates the loads due to structural weight. Both distributed mass and concentrated mass can be handled to formulate the mass matrix. The output of the structural loads program is available on cards, tape, and/or printed form.

Multiple Level Substructuring Approach

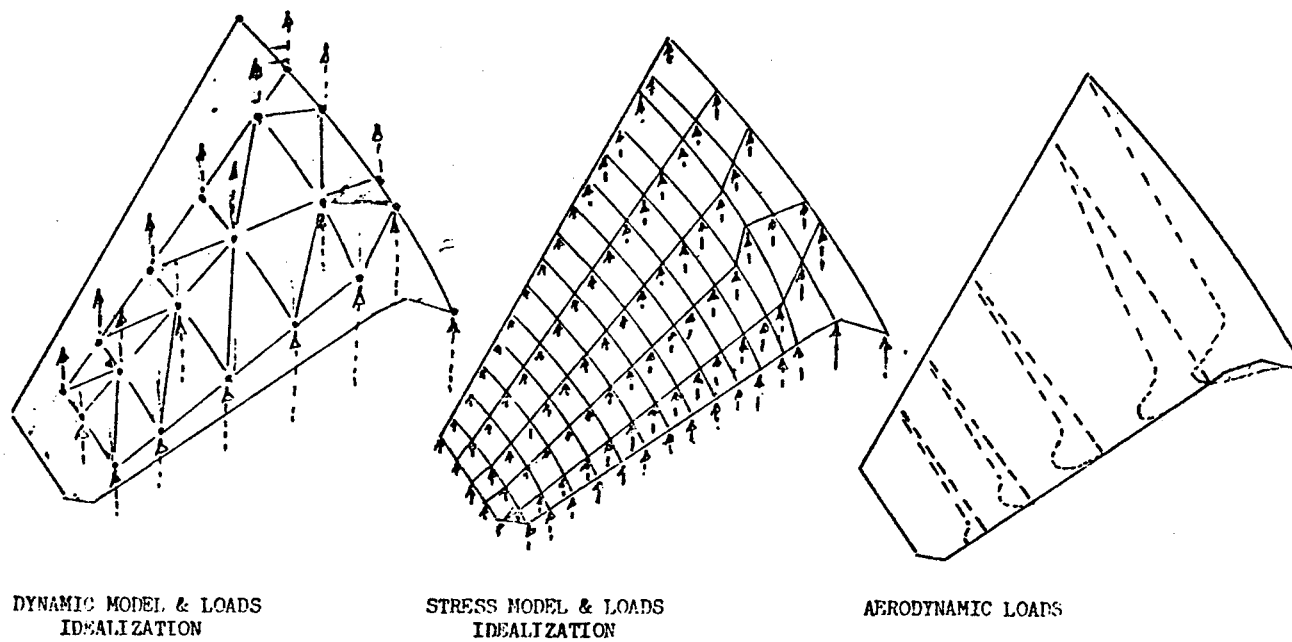
Many configuration requirements almost dictate the necessity of a multiple level substructuring analysis program. This can help reduce the cost of the MMLS analysis, to reduce errors, and to meet contract schedule requirements of various components, subassemblages and assemblages. For intermediate structures, the need for single level substructuring may be satisfactory. Reference 6 suggests the need of a substructuring program as an auxiliary processor to NASTRAN. The NARSESA program (which stands for North American Rockwell Structural Elastic Substructuring Analysis) is a multiple level substructuring program (see Refs. 7 and 8). The multiple level analysis of reference 7 is an extension to reference 9. Many user's options exist. The program can be used for substructuring as well as a matrix manipulator for reordering, gathering, decomposing, and reducing large matrices that must be handled in and out of core.



MODE ASPECT RY RZ PROJECTION RX 0.0 RY 45.0 RZ -45.0

Figure 4 - TYPICAL THREE-DIMENSIONAL MODEL ILLUSTRATING A ROTATED CRT
PLOT VIEW

Figure 5 - TYPICAL LOAD IDEALIZATION MODELING



Various product matrices obtained during the subset development are saved for future substructuring steps. Since a great portion of the computer time is spent on the decomposition, considerable effort was made to have an efficient matrix algorithm. A partitioned blocked data set technique was used to decrease the input/output data handling. The same blocking technique was applied for the forward and backward sweeps in the Cholesky-reduction routine.

The NARSESA program performs an automated coordinate description check between mating substructures prior to any assembly to assure that the mating nodes are compatible in spatial coordinates. The node numbers are generally not the same at mating boundaries since each substructure may be numbered independently of one another. An option was included to either manually order the rows or let the program automatically order the rows during gathering. This renumbering essentially reduces the combined assembly boundary matrix bandwidth. Hence, the computer time for decomposition decreases sharply. The substructuring program will automatically keep track of all degrees of freedom at all levels and assemblages. Printouts have a table of equivalence or an "Mcode" table to correlate user node numbers to program computer numbers for every substructure at every level and assemblage.

The static solution for the substructuring boundary is determined at the highest substructure level for each load vector. These boundary displacements are then automatically distributed back to the lower level substructures in order to compute the interior displacements. The cycle is repeated automatically until all of the displacements are determined. Here again the output displacements for each substructure are in the user's original notation.

The substructuring program is also used as a reduction routine to formulate the dynamics model from the statics model. The first level substructuring can be used to perform the assemblage and reduction. In general, the modal characteristics solution of each substructure will give indications as to obvious errors in either the mass matrix or stiffness matrix. Hence, considerable computer and modeling support time can be saved by correcting any errors, human or otherwise, before proceeding onward.

POST PROCESSOR DATA HANDLING

The post processor data handling on the MMLS solution involves the determination of the loads and stresses. Additional input data on the control system, aerodynamics, propulsion, trajectories, impact loads, and constraints are used during the dynamics stability and POGO investigations. However, these are usually analyzed by themselves in their functional area. In the event that the structure is unstable, then a resizing of the mathematical model is performed. If the structure is stable, the internal loads and stresses are computed from the NARSAMS program by the STOM job option.

The NARSAMS program options include START, MTOS and STOM. The START jobs read in model data and compute deflections, internal loads and stresses. The MTOS jobs read in model data and generate the stiffness matrix and loads vectors, renumbering identification, and restart information. The STOM jobs read in model data and deflections for all nodes (obtained from another program such as NARSESA) to compute the internal loads and stresses. Only a few cards are changed from the MTOS job. The stresses are computed based upon the plain stress, quadratic field, and/or best-fit formula for the nodes (as in reference 10). A user option to compute the stresses at each node of an element exists, however the stresses for sandwich elements are computed per element rather than per node. The stresses in the facing sheets and the shear stresses in the sandwich core are determined. A user option also permits computing stresses at only certain portions of the structure. Another option is to choose the quantity of specific nodes and their numbers. Similar options for sandwich elements are also available. The post processor will print the output in meaningful fashion for direct documentation into a report. In order to eliminate the data handling of thousands of pages, and automated data search is being incorporated. The material allowable data will be used to compute the margin of safety.

DISCUSSION

Today's structures engineer must have insight into modeling techniques, data disposition (either by cards, tapes, and/or disk packs), and be cost minded. More and more the engineer's use of general purpose and auxiliary programs also requires some programming knowledge. The adaptation of various post, intermediate, and pre-processor programs now developed can be made to large computer programs like NASTRAN and ASKA. Some work along this subject has already been done.

As computers become bigger and faster the number of degrees of freedom problem will probably continue to grow. With this growth, there will be greater data handling requirements. The use of auxiliary processors will help eliminate most major errors, thus helping meet budget and schedule requirements.

REFERENCES

1. Mac Neal, R. H., editor: The NASTRAN Theoretical Manual. NASA SP-221, Oct. 1969.
2. Douglas, F. J., editor: The NASTRAN Programmer's Manual. Parts I and II. NASA SP-223, Oct. 1969.
3. McCormick, C. W., editor: The NASTRAN User's Manual. NASA SP-222, Sept. 1970.
4. Martens, M. A., Grooms, H. R., Kitagawa, M., and Bentley, H. C.,: NARFEM User's Manual - North American Rockwell Finite Element Model. SD71-302, Space Division, North American Rockwell, Dec. 1970.
5. Yahata, S., Furuike, T., and Feick, D. Jr.: NARSAMS - North American Rockwell Structural Analysis and Matrix System - User's Manual. STR 249, Sept. 1970.
6. Yahata, S. and Grooms, H. R.: The Need for Substructuring. NASTRAN User's Colloquium, Langley, Va. 1971.
7. Furuike, T.: Multiple Level Substructuring - NARSESA, STR 248, North American Rockwell, Space Division, Sept. 1970.
8. Yahata, S., Grooms, H. R., and Furuike, T.: User's Manual to Multiple Level Substructuring - NARSESA, STR 247, North American Rockwell, Space Division, Sept. 1970.
9. Przemieniecki, J. S.: Theory of Matrix Structural Analysis, McGraw Hill Book Company, N. Y., 1968.
10. Utku, S. and Akyuz, F. A.: ELAS - A General-Purpose Computer Program for the Equilibrium Problems of Linear Structures. Vols. I and II. JPL Technical Report 32-1240, 1968.

NASTRAN PLOTTING CAPABILITIES

By John R. McDonough

Computer Sciences Corporation

SUMMARY

There are numerous options and features included in the NASTRAN plot package that are available to the user. To provide the analyst with a visual presentation of his results, the basic static, modal, and transient analyses plots may be enhanced and clarified with the aid of model or lay-out specifications. As described in the NASTRAN documentation, the program is compatible with five plotter manufacturers' equipment. The results presented here were obtained from a Stromberg-Carlson model 4020 plotter.

INTRODUCTION

Recent development work on NASTRAN has produced significant improvements in the plotting software, not the least of which is a better understanding of how to more effectively use the three basic programmed modules: e.g. the Structural Plotter (PLØT), X-Y Plotter (XYPLØT), and the Matrix Plotter (SEEMAT). The intent of this paper is to demonstrate some of the more important plotting improvements and techniques for better use of the graphic routines.

NASTRAN, as described in references 1 and 2, provides the capability for generating on any of several different plotters the following kinds of plots:

- a. Undeformed geometric projections of the structural model,
- b. Static deformations of the structural model by either displaying the deformed shape (alone or superimposed on the undeformed shape), or displaying the displacement vectors at the grid points (superimposed on either the deformed or undeformed shape),
- c. Modal deformations (sometimes called mode shapes or eigenvectors) resulting from real eigenvalue analysis by the same options stated in "b" above,

Preceding page blank

- d. Transient deformations of the structural model by displaying either vectors or the deformed shape for specified times,
- e. X-Y graphs of transient response or frequency response,
- f. Topological displays of matrices.

The plots presented here include those which are possible because of corrections to Level 12.0 and those which result from capabilities inaugurated for Level 14.0.

NASTRAN PLOTTER SOFTWARE OVERVIEW

Figure 1 shows the five common software functions performed by all the plot generating routines in NASTRAN to provide the above capabilities. Each of these major functional areas has been the source of errors or difficulties experienced by the users either because of misunderstanding of instructions and supporting documentation, or due to problems with the hardware and software. A short discussion of each major function follows in order to place in context the error avoidance techniques and enhancements implemented in later versions of NASTRAN. These are the subjects of subsequent sections of this paper.

Parameter definition refers to the various plot request packet card entries and calling sequence parameters covered in the User's Manual respectively under Structure Plotting, X-Y Plotting, and matrix pictures generated by the Utility Module SEEMAT. In general, the parameters define the plotter name and model as well as the physical constraints and modes of operation. In most cases default options are allowed.

The program structure itself is common with creation of one DMAP parameter (PLTNUM) for passing the plot number, and two named common blocks which contain the values of all other physical parameters. Typical problems that have been encountered in the parameter definition area include:

- specifications for time and eigenvalues greater than 10^8 ,
- creation of extraneous lines when plotting structures or curves containing over 100 distinct lines,
- the misunderstanding and misuse of the MAXIMUM DEFORMATION card and the maximum deformation field on the PLOT card,

- excessive computer time for creation of complicated plots.

Parameter initialization refers to the programmed instructions that set various counters, switches, and addresses to zero or other starting values at the beginning or other prescribed points in the computer program. In the NASTRAN case, two subroutines initialize all parameters in two common blocks and provide the capability of the system to default to standard plotter and model indices as well as initializing such parameters as paper size and plot tape buffer size. Once initialization is complete, none of the parameters in the common blocks can be changed without repeating the initialization step. A case in point was that in the event of a failure in module PLOT (or PRTMSG) and a subsequent restart, then the entire plot DMAP sequence had to be removed by the ALTER capability in order to obtain proper initialized parameters. Additional parameters have been added to NASTRAN in Level 14.0 to overcome such troublesome problems as obtaining vectors without an underlay structure. This is achieved by a new parameter 'N' which may be initialized by the VECTOR option on the PLOT card, and thereby not draw any shape(s), but allow all other plot options to be exercised.

Plot initiation follows parameter initialization and refers to starting the plotter. Prior to the start, the plot number is incremented. The actual starting is accomplished by one subroutine which, when appropriate, will select the proper medium, generate an identification plot, and insert the specified number of blank frames. A typical problem involving this area involved obtaining plots sequentially numbered on rigid formats 8 and 11 if both structure and X-Y plots were requested. A particular rigid format ALTER was required in the executive control deck to obtain the sequentially numbered plots.

Plot creation in NASTRAN is accomplished by seven subroutines for performing the various tasks: e.g. AXIS, LINE, PRINT, SYMBOL TIPE, TYPFLT, TYPINT. There are three operating modes defined in these subroutines:

- axis mode,
- straight line mode,
- typing mode.

These three modes are totally independent of each other and are mutually exclusive. This implies that only one mode can be active at any one point in time. Subroutine AXIS operates in the axis mode; subroutine LINE operates in the straight line mode. The problems with this area of NASTRAN plotter software have been relatively minor based on the number of reports from the user community and involve such things as peculiarities with particular plotter pens.

The final common function of NASTRAN graphic program modules is terminating the plot. This is a relatively simple function and is accomplished by the same subroutine that initiated the plot. The routine, upon sensing a negative argument, will terminate the current subset of plot commands (as appropriate), skip to a new frame, and, if necessary, write an end-of-file mark on the plot tape.

THE TEST PROBLEM

The test problem chosen to illustrate the three types of rigid format plotting is the delta wing. The problem itself, i. e. the bulk data, is the same as the standard NASTRAN Demonstration Problem 1-1, which is described in reference 3. Figure 2 is a simplified sketch of the original model but is the configuration used during the plotting exercises presented here. The bulk data is essentially unchanged since it resides on the deliverable NASTRAN User's Master File Tape. Since the object of this presentation is to demonstrate plot output (as opposed to specific numerical results), no adjustment was made to convert the problem's existing English system units to international units. Therefore, where data changes were required in order to perform the run, these data were in English units. Data input in accordance with the allowable options and requirements of the program was chosen to obtain the desired responses in each of the three rigid formats used: rigid format 1 (static analysis), rigid format 3 (modal analysis), and rigid format 12 (transient analysis).

The delta wing model is composed of membrane, shear panel and rod elements. Due to the existence of symmetry or antisymmetry in the structure and loading conditions, only one-quarter of the wing needs to be modeled. The midplane of the wing (the plane dividing the wing into upper and lower halves) is a plane of symmetry as is the center plane that divides the wing into left and right halves). The loading conditions are antisymmetrical with respect to the midplane of the wing and symmetric with respect to the center plane.

The surface skin of the wing is modeled with membrane elements while the ribs and spars are modeled with a combination of shear panels and rods. The shear load carrying capability of ribs and spars is represented by shear panels. The bending stiffness of the ribs and spars is modeled with rod elements placed in the plane of the skin surface.

Since a quarter model is used, the loading conditions require that an antisymmetric boundary be provided on the midplane and a symmetric boundary must be provided on the center plane. These boundary conditions are provided by constraining all grid points on the midplane in the X and Y directions and all grid points on the center plane in the X direction. Supports for the structure are provided by constraining grid points 13, 33, 53, 73 and 93 in the Z direction. Since no rotational rigidity is provided by the elements used in the model, all rotational degrees of freedom have been removed by the use of the GRDSET bulk data card.

Static Rigid Format Plots

The first series of examples, of primary consideration here, is the static loading of the sample delta wing at two points on the wing tip. The first load is applied at point 16 on the trailing edge, which is called subcase 1, and the second load is applied independently at point 36 on the leading edge, which is called subcase 2. The loads are both equivalent to 2230 newtons, although 500 pounds is the actual value used during the computer run.

The major cards in the case control deck for the rigid format 1 plots are:

SPC = 1	referencing the constraints previously discussed
SUBCASE 1	containing the load set 1
SUBCASE 2	containing the load set 2

The set definition cards are:

SET 1 = 1 THRU 17	the upper surface
SET 2 = 18 THRU 22	the trailing surface
SET 3 = 50	the tip surface
SET 4 = 1 THRU 22	
SET 5 = 1 THRU 22, 50	

Each set is individually plotted in its undeformed shape such as:

```
FIND SCALE, ORIGIN 1, SET 5
PLOT SET 5, ORIGIN 1, DENSITY 2, SYMBOLS 6, LABEL GRID POINTS
```

This is shown in figure 3 at the default values for AXES and VIEW.

To view the sets at other than default values, the AXES and VIEW cards are used. For example:

```
AXES Z, X, Y
VIEW 0.0, 0.0, 0.0
FIND SCALE, ORIGIN 2, SET 1
PLOT SET 1, ORIGIN 2, DENSITY 2, SYMBOLS 6, LABEL GRID POINTS
```

The top surface is shown in figure 4 rotated from the original bulk data orientation to the plotter orientation so that a truly scaled orthographic projection results. The other defined sets may be positioned by similar orientation commands.

The set chosen for plotting deformed shapes is the trailing surface of the wing because the effects of the tip loads can be seen with respect to the line of action.

A maximum deformation parameter is required for scaling by the program:

MAXIMUM DEFORMATION 30.0

Since the plots depend on orientation, new AXES and VIEW cards are used:

```
AXES Y, X, Z  
VIEW 0.0, 0.0, 0.0  
FIND SCALE, ØRIGIN 5, SET 2
```

To this point the set and orientation are defined and all following commands apply to the same definitions:

```
PLØT STATIC DEFØRMATION 0, 1, 2, ØRIGIN 5, SET 2, DENSITY 2,  
SYMBOLS 6, LABEL GRID PØINTS, VECTOR Z, SHAPE
```

This command results in a deformed plot with an undeformed underlay for both subcases 1 and 2. The plot obtained from subcase 1 is shown in figure 5. The original location of the grid points are marked with an asterisk and the final location with the chosen symbol (the open circle). The vectors appear to be double density but this is a result of two grid point displacement vectors being colinear. These same plots could have been obtained without the subcase integers if the integer 0 were used alone because all subcases are default.

```
PLØT STATIC DEFØRMATION 1, 2, ØRIGIN 5, SET 2, DENSITY 2,  
SYMBOLS 6, LABEL GRID PØINTS, VECTOR Z, SHAPE
```

Figure 6 is the resulting plot for the subcase 1 load. This is similar to the preceding plot except that the underlay flag, integer 0, is missing so the result is only the deformed shape. This kind of plot could be obtained without the subcase integers or the SHAPE option because the deformed shape for all subcases is default. However, because the VECTOR option was used without the 0 integer, the direction of the vectors is reversed.

```
PLØT STATIC DEFØRMATION 0, 1, 2, ØRIGIN 5, SET 2, SYMBOLS 6,  
LABEL GRID PØINTS, VECTOR Z
```

One of the resulting plots, shown in figure 7, is the undeformed structure with vectors from the original grid point positions to the deformed positions. The same plot could be obtained without the 0 integer. The vectors can be omitted by either not using the VECTOR option or using VECTOR N.

```
PLØT STATIC DEFØRMATION 1, 2, ØRIGIN 5, SET 2, DENSITY 2,  
SYMBOLS 6, LABEL GRID PØINTS, VECTOR NZ
```


The plot for subcase 2 is shown in figure 8. The structure is not plotted but the vectors are shown at their deformed and undeformed positions. The original positions are marked with an asterisk and the final positions are marked with the chosen open circles. This plot can also be obtained with the integer 0.

PLØT STATIC DEFØRMTØN 1, 2, ØRIGIN 5, SET 2, DENSITY 2,
SYMBOLS 6, LABEL GRID PØINTS, VECTOR NZ, SHAPE

Figure 9 is the plot obtained from subcase 1 conditions. The structure is not plotted but the vector directions are reversed from the previous example.

Modal Rigid Format Plots

The second series of plots obtained are those due to the unloaded wing whereby the natural vibration frequencies are calculated and the normalized mode shapes are plotted. The method chosen to extract the eigenvalues from the dynamic matrix equation $[K - \lambda M] \{u\} = \{0\}$ is the Givens method. (In the above equation K is the stiffness matrix, M is the mass matrix, and u is the displacement matrix. The quantity, λ , represents the eigenvalues which are the squares of the natural frequencies.) The eigenvector normalization method chosen is normalization to unit generalized mass. The delta wing is an 86 order problem, and as expected, the Givens method outputs all eigenvalues at once. Only ten eigenvectors are chosen for consideration as optioned on the EIGR bulk data card.

In order to produce the desired results the case control deck is constructed to conform to the adjusted bulk data deck. Specifically, the two forces from the static case are dropped and an eigenvalue method is adopted. Everything else remains the same.

In addition, the case control deck output requests are set up so that the eigenvectors reference a subcase by use of the MØDES card. This is accomplished by the following technique:

SUBCASE 1	
MØDES = 2	implies two subcases (modes)
DISP = NØNE	no output for the first two modes
SUBCASE = 3	
DISP = 1	output for the third mode for a selected set
SUBCASE 5	implies fourth mode displacements after subcase 3
DISP = NØNE	
SUBCASE 7	implies sixth mode suppression after subcase 5
DISP = 1	
SUBCASE 8	
DISP = NØNE	no output beyond the seventh mode

The plot package contains the upper wing surface element set selection:

SET 1 = 1 THRU 17

A maximum deformation is set:

MAXIMUM DEFORMATION 25.0

The command

FIND SCALE, ORIGIN 1, SET 1

positions the plotter and scales the object.

The plot from the command

PLOT ORIGIN 1, SET 1, DENSITY 2, SYMBOLS 6, LABEL GRID POINTS

is shown in figure 10.

The plots resulting from

PLOT MODAL DEFORMATION 3, 4, 7, ORIGIN 1, SET 1, DENSITY 2,
SHAPE

are shown in figures 11 and 12.

These two plots indicate a need for further investigation because they are not as expected. It is suspected at this time that a problem exists in the subcase counting method because of the following table of results:

SUBCASE	OUTPUT	PLOT
1	NO (ok)	NO (ok)
2	NO (ok)	NO (ok)
3	YES (ok)	YES (no)
4	YES (no)	YES (3rd mode)
5	NO (ok)	NO (ok)
6	NO (ok)	NO (ok)
7	YES (5th mode)	YES (5th mode)
8	NO (ok)	NO (ok)
9	NO (ok)	NO (ok)
10	NO (ok)	NO (ok)

It can be seen that the modal deformations, however selected, yield a mode shape for a particular eigenvalue.

Transient Rigid Format Plots

The final series of plots are obtained from the transient analysis of the wing which is subjected to a time dependent force. The dynamic matrix equation employed in transient analysis is $[p^2 M + pB + K] \{u\} = \{P\}$ where P represents a force, sinusoidally varying with time, p is the differential operator d/dt , B is the damping matrix, and the other quantities are as previously defined.

The case control deck parameters required to augment the adjusted bulk data deck include the omission of the static forces and the use of a dynamic force, a damping force, and a time step flag. The eigenvalue selection method is the same as that employed previously.

The dynamic force used is one described by the equation associated with a TLOAD2 bulk data card. After certain options, obtained with the aid of a DAREA bulk data card, the loading equation evolves to $P(t) = 50.0 \cos [2\pi (40.0) t + 45^\circ]$ applied at point 36 in the positive Z direction. The peak amplitude force of 223.0 newtons (50.0 pounds used), at a forcing frequency of 40.0 hertz is 45° out of phase from the undamped natural frequency. In addition a structural damping force linearly varying with frequency is described by:

$$G = \begin{cases} 0.01 f & 0 \leq f < 10.0 \\ 0.1 f & 10.0 \leq f < 100.0 \\ 1.0 f & 100.0 \leq f < 1000.0 \end{cases}$$

and appears on a TABDMP1 bulk data card. A TSTEP card describes ten time steps, one second apart and the LFREQ and HFREQ PARAM cards were the other cards added to the bulk data deck.

Since both the structure plotter and the X-Y plotter are employed for this series, the two sections of the plot package are separated by the output requests OUTPUT(PLOT) and OUTPUT(XYPLØT) respectively. Other parameters related to the SC 4020 X-Y plotter will be discussed later.

The upper surface of the wing is chosen as the plot package set:

SET 1 = 1 THRU 17

The deformation and scale initializations are:

MAXIMUM DEFØRMATION 25.0
FIND SCALE, ØRIGIN 1, SET 1

The command

PLØT TRANSIENT DEFØRMATION TIME 0.0, 10.0, SET 1, ØRIGIN 1,
DENSITY 2, VECTOR Z, SHAPE

results in ten plot frames for each of the ten time steps chosen but only nine plots result. This is because the SHAPE option suppresses the undeformed shape and no plot results for time zero. Figure 13 shows the plot at time of 1.0 second.

The command

```
PLOT TRANSIENT DEFORMATION, TIME 0.0, 10.0, SET 1, ORIGIN 1,  
DENSITY 2, VECTOR Z
```

results in the ten plot frames with a plot in every frame. Since the SHAPE option was dropped, all ten plots are in the undeformed shape. Figures 14 and 15 show the plots at time zero and time of 1.0 second.

For the X-Y plotter package, some of the parameters are stated in a different manner from the structure plotter.

The microfilm plotter DENSITY 2 option which appears in all the structure plotter commands is now changed to a separate card:

```
DENSITY = 2
```

The frame skip counter is optional to suppress the default skip of one between each frame with

```
SKIP = 0 (or SKIP BETWEEN FRAMES = 0)
```

It should be noted that in the structure plotter case, the skip between each frame is always zero except between the undeformed and deformed plots (where the skip is one), so skip commands in that series were not necessary.

In the case of the SC 4020 plotter the equipment flag must be set to choose the option of plotting on paper only. Thus CAMERA = 2 suppresses the creation of a film strip.

One plot frame (figure 16) is produced to demonstrate the various options available in the X-Y plotter package:

```
XYPLOT DISP / 36 ( T3, T3 )
```

The command itself provides an X-Y plot of the displacement (response by default) of grid point 36 (the loaded point in the example). There is one frame with two graphs (one upper and one lower), both depicting the response in the Z (T3) direction. With the exception of the symbols, the upper graph plot was obtained completely by the defaults available in the X-Y plotter package.

The parameters which define the graphs of the upper and lower half frames are summarized in the following table:

Lower Half Frame Commands	Upper Half Frame Defaults
XBAXIS = YES	No
XBGRID LINES = YES	No
YBGRID LINES = YES	No
YBVALUE PRINT SKIP = 1	0
YBDIVISIONS = 10	5
YBTITLE = RESPONSE	None

These commands provide that the lower graph has an X-axis, grid lines parallel to the Y-axis, grid lines parallel to the X-axis, values placed on tick marks with one tick skipped between labels along the Y-axis, 10 tick divisions along the Y-axis, and Y-axis title, respectively. By default the maximum and minimum values along the Y-axis are obtained to accommodate all values on both graphs and the X-axis is drawn at $y = 0$. Since symbols placed on the curves is not separable, one command `CURVELINESYMBOL = 2` places the symbol X on both graphs at plotted points.

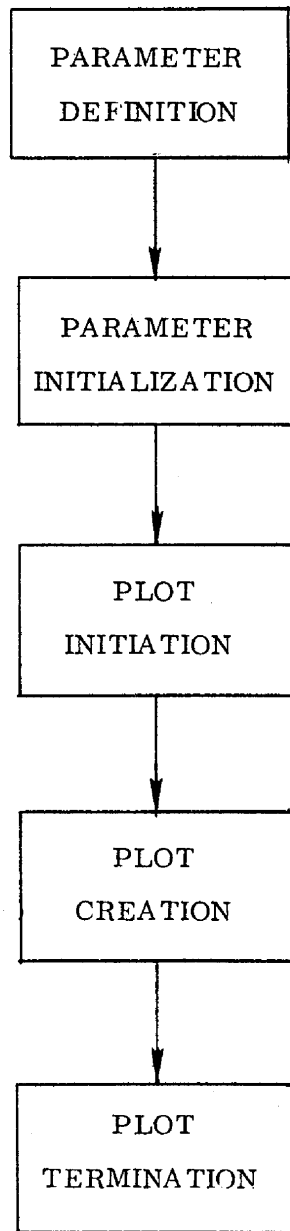
The maximum deflection occurring at time of 1.0 second is of the order 10^{-5} while all other values from time 2.0 to 10.0 seconds are so small, they appear nearly equal to zero.

CLOSURE

The static analysis rigid format plot package presently seems the most versatile. Aside from the problem encountered in the modal analysis plot it remains for further study to investigate the possibility of employing all the static plot features to the two dynamic plot rigid formats.

REFERENCES

1. The NASTRAN Theoretical Manual, NASA SP-221, September, 1970, Section 13.
2. The NASTRAN User's Manual, NASA SP-222, September, 1970, Section 4.
3. NASTRAN Demonstration Problem Manual, NASA SP-224, September, 1970, pp. 1.1-1 through 1.1-8.



COMMON SOFTWARE FUNCTIONS

Fig. 1

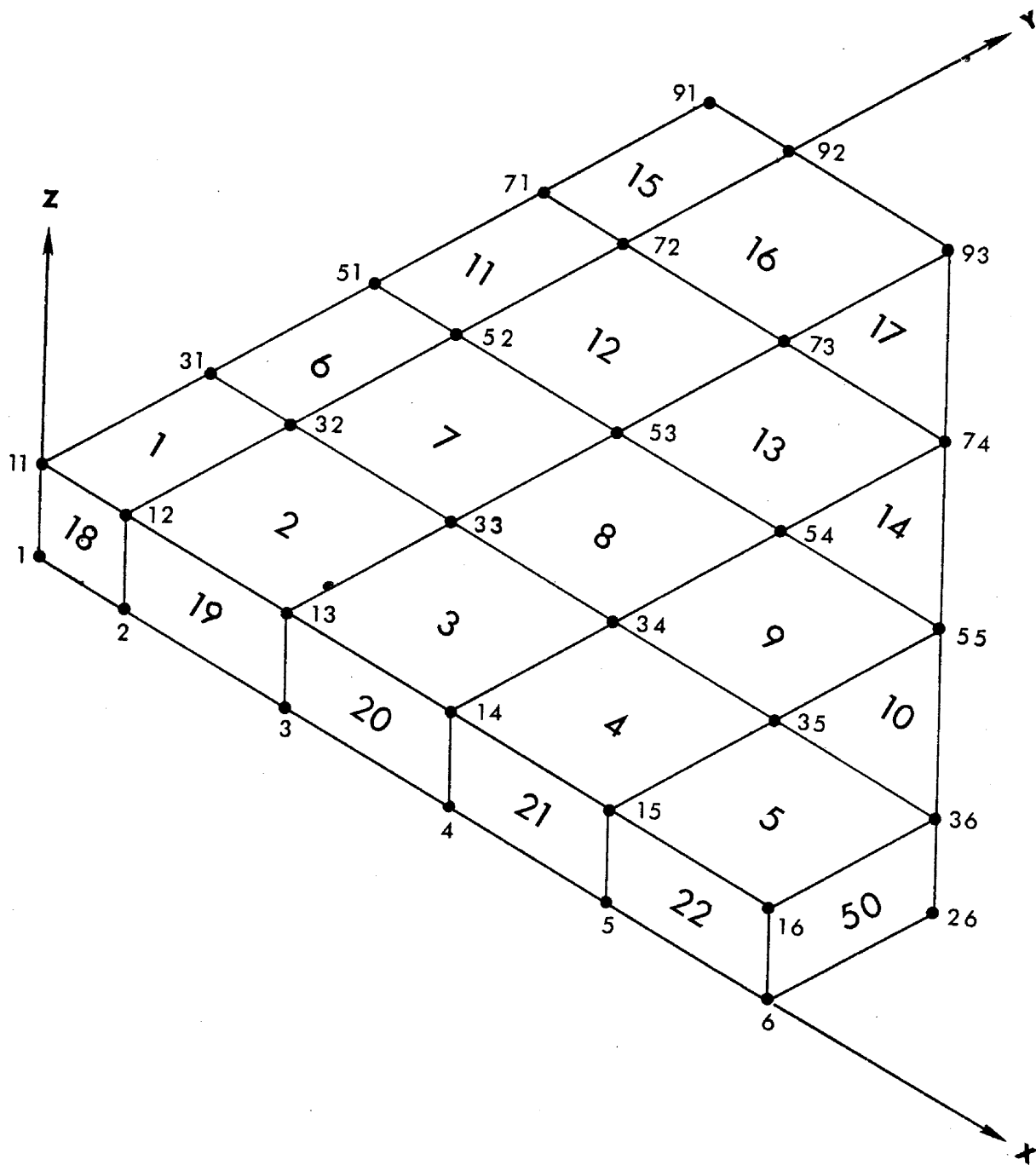
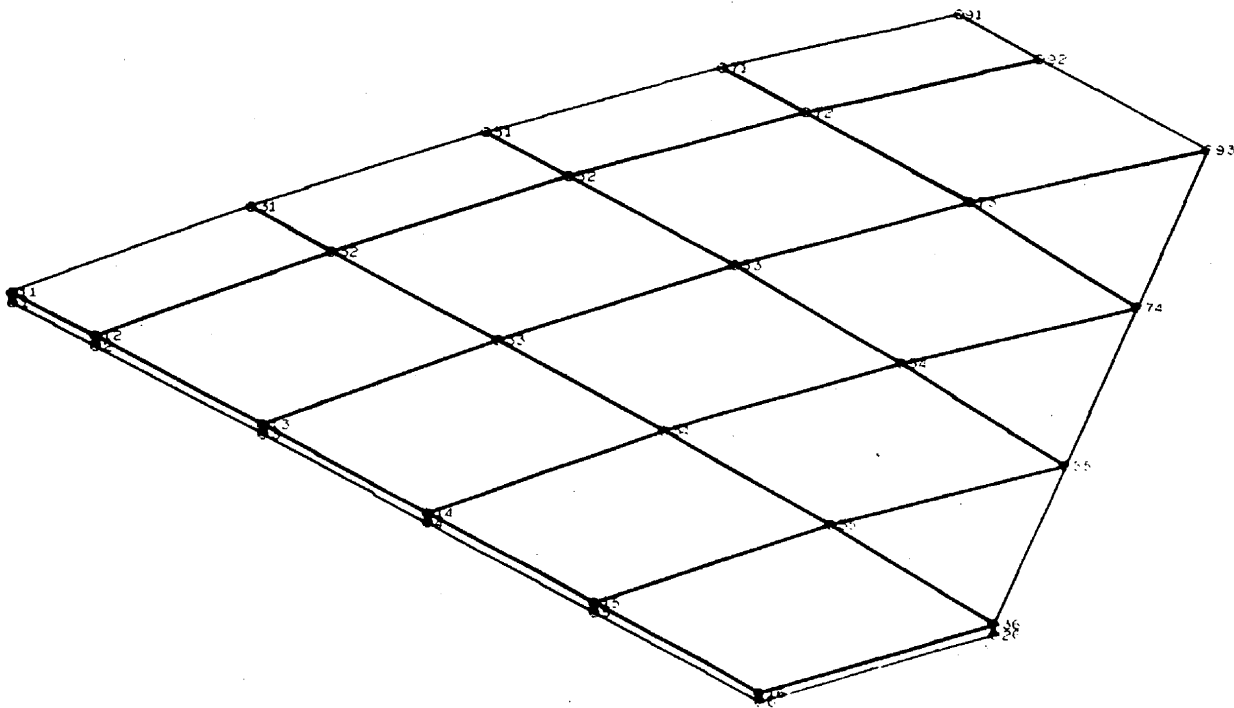


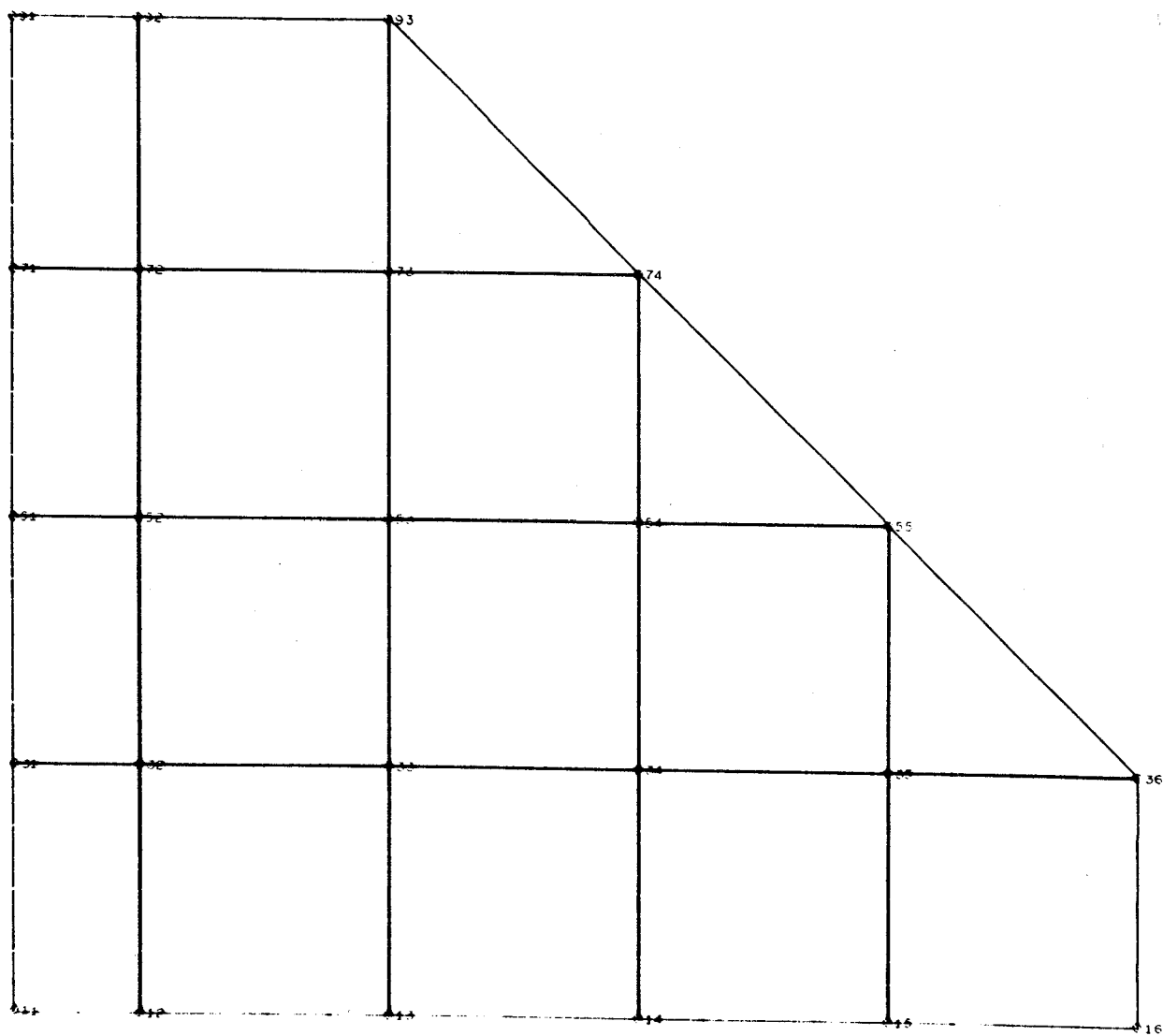
Fig. 2



STATIC ANALYSIS OF A DELTA WING

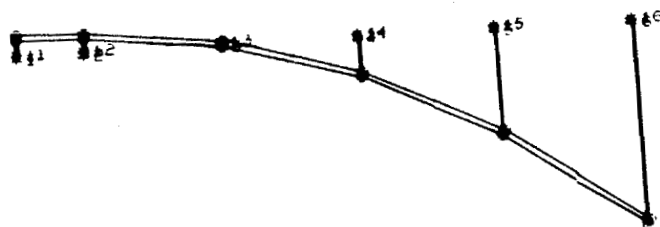
UNDEFORMED SHAPE

Fig. 3



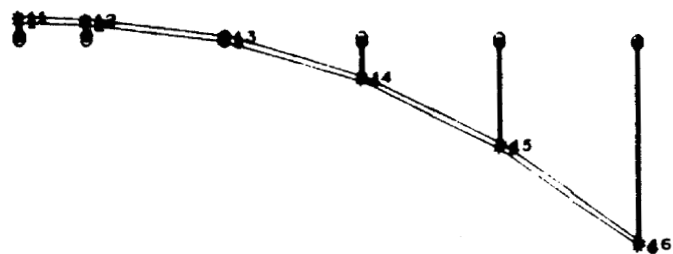
STATIC ANALYSIS OF A DELTA WING

Fig. 4



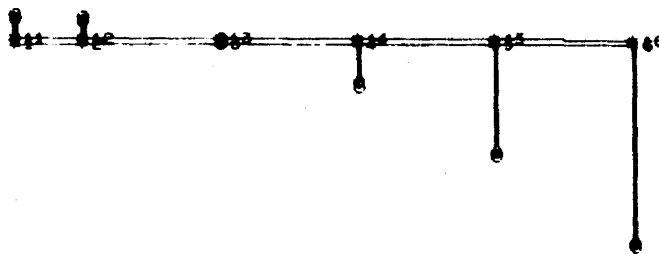
STATIC ANALYSIS OF A DELTA WING
LOAD ON TRAILING EDGE
STATIC DEFORMATION - SUBCASE 1 LOAD SET 1

Fig. 5



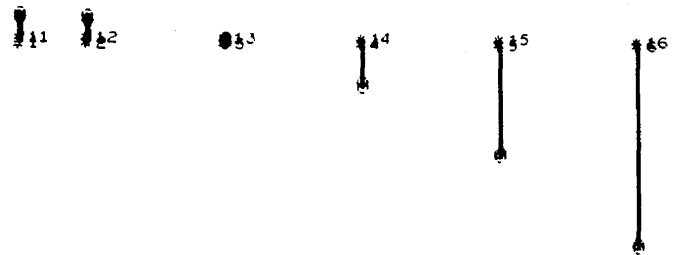
STATIC ANALYSIS OF A DELTA WING
 LOAD ON TRAILING EDGE
 STATIC DEFORMATION - SUBCASE 1 LOAD SET 1

Fig. 6



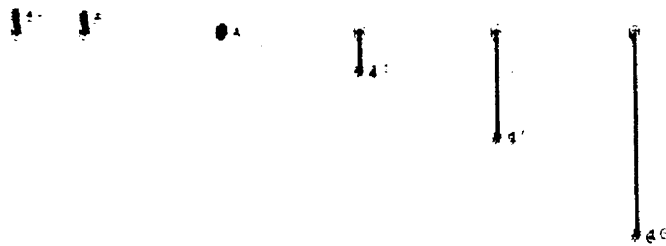
STATIC ANALYSIS OF A DELTA WING
 LOAD ON LEADING EDGE
 STATIC DEFORMATION - SUBCASE 2 LOAD SET 2

Fig. 7



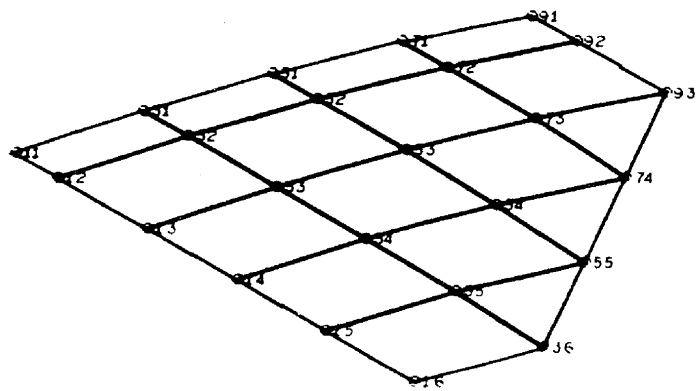
STATIC ANALYSIS OF A DELTA WING
LOAD ON LEADING EDGE
STATIC DEFORMATION - SUBCASE 2 LOAD SET 2

Fig. 8



STATIC ANALYSIS OF A DELTA WING
 LOAD ON TRAILING EDGE
 STATIC DEFORMATION SUBCASE 1 LOAD SET 1

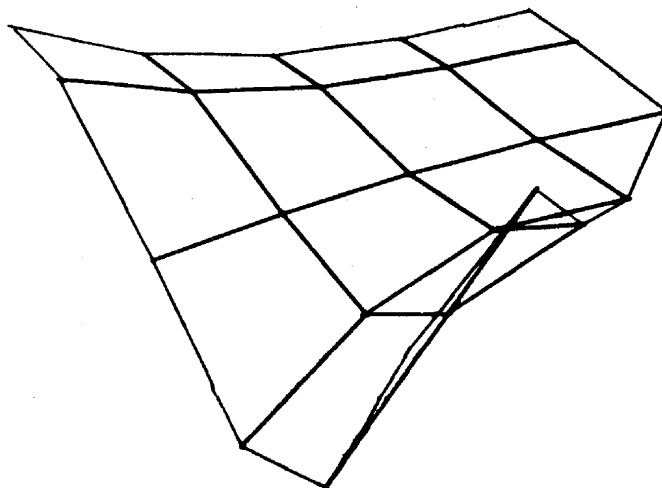
Fig. 9



MODAL ANALYSIS OF A DELTA WING

UNDEFORMED SHAPE

Fig. 10



MODAL ANALYSIS OF A DELTA WING

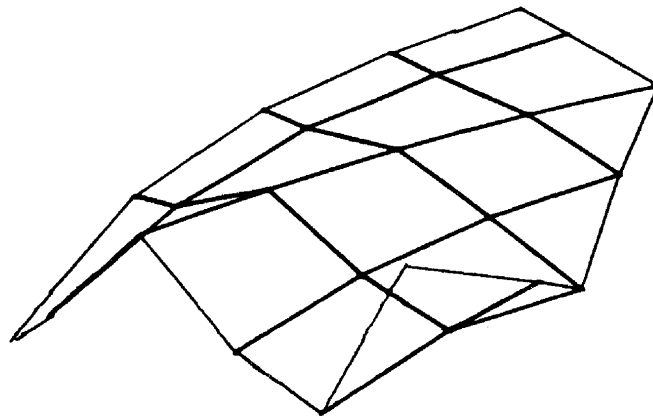
THIRD AND FOURTH MODES

MODAL DEFORMATION - SUBCASE 4

MODE 3

EIGENVALUE = 962977.19000

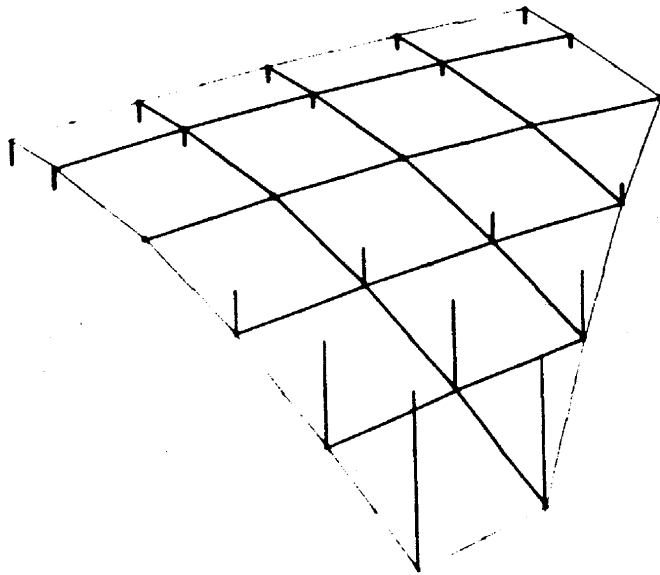
Fig. 11



MODAL ANALYSIS OF A DELTA WING

MODE 7
MODAL DEFORMATION - SUBCASE 7 MODE 5 EIGENVALUE = 1612740.4000

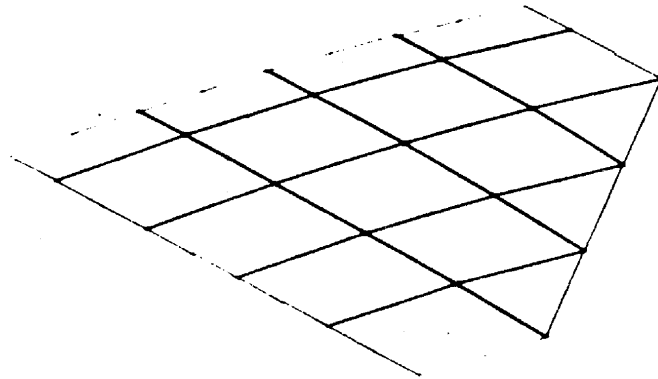
Fig. 12



TRANSIENT ANALYSIS OF A DELTA WING

TRANSIENT DEFORMATION - SUBCASE 1 LOAD SET 100 TIME = 0.9999999900

Fig. 13



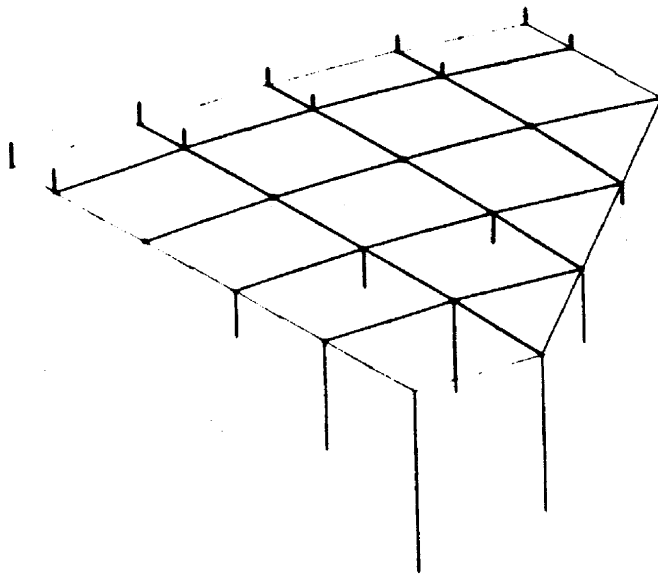
TRANSIENT ANALYSIS OF A DELTA WING

TRANSIENT DEFORMATION - SUBCASE 1

LOAD SET 100

TIME = 0.

Fig. 14



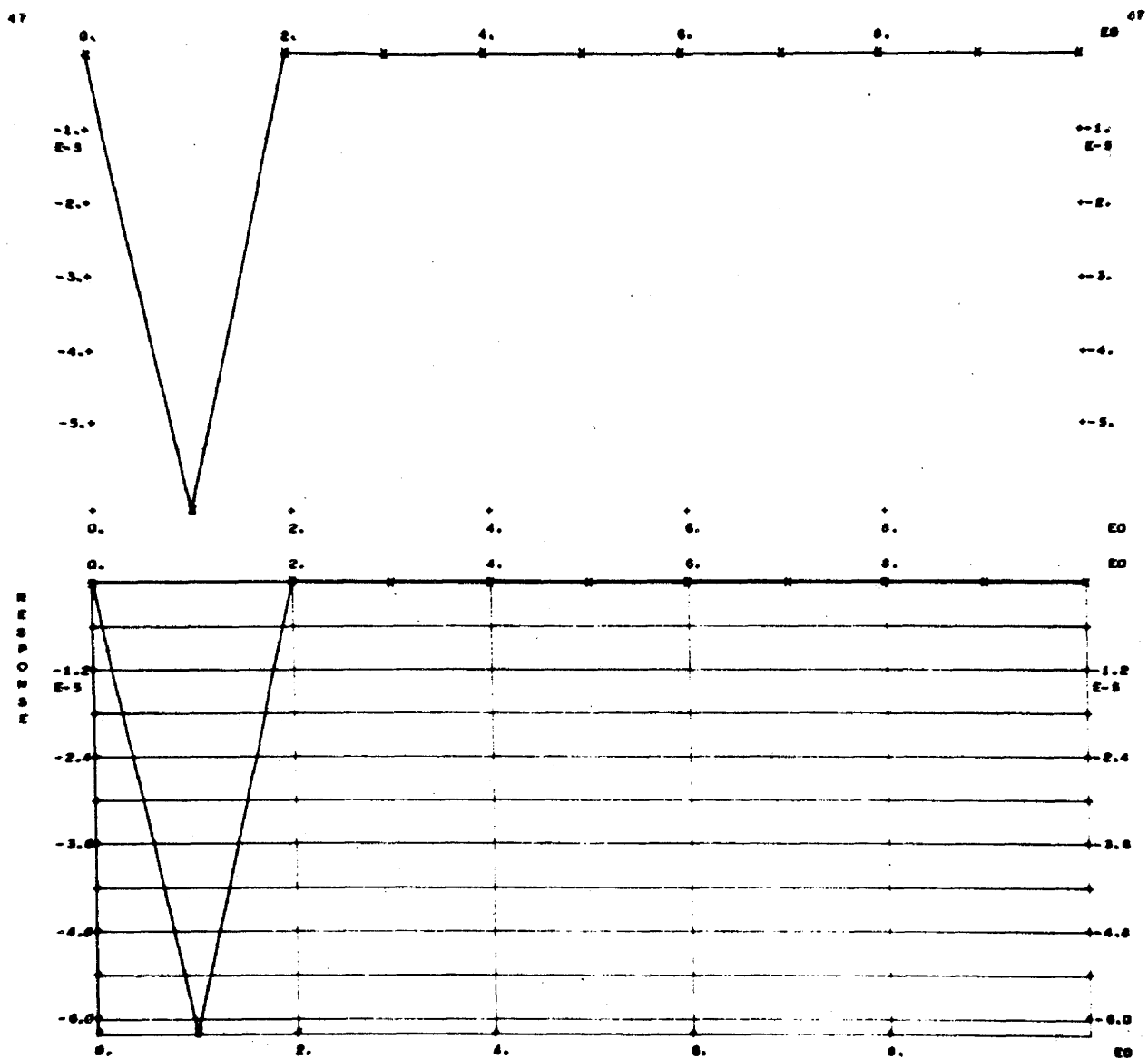
TRANSIENT ANALYSIS OF A DELTA WING

TRANSIENT DEFORMATION - SUBCASE 1

LOAD SET 100

TIME = 0.9999999900

Fig. 15



UPPER HALF DEFAULT, LOWER HALF DEFINED
TRANSIENT ANALYSIS OF A DELTA WING

Fig. 16

Preceding page blank

A NASTRAN POSTPROCESSOR FOR STRUCTURAL MODIFICATION REANALYSIS*

By Roy Levy

Jet Propulsion Laboratory

SUMMARY

An efficient procedure is described for reanalysis of space-truss structural frameworks. The procedure has been programmed to operate as a postprocessor to determine response changes from sets of displacements developed for the initial structure by an independent structural analysis system. Examples given show substantial savings in computation time when operating in conjunction with the NASTRAN structural analysis system.

INTRODUCTION

Efficient methods of reanalysis are useful to assess the changes in structural response as a function of modifications to the properties of the individual member components of the structure. The applications encompass all design phases through inception and future alteration, particularly in conjunction with the implementation of the techniques for structural optimization.

Currently, a number of diverse procedures for reanalysis have evolved to operate within the overall formulation chosen for analytical solution of the response problem. Some have been designed to be used in conjunction with force method, displacement method, or mixed formulations. Additional alternatives depend for their attractiveness upon whether or not the number of members for which modifications are considered form a relatively large or a relatively small set, or possibly whether or not the modified members can be readily localized to occur within restricted regions of the structure. Reference 1 describes several of the currently prevalent and useful reanalysis procedures.

*This paper presents the results of one phase of research carried out at the Jet Propulsion Laboratory, California Institute of Technology, under Contract No. NAS 7-100, sponsored by the National Aeronautics and Space Administration.

Some procedures are mathematically exact in the sense that the solutions will be exactly equivalent to solutions that would be obtained from analysis of the modified structure ab initio. Others develop approximate solutions that are sufficiently accurate to serve during intermediate stages of structural optimization techniques. All methods usually appear to fall within either of two classes:

- (1) Given the inverse of the stiffness matrix for the initial structure, the inverse for the modified structure is developed by perturbation (refs. 2, 3, and 4). An alternative to avoid dealing with the inverse of the stiffness matrix is to operate in terms of its decomposition (ref. 1).
- (2) The solution for the modified structure is developed as a linear combination of solutions for the initial structure (refs. 5, 6, and 7).

PROPOSED METHOD

In the following, an exact method of solution will be described that develops displacements and member forces for the modified structure from linear combinations of displacement function solutions developed for the initial structure. Conceptually, the method is based upon a parallel element approach. For each component member to be modified, a hypothetical parallel member is postulated. Cross-sectional properties of the parallel member are taken as exactly equal to the changes in properties of the parent (original) member and the connectivity is duplicated. The final member forces for the modified structure are the sums of the member forces on parent and parallel members. A condition of the solution is to maintain compatibility of the parent and parallel member distortions. Figure 1 illustrates the approach for compatibility enforcement and displacement superposition for a plane truss structure subjected to a single loading condition and with only one member to be changed. In this case, the member distortion consists of the axial extension.

Reanalysis is performed by a postprocessor computer program that uses input displacement functions developed previously by an independent structural analysis program. Because the only computed data that are input are the displacement functions, the analytical formulation procedure used to process the initial structure and develop these displacements is immaterial. The present implementation of the program is designed to accept input specifically in the format of the NASTRAN analysis system. A present limitation is the restriction to process only changes in the cross-sectional area property for one-dimensional bars. This limitation, however, is compatible with the design requirements of space-truss structures, such as the frameworks of antenna reflectors. Nevertheless, it is feasible to extend the procedure to include beam-type bars. The advantages of this method are the simplicity of program operation and input requirements and the efficiency with which parameter studies can be developed for the response as a function of a spectrum of property changes for particular bars. Entirely new members can be added

by parallel members, and original members can be completely removed by assigning duplicate properties of negative magnitude to the parallel member.

MATHEMATICAL FORMULATION

At first, we will make the conventional assumption that the change in external loading caused by the changes in the weights of modified bars need not be considered. Subsequently, an adjustment to include these effects will be indicated. Consequently, the displacements of the modified structure U_M are obtained by superposition of displacements of the initial structure U_I (assumed as invariant with respect to property changes) and the displacements ΔU caused by the internal forces of the parallel members acting as loads on the initial structure. That is,

$$[U_M] = [U_I] + [\Delta U] \quad (1)$$

The order of the matrices in equation (1) is $m \times k$, where m is the number of unconstrained degrees of freedom and k is the number of external loading vectors.

To evaluate ΔU , it is convenient to express these displacements as the product of the displacements for unit values U_S of the parallel member forces postmultiplied by the forces R of the parallel members, or

$$[\Delta U] = [U_S] [R] \quad (2)$$

(m × k) (m × b) (b × k)

In equation (2), the index b is equal to the number of property changes summed over all the members.

To enforce compatibility, let

e_F = final distortions of parent members = distortions of parallel members

e_I = initial distortion of parent member for the external loads

e_S = distortions of parent member for unit values of forces of the parallel members

e_0 = distortions of parallel members for unit forces

Therefore, from superposition

$$\begin{matrix} [e_F] & = & [e_I] & + & [e_S] & [R] \\ (b \times k) & & (b \times k) & & (b \times b) & (b \times k) \end{matrix} \quad (3)$$

But e_F can be determined directly as the distortions of the parallel members,

$$[e_F] = [e_0] [R] \quad (4)$$

After combining equations (3) and (4) and rearranging, R can be obtained by solving

$$([e_0] - [e_S]) [R] = [e_I] \quad (5)$$

The solution of equation (5) for R can be obtained readily in many instances because the order of the coefficient matrix is equal only to the total number of property changes.

Examination of equation (5) shows that relatively little additional computational effort is necessary to process more than one property change for a given member. This can be done by saving the e_S and e_I matrices in equation (5) and repeating only the relatively minor effort in regenerating new e_0 matrices. In this manner, the responses for sequences of property changes for given members can be obtained efficiently.

After combining equations (1) and (2), the final displacements of the modified structure are obtained from

$$\begin{matrix} [U_M] & = & [U_I] & + & [U_S] & [R] \\ (m \times k) & & (m \times k) & & (m \times b) & (b \times k) \end{matrix} \quad (6)$$

The final member forces can be found either by summing forces on parent and parallel bars, or else by expanding the indices of equation (3) to cover all of the members of interest and then applying the internal force-distortion relationship for these members.

In the limited case of one-dimensional bar members, the member distortion is the extension of a bar along its axis and is given by

$$e_i = \frac{S_i L_i}{A_i E_i} \quad (7)$$

where S_i , L_i , A_i , and E_i are, respectively, the member force, length, area, and modulus of elasticity for the i^{th} member. As an alternative to equation (7), the present implementation computes the extension from the grid coordinates and displacements associated with the bar as follows:

$$e_i = \sum_{\alpha=1}^3 \frac{q_i^\alpha H_i^\alpha}{L_i}, \quad i = 1, 2, \dots, b \quad (8)$$

where q_i^α is the difference in displacements of the terminal nodes of the bar in the direction of the α^{th} axis of Cartesian coordinates, H_i^α is the projection of the bar axis along the α^{th} axis, and

$$L_i = \left(\sum_{\alpha=1}^3 [H_i^\alpha]^2 \right)^{1/2} \quad (9)$$

The computations for equations (8) and (9) are performed by using the member connection cards to define the terminal nodes and the grid cards to give the nodal coordinates. These data can be duplicates of the input for the original structural analysis program. The displacements used to generate the e_I set are the responses to the applied loading. The displacements that generate the e_S set are obtained by applying a pair of unit loads directed towards each other at the terminal nodes associated with each parallel member; each pair of loads forms one loading vector and contributes one column of displacements to the U_S matrix, which is used to compute one column of distortions in the e_S matrix. The U_S columns are readily produced by NASTRAN using FORCE1 bulk data cards to define the loadings.

The unit loads that produce the e_S set are equilibrated by corresponding unit loads that extend the parallel member. Consequently, the e_0 matrix is a diagonal matrix of distortions for unit tensile loads, with each diagonal element of the form

$$e_0 = \frac{L_i}{A_i E_i} \quad (10)$$

where A_i is the change in area for the i^{th} member and this can be positive or negative, depending upon whether the area of the i^{th} member is to be increased or decreased.

The foregoing procedures can be adjusted to include changes in loading caused by modified member properties. To do this, additional loading vectors that are the result of unit areas for the parallel members are processed by the initial analysis program. The corresponding new displacement functions

are supplied to the postprocessor program, which multiplies these by the area currently being processed for the parallel member and adds the result to the U_I displacements. Consequently, in equation (5), it is necessary to generate a new e_I vector for each property change in a sequence.

PROGRAM EXECUTION AND CONCLUSIONS

A flow chart of the reanalysis program described for invariant external loading is shown in figure 2. The program is developed either to process property changes for individual bars or common property changes to groups of bars.

Table 1 contains a summary of the central processing unit times for program operation (Univac 1108 Exec 8 computer) for two different structures that have been reanalyzed by this program. For both structures, the input displacements were read from a tape which was created by suppressing NASTRAN output punch card images by means of the executive breakpoint feature of the 1108 computer. The central processing unit (CPU) times shown include, in addition to computation time, the time used for data input (card and tape reading) and a substantial amount of printed output.

Two NASTRAN runs were made in each case of table 1. The first run was made independently of reanalysis requirements. The purpose was to check stability of the analytical model and to provide some insight into which members were the most desirable candidates for revision. When the checking can be eliminated and the members to be changed are known in advance, reanalysis can start from the second run, which generates all needed information. The time used for the first run, however, gives an indication of the time required to process one additional group change of member properties in lieu of using the reanalysis postprocessor program.

Table 2 illustrates the advantages in computation total time that can be obtained by using the reanalysis procedure to process up to four property changes for a given bar group for the two structures. The tabulations show the time to analyze each modification as a new structure by using NASTRAN only and the time to process the modifications by the reanalysis program. The "NASTRAN only" column does not consider program restarts, because experience does not show significant economies in restarting when the basic structure is modified. Although table 2 shows substantial advantages for reanalysis postprocessing when at least two changes are considered, the benefits would be even more pronounced whenever the first NASTRAN run is eliminated and only the second NASTRAN run (table 1) is used.

Because the number of computations depends upon the number of changes, computational time savings are the largest when the number of members with changes is a relatively small proportion of all of the members.

Whenever a large number of members are jointly to be given a small number of changes, the advantages of reanalysis tend to diminish. For example, if all members were to be changed, the time to generate the U_S displacements would be equivalent to the generation of the full flexibility matrix. In addition, it has been found that when changes in the external loadings are included, the postprocessor program takes about 50% more computation time. Therefore, the relative efficiency of complete reanalysis within the initial program should be considered.

REFERENCES

1. Kavlíe, D., and Powell, G. H., Efficient Reanalysis of Modified Structures. Proc. ASCE: J. Struct. Div., Vol. 97, No. ST1, Jan. 1971, pp. 377-392.
2. Sack, R. J., Carpenter, W. C., and Hatch, G. L., Modification of Elements in the Displacement Method. AIAA. J., Vol. 5, No. 9, Sept. 1967, pp. 1708-1710.
3. Von Hoerner, S., Homologous Deformations of Tilttable Telescopes. Proc. ASCE: J. Struct. Div., Vol. 93, No. ST5, Oct. 1967, pp. 461-485.
4. Romstead, K. M., and Wang, C. K., Optimum Design of Framed Structures. Proc. ASCE: J. Struct. Div., Vol. 94, No. ST12, Dec. 1968, pp. 2817-2845.
5. Sobieszczanski, J., Matrix Algorithm for Structural Modification Based on the Parallel Element Concept. AIAA. J., Vol. 7, No. 11, Nov. 1969, pp. 2132-2139.
6. Melosh, R. J., and Luik, R., Multiple Configuration Analysis of Structures. Proc. ASCE: J. Struct. Div., Vol. 94, No. ST11, Nov. 1968, pp. 2581-2595.
7. Cella, A., and Logcher, R. D., Automated Optimum Design from Discrete Components. Proc. ASCE: J. Struct. Div., Vol. 97, No. ST1, Jan. 1971, pp. 175-189.

Table 1. CPU times^a for Univac 1108 Exec 8 computer

Parameter	Structure I	Structure II
Matrix order m	48	1350
Total number of bars	60	1492
Number of loading vectors k	2	2
Number of bars in change group b	6	37
NASTRAN CPU times ^a		
Original structure: for U_I	32 s	12 min 44 s
Original structure: for U_I and U_S	45 s (cold start)	11 min 41 s (restart)
Reanalysis program CPU times ^a		
Generate U_M for first area change	2.7 s	37.0 s
Generate U_M for each additional area change	0.3 s	2.3 s
^a CPU times are central processing unit times for all operations of computations plus input/output, exclusive of compilation time.		

Table 2. CPU times^a for reanalysis of multiple property changes of a bar group

Structure	Number of property changes	Time, s	
		NASTRAN only	NASTRAN + postprocessor reanalysis
I	1	32	47.7
	2	64	48.0
	3	96	48.3
	4	128	48.6
II	1	768	738
	2	1536	740
	3	2304	743
	4	3072	746
^a CPU times are central processing unit times for all operations of computations plus input/output, exclusive of compilation time.			

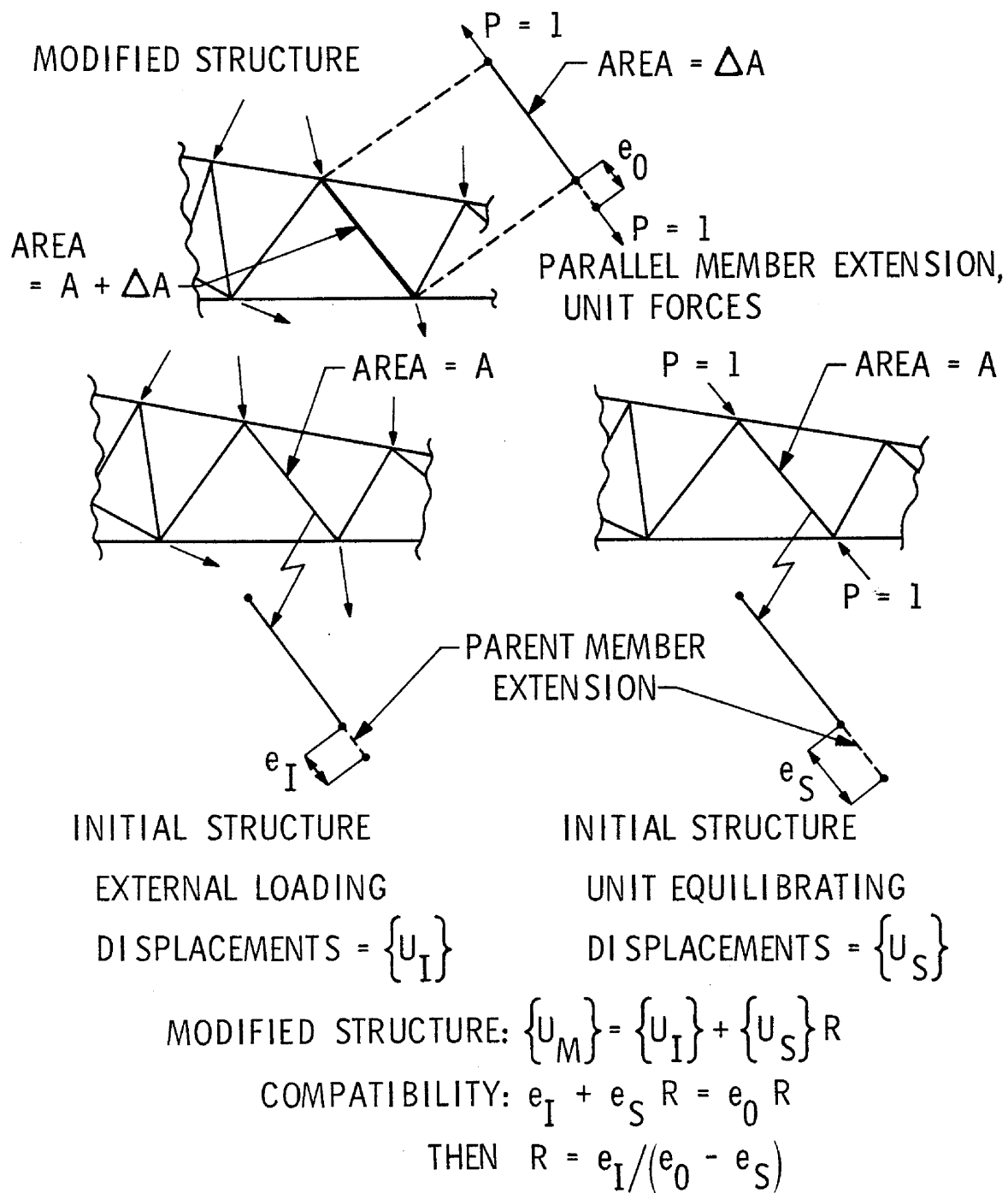


Figure 1. - Parallel element distortion compatibility approach

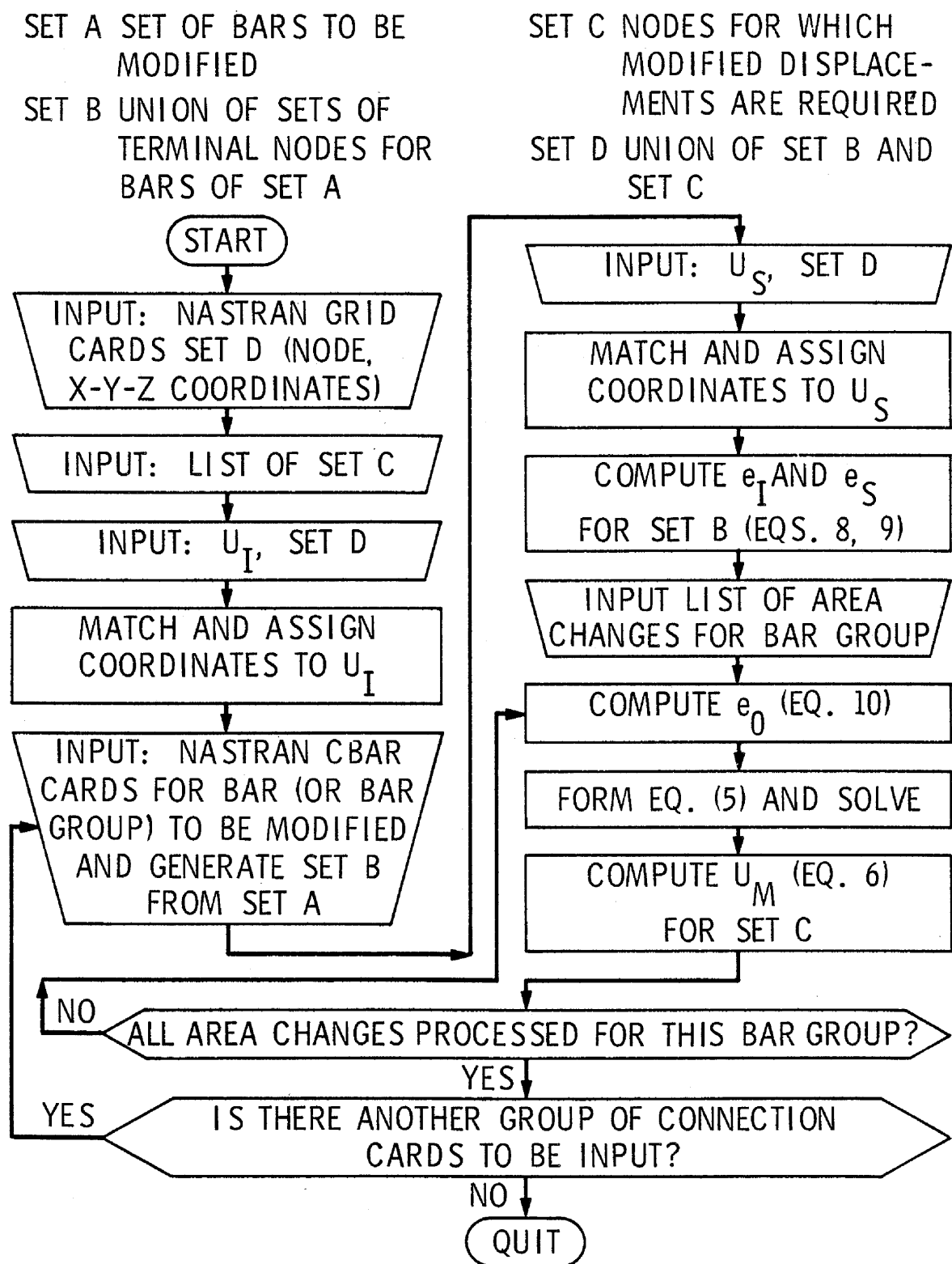


Figure 2. - Flow chart for computations of modified structure displacements (NASTRAN postprocessor)

CONVERGENCE OF THE NASTRAN PLATE ELEMENTS FOR SHELL STRESS ANALYSIS

By Michael T. Wilkinson and Robert E. Fulton
NASA Langley Research Center

SUMMARY

The procedure of approximating thin elastic shells with flat plate finite elements has been accepted practice for several years, and the initial version of the NASTRAN program is restricted to this procedure for the analysis of general shell shapes. The present paper investigates the convergence properties of the QUAD2 element contained in NASTRAN for approximating shell structures. Application is made to the stress analysis of cylindrical and conical shells, and NASTRAN results are compared with those obtained from classical shell theory. The results converge monotonically to the exact shell theory results as the mesh size is reduced. They also indicate that, for the cylindrical shell, the flat plate approximation has a principal truncation error of the order of the square of the element size.

INTRODUCTION

The procedure of approximating thin elastic shells with flat plate finite elements has been an accepted structural practice for several years (see, for example, refs. 1-4). Partly as a result of this practice, the initial version of the NASTRAN system (ref. 5) contains only flat elements to model general shell structures.

The present work investigates the quality and convergence of results obtained by using the NASTRAN flat elements to model shell structures for static stress analysis. The element used in the modeling is the quadrilateral plate element designated in NASTRAN as the QUAD2 element. This element contains both bending and extensional behavior and could be considered a reasonable model for approximating shell bending behavior.

The procedure used in the study is to compare NASTRAN finite element results for decreasing element sizes with results obtained with classical shell theory. Two isotropic shell problems are studied which undergo asymmetric behavior and for which the essentially exact solution can be obtained. The first is a simply supported cylindrical shell subjected to normal pressure which is harmonic in both the axial and circumferential directions. The second is a simply supported conical shell subjected to normal surface pressure which varies harmonically in the circumferential direction.

Preceding page blank

SYMBOLS

a, a_1, a_2	shell radius (figs. 1 and 6)
A, B, C	displacement amplitudes in equations (1)
E	Young's modulus
L	shell length (figs. 1 and 6)
m	circumferential harmonic
M_x	bending stress resultant in the axial direction
N	number of elements in the axial direction
N_x	membrane stress resultant in the axial direction
p	normal pressure loading (perpendicular to shell surface)
r	error measurement of deflections or stresses
t	shell thickness
u, v, w	axial, circumferential, and radial displacements
$\bar{u}, \bar{v}, \bar{w}$	functional coefficients in the conical shell problem defined in equations (2)
x	axial coordinate
ν	Poisson's ratio
σ_θ	circumferential stress
θ	circumferential angle

A subscript s indicates the variable is obtained using Sanders' theory.

CYLINDRICAL SHELL EXAMPLE

Consider an isotropic circular cylinder described in the cylindrical coordinate system shown in figure 1. The cylinder is subjected to a normal pressure

$$p = \sin \frac{\pi x}{L} \cos m\theta$$

where m is an integer constant and L is the cylinder's length. For the case of simply supported boundary conditions ($N_x = v = w = M_x = 0$), the normal, axial, and circumferential displacements of the cylinder are of the form

$$w = A \sin \frac{\pi x}{L} \cos m\theta \quad (1a)$$

$$u = B \cos \frac{\pi x}{L} \cos m\theta \quad (1b)$$

$$v = C \sin \frac{\pi x}{L} \sin m\theta \quad (1c)$$

where A , B , and C are displacement amplitudes. This problem has several attractive features for comparing shell modeling results. It includes both axisymmetric ($m = 0$) and asymmetric deformations ($m \geq 1$). It also includes deformations which are predominantly membrane ($m = 0$) and those which are primarily inextensional ($m = 2$).

The general shell behavior is modeled by QUAD2 elements and the calculations are simplified by taking advantage of symmetry in both the axial and circumferential directions. Using this symmetry, one-quarter of the cylinder was modeled with the four grids shown in figure 2. This grid refinement provides a finite element model which has a constant aspect ratio of arc length to axial length and lends itself to extrapolation procedures.

The shell properties in the example are:

$$a = 76.20 \text{ cm (30 in.)}$$

$$L = 4.572 \text{ m (180 in.)}$$

$$t = 2.540 \text{ cm (1.0 in.)}$$

$$E = 206.8 \text{ GN/m}^2 \text{ (30 x 10}^6 \text{ psi)}$$

$$\nu = 0.3$$

The finite element results are compared with two shell solutions to the cylindrical shell. A highly accurate solution to Sanders' shell equations (ref. 6) based on finite difference techniques was obtained with the SALORS shell of revolution program (ref. 7).^{*} A second solution was obtained from an exact solution to the Flügge theory (ref. 8), taking advantage of the harmonic character of the solution. In NASTRAN, the finite element results provide displacements at node points and stresses at each element's centroid. The

^{*}A sufficient number of finite difference stations was taken to ensure that the SALORS results had converged to an essentially exact solution.

amplitude of the finite element results can be compared with the amplitude of the results obtained from the exact solutions since for the example problem both results are doubly harmonic in the x and ϕ directions.

Results are given in figures 3-5 for the ratio of the amplitude of the finite element results to the amplitude of the Sanders theory results obtained from SALORS for the four grid sizes $N \times N$ where N is the number of elements in each direction and has the value 3, 6, 12, or 24. Results are given for the amplitude of the lateral and longitudinal displacement and the circumferential stress on the outside surface σ_ϕ . The abscissa of these plots is the square of the ratio of m , the circumferential harmonic, to N , the grid size parameter. In the special case of axisymmetric loading where $m = 0$, the abscissa is taken to be $(1/N)^2$.

The results show that, as the element size is reduced, the finite element results for both displacement and stress converge to the exact shell theory results. Furthermore, as the exact result is approached the plots appear to become linear; thus the convergence rate becomes of the principal order of the square of the element size denoted herein as quadratic convergence.

To further investigate the convergence, the four NASTRAN solutions have been extrapolated using the Richardson h^6 extrapolation procedure (ref. 9) and the results are given in table 1 together with the results obtained with the Sanders and Flügge shell theories. In all instances, application of this extrapolation procedure to the data virtually eliminates any error in the numerical results when compared with either shell theory. Thus, the results corroborate the error analysis of reference 10 and show that the NASTRAN QUAD2 element has quadratic convergence properties for this problem.

CONICAL SHELL EXAMPLE

As a second example consider the conical shell shown in figure 6 loaded with a normal pressure

$$p = \cos m\phi$$

The ends are geometrically constrained against motion; that is, $u = v = w = 0$ at $x = 0$ and $x = L$, and the meridional moment also vanishes. For this problem the displacements in cylindrical coordinates are of the form

$$w = \bar{w}(x) \cos m\phi \quad (2a)$$

$$u = \bar{u}(x) \cos m\phi \quad (2b)$$

$$v = \bar{v}(x) \sin m\phi \quad (2c)$$

where the coefficients \bar{w} , \bar{u} , and \bar{v} are functions of the axial coordinate x . Taking advantage of symmetry in the circumferential direction half of the cone is modeled with finite elements using mesh sizes $N \times 2N$ where $N = 2, 4, 8$ (see fig. 7). Finite element results were compared with converged results from Sanders' shell theory obtained with the SALORS program for the following problem:

$$a_1 = 25.4 \text{ cm (10 in.)}$$

$$a_2 = 101.6 \text{ cm (40 in.)}$$

$$L = 101.6 \text{ cm (40 in.)}$$

$$t = 0.254 \text{ cm (0.1 in.)}$$

$$E = 206.8 \text{ GN/m}^2 \text{ (30 x 10}^6 \text{ psi)}$$

$$\nu = 0.3$$

The NASTRAN solutions for this cone problem have a harmonic variation in the circumferential direction and a nonharmonic variation with x along the meridian. Thus, to understand the difference between the finite element and exact results, one must compare the axial function coefficients, for example, the $\bar{w}(x)$ of equation (2a), with the corresponding NASTRAN output. Similar functions may be compared for each stress component.

Several of these function coefficients for the radial displacement and the circumferential stress at the outer surface have been plotted in figures 8 through 10. The figures demonstrate the convergence of the NASTRAN solution to the shell solution. Note that the results from the NASTRAN model generally approximate the shell solution but have significant error near the shell ends. These errors could be significantly reduced by using a finer grid mesh near the shell boundary, but such grid refinements are inconsistent with the present uniform convergence study.

To investigate the convergence of the results, it is convenient to reduce each function coefficient to a single scalar quantity. The procedure used is to calculate the error measurement

$$r = \frac{\sum \bar{w}_s^2}{\sum (\bar{w}_s)^2}$$

where w_s is the radial displacement obtained from the SALORS solution. The quantity r is equal to unity only when the NASTRAN and Sanders theory solutions are identical.*

These error ratios for both the deflections and stresses shown in figures 8 - 10 are given in table 2 and plotted in figure 11. The results show that in all cases the error ratios tend toward unity as the grid is refined. However, it is apparent they are not as accurate as occurred for the cylinder. Furthermore, the fact that these plots have pronounced curvature indicates that the principal terms in the convergence rate of r are not quadratic. A possible explanation for this behavior is contained in reference 10 where it was shown that adjacent elements had to be the same size in plate problems in order for the convergence to be quadratic. This condition is clearly violated with the model of this cone problem.

CONCLUDING REMARKS

A study has been carried out on the use of the NASTRAN quadrilateral plate element to model the behavior of shell structures for static stress analysis. Results have been obtained for cylindrical and conical shell examples. The results indicate that a simply supported elastic cylinder can be successfully modeled with the QUAD2 flat plate finite elements of NASTRAN. Several forms of harmonic pressure loading were investigated. As the grid was reduced the finite element solutions of the cylindrical shell examples converged monotonically to the shell solution with quadratic order of error terms. A similar investigation of a simply supported elastic cone also produced results which compared favorably with classical theory; however, the magnitude of error was substantially greater than the cylinder for a comparable mesh size. Furthermore, although convergence was monotonic it did not appear to be quadratic. These studies suggest that the QUAD2 flat plate finite element contained in NASTRAN can be used to model the general behavior of thin elastic shells and, if sufficient elements are used, will be expected to converge to results obtained with classical shell theory.

*Application of this error measurement to the previous cylinder problem produces the same error values as those previously cited. This occurs because both the exact and NASTRAN solutions are doubly harmonic in the x and θ directions.

REFERENCES

1. B. E. Greene, D. R. Strome, and R. C. Weikel, "Application of the Stiffness Method to the Analysis of Shell Structures," Proc. Aviation Conf., Amer. Soc. Mech. Eng., Los Angeles, March 1961.
2. O. C. Zienkiewicz, and Y. K. Cheung, The Finite Element Method in Structural and Continuum Mechanics. McGraw-Hill, New York, 1967.
3. R. W. Clough, and C. P. Johnson, "A Finite Element Approximation for the Analysis of Thin Shells," Internat. Jour. Solids Structures, Vol. 4, 1968, pp. 43-60.
4. L. R. Herrmann, and D. M. Campbell, "A Finite Element Analysis of Thin Shells," AIAA Journal, Vol. 6, 1968, pp. 1842-1847.
5. C. W. McCormick, "The NASTRAN User's Manual," NASA SP-222, 1970.
6. J. L. Sanders, "An Improved First-Approximation Theory for Thin Shells," NASA TR R-24, 1959.
7. M. S. Anderson, R. E. Fulton, W. L. Heard, Jr., and J. E. Walz. "Stress, Buckling, and Vibration Analysis of Shells of Revolution," paper presented at the Conference of Computer Oriented Analysis of Shell Structures, Palo Alto, Calif., August 10-14, 1970.
8. W. Flügge, Stresses in Shells, Springer-Verlag, Berlin, 1970.
9. Z. Kopal, Numerical Analysis. John Wiley and Sons, New York, 1955.
10. J. E. Walz, R. E. Fulton, N. J. Cyrus, and R. T. Eppink, "Accuracy of Finite Element Approximations to Structural Problems," NASA TN D-5728, 1970.

TABLE 1

CYLINDRICAL SHELL RESULTS

(a) DEFLECTIONS IN CENTIMETERS AND STRESSES IN GN/m²

Mesh	$p = \sin \frac{\pi x}{L}$			$p = \frac{\sin \pi x}{L} \cos \phi$			$p = \sin \frac{\pi x}{L} \cos 2\phi$		
	$u \times 10^4$	$w \times 10^4$	$\sigma_\phi \times 10^5$	$u \times 10^3$	$w \times 10^3$	$\sigma_\phi \times 10^5$	$u \times 10^3$	$w \times 10^2$	$\sigma_\phi \times 10^5$
3 x 3	0.3457	0.6175	16.2	-0.3782	1.3109	10.1	-0.2822	0.2106	15.7
6 x 6	0.4122	0.7234	19.5	-0.4575	1.5558	18.1	-1.1024	0.9418	137.3
12 x 12	0.4303	0.7521	20.4	-0.4796	1.6228	20.5	-1.4978	1.3193	209.5
24 x 24	0.4351	0.7595	20.6	-0.4851	1.6398	21.1	-1.6165	1.4351	231.3
h ⁶ Extrap	0.4366	0.7620	20.7	-0.4869	1.6454	21.3	-1.6579	1.4757	239.0
Sanders	0.4366	0.7620	20.7	-0.4872	1.6457	21.3	-1.6571	1.4745	239.9
Flügge	0.4366	0.7620	20.3	-0.4872	1.6457	21.3	-1.6525	1.4712	240.5

(b) DEFLECTIONS IN INCHES AND STRESSES IN PSI

Mesh	$p = \sin \frac{\pi x}{L}$			$p = \frac{\sin \pi x}{L} \cos \phi$			$p = \sin \frac{\pi x}{L} \cos 2\phi$		
	$u \times 10^4$	$w \times 10^4$	σ_ϕ	$u \times 10^3$	$w \times 10^3$	σ_ϕ	$u \times 10^3$	$w \times 10^2$	σ_ϕ
3 x 3	0.1361	0.2431	23.5	-0.1489	0.5161	14.6	-0.1111	0.0829	22.8
6 x 6	0.1623	0.2848	28.3	-0.1801	0.6125	26.2	-0.4340	0.3708	199.1
12 x 12	0.1694	0.2961	29.6	-0.1888	0.6389	29.7	-0.5897	0.5194	303.8
24 x 24	0.1713	0.2990	29.9	-0.1910	0.6456	30.6	-0.6364	0.5650	335.5
h ⁶ Extrap	0.1719	0.3000	30.0	-0.1917	0.6478	30.9	-0.6527	0.5810	346.6
Sanders	0.1719	0.3000	30.0	-0.1918	0.6479	30.9	-0.6524	0.5805	348.0
Flügge	0.1719	0.3000	29.5	-0.1918	0.6479	30.9	-0.6505	0.5792	348.8

TABLE 2
CONICAL SHELL RESULTS

$$r = \frac{\sum \bar{w}_s \bar{w}_s}{\sum (\bar{w}_s)^2}$$

GRID	<u>p = 1</u>	<u>p = cos θ</u>	<u>p = cos 2θ</u>
2 x 4	0.803	0.664	0.342
4 x 8	0.892	0.872	0.747
8 x 16	0.931	0.946	0.917
16 x 32	0.951	0.971	0.978

$$r = \frac{\sum \bar{\sigma}_\theta \bar{\sigma}_\theta}{\sum (\bar{\sigma}_\theta)^2}$$

GRID	<u>p = 1</u>	<u>p = cos θ</u>	<u>p = cos 2θ</u>
2 x 4	0.409	0.257	0.043
4 x 8	0.678	0.606	0.440
8 x 16	0.802	0.774	0.703
16 x 32	0.925	0.916	0.892

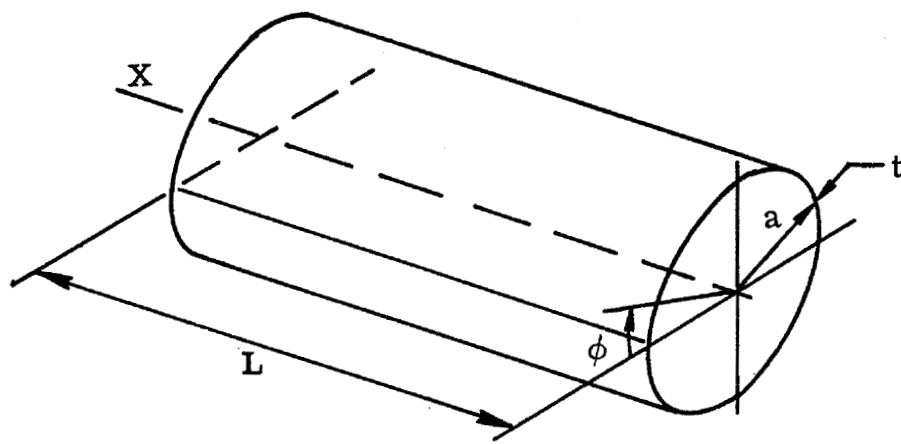


Figure 1. - Cylindrical shell.

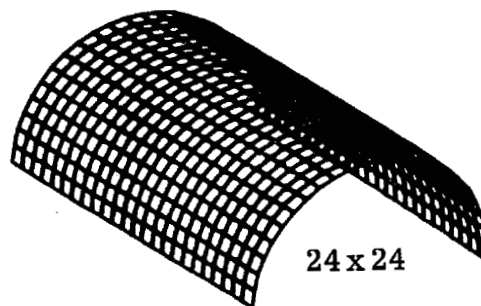
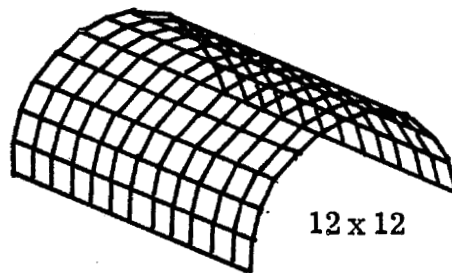
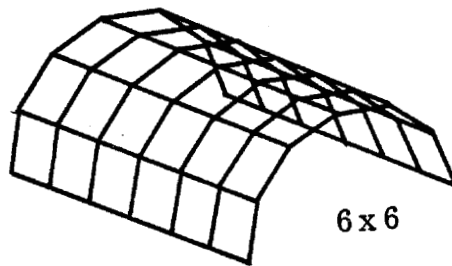
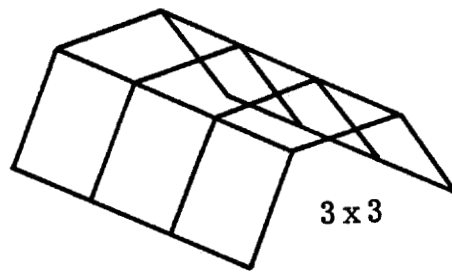


Figure 2. - NASTRAN plots of grids for cylindrical shell.

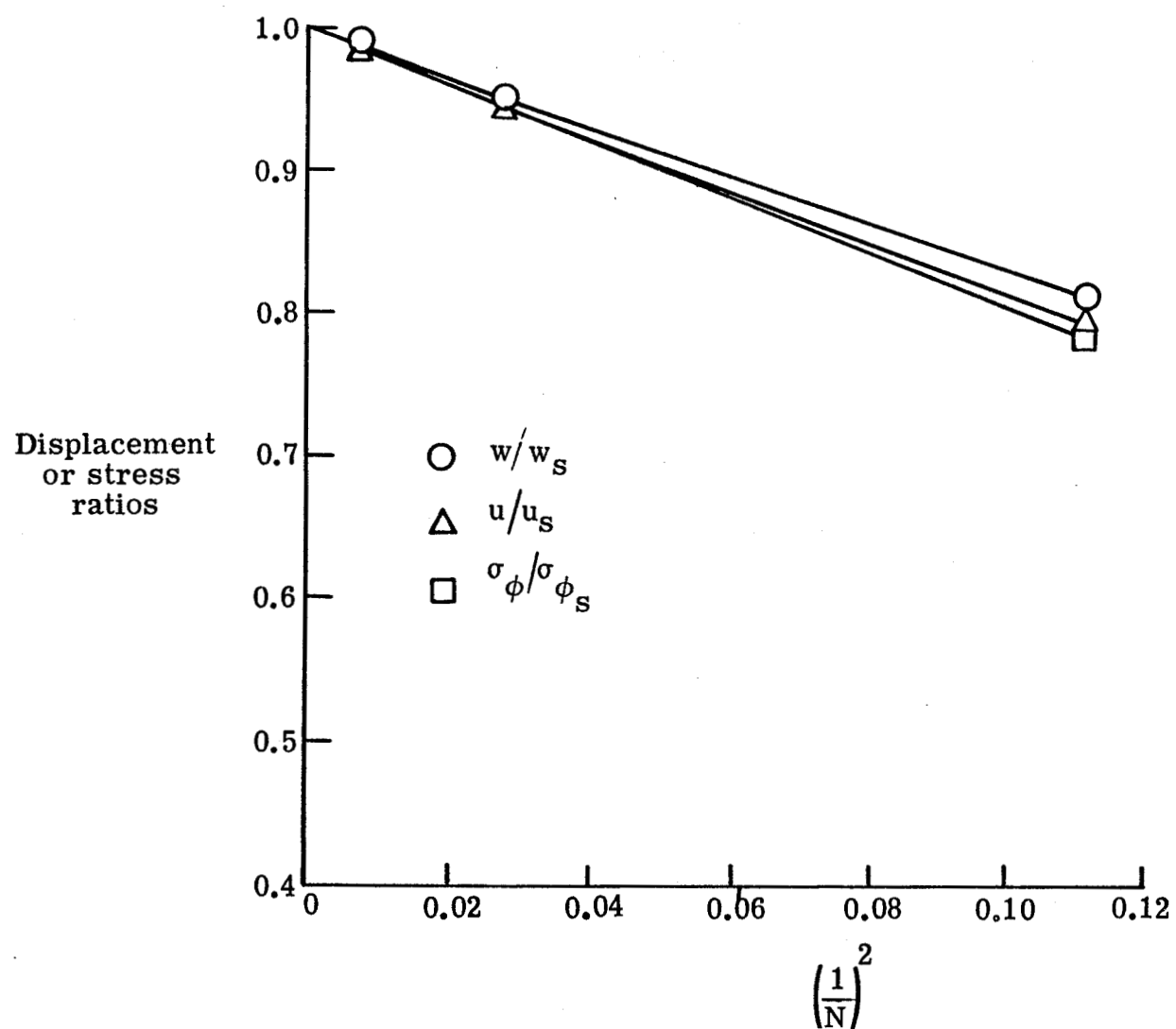


Figure 3. - Convergence of results for simply supported cylinder with $p = \text{SIN } \frac{\pi x}{L}$.

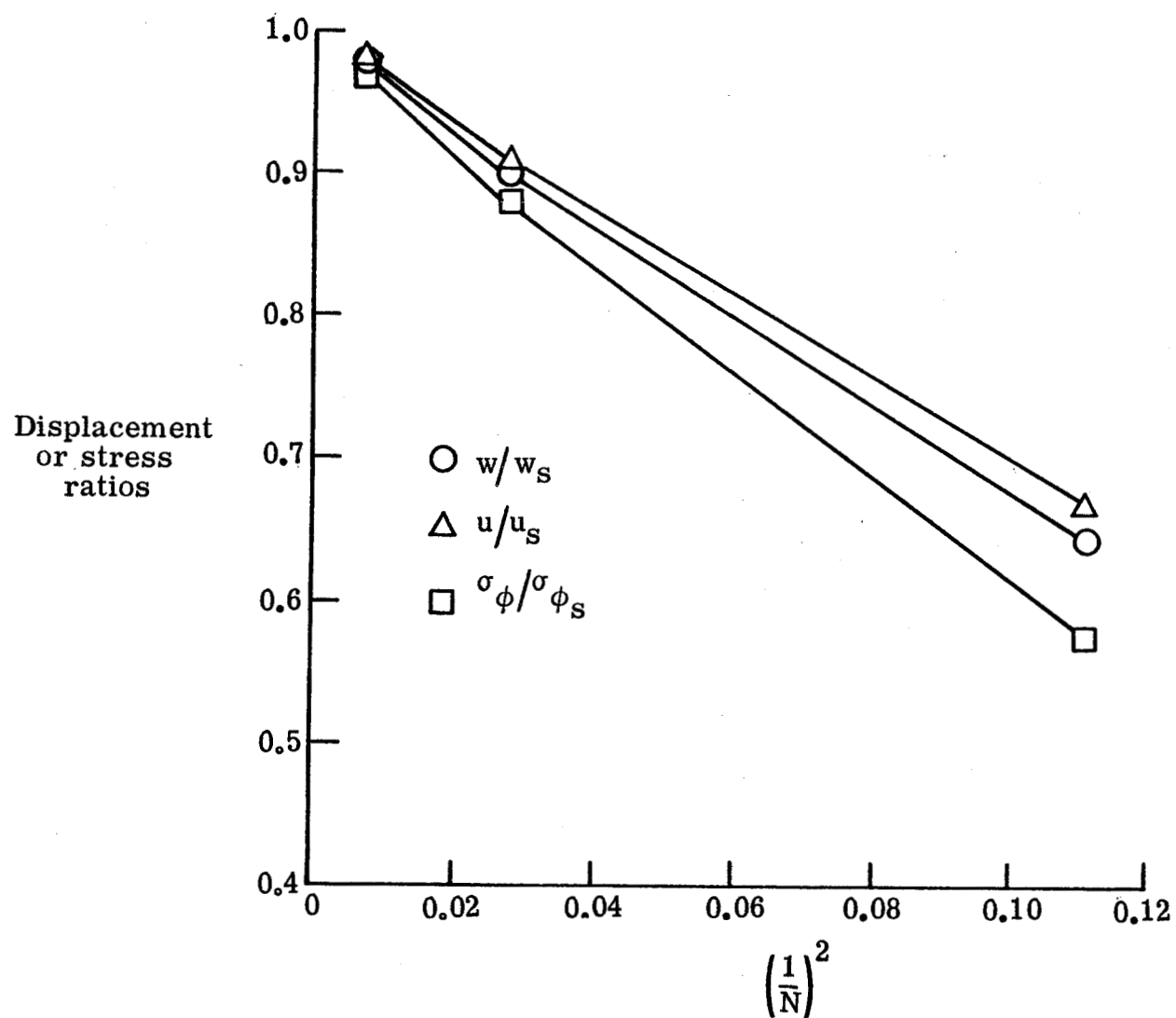


Figure 4.- Convergence of results for simply supported cylinder with $p = \sin \frac{\pi x}{L} \cos \phi$.

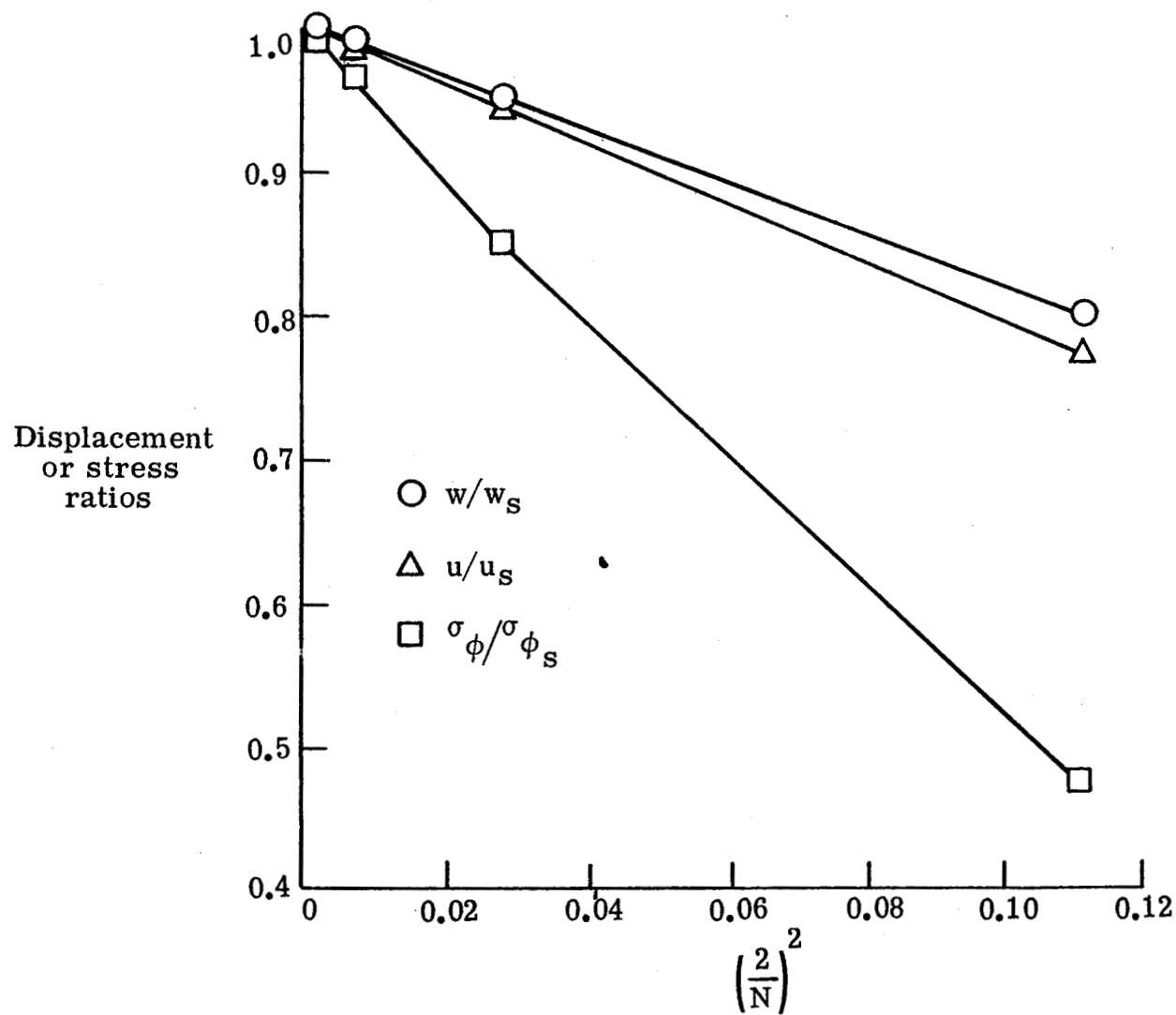


Figure 5. - Convergence of results for simply supported cylinder with $p = \sin \frac{\pi x}{L} \cos 2\phi$.

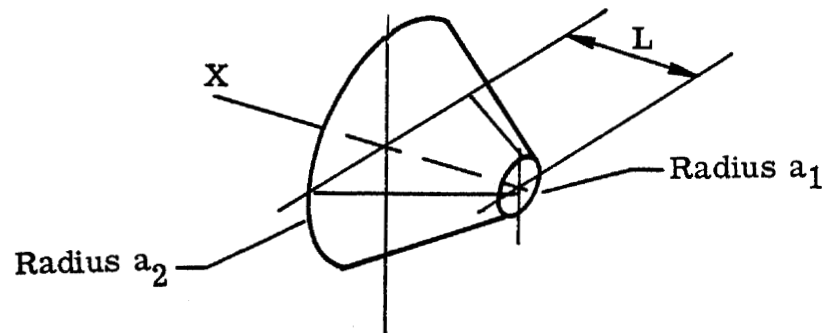


Figure 6. - Conical shell.

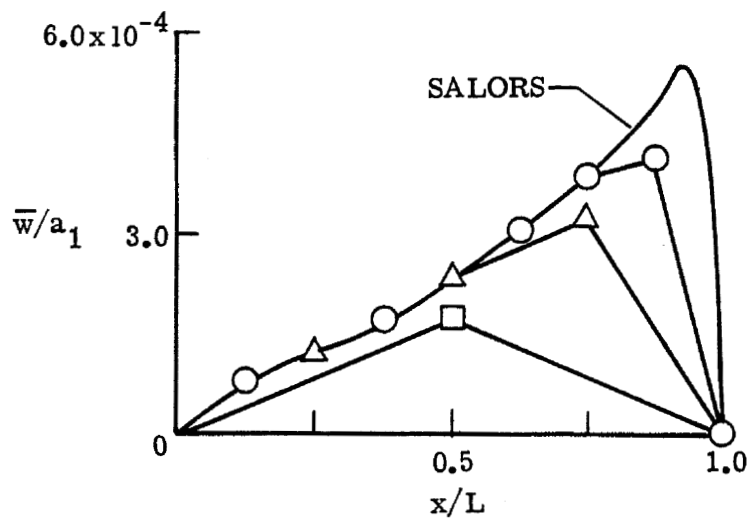


2 x 4

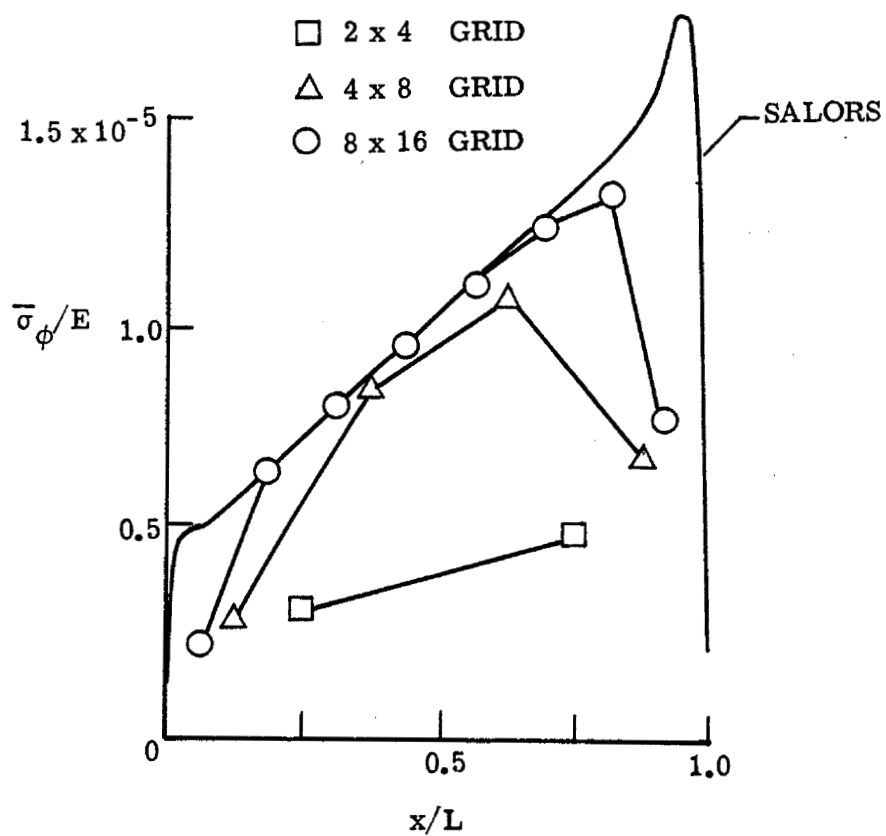


4 x 8

Figure 7. - Finite element models of conical shell.

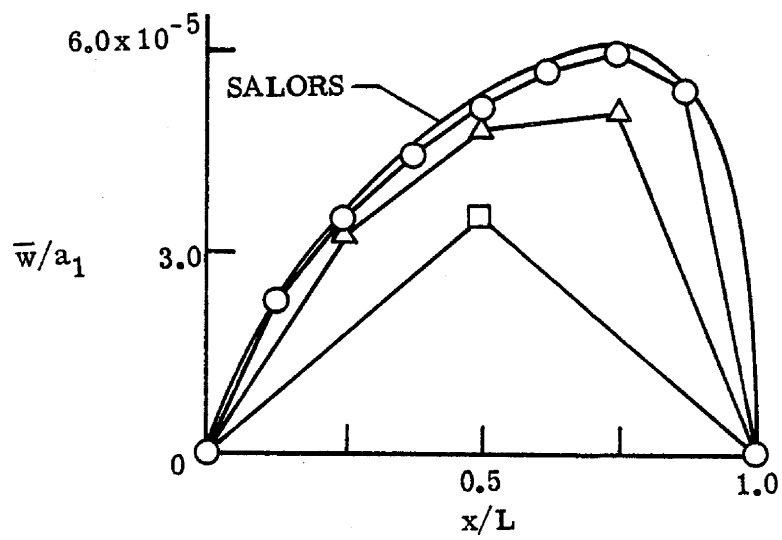


(a) Radial displacement

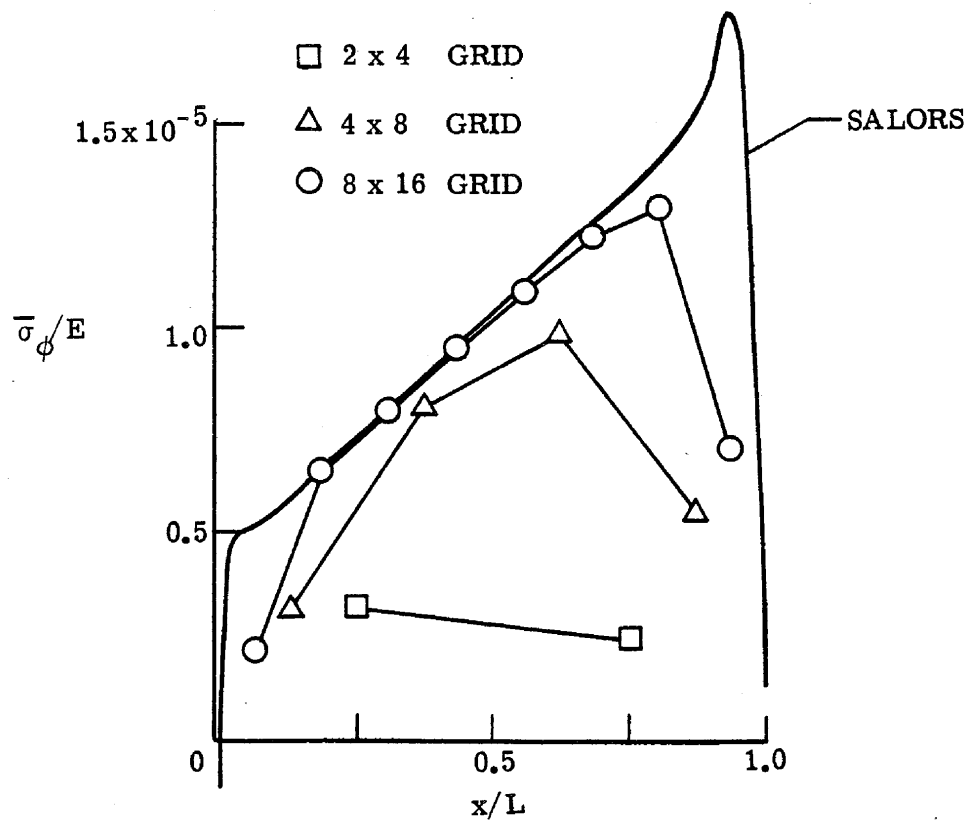


(b) Circumferential stress

Figure 8. - Function coefficients for simply supported cone with $p = 1$.

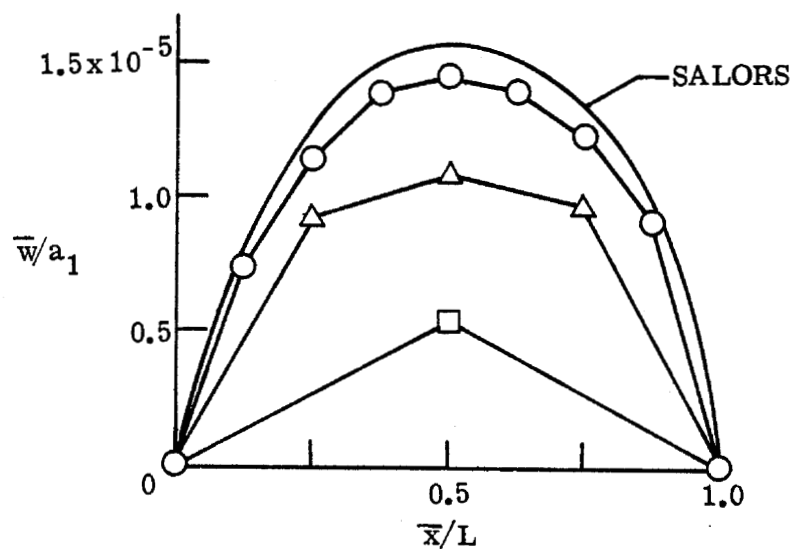


(a) Radial displacement.

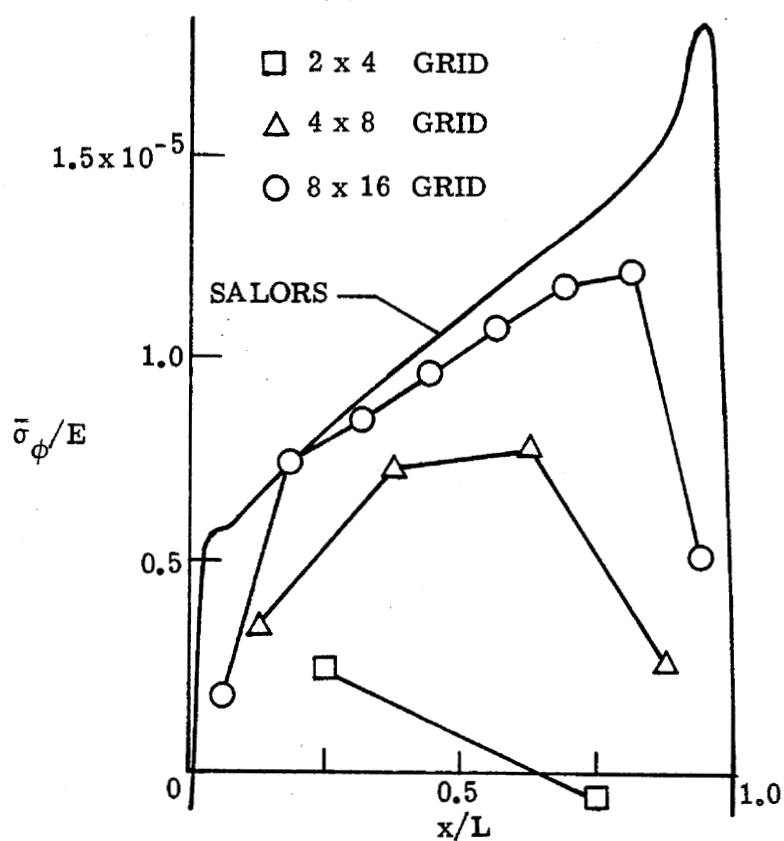


(b) Circumferential stress.

Figure 9. - Function coefficients for simply supported cone with $p = \cos \phi$.



(a) Radial displacement.



(b) Circumferential stress.

Figure 10. - Function coefficients for simply supported cone with $p = \cos 2\phi$.

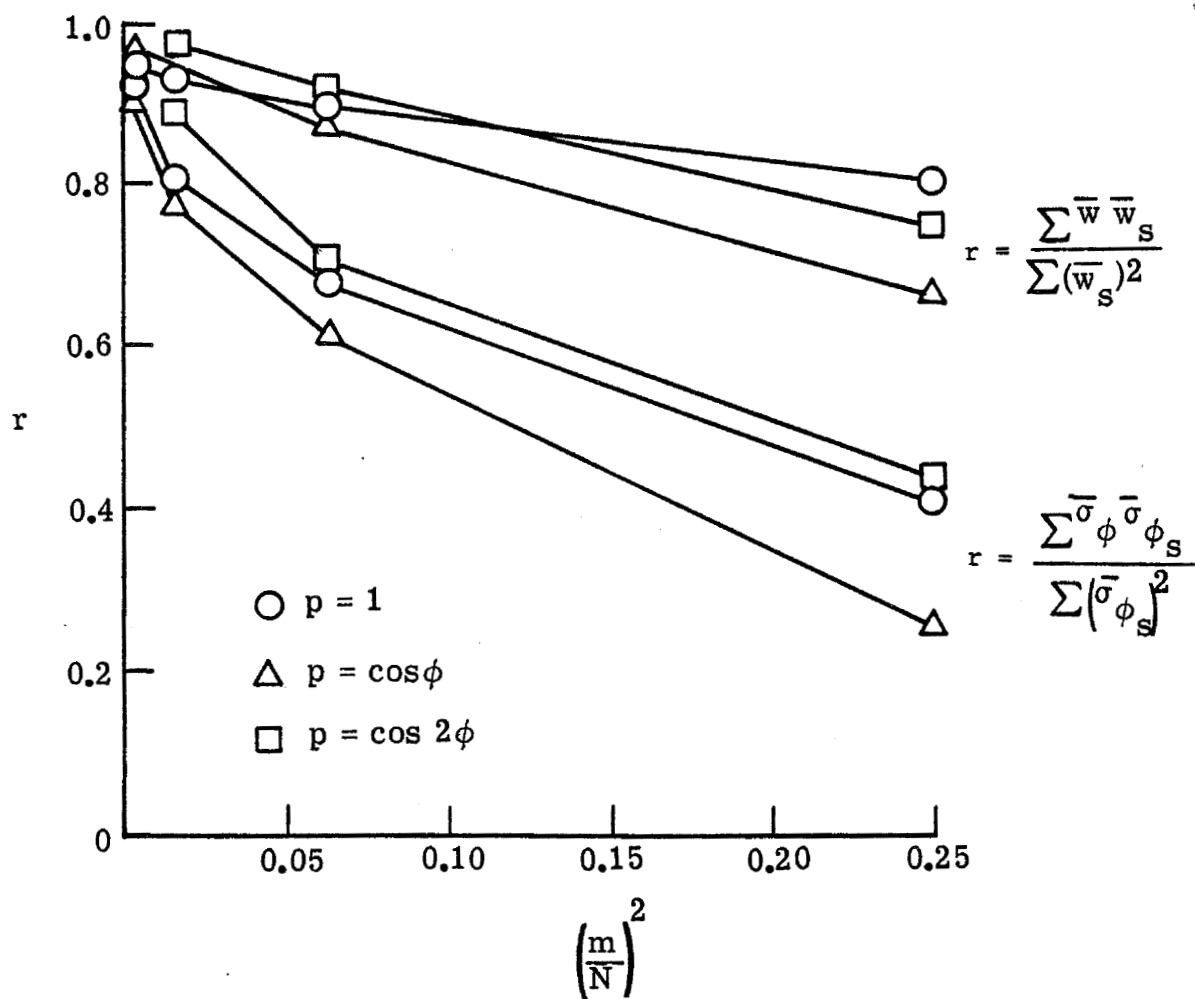


Figure 11. - Plot of error ratios for cone.

SPACE SHUTTLE -

THE NEED FOR SUBSTRUCTURING

By H. R. Grooms and S. Yahata

Space Division, North American Rockwell

SUMMARY

A brief sketch of the method of substructuring is given. The benefits which accrue from using this method of analysis on complex structures are discussed.

INTRODUCTION

While substructuring, in principle, is not really a new idea its application has not been widespread. Substructuring has probably been in use for at least two decades although the mathematical foundation was published by Przemieniecki in 1963 (Reference 1). A somewhat different method has been presented by Rosen and Rubinstein (Reference 2). Explanations of the method also can be found in several other places (References 3 and 4). In structural engineering (as well as most other branches of engineering) too often the problem is forced to fit the existing analytical tools rather than developing the tools to solve the problem. This particular phenomenon seems to account for the minimal use of substructuring.

The shuttle vehicle basically consists of two mated elastic bodies; the booster and the orbiter. The structural analysis of this vehicle lends itself very naturally to multiple level substructuring. This approach inherently resolves some of the more troublesome problems that occur when an analysis of a complex structure like the shuttle vehicle is undertaken. The main advantages of using substructuring are:

- (1) Investigation of various configurations
- (2) Design studies
- (3) Segmented model verification
- (4) Ease and cost of solution

Preceding page blank

Each of these items is discussed in detail in a separate section of this paper.

While NASTRAN does not explicitly include substructuring, it has all the matrix routines necessary to accomplish it. That is, with some effort, NASTRAN could perform substructuring. Substructuring could also be performed by using NASTRAN in conjunction with an existing substructuring program such as NARSESA (Reference 5).

In order to make some of the later concepts discussed in this paper clear a brief outline of the computations involved in substructuring (using the displacement method) is now given. A stiffness matrix (free-free) is generated for each of the substructures. Each of these ($K^{(r)}$, where the superscript denotes the substructure number) is then partitioned:

$$[K^{(r)}] = \begin{bmatrix} [K_{ii}^{(r)}] & [K_{ib}^{(r)}] \\ [K_{bi}^{(r)}] & [K_{bb}^{(r)}] \end{bmatrix}$$

The subscript i denotes interior nodes while the subscript b stands for boundary nodes (nodes that tie to other substructures). A reduced matrix, $K^{(r)}$, is then obtained using

$$[K_b^{(r)}] = [K_{bb}^{(r)}] - [K_{bi}^{(r)}] [K_{ii}^{(r)}]^{-1} [K_{ib}^{(r)}]$$

Operations are also performed with the load and displacement vectors but the details, because of space considerations, are not included (see Reference 1).

After reduced boundary matrices are obtained for each of the substructures these reduced matrices are then superposed. This is done in the following manner:

$$[K_b^{\text{total}}] = \begin{bmatrix} [K_b^1] & & & \\ & [K_b^2] & & \\ & & \ddots & \\ & & & [K_b^n] \end{bmatrix}$$

The double cross-hatched region represents the ties between substructures. This final reduced matrix, $[K_b^{\text{total}}]$, can then be inverted (decomposed) and used with the transformed load vectors to obtain boundary deflections. These boundary deflections are then used along with the substructure stiffness matrices to compute deflections for the entire structure.

INVESTIGATION OF VARIOUS CONFIGURATIONS

Figure 1 shows a sketch of the mated booster-orbiter. Figures 2 and 3 show finite element models for the orbiter and booster, respectively.

The analysis of the shuttle vehicle consists of analyzing three distinct structures: (1) booster alone, (2) orbiter alone, and (3) orbiter and booster mated. Under the one-pass (i.e., without substructuring) system of analysis three separate mathematical models would be required. The computational effort required to obtain these three solutions could be considerable.

However, if substructuring (multiple-level) were used, a significant reduction in the computational effort would occur. The booster and the orbiter could each be formulated as large substructures and solved individually. Then a great portion of the computations required to analyze the third configuration (booster and orbiter mated) would have already been done and saved. This is illustrated by Figure 4. Specifically, the K_b matrices for the booster and orbiter will already be available and can be readily superposed (after partitioning, etc.) to yield a K_b matrix for the mated configuration. Thus the work required to obtain a solution for configuration 3, after configurations 1 and 2 have been handled, is relatively minimal.

DESIGN STUDIES

When design changes are made they usually dictate that a whole new analysis be performed. Consider the case where the three configurations enumerated in the previous section are of interest. A portion of the orbiter wing is changed (e.g., different stiffener size). If a one-pass solution had been obtained for each of the configurations then two (orbiter and orbiter and booster mated) of the three analyses would have to be completely redone.

If the multiple level substructuring scheme outlined in Figure 4 is used then for configuration 2 the following computations have to be redone: 1u and 3b. For configuration 3 computations 1u, 3b, and 4a have to be redone. For configuration 1 none of the computations have to be redone.

The use of substructuring makes the process of structural optimization (e.g., minimum weight, fully stressed, etc.) more feasible than it has been. Different designs (anything can be varied except location of tie points) can be investigated without requiring a complete reanalysis.

SEGMENTED MODEL VERIFICATION

For the analysis of a large complex structure such as the shuttle vehicle the prevention and rectification of modeling errors is a huge task. If a one-pass analysis is undertaken a considerable number of complete runs might be required before all modeling errors could be detected and eliminated. Since these runs would probably be fairly long, the cost of verifying the mathematical model could be enormous. However, if substructuring were used the model could be verified by making much smaller runs - analyzing each substructure separately before forming the assemblage. Also, it is quite possible to have each substructure modeled by a different individual and hence reduce the calendar time required for the analysis.

An analysis of each substructure with its boundaries (tie points) fixed requires few additional computations. An inverse for each substructure, $[K_{ii}^{(r)}]^{-1}$, will have been computed and can be used with any load vectors to obtain deflections. Gross modeling errors should become apparent when these deflections are studied.

EASE AND COST OF SOLUTION

When a one-pass solution is attempted the analysis of a structure with appendages (e.g., space shuttle vehicle) can cause considerable difficulties. If the vehicle were modeled without using substructuring, the bandwidth of the stiffness matrix might be very large. With the use of substructuring the vehicle could be divided into several substructures where each of these has a reasonable bandwidth. Therefore, it can be readily shown that for certain classes of structures the solution using substructuring can be cheaper than a one-pass solution.

Also, when a one-pass solution of a large structural problem is attempted a great deal of faith is inherently put in the reliability of the computer. This can be hazardous when the time required for a particular step is longer than the usual "up" time of the machine. Substructuring helps to reduce this danger by doing the computations in relatively small independent portions. Additionally, depending on the particular installation, it is usually easier to run many small jobs instead of one large job.

An analysis was performed at Space Division, North American Rockwell, of the Space Shuttle vehicle. The orbiter (Figure 2) and the booster (Figure 3) were each divided into a number of substructures. Table 1 gives the total number of degrees of freedom (DOF), maximum semi-bandwidth (SBW), and a description of each of the substructures in the booster. Table 2 gives similar information for the orbiter. Because of symmetry only half of each structure was modeled. For comparison purposes, the size and maximum semi-bandwidth of the booster and orbiter (for a one-pass solution) stiffness matrices are given in Table 3. Substructures 2, 6, 8, 9, and 11 were joined as one assemblage (Figure 4) in order to easily investigate the effects of varying the bulkhead

thicknesses and linkage stiffness.

CONCLUDING REMARKS

A discussion of the reasons for applying substructuring to large complex structures has been given. These reasons, when considered together, form a strong argument for including such a capability in a general purpose program such as NASTRAN. For any substructuring program particular attention should be given to:

1. Internal bookkeeping (including reordering)
2. Compatibility of common boundaries
3. Method of storing arrays
4. Matrix algorithms

REFERENCES

1. Przemieniecki, J. S., "Matrix Structural Analysis of Substructures", JATAA, Vol. 1, No. 1 (Jan. 1963), pp. 138-147.
2. Rosen, R., and Rubinstein, M. F., "Substructure Analysis by Matrix Decomposition", Journal of the Structural Division, ASCE, Vol. 96, St. 3 (March 1970), pp. 663-670.
3. Przemieniecki, J. S., Theory of Matrix Structural Analysis, McGraw-Hill Book Co., New York, 1968.
4. Rubinstein, M. F., Matrix Computer Analysis of Structures, Prentice Hall, Inc., New Jersey, 1966.
5. Yahata, S., Grooms, H. R., Furuike, T., "User's Manual to Multiple Level Substructuring: NARSESA", STR-247, North American Rockwell Corp., Space Division, 1970.

TABLE 1 - BOOSTER

SUBSTRUCTURE NO.	DOF/SBW	DESCRIPTION OF SUBSTRUCTURE
1	588/366	Thrust Structure
2	240/90	Aft Bulkhead H ₂ Tank
3	810/180	Aft Section H ₂ Tank
4	372/246	Mid Section H ₂ Tank
5	390/90	Forward Section H ₂ Tank
6	240/90	Forward Bulkhead H ₂ Tank
7	420/276	Inter-Tank Structure
8	42/18	Orbiter-Booster Forward Linkage
9	240/90	Aft Bulkhead O ₂ Tank
10	474/90	O ₂ Tank & Forward Skirt
11	240/90	Forward Bulkhead O ₂ Tank
12	588/90	Delta Wing
13	252/54	Canard
14	252/54	Vertical Stabilizer

TABLE 2 - ORBITER

SUBSTRUCTURE NO.	DOF/SBW	DESCRIPTION OF SUBSTRUCTURE
1	540/126	Forward Fuselage
2	744/126	Forward Intermediate Fuselage
3	744/126	Aft Intermediate Fuselage
4	620/192	Aft Fuselage
5	576/66	Vertical Tail
6	426/120	Delta Wing

TABLE 3

DOF/SBW	STRUCTURE
4500/420	Booster
3000/216	Orbiter

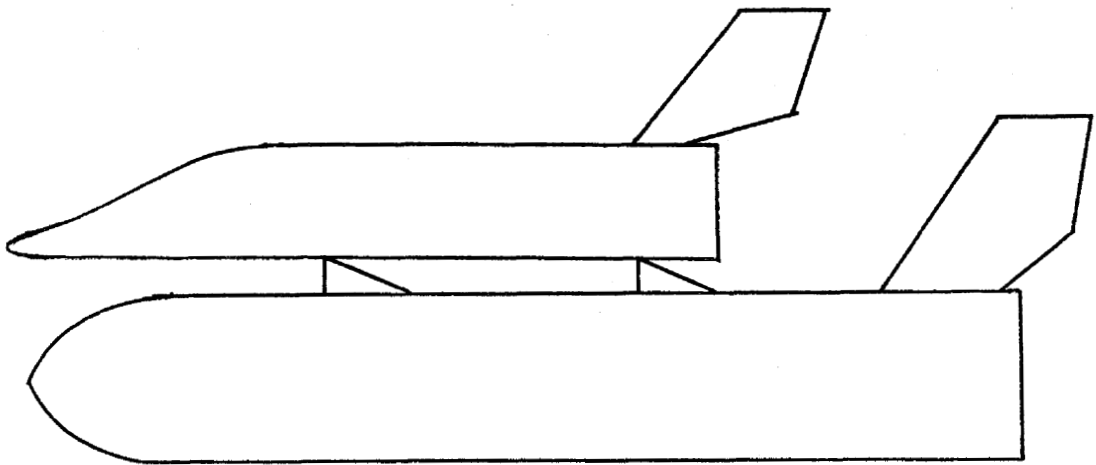


FIGURE 1 - MATED BOOSTER-ORBITER.

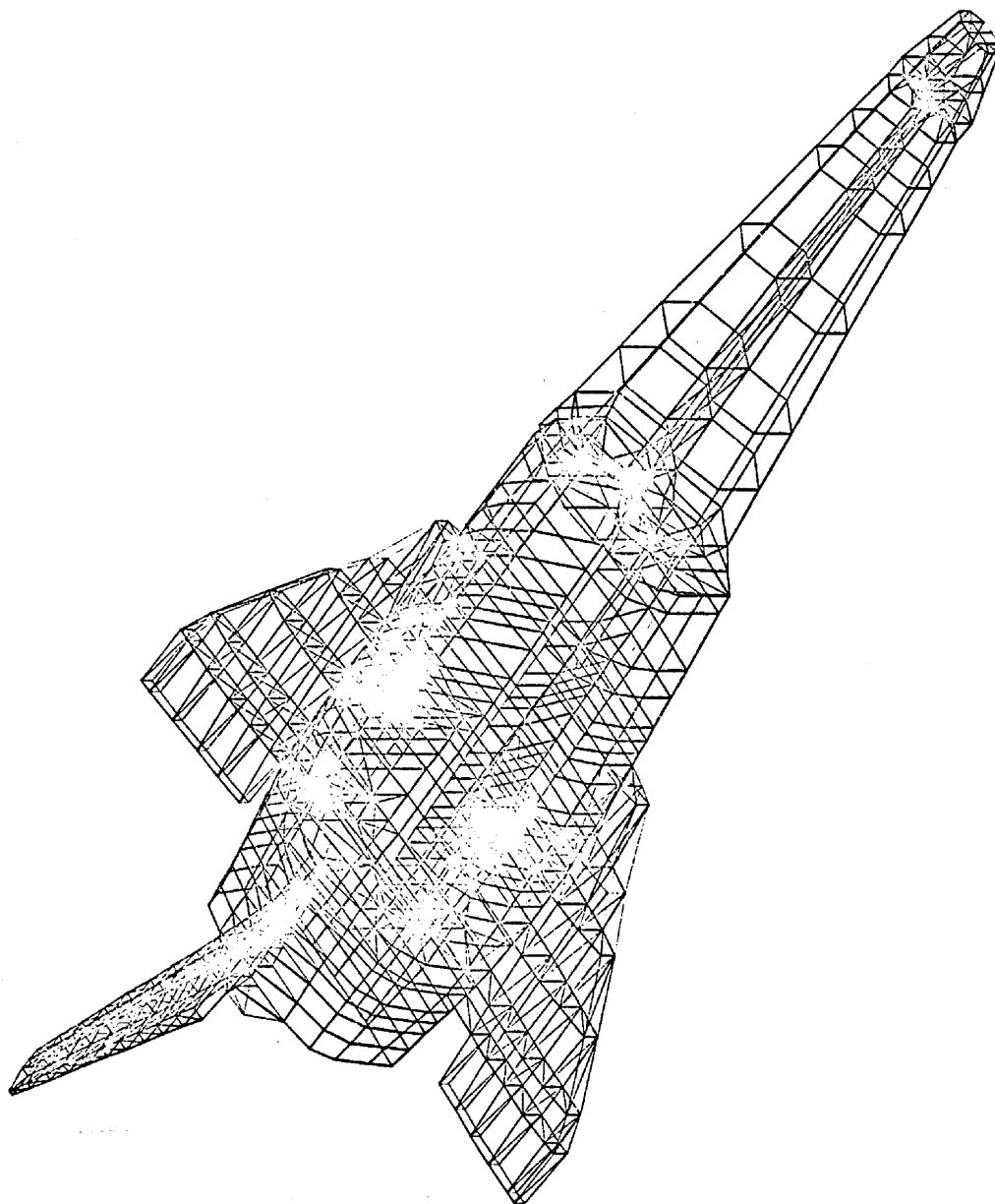


FIGURE 2 - ORBITER.

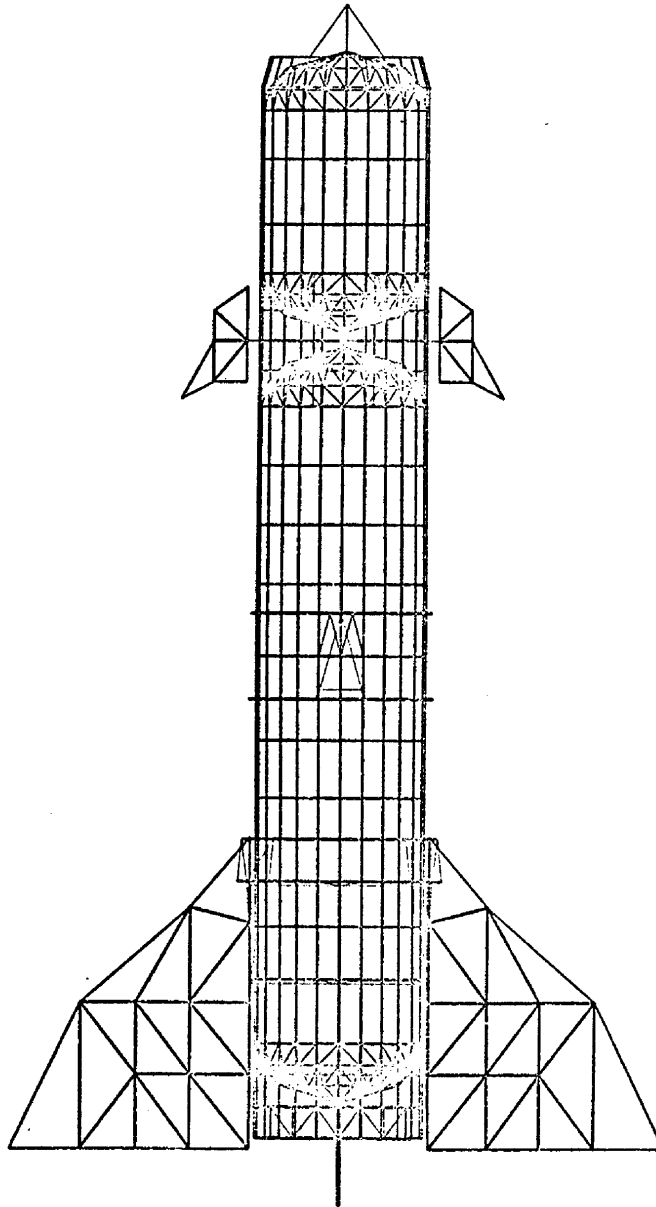


FIGURE 3 - BOOSTER.

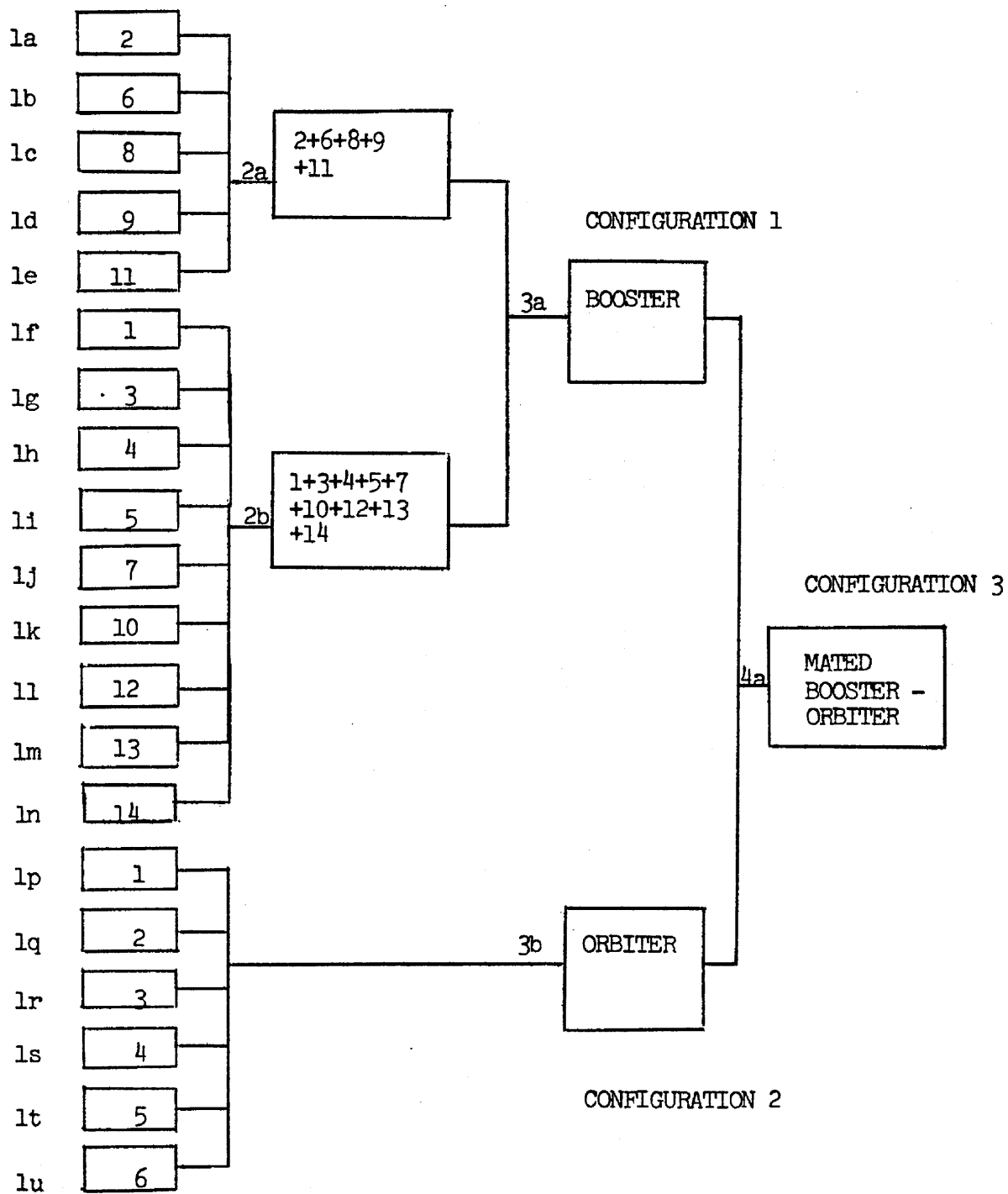


FIGURE 4 - MULTIPLE LEVEL SUBSTRUCTURING APPLIED TO SPACE SHUTTLE.

A DESIGN STUDY FOR THE INCORPORATION OF AEROELASTIC CAPABILITY INTO NASTRAN

By Robert L. Harder*, Richard H. MacNeal*, and Robert V. Doggett, Jr.**

*The MacNeal-Schwendler Corporation

**NASA Langley Research Center

SUMMARY

This paper summarizes a study whose results are presented in detail in reference 1. The purpose of the study was to define the modifications required to add aeroelastic capability to NASTRAN. A preliminary design for the new capability was developed, including the subdivision of the task into functional modules, the specifications of the mathematical content of the modules, and the arrangement of modules into flow diagrams for new NASTRAN rigid formats. The development of the preliminary design revealed the existence of a number of computational problems to whose solution particular attention was directed. The mathematical and computational details of the study are contained in reference 1.

PRESENT NASTRAN CAPABILITIES

The NASTRAN digital computer program for structural analysis is a finite element program with an extremely broad range of applications. Its problem solving capabilities are, at present, separated into the following twelve "rigid formats," each of which entails a predetermined sequence of calculations that are performed by "functional modules" under the control of a flexible executive system:

Static Analysis

1. (Basic) Static Analysis
2. Static Analysis with Inertia Relief
3. Static Analysis with Differential Stiffness
4. Piecewise Linear Analysis

Elastic Stability

5. Buckling

Dynamics

6. Vibration Mode Analysis
7. Direct Complex Eigenvalue Analysis
8. Direct Frequency and Random Response Analysis

9. Direct Transient Response Analysis
10. Modal Complex Eigenvalue Analysis
11. Modal Frequency and Random Response Analysis
12. Modal Transient Response Analysis

It will be noted that dynamic response and complex eigenvalue problems may be solved either by a "direct" method or by a "modal" method. In a direct method the degrees of freedom are physical components of displacement. In a modal method the degrees of freedom are generalized modal coordinates. Like all other general purpose structural programs, NASTRAN employs the finite element approach. The structural model that is analyzed consists of "elements" such as beams, plates, and concentrated springs, that are connected together at a finite number of "grid points." The equilibrium equations of the model are expressed and solved in terms of the components of motion at grid points. The solution of large problems, with hundreds or thousands of structural elements, is emphasized in the design of NASTRAN. It is, in addition, a highly user-oriented program with a large number of convenience features including automatic load generation, plotting, and restart capabilities. It also includes provisions for incorporating nonstructural components, such as control systems, in the structural model.

At present, the solution of aeroelastic problems is accomplished in NASTRAN by means of "direct input" matrices which may be real or complex and which may be added to the structural mass, damping, or stiffness matrices and included in the solution of any of the seven dynamic rigid formats. This provision is regarded as inadequate for the following reasons:

- a. It requires the use of separate computer programs for the generation of the aerodynamic input matrices, thereby causing delays and increasing the frequency of errors.
- b. It places the burden of achieving geometric compatibility between the aerodynamic forces and the structure entirely on the user of the program.
- c. It provides very little static aeroelastic capability and it automates none of the specialized features of aeroelastic analysis, such as the selection of control surface deflections for trimmed flight, and the plotting of V-g flutter curves.

OBJECTIVES

The purpose of the study was to define the modifications that will be required to make NASTRAN an effective tool for aeroelastic analysis. Due to its modular character, the addition of new capability to NASTRAN is not inherently difficult. The modifications required to add a particular new capability may involve changes in existing functional modules, the generation of new functional modules, or the compilation of new rigid formats. All of these measures will be required to add aeroelastic capability.

One of the major objectives of the study was to define an aeroelastic capability for NASTRAN which will provide a degree of automation and a range of application comparable to that which presently exists for the solution of purely structural problems. Advanced aerodynamic configurations, such as the Space Shuttle, indicate a need for a more sophisticated approach to aeroelasticity in order to cope with the attendant structural and aerodynamic complexities. Our study of these matters has led to the following list of requirements for a general purpose aeroelastic program:

1. Broad Application
 - a. Many types of structures
 - b. Many aerodynamic configurations
 - c. Subsonic to hypersonic flow regimes
 - d. Many classes of static and dynamic analysis
 - e. Compatibility with other aspects of structural analysis, such as stress analysis, and control system interaction
2. Sophistication
 - a. Ability to use advanced aerodynamic theories
 - b. Accurate and efficient computational procedures
 - c. Many degrees of freedom
3. Automation
 - a. Minimum user effort, for both clerical and intellectual tasks
 - b. Checkpoint and restart capabilities
4. Ease of modification to include new or improved features

The requirement for broad application is important from an economic viewpoint, because it reduces the number of separate computer programs, and, therefore, reduces development cost. It also eliminates the time that the user would spend in learning to apply several separate programs, and in preparing several different sets of input data.

The qualities listed under Sophistication and Automation are the qualities that are usually associated with large user-oriented computer programs, and they are now largely taken for granted in structural analysis, if not yet in aeroelastic analysis. Ease of modification to include new or improved features is particularly important due to the long length of the development cycle for large scale computer programs, and the rapidity of recent technical progress.

The heart of an aeroelastic analysis is the theory used to calculate aerodynamic forces, and the requirements listed above for the complete computer program can also, very largely, be applied to the selection of aerodynamic theories. Since no existing theory has the desired range of application, the

ability to include several different aerodynamic theories, perhaps even in the same problem, is recognized as a requirement. Advanced theories should be included, and also simple theories which are usually better from the standpoint of computational efficiency. One of the tasks undertaken in the study was to investigate candidate unsteady aerodynamic theories with respect to their range of application, accuracy, efficiency, user convenience, and general compatibility with a finite element approach to aeroelastic analysis.

CLASSIFICATION OF AEROELASTIC PROBLEMS

It is expected that aeroelastic capability will be implemented in NASTRAN by a number of different rigid formats with names such as "Divergence," "Flutter," and "Frequency Response" that correspond to different types of analysis. A first task, before discussing the proposed measures for including aeroelasticity in NASTRAN, is to classify aeroelastic problems according to type of solution. The classification will be separated, for convenience, into static aeroelastic problems, flutter, and dynamic response problems.

Static Aeroelastic Problems

A static aeroelastic problem may be defined as a problem involving the response of a flexible structure to aerodynamic loading in which terms proportional to the velocities and accelerations of the structure are assumed to be independent of time. Thus, inertia forces, if they enter at all, are assumed to be constant in time. The three common types of static aeroelastic problems are

- a. Calculation of static response, including loads and stresses in the structure.
- b. Calculation of stability and control derivatives, i.e., the calculation of the changes in the aerodynamic loading (and, more particularly, of the changes in its resultants) due to small changes in the motions of the vehicle and of control surface deflections.
- c. Divergence, which is an idealized stability problem in which the determinant of the stiffness matrix, including both structural and aerodynamic terms, vanishes.

Each of the above static aeroelastic problems may be further classified as to whether the structure is supported or free to move. If it is free to move, the inertia forces due to (steady) accelerations must be taken into account.

An additional distinction occurs in the determination of the static response of a freely moving structure, with respect to the manner in which the velocity components and the control surface deflections of the structure are determined. In some cases the analyst specifies all of the components of velocity and the control surface deflections and accepts whatever accelerations

they produce. He may, on the other hand, request that some of the velocity components and control surface deflections be evaluated so as to put the forces on the vehicle into equilibrium, i.e., into a trimmed flight condition.

The general task of formulating and classifying static aeroelastic problems for solution in NASTRAN is addressed in Appendix B of reference 1. It is shown there that all of the problem types mentioned above may be solved with the following three rigid formats:

- Aeroelastic Divergence
- Untrimmed Static Aeroelastic Response
- Trimmed Static Aeroelastic Response

In particular, the calculation of stability and control derivatives is treated as a subcase of static aeroelastic response.

Flutter

Flutter is the dynamic aeroelastic stability problem and it is appropriately analyzed as an eigenvalue problem. It is, however, a multiple eigenvalue problem because the speed and altitude at which the oscillations become unstable are desired items of information. The unsteady aerodynamic forces are functions of reduced frequency (or Strouhal number), Mach number, air density, and perhaps of other parameters. A standard general approach to flutter analysis is to evaluate the frequency of the oscillations and their damping (or equivalently the structural damping required to make them neutrally stable) for different values of the parameters, and then to cross-plot the results to find stability boundaries in the parameter space. Several variations of the general approach are explored in reference 1, resulting in the recommendation that two different methods of flutter-eigenvalue analysis be implemented in NASTRAN. These methods, which are the conventional reduced frequency method and the Hassig P-K method, reference 2, can be implemented with the same rigid formats.

The ability to have both "direct" and "modal" methods of solution, noted earlier as an existing NASTRAN capability, is also important for flutter analysis, although the modal method is usually more efficient. Separate "direct" and "modal" rigid formats are proposed for flutter analysis.

Dynamic Response

The steady state response of an aeroelastic system to sinusoidal excitation can provide the basis for the calculation of deflections and stresses due to loads caused by oscillatory vibration, random vibration, and transient excitation. The frequency response calculation requires the solution of a system of simultaneous complex algebraic equations. The transfer functions that result from the calculation can be used to compute the statistical properties of the response of linear systems to stationary random excitation. In

addition, Fourier integral transform theory provides the basis for using frequency response data to compute the response of linear systems to transient excitation.

The latter ability is particularly important for aeroelastic analysis because all advanced unsteady aerodynamic theories are formulated in the frequency domain. Their conversion to the time domain in order to numerically integrate the equations of motion appears to be prohibitively awkward unless gross approximations are made. For this reason, the study concludes that transient aeroelastic response calculation should be implemented by the Fourier Integral Method only, at least initially.

Dynamic aeroelastic response, therefore, results in four NASTRAN rigid formats corresponding to frequency response analysis and transient response analysis (by the Fourier Integral Method) using either a direct or a modal formulation. Random analysis is treated, as in the present NASTRAN rigid formats, as a subcase of frequency response.

THE MAJOR TASKS

The process of solving a linear aeroelastic problem with the aid of a structural analysis computer program is conceived as consisting of the following steps:

1. Define the properties of the structure in terms of matrices of stiffness, mass and (perhaps) damping coefficients that refer to the components of motion at structural grid points (or to generalized modal coordinates in a modal formulation).
2. Compute a matrix of aerodynamic influence coefficients, relating forces to motions, at a set of aerodynamic control points.
3. Transfer the aerodynamic influence coefficients to the structural grid points (or to modal coordinates) and combine them with the structural matrices.
4. Solve the resulting matrix equations by whatever methods are appropriate for the type of results desired, e.g., by eigenvalue extraction for a flutter analysis.
5. Recover stresses, aerodynamic forces, etc., by means of equations relating these quantities to the degrees of freedom evaluated in Step 4.

In the above list of steps,

- Step 1 requires no modification of NASTRAN;
- Steps 2 and 3 are wholly new;

- Step 4 requires some new solution techniques to accommodate special features of aeroelastic analysis;
- Step 5 requires modification of NASTRAN only to the extent of adding routines to recover aerodynamic quantities.

Major emphasis was placed, during the study, on formulating an approach for the implementation of steps 2 and 3. The foremost objectives were to provide a broad range of options with respect to configuration parameters and available theories, and to minimize user effort.

Step 2 was divided into two tasks: first, subdivision of aerodynamic surfaces into subregions (called aerodynamic elements) and the definition of their geometric properties; and second, the calculation of aerodynamic matrices for the selected aerodynamic theories. By restricting the range of permitted aerodynamic element shapes and orientations, the design of a module to perform the first task is made independent of the second task. The work required to add new aerodynamic theories is thereby minimized for theories that conform geometrically to the restrictions that are imposed. For this reason considerable attention was paid in the study to the geometric requirements of current aerodynamic theories.

Step 3 was divided into four tasks as follows, each performed by a different functional module:

- 3.1 Generate a transformation matrix that linearly relates displacements at aerodynamic control points to displacements at structural grid points. Calculation of the transformation matrix involves the use of interpolation procedures, for which a variety of options were proposed in the study.
- 3.2 Compute aerodynamic matrices as seen at the structural grid points (or modal coordinates) for a selected list of aerodynamic parameter sets (reduced frequency and Mach number), using the transformation matrix from task 3.1, the aerodynamic matrices generated in step 2, and, if needed, the matrix of structural eigenvectors.
- 3.3 Interpolate the aerodynamic matrices to other values of the aerodynamic parameters.
- 3.4 Combine the aerodynamic and structural matrices in the functional module that generates each particular type of solution.

The accomplishment of step 4, solution of matrix equations, will require new routines for flutter analysis, divergence and static aeroelastic response. In our judgement, the existing NASTRAN procedures are not adequate to accommodate the special features of these analysis types, although in all cases the new routines resemble existing routines.

The effort required to formulate computational procedures for the above tasks resulted in some innovations that may be worthy of consideration in other

contexts. These include the use of elastic plates for surface interpolation, reference 1, appendix E, and the derivation of a kernel function, reference 3, that permits extension of the subsonic aerodynamic theory known as the Doublet-Lattice Method, reference 4, to supersonic speeds.

FLOW DIAGRAMS

A computer program consists of a set of instructions that are organized to solve a variety of mathematical problems. The problems themselves are described by parameter values supplied by the user of the program. The computational task is subdivided into steps that are performed by discrete blocks of code called "Functional Modules." In NASTRAN, calls to functional modules are controlled by the "Executive System." A number of sequences of module calls, called "Rigid Formats," are stored in the program. Each rigid format is designed to solve a particular class of problems such as "Basic Static Analysis," "Buckling," "Modal Transient Response Analysis," etc.

The subdivision of computational steps into Functional Modules is arbitrary at least to the degree that the dividing points that they insert in the sequence of calculations can be placed arbitrarily. In some cases it is also possible to rearrange the order of calculations. Computational efficiency (and common sense) dictates the insertion of division points at places where the data transmitted across the interfaces are minimal (NASTRAN requires that all data blocks transferred from one module to another be first placed in peripheral storage). Other factors, such as the requirement that restarts can only be scheduled at the beginning of a module, or that certain calculations are useful in several different types of problems, influence the subdivision into Functional Modules.

The subdivision of aeroelastic analysis into NASTRAN Functional Modules and Rigid Formats, as recommended by the study, is summarized in the following exhibits:

Table 1: Simplified Flow Diagram for Dynamic Aeroelastic Analysis

Table 1 presents a sequence of functional module calls for all forms of dynamic aeroelastic analysis. It also provides a very brief statement of the operations performed by each module and indicates whether the module is an existing module or a new module.

Table 2: Simplified Flow Diagram for Static Aeroelastic Analysis

Table 2 is analogous to Table 1.

Table 3: New Functional Modules

Table 3 lists the names of the new functional modules contained in Tables 1 and 2 in three categories:

- A. Modules used in both static and dynamic analysis.
- B. Modules used only in dynamic analysis.
- C. Modules used only in static analysis.

Table 4: New Rigid Formats

Table 4 lists nine new rigid formats for the solution of aeroelastic problems. Each rigid format corresponds to a particular type of aeroelastic analysis and, in the case of dynamic aeroelasticity, to a particular method of analysis. Additional rigid formats will be required for transient analysis with aerodynamic forces represented directly in the time domain, but this topic has not been researched sufficiently. The different rigid formats correspond to alternate paths in the flow diagrams of Tables 1 and 2, or to the deletion of some modules, or, in some cases, simply to alternate paths within modules. Separate rigid formats are provided for direct and modal dynamic analyses, which is consistent with existing NASTRAN practice for structural dynamics. A separate rigid format does not exist for the calculation of stability derivatives, because this task can be accomplished with Format No. 8A, Untrimmed Static Aeroelastic Response.

CONCLUDING REMARKS

The addition of aeroelastic capability to NASTRAN is seen to be a sizeable task involving the generation of nine new rigid formats and seventeen new functional modules. The magnitude of the task is inherent in the breadth of the subject matter and in the requirements for automation and generality that were assumed. NASTRAN itself is relatively easy to modify.

The question remains as to whether or not the recommendations of the study should be implemented. The answer to this question depends in turn, on the answers to the following three questions.

1. Is there a requirement for an aeroelastic analysis capability with the degree of automation and the range of application that were assumed in the study?
2. Does any existing computer program meet the requirements?
3. Is NASTRAN the best program to use as a basis for the new capability?

The first question can be answered by even a brief examination of the configurations proposed for the Space Shuttle, all of which are characterized by a multiplicity of interfering aerodynamic surfaces and a high degree of

structural complexity. As was mentioned earlier, the examination of the aeroelastic properties of the Space Shuttle and of other advanced configurations generated the list of requirements that were assumed in the study.

The answer to the second question is that no computer program exists in the public domain that even remotely approaches satisfaction of the requirements. The closest approach is probably the COFA series of computer programs for flutter analysis, reference 5, developed under sponsorship of the Naval Air System Command, which includes capability for the entire Mach number range but which is severely configuration limited.

The answer to the third question depends mostly on one's opinion of NASTRAN relative to other available general purpose structures programs. Certainly there can be little question that the modularity and sophistication provided by general purpose programs are needed, or that the largest and most advanced general purpose programs have been developed for structural analysis. NASTRAN's chief competitor would appear to be FØRMAT II, reference 6, developed under Air Force sponsorship. It seems likely at this date that aeroelastic capability will be added to both programs.

REFERENCES

1. Harder, R. L.; MacNeal, R. H.; and Rodden, W. P.: A Design Study for the Incorporation of Aeroelastic Capability into NASTRAN. NASA CR-111918, 1971.
2. Hassig, H. J.: An Approximate True Damping Solution of the Flutter Equation by Determinant Iteration. To be published in Journal of Aircraft, Nov. or Dec. 1971.
3. Harder, R. L.; and Rodden, W. P.: Kernel Function for Nonplanar Oscillating Surfaces in Supersonic Flow. Journal of Aircraft, vol. 8, no. 8, Aug. 1971, pp. 677-679.
4. Albano, E.; and Rodden, W. P.: A Doublet-Lattice Method for Calculating Lift Distributions on Oscillating Surfaces in Subsonic Flows. AIAA Journal, vol. 7, no. 2, Feb. 1966, pp. 279 - 285.
5. Collocation Flutter Analysis. Missile Systems Division Report No. MSD-P69-144, Hughes Aircraft Co., April 1969.
6. Picard, J: Format II - Second Version of Fortran Matrix Abstraction Technique. Vol. 1, User's Manual, AFFDL TR-66-207, Air Force Flight Dynamics Lab, WPAFB, Ohio, Dec. 1966.

TABLE 1. Simplified Flow Diagram for Dynamic Aeroelastic Analysis

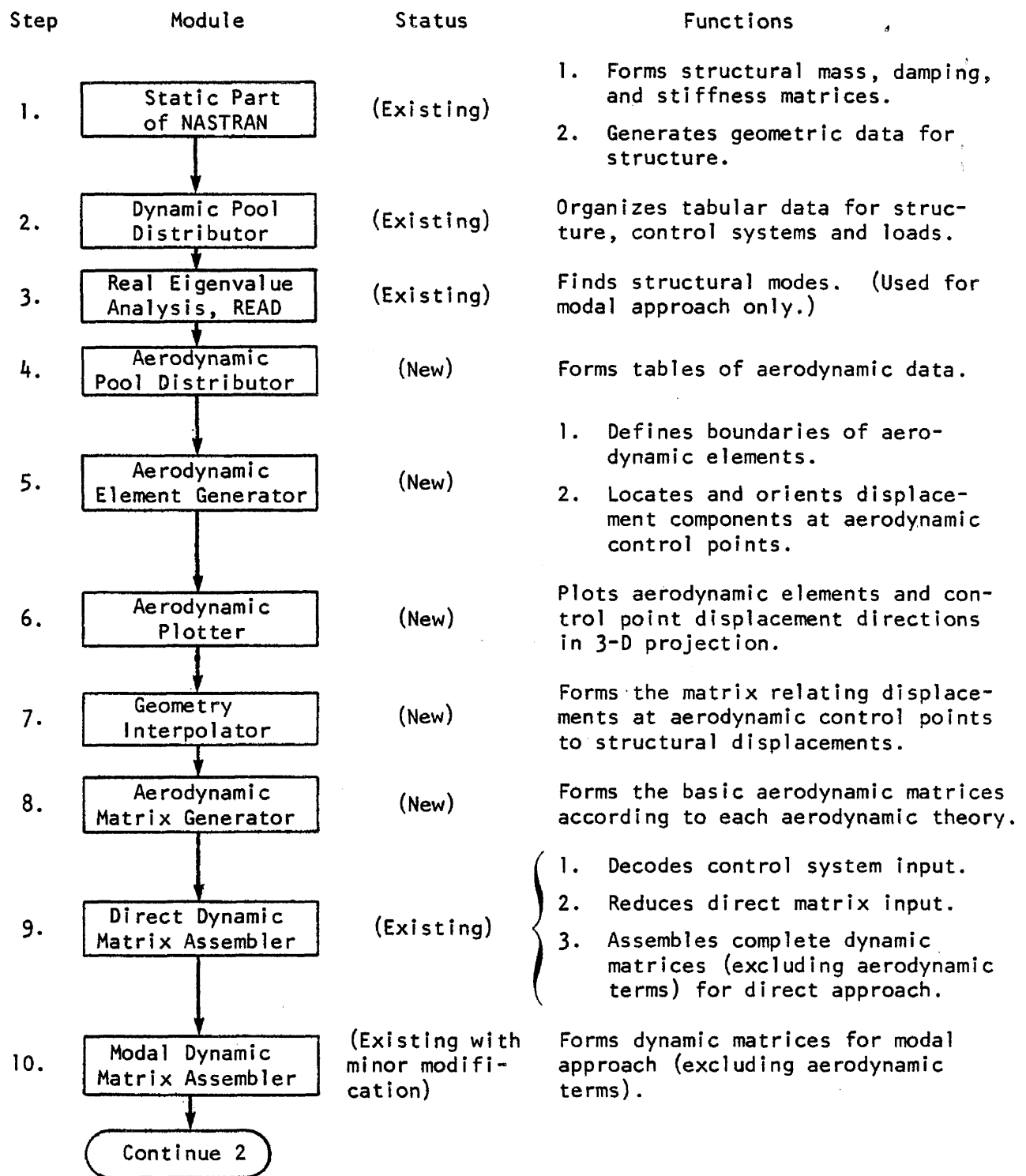


TABLE 1. Simplified Flow Diagram for Dynamic Aeroelastic Analysis
(Cont.)

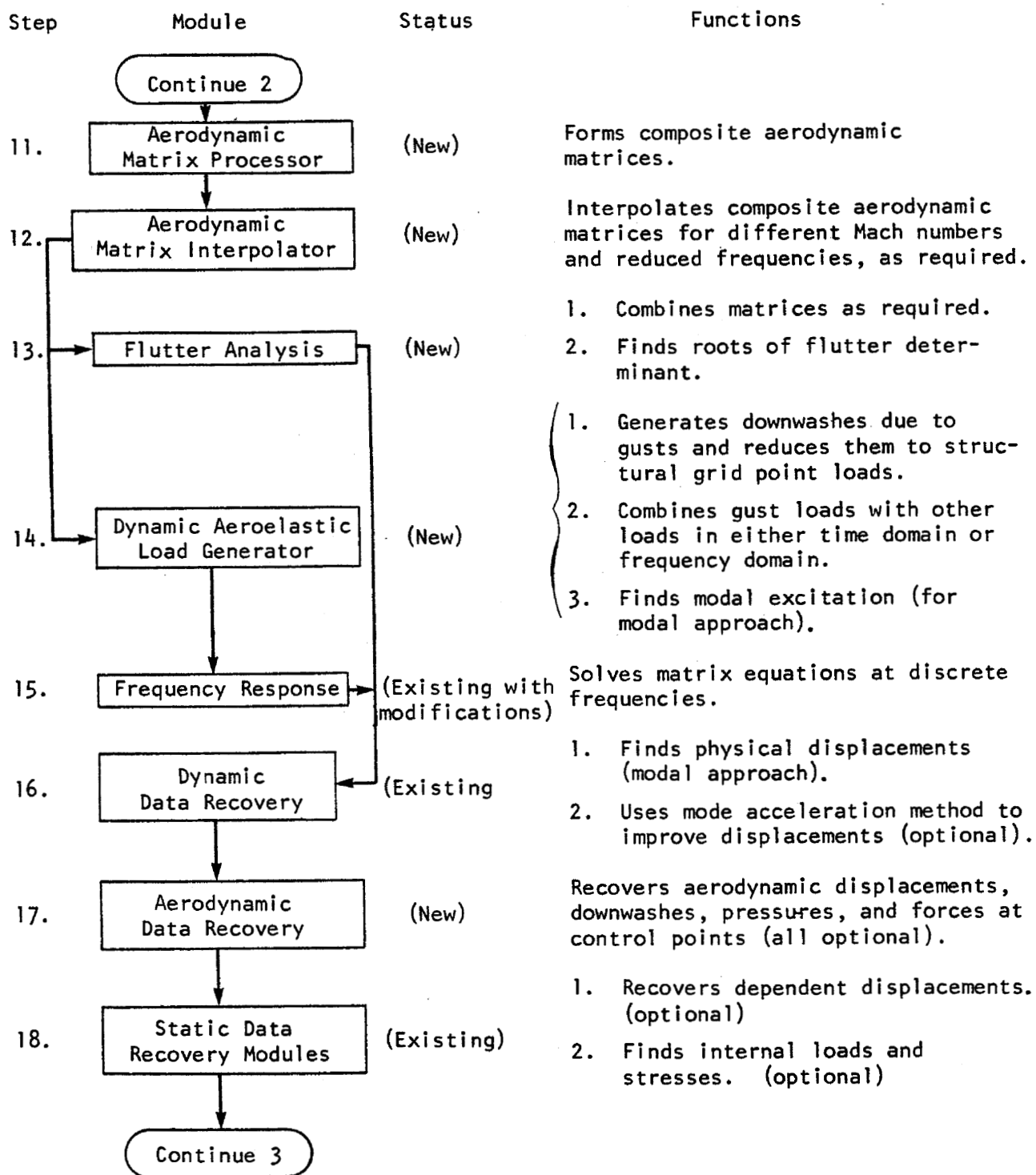


TABLE 1. Simplified Flow Diagram for Dynamic Aeroelastic Analysis
(Cont.)

Step	Module	Status	Functions
	Continue 3		
19.	Random Analysis	(Existing)	Finds psd, rms value and/or auto-correlation function for <u>any</u> response quantity. (Optional)
20.	Inverse Fourier Transform	(New)	Finds time history of <u>any</u> response quantity for Fourier transform method of transient analysis.
21.	Output File Processor	(Existing)	Organizes output data for printing and plotting.
22.	X-Y Plotter	(Existing with modifications)	<ol style="list-style-type: none"> 1. Plots time histories (optional). 2. Makes Bode plots of frequency response output. (Optional) 3. Makes V-g and V-f plots of flutter roots. (New feature, optional)
23.	Deformed Structures Plotter	(Existing with modifications)	<ol style="list-style-type: none"> 1. Plots structural modes in 3-D projection. (Optional) 2. Plots real and imaginary parts of flutter modes in 3-D projection (new feature, optional).

TABLE 2. Simplified Flow Diagram for Static Aeroelastic Analysis

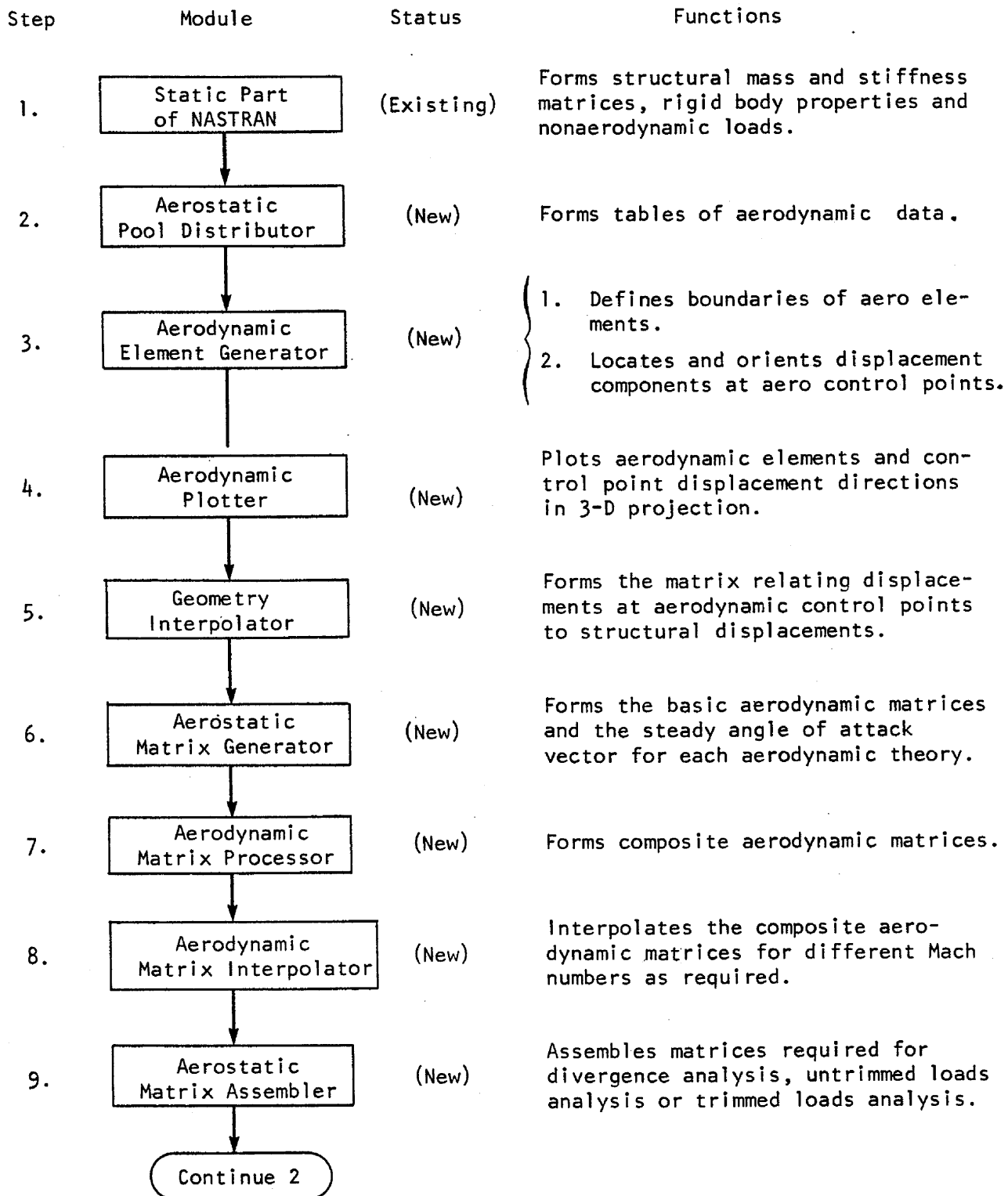


TABLE 2. Simplified Flow Diagram for Static Aeroelastic Analysis
(Cont.)

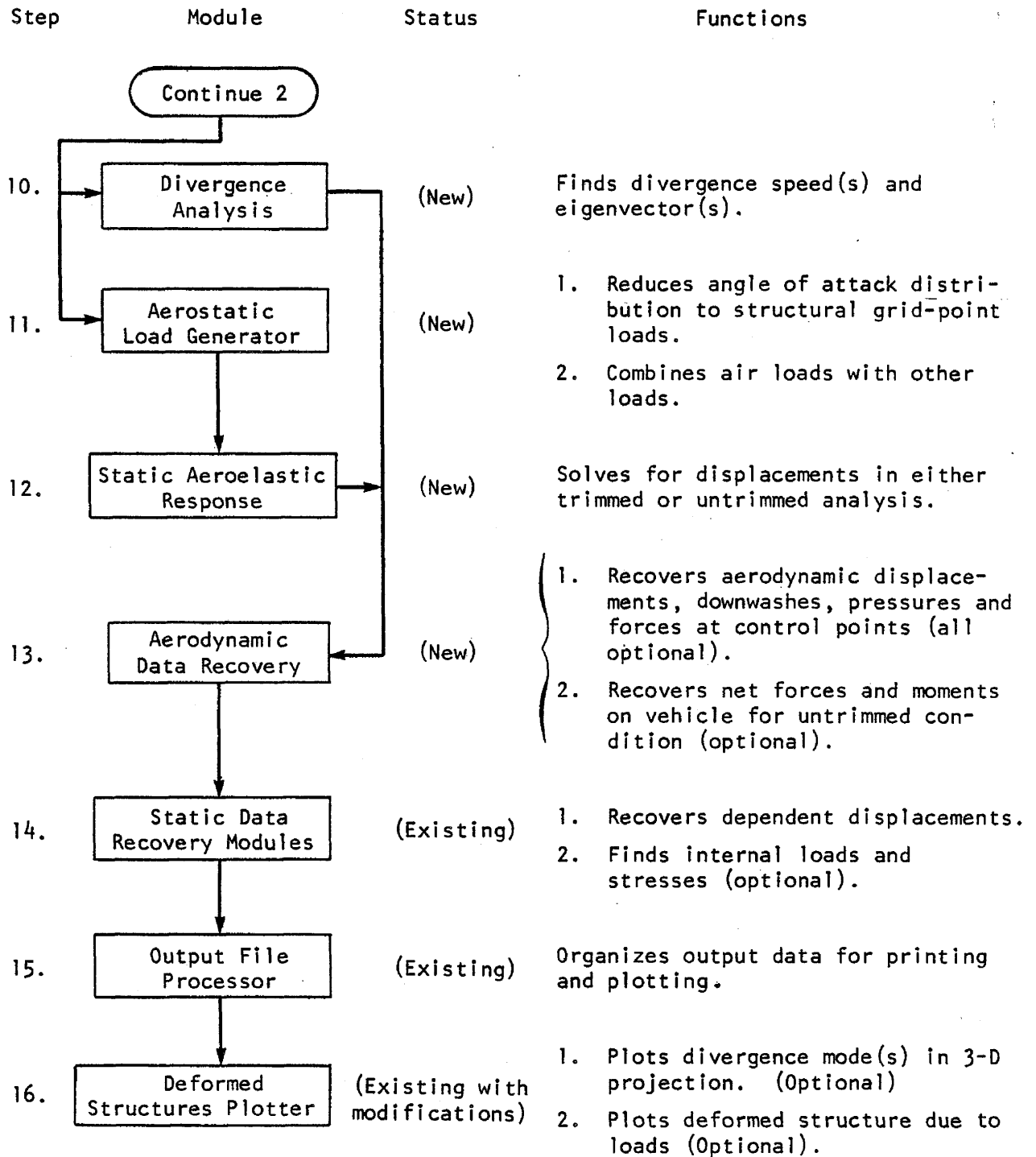


TABLE 3. New Functional Modules

A. Modules used in both static and dynamic aeroelastic analysis

1. Aerodynamic Element Generator
2. Aerodynamic Plotter
3. Geometry Interpolator
4. Aerodynamic Matrix Processor
5. Aerodynamic Matrix Interpolator
6. Aerodynamic Data Recovery

B. Modules used only in dynamic aeroelastic analysis

7. Aerodynamic Pool Distributor
8. Aerodynamic Matrix Generator
9. Flutter Analysis
10. Dynamic Aeroelastic Load Generator
11. Inverse Fourier Transform

C. Modules used only in static aeroelastic analysis

12. Aerostatic Pool Distributor
13. Aerostatic Matrix Generator
14. Aerostatic Matrix Assembler
15. Divergence Analysis
16. Aerostatic Load Generator
17. Static Aeroelastic Response

TABLE 4. New Rigid Formats

- 1A. Direct Flutter Analysis
- 2A. Direct Aeroelastic Frequency and Random Response
- 3A. Direct Aeroelastic Transient Response by Fourier Integral Method
- 4A. Modal Flutter Analysis
- 5A. Modal Aeroelastic Frequency and Random Response
- 6A. Modal Aeroelastic Transient Response by Fourier Integral Method
- 7A. Aeroelastic Divergence
- 8A. Untrimmed Static Aeroelastic Response
- 9A. Trimmed Static Aeroelastic Response.

Note: There are twelve NASTRAN rigid formats at the present time. The (A) after each rigid format number in the above list is intended to symbolize aeroelastic analysis.

SOLID ELEMENT REQUIREMENT FOR NASTRAN

By Stig Wahlstrom

THE BOEING COMPANY

RENTON, WASHINGTON

Preceding page blank

SUMMARY

Finite element analysis of structures using solid elements has received increasing attention over the past few years. Practical experience is currently rather limited. It is anticipated that most immediate principal applications will be for stress analysis. This paper presents coding considerations for implementation of general isoparametric solids into a displacement method analysis program. The user interfaces (input and output) with such a program are discussed. The thoughts presented herein have been or are being implemented into ATLAS, Boeing's integrated structural analysis and design program. No discussion of structural synthesis using solid elements is presented here, nor does this paper concern itself with axisymmetric elements or contain any new theoretical developments.

INTRODUCTION

A constant strain tetrahedron was introduced by Argyris (ref. 1) in 1965. General solid elements using three degrees of freedom per node include the 4 corner tetrahedron, the 6 corner wedge and the 8 corner brick (fig. 1) with nodes coinciding with the corners as well as higher order elements with additional nodes along the edges, on the boundary surfaces or in the interior. General elements with more than three degrees of freedom per node have also been introduced, see ref. 2. Such elements will not be considered in this paper. Reference 3 contains a recent state-of-the-art review of solid elements and a comparison of some isotropic tetrahedra and hexahedra. This reference points out clearly the advantage of elements with varying strain capability over those with constant strain for stress analysis. This effect is more pronounced in three- than in two-dimensional problems.

The family of isoparametric solid elements represents the current state-of-the-art for three-dimensional analysis, using the displacement method with translational freedoms only. (In this paper, "isoparametric" connotes shape functions identical to coordinate mapping functions and thus includes volume coordinate representations). All but the simplest of the members of this family are capable of inclusion of varying strain. They all have an inherent monotonic convergence to the true solution (assuming no numerical problems) and the element derivation is concise and elegant and lends itself to a powerful, general purpose coding. The use of numerical integration should be considered only a minor disadvantage that

can be offset by efficient coding but the ability of higher order members of the family to conform accurately to curved boundaries is a major asset.

For the initial implementation of solid elements into NASTRAN, the isoparametric brick, tetrahedron and wedge should be chosen (in that order of priority). The coding should be arranged to recognize commonalities between the different topological types and the principles of the "deviation from linearity" technique should be used for easy implementation of higher order elements. Generation CP-times are relatively high for these elements and major areas of CP-time consumption (congruent transformations) should be identified and coded as separate, general routines that can be replaced with FORTRAN callable routines coded in assembly language which can reduce the run time by recognizing the particular hardware characteristics. This principle applies to all types of element generation but is becoming more important for higher order isoparametric solid elements.

Although it is assumed throughout this paper that the reader is familiar with isoparametric elements, some derivations for the 8 vertex brick are contained in Appendix A to establish referenceable notations. The ideas presented in this paper are applicable to all solid isoparametric elements but expressed specifically for the 8 corner brick.

NOTATIONS

B	Matrix transforming elemental nodal displacements into strain
D	6 x 6 matrix transforming strain into stress in local (material) reference frame
D'	6 x 6 matrix transforming strain into stress in global reference frame
f	Matrix of body force loads
I	Unit matrix
J	Jacobian matrix (3 x 3)
K	Elemental stiffness matrix, transforming elemental global displacements into elemental global loads
N	Matrix of displacement shape functions
N_k	Displacement shape function
N^f	Body force interpolation matrix
N^p	Surface load interpolation matrix

N^t	Thermal load interpolation matrix
N^{ϵ_0}	Initial strain interpolation matrix
p	Matrix of surface loads
R	Elemental structural nodal loads
R_f	Nodal loads equivalent to body forces
R_p	Nodal loads equivalent to surface loads
R_t	Nodal loads equivalent to thermal loads
R_{ϵ_0}	Nodal loads equivalent to initial strain
r	Matrix of elemental nodal global displacements
r'	Matrix of elemental nodal local displacements
r_i	Elemental nodal global displacements in the x_i direction
T	Coordinate transformation matrix
t	Matrix of thermal loads
u_i	Displacement in the x_i direction
u_i^k	Nodal value (at node k) of u_i
W	Integration weights
x_i	Global coordinate
α_e	$\alpha_e - 8$ is number of edge nodes
α_i	$\alpha_i - \alpha_s$ is number of interior nodes
α_s	$\alpha_s - \alpha_e$ is number of boundary surface nodes
β	Matrix expressing deviations from "earlier displacements", see appendix A
γ	Matrix transforming r into r'
ϵ	Matrix of elemental strain
ϵ_0	Matrix of initial strain
ξ_i	Local coordinate
η	Matrix of thermal expansion coefficients

σ Matrix of element stresses

σ_m Stress matrix

CODING ORGANIZATION

There are three areas of major concern for the coding of matrix generation for solid isoparametric elements. They are (a) the number of arithmetic operations involved, particularly for the congruent matrix transformation $B^T D' B$ that is required at each integration point of the stiffness matrix generation; (b) the amount of core storage required for higher order members of the family of solid elements that may make the generation phase core storage critical (which it may be anyhow) if the traditional (and simplest) approach with a core contained generation is used; (c) the desire to be as general as possible by recognizing commonalities between different solid elements and organize a library of "element generation support routines". To illustrate points (a) and (b) above let us examine how many multiplications and words of storage the congruent transformations $\gamma^T (B^T D' B) \gamma$ require if we disregard matrix sparseness.

	8-node	20-node	32-node
N mult	40000	680000	3300000
6600 CP time	.3 s	4 s	20s
Storage	1500	7500	20000
N int. points	8	27	64

For timing purposes etc., values typical for a Control Data 6600 computer will be used through this paper. The central processor (CP) times are computed assuming 6 microseconds (μs)/mult and add for matrix multiplications which is typical for FORTRAN-generated code. The storage is what is required to hold D' , B , γ , K , $B^T D' B$ in core simultaneously. It is quite obvious from the table that both the storage requirement and the computer time increase rapidly with the number of nodes. It is also quite obvious that an integration technique should be used which requires as few integration points as possible for a certain level of accuracy. Gauss' method (ref. 4) meets this requirement.

To decrease the computer CP-time there are two possible improvements to make: avoid zero operations and use assembly code for the most critical operations. The number of non-zero multiplications is approximately 50% of the total number (B and γ are approximately "half-populated") and the CP-time per multiplication can be reduced to 1 μs /mult with appropriate

COMPASS code. Thus the CP-time reductions due to fast "inner loops" in the matrix multiply operations are much more pronounced than those of coding for non-zero "custom-made" arithmetic. For this reason and because the assembly-coded routines will be more generally applicable, they should be preferred to "custom-made" FORTRAN code. However, a vector inner-product subroutine will still be less than optimum since the inner products are very short for the bulk of the operations (6 or 3 depending upon if zeros are recognized or not) and calling times of 20-30 μ s are typically required for such subroutines. Therefore a FORTRAN-callable routine to multiply a matrix by a vector should be used.

No out-of-core generation should presently be considered for the reasons that: (1) the performance of higher order elements is now known well presently and they may prove to have in some cases the deficiencies that least square fits with higher order polynomials quite often display (2) analyses using higher order solids will normally require so much arithmetic that they will be performed on hardware on which sufficient core should be available. However, the allocation of core for the elemental matrices should be dynamic (typically using the FORTRAN idea of blank common) to allow for execution on smaller core when lower order elements are used.

To make the code for stiffness matrix generation as general as possible the following steps should be recognized:

1. Set up vectors of integration coordinates and weights
2. Set up $D' = T^{-1} D T$
3. For each integration point,
 - 3a. Establish $\frac{\partial N_i}{\partial \xi_j}$ and 3 rows of I- β
 - 3b. Set up and invert the Jacobian J and establish $\frac{\partial N_i}{\partial x_j}$
 - 3c. Establish B
 - 3d. Add $\Sigma B^T D' B$
4. Finally after the loop compute

$$K = \gamma^T (\Sigma B^T D' B) \gamma$$

The number of integration points (which may be different in different directions) should be set to default values that are consistent with the element order. The user should have the option to overrule these default values. Successful numerical integration using only a few integration points has been reported (ref. 4).

* "custom-made" means that the code is organized to recognize the particular features of the problem, i.e. locations of zeros in matrices, etc.

Use of fewer points for the shear term contributions is not recommended since it is undesirable to bias an element intended for general application toward any strain energy component.

For other types of isoparametric elements, only step 3a of the proposed coding sequence needs to be modified in essence. Further it is noted that variable material properties are available by forming D' (step 2) inside the integration loop (step 3).

Six rows of the stress matrix are obtained from the matrix product DTB_y , where the B-matrix (and D, if variable material properties are used) must be evaluated at the point where the stresses are to be determined. This is done simply by coding step 3 of the stiffness matrix generation so that $\frac{\partial N_i}{\partial \xi_j}$ may be obtained at any point. The coding in steps 4 and 5 then apply directly to the stress matrix generation. As a default option, stresses should be generated at the corner nodes (48 stress components); but, evaluation at other points should also be available at the user's option.

Equivalent nodal load matrices should be generated using the same shape functions to describe the loading that are used for the displacements. For most practical applications there are relatively few load cases and the nodal load matrices should be kept inside the summation. Integration is performed as for the stiffness matrix generation.

Dynamic core allocation is recommended both for stress matrices and equivalent nodal loads matrices.

INPUT

Convenient input data formats are important for any structural analysis program. The problem of devising simple but powerful formats is particularly pronounced for (higher order) solid elements since only a few elements suffice to describe the total structure and each element will require a substantial amount of information. Many users think this information should be determined by the program itself. In this section we shall study the 8 corner brick element with edge nodes only but what is stated applies in principle to other bricks and to tetrahedra and wedges as well. Both direct element input requirements and some thoughts on a grid generator for solid elements are presented. Data generation by modified repetition etc. is naturally desired and normally available in a state-of-the-art program but does not apply to solid elements in particular and will not be discussed.

Direct Input

For stiffness matrix generation one needs the element type, its user identification, node numbers and material data (code, property orientation and temperature). Input formats for this except the node list are trivial. The list of nodes should begin with the eight corner nodes in the order

defined in fig. 2 and contain additional nodes if there are nodes on one or more edges of the brick. The following formats of nodal input are proposed:

- 1) $N_1, N_2, \dots, N_8, N_{E_1}^p, N_{E_2}^p, \dots, N_{E_{12}}^p$
- 2) $N_1, N_2, \dots, N_8, \text{Nodes on } E_1, N_2, \text{Nodes on } E_2, N_3, \dots,$
 $\text{Nodes on } E_{12}, N_i$
- 3) $N_1, N_2, \dots, N_8 R_{NC}$

where N_1, \dots, N_8 denote corner nodes; E_1, \dots, E_{12} stand for edge 1 through edge 12 (with directions defined, see Fig. 2). In 1) there are exactly p nodes in each set $N_{E_i}^p$ ($p = 0, \dots$). Thus the total number of nodes input is $8 + 12p$. Zero end fill in $N_{E_i}^p$ is used to degenerate the edge to a lower order form. In the second format which uses delimiters (the end corner of the edge) zero fill within the edge node lists is not allowed. The program should distinguish between formats 1 and 2 by checking for occurrence of corner nodes in the nodes following N_8 . Format 3) contains only corner nodes and a radius R_{NC} (real) which instructs the program to include all nodes enclosed within a cylinder with the given radius along straight lines defining the edges.

If non-default stress generation is desired (default is stresses with respect to material axes at the eight corners), additional information is needed. Available options would be stresses computed at any node or at any specified coordinate (global). In each case 6 stress components will be computed at each user specified point and in the order they are specified by the user (order of rows of the stress matrix). Input of stress generation information should be done in a separate record in which node numbers (integers) are mixed with triplets of floating point numbers. The program should distinguish the type of the number input.

Element loading input is more complex. Primarily due to the input volume, it should not be contained in the basic element input record. Thermal loads, initial strains and body force loads require exactly as many values per load case as there are nodes (input in the nodal data order). One input value by default refers to constant loads (strains) while 8 input values refer to the corner nodes and imply that the basic corner shape functions should be used as load interpolation functions. Surface loading is input as nodal values surface by surface. The surface is identified by an integer between 1 and 6 and the nodal values are input according to edge order (from lower to higher, last node on edge not included). For any one load component, there should be default options of one or four values available indicating constant load or load at the four corners. Loading values refer to intensities per actual area of the surface.

Due to the large amount and complexity of input data for solid brick elements, it is important to define and implement as many data checks as possible. Such checks would include tests for

- (a) reentrant corners and warping of the 6 quadrilaterals formed by the eight corners
- (b) determining that intermediate edge nodes fall within a user defined cylinder between corner nodes
- (c) determining that each element defined is topologically feasible (has a single interior)
- (d) determining that points where stresses are to be computed lie on or within the element

Grid Generator

A typical feature of input data for solid elements is that many of the nodes are not used to define the geometrical configuration of the structure but rather to obtain a certain refinement of the results. Thus a grid generator for solid elements should prove to be very efficient. The user only needs to input the surface geometry and the desired grid refinement and the grid generator can then produce nodal and elemental data. If a grid generator is used for nodes and elements, it is imperative that it be extended to element loads, nodal loads and boundary constraints as well; since the user loses control over details of the produced data. Some work has been in progress within Boeing over the past year to generate data for solid finite element analysis. Currently a simple grid generator for 8-node bricks is available. The basic principle used is that any body that is topologically equivalent to a brick can be assigned a rectangular user grid (and thereby "userbrick" elements) to define its geometry. Within each "userbrick" the nodal refinement and any nodal loads may be defined. Known deficiencies are the requirement of topological equivalence to a cube, that grid refinements do not utilize higher order elements and that a grid generator is not very useful unless there is a post processor available for the results, since there is no detail user control over node and element numbers.

OUTPUT

Preparation of input data for analysis with solid elements is quite cumbersome but the interpretation and use of the output (primarily stresses) is even more so if non-selective printout of stress components in global coordinates is the only available option. Selective display of stress data is necessary for efficient analysis of solids, at least this is strongly indicated by recent experience within The Boeing Company. If a grid generator is used for data preparation, selective output for geometrically defined regions is imperative.

The reason that extraction of stresses is the most valuable output feature is the fact that no or little additional processing is needed for the stresses. However other options such as computation and display

of principal stresses and their directions would also be valuable. Of particular interest is the employment of some yield or failure criteria such as Hill's yield function (ref. 5) to allow for a computerized search for critical conditions. To simplify fatigue analysis it would be useful to have the program find the maximum tensile stress in certain surfaces of the structure.

REFERENCES

1. "Matrix Analysis of Three Dimensional Elastic Media, Small and Large Displacements", Argyris, J. H., AIAA Journal, Vol. III, 1965
2. "Three-Dimensional Theory of Elasticity", Fjeld, S. A., Finite Element Methods in Stress Analysis, Tapir, Trondheim, Norway, 1969
3. "Comparison of Three Dimensional Finite Elements", Clough, R. W., Proc. Symposium on Application of Finite Elements in Civil Engineering, Nashville, Tenn., ASCE, Nov. 1969
4. "Numerical Integration Applied to Finite Element Methods", Irons, B. M., Conf. Use of Digital Computers in Structural Engineering, Univ. of Newcastle, July 1966
5. "The Mathematical Theory of Plasticity", Hill, R., Oxford Univ. Press, New York, 1950
6. "Refined Finite Element Analysis of Linear and Nonlinear Two-Dimensional Structures", Felippa, C. A., Report SESM 66-22, Struct. Eng. Lab., Univ. of Calif., Berkeley, Oct. 1966
7. "Iso-parametric and Associated Element Families for Two- and Three-Dimensional Analysis", Zienkiewicz, O. C. et al, Finite Element Methods in Stress Analysis, Tapir, Trondheim, Norway, 1969

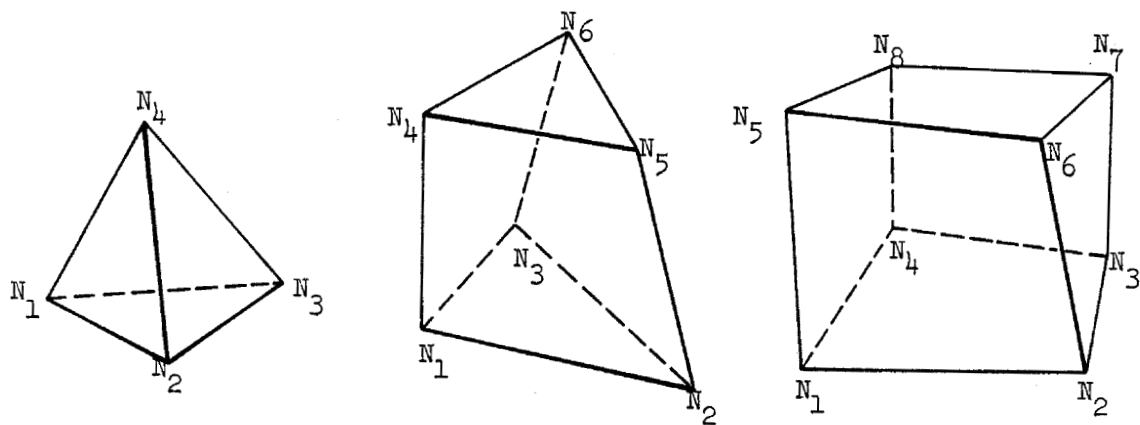


Figure 1 Tetrahedron, wedge and brick solids

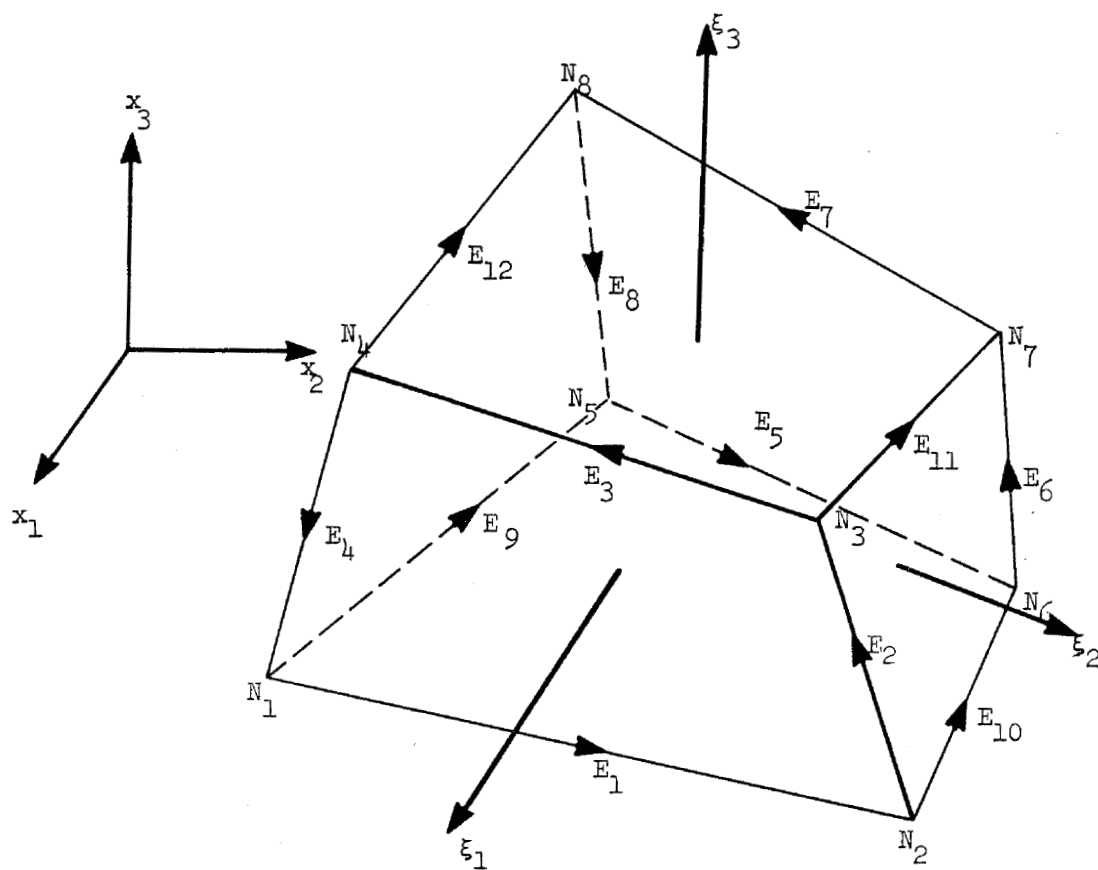


Figure 2 8 node brick

APPENDIX A

DERIVATION OF ELEMENTAL MATRICES FOR AN EIGHT CORNER ISOPARAMETRIC BRICK

The derivations outlined herein are brief. For additional information on displacement method theory in general, the reader is referred to C. A. Felippa's excellent report on the subject, ref. 6, while for particulars on isoparametric elements he is referred to ref. 7.

Stiffness Matrix

Let the displacement u_i (component along global x_i axis) be

$$\begin{aligned}
 u_i = & \sum_{k=1}^8 N_k u_i^k + & (\text{basic 8 node brick}) \\
 & + \sum_{k=9}^{\alpha_e} N_k (u_i^k - \sum_{j=1}^8 \beta_{kj} u_i^j) & (\text{addition for nodes on edges}) \\
 & + \sum_{k=\alpha_e+1}^{\alpha_s} N_k (u_i^k - \sum_{j=1}^{\alpha_e} \beta_{kj} u_i^j) & (\text{addition for nodes on boundary surfaces}) \\
 & + \sum_{k=\alpha_s+1}^{\alpha_i} N_k (u_i^k - \sum_{j=1}^{\alpha_s} \beta_{kj} u_i^j) & (\text{additions for nodes in the interior})
 \end{aligned}$$

The shape functions N_k for the edge nodes ($k = 9, \dots, \alpha_e$) are zero-valued for the corners (as well as for the other edge nodes), those for the boundary surfaces have zero values on the edges (and corners) and for other surface nodes while those for the interior disappear on the total boundary and on other interior points. The coefficients β_{kj} simply take the values of N_j at point k . Using matrix notation the displacement function u_i can be written as

$$u_i = N r_i - N \beta r_i = N(I - \beta) r_i = N r'_i$$

where N is a (row) vector of shape functions, r_i a matrix of nodal displacements in the x_i -direction, β a (lower diagonal) matrix that represents "deviations from previous displacements." $r'_i = (I - \beta)r_i$ is an independent set of linear combinations of nodal displacements (in the x_i -direction).

The functions N_k are easily expressed as functions of the natural coordinates ξ_i rather than as functions of the global (cartesian) coordinates x_i . The transformation from natural coordinates to global coordinates is expressed by

$$x_i = \sum_k N_k (x_i^k - \sum_j \beta_{kj} x_i^j)$$

where x_i^k is the x_i -coordinate of node k .

The vector ϵ of element strain is

$$\epsilon = \begin{bmatrix} \frac{\partial u_1}{\partial x_1} \\ \frac{\partial u_2}{\partial x_2} \\ \frac{\partial u_3}{\partial x_3} \\ \frac{\partial u_1}{\partial x_2} + \frac{\partial u_2}{\partial x_1} \\ \frac{\partial u_1}{\partial x_3} + \frac{\partial u_3}{\partial x_1} \\ \frac{\partial u_2}{\partial x_3} + \frac{\partial u_3}{\partial x_2} \end{bmatrix} = B r' = B \gamma r$$

where

$$B = \begin{bmatrix} \frac{\partial N}{\partial x_1} & 0 & 0 \\ 0 & \frac{\partial N}{\partial x_2} & 0 \\ \frac{\partial N}{\partial x_2} & \frac{\partial N}{\partial x_1} & 0 \\ \frac{\partial N}{\partial x_3} & 0 & \frac{\partial N}{\partial x_1} \\ 0 & \frac{\partial N}{\partial x_3} & \frac{\partial N}{\partial x_2} \end{bmatrix}$$

in which $\frac{\partial N}{\partial x_i}$ is a row vector, the k th element of which is $\frac{\partial N_k}{\partial x_i}$ and r is a vector of all nodal displacements (in nodal order). r' is a vector of linear combinations of r (in freedom order rather than nodal order) and γ is a 3×6 square matrix that is made up from elements of the matrix $(I - \beta)$. (Other transformations such as change of coordinates, offsets, etc. can be included in γ).

The element stiffness matrix K relating global displacements r to associated nodal forces R (force components expressed in a dual base) is then

$$K = \int_{x_1} \int_{x_2} \int_{x_3} \gamma^T B^T T^{-1} D T B \gamma dx_1 dx_2 dx_3$$

where the integral is to be taken over the total volume of the element. The matrix D (6 x 6) represents the constitutive equations with respect to material axis directions which could be different from those of the global coordinate system and T is a (6 x 6) matrix that transforms stresses or strains from the global reference system to the material reference frame. $T^{-1} D T$ is symmetric.

No closed form expression for the K -matrix is known and it is evaluated by means of numerical integration. Most conveniently it is evaluated after the change of integration variables to those of the natural coordinate system is made which leads to the following summation:

$$K = \gamma^T \left[\sum_{i_1} \sum_{i_2} \sum_{i_3} W_{i_1} W_{i_2} W_{i_3} B^T(\xi_{i_1}, \xi_{i_2}, \xi_{i_3}) D'(\xi_{i_1}, \xi_{i_2}, \xi_{i_3}) B(\xi_{i_1}, \xi_{i_2}, \xi_{i_3}) |\text{Det } J(\xi_{i_1}, \xi_{i_2}, \xi_{i_3})| \right] \gamma$$

where J is the (3 x 3) Jacobian matrix for the transformation defined by

$$J_{ij} = \frac{\partial x_j}{\partial \xi_i} = \sum_k \frac{\partial N_k}{\partial \xi_i} x_j^k$$

By use of J^{-1} , partial derivatives of N_k with respect to global coordinates can be obtained from those of N_k with respect to natural coordinates. The choice of integration weights W_k and abscissas ξ can be done according to a variety of numerical techniques but Gauss numerical integration is preferred by many since it will require few integration points for high accuracy.

Stress Matrix

The stress vector σ (components with respect to the material axes) is

$$\sigma = D T B \gamma r$$

where the matrices D , T and B are established at the point where the stresses are sought. If stress components with respect to another reference frame are desired then T'^{-1} will transform σ to the proper reference frame. T' is an appropriate stress transformation matrix. The product $T'^{-1} D T B \gamma$ makes up 6 rows of the stress matrix σ_m .

Surface Loading

Let the loading \tilde{p} on the surface B_p be

$$\tilde{p} = N^p p$$

where p is a vector of nodal intensities of the pressure loading (components in global system) and N^p the load interpolation functions. The vector R_p (of equivalent nodal loads is)

$$R_p = \int_{B_p} \gamma^T N^T N^p dA p$$

Body Forces

The loading \tilde{f} is expressed by the interpolation formula

$$\tilde{f} = N^f f$$

where f is a vector of nodal intensities of the body forces (components in global system) and N^f the body force interpolation functions. The vector R_f of equivalent nodal loads is

$$R_f = \int_V \gamma^T N^T N^f dV f$$

Initial Strain

The initial strain $\tilde{\epsilon}_0$ in terms of nodal strain values ϵ_0 is

$$\tilde{\epsilon}_0 = N^{\epsilon_0} \epsilon_0$$

where N^{ϵ_0} is a matrix of initial strain interpolation functions. The vector R_{ϵ_0} of equivalent nodal loads is

$$R_{\epsilon_0} = \int_V \gamma^T B^T D' N^{\epsilon_0} dV \epsilon_0$$

Thermal Loads

The temperature \tilde{t} in terms of nodal temperature values t is

$$\tilde{t} = N^t t$$

where N^t is a matrix of initial strain interpolation functions. The strain equivalent to \tilde{t} is

$$\epsilon = \eta \tilde{t}$$

where η is a matrix of thermal expansion coefficients. The vector R_t of

equivalent thermal nodal loads is

$$R_t = \int_V \gamma^T B^T D' \eta N^t dV t$$

Preceding page blank

ON THE REDUCTION OF PROLIFERATION OF
FINITE ELEMENT PROGRAMS

By T. G. Butler

NASA Goddard Space Flight Center

INTRODUCTION

Even in the face of a prodigious amount of structural analysis capability by finite element methods, some organizations are generating new programs which essentially duplicate the characteristics of current programs. The purpose of this paper is to examine the effects of proliferation. Arguments are presented which will show that the benefits derived from a reduction in proliferation result in better communication, reduced cost, and increased dissemination of capability.

Large finite element programs are expensive to generate because they contain great volumes of code. Technology is moving so fast in the mechanics of finite elements, in numerical analysis in finite fields, and in computer hardware and software, that these large finite element programs rapidly become outdated. The combinations of paths through large programs are so great that we can say that they will never be fully checked out, so they are constantly in need of servicing as usage broadens. To stay abreast of technology changes and error discoveries, large finite element programs should be maintainable and should be maintained in order to achieve user confidence. Maintenance is costly but much less so than complete program replacement in both dollars and time. Anything that would compound the cost of providing finite element analysis capability to the structural community would be considered undesirable; therefore, proliferation is bad. There are many other factors besides cost that would determine an attitude toward proliferation, but cost is a sufficient basis.

Before we can champion a cause, we have to get definition of it. What constitutes proliferation of finite element programs in the eyes of structural analysts? If a known capability exists and an effort is initiated to duplicate that capability, there is proliferation so long as there is not something unique that is being offered with respect to the following general characteristics:

Problem size

Object of the analysis { General purpose
Special purpose

Method of approach

Solution capability

Mode of operation { Applications
Experimentation

Accuracy

Efficiency

Convenience

Let us also get a definition of proliferation from a negative sense. In no wise is there an implication that existing programs that are in use which have overlapping capability constitute proliferation in the sense of this discussion. Programs such as Boeing's SAMECS, Jet Propulsion Lab's SAMIS, or Wright Field's FORMAT have been in use long enough to have proven themselves as production tools. In terms of efficiency for certain types of problems it would take analysts, who have become expert at operating these existing programs, much longer to convert to a new program than to continue using those with which they are familiar. Only when analytical needs exceed the capabilities of the older programs should the analyst be coaxed toward programs with prospects for extensive longevity. It becomes proliferation only when attempts are made to put new capability into programs that are not readily maintainable. Programs with limited capability which are costly to modernize should be allowed to phase out in favor of the maintainable programs when the technological advancements render them out-of-date.

MAINTAINABILITY

The policy which I hope to convince you of is that with a good, modular, maintainable program any characteristic which is found to be insufficient can be arighted by directly modifying the offending portion. Since this is a NASTRAN User's Colloquium, it is forgivable if we examine the suitability of this policy with respect to NASTRAN as being representative of a good, modular, maintainable program. Its suitability will be examined according to the above set of characteristics.

Problem Size

Right now NASTRAN does a creditable job handling problems from 100 to 10,000 degrees of freedom. For problems under 100 degrees of freedom the overhead cost of arraying the large amount of general purpose software onto the computer and stepping through the options accounts for over 95% of the central processing unit (CPU) charge time. If one is confronted with heavy traffic in small sized jobs it would definitely pay to abandon a general purpose program and go to a special purpose program. The overhead cost of NASTRAN on various sizes of computers is tabulated as follows:

<u>Computer</u>	<u>CPU Overhead Time</u>
IBM 360 Model 95	20 Sec
IBM 360 Model 85	20 Sec
IBM 360 Model 75	35 Sec
IBM 360 Model 65	52 Sec
IBM 360 Model 50	217 Sec
CDC 6600	12 Sec
CDC 6400	18 Sec
UNIVAC 1108	17 Sec

A problem in statics or eigenvalues for a small problem of less than 100 degrees of freedom using a special purpose program should take about 3 seconds on the 360/95. General purpose programs cannot compete with special purpose programs on small sized problems.

For very large problems a computer strategy of breaking the problem up into pieces and condensing the pieces before joining them to represent the total structure is called structural partitioning. Experimental versions of structural partitioning for NASTRAN are already working, so the extensions to very large sized problem is already established for both statics and dynamics.

Type of Computer

The scheme for making NASTRAN adaptable to many different computers was to make the program modular. Some modules deal only with the management of the program and are called executive

modules, while other modules deal with the operation of the solution process and are called functional, mathematical, and utility modules. All except some of the executive modules are machine independent, so the problem of adapting NASTRAN to a new computer is to rewrite only certain of the executive modules which are machine dependent. The feasibility for making an adaption was demonstrated in the pilot conversion that was done for the IBM 360 Model 67 computer operating under time sharing operating system. The adaptability is further being attested by the work that is currently underway to convert NASTRAN to the Honeywell 635 computer. Active interest is being shown in adapting it also to the Xerox Sigma class of computers.

Object of the Analysis

A program can be designed for general purpose operation or for special purpose solutions. NASTRAN is obviously already a general purpose program, and, if it is not already obvious, it will be amply shown subsequently that it can be extended into further generalization. The real question is what can we do about special purpose needs? Can one truncate the program? Can one strip out the options? The answer to both of these questions is yes. Take for example, the need for a special purpose sub program to solve truss-like statics problems for large bridges described in rectangular coordinates, subject to point force loads at grid points only. The source code would be culled of all executive control functions except restart. The case control would retain only labelling; subcases for regulating: load sets, boundary sets, multi-point constraint sets, output sets of forces, displacements, and stresses; and plots of only rod elements. The executive routines would be reduced to a skeleton amount of input data checking, a fixed assignment of data blocks to discs and tapes instead of dynamic assignment, a fixed OSCAR (operating sequence control array) with a few variable flags instead of variable arrays, and a small parameter table. The bulk data cards would consist of a GRID, a CONROD, a MAT 1, a FORCE, an SPC, an MPC, a delete, and an OMIT. The organization into links would be abandoned but an overlay structure would probably be kept.

The beauty of having the rigid formats written in DMAP language is that the logic of reducing the program to special purpose form can be tested by operating it in the environment of the existing general organization by using ALTER cards to eliminate batches of operations. Plot routines would be kept, but their framework would be whittled to necessities. Analysts involved in production-like repetitive analyses of the same type may want to do a scaling down operation like this as a routine matter.

There is even another kind of special reduction in which a given structure is frozen into the program and the only variability that is retained is in the type of load or the solution case type. Thus all sorts of unneeded data checking routines and decomposition routines could be eliminated in favor of load vector formation and forward-backward pass operations.

Recapitulating then, it is possible to strip out generality from the code to reduce some portions to a minimum of operations and options. The remaining portions of the code could successfully function in special purpose form to gain the advantages of tailored programs.

Method of Approach

Provision was made originally in NASTRAN to solve finite element problems by the displacement method, the force method, and by DMAP (direct matrix abstraction). One whole link is still reserved for the force method that never did get integrated. If a new force method such as an approach via stress functions were developed it could be incorporated by locating it in the reserved force link or by adding entirely new links, because the organization is open-ended with respect to links. Entries would have to be made in executive tables and to output processors, but these tables and processors are also open-ended. This implies that distinct new approaches to finite element analysis can be added or existing ones can be replaced by improved ones because of the modularity and open-endedness to the overall program design.

Solution Capability

If a better method of decomposition is found, if an improved eigenvalue routine appears, or if a differential equation integration routine has a special feature, one of two possibilities can be invoked in each instance. The existing routine can be replaced by the candidate routine within the respective modules or new logic can be introduced to allow an option between the existing routine and the added capability. The second alternative will involve additional new entries in case control and bulk data. The fact to note here is that the new routines can be entered without disturbing the code outside of the module.

Turning our attention to the next level of complexity above a subroutine to a module, it is possible to replace modules without disturbing any other part of the program. Each module has a prescribed interface with the executive only and definitely eschews any interaction with any other module. A module can be drastically overhauled and will cause no repercussions outside of this module so long as the replacement module retains the

same interface with the executive that the previous module did. A particularly convenient facility called a dummy module has been provided in NASTRAN to test out a new module within the NASTRAN environment without disrupting anything. All entries for dummy modules have been made in tables and lists. When a module is ready to be tested, the symbolic dummy entries are replaced by named quantities pertaining to the new module. In this test mode, the final grooming can be worked on with impunity. Its ultimate performance after integration can be precisely predicted from its performance in the dummy module mode.

Going back now to the topic of routines, there is a new capability being developed called a Dummy Element. Input cards, table entries, parameter entries, material calls, and plot calls will all have symbolic dummy entries. This will soon allow a new element routine to be added or be substituted in a fashion similar to the dummy module by simply providing named quantities for the symbolic dummy entries at the time of inserting the element routine code. Element routines are the only routines being provided for testing in a specific dummy fashion. If one desires to test other routines in dummy fashion the module for which it is destined can be copied except for the new routine and be operated as a separate dummy module so that the new and old can be directly compared.

At the highest level of complexity a complete rigid format (i.e. a structural case type) can be created and can be entered as an additional solution string. The number of rigid formats like many other systems in NASTRAN is open-ended. DMAP language is used to write the rigid format operations. Entries are made in the executive solution table, the executive module property list, and the catalog of restart options is put in. All of these new features operate distinctly from any other solution strings, so they can be added or deleted with freedom.

As proof of this power to add rigid formats, the ability to solve hydro-elastic problems was implemented as several new rigid formats. Aero-elasticity solutions are being contemplated as several more. Thermal analyzer modules may eventually occupy over five rigid formats. Existing rigid formats will be revamped to include structural partitioning. What is indicated here is solid activity in replacing and augmenting the number of rigid formats, proving that the claim to maintainability is really so.

Mode of Operation

Programs can usually be classified as either for applications work or for developmental work. Some excellent development work is being carried out at the University of Wales, Brown,

Liege, Cornell, Vermont, Arizona, Hawaii, M.I.T., and California. Most of the well known programs, however, are applications type. It was the intention also that NASTRAN be an application program; but because of its link structure, a link can be devoted entirely to developmental purposes without impeding any of the applications features. A link can be organized to have counterpart operations overlaid at the same level with an option to choose between them for comparison purposes. All of the applications links will be entirely insensitive to all of the features within the experimental link. Therefore, unless the experimentation would involve executive operations, NASTRAN can readily provide a handy vehicle for module experimentation, and thus obviate the expense of generating experimental programs.

I must not overlook the impractical aspects of using NASTRAN as an experimental program in its present form. There is an expensive, fixed overhead in its present form. It would be folly to exercise the whole program in an experimental mode for an extensive schedule of experimental work. It would be better to strip the unnecessary routines out of the executive to minimize the overhead, and to condense all operations into a single link program for conserving storage space. In some respects the distilling of an experimental version from the complete program is akin to separating out of a special purpose program. The amount of work to extract an experimental version from NASTRAN is much smaller than writing an entirely new program and worry through a check-out phase.

A distinct mode of operation within the realm of applications programs, is the on-line, direct-interaction mode operating from a cathode ray scope command terminal. There is no technical impediment towards adapting NASTRAN to an on-line mode. Money is needed to subsidize such capability, but prior to this, a design study should be conducted in order to determine (a) the suitability of relative sizes of core residency between the scope graphics and the analysis program, (b) the degree of antiquity of recallable, prior analyses, (c) and the organization of scope displays for rapid interpretation and subsequent analysis commands. Such on-line operation is the apogee toward which a completely general purpose program should aim.

Here we have shown that the link/overlay/modular construction allows for adjusting to a desired mode of operation.

Accuracy

There are times when routines or modules have poor convergence properties except for particular ranges of parameter values. There is continual activity to remove these imperfections.

When algorithms with improved accuracy are perfected a proper course of action would be to expedite its incorporation into appropriate modules of a maintainable program like NASTRAN. It is insupportable to make an isolated advancement in the state of the arts the basis to launch into a competitive or redundant venture. Recent activities along these lines to create all new code are unjustified and should be interdicted.

Efficiency

Large, maintainable programs are being scrutinized from many different points of view. The multiplicity of paths versus the independent range of parameter values can produce instances of sluggishness. Such instances should be rectified and not be made occasions of scorn. The stamp of inefficiency can be affixed to an algorithm when improvements in numerical analysis or supporting software admit of designs of swifter execution. In this event the module containing the offending code should be replaced with due haste. There is current activity along these lines in NASTRAN. Inefficiencies in plotting, matrix packing, reading a matrix into core, and multiplications are being attended with consequent individual running time reductions by factors of 2 up to 10 and in combination as high as 40. Such instances are not surprising. In fact it is expected that attention to efficiency will be a continuing maintenance activity.

Convenience

Needs of analysts in organizing input data, in successive manipulations of incremental solutions, and in the production of plots are as mutable as slang in a modern language. Dissatisfaction with an existing method of treating a situation is no cause for abandoning a maintainable program in favor of the development of a new program. The very word maintainable implies that replacements are possible and economically feasible.

Using NASTRAN as an example again, a basic policy was decreed towards generation of input data. The format of bulk data input was to be as convenient yet general as possible. On the other hand automatic generation of input data was not to be made part of the basic program. Generator programs were to be auxiliary and separate. The rationale behind this policy was an attempt to keep things manageable. NASTRAN was a sizeable task to manage without having to burden it with data processors. More important, however, was the prospect that small generator programs were expected to spring up frequently and would very likely have short lives. Rather than incorporate these programs into the mainbody of NASTRAN and require a link editing of the

overlay structure every time one of them became supplanted, it appeared much more logical to require these generator programs to be distinct entities that would be simple to operate.

Returning to the topic of convenience within the program, there has been a recent rash of improvements in diagnostics. A major revision of curve plotting has been proposed to give more versatility. A modification to the eigenvalue rigid format to allow multiple subcases for boundary value changes has been put forward. All such convenience features and service code are readily implementable because of the modular nature of NASTRAN. Constant attention to items of convenience will bring about remarkable streamlining.

Hopefully, it has been demonstrated that a large general purpose program like NASTRAN is maintainable in each of the categories deemed important. Thus it should be possible to stay abreast of the state-of-the-arts by continual enhancement of a maintainable program without having to recreate entirely new programs as technology advances.

BENEFITS

One of the strongest arguments to inhibit duplication of effort is the amount of direct benefit that would be derived. The argument is based on the assumption that finite element structural analysis is needed and that the many different organizations which do analysis would have access to the generally accepted programs.

The first benefit would be in communication. Engineers working on the same mission and doing analysis with the same program can feed data between each other in situations where one analysis needs to have information supplied from several sources. An example of this would be a vibration analysis of a space mission launch configuration. The vibration analyst could draw on analysts who had used the common program to study the rocket, the spacecraft, the shroud, and the experiments mounted within the spacecraft. Models of each of these components could already have been on magnetic tape. The vibration analyst need only read the structural modelling data from the tape resulting from each portion of the launch configuration and add a few control cards to his computer run to do an analysis for finding the important frequencies and mode shapes of the entire structure at launch. To make things go smoothly it would be well to anticipate such an overall analysis so that the interface compatibility conditions could be provided for in advance of the final analysis. General Purpose programs which are adaptable to many computers can provide this communication vehicle.

The second benefit would be cost savings. Big, general purpose, finite element programs are expensive to build and to maintain. Rather than have each organization that does analysis bear the cost of developing its own finite element program and continue to pay for maintenance, a well subsidized, single development and maintenance effort to provide a program that meets the requirements of the individual organizations, would suppress the unnecessary duplication of expense. There can be an obverse to this expense picture in that organizations can save their fellow organizations new development costs. Consider the situation in which a program in wide use has a published program of planned enhancement. Consider also an organization that has need of a capability earlier than it is scheduled in the enhancement plan. If this organization were to accelerate the development of the subject capability by doing it or paying to have it done in time for its own use, this cost could be amortized against the budget for the mission needing the analysis. This added capability could then be donated to the general program for distribution to all users, thus freeing funds, earmarked for this particular capability, to be reassigned to augment some other facet of the program.

The third benefit would be the rapid dissemination of advancements in analytical tools. Many active program developers might consider this dissemination a handicap rather than a benefit. Let me frame the argument for dissemination on the basis of what our Ad Hoc Group found when it canvassed the aerospace industry in 1964. Most programs were proprietary in 1964 and each company was anxious to hoard its advantage. As a result each company's program had some remarkably attractive features, but each also had a great many defects, considering all three disciplines. The whole aerospace industry suffered from analyses not being up to their full potential, because of mismatches within these programs. No doubt the prospect of a technical advantage was a spur to some of the advancements that were made in that period. In the future we should turn to other spurs to stimulate technical break-throughs. Nineteenth century Europe awarded prizes and other prestigious recognitions. Possibly the honor associated with such awards from their peers would inspire men to equal or more lofty pursuits than before. The point to be made here is that dissemination of the latest finite element analysis capability benefits not just aerospace, but machinery, automotive and building segments of the structures community. It will lift the calibre of analytical determinations with the ultimate effect of raising the stature of our profession.

If I have been persuasive on the merits of reducing proliferation, it will establish a credo for us, but it falls short of how to put the credo into practice. Our problem is similar

to the practice of eugenics. We know that we want to preserve and promote only the best. But, who does the choosing? Who declares what is worthy and what shall be expended? To give the problem even more reality, here in alphabetical order by organization are the important, extant finite element programs:

<u>Organization</u>	<u>Program Name</u>
Bell Aerosystems Co.	MAGIC
Boeing Co.	{ COSMIC
	SAMECS
	ASTRA
Brown University	Pedro Marcal's Experimental Program
University of California	Wilson Code
Control Data Corp./MRI	Stardyne
Convair/San Diego	DYNES
Cornell University	Dick Gallagher's Experimental Program
Douglas Aircraft Co.	DEMON
General Electric Co.	MASS
Grumman	ASTRAL
Jet Propulsion Laboratory	{ SAMIS
	ELAS
University of Liege	F. DeVuebeckes' Experimental Program
Lockheed Aircraft Co.	{ FAMAS
	DAISY
Marshall Space Flight Center	SNAP
Martin Co.	SB038
Massachusetts Inst. of Tech.	{ Ted Pian's Experimental Program
	ICES/STRU DL
National Aeronautics & Space Administration	NASTRAN
University of Stuttgart	ASKA
University of Wales	Olgierd Zinkiewicz's Experimental Program
Wright-Patterson Air Force Base	FORMAT

There is a fear that if government programs are among the ones chosen to be promoted, the free enterprise system will be threatened, industry will be bullied by government dictatorship, and the government will dominate all of the developmental activity and leave industry on the sidelines as spectators. I can only speak for NASA in trying to assuage your fears. An attitude that has been expressed at NASA Headquarters has urged that NASA should not force anyone to use NASTRAN. The attitude is that if NASTRAN is a good program, people will use it voluntarily; if it is not, people will disregard it.

I will let our host the NASTRAN System Management Office (NSMO) at Langley Research Center speak for themselves, but I have their assurance that they want to see active competition in future NASTRAN improvements. After all, in the six years since the design was set until today when long range maintenance has begun, there have been steady technological strides made that have inevitably invalidated some of the NASTRAN code. There is a need for reworking a sufficient number of modules and routines that there is room for all to compete and contribute. In fact the spirit in which NSMO was set up was very much in the spirit of partnership between government and industry that pertained in the old NACA days. In this spirit Dick Martin of Convair/San Diego several years ago expressed an industry opinion to me that is distinctly in this partnership vein. He said, "At first I was opposed to government incursion into the industry province of analysis program development. The longer I reflected however, the more I began to realize that there is a proper role for government here. The quantity of analytical routines that have achieved competence is so great today compared to several years ago that the cost of developing these big, general purpose finite element programs is so great that individual companies can no longer afford to write their own programs. I think it is a proper role for government to shoulder the cost and responsibility for our modern finite element programs and serve all industry with such up-to-date analytical tools. It doesn't make sense any more for everyone to go his own separate way. I personally endorse what you are doing in the NASTRAN project."

I have somewhat begged the question by a tangential excursion into government programs. To get back, regardless of which are chosen, the method of how we should practice our computer program eugenics is the knotty question. I would suggest a committee. Horrors, some are no doubt saying. I developed a confidence in decision by committee after my experience with the dedicated, hard work that the NASA Ad Hoc Group on Computer Methods in Structural Analysis did over the years. A committee with representatives from the finite element community including government, industry, and universities should set up criteria of suitable program maintainability, solution commensurability, user convenience, and machine independence that a program should have to be recognized as maintenance-worthy. A criterion is also needed for an acceptable rate of modernization with respect to the rate of state-of-the-arts advancement for budgetary purposes. Finally, a criterion is needed for obsolescence of analysis state-of-the-arts compared to synthesis state-of-the-arts so that there won't be an unnecessary commitment of maintenance to a passé discipline.

Once the committee has promulgated its set of criteria, then that committee should scrutinize all extant finite element programs to determine which of them qualify as maintainable. If these findings receive general acceptability by all segments of the analytical community that are concerned then the remaining task is to obtain a solid commitment from a reliable source to subsidize the maintenance activity - with the participation of an advisory group, of course.

It could very well be that a more sage approach to the whole topic of proliferation of programs may be to let nature take its course. There could very well be a law of natural selection at work which should be allowed to work. Those programs which become outdated for lack of maintenance (for whatever reason) might naturally be ignored by analysts and only those that satisfy the continuing needs would survive.

CONCLUSION

There is one fundamental precept for which I would plead. So long as there is no revolutionary break-through in computer technology; there are enough good, maintainable programs in existence today to vitiate against the inauguration of any new programs. Proliferation should subside as the number of programs that are properly maintained reduce to a vigorous few. Proliferation impedes the benefits of good communication, economy, and dissemination which can be derived from maintaining a small number of programs. Before any of today's programs are retired, however, there should be a consensus within the profession as to how best to proceed in the future.